O'ZBEKISTON RESPUBLIKASI
FANLAR AKADEMIYASI

Mexanika va inshootlar seysmik mustahkamligi instituti
MISMI

International Conference: Mechanics, Earthquake Engineering, Machinery Building

Международная конференция: Механика, Сейсмостойкость, Машиностроение

«Ensuring seismic safety and seismic stability of buildings and structures, applied problems of mechanics»

dedicated to the 90th anniversary of Academician T.R. Rashidov

«Обеспечение сейсмической безопасности и сейсмостойкости зданий и сооружений, прикладные задачи механики»

посвященная 90-летию академика АН РУз Т.Р. Рашидова

II-ТОМ

May 27-29, 2024. Tashkent, Uzbekistan
27-29 мая 2024 г. Ташкент, Узбекистан

Кабинет Министров Республики Узбекистан
Академия наук Республики Узбекистан
Институт механики и сейсмостойкости сооружений им. М.Т.Уразбаева
Институт сейсмологии им. Г.О. Мавлянова
Национальный университет Узбекистана им. Мирзо Улугбека
Самаркандский государственный университет
Ташкентский архитектурно-строительный университет
Самаркандский государственный архитектурно-строительный университет
Санкт-Петербургский политехнический университет Петра Великого
Калифорнийский университет в г. Беркли

СБОРНИК МАТЕРИАЛОВ МЕЖДУНАРОДНОЙ КОНФЕРЕНЦИИ: МЕХАНИКА, СЕЙСМОСТОЙКОСТЬ, МАШИНОСТРОЕНИЕ

ПО ПРОБЛЕМАМ

ОБЕСПЕЧЕНИЯ СЕЙСМИЧЕСКОЙ БЕЗОПАСНОСТИ И СЕЙСМОСТОЙКОСТИ ЗДАНИЙ И СООРУЖЕНИЙ, ПРИКЛАДНЫЕ ЗАДАЧИ МЕХАНИКИ

посвященная 90-летию академика АН РУз Т.Р. Рашидова
27-29 мая 2024 года

II – ТОМ

Ташкент

Сборник материалов международной научной конференции: Механика, Сейсмостойкость, Машиностроение по проблемам «Обеспечения сейсмической безопасности и сейсмостойкости зданий и сооружений, прикладные задачи механики», посвященной 90-летию академика АН РУз Т.Р. Рашидова.

Сборник материалов состоит из 3х томов:

I-Том содержит материалы секций 1 «Сейсмостойкость зданий и сооружений»,
2 «Инженерная сейсмология и сейсмический риск»;

II-Том содержит материалы секции 3 «Механика деформируемого твердого тела, геотехника»;

III-Том содержит материалы секций 4 «Механика жидкости, газа и многофазных сред»,
5 «Динамика и прочность машин».

В сборнике международной конференции представлены научные доклады из научно-исследовательских организаций и университетов Узбекистана, Казахстана, Кыргызстана, США, России, Таджикистана.

В сборнике материалы посвящены актуальным проблемам обеспечения сейсмической безопасности и сейсмостойкости зданий и сооружений, а также решению прикладных задач механики. Материалы сборника освещают широкий круг вопросов по междисциплинарным исследованиям проблем теоретической и прикладной механики: представлены последние инновационные результаты научных исследований, а также новейшие разработки и тенденции широкого спектра задач механики, включая эксперименты, численные результаты и приложения. Избранные доклады будут опубликованы в Узбекском журнале Проблемы механики, AIP Conference Proceedings и Magazine of Civil Engineering. В сборнике все статьи представлены в авторской редакции.

Сборник материалов будет полезен научным работникам, преподавателям, докторантам и студентам вузов.

Collection of materials of the International Scientific Conference: Mechanics, Seismic Resistance, Mechanical Engineering on the problems of "Ensuring Seismic Safety and Seismic Resistance of Buildings and Structures, Applied Problems of Mechanics", dedicated to the 90th anniversary of Academician of Academy of Sciences of RUz T.R. Rashidov

The collection of materials consists of 3 volumes:

Volume I contains materials of sections 1 “Seismic resistance of buildings and structures” and
2 “Engineering seismology and seismic risk”;

Volume II contains materials of section 3 “Mechanics of deformable rigid bodies, geotechnics”;

Volume III contains materials of sections 4 “Mechanics of liquids, gases, and multiphase media” and
5 “Dynamics and strength of machines.”

The proceedings of the International Conference of present scientific reports from research institutions and universities of Uzbekistan, Kazakhstan, Kyrgyzstan, the USA, Russia, and Tajikistan.

Materials of the collection of reports are devoted to current problems of ensuring seismic safety and seismic resistance of buildings and structures and solving applied problems of mechanics. The proceedings cover a wide range of issues in interdisciplinary research into problems of theoretical and applied mechanics: the latest innovative results of scientific research and the latest developments and trends in numerous mechanics problems, including experiments, numerical results, and applications. Selected reports will be published in the Uzbek Journal of Problems of Mechanics, AIP Conference Proceedings and Magazine of Civil Engineering. In the collection, all articles are presented in the author's edition.

The collection of reports will be useful to researchers, lecturers, doctoral students, and university students.

© Институт механики и сейсмостойкости сооружений им. М.Т. Уразбаева, 2024

ОРГАНИЗАТОРЫ

Юлдашев Бехзод Садыкович
Президент Академии наук Республики Узбекистан

Закиров Батир Иркинович
Министр строительства и жилищно-коммунального хозяйства Республики Узбекистан

Кулдашев Абдулла Хамидуллаевич
Министр по чрезвычайным ситуациям Республики Узбекистан

Бекмирзаев Диёрбек Абдугаппорович
Заместитель начальника отдела координации вопросов обеспечения сейсмической безопасности Кабинет Министров Республики Узбекистан

ОРГАНИЗАЦИОННЫЙ КОМИТЕТ КОНФЕРЕНЦИИ

Юлдашев Бехзод Садыкович (*председатель*)
Президент Академии наук Республики Узбекистан, доктор физико-математических наук, профессор. Ташкент, Узбекистан

Султанов Карим Султанович (*сопредседатель*)
доктор физико-математических наук, профессор, директор Института механики и сейсмостойкости сооружений АН РУз. Ташкент, Узбекистан

Ватин Николай Иванович (*сопредседатель*)
доктор технических наук, профессор, Санкт-Петербургский политехнический университет Петра Великого. Санкт-Петербург, Россия

МЕЖДУНАРОДНЫЙ КОНСУЛЬТАТИВНЫЙ КОМИТЕТ

Нигматулин Р.И. – Академик РАН, д.ф.-м.н., профессор, Московский государственный университет имени М.В.Ломоносова. Москва, РОССИЯ

Марко Амабили – профессор, Инженерный факультет Университета Вестлейка, Ханчжоу, Китай.

Амаржит Сингх – профессор, Машиностроительный факультет, Национальный технологический институт Хамирпур, Индия.

Быковцев А.С. – д.т.н., профессор, Региональная академия естественных наук, Калифорния, США.

Рашид Зегаид – профессор, Университет Касди Мерба Уаргла, Уаргла, Алжир.

Бассас А. Тайах – профессор, Строительный факультет, Исламский университет Газы, Газа.

Энрике Да Сильва Пиззо – Строительство/Водные ресурсы, Факультет гидравлический измерений, Муниципальная санитарно-техническая компания Жуис де Фора, Минас Жераис, Бразилия.

Мирсаидов М.М. – Академик АН РУз, доктор технических наук, профессор, Национальный исследовательский университет "Ташкентский институт инженеров ирригации и механизации сельского хозяйства". Ташкент, Узбекистан.

Бахадиров Г.А. – профессор, Институт механики и сейсмостойкости сооружений АН РУз. Ташкент, Узбекистан.

Саурав Диксит – профессор, Профессиональный университет Ловли, Пенджаб, Индия

Тахиров Ш.М. – профессор, Калифорнийский Университет в Беркли, США.

Ху Донгшенг – профессор, Технологический университет Уханя, Ухань, Китай

Абиров Р.А. – старший научный сотрудник, Институт механики и сейсмостойкости сооружений АН РУз. Ташкент, Узбекистан.

ПРОГРАММНЫЙ КОМИТЕТ КОНФЕРЕНЦИИ

Абдуллабеков К.Н. Академик АН РУз. г. Ташкент.
Негматуллаев С.Х. Академик НАН РТ, г. Душанбе.
Мамасаидов М.Т. Академик НАН КР, г. Ош.
Ильичев В.А. Академик РААСН, г. Москва.
Алексеева Л.А. д.ф.-м.н., проф. г. Алматы.
Абдикаримов Р.А. д.ф.-м.н., проф. г. Ташкент.
Абдусаттаров А.А. д.т.н., проф. г. Ташкент.
Ахмедов А.Б. д.ф.-м.н., проф. г. Ташкент.
Бегалиев У.Т. д.т.н., проф. г. Бишкек.
Бегматов А.Б. д.ф.-м.н., проф. г. Ташкент.
Георгиевский Д.В. д.ф.-м.н., проф. г. Москва.
Исаханов Е.А. д.т.н., проф. г. Алматы.
Исмаилов В.А. д.г.-м.н., проф. г. Ташкент.
Исмоилова С.И. д.т.н. г. Ташкент.
Исраилов М.Ш. д.ф.-м.н., проф. г. Грозный.
Халджигитов А.А. д.ф.-м.н., проф. г. Ташкент.
Хожметов Г.Х. д.т.н., проф. г. Ташкент.
Худайназаров Х.Х. д.т.н., проф. г. Ташкент.
Хужаев И.К. д.т.н., проф. г. Ташкент.
Хусанов Б.Э. д.ф.-м.н. г. Ташкент.
Хужаёров Б.Х. д.ф.-м.н., проф. г. Самарканд.
Коршунова Н.А. д.ф.-м.н., проф. г. Ташкент.
Кузнецов С.В. д.ф.-м.н., проф. г. Москва.
Маликов З.М. д.т.н., проф., г. Ташкент.
Мухаммадиев Д.М. д.т.н., проф. г. Ташкент.
Мардонов Б.М. д.ф.-м.н., проф. г. Ташкент.
Мирзаев И.М. д.ф.-м.н., проф. г. Ташкент.
Москвитин Г.В. д.ф.м.н., проф. г. Москва.
Овчинникова Н.В. к.ф.-м.н. г. Москва.
Ризаев А.А. д.т.н., проф. г. Ташкент.
Усаров М.К. д.ф.-м.н., проф. г. Ташкент.
Ювмитов А.С. PhD., ст.н.с. г. Ташкент.
Уздин А.М. д.т.н., проф. г. Санкт-Петербург.
Жусупбеков А.Ж. д.т.н., проф. г. Астана.

СЕКРЕТАРИАТ

Нишонов Н.А. (отв. секр.)	PhD.	Ташкент
Ан Е.В.	PhD.	Ташкент
Джураева Н.Б.	PhD.	Ташкент
Логинов П.В.	PhD.	Ташкент
Набиев А.М.	PhD.	Ташкент
Умархонов С.И.	к.т.н.	Ташкент
Хамдамов М.	PhD.	Ташкент

PARAMETRIC VIBRATIONS OF A VISCOELASTIC SHELL OF VARIABLE THICKNESS

Abdikarimov R.A.[1], Ishmatov A.N.[2], Khodzhaev D.A.[2], Normuminov B.A.[2]
[1]*Tashkent University of Architecture and Civil Engineering, Tashkent, Uzbekistan*
[2]*National Research University "TIIAME", Tashkent, Uzbekistan*
E-mail: normuminovb_77@inbox.ru

Abstract: *The problem of parametric vibrations of a doubly-curved viscoelastic shell of variable thickness under the influence of a periodic load is considered in the article. Under the Kirchhoff-Love hypothesis in a geometrically nonlinear statement, a mathematical model of the problem was developed considering the viscoelastic properties of the material. Using the Bubnov-Galerkin method, a resolving system of equations was obtained as a system of ordinary integrodifferential equations. The resulting system is solved by the proposed numerical method. Based on this method, a computational algorithm for numerical solution was developed and a package of programs was created in the Delphi algorithmic language.*

Keywords: *viscoelastic shell, variable thickness, periodic load, parametric vibrations, mathematical model, numerical method*

1. Introduction

Complex structures are now widely used in modern technology and engineering and ensuring their strength and reliability is of great importance. The optimal design of such structures is impossible without creating mathematical models that allow considering the maximum possible number of factors affecting their performance. Lightweight and durable thin-walled structures such as plates, panels, and shells can be subject to various loads. Thin plates or shells can have smooth thickenings to provide the necessary thickenings in the right places. Therefore, their design scheme must be built considering the smooth variable or stepwise variable thickness of the shell. Under significant impacts, large deflections occur in such elements, and to calculate such structures, it is necessary to conduct studies in a geometrically nonlinear statement.

A series of publications is devoted to studying the behavior of plates, panels, and shells of constant thickness under dynamic loads in an elastic statement. A review of the results of these studies can be found in [1, 2].

The nonlinear dynamics of plates and shallow shells was considered by A.S. Volmir [2], V.A. Krysko [3], and other researchers. V.V. Karpov [4] developed the geometrically nonlinear theory of shells of stepwise variable thickness.

Recently, special attention has been paid to lightweight composite materials in construction, resulting in the need to consider structures with both homogeneous and non-homogeneous material properties. The behavior of thin-walled structures with various types of features, considering the viscoelastic properties of the material and geometric nonlinearity under dynamic loading, was not sufficiently studied due to the complexity of accounting for the above factors and the need to solve cumbersome nonlinear boundary value problems.

A review of the study on the behavior of plates and shells under dynamic loads, considering the viscoelastic properties of the material, can be found in [5].

Parametric vibrations were the subject of numerous studies in application to a variety of mechanical systems with distributed parameters, in particular rods, plates, and shells.

In [6], models with four degrees of freedom were studied, describing the parametric vibrations of a cylindrical shell under geometrically nonlinear strain. The dynamics of the system are described by the Donnell-Mushtari-Vlasov equations. Discretization is conducted by the Bubnov-Galerkin method.

Based on the V.Z. Vlasov semi-momentless theory [7], the problem of dynamic stability of an isotropic cylindrical shell of variable thickness and density along the generatrix under the influence of a symmetrical variable external pressure along the generatrix was considered under various boundary conditions.

Based on the simplified theory of nonlinear shells proposed by V.V. Novozhilov, in [8], nonlinear vibrations of composite shells of variable thickness were studied.

In [9], a new numerical-analytical method was proposed for studying nonlinear vibrations of shells of variable thickness of the layer in a geometrically nonlinear formulation. The problem was reduced to solving a sequence of linear problems, including the ones related to linear vibrations with a special form of elasticity.

The study in [10] is devoted to vibrations of various types of composite plates and shells of variable thickness. The resulting equations were solved by the proposed numerical method, the accuracy of which was confirmed by comparison with the results of other researchers, obtained analytically and numerically.

In [11], the stability of thin cylindrical shells of variable thickness under dynamic axial load was studied. The effect of thickness variation and loading rate on the critical load of stability loss was investigated.

A technique for buckling optimization of thin-walled cylindrical shells of variable stiffness under the axial load is described in [12].

Reference [13] is devoted to the experimental and numerical study of buckling and free vibrations of cylindrical shells of constant and variable rigidity.

In [14], free vibrations of cylindrical shells of variable thickness were studied under various boundary conditions using numerical results. To solve the problem, the finite element method was used. The influence of variation in thickness, boundary conditions, and material properties on the frequency and amplitude of vibrations was studied.

The study in [15] was devoted to vibrations of a doubly-curved shell of variable thickness. Various types of thickness profiles were considered.

Free vibrations of composite shells of variable thickness are considered in [16].

In [17], the finite element method for calculating plates and shells of variable thickness is described. In this case, elements of various shapes are used and their advantages in solving specific problems are shown.

In [18], a three-dimensional rectangular plate (shell) element was proposed based on the formulation of the finite element method for absolute nodal coordinates.

Despite the large number of published works devoted to parametric vibrations of thin-walled structures, the number of studies on parametric vibrations of thin-walled structures considering the viscoelastic properties of their material is limited.

2. Materials, methods, and object of study.

Let us consider a doubly-curved viscoelastic shell with sides *a* and *b*, variable thickness *h=h(x,y)* and radii of curvature of the middle surface R_1 and R_2 under the action of axial dynamic loads. The shell is located under the specified external static loads of intensity p_x, p_y, q applied to the shell element in the *x*, *y* and *z* directions, respectively. Let the shell be subjected to dynamic loading along side *a* by periodic load $P(t)=P_0+P_1\cos\Theta t$ (P_0, P_1=const; Θ - is the frequency of the external periodic load).

Under the accepted assumptions, with force $P(t)\frac{\partial^2 w}{\partial x^2}$, the mathematical model of this problem regarding deflection *w=w(x,y,t)* and displacements *u=u(x,y,t), v=v(x,y,t)* is described by the following equation [19]:

$$\left(1-\Gamma^*\right)\left\{h\left[\frac{\partial^2 u}{\partial x^2}-\left(k_x+\mu k_y\right)\frac{\partial w}{\partial x}+\frac{1-\mu}{2}\frac{\partial^2 u}{\partial y^2}+\frac{1+\mu}{2}\frac{\partial^2 v}{\partial x\partial y}+\frac{\partial w}{\partial x}\frac{\partial^2 w}{\partial x^2}+\right.\right.$$

$$\left.+\frac{1-\mu}{2}\frac{\partial w}{\partial x}\frac{\partial^2 w}{\partial y^2}+\frac{1+\mu}{2}\frac{\partial w}{\partial y}\frac{\partial^2 w}{\partial x\partial y}\right]+\frac{\partial h}{\partial x}\left[\frac{\partial u}{\partial x}+\mu\frac{\partial v}{\partial y}-\left(k_x+\mu k_y\right)w+\right.$$

$$+\frac{1}{2}\left(\frac{\partial w}{\partial x}\right)^2+\frac{\mu}{2}\left(\frac{\partial w}{\partial y}\right)^2\Bigg]+\frac{1-\mu}{2}\frac{\partial h}{\partial y}\left(\frac{\partial u}{\partial y}+\frac{\partial v}{\partial x}+\frac{\partial w}{\partial x}\frac{\partial w}{\partial y}\right)\Bigg\}+p_x-\frac{\left(1-\mu^2\right)\rho h}{E}\frac{\partial^2 u}{\partial t^2}=0\,,$$

$$\left(1-\Gamma^*\right)\Bigg\{h\Bigg[\frac{\partial^2 v}{\partial y^2}-\left(k_y+\mu k_x\right)\frac{\partial w}{\partial y}+\frac{1-\mu}{2}\frac{\partial^2 v}{\partial x^2}+\frac{1+\mu}{2}\frac{\partial^2 u}{\partial x\partial y}+\frac{\partial w}{\partial y}\frac{\partial^2 w}{\partial y^2}+$$

$$+\frac{1-\mu}{2}\frac{\partial w}{\partial y}\frac{\partial^2 w}{\partial x^2}+\frac{1+\mu}{2}\frac{\partial w}{\partial x}\frac{\partial^2 w}{\partial x\partial y}\Bigg]+\frac{\partial h}{\partial y}\Bigg[\frac{\partial v}{\partial y}+\mu\frac{\partial u}{\partial x}-\left(k_y+\mu k_x\right)w+ \qquad (1)$$

$$+\frac{1}{2}\left(\frac{\partial w}{\partial y}\right)^2+\frac{\mu}{2}\left(\frac{\partial w}{\partial x}\right)^2\Bigg]+\frac{1-\mu}{2}\frac{\partial h}{\partial x}\left(\frac{\partial u}{\partial y}+\frac{\partial v}{\partial x}+\frac{\partial w}{\partial x}\frac{\partial w}{\partial y}\right)\Bigg\}+p_y-\frac{\left(1-\mu^2\right)\rho h}{E}\frac{\partial^2 v}{\partial t^2}=0\,,$$

$$\left(1-\Gamma^*\right)h^3\left(\frac{\partial^4 w}{\partial x^4}+2\frac{\partial^4 w}{\partial x^2\partial y^2}+\frac{\partial^4 w}{\partial y^4}\right)+3\left(1-\Gamma^*\right)\left[2h\left(\frac{\partial h}{\partial x}\right)^2+h^2\frac{\partial^2 h}{\partial x^2}\right]\left(\frac{\partial^2 w}{\partial x^2}+\mu\frac{\partial^2 w}{\partial y^2}\right)+$$

$$+6\left(1-\Gamma^*\right)h^2\frac{\partial h}{\partial x}\left(\frac{\partial^3 w}{\partial x^3}+\frac{\partial^3 w}{\partial x\partial y^2}\right)+6\left(1-\Gamma^*\right)h^2\frac{\partial h}{\partial y}\left(\frac{\partial^3 w}{\partial y^3}+\frac{\partial^3 w}{\partial x^2\partial y}\right)+$$

$$+3\left(1-\Gamma^*\right)\left[2h\left(\frac{\partial h}{\partial y}\right)^2+h^2\frac{\partial^2 h}{\partial y^2}\right]\left(\frac{\partial^2 w}{\partial y^2}+\mu\frac{\partial^2 w}{\partial x^2}\right)+6\left(1-\mu\right)\left(1-\Gamma^*\right)\left[2h\frac{\partial h}{\partial x}\frac{\partial h}{\partial y}+h^2\frac{\partial^2 h}{\partial x\partial y}\right]\frac{\partial^2 w}{\partial x\partial y}-$$

$$-12\left(1-\Gamma^*\right)h\Bigg[\left(k_x+\mu k_y\right)\frac{\partial u}{\partial x}+\left(\mu k_x+k_y\right)\frac{\partial v}{\partial y}-\left(k_x^2+k_y^2+2\mu k_x k_y\right)w+$$

$$+\frac{k_x+\mu k_y}{2}\left(\frac{\partial w}{\partial x}\right)^2+\frac{k_y+\mu k_x}{2}\left(\frac{\partial w}{\partial y}\right)^2\Bigg]-12\frac{\partial w}{\partial x}\left(1-\Gamma^*\right)\Bigg\{h\Bigg[\frac{\partial^2 u}{\partial x^2}-\left(k_x+\mu k_y\right)\frac{\partial w}{\partial x}+$$

$$+\frac{1-\mu}{2}\frac{\partial^2 u}{\partial y^2}+\frac{1+\mu}{2}\frac{\partial^2 v}{\partial x\partial y}+\frac{\partial w}{\partial x}\frac{\partial^2 w}{\partial x^2}+\frac{1-\mu}{2}\frac{\partial w}{\partial x}\frac{\partial^2 w}{\partial y^2}+\frac{1+\mu}{2}\frac{\partial w}{\partial y}\frac{\partial^2 w}{\partial x\partial y}\Bigg]+\frac{\partial h}{\partial x}\Bigg[\frac{\partial u}{\partial x}+$$

$$+\mu\frac{\partial v}{\partial y}-\left(k_x+\mu k_y\right)w+\frac{1}{2}\left(\frac{\partial w}{\partial x}\right)^2+\frac{\mu}{2}\left(\frac{\partial w}{\partial y}\right)^2\Bigg]+\frac{1-\mu}{2}\frac{\partial h}{\partial y}\left(\frac{\partial u}{\partial y}+\frac{\partial v}{\partial x}+\frac{\partial w}{\partial x}\frac{\partial w}{\partial y}\right)\Bigg\}-$$

$$-12\frac{\partial^2 w}{\partial x^2}\left(1-\Gamma^*\right)h\Bigg[\frac{\partial u}{\partial y}+\mu\frac{\partial v}{\partial y}-\left(k_x+\mu k_y\right)w+\frac{1}{2}\left(\frac{\partial w}{\partial x}\right)^2+\frac{\mu}{2}\left(\frac{\partial w}{\partial y}\right)^2\Bigg]-$$

$$-12\frac{\partial w}{\partial y}\left(1-\Gamma^*\right)\Bigg\{h\Bigg[\frac{\partial^2 v}{\partial y^2}-\left(k_y+\mu k_x\right)\frac{\partial w}{\partial y}+\frac{1-\mu}{2}\frac{\partial^2 v}{\partial x^2}+\frac{1+\mu}{2}\frac{\partial^2 u}{\partial x\partial y}+$$

$$+\frac{\partial w}{\partial y}\frac{\partial^2 w}{\partial y^2}+\frac{1-\mu}{2}\frac{\partial w}{\partial y}\frac{\partial^2 w}{\partial x^2}+\frac{1+\mu}{2}\frac{\partial w}{\partial x}\frac{\partial^2 w}{\partial x\partial y}\Bigg]+\frac{\partial h}{\partial y}\Bigg[\frac{\partial v}{\partial y}+\mu\frac{\partial u}{\partial x}-$$

$$-\left(k_y+\mu k_x\right)w+\frac{1}{2}\left(\frac{\partial w}{\partial y}\right)^2+\frac{\mu}{2}\left(\frac{\partial w}{\partial x}\right)^2\Bigg]+\frac{1-\mu}{2}\frac{\partial h}{\partial x}\left(\frac{\partial u}{\partial y}+\frac{\partial v}{\partial x}+\frac{\partial w}{\partial x}\frac{\partial w}{\partial y}\right)\Bigg\}-$$

$$-12\frac{\partial^2 w}{\partial y^2}\left(1-\Gamma^*\right)h\Bigg[\frac{\partial v}{\partial y}+\mu\frac{\partial u}{\partial y}-\left(k_y+\mu k_x\right)w+\frac{1}{2}\left(\frac{\partial w}{\partial y}\right)^2+\frac{\mu}{2}\left(\frac{\partial w}{\partial x}\right)^2\Bigg]-$$

$$-12\left(1-\mu\right)\frac{\partial^2 w}{\partial x\partial y}\left(1-\Gamma^*\right)h\left(\frac{\partial u}{\partial y}+\frac{\partial v}{\partial x}+\frac{\partial w}{\partial x}\frac{\partial w}{\partial y}\right)+\frac{12\left(1-\mu^2\right)\rho h}{E}\frac{\partial^2 w}{\partial t^2}-P(t)\frac{\partial^2 w}{\partial x^2}=\frac{12\left(1-\mu^2\right)}{E}q\,,$$

where $k_x=1/R_1$, $k_y=1/R_2$.

Let the shell thickness change by the following law $\square(x)=\frac{1}{2}\square_0(1+\alpha*x)$, ($\alpha*-$ is the

thickness variation parameter), i.e., the change leads to a linear increase in shell thickness. We will assume that the shell has initial deflections $w_0=w_0(x, y, t)$.

We approximate the total and initial deflections and shell displacements, in the following form:

$$u(x,y,t)=\sum_{n=1}^{N}\sum_{m=1}^{M}u_{nm}(t)\varphi_{nm}(x,y),\quad v(x,y,t)=\sum_{n=1}^{N}\sum_{m=1}^{M}v_{nm}(t)\phi_{nm}(x,y),$$

$$w(x,y,t)=\sum_{n=1}^{N}\sum_{m=1}^{M}w_{nm}(t)\psi_{nm}(x,y),\quad w_0(x,y)=\sum_{n=1}^{N}\sum_{m=1}^{M}w_{0nm}\psi_{nm}(x,y), \tag{2}$$

where $u_{nm}=u_{nm}(t), v_{nm}=v_{nm}(t),\ \ w_{nm}=w_{nm}(t)$ – are the unknown functions of time; $\phi_{nm}(x,y)$, $\varphi_{nm}(x,y)$, $\psi_{nm}(x,y)$, $n=1,2,...,N$; $m=1,2,...,M$ are the coordinate functions that satisfy given boundary conditions of the problem.

Substituting (2) into the system of equations (1) and performing the Bubnov-Galerkin procedure, while introducing the following dimensionless quantities

$$\frac{u}{h_0},\ \frac{v}{h_0},\ \frac{w}{h_0},\ \frac{w_0}{h_0},\ \frac{x}{a},\ \frac{y}{b},\ \frac{h}{h_0},\ \lambda=\frac{a}{b},\ \ \delta=\frac{b}{h_0},\ \bar{k}_x=\frac{a^2}{h_0R_1},\ \bar{k}_y=\frac{b^2}{h_0R_2},$$

$$\bar{q}=\frac{q}{E}\left(\frac{b}{h_0}\right)^4,\ \ \bar{p}_x=\frac{p_x}{E},\ \ \bar{p}_y=\frac{p_y}{E},\ \ \frac{\Theta}{\omega},\ \ \omega t,\ \ \frac{\Gamma(t)}{\omega},\ \ \delta_0=\frac{P_0}{P_{кр}},\ \ \delta_1=\frac{P_1}{P_{кр}},$$

and keeping the same notation to determine the unknowns $w_{nm}=w_{nm}(t),\ u_{nm}=u_{nm}(t),\ v_{nm}=v_{nm}(t)$, we obtain the following system of nonlinear integro-differential equations:

$$\sum_{n=1}^{N}\sum_{m=1}^{M}a_{klnm}\ddot{u}_{nm}-\eta_1\left(1-\Gamma^*\right)\left\{\sum_{n=1}^{N}\sum_{m=1}^{M}\left(d_{1klnm}u_{nm}+\lambda e_{1klnm}v_{nm}\right)-\right.$$

$$\left.-\frac{k_x+\lambda^2\mu k_y}{\lambda\delta}f_{1klnm}\left(w_{nm}-w_{0nm}\right)\right)+\frac{1}{\delta}\sum_{n,i=1}^{N}\sum_{m,j=1}^{M}g_{1klnmij}\left(w_{nm}w_{ij}-w_{0nm}w_{0ij}\right)\Bigg\}=0,$$

$$\sum_{n=1}^{N}\sum_{m=1}^{M}b_{klnm}\ddot{v}_{nm}-\eta_2\left(1-\Gamma^*\right)\left\{\sum_{n=1}^{N}\sum_{m=1}^{M}\left(\frac{1}{\lambda}d_{2klnm}u_{nm}+e_{2klnm}v_{nm}\right)-\right.$$

$$\left.-\frac{\lambda^2k_y+\mu k_x}{\lambda^2\delta}f_{2klnm}\left(w_{nm}-w_{0nm}\right)\right)+\frac{1}{\delta}\sum_{n,i=1}^{N}\sum_{m,j=1}^{M}g_{2klnmij}\left(w_{nm}w_{ij}-w_{0nm}w_{0ij}\right)\Bigg\}=0,$$

$$\sum_{n=1}^{N}\sum_{m=1}^{M}c_{klnm}\ddot{w}_{nm}+\eta_3\sum_{n=1}^{N}\sum_{m=1}^{M}p_{klnm}^2\left(1-2\mu_{klnm}\cos\Theta t\right)w_{nm}+ \tag{3}$$

$$+\eta_3\left(1-\Gamma^*\right)\left\{\sum_{n=1}^{N}\sum_{m=1}^{M}\left(d_{3klnm}u_{nm}+e_{3klnm}v_{nm}+f_{3klnm}\left(w_{nm}-w_{0nm}\right)\right)-\sum_{n,i=1}^{N}\sum_{m,j=1}^{M}g_{3klnmij}\left(w_{nm}w_{ij}-w_{0nm}w_{0ij}\right)\right\}-$$

$$-\eta_3\left\{\sum_{n,i=1}^{N}\sum_{m,j=1}^{M}w_{nm}\left(1-\Gamma^*\right)\left(d_{4klnmij}u_{ij}+e_{4klnmij}v_{ij}+f_{4klnmij}\left(w_{ij}-w_{0ij}\right)\right)+\right.$$

$$+e_{4klnmij}v_{ij}+f_{4klnmij}\left(w_{ij}-w_{0ij}\right)\Big)+$$

$$\left.+\sum_{n,i,r=1}^{N}\sum_{m,j,s=1}^{M}g_{klnmijrs}w_{nm}\left(1-\Gamma^*\right)\left(w_{ij}w_{rs}-w_{0ij}w_{0rs}\right)\right\}=12\eta_3\left(1-\mu^2\right)\lambda^4q_{kl},$$

$$u_{nm}(0)=u_{0nm},\ \dot{u}_{nm}(0)=\dot{u}_{0nm},\ v_{nm}(0)=v_{0nm},\ \dot{v}_{nm}(0)=\dot{v}_{0nm},\ w_{nm}(0)=w_{0nm},\ \dot{w}_{nm}(0)=\dot{w}_{0nm},$$

where $P_{кр} = \frac{\pi^2}{3(1-\mu^2)} E\left(\frac{h_0}{b}\right)^2$ – is the static critical load; $\omega = \sqrt{\pi^2 E h_0^2 P_{кр}^* / (\rho b^4)}$ – is the frequency of the fundamental mode of oscillations; $p_{klnm}^2 = f_{klnm}^{п} - 4\pi^2\lambda^2 p_{klnm}^* \delta_0$; $\mu_{klnm} = \frac{2\pi^2\lambda^2 p_{klnm}^*}{p_{klnm}^2}\delta_1$; the remaining constant coefficients included in this system are related to coordinate functions and their derivatives.

System (3) was integrated using the numerical method proposed in [20]. The weakly singular Koltunov-Rzhanitsyn kernel of the following form [21-23] is used as a relaxation kernel:

$$\Gamma(t) = Ae^{-\beta t} t^{\alpha-1}, \quad (0 < \alpha < 1)$$

Here: A – is the viscosity parameter; α, β – are other rheological parameters.

3. Results and discussion

The results of calculations performed on a computer are shown in graphs, Fig. 1-3. Fig. 1 shows the influence of the viscoelastic properties of the shell material on its behavior. Analysis of the results obtained shows that the consideration of the viscoelastic properties of the material leads to a narrowing of the region of dynamic instability.

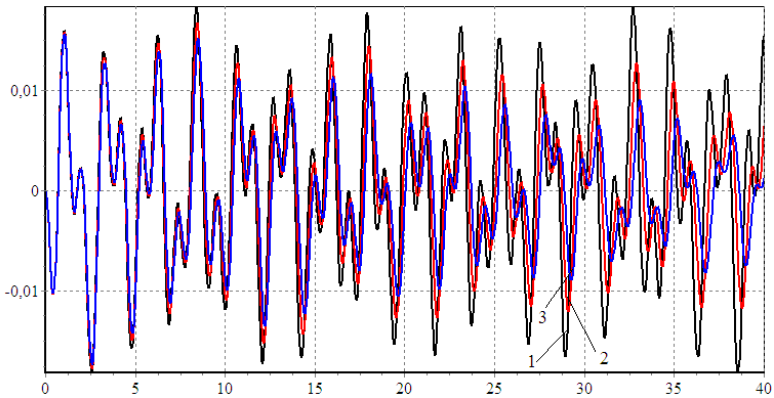

Figure 1. - **Deflection as a function of time for *A*=0 (1); 0.05 (2); 0.1 (3)**

The results of studying the behavior of the shell at different values of the thickness variation parameter α^* are shown in Fig. 2. Changing the thickness of the viscoelastic shell by the above law, with equal volumes of shell of constant and variable thickness, leads to a decrease in maximum displacements. The results of the study show that an increase in this parameter leads to an increase in the amplitude of oscillations and a phase shift.

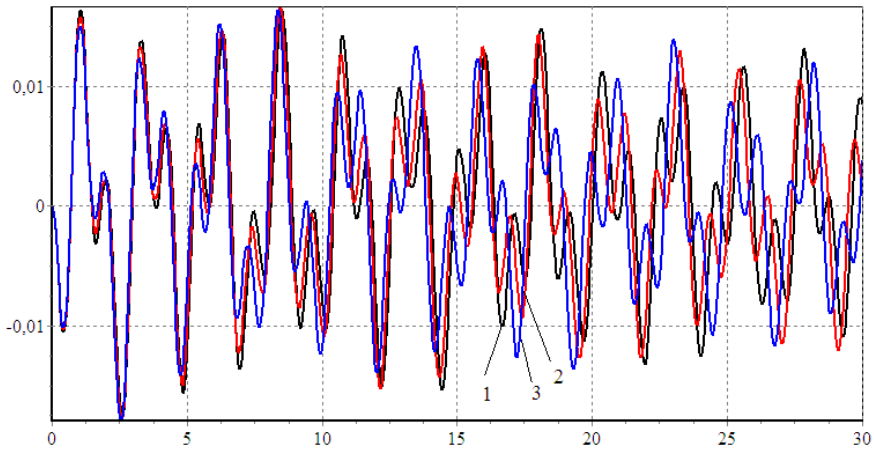

Figure 2. - **Deflection as a function of time for α*=0.3 (1); 0.5 (2); 0.8 (3)**

Fig. 3 shows the results of studying the behavior of the shell at different values of curvature k_x. The figure shows that an increase in this parameter leads to an increase in the oscillation amplitude and a phase shift.

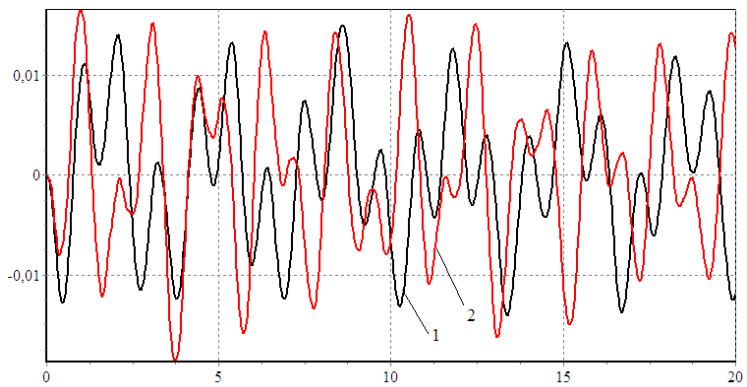

Figure 3. - **Deflection as a function of time for k_x=0 (1); 20 (2)**

4. Conclusion

Based on a polynomial approximation of deflections, the dynamic behavior of a doubly-curved shell of variable thickness was studied.

The influence of variations in the physical, mechanical, and geometric parameters of the shell material on the amplitude-time characteristics and the stress-strain state was assessed, and a number of new mechanical effects were identified:

variations in the thickness at the same volume of thin-walled structures lead to a decrease in the maximum values of deflections;

variations in the thickness of the shell lead to a redistribution of bending and chain stresses.

References

1. *Bolotin V.V.* Dynamic stability of elastic systems / M.: Gostekhizdat, 1956, 600 p.
2. *Volmir A.S.* Stability of deformable systems / M.: Nauka, 1967, 1984 p.
3. *Krysko V.A.* Nonlinear statics and dynamics of inhomogeneous shells / Saratov: Publishing House of Saratov Univ., 1976, 216 p.
4. *Karpov V.V.* Geometrically nonlinear problems for plates and shells and methods for their solution / St. Petersburg: Publishing house ASV; SPbGASU, 1999, 154 p.
5. *Rzhanitsyn A.R.* Theory of creep / M.: Nauka, 1968, 416 p.
6. *Kochurov R.E., Avramov K.V.* Models of nonlinear parametric vibrations of cylindrical shells // Problems of mechanical engineering, 2010, vol.13, No. 3, pp. 55-61.
7. *Mochalin A.A.* Parametric vibrations of an inhomogeneous circular cylindrical shell of variable density under various boundary conditions // News of Saratov University. New Series. Series: Mathematics. Mechanics. Informatics, 2015, vol.15, No. 2, pp. 210-215.
8. *Datta P., Ray M.C.* Smart damping of large amplitude vibrations of variable thickness laminated composite shells. Thin-Walled Structures. 2018. 127. pp. 710–727. DOI:10.1016/j.tws.2018.03.009.
9. *Awrejcewicz J., Kurpa L., Shmatko T.* Investigating geometrically nonlinear vibrations of laminated shallow shells with layers of variable thickness via the R-functions theory. Composite Structures. 2015. 125. pp. 575–585. DOI:10.1016/j.compstruct.2015.02.054.
10. *Bacciocchi M., Eisenberger M., Fantuzzi N., Tornabene F., Viola, E.* Vibration analysis of variable thickness plates and shells by the Generalized Differential Quadrature method. Composite Structures. 2016. 156. pp. 218–237. DOI:10.1016/j.compstruct.2015.12.004.
11. *Fan H., Chen Z., Cheng J., Huang S., Feng W., Liu L.* Analytical research on dynamic buckling of thin cylindrical shells with thickness variation under axial pressure. Thin-Walled Structures. 2016. 101. pp. 213–221. DOI:10.1016/j.tws.2016.01.009.
12. *Pitton S.F., Ricci S., Bisagni C.* Buckling optimization of variable stiffness cylindrical shells through artificial intelligence techniques. Composite Structures. 2019. 230. 111513. DOI:10.1016/j.compstruct.2019.111513.
13. *Labans E., Bisagni C.* Buckling and free vibration study of variable and constant-stiffness cylindrical shells. Composite Structures. 2019. 210. pp. 446–457. DOI:10.1016/j.compstruct.2018.11.061.
14. *Golpayegani I.F., Arani E.M., Foroughifar A.A.* Finite Element Vibration Analysis of Variable Thickness Thin Cylindrical FGM Shells under Various Boundary Conditions. Materials Performance and Characterization. 2019. 8(1). 20180148. DOI:10.1520/mpc20180148.
15. *Tornabene F., Fantuzzi N., Bacciocchi M.* The local GDQ method for the natural frequencies of doubly-curved shells with variable thickness: A general formulation. Composites Part B: Engineering. 2016. 92. pp. 265–289. DOI:10.1016/j.compositesb.2016.02.010.

16. *Venkatachari A., Natarajan S., Ganapathi M.* Variable stiffness laminated composite shells – Free vibration characteristics based on higher-order structural theory. Composite Structures. 2018. 188. pp. 407–414. DOI:10.1016/j.compstruct.2018.01.025.
17. *Agapov V.* The family of multilayered finite elements for the analysis of plates and shells of variable thickness. E3S Web of Conferences. 2019. 91. Pp. 02013. DOI:10.1051/e3sconf/20199102013.
18. *Abbas L.K., Rui X., Hammoudi Z.S.* Plate/shell element of variable thickness based on the absolute nodal coordinate formulation. Proceedings of the Institution of Mechanical Engineers, Part K: Journal of Multi-body Dynamics. 2010. 224. pp. 127–141.
19. *Abdikarimov R.A., Zhgutov V.M.* Mathematical models of problems of nonlinear dynamics of viscoelastic orthotropic plates and shells of variable thickness // Engineering and Construction Journal, 2010, No. 6, pp. 38-47.
20. *Verlan A.F., Abdikarimov R.A., Eshmatov Kh.* Numerical modeling of nonlinear problems of dynamics of viscoelastic systems with variable stiffness // Electronic modeling, 2010, V.32, No. 2, pp. 3-14.
21. *Koltunov M.A.* Creep and relaxation / M.: Higher School, 1976, 276 p.
22. *Normuminov B., Abdikarimov R., Mirsaidov M., Khodzhaev D., Mirzaev B.* Parametric vibrations of viscoelastic orthotropic cylindrical panels of variable thickness. IOP Conference Series: Materials Science and Engineering, 2020, 869(5), 052034.
23. *Normuminov B., Abdikarimov R., Khodzhaev D., Khafizova Z.* Parametric oscillations of viscoelastic orthotropic plates of variable thickness. IOP Conference Series: Materials Science and Engineering, 2020, 896(1), 012029.

DESIGN AND CALCULATION OF SURFACE ROAD CONDUCTORS

Abdukadirov F.E.[1], Hasanov T.M.[1]
[1] *Tashkent State Transport University, Tashkent, Uzbekistan*
E-mail: farkhod.toshkent@gmail.com

Abstract: *This in the article important factors of design and calculation of overhead conductors, their basics are explained. It is also presented to determine stress-deformation states of beam-type load-bearing structures for various loads, and to evaluate their performance using ANSYS software.*
Keywords: *bridge, pier, displacement, tension, ANSYS software.*

1. Introduction

Bridge, overpass, road In order to be considered an important engineering structure, the conductors must meet a number of requirements for it: architecture and planning, production and operation, economic, environmental, design and calculation requirements.

The design and calculation requirements include the condition of strength of the structure, the condition of the unity of the overpass, and the priority conditions of the structure.

The construction of buildings and structures, as well as the design of various structures, are being rapidly implemented in our republic, including many artificial structures such as reinforced concrete girder bridges, overpasses, viaducts, underground and surface metros.

T.R.Rashidov, U.Z.Shermukhamedov [1] methods of designing and calculating special seismic protection systems of bridges, damping devices and dynamic vibration dampers used in seismic protection of bridges, influence of seismic isolation on operational characteristics of railway bridges, design of calculation schemes of bridge structures, seismic safety the analysis of the modern state of the problems of provision, the main requirements and measures to ensure earthquake resistance are presented.

V.M. Brodsky, D.A. Ilyushin's article [2] used two different methods to determine the dynamic properties of bridges with reinforced concrete intermediate structures, i.e. calculation and experimental results. In this case, the experiment was carried out with the help of temporary motor vehicle loads specified in the regulatory documents using the measurement-calculation method. Theoretical calculations are based on the use of dynamic influence lines, and the results are calculated for different combinations of loads and speeds. The use of dynamic influence lines allows to estimate the possible changes in dynamic properties by calculation even before the test, but it is described that the analysis of dynamic properties obtained as a result of actual measurements is necessary and urgent when testing bridge intermediate devices with an existing variable load.

In the manual of A.I.Vasilev [3], the main focus is on possible natural loads affecting bridges and the strength of construction materials, where the strength limits of bridge elements are analyzed in terms of reliability theory. Also, the rules of the calculation methodology based on the limit states of building constructions and the probable basis for the determined coefficients are presented. In addition, the load-carrying capacity of the structure and the remaining service life are highlighted in terms of reliability indicators.

A.S.Efremenko, E.A.Ivanovskaya in their article [4] emphasized that the main emphasis is on choosing the most optimal option in the design of overpass supports, and used the method of designing different types of supports to choose the most optimal option. In this work, overpass supports made of metal, precast reinforced concrete, monolithic reinforced concrete structures and reinforced concrete combined structures were compared, taking into account efficiency indicators.

In the article of V.N.Smirnov [5], the main attention is given to the fact that during the construction of a continuous rail track in ballasted bridges, additional forces appear in the supports and other elements of the bridge structure, which are not taken into account in the standards. It is shown that when designing bridge supports on high-speed railways, it is necessary to take into account the interaction of the elements of the "most-besstykovoy put" system on highways.

U.Z. Shermuhamedov , M.A. Abduakhatovalar [6] in the article city transport facilities city of infrastructure important element to be considered , his main of duties one is water roads , car ways intersections and another kind of barriers is available when complicated from the city transport connection normal use conditions provide about information giving , last It is about the reforms implemented in the field of transportation in Tashkent city in 2012 , that is, about the construction of surface transport facilities, suspension roads designed for pedestrian traffic, and three-story overpasses that are planned to be built in the future.

In the article by A.A. Loktev et al. [7], it was found that the speed of vehicles, axle loads and the total mass of the train, as well as the reduction of the time interval between the trains have significantly increased, and the factors lead to a significant increase in dynamic effects, and the classic for artificial structures of the transport infrastructure suggests that non-structural schemes should be used. In the research work, it is proposed to take a three-span arch bridge with a central span structure as the basis for the bridge. The design of the structure of this type allows to change the length of the central span in a very wide range, to reduce the total number of supports while increasing the total length of the bridge crossing, as well as two-track railway and two or four row road bridge from the structure to use possibility gives

T.S. Velichko , S.B. In the article of Kolokolov [8]. city car on the roads security of provision current problems with depends issues will be discussed . Spacing for pedestrian crossings in the article and road of conductors is available structures analysis to do and systematization results given. Analysis as a result work developed of intervals classification use of force principle, basis conditions, project complexity , construction technology and pedestrians for convenience based on given Research from the results city dense is located in places road conductors when designing use can

2. Materials and methods

The load-bearing elements of constructions and structures - the metro overpass under the influence of various loadings were taken, and the laws of elasticity and plasticity of its elements, finite differences and mathematical modeling methods were used in the research process.

Currently, more than 7000 highway bridges are in operation on the public roads of the Republic of Uzbekistan. The total number of bridge structures on highways is 14331, including 604 of international importance, 2722 of national importance, 4302 of local importance, and 6703 of urban and rural internal roads. As it is known, most of the bridges in our Republic are reinforced concrete bridges [9].

These problems are solved by variational or numerical methods. Variational method - Ritts, Bubnov-Galerkin, Treffits as an example, numerical methods - finite element method, finite difference method, boundary element method, spectral method, etc. can be mentioned. The most

common numerical methods are LIRA, ADINA, ANSYS, MARC, MSC/NASTRAN, COSMOS, HERCULE, MODULEF.

3. Results and discussion

A methodology for calculating the state of stress-deformation was developed based on the use of ANSYS software for a spatial structure under different loads - subway-overpass rigging Below is a technical implementation of the calculation method using the ANSYS software for the example of a load-bearing structural element - bridge girders. ANSYS software is an advanced suite of computer engineering modeling tools. ANSYS tools make it possible to solve many problems in various fields of technology using the finite element method [10-11].

Calculation of reinforced concrete structures and foundations based on the limit states of the first and second groups should be carried out taking into account the most unfavorable combinations of loads or forces corresponding to them. The effect of loads is established as a result of the analysis of the actual options for the simultaneous effect of various loads for the considered operation stage of the structure. . The construction of the overpass is a composite-monolithic one, consisting of intermediate supports and spacers that cover the space between the supports and transfer the weight of the loads through the supports to the foundation soil.

Figure 1. a shows the variant of reinforced concrete structures of the type of trestle , and this type of structures is the most useful in terms of technical and economic indicators and economical in terms of material resources.

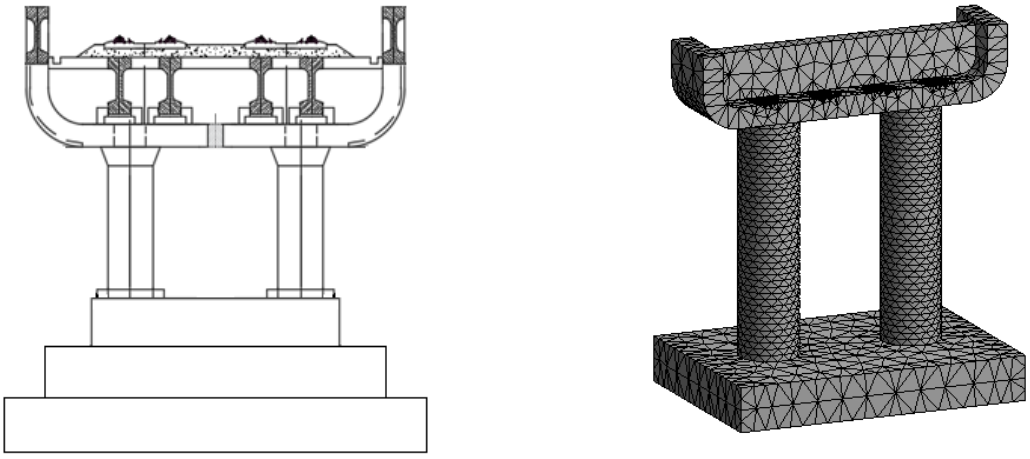

a) b)

Figure 1 - **a) overpass type of reinforced concrete construction s scheme ; b) e stack finite elements appearance .**

The overpass is made of reinforced concrete consists of : concrete B25, reinforcement A-400 (A- III). Rated seismicity - 8 points (Tashkent region for). ANSYS software provided reinforced concrete piers of the metro count for spatial scheme 1.b is shown in Fig.

Calculation of the two-column support of the subway overpass for the main and special combination of loads ShNQ 2.05.03-12 "Bridges and pipelines" and QMQ 2.01.20-16. "Construction of transport facilities in seismic areas". performed in accordance with the requirements.

4. Calculation results and discussion

Spatial calculation of the stress-deformation state of the overpass column was carried out using the ANSYS program. According to the calculation results, self-weight loading, two-span single road loading and two-span two-span loading were analyzed. The distribution of displacement - u_z and normal stress - s_z from two intermediate loadings of the finite element nodes is shown in Fig. 2.

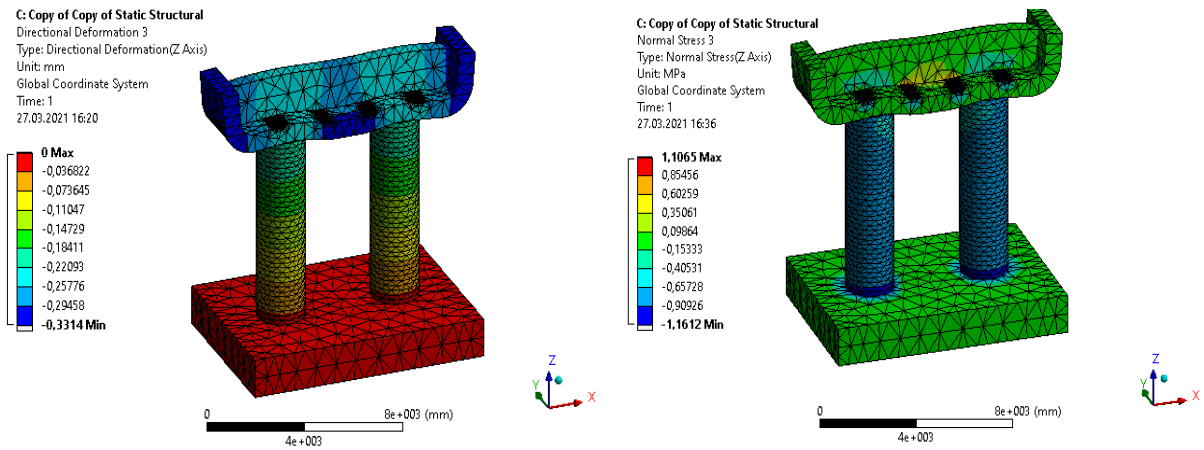

Figure 2. - **Displacement u $_z$ and normal stress σ_z distribution from two span loadings**

Graphs of displacements, deformations and changes in stresses along the length of the cross-section were also obtained. The maximum and minimum values of column node quantities in spatial position (along *the x, y, z axes) were obtained for three types of loading.*

5. Analysis of results

Based on the obtained results, the graph is built of the trestle bridge length across displacements, deformations and of voltages change shown (Fig. 3).

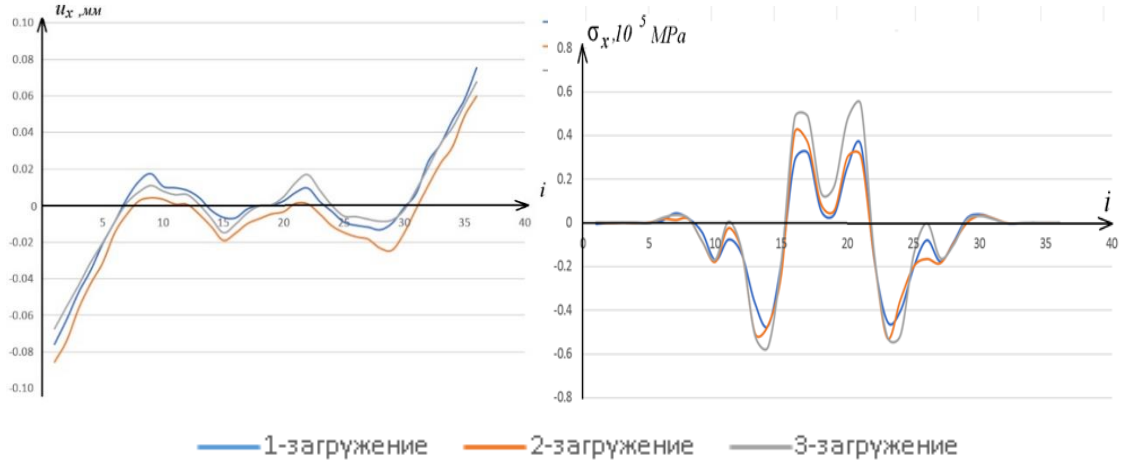

Figure 3. - **Rigel length across a) displacements b) stresses**

Table 1 below three kind of download for in space (*x* , *y* , *z* arrows along) rigels finite element nodes maximum of values values shown.

Table 1

Moving and of voltages maximum values.

Indicators		Download 1:	Download 2:	Download 3:
displacement , mm	u $_x$	0 . 075954	0.08726	0.09776
	he $_y$	0 . 015173	0.01699	0.01931
	he	0 . 31277	0.32959	0.33140
stress , MPa.	σ_x	13 , 0032	1 4 , 9912	1 6 , 5984
	σ_y	24 , 0296	27 , 0186	30.8210
	σ_z	1 5 .0 178	15 , 4966	1 6 , 2568

The results show that the values of the self-weight normal stresses along the *z* -axis are 12.3% less than the two-span one-way loading and 28.4% less than the two-span two-span loading.

6. Conclusions

Based on the above research, the use of advanced modern software in the design and calculation of overhead conductors, as well as a methodical approach to the calculation of load-

bearing structural elements using ANSYS complex programs, as an example - rigel, and a scheme for its implementation are proposed. Deformation-stress state of Rigel is constructed by taking into account the effects of seismic forces, depending on the types of loading, displacement, tension force and moments. a methodology for calculating the load-bearing elements of reinforced concrete structures - metro overpasses and an implementation scheme have been developed.

References

1. *Rashidov T.R., Shermukhamedov U.Z.* Transport facilities earthquake resistance. OROvaOMTV. 2020.- 408 p.
2. *Brodsky V.M., Ilyushin D.A.* Ispolzovanie dynamicheskikh linear vliyaniya progibov pri analize raboty balochnyx proletnyx stroeniy mostov // Vestnik TGASU No. 3, 2009.
3. *Vasiliev A.I.* Osnovy teorii nadejnosti mostov: uchebnoe posobie - M.: MADI, 2021. - 96 p.
4. *Efremenko A.S., Ivanovskaya E.A.* Технико-економическое sravnenie variantov konstruktivnogo spolneniya opor treskad // Universum: Teknicheskie nauki: elektron. nauchno Journal. 2019. No. 6(63).
5. *Smirnov V.N.* "Osobennosti raboty opor mostov skorostnykh zhelenodorojnykh magistraley" Izvestia Petersburg University putey soobshcheniya 2004/2
6. *Shermukhamedov U.Z., Abduakhatova M.A.* "Current state and prospective design and construction of urban transport infrastructure of the Republic of Uzbekistan" road navigator 2019.
7. *Loktev A.A. i dr* . "Perspektivnye konstruktsii bridge crossings and transport highways". Vestnik Nauchno-issledovatelskogo instituta zhelenodorozhnogo transporta (Vestnik VNIIJT), 2018.
8. *Velichko T. S., Kolokolov S.B. i dr.* "Overground pedestrian crossing: problem choice konstruktsii" Shag v nauku 1 2020.
9. *Basov K.A.* ANSYS : Reference. - Moscow, DMK Press, 2005, 640 p.
10. *Abdusattarov A., Abdukadirov F. E.* Realization method of calculation of load- bearing elements construction with use of PK ANSYS Mejdunarodnaya nauchno-prakticheskaya conference, "Computer science and engineering technology". Djizak, 2022, c.210-213.

ON STRENGTHENING OF MATERIALS WITH ONE CENTRAL CRACK

Adilov F.F.[1]

[1]*Institute of Mechanics and Seismic Stability of Structures, Tashkent, Uzbekistan*

E-mail: mahzun86@gmail.com

Abstract. *In structures operating under certain external loads and modes of change, the presence of stable cracks is not dangerous. The service life of such structures can be significantly extended by artificially strengthening them with rivets and plates, drilling holes in the path of crack propagation, etc. The article presents one of the ways to strengthen a plate with cracks. For this purpose, a numerical boundary element method is described, which implements the displacement discontinuity method in plane. The advantage of this method is that only the boundary of the body and the crack surface, which simulates the rupture of an elastic medium, are divided into boundary elements. This reduces the dimension of the problem at the stage of its solution. In this article, the author analyzes numerical solutions to boundary value problems of the theory of cracks under various boundary conditions and determines the degree of stress concentration at the crack tip.*

Keywords: *crack theory, displacement discontinuity method, mixed boundary conditions.*

1. Introduction

Many structural elements and machine parts contain initial or acquired stress concentrators in the form of cracks, notches, etc. They may be partly due to technological necessity, but for the most part, they arise during operation. One of the urgent problems of modern fracture mechanics is the study of stress concentration in the vicinity of a crack.

In practice, numerical methods are used to solve boundary value problems of complex geometry and loading conditions. According to the finite element method (FEM) procedure, the domain under consideration is partitioned into finite elements that can have a linear, quadratic, or other parametric description. The finite difference method (FDM) is based on replacing differential equations with corresponding finite difference equations. Numerical solutions based on boundary integral equations have now achieved a certain dynamism. The boundary element method (BEM) [1-3] is successfully used nowadays as a universal numerical method for solving boundary value problems. It can be used to solve problems of discretization of only the boundary of the domain, whereas FEM and FDM do not allow this.

2. Materials, methods, and object of study

By geometric characteristics, cracks are divided into 3 types (separation, transverse shear, longitudinal shear). The first type (I) includes the formation of cracks of normal separation, i.e., displacement of points on the crack surface under the influence of load in the direction perpendicular to the plane of the crack; the crack tends to open. A crack of transverse shear (type II) corresponds to the case when surface points are displaced across the crack front. A longitudinal shear crack (type III) is characterized by the displacement of crack surface points along the crack front [4]. Types I and II can be considered plane problems of elasticity theory. Symmetric and oblique symmetric parts can be distinguished for the displacements of the crack surfaces.

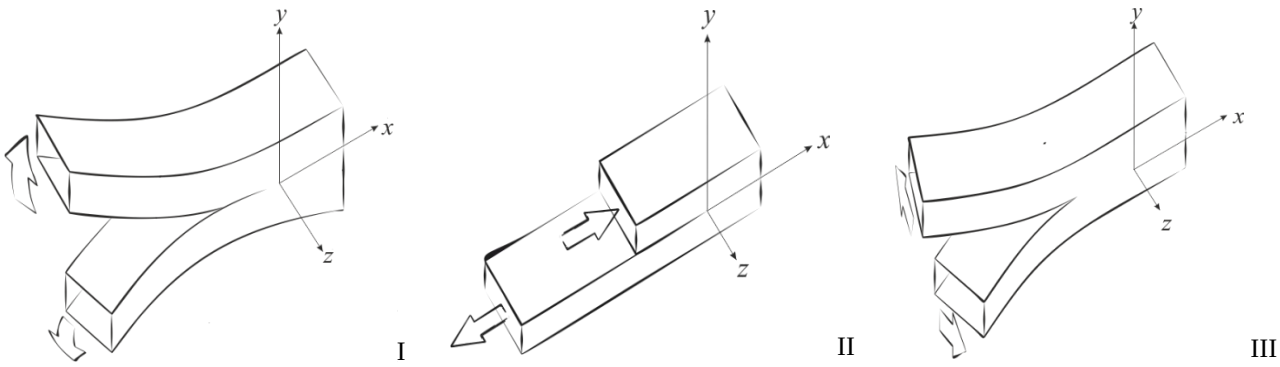

Figure 1. **Main types of crack surface displacements**

The solution to the elastic problem for cracks of types I and II was obtained in displacements (fundamental solution) based on the Papkovich–Neuber solution [5].

The equilibrium equation is:

$$div\,\bar{\sigma} + \bar{X} = 0. \tag{1}$$

In displacements, we obtain:

$$\frac{G}{1-2\nu} grad\, div\,\bar{u} + G\nabla^2\bar{u} + \bar{X} = 0, \tag{2}$$

From (2), we obtain:

$$G\frac{2(1-\nu)}{1-2\nu}\nabla^2\, div\bar{u} + div\bar{X} = 0,$$

In general form the solution is sought as:

$$\bar{u} = 4(1-\nu)\bar{B} - grad\left(\bar{i}_k x_k \bar{B} + B_0\right), \tag{3}$$

where B_0 is an arbitrary scalar.

Under plane strain conditions for the direction of the y coordinate, the components of displacement along the x- and y-axes in a homogeneous, isotropic, linearly elastic body are determined by expressions based on Eq. (3):

$$\left.\begin{aligned} u_x &= B_x - \frac{1}{4(1-\nu)}\frac{\partial}{\partial x}(xB_x + yB_y + \beta), \\ u_y &= B_y - \frac{1}{4(1-\nu)}\frac{\partial}{\partial y}(xB_x + yB_y + \beta), \end{aligned}\right\} \tag{4}$$

where ν is Poisson's ratio, B_x, B_y, and β are the Papkovich functions, which, in the absence of body forces, satisfy the Laplace equation:

$$\nabla^2 B_x = 0, \nabla^2 B_y = 0, \nabla^2\beta = 0.$$

It will be appropriate to choose two particular forms of the Papkovich set function, one set corresponding to a body in plane $y = 0$, free from transverse load, and the other - to a body in the same plane, free from normal forces. These two specific solutions are found by substituting equations (6) into the stress-strain relationships for the plane strain; and choosing B_x, B_y, and β such that either $\sigma_{xy}=0$, or $\sigma_{yy}=0$ on $y=0$. Omitting the details, this leads to the following results:

if the Papkovich functions are chosen in the following form:

$$\left.\begin{aligned} B_x &= 0, \\ B_y &= 4(1-\nu)\frac{\partial\phi}{\partial y}, \\ \beta &= 4(1-\nu)(1-2\nu)\phi, \end{aligned}\right\}$$

where $\Delta\phi = 0$, displacements can be expressed through a harmonic function in the following form:

$$\left.\begin{aligned} u_x &= -(1-2\nu)\frac{\partial\phi}{\partial x} - y\frac{\partial^2\phi}{\partial x\partial y}, \\ u_y &= 2(1-\nu)\frac{\partial\phi}{\partial y} - y\frac{\partial^2\phi}{\partial y^2}+, \end{aligned}\right\} \tag{5}$$

and stresses, respectively:

$$\left.\begin{aligned} \sigma_{xx} &= 2G\left(\frac{\partial^2\phi}{\partial y^2} + y\frac{\partial^3\phi}{\partial y^3}\right), \\ \sigma_{yy} &= 2G\left(\frac{\partial^2\phi}{\partial y^2} - y\frac{\partial^3\phi}{\partial y^3}\right), \\ \sigma_{xy} &= -2Gy\frac{\partial^3\phi}{\partial x\partial y^2}, \end{aligned}\right\} \tag{6}$$

where G is the shear modulus. The expression for σ_{xx} shows that the shear stress vanishes at $y = 0$ (assuming that $\frac{\partial^3\phi}{\partial x\partial y^2}$ is bounded at $y = 0$).

If the Papkovich functions are taken in the following form:

$$\left.\begin{aligned} B_x &= 0, \\ B_y &= 4(1-\nu)\frac{\partial\chi}{\partial x}, \\ \beta &= 8(1-\nu)^2\int\frac{\partial\chi}{\partial x}dy, \end{aligned}\right\}$$

where $\Delta\chi = 0$, displacements and stresses can be expressed through a harmonic function as:

$$\left.\begin{aligned} u_x &= 2(1-\nu)\frac{\partial\chi}{\partial y} + y\frac{\partial^2\chi}{\partial y^2}, \\ u_y &= (1-2\nu)\frac{\partial\chi}{\partial x} - y\frac{\partial^2\chi}{\partial x\partial y}, \end{aligned}\right\} \tag{7}$$

$$\left.\begin{aligned} \sigma_{xx} &= 2G\left(2\frac{\partial^2\chi}{\partial x\partial y} + y\frac{\partial^3\chi}{\partial x\partial y^2}\right), \\ \sigma_{yy} &= -2Gy\frac{\partial^3\chi}{\partial x\partial y^2} - \sigma_{yy}^{pl}, \\ \sigma_{xy} &= 2G\left(\frac{\partial^2\chi}{\partial y^2} + y\frac{\partial^3\chi}{\partial y^3}\right). \end{aligned}\right\} \tag{8}$$

The expression for σ_{xx} shows that the shear stress vanishes at $y=0$ (assuming that $\frac{\partial^3\chi}{\partial x\partial y^2}$ is bounded at $y=0$).

The given solutions are special cases that, individually or in combination, can be used to construct solutions to some boundary value problems for infinite and semi-infinite bodies. From this perspective, one solution for an infinite body is of particular interest, namely, a solution with a constant displacement discontinuity (dislocation) on a finite segment of a straight line, say, between $x=-a$ and $x=a$ at section $y=0$. It is appropriate to solve this problem in parts, the first - for the discontinuity along the normal u_y and the second - for the discontinuity along the transverse displacement u_x - dislocation (shear). Here we use a superposition, which, generally speaking, is not completely correct in the nonlinear case. However, this approach is justified as shown below.

The boundary conditions for the problem of a constant discontinuity (Fig. 2) have the following form:

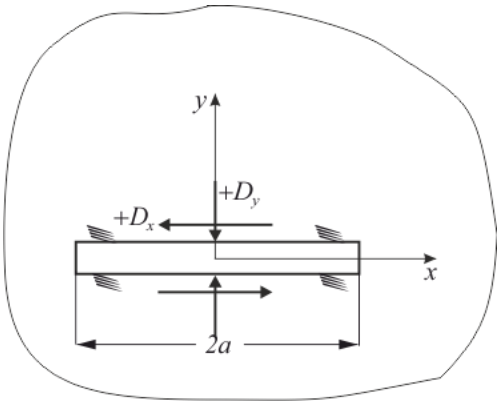

Figure 2. **Components of a constant displacement discontinuity**

$$\left.\begin{aligned} &\sigma_{xy}(x,0)=0, \quad -\infty<x<\infty, \\ &u_y(x,0)=0, \quad |x|>a, \\ &\lim_{y\to 0_+} u_y(x,y)-\lim_{y\to 0_-} u_y(x,y)=D_y, \quad |x|<a, \end{aligned}\right\} \tag{9}$$

for which solutions are the representations of equations (5) and (6) in the form ϕ. Function ϕ under conditions (9) is easy to find by noting that function *arctg(x/y)* (which is harmonic) has the following properties:

$$\lim_{y\to 0} arctg\,\frac{x}{y}=\begin{cases} \dfrac{\pi}{2}; & for \quad x>0, \\ -\dfrac{\pi}{2}; & for \quad x<0. \end{cases}$$

$$\lim_{x\to 0} arctg\,\frac{x}{y}=\begin{cases} -\dfrac{\pi}{2}; & for \quad x>0, \\ \dfrac{\pi}{2}; & for \quad x<0. \end{cases}$$

From these results, with expression for u_y in equation (5), we can conclude that ϕ for problem (9) is defined as:

$$\frac{\partial}{\partial y}\phi(x,y)=\frac{D_y}{4\pi(1-\nu)}\left[\arctan\frac{(x+a)}{y}-\arctan\frac{(x-a)}{y}\right].$$

Next, by integrating, we find:

$$\phi(x,y)=\frac{D_y}{4\pi(1-\nu)}\left[y\arctan\left(\frac{x+a}{y}\right)-y\arctan\left(\frac{x-a}{y}\right)+\right.$$
$$\left.(x+a)\ln\sqrt{(x+a)^2+y^2}-(x-a)\ln\sqrt{(x-a)^2+y^2}\right].$$

This function is harmonic and in equations (5) and (6), displacements and stresses vanish at infinity and are continuous everywhere in the infinite domain, except for section *(-a, a)* at $y = 0$, where u_y undergoes a discontinuity.

Next, we assume (dislocation):

$$\left.\begin{aligned}&\sigma_{yy}(x,0)=0, \quad -\infty<x<\infty,\\&u_x(x,0)=0, \quad |x|>a,\\&\lim_{y\to 0_+}u_x(x,y)-\lim_{y\to 0_-}u_x(x,y)=D_x, \quad |x|<a.\end{aligned}\right\}$$

Similar reasoning for the problem of a constant discontinuity, for example, D_x in u_x for section *(-a, a)* at $y = 0$ leads to the following expression for χ:

$$\chi(x,y)=\frac{D_x}{4\pi(1-\nu)}\left[y\arctan\left(\frac{x+a}{y}\right)-y\arctan\left(\frac{x-a}{y}\right)\right.$$
$$\left.+(x+a)\ln\sqrt{(x+a)^2+y^2}-(x-a)\ln\sqrt{(x-a)^2+y^2}\right].$$

This function is the solution to Eqs. (7) and (8).

The terms after D_x and D_y are the same. Therefore, we denote them as follows:

$$\phi(x,y)=D_y f(x,y),$$
$$\chi(x,y)=D_x f(x,y),$$

where

$$f(x,y)=-\frac{1}{4\pi(1-\nu)}\left[y\left(\arctan\left(\frac{y}{x+a}\right)-\arctan\left(\frac{y}{x-ay}\right)\right)+\right.$$
$$\left.(x-a)\ln\sqrt{(x-a)^2+y^2}-(x+a)\ln\sqrt{(x+a)^2+y^2}\right].$$

For constant elements (each element is assumed to be constant), the displacement discontinuity method has the following form:

$$\begin{aligned}u_x&=D_x\left[2(1-\nu)f_{,y}-yf_{,xx}\right]+D_y\left[-(1-2\nu)f_{,x}-yf_{,xy}\right],\\u_y&=D_x\left[(1-2\nu)f_{,x}-yf_{,xy}\right]+D_y\left[2(1-\nu)f_{,y}-yf_{,yy}\right],\\\sigma_{xx}&=2GD_x\left[2f_{,xy}+yf_{,xyy}\right]+2GD_y\left[f_{,yy}+yf_{,yyy}\right],\\\sigma_{yy}&=2GD_x\left[-yf_{,xyy}\right]+2GD_y\left[f_{,yy}-yf_{,yyy}\right],\\\sigma_{xy}&=2GD_x\left[f_{,yy}+yf_{,yyy}\right]+2GD_y\left[-yf_{,xyy}\right],\end{aligned}$$

where D_i are the displacement discontinuities.

Since the orientation of cracks can be arbitrary in plane, it is more appropriate to use a local coordinate frame on each boundary element. In this case, only normal stress ***n*** (normal to the boundary) and shear stress ***s*** will be determined.

The displacement discontinuity method (DDM) for two-dimensional problems with cracks was proposed by Crouch [5]. Here, the crack is approximated by segments with constant displacement discontinuity *D* along each segment. Using the exact solution for such a segment, stresses σ in the center of the *j*-th element of the crack are expressed through displacement discontinuities *D* as a superposition of solutions to all *i*-th elements:

$$\sigma_s^i=\sum_{j=1}^{N}A_{ss}^{ij}D_s^j+\sum_{j=1}^{N}A_{sn}^{ij}D_n^j$$
$$\sigma_n^i=\sum_{j=1}^{N}A_{ns}^{ij}D_s^j+\sum_{j=1}^{N}A_{nn}^{ij}D_n^j$$

where subscripts *s* and *n* denote the shear and normal components of vectors σ and *D*; functions A_{ss}, A_{sn}, A_{ns}, A_{nn} are the exact solutions to constant displacement discontinuities on a segment, obtained using the Papkovich functions. A system of linear algebraic equations (SLAE) was formed and the unknowns *D* were determined from its solution. The problem was solved using the developed software package, and the SLAE was solved by the Gaussian method [6].

In [7], using this method, the calculation of continuous media with an initial crack of various orientations was presented. The problem is solved under conditions of a plane stress state by the displacement discontinuity method. The solution method is based on the fundamental Papkovich-Neuber solution. In the numerical implementation, the values of the sought-for functions in each section of the boundary element were considered constant. Based on the plotted graphs, the effect of crack orientation on the stress state of the body was determined.

3. Statement of the problem

Since cracks are mainly type I cracks (Fig. 1), let us consider this type as an example. We consider the problem of loading a plate (plane stress state). The presence of side hinges makes it possible to reduce stress concentration under tension (or shear); however, this approach is not always applicable. Let us consider another way and define a general principle for creating devices that make it possible to slow down the development (initiation) of a crack. Below we consider the problem with side hinges (Fig. 3) and without them (Fig. 4).

Consider the problem with the following physical and geometric parameters of the sample: $P=5$, $E=2$, $\nu=0.3$; $r=0.1$ is the notch radius; p is the distributed compression load in the notches ($\Delta\alpha=\pi/3$). The boundary conditions are specified as follows:

$$\begin{aligned} &for\ \ 0 \le y \le 5, \quad \begin{matrix} u_x(0,y)=0;\ P_y(0,y)=0; \\ u_x(5,y)=0;\ P_y(5,y)=0; \end{matrix} \\ &for\ \ 0 \le x \le 5, \quad \begin{matrix} P_x(x,0)=0;\ P_y(x,0)=P; \\ P_x(x,5)=0;\ P_y(x,5)=P. \end{matrix} \end{aligned} \tag{22}$$

Next, we will consider the same problem under other boundary conditions - a free boundary (Fig. 4), generally observed in practice.

$$\begin{aligned} &for\ \ 0 \le y \le 5, \quad \begin{matrix} P_x(0,y)=0;\ P_y(0,y)=0; \\ P_x(5,y)=0;\ P_y(5,y)=0; \end{matrix} \\ &for\ \ 0 \le x \le 5, \quad \begin{matrix} P_x(x,0)=0;\ P_y(x,0)=P; \\ P_x(x,5)=0;\ P_y(x,5)=P. \end{matrix} \end{aligned} \tag{23}$$

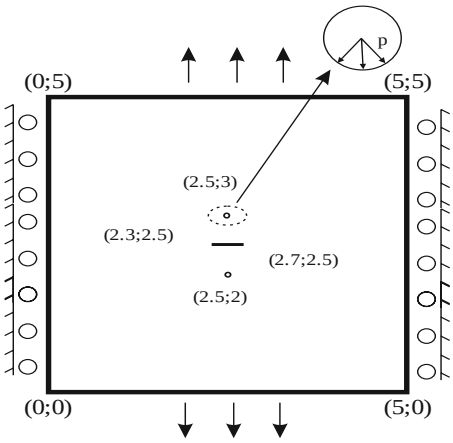

Figure 3. **Loading of a sample with one central crack (hinged support)**

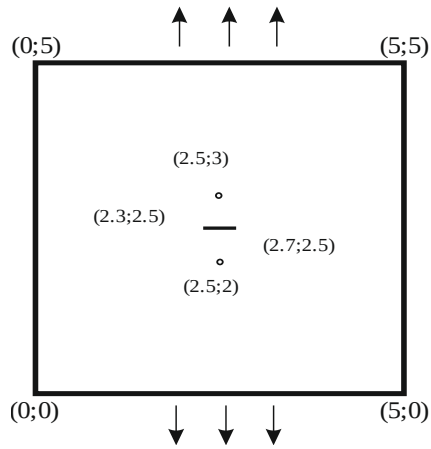

Figure 4. **Loading of a sample with one central crack (free boundary)**

4. Results

Below are graphs of normal stresses along the crack line with side hinges (Fig. 5) and without them (Fig. 6).

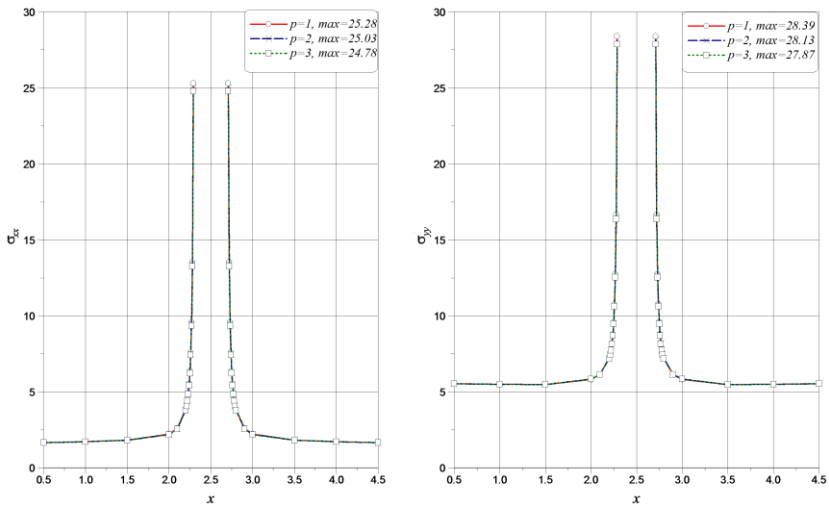

Figure 5. **Comparative graphs for different values of *p***

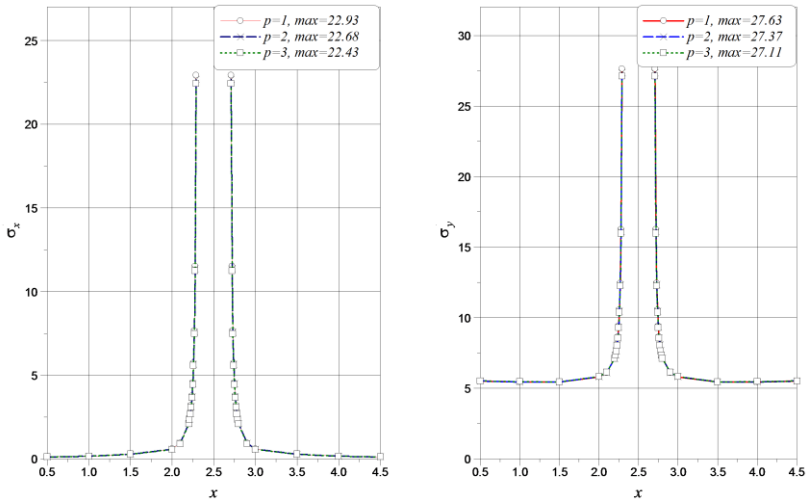

Figure 6. **Comparative graphs for different values of *p***

Below is a comparison of normal stresses for a hinge plate with and without a crack arrester.

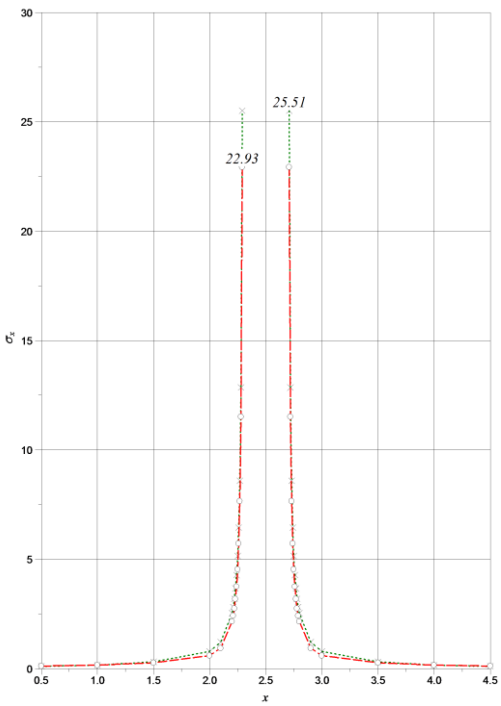

Figure 7. **- Comparative graphs with and without rivets**

5. Analysis of results

As seen from the graphs (Fig. 5), at *p=P·0,2 (20% of P)* of the external load, the stress concentration does not decrease significantly with an increase in the distributed compression load. As the solution to the problems shows (Fig. 6), the situation remains similar for a free boundary.

Figure 7 shows that the normal stresses at the crack tip are reduced by *10%* when the device is placed relative to the center of the crack to slow down crack growth on a hinged side plate with a central crack. It is also necessary to consider that the magnitude of normal stresses at the crack tip depends on the location and number of stringers. The differences are relatively small, so the evaluation with a single stringer is considered in this article.

6. Conclusion

Under compression load in the notches (where stringers can be installed) *p=P·0,2*, the stress concentration values stabilize. In the above problems, all stress components grow asymptotically at the crack tip. This is consistent with the principles of brittle fracture mechanics.

References

1. *Fedelinski P.* Analysis of closed branched and intersecting cracks by the boundary element method // Acta Mech., 2022, pp. 1213-1230
2. *Watson J. O.* Boundary elements for cracks and notches in three dimensions // Int. J. Numer. Methods Eng., Feb. 2006, vol. 65, No. 9, pp. 1419-1443
3. *Xu Y. and Jackson R. L.* Boundary element method (BEM) applied to the rough surface contact vs. BEM in computational mechanics // Friction, Aug. 2019, vol. 7, No. 4, pp. 359-371
4. *Yu.G. Matvienko.* Models and criteria of fracture mechanics / «FIZMATLIT» M., 2006, 328 p.
5. *Crouch, S., Starfield, A.* Boundary Element Methods in Solid Mechanics / «George Allen & Unwin» London, 1983, 328 p.
6. *Demidovich B.P., Maron I.A.* Fundamentals of computational mathematics / «Nauka» Moscow, 1966, 664 p.
7. *Adilov F.F.* On a Method of Calculating of Continua with an Initial Crack // 4th International Conference on Trends in Material Science and Inventive Materials (ICTMIM - 2022) 24-25, March 2022, vol. 243-253, https://link.springer.com/chapter/10.1007/978-981-19-5395-8_21

APPLIED PROBLEMS OF EQUILIBRIUM PLATES IN STRESSES

Akhmedov A.B.[1]

[1]*The National University of Uzbekistan named after Mirzo Ulugbek, Tashkent, Uzbekistan*

E-mail: Ahmedov-1956@mail.ru

Abstract. *In this paper, a new theory of plates in stresses is proposed. The resolving equations are obtained in terms of longitudinal forces, shear forces and internal moments. Boundary conditions for plates in stresses are formulated. The resulting stress solutions simultaneously satisfy the equilibrium and stress compatibility equations of Beltrami-Mitchell. The boundary value problem for a plate under the action of self-balanced loads in stress potentials is formulated.*

Keywords: *plate theory, stress problem, parallelepiped, stress potential, mutually balanced loads, Beltrami-Mitchell equation system.*

1. Introduction

As is known, in engineering applications for calculating the strength and stiffness of structural elements, components of the stress tensor are used, while the magnitude of the displacement vector is of purely academic interest. At the same time, the correct formulation of the problem of elasticity theory is formulated in displacements, therefore, it is not possible to directly calculate the components of the stress tensor in spatial problems.

The classical formulation of the problem of the theory of elasticity in stresses consists in solving three equilibrium equations:

$$\sigma_{ij,j} + X_i = 0,\ x \in V \tag{1.1}$$

when three static boundary conditions are met:

$$\sigma_{ij} n_j \big|_G = S_i,\ x \in G \tag{1.2}$$

where σ_{ij} - are the components of the symmetric stress tensor. X_i *and* S_i are components of mass and surface forces, respectively. $n_j -$ are the components of the vector of the external normal. At the same time, the incorrectness of setting spatial tasks in stresses is shown.

In plane problems of elasticity theory, using the Erie stress function, an exact satisfaction of the equilibrium equations is achieved. The Saint-Venant strain compatibility equation is used to determine the unknown stress potential. Consequently, in the plane problems of elasticity theory there is a correct statement of the problem in stresses.

The first attempts to formulate spatial problems of the theory of elasticity in stresses were made in the works of Konovalov A.N. [1], in which the spatial equilibrium equations using the deformation operation are reduced to six stress equations:

$$\sigma_{ik,kj} + \sigma_{jk,kj} + X_{i,j} + X_{j,i} = 0, x \in V \tag{1.3}$$

however, only three static boundary conditions (1.2) in stresses remain available.

In the fundamental work of Pobedrya B.E. [2], a new correct formulation of the problem of the theory of elasticity in stresses is proposed. Let's briefly outline the essence of the approach.

As is known [3], the compatibility equation is fulfilled for the symmetric strain tensor:

$$\Delta\varepsilon_{ij} + \varepsilon_{kk,ij} - \varepsilon_{ik,kj} - \varepsilon_{jk,ki} + (\varepsilon_{nk,kn} - \Delta\varepsilon_{nn})\delta_{ij} = 0 \tag{1.4}$$

Hooke's law for the six symmetric components of the stress tensor σ_{ij}_ij and deformations ε_{ij} has the form

$$\varepsilon_{ij} = \frac{1}{2\mu}\left(\sigma_{ij} - \frac{\nu}{1+\nu} \sigma_{kk}\delta_{ij}\right) \tag{1.5}$$

which, substituting in (1.4), taking into account the equilibrium equation (1.1), after some calculations we will have a system of Beltrami-Mitchell equations in stresses:

$$\Delta\sigma_{ij} + \frac{1}{1+\nu}\sigma_{kk,ij} + X_{i,j} + X_{j,i} + \frac{\nu}{1-\nu}X_{k,k}\,\delta_{ij} = 0 \tag{1.6}$$

Folding the obtained equations, we will have:

$$\Delta\sigma_{kk} + \frac{1+\nu}{1-\nu}X_{k,k} = 0 \tag{1.7}$$

hence, it immediately follows that the symmetric stress tensor is a biharmonic function:

$$\Delta\Delta\sigma_{ij} + \Delta X_{i,j} + \Delta X_{j,i} + \frac{1}{1-\nu}\left(\nu\Delta X_{k,k}\,\delta_{ij} - X_{k,kij}\right) = 0 \tag{1.8}$$

The system of Beltrami-Mitchell equations-(1.6), differentiating by the coordinate x_j, we will have:

$$\Delta\left(\sigma_{ij,j} + X_i\right) = 0 \tag{1.9}$$

and requiring the fulfillment of the equilibrium equation at the boundary:

$$\left(\sigma_{ij,j} + X_i\right)\Big|_G = 0 \tag{1.10}$$

satisfaction of the equilibrium equation over the entire volume of the object under consideration is achieved. This is the essence of the formulation of spatial problems of the theory of elasticity in stresses proposed by B.E.Pobedrya. Here, the spatial problem of elasticity theory under consideration becomes closed, i.e. for the six components of the symmetric stress tensor, we will have six resolving equations – (1.6) and six boundary conditions (1.2) and (1.10).

In [4], a variational-difference method for solving the problem in stresses is proposed. In [5], the problems of quasi-static equilibrium of a viscoelastic parallelepiped in stresses under the action of self-balanced loads, including concentrated forces, were solved by the variational-difference method.

In [6], by introducing three stress potentials, using the formulation of the problem in stresses by B.E.Pobedrya, the problems of equilibrium of a parallelepiped under the influence of various self-balanced surface and volumetric loads were solved. Here, it is shown that for plates and rods, as the limiting cases of a parallelepiped, the solutions obtained precisely satisfy the equilibrium equations in the regions under consideration.

In plate theory, usually by the introduction of longitudinal forces, shear forces and internal moments are reduced to two-dimensional problems. In [7-10], a non-classical theory of plates is proposed without simplifying assumptions and hypotheses in displacements.

In this paper, a correct theory of plates in stresses is proposed.

2. Main part

In order to simplify calculations for the problem under consideration, assume that only surface loads ($X_i = 0$) act on the plate and a rectangular Cartesian coordinate system is located in the geometric center of the plate under consideration. The coordinate normal to the middle plane of the plate, denoted by – z, will have the coordinate system- Ox_1x_2z, then the replacement $3 \to z$ should be introduced in the stress tensor indices, hence the equilibrium equations (1.1):

$$\begin{cases} \sigma_{ij,j} + \sigma_{iz,z} = 0 \\ \sigma_{zj,j} + \sigma_{zz,z} = 0 \end{cases} \tag{2.1}$$

and Beltrami-Mitchell (1.6) will take the form:

$$\begin{cases} \Delta\sigma_{ij} + \sigma_{ij,zz} + \frac{1}{1+\nu}(\sigma_{kk} + \sigma_{zz})_{,ij} = 0 \\ \Delta\sigma_{iz} + \sigma_{iz,zz} + \frac{1}{1+\nu}(\sigma_{kk} + \sigma_{zz})_{,iz} = 0 \\ \Delta\sigma_{zz} + \frac{2+\nu}{1+\nu}\sigma_{zz,zz} + \frac{1}{1+\nu}\sigma_{kk,zz} = 0 \end{cases} \tag{2.2}$$

Suppose that on opposite planes of the plate, along the normal coordinate -z, normal $-q_z^{\pm}(x_1, x_2)$, and tangential loads $-q_z^{\pm}(x_1, x_2)$, act. Then, taking into account the equilibrium equations on this face, we will have six boundary conditions with respect to the six components of the symmetric stress tensor:

$$\begin{cases} \sigma_{zi} = q_i^{\pm}(x_1, x_2), \\ \sigma_{zz} = q_z^{\pm}(x_1, x_2), \\ \sigma_{iz,z} = -\sigma_{ij,j}, \\ \sigma_{zz,z} = -q_i^{\pm}{}_{,i}(x_1, x_2), \end{cases} \quad \text{at} \quad z = \pm\frac{h}{2} \tag{2.3}$$

For the plate, the desired stress solution is represented as a polynomial in the normal z coordinate [7]:

$$\begin{cases} \sigma_{zz} = \frac{1}{h}N_z + \frac{12}{h^3}M_z z - \Phi_2(z)C - \Phi_3(z)D \\ \sigma_{iz} = \frac{Q_i}{h} + \frac{12}{h^3}\mathcal{T}_i z - \Phi_2(z)C_i - \Phi_3(z)D_i \\ \sigma_{ij} = \frac{N_{ij}}{h} + \frac{12}{h^3}M_{ij} z - \Phi_2(z)C_{ij} - \Phi_3(z)D_{ij} \end{cases} \tag{2.4}$$

where,

$$\begin{pmatrix} N_z \\ Q_i \\ N_{ij} \end{pmatrix} = \int_{-h/2}^{h/2} \begin{pmatrix} \sigma_{zz} \\ \sigma_{iz} \\ \sigma_{ij} \end{pmatrix} dz, \quad \begin{pmatrix} M_z \\ \mathcal{T}_i \\ M_{ij} \end{pmatrix} = \int_{-h/2}^{h/2} \begin{pmatrix} \sigma_{zz} \\ \sigma_{iz} \\ \sigma_{ij} \end{pmatrix} z dz,$$

$$\Phi_2(z) = \frac{h^2}{12}\left(1 - 12\frac{z^2}{h^2}\right), \Phi_3(z) = \frac{3h^2}{20}\left(1 - \frac{20}{3}\frac{z^2}{h^2}\right)z,$$

At the same time, there is a $\int_{-h/2}^{h/2} \Phi_r(z)dz$=0, $\int_{-h/2}^{h/2} \Phi_r(z)zdz$=0, r=2,3.

After satisfying the boundary conditions (2.3) at $z=\pm\frac{h}{2}$, for normal σ_{zz} and tangential σ_{iz} stresses we will have the following expressions:

$$\begin{cases} \sigma_{zz} = \left[\frac{3}{2h}N_z + \frac{30}{h^3}M_z z\right]\left(1 - 4\frac{z^2}{h^2}\right) - \frac{1}{4}\left(1 - 12\frac{z^2}{h^2} + 6\frac{z}{h} - 40\frac{z^3}{h^3}\right)q_z^+ - \\ \qquad \frac{1}{4}\left[\left(1 - 12\frac{z^2}{h^2} - 6\frac{z}{h} + 40\frac{z^3}{h^3}\right)\right]q_z^-, \\ \sigma_{iz} = \left(\frac{3}{2h}Q_i + \frac{30}{h^3}\mathcal{T}_i z\right)\left(1 - 4\frac{z^2}{h^2}\right) - \frac{1}{4}\left(1 - 12\frac{z^2}{h^2} + 6\frac{z}{h} - 40\frac{z^3}{h^3}\right)q_i^+ \\ \qquad -\frac{1}{4}\left(1 - 12\frac{z^2}{h^2} - 6\frac{z}{h} + 40\frac{z^3}{h^3}\right)q_i^- \end{cases} \tag{2.5}$$

where,

$$\begin{cases} N_z = hm_z + \frac{h^2}{12} p_{k,k} \\ M_z = \frac{h^2}{10} p_z - \frac{h^3}{60} m_{k,k} \end{cases}$$

$$\begin{cases} Q_i = -\frac{h^5}{240} D_{ij,j} \\ \mathcal{T}_i = \frac{h^5}{180} C_{ij,j} + \frac{h^2}{3} p_i \end{cases} \tag{2.6}$$

$$m_z = \frac{q_z^+ + q_z^-}{2}, p_z = q_z^+ - q_z^-, \quad m_i = \frac{q_i^+ + q_i^-}{2}, \quad p_i = q_i^+ - q_i^-.$$

After substituting (2.5) into (2.4), we obtain the final formula for σ_{zz}

$$\sigma_{zz} = -\frac{h}{4}\left\{p_{k,k} + m_{k,k}\frac{z}{h}\right\} f(z) + \frac{1}{2}\left(1 + 3\frac{z}{h} - 4\frac{z^3}{h^3}\right) q_z^+ + \frac{1}{2}\left(1 - 3\frac{z}{h} + 4\frac{z^3}{h^3}\right) q_z^- \tag{2.7}$$

where $f(z) = \left(1 - 4\frac{z^2}{h^2}\right)$.

In particular, it follows from the resulting expression for σ_{zz} and (2.5) that, when

$$q_z^+ = q_z^- = q_z, \; q_i^+ = q_i^- = 0,$$

we will have:

$$N_z = hq_z, \; M_z = 0, \; \sigma_{zz} = q_z, \; \sigma_{iz} = \left(\frac{3}{2h} Q_i + \frac{30}{h^3}\mathcal{T}_i z\right) f(z)$$

and for the case $q_z^+ = q_z, \; q_z^- = 0, \; q_i^+ = q_i^- = 0,$ we will have:

$$N_z = \frac{h}{2} q_z, \; M_z = \frac{h^2}{10} q_z, \quad \sigma_{zz} = \frac{1}{2}\left(1 + 3\frac{z}{h} - 4\frac{z^3}{h^3}\right) q_z.$$

The last expression for normal stress is $-\sigma_{zz}$, which corresponds to the proposed a priori Reissner formula [11] for bending plates. The components of the stress tensor σ_{zz} and σ_{iz}, contrary to the well-known classical and refined plate theories [8], are nontrivial and precisely satisfy the specified boundary conditions.

The remaining unknown functions of the Ox_1x_2, coordinates involved in expressions (2.4)-(2.7) are subject to definition. In order to determine them in the equilibrium equations (2.1) and Beltrami-Mitchell (2.2), we perform a standard integration procedure over the thickness of the plate in question:

$$\begin{cases} N_{ij,j} + p_i = 0 \\ M_{ij,j} - Q_i + hm_i = 0 \\ Q_{i,i} + p_z = 0 \\ \mathcal{T}_{i,i} - N_z + hm_z = 0 \end{cases} \tag{2.8}$$

$$\begin{cases} \Delta N_{ij} + \sigma_{ij,z}\Big|_{-\frac{h}{2}}^{\frac{h}{2}} + \frac{1}{1+\nu}(N_{kk} + N_z)_{,ij} = 0 \\ \Delta M_{ij} + z\sigma_{ij,z}\Big|_{-\frac{h}{2}}^{\frac{h}{2}} - \sigma_{ij}\Big|_{-\frac{h}{2}}^{\frac{h}{2}} + \frac{1}{1+\nu}(M_{kk} + M_z)_{,ij} = 0 \\ \Delta Q_i + \sigma_{iz,z}\Big|_{-\frac{h}{2}}^{\frac{h}{2}} + \frac{1}{1+\nu}(\sigma_{kk} + \sigma_{zz})_{,i}\Big|_{-\frac{h}{2}}^{\frac{h}{2}} = 0 \\ \Delta\mathcal{T}_i + z\sigma_{iz,z}\Big|_{-h/2}^{h/2} - \sigma_{iz}\Big|_{-\frac{h}{2}}^{\frac{h}{2}} + \frac{1}{1+\nu}\left[z(\sigma_{kk} + \sigma_{zz})_{,i}\Big|_{-\frac{h}{2}}^{\frac{h}{2}} - (N_{kk} + N_z)_{,i}\right] = 0 \\ \Delta N_z + \frac{2+\nu}{1+\nu}\sigma_{zz,z}\Big|_{-h/2}^{h/2} + \frac{1}{1+\nu}\sigma_{kk,z}\Big|_{-h/2}^{h/2} = 0 \\ \Delta M_z + \frac{2+\nu}{1+\nu}\left(z\sigma_{zz,z}\Big|_{-h/2}^{h/2} - \sigma_{zz}\Big|_{-\frac{h}{2}}^{\frac{h}{2}}\right) + \frac{1}{1+\nu}\left(z\sigma_{kk,z}\Big|_{-\frac{h}{2}}^{\frac{h}{2}} - \sigma_{kk}\Big|_{-\frac{h}{2}}^{\frac{h}{2}}\right) = 0 \end{cases} \tag{2.9}$$

Taking into account the expressions for σ_{ij} in (2.4), we will have:

$$\begin{cases} \sigma_{ij,z}\left(\frac{h}{2}\right) - \sigma_{ij,z}\left(-\frac{h}{2}\right) = 2hC_{ij}, \sigma_{ij,z}\left(\frac{h}{2}\right) + \sigma_{ij,z}\left(-\frac{h}{2}\right) = \frac{24}{h^3} M_{ij} + \frac{6h^2}{5} D_{ij} \\ \sigma_{ij}\left(\frac{h}{2}\right) - \sigma_{ij}\left(-\frac{h}{2}\right) = \frac{12}{h^2} M_{ij} + \frac{h^3}{10} D_{ij}, \; \sigma_{ij}\left(\frac{h}{2}\right) + \sigma_{ij}\left(-\frac{h}{2}\right) = 2\frac{N_{ij}}{h} + \frac{h^2}{3} C_{ij} \end{cases} \tag{2.10}$$

and substituting them in (2.9), from the first two equations of this system, it is possible to determine the components of the tensors C_{ij} and D_{ij}:

$$\begin{cases} C_{ij} = -\frac{1}{2h}\left[\Delta N_{ij} + \frac{1}{1+\nu}(N_{kk} + N_z)_{,ij}\right] \\ D_{ij} = -\frac{2}{h^3}\left[\Delta M_{ij} + \frac{1}{1+\nu}(M_{kk} + M_z)_{,ij}\right] \end{cases} \tag{2.11}$$

by collapsing the resulting and taking into account the expression for N_z and M_z from (2.5) we will have:

$$\begin{cases} C_{kk} = -\frac{1}{2h}\left[\frac{2+\nu}{1+\nu}\Delta N_{kk} + \frac{1}{1+\nu}h\Delta\left(m_z + \frac{h}{12}p_{k,k}\right)\right] \\ D_{kk} = -\frac{2}{h^3}\left[\frac{2+\nu}{1+\nu}\Delta M_{kk} + \frac{1}{1+\nu}\frac{h^2}{10}\Delta\left(p_z - \frac{h}{6}m_{k,k}\right)\right] \end{cases} \tag{2.12}$$

From the boundary conditions (2.3) we will have:

$$\sigma_{zz}\left(\frac{h}{2}\right) \pm \sigma_{zz}\left(-\frac{h}{2}\right) = q_z^+ \pm q_z^-, \sigma_{zz,z}\left(\frac{h}{2}\right) \pm \sigma_{zz,z}\left(-\frac{h}{2}\right) = -(q_i^+{}_{,i} \pm q_i^-{}_{,i}) \tag{2.13}$$

and (2.13), (2.10) substituting into the last two equations (2.9), we obtain:

$$\begin{cases} \Delta N_z - \frac{2+\nu}{1+\nu}p_{k,k} + \frac{2h}{1+\nu}C_{kk} = 0 \\ \Delta M_z - \frac{2+\nu}{1+\nu}(hm_{k,k} + p_z) + \frac{1}{1+\nu}\frac{h^3}{2}D_{kk} = 0 \end{cases} \tag{2.14}$$

and in (2.14) substituting the expression C_{kk} and D_{kk} from (2.12) after some calculations, taking into account (2.13) we obtain the final equation with respect to normal forces N_{kk} and internal bending moments - M_{kk}:

$$\begin{cases} \Delta N_{kk} = \nu h\Delta\left(m_z + \frac{h}{12}p_{k,k}\right) - (1+\nu)p_{k,k} \\ \Delta M_{kk} = \nu\frac{h^2}{10}\Delta\left(p_z - \frac{h}{6}m_{k,k}\right) - (1+\nu)(hm_{k,k} + p_z), \end{cases} \tag{2.15}$$

Similarly, from the boundary conditions (2.3) we have:

$$\sigma_{iz}\left(\frac{h}{2}\right) - \sigma_{iz}\left(-\frac{h}{2}\right) = q_i^+ - q_i^-, \quad \sigma_{iz,z}\left(\frac{h}{2}\right) \pm \sigma_{iz,z}\left(-\frac{h}{2}\right) = -\sigma_{ij,j}\left(\frac{h}{2}\right) \mp \sigma_{ij,j}\left(-\frac{h}{2}\right) \tag{2.16}$$

and (2.16), (2.10) substituting into the third and fourth equations (2.9) , we obtain a system of differential equations of relative shear forces $-Q_i$ and internal moments of depletion:

$$\begin{cases} \Delta\mathcal{T}_i - \frac{30}{h^2}\mathcal{T}_i + T_i = 0 \\ \Delta Q_i + \frac{24}{h^2}Q_i + \frac{1}{1+\nu}\frac{12}{h^2}M_{kk,i} + F_i = 0 \end{cases}, \tag{2.17}$$

where $F_i = \frac{1}{1+\nu}p_{z,i} - \frac{12}{h}m_i - \frac{1}{5}\frac{1}{1+\nu}\left[\frac{h^2}{10}\Delta\left(p_z - \frac{h}{6}m_{k,k}\right) - (2+\nu)(hm_{k,k} + p_z)\right]_{,i}$,

$$T_i = 10p_i + \frac{1}{1+\nu}\left\{-\frac{h^2}{12}\left[h\Delta\left(m_z + \frac{h}{12}p_{k,k}\right) - (2+\nu)p_{k,k}\right] - \frac{h}{2}m_z + \frac{h^2}{12}p_{k,k}\right\}_{,i}$$

Differentiating equations (2.17) by x_i and folding the resulting expression, taking into account the third equation (2.8) after some calculations, we obtain self-balancing conditions for external loads:

$$\begin{cases} \frac{15}{2}p_{k,k} + \frac{1}{1+\nu}\Delta\left\{-\frac{h^3}{12}\Delta\left(m_z + \frac{h}{12}p_{k,k}\right) - \frac{h}{2}m_z + \frac{h^2}{6}(2+\nu)p_{k,k}\right\} = 0 \\ \frac{12}{5}\Delta p_z + \frac{12}{h^2}(1-\nu)p_z + \frac{2}{1+\nu}\frac{h}{5}\Delta m_{k,k} - (2+\nu)\frac{12}{h}m_{k,k} \\ -\frac{1}{5}\frac{1}{1+\nu}\frac{h^2}{10}\Delta\Delta\left(p_z - \frac{h}{6}m_{k,k}\right) = 0 \end{cases} \tag{2.18}$$

Thus, with respect to the unknowns $M_{ij}, N_{ij}, Q_i, \mathcal{T}_i$, we will have the following systems of interrelated equations:

$$\begin{cases} N_{ij,j} + p_i = 0 \\ \Delta N_{kk} = \nu h\Delta\left(m_z + \frac{h}{3}p_{k,k}\right) - (1+\nu)p_{k,k} \\ \Delta\mathcal{T}_i - \frac{30}{h^2}\mathcal{T}_i + T_i = 0 \end{cases} \tag{2.19}$$

$$\begin{cases} M_{ij,j} - Q_i + hm_i = 0 \\ \Delta M_{kk} = \nu \frac{h^2}{10} \Delta \left(p_z - \frac{h}{12} m_{k,k} \right) - (1+\nu)(p_z - hm_{k,k}) \\ \Delta Q_i + \frac{24}{h^2} Q_i + \frac{1}{1+\nu} \frac{12}{h^2} M_{kk,i} + F_i = 0 \end{cases} \tag{2.20}$$

The system (2.19) and (2.20), consisting of 10 interrelated partial differential equations, allows us to determine 10 unknown integral quantities $-N_{ij},\ M_{ij},\ Q_i, \mathcal{T}_i$.

1. Let the faces of the parallelepiped perpendicular to the Ox_i axes be free from loads. Then the corresponding boundary conditions in stresses on arbitrary faces of the parallelepiped can be written as follows:

$$\begin{cases} \sigma_{11} = 0,\ \ \sigma_{12} = 0,\ \ \ \sigma_{1z} = 0, \\ \sigma_{ij,j} + \sigma_{iz,z} = 0, \sigma_{zz,z} + \sigma_{zi,i} = 0, \end{cases} \quad \text{at} \quad x_1 = -\frac{l_1}{2}, \frac{l_1}{2} \tag{2.21}$$

$$\begin{cases} \sigma_{21} = 0,\ \ \sigma_{22} = 0,\ \ \ \sigma_{2z} = 0, \\ \sigma_{ij,j} + \sigma_{iz,z} = 0, \sigma_{zz,z} + \sigma_{zi,i} = 0, \end{cases} \quad \text{at} \quad x_2 = -\frac{l_2}{2}, \frac{l_2}{2} \tag{2.22}$$

From the obtained boundary conditions at the edges of the plate, we will have the corresponding boundary conditions for these integral quantities:

$$\begin{cases} N_{11} = 0, N_{12} = 0, M_{11} = 0, M_{12} = 0, \mathcal{T}_1 = 0, \mathcal{T}_{i,i} - N_z + hm_z = 0 \\ N_{ij,j} + p_i = 0,\ \ M_{ij,j} - Q_i + hm_i = 0,\ \ Q_1 = 0,\ \ Q_{i,i} + p_z = 0, \end{cases} \quad \text{at } x_1 = -\frac{l_1}{2}, \frac{l_1}{2} \tag{2.23}$$

$$\begin{cases} N_{22} = 0, N_{12} = 0, M_{22} = 0, M_{12} = 0, \mathcal{T}_2 = 0, \mathcal{T}_{i,i} - N_z + hm_z = 0 \\ N_{ij,j} + p_i = 0,\ \ M_{ij,j} - Q_i + hm_i = 0,\ \ Q_2 = 0,\ \ Q_{i,i} + p_z = 0, \end{cases} \quad \text{at } x_1 = -\frac{l_1}{2}, \frac{l_1}{2} \tag{2.24}$$

2. Let the faces perpendicular to the Ox_i axes be rigidly pinched, therefore

$$u_1=0,\ u_2=0,\ u_z=0 \quad \text{at} \quad x_i = -\frac{l_i}{2}, \frac{l_i}{2} \tag{2.25}$$

from where, for the components of the strain tensor, we will have

$$\begin{cases} \varepsilon_{22} = 0, \varepsilon_{zz} = 0, \quad \text{at } x_1 = -\frac{l_1}{2}, \frac{l_1}{2} \\ \varepsilon_{11} = 0, \varepsilon_{zz} = 0, \quad \text{at } x_2 = -\frac{l_2}{2}, \frac{l_2}{2} \end{cases} \tag{2.26}$$

Using Hooke's law with respect to the normal components of the stress tensor, instead of (2.26), we will have boundary conditions in stresses $-\sigma_{ij}$:

$$\begin{cases} \sigma_{22} = \sigma_{zz},\ \sigma_{11} = \frac{1-\nu}{\nu} \sigma_{zz}, \sigma_{ij,j} + \sigma_{iz,z} = 0, \sigma_{zz,z} + \sigma_{zi,i} = 0, \ \text{at } x_1 = -\frac{l_1}{2}, \frac{l_1}{2}, \\ \sigma_{11} = \sigma_{zz},\ \sigma_{22} = \frac{1-\nu}{\nu} \sigma_{zz}, \sigma_{ij,j} + \sigma_{iz,z} = 0, \sigma_{zz,z} + \sigma_{zi,i} = 0, \ \text{at } x_2 = -\frac{l_2}{2}, \frac{l_2}{2}, \end{cases} \tag{2.27}$$

Here, it should be noted that for incompressible (ν = 0.5) materials, the boundary conditions for both faces become the same.

3. Let the faces perpendicular to the Ox_i, axes be pivotally fixed, therefore

$$\begin{cases} \sigma_{11} = 0, \quad u_2 = 0,\ at \qquad x_1 = -\frac{l_1}{2}, \frac{l_1}{2} \\ u_1 = 0, \quad \sigma_{22} = 0,\ at \qquad x_2 = -\frac{l_2}{2}, \frac{l_2}{2} \end{cases} \tag{2.28}$$

For this case of anchoring, the normal component of the displacement vector in the middle of these faces is zero. Acting similarly to the rigid pinching, for the hinge fastening from (2.28), we will have:

$$\begin{cases} \sigma_{11} = 0, \sigma_{22} = \nu\sigma_{zz}, \sigma_{ij,j} + \sigma_{iz,z} = 0, \sigma_{zz,z} + \sigma_{zi,i} = 0, \quad \text{at } x_1 = -\frac{l_1}{2}, \frac{l_1}{2}, \\ \sigma_{11} = \nu\sigma_{zz}, \sigma_{22} = 0, \sigma_{ij,j} + \sigma_{iz,z} = 0, \sigma_{zz,z} + \sigma_{zi,i} = 0, \quad \text{at } x_2 = -\frac{l_2}{2}, \frac{l_2}{2}, \end{cases} \tag{2.29}$$

The peculiarity of rigid and hinged fastening of the edges of the plate, unlike normal stresses, does not formulate conditions for tangential stresses in the appropriate boundary conditions.

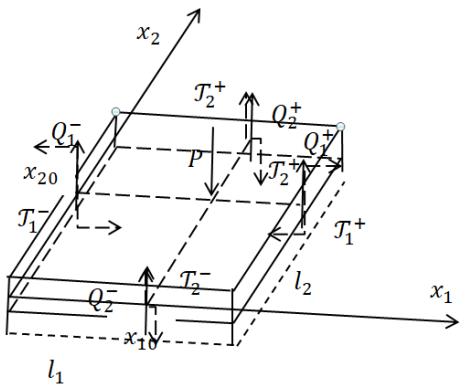

Figure 1. - **The equilibrium of the plate under the action of the linear force P_i**

The linear forces from the action of a distributed transverse load are calculated in the following form $P_i = \int q_z dx_i$, which is balanced by the shearing forces $Q_i = \int \sigma_{iz} dz$, set at the edges of the plate $-x_i = -\frac{l_i}{2}, \frac{l_i}{2}$ (fig. 1.):

$$Q_i^+ + Q_i^- = P_i \tag{2.30}$$

Relative to the line passing through the center of gravity $M_0(x_{10}, x_{20})$, we calculate the resulting moments

$$\begin{cases} (l_1 - x_{10})Q_1^+ - x_{10}Q_1^- = 0 \\ (l_2 - x_{20})Q_2^+ - x_{20}Q_2^- = 0 \end{cases}. \tag{2.31}$$

From where we will have

$$Q_r^- = \frac{l_r - x_{r0}}{l_r} P_r, \qquad Q_r^+ = \frac{x_{r0}}{l_r} P_r \;\; r = 1,2.$$

At the same time, the moments arising at the edges of the plate – $\mathcal{T}_i^{\pm}$ it is calculated as follows

$$\mathcal{T}_r^{\pm} = \pm \frac{l_r - x_{r0}}{l_r} x_{r0} P_r, \;\; r = 1,2$$

Thus, for a rigidly pinched plate, the boundary conditions with respect to integral quantities have the form

$$\begin{cases} N_{11} = \frac{1-\nu}{\nu} N_z, \quad N_{22} = N_z, M_{11} = \frac{1-\nu}{\nu} M_z, \; M_{22} = M_z, \\ N_{ij,j} + p_i = 0, \quad M_{ij,j} - Q_i + hm_i = 0, \quad Q_{i,i} + p_z = 0, \\ Q_1 = Q_1^{\mp}, \quad \mathcal{T}_1 = \mathcal{T}_1^{\mp}, \quad \mathcal{T}_{i,i} - N_z + hm_z = 0, \end{cases} \text{ at } \quad x_1 = -\frac{l_1}{2}, \frac{l_1}{2} \tag{2.32}$$

$$\begin{cases} N_{22} = \frac{1-\nu}{\nu} N_z, \quad N_{11} = N_z, M_{22} = \frac{1-\nu}{\nu} M_z, \; M_{11} = M_z, \\ N_{ij,j} + p_i = 0, \quad M_{ij,j} - Q_i + hm_i = 0, Q_{i,i} + p_z = 0, \\ Q_2 = Q_2^{\mp}, \quad \mathcal{T}_2 = \mathcal{T}_2^{\mp}, \quad \mathcal{T}_{i,i} - N_z + hm_z = 0 \end{cases} \text{ at } \quad x_2 = -\frac{l_2}{2}, \frac{l_2}{2} \tag{2.33}$$

For a hinged plate, taking into account (2.30) and (2.31), the corresponding boundary conditions will take the form:

$$\begin{cases} N_{11} = 0, N_{22} = \nu N_z, M_{11} = 0, M_{22} = \nu M_z, \\ N_{ij,j} + p_i = 0, \quad M_{ij,j} - Q_i + hm_i = 0, \quad Q_{i,i} + p_z = 0, \\ Q_1 = Q_1^{\mp}, \quad \mathcal{T}_1 = \mathcal{T}_1^{\mp}, \quad \mathcal{T}_{i,i} - N_z + hm_z = 0, \end{cases} \text{ at } \quad x_1 = -\frac{l_1}{2}, \frac{l_1}{2} \tag{2.34}$$

$$\begin{cases} N_{22} = 0, N_{11} = \nu N_z, \; M_{11} = 0, M_{22} = \nu M_z, \\ N_{ij,j} + p_i = 0, \quad M_{ij,j} - Q_i + hm_i = 0, \quad Q_{i,i} + p_z = 0, \\ Q_2 = Q_2^{\mp}, \quad \mathcal{T}_2 = \mathcal{T}_2^{\mp}, \quad \mathcal{T}_{i,i} - N_z + hm_z = 0 \end{cases} \text{ at } \quad x_2 = -\frac{l_2}{2}, \frac{l_2}{2} \tag{2.35}$$

Thus, we have a correct formulation of the problem of plate equilibrium in longitudinal forces, shear forces and internal moments, under various boundary conditions, with the help of which the components of the symmetric stress tensor for various applied problems are directly calculated.

3. Discussion

1. Boundary value problem for self-balanced loads.

Let the external influences be self-balanced $q_i^+ = q_i^- = q_i, q_z^+ = q_z^- = q_z$, then $p_i = 0$, $m_i = q_i$, $m_z = q_z, p_z = 0$. In this case, the following system of equations for self-balanced loads can be written in place of the system of equations (2.19) and (2.20):

$$\begin{cases} N_{ij,j} = 0, \quad \Delta N_{kk} = \nu h \Delta q_z \\ \Delta \mathcal{T}_i - \frac{30}{h^2}\mathcal{T}_i + \frac{1}{1+\nu}\left[-\frac{h^3}{12}\Delta q_z - \frac{h}{2}q_z\right]_{,i} = 0 \end{cases} \tag{3.1}$$

$$\begin{cases} M_{ij,j} - Q_i + hq_i = 0 \\ \Delta M_{kk} = -\nu\frac{h^3}{120}\Delta q_{k,k} - (1+\nu)\frac{h}{2}q_{k,k} \\ \Delta Q_i + \frac{24}{h^2}Q_i + \frac{1}{1+\nu}\frac{12}{h^2}M_{kk,i} - \frac{12}{h}q_i + \frac{1}{5}\frac{1}{1+\nu}\left[\frac{h^3}{60}\Delta q_{k,k} - (2+\nu)hq_{k,k}\right]_{,i} = 0 \end{cases} \tag{3.2}$$

It should be noted here that for self-balanced loads, longitudinal forces and moments of depletion arise under the action of transverse loads, while internal bending moments and shearing forces are accompanied by tangential loads, i.e. the general task is divided into two subgroups.

2. The boundary value problem in the potentials of internal efforts and moments.

Let tangential loads are potential: $q_i^{\pm} = q_{,i}^{\pm}$, then $p_i = p_{,i}$. $m_i = m_{,i}$. Let's introduce the Eri function into consideration:

$$N_{ij} = (\Delta N - p)\delta_{ij} - N_{,ij}, M_{ij} = (\Delta M - hm + Q)\delta_{ij} - M_{,ij}, Q_i = Q_{,i}\, \mathcal{T}_i = \mathcal{T}_{,i} \tag{3.3}$$

thus, the equation of equilibrium in bending moments and lateral efforts in (2.19)-(2.20) become identities. Therefore, we will have the following system of partial differential equations:

$$\begin{cases} \Delta\Delta N = \nu h \Delta\left(m_z + \frac{h}{3}\Delta p\right) - (1+\nu)\Delta p, \\ \Delta\mathcal{T} - \frac{30}{h^2}\mathcal{T} + 10p + T = 0, \\ \Delta\Delta M + 2\Delta Q = \nu\frac{h^2}{10}\Delta\left(p_z - \frac{h}{12}\Delta m\right) - (1+\nu)p_z - (1-\nu)h\Delta m \\ \Delta Q + \frac{24}{h^2}Q + \frac{1}{1+\nu}\frac{12}{h^2}\Delta M + \frac{1}{1+\nu}p_z + F = 0, \end{cases} \tag{3.4}$$

where

$$T = \frac{1}{1+\nu}\left\{-\frac{h^2}{12}\left[h\Delta\left(m_z + \frac{h}{12}\Delta p\right) - (2+\nu)\Delta p\right] - \frac{h}{2}m_z + \frac{h^2}{12}\Delta p\right\},$$

$$F = -\frac{12}{h}m - \frac{1}{5}\frac{1}{1+\nu}\left[\frac{h^2}{10}\Delta\left(p_z - \frac{h}{6}\Delta m\right) - (2+\nu)(h\Delta m + p_z)\right],$$

Boundary conditions (2.23), (2.24), (2.32)-(2.35) at the edges of the plate, in terms of the potentials of longitudinal forces $-N$, shear forces $-Q$ and internal moments $-M$, $\mathcal{T}$, taking into account the identical fulfillment of the corresponding equilibrium equations at the boundary, for a free boundary, it will take the following form:

a). Free edge

$$\begin{cases} N = 0, N_{,1} = 0, M = 0, M_{,1} = 0,\ \mathcal{T}_{,1} = 0,\ Q_{,1} = 0, \text{at}\ \ x_1 = -\frac{l_1}{2}, \frac{l_1}{2}, \\ N = 0, N_{,2} = 0, M = 0, M_{,2} = 0,\ \mathcal{T}_{,2} = 0,\ Q_{,2} = 0, \text{at}\ \ x_1 = -\frac{l_1}{2}, \frac{l_1}{2}, \end{cases} \tag{3.5}$$

b). Hard-pinched edge

$$\begin{cases} N_{,22} = p + \frac{1-\nu}{\nu}N_z,\ \ N_{,11} = p + N_z, Q_{,1} = Q_2^{\mp}, \quad \mathcal{T}_{,1} = \mathcal{T}_2^{\mp} \\ M_{,22} = mh - Q + \frac{1-\nu}{\nu}M_z,\ \ M_{,11} = mh - Q + M_z, \end{cases} \quad \text{at}\ \ x_1 = -\frac{l_1}{2}, \frac{l_1}{2} \tag{3.6}$$

$$\begin{cases} N_{,11} = p + \frac{1-\nu}{\nu}N_z,\ \ N_{,22} = p + N_z, Q_{,2} = Q_2^{\mp}, \quad \mathcal{T}_{,2} = \mathcal{T}_2^{\mp} \\ M_{,11} = mh - Q + \frac{1-\nu}{\nu}M_z,\ \ M_{,22} = mh - Q + M_z, \end{cases} \quad \text{at}\ \ x_2 = -\frac{l_2}{2}, \frac{l_2}{2} \tag{3.7}$$

c). Hinged edge

$$N_{,22} = 0, N_{,11} = \nu N_z, Q_{,1} = Q_1^{\mp}, \mathcal{T}_{,1} = \mathcal{T}_1^{\mp}, M_{,22} = 0,\ M_{,11} = \nu M_z \text{ at } x_1 = -\frac{l_1}{2}, \frac{l_1}{2} \quad (3.8)$$

$$N_{,11} = 0, N_{,22} = \nu N_z, Q_{,2} = Q_2^{\mp}, \mathcal{T}_{,2} = \mathcal{T}_2^{\mp}, M_{,11} = 0,\ M_{,22} = \nu M_z \text{ at } x_2 = -\frac{l_2}{2}, \frac{l_2}{2} \quad (3.9)$$

Thus, we have a correct formulation of the problem in the potentials of internal efforts and moments.

4. Conclusions

1. The non-classical theory of plates in stresses is proposed for the first time.

2. Unlike the known approaches, the obtained resolving equations and boundary conditions in stresses are correct and closed in plate theory.

3. In the proposed theory of plates, simultaneous fulfillment of the equations of equilibrium and compatibility of the Beltrami-Mitchell stresses has been achieved.

References

1. *Konavalov A.N.* Numerical methods in dynamic problems of elasticity theory // Siberian Mathematical Journal, 1997, vol. 38, No. 3, pp. 551-568.

2. *Pobedrya B.E.* On the problem of static in voltages // Bulletin of the Moscow State University.ser. Math., mech., 2003, No. 3, pp. 61-67.

3. *Timoshenko S.P., Guder D.J.* Theory of elasticity / M.: Nauka, 1975, 576 p.

4. *Kholmatov T.* On methods of solving the problem in stresses // DAS USSR, 1980, vol. 1, p. 252 No. 2, pp. 315-317.

5. *Akhmedov A.B.* Numerical solution of spatial problems of the theory of viscoelasticity in stresses / Abstract of the candidate's thesis. Tashkent, 1984, 12 p.

6. *Akhmedov A.B.* Solving spatial problems of the theory of elasticity in stress potentials // Uzbek Journal of Problems of Mechanics, No. 1, 2022, pp. 3-16.

7. *Akhmedov A.B., Sheshenin S.V.* Nonlinear equations of motion of orthotropic plates // Bulletin of the Moscow State University of Mechanics and Mathematics, 2012, pp.66-68.

8. *Akhmedov A.B.* Qualitative analysis of the theory of plates made of composite materials // DAN RUz. – 2011. – No.1. pp. 81 -84.

9. *Akhmedov A.B, Grigorev P.S, Ibodulloev Sh.R, Kuldibaeva L.A.* Imitating Simulation of Thermomechanical Processing of Metals // J:Turkish Journal of Computer and Mathematics Education, 2021 Vol.12 №.4, pp. 31-36.

10. *Altenbach H., Eremeyev V.A.* (Eds). Shell like Structures: Nonclassical Theories and Applications / Advanced Structured Materials. Volume 15, Springer, Berlin et al. 2011, 761 p.

11. *Reissner E.* On the bending of elastic plates // Quart. Appl. Math. - 1947.- V. 5, № 1, pp 11-22.

12. *Tyukalov Yu.Ya.* Equilibrium finite elements for plane problems of the elasticity theory // Magazine of Civil Engineering. 2019. 91(7). pp. 80-97.

NON-CLASSICAL THEORY OF THE EQUILIBRIUM OF LAYERED PLATES

Akhmedov A.B.[1], Kuldibaeva L.A.[1]
[1]*National University of Uzbekistan named after Mirzo Ulugbek, Tashkent, Uzbekistan*
E-mail: Ahmedov-1956 @ mail.ru

Abstract. *An improved non-classical theory [10] on the equilibrium of layered plates is proposed in this article based on three-dimensional equations of elasticity theory without hypotheses. Here, all boundary conditions specified in the front and interlayer planes of the layered plate are met. Recurrence relations are obtained that ensure the fulfillment of interlayer continuity conditions for the components of the displacement vector and stress tensor. Equilibrium equations are derived in terms of the components of the longitudinal force tensor, internal moments, and vector of shearing forces for each "package" of layers of plates.*

Keywords: *layered plates, interlayer stress-strain conditions, approximate analytical Navier method.*

1. Introduction

As is known, layered composites, which, along with low specific density, have high specific strength, are widely used in various fields of mechanical engineering, construction, and modern technologies for creating high-strength ultra-light aircraft [1, 2]. At present, with the development of the latest technologies for high-strength materials made from composites, there is a need to study problems with a more exact solution to the equation of motion of layered plates [3-7].

In this study, without preliminary hypotheses, a new approach to constructing a non-classical theory of layered plates is proposed.

2. Statement of the problem

The equilibrium equation of the stress state of a three-dimensional body in a Cartesian coordinate frame $Ox_1x_2x_3$, under the influence of a system of surface and volumetric forces, has the following form [8]:

$$\sigma_{ij,j} + X_i - \rho \ddot{U}_i = 0 \ , \tag{1}$$

which defines relations between the stress σ_{ij} and strain ε_{ij} tensors

$$\sigma_{ij} = C_{ijkl}\varepsilon_{kl} \tag{2}$$

and geometric Cauchy relations between ε_{ij} and components of the displacement vector U_i

$$\varepsilon_{ij} = \frac{1}{2}\left(U_{i,j} + U_{j,i}\right) \tag{3}$$

and boundary conditions

$$U_i\big|_{\Sigma} = U_i^{\Sigma} \ , \ \ \sigma_{ij} n_j\big|_{\Sigma} = S_i \tag{4}$$

where X_i, S_i are the volumetric and surface forces, U_i^{Σ} are specified on part of the displacement boundary, n_j is the external normal, ρ - is the density, $C_{ijkl}(x)$ - are the elastic moduli, $i, j, k, l = 1,2,3$. For isotropic materials, the following relations for the components of the elastic modulus tensor hold:

$$C_{ijkl} = \lambda\delta_{ij}\delta_{kl} + \mu\left(\delta_{ik}\delta_{jl} + \delta_{il}\delta_{jk}\right), \tag{5}$$

Where $\lambda = \dfrac{E\nu}{(1-2\nu)(1+\nu)}$, $\mu = \dfrac{E}{2(1+\nu)}$

are the Lamé coefficients, E – modulus of elasticity ν – Poisson's ratio.

Here the Cartesian coordinate frame Ox_1x_2z is located in the lower plane of the layered plate with constant thickness h. The dependence of the elastic modulus of a layered plate along the coordinate z is given in the following form [9]:

$$C_{ijkl}(x_1,x_2,z)=C^{(1)}{}_{ijkl}(x_1,x_2)H(z_1-z)+C^{(N)}{}_{ijkl}(x_1,x_2)H(z-z_{N-1})+\sum_{r=2}^{N-1}C^{(r)}{}_{ijkl}(x_1,x_2)H(z_r-z)H(z-z_{r-1}) \quad (6)$$

where z_r are the coordinates of the interface between the layers of the composite plate. $H(z)$ is the Heaviside function. Here, $h_r=z_{r+1}-z_r,\quad r=1,3,\cdots N-1,\quad z_1=0,\quad z_N=h$.

The sought-for solution to problem (1)-(5) for layered plates considering (6) is presented in the following form [9]:

$$\begin{cases} U_I(x_1,x_2,z)=U_I^{(1)}(x_1,x_2,z)H(z_1-z)+U_I^{(N)}(x_1,x_2,z)H(z-z_{N-1})+\sum_{r=2}^{N-1}U_I^{(r)}(x_1,x_2,z)H(z_r-z)H(z-z_{r-1}) \\ U_Z(x_1,x_2,z)=U_Z^{(1)}(x_1,x_2,z)H(z_1-z)+U_Z^{(N)}(x_1,x_2,z)H(z-z_{N-1})+\sum_{r=2}^{N-1}U_Z^{(r)}(x_1,x_2,z)H(z_r-z)H(z-z_{r-1}) \end{cases} \quad (7)$$

Consequently, the components of the stress and strain tensors are also represented in a similar form, where $U_Z^{(r)}, U_I^{(r)}$, $I=1,2$ is the sought-for solution for each "package" of layers. Here and below, capital indices take the values 1.2. Then each "package" has its corresponding system of equilibrium equations.

$$\begin{cases} \sigma_{IJ,J}^{(r)}+\sigma_{IZ,Z}^{(r)}+X_I^{(r)}=0 \\ \sigma_{ZJ,J}^{(r)}+\sigma_{ZZ,Z}^{(r)}+X_Z^{(r)}=0 \end{cases} \quad (8)$$

Let us introduce "fast" variable ξ for each r-"package" by the change of variables $z_r=h_r\xi$, $\xi=[0,1]$. We present the sought-for solution for each r layer as a polynomial in ξ,

$$\begin{cases} U_K^{(r)}=u_K{}^{(r)}+\xi h_r\psi_K{}^{(r)}+\xi^2h_r{}^2C_K{}^{(r)}+\xi^3h_r{}^3D_K{}^{(r)} \\ U_Z^{(r)}=w^{(r)}+\xi h_rV^{(r)}+\xi^2h_r{}^2\theta^{(r)} \end{cases} \quad (9)$$

At the interface $z=z_r$, for each r-"package" the conditions of continuity of displacements and stress tensor are met:

$$U_I^{(r+1)}=U_I^{(r)}, U_Z^{(r+1)}=U_Z^{(r)}, \sigma_{IZ}^{(r+1)}=\sigma_{IZ}^{(r)},\ \sigma_{ZZ}^{(r+1)}=\sigma_{ZZ}^{(r)},\ r=2,\ldots,N-1 \quad (10)$$

where, with (2)-(5) and (9), we have the following expressions for the stress tensor components $\sigma_{IZ}^{(r)}, \sigma_{ZZ}^{(r)}$:

$$\begin{cases} \sigma_{IZ}^{(r)}(x_1,x_2,\xi)=\mu_r\left[\psi_I{}^{(r)}+2\xi h_rC_I{}^{(r)}+3\xi^2h_r{}^2D_I{}^{(r)}+\left(w^{(r)}+\xi h_rV^{(r)}+\xi^2h_r{}^2\theta^{(r)}\right)_{,I}\right] \\ \sigma_{ZZ}^{(r)}(x_1,x_2,\xi)=\lambda_r\left[\left(u_K{}^{(r)}+\xi h_r\psi_K{}^{(r)}+\xi^2h_r{}^2C_K{}^{(r)}+\xi^3h_r{}^3D_K{}^{(r)}\right)_{,K}+\frac{1-\nu_r}{\nu_r}\left(V^{(r)}+2\xi h_r\theta^{(r)}\right)\right] \end{cases} \quad (11)$$

At the interface between the layers, considering (9)-(11), we have

$U_I^{(r+1)}(x_1,x_2,0)=U_I^{(r)}(x_1,x_2,1), U_Z^{(r+1)}(x_1,x_2,0)=U_Z^{(r)}(x_1,x_2,1),$
$\sigma_{IZ}^{(r+1)}(x_1,x_2,0)=\sigma_{IZ}^{(r)}(x_1,x_2,1),\ \sigma_{ZZ}^{(r+1)}(x_1,x_2,0)=\sigma_{ZZ}^{(r)}(x_1,x_2,1).$

Therefore,

$$\begin{cases} u_I{}^{(r+1)}=u_I{}^{(r)}+h_r\psi_I{}^{(r)}+h_r{}^2C_I{}^{(r)}+h_r{}^3D_I{}^{(r)} \\ w^{(r+1)}=w^{(r)}+h_rV^{(r)}+h_r{}^2\theta^{(r)} \\ \mu_{r+1}\psi_I{}^{(r+1)}=\mu_r\left(\psi_I{}^{(r)}+2h_rC_I{}^{(r)}+3h_r{}^2D_I{}^{(r)}\right)+(\mu_r-\mu_{r+1})w,_I{}^{(r+1)} \\ \lambda_{r+1}\frac{1-\nu_{r+1}}{\nu_{r+1}}V^{(r+1)}=(\lambda_r-\lambda_{r+1})u_{I,I}{}^{(r+1)}+\lambda_r\frac{1-\nu_r}{\nu_r}\left(V^{(r)}+2h_r\theta^{(r)}\right) \end{cases}, \quad (12)$$

hence, after some calculations, we have the following recurrence relations:

$$\begin{cases} u_I^{(r)} = u_I^{(1)} + \sum_{l=2}^{r-1}\left(h_l\psi_I^{(l)} + h_l^2 C_I^{(l)} + h_l^3 D_I^{(l)}\right) \\ w^{(r)} = w^{(1)} + \sum_{l=2}^{r-1}\left(h_l V^{(l)} + h_l^2\theta^{(l)}\right) \\ \psi_I^{(r)} = \psi_I^{(1)} + \frac{1}{\mu_r}\sum_{l=1}^{r-1}\left[\mu_l\left(2h_l C_I^{(l)} + 3h_l^2 D_I^{(l)}\right) + (\mu_l - \mu_r)\left(h_l V^{(l)} + h_l^2\theta^{(l)}\right)_{,I}\right] \\ V^{(r)} = \frac{\nu_{r+1}}{1-\nu_{r+1}}\left[\frac{1-\nu_1}{\nu_1}V^{(1)} + \frac{1}{\lambda_r}\sum_{l=1}^{r-1}\left((\lambda_l - \lambda_r)\left(h_l\psi_I^{(l)} + h_l^2 C_I^{(l)} + h_l^3 D_I^{(l)}\right)_{,I} + \frac{2\lambda_l(1-\nu_l)}{\nu_l}h_l\theta^{(l)}\right)\right] \end{cases} \tag{13}$$

In this study, we assume that only the normal distributed load $q(x_1, x_2)$ acts on the upper plane of the layered plate, and there are no body forces.

In the problem under consideration, the boundary conditions on the lower plane of the layered plate, i.e., in the first layer $(\xi = 0)$, have the following form for stresses:

$$\begin{cases} \sigma_{IZ}^{(1)} = \mu_1\left[\psi_I^{(1)} + w,_I^{(1)}\right] \\ \sigma_{ZZ}^{(1)} = \lambda_1\left[u_{K,K}^{(1)} + \frac{1-\nu_1}{\nu_1}V^{(1)}\right] \end{cases}.$$

Hence, we obtain:

$$\begin{cases} w,_I^{(1)} = -\psi_I^{(1)} \\ u_{K,K}^{(1)} = -\frac{1-\nu_1}{\nu_1}V^{(1)} \end{cases} \tag{14}$$

On the upper plane, to which the last layer corresponds, the boundary conditions for $\xi = 1$ have the following form:

$$\sigma_{IZ}^{(N)} = 0,\ \sigma_{ZZ}^{(N)} = q,$$

hence, considering recurrent formulas (12) and relation (14), we obtain the following system of differential equations:

$$\begin{cases} \psi_I^{(N)} + 2h_N C_I^{(N)} + 3h_N^2 D_I^{(N)} + \left(w^{(N)} + h_N V^{(N)} + h_N^2\theta^{(N)}\right)_{,I} = 0 \\ \left(u_K^{(N)} + h_N\psi_K^{(N)} + h_N^2 C_K^{(N)} + h_N^3 D_K^{(N)}\right)_{,K} + \frac{1-\nu_N}{\nu_N}\left(V^{(N)} + 2h_N\theta^{(N)}\right) = \frac{q}{\lambda_N} \end{cases} \tag{15}$$

From (14) and (15), we can obtain the following expressions for the unknown functions of the first layer:

$$\begin{cases} h_1 V,_I^{(1)} = -\sum_{r=2}^{N} h_r V,_I^{(r)} - \sum_{r=1}^{N}\left(2h_r C_I^{(r)} + 3h_r^2 D_I^{(r)} + h_r^2\theta,_I^{(r)}\right) \\ \lambda_1 h_1\psi_{K,K}^{(1)} = q - \sum_{r=1}^{N}\lambda_r\left[\left(h_r^2 C_K^{(r)} + h_r^3 D_K^{(r)}\right)_{,K} + \frac{2(1-\nu_r)}{\nu_r}h_r\theta^{(r)}\right] - \sum_{r=2}^{N}\lambda_r h_r\psi_{K,K}^{(r)} \\ w,_I^{(1)} = -\psi_I^{(1)}, \quad u_{K,K}^{(1)} = -\frac{1-\nu_1}{\nu_1}V^{(1)} \end{cases} \tag{16}$$

Thus, we have expressions for the unknown functions of the first layer of the plate under consideration.

In the absence of body forces, we transfer the equilibrium equations relative to the Ox_1x_2z coordinate frame into the $Ox_1x_2\xi$ coordinate frame:

$$\sigma_{IJ,J}^{(r)} + \frac{\sigma_{IZ,\xi}^{(r)}}{h_r} = 0$$
$$\sigma_{ZJ,J}^{(r)} + \frac{\sigma_{ZZ,\xi}^{(r)}}{h_r} = 0 \tag{17}$$

In this case, for the longitudinal components of the stress tensor $\sigma_{IJ}^{(r)}$, we have the following expressions:

$$\sigma_{IJ}^{(r)}(x_1, x_2, \xi) = \lambda_r \left[u_{K,K}{}^{(r)} + \xi h_r \psi_{K,K}{}^{(r)} + \xi^2 h_r{}^2 C_{K,K}{}^{(r)} + \xi^3 h_r{}^3 D_{K,K}{}^{(r)} + V^{(r)} + 2\xi h_r \theta^{(r)} \right] \delta_{IJ} +$$
$$\mu_r \left[\left(u_{I,J}{}^{(r)} + u_{J,I}{}^{(r)} \right) + \xi h_r \left(\psi_{I,J}{}^{(r)} + \psi_{J,I}{}^{(r)} \right) + \xi^2 h_r{}^2 \left(C_{I,J}{}^{(r)} + C_{J,I}{}^{(r)} \right) + \xi^3 h_r{}^3 \left(D_{I,J}{}^{(r)} + D_{J,I}{}^{(r)} \right) \right] \tag{18}$$

Using expressions (11) and (18), we calculate the longitudinal forces $N_{IJ}^{(r)} = h_r \int_0^1 \sigma_{IJ}^{(r)} d\xi$, internal moments $M_{IJ}^{(r)} = h_r{}^2 \int_0^1 \sigma_{IJ}^{(r)} \xi d\xi$, and shearing forces $Q_I^{(r)} = h_r \int_0^1 \sigma_{ZI}^{(r)} d\xi$:

$$N_{IJ}^{(r)} = \lambda_r h_r \left[u_{K,K}{}^{(r)} + \frac{1}{2} h_r \psi_{K,K}{}^{(r)} + \frac{1}{3} h_r{}^2 C_{K,K}{}^{(r)} + \frac{1}{4} h_r{}^3 D_{K,K}{}^{(r)} + V^{(r)} + h_r \theta^{(r)} \right] \delta_{IJ} +$$
$$\mu_r h_r \left[\left(u_{I,J}{}^{(r)} + u_{J,I}{}^{(r)} \right) + \frac{1}{2} h_r \left(\psi_{I,J}{}^{(r)} + \psi_{J,I}{}^{(r)} \right) + \frac{1}{3} h_r{}^2 \left(C_{I,J}{}^{(r)} + C_{J,I}{}^{(r)} \right) + \frac{1}{4} h_r{}^3 \left(D_{I,J}{}^{(r)} + D_{J,I}{}^{(r)} \right) \right] \tag{19}$$

$$M_{IJ}^{(r)} = \lambda_r h_r{}^2 \left[\frac{1}{2} u_{K,K}{}^{(r)} + \frac{1}{3} h_r \psi_{K,K}{}^{(r)} + \frac{1}{4} h_r{}^2 C_{K,K}{}^{(r)} + \frac{1}{5} h_r{}^3 D_{K,K}{}^{(r)} + \frac{1}{2} V^{(r)} + \frac{2}{3} h_r \theta^{(r)} \right] \delta_{IJ} +$$
$$\mu_r h_r{}^2 \left[\frac{1}{2} \left(u_{I,J}{}^{(r)} + u_{J,I}{}^{(r)} \right) + \frac{1}{3} h_r \left(\psi_{I,J}{}^{(r)} + \psi_{J,I}{}^{(r)} \right) + \frac{1}{4} h_r{}^2 \left(C_{I,J}{}^{(r)} + C_{J,I}{}^{(r)} \right) + \frac{1}{5} h_r{}^3 \left(D_{I,J}{}^{(r)} + D_{J,I}{}^{(r)} \right) \right]$$
(20)

$$Q_I^{(r)} = \mu_r h_r \left[\psi_I{}^{(r)} + h_r C_I{}^{(r)} + h_r{}^2 D_I{}^{(r)} + \left(w^{(r)} + \frac{1}{2} h_r V^{(r)} + \frac{1}{3} h_r{}^2 \theta^{(r)} \right)_{,I} \right] \tag{21}$$

To derive the equilibrium equation in terms of longitudinal forces, internal moments, and shear forces, considering boundary conditions (10) and expressions for normal stresses (18) in the equilibrium equations (17), we perform the standard integration procedure over the thickness of each layer:

$$\begin{cases} N_{IJ,J}^{(r)} + \sigma_{IZ}^{(r+1)}\Big|_{\xi=0} - \sigma_{IZ}^{(r)}\Big|_{\xi=0} = 0 \\ M_{IJ,J}^{(r)} - Q_I^{(r)} + h_r \sigma_{IZ}^{(r+1)}\Big|_{\xi=0} = 0 \\ Q_{I,I}^{(r)} + \sigma_{ZZ}^{(r+1)}\Big|_{\xi=0} - \sigma_{ZZ}^{(r)}\Big|_{\xi=0} = 0 \end{cases} \tag{22}$$

Substituting (19)-(21) into (22) and considering (11), we obtain

$$
\begin{cases}
\lambda_r h_r\left(u_{K,K}{}^{(r)}+\frac{1}{2}h_r\psi_{K,K}{}^{(r)}+\frac{1}{3}h_r{}^2C_{K,K}{}^{(r)}+\frac{1}{4}h_r{}^3D_{K,K}{}^{(r)}+V^{(r)}+h_r\theta^{(r)}\right)_{,I}+ \\
\mu_r h_r\left(\left(u_{I,J}{}^{(r)}+u_{J,I}{}^{(r)}\right)+\frac{1}{2}h_r\left(\psi_{I,J}{}^{(r)}+\psi_{J,I}{}^{(r)}\right)+\frac{1}{3}h_r{}^2\left(C_{I,J}{}^{(r)}+C_{J,I}{}^{(r)}\right)+\frac{1}{4}h_r{}^3\left(D_{I,J}{}^{(r)}+D_{J,I}{}^{(r)}\right)\right)_{,J}+ \\
\mu_{r+1}\left[\psi_I{}^{(r+1)}+w,_I{}^{(r+1)}\right]-\mu_r\left[\psi_I{}^{(r)}+w,_I{}^{(r)}\right]=0 \\
\lambda_r h_r{}^2\left(\frac{1}{2}u_{K,K}{}^{(r)}+\frac{1}{3}h_r\psi_{K,K}{}^{(r)}+\frac{1}{4}h_r{}^2C_{K,K}{}^{(r)}+\frac{1}{5}h_r{}^3D_{K,K}{}^{(r)}+\frac{1}{2}V^{(r)}+\frac{2}{3}h_r\theta^{(r)}\right)_{,I}+ \\
\mu_r h_r{}^2\left(\frac{1}{2}\left(u_{I,J}{}^{(r)}+u_{J,I}{}^{(r)}\right)+\frac{1}{3}h_r\left(\psi_{I,J}{}^{(r)}+\psi_{J,I}{}^{(r)}\right)+\frac{1}{4}h_r{}^2\left(C_{I,J}{}^{(r)}+C_{J,I}{}^{(r)}\right)+\frac{1}{5}h_r{}^3\left(D_{I,J}{}^{(r)}+D_{J,I}{}^{(r)}\right)\right)_{,J}- \\
\mu_r h_r\left[\psi_I{}^{(r)}+h_rC_I{}^{(r)}+h_r{}^2D_I{}^{(r)}+\left(w^{(r)}+\frac{1}{2}h_rV^{(r)}+\frac{1}{3}h_r{}^2\theta^{(r)}\right)_{,I}\right]+h_r\mu_{r+1}\left[\psi_I{}^{(r+1)}+w,_I{}^{(r+1)}\right]=0 \\
\mu_r h_r\left(\psi_I{}^{(r)}+h_rC_I{}^{(r)}+h_r{}^2D_I{}^{(r)}+\left(w^{(r)}+\frac{1}{2}h_rV^{(r)}+\frac{1}{3}h_r{}^2\theta^{(r)}\right)_{,I}\right)_{,I}+ \\
\lambda_{r+1}\left[u_{K,K}{}^{(r+1)}+\frac{1-\nu_{r+1}}{\nu_{r+1}}V^{(r+1)}\right]-\lambda_r\left[u_{K,K}{}^{(r)}+\frac{1-\nu_r}{\nu_r}V^{(r)}\right]=0
\end{cases}
\tag{23}
$$

Thus, we have a system of equations (23), boundary conditions on the upper plane (15), recurrent relations (13) on the interface of layered plates for N layers, and boundary conditions on the lower plane of the plate under consideration (14) with a total number of 11 N relative to unknowns $u_I{}^{(r)}, \psi_I{}^{(r)}, C_I{}^{(r)}, D_I{}^{(r)}, w^{(r)}, V^{(r)}, \theta^{(r)}$, i.e. a closed system of partial differential equations.

At the ends of the layered plate, there are generally three types of fixing, which in terms of stresses and displacements can be written as [10]:

I. $\sigma_{IJ}{}^{(r)}n_J\big|_\Sigma=0,\ \ U_Z{}^{(r)}\big|_\Sigma=0$ - hinged fixing;

II. $U_I{}^{(r)}\big|_\Sigma=0,\ \ U_Z{}^{(r)}\big|_\Sigma=0$ - rigid fixing; (24)

III. $\sigma_{IJ}{}^{(r)}n_J\big|_\Sigma=0,\ \ \sigma_{IZ}{}^{(r)}n_I\big|_\Sigma=0$ - free edge.

In terms of integral quantities, the given boundary conditions are, accordingly, written in the following form:

I. $N_{IJ}{}^{(r)}n_J\big|_\Sigma=0,\ \ M_{IJ}{}^{(r)}n_J\big|_\Sigma=0,\ w^{(r)}\big|_\Sigma=0,\ V^{(r)}\big|_\Sigma=0,\ \theta^{(r)}\big|_\Sigma=0$

II. $u_I^{(r)}\big|_\Sigma=0,\ \ \psi_I^{(r)}\big|_\Sigma=0,\ w^{(r)}\big|_\Sigma=0,\ V^{(r)}\big|_\Sigma=0,\ \theta^{(r)}\big|_\Sigma=0$ (25)

III. $N_{IJ}{}^{(r)}n_J\big|_\Sigma=0,\ \ M_{IJ}{}^{(r)}n_J\big|_\Sigma=0,\ Q_I^{(r)}n_I\big|_\Sigma=0,\ V,_I{}^{(r)}n_I\big|_\Sigma=0,\ \theta,_I{}^{(r)}n_I\big|_\Sigma=0$

In the boundary conditions obtained for the first two types, there is no normal displacement at the edges of the plate, therefore, V,θ are trivial; for the third type in (24), it is assumed that there is no gradient for compression along the free edges of the plate. It should be noted that here typical boundary conditions are formulated. The remaining types of boundary conditions can be either obtained by a linear combination of the above conditions or formulated in each case separately.

3. Discussion of results

In the problem under consideration, assuming longitudinal displacements to be potentials $U_I{}^{(r)}=U,_I{}^{(r)}$, we obtain a more simplified problem:

$$\begin{cases}(\lambda_r+2\mu_r)h_r\Delta\left(u^{(r)}+\frac{1}{2}h_r\psi^{(r)}+\frac{1}{3}h_r^2C^{(r)}+\frac{1}{4}h_r^3D^{(r)}\right)+\lambda_r h_r\left(V^{(r)}+h_r\theta^{(r)}\right)+\mu_{r+1}\left[\psi^{(r+1)}+w^{(r+1)}\right]-\mu_r\left[\psi^{(r)}+w^{(r)}\right]=0\\ (\lambda_r+2\mu_r)h_r^2\Delta\left(\frac{1}{2}u^{(r)}+\frac{1}{3}h_r\psi^{(r)}+\frac{1}{4}h_r^2C^{(r)}+\frac{1}{5}h_r^3D^{(r)}\right)+\lambda_r h_r^2\left(\frac{1}{2}V^{(r)}+\frac{2}{3}h_r\theta^{(r)}\right)\\ -\mu_r h_r\left[\psi_I^{(r)}+h_rC^{(r)}+h_r^2D^{(r)}+w^{(r)}+\frac{1}{2}h_rV^{(r)}+\frac{1}{3}h_r^2\theta^{(r)}\right]+\mu_{r+1}h_r\left[\psi^{(r+1)}+w^{(r+1)}\right]=0\\ \mu_r h_r\Delta\left(\psi^{(r)}+h_rC^{(r)}+h_r^2D^{(r)}+w^{(r)}+\frac{1}{2}h_rV^{(r)}+\frac{1}{3}h_r^2\theta^{(r)}\right)+\lambda_{r+1}\left[\Delta u^{(r+1)}+\frac{1-\nu_{r+1}}{\nu_{r+1}}V^{(r+1)}\right]-\lambda_r\left[\Delta u^{(r)}+\frac{1-\nu_r}{\nu_r}V^{(r)}\right]=0\end{cases}\tag{26}$$

System (12) is reduced to the following form considering the potentials:

$$\begin{cases}u^{(r+1)}=u^{(r)}+h_r\psi^{(r)}+h_r^2C^{(r)}+h_r^3D^{(r)}\\ w^{(r+1)}=w^{(r)}+h_rV^{(r)}+h_r^2\theta^{(r)}\\ \mu_{r+1}\psi_I^{(r+1)}=\mu_r\left(\psi^{(r)}+2h_rC^{(r)}+3h_r^2D^{(r)}\right)+\left(\mu_r-\mu_{r+1}\right)w^{(r+1)}\\ \lambda_{r+1}\frac{1-\nu_{r+1}}{\nu_{r+1}}V^{(r+1)}=\left(\lambda_r-\lambda_{r+1}\right)\Delta u^{(r+1)}+\lambda_r\frac{1-\nu_r}{\nu_r}\left(V^{(r)}+2h_r\theta^{(r)}\right)\end{cases}\tag{27}$$

Then expression (26) has the following form:

$$\begin{cases}(\lambda_r+2\mu_r)h_r\Delta\left(u^{(r)}+\frac{1}{2}h_r\psi^{(r)}+\frac{1}{3}h_r^2C^{(r)}+\frac{1}{4}h_r^3D^{(r)}\right)+\mu_r h_r\left(2C^{(r)}+3h_rD^{(r)}\right)+\left(\lambda_r+\mu_r\right)h_r\left(V^{(r)}+h_r\theta^{(r)}\right)=0\\ (\lambda_r+2\mu_r)h_r^2\Delta\left(\frac{1}{2}u^{(r)}+\frac{1}{3}h_r\psi^{(r)}+\frac{1}{4}h_r^2C^{(r)}+\frac{1}{5}h_r^3D^{(r)}\right)+\mu_r h_r^2\left[C^{(r)}+2h_rD^{(r)}\right]+\left(\lambda_r+\mu_r\right)h_r^2\left(\frac{1}{2}V^{(r)}+\frac{2}{3}h_r\theta^{(r)}\right)=0\\ \left(\lambda_r+\mu_r\right)\Delta\left(\psi^{(r)}+h_rC^{(r)}+h_r^2D^{(r)}\right)+\mu_r\Delta\left(w^{(r)}+\frac{1}{2}h_rV^{(r)}+\frac{1}{3}h_r^2\theta^{(r)}\right)+2\lambda_r\frac{1-\nu_r}{\nu_r}\theta^{(r)}=0\end{cases}\tag{28}$$

We multiply the first line by $\frac{1}{(\lambda_r+2\mu_r)h_r}$, the second line by $\frac{1}{(\lambda_r+2\mu_r)h_r^2}$, and the third line by $\frac{1}{(\lambda_r+\mu_r)}$ and obtain the following system:

$$\begin{cases}\Delta\left(u^{(r)}+\frac{1}{2}h_r\psi^{(r)}+\frac{1}{3}h_r^2C^{(r)}+\frac{1}{4}h_r^3D^{(r)}\right)+\frac{1}{2(1-\nu_r)}\left[(1-2\nu_r)\left(2C^{(r)}+3h_rD^{(r)}\right)+V^{(r)}+h_r\theta^{(r)}\right]=0\\ \Delta\left(\frac{1}{2}u^{(r)}+\frac{1}{3}h_r\psi^{(r)}+\frac{1}{4}h_r^2C^{(r)}+\frac{1}{5}h_r^3D^{(r)}\right)+\frac{1}{2(1-\nu_r)}\left[(1-2\nu_r)\left(C^{(r)}+2h_rD^{(r)}\right)+\frac{1}{2}V^{(r)}+\frac{2}{3}h_r\theta^{(r)}\right]=0\\ \Delta\left(\psi^{(r)}+h_rC^{(r)}+h_r^2D^{(r)}\right)+(1-2\nu_r)\Delta\left(w^{(r)}+\frac{1}{2}h_rV^{(r)}+\frac{1}{3}h_r^2\theta^{(r)}\right)+4(1-\nu_r)\theta^{(r)}=0\end{cases}\tag{29}$$

Thus, we have a system of three partial differential equations (29) and a system of recurrence relations (27) to determine unknowns $u^{(r)},\psi^{(r)},C^{(r)},D^{(r)},w^{(r)},V^{(r)},\theta^{(r)}$. Here, for the sought-for variables, the approximate analytical Navier method can be used, ensuring the selection of basic functions that satisfy the corresponding boundary conditions. Without specifying the boundary conditions and solving the corresponding spectral problem, in (29) instead of the Laplace operator we introduce a formal substitution $-\gamma^2$ and system (29) acquires the following form:

$$\begin{cases}-2(1-\nu_r)\gamma^2\left(u^{(r)}+\frac{1}{2}h_r\psi^{(r)}+\frac{1}{3}h_r^2C^{(r)}+\frac{1}{4}h_r^3D^{(r)}\right)+(1-2\nu_r)\left(2C^{(r)}+3h_rD^{(r)}\right)+V^{(r)}+h_r\theta^{(r)}=0\\ -2(1-\nu_r)\gamma^2\left(\frac{1}{2}u^{(r)}+\frac{1}{3}h_r\psi^{(r)}+\frac{1}{4}h_r^2C^{(r)}+\frac{1}{5}h_r^3D^{(r)}\right)+(1-2\nu_r)\left(C^{(r)}+2h_rD^{(r)}\right)+\frac{1}{2}V^{(r)}+\frac{2}{3}h_r\theta^{(r)}=0\\ -\gamma^2\left(\psi^{(r)}+h_rC^{(r)}+h_r^2D^{(r)}\right)-(1-2\nu_r)\gamma^2\left(w^{(r)}+\frac{1}{2}h_rV^{(r)}+\frac{1}{3}h_r^2\theta^{(r)}\right)+4(1-\nu_r)\theta^{(r)}=0\end{cases}\tag{29}$$

Then from (29), we can determine $C^{(r)}$, $D^{(r)}$, $\theta^{(r)}$

$$\begin{cases} C^{(r)} = \dfrac{1}{(1-2\nu_r)}\left((1-\nu_r)\gamma^2 u^{(r)} - \dfrac{1}{2}V^{(r)}\right) \\ D^{(r)} = -\dfrac{\gamma^2}{12(1-\nu_r)(1-2\nu_r)}\left(\psi^{(r)} + w^{(r)}\right) \\ \theta^{(r)} = \dfrac{\gamma^2}{4}\left(\dfrac{1}{(1-\nu_r)}\psi^{(r)} + \dfrac{(1-2\nu_r)}{(1-\nu_r)}w^{(r)} + \dfrac{2}{(1-2\nu_r)}h_r V^{(r)}\right) \end{cases} \tag{30}$$

Considering the introduced potentials for the sought-for functions, substituting the expressions from system (16) into system (13) using (30) we obtain the following system

$$\begin{cases} u^{(1)} = \dfrac{(1-\nu_1)(1-2\nu_1)}{\lambda_1\gamma^2 h_1^2 \nu_1(3-2\nu_1)}\left[\dfrac{2q}{\gamma^2} + \sum\limits_{k=2}^{N}\dfrac{\lambda_k h_k^2}{1-2\nu_k}\left[2\gamma^2(1-\nu_k)u^{(k)} - \dfrac{1}{h_k}\left(\dfrac{(1-2\nu_k)^2}{\nu_k} + \dfrac{\gamma^2 h_k^2}{6(1-\nu_k)}\right)\left(\psi^{(k)} + w^{(k)}\right) - \dfrac{2-\nu_k}{\nu_k}V^{(k)}\right]\right] \\ V^{(1)} = \dfrac{1-2\nu_1}{\lambda_1 h_1^2(3-2\nu_1)}\left[\dfrac{2q}{\gamma^2} + \sum\limits_{k=2}^{N}\dfrac{\lambda_k h_k^2}{1-2\nu_k}\left[2\gamma^2(1-\nu_k)u^{(k)} - \dfrac{1}{h_k}\left(\dfrac{(1-2\nu_k)^2}{\nu_k} + \dfrac{\gamma^2 h_k^2}{6(1-\nu_k)}\right)\left(\psi^{(k)} + w^{(k)}\right) - \dfrac{2-\nu_k}{\nu_k}V^{(k)}\right]\right] \\ \psi^{(1)} = -\dfrac{2(1-2\nu_1)}{\gamma^2 h_1 \nu_1}\left[\dfrac{aq}{\gamma^2} + \sum\limits_{k=2}^{N}\left[\begin{array}{l} \dfrac{\gamma^2(1-\nu_k)}{(1-2\nu_k)}\left(a\lambda_k h_k^2 + \dfrac{2h_k}{h_1}\right)u^{(k)} - \left(ab + \dfrac{\gamma^2 h_k^2 \nu_k}{2h_1(1-2\nu_k)(1-\nu_k)}\right)\psi^{(k)} - \left(ab - \dfrac{\gamma^2 h_k^2 \nu_k}{h_1(1-2\nu_k)}\right)w^{(k)} \\ + \dfrac{h_k}{2(1-2\nu_k)}\left(\dfrac{\gamma^2 h_k^2 - 4\nu_k}{h_1} - \dfrac{a\lambda_k h_k(2-\nu_k)}{\nu_k}\right)V^{(k)} \end{array}\right]\right] \\ w^{(1)} = \dfrac{2(1-2\nu_1)}{\gamma^2 h_1 \nu_1}\left[\dfrac{aq}{\gamma^2} + \sum\limits_{k=2}^{N}\left[\begin{array}{l} \dfrac{\gamma^2(1-\nu_k)}{(1-2\nu_k)}\left(a\lambda_k h_k^2 + \dfrac{2h_k}{h_1}\right)u^{(k)} - \left(ab + \dfrac{\gamma^2 h_k^2 \nu_k}{2h_1(1-2\nu_k)(1-\nu_k)}\right)\psi^{(k)} - \left(ab - \dfrac{\gamma^2 h_k^2 \nu_k}{h_1(1-2\nu_k)}\right)w^{(k)} \\ + \dfrac{h_k}{2(1-2\nu_k)}\left(\dfrac{\gamma^2 h_k^2 - 4\nu_k}{h_1} - \dfrac{a\lambda_k h_k(2-\nu_k)}{\nu_k}\right)V^{(k)} \end{array}\right]\right] \end{cases} \tag{31}$$

where $a = \dfrac{4(1-2\nu_1) + \gamma^2 h_1^2 \nu_1}{\lambda_1 h_1^2 \nu_1(3-2\nu_1)}$, $b = \dfrac{\lambda_k h_k}{2}\left(\dfrac{1-2\nu_k}{\nu_k} - \dfrac{\gamma^2 h_k^2}{6(1-\nu_k)(1-2\nu_k)}\right)$.

From (27) after some calculations, we will have the following recurrence relations:

$$\begin{cases} u_I^{(r)} = u_I^{(1)} + \sum\limits_{k=2}^{r-1} h_k\left(h_k\psi^{(k)} + h_k^2 C^{(k)} + h_k^3 D^{(k)}\right) \\ w^{(r)} = w^{(1)} + \sum\limits_{k=2}^{r-1}\left(h_k V^{(k)} + h_k^2\theta^{(k)}\right) \\ \psi_I^{(r)} = \psi_I^{(1)} + \dfrac{1}{\mu_r}\sum\limits_{k=1}^{r-1}\left[\mu_k\left(2h_k C^{(k)} + 3h_k^2 D^{(k)}\right) + (\mu_k - \mu_r)\left(h_k V^{(k)} + h_k^2\theta^{(k)}\right)\right] \\ V^{(r)} = \dfrac{\nu_r}{1-\nu_r}\left[\dfrac{1-\nu_1}{\nu_1}V^{(1)} - \dfrac{1}{\lambda_r}\sum\limits_{k=1}^{r-1} h_k\left(\gamma^2(\lambda_k - \lambda_r)\left(\psi^{(k)} + h_k C^{(k)} + h_k^2 D^{(k)}\right) - \dfrac{2\lambda_k(1-\nu_k)}{\nu_k}\theta^{(k)}\right)\right] \end{cases} \tag{32}$$

and (31) substituting into (32), we will ultimately have a system of 4 N algebraic equations for unknowns $u^{(r)}, \psi^{(r)}, w^{(r)}, V^{(r)}$.

It should be especially noted here that it is possible to study the stress-strain state of plates with an arbitrary number of layers. This fact is especially important when studying layered structural elements using advances in nanotechnology.

4. Conclusions

1. A non-classical theory of layered plates was proposed, ensuring interlayer continuity conditions without simplifying assumptions and hypotheses.

2. When solving applied problems, there are no restrictions on the number of layers and interlayer connection conditions.

3. In future studies, each “package” of layers can be anisotropic and thermoplastic.

References

1. *Christensen P.M.* Introduction to the mechanics of composites. M.: Mir, 1982.
2. *Pobedrya B.E.* Mechanics of composite materials – M.: Moscow State University Publishing House 1984 -336 p.
3. *Dimitrienko Yu.I., Gubareva E.A., Yakovlev D.O.* Calculation of multilayer plates based on the asymptotic theory of averaging - M.: Publishing house of MSTU named after N.E. Bauman, 2013, p. 7.
4. *Volchkov Yu.M.* Modified equations of finite-size layered plates made of orthotropic material. Comparison of the results of numerical calculations with analytical solutions // Applied mechanics and technical physics. – 2017. V. 58 – No. 5. – pp. 167-177.
5. *Usarov M.K., Usarov D.M.* To the solution of the problem of bending and vibration of three-layer plates with thick filler // Higher school scientific and practical journal. – No. 18. Ufa. – 2017 – pp. 40-43.
6. *Niyazova N.A., Usarov M.K.* On the theory of bending and stability of three-layer plates with orthotropic three-dimensional filler // Eighth All-Russian Congress on Theoretical and Applied Mechanics. – Perm, August 23-29, 2001. – pp.458–459.
7. *Akhmedov A.B., Sheshenin S.V.* To the construction of nonlinear equations of motion of orthotropic plates // Bulletin of Moscow State University, Series of Physical and Mathematical Sciences. – Moscow, 2012. – No. 3. – P.36-39.
8. *Novatsky V.* Theory of elasticity. -M.: Mir, 1975.
9. *Akhmedov A.B., Shamsiev D.* Nonclassical theory of layered composite plates. Vestnik TSTU 2015, No. 2.
10. *Akhmedov A.B.* Nonclassical problems of plates and shallow shells and development of numerical methods for solution. //Dissertation Doctor of Phys.-Math. Sci. - Tashkent, 2016. 243 p.

MATHEMATICAL MODELING AND NUMERICAL SOLUTION OF PROBLEMS OF UNDERGROUND PIPELINES UNDER SPATIAL SEISMIC EFFECT

Bekmirzaev D.A.[1], Mansurova N.Sh.[1]

[1]*Institute of Mechanics and Seismic Stability of Structures named after M.T.Urazbaev,*
Uzbekistan Academy of Sciences. Tashkent, Uzbekistan.
E-mail: diyorbek_84@mail.ru

Abstract. *Mathematical modeling and numerical solution of problems of underground pipelines under spatial seismic effects are discussed in the paper. The systems of differential equations of motion are obtained for the problems of seismodynamics of underground pipelines with complex conditions of interacting with soil, at arbitrary direction of seismic load, based on Hamilton–Ostrogradsky variation principle, this allows in general form to consider a number of classes of problems. An analysis of results was made for an extended pipeline with joints located on the Oxy plane and interacting with surrounding soil. Applied software was created for calculation and visual representation of the results of solving problems in the form of graphs of changes in displacements, forces and moments over time at selected nodal points of the structure and in the form of animation. Results obtained present a new contribution into seismodynamic theory; they open wide possibilities for their use in optimal design of the complex of life support in seismic zones.*

Keywords*: model, underground pipeline, seismic wave, interaction, soil, numerical method.*

1. Introduction.

At present, the case-history of strong earthquakes that have occurred in the world shows that a preliminary hazard assessment of earthquakes and timely consideration of appropriate measures (problems of assessing seismic risk and their mitigation) are of great importance for the reduction of catastrophic aftermath. Thus, it is necessary to ensure the strength and stability of underground structures subjected to seismic loads. In this sense, the implementation of targeted scientific research to improve numerical methods for solving problems, to calculate the earthquake resistance of underground pipeline systems under random seismic effects is a relevant issue [1-8].

The current capability of computing facilities makes it possible to more fully account for numerous factors and, with a greater degree of reliability, determine the actual stress-strain state of an underground pipeline. Severe earthquakes all over the world in recent years (Nepal, 15–26 April, 2015; Chile, 2 April, 2014; Cephalonia, 26 January and 3 February, 2014; Japan, 13 April, 2013 and others) affected normal operation of underground support nerworks; their number growing considerably high in 1960-1980 years of the last century due to urbanization of towns and villages.

In the second half of the twentieth century to calculate the complex system of underground pipelines with a large number of branches and inclusions (water supply, drainage systems, etc.) T.R. Rashidov has proposed “Dynamic theory of seismic stability of complex systems of underground structures”, based on the presentation of linear part of the pipeline by core elements of finite length

and joint connections (structural inclusion) – by absolutely rigid bodies. Here all the relevant elements and units are in interaction with surrounding soil medium. In the future, the work has been carried out to improve this technique in terms of taking into account different kinds of nonlinearities (joints deformation, slip on the ground, etc.) [1-4].

In works of H. Zhuang, Z. Hu, X. Wang, G. Chen, S. Sarioletlagh, V. Corrado, B. D'Acunto, N. Fontana M. Nekooei, A.V. Oskouei, A. Aziminejad, D. Ha, T.H. Abdoun, M.J. O'Rourke, M.D. Symans, M. Saberi, H. Arabzadeh, A. Keshavarz, P. Vazouras, S.A. Karamanos, S.C. Chian, S.P.G. Madabhushi, et al. the use of different mechanical mathematical models was analyzed and a number of urgent problems of underground and ground structures were solved [5-14].

Analysis of the aftermath of severe earthquakes shows that seismic stability of underground structures depends on the direction of seismic wave. Since underground structures during the earthquakes are stresses by arbitrary directed loading, the evaluation of stress-strain state of underground pipelines under spatial oscillations is an actual problem and it serves to the determination of potential seismic hazard [17-21].

This paper is devoted to the study of the underground pipelines dynamics based on the seismodynamic theory of underground structures, using a mathematical model of the theory of rods, considered in [1-4] for the case of rod point displacements under combined action of longitudinal and transverse forces.

2. Methodology.

The main problem of seismodynamics of underground pipelines is a simulatiuon of interaction in the system "pipe-soil". The main parameters determining stressed state of life support systems (underground pipelines) are the coefficients of interaction of these structures with surrounding soil [1-3].

To study the longitudinal, torsional and transverse vibrations of underground pipelines under randomly directed seismic load, the applied theory of rod vibrations was used. The Hamilton–Ostrogradsky variational principle for an underground pipeline has the form [22-24]

$$\int_t \left(\delta \mathrm{T} - \delta \Pi + \delta \mathrm{A}\right) dt = 0\,, \tag{1}$$

where δT, $\delta\Pi$ are the variations of kinetic and potential energies; δA is the variation of the work of external forces; t is time.

The pipeline is modeled as a rod. Displacements are defined as follows [15, 18]:

$$u_1 = u - y\alpha_1 - z\alpha_2\,,\; u_2 = \mathrm{v} + z\theta\,,\; u_3 = w - y\theta\,, \tag{2}$$

where the components u_1, u_2, u_3 are the displacements of any point in the pipeline; u, v, w – are the longitudinal, transverse horizontal and vertical displacements of the pipeline axis; α_1, α_2 are the angles of rotation of the pipeline axis under pure bending; θ is the torsion of the pipeline.

Variations in kinetic energy of the pipeline. Kinetic energy variations can be represented as

$$\int_t \delta \mathrm{T} dt = \int_t \int_V \left[\rho \frac{\partial u_1}{\partial t} \delta \frac{\partial u_1}{\partial t} + \rho \frac{\partial u_2}{\partial t} \delta \frac{\partial u_2}{\partial t} + \rho \frac{\partial u_3}{\partial t} \delta \frac{\partial u_3}{\partial t} \right] dV dt. \tag{3}$$

Variations in potential energy of the pipeline. Consider the potential energy variations

$$\int_t \delta \Pi dt = \int_t \int_V \left(\sigma_{11}\delta\varepsilon_{11} + \sigma_{12}\delta\varepsilon_{12} + \sigma_{13}\delta\varepsilon_{13}\right) dV dt\,. \tag{4}$$

Metal pipelines are strained within the elastic limit. Therefore, for a metal pipeline the Hooke's law is considered

$$\sigma_{11} = E\left(\frac{\partial u}{\partial x} - y\frac{\partial \alpha_1}{\partial x} - z\frac{\partial \alpha_2}{\partial x}\right),\; \sigma_{12} = G\left(\frac{\partial v}{\partial x} + z\frac{\partial \theta}{\partial x} - \alpha_1\right),\; \sigma_{13} = G\left(\frac{\partial w}{\partial x} - y\frac{\partial \theta}{\partial x} - \alpha_2\right). \tag{5}$$

For underground polymer pipelines, the stress-strain relation is:

$$\sigma_{11} = E\left(\frac{\partial u}{\partial x} - y\frac{\partial \alpha_1}{\partial x} - z\frac{\partial \alpha_2}{\partial x}\right)(1 - \int_0^t \Gamma(t-\tau)d\tau),$$

$$\sigma_{12} = G\left(\frac{\partial v}{\partial x} + z\frac{\partial \theta}{\partial x} - \alpha_1\right)(1 - \int_0^t \Gamma(t-\tau)d\tau), \tag{6}$$

$$\sigma_{13} = G\left(\frac{\partial w}{\partial x} + y\frac{\partial \theta}{\partial x} - \alpha_2\right)(1 - \int_0^t \Gamma(t-\tau)d\tau).$$

Based on stresses $\sigma_{i\,j}$ (5) and (6), the longitudinal and transverse forces N_x and $Q_{i\,j}$, and the moments of bending and torques $M_{i\,j}$ were calculated.

Variations in external forces work of the pipeline. Variations in external forces work of the pipeline in a general way are as follows

$$\int_t \delta A dt = \int_t \int_V [P_1\delta u_1 + P_2\delta u_2 + P_3\delta u_3] dV dt +$$
$$+ \int_t \int_S [q_1\delta u_1 + q_2\delta u_2 + q_3\delta u_3] dS dt + \int_t \int_{S_1} [\varphi_1\delta u_1 + \varphi_2\delta u_2 + \varphi_3\delta u_3] dS_1 dt\Big|_x. \tag{7}$$

Here P_1, P_2, P_3 are the volume forces, q_1, q_2, q_3 are the surface forces, φ_1, φ_1, φ_1 are the lateral forces acting on the pipeline.

After setting the variation of kinetic (3), potential (4) energy and the work of external forces (7) based on the Hamilton-Ostrogradsky variational principle (1) and performing the operation of similar terms reduction, we obtain the variational equation of underground pipelines with the corresponding initial and boundary conditions.

$$\int_t (\delta\Gamma - \delta\Pi + \delta A) dt = \int_x \left[\rho\left(F\frac{\partial u}{\partial t}\delta u + I_z\frac{\partial \alpha_1}{\partial t}\delta\alpha_1 + I_y\frac{\partial \alpha_2}{\partial t}\delta\alpha_2 + F\frac{\partial v}{\partial t}\delta v + F\frac{\partial w}{\partial t}\delta w + I_p\frac{\partial \theta}{\partial t}\delta\theta\right)\right] dx\Big|_t +$$
$$+ \int_t \int_x \left\{\left[-\rho F\frac{\partial^2 u}{\partial t^2} + \frac{\partial N_x}{\partial x} + N_x(P_1) + N_x(q_1)\right]\delta u + \left[-\rho I_z\frac{\partial^2 \alpha_1}{\partial t^2} - \frac{\partial M_z}{\partial x} + Q_{12} - M_z(P_1) - M_z(q_1)\right]\delta\alpha_1 +\right.$$
$$+ \left[-\rho I_y\frac{\partial^2 \alpha_2}{\partial t^2} - \frac{\partial M_y}{\partial x} + Q_{13} - M_y(P_1) - M_y(q_1)\right]\delta\alpha_2 + \left[-\rho F\frac{\partial^2 v}{\partial t^2} + \frac{\partial Q_{12}}{\partial x} + Q_{12}(P_2) + Q_{12}(q_2))\right]\delta v +$$
$$\left. + \left[-\rho F\frac{\partial^2 w}{\partial t^2} + \frac{\partial Q_{13}}{\partial x} + Q_{13}(P_3) + Q_{13}(q_3)\right]\delta w + \left[-\rho I_p\frac{\partial^2 \theta}{\partial t^2} + \frac{\partial M_x}{\partial x} + M_x(P_2, P_3) + M_x(q_2, q_3)\right]\delta\theta\right\} dx dt +$$
$$+ \left\{\left[\left(-N_x + N_x(\varphi_1)\right)\delta u + (M_z - M_z(\varphi_1))\delta\alpha_1 + (M_y - M_y(\varphi_1))\delta\alpha_2 + (-Q_{12} + Q_{12}(\varphi_2))\delta v +\right.\right.$$
$$\left.\left. + (-Q_{13} + Q_{13}(\varphi_3))\delta w + (-M_x + M_x(\varphi_2, \varphi_3))\delta\theta\right]\Big|_x\right\} dt = 0.$$

where

$$N_x = EF\frac{\partial u}{\partial x},\ M_z = -EI_z\frac{\partial \alpha_1}{\partial x},$$
$$M_y = -EI_y\frac{\partial \alpha_2}{\partial x},\ Q_{12} = GF\frac{\partial v}{\partial x} - GF\alpha_1, \tag{8}$$
$$Q_{13} = GF\frac{\partial w}{\partial x} - GF\alpha_2,\ M_x = GI_p\frac{\partial \theta}{\partial x}.$$

Based on this statement, a system of differential equations, natural boundary and initial conditions is obtained from the variational equation. The resulting systems of differential equations and natural boundary and initial conditions can be represented in a vector form.

The system of differential equations for linear sections of underground pipelines in a local (for each linear section) spatial coordinate system (*Oxyz*) under random seismic action, with corresponding boundary conditions at the ends and initial conditions, has a vector form

$$M\frac{\partial^2 U}{\partial t^2}+A\frac{\partial^2 U}{\partial x^2}+B\frac{\partial U}{\partial x}+CU=CU_0, \tag{9}$$

$$D\frac{\partial U}{\partial x}+QU=QU_0, \tag{10}$$

$$U=0,\quad \frac{\partial U}{\partial t}=0, \text{ at } t=0. \tag{11}$$

where M, A, B, C, D, Q are the sixth-order matrices, U are the pipeline and nodes displacements, U_0 are the given displacements of soil under the effect of seismic waves, depending on time and coordinates.

The stresses in the underground pipeline generated from axial force N and the combined action of axial force and the force moment M under random action are calculated according to the following formulas [2]

$$\sigma=\frac{N}{F}, \tag{12}$$

$$\sigma_{y,z}^{\pm}=\frac{N}{F}\pm\frac{M_{y,z}\cdot R_H}{I_{y,z}}. \tag{13}$$

The finite element method (FEM) in spatial coordinates and the implicit finite difference method (FDM) in time to discretize the pipeline problem under the action of random seismic waves are used as numerical methods for solving the equation of motion (9) with account for (10) and (11) [2].

In this paper, an approach is proposed for determining the stress-strain state of a pipeline subjected to randomly directed plane longitudinal unsteady-state seismic wave. Its propagation direction makes an angle α with the pipeline axis *Ox* and β is the angle between the projection of this wave direction vector onto the *Oyz* plane and the *Oy* axis of the pipeline [2].

Consider an extended pipeline with joints located on the *Oxy* plane and interacting with surrounding soil according to a simplified elastic model. Let the length of underground pipeline be 200 m and the length of each section - 5 m (Figure 1).

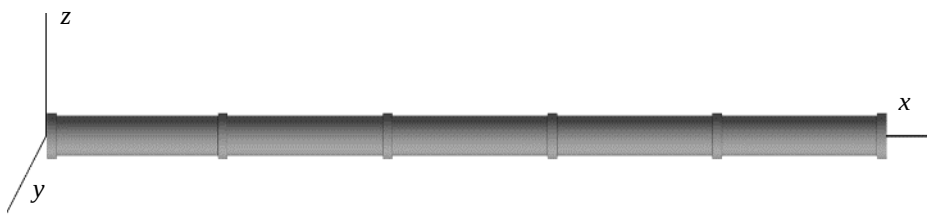

Figure. 1. - **Underground pipeline with joint**

The left and right ends of the pipeline are embedded into the ground, and the seismic wave is given as a harmonic function with incidence angles α=30°, β=30°. In general, the problem is an unsteady-state spatial one for studying the processes in underground pipelines under the action of seismic waves. Mechanical and geometrical parameters of underground pipeline and soil are taken as follows:

Problem. $E=1.2\cdot10^5$ MPa; $\rho=7.0\cdot10^3$ kg/m^3; $l=200$ m; $D_H=0.5$ m; $D_B=0.49$ m; in a straight section $k_x=1.5\cdot10^4$ kN/m^3; $k_{y,z}=3.9\cdot10^4$ kN/m^3; $u_0=a_0\cdot\sin\omega(t-x\cdot\cos\alpha/C_p)\cdot H(t-x\cdot\cos\alpha/C_p)$; $\nu_{soil}=0.2$; $\nu_{pipe}=0.3$; $a_0=0.01$ m; $\omega=2\pi/T$; $T=0.3$ s; $C_p=700$ m/s; $u_{0x}=u_0\cdot\cos\alpha$; $u_{0y}=u_0\cdot\sin\alpha\cdot\cos\beta$; $u_{0z}=u_0\cdot\sin\alpha\cdot\sin\beta$.

The amplitude of ground vibrations a_0 corresponds to a 9 point earthquake on the MSK-64 scale. Joint stiffness factors are

$$K_N=80\cdot10^4 \text{ kN/m}; \; K_Q=200\cdot10^4 \text{ kN/m};$$

$$K_{M_u}=9\cdot10^2 \text{ kNm}; \; K_{M_k}=8\cdot10^4 \text{ kNm}.$$

Here E, D_H are the elastic modulus of the pipeline material and the outer diameter of the pipe, respectively; ρ is the density of the pipeline material; k_x, $k_{y,z}$ are the coefficients of longitudinal, transverse and vertical interaction of the pipe with soil; a_0 is the amplitude of ground vibration; ω is the vibration frequency; C_p is the propagation velocity of seismic waves in soil.

3. Results and Discussions.

The results on Fig. 2 shows the changes in longitudinal displacements along the pipeline at a fixed time. The wave distribution along the pipeline in the time range t=0.05÷0.3 s is presented here. At t=0.286 s the wave propagating in soil reaches the right end of the pipeline.

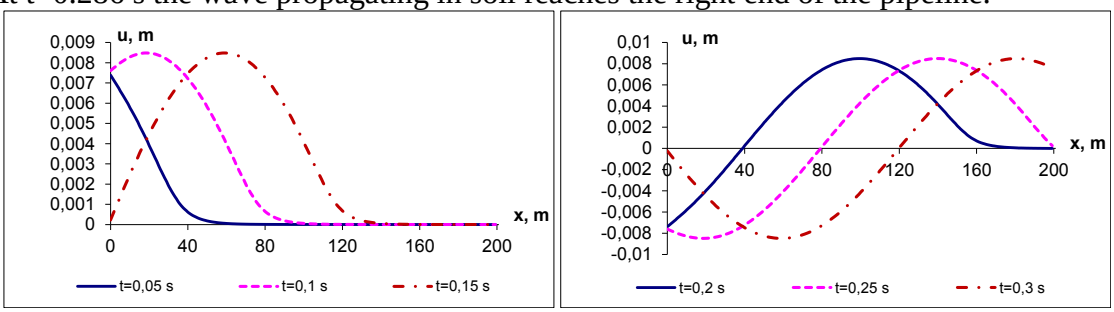

Figure 2. - **Changes in longitudinal displacements along the pipeline axis at a fixed time**

Figure 3 shows the changes in transverse and vertical displacements along the pipeline axis at a fixed time. The results show that the displacements in each section of the underground pipeline along the coordinate are complex in nature with certain small bursts associated with the presence of flexible joints.

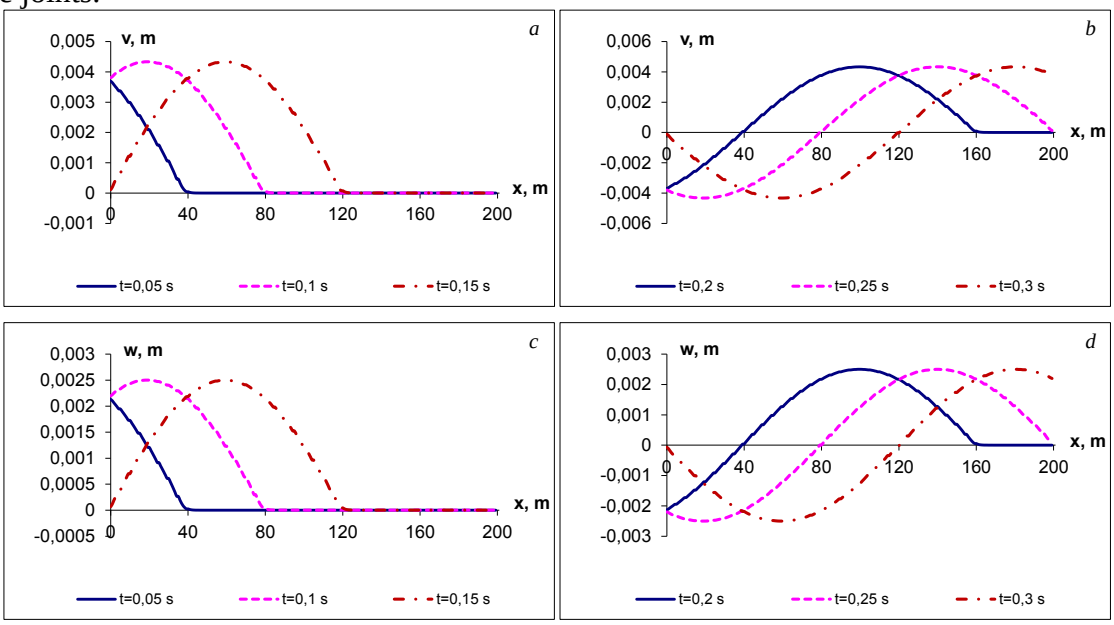

Figure 3. - **Changes in transverse (*a*, *b*) and vertical (*c*, *d*) displacements along the pipeline axis at a fixed time**

Figure 4 shows the changes in compressive (tensile) stress along the axis of underground pipeline at a fixed time.

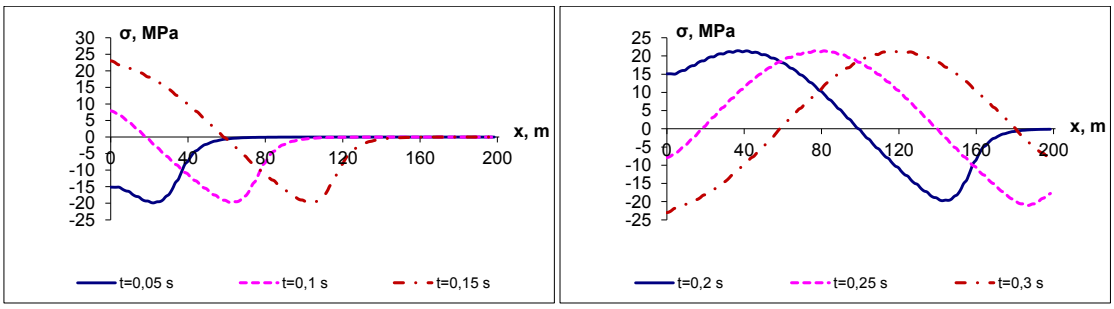

Figure 4. - **Changes in compressive (tensile) stress along the axis of underground pipeline at a fixed time**

The results show that in each joint, the compressive (tensile) stress of underground pipeline along the coordinate has a value distinctive for this joint with certain small bursts. This is due to the wave reflection from the joint and the wave propagation through the joint to the adjacent section of the pipeline.

Figure 5 shows the changes in total stresses (σ_y^+, σ_y^-) along the axis of the underground pipeline at a fixed time.

It is seen that at each joint, the values of total stresses of the underground pipeline along the coordinate are of a different nature and have certain small bursts due to the joints flexibility.

The results show that at each joint, as in the case in Figure 5, the values of total stresses in underground pipeline along the coordinate have different pattern with certain small burst.

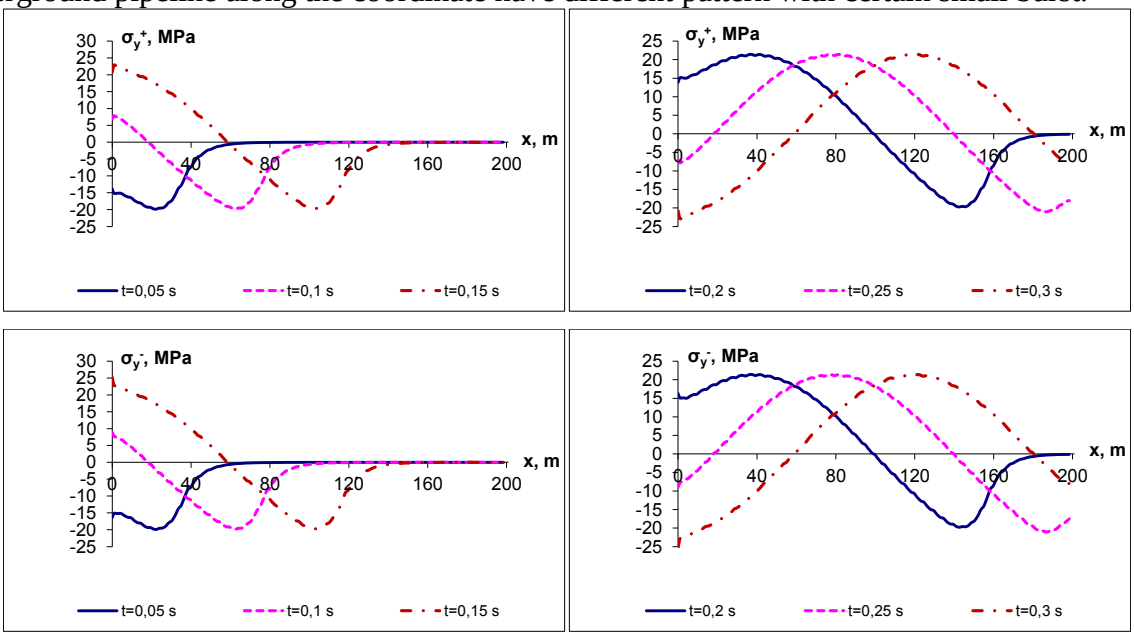

Figure 5. - **Changes in total stresses (σ_y^+, σ_y^-) along the underground pipeline axis at a fixed time**

Figure 6 shows the changes in total stresses (σ_z^+, σ_z^-) along the underground pipeline axis at a fixed time.

From the graphs in Figures 5 and 6, it is seen that each section of the underground pipeline affects the values of bending moments.

It can be seen from the results, the values of bending moment of the underground pipeline are separately formed at each section of the pipeline and at the joints.

At the joints, the values of bending moments are much smaller, compared with their values in sections, due to the flexibility of joints. The burst in value of bending moment near the wave front is associated with the pipeline end embedding in the deflection points.

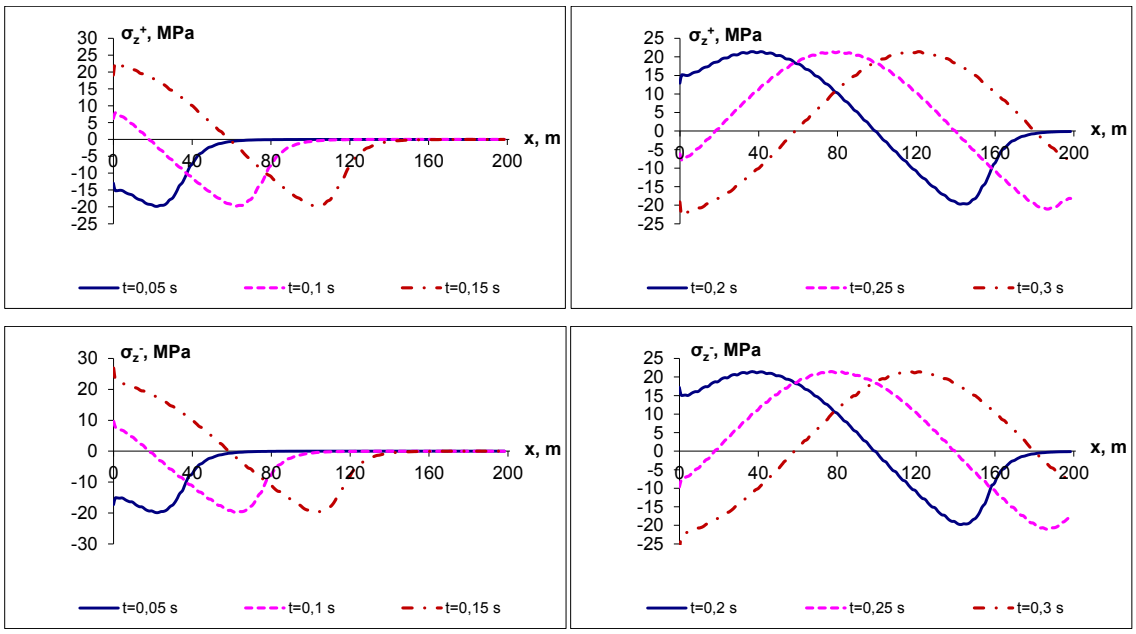

Figure 6. - **Changes in total stresses (σ_z^+, σ_z^-) along the underground pipeline axis at a fixed time**

For visualization, Figure 7 shows the change in bending moments values (M_y, M_z) for a different range of lengths (x=5÷25 m and x=170÷195 m) of the underground pipeline at a fixed time. The figures show that the bending moments (M_y, M_z) change along the length of the underground pipeline section; they increase from the left joint and then decrease to the right joint (see Figure 7), and at the joint the values of bending moment are less than in the middle of the section.

The previous graphs show the flexibility effect of section joints of the pipeline on the forces and moments distribution along the pipeline.

From the results obtained for the bending moment, it is seen that a separate bending moment arises in each section of the joined underground pipeline during earthquakes. Therefore, the dynamic process in an underground pipeline is of a complex pattern and the values of total stress increase. A seismic wave acts on a joined pipeline; calculations should be carried out at an angle to its longitudinal axis using a composite model of the pipeline, where each section of a pipeline and each of its joints are taken into account.

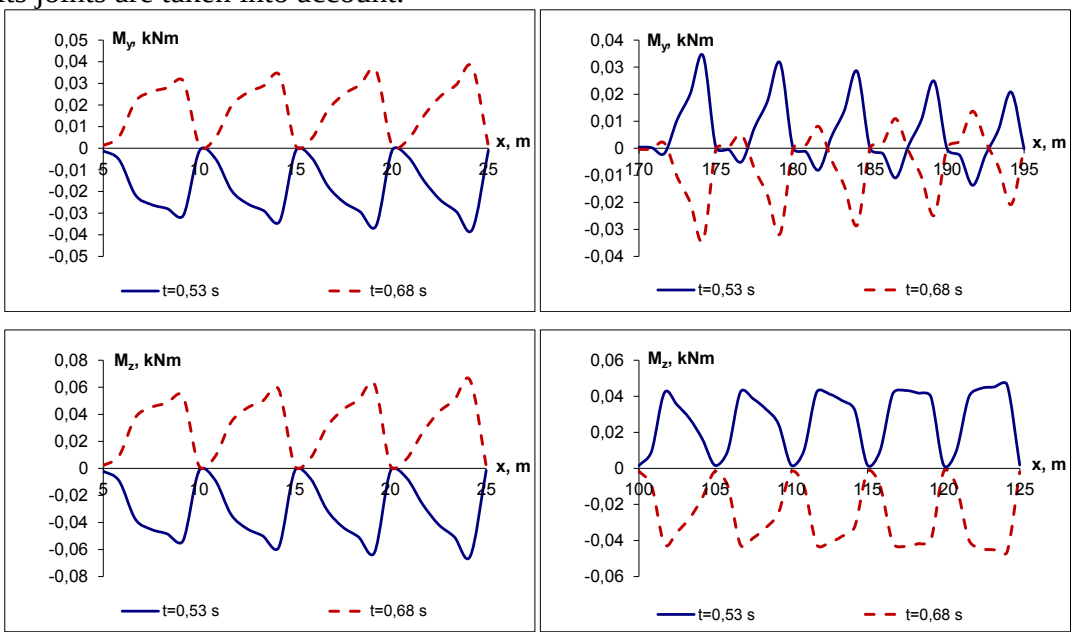

Figure 7. - **Change in bending moment (bending relative to axes *Oy* and *Oz*) in different sections of the underground pipeline at a fixed time**

4. Conclusions

A generalized system of differential equations of underground pipeline spatial vibrations under random seismic actions at natural initial conditions based on the Hamilton–Ostrogradsky variational principle was developed. The system of differential equations with corresponding boundary and initial conditions is derived.

As seen from results of numerical experiments, based on hypothesis taken in calculations concerning the forces of interaction between long underground structures (pipelines) and soil, a good agreement is stated with actual data obtained from analysis of earthquake aftermath.

Joints of the underground pipeline play an important role in the stress-strain state formation, since the total stresses change in each section of underground pipeline due to the bending strains in the sections.

The problems were solved by the Finite difference method with consideration of combined longitudinal and transverse equations of oscillations of the system of pipelines, various mechanical, geometrical parameters and the modes of seismic loads. Developed mathematical models, algorithms and a complex of applied programs for the study of combined longitudinal and transverse oscillations of underground pipelines are described in details at arbitrary direction of seismic loading. So, new results were obtained for the systems of life support in seismodynamics of underground pipelines.

References

1. *Rashidov T.R.* Dynamic Theory of Seismic Resistance of Complex Systems of Underground Structures. Tashkent. “FAN”. 1973. – 179 p.
2. *Rashidov T.R., Xojmetov G.X.* Seismic Stability of underground pipelines. Fan, Tashkent, 1985. 152 p.
3. *Rashidov T.R., Bekmirzaev D.A.* “Seismodynamics of Pipelines Interacting with Soil”, Soil Mechanics and Foundation Engineering, Issue 3, Vol. 52, No. 3, pp. 149-154, 2015.
4. *Rashidov T.R., Yuldashev T., Bekmirzaev D.A.* “Seismodynamics of underground pipelines with arbitrary direction of seismic loading”, Soil Mechanics and Foundation Engineering, Issue 4, Vol. 55, No. 4, pp. 243-247, 2018.
5. *Liu W., Huang Ch., Wang Yu., Shi P.* Seismic analysis of connections of buried continuous pipelines // Hindawi Advances in Civil Engineering, pp.20 (2020), http://doi.org/10.1155/2020/8839380.
6. *Wei L., Sun Q., Miao H., Li J.* Nonlinear stochastic seismic analysis of buried pipeline systems // Soil Dynamics and Earthquake Engineering. 2015. Vol. 74, pp. 69–78.
7. *Saberi M., Arabzadeh H., Keshavarz A.* Numerical Analysis of Buried Pipelines with Right Angle Elbow under Wave Propagation // Procedia Engineering. Vol. 14. Published by Elsevier Ltd, 2011.– P. 3260–3267.
8. *Z Chen, P Wang, Y Wan, X Sun, X Guo, Y Cao, S Li.* Coupled surface-internal deformation monitoring in three-dimensional space for freezing-thawing soil // Soils and Foundation. Volume 64, Issue 3, June 2024, 101468. https://doi.org/10.1016/j.sandf.2024.101468.
9. *Corrado V., D’Acunto B., Fontana N., Giugni M.* Estimation of dynamic strains in finite end-constrained pipes in seismic areas // Mathematical and Computer Modelling. Vol. 49. United Kingdom, 2009. № 3–4, P. 789–797.
10. *Xie X., Symans M.D., O’Rourke M.J., Abdoun T.H., O’Rourke T.D., Palmer M.C., Stewart H.E.* Numerical modeling of buried HDPE Pipelines subjected to strike-slip faulting // Journal of Earthquake Engineering. Vol. 15. 2011. –No. 8. Taylor & Francis. – P. 1273–1296.
11. *Ha D., Abdoun T.H., O'Rourke M.J., Symans M.D.* “Centrifuge Modeling of Earthquake Effects on Buried High-Density Polyethylene (HDPE) Pipelines Crossing Fault Zones”, Journal of Geotechnical and Geoenvironmental Engineering, Vol. 134, No. 10, pp. 1501-1515, 2008.
12. *Kuwata Y., Takada S., Yamasaki S.* Seismic performance of complicated pipeline network // The 14th World Conference on Earthquake Engineering. – China, 2008. – Pdf. (06–0127).
13. *Chian S.C., Tokimatsu K., Madabhushi S.P.G.* “Soil Liquefaction-Induced Uplift of Underground Structures: Physical and Numerical Modeling”, Journal of Geotechnical and Geoenvironmental Engineering, Vol. 140, pp. 04014057-18, 2014.
14. *Toprak S., Taskin F.* Estimation of earthquake damage to buried lifelines caused by ground shaking // Natural Hazards. Vol. 40: 2007. – P.1–24.
15. *H Guo, R.G. Rinaldi, M Broudin, S Tayakout, O Lame.* Anisotropic deformation and failure behaviors of the necked HDPE materials induced by oligo-cyclic loading. Polymer, Volume 234, 8 November 2021, 124232
16. *Zhuang H., Hu Z., Wang X., Chen G.* “Seismic responses of a large underground structure in liquefied soils by FEM numerical modelling”, Bulletin of Earthquake Engineering,Vol. 13,pp. 3645-3668, 2015.

17. *Bekmirzaev D.A., Mirzaev I.* "Dynamic processes in underground pipelines of complex orthogonal configuration at different incidence angles of seismic effect", International Journal of Scientific & Technology Research, Vol. 9, No. 4, pp. 2449–2453, 2020.
18. *Kishanov R., Bekmirzaev D., Nishonov N., Rakhmanov U., Ismailova G.* Response of underground polymer pipelines considering viscoelastic interaction under seismic impact. AIP Conference Proceedings 2612, 040032. https://doi.org/10.1063/5.0113061. 15 March 2023.
19. *Bekmirzaev D., Mirzaev I., Kishanov R., Mansurova N., Sabirova Sh.* Study of the Mass Effect of a Complex Node of Underground Pipelines of Orthogonal Configuration Based on Real Earthquake Records. Proceedings of MPCPE 2021, Lecture Notes in Civil Engineering 182, https://doi.org/10.1007/978-3-030-85236-8_34.
20. *Sarioletlagh S., Nekooei M., Oskouei A.V., Aziminejad A.* "Experimental and numerical modeling of horizontally-bent buried pipelines crossing fault slip", Latin American Journal of Solids and Structures, Vol. 16, No. 3, pp. 1-16, 2019.
21. *Vazouras P., Karamanos S.A., Dakoulas P.* "Finite element analysis of buried steel pipelines under strike-slip fault displacements", Soil Dynamics and Earthquake Engineering, Vol. 30, pp. 1361-1376, 2010.
22. *Kabulov V.K.* Algorithmization in the theory of elasticity and deformation plasticity. Tashkent: Fan, 1966. – 386 p.
23. *Mirzaev I., Nishonov N., Bekmirzaev D., Kosimov E.* Seismodynamics of the cross-shaped underground pipeline under real earthquakes. AIP Conf. Proc.Volume 2432, 030107 (2022). https://doi.org/10.1063/5.0089585.
24. *Ishanxodjaev A.A., Bekmirzaev D.A., Ospanov R.S., Axmedov Sh.B., Usmonov D.T.* Influence of the inertia force of underground pipeline systems under seismic loads. AIP Conf. Proc. Volume 2637, 050002 (2022). https://doi.org/10.1063/5.0119606.

RATIONALE FOR STRUCTURAL HEALTH MONITORING SYSTEMS IMPLEMENTATION ON MOVABLE BRIDGES

Belyi A.A.[1], Antonyuk A.A. [2], Makhonko A.A.[3]
[1]*K2 Engine LLC, Tashkent, Uzbekistan*
[2]*Petersburg State Transport University, Saint-Petersburg, Russia*
[3]*OSA-Sever LLC, Saint-Petersburg, Russia*
E-mail: AndreiABelyi@gmail.com

Abstract: *The justification for implementing a monitoring system on movable bridges is presented as one of the key components ensuring the necessary level of safety in accordance with modern norms and standards of the Russian Federation. The specifics of the functioning of the main elements of the structure of movable spans are described, in particular, the movable spans of the lifting system. The positive experience of implementing a monitoring system on the movable bridge across the Neva River in St. Petersburg using automated technologies is provided. Based on the implementation of this project, the concept of "integrated monitoring" was proposed, which includes several different subsystems with various algorithms and measurement methods to ensure the safety of operating movable bridges. According to the authors of the article, the proposed concept can be applied not only to transportation structures, in particular, movable bridges, but also to other engineering objects, which will significantly increase the level of safety and reliability of buildings and structures of various purposes during their operation.*

Keywords: *movable bridge, monitoring of artificial structures; transportation infrastructure object; safety; stress-strain state; reliability.*

1. Introduction

During the operation of the expanding system of movable bridges, specifically during the opening and closing of the movable span, spatial work of the structure occurs, leading to a change in the static scheme. As a result, it becomes difficult to assess the changes in individual operational characteristics that directly affect the consumer properties of the considered type of transport structures. One of the key features to highlight as a result of such spatial work of the structure, accompanied by a change in the static scheme, is the alteration of the stress-strain state. Such changes, without the ability to account for and control them, can be the primary cause of an emergency situation with the potential to harm the lives and health of citizens, surrounding buildings, property, and the environment, directly linked to the absence or timeliness of a decision aimed at ensuring safety. A timely and, most importantly, correct decision is the main catalyst for the implementation of monitoring systems during the operation phase of the structure.

At present, the implementation of monitoring systems can confidently be considered as the most effective and precise method of control and inspection of the state of civil and transport

construction objects both during their construction and in the operational period, which, in the modern conditions of global digitalization, is a mandatory requirement to ensure the required level of safety within the existing regulatory framework, including for reducing the risk of economic and social losses. Monitoring systems are widely used in various transport objects: bridges, tunnels, embankments, dams, hydraulic structures, as well as in individual elements of transport infrastructure, with particular attention being paid to bridge structures. This increased attention is due to the complex operating conditions of bridges, which directly impacts the complexity of repair and maintenance work, and in the case of movable bridges, raises the issue associated with accounting for their spatial movement.

A monitoring system, as a means of control and accountability, represents a technology of informational support for the decision-making process regarding the monitoring of parameters of engineering structures and individual construction elements at all stages of their life cycle, carried out through systematic or periodic observation of their technical condition [1-5].

The main tasks of monitoring systems include:

1. Evaluation of the stress-strain state of structural elements and the entire structure taking into account existing defects and damages;
2. Analysis and assessment of the impact of external factors on the load-bearing capacity at the current moment and for the projected period;
3. Prediction of the service life of the structure considering external influences and degradation processes;
4. Development of strategies for restoring or improving consumer characteristics in existing or planned structures.

The authors of the article formulated and solved the following tasks based on the implementation of a project to introduce automated monitoring systems for the technical condition of the bascule bridge of Alexander Nevsky across the Neva River in the city of St. Petersburg:

1. Analysis of the peculiarities of the spatial operation of the bascule spans of bridges with an opening system;
2. Analysis of the selection of monitoring subsystems for an integrated assessment of the technical condition using the example of implementing this system on the bascule span of the Alexander Nevsky Bridge;
3. Analysis of the positive experience of implementing and the operational efficiency of the monitoring system on bascule bridges.

The choice of the Alexander Nevsky Bridge was motivated by the personal involvement of the authors in the project to implement an automated monitoring system for the technical condition of this structure, as well as its uniqueness, technical features, and the challenges faced by builders and maintenance specialists over the more than half-century period of service of this structure. These facts are widely known in the professional and scientific community, making this bridge preferable for the analysis and study of this issue.

2. Features of the spatial operation of the bascule spans of bridges with an opening system

Bascule bridges, as part of the transportation infrastructure, play a crucial role in shaping urban spaces and future development. Especially in central city areas, bascule bridges exhibit architectural expressiveness, emphasizing their significance in capital and culturally important metropolises worldwide. An example can be seen in the city of St. Petersburg, where bascule bridges crossing the Neva River, flowing through its territory, are part of the federal transport waterway - the "Volga-Baltic Waterway named after V. I. Lenin" (see Fig. 1). This waterway holds immense importance for the economic prosperity of the city, evidenced by its long history and continuous intense vessel traffic.

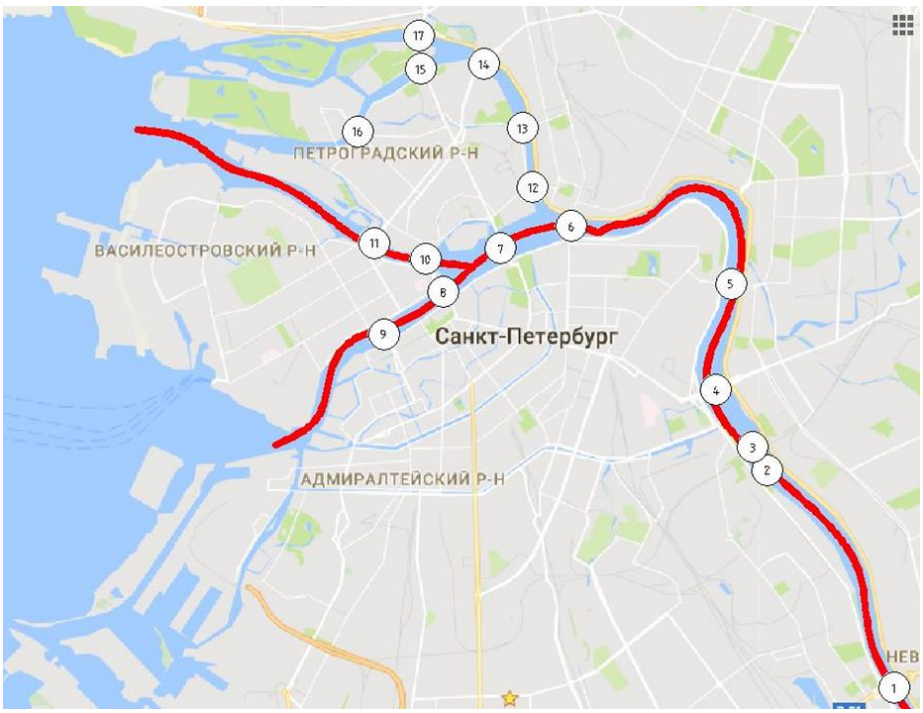

1 - Volodarsky Bridge; 2 - First path of the Finland Bridge; 3 - Second path of the Finland Bridge; 4 - Alexander Nevsky Bridge; 5 - Bolshoy Ohtinsky Bridge; 6 - Liteyny Bridge; 7 - Troitsky Bridge; 8 - Dvorcovyi Bridge; 9 - Blagoveschensky Bridge; 10 - Birjevoy Bridge; 11 - Tuchkov Bridge; 12 - Sampsonievsky Bridge; 13 - Grenadersky Bridge; 14 - Kantemirovsky Bridge; 15 - Kamennoostrovsky Bridge; 16 - Bolshoy Krestovsky Bridge; 17 - Ushakovsky Bridge;
- fairway.

Figure. 1 – **Diagram of the location of bascule bridges in St. Petersburg**

Based on the above, it is evident that in St. Petersburg, the majority of bascule bridges use an opening system. Considering the importance of high-traffic bridges for both the transportation and navigational infrastructure on the Neva River, let's take a closer look at this type of bascule bridges. In general, the structure of opening bascule spans and mechanisms includes the following main components: an electro-hydraulic drive providing the force to operate the spans during opening and closing; the bascule span (leaf), typically made of solid-walled metal beams; an external orthotropic plate; a covering for the external plate that withstands the main impact from the moving traffic flow; counterweights; a rotation axis and its unloading mechanism; locks; span supports; power supply, and control system. The diagram (Fig. 2) shows the opening span of the opening system with an unloaded rotation axis using a rocking pillar.

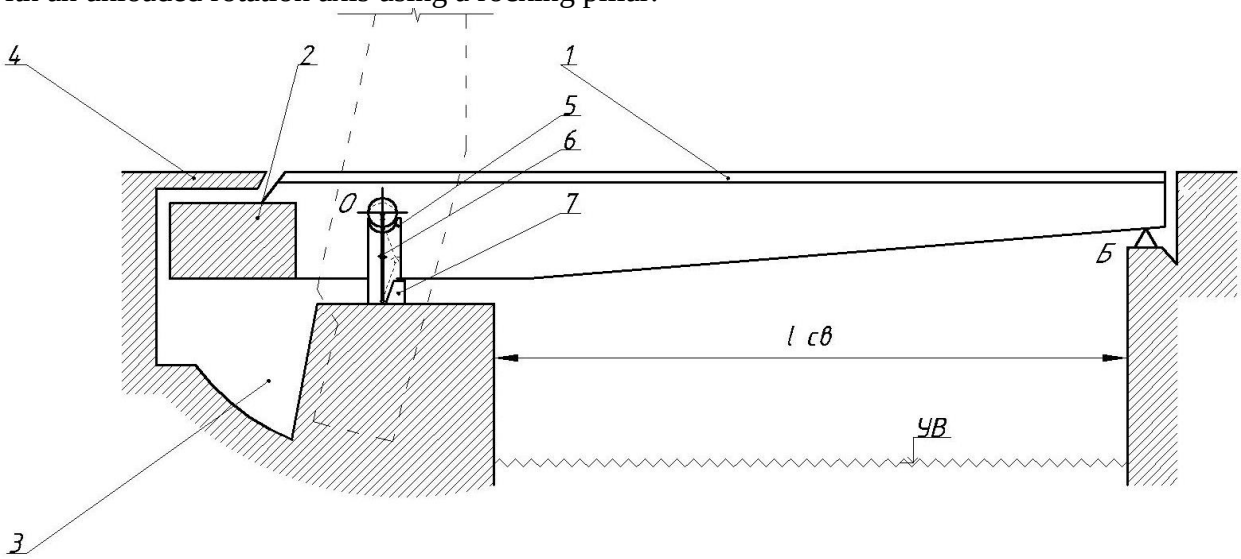

1 - bascule leaf, 2 - counterweight, 3 - counterweight well, 4 - cover of the counterweight well, 5 - guides of the horizontal axis, 6 - rocking pillar, 7 - lower support of the rocking pillar hinge, УВ - water level, O - rotation axis, B - support of the bascule span.

Figure. 2 – **Diagram of a single-leaf bascule bridge of the opening system with an unloaded rotation axis using rocking pillars:**

During the spatial operation - opening/closing (Fig. 3), the direction of the supporting reaction changes in the bascule span structure of the opening system, resulting in a change in the stress-strain state of the main structural elements.

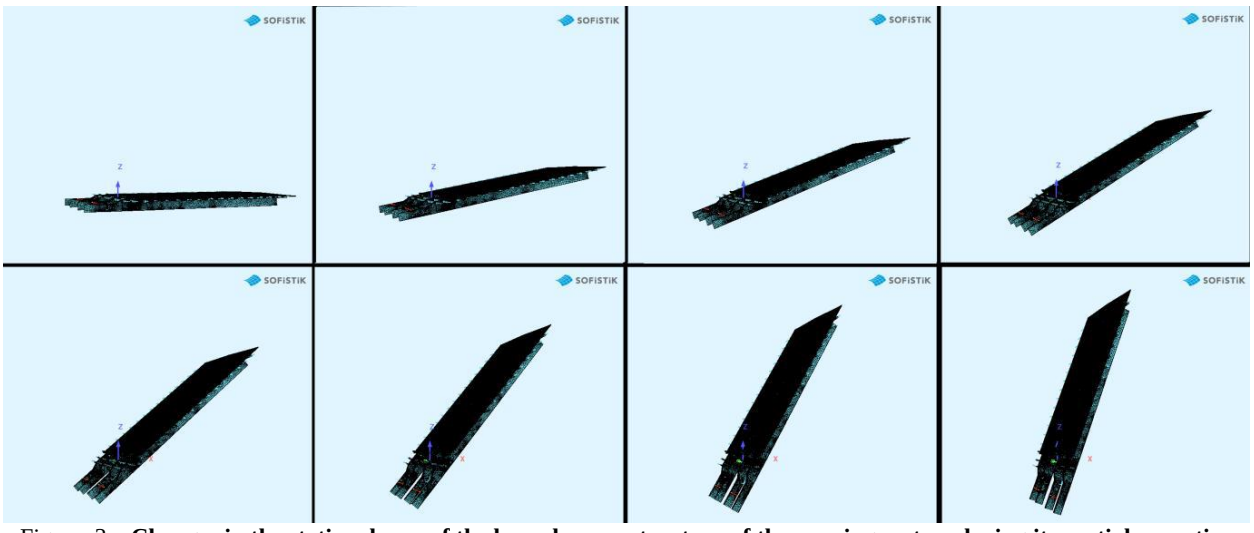

Figure. 3 – **Changes in the static scheme of the bascule span structure of the opening system during its spatial operation**

As a result of such complex spatial operation - the alternating change of compressive and tensile forces in the main elements of similar structures, the most common defect is the formation of cracks in welded joints, which poses a direct threat to safety in the broadest sense of the term [11-20].

Taking all of the above into account, the group of authors, despite the requirements outlined in GOST R 59943-2021, which stipulates that the main objects of monitoring are bridge structures with a span length of more than 100 m or pillar height exceeding 15 m, strongly recommend, as a matter of priority, to implement such systems on facilities that, due to their functionality and purpose, are subject to multiple changes in the static scheme and significant alterations in the stress-strain state during operation [21-29].

3. Research Object - Alexander Nevsky Bridge across the Neva River. Description and monitored parameters

One of the bascule bridges across the Neva River, named the Alexander Nevsky Bridge, was constructed between 1960 and 1965. This bridge is a reinforced concrete structure consisting of seven spans with a bascule span in the middle and inclined ramps at both ends. The main spans consist of three beams with rigid connections at the intermediate support (49.9 + 109.8 + 123.5 m). A feature of this bridge is the rigid connection of the support to the bridge structure, which requires constant monitoring of the bridge's behavior during its operation.

In the cross-section, the stationary part of the bridge structure consists of two widely spaced main beams, between which there is a system of transverse and longitudinal beams. The main beams have a curved shape of the lower flange and a three-chambered box rectangular section. They are made of prestressed reinforced concrete. The transverse beams have an I-beam section and are made of ordinary reinforced concrete.

Since the commissioning of the Alexander Nevsky Bridge, there have been several emergency situations at this site, the resolution of which has occurred retroactively, as an example:

- Multiple breakages of reinforcement cables (from 1964 to 1980);
- Detachment of a 700-ton counterweight beam (1982).

The incidents listed led to significant social and economic consequences, as the movement on this bridge was completely halted for their comprehensive resolution. It was only in 1983 that traffic on the bridge was fully restored.

Taking into account the existing problems associated with the operation of this structure and the increase in traffic intensity in 2000, during the period of the start of the full reconstruction of the

bridge, an Information Measurement Monitoring System (IIMS) was developed and implemented to assess the condition of the stationary reinforced concrete spans and the bascule span of the Alexander Nevsky Bridge across the Neva River in the city of St. Petersburg, developed by the company JSC NPP "Promtransavtomatika". This monitoring system included the following parameters for control:

–changes in the stress-strain state of the concrete structures of the main beams of stationary spans;

–appearance of new cracks in the concrete of stationary spans;

–crack opening widths in the concrete of stationary spans;

–longitudinal deformations of stationary spans;

–condition of reinforcement cables for possible breakages;

–**changes in the stress-strain state of the metal structures of the bascule span**;

–temperature changes inside and outside the boxes of the main beams of stationary spans.

Testing of the Information Measurement Monitoring System (IIMS) continued until April 2004. During this time, the necessary stability of the IIMS operation could not be achieved. Failures occurring during the operation of the IIMS were attributed to malfunctions in the sensors and connecting cables - the presence of mechanical damages resulting from natural and man-made impacts. Additionally, computational power (computers), periodic power outages, and other factors led to "freezes" and malfunctions in program operation and database damage. In 2009, the IIMS was disconnected, and the question of developing a new monitoring system was raised.

When developing the new monitoring system for the Alexander Nevsky Bridge in 2018, all the negative operational experience of the "old" system was taken into account, with the following aspects forming the basis of its operation:

- justification of the placement of monitoring equipment and determination of quantitative indicators for comprehensive risk assessment of emergency situations;
- use of modern monitoring equipment (sensors) with improved reliability, efficiency (especially in terms of energy consumption), universality (ease of interaction with each other), and reduced installation and maintenance costs;
- development of unique software that takes into account all the peculiarities of the structure's operation, including the spatial work of the bascule span, and possesses high reliability and ergonomics with the ability to archive obtained values using modern databases;
- development and implementation of an algorithm to prevent false system activations.

Table 1

Subsystems and the number of monitoring tools in the new system

№	Monitoring Subsystem Name	Bridge Elements with Monitoring Tools	Sensors Used
1	Dynamic Parameter Change Subsystem (Vibration subsystem/Acceleration control system)	External reinforcement cables (48 pcs.) Internal cables (96 pcs.) P-shaped reinforcement cables (976 pcs.)	Accelerometers
2	Inclination Angle Control Subsystem	Beams of stationary spans (120 pcs.)	Inclinometers
3	Stress-Strain State Monitoring Subsystem	Beams of stationary spans (400 pcs.) Bascule span structures (64 pcs.)	Strain gauges
4	Displacement Control	Sensors on expansion joints (8 pcs.)	Displacement sensors
5	Crack Opening Control	Beams of stationary spans (80 pcs.)	Displacement sensors
6	Satellite Positioning Subsystem	Beams of stationary spans (17 pcs.)	GLONASS or GPS navigation system
7	Structural Element Temperature Control	Beams of stationary spans (200 pcs.)	Temperature sensors

As part of the implementation of this project, it was proposed to create a monitoring system that would integrate a comprehensive approach to achieve the main goal - the ability to obtain an accurate, comprehensive, and adequate assessment of the bridge's condition. Ultimately, such a

system included several subsystems with completely different physical and geometric databases - "integrated monitoring," that is, monitoring the state of structures, taking into account data from sensors as a whole, using internal program algorithms that are based on the reliability of structural elements, signal duplication, cyclic repetition, and protection against false activations.

The working principle and importance of each of the subsystems presented in the table of the "integrated monitoring system" are described below.

4. Operating principle of the subsystems of the "integrated monitoring system"

Measurement of the stress-strain state is carried out using the strain gauge method. Specialized sensors called strain gauges are used for this purpose. They record deformation at a specific point (zone) of the structural element, after which, using Hooke's Law, stresses are determined. Deformations measured in the segment, called the S-base, in the elastic stage are characterized by insignificant values. Strain gauges (fig. 4, a) measure the absolute elongation (or contraction) ΔS, which is then used to determine the average relative deformation.

$$\varepsilon = \frac{\Delta S}{S} \tag{1}$$

The S-base should be as small as possible to more accurately reflect the true average relative deformation.

Based on the obtained value and the known modulus of elasticity E, the stress is calculated using the formula.:

$$\sigma = \varepsilon E \tag{2}$$

When a flat stress-strain state occurs in the structural element at a given point, the system measures deformations in two or three directions. In such cases, strain gauges need to be placed along the principal stresses σ1 and σ2, or (if the directions of action of the principal stresses are unknown) one strain gauge can be placed arbitrarily, while the remaining two are placed at angles of 45° and 90° or 60° and 120° relative to the first strain gauge. In the first case, when the directions of action of the principal stresses are known, σ1 and σ2 are determined as follows:

$$\left.\begin{aligned} \sigma_2 &= \frac{E}{1-\mu^2}(\varepsilon_2 + \mu\varepsilon_1), \\ \sigma_1 &= \frac{E}{1-\mu^2}(\varepsilon_1 + \mu\varepsilon_2); \end{aligned}\right\} \tag{3}$$

where, μ – Poisson's ratio.

In the second case, calculating the final voltage value is more difficult.

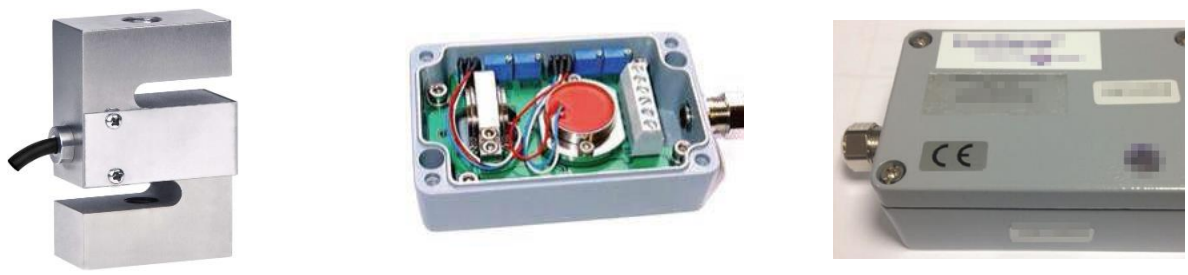

а) б) в)

Figure. 4 - **Overview of the main monitoring tools: a) - strain gauge; b) - accelerometer; c) - inclinometer.**

The vibration monitoring subsystem provides dynamic parameters of structures in the form of sets of accelerations and frequency characteristics of vibrations using accelerometers (see fig. 4, b). These parameters include information about the stiffness, mass of the structure, and external forces. The results of measurements within dynamic monitoring allow for the detection of hidden changes in the structural properties of the constructions. Thus, the tasks of dynamic monitoring include the following:

- determining the predominant frequencies of free vibrations;
- assessing the impact of seismic activity on the dynamic behavior of the structure as a whole;

• establishing the level of influence of loads and effects from vehicle movement on dynamic characteristics;

• analyzing vibration frequencies to assess and predict possible changes in the technical condition of the structure and its individual elements.

The importance and necessity of solving the tasks outlined above in the framework of dynamic monitoring open up a wide field for both researching such structures considering the development of hidden damages and defects, and from the perspective of developing new methodologies and tools for upgrading the monitoring system.

The subsystem for monitoring angles and displacements is carried out to assess the stability of the structure, allowing for the evaluation of the stability of a bridge structure and the detection of any anomalies or undesired deformations that may indicate potential issues. The use of inclinometers (see fig. 4, c) within this subsystem enables the detection of even minor changes in the angle of rotation and displacements of the structure, aiding in preventing possible damages or accidents.

In combination with the subsystem responsible for measuring the stress-strain state of structural elements, employees of operating organizations and researchers can determine the degree of influence and dependence of the acting loads on the displacements of the structure, which is an important aspect for ensuring the safety and durability of the structure as a whole.

Monitoring subsystems for displacements of span structures in deformation joint zones and crack opening in beams of stationary span structures use the same sensors with different measurement bases. Potentiometric sensors are designed to convert linear displacements into an electrical signal, as well as to establish simple functional dependencies in continuous-type automatic devices. These sensors consist of a variable resistor to which a supply voltage is applied. Their input parameter is the linear displacement of the current-carrying contact, and the output parameter is the voltage taken from this contact, which varies depending on its position.

Subsystem of Global Navigation Satellite System (GNSS).

Global Navigation Satellite Systems (GNSS) provide high accuracy and reliability in monitoring transportation infrastructure objects, allowing for real-time data on movements and structural deformations with a high degree of precision.

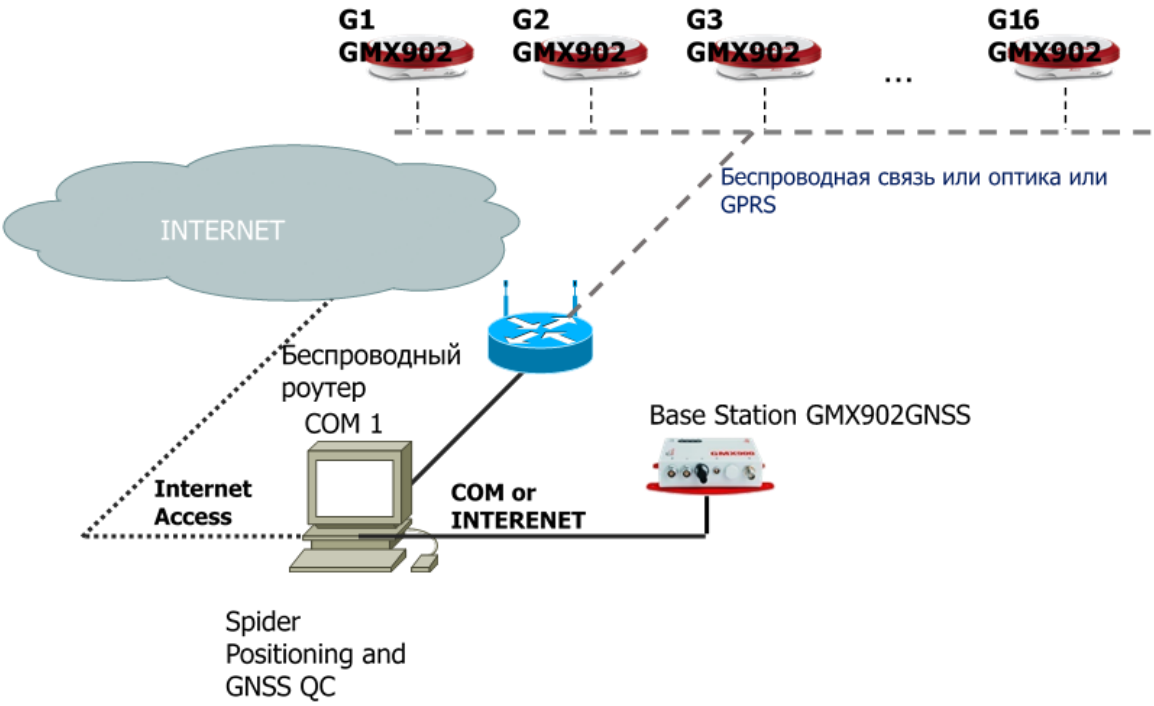

Figure. 5 - **Diagram of the operation of GNSS equipment in the "integrated system" for deformation monitoring on the Alexander Nevsky Bridge**

As mentioned earlier, the key task of an "integrated system" monitoring is to provide up-to-date information on the structure's condition in real-time. GNSS systems enable continuous monitoring of bridge conditions in a "non-stop" mode, allowing for prompt responses to any changes and potential safety threats. Additionally, GNSS systems facilitate the analysis of long-term changes in the behavior of bridge structures, helping to identify trends and forecast possible issues or risks.

The general principle of operation of GNSS equipment implemented in the monitoring system on the Alexander Nevsky Bridge is shown in fig. 5, while the actual installed elements are depicted in fig. 6.

Figure. 6 - **Locations of GNSS equipment installation on the Alexander Nevsky Bridge as part of the "integrated system" monitoring**

The satellite automated deformation monitoring system receives data on coordinates and displacements in three directions at each receiver point, both in absolute values and in the bridge structure's coordinate system.

5. Results and conclusions

After analyzing the spatial characteristics of the operation of the movable spans of bridges of the opening system and taking a comprehensive approach to designing monitoring systems using the example of implementing a project to introduce an automated monitoring system for the technical condition of the Alexander Nevsky Bridge across the Neva River in the city of St. Petersburg, the authors of the article formulated the following conclusions:

1. Considering the spatial characteristics of the operation of the movable spans of bridges of the opening system and the over 50 years of experience in operating the Alexander Nevsky Bridge located in St. Petersburg, the authors of the article emphasize the importance and necessity of implementing monitoring systems on similar structures. This will allow for timely response to any changes related to the risks of security threats.
2. The approach to designing monitoring systems for the technical condition of engineering structures implemented on the Alexander Nevsky Bridge is comprehensive and, in the authors' opinion, can be recommended not only for monitoring bridge structures but also for buildings and structures of various purposes.
3. The "integrated system" of monitoring, as an approach to designing such systems, has proven itself very positively and has been implemented in other engineering structures in St. Petersburg, for example, in the transportation infrastructure objects on the private, toll general-purpose road "Western High-Speed Diameter."

References

1. *Sumitro S.* Structural Health Monitoring System Applications in Japan // In: Ansari F. (eds) Sensing Issues in Civil Structural Health Monitoring. Springer, Dordrecht, 2005. – pp. 495-504. https://doi.org/10.1007/1-4020-3661-2_49.

2. *Rucker W., Hille F., Rohrmann R.* Guideline for structural health monitoring. Final report / SAMCO, Berlin, 2006. – 63 p.

3. *Li J and Hao H.* Damage detection of shear connectors under moving loads with relative displacement measurements. // Mech Syst Signal Pr 2015; 60–61: 124–150.

4. *Ana Paula Camargo Larocca, João Olympio De Araújo Neto, Jorge Luiz Alves Trabanco, Augusto César Barros Barbosa, André Luiz Barbosa Nunes Da Cunha, Ricardo Ernesto Schaal*. Usage of 100 HZ GPS receivers in detecting millimetric vertical deflections of small concrete bridges. // Bol. Ciênc. Geod., sec. Artigos, Curitiba, v. 21, no 2, p.290-307, Apr-Jun, 2015. http://dx.doi.org/10.1590/S1982-21702015000200017
5. *Lienhart, W., Ehrhart, M.* State of the art of geodetic bridge monitoring Structural Health Monitoring 2015: System Reliability for Verification and Implementation // Proceedings of the 10th International Workshop on Structural Health Monitoring, IWSHM 2015 DOI: 10.12783/SHM2015/58
6. *Mosbeh R. Kaloop and Jong Wan Hu*. Dynamic Performance Analysis of the Towers of a Long-Span Bridge Based on GPS Monitoring Technique // Journal of Sensors Volume 2016 (2016), Article ID 7494817, 14 pages http://dx.doi.org/10.1155/2016/7494817
7. *Yang Y, Q. S. Li, B. W. Yan*. Specifications and applications of the technical code for monitoring of building and bridge structures in China. // Advances in Mechanical Engineering. – 2017. – Vol. 9 (1). p. 1–10. DOI: 10.1177/1687814016684272.
8. *Geoffrey R. Thomas, Akbar A. Khatibi*. Durability of structural health monitoring systems under impact loading. // Procedia Engineering 188 (2017) 340 – 347
9. *Makhonko A. A., Malkov A. V., Bely A. A., Antonyuk A. A.* Features of the monitoring system of a cable-stayed bridge across the Petrovsky Canal in the alignment of the "Western High-Speed Diameter" highway in St. Petersburg // Putevoy navigator. – 2023. – No. 56(82). – P. 68-77. – EDN JEYBWL.
10. *Makhonko A. A., Malkov A. V., Bely A. A., Antonyuk A. A.* Experience of operating the monitoring system of a cable-stayed bridge across the Petrovsky Canal in the alignment of the "Western High-Speed Diameter" highway in St. Petersburg // Innovative transport systems and technologies. – 2023. – Vol. 9, No. 2. – P. 83-96. – DOI 10.17816/transsyst20239283-96. – EDN NUIUJE.
11. *Bely A. A., Belov A. A., Yashchenko A. I., Antonyuk A. A.* Integral monitoring of the Alexander Nevsky Bridge // Putevoy navigator. – 2020. – No. 45(71). – P. 38-45. – EDN ZDBIAB.
12. *Yashchenko A.I.* From water level to high-precision inclinometer // Geoprofi Journal, No. 4/2010. – Moscow: Information Agency "GROM", 2010 – P. 17 - 19.
13. *Yashnov A.N., Baranov T.M.* Some results of the work of the dynamic monitoring system of the academic bridge across the Angara River in Irkutsk. // Bulletin of the Tomsk State University of Architecture and Building. – 2017.- No.1(60). P. 199-209.
14. *Belyi A.A., Karapetov E.S., Efimenko Yu. S.* Structural health and geotechnical monitoring during transport objects construction and maintenance (Saint-Petersburg example). // Procedia Engineering. – 2017. – Vol. 189. p.145–151. PII:S1877-7058(17)32145-8 DOI:10.1016/j.proeng.2017.05.024
15. *Lazarev Yu.G., Yermoshin N.A., Sentsov I.V.* Development planning of road network considering multi-criteria optimization principles // Putevoy Navigator, No. 38 (64), 2019 – St. Petersburg: ANP "Union "DORMOST", 2019. – P. 24-31.
16. *Bely A.A., Zaitsev V.M., Karapetov E.S.* On the operation of reinforced concrete bridge structures in St. Petersburg // Putevoy Navigator, No. 32(58), 2017. – P. 66-73.
17. *Korobova O.A., Maksimenko L.A.*. Current state of monitoring underground structures at the present stage //. Interexpo Geo-Siberia. – 2017, vol. 3, No.2. P. 269-275.
18. *Hiller B., Yambaev Kh.K.* Investigation of an automated deformation monitoring system for lock chambers. // Proceedings of Higher Educational Institutions. Geodesy and Aerial Photography. – 2016.-No.3. P. 33-38.
19. *Efanov D.V.* Functional control and monitoring of railway automation and telemechanics devices. Monograph. / St. Petersburg: PGUPS, 2016. – 171 p.
20. *Hiller B.* Digital inclinometers in automated geodetic deformation monitoring systems // Proceedings of Higher Educational Institutions. Geodesy and Aerial Photography, No.6, 2015. – Moscow: Moscow State University of Geodesy and Cartography, 2015. – P. 23-30.
21. *Efanov D.V., Osadchiy G.V., Sedykh D.V., Barch D.V.* Organization of continuous monitoring of the inclination angles of the supports of the railway contact network // Transport of the Urals. – 2017. – No:2 (53) P: 37-41 DOI: 10.20291/1815-9400-2017-2-37-41
22. *Bryn M.Y., Tolstov E.G., Nikitchin A.A., Reznik B., Yashchenko A.I., Evstaev O.V., Kuchumov V.A.* Geodetic monitoring of deformations of cable-stayed bridges based on satellite technologies. // "Proceedings of the St. Petersburg University of Communications", issue 2(19)– St. Petersburg: PGUPS, 2009 – P.120-128.
23. *Syrkov A.V., Krutikov O.V.* Lifecycle optimization of the bridge on Russky Island in Vladivostok using risk analysis and monitoring // Automation in Industry. – 2012. - No.9. P. 45-50.
24. *Bely A.A., Belov A.A., Osadchiy G.V., Dolinskiy K.Y.* Concept of monitoring artificial structures in St. Petersburg // Journal "Roads. Innovations in construction", No. 71/2018 – St. Petersburg: LLC "Technical Information Center "TechInform", 2018 – P. 58-62.
25. *Bely A.A., Belov A.A., Osadchiy G.V., Osetinsky O.V., Dolinskiy K.Y* // Automation in Transport, No.3, vol. 4, 2018 – St. Petersburg: PGUPS, 2018. – P. 380-406.
26. *Karapetov E.S., Bely A.A.* Monitoring of bridge structures in St. Petersburg. History. Purpose. Examples. Perspectives // "Zodchii. 21st century" Bulletin, No. 4(29)/2008 – St. Petersburg: Publisher "Zodchii", 2008. – P. 80-83.
27. *Federal Law* No. 384 "Technical Regulation on Safety of Buildings and Structures", 30.12.2009.

28. *Andrei Belyi, German Osadchy, Kirill Dolinskiy*. Practical Recommendations for Controlling of Angular Displacements of High-Rise and Large Span Elements of Civil Structures // Proceedings of IEEE East-West Design & Test Symposium (EWDTS'2018) – pp. 176-183. DOI 10.1109/EWDTS.2018.8524743

29. *Shermukhamedov U., Sobirova M.,. Azamov. N., Ibrokhimova. S.* Analysis of technical and operational condition of urban reinforced concrete bridge structures // Conference Paper • Open access. 2023. E3S Web of Conferences. 365, 02015.

30. *Shermukhamedov U.Z., Karimova A.B., Abdullaev A.R., Khakimova Ya.T.* Comparison of operating costs of reinforced concrete bridges and overpasses with different static schemes // Conference Paper • Open access. 2023. E3S Web of Conferences, 401, 02035.

ENSURING THE STRENGTH OF COHESIVE CLAY SOILS RAILWAY EMBANKMENT

Bondar I.S.[1], Mamedova J.E.[2]

[1]*Kazakh National research technical university, Almaty, Kazakhstan*

[2]*Academy of Logistics and Transport, Almaty, Kazakhstan*

E-mail: ivan_sergeevich_08@mail.ru

Abstract. *A method of determining the strength characteristics of cohesive soils in shear devices for the purpose of their use in calculations of the stability of soil transport structures is proposed. The result of any shear tests, the most common method of laboratory determination of strength characteristics of soils, is a set of values of ultimate shear resistance and its corresponding normal pressure along the shear area. The theoretical basis for analysing the results of shear tests of soils is probability theory and mathematical statistics. At the same time, some questions remain concerning the determination of design values of soil strength parameters, when processing the results of shear tests according to the consolidated-drained scheme for soft-plastic loam. In the article dependences between tangential stress and absolute deformation for soft-plastic loam of natural structure in conditions of absence of normal pressure at initial and repeated shear are considered. the influence of dynamic influence can lead to reduction of shear resistance. Change of shear resistance of soft-plastic loams under vibrodynamic impacts depends on moisture content, change of stress state and is characterised by a change in the value of adhesion, depending on the type and nature of interactions between soil particles and the possibility of their changes in the process of shear. In calculations of stability of soils of transport structures consisting of non-water-saturated cohesive soils of disturbed structure, it is recommended to take the angle of internal friction determined by the Tertsagi-Kulon method in the kinematic loading mode as a design parameter, and the cohesion of contact bonds determined by the results of soil tests without normal load under repeated shear as a design parameter.*

Keywords: *Railway embankment, clayey soils, strength, shear characteristics.*

1. Introduction

For the most effective use of the infrastructure of the transport and logistics potential of the Turkestan-Siberian railway it is necessary to ensure the possibility of its safe operation with rational management of transport hubs [1]. The stability of artificial structures (embankments and excavations, retaining walls on railways) consisting of clay soils is one of the most important engineering problems of reliability [2, 3]. The solution of this problem is possible only on the basis of the complex approach connected with the research of influence on stability of geometry of slopes, physical and mechanical properties of soils, features of influence of static, dynamic, seismic, shock loads [4-8] and many other factors in system wheel-rail-sleeper-ballast-soil [9].

The authors have carried out experiments to determine the effect of pre-compaction pressure on the strength of cohesive soils. The tests were carried out according to the following scheme: soil samples of a given density-humidity were kept until full consolidation in the device of preliminary compaction at normal pressures of 100, 200, 300 kPa for 72 hours, and then tested in the shear device without applying normal pressure with repeated shear [10-13]. Shear tests are the most common method for laboratory determination of strength characteristics of soils - specific cohesion c and internal friction angle φ. The wide popularity of shear tests is due to the high reliability of the technological operations of soil sampling, preparation for testing and realization of the shear process in laboratory conditions [14].

2. Materials and methods

Reconnaissance survey of the railway embankment site to identify groundwater affecting dangerous engineering and geological processes (waterlogging, overwatering and slumping of the embankment slope) [15-16].

Drilling of boreholes was carried out to: study the lithological section; determine the depth of occurrence of soil layers; take samples of soils and rocks to study their composition, salinity and physical and mechanical properties.

Drilling was carried out with a 180 mm diameter drill rig PBU-2. Engineering-geological description of the lithological section and soil sampling were carried out during drilling. Undisturbed structure (monoliths) was sampled by means of pressurizing soil carriers (Figure 1).

Figure 1. - **Monolith sampling in the section along the railway embankment**

To conduct experimental studies, the authors used a modified version of a single-plane shear instrument VSV-25 designed by Gidroproekt, the general view of which is shown in Figure 2.

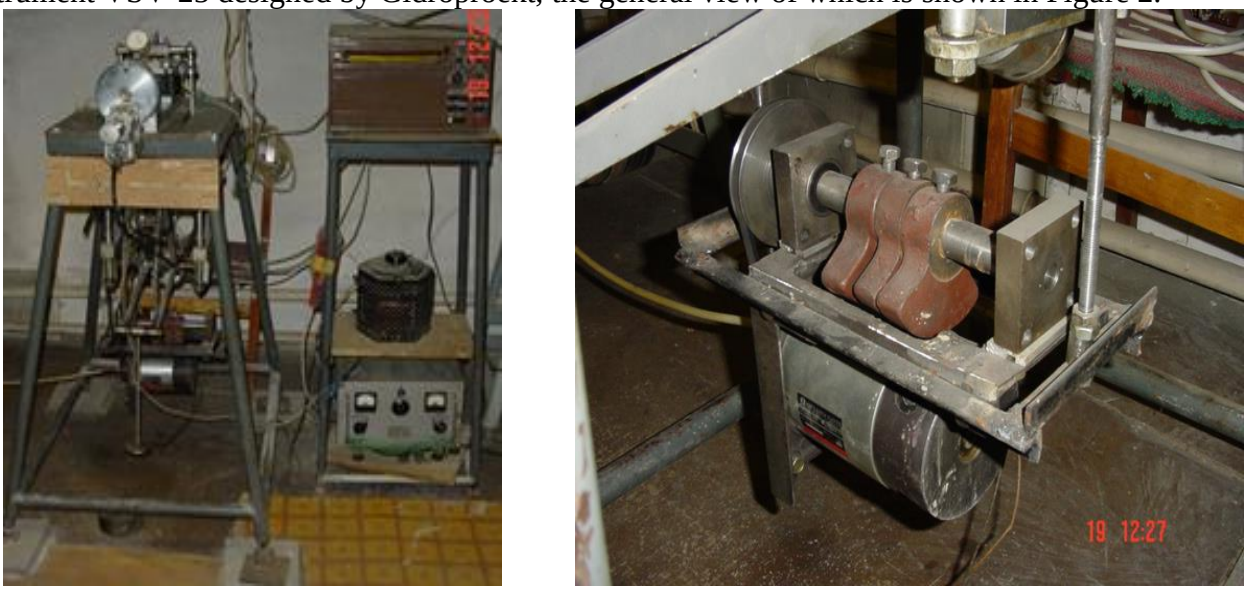

General view Eccentric rotary vibrator

Figure 2. - **VSV-25 single plane shear instrument.**

The advantage of this device over domestic analogues is a more uniform distribution of stresses over the shear area due to the symmetrical impact of vertical and horizontal forces. Increasing the wall thickness of the device cages allowed to reach the value of relative shear deformation of the specimen of the value equal to 27% of the inner diameter of the carriage.

To create vibrodynamic loading on the soil sample, an eccentric rotary vibrator (Figure 2 right) with a drive from a DC motor of PJK-25/3 brand was specially designed.

Changing the location of eccentrics on the drive shaft allows changing the amplitude of the pulsating load. The device operates in the controlled deformation mode (kinematic mode) and has

additional equipment for temporary fixation of absolute shear deformations of the soil sample. The shear rate can vary from 0.5 to 0.01 mm/min. Variation of shear rate is regulated by changing the current of the power supply VSA-5K.

The reciprocating motion of the lower movable cage of the device is created by the reduction reducer MPK-13I-5 through the spindle. The general drive of the shear force system is carried out by a DC motor D-10ARU. At vibrodynamic influence frequency of oscillations is regulated by laboratory automatic transformer "LATR". The value of the oscillation frequency is determined by the tachometer. The tachometer is driven through the speedometer cable of the GAZ-53 car connected to the driven shaft of the rotary vibrator. The device design allows to create vibration frequency in the range from 0 to 30 Hz.

Control and measuring equipment allow to obtain quantitative values of alternating normal load N±DN both at static and vibrodynamic influences, as well as horizontal shear force T and displacement of the device cage U.

3. Results

According to the results of the experiments, the stress-strain relationship graphs were plotted using the mean values of the experimental points corresponding to the tangential stresses.

A characteristic plot of the relationship between tangential stress and absolute strain for soft-plastic loam of natural structure in the absence of normal pressure under initial and repeated shear is shown in Figure 3.

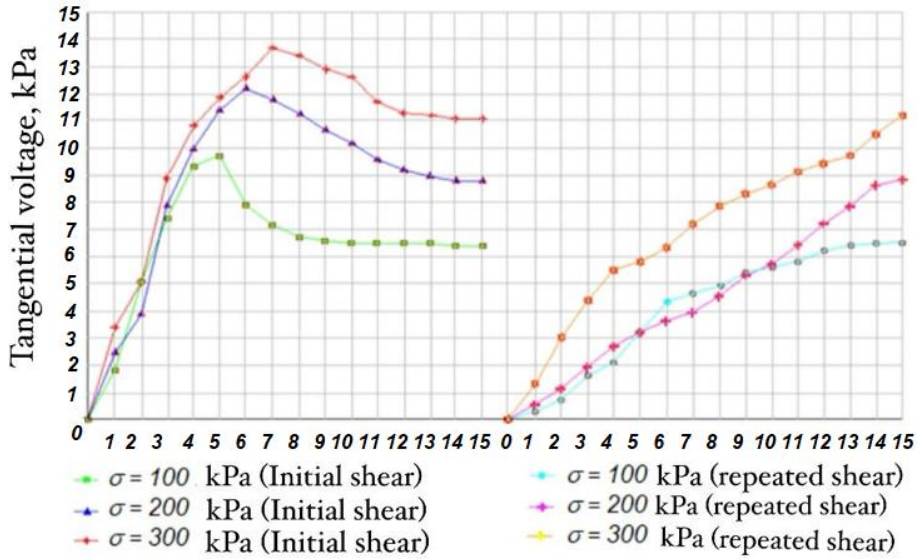

Figure 3 - **Graph of the relationship between absolute strain and tangential stress (soft-plastic loam)**

Soil cohesion can be divided into two components - primary (initial) cohesion and strengthening cohesion:

$$C = c_n + c_y$$

where C – the total cohesion of clayey rock;

c_n– primary (initial) cohesion;

c_y – hardening cohesion.

In our experiments, the peak values of tangential stresses correspond to the full bond C, and the minimum values correspond to the primary bond. In other words, full cohesion is characteristic of the peak strength of cohesive soil, and primary cohesion determines the residual strength.

From the plots of the "tangential stress - absolute strain" relationship, it followed that the shear resistance differs in the region of peak strength determination, i.e. in the region of fully realised bonding. In the residual strength region, however, the primary coupling tends to a single asymptote. Since the values of full coupling and primary coupling, which depend on the history of the stress state (in this case, on the pre-compaction pressure), differ insignificantly from each other,

their determination by average values can be assumed. Thus, for soft-plastic loam, the full cohesion is determined (Figure 2):

$$C = \frac{9{,}7+12{,}2+13{,}7}{3} = 11{,}9 \text{ kPa.}$$

Primary clutch:

$$C_{п} = \frac{6{,}5+8{,}8+11{,}1}{3} = 8{,}8 \text{ kPa.}$$

It follows from expression (1) that:

$$C_y = C - C_n$$

Clutch hardening from expression (2):

$$C_y = 11{,}9 - 8{,}8 = 3{,}3 \text{ кkPa}$$

Based on the graphs "tangential stress - absolute strain" for the studied soils, diagrams of shear resistance dependence on pre-compaction pressure were constructed (Figure 4).

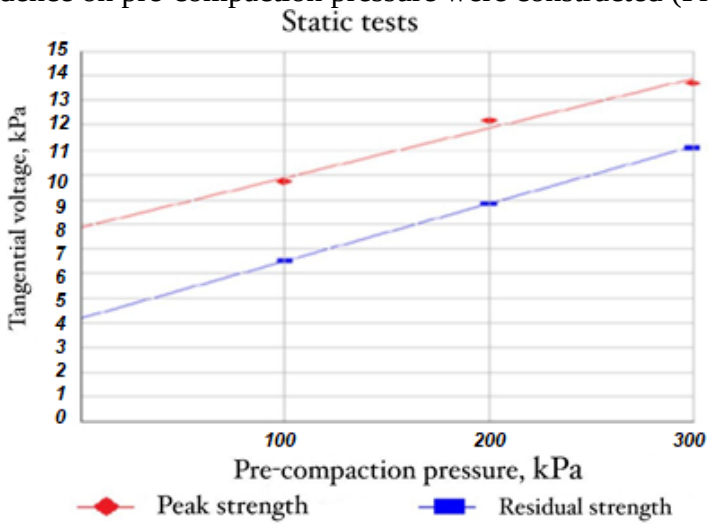

Figure 4 - **Graph of the relationship between tangential stress and pre-compaction pressure (soft-plastic loam)**

From the experimental studies it followed that the relationship between tangential stress and pre-compaction pressure is linear and is approximated by the equation:

$$y = ax + b$$

According to the theory of N. N. Maslov:

$$C = \Sigma_{\omega} + C_c$$

Here C – the total cohesion;

Σ_{ω} – cohesion of water-colloidal character;

C_c – structural cohesion, which does not depend on the density - humidity of the soil and is very sensitive to any disturbance of the soil structure.

The final expression of this theory was the dependence:

$$\tau_{p\omega} = \sigma tg\varphi_{\omega} + \Sigma_{\omega} + C_c$$

where $\tau_{p\omega}$ − the shear resistance of the soil at a certain density, moisture content and load acting on it;

φ_{ω} − the true angle of internal friction, independent of the cohesion of the soil increasing with the load;

As it was mentioned above, peak strength is characterised by full cohesion, and residual strength is characterised by primary (initial) cohesion Cp or cohesion Sw (according to Maslov N.N.). From expression (4) follows

$$C_c = C - \Sigma_{\omega}.$$

Results of IGE-3: The loans are soft-plastic, occur in the form of interlayers in the lower parts of the section, their thickness is from 0.2 to 2.0 meters. Partial indicators of physical and mechanical properties are given in Table 1.

Table 1.

Estimated values of physical and mechanical properties of soils

Indicator name	Unit of measurement	Normative values	Estimated values	
			At α=0,85	At α=0,95
Natural moisture	unit shares	0,14	-	-
Moisture at the boundary of fluidity	unit shares	0,19	-	-
Humidity at the plasticity boundary	unit shares	0,11	-	-
Plasticity number	unit shares	0,80	-	-
Fluidity index	unit shares	0,69	-	-
Water saturation coefficient	unit shares	0,860	-	-
Density of soil particles	g/cm^3	2,69		
Density of natural soil (safety factor)	g/cm^3	2,10	2,09 (1,004)	2,08 (1,007)
Density of dry soil (safety factor)	g/cm^3	1,83	1,82 (1,004)	1,81 (1,007)
Porosity	%	32,1	-	-
Porosity coefficient		0,47	-	-
Angle of internal friction at natural moisture (safety factor)	hail	30	30 (1,006)	26 (1,15)
Angle of internal friction at water saturation (safety factor)		19	19 (1,005)	16,5 (1,15)
Cohesion at natural humidity (safety factor)	kPa	55	55 (1,010)	36,6 (1,5)
Cohesion at water saturation (safety factor)		40	40 (1,010)	27 (1,5)
Modulus of deformation at natural humidity	MPa	8	8	-
Modulus of deformation under water saturation		7	7	-
Relative subsidence	unit shares	0,009	Non-sagging soils	
Compressibility coefficient, MPa-1	m_0	0,184	Low-compressible oils	
Design resistance at yield strength I=1 (SP 5.01-102-2013 tb. B3)	кПа	200		

4. Discussion

From the plots of the relationship between tangent stress and pre-compaction pressure (Fig.3), using expression (6) the structural cohesion of the investigated soils is easily determined. In particular, for soft plastic loam C_c = 7,9 – 4,2 = 3,7 kPa.

Unlike the structural cohesion C_c, the cohesion (Σ_ω) of clayey soils is of a water-colloidal nature and is reversible.

In the absence of phase and transition contacts, the cohesion of clayey rocks is determined solely by coagulation contacts, i.e. $C = \Sigma_\omega$. Therefore, the cohesion value depends significantly on the density and humidity of the rock, dispersity and hydrophilicity of the constituent minerals, the degree of orientation of particles in the shear plane, etc. In rocks with predominance of phase contacts, the cohesion is almost entirely determined by C_c, the value of which depends weakly on the moisture content and composition of the clay rock.

In soils with mixed type of contacts, cohesion is determined by both components, i.e. $C = \Sigma_\omega + C_c$. At normal loads lower than the structural strength ($\sigma < P_c$), the value of C_c plays the greatest role, and at σ > Pc - the value of Sw. Consequently, depending on the type of contact bonds (Fig.5), not only the magnitude but also the nature of cohesion changes in clayey soils.

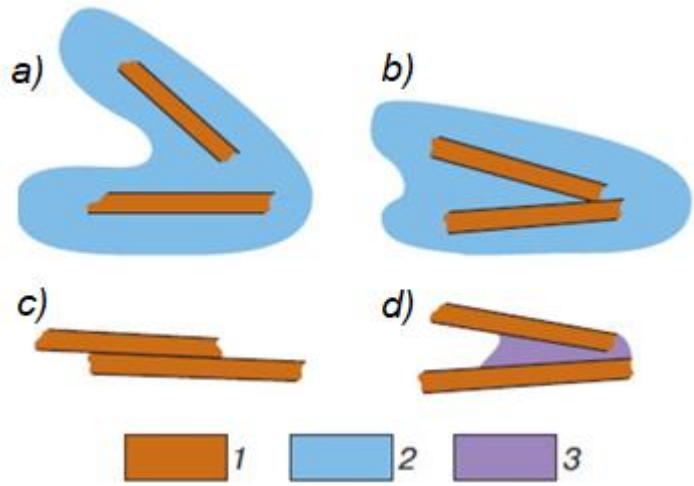

a - coagulation; b - transient (point); c, d - phase; 1 - particles; 2 - water films; 3 - cementitious substance.

Figure 5 - Types of contacts in cohesive soils

The investigated soils with a sufficient degree of certainty can be attributed to latently plastic normally compacted cohesive soils used in construction practice for the erection of unpaved transport structures (retaining walls, embankments and excavations of the earth bed of roads and railways).

Introducing the following notations into expression (3): $y = \Sigma_\omega$; $a = P_p$; $x = tg\alpha$; $b = C_{cont.}$, we get:

$$\Sigma_\omega = P_p tg\alpha + C_{cont.},$$

where Σ_ω − water-colloidal cohesion (according to Maslov N.N.);

P_p – pressure, which was experienced by the rock in its prehistory;

$C_{cont.}$ – cohesion of contact bonds, depending on the type of contacts between particles;

$tg\alpha$ − bonding angle of contact bonds, depending on the history of soil stress state.

Under conditions of sufficiently slow (quasi-equilibrium) loading, the shear resistance of non-water-saturated soils obeys Coulomb's law of dry friction at constant values of the strength parameter φk for the soil of a given material composition.

From expressions (5) and (7), taking into account C(c) = 0, for the limit state follows:

$$\tau_p = \begin{cases} P_p \mathrm{tg}\alpha + Ccont, & 0 < \sigma < \sigma_0 \\ \sigma \mathrm{tg}\phi - \mathrm{C}, & \sigma_0 < \sigma < \infty \end{cases}$$

Here σ_o - is the initial pressure of dry Coulomb friction.

Graphical interpretation of expression (8) is presented in Figure 6.

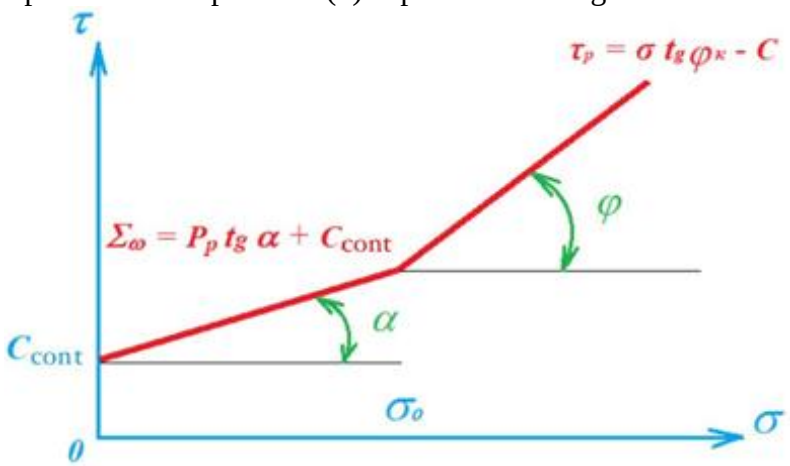

Figure 6 - **Shear criterion for non-water saturated latently plastic normally compacted cohesive soils**

Expression (8) is the equation of limit equilibrium of latent plastic normally compacted cohesive soils without structural cohesion. Thus, it can be concluded from equation (8) that the shear resistance of non-water saturated latent plastic normally compacted cohesive soils depends

not only on the acting pressure, but also on the pressure experienced by the rock in its prehistory. In addition, shear resistance depends on the cohesion of the soil [11, 12], which is determined by the nature of contact interactions between particles [13].

5. Conclusion

According to the results of laboratory tests, the following conclusions can be drawn:

- Shear resistance of soft-plastic loams is characterised by peak and residual strength under both static and vibrodynamic effects;

- for conditions of plane deformation (under static and vibrodynamic influences) the characteristics of shear resistance of soft-plastic loams corresponding to residual strength and obeying Coulomb's law are established. The parameter $\varphi_к$ of the limit equilibrium equation is found to be constant and is determined only by the material composition of the soil. It is established that the angle of internal friction of soft-plastic loams under static and vibrodynamic loading conditions is invariant;

- the influence of dynamic action can lead to a decrease in shear resistance. Change of shear resistance of soft-plastic loams under vibrodynamic impacts depends on moisture content, change of stress state and is characterised by a change in the value of adhesion, depending on the type and nature of interactions between soil particles and the possibility of their changes in the process of shear.

In calculations of stability of soils of transport structures consisting of non-water-saturated cohesive soils of disturbed structure[17-21], it is recommended to take as design parameter φ the angle of internal friction $\varphi_к$ determined according to the Tertsagi-Kulon method in the kinematic loading mode, and as design parameter C - the cohesion of contact bonds C_{cont}, determined according to the results of tests of soil without normal load under repeated shear.

References

1. *Pokrovskaya O.D.,* Samuilov V.M. International logistics of the Trans-Siberian Railway: the use of transit potential of Russia // Innovative transport. - 2016. - № 3 (21). - pp. 3-7.
2. *Blazhko L.S., Vasiliev S.G., Romanov A.V.* Risk assessment in the system of technical regulation of infrastructure // Transport of the Russian Federation. - 2019. - № 1 (80). - pp. 4-7.
3. *Blazhko L.S., Chuyan S.N., Zakharov V.B., Chernyaev E.V.* Analysis of the ways to increase the bearing capacity of soils of the main site of the earth bed // Izvestiya PSUPSa. - 2016. - T. 13. - № 3 (48). - pp. 328-336.
4. *Kvashnin M.Ya., Kosenko S.A., Kvashnin N.M., Bondar I.S.* Experimental studies of the vibrodynamic impact of the mobile load on the main site of the subgrade in cold regions // Proceedings of the Second International Symposium on the problems of the subgrade in cold regions: SGUPS, Novosibirsk, 2015, pp. 147-151.
5. *Kvashnin M.Y., Bondar I.S., Zhumaseitova A.B., Bikhozhaeva G.S.* To the issue of vibrodynamic impact of mobile load on the main site of the earth bed // Bulletin of KazATK №1 (96) 2016 - pp. 7-12.
6. *Zamukhovsky A.V., Burombaev S.A., Kvashnin M.Y., Bondar I.S., Shmakov A.P.* Vibrations of the earth bed soil on the approaches to the bridges // Proceedings of the XIV International Scientific and Technical Conference "Modern problems of design, construction and operation of railway track". Readings in memory of Professor G.M. Shakhunyants: RUT(MIIT), Moscow, 2017, pp 104-106.
7. *Lanis A. L., Razuvaev D.A.* Strengthening of the earth bed soils on the approaches to the bridges and overpasses // Vestnik of Rostov State University of Railway Engineering. - 2016. - № 3 (63). - pp. 97-104.
8. *Kvashnin M.Ya., S.A. Kosenko, Bondar I.S.* Vibrodiagnostics of the approach embankment of the railway bridge // Vestnik of SGUPS. - 2017. - № 2 (41). - pp 34-39.
9. *Fedorov I.V., Vorobyev A.A., Samarkina I.K., Konograi O.A., Bunkova T.G.* Investigation of the stress state in the contact "wheel-rail" in the presence of a chipping // Izvestia PSUPS. - St. Petersburg, 2019, No. 4. - pp 78-86.
10. *Khomyakov V.A., Isakhanov E.A., Kvashnin M.Ya.* Some peculiarities of soil testing in shear devices. // Proceedings of the International geotechnical symposium. St. Petersburg, 2003, pp. 235 - 237.
11. *Kvashnin M.Ya.* Experimental Investigations of Strength Characteristics of Clayey Soils for Forecasting of Transport Structures Stability. Dissertation for the degree of Candidate of Technical Sciences, Almaty, 2005.
12. *Kvashnin M.Ya., Abiev B.A., Bondar I.S.* Influence of loading conditions on soil shear resistance // Bulletin of KazATK № 1 (56), 2009 – pp. 5-12.
13. *Bondar I.S.* Shear tests of cohesive soils under different loading trajectories // Engineering and Construction Journal, No.7, 2012 - pp 50-57.
14. *Karaulov A.M., Korolev K.V., Bartolomei L.A., Bragar E.P.* Statistical processing of the results of shear tests of soils (in Russian) // Construction and Geotechnics. - 2020. - T. 11, № 3. - pp 8-17.

15. *Shuvaev A.N., Smirnov A.P., Kartavy S.V.* The Construction of Roadbeds on Permafrost and in Swamps from Reinforced Soils of Increased Strength // Civil Engineering Journal. – 2020. – Vol. 6, Issue 10. – pp 1922–1931.

16. *Kulikov A.V., Vorontsov V.V., Shuvaev A.N.* Investigation of physical and mechanical properties of peat // International Journal of Engineering and Technology. – 2018. – Vol. 7, Issue 3. – pp 1056–1058.

17. *Bogomolov A.N., Kuznetsova S.V., Bogomolova O.A., Shiyan S.I., Babakhanov B.S., Soloviev A.V., Nesterov N.S., Prokopenko A.V.* Risk assessment of landslide process occurrence and assignment of reserve coefficients when calculating slopes of soil structures for stability // Engineering problems of building materials science, geotechnical and road construction. Volgograd. 2012. pp 85-94.

18. *Vasiliev V.P.* Geosynthetics strengthens the position Road reliability is one of the key aspects of the industry // Automobile roads. 2023. pp 74-77.

19. *Krasnikova T.R.* Modern ways of the high embankment strengthening in the road construction. Volgograd. 2020. pp 657-660.

20. Frolov, A.Yu., Tsvetkova, E.V. Stress state analysis of a loaded reinforced slope (in Russian) // Low-rise construction. Volgograd. 2009. C. 257-260.

21. Bogomolov, A.N.; Ofrichter, V.G.; Redin, A.V.; Bogomolova, O.A.; Bogomolov, S.A. Stability estimation of a loaded slope in the complicated engineering-geological conditions (in Russian) // Construction and geotechnics. Perm. 2022. C. 70-85.

ON THE RHEOLOGICAL MODEL OF ASPHALT CONCRETE

Djumaev Kh[1].

[1]*Tashkent State Transport University, Tashkent, Uzbekistan*

E mail: djumaev1959@mail.ru

Abstract: *Since asphalt concrete exhibits elastic, plastic, and viscous properties in response to changes in tempe-rature and external influences, establishing a relationship between stress and deformation is an important issue. The study of the elastic and viscosity properties of physical bodies began in 1868 with the introduction of the concept of relaxation by Maxwell. Different models have been proposed to establish the above-mentioned relationship. Despite the large number of models offered, they are based on and are a combination of Hooke, Newton, and Saint-Venan models for elastic, viscous, and plastic bodies.*

Keywords: *asphalt concrete, models, relaxation, retardation, stress, deformation, geometric progression.*

1. Introdicton, materials, methods and object of research.

The Maxwell model consisted of the sum of the Hooke and Newton models (Fig.1). The Max-well model did not take retardation (delay of deformation) into account when considering relaxation. In the model (Fig.2), relaxation is not observed [2]. Similarly, the advantages and disadvantages of the remaining models can be shown (Fig.3).

Figure.1. - **Maxwell model.**

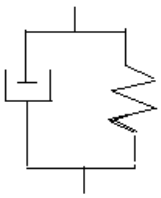

Figure.2. - **Kelvin-Foyxt model**

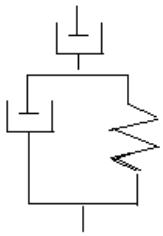

Figure.3. - **Lesersich model.**

In 1874, a general linear connection was proposed by L.Boltzmann, and all the models shown were described by L. Boltzmann. It can be obtained as a special case of the Boltzmann's connection [4].

The movement of a viscoplastic medium is characterized by peculiar features. Thus, when a vis-coplastic medium is pushed through a round pipe, the central part of the flow is not deformed and mo-ves like a solid, only a certain annular layer adjacent to the pipe walls is deformed.

The description of complex mechanical properties of materials requires the use of multielement models characterized by a large number of parameters. The models discussed in the previous paragraphs contained two parameters (E, σ_s or E, μ or σ_s, μ). The model shown in Fig. 4. contains three parameters E_1 E_2, μ_1. The defor-mation law of such a medium can be obtained as follows: we write the deformation laws of simple elements I, II, III.

$$\sigma_1 = E\varepsilon_1, \sigma_2 = \mu_1 \frac{d\varepsilon_2}{dt}, \sigma_3 = E\varepsilon_3 \tag{1}$$

and conditions of equilibrium and continuity

$$\sigma_1 + \sigma_2 = \sigma \ , \sigma_3 = \sigma \ , \varepsilon_1 + \varepsilon_3 = \varepsilon, \varepsilon_1 = \varepsilon_2 \tag{2}$$

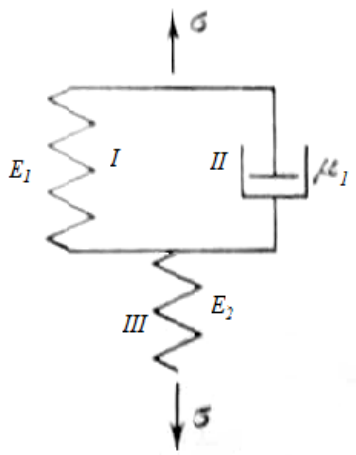

Figure.4. - **Model with three parameters**

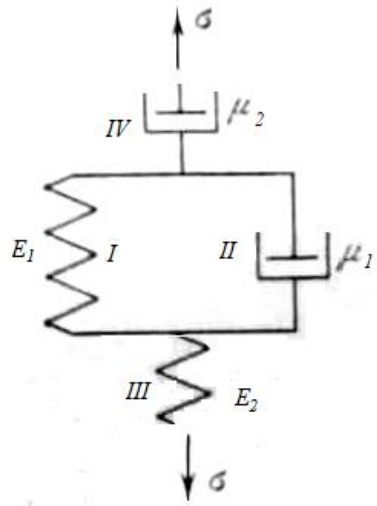

Figure. 5. - **Model with four parameters**

From here we easily find:

$$E_1\varepsilon + \mu_1 \frac{d\varepsilon}{dt} = \left(1 + \frac{E_1}{E_2}\right)\sigma + \frac{\mu_1}{E_2}\frac{d\varepsilon}{dt}. \tag{3}$$

An example of a model with four parameters E_1, E_2, μ_1, μ_2 is shown in Fig.5. An example of a 2*n*-parametric model is shown in Fig.6.

With a large number of elements of the same type, it is convenient to switch to a model with a continuous distribution of parameters; deformation of such a model will be defined by some integral.

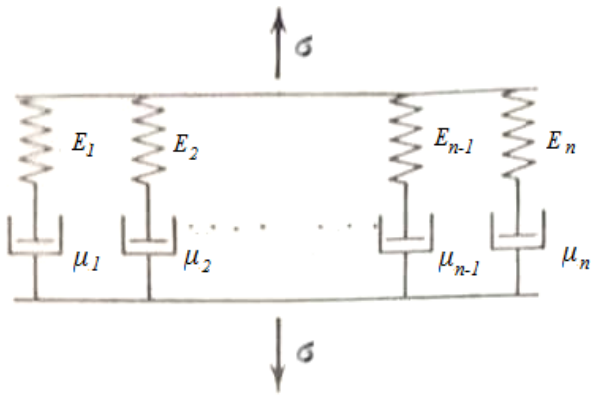

Figure.6. - **2*n*-parametric model**

The properties of many real materials cannot be satisfactorily described using the considered mo-dels, even with the introduction of a significant number of parameters. On the other hand, the use of complex multielement models is associated with the cumbersomeness of the mathematical apparatus.

A compact form of the general linear law of deformation was proposed by L. Boltzmann. This law is based on the principle of superposition of deformations.

Let the stress σ (τ) be applied to the body at the moment of time τ during a small time interval Δτ; the latter caused some deformation, which, when the stress is removed, will not disappear immediately, but will gradually decrease. Let us assume that this deformation at an arbitrary moment t>τ is proporti-onal to the magnitude of the acting stress σ(τ), the duration of the action Δτ, and some decreasing function depending on the time elapsed since the moment τ. Thus, at the moment t>τ the deformation will have the value

$$\varphi(t-\tau)\sigma(\tau)\Delta\tau \tag{4}$$

here $\varphi(t-\tau)$ is a monotonically decreasing function characteristic of a given material .

If, in addition, at the moment t the stress σ (τ) acts on the body,then the latter, according to Hooke's law, will cause instant deformation; total deformation at time t has the form:

$$\varepsilon(t) = \frac{\sigma(t)}{E} + \varphi(t-\tau)\sigma(\tau)\Delta\tau. \tag{5}$$

By virtue of the superposition principle, the influence of the stress σ (τ) acting at the moment τ is not disturbed by the stresses applied at other moments of time. Therefore, if stresses σ (τ_j) acted at different times τ_j during time intervals $\Delta\tau_j$, then the deformation at time t is determined by the sum

$$\varepsilon(t) = \frac{\sigma(t)}{E} + \sum \varphi(t-\tau_j)\sigma(\tau_j)\Delta\tau_j \tag{6}$$

2. Statement of problem.

Today, the above-mentioned complex properties of asphalt concrete are almost taken into account in the Boguslavsky model (Fig. 8), which generalizes the Maxwell (Fig.1), Kelvin-Foyxt model (Fig.2), Lesersich (Fig.3), and Burgers (Fig.7) models [3-6].

In the Boguslavsky model, the differential equation between the stress and defor-mation formed in asphalt concrete takes the following form [2]:

$$\theta\tau E\frac{d^2\varepsilon}{dt^2} + \frac{d\varepsilon}{dt}(2\eta + \tau E) + \varepsilon E = \theta\frac{d\sigma}{dt} + \sigma \tag{7}$$

The solution of this equation concerning eating a single load is as follows.

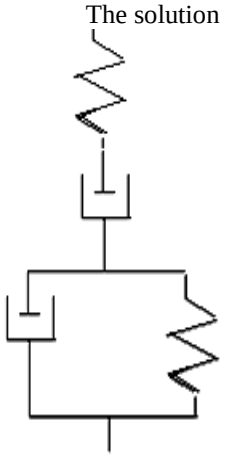

Figure.7. - **Burgers model.**

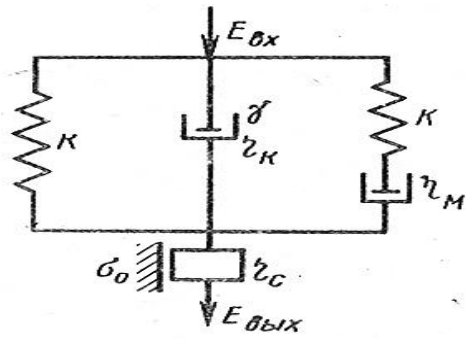

Figure. 8. - **Generalized model**.

$$\varepsilon_D = \varepsilon_{EV} + \varepsilon_P = \frac{(1+P_1\theta)P_2}{(P_1-P_2)}\cdot\frac{\sigma}{E}e^{-P_1 t} + \frac{\sigma}{E}\left[1 + \frac{(1+P_2\theta)P_1}{P_1-P_2}e^{-P_2 t}\right] + \frac{\sigma t}{\eta}, \tag{8}$$

The quantities involved in this equation and their units of measurement are as follows: P_1 and P_2 - kinetic characteristics of asphalt concrete, 1 / s; θ - relaxation time, s; σ - stress, MPa; τ - retardation time, s; t - stress exposure time, s; $\eta -$ viscosity coefficient N· s/sm^2; ε_p - plastic deformation; ε_{EV} - elastic-viscous part of deformation; $\varepsilon_D -$ total deformation; E- modulus of elasticity, MPa ; e- natural logarithm basis.

$$P_1, P_2 = -\frac{\theta + 0{,}5\tau}{\theta\tau} \pm \sqrt{\left(\frac{\theta + 0{,}5\tau}{\theta\tau}\right)^2 - \frac{1}{\theta\tau}} \tag{9}$$

The relative deformation after multiple loads is determined as follows [7-10]:

$$\varepsilon_{D\Sigma} = \frac{K_r\sigma}{E}(0{,}5 - e^{-P_2 t})T_1\sum_{i=0}^{i=n-1}(0{,}5e^{-P_1\lambda})^i + \frac{K_r\sigma\tau'}{\eta}(1 - e^{-(\tau')^{-0,5}}) \tag{10}$$

K_r - coefficient of reduction of vertical stress to horizontal stress, T_1 - the number of loads of imported vehicles, $T_1 = K_0 K_P\, m_1\, m_2$, n- the number of downloads per hour, m_1- coating temperature 50^0C and the number of hours per day that are higher, m_2 - coating temperature in three years 50^0C and the number of days higher, K_0 - coefficient taking into account the number of arrows, K_P - a factor that takes into account the width of the pavement and the location of the plot. λ - rest duration between downloads, τ' - total duration of downloads,

$$\tau' = tnT_1$$

P_1, P_2 are the kinetic characteristics of the deformation process (9) spreading the equation to Taylor's row, dropping infinitely small terms, we obtain the following:

$$P_1 = -\frac{0{,}5}{\theta},\ P_2 = -\frac{2}{\tau},\ \text{and } P_1/P_2 = 0{,}25\ \tau/\theta \qquad (11)$$

3. Results and analysis of the results.

The result (10) looks like this:

$$\varepsilon_{D\Sigma} = \frac{K_r\sigma}{2E}(1 - e^{\frac{2t}{\tau}})T_1\sum_{i=0}^{i=n-1}(0{,}5e^{\frac{0.5\lambda}{\theta}})^i + \frac{K_r\sigma\tau'}{\eta}(1 - e^{-(\tau')^{-0,5}}) \qquad (12)$$

After unloading

$$\varepsilon^0_{D\Sigma} = \frac{K_r\sigma}{2E}(1 - e^{\frac{2t}{\tau}})T_1\sum_{i=0}^{i=n}(0{,}5e^{\frac{0.5\lambda}{\theta}})^i + \frac{K_r\sigma\tau'}{\eta}(1 - e^{-(\tau')^{-0,5}}) \qquad (13)$$

This is the denominator under the sum sign in the equation $0{,}5e^{\frac{0.5\lambda}{\theta}} < 1$ is a geometric progression. Use the formula for the sum of the steps, instead (12) we create an equation

$$\varepsilon_{D\Sigma} = \frac{K_r\sigma}{2E}(1 - e^{\frac{2t}{\tau}})T_1\frac{(0{,}5e^{\frac{0.5\lambda}{\theta}})^{n-1} - 1}{0{,}5e^{\frac{0.5\lambda}{\theta}} - 1} + \frac{K_r\sigma\tau'}{\eta}(1 - e^{-(\tau')^{-0,5}}) \qquad (14)$$

To verify this equation, a sample (similar to practical experiments) was calculated by taking the problem.

$\tau = 46s$, $\theta = 4000s$; $P_1/P_2 = 0{,}003$; $E = 70Mpa$; $\sigma = 0{,}8\,Mpa$; $\lambda = 60s$

$\eta = 280000Mpa \cdot s$; t= 0,05s (speed 30km/h); $K_r = 0{,}3$; n=40/h; m_1 =2; m_2 =124; $T_1 = 50$; $\tau' = 100$ in values, after some simplification, the numerical expression of (12) is equal to:

$$\varepsilon_{D\Sigma} = \frac{0.24}{140}(1 - e^{\frac{0.1}{46}})\sum_{i=0}^{39}[(0{,}5\ e^{\frac{3}{400}})^0 + \ldots + (0{,}5e^{\frac{3}{400}})^{39}] + \frac{0.24}{280000}(1 - e^{-\frac{1}{10}}) = 0{,}00172 \qquad (15)$$

After unloading according to(13), $\varepsilon^0_{D\Sigma}$=0,00078+0,00002=0,0008.

The calculations using the equation (14) overlapped with the results of the equation in which the sum was involved.

References

1. *Gezentsvey L.B.* Road asphalt concrete // M. «Transport», 1976. 336p.
2. *Boguslavskiy A.M., Boguslavskiy L.A.* Basic rheology of asphalt concrete // M. "High School",1972. 200p.
3. *Gezentsvey L.B.* Road asphalt concrete //M. «Transport», 1985. 352p.
4. *Kachanov L.M.* Theory of plasticity //M. GITTL.1986. 324 p.
5. *Burakov A.V., Sobolev E.E.* Rheological model of stress-strain state bitumen-polymer airfield sealant in an expansion joint // Modern innovations,№ 2(30) 2018, Moscow. Publishing house "Problems of Science".

6. *Bogomolov V. A.* Improved rheological model of asphalt concrete when working on compression // Bulletin of KhNADU, issue 55, 2011.
7. *Kuzin N.V.* Accounting for elastoviscoplatic properties of asphalt concrete pavements // Dissertation work. Omsk, 2008, 176 p.
8. *Khvoinsky JI.A.* Research and development of methods for ensuring road sustainability structures of highways in Western Siberia // Author's abstract. PhD dissertation in technical sciences. Omsk,2001,17 p.
9. *Kanygina S.Yu.* Prediction of residual deformations of nonrigid road pavements on a subgrade made of clay soils // Author's abstract. dis. Ph.D. tech. Sci. -M.: MADI, 1999, 20 p.
10. *Alexandrov A.S.* Modeling of deformation processes occurring in connected soils // Science and technology in the road industry. 2002. No. 4.s. 16 – 19pp.

ELASTIC-PLIABLE LINKS TO REGULATE THE FORCES IN THE SUPERSTRUCTURES OF TRANSPORT STRUCTURES

Dostanova S.Kh.[1], Issakhanov Y.[2], Kasymova G.T.[3], Tokpanova K.E.[4]
[1]*K. Satpayev National Research Technical University, Almaty, Kazakhstan*
[2]Research Institute of Railway Development, *Almaty, Kazakhstan*
[3]*Kazakh Head Architectural and Construction Academy, Almaty, Kazakhstan*
[4]*Eurasian Technologiical University, Almaty, Kazakhstan*
E-mail: dostanova0109@mail.ru

Abstract: *An algorithm is presented for the dynamic calculation of superstructures of transport structures using elastic-yielding supports, which allows you to regulate the forces and deformation under the action of moving loads. Its implementation is based on variational principles using approximate methods. Equations for determining natural frequencies and forces under the action of a moving load are presented, taking into account the stiffness of flexible supports. Using the example of an existing three-span highway overpass, the calculation results are presented for various stiffness values, and optimal options for forces and deformations are identified. Comparisons of the results obtained with the case of rigid supports are made.*

Keywords: *Vibrations, frequencies, rigidity, regulation, connections, pliability.*

1. Introduction

The issues of dynamics in the study of reliability and safety of transport structures are relevant and timely. This is caused by the constantly increasing intensity of traffic and operational load, which leads to the exhaustion of the strength reserve and to emergency situations. This is especially important for seismic areas.

The traditional method of ensuring the strength of structures involves increasing the load-bearing capacity of the main structural elements by increasing their size and strength. This type of self-defense is passive. The use of passive self-defense elements leads to an increase in the cross-sections of structural elements, which in turn leads to an increase in the rigidity and weight of the structure. This causes an increase in the inertial load, and, therefore, in order to perceive it, the rigidity of the structure should be reviewed once again. This will lead to an increase in the cost of construction

Currently, to ensure the resistance of structures under intense dynamic impacts, active methods of protection are becoming increasingly widely used: vibration damping, vibration damping, vibration isolation, etc. [1-6].

The use of active protection methods in the form of flexible supports allows increasing the energy intensity of the support-structure system and reducing the intensity of dynamic impact. As a result, the cost of structures and the complexity of their restoration is reduced. The development and implementation of active methods for protecting reinforced concrete structures under dynamic loading requires the development and improvement of effective methods for dynamic calculation of systems that include both the structures themselves and the means of active protection. At the same time, for a reliable assessment of the stress-strain state, the developed calculation methods should take into account not only the basic physical laws of deformation of reinforced concrete under dynamic influences, but also the features of deformation of flexible supports.

Recently, the use of flexible support devices under dynamic impacts is widely used. This is especially true for complex structures in seismic areas. Their use makes it possible to artificially

regulate the state of the structure with significant fluctuations in the system, so the task of improving methods for calculating reinforced concrete transport structures on flexible supports under dynamic loading is an important task [1-6].

The task of regulation is to foresee in advance the possible dangerous state of the system and in time to positively influence the stress-strain state of the system by regulating of forces and deformations. Then artificial forces arise in the structures that are opposite in sign to those that arise from operational loads. Due to this, stresses and deformations in the elements from the operating load can be significantly reduced. At the same time, great opportunities open up for creating effective structures [1-5,7].

At the same time, transport structures with regulating support devices have not become widespread due to insufficient theoretical and experimental studies of the operation of superstructures. In particular, the effect of operational loads on the operation of the span of a beam bridge with regulating support devices has not been studied, the effect of dynamic loads on the superstructures has not been studied. Regulating support devices change the dynamic design scheme and dynamic characteristics of the superstructure (periods of natural oscillations, attenuation coefficient, oscillation forms) during its fluctuations.

An important parameter in dynamic analysis is damping, which reduces the response of the superstructure to dynamic impact. There are many sources of damping of bridge structures, which include internal friction of building materials, cracks, elastically pliable support links, friction in the support parts, aerodynamic resistance of the structure or viscoelastic properties of the foundation soils.

Further, the use of elastically flexible supports in the superstructures of road overpasses is considered.

2. Materials, methods and object of research

The object of research is the load-bearing beams of spans of automobile overpasses. Figure 1 shows a general view of the overpass. The overpass in the longitudinal direction is made three-span. Static system of superstructures – beam-split. Support of beams on supports-hinged. The superstructure is reinforced concrete, three–span, superstructures No. 1 and No. 3 consist of T-shaped reinforced concrete beams with a length of 11.36 m, made according to a standard design of reinforced concrete prefabricated superstructures without diaphragms with frame reinforcement of a periodic profile [8-9]. Superstructure No. 2 consists of prefabricated I-beams with a length of 16.76 m.

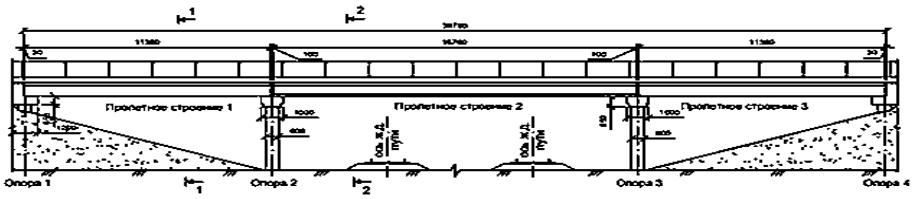

Figure 1. - **General view of the overpass**

Superstructures are considered as beams on two elastically flexible supports with stiffness C1 and C2 (Fig. 2). It is assumed that each span of the split bridge operates independently of each other. The free vibrations of a beam with a uniformly distributed mass are described by a fourth-order differential equation [8-9].

The differential equation of free vibrations without taking into account the resistance forces has the form [7-8]:

$$EI\frac{\partial^4 y}{\partial x^4}+m(x)\frac{\partial^2 y}{\partial t^2}=0 \qquad (1)$$

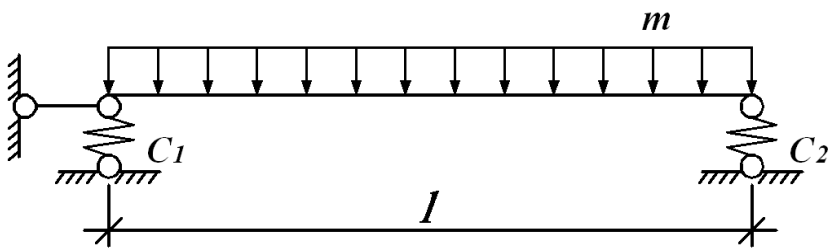

Figure 2. - **Design scheme of a beam on regulating supports**

In (1) deflection $y(x,t)$, EI – bending stiffness, $m(x)$ – linear mass. We restrict ourselves to finding only such solutions of equation (1) that determine standing waves, i.e., the bending shape that does not depend on time. These solutions correspond to the main waveforms. Using the method of separation of variables, equation (1) decomposes into two independent systems of ordinary differential equations:

$$y_k^{IV}(x) - \lambda_k^4 y_k(x) = 0, \qquad k = 1,2,3,\ldots.$$
$$\lambda_k^4 = \frac{m(x)\cdot\omega_k^2}{EI} \tag{2}$$
$$(T_k^{//}(t) + \omega_k^2 T_k\ (t) = 0, \qquad k = 1,2,3,\ldots. \tag{3}$$

Using the Euler method for solving linear ordinary equations, the solutions of equations (2) and (3) can be represented as:

$$y(x,t) = \sum_{k=1}^{\infty} y_k\,(x) T_k(t),$$
$$y_k(x) = Ach\,(\lambda kx)_k + Bsh\,(\lambda kx_k) + C\mathrm{Cos}(\lambda kx_k) + D\mathrm{Sin}(\lambda kx_k x),$$
$$T_k(t) = A_k \mathrm{Sin}\omega_k t + B_k \mathrm{Cos}\omega_k t,$$
$$\text{General solution for deflections:} \tag{4}$$
$$y(x,t) = \sum_{k=1}^{\infty} \begin{matrix} \left(\mathrm{A}ch(\lambda_k x) + Bsh(\lambda_k x) + C\mathrm{Cos}(\lambda_k x) + D\mathrm{Sin}(\lambda_k x)\right)\cdot \\ (A_k \mathrm{Sin}\omega_k t + B_k \mathrm{Cos}\omega_k t) \end{matrix}$$

In (4), the values A, B, C, and D are constants determined from the fastening conditions (boundary conditions), and A_k, B_k are constants determined from the initial conditions, i.e., displacements and velocities at the initial time t=0.

The expression for $y_k(x)$ defines the main form of vibrations corresponding to the frequency ω_k, it defines a static elastic line caused by the linear load $q_k=m(x)\omega^2_k y_k$. If the linear mass is constant over the length of the span, then $m(x)=m$=const, then we can write for the parameter s_k:

$$\lambda_k = l\sqrt[4]{\frac{m\omega_k^2}{EI}} \tag{5}$$

For the case when the beam is hinged at the edges, the boundary conditions will be:

when $x = 0$ $\quad M_0 = 0,\ Q_0 = y_0 \cdot C_1,$

for $x=l$ $\quad M_l = 0, \quad Q_l = -y_l \cdot C_2,$ (6)

where y_0 – displacement at the origin, y_l-beam displacement at $x=l$; M_0 и M_l are moments at x=0 and $x=l$, respectively, Q_0 и Q_l are transverse forces at x=0 and $x=l$, C_1, C_2 are stiffness of flexible supports at the left and right ends, respectively.

Expressing the coefficients A, B, C and D through initial parameters y_0, φ_0, M_0, and Q_0, then the standing waves can be represented as:

$$\left.\begin{aligned} y_x &= y_0 S_x + \frac{\varphi_0}{\lambda} T_x - \frac{y_0 \mathrm{With1}}{\lambda^3 EI} V_x, \\ \varphi_x &= y_0 \lambda V_x + \varphi_0 S_x - \frac{y_0 \mathrm{With1}}{\lambda^2 EI} U_x, \\ M_x &= -y_0 \lambda^2 EI U_x - \varphi_0 \lambda EI V_x + \frac{y_0 \mathrm{With1}}{\lambda} T_x, \\ Q_x &= -y_0 \lambda^3 EI T_x - \varphi_0 \lambda^2 EI U_x + y_0 \mathrm{With1} S_x. \end{aligned}\right\} \tag{7}$$

In (7), S_x, T_x, U_x, V_x represent Krylov's functions:

$$S_x = \frac{ch\lambda x\ \ + \cos\lambda x}{2}, \qquad T_x = \frac{Sh\lambda x + \mathrm{Sin}\lambda x}{2},$$

$$U_x = \frac{ch\lambda x \ -\cos\lambda x}{2}, \qquad V_x = \frac{Sh\lambda x - \mathrm{Sin}\lambda x}{2}.$$

Using the boundary conditions (6), we write the expressions for deflection, moment, and transverse force at $x=l$. As a result, we obtain a system of three homogeneous equations with respect to three unknowns: y_0, y_l, φ_0. Equating the determinant of this system at unknowns to zero, we obtain a transcendental equation with respect to the unknown quantity λ.

$$\begin{vmatrix} (S_{x=l} - \frac{C1}{\lambda^3 EI} V_{x=l} \ -1) & \frac{1}{\lambda} T_{x=l} & -1 \\ -(\lambda^2 EIU_{x=l} - \frac{C1}{\lambda} T_{x=l}) & -\lambda EIV_{x=l} & 0 \\ -(\lambda^3 EIT_{x=l} - C1 S_{x=l}) & -\lambda^2 EIU_{x=l} & C2 \end{vmatrix} = 0 \tag{8}$$

$$S_{x=l} = \frac{ch\lambda l + \cos\lambda x l}{2}, \quad T_{x=l} = \frac{Sh\lambda l + \mathrm{Sin}\lambda l}{2},$$
$$U_{x=l} = \frac{ch\lambda l \ -\cos\lambda l}{2}, \quad V_{x=l} = \frac{Sh\lambda l - \mathrm{Sin}\lambda l}{2}.$$

The determinant (8) is a transcendental equation from which the parameters of the natural oscillations λ are determined:

$$F(\lambda) = \left(S_{x=l} - \frac{C1}{\lambda^3 EI} T_{x=l} - 1\right)(-\lambda EIV_{x=l} C2) - \frac{1}{\lambda} T_{x=l}\left(-\lambda^2 EIU_{x=l} + \frac{C1}{\lambda} T_{x=l}\right) C2 +$$
$$+\left(-\lambda^2 EIU_{x=l} + \frac{C1}{\lambda} T_{x=l}\right)\lambda^2 EIU_{x=l} + \lambda EIV_{x=l}(-\lambda^3 EIT_{x=l} + C1 S_{x=l}) = 0 \tag{9}$$

Equation (9) includes the stiffness of elastically flexible supports C1, C2. Assuming one of the supports or two supports are rigid, we can consider 3 special cases:

1. $C_1=\infty$; 2. $C_2=\infty$; 3. $C_1=C_2=\infty$

The frequency of natural vibrations is expressed through the parameter λ:

$$\omega_k = l^2 \lambda_k \sqrt{\frac{EI}{m}}. \tag{10}$$

Knowing the natural frequencies, we can use formula (7) to determine deflections, rotation angles, bending moments, and transverse forces.

The solution of equation (9) is determined by approximate methods. Using an iterative process over the parameter λ in the range of variation ω [$\pi/2 - 2\pi$], λ is determined. The iterative process continues until the value of the function reaches the required $F(\lambda_k)<\varepsilon$.

When considering forced vibrations of load-bearing beams, an external moving load acts on spans with a uniformly distributed mass m. We assume that it varies according to the harmonic law with a frequency θ (for the case of an arbitrary load, we use decomposition according to the norms of natural oscillations) (Fig. 3):

$$F = F_0 Sin(\frac{\pi t}{T_0}), \tag{11}$$

where F_0 is the wheel load distributed over the area of a circle of diameter D, $T_0 = D/V$, V is the speed of horizontal movement of the load, and t is the current time. Denoting the ratio π/T_0 by θ, then the external load can be represented as: $F = F_0 Sin(\theta \cdot t)$, where θ is the frequency of fluctuations of the external load.

The differential equation of transverse vibrations and its solution have the form:

$$EI\frac{\partial^4 y}{\partial x^4} + m\frac{\partial^2 y}{\partial t^2} = F_0 \mathrm{Sin}\theta t,$$
$$y = y_o + y_{pr} \tag{12}$$

y_0 – homogeneous equation solution, y_{pr} – private solution.

The amplitude values of normal inertial forces are determined by the formula:

$$I = \frac{\gamma h \theta^2 y(x)}{g},$$

where γ is the specific weight of the beam material, g is the acceleration of a free-falling body, and y(x) is the deflections. Consider the steady-state forced vibrations of a beam (y_o=0), assuming that

the displacements $y(x,t) = y(x)Sin\theta t$ are harmonic vibrations with a frequency θ, where y(x) is an unknown deflection function. Equation (12) can be written in the form:

$$\frac{\partial^4 y}{\partial x^4} + \frac{m\theta^2}{EI}\frac{\partial^2 y}{\partial t^2} = \frac{F}{EI}, \qquad u = l\sqrt[4]{\frac{m\theta^2}{EI}} = kl, \qquad k = \sqrt[4]{\frac{m\theta^2}{EI}}, \tag{13}$$

$$y = y_{pr}\ (u,x)$$

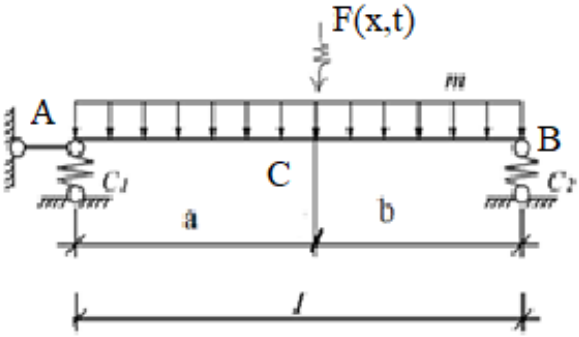

Figure 3. - **Forced vibrations of a beam with elastically flexible supports**

Considering 2 sections (AC, CB), the solution of equation (13) is compiled at each section using the interface conditions at the boundary of the sections. For example, in section 1 there is no external load $\leq a$, so equation (13) can be considered as homogeneous and the solution (7) can be used for the amplitude values of displacements and internal forces.

In the second section, the solution will be summed up from the solution of the first section and additional terms, i.e., using the initial parameter method, we can write:

For (a+b) ≥x≥ a

$$y_2(x) = y_0 S_x + \frac{\varphi_0}{u}T_x - \frac{Q_0}{u^3 EI}V_x - \frac{F_0}{u^3 EI}V_{x-a}$$

$$\varphi_2(\mathrm{x}) = y_0 u V_x + \varphi_0 S_x - \frac{Q_0}{u^2 EI}U_x - \frac{\mathrm{F}_0}{u^2 EI}U_{x-a}$$

$$M_2(\mathrm{x}) = -y_0 u^2 EIU_x - \varphi_0 uEIV_x + \frac{Q_0}{u}T_x + \frac{\mathrm{F}_0}{u}T_{x-a}$$

$$Q_2(\mathrm{x}) = -y_0 u^3 EIT_x - \varphi_0 u^2 EIU_x + Q_0 S_x + \mathrm{F}_0 S_{x-a} \tag{14}$$

To determine the initial parameters Q_0, φ_0 and reference deflections $y_1(x=0)=y_{1,0}$, $y_2(x=a+b)=y_l$ we use the boundary conditions and conditions for the compatibility of deformations at the boundary of the sections (Fig. 3):

On the 1st section at x=0 $M_{1,0}=0$; $Q_{1,0}=C1\cdot y_0$

On the 2nd section at x=a+b $M_2(x=a+b)=0$; $Q_2=C2\cdot y_2(x=a+b)=$ $C2y_{2l}$; $y_2(x=a+b)=y_l$

On the border of sections: $y_1(x=a) = y_2(x=a)$, $\varphi_1(x=a) = \varphi_2(x=a)$

Using the boundary conditions, the system of three algebraic equations with respect to 3 unknowns y_0, φ_0, y_l has following form:

$$M_2(\mathrm{x} = l) = -y_0 u^2 EIU_{x=a+b} - \varphi_0 uEIV_{x=a+b} + \frac{\mathrm{C1}\cdot \mathrm{y}_0}{u}T_{x=a+b} + \frac{\mathrm{F}_0}{u}T_{x=b} = 0$$

$$y_{2l} = \ y_{10}S_{x=a+b} + \frac{\varphi_0}{u}T_{x=a+b} - \frac{C1y_0}{u^3 EI}V_{x=a+b} - \frac{\mathrm{F}_0}{u^3 EI}V_{x=a+b}, \tag{15}$$

$$Q_2(\mathrm{x} = l) = -y_0 u^3 EIT_{x=a+b} - \varphi_0 u^2 EIU_{x=a+b} + C1y_0 S_{x=a+b} + \mathrm{F}_0 S_{x=b} = \mathrm{C2}y_{2l}$$

a+b=l – beam length.

The solution of equations (15) can be represented as:

$$y_0 = f_2(u,C1,C2),\ \ \varphi_0 = f_1(u,C1,C2),\ \ y_l = f_3(u,C1,C2) \tag{16}$$

The functions f_i (i=1,2,3) depend on the stiffnesses C1, C2 and on the parameter $u = \sqrt[l4]{\frac{m\theta^2}{2\ 2\ EI}}$. In (15), the initial parameters y_0 are the deflection in the left support, φ_0 is the angle of rotation in the left support, y_l is deflection in the right support, C1, C2 are the stiffness of elastic supports.

Using formulas (7) and (15), deflections, rotation angles, bending moments, and transverse

forces from an external load can be determined.

3. Problem statement

For a given design of a three-span overpass with elastic-flexible connections (Fig. 1), it is necessary to determine the natural frequencies and optimal values of the stiffness of flexible supports C_1, C_2, which increase the load-bearing capacity under the action of a moving load F(x) at speed V..

To find the optimal values of parameters C_1, C_2 we use the variational method. Condition for the minimum of the total energy E for unknown parameters:

$$\frac{\partial E}{\partial C1} = 0, \frac{\partial E}{\partial C2} = 0 \tag{17}$$

Equations (17) are a system of two nonlinear algebraic equations with respect to 2 unknown parameters C1, C2. The stable solution corresponds to the following inequality:

$$\frac{\partial^2 \mathrm{E}}{\partial \mathrm{C1}\, \partial \mathrm{C2}} > 0 \tag{18}$$

For the case of a single moving load, the total potential energy expression can be written as:

$$E = \int_0^a EI \frac{y_1^2(x)dx2}{2} + \int_a^b EI \frac{y_2^2(x)dx2}{2} - \frac{C1\mathrm{f}3^2(\mathrm{u,C1,C2})}{2} - \frac{\mathrm{C2f}4^2((\mathrm{u,C1,C2})}{2} - \int F_0 y(x)dx \tag{19}$$

The functions $\mathrm{f2(u, C1, C2)}$, $\mathrm{f3(u, C1, C2)}$ depend on the stiffness of the supports C1, C2, which are determined from equations (17). To simplify the calculation in (19), the deflection function can be taken in the following form:

$$y(x) = \frac{F_0 x^3}{12EI}(1\text{-}\frac{x}{l}),$$

where F_0 is the amplitude value of the mobile load.

4. Results of instrumental and theoretical studies

Using the proposed algorithm, the natural frequencies of transverse vibrations of the spans are determined for the case of hinge fastening of the ends of the bearing beams (C1=C2=∞) and for the case of elastic supports with different stiffness values. At the speed of movement of the moving load V =20.2 m/cm, the values of the dynamic coefficient 1 + μ are determined. Table 1 shows the values of the natural oscillation frequencies at different values of the stiffness of the flexible bonds and the corresponding values of the dynamic coefficient at a speed of movement V = 20.2 m/cm (F_0 =12ton). With an increase in the speed of movement of the load, the dynamic coefficient increases. Instrumental measurements of natural frequencies (C1=C2=∞), carried out using the multifunctional measuring complex "Tensor MS", are close to the theoretical values presented.

Table 1.

Calculated values depending on the stiffness of flexible supports

Span number	Anchoring conditions	Natural frequencies ω1, hz	Oscillation periods sec	Instrumental measurements ω1	Dynamic. coefficients (1+μ)
1,3	(C1=C2=∞)	9,82	0,64	10,40	1,37
2		5,86	1,07	6,21	1,41
1,3	(C1=C2=100kN/cm)	5,52	1,14	-	1,14
2		4,84	1,55	-	1,13
1,3	(C1=C2=200kN/cm)	5,44	1,15	-	1,12
2		4,44	1,25	-	1,11
1,3	(C1=C2=400kN/cm)	7,66	0,82	-	1,33
2		5,32	1,18	-	1,23
1,3	(C1=C2=800kN/cm)	8,55	0,74	-	1,42
2		5,38	1,17	-	1,35

Fig. 4 shows a graph of changes in the frequency of natural vibrations ω in hz depending on the stiffness of elastic supports C1 in kN/cm for two spans of an automobile overpass. Curve 2 corresponds to the first span, and curve 4 corresponds to the second span. The graph shows two asymptotes: (1) for the first and (3) for the second spans corresponding to rigid supports.

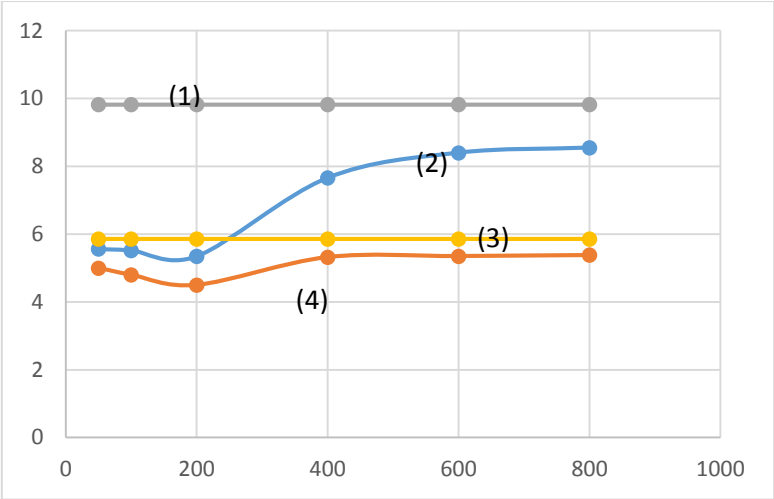

Figure 4. - **Graph of the natural oscillation frequency ω in hz as a function of the stiffness of elastic supports C1 in kN/cm for two spans of an automobile overpass: (1) for the first and (3) for the second span with rigid supports, (2) corresponds to the first and (4) to the second span for elastic supports.**

Table 2.

Values of internal forces in the middle of the beam spans

Efforts t/m^2	1 span L=11,36m	2 span L=16,76m	3 span L=11.36m
Static calculation (C1=C2=∞)			
$(Mc)_{max}$	34.08.08	50.20	34.08.08
$(\sigma_s)_{min}$	-1072,0	-1435.6	-1072
$(\sigma_c)_{max}$	1594.0	1867.10	1594.0
Dynamic calculation (C1=C2=∞)			
$(Mc)_{max}$	44.30	65.26	44.30
$(\sigma_s)_{min}$	-1394,0	-2053,0	-1394,0
$(\sigma_s)_{max}$	2072.20	2180.20	2072.20
(C1=C2=100kN/cm)			
$(Mc)_{max}$	38.85	56.72	38.85
$(\sigma_s)_{min}$	-1225,51	-1622,20	-1225,50
$(\sigma_s)_{max}$	1817.16	2109.82	1817.16
(C1=C2=200kN/cm)			
$(Mc)_{max}$	37.50	55.72	37.50
$(\sigma_s)_{min}$	-1200,64	-1593,16	-1200,64
$(\sigma_s)_{max}$	1785.28	2072.48	1785.28
(C1=C2=400kN/cm)			
$(Mc)_{max}$	45.33	56.52	45.33
$(\sigma_c)_{min}$	-1425,76	-1622,23	-1425,76
$(\sigma_s)_{max}$	2120.02	2296.47	2120.02
(C1=C2=800kN/cm)			
$(Mc)_{max}$	48.39	67.77	48.39
$(\sigma_s)_{min}$	-1522,24	-1938,06	-1522,24
$(\sigma_c)_{max}$	2263.48	2520.58	2263.48

With an amplitude value of the external moving load equal to F_0 = 12ton Table 2 shows the values of dynamic internal forces in the middle of the beam spans (Fig. 3) at different values of stiffness of elastic bonds.

Table 3 shows the values of deflections for 3 spans with different values of stiffness of bonds obtained by analytical methods. Comparing the work of 3 spans, it is clear that the largest deflections correspond to the average span.

Table 3.

Deflection values for girder spans under various boundary conditions

Span number	Conditions of fastening	Deflections W [m]
Static solution		
1.3	(C1=C2=∞)	0.028
2		0.042
Dynamic calculation		
1.3	(C1=C2=∞)	0.038
2		0.059
1.3	(C1=C2=100kN/cm)	0.036
2		0.047
1.3	(C1=C2=200kN/cm)	0.031
2		0.046
1.3	(C1=C2=400kN/cm)	0.037
2		0.047
1.3	(C1=C2=800kN/cm)	0.039
2		0.057

5. Analysis of results

Table 1 shows that the natural vibration frequencies and dynamic coefficients for elastic supports decrease in comparison with rigid ones. This makes it possible to avoid resonance. The smallest value of the dynamic coefficient corresponds to the value of stiffness of elastically flexible bond equal to C1=200kN/cm. In comparison with other values of C1, the dynamic coefficient (1+μ) decreased by 17.5% in comparison with rigid bonds. It can be seen from graph (4) that as the stiffness of the supports increases, the natural oscillation frequencies approach values close to rigid supports.

Table 2 shows that with the stiffness of an elastic support equal to C1=200kN/cm, the values of dynamic internal forces in the middle of the second span in comparison with rigid supports, respectively, decrease for bending moments by 14.6%, for compressive normal stresses by 22.4%, for tensile stresses by 5%.

Table 3 shows that with the stiffness of an elastic support equal to C1=200kN/cm, the largest deflection values in comparison with rigid supports decrease for the 1st span by 18.42% for the 2nd by 22%.

6. Discussion

A constant increase in cargo loads on transport structures requires a constant search for strengthening their dynamic strength reserve, one of the promising ways in this direction is the use of elastically flexible supports. Basically, modern research in this direction is focused on the technical side, improving the technology of manufacturing spatial supports. For a reliable assessment of the stress-strain state of transport structures, in addition to the physical patterns of deformation of reinforced concrete under dynamic influences, it is necessary to identify the features of deformation of flexible supports.

To increase the effectiveness of increasing the resistance of reinforced concrete structures to dynamic impacts, it is advisable to use flexible supports of variable stiffness. For this purpose, it is necessary to optimize the stiffness of flexible supports, taking into account the physical and geometric parameters of spans.

The use of elastically flexible supports makes it possible to regulate forces and deformations and increase the load-bearing capacity of existing transport structures. When calculating the 1st and 2nd limit states, it is necessary to clarify the current regulatory documents, taking into account the engineering analysis of the state of road bridge structures and their reconstruction, taking into account the use of flexible supports.

For the safe operation of transport structures, it is necessary to improve and develop scientific research in the field of searching for new structural forms and protection systems for transport structures under significant dynamic influences.

7. Conclusion

Based on the above calculations, the following conclusions can be drawn:

1. The use of regulatory support links in bridge structures can reduce the dynamic coefficient from 18% or more in comparison with rigid links.
2. According to numerical calculations, regulating support links reduce dynamic deflections in superstructures from a moving load in comparison with its static effect by 18-20%, bending moments up to 15% and normal stresses up to 22%.
3. Regulating support devices reduce the natural vibration frequencies of the beam, thereby removing it from the resonant zone by 9% or more.
4. An increase in the length of the span beams leads to a decrease in natural frequencies and an increase in internal forces and deflections by up to 32% on average.

References

1. *Kumpyak O.G., Galyautdinov Z.R.* Deformation of reinforced concrete beams on flexible supports under short-term dynamic loading, In: Proceedings of the Materials of the international scientific and technical conference "Modern problems of building materials, structures, soil mechanics and complex rheological systems". – Samarkand, 2013. – pp. 31-35.

2. *Galutdinov Z.R.* Investigation of a reinforced concrete ball on an auxiliary support under short–term dynamic loading // Reinforced concrete structures. handiwork.-Tomsk, 2023.1(1). pp. 28-36.

3. *Kumpyak O.G., Galyautdinov Z.R., Kokorin D.N.* Experimental and theoretical studies of reinforced concrete beams on pliable supports along inclined sections under seismic and other dynamic loads // Earthquake-resistant construction. Safety of structures. 2013. No. 1. pp. 40-45.

4. *Aidaraliev A.E.* Calculation of the bridge span for a moving load // KGUSTA Bulletin. 2010, Issue 1 (27). Bishkek, pp. 21-24.

5. *Aidaraliev A.E.* Regulation of forces in beams with a change in the geometric scheme of structures // Bulletin of the Kazakh Academy of Transport and Communications named after M. Tynyshpaev – Almaty, 2010, No. 3. pp. 45-48.

6. *Gridnev S.Yu.* Development of the theory of dynamic calculation of road bridges for mobile load. Abstract of the Candidate of Sciences. dissert., Voronezh, 2013, 41 p.

7. *Dostanova S.Kh., Tokpanova K.E., Saleh G.S.* Advantages of seismic insulation of buildings and structures. Bulletin of KAZGAS, 2020, 3 (77), pp. 119-124.

8. *Dostanova S.H., Tokpanova K.E., Saleh G.* Modern methods of seismic isolation and seismic protection of buildings and transport structures. Proceedings of the ISPC "Modern trends in architecture and construction: energy efficiency, energy conservation, BIM technologies, problems of the urban environment". Almaty, 2021, pp. 153-161.

9. *Dostanova S.Kh., Shayakhmetov S., Tokpanova K., Kalpenova Z.* Accounting for the dynamic characteristics of automobile overpasses, In: Proceedings of the X International Annual Conference "Industrial Technologies and Engineering". ICITE -2023, Vol. II, Shymkent, Kazakhstan. pp.144-153.

BENDING OF FIBER-REINFORCED COMPOSITE WING-LIKE PLATES

Eshmatov B.Kh.[1], Abdikarimov R.A.[2]

[1] *Department of Mathematics, Branch of University of Science and Technology "MISIS", Almalyk, Uzbekistan*

[2] *Department of Civil Engineering, Tashkent University of Architecture and Civil Engineering, Tashkent, Uzbekistan*

E-mail: ebkh@mail.ru

Abstract: *In this work, studies are carried out on the bending of anisotropic reinforced quadrangular composite plates of various geometric configurations, in each of which one side is clamped, and the other sides are free (cantilever plate). The influence of the mechanical and geometric parameters of the plate on its stress-strain state has been studied. The ABAQUS finite element analysis package was used to study the bending problem of anisotropic reinforced plate of non-rectangular shape.*

Keywords: *bending, cantilever reinforced plate, feathering, twisting.*

1. Introduction

The development of composite materials that are lightweight and highly resistant to temperature changes is essential for creating aircraft designs with high performance and efficiency. The use of such materials makes it possible to reduce fuel consumption, increase efficiency and reduce the direct operating costs of the aircraft. Composite materials provide the opportunity to create various shapes and, if necessary, strengthen the fibers to increase strength. One of the useful features of composites is their layered structure, in which the fibers in each layer are oriented in different directions. This allows the engineer to design structures with unique properties. For example, you can design a structure that will bend only in a certain direction, and will not allow bending in others.

One of the main structural elements of the aircraft, where reinforced composites are most often used, is the wing of the aircraft. A wing is a structural element of an aircraft that is used to create lift during flight. The wing is initially tilted at a certain angle of attack and therefore the flow passing over it, due to the pressure difference on the upper and lower surfaces of the wing, creates lift, allowing the structure to take off and maneuver in flight. It is important to understand here that under the influence of various static and dynamic loads (for example, aerostatic or aerodynamic pressures), aircraft wing structures made of reinforced composites (due to its heterogeneity) behave differently than the same structures made of conventional traditional aluminum. In addition, the movement of the aircraft in the air largely depends on its geometric configuration.

The problems of bending a rectangular isotropic cantilever thin plate subjected to arbitrary loads using the method of double finite integral transformation were considered in [1].

The article [2] discusses the results of the analysis of bending and vibration of plates of medium thickness reinforced with a thin composite plate. In the analytical formulation, the layer is modeled as a shear deformable plate.

In [3], the analysis of free vibrations and static bending of piezoelectric plates made of functionally ordered material based on one region of a two-parameter elastic base was carried out. Verification tasks are performed to assess the accuracy of the proposed theory and mathematical model. To determine the influence of geometric, physical properties and material, such as plate size, volume fraction index, piezoelectric effect, base elasticity coefficients and the square size of the base area, on free vibration and static bending of a piezoelectric functionally graded material, a wide range of plate parameters is studied.

However, the problems associated with the research of shell structures, which are components of aircraft, have not yet been sufficiently studied. Due to the structural features of reinforced composite materials, deformations that differ from those of conventional materials occur in them. The paper investigates the problems of bending a rectangular and trapezoidal cantilever plate, which in shape represent a mock-up of an airplane wing. Twisting and feathering occurring in reinforced composites, under the influence of various loads, play an important role in the formation of lifting force.

2. Mathematical model

Consider a rectangular composite reinforced plate subjected to a transverse load $q = q(x, y)$. Suppose that one of the sides of the plate is clamped, and the rest are free (Fig. 1). Epoxy graphite plastic with the following mechanical characteristics is selected as the plate material: $E_1 = 181\ GPa, E_2 = 10.3\ GPa, G_{12} = 7.17\ GPa, \mu_{12} = 0.28$. Unless otherwise stated, as input data we take: $a = b = 1\ m$. (sides of the plate), $h = 0.01\ m$. (thickness), $q = 100\ N/m^2$. Such a design represents the profile of an aircraft wing and therefore the issues of studying their stress-strain state are very relevant in modern aircraft engineering.

To solve this boundary value problem, its solution satisfying the boundary conditions we will take in the following form [4]:

$$w(x, y) = \sum_{m=1}^{M} \sum_{n=1}^{N} X_m(x) Y_n(y), \tag{1}$$

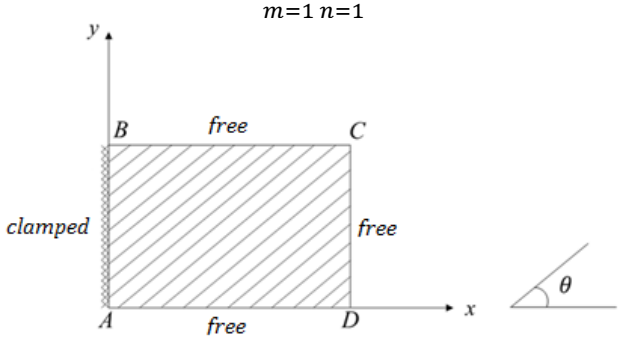

Figure 1. **- Geometry of an anisotropic rectangular cantilever plate reinforced with fibers at an angle of θ degrees**

$$X_m(x) = \frac{cos\lambda_m + cosh\lambda_m}{sin\lambda_m - sinh\lambda_m}\left(cos\frac{\lambda_m x}{a} - cosh\frac{\lambda_m x}{a}\right) + sin\frac{\lambda_m x}{a} - sinh\frac{\lambda_m x}{a},$$

$$Y_1(y) = 1, \quad Y_2(y) = 1 - \frac{2y}{b},$$

$$Y_n(y) = cos\alpha_n\left(\frac{y}{b} - \frac{1}{2}\right) - \frac{sin(\alpha_n/2)}{sinh(\alpha_n/2)} cosh\alpha_n\left(\frac{y}{b} - \frac{1}{2}\right) \quad (n = 3,5,7, \dots)$$

$$Y_n(y) = sin\beta_n\left(\frac{y}{b} - \frac{1}{2}\right) + \frac{sin(\beta_n/2)}{sinh(\beta_n/2)} sinh\alpha_n\left(\frac{y}{b} - \frac{1}{2}\right) \quad (n = 4,6,8, \dots)$$

where λ_m, α_n, β_n are determined from the transcendental equations:

$$cos\lambda_m cosh\lambda_m = -1,\ tan\left(\frac{\alpha_n}{2}\right) + tanh\left(\frac{\alpha_n}{2}\right) = 0,\ tan\left(\frac{\beta_n}{2}\right) - tanh\left(\frac{\beta_n}{2}\right) = 0$$

Substituting (1) into the equations of motion [5,6] and performing the Bubnov-Galerkin procedure, we obtain a system of differential equations describing the stress-strain state of an anisotropic reinforced rectangular cantilever plate, similar to those obtained in [7-9].

3. Results and discussion

Fig. 2 (a,b,c) illustrate the deflection shapes of a square reinforced cantilever plate with different fiber directions at a constant transverse load q. As expected, in the case of orthotropic plates (fiber direction 0 and 90 degrees), the edge of the plate, located opposite the clamped side, does not twist. In these cases, the deviation values are the same for each point along the lines at the intersections of the plate with the $x = const$ plane. The deflection has its maximum value at points on the line, which is the intersection of the plate with the plane $x = a$ (on the CD line in Fig. 1). The value of the maximum deflection of the plate with the fiber direction 90^0 is greater than that of the plate with the fiber direction 0^0.

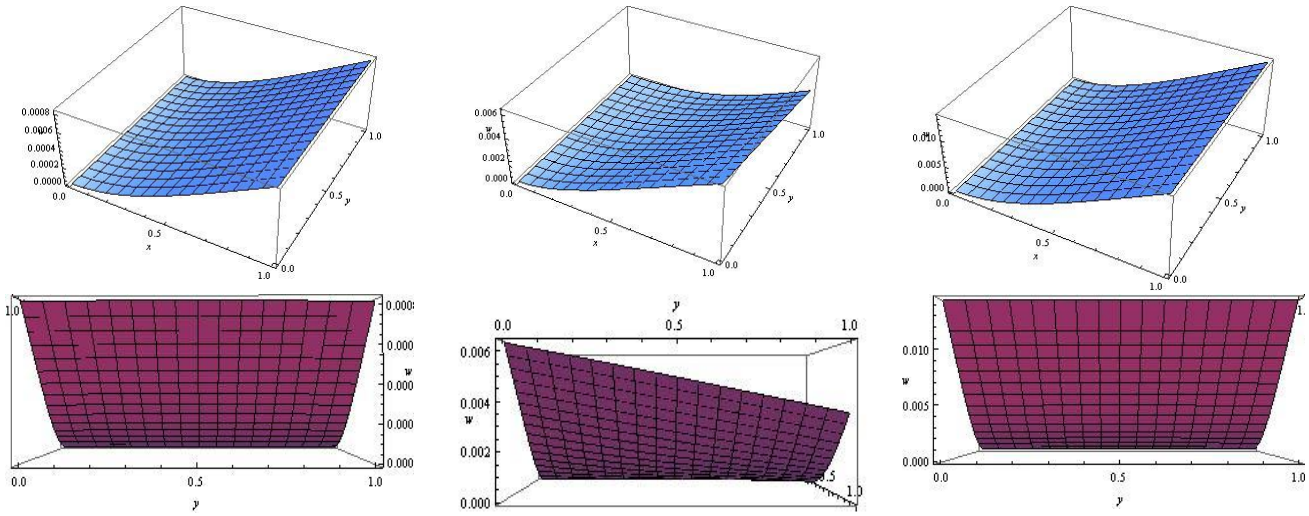

(a) (b) (c)

Figure 2. **- Bending of anisotropic CFFF square plate under transverse load $q = const$ with (a) – 0^0; (b) – 45^0 and (c) – 90^0 fiber orientations**

In contrast to specially orthotropic plates, we can see twisting in the anisotropic plates. Here, the values of deflections are not same at points on intersections of a plate with the plane $x = const$. The extreme values of deflection are reached at points C and D (Fig. 1). Moreover our results show that the edge $x = a$ located opposite to the clamped edge has the form of a straight line. This means that the plate has no "feathering"; a schematic of this is shown in the one of the following figures.

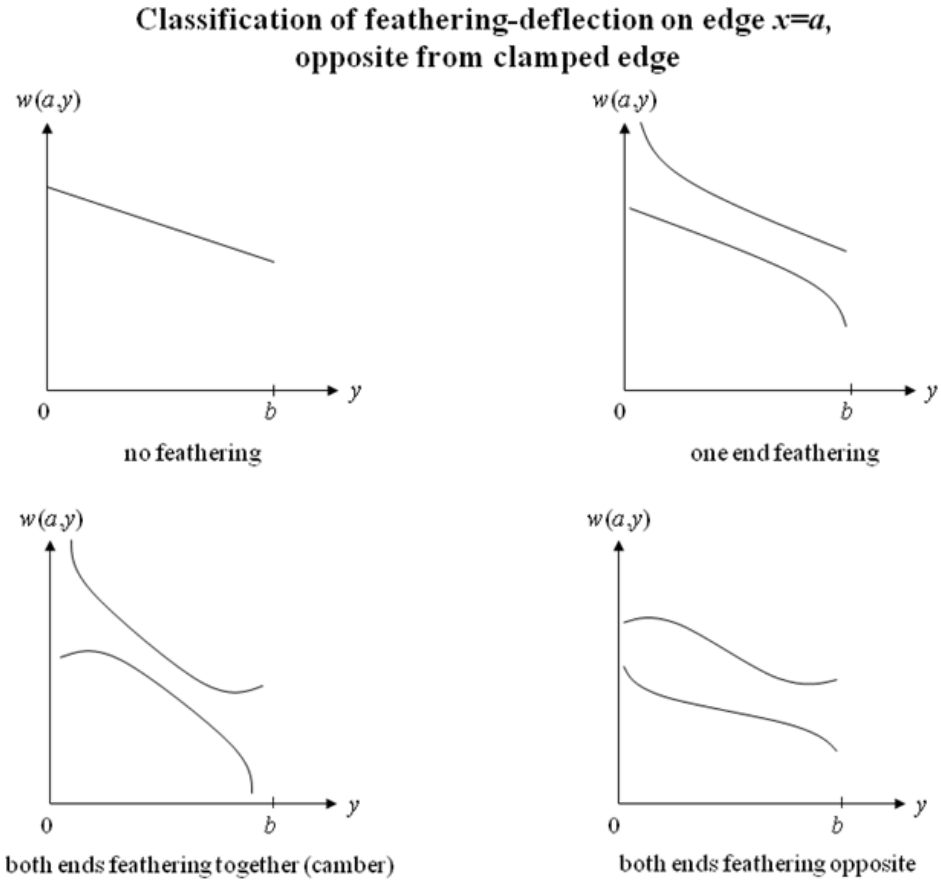

The edges in feathering can move in the same or in opposite directions. The feathering is related to camber, which describes the curvatures on the top and bottom surfaces of an airfoil. This can be built into the shape of the airfoil surfaces or can be created in a membrane by interaction with the airflow. We produce these curvatures by elastic coupling, and we define a feathering metric at either end of the plate as $f = d/t$ (see figure below).

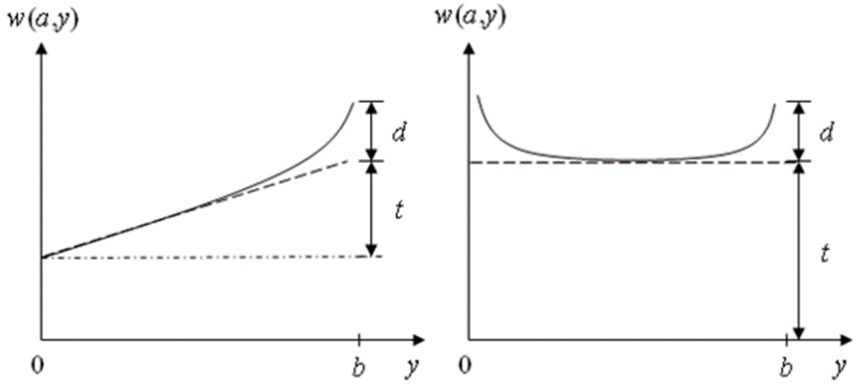

We define that the edge located opposite to clamped edge has feathering only if the value of d/t is more than 2% as defined by the figures above.

We now turn to the case when a CFFF anisotropic plate is located in the air flow such that the pressure varies over the plate surface. In this case the transverse load is assumed to vary according to a linear law. The deflections of a square anisotropic plate under transverse load $q = q_0(1 - 2y/b)$ are shown in Fig. 3 (a,b,c). The value of q_0 is set to 100 N/m^2.

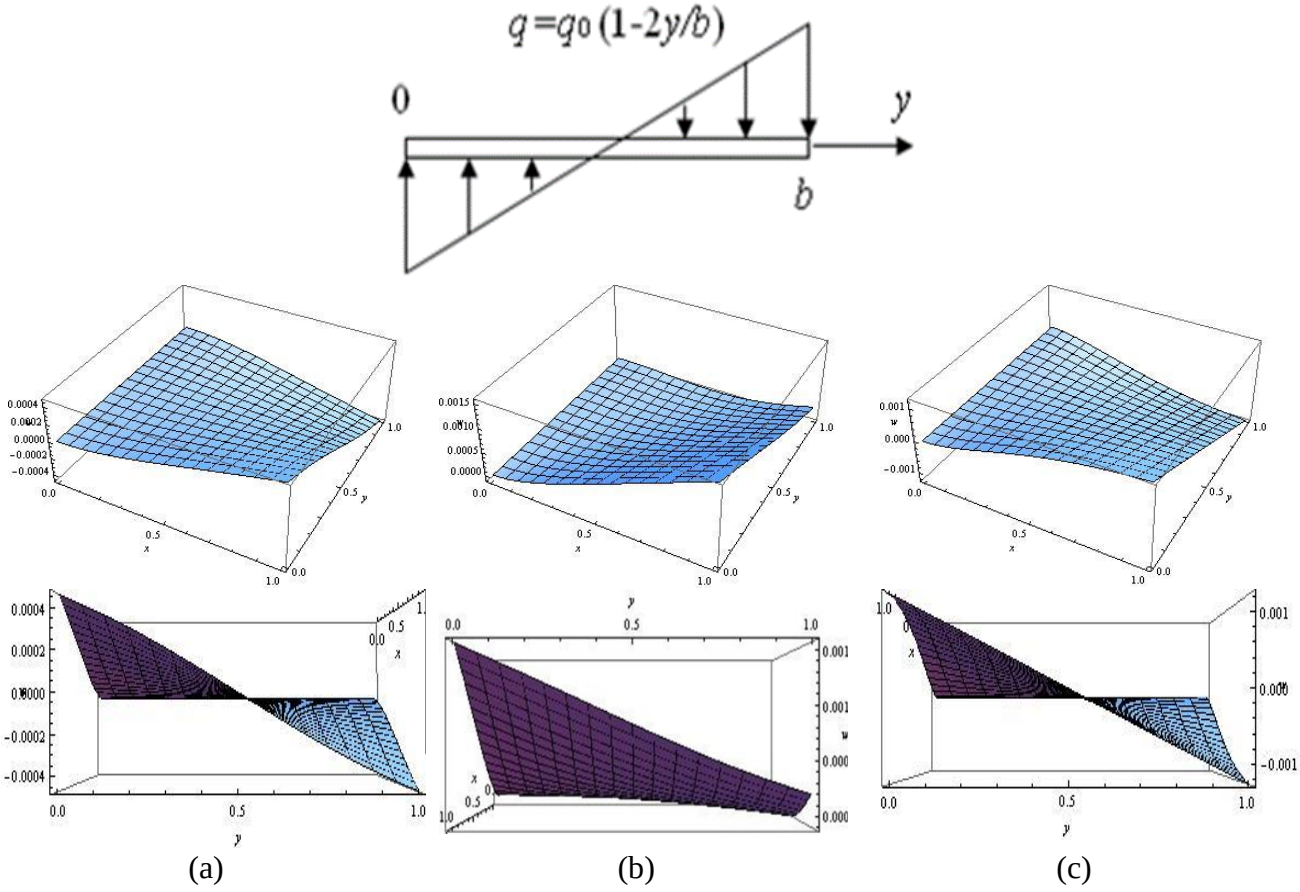

Figure 3. - **Bending of anisotropic CFFF square plate under transverse load $q = q_0(1 - 2y/b)$ with (a) – 0^0; (b) – 45^0 and (c) – 90^0 fiber orientations**

Here we can observe twisting in both the specially orthotropic and anisotropic cases. Although the maximum deflections of orthotropic plates are different, the forms of their deformations are the same. Both plates with 0 and 90 degree fiber orientations have maximum deflection at the point *D* and minimum deflection at the point *C*. In specially orthotropic plate with 90 degree fiber orientation, the edge located to the opposite of the clamped edge has the form of a straight line while in the plate with 0 degree fiber orientation there is a feathering of both ends

opposite. As in the previous cases there is no feathering here. The effect of q dominates twisting and the effect of fiber orientation dominates the bending and feathering.

In the anisotropic case we can see (visually) that there is feathering of one end, but this occurs at opposite ends of the edge $x = a$. The twisting and feathering characteristics of an anisotropic CFFF square plate under various loadings is presented in Table 1. In the last column of table one can find the values of slopes of the curve $\partial w/\partial y$ at point *x=a, y=b/2*. This point is a center of the edge located opposite to the clamped edge ($x = a, y\epsilon(0, b)$).

Next, we consider the bending problem of an anisotropic CFFF trapezoidal cantilever plate under the uniform transverse load q=100 N/m^2 (Fig. 4). Unless otherwise stated, as input data we take: $a = 0.5\ m, b = c = 1\ m$ (area of the plate is 0.75 m^2), $h = 0.01\ m$. To solve this problem we use ABAQUS, since the boundary conditions for an approximation method such as Ritz are not easily satisfied for non-rectangular plates.

Table 1.

Twisting and feathering of the anisotropic and isotropic CFFF square plate

Fiber orientation	Sizes of the plate	Loading	Twisting/ Feathering	Coefficient of feathering f	$w(a, b/2)$, m	$\frac{\partial w}{\partial y}(a, b/2)$
0^0	Square a=1 m., b=1 m.	q=const	No/No	-	$0.821*10^{-3}$	0
90^0			No/No	-	$14.52*10^{-3}$	0
45^0			Yes/No	-	$4.985*10^{-3}$	$-2.78*10^{-3}$
-45^0			Yes/No	-	$4.985*10^{-3}$	$2.78*10^{-3}$
0^0		$q=q_0(1-2y/b)$	Yes/Yes (both ends opposite)	0.085	0	$-1.07*10^{-3}$
90^0			Yes/No	-	0	$-2.486*10^{-3}$
45^0			Yes/Yes (one end)	0.092	$0.831*10^{-3}$	$-1.426*10^{-3}$
-45^0			Yes/Yes (one end)	0.084	$-0.831*10^{-3}$	$-1.426*10^{-3}$
Isotropic (Aluminum)			Yes/No	-	0	$-0.635*10^{-3}$

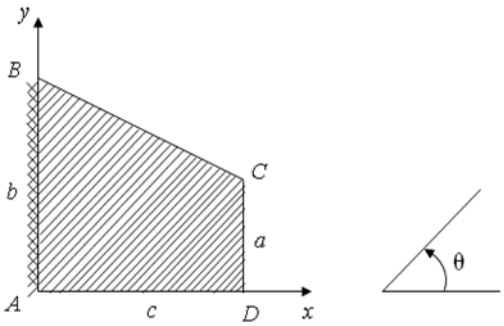

Figure 4. - **Trapezoidal wing-like anisotropic CFFF plate with *θ* degree fiber orientation**

The values of maximum deflections of the trapezoidal wing-like anisotropic plates made from different composite materials are presented in Table 2.

Table 2.

The values of the maximum deflections of the trapezoidal wing-like plates made from different types of composite materials

Material	E_1, GPa	E_2, GPa	E_1/E_2	G_{12}, GPa	w_{max}		
					0^0	45^0	90^0
Glass Epoxy	38.6	8.27	4.67	4.14	$3.505\cdot10^{-3}$	$10.68\cdot10^{-3}$	$14.26\cdot10^{-3}$
High Strength Carbon Epoxy	145	9	16.11	4.5	$1.065\cdot10^{-3}$	$7.860\cdot10^{-3}$	$13.19\cdot10^{-3}$
High Modulus Carbon Epoxy	181	10.3	17.57	7.17	$0.828\cdot10^{-3}$	$6.159\cdot10^{-3}$	$11.26\cdot10^{-3}$
Boron Epoxy	204	18.5	11.03	5.59	$0.775\cdot10^{-3}$	$4.704\cdot10^{-3}$	$6.696\cdot10^{-3}$

It is noteworthy that the inter-relationship of the mechanical properties produces different patterns and deflections. For orthotropic zero degree fiber oriented wing-like structures, the increase of E_1 (Longitudinal Young's Modulus) leads to proportional decrease of the maximum deflection. Similar behavior can be observed for structures with 90 degree fiber orientation. In this case, an increase of E_2 (Transverse Young's Modulus) leads to proportional decrease of maximum deflections. Note that changing of the values of G_{12} (In-Plane Shear Modulus) doesn't affect the bending of the orthotropic plates. The values of mechanical properties of composite materials used in this work were taken from [10].

The behavior of the anisotropic trapezoidal wing-like plates under uniform transverse load is presented in Fig. 5-7. Here it should be noted that contour of constant deflections (see Fig. 5-6) are almost parallel to the directions of fibers for plates with 45 and 90 degree fiber orientations. In all cases the deflection has maximum at the same point (at point *D* of Fig. 4). Comparing these values of maximum deflections with one obtained for a square plate we can conclude that they are almost the same for plates with 0 and 45 degree fiber orientations. For example, the difference between the maximum values of deflections obtained for 45 degree fiber oriented square and trapezoidal plates is about 6.1%, and for 0 degree is about 0.16%.

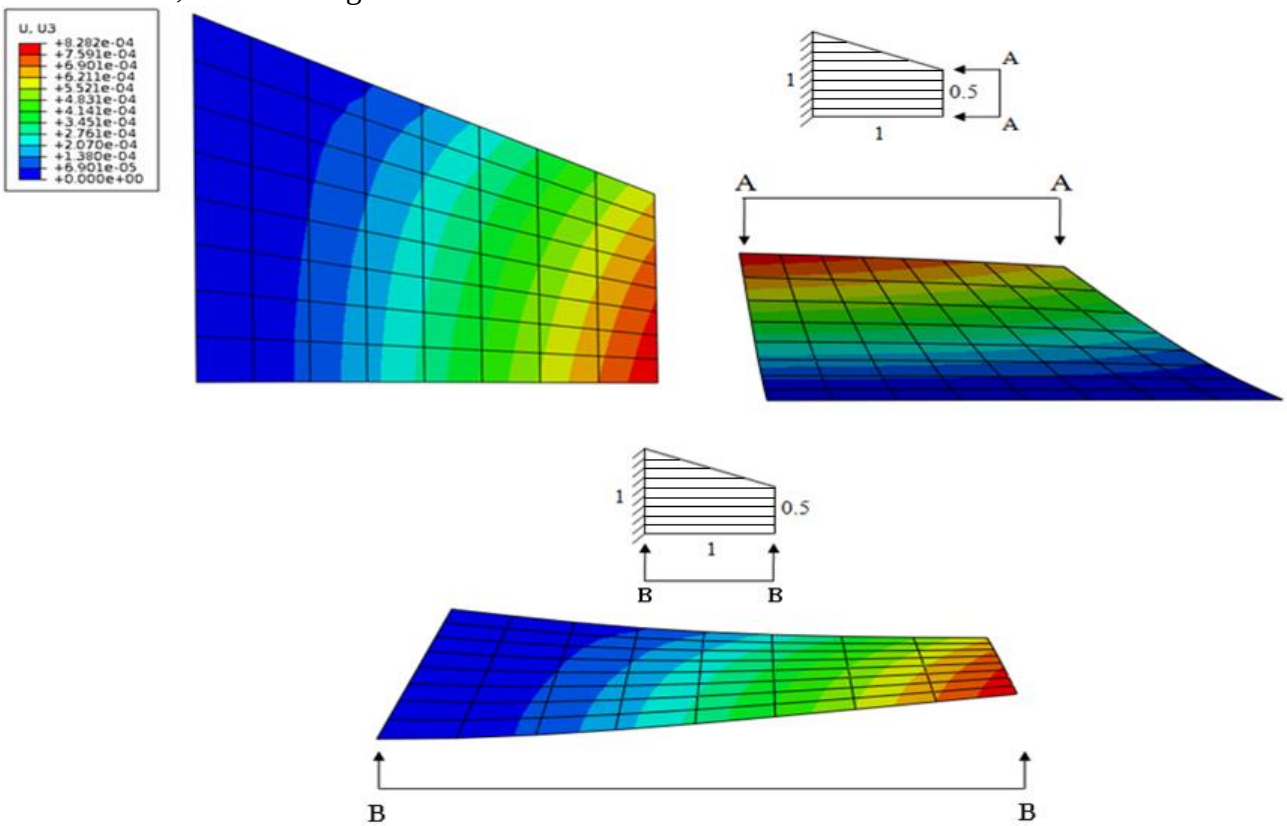

Figure 5. - **Bending of trapezoidal wing-like orthotropic plate (Graphite/Epoxy, 0^0 fiber orientation)**

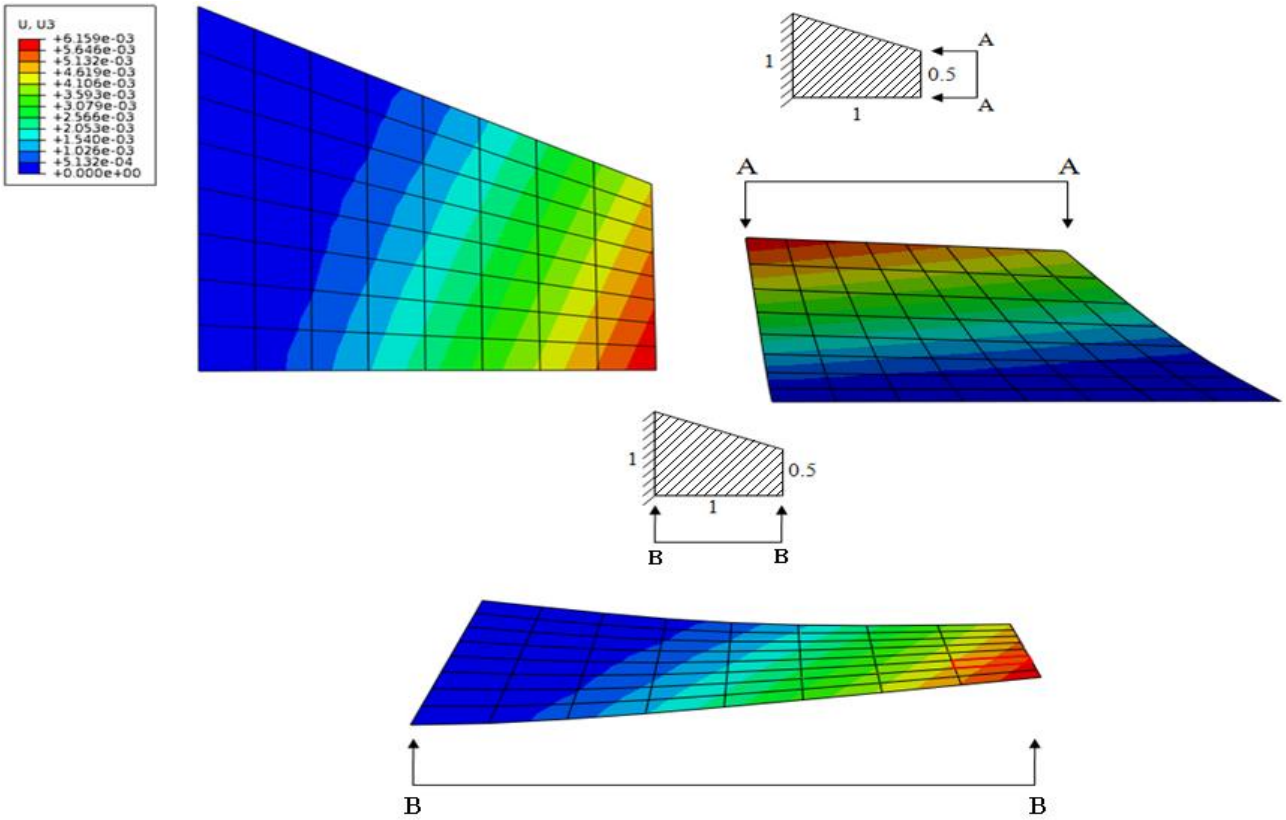

Figure 6. - **Bending of trapezoidal wing-like orthotropic plate (Graphite/Epoxy, 45^0 fiber orientation)**

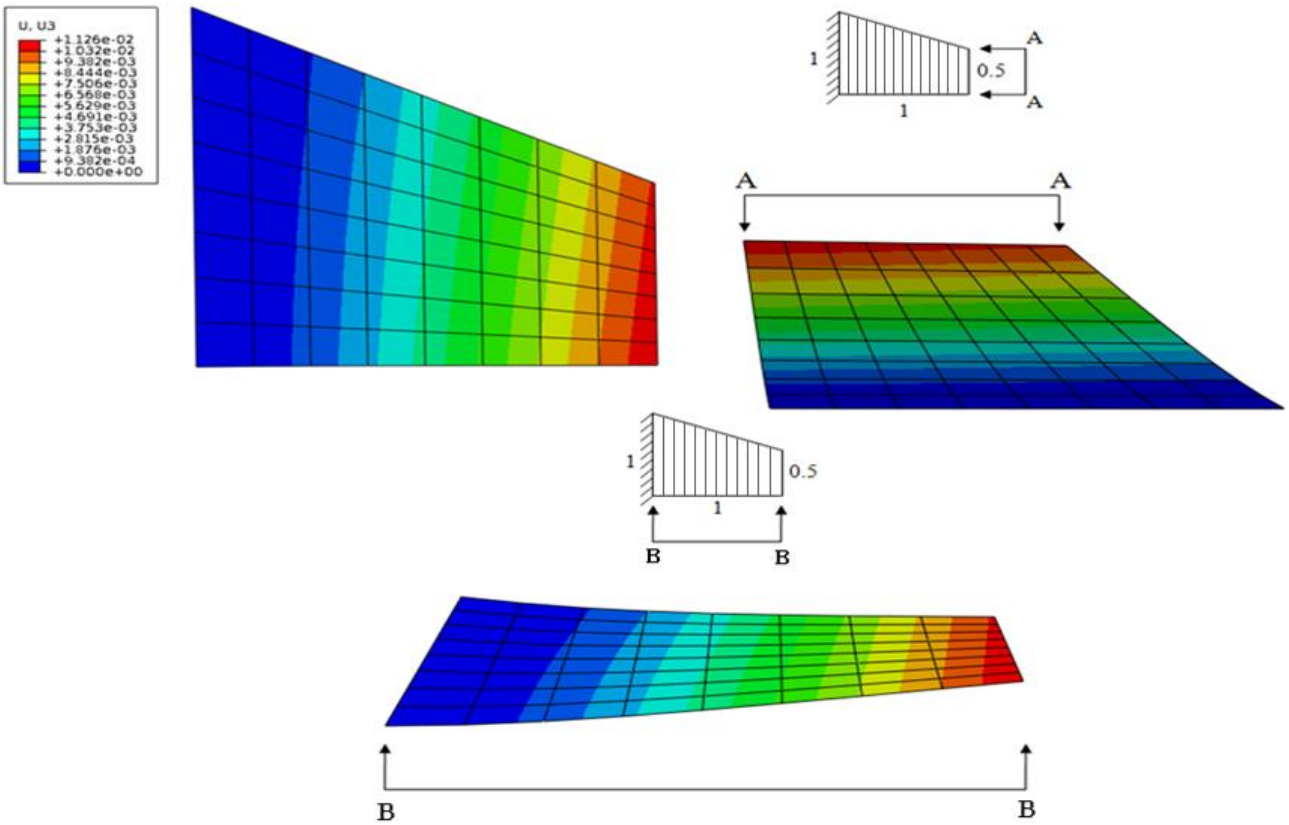

Figure 7. - **Bending of trapezoidal wing-like orthotropic plate (Graphite/Epoxy, 90^0 fiber orientation)**

The summary of the twisting and feathering of the anisotropic CFFF trapezoidal plate under uniform transverse load q is presented in Table 3. In the last column of table one can find the values of slopes of the curve $\partial w/\partial y$ at point $x = a, y = b/2$. To find the function w to determine the

slope, we use the interpolation method using the values of the deflections at the modes and passing the values to interpolation function.

Table 3.

Twisting and feathering of the anisotropic CFFF trapezoidal plate

Fiber orientation	Sizes of the plate	Loading	Twisting/ Feathering	Coefficient of feathering, f	$w(a, b/2)$, m	$\frac{\partial w}{\partial y}(a, b/2)$
0^0	a=0.5 m, b=c=1 m	q=const	Yes/Yes (both ends together)	0.146	$0.748*10^{-3}$	$-0.418*10^{-3}$
90^0			Yes/No	-	$10.86*10^{-3}$	$-1.604*10^{-3}$
45^0			Yes/No	-	$5.391*10^{-3}$	$-3.145*10^{-3}$
-45^0			Yes/Yes (both ends together)	0.058	$2.785*10^{-3}$	$1.138*10^{-3}$

Note that in all cases, the maximum deflections of plates with 0 degree fiber orientations are the smallest among the fiber orientations considered. However, the deflections depend on the geometry and mechanical properties of the plate.

4. Conclusions

- the analytical expansion and finite element methods were used to investigate the behavior of anisotropic wing-like (rectangular, trapezoidal) plates under buckling loads;

- by changing physical and geometric parameters, it was determined which fiber orientations and wing planforms give useful couplings (bending-twisting) and useful “feathering” at useful frequencies for interacting with airstream;

- in almost all considered cases we can see twisting. The feathering is most typical for the following cases: a. Square CFFF anisotropic plate with 0 and 45 degree fiber orientations under transverse load changing according to linear law; b. Trapezoidal CFFF anisotropic plate with 0 degree fiber orientations under uniform transverse load.

References

1. *Tian B., Zhong Y., Li R.* Analytic bending solutions of rectangular cantilever thin plates // Archives of Civil and Mechanical Engineering. 2011, vol. 11, No. 4, pp. 1043-1052.
2. *Shen H.-S., Chen Y., Yang J.* Bending and vibration characteristics of a strengthened plate under various boundary conditions // Engineering Structures. 2003, vol. 25, No. 9, pp.1157-1168.
3. *Thi H.N.* Free Vibration and Static Bending Analysis of Piezoelectric Functionally Graded Material Plates Resting on One Area of Two-Parameter Elastic Foundation // Mathematical Problems in Engineering. 2020, vol. 2020, No. 9236538.
4. *Leissa A.W.* Vibration of Plates / «Acoustical Society of America» Washington, 1993, 353 p.
5. *Volmir A.S.* Nonlinear dynamics of plates and shells / «Nauka» Moscow, 1972, 432 p.
6. *Ashton J.E., Whitney J.M.* Theory of Laminated Plates / «Technomic publication» Stamford, 1970, 153 p.
7. *Eshmatov B.Kh., Abdikarimov R.A., Amabili M., Vatin N.I.* Nonlinear vibrations and dynamic stability of viscoelastic anisotropic fiber reinforced plates // Magazine of Civil Engineering, 2023, vol. 118, No. 2, No.11811.
8. *Abdikarimov R., Amabili M., Vatin N.I., and Khodzhaev D.* Dynamic Stability of Orthotropic Viscoelastic Rectangular Plate of an Arbitrarily Varying Thickness // Applied Sciences, 2021, vol. 11, No. 13 – 6029.
9. *Eshmatov B.Kh.* Nonlinear vibrations of viscoelastic anisotropic fiber reinforced plate // Mechanics of Solids. 2018, No. 5, pp. 106-111.
10. *Kaw A.* Mechanics of Composite Materials // 2nd edition, Boca Raton: CRC Press, Taylor&Francis, 2006, 473 p.

SIMULATION OF A DYNAMIC CONFLICT SITUATION IN REAL TIME FLIGHT OF A RESTORED AIRCRAFT VESSEL

Eshmuradov D.E [1], Dzhumamuratov B.A[2], Elmuradov T.D[2], Sharipov G. N.[2]

[1]*Tashkent University of Information Technologies named after Muhammad al- Khwarizmi, Tashkent, Uzbekistan*

[2]*Tashkent State Technical University named after Islam Karimov, Tashkent, Uzbekistan*

E-mail: e_dilshod69@mail.ru

Abstract. *An aircraft (AC) is one of the most complex and dynamic objects; during operation, they are under the influence of forces (various loads), vibration, dust, various gases, high temperatures and atmospheric conditions. All these factors cause natural wear of parts and assemblies, which consists of a gradual change in their size, shape, surface quality and strength properties. These changes lead to a decrease in reliability and, ultimately, to failure of parts and assemblies of aircraft and aircraft engines. One example of an integrated approach to aircraft design is the use of composite materials. Composite materials make it possible to reduce the weight of aircraft, which leads to increased efficiency. At the same time, they also provide the necessary strength and safety of the aircraft. In this article we will consider the main aspects of modeling dynamic conflict situations in real time of the flight of an aircraft with a restored fairing.*

Keywords: *aircraft, fairing, conflict situation, algorithms, modeling, radome test, models.*

1. Introduction

In the airspace there are many different objects such as airplanes, helicopters, drones and other aircraft that move through the air at high speed and can collide with each other at any given time. To ensure air traffic safety, various systems are used, such as radio navigation systems, flight control systems, etc. However, despite this, conflict situations still arise that can lead to accidents and major disasters. One of the ways to prevent conflict situations is to simulate dynamic conflict situations in airspace in real time. This allows you to predict possible conflicts and take measures to prevent them.

2. Basic principles of modeling.

Numerous methods have been developed for calculating the motion parameters of aircraft, including maneuvering ones. Usually, for this purpose, a system of differential equations is compiled that describes the control and disturbing forces acting on the aircraft, and the initial data for modeling are the characteristics of the aircraft and the purpose of its movement [1,2].

Modeling of dynamic conflict situations in airspace [3,4,7,8] in real time is based on the following principles:

1. Modeling the movement of aircraft. To simulate dynamic conflict situations, it is necessary to have an accurate model of the movement of aircraft. This model must take into account all factors that can affect the movement of the aircraft, such as weather conditions, technical condition of the aircraft, navigation data, etc.

2. Simulation of conflict situations. To simulate conflict situations, it is necessary to have an accurate model of all objects that may collide with each other in the airspace. This model must take into account all parameters of objects, such as speed, direction of movement, height, etc.

3. Modeling reactions to conflict situations. To model the response to conflict situations, it is necessary to have an accurate model of the behavior of aircraft when a conflict occurs. This model must take into account all possible behavior of the aircraft under various conditions.

4. Modeling of the control system. To model dynamic conflict situations, it is necessary to have an accurate model of the control system that will make decisions about conflict prevention. This model must take into account all the parameters of the aircraft and determine the optimal path and time to prevent a conflict.

A possible example of modeling dynamic conflict situations in airspace in real time could be the automatic air traffic control (ATC) system in Fig. 1, used at airports and on airlines. [9,10,11,12,13,14].

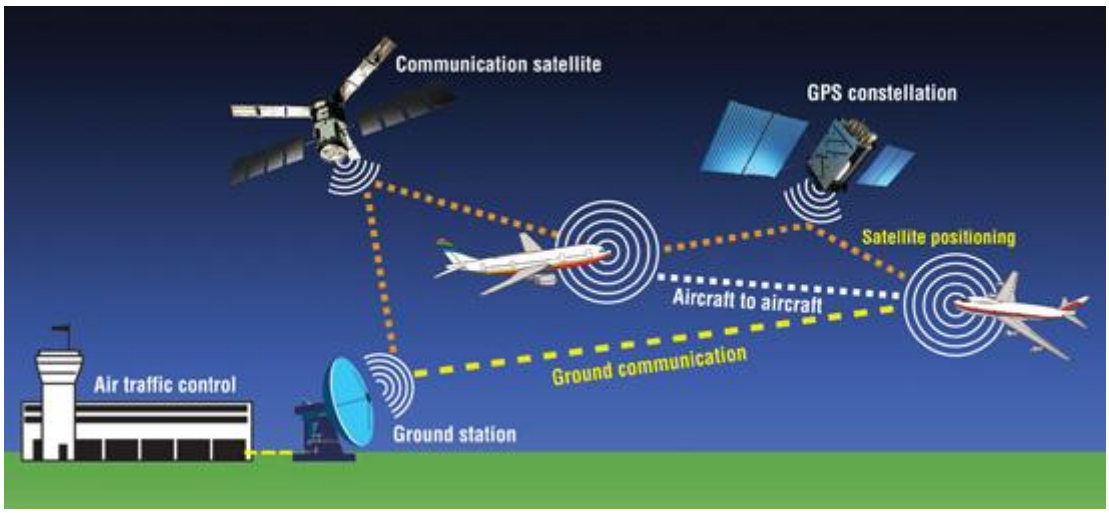

Figure.1. **- Automatic Air Traffic Control (ATC) system.**

The system uses data about the position and speed of aircraft, as well as weather conditions and other factors, to identify potentially dangerous situations and prevent collisions between aircraft. The ATC model may include various algorithms and rules that determine what actions must be taken to prevent conflicts. For example, the system can automatically change flight routes or aircraft speeds to avoid collisions. Such a model can be used to train and train air traffic controllers, as well as to test new algorithms and airspace management strategies.

3. Examples of using modeling.

Real-time simulation of dynamic airspace conflict situations can be used for various purposes, for example:

1. Prevention of accidents. Modeling can help prevent accidents and major disasters by predicting possible conflicts and taking measures to prevent them.

2. Optimization of the control system. Simulation can help optimize an air traffic control system by determining the optimal path and timing for each aircraft.

3. Pilot Training Simulation can be used to train pilots and other aviation professionals by creating different scenarios and practicing how to react to them.

The absorber was measured by using a HP 5610B network analyzer that covers the range of 9–12 GHz, and two broadband horn antennas in a microwave anechoic chamber, as shown in Figure 3. As shown in Figure 3(b), the peak reflection is obtained, and then the maximum peak is remained by using bandpass time gating in vector network analyzer. The wire grid mesh ground plane can act as the metal plane at the microwaves. The fabricated structure shows absorption greater than 88% is in the frequency range of 6.4-12.1GHz and the bandwidth is 61.8% of center frequency. Figure 3 shows the measured absorptions for different polarizations of the incident wave. The optical transmittance of total structure is more than 62.4% as shown in Figure 3(b) [26,27].

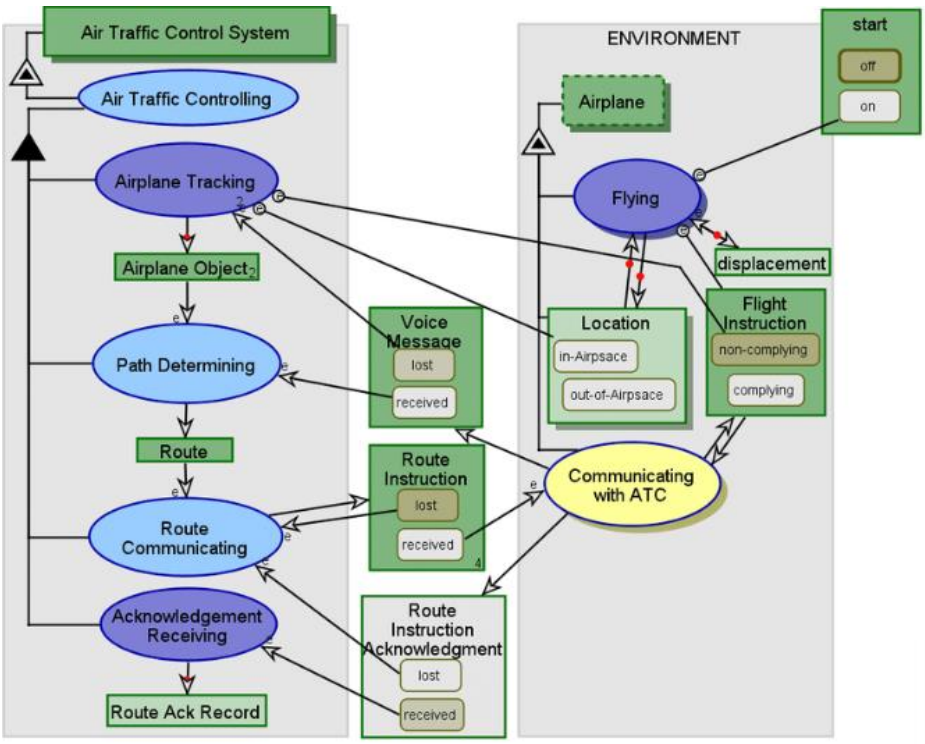

Figure. 2. **- Fault-tolerant model of air traffic control system.**

4. Algorithms for the automatic air traffic control system model

1. Hazard Identification Algorithm: This algorithm uses aircraft position and speed data, as well as weather conditions and other factors, to determine when a collision between aircraft is likely.

It involves obtaining data on the position and speed of aircraft, determining the distance between them, calculating the time to collision and checking that time against a threshold. If the time to collision is less than a threshold, the program displays a message about a potentially dangerous situation. This algorithm can be used in automatic air traffic control systems to prevent emergency situations and ensure flight safety [17-19].

An algorithm for identifying potentially dangerous situations involving a collision between aircraft may consist of the following steps:

Step 1. Obtaining data on the position and speed of aircraft;

Step 2. Determining the distance between them;

Step 3. Calculation of time to collision using the formula: time = distance / speed;

Step 4. Checking the time to collision against a threshold value;

Step 5. If the time to collision is less than the threshold value, a message about a potentially dangerous situation is displayed;

Step 6. The program repeats steps 1-5 for all pairs of aircraft in the observation area;

Step 7. The algorithm can be integrated into automatic air traffic control systems to prevent emergency situations and ensure flight safety.

2. Conflict Prevention Algorithm: This algorithm determines what actions should be taken to prevent conflicts. For example, the system can automatically change flight routes or aircraft speeds to avoid collisions. The algorithm may consist of the following steps:

Step 1. Obtaining data on the position and speed of aircraft from a radar surveillance system;

Step 2. Determining the distance between all pairs of aircraft;

Step 3. Calculation of time to collision using the formula: time = distance / speed;

Step 4. Setting a threshold value of time before a collision at which it is considered that an emergency situation is possible;

Step 5. Checking the time to collision for each pair of aircraft against a threshold value;

Step 6. If the time to collision is less than a threshold value, a message about a potentially dangerous situation is displayed and automatic notification of aircraft crews and regulatory authorities occurs;

Step 7. The program repeats steps 1-6 at specified intervals to ensure continuous monitoring of the airspace;

Step 8. The algorithm can be integrated into automatic air traffic control systems to prevent emergency situations and ensure flight safety.

3. Aircraft Flow Control Algorithm: This algorithm determines which aircraft should be allowed to take off and land, and what route they should take. It can also take into account airspace restrictions such as restricted areas or low visibility areas. Algorithm steps:

Step 1. Determination of aircraft flight routes based on planned flights and current airspace load;

Step 2. Distribution of aircraft along routes taking into account their speed and flight priority;

Step 3. Monitoring the position and speed of aircraft on routes;

Step 4. Analysis of the current airspace load and adjustment of aircraft routes if necessary;

Step 5. Determination of optimal time intervals between departures and arrivals of aircraft at airports;

Step 6. Monitoring the implementation of flight schedules and timely departure and arrival of aircraft;

Step 7. Regulating the flow of aircraft by delaying or accelerating aircraft departures and arrivals;

Step. 8. Ensuring flight safety by preventing aircraft from crossing routes and preventing collisions;

Step 9. Integration of an algorithm for controlling the flow of aircraft into automatic air traffic control systems to optimize the work of regulatory authorities and ensure flight safety.

4. Delay Allocation Algorithms: These algorithms are used to distribute landing and takeoff delays among different aircraft. They can take into account airline priorities and requirements, as well as airspace restrictions. Algorithm steps:

Step. 1. Determination of the current load of airspace and the predicted load in the near future;

Step. 2. Determining the priority of aircraft flights based on their type, flight direction and the presence of passengers who must transfer to another flight;

Step 3. Calculation of the optimal delay time for each aircraft, taking into account its speed and flight priority;

Step. 4. Determination of a new departure time for each delayed aircraft;

Step. 5. Notifying pilots and airlines about new departure and arrival times;

Step. 6. Monitoring the implementation of delays and adjusting the schedule if necessary;

Step. 7. Ensuring flight safety by preventing aircraft from crossing routes and preventing collisions;

Step. 8. Integration of an algorithm for controlling the flow of aircraft into automatic air traffic control systems to optimize the work of regulatory authorities and ensure flight safety.

5. Emergency Handling Algorithms: These algorithms are used to handle emergency situations such as engine failure or other technical problems. These may include evacuation procedures and other safety measures. Algorithm steps:

Step. 1. Detection of an emergency situation in the airspace or on board an aircraft;

Step. 2. Collection and analysis of data on the condition of the aircraft, its location, weather conditions and other factors that may affect further actions.

Step. 3. Identification of possible solutions to resolve the emergency and their assessment, taking into account flight safety and available resources.

Step. 4. Decide on the best course of action and implement it, including communication with pilots, airlines and other regulatory authorities.

Step. 5. Monitoring the implementation of the decision and adjustments if necessary.

Step. 6. Notifying the relevant services about the emergency situation that has occurred and the measures taken to eliminate it.

Step. 7. Analysis of the emergency situation and its consequences to determine possible improvements in the air traffic control system and prevent similar situations in the future.

Step. 8. Ensuring timely information to passengers and airlines about the emergency that has occurred and its consequences.

6. Algorithms for handling changes in weather conditions : These algorithms are used to handle changes in weather conditions such as thunderstorms or strong winds. These may include changing flight routes or aircraft speeds to avoid hazardous conditions. Algorithm steps:

Step. 1. Collection of information about current weather conditions in the flight area and at destination and departure airfields.

Step. 2. Analyze the data obtained and determine possible weather changes that could affect the flight.

Step. 3. Risk assessment and decision-making on the need to change the route, departure time or other actions to ensure flight safety.

Step. 4. Communication with pilots, airlines and other regulatory authorities to discuss measures taken and coordinate actions.

Step. 5. Monitoring weather changes and adjusting decisions if necessary.

Step. 6. Update flight plans and prepare for changes in real time.

Step. 7. Notifying passengers and airlines about possible delays or schedule changes.

Step. 8. Analysis of weather changes that have occurred and measures taken to determine possible improvements in the air traffic control system and prevent similar situations in the future.

7. Emergency Handling Algorithms : These algorithms are used to handle emergency situations such as terrorist attacks or other security threats. These may include evacuation procedures and other safety measures. Algorithm steps:

Step. 1. Detection of an abnormal situation in the flow of aircraft, for example, an engine failure on board an aircraft or a violation of the safe distance between aircraft.

Step. 2. Collection of information about the situation, including data on the position and speed of aircraft, weather conditions and other factors that may affect the further development of the situation.

Step. 3. Analysis of the data obtained and determination of possible consequences for the safety of the flight and the lives of people on board.

Step. 4. Deciding on measures to eliminate an emergency situation, for example, changing the flight route, changing the flight altitude or evacuating passengers.

Step. 5. Communication with pilots, airlines and other regulatory authorities to discuss measures taken and coordinate actions.

Step. 6. Monitoring changes in the situation and adjusting decisions if necessary.

Step. 7. Notifying passengers and airlines about changes and possible delays.

Step. 8. Analysis of changes that have occurred and measures taken to determine possible improvements in the air traffic control system and prevent similar situations in the future.

Program written in Python uses data about the position and speed of two aircraft to determine the distance between them and the time before collision. If the time to collision is less than 10 seconds, the program displays a message about a potentially dangerous situation.

5. Radome Test Range Design

The radome test range design is shown in Figure 1. The size of the test room was determined by considering the range length as well as providing adequate room for the positioner and radome handling space. The example shown below will test radome up to and including the Boeing 667 radome. The room dimensions are nominally 4.4 M height x 4.5 M width x 12.5M Length (14' H x 14'W x 38' L). The range antenna and the system antenna are precisely and permanently aligned with each other and do not move during the measurements.

The range antenna is transmitting and all testing is performed at the single frequency of operation of the weather radar which is typically within 9 to 9.8 GHz. A narrow band filter is used on the input of the measurement device to filter out any out of band signals.

Because the two directive antennas stay precisely aligned to each other throughout the test and because the filtering rejects any out of band signals, the measurement is largely impervious to off axis or out of band stray signals. As a result of this, the requirements for the test room are significantly reduced. Provided that there is not a significant source of in band stray radiation near by, a full fledged shielded anechoic chamber is not required. Eight (2) inch absorber is only needed on the end walls to knock down potential mutual coupling [24,27].

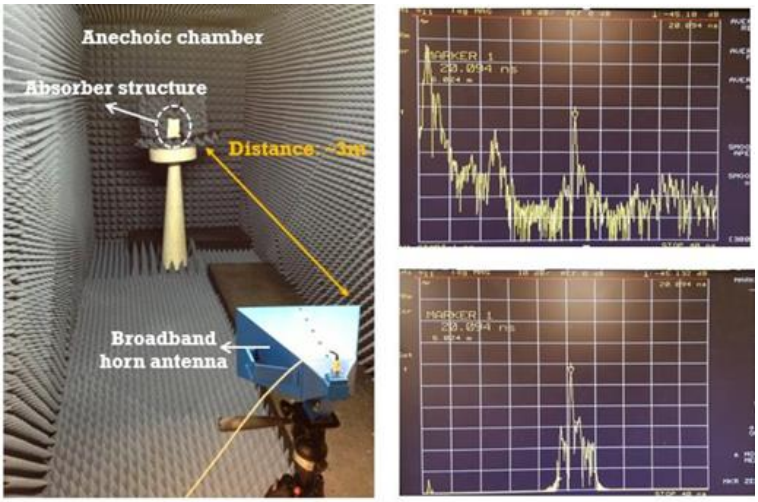

(a) (b)

Figure 3. - (a) Measurement set-up (b) Time gating in vector network analyzer.

6. Conclusion.

Real-time simulation of dynamic airspace conflict situations is a very important tool for ensuring air traffic safety. It allows you to predict possible conflicts and take measures to prevent them. In addition, simulation can be used to optimize control systems and pilot training.

References

1. *Ивахненко Ю. А., Варрик Н. М., Максимов В. Г.* Высокотемпературные радиопрозрачные керамические композиционные материалы для обтекателей антенн и других изделий авиационной техники (обзор)
2. *Абросимов В. К., Гончаренко В. И.* Моделирование движения и маневрирования летательных аппаратов на нейронных сетях // Известия ЮФУ. Технические науки. 2013. №3 (140).
3. *Каблов Е.Н.* Инновационные разработки ФГУП «ВИАМ» ГНЦ РФ по реализации «Стратегических направлений развития материалов и технологий их переработки на период до 2030 года» // Авиационные материалы и технологии. 2015. №1 (34). С. 3–33.
4. *Трофимов Д.А., Шалгунов С.И., Симонов-Емельянов И.Д.* / Модель и анализ построения свободного пространства в армирующем материале и оптимизации технологии получения конструкционных изделий из полимерных композитов // Конструкции из композиционных материалов. №.Э, 2022. С. 19 - 23.
5. *Кузнецов В.А., Амбросов Д.В.* Динамическая модель пространственно-распределенной воздушной цели // Системы управления, связи и безопасности. 2019. №2. С. 215-235.
6. *Шалгунов .И. Трофимов А.Н, Соколов В.И. Морозова И.В Прохорова Ю.С.* Особенности проектирования и разработки радиопрозрачных обтекателей и укрытий, работающих в сантиметровом и миллиметровом диапазонах радиоволн ОАО «НПО Стеклопластик» №3 ст-6 2014.
7. *Баяндина Т.А., Балакин В.Л.* Математические модели движения летательных аппаратов: электрон. курс лекций / В.Л. Балакин, Т.А. Баяндина; Минобрнауки России, Самар. гос. аэрокосм. ун-т им. С. П. Королёва (Нац. исслед. ун-т). - Электрон. текстовые и граф. дан. (1,14 Мбайт). - Самара, 2013. - 1 эл. опт. диск (CD-ROM). - Систем. требования: ПК Pentium; Windows 98 или выше
8. *Петров Н.А.* Разработка универсального алгоритма разрешения конфликтных ситуаций в воздушном пространстве при полете магистрального самолета // Научный вестник МГТУ ГА. 2014. №205.
9. *Акиншин Р.Н., Костромин А.Ю.* Обобщенный анализ информационных процессов в автоматизированных системах управления воздушным движением // Научный вестник МГТУ ГА. 2010. №158.

10. *Eshmuradov D.E., Jumamuratov B.A., Nabikhanova A.D.* Kompozit materiallarning radioshaffofligini monitoring qilishning zamonaviy tizimlari va vositalari // International Scientific Journal Science and innovation special issue “Modern problems and prospects of development of energy supply of digital technology facilities” March, 2024, 434c.

11. *Djumamurotov B.A., Sharipov G‘.N., O‘rolov J.A.* Samolyotning tumshuq qismi (обтекатель) ta'mirlash va sinovdan o'tkazishning metrologik ta'minoti, https://doi.org/10.5281/zenodo.10719692 International Scientific Journal Science and innovation special issue “Modern problems and prospects of development of energy supply of digital technology facilities” March, 2024, 49c.

12. *Эшмурадов Д. Э.* Зональная навигация в Республике Узбекистан. Монография. Т.: ТГТУ (2016).

13. *Поединок В. М.* Алгоритм автоматического управления траекторией самолета, обеспечивающий безопасный полет в условиях сложного рельефа местности // Ученые записки ЦАГИ. 2004. №1-2.

14. *Исмаилов О.М., Мирзахалилов С., Исмаилов М.О.* Исследование методов и алгоритмов репликации в системах с распределенной базой данных // Проблемы вычислительной и прикладной математики. – 2023. – №1(46). – С. 116-122.

15. *Исмаилов О.М., Исаков А.Ф., Маллаев Р.К.* "Алгоритм быстрого строкового сопоставления сетевых систем обнаружения вторжений." Актуальные проблемы оптимизации и автоматизации технологических процессов и производств 1.1 (2017): 132-137.

16. *Людомир А.В., Орлов В.С.* Имитационное моделирование динамической воздушной обстановки в управляемом воздушном пространстве // Прикладная информатика. 2014. №5 (53).

17. *Перунов Ю.М., Мацукевич В.В., Васильев А.А.* Зарубежные радиоэлектронные средства. Книга 3: Антенны Радиотехника, 2010. — 304 с.: ил. — ISBN: 978-5-88070-273-2.

18. *O. Russo, A. Colasante, G. Bellaveglia, F. Maggio L. Marcellini, L. Scialino, L. Rolo, J.C. Angevain& R. Midthasse* “State of the Art Materials for KU and KA Band Satellite Antenna Radome”, Telecommunications Ground Segments Workshop, Esa/Estec, 2012

19. *Огунвоул Блессинг Деле, Баланчук Е.А., Кандыба К.С.* Моделирование отказов в автоматизированной системе управления воздушным судном // Научный вестник МГТУ ГА. 2017. №4.

20. Технологические аспекты создания радиопрозрачных стеклокристаллических материалов на основе высокотемпературных алюмосиликатных систем (обзор) / А. С. Чайникова, М. Л. Ваганова, Н. Е. Щеголева, Ю. Е. Лебедева // Труды ВИАМ. – 2015. – № 11. – С. 26-39. – Библиогр.: 37-39 (51 назв.).

21. *N.P. Suprun; J.I. Ostrovetskaya; Yu.A. Scripnic; A.F. Yanenko*. Research of radiotransparency of materials for clothes at change of their moisture capacity. 13th International Crimean Conference Microwave and Telecommunication Technology, 2003. CriMiCo 2003. IEEE. Sevastopol, Ukraine. 30 January 2004. (https://ieeexplore.ieee.org/document/1256681).

22. *А.В.Любченков.* Методики измерения отражательнных характеристик радиопоглощающих материалов в радиолокационном диапазоне длин воли в интересах защиты информации на объектах информатизации.

23. *Шумов А.В., Плахотниченко А.А., Титова М.В.* Применение композитных материалов в радиолокационной технике. Отражатель антенного устройства Доплеровского метеорологического радиолокатора.

24. *О.Г.Жидкова, А.В.Бородавин, Д.В.Митюшкина, Н.В.Берсекова* “Проектирование радиопрозрачных конструкций из композиционных материалов”. Специальное конструкторско-технологическое бюро "Пластик", г. Сызрань, Самарская обл., Россия.

25. *Нестеренко Р.А., Магдин А.Г., Кудрявцев Д.В.,* Жанзакова Д.К. Применение композиционных материалов при проектировании носовых обтекателей летательных аппаратов. Вестник Брянского государственного технического университета Том 2021 № 2 (99).

26. *T. Bertuch, M. Pamies and others.* System aspects of a low-cost coherent radar system with AESA antenna for maritime applications. International Kharkov symposium on physics and engineering of microwaves, millimeter and submillimeter waves. 21-26 June 2010. Kharkiv, Ukraine. 10.1109/MSMW.2010.5545998.

27. *John Wilber.* Low Cost, Automated RTCA/DO-213 Compliant – Radome Test System P. 1-6

EVALUATION OF STRENGTH PROPERTIES IN SOILS ENHANCED BY LARGE CRUSHED STONE PARTICLES

Ibragimov B.T.[1], Nishonboev Sh.Z.[2], Abdusattorov A.A.[2], Rashidov J.[3]

[1]Academy of the Ministry of Emergency Situations of the Republic of Uzbekistan, Tashkent, Uzbekistan
[2]Tashkent State Transport University, Tashkent, Uzbekistan;
[3]Tashkent University of Architecture and Civil Engineering, Tashkent, Uzbekistan
E-mail: jasrash55@gmail.com

Abstract: *This paper explores how the strength of soil structures relies on various factors affecting the strength characteristics of coarse crushed stone soil. These factors include particle size, particle shape, normal stress levels, structural density, pressure impact on displacement resistance, and the correlation between displacement angle and packing density.*

Keywords: *broken rock, rocky soil, soil structure, soil particles, magnitude of stress, pressure, displacement, strength.*

1. Introduction

Based on information gleaned from research publications conducted both in the Commonwealth of Independent States and abroad, several factors influence the strength characteristics of large crushed rock soils. These factors include the integrity of the soil structure, the size and shape of soil particles, and the levels of normal stress [1-9]. Researchers have underscored the significance of structural density in determining the strength properties of large crushed stone soils and sands, particularly in the context of tunnel construction in mountainous regions. They unanimously assert that as the total volumetric weight of a given soil skeleton increases, thereby reducing its porosity, the angle of internal friction also increases correspondingly. This correlation mirrors findings by S.M. Atayya [10] in the examination of Nurek limestone.

2. Methods of research

The tests were carried out in a triaxial compression vacuum apparatus with a height of 500 mm and a diameter of 250 mm. The axial pressure on the sample did not exceed 7.5 kg/cm^2 , and the lateral pressure did not exceed 0.9 kg/cm^2 .

By comparing (comparing) the results shown in Table 1, we get the following: for 5-10 mm fractions, when σ_1 increases φ from 2.45 to 6-6.3 kg/cm^2 ، 2-2° decreases by 30, for 10-20 mm fractions, this value 2-2° was 30, and for fractions 20-30 mm it was equal to -4° .Thus, the effect of these pressures on the angle of internal friction was observed even at normal pressures that were not too large compared to each other.

Table 1

Effect of pressure on shear resistance

Material	Sizes of fractions,mm	Initial density, ρ, g/cm ^{3}	n, %	Lateral pressure, σ_3 , kg/cm ^{2}	Axial pressure, σ_1, kg/cm ^{2}	Angle of internal friction,φ
Nurek limestone	5-10	1.50	45	0.37	2.45	51 °20′
			45.5	0.36	2.7	50 °30′
			45.5	0.6	4.5	50°
			45	0.6	4.6	50 °30′
			46	0.9	6.0	48°
			45	0.9	6.3	48 °40′
	10-20	1.50	45.5	0.3	2.4	51 °30′
			45	0.3	2.44	51 °15′
			45.5	0.6	4.6	50 °30′
			45	0.6	4.5	50°
			46	0.9	5.8	47°
			46	0.9	6.2	48 °30′
	20-30	1.50	45	0.3	2.75	53°
			45.5	0.6	5.0	51 °30′
			45	0.9	6.4	49°
	30-55	1.77	35	0.5	4.1	52°
			35	0.9	7.5	52°

Consists of the products of weathering of argillaceous shales filled with sandstones, limestones, and tufforphyritic rocks [11-26]. The strength of large crushed stone soils is determined in laboratory conditions in large-scale rigs. the strength of large crushed stone soils is rarely determined directly in natural conditions, because their methodology is not fully developed.

In the mining of rocky rocks, depending on the strength of the rocks being mined, the amount of cracks, and the layers of weaker rocks in the base massif, a rock mass with different coefficients of polyhedra is obtained. The recommended granular composition of the pile mass for laying on the base prism of the Piskom dam: granular composition No. 1; 2; It is divided into three zones by curves 3 and 4 (Fig. 1).

3. Results

These compositions differ from each other in terms of the size of fine (fr.<5mm) particles of the mixture, large fractions, and coefficients of heterogeneity. Therefore, it is necessary to experimentally establish the calculation characteristics included in the project in each specific case . The task (problem) carried out includes the establishment of calculation characteristics of the rock mass for the most probable granular composition and the assessment of the change of the angle of displacement in the limit of 1-4 granular compositions. When conducting BPI (drilling and blasting operations), it is ~very difficult to obtain the minimum amount of 5% of small (fr.<5mm) particles of ground (limestones) in the grain composition of the rock mass, therefore, the range between 1-3 curves is adopted for the main composition. The curve of grain composition No. 2 is the average grain composition for this range, the calculation characteristics of which are determined by the appropriate amount of displacements according to the regulatory requirements for this composition.

For grain sizes 1-4, two tests were performed at each recorded load and density corresponding to the grain size. Such tests can only give approximate values of strength and allow evaluation of strength parameters within the limits of selected grain sizes of the stone. Experiments were carried out on large-scale devices, the use of such devices made it possible to conduct tests on the material containing 140 mm fractions fulfilling the $5D_{max} \leq d_{min}$ condition of the device. The presence of fractions of 500-900 mm in the natural material forces the transition to the model composition of the material. The granular compositions of the soil obtained on the basis of experiments and their model mixtures are shown in Fig. 1. The material presented for testing was divided into fractions that form model mixtures. Various compressive loads of samples: 2; 0.4; 0.8; Displacement at 1.2 MPa was carried out according to the guidelines. Based on the results of the displacement tests, Table 2 was created, according to this table, graphs of the displacement coefficient depending on the vertical load and density were constructed (Fig. 1).

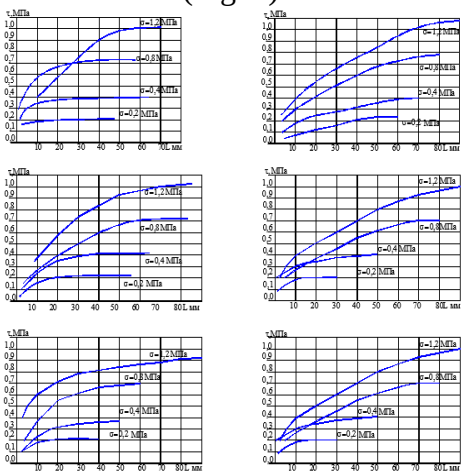

Figure 1. - **Granularity (m<5=18%) results of tests №1÷№24, carried out on the test of quarry soil № 7 with respect to displacement for curve № 2 of composition**

By cutting these graphs with horizontal straight lines, it was determined that the displacement angle depends on the density of the rock mass and the vertical stresses . It follows from the graphs that it is possible to regulate the strength properties of the material at different stresses with the

deposit density of the rock mass. Here $\rho_{d<140}$ - the density of the model mixture, t/m ^{3}; ρ_d^s - density of individual fractions (ρ_d^s =2.66 t/m ^{3}); m $_{<140}$ – amount of fractions smaller than 140 mm in natural soil.

Table 2

Results of the tests conducted to determine the displacement characteristics of pit soil No. 7

№	ρ_n -initial, ρ_k -final densities	Vertical loads, MPa							
		σ=0.2		σ=0.4		σ=0.8		σ=1.2	
		K $_{sd}$	τ, MPa	K $_{sd}$	τ, MPa	K $_{sd}$	τ, MPa	K $_{sd}$	τ, MPa
1	ρ_n	1,125 / 1.90	0.225	1.00 / 1.93	0.400	0.913 / 1.95	0.730	0.85 / 2.01	1.02
	ρ_k	1.92		1.94		2.07		2.05	
2	ρ_n	1,175 / 1.96	0.235	1,075 / 2.02	0.430	0.92 / 1.98	0.736	0.875 / 2.07	1.05
	ρ_k	1.96		2.05		2.02		2.10	
3	ρ_n	1.10 / 1.86	0.220	0.95 / 1.86	0.380	0.875 / 1.90	0.700	0.788 / 1.97	0.94
	ρ_k	1.87		1.87		1.94		1.99	
4	ρ_n	1.15 / 1.91	0.230	1,025 / 1.94	0.410	0.969 / 1.99	0.775	0.896 / 2.06	1.07
	ρ_k	1.93		1.94		2.02		2.08	
5	ρ_n	1,075 / 1.88	0.215	0.99 / 1.90	0.396	0.90 / 1.93	0.720	0.875 / 2.04	1.05
	ρ_k	1.89		1.90		1.96		2.06	
6	ρ_n	1.05 / 1.84	0.210	1.86 / 1.98	0.371	0.85 / 1.88	0.680	0.83 / 2.01	1,0
	ρ_k	1.85		1.99		1.93		2.03	

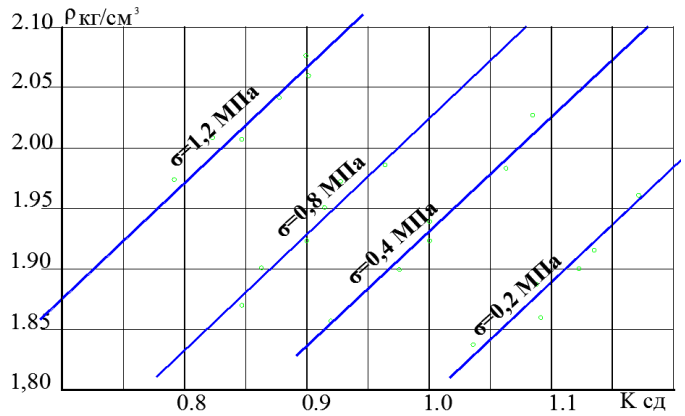

Figure 2. - **Graphs of dependence of angles on density and vertical loads (mixture No. 2, m $_{<5}$ =18%)**

Determining the required densities of laying the soil mass for natural soil αwas carried out at the time of determining the densities of stone laying depending on the grain composition and a reliable probability =0.95.

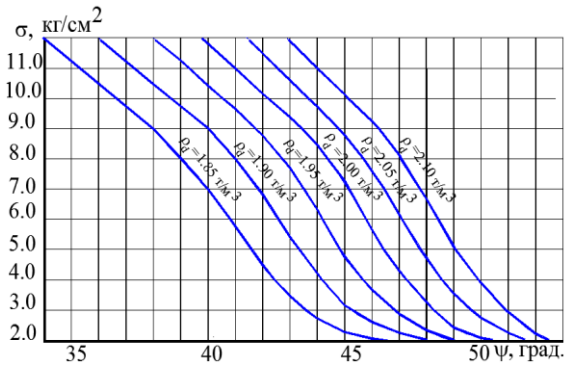

Figure 3. - **Graphs of dependence of rock mass displacement angles of quarry No. 7 on normal stresses and density of deposited material (curve No. 2, mixture No. 2, m<5=18%)**

mixture №4, $m_{<5}$ =5%, ρ_d^{mp} =1.75 t/m ^{3}; mixture #3, $m_{<5}$ =10%, ρ_d^{mp} =1.84 t/m ^{3}; mixture #2, $m_{<5}$ =18%, ρ_d^{mp} =2.02 t/m ^{3}; smes #1, $m_{<5}$ =25%, ρ_d^{mp} =2.18 t/m ^{3}; tg φ^n i c^n is presented in Table 4. The calculation of the normative and computational characteristics of τ=σtgφ+c was carried out according to the formulas of the method of least squares of linear correlations in the form of "tgφ" and "s" for the entire set of data obtained from experiments.

Table 3

Calculation of normative values

№	σ_i, kgs/cm ^{2}	σ_i^2, kgs/cm ^{2}	τ_i, kgs/cm ^{2}	$\sigma_i \cdot \tau_i$ kgs/cm ^{2}
1	2	4	2.20	4.40
2	2	4	2.30	4.60
3	2	4	2.15	4.30
4	2	4	2.10	4.20
5	2	4	2.35	4.70
6	2	4	2.25	4.50
7	4	16	3.80	15.20
8	4	16	4.0	16.40
9	4	16	3.96	15.84
10	4	16	3.71	14.84
11	4	16	4.30	17.20
12	4	16	4.00	16.00
13	8	64	7.0	56.0
14	8	64	7.75	62.0
15	8	64	7.20	57.6
16	8	64	6.80	54.4
17	8	64	7.36	58.88
18	8	64	7.30	58.40
19	12	144	9.45	113.40
20	12	144	10.75	129.0
21	12	144	10.50	126.0
22	12	144	10.00	120.0
23	12	144	10.50	126.0
24	12	144	10.20	122.4
Σ	**156**	**1368**	**142.03**	**1206.26**

The calculated values of the strength were obtained by applying pressure to the soil reserve coefficient, the physical essence of which is that the actual (actual) values of the strength characteristics do not exceed the limits of the limit strengths of the soil strength with a reasonable probability. The soil reserve coefficient is calculated by summing up the measurements of vertical stresses and displacement loads in pairs from σ_{min} to σ_{max}, and it depends on the change (variation) of these quantities, i.e., the "V" coefficient.

For the average curve of granular composition No. 2, we obtain the following using the calculation characteristics of the rock mass strength and the methodical instructions for calculating the dependences on the strength characteristics in the statically stressed state:

$$tg\psi = tg\varphi^{P} + \frac{c^{P}}{\sigma} \quad (1)$$

Table 4

Results of calculation of strength characteristics of rock mass in statically stressed condition

σ, MPa	0.2	0.4	0.6	0.8	1.0	1.2
tgψ	1.103	0.932	0.874	0.846	0.828	0.817
ψ°	47.8	43.0	41.2	40.2	39.6	39.2

As can be seen from the table, according to it, as the stresses increase, the strength decreases, which, in turn, allows us to conclude that the support prism of the dam should be restored from the state of tension, that is, in order to obtain homogeneity in terms of physical and mechanical properties of the material, the material should be distributed to different zones of the dam body. laying of this material is subject to requirements that ensure homogeneity of strength. According to the results of the conducted tests, the predicted approximate indicators of strength in the range of granularity material were obtained. Tests were carried out with two repetitions for each load on the sum of even values of normal and shear stresses for each granular composition of "Rybki" bounded by curves 1-4.

For each recorded value of the normal stress, the ultimate yield stress was determined based on the results obtained by the shearing (displacement) method. Displacement tests were performed in duplicate for each curve of #1-4 grain compositions. In the strength tests of the samples (mixtures No. 1-4) at the shear strength, after applying all steps of the vertical load of 0.2-3 MPa, the soil density in the pile that is more compatible with the shear moment than the initial density or the density after the shear was adopted. Experiments were conducted at densities close to the allowable density for the selected average range of densities. When carrying out experimental experiments with respect to displacement, the sample is placed in the installation by manual compaction of the soil and the same sample is tested, so the compactions performed cannot have a constant strength. It is worth noting the improper compaction of the samples in the optimal size of overcompaction when the amount of fine-grained soil in the soil composition is small. Bringing the obtained values of strength properties to the limits of single-grain content and required density was carried out according to the empirical formula.

$$tg\psi_2 = tg\psi_1 (\frac{\rho_{d2}}{\rho_{d1}})^{2/3} \quad (2)$$

where tg ψ_1 ; tg ψ_2 – required and obtained in experiments ρ_{d1} ; ρdisplacement angles corresponding to $\div_{d2}$. This calculation was performed for the required densities for each grain composition represented by curves 1 4 . The results of the displacement tests for each curve are shown in Table 5.

According to the results of tests of different granularities of the soil against displacement and the parameters of the displacements to the densities required for laying soils of this composition, ÷ diagrams of displacements were obtained for the entire range of changes in the granularity (1- 4 curves) (Fig. 4).

Table 5

Results obtained from tests against displacement of soil mass №7 for each granular composition represented by curves №1 4÷

Numbers of mixtures with fractions of less than 5 mm	Vertical load, MPa			
	0.2	0.4	0.8	1.2
t/r $_d$ τ-horizontal load, ρ_d -density (t/m ^{3})				
Mixture №3 m $_{<5}$ =10%	$\frac{2,35}{1,81};\frac{2,10}{1,80}$	$\frac{4,10}{1,84};\frac{3,90}{1,81}$	$\frac{7,80}{1,88};\frac{7,20}{1,84}$	$\frac{10,10}{1,89};\frac{10,50}{1,90}$
Mixture №2 m $_{<5}$ =18%	$\frac{2,25}{1,90};\frac{2,35}{1,96}$	$\frac{4,00}{1,93};\frac{4,3}{2,02}$	$\frac{7,30}{1,95};\frac{7,36}{1,98}$	$\frac{10,20}{2,01};\frac{10,5}{2,07}$
Mixture №1 m $_{<5}$ =25%	$\frac{2,52}{1,96};\frac{2,30}{2,01}$	$\frac{4,10}{1,97};\frac{4,6}{2,03}$	$\frac{6,8}{2,00};\frac{8,3}{2,07}$	$\frac{11,00}{2,04};\frac{11,0}{2,10}$

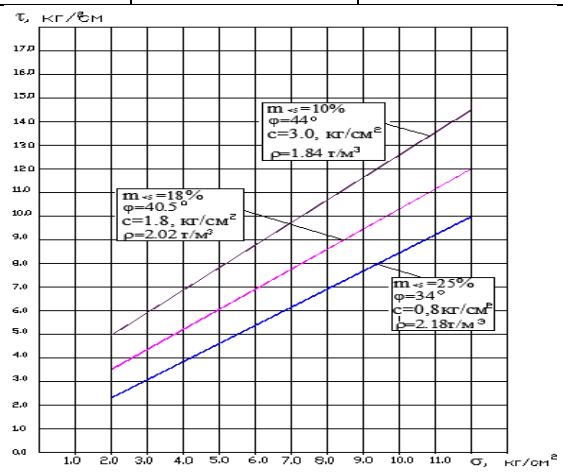

Figure 4. - **Dependence of t and s in different percent granularity of fine (fr. m $_{<5\ mm)}$ particle fractions**

4. Conclusion.

The strength properties remain consistently stable within the specified range when the material is deposited within the dam body at densities aligned with the grain composition. Regarding strength characteristics, the stone material exhibits minimal variation, with differences primarily observed in the coefficient of cohesion (maintaining a strength level within 5% of the absolute value). This coefficient demonstrates an increase as the soil composition of fine particles approaches its optimal composition.

References:

1. *Ahmad, Z., & Wah, K. H.* (2019). Strength characteristics of crushed stone aggregate. International Journal of Advanced Science and Technology, 28(12), 226-234.
2. *Al-Homoud, A. S.* (2003). Properties of concrete incorporating fine recycled aggregate. Cement and Concrete Research, 33(7), 1001-1006.
3. *Rashidov, J., Ibragimov, B., Chulliyev, F., & Salimova, I.* (2023). Structure of refractory materials based on local mineral raw. In E3S Web of Conferences (Vol. 401, p. 02057). EDP Sciences.
4. *Bagheri, A., & Abolfazli, M.* (2019). Influence of different amounts of crushed stones on the strength properties of cohesive soils. Construction and Building Materials, 211, 589-598.
5. *Baziar, M. H., Abedini, M., & Moghaddas Tafreshi, S. N.* (2012). Effect of crushed rock powder and polypropylene fibers on freeze-thaw resistance of high performance concrete. Cold Regions Science and Technology, 81, 42-51.
6. *Gao, L., Zhang, G., Wei, W., & Wang, C.* (2017). Mechanical properties of crushed stone materials with irregular shapes. Construction and Building Materials, 156, 974-980.
7. *Hamed, M. N. A., Abidin, M. H. Z., & Azmi, M.* (2020). Effect of coarse crushed stone on the geotechnical properties of soft cohesive soil. IOP Conference Series: Earth and Environmental Science, 499(1), 012074.
8. *Indraratna, B., Salim, W., Rujikiatkamjorn, C., & Christie, D.* (2012). Strength and deformation characteristics of railway ballast under monotonic and cyclic loading. Géotechnique, 62(10), 939-953.

9. *Khandelwal, M., Singh, T. N., & Verma, A. K. (*2019). Evaluation of strength characteristics of crushed stone aggregate composite. International Journal of Engineering Research and Technology, 12(1), 138-144.
10. *Ataya, S. M., Osman, S. E. M., Diab, S. M., & Wassif, O. M.* (2022). Improving of hayany date palm production by using K-Humate as soil application and magnetic water irrigation at south Sinai governorate Egypt. Egyptian Journal of Horticulture, 49(2), 129-146.
11. *Li, L., & Zou, Q.* (2020). Experimental study on the strength characteristics of graded crushed stone soil. Advances in Civil Engineering, 2020, 1-12.
12. *Lu, X., Wang, H., Ma, W., & Yin, Z.* (2021). Influence of graded crushed stone soil on bearing capacity and deformation properties of subgrade. Advances in Civil Engineering, 2021, 1-10.
13. *Manjunatha, C., & Nagaraj, T. S.* (2014). Strength and permeability characteristics of crushed stone aggregate layers stabilized with fly ash and lime. Geotechnical and Geological Engineering, 32(6), 1411-1421.
14. *Maraseni, T. N., & Son, H. T.* (2012). Technological advancements in CO2 emissions reduction in cement production. Renewable and Sustainable Energy Reviews, 16(2), 921-939.
15. *Naseri, M. S., Namazi, E., Soltanmohammadi, J., & Ghasemi, Y.* (2020). Shear strength of sandy soil reinforced with randomly distributed crushed stones. International Journal of Civil Engineering, 18(2), 193-206.
16. *Narov, R., Rashidov, J., & Turgunbayev, U.* (2023). Influence of type of modified fillers based on dune sand on properties of cement paste, stone, and on technological and strength properties of concrete. In E3S Web of Conferences (Vol. 401, p. 01076). EDP Sciences.
17. *Rao, M. N.* (2016). Strength characteristics of crushed stone aggregate as per IS 2386 Part IV–1963. International Journal of Civil Engineering and Technology, 7(4), 106-112.
18. *Rao, S. M., & Vijayasai, A.* (2018). Effect of crushed stone on the engineering properties of black cotton soil. International Journal of Innovative Research in Science, Engineering and Technology, 7(6), 6888-6892.
19. *Sajjad, M., Nazim, M., Rafiq, M., & Riaz, M.* (2018). Evaluation of geotechnical properties of crushed stone aggregate soil. International Journal of Engineering Trends and Technology, 59(4), 228-233.
20. *Sivapullaiah, P. V., Sridharan, A., & Prashanth, J. P.* (2010). Influence of crushed stone aggregate on consolidation characteristics of silty soils. Geotechnical Testing Journal, 33(2), 92-97.
21. *Taghavi, H. R., Khosravi, A., & Rashid, A. S. A.* (2019). A novel approach to predict the mechanical properties of a soil stabilized with crushed stones. Arabian Journal of Geosciences, 12(6), 1-14.
22. *Narov, R., Rashidov, J., & Yusupov, K.* (2023). Influence of compound additive on concrete in hot and dry climate. In E3S Web of Conferences (Vol. 365, p. 02012). EDP Sciences.
23. *Tang, C. S., & Shi, B.* (2011). Particle crushing and its effect on particle-size distribution and particle shape of a sand and gravel deposit. Engineering Geology, 126(1-2), 101-107.
24. *Vasan, R. M., & Devaraj, N.* (2017). Study on strength characteristics of crushed stone aggregate soil reinforced with geogrid. International Journal of Engineering and Techniques, 3(4), 26-31.
25. *Veiskarami, M., Rahmannejad, R., & Dehghan, S. H.* (2013). Effect of crushed stone dust on some properties of concrete. Cement and Concrete Research, 43, 112-117.
26. *Raupov, C., Shermuxamedov, U., & Karimova, A.* Assessment of strength and deformation of lightweight concrete and its components under triaxial compression, taking into account the macrostructure of the material. In E3S Web of Conferences (Vol. 264, p. 02015). CONMECHYDRO-2023, EDP Sciences. (2021)
27. *Shermukhamedov, U., Mirzaev, I., Karimova, A.B., & Askarova, D.* (2023) Calculation of the stress-strain state of monolithic bridges on the action of real seismic impacts. In E3S Web of Conferences (Vol. 401, p. 05080). EDP
28. *Shermukhamedov, U., Karimova, A.B., Abdullaev, A.R., & Khakimova, Ya.T.* (2023) Comparison of operating costs of reinforced concrete bridges and overpasses with different static schemes. In E3S Web of Conferences (Vol. 401, p. 02035). EDP Sciences. https://doi.org/10.1051/e3sconf/202340102035.
29. *Raupov, C., Karimova, A., Zokirov, F., Khakimova, Y.* Experimental and theoretical assessment of the long-term strength of lightweight concrete and its components under compression and tension, taking into account the macrostructure of the material. In E3S Web of Conferences 264, 02024 CONMECHYDRO-2021. (2021)
30. *Shermukhamedov U.Z., Karimova A.B., Khakimova Ya.T., Abdusattorov A.A.* Modern techniques for the construction of monolithic bridges // "Science and innovation" international scientific journal. Volume 1 Issue 8, UIF-2022: 8.2. ISSN: 2181-3337. – p. 790-799. https://doi.org/10.5281/zenodo.7441336.
31. *Shermukhamedov, U.Z., Karimova, A.B., & Zakirov, B.S.* (2023) Calculation of Continuous Reinforced Concrete Bridges And Overpasses Inseismically Hazardous Areas. In E3S Web of Conferences (Vol. 401, p. 01078). EDP.
32. *Mahamadazizovna, Mirzaeva Z., and Rasulmukhamedov M. Mahamadaminovich.* "Mathematical Modeling Of Calculation Of Spatial Structures Under Variable Loads." JournalNX, vol. 7, no. 05, 2021, pp. 246-249, doi:10.17605/OSF.IO/N9M47.
33. *Абдураимов УК, Абдусатторов АА.* (2022). Определение и оценки устойчивости откосов железнодорожного земляного полотна. Международная конференция академических наук 2. (Выпуск 22,), 70-75.
34. *Yadav, R. K., Kharade, P. P., & Khandelwal, M.* (2016). Assessment of strength characteristics of crushed stone aggregate soil stabilized with fly ash and phosphogypsum. International Journal of Advanced Research in Engineering and Technology, 7(3), 319-324.

NONLINEAR STRAIN OF FLEXIBLE SHELLS IN A MAGNETIC FIELD

Indiaminov R.[1], Djuraev A.[1], Shodmonov J.[2], Indiaminov M.[3]
[1]*Samarkand Branch Tashkent University of Information Technologies, Samarkand, Uzbekistan*
[2] *Kattakurgan branch of Samarkand State University, Kattakurgan, Uzbekistan*
[3]*Tashkent University of Information Technologies named after Muhammad al-Khwarizmi, Tashkent, Uzbekistan*
E-mail: r_indiaminov@mail.ru

Abstract: In models of motion of a continuous medium when considering electromagnetic effects in the mechanics of conjugate fields, the influence of the electromagnetic field on the thermomagnetomechanical behavior of the current-carrying body is accounted for through ponderomotive forces and their moments, and sources of complementary energy arising from the interaction of the current-carrying body with an external electromagnetic field. Ponderomotive forces act upon a current-carrying body placed in a non-uniform electromagnetic field. These forces arise from the interaction of electric and magnetic fields with the polarization and magnetization of the body. Sources of complementary energy arise from the interaction of the electromagnetic field with the movement of charged particles in a current-carrying body. Electromagnetic effects consideration in continuum mechanics is important for understanding the behavior of many conductive materials and devices, such as piezoelectrics and magnetostrictors. These materials are widely used in various fields, including acoustics, microelectronics, micromagnetoelectronics, optoelectronics, and robotics. Current-carrying shells are widely used in various engineering applications. Modeling nonlinear coupled magnetoelasticity problems of current-carrying shells is an important tool for understanding the behavior of these structures. Problems of nonlinear coupled magnetoelasticity describe the complex interaction between mechanical strains and electromagnetic fields in current-carrying shells. Using numerical simulation methods, the design of current-carrying shells can be analyzed and optimized to improve their performance and reliability. A two-dimensional model of magnetoelasticity of a current-carrying shell under the influence of non-stationary electromagnetic forces and mechanical loads was constructed. Numerical results were obtained, the influence of external electric current on the stress state was studied, and electromagnetic effects and the stress-strain state of the current-carrying shell were analyzed.

Keywords: Coupled problems of magnetoelasticity, current-carrying body, ponderomotive forces, conductivity, shell, electromagnetic field, geometric nonlinearity

1. Introduction.

Conjugate field mechanics studies systems in which several physical fields are simultaneously present and interact with each other. Examples of such systems are electromagnetic systems with electric and magnetic fields. The main method of conjugate field mechanics is the principle of virtual displacements, which allows one to establish a connection between external forces acting on the system and displacements of the system. This principle states that for any virtual system, that is, a system that satisfies all geometric relationships, the work of external forces is equal to the work of internal forces. The use of variational principles and theorems made it possible to formulate problems of analysis of conjugate fields in the form of minimization problems. This led to the development of powerful numerical methods that could solve these problems efficiently. The mechanics of conjugate fields has wide application in various fields of science and technology. It is used for the analysis and design of electromechanical and microelectromechanical systems. Magnetoelastic shells arise in many engineering applications such as magnetic bearings, actuators, and sensors; current-carrying materials are widely used in various fields including acoustics, microelectronics, micromagnetoelectronics, optoelectronics, and robotics. These shells are subject to mechanical and magnetic fields, resulting in complex interactions between stress fields, displacement fields, and magnetic fields. Analysis of these interactions requires two-dimensional magnetoelasticity models that consider the effects of mechanical loading and magnetic fields.

In recent years, rigorous mathematical methods for analyzing the conjugate fields of electrically conductive elements have been intensively developed within the mechanics of deformable electromagnetothermoelastic media [1-15].

In general, rigorous mathematical methods play an important role in understanding and analyzing conjugate fields in electrically conductive elements. These methods continue to evolve and find new applications in various fields of science and technology.

2. Statement of the problem. Models of magnetic elasticity.

When non-stationary magnetic fields affect metal structures, volumetric electrodynamic forces arise. These forces can have a significant impact on thin-walled elements, plates, and shells due to the nature of their structure and material. Electrodynamic forces arise due to the interaction of a magnetic field with conductors, which causes the induction of currents in the material. In this case, magnetic forces arise that act on the conductor and lead to the appearance of electro-dynamic forces. A class of nonlinear boundary value problems for thin-walled plates and shells describes the processes of strain in electrically conductive flexible bodies under the influence of forces and electromagnetic loads. Below we will consider one problem from this class - the stress-strain state calculation of a current-carrying shell of rotation of variable thickness subject to the combined action of a compressive axial force, an external non-stationary magnetic field, and an external non-stationary electric current. We assume that the electromagnetic hypotheses of magnetoelasticity of thin bodies are satisfied for the electric field strength $\vec{E}$ and magnetic field strength $\vec{H}$ [1]. Accepting these hypotheses allows us to reduce the problem of strain in a three-dimensional body to the problem of strain in an arbitrarily chosen coordinate surface.

Applying the principle of virtual displacements to the equation and the relationship between flexible shells of revolution in a magnetic field, according to the results given in [2,3,5,10,11], and considering the geometry of the shell, the complete system of equations that makes it possible to mathematically describe the nonlinear two-dimensional model of magnetoelasticity of flexible shells of revolution consists of magnetoelasticity equations

$$\frac{\partial}{\partial s}(rN_s) - \cos\varphi\, N_\theta + \frac{\partial S}{\partial \theta} + \frac{1}{R_s}\frac{\partial H}{\partial \theta} + \frac{r}{R_s}Q_s + r(P_s + \rho F_s^{\wedge}) = r\rho h\frac{\partial^2 u}{\partial t^2};$$

$$\frac{\partial N_\theta}{\partial \theta} + \frac{1}{r}\frac{\partial}{\partial S}(r^2 S) + \frac{\partial}{\partial s}(\sin\varphi\, H) + \frac{\cos\varphi}{R_s}H +$$

$$+\sin\varphi\, Q_\theta + r\left(P_\theta + \rho F_\theta^{\wedge}\right) = r\rho h\frac{\partial^2 v}{\partial t^2};$$

$$\frac{\partial}{\partial s}(rQ_s) + \frac{\partial Q_\theta}{\partial \theta} - \frac{r}{R_s}N_s - \sin\varphi\, N_\theta + r(P_z + \rho F_z^{\wedge}) = r\rho h\frac{\partial^2 w}{\partial t^2}; \qquad (1)$$

$$\frac{\partial H}{\partial \theta} + \frac{\partial}{\partial s}(rM_s) - \cos\varphi\, M_\theta - rQ_s - r\left(N_s - \frac{\sin\varphi}{r}M_\theta\right)\vartheta_s - rS\vartheta_\theta = 0;$$

$$\frac{1}{r}\frac{\partial}{\partial S}(r^2 H) + \frac{\partial M_\theta}{\partial \theta} - rQ_\theta - r\left(N_\theta - \frac{1}{R_s}M_s\right)\vartheta_\theta - rS\vartheta_s = 0;$$

$$-\frac{\partial B_z}{\partial t} = \frac{1}{r}\left(\frac{\partial(rE_\theta)}{\partial s} - \frac{1}{r}\frac{\partial E_s}{\partial \theta}\right);$$

$$\sigma\left[E_s - \frac{\partial v}{\partial t}B_z - 0{,}5\frac{\partial w}{\partial t}(B_\theta^+ + B_\theta^-)\right] = \frac{1}{r}\frac{\partial H_z}{\partial \theta} + \frac{H_\theta^+ - H_\theta^-}{h};$$

$$\sigma\left[E_\theta - \frac{\partial u}{\partial t}B_z + 0{,}5\frac{\partial w}{\partial t}(B_\theta^+ + B_\theta^-)\right] = -\frac{\partial H_z}{\partial s} + \frac{H_\theta^+ - H_\theta^-}{h};$$

expressions for strains:

$$\varepsilon_{ss} = \frac{\partial u}{\partial s} + \frac{w}{R_s} + \frac{1}{2}\vartheta_s^2;\ \ \varepsilon_{\theta\theta} = \frac{1}{r}\frac{\partial v}{\partial \theta} + \frac{\cos\varphi}{r}u + \frac{\sin\varphi}{r}w + \frac{1}{2}\vartheta_\theta^2;$$

$$\varepsilon_{s\theta} = \frac{1}{r}\frac{\partial u}{\partial \theta} + r\frac{\partial}{\partial s}\left(\frac{v}{r}\right) + \vartheta_s\vartheta_\theta;\ \ \chi_{ss} = \frac{\partial \vartheta_s}{\partial s},\ \ \chi_{\theta\theta} = \frac{1}{r}\frac{\partial \vartheta_\theta}{\partial \theta} + \frac{\cos\varphi}{r}\vartheta_s; \qquad (2)$$

$$\chi_{s\theta} = \frac{\partial \vartheta_\theta}{\partial s} + \frac{1}{r}\frac{\partial \vartheta_s}{\partial \theta} - \frac{\cos\varphi}{r}\vartheta_\theta + \frac{1}{R_s}\left(\frac{1}{r}\frac{\partial u}{\partial \theta} - \frac{\cos\varphi}{r}v\right) + \frac{\sin\varphi}{r}\frac{\partial v}{\partial s},$$

where $\vartheta_s = -\frac{\partial w}{\partial s} + \frac{u}{R_s}$; $\vartheta_\theta = -\frac{1}{r}\frac{\partial w}{\partial \theta} + \frac{\sin\varphi}{r}v$ are the rotation angles of the normal;

elasticity relations:

$$N_s = \frac{Eh}{1-\nu^2}\,[\varepsilon_{ss} + \nu\varepsilon_{\theta\theta}];$$

$$N_\theta = \frac{Eh}{1-\nu^2}[\varepsilon_{\theta\theta} + \nu\varepsilon_{ss}];$$
$$S = \frac{Eh}{2(1+\nu^2)}\varepsilon_{s\theta}; \quad H = \frac{Eh}{12(1+\nu^2)}\chi_{s\theta};$$
$$M_s = \frac{Eh^3}{12(1-\nu^2)}[\chi_{ss} + \nu\chi_{\theta\theta}];$$
$$M_\theta = \frac{Eh^3}{12(1-\nu^2)}[\chi_{\theta\theta} + \nu\chi_{ss}]; \tag{3}$$

Lorentz force components:

$$\rho F_s^{\wedge} = hJ_{\theta st}B_z + \sigma hE_\theta B_z + \sigma h\Big\{0{,}5\frac{\partial w}{\partial t}(B_s^+ + B_s^-)B_z -$$
$$-\frac{\partial u}{\partial t}B_z^2 - \frac{\partial u}{\partial t}\left[0{,}25(B_\theta^+ + B_\theta^-)^2 + \frac{1}{12}(B_\theta^+ + B_\theta^-)^2\right] +$$
$$+\frac{\partial v}{\partial t}\left[0{,}25(B_s^+ + B_s^-)(B_\theta^+ + B_\theta^-) + \frac{1}{12}(B_s^+ - B_s^-)(B_\theta^+ - B_\theta^-)\right]\Big\};$$
$$\rho F_\theta^{\wedge} = -hJ_{s\,st}B_z - \frac{h}{r\mu}\frac{\partial B_z}{\partial\theta}B_z +$$
$$+\sigma h\Big\{\frac{\partial u}{\partial t}\left[0{,}25(B_s^+ + B_s^-)(B_\theta^+ + B_\theta^-) + \frac{1}{12}(B_s^+ - B_s^-)(B_\theta^+ - B_\theta^-)\right] -$$
$$-\frac{\partial v}{\partial t}\left[0{,}25(B_\theta^+ + B_\theta^-)^2 + \frac{1}{12}(B_\theta^+ - B_\theta^-)^2\right] - \frac{B_\theta^+ - B_\theta^-}{\mu}B_z; \tag{4}$$
$$\rho F_z^{\wedge} = 0{,}5h[J_{scm}(B_\theta^+ + B_\theta^-) - J_{\theta st}(B_s^+ + B_s^-)] + \frac{h}{2r\mu}\frac{\partial B_z}{\partial\theta}(B_\theta^+ + B_\theta^-) -$$
$$-0{,}5\sigma hE_\theta(B_s^+ + B_s^-) + \sigma h\Big\{0{,}5\frac{\partial u}{\partial t}(B_s^+ + B_s^-)B_z - \frac{\partial w}{\partial t}[0{,}25(B_s^+ + B_s^-)^2 +$$
$$+\frac{1}{12}(B_\theta^+ - B_\theta^-)^2 + \frac{1}{12}(B_s^+ - B_s^-)^2]\Big\} + \frac{(B_\theta^+)^2 - (B_\theta^-)^2}{\mu}.$$

Here N_s, N_θ are the normal and shear forces; S is the shear force; Q_s, Q_θ are the transverse forces; M_s, M_θ, H are the bending and torque moments, respectively; u,v,w are the components of displacements; E_s, E_θ are the components of the electric field strength; B_z is the normal component of magnetic induction; $B_s^\pm, B_\theta^\pm$ are the known components of magnetic induction on the surface of the shell; $J_{sст}$, $J_{\theta ст}$ are the components of electric current density from an external source; σ is the electrical conductivity; $h = h(\alpha,\beta)$ is the shell thickness; E is Young's modulus; ν is Poisson's ratio; $\varepsilon_{ss}, \varepsilon_{\theta\theta}, \varepsilon_{s\theta}, \chi_{ss}, \chi_{\theta\theta}, \chi_{s\theta}$ are the shell strain characteristics; R_s, R_θ are the radii of principal curvatures.

Systems of equations (1)-(3) constitute a complete closed coupled system of nonlinear differential equations for the magnetoelasticity of a current-carrying flexible shell.

We assume that all components entering the equations do not depend on coordinate θ from relations (1)-(3) and obtain the following coupled system:

$$\frac{\partial u}{\partial s} = \frac{1-\nu^2}{Eh}N_s - \frac{\nu\cos\varphi}{r}u - \left(\frac{1}{R_s} + \frac{\nu\sin\varphi}{r}\right) - \frac{1}{2}\vartheta_s^2, \qquad \frac{\partial w}{\partial s} = -\vartheta_s + \frac{u}{R_s},$$
$$\frac{\partial\vartheta_s}{\partial s} = \frac{12(1-\nu^2)}{Eh^3}M_s - \frac{\nu\cos\varphi}{r}\vartheta_s,$$
$$\frac{\partial N_s}{\partial s} = \frac{\cos\varphi}{r}[\nu - 1]N_s + Eh\left(\frac{\cos\varphi}{r}u + \frac{\sin\varphi}{r}w\right) - \frac{1}{R_s}Q_s - P_s -$$
$$-hJ_{\theta ст}B_\gamma - \sigma h\left[E_\theta B_\gamma + 0{,}5\frac{\partial w}{\partial t}B_\gamma(B_s^+ + B_s^-) - \frac{\partial u}{\partial t}B_\gamma^2\right] + \rho h\frac{\partial^2 u}{\partial t^2},$$
$$\frac{\partial Q_s}{\partial s} = -\frac{\cos\varphi}{r}Q_s + \left(\frac{1}{R_s} + \frac{\nu\sin\varphi}{r}\right)N_s + Eh\frac{\sin\varphi}{r}\left(\frac{\cos\varphi}{r}u + \frac{\sin\varphi}{r}w\right) - P_\gamma +$$

$$+0{,}5hJ_{\theta\text{СТ}}(B_s^+ + B_s^-) + \sigma h\left[0{,}5E_\theta(B_s^+ + B_s^-) + 0{,}25\frac{\partial w}{\partial t}(B_s^+ + B_s^-)^2 + \right.$$
$$\left. + \frac{1}{12}\frac{\partial w}{\partial t}(B_s^+ - B_s^-)^2 - 0{,}5\frac{\partial u}{\partial t}B_\gamma(B_s^+ + B_s^-)\right] + \rho h\frac{\partial^2 w}{\partial t^2}, \qquad (5)$$
$$\frac{\partial M_s}{\partial s} = \frac{\cos\varphi}{r}\left[(\nu - 1)M_s + \frac{Eh^3}{12}\frac{\cos\varphi}{r}\vartheta_s\right] + Q_s + N_s v_s -$$
$$-\frac{\sin\varphi}{r}\left(\nu M_s + \frac{Eh^3}{12}\frac{\cos\varphi}{r}\vartheta_s\right)\vartheta_s, \qquad \frac{\partial E_\theta}{\partial s} = -\frac{\partial B_\gamma}{\partial t} - \frac{\cos\varphi}{r}E_\theta,$$
$$\frac{\partial B_\gamma}{\partial s} = -\sigma\mu\left[E_\theta + 0{,}5\frac{\partial w}{\partial t}(B_s^+ + B_s^-) - \frac{\partial u}{\partial t}B_\gamma\right] - \frac{(B_s^+ - B_s^-)}{h}.$$

Here the sought-for functions are $u, w, \vartheta_s, N_s, Q_s, M_s, E_\theta, B_\gamma$. The resulting system of eighth-order nonlinear differential equations describes mathematical models of the magnetoelasticity of a flexible shell of revolution located in a non-stationary magnetic field.

3. Methodology for solving the magnetoelasticity problem.

To numerically solve the magnetoelastic boundary value problem, according to [2,3,5,10,11,16,17,18,19,20], a technique is proposed that uses the methods of Newmark, quasi-linearization, and discrete orthogonalization. When studying the stressed state of flexible current-carrying shells of rotation of arbitrary cross-section, and conjugate shells of various shapes under the influence of a non-stationary magnetic field, we select the following functions as the sought-for ones:

$$u_x, u_z, \vartheta_s, N_x, N_z, M_s, E_\theta, B_\gamma, \qquad (6)$$

where u_x, u_z are radial and axial displacements, ϑ_s is the normal rotation angle, N_x, N_z are radial and axial forces, M_s is the bending moment, E_θ is the electric field strength, B_γ is the magnetic field induction.

These quantities are related to displacements u, w and forces N_s, Q_s as:

$$N_x = N_s\cos\varphi + Q_s\sin\varphi, \quad u_x = u\cos\varphi + w\sin\varphi,$$
$$N_z = N_s\sin\varphi - Q_s\cos\varphi, \qquad u_z = u\sin\varphi - w\cos\varphi. \qquad (7)$$

The use of these functions makes it possible to construct an algorithm for solving problems for shells of revolution of an arbitrary cross-section when the conditions for the simplest conjugation of shells of revolution are met. In this case, the elasticity relations [2,3] are written in the following form:

$$\varepsilon_{ss} = \frac{1-\nu^2}{Eh}(N_x\cos\varphi + N_z\sin\varphi) - \frac{\nu}{r}u_x, \qquad \varepsilon_{\theta\theta} = \frac{u_x}{r},$$
$$\chi_{ss} = \frac{12(1-\nu^2)}{Eh^3}M_s - \frac{\nu\cos\varphi}{r}\vartheta_s, \qquad \chi_{\theta\theta} = \frac{\cos\varphi}{r}\vartheta_s, \qquad (8)$$
$$N_\theta = \nu(N_x\cos\varphi + N_z\sin\varphi) + \frac{Eh}{r}u_x, \qquad M_\theta = \nu M_s + \frac{Eh^3}{12}\frac{\cos\varphi}{r}\vartheta_s.$$

Considering ((6), (7)), we obtain a resolving system of nonlinear differential equations of magnetoelasticity that describes the stress-strain state of shells of rotation of an arbitrary cross-section:

$$\frac{\partial u_x}{\partial s} = \frac{1-\nu^2}{Eh}(\cos\varphi\, N_x + \sin\varphi\, N_z)\cos\varphi + \frac{\nu\cos\varphi}{r}u_x + \frac{1}{R_s}u_z - \sin\varphi\,\vartheta_s - \frac{\cos\varphi}{2}\vartheta_s^2$$
$$\frac{\partial u_z}{\partial s} = \frac{1-\nu^2}{Eh}(\cos\varphi\, N_x + \sin\varphi\, N_z)\sin\varphi + \frac{\nu\sin\varphi}{r}u_x - \frac{1}{R_s}u_x + \cos\varphi\,\vartheta_s - \frac{\sin\varphi}{2}\vartheta_s^2$$
$$\frac{\partial\vartheta_s}{\partial s} = \frac{12(1-\nu^2)}{Eh^3}M_s - \frac{\nu\cos\varphi}{r}\vartheta_s, \qquad (9)$$
$$\frac{\partial N_x}{\partial s} = \frac{\cos\varphi}{r}(\nu - 1)N_x + \left(\frac{1}{R_s} + \frac{\nu\sin\varphi}{r}\right)N_z + \frac{Eh}{r^2}u_x - (P_r + \rho\hat{F_r}) +$$

$$+\rho h\left(\frac{\partial^2 u_x}{\partial t^2}\cos\varphi+\frac{\partial^2 u_z}{\partial t^2}\sin\varphi\right),$$

$$\frac{\partial N_z}{\partial s}=-\frac{\cos\varphi}{r}N_z-\frac{1}{R_s}N_x-(P_z+\rho F_z^{\wedge})+\rho h\left(\frac{\partial^2 u_x}{\partial t^2}\sin\varphi-\frac{\partial^2 u_z}{\partial t^2}\cos\varphi\right),$$

$$\frac{\partial M_s}{\partial s}=\frac{\cos\varphi}{r}(\nu-1)M_s+\frac{Eh^3}{12}\frac{\cos^2\varphi}{r^2}\vartheta_s+\cos\varphi\,N_x-\sin\varphi\,N_z+$$

$$+(\cos\varphi\,N_x+\sin\varphi\,N_z)\vartheta_s-\frac{\nu\sin\varphi}{r}M_s\vartheta_s-\frac{Eh^3}{12}\frac{\cos\varphi\sin\varphi}{r}\vartheta_s^2\,,$$

$$\frac{\partial E_\theta}{\partial s}=-\frac{\partial B_\gamma}{\partial t}-\frac{\cos\varphi}{r}E_\theta\,,$$

$$\frac{\partial B_\gamma}{\partial s}=-\sigma\mu\left[E_\theta+0{,}5\left(\frac{\partial u_x}{\partial t}\sin\varphi-\frac{\partial u_z}{\partial t}\cos\varphi\right)(B_s^+ + B_s^-)-\mu J_{\theta\text{ст}}-\right.$$

$$\left.-\left(\frac{\partial u_x}{\partial t}\cos\varphi+\frac{\partial u_z}{\partial t}\sin\varphi\right)B_\gamma\right]+\frac{B_s^+ - B_s^-}{h},$$

where

$$P_r=P_s\cos\varphi+P_\gamma\sin\varphi,\quad P_z=P_s\sin\varphi-P_\gamma\cos\varphi\,,$$

$$F_r^{\wedge}=F_s^{\wedge}\cos\varphi+F_\gamma^{\wedge}\sin\varphi,\quad F_z^{\wedge}=F_s^{\wedge}\sin\varphi-F_\gamma^{\wedge}\cos\varphi.$$

The Lorentz force components $F_s^{\wedge}, F_\gamma^{\wedge}$ take the following form:

$$\rho F_r^{\wedge}=hJ_{\theta\text{ст}}B_\gamma+\sigma h\left[E_\theta B_\gamma+0{,}5\left(\frac{\partial u_x}{\partial t}\sin\varphi-\frac{\partial u_z}{\partial t}\cos\varphi\right)(B_s^+ + B_s^-)B_\gamma-\right.$$

$$\left.-\left(\frac{\partial u_x}{\partial t}\cos\varphi+\frac{\partial u_z}{\partial t}\sin\varphi\right)B_\gamma^2\right]$$

$$\rho F_z^{\wedge}=-0{,}5hJ_{\theta\text{ст}}(B_s^+ + B_s^-)-\sigma h\{0{,}5E_\theta(B_s^+ + B_s^-)+\left(\frac{\partial u_x}{\partial t}\sin\varphi-\frac{\partial u_z}{\partial t}\cos\varphi\right)$$

$$\times\left[0{,}25(B_s^+ + +B_s^-)^2\right.$$

$$\left.+\frac{1}{12}(B_s^+ - B_s^-)^2\right]-0{,}5\left(\frac{\partial u_x}{\partial t}\cos\varphi+\frac{\partial u_z}{\partial t}\sin\varphi\right)B_\gamma(B_s^+ + B_s^-)\Big\}. \qquad (10)$$

Here, $B_s^{\pm}$ refers to the value of magnetic induction on the surfaces of the shell:

$$B_s\left(s,\pm\frac{h}{2},t\right)=B_s^{\pm}(s,t). \qquad (11)$$

After applying the Newmark scheme and the quasi-linearization method to a resolving system (9), we obtain a coupled system in the following form:

$$\frac{du_x^{(k+1)}}{dm}=\frac{1-\nu_s\nu_\theta}{\rho e_s h}\left(cos\varphi N_x^{(k+1)}+sin\varphi N_z^{(k+1)}\right)cos\varphi-\frac{\nu_\theta cos\varphi}{\rho r}u_x^{(k+1)}+$$

$$+\frac{1}{\rho R_s}u_z^{(k+1)}-\frac{sin\varphi\theta_s^{(k+1)}}{\rho}-\frac{cos\varphi}{2\rho}\left(-\left(\theta_s^{(k)}\right)^2+2\theta_s^{(k+1)}\theta_s^{(k)}\right);$$

$$\frac{du_z^{(k+1)}}{dm}=\frac{1-\nu_s\nu_\theta}{\rho e_s h}\left(cos\varphi N_x^{(k+1)}+sin\varphi N_z^{(k+1)}\right)sin\varphi-\frac{\nu_\theta sin\varphi}{\rho r}u_x^{(k+1)}+$$

$$+\frac{1}{\rho R_s}u_z^{(k+1)}-\frac{cos\varphi\theta_s^{(k+1)}}{\rho}-\frac{sin\varphi}{2\rho}\left(-\left(\theta_s^{(k)}\right)^2+2\theta_s^{(k+1)}\theta_s^{(k)}\right);$$

$$\frac{d\theta_s^{(k+1)}}{dm}=\frac{12(1-\nu_s\nu_\theta)}{\rho e_s h^3}M_s^{(k+1)}-\frac{\nu_\theta cos\varphi}{\rho r}\theta_s^{(k+1)};$$

$$\frac{dN_x^{(k+1)}}{dm}=\frac{cos\varphi}{\rho r}\left(\nu_s\frac{e_\theta}{e_s}-1\right)N_x^{(k+1)}+\frac{1}{\rho}\left(\frac{1}{R_s}+\frac{\nu_\theta sin\varphi}{r}\right)N_z^{(k+1)}+\frac{e_\theta h}{\rho r^2}u_z^{(k+1)}-$$

$$-\frac{cos\varphi}{\rho}P_s^{(k+1)}-\frac{cos\varphi}{\rho}\Big[-hJ_{\theta CT}B_\zeta^{(k+1)}+\sigma_1 h\Big\{\Big(-E_\theta^{(k)}B_\zeta^{(k)}+E_\theta^{(k+1)}B_\zeta^{(k)}+$$

$$+E_\theta^{(k)}B_\zeta^{(k+1)}\Big)+0{,}5\Big(\Big(-\Big(\dot{u}_x^{(t+\Delta t)}\Big)^{(k)}B_\zeta^{(k)}+\Big(\dot{u}_x^{(t+\Delta t)}\Big)^{(k+1)}B_\zeta^{(k)}+$$

$$+\Big(\dot{u}_x^{(t+\Delta t)}\Big)^{(k)}B_\zeta^{(k+1)}\Big)sin\varphi-\Big(-\Big(\dot{u}_z^{(t+\Delta t)}\Big)^{(k)}B_\zeta^{(k)}+\Big(\dot{u}_z^{(t+\Delta t)}\Big)^{(k+1)}B_\zeta^{(k)}+$$

$$+\Big(\dot{u}_z^{(t+\Delta t)}\Big)^{(k)}B_\zeta^{(k+1)}\Big)cos\varphi)(B_s^++B_s^-)-\Big(-\Big(B_\zeta^{(k)}\Big)^2\Big(\dot{u}_x^{(t+\Delta t)}\Big)^{(k)}+$$

$$+\Big(B_\zeta^{(k)}\Big)^2\Big(\dot{u}_x^{(t+\Delta t)}\Big)^{(k+1)}+2B_\zeta^{(k+1)}B_\zeta^{(k)}\Big(\dot{u}_x^{(t+\Delta t)}\Big)^{(k)}\Big)cos\varphi+\Big(-\Big(B_\zeta^{(k)}\Big)^2\cdot$$

$$\cdot\Big(\dot{u}_z^{(t+\Delta t)}\Big)^{(k)}+\Big(B_\zeta^{(k)}\Big)^2\Big(\dot{u}_z^{(t+\Delta t)}\Big)^{(k+1)}+2B_\zeta^{(k+1)}B_\zeta^{(k)}\Big(\dot{u}_z^{(t+\Delta t)}\Big)^{(k)}\Big)sin\varphi\Big\}\Big]-$$

$$-\frac{sin\varphi}{\rho}P_\zeta^{(k+1)}-\frac{sin\varphi}{\rho}\Big[0.5hJ_{\theta CT}(B_s^++B_s^-)+\sigma_3 h\Big\{-0.5E_\theta^{(k+1)}(B_s^++B_s^-)-$$

$$-\Big(\Big(\dot{u}_x^{(t+\Delta t)}\Big)^{(k+1)}sin\varphi-\Big(\dot{u}_z^{(t+\Delta t)}\Big)^{(k+1)}cos\varphi\Big)(0.25(B_s^++B_s^-)^2+$$

$$+\frac{1}{12}(B_s^++B_s^-)^2\Big)+0.5\Big(\Big(-\Big(\dot{u}_x^{(t+\Delta t)}\Big)^{(k)}B_\zeta^{(k)}+\Big(\dot{u}_x^{(t+\Delta t)}\Big)^{(k+1)}B_\zeta^{(k)}+$$

$$+\Big(\dot{u}_x^{(t+\Delta t)}\Big)^{(k)}B_\zeta^{(k+1)}\Big)sin\varphi-\Big(-\Big(\dot{u}_z^{(t+\Delta t)}\Big)^{(k)}B_\zeta^{(k)}+\Big(\dot{u}_z^{(t+\Delta t)}\Big)^{(k+1)}B_\zeta^{(k)}+$$

$$+\Big(\dot{u}_z^{(t+\Delta t)}\Big)^{(k)}B_\zeta^{(k+1)}\Big)cos\varphi\Big)(B_s^++B_s^-)\}\Big]+h\Big(\ddot{u}_x^{(t+\Delta t)}\Big)^{(k+1)};$$

$$\frac{dN_z^{(k+1)}}{dm}=-\frac{cos\varphi}{\rho r}N_z^{(k+1)}+\frac{1}{\rho R_s}N_x^{(k+1)}-\frac{sin\varphi}{\rho}P_s^{(k+1)}-\frac{sin\varphi}{\rho}\Big[-hJ_{\theta CT}B_\zeta^{(k+1)}+$$

$$+\sigma_1 h\Big\{\Big(-E_\theta^{(k)}B_\zeta^{(k)}+E_\theta^{(k+1)}B_\zeta^{(k)}+E_\theta^{(k)}B_\zeta^{(k+1)}\Big)+0{,}5\Big(-\Big(\dot{u}_x^{(t+\Delta t)}\Big)^{(k)}B_\zeta^{(k)}+$$

$$+\Big(\dot{u}_x^{(t+\Delta t)}\Big)^{(k+1)}B_\zeta^{(k)}+\Big(\dot{u}_x^{(t+\Delta t)}\Big)^{(k)}B_\zeta^{(k+1)}\Big)sin\varphi-\Big(-\Big(\dot{u}_z^{(t+\Delta t)}\Big)^{(k)}B_\zeta^{(k)}+$$

$$+\Big(\dot{u}_z^{(t+\Delta t)}\Big)^{(k+1)}B_\zeta^{(k)}+\Big(\dot{u}_z^{(t+\Delta t)}\Big)^{(k)}B_\zeta^{(k+1)}\Big)cos\varphi)(B_s^++B_s^-)-$$

$$-\Big(-\Big(B_\zeta^{(k)}\Big)^2\Big(\dot{u}_x^{(t+\Delta t)}\Big)^{(k)}+\Big(B_\zeta^{(k)}\Big)^2\Big(\dot{u}_x^{(t+\Delta t)}\Big)^{(k+1)}+2B_\zeta^{(k+1)}B_\zeta^{(k)}\Big(\dot{u}_x^{(t+\Delta t)}\Big)^{(k)}\Big)$$

$$\cdot cos\varphi+\Big(-\Big(B_\zeta^{(k)}\Big)^2\Big(\dot{u}_z^{(t+\Delta t)}\Big)^{(k)}+\Big(B_\zeta^{(k)}\Big)^2\Big(\dot{u}_z^{(t+\Delta t)}\Big)^{(k+1)}+$$

$$+2B_\zeta^{(k+1)}B_\zeta^{(k)}\Big(\dot{u}_z^{(t+\Delta t)}\Big)^{(k)}\Big)sin\varphi\Big\}\Big]-\frac{cos\varphi}{\rho}P_\zeta^{(k+1)}-$$

$$-\frac{cos\varphi}{\rho}\Big[0.5hJ_{\theta CT}(B_s^++B_s^-)+\sigma_3 h\Big\{-0.5E_\theta^{(k+1)}(B_s^++B_s^-)-$$

$$-\Big(\Big(\dot{u}_x^{(t+\Delta t)}\Big)^{(k+1)}sin\varphi-\Big(\dot{u}_z^{(t+\Delta t)}\Big)^{(k+1)}cos\varphi\Big)(0.25(B_s^++B_s^-)^2+$$

$$+\frac{1}{12}(B_s^++B_s^-)^2\Big)+0.5\Big(\Big(-\Big(\dot{u}_x^{(t+\Delta t)}\Big)^{(k)}B_\zeta^{(k)}+\Big(\dot{u}_x^{(t+\Delta t)}\Big)^{(k+1)}B_\zeta^{(k)}+$$

$$+\Big(\dot{u}_x^{(t+\Delta t)}\Big)^{(k)}B_\zeta^{(k+1)}\Big)sin\varphi-\Big(-\Big(\dot{u}_z^{(t+\Delta t)}\Big)^{(k)}B_\zeta^{(k)}+\Big(\dot{u}_z^{(t+\Delta t)}\Big)^{(k+1)}B_\zeta^{(k)}+$$

$$+\Big(\dot{u}_z^{(t+\Delta t)}\Big)^{(k)}B_\zeta^{(k+1)}\Big)cos\varphi\Big)(B_s^++B_s^-)\}\Big]+h\Big(\ddot{u}_z^{(t+\Delta t)}\Big)^{(k+1)};$$

$$\frac{dM_s^{(k+1)}}{dm}=-\frac{cos\varphi}{\rho r}\Big(\nu_s\frac{e_\theta}{e_s}-1\Big)M_s^{(k+1)}+\frac{e_\theta h^3}{12}\frac{cos\varphi}{\rho r^2}\theta_s^{(k+1)}+\frac{cos\varphi}{\rho}N_x^{(k+1)}-$$

$$-\frac{sin\varphi}{\rho}N_z^{(k+1)}+\frac{cos\varphi}{\rho}\Big(-N_x^{(k)}\theta_s^{(k)}+N_x^{(k+1)}\theta_s^{(k)}+N_x^{(k)}\theta_s^{(k+1)}\Big)+$$

$$+\frac{sin\varphi}{\rho}\left(-N_z^{(k)}\theta_s^{(k)}+N_z^{(k+1)}\theta_s^{(k)}+N_z^{(k)}\theta_s^{(k+1)}\right)-\nu_s\frac{e_\theta}{e_s}\frac{sin\varphi}{\rho r}\left(-M_s^{(k)}\theta_s^{(k)}+\right.$$

$$\left.+M_s^{(k+1)}\theta_s^{(k)}+M_s^{(k)}\theta_s^{(k+1)}\right)-\frac{e_\theta h^3}{12}\frac{cos\varphi sin\varphi}{\rho r}\left(-\left(\theta_s^{(k)}\right)^2+2\theta_s^{(k+1)}\theta_s^{(k)}\right);\quad (12)$$

$$\frac{dB_\zeta^{(k+1)}}{dm}=-\frac{\sigma_2\mu_3}{\rho}\left[E_\theta^{(k+1)}+0.5\left(\left(\dot{u}_x^{(t+\Delta t)}\right)^{(k+1)}sin\varphi-\left(\dot{u}_z^{(t+\Delta t)}\right)^{(k+1)}cos\varphi\right)(B_s^+ + B_s^-)\right.$$

$$-\left(\left(-\left(\dot{u}_x^{(t+\Delta t)}\right)^{(k)}B_\zeta^{(k)}+\left(\dot{u}_x^{(t+\Delta t)}\right)^{(k+1)}B_\zeta^{(k)}+\left(\dot{u}_x^{(t+\Delta t)}\right)^{(k)}B_\zeta^{(k+1)}\right)cos\varphi+\right.$$

$$\left.\left.+\left(-\left(\dot{u}_z^{(t+\Delta t)}\right)^{(k)}B_\zeta^{(k)}+\left(\dot{u}_z^{(t+\Delta t)}\right)^{(k+1)}B_\zeta^{(k)}+\left(\dot{u}_z^{(t+\Delta t)}\right)^{(k)}B_\zeta^{(k+1)}\right)sin\varphi\right)\right]+\frac{(B_s^+ + B_s^-)\mu_3}{\mu_1\rho h};$$

$$\frac{dE_\theta^{(k+1)}}{dm}=-\frac{1}{\rho}\left(\dot{B}_\zeta^{(t+\Delta t)}\right)^{(k+1)}-\frac{cos\varphi}{\rho r}E_\theta^{(k+1)},\quad (k=0,1,2,\dots)$$

4. Analysis of numerical results

Let us study the stress-strain state of geometrically nonlinear shells of rotation of variable thickness depending on changes in external electric current.

$$u=0,\quad w=0,\quad M_S=0,\quad B_\zeta=0.3\sin\omega t\quad hinged, for\ \ s=s_0=0,$$
$$w=0,\quad \theta_S=0,\quad N_S=0,\quad B_\zeta=0\quad sliding, for\quad s=s_N=0.05\,m,$$

The parameters of the shell and material are taken as follows:

$$s_0=0, s_N=0.05\,m, h=5\cdot10^{-4}\left(1-0.5\ {}^{s}/_{s_N}\right)m, r=r_0+s\cos\varphi, r_0=0.05\text{ м},$$
$$\omega=\pi\times10^2 sec^{-1},\ \ \rho=2670\ kg/m^3,\ \ B_s^+=B_s^-=0.1\,Tl, \varphi={}^{\pi}/_{30}, B_{S0}=0.1\,Tl,$$
$$\sigma=3{,}63\times10^7(\Omega\cdot m)^{-1},\ \ \mu=1{,}256\times10^{-6}\,H/m,\ \ J_{\theta\text{CT}}=5\cdot10^5\sin\omega t\,A/m^2,\ \ \sigma$$
$$=3{,}63\times10^7(\Omega\cdot m)^{-1},\qquad P_\zeta=5\cdot10^3\sin\omega t\ N/m^2,\ E=7{,}1\times10^{10}\,N/m^2,$$

In the figures below (Fig. 1-5), correspond to the following options of variation in external electric current: 1. $J_{\theta\text{CT}}=5\cdot10^5\sin\omega t$; 2. $J_{\theta\text{CT}}=5\cdot10^7\sin\omega t$; 3. $J_{\theta\text{CT}}=-5\cdot10^5\sin\omega t$;

4. $J_{\theta\text{CT}}=-8\cdot10^7\sin\omega t$; 5. $J_{\theta\text{CT}}=-1\cdot10^8\sin\omega t$.

Figure 1 shows the distribution of the shell deflection depending on time for $s=0.4\,m$; for all options of variation in external electric current $J_{\theta\text{CT}}$.

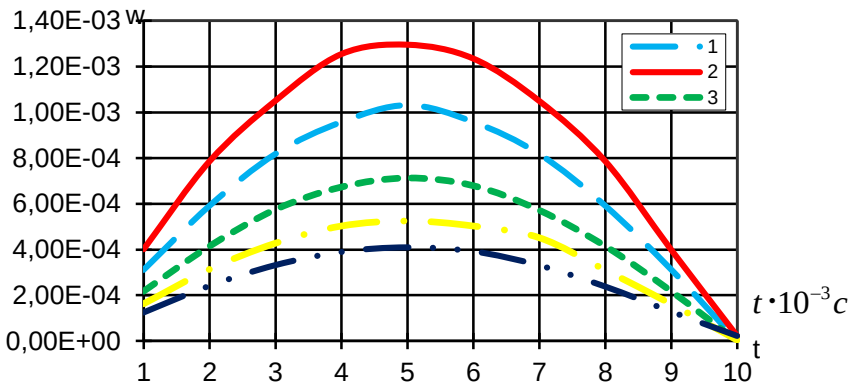

Figure 1. - **Distribution of shell deflection depending on time for all options of variation in external electric current $J_{\theta\text{CT}}$.**

5. Conclusion.

A two-dimensional model of magnetoelasticity of flexible shells of rotation of variable thickness was constructed under the influence of a time-varying mechanical force and external electric current in an external electromagnetic field. Two-dimensional magnetoelasticity models of current-carrying shells are a powerful tool for understanding their behavior in magnetic fields. These models can be used to analyze and design electromagnetic devices, and study fundamental

aspects of magnetoelastic interactions. Numerical results of the coupled magnetoelastic problem were obtained. From the results obtained, it is clear that an increase in the positive values of the external electric current leads to an increase in the shell deflection, and at a negative direction of the external current, the shell deflection decreases. This is explained by the fact that the action of ponderomotive forces associated with the direction of an external electric current coincides with the direction of action of the normal component of the mechanical load and causes corresponding variations in the stress-strain state of the shell. The presented results make it possible to evaluate the influence of external electric current on the stress-strain state of the current-carrying shell.

References

1. *Ambartsumyan A., Bagdasaryan G.E., Belubekyan M.V.* Magnetoelasticity of Thin Shells and Plates [in Russian], Nauka, Moscow (1977).
2. *Grigorenko Y.M., Mol'chenko L.V.* Fundamentals of the Theory of Plates and Shells with Elements of Magnetoelasticity (Textbook) (IPTs, 2010). Google Scholar
3. *Budak V. D., Mol'chenko L. V., Ovcharenko A. V.* Nonlinear Magnetoelastic Shells [in Russian], Ilion, Nikolaev (2016).Google Scholar
4. *Kuang, Z.B.* (2014) An applied electro-magneto-elastic thin plate theory. Acta Mechanica, 225: 1153–1166.
5. *Mol'chenko L. V., Loos I. I., Indiaminov R. S.* Determining the stress state of flexible orthotropic shells of revolution in magnetic field // Int. Appl. Mech **44**, 882–891 (2008).). https://doi.org/10.1007/s10778-008-0102-6, Google ScholarCrossref
6. *Mol'chenko L. V., Loos I. I., Indiaminov R. S.* Stress–strain state of flexible ring plates of variable stiffness in a magnetic field // Int. Appl. Mech. **45**, 1236–1242 (2009).
7. *Indiaminov R.* On the absence of the tangential projection of the lorenz force on the axsymmetrical stressed state of current-carrying conic shells // Int. Jour.Comp. Techn. **13**, 65–77 (2008).
8. *Mol'chenko L. V. Loos I. I.* The stress state of a flexible orthotropic spherical shell subject to external current and mechanical force in a magnetic field // Int. Appl. Mech. 49, 528–533 (2013).
9. *Indiaminov R.Sh., Abdullaev A., Indiaminov M.Sh.* Numerical solution of the problems of magnetoelasticity of plates // International journal of theoretical and applied issues of digital technologies vol. 3 № 1, 2023.
10. *Bian Y. H., Zhao H. T.,* Analysis of thermal-magnetic-elastic stresses and strains in a thin current-carrying cylindrical shell // Int. Appl. Mech., 52, No. 4, 437–448 (2016).
11. Bian Y. H. Analysis of nonlinear stresses and strains in a thin current-carrying elastic plate // Int. Appl. Mech., **51**, No. 1, 108–120 (2015).
12. *Bian Y.H., You Q., Zhang C.* (2018) Coupling effect analysis of a conductive bar-shell in a magnetic field // Advances in Engineering Research, 170: 677–681.
13. *Indiaminov R. Sh.,* Magnetoelastic deformation of a current-carrying orthotropic conical shell with an orthotropy of conductive properties // Bulletin of the University of Kiev 5, 81–86 (2015)
14. *Indiaminov R., Narkulov A., Butaev R.* Magnetoelastic strain of flexible shells in nonlinear statement // AIP Conference Proceedings, 2021, 2365, 02 0002.
15. *Indiaminov R., Butaev R., Narkulov A.* Nonlinear deformation of a current shell in a magnetic field // AIP Conference Proceedings, 2021, 2365, 02 0001.
16. *Indiaminov R., Yusupov N.*, "Mathematical Modeling of Magnetoelastic Vibrations of Current Conductive Shells in the Non Stationary Magnetic Field," *2021 International Conference on Information Science and Communications Technologies (ICISCT)*, 2021, pp. 1-4, https://ieeexplore.ieee.org/ document/9670308
17. *Indiaminov R., Abdullaev A., et al.* Nonlinear Strain of a Current-Conducting Annular Plate in a Magnetic Field // AIP Conference Proceedings 2467, 060026 (2022); https://doi.org/ 10.1063/5.0092485
18. *Indiaminov R., Yusupov N., et al.* Nonlinear Oscillations of a Current-Carrying Shell in Magnetic Field // AIP Conference Proceedings 2467, 020013 (2022); https://doi.org/ 10.1063/5.0092465
19. *Indiaminov R.Sh., Shodmonov J.* (2022). Mathematical modeling of magnetoelastic vibrations of a conducting shell in a magnetic field // ISJ Theoretical & Applied Science, 04 (108), 664-669.
20. *Indiaminov R.Sh., Kholjigitov S.M., Djuraev A.A.* Magnetoelastic deformation of a truncated flexible paraboloid of rotation in a magnetic field // International journal of theoretical and applied issues of digital technologies vol. 6 № 4, 2023. http://ijdt.uz/index.php/ijdt

ON THE METHODOLOGY OF REINFORCEMENT OF T-SHAPED REINFORCED CONCRETE BEAMS WITH CARBON FIBER MATERIALS

Ishankhodjayev A.A.[1], Akhmedov Sh.B.[1]

[1]*Tashkent state transport university, Tashkent, Uzbekistan*

E-mail: ahmedovsherzod911@gmail.com

Abstract: *The work is devoted to the rehabilitation of damaged brand reinforced concrete bridge beams with carbon fiber materials. The resistance of the beams during shearing was assessed depending on the percentage of longitudinal working reinforcement – μ, the ratio of the cut span to the working height of the section–a_v/h_o, the interval, the number and orientation of the CFRP strips. The mechanism of destruction and evaluation of the bearing capacity of reinforced damaged and undamaged T-beams during shearing are investigated. The test results are presented in the form of deflections in the middle of the span, deformations of the stretched working and transverse reinforcement, deformations of concrete along the height of the beams and in the bands of the CFRP from the load. The influence of CFRP on the bearing capacity and the nature of the destruction of beams is investigated.*

Keywords: *bridges, superstructures, corrosion, reinforcement, carbon fiber material.*

1. Introduction

The issues of assessing the technical condition and strengthening of reinforced concrete bridges and structures are the main ones in their operation, since in many of them, serious damage from the combined action of operational loads and the environment is found during inspection. These damages, accumulating and developing over time, reduce their bearing capacity and can lead to catastrophic consequences. The most dangerous defects are reductions in the cross-sectional area of the reinforcement as a result of its corrosion and cracks developing in the supporting inclined sections of the girder superstructures of bridges. In this regard, structural systems must be continuously diagnosed during operation and, if necessary, be strengthened with the help of available means. It should be noted that there are still no building codes or standards for new constructive methods of repair and reinforcement. In this regard, experimental and theoretical studies are required to create basic regulatory documents and standards for methods of design and calculation of repair and reinforcement of such structures. Many traditional methods of reinforcement are known, including a common method of reinforcing the wall of beams with a steel plate or strengthening the stretched zone using steel linings and strands. At the same time, in recent years, the most effective method of strengthening concrete structures is the use of polymer, including carbon fiber materials (CFRP), which, characterized by high strength and technological characteristics, are used for external reinforcement of the damaged area of structures. During loading, the moments of formation of the first inclined cracks in each beam were noted, their transition to critical ones, the separation of the CFRP strips from the concrete surface, and the type of beam destruction was revealed.

2. Materials, methods and object of research

To study the mechanism of destruction and assess the bearing capacity of damaged and reinforced reinforced concrete bending elements (rectangular and T-shaped beams) during cutting, we conducted comprehensive experimental studies. This work is part of these studies and is devoted to the methodology of reinforcing reinforced concrete beams with the help of CFRP sheets glued to their surface, consisting of two main components – epoxy resin and fibers with a mutually orthogonal orientation. The cohesive strength of the epoxy resin is 4 MPa, the tensile strength is 30 MPa, the modulus of elasticity is 3.80 MPa, the tensile strength of the fiber sheet is 3.80 MPa and the modulus of elasticity is 230.0 MPa (according to the manufacturer's specification). The CFRP were supplied by Sikadur–330 (Switzerland) in the form of a rolled sheet with a thickness of 0.09 mm, a width of 600 mm and a length of 5 m with an orientation of the fibers at an angle of 0/90°. CFRP sheets were glued to the surface of concrete pre-coated with epoxy resin, rolled with a roller, and then covered with a final layer of epoxy resin. The resistance of the beams during shearing was assessed depending on the percentage of longitudinal working reinforcement – μ, the ratio of the cut span to the working height of the section – av/ho, the interval, number and orientation of the CFRP strips (Fig. 1 and Table 1).

Table 1.

List of tested T-beams

Description of samples	Step and orientation of the CFRP strip, mm–degree	R, MPa	a_v/h_o	The diameter of the stretched reinforcement, mm	Number, diameter–the pitch of the clamps, mm
[1]TS1a	—	16,73	2,5	Ø 16	2 Ø 8–210
[2]TS1–1	U– stripe 150–0/90				
[2]TS1–2	U– stripe 200–0/90				
[3]TS1–1I	U– stripe 200–0/90				
[1]TT1a	—	27,38	2,5	Ø 20	4 Ø 6–120
[2]TT1–1	U– stripe 150–0/90				
[2]TT1–2	U– stripe 200–0/90				
[3]TT1–1I	U– stripe 200–0/90				
[1]TS2a	—	16,73	4,0	Ø 16	2 Ø 8–145
[2]TS2–1	U– stripe 200–0/90				
[2]TS2–2	L– stripe 150–45/135				
[3]TS2–21	L– stripe 150–45/135				
[1]TT2a	—	27,38	4,0	Ø 20	4 Ø 6–90
[2]TT2–1	U– stripe 150–0/90				
[2]TT2–2	L– stripe 150–45/135				
[3]TT2–2I	L– stripe 150–45/135				

[1]– control samples without reinforcement;[2]– reinforced samples with damage;[3]– reinforced samples without damage.

This series (series T) consisted of sixteen beams. They were divided into two groups, TT (p = 1.69%) and TS (p = 1.08%), which differed in the percentage of longitudinal working reinforcement. All beams were reinforced with transverse steel clamps at different intervals (Table 1 and Fig.1, a). The TT and TS groups included two subgroups each, differing in the ratio of the cut span to the working height, av/ho (Table 1). All samples were tested during static loading. Each subgroup had four samples. Of these, one beam was reinforced with CFRP sheets before the test, i.e. it remained "undamaged", and two other similar beams were subjected to preloading (60% of the destructive), or "damaged", to obtain the main system of cracks characteristic of beams operating under real operating conditions of bridges and after unloading were reinforced with CFRP sheets. One beam from each subgroup remained the control one, i.e. without any reinforcement. In addition, six cylinders with a diameter of 150 mm and a height of 300 mm and six cubes with an edge of 150 mm were manufactured and tested. Table 1 shows a list of tested samples. All samples of the working fittings were tested under uniaxial tension on a bursting machine. The average tensile strength of a rod made of high–strength steel with a diameter of 16 mm is 311.22 MPa, with a diameter of 20 mm – 554.17 MPa, and a rod made of mild steel with a diameter of 6 mm – 660.82 MPa, with a diameter of 8 mm – 620.31 MPa. Fig. 1,a shows the details of reinforcement and the location of load cells on the stretched working longitudinal rods and clamps of the TS1 and TT1 subgroups. The sample loading schemes are shown in Fig.1,b. The samples of the BT1, BS1, TT1 and TS1 groups were subjected to two–point bends, and the samples of the BT2, BS2, TT2 and TS2 groups were subjected to a concentrated load in the middle of the beam (Fig.2). The reinforcement scheme and orientation of the CFRP strips, the location of sensors on the surface of the CFRP strip and concrete are shown in Fig.2. During the test, deflection in the middle of the span and deformations in the stretched working fittings and clamps, deformations on the side surface in the average normal section of the beam and along the inclined section, as well as in the glued strips of the CFRP were measured at each load stage. According to the test results, the types of destruction and the nature of cracking under extreme load were determined, and the degree of increase in load-bearing capacity with this type of reinforcement was revealed. Strain gauges with a measuring base of 10 mm were used to measure the magnitude of deformations of internal steel reinforcement, and strain gauges with a measuring base of 30 mm were used on the concrete surface and in the CFRP strips (Fig.1,a). In addition, deformations on the concrete surface within the middle span of the T-beams were also measured using reference points L1, L2, L3, L4, L5 and L6 with a measurement base of 150 mm, located at a distance of 10 mm, 40 mm, 73 mm, 135 mm, 220 mm and 310 mm

from the top, respectively the surface of the beam (fig. 1,b). One linear strain transducer and two dial indicators were also installed in the center of the beam on the samples (Fig.1,b). During loading, the formation of the first cracks, critical crack opening, separation of sheets from the concrete surface or rupture of reinforcing strips with concrete staining were recorded. Crack propagation was clearly observed at each load increment throughout the test. The test results were presented in the form of "load–deflection" dependencies in the middle of the span, "load–deformation" of stretched rebars and transverse clamps, in the CFRP strips and on the concrete surface.

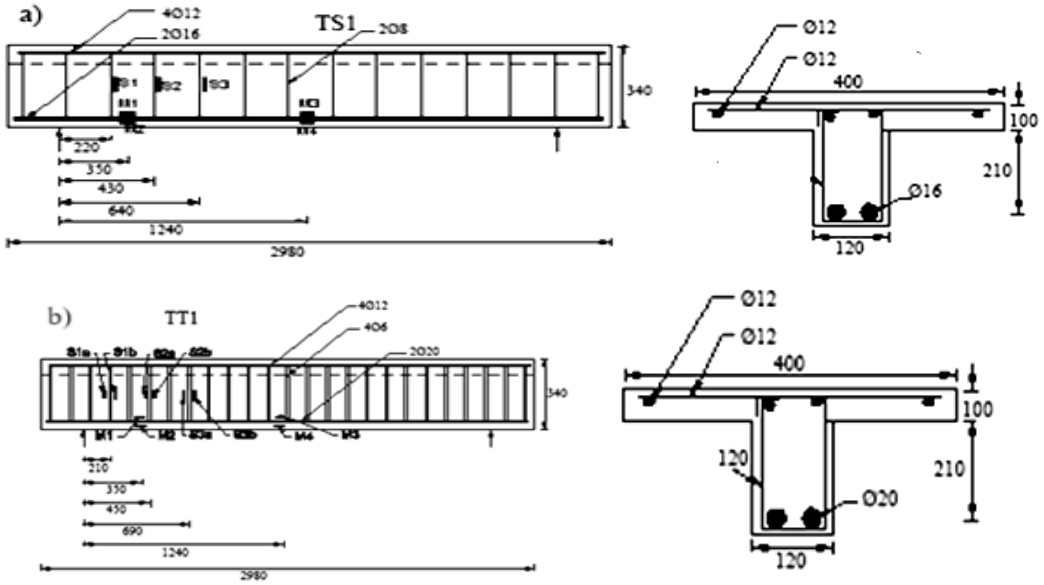

Figure 1. **- The scheme of reinforcement and arrangement of load cells: a) on the fittings of samples; b) on the surface of concrete and strips of CFRP, as well as the scheme of loading samples**

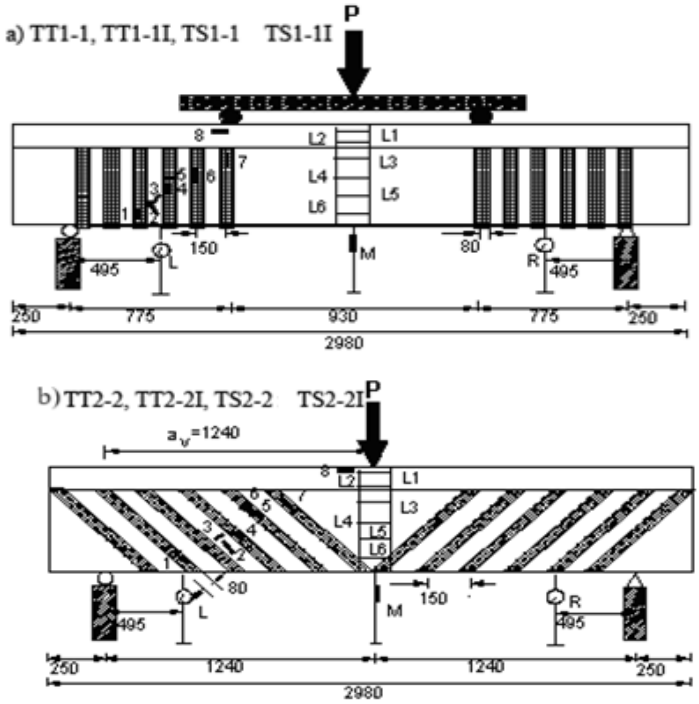

Figure 2. **- The reinforcement scheme and orientation of the CFRP strips, the location of sensors on the surface of the CFRP strip and concrete**

To study the mechanism of destruction and assess the bearing capacity of reinforced structures (rectangular, T-shaped beams and special samples) during cutting, we conducted comprehensive experimental studies. This work is part of these studies and is devoted to the

rehabilitation of T-shaped reinforced concrete beams (series T) of bridges with carbon fiber materials (CFRP) consisting of two main components – epoxy resin and fibers with a mutually orthogonal orientation. This series consisted of sixteen T-beams, which were divided into two groups with different percentages of reinforcement of the stretched zone TT (p = 1.69%) and TS (p = 1.08%). All the T-beams were reinforced with clamps at various intervals. The TT and TS groups were divided into two subgroups TT1, TS1 and TT2, TS2 with the ratio of the cut span to the working height (a_v/h_o) equal to 2.5 and 4.0, respectively. All samples were tested during static loading. The samples of the TT1 and TS1 subgroups were subjected to two-point bending, and the samples of the TT2 and TS2 subgroups were loaded with a load in the middle of the span. Each subgroup consisted of four samples. Of these, one beam was initially reinforced without creating a system of preliminary cracks, the other two beams were pre-destroyed by preload (up to 60% of the destructive load) and reinforced with CFRP sheets. One beam remained the control beam without any reinforcement. During loading, the moments of formation of the first inclined cracks in each beam were noted, their transition to critical ones, the separation of the CFRP strips from the concrete surface, and the type of beam destruction was revealed. The test results are presented in the form of deflections in the middle of the span, deformations of the stretched working and transverse reinforcement, deformations of concrete along the height of the beams and in the CFRP bands from the load (Fig.1 and 2). The influence of the CFRP on the bearing capacity and the nature of the destruction of beams was also studied. The cubic strength of the samples of the TT1, TT2 and TS1, TS2 groups is 27.38 and 16.73 MPa, respectively.

3. Results

1. The results of the experiment show that CFRP strips with fibers oriented in two directions can be used to significantly increase the bearing capacity of beams during cutting. For the TT1, TS1, TT2 and TS2 subgroups, the shear load capacity increased by 38,08%-60,94%, 19,74%-39,51%, 17,98%-44,93% and 12.29%-36.9%. In general, the bearing capacity when cutting the T–beams was 12.29% - 60.94% higher compared to the control beams. The results show that an increase in the number of internal (steel clamps) and external (CFRP strips) reinforcement does not so much proportionally increase the bearing capacity of the beams during shearing, as it changes the type of their destruction from a shear mechanism to a bending one (with a gap in the reinforcement bands) due to the presence of a large number of shear reinforcement. In T–beams, the increase in the bearing capacity of reinforced samples without damage was by 7% - 17% compared to reinforced samples with damage. According to the results of the experiment, it was found that the use of CFRP strip systems as a reinforcement method is the most effective for the rehabilitation of damaged beams operating in real conditions and allows to increase the bearing capacity of reinforced concrete beams during cutting.

2. The results of the load–deflection ratio in the middle of the span show that the stiffness of the damaged and undamaged T-beams reinforced with CFRP was similar to the stiffness of the control beam due to the presence of internal reinforcement (Fig.3). In T-beams, the average deflection of samples loaded in the middle of the span reached a higher value compared to samples tested with two-point loading at the same load. This effect may occur due to the influence of the upload form. It was also found that the average deflection of the samples reinforced with CFRP sheets was less than that of the control beam for the same load, whereas they achieved more in the maximum load compared to the control beam.

The load–strain relationships in the longitudinal and transverse reinforcement of reinforced damaged and undamaged beams show linear behavior as in the control beam. The observed strain values in the stretched work fittings and clamps were less than those of the control beam for the same load. In general, the proportionate deformations in damaged and undamaged beams reinforced with CFRP were greater under destructive load than in the control beam. It was also noted that the deformations of the CFRP strips in reinforced damaged and undamaged beams were less compared to the deformations of the clamps.

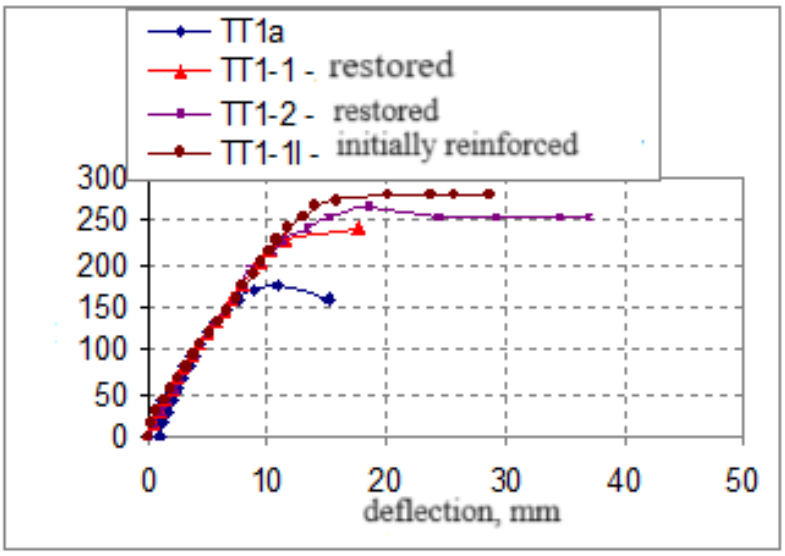

Figure 3. - **Comparison of the load–deflection curves in the middle of the span of the TT1 subgroup (after reinforcement)**

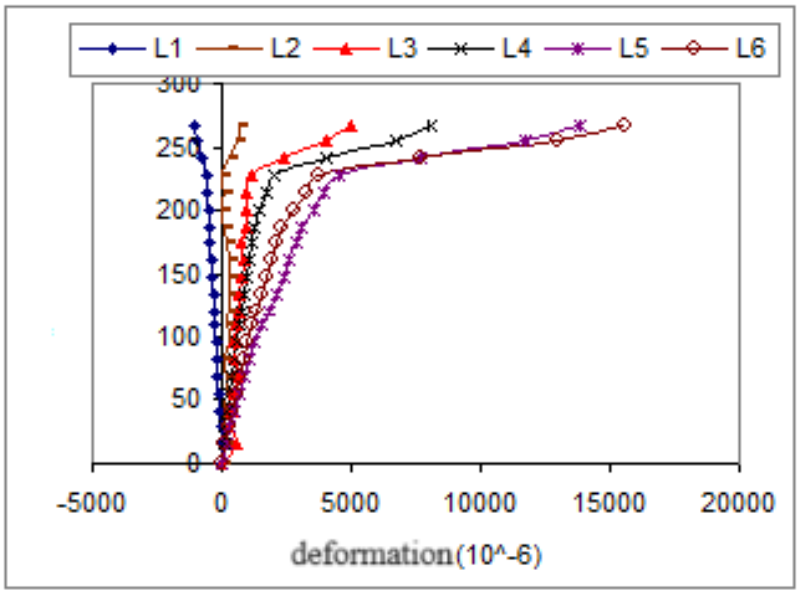

Figure 4. - **The "load–strain" curve in the middle of the span of a reinforced beam with TT1-2 damage**

The results also showed that the deformation of the CFRP strips used in the beams is below their maximum deformation in the non-glued state. It was found that in samples with an inclined orientation of the CFRP 45/135^0 bands (L-bands), a smaller number, smaller width and length of the cracks formed were observed than in samples with the orientation of the CFRP 0/90^0 bands (U-bands) to the longitudinal axis. The bearing capacity of samples with the orientation of the CFRP 45/135^0 bands was higher than that of samples with the orientation of the CFRP 0/90^0 bands to the longitudinal axis (Table.2).

These results show that the orientation of the CFRP strips not only affects the type of fracture, but also the bearing capacity of the beam during shearing. As an exception, the TS2 subgroup sample with inclined L-bands achieved a lower increase in load-bearing capacity compared to the sample with vertical U-bands. The damaged and undamaged beams reinforced by the CFRP showed good elastic behavior.

Table 2.

The deformation on the concrete surface (that is, between the strips of the CFRP) is greater than the surface deformation of the strips of the CFRP

Name of the sample	The pitch and orientation of the CFRP strip, mm–degree	Total destructive load, kN	Cracking load, (kN)	The proportion of Q perceived CFRP, kN	Increasing the carrier capacity beams when cut (%)
[1]TT1a	---	174,65	87,325	–	–
[2]TT1-1	U- stripe 200–0/90	241,16	120,58	66,51	>38,08
[2]TT1-2	U- stripe 150–0/90	267,77	133,885	93,12	>53,32
[3]TT1-1I	U- stripe 200–0/90	281,08	140,54	106,43	>60,94
[1]TS1a	---	134,74	67,37	–	–
[2]TS1-1	U- stripe 150–0/90	187,98	93,99	53,24	>39,51
[2]TS1-2	U- stripe 200–0/90	161,34	80,67	26,6	>19,74
[3]TS1-1I	U- stripe 200–0/90	121,44	60,72	–	–
[1]TT2a	---	148,04	74,02		–
[2]TT2-1	U- stripe 150–0/90	174,65	87,32	26,61	>17,98
[2]TT2-2	L- stripe 150–45/135	201,26	100,63	53,22	>35,95
[3]TT2-2I	L- stripe 150–45/135	214,56	107,28	66,52	>44,93
[1]TS2a	---	108,14	54,07		–
[2]TS2-1	U- stripe 200–0/90	148,04	74,02	39,9	>36, 90
[2]TS2-2	L- stripe 150–45/135	134,74	67,37	26,6	>24,59
[3]TS2-1I	L- stripe 150–45/135	121,44	60,72	13,3	>12,29

[1]– control samples without reinforcement;[2]– reinforced samples with damage; [3]– reinforced samples without damage.

Experiments show that in the limiting state, the beams were destroyed either by bending or shear mechanisms with the rupture of the strips. The results show that the percentage of longitudinal reinforcement, the number and pitch of steel clamps, the number, pitch and orientation of the CFRP strips and the ratio of the cut span to the working height affect the effectiveness of reinforced concrete beams. The interval of the CFRP strips also affects the load-bearing capacity of the beam during cutting. With an increase in the interval between the strips of the CFRP, the bearing capacity of the beam section decreases. In the TT1 subgroup, the bearing capacity of the TT1-2 sample (band interval–150 mm) was 15% greater than that of the TT1-1 sample (band interval–200 mm). Reinforced samples without damage of the TS2 and TS1 subgroups did not show an increase in load-bearing capacity compared to "damaged" reinforced samples with a similar orientation of the CFRP bands. The bidirectional CFRP strip not only increases the bearing capacity when cutting reinforced samples, but also prevents the spread of cracks and the strip from peeling off the concrete surface, acting as a deformation limiter. The results show that the shear load capacity does not increase with an increase in the ratio of the shear span to the working height of reinforced samples - "damaged" and "undamaged" (Table 1). The use of external reinforcement with CFRP sheets for "damaged" beams prevents the development of preliminary cracks at the stage of destruction [16-20].

The results show that the reinforcement of reinforced concrete beams with bidirectional strips of CFRP significantly (12-61%) increases the bearing capacity of the beam section. In T-beams, the increase in the bearing capacity of reinforced samples without damage was 7-17% higher compared to similarly reinforced samples with damage. The test results showed that the CFRP strip with orthogonally directed fibers is the most effective and economical for strengthening damaged beams and allows increasing their shear bearing capacity during the restoration or modernization of reinforced concrete beams.

4. Conclusion

As the results of this study have shown, the stress-strain state of reinforced concrete and composite concrete structures are of a different nature. To ensure the reliability and durability of composite concrete structures, as well as to increase their efficiency, it is necessary to further improve the calculation of the bearing capacity and deformability of such structures. The use of basalt reinforcement in the construction of bridge structures in certain cases can be effective and

economically feasible. This will lead to a reduction in the cost of the structure per unit of operational time. During the search for a solution to the problem of durability of reinforced concrete structures of bridge structures, it was found that to a large extent this problem can be solved by the use of certain types of non-metallic composite reinforcement, which has increased resistance to corrosion in seawater [21,22]. Based on the analysis of corrosion resistance of composite reinforcement available on the Uzbek market, it was concluded that basalt reinforcement has the best corrosion resistance to aggressive external environments, including water environments, in conditions of 100% humidity and aggressive alkaline environment of concrete. This property of basalt reinforcement opens up wide prospects for its application in bridge structures. When determining the bearing capacity of non-centrally compressed and bent concrete structures of bridge structures reinforced with basalt reinforcement, the conclusion is made, that in order to obtain more accurate results of bearing capacity, it is necessary to take into account the work of basalt reinforcement in the compressed zone of concrete. Taking into account the results of the research carried out in the work, calculations were made of the structures of a specific object - a dry dock - with the replacement of steel reinforcement with basalt. The economic efficiency of such a replacement is evaluated. As a result of the analysis of the results of the replacement of steel reinforcement with basalt in the structures of dry.

References

1. *Akhmedov Sh., Saatova N., Radjabov T., Shojalilov Sh., Safarov Sh.* Investigation of stress transfer through cracks in reinforced concrete elements // E3S Web of Conf. vol. 401, 2023, https://doi.org/10.1051/e3sconf/202340103023
2. *Akhmedov Sh., Aripov Kh., Ospanov R., Mirzaolimov I., Kenjayev T.* Strength of reinforced concrete T-beams of bridges reinforced with external reinforcement from fabric polymeric composites // E3S Web of Conf. vol. 401, 2023. https://doi.org/10.1051/e3sconf/202340101068
3. *Ishanxodjaev A.A., Bekmirzaev D.A., Ospanov R.S., Axmedov Sh.B., Usmonov D.T.* Influence of the inertia force of underground pipeline systems under seismic loads // AIP Conf. Proc. 2637, 050002 (2022). https://doi.org/10.1063/5.0119606
4. *Ahmedov Sh.B., Rajabov T.Yu., Shojalilov Sh.Sh., Ergashev A.T., Mirzaolimov I. Yu.* Multivariate statistical modeling of strength and parameters of diagrams *σb–εb* for expanded clay concrete // AIP Conf. Proc. 2637, 050002 (2022). https://doi.org/10.1063/5.0120127
5. *Miralimov M., Ishankhodjaev A., Almenov Kh., Muminov E.* Influencing of land transport load on structure of backfill arched Road Bridge // E3S Web Conf. vol. 264, 2021, https://doi.org/10.1051/e3sconf/202126402013
6. *Saatova N., Shozhalilov Sh., Safarov Sh.* Methodology of Techno-Economic Feasibility Study for the Reconstruction of Road Bridges // AIP Conf. Proc. 2432, 030096 (2022). https://doi.org/10.1063/5.0089536
7. *Miralimov M., Ospanov R., Mengliev I.* Modeling of dissipation of vibration energy in problems of structural dynamics // E3S Web of Conf. vol. 401, 2023, https://doi.org/10.1051/e3sconf/202340105025
8. *Miralimov M.* Numerical Approach for Assessment of Stress Strain State of Road Culverts // AIP Conf. Proc. 2637, 050002 (2022). https://doi.org/10.1063/5.0119096
9. *Miralimov M., Abirov R.A.*Cement concrete pavements technology at construction of main roads in Uzbekistan conditions // E3S Web of Conf, vol. 458, 2023, https://doi.org/10.1051/e3sconf/202345807018
10. *Abirov R., Miralimov M.* Calculation of the Lining of Construction of the Shallow Subway Tunnel // Hydraulic and Civil Engineering Technology VIII, pp.42-48. http://dx.doi.org/10.3233/ATDE230700
11. *Abirov R., Miralimov M.* On Mitigation of Damages on Landslide Prone Regions of Uzbekistan // Hydraulic and Civil Engineering Technology VIII, pp. 1240-1245, http://dx.doi.org/10.3233/ATDE230856
12. *Miralimov M.,Normurodov Sh.* Ground behaviour and settlements analysis on tunnelling of shallow-buried metro in Tashkent city // E3S Web of Conf, vol. 401, 2023, https://doi.org/10.1051/e3sconf/202340101062
13. *Miralimov M., Normurodov Sh., Akhmadjonov M., Karshiboev A.* Numerical approach for structural analysis of Metro tunnel station // E3S Web Conf. vol. 264, 2021 https://doi.org/10.1051/e3sconf/202126402054
14. *Adilov F.F., Miralimov M.H., Abirov R.A.*To the stability of the roadbed reinforced with gabions // IOP Conf. Ser.: Mater. Sci. Eng. 913 042066. https://doi.org/10.1088/1757-899X/913/4/042066
15. *Miralimov M., Adilov F., Abirov R., Juraev D., Khazratkulov I.*·To numerical approach for calculation of underground structures // IOP Conf. Ser.: Mater. Sci. Eng. 883 012204. https://doi.org/10.1088/1757-899X/883/1/012204
16. *Ergashov A., Shojalilov Sh., Djumaniyazova R. Shipilova K.* Evaluation of effect of deviations in width of cross-section of connected elements // E3S Web of Conf. vol. 401, 2023, https://doi.org/10.1051/e3sconf/202340102049

17. *Mardonov B., An E., Shojalilov Sh., Khakimova Y., Ismoilova G.* Transverse Vibrations of Underground Pipelines with Different Interaction Laws of Pipe with Surrounding Soils // E3S Web Conf. vol. 264, 2021, https://doi.org/10.1051/e3sconf/202126402035
18. *Nishonov N., Bekmirzaev D., Ergashov A., Rakhimjonov Z., Khurramov A.* Underground polymeric l-shaped pipeline vibrations under seismic effect. E3S Web Conf. vol. 264, 2021 https://doi.org/10.1051/e3sconf/202126402037
19. *Miralimov M., Shojalilov Sh., Karshiboev A., Usmanov D.* Calculation method of reinforced concrete structures with account of nonlinear deformation of the material // AIP Conf. Proc. 3045, 030078 (2024). https://doi.org/10.1063/5.0197797
20. *Ospanov R.S.* Calculation of the intermediate support of a three-span overpass // Universum. 2023. 5(110). https://7universum.com/ru/tech/archive/item/15557
21. *Miralimov M., Ospanov R.* Seismic resistance of supports in bridge structures, modern problems of bridge structures. Railway transport: topical issues and innovations, 2023. №4. pp. 26-33.
22. *Akhmedov Sh., Mirzaolimov I.* Feasibility study of the use of basalt reinforcement in the construction of bridge structures // Railway transport: topical issues and innovations, 2023. №4. pp. 34-41.

INFLUENCE OF ELASTIC, VISCOUS, AND PLASTIC PROPERTIES ON THE STRESS-STRAIN STATE OF YARNS UNDER IRREGULAR DYNAMIC LOADS

Ismoilova S.I.[1], Khazratova T.Ya.[1], Begmanov R.A.[1]
Institute of Mechanics and Seismic Stability of Structures named after M.T. Urazbaev, Tashkent, Uzbekistan
E-mail:ismailova.sabida@mail.ru

Abstract. *The influence of elastic, viscous, and plastic properties of yarns on the qualitative and quantitative patterns of the stress-strain state of yarns subject to tension and recovery under the effect of semicyclic and irregular dynamic changes under the yarn stretching is considered in the article. The proposed law considers the elastic, viscous, and plastic properties of cotton yarn with different linear densities. The parameters of the law can be determined from the results of experiments on yarn tension on standard tensile installations for stretching yarn. The nonlinear elastic-viscoplastic law of cotton yarn strain can be used in solving applied problems to study the process of deformation and breakage of cotton yarns.*

Keywords*: yarn, tension, strength, strain, elongation, breakage, load.*

1. Introduction.

The fundamentals of the mechanics of textile yarns were developed in [1-4]. The basic task is to determine the tensile force of the yarn when stretched. The tensile force was determined following the textile production requirements.

The strength of textile products and materials is inextricably linked with the strength of the yarns, from which they are made, in the most complex technological processes of textile production. To directly determine and evaluate strength, first, it is necessary to reliably know the law of yarn strain under tensile loads that the yarn experiences in certain operations. There is a need to turn to the mechanics of a deformable rigid body, as the scientific basis of the technology of textile materials [4].

Analysis of the results of experiments on breaking extension [5] shows that yarn, when strained, has three main mechanical properties - elasticity, plasticity, and viscosity. These properties manifest themselves to varying degrees depending on the yarn structure, temperature, moisture content, and type of load - static or dynamic.

In textile production, quality problems arise as machine speed increases due to high dynamic stresses in the yarn feeding system. Given the large number of factors influencing this process, analysis of the cause of errors is possible with large experimental efforts while, in the case of sporadic errors, is not possible at all. Yarn tension is a critical parameter and its modeling throughout the yarn feeding process opens up wide possibilities for analysis and optimization. First, a mathematical model is built based on the invariance of the mass of a length of yarn, the nonlinear behavior of yarn during elongation, the influencing factors of the main elements of the yarn feed cone, feeder, and loop on the tension force of the yarn [6-8].

Various factors influence the strength of yarn. Yarn breakage occurs due to fiber breakage and slippage; some fibers slip and others break [9].

The yarn strength is calculated by simulating the random arrangement of fibers in the yarn. From the calculation results, it can be seen that the critical slip length decreases as the yarn twisting coefficient increases. Meanwhile, as the twisting coefficient increases, the design strength of the yarn increases to a maximum point and then decreases, which is consistent with the conventional spinning theory. Therefore, the calculation of yarn strength based on the critical slip length can reflect the breaking mechanism of yarn when the twisting coefficient of yarn changes and these calculations can be used to predict yarn strength [10].

To ensure yarn vibration control and quality improvement, it is critical to study yarn tension fluctuations and their effects on the process [11].

Simulation of yarn and filament behavior is important due to its role in optimizing the production processes of different types of yarns. Virtual models of yarn allow us to more accurately simulate the behavior of fabrics and realistically simulate the behavior of yarns in seam lines. The structure of yarns is an important factor influencing their behavior. However, most studies in filament modeling ignore the structure of filaments and model them as single fibers [12-13].

2. Materials, methods, and object of study.

Analysis of the qualitative and quantitative dynamics of the stress-strain state of yarn is important for understanding its mechanical properties and behavior under various operating conditions. Consideration of elastic, viscous, and plastic characteristics of yarns allows more accurate modeling of their behavior and predicts possible damage and breakage [14-15].

The theoretical description of this diverse behavior of the yarn is made using mechanical and mathematical models, which is an idealization of the mechanical behavior of the yarn under straining.

3. Statement of the problem.

To describe the process of yarn strain under tension and recovery, considering the viscous and plastic properties of the yarn material, a nonlinear law of yarn strain (1) was proposed [5]:

$$E_D^{-1}(\varepsilon)\frac{d\sigma}{dt} + E_S^{-1}(\varepsilon)\mu(\varepsilon)\sigma = \frac{d\varepsilon}{dt} + \mu(\varepsilon)\varepsilon \tag{1}$$

The law of yarn strain (1) describes the process of yarn stretching until it breaks, however, in technological processes of textile production it is also necessary to account for the recovery of yarn strain [1]. Experimental data is needed to describe the recovery (unloading) process. Currently, there are no experimental data on the strain unloading of yarn when it is stretched.

Based on this, a phenomenological law of yarn unloading is proposed, based on the general principles of the theory of plasticity [2].

It is proposed to describe the recovery of yarn strain at any stage of loading by the following equation:

$$\frac{d\sigma}{E_R(\varepsilon)dt} = \frac{d\varepsilon}{dt} \quad \text{for} \quad \frac{d\varepsilon}{dt} < 0 \tag{2}$$

where $E_R(\varepsilon)-$ is the variable unloading modulus, considering the plastic properties of yarn strain.

To determine the value of the unloading modulus under yarn stretching, the following relations were phenomenologically proposed:

$$E_R(\varepsilon) = E_T \quad \text{for} \quad 0 \le \varepsilon \le \varepsilon_e \tag{3}$$

$$E_R(\varepsilon) = E_T \exp\left[\varphi\left(I_S - 1\right)\right] \quad \text{for} \quad \varepsilon_e < \varepsilon < \varepsilon_m \tag{4}$$

$$E_R = E_T \exp\left[\varphi\left(\frac{\varepsilon_m}{\varepsilon_e} - 1\right)\right] \quad \text{for} \quad \varepsilon \ge \varepsilon_m \tag{5}$$

where E_T- is the current value of the strain modulus at the time of unloading; $\varphi-$ is the dimensionless coefficient characterizing the slope of the unloading curve to the strain axis $\sigma(\varepsilon)$ in

the diagram; K_R – is the dimensionless coefficient characterizing the maximum possible value of the unloading modulus; I_S – is the parameter characterizing the dependence of the plastic properties of yarn under tension on changes in its structure [5].

According to equations (3)–(5), the process of yarn unloading in the strain range $[0 \le \varepsilon \le \varepsilon_e]$ is linear and completely reversible, in the range $[\varepsilon_e < \varepsilon \le \varepsilon_m]$, it is nonlinear and partially reversible. For $\varepsilon = \varepsilon_e$, $I_S = 1$ and $E_R(\varepsilon) = E_T$, and for $\varepsilon = \varepsilon_m$, $I_S = I_{S_{\max}} = \dfrac{\varepsilon_m}{\varepsilon_e} > 1$, $E_R(\varepsilon)$ reaches its maximum value and then remains constant in the range $[\varepsilon_m < \varepsilon \le \varepsilon_k]$, according to equation (5).

Equation (1) with the defining relations (2)–(5) is a physically nonlinear elastic-viscoplastic law of yarn strain considering unloading.

Consider the work of equation (1) with equation (2), i.e. with yarn unloading. To do this, following the experiment, we set the change in strain by the following equation:

$$\varepsilon = \varepsilon_k \sin \frac{\pi t}{2t_k} \tag{6}$$

Let us make the following changes to equation (6):

$$\varepsilon(t) = abs\left(\varepsilon_a \sin \frac{\pi t}{2t_k} \right) \tag{7}$$

where ε_a – is the amplitude (he maximum value) of strain at which unloading occurs.

According to equation (7), the current strain value is always positive, since the yarn only stretches and does not work under compression. Using equations (1)–(7), we consider the unloading of yarn over the range of strain changes $0 \le \varepsilon \le \varepsilon_e$. The original problems remains unchanged, except for $\varepsilon_a = \varepsilon_e$, $\mu_N = 100$ s^{-1}, $K_R = 1$ and the calculation step here and below is $\Delta t = 0.001$s [5].

4. Results.

The calculation results are shown in Fig. 1; changes in strain over time are shown in Fig. 2 (curve 2). The loading (stretching) of the yarn occurs along curve 1. After the strain reaches the value of $\varepsilon_a = \varepsilon_e$ for $d\varepsilon/dt < 0$, unloading occurs along line 2. With repeated changes in strain in section $0 \le \varepsilon \le \varepsilon_e$, the «loading-unloading» process occurs in a closed circle along lines 1 and 2 (Fig. 1). The change in strain occurs in half-cycles of a sinusoid, Fig. 2 (curve 1).

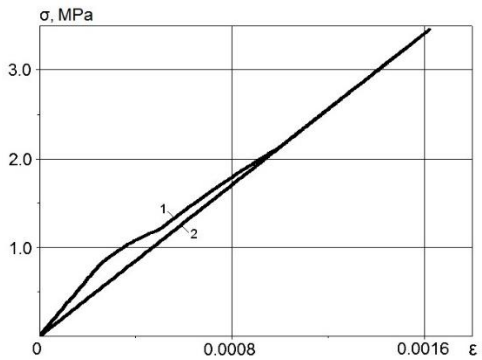

Figure 1. - **Load-unload diagram at the viscoelastic stage of strain**

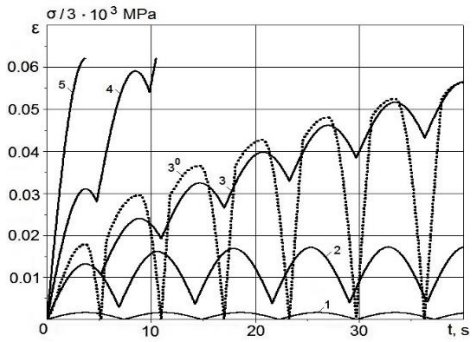

Figure 2. - **Options for changing the tensile strain of yarn**

In Fig. 2: 1 curve – $E_R = E_T$; curve 2 – $E_R = \gamma E_T$; curve 3 – $E_R = 5\gamma E_T$; curve 4 – $E_R = 10\gamma E_T$; curve 5 – $E_R = 10\gamma E_T$; and curve 3^0 – change in $\sigma(t)$.

According to these results, the laws of strain (1) and (2) work quite adequately in the area of elastic strain of the yarn.

For cases $\varepsilon_a = \varepsilon_m$ and $K_R = 2$, when unloading begins after the strain reaches the value of ε_m, the change in $\sigma(\varepsilon)$ is shown in Fig. 3. Changes in strain over time for this option are shown in Fig. 2 (curve 2).

In the first half-cycle, loading occurs along curve 1 (Fig. 3). After the strain reaches the value of ε_m, at point (a), unloading occurs along line 2, re-loading also occurs along line 2 to point (a), then along line 1. At point (b), the strain again reaches the value of ε_m, in a new half-cycle and unloading occurs along line 3. This cyclic pattern of the «loading-unloading» process occurs until the strain reaches the critical value of ε_k. At $\varepsilon = \varepsilon_k$, the yarn breaks.

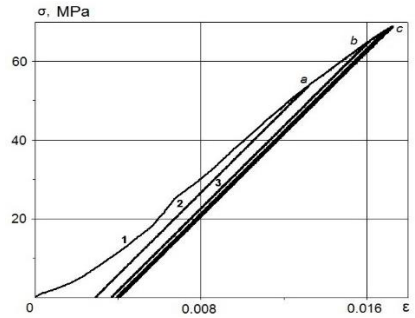

Figure 3. - **«Loading-unloading» diagram at the elastoplastic stage of yarn strain for $K_R=\gamma$ under «soft» unloading**

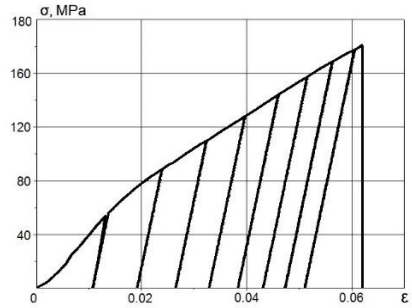

Figure 4. - **«Loading-unloading» diagram at the elastoplastic stage of yarn strain for $K_R=5\gamma$ under «hard» unloading**

Different changes in strain over time occur with the increase in parameter $K_R = E_R / E_T$ (Fig. 2, curves 2 and 3).

The changes in the diagrams $\sigma(\varepsilon)$ for $K_R = 10$ corresponding to the strain change curve (Fig. 2, curve 3) are shown in Fig. 4. In this option, the values of the remaining source data did not change.

As seen from Fig. 4, an increase in the slope of the unloading line to the strain axis, i.e. an increase in the value of K_R, leads to an increase in the strain value compared to the previous case (Fig. 2, curves 2 and 3). The change in stress over time corresponding to this case is shown in Fig. 2 (dashed curve 3^0). Here, in each half-cycle, the stress decreases to zero at a significant residual strain. Similar changes in stress occur in all other cases of strain changes.

When the value increases to $\varepsilon_a = 0.5\varepsilon_k$ (Fig. 2, curve 4), after two half-cycles of change in strain, the yarn breaks (Fig. 5).

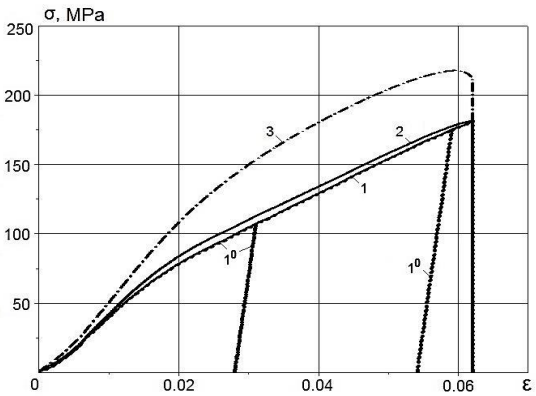

Figure 5. - **Stress-strain diagram of yarns of different viscous properties at unloading to breakage**

The change in $\sigma(\varepsilon)$ for this option is shown in Fig. 5 (curve 1^0). Loading proceeds as in case $\varepsilon_a = \varepsilon_k$ (curve 1), but with unloading at times when the strain reaches the value of $\varepsilon_a = 0.5\varepsilon_k$.

For $\varepsilon_a = \varepsilon_k$ (curve 5, Fig. 2), in the first half cycle the strain reaches a critical value and at $t_k = 3.72$ s, the yarn breaks. Curve 1 in Fig. 5 corresponds to this case.

The effect of the change in the value of μ_N on dependencies $\sigma(\varepsilon)$ is also shown in Fig. 5. Here curve 1 corresponds to the experimental curve $\sigma(\varepsilon)$ for $\mu_N = 100$ s^{-1}. Curve 2 was obtained for $\mu_N = 10$ s^{-1}, and curve 3 for $\mu_N = 1$ s^{-1}. As can be seen, with a decrease in the value of the yarn viscosity parameter μ_N, which corresponds to an increase in the value of the viscosity coefficient η, the discrepancies between the experimental and calculated dependencies $\sigma(\varepsilon)$ increase. It follows that by varying the values of μ_N for known functions $E_S(\varepsilon)$ and $E_D(\varepsilon)$, based on equation (1) and comparisons of experimental and calculated curves $\sigma(\varepsilon)$, it is possible to determine approximate values of μ_N. As seen from Fig. 5, an increase in the value of the bulk viscosity coefficient η (a decrease in the bulk viscosity parameter η) leads to an increase in the yarn breakage stresses (curve 3).

The analysis results of the proposed physically nonlinear law of yarn strain show that equations (1) and (2) with the defining relations correspond to the results of experiments on yarn stretching to breakage. The proposed law also describes the «loading-unloading» process with semi-cyclic or variable changes in strain over time.

Consider the process of yarn strain, described by equations (1)–(5), under irregular dynamic loads, the analysis of which is given in [8-11]. By [8-11], the strain change is set by the following equation:

$$\varepsilon = \varepsilon_{\max} \sin\left(\pi n\left(t - t_R\right)/2t_k\right) \tag{8}$$

where $\varepsilon_{\max}$ – is the maximum value of strain, after reaching which unloading begins; n – is the number of irregular loading cycles in the time interval $0 \le t \le t_k$; t_k – is the time of yarn breakage after ε reaches the critical strain ε_k; t_R – is the end time of each loading-unloading cycle. The initial values of the parameters of the elastic-viscoplastic model of yarn strain (1)–(5) are $T = 10$ tex; $\gamma_N = 1.02$; $\gamma_m = 1.07$; $\mu_N = 10$ s^{-1}; $K_R = 100$; $n = 5$. In this case, the equations of the model correspond to the elastic-plastic strain of the yarn since $E_D \approx E_S$ [5].

Following the results of publications [1-4], in computer calculations, the strain values determined from equation (8) were taken only with a positive sign since the yarn does not work in compression:

$$\varepsilon = \left|\varepsilon_{\max} \sin\left(\pi n\left(t - t_R\right)/\left(2t_k\right)\right)\right| \tag{9}$$

Considering (9), yarn stretching occurs in a semi-cyclic mode.

The loading-unloading process depends on the value of $\varepsilon_{\max}$. By varying $\varepsilon_{\max}$, it is possible to obtain unloading of the yarn in any range of strain changes.

Consider the «loading-unloading» process in the range of elastic strains $\varepsilon \le 0 \le \varepsilon_e$. For this case, $\varepsilon_{\max}$ is taken as $\varepsilon_{\max} = 0.97\varepsilon_e$. All other parameters of the model are determined from the relationships given in [5]. The strain changes over time are shown in Fig. 6. Seven half-cycles of «loading-unloading» occur at $t =$ 10.

Fig. 7 shows the changes in stresses over time.

Due to the manifestation of the viscous properties of the yarn, a time «delay» of strain from stress occurs (Fig. 6).

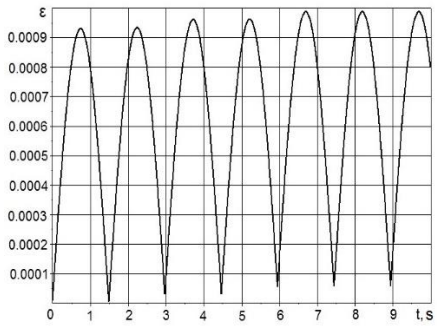

Figure 6. - **Changes in strains over time for ε_{max}=0.97ε_e**

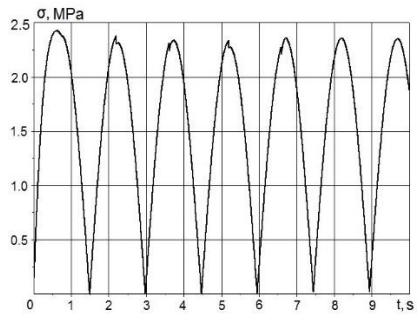

Figure 7. - **Changes is stresses over time for ε_{max}=0.97ε_e**

The stress is zero ($\sigma = 0$) at the strain value of $\varepsilon \neq 0$. Then the stresses increase in the next cycle, i.e. non-zero strain values are not residual strains (Fig. 8). As stated, diagrams $\sigma(\varepsilon)$ are built based on graphs $\sigma(t)$ and $\varepsilon(t)$, shown in Figs. 6 and 7.

In the first cycle, the yarn is loaded along curve 1. As seen, under loading, dependence $\sigma(\varepsilon)$ is highly nonlinear. After reaching strain value $\varepsilon = \varepsilon_{\max}$, unloading occurs along the line $E_R = E_D \approx E_S = E_e$ (line 2) without the formation of residual strain. Secondary loading occurs along unloading line 2 and then this process repeats along lines 2, 3, 4, etc. As noted, in this range the process of yarn strain is reversible.

When unloading occurs in the range $0 \le \varepsilon \le \varepsilon_m$, i.e. $\varepsilon_{\max} = 0.97\varepsilon_m$, the strain process changes completely (Fig. 9). In this option, the initial data of the problem do not change, except for the value of $\varepsilon_{\max}$. The strain changes related to this option are shown in Fig. 10.

While in the previous case, unloading occurred in the range of strains $\varepsilon \le 0 \le \varepsilon_e$, according to equation (3) along the loading line (along E_D), in this case, unloading occurs by equation (4), and the slope of the unloading modulus to the strain axis is quite large.

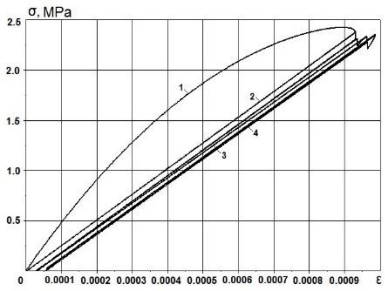

Figure 8. - **Elastic process of yarn loading-unloading**

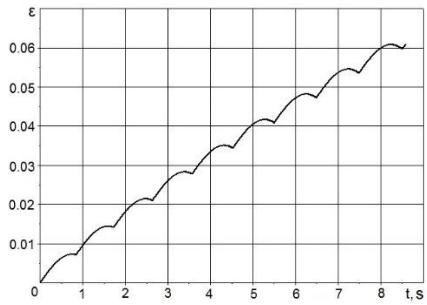

Figure 9. - **Change in strains over time for ε_{max}=0.97ε_m**

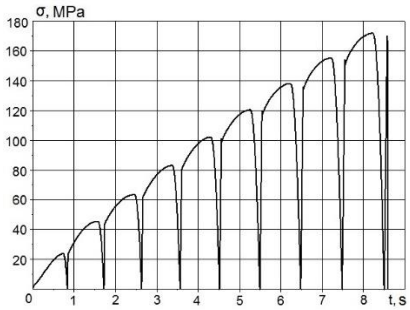

Figure 10. - **Change in stresses over time for ε_{max}=0.97ε_m**

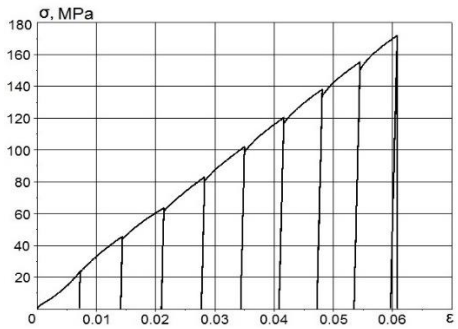

Figure 11. - **Dependencies $\sigma(\varepsilon)$ for ε_{max}=0.97ε_m**

Therefore, a slight decrease in the strain values after reaching the maximum is enough to completely unload the yarn. As a result, wave-like changes in strain values over time occur (Fig. 9).

Fig.10 shows the changes in stresses time-related to this case. As seen from Fig. 10, a slight decrease in strain after reaching $\varepsilon = \varepsilon_{\max}$ leads to the decrease in stress to zero due to the

manifestation of the viscous properties of the yarn and the large value of E_R determined from $K_R = E_R / E_D$, where $K_R = 100$, and accordingly, $E_R = 100\ E_D$.

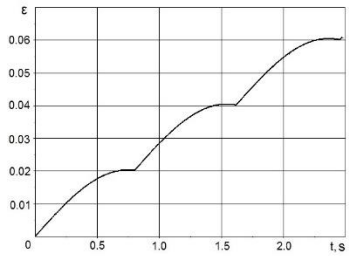

Figure 12. - **Changes in strains over time for ε_{max}=0.97ε_S**

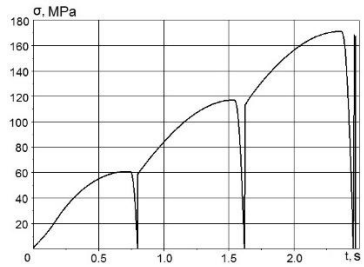

Figure 13. - **Changes in stresses over time for ε_{max}=0.97ε_S**

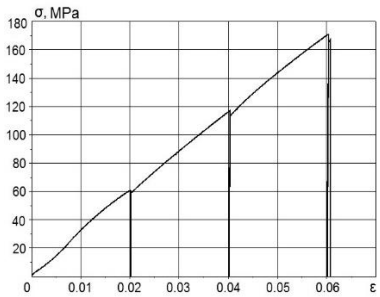

Figure 14. - **Dependencies $\sigma(\varepsilon)$ for ε_{max}=0.97ε_S**

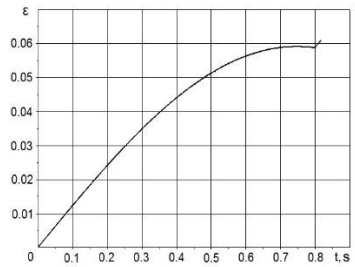

Figure 15. - **Changes in strains over time for ε_{max}=0.97ε_k**

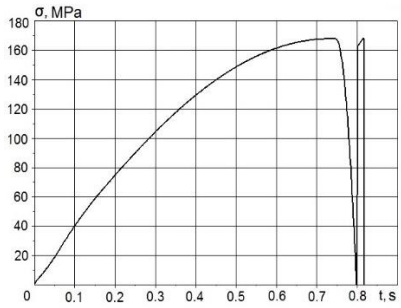

Figure 16. - **Changes in stresses over time for ε_{max}=0.97ε_k**

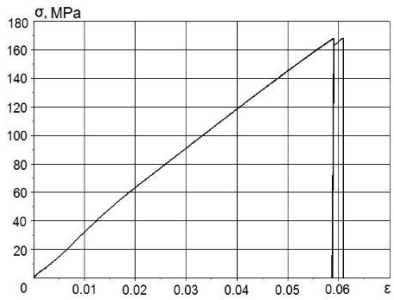

Figure 17. - **Dependencies $\sigma(\varepsilon)$ for ε_{max}=0.97ε_k**

Diagrams $\sigma(\varepsilon)$ for this option are shown in Fig. 11. Here, too, almost vertical stress relief is observed under a slight decrease in strain. According to the accepted model of strain near the maximum value of $(\varepsilon_{\max} = 0.97\varepsilon_m)$, the process of yarn tension is completely irreversible. According to this, vertical unloading $(E_R = 100\ E_D)$ occurs in diagram $\sigma(\varepsilon)$ in Fig. 11. Then, the changes in the stress-strain over time and diagrams $\sigma(\varepsilon)$ in the range $\varepsilon_m \le \varepsilon \le \varepsilon_k$ are shown in Figs. 12-17.

The following values are taken for these options $\varepsilon_{\max} = 0.97\varepsilon_S$ (Figs. 12–14) and $\varepsilon_{\max} = 0.97\varepsilon_k$ (Figs. 15–17). In these cases, in nonlinear dependencies $\sigma(\varepsilon)$ under loading, it is observed that unloading occurs almost instantly.

In the cases discussed above, for $\gamma_N = 1{,}02$; $\gamma_m = 1.07$, the equations of model (1) practically pass to the Hooke model of an elastic medium.

To consider the influence of the viscous properties of yarn under semi-cyclic (dynamically irregular) loads, we will analyze the results of computer calculations for different values of γ_N, γ_m, and μ.

The following values of the initial data remain unchanged for this case $T = 10$ tex; $\gamma_N = 1.1$; $K_R = 100$; $n = 5$; $\varepsilon_{\max} = 0.97\varepsilon_m$. The values of parameters γ_N and μ_N varied (Fig. 18).

For $\gamma_N = 1.1$; $\gamma_m = 2$ (Fig. 18), unloading occurs almost vertically and the residual strain is significant, i.e. the process is almost completely irreversible (curves 1, 2). With an increase in the viscous characteristics of the yarn ($\gamma_N = 1.1$; $\gamma_m = 4$ and $\mu_N = 5$ s^{-1}) the course of curves $\sigma(\varepsilon)$ also changes (curve 3). A decrease in the initial value of the viscosity parameter to $\mu_N = 1$ s^{-1} corresponds to an increase in the viscosity coefficient, which leads, as in the case before the breakage, to an increase in stress values at the same yarn strains (curve 4).

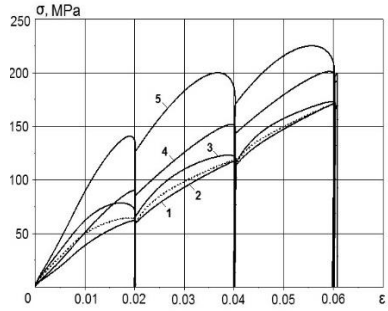

Figure 18. - **Elastic-viscoplastic strain of cotton yarn**

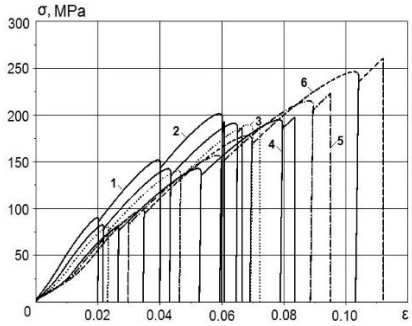

Figure 19. - **Elastic-viscoplastic model of strain depending on the linear density of yarn**

For the case when $\gamma_N = 1.1$; $\gamma_m = 2$ and $\mu_N = 1$ s^{-1}, which corresponds to a stronger manifestation of the viscous and plastic properties of the yarn, high nonlinearity appears in dependences $\sigma(\varepsilon)$ (curve 5). The maximum stress values also increase with increasing viscous properties of different types of yarns (Fig. 18).

Fig. 19 shows the «loading-unloading» half-cycles for linear densities $T = 10$, 20, 30, 50, 70, and 100 tex, obtained on a computer (curves 1–6, respectively). In this option, the initial parameter values are $\gamma_N = 1.1$; $\gamma_m = 2$ and $\mu_N = 1$ s^{-1}; $K_R = 100$; $n = 5$; $\varepsilon_{\max} = 0.97\varepsilon_m$. In the calculations performed on a computer, only the linear yarn densities T changed.

As seen from Fig. 19, with an increase in the linear density of the yarn, the value of the critical strain increases, accordingly, the critical stress at which the yarn breaks increases. Dependence $\sigma(\varepsilon)$ is nonlinear, and the process of yarn strain is irreversible.

5. Conclusions.

The conducted studies showed that the elastic-viscoplastic law, developed based on experimental results on yarn tension, fully describes the process of yarn strain under various loads, including semi-cyclic-irregular dynamic loads that arise in technological processes of textile production.

The proposed law considers the elastic, viscous, and plastic properties of cotton yarn with different linear densities. The parameters of the law can be determined from the results of experiments on yarn tension on standard tensile installations for stretching yarn.

The nonlinear elastic-viscoplastic law of cotton yarn strain can be used in solving applied problems to study the process of deformation and breakage of cotton yarns.

References

1. *Sultanov K.S., Ismoilova S.I.* Strength of the yarns at high velocities of their motion in technological processes of textile production, In: Proceedings of the International Conference on Actual Problems of Applied Mechanics - APAM - 2021. 2637, 030020, 2022, 20 October 2022. 030020-1-16.

2. *Ismoilova S.I.* Deterministic method to calculate the strength of cotton yarns, In: Proceedings of the International Conference on Actual Problems of Applied Applied Mechanics - APAM - 2021. 2637, 030018, 20 October 2022. 030018-1-9.

3. *Sultanov K.S., Ismailova S.I.* Determination of the strength of cotton yarn based on a nonlinear elastoviscoplastic deformation model // Izvestia of Universities. Textile industry technology. Ivanovo. 2018, No. 3 (375). pp. 95-101.

4. *Sultanov, K., Ismoilova, S., Begmanov R., Khazratova T.* Influence of textile yarn velocity in technological processes on its strength, In: Proceedings of the AIP Conference, 2024, 3045(1), 040028. Vol. 3045, Issue 1, 11 March 2024. 040028-1-6.
5. *Sultanov K.S., Ismailova S.I.* Nonlinear Elastic-Viscoplastic Law of Cotton Yarn Deformation, In: Proceedings of the AUTEX 2017 World Textile Conference. 2017. pp. 956-958.
6. *Matthes A., Pusch T. Cherif C.* Numerical simulation of yarn tensile force for dynamic yarn supply systems of textile machines // The Journal of The Textile Institute, 2012, 103(1), pp. 70-79.
7. *Liu K., Zhou Y., Xu W.* Numerical analysis of the tension and twist of staple strands in embeddable and locatable spinning // Textile Research Journal. 2019, 89(8), pp. 1582-1592.
8. *Grechukhin A.P., Seliverstov V.Yu., Rudovskiy P.N.* The method of determination of yarn bending rigidity and friction factor during interaction of fibers // The Journal of The Textile Institute, 2017, 108(12), pp. 2067-2072.
9. *Halfaou R., Chemani B.* The influence of cyclic deformation on the strength and elongation at break of carded and combed wool yarns // The Journal of The Textile Institute, 2013, 104(11), pp. 1156-1163.
10. *Jiang Z., Yu C., Yang J., Han G., Xing M.* Estimation of yarn strength based on critical slipping length and fiber length distribution // Textile Research Journal. 2019, 89(2), pp. 182-194.
11. *Gao X., Li Y., Chen H.* On the dynamic model of yarn with time-dependent tension // The Journal of The Textile Institute, 2014, 105(4), PP.454-459.
12. *Kargar M., Payvandy P.,Mozafary V.* A numerical structure-based method of simulating filament yarns // The Journal of The Textile Institute, 2022, 113(12), pp. 2681-2693.
13. *Mei D., Xia F., Wan A., Ma P.* Mechanical properties and hairiness characterizations of compact-spinning cotton yarn in warp-knitting processing // The Journal of The Textile Institute, 2022, 113(9), pp.1950-1957.
14. *Zubair M., Neckar B., Eldeeb M., Gulzar A.* Tensile behavior of staple fiber yarns, part IV: experimental verification of predicted stress–strain curves // The Journal of The Textile Institute, 2017, 108:8, pp.1291-1296.
15. *Zubair M., Eldeeb M., Neckar B.* Tensile behavior of staple fiber yarns part III: comparison of mathematical models // The Journal of The Textile Institute, 2017, 108:7, pp. 1234-1237.

DETERMINATION OF STRAIN MODULI PARAMETERS OF COTTON YARN UNDER THE CHANGE IN ITS STRUCTURE

Ismoilova S.I.[1], Khazratova T.Ya.[1], Begmanov R.A.[1], Mamatova N.R.[2]
[1]*Institute of Mechanics and Seismic Stability of Structures named after M.T.Urazbaev, Tashkent, Uzbekistan*
[2]*Institute of Textile and Light Industry, Tashkent, Uzbekistan*
E-mail: ismailova.sabida@mail.ru

Abstract*. The results of experimental and theoretical studies of the strength of cotton yarns, when stretched to breakage, are presented in the article. The functions of changing the parameters of the physically nonlinear elastic-viscoplastic law of strain of cotton yarn are determined based on the results of processing experimental data on tension to breakage. These functions make it possible to determine the averaged values of the nonlinear law parameters, which allows its use in practice when solving applied problems of yarn mechanics, determining and assessing the strength of cotton yarns.*

Keywords*: cotton yarn, strain modulus, breakage, stress, strain, tension, nonlinear law, linear density.*

1. Introduction.

The mechanical properties of cotton yarns (hereinafter, yarns) are determined by their structure. There is an opinion [1], that it is impossible to construct laws for the yarn behavior under loading if ignore the yarn structure and the characteristics of fibers (length, heterogeneity along the length, inter-fiber friction, how the moduli of individual fibers are transferred to the yarn modulus, etc.).

The mechanical properties of yarn are described quantitatively and qualitatively by mathematical relationships between the stressed state (stress tensor), configuration (strain tensor and tensors derived from it), and time. These relationships are found in experiments for yarn testing under different loads [2].

The experiment accounts for the internal processes occurring in yarns under strain, i.e. in the experiment on yarn tension, all the characteristics of the internal process appear under its stretching. The experimental diagrams $F(\varepsilon)$ are quantitative and qualitative results of these phenomena, including the influence of the geometric and mechanical characteristics of cotton fiber and inter-fiber friction on the process of yarn strain, as a whole. Thus, the experimental laws of yarn strain $F(\varepsilon)$ consider the complex structure of yarns, including staple fibers and changes in their structure

when stretched (strained). The laws $F(\varepsilon)$ obtained from experiments are a consequence of the size effect (fiber length), fiber length heterogeneity (cross-sectional variation), strain rate, and how the fiber moduli are transferred to the yarn modulus when the yarn is strained (stretched).

The point is that all physical-mechanical, geometric properties of fibers and their interaction are taken into account by the experimental law of yarn tension, i.e. by dependence $F(\varepsilon)$ obtained from experiments. The development of the law of yarn strain that corresponds to the experimental law will lead to the creation of physically nonlinear equations of yarn state. When developing the laws of physically nonlinear yarn strain, it is necessary to determine the variable strain moduli and viscosity coefficient of yarn. In [3], such studies were conducted phenomenologically for the Voigt model. There are two solutions here.

The first way is, following [4-7], to construct mathematical relationships for determining the yarn modulus through the fiber moduli. These relationships must take into account the arrangement of fibers in the yarn, inter-fiber friction forces, fiber length, heterogeneity along the length, etc. There are a number of physical and mathematical difficulties here. To overcome them, some simplifications and idealization of the yarn structure are assumed.

The second way is to determine the strain moduli directly based on experimental tensile diagrams. In this case, as noted, the experimental diagram considers all of the above properties of fibers in the yarn, which manifest themselves in the experiment and are reflected in the tensile diagrams. The strain moduli obtained from this diagram are obviously more accurate than in the first case, so the second way was applied in determining the strain modulus of yarns.

2. Materials, methods, and object of study.

To determine the experimental laws of the strain of cotton yarn, i.e. «tensile force-strain» diagrams, experiments were conducted on a standard tensile testing device «Tenso Master» in accordance with state standards GOST 6611.2-73.

The software in-built inTenso Master device partially processes statistics of the experimental data obtained. To conduct the experiments, we used homogeneous carded yarn, produced on a pneumo-mechanic spinning machine from medium-staple cotton of the 1st grade, 1st maturity group, 4th fiber type, according to state standards Uz DSt 2321:2011.

Yarns with nominal linear densities were selected for testing (the number of bobbins is indicated in parentheses): $T = 14.0$ (2); 15.4 (2); 16.5 (2); 18.5 (5); 29.0 (16); 50.0 (10); 72.0 (4); 100.0 (3) and 160.0 (1) tex.

For a given nominal linear density of $T = 14.0$ tex: 14.56 and 14.6 tex; for $T = 15.4$ tex: 14.7 and 15.0 tex; for $T = 16.5$ tex: 16.7 and 16.9 tex; for $T = 18.5$ tex: 17.73; 18.41; 18.6; 19.2 and 20.2 tex; for $T = 29.0$ tex: 27.7; 28.10; 28.30; 28.50; 28.52; 28.61; 28.63; 28.7; 28.96; 29.03; 29.1; 29.27; 29.4; 29.5; 29.56 and 31.3 tex; for $T = 50.0$ tex: 48.18; 48.2; 48.54; 49.10; 49.16; 49.32; 49.8; 50.03; 50.02 and 50.7 tex; for $T = 72.0$ tex: 70.68; 71.41; 71.21 and 71.42 tex; for $T = 100.0$ tex: 97.36; 97.4; 102.76 tex and $T = 162.13$ tex.

The selection of yarns with these linear densities was random [8-13]. Before conducting the experiments, the actual linear density of yarn for each bobbin was determined separately according to GOST 6611.1-73. To measure the linear density of yarn, 50 small balloons of yarn (skeins) 112.5 m long (100 revolutions of bobbin reel) were wound automatically using an NM-3 reeling machine. After this, the wound samples were weighed one by one on an SK-60H scale.

Using the results of linear density measurements for each reel, the coefficients of variation of linear density irregularity (quadratic irregularity) were determined according to GOST 6611.1-73 and the methods given in [8-9]. The values of the coefficients of variation for 45 bobbins of yarn examined in experiments varied from 0.6 to 2%, which corresponds to the Republican standard Uz DSt 604:2016.

Yarn from each bobbin was tested 50 times in succession, i.e. experiments were repeated 50 times. The resulting 50 curves of tensile force F (cH) versus strain ε (%) were averaged by the software of the device.

3. Statement of the problem.

Based on fundamental ideas [1-7] in [8,9], a physically nonlinear elastic-viscoplastic law of yarn strain under tension considering the unloading was proposed in the following form:

$$E_D^{-1}(\varepsilon)\frac{d\sigma}{dt}+E_S^{-1}(\varepsilon)\mu(\varepsilon)\sigma=\frac{d\varepsilon}{dt}+\mu(\varepsilon)\varepsilon \quad \text{for } \frac{d\varepsilon}{dt}>0 \tag{1}$$

$$E_R^{-1}(\varepsilon)\frac{d\sigma}{dt}=\frac{d\varepsilon}{dt} \quad \text{for } \frac{d\varepsilon}{dt}\le 0 \tag{2}$$

where $\sigma-$is the longitudinal tensile stress, $\varepsilon-$is the longitudinal strain of yarn, and $t-$ is time.

In [9], the nonlinear function $E_S(\varepsilon)-$the quasi-static modulus of strain under yarn tension is defined. There, the methods for determining $E_D(\varepsilon)-$the function of the dynamic modulus of strain, $\mu(\varepsilon)-$the function of the viscosity parameter, and $E_R(\varepsilon)-$the function of the unloading modulus are considered [9]. The strain law (1) is developed based on a linear viscoelastic model of a standard linear body.

In [9], it is shown that the nonlinear function of change in the yarn strain modulus $E_S(\varepsilon)$ has the following parameters: E_N- the initial value for $\varepsilon=\varepsilon_N=0$; E_e- the minimum value for $\varepsilon=\varepsilon_e$; $E_m-$the maximum value for $\varepsilon=\varepsilon_m$; $E_k-$the critical value of the strain modulus for $\varepsilon=\varepsilon_k$ at the time of yarn breakage.

In [9], another value of the strain modulus was introduced in interval $[\varepsilon_m\ \varepsilon_k]$ indicated E_S for $\varepsilon=\varepsilon_S$. The fact is that a decrease in strain in interval $[\varepsilon_m\ \varepsilon_k]$ is not always observed. In some cases, after reaching E_m, in a further increase in strain, the decrease in E stops and remains approximately constant or increases. This time point for $\varepsilon=\varepsilon_S$ and $E=E_S$ in [10] is fixed as an additional point. Beyond this point the value of E either decreases, remains constant, or increases.

Thus, the parameters for changing the strain modulus $E(\varepsilon)$ under yarn tension to breaking are E_N, E_e, E_m and E_k. Using these data, we consider the patterns of changes in these parameters on linear density T based on experimental data [9-11]. These patterns are essential for assessing and predicting strength and for constructing a physically nonlinear law of cotton yarn strain.

Fig. 1 shows 50 dependences of tensile force on relative strain $F(\varepsilon)$, obtained for yarn of a linear density of 29.0 tex [11].

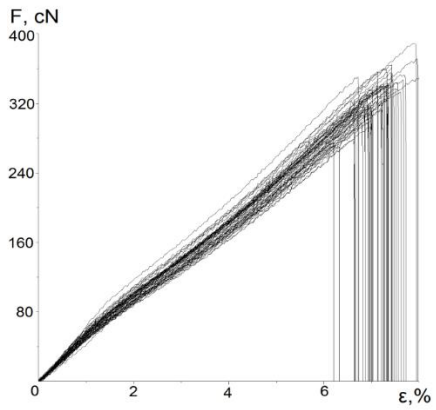

Figure 1. - **Experimental Dependencies *F*(*ε*) for yarn with a linear density of *T*=29.0 tex**

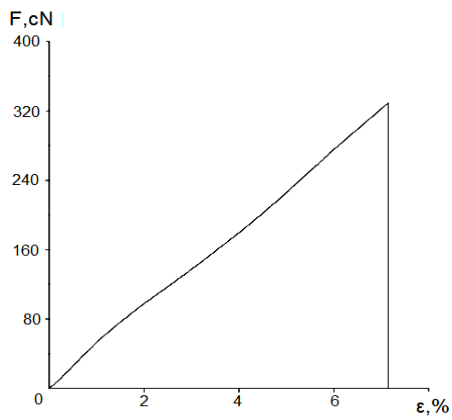

Figure 2. - **Average diagram *F*(*ε*) for yarn with linear density *T*=29.0 tex**

The nonlinearity of dependencies $F(\varepsilon)$ is related to changes in the yarn structure under tension. When yarn is stretched, a complex process of its structure change occurs, associated with

relative displacements of cotton fibers, which primarily determines the nature of the change in dependence $F(\varepsilon)$, that is, the pattern of yarn tension. As seen in Fig. 1, the experimental laws of yarn strain $F(\varepsilon)$ consider its complex structure consisting of staple fibers [11].

The experiment registers the internal processes occurring in the yarn under strain. The experimental results or experimental diagrams $F(\varepsilon)$ are quantitative and qualitative consequences of these phenomena, including the influence of the geometric and mechanical characteristics of cotton fiber, inter-fiber friction on the strain process of yarn as a whole. The point is that the experimental law of yarn tension accounts for all physical, mechanical, and geometric properties of fibers, as seen in dependence $F(\varepsilon)$ obtained in experiments.

When developing the laws of nonlinear strain of yarn, it is necessary to determine the variable strain modulus and viscosity coefficient of yarn.

The first way is, following [5–8], to construct mathematical relationships to determine the yarn modulus through the fiber moduli. The second way is to determine the strain modulus based on experimental tensile diagrams. We applied the second way.

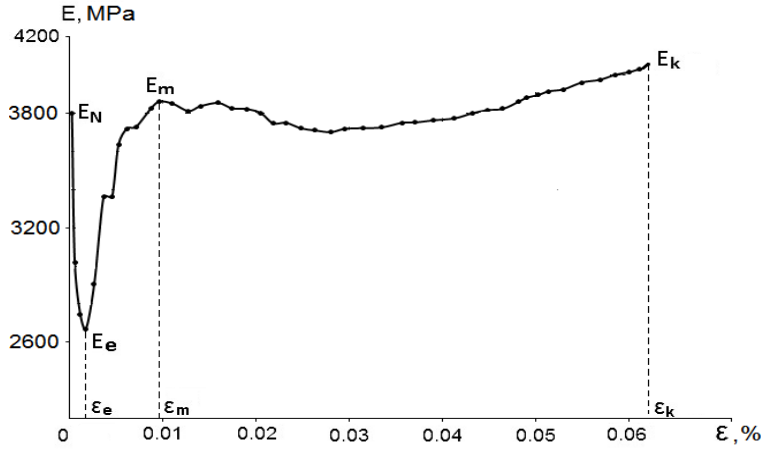

Figure 3 - **Change in strain modulus *E* depending on longitudinal strain ε for cotton yarn of a linear density of *T*=29.0 tex**

To determine the strain modulus, we used the averaged dependence $F(\varepsilon)$ (Fig. 2), given by the Tenso Master tensile device for each series of experiments. To do this, curve $F(\varepsilon)$ in Fig. 2 is divided into 50 intervals with approximately the same step $\Delta\varepsilon$. The strain modulus for these points of intervals is defined as $E = F/\varepsilon$, where F and $\varepsilon -$are the values of the longitudinal tensile force and strain in %, at the boundaries of intervals [8,9].

Fig.3 shows the dependencies of the secant modulus of strain on strain $E(\varepsilon)$, determined from the averaged dependencies $F(\varepsilon)$ in Fig. 2.

The pattern of change in strain modulus $E(\varepsilon)$ in Fig. 3 shows that at the beginning of the process of cotton yarn strain, the strain modulus drops abruptly from the initial value E_N to the value E_e for $\varepsilon = \varepsilon_e$. Next, there is an increase in the value E to the maximum E_m, for $\varepsilon = \varepsilon_m$, then modulus E decreases to E_k for $\varepsilon = \varepsilon_k$. When $\varepsilon = \varepsilon_k$ reaches $E = E_k$, the cotton yarn breaks.

From each dependence $E(\varepsilon)$, the values of parameters E_N, E_e, E_m, E_k were determined according to the methods given in [9-11].

Thus, the parameters for strain modulus $E(\varepsilon)$ variation under yarn tension to breaking are E_N, E_e, E_m, E_k. Using these data, we first consider the patterns of change in the strain modulus as a function of linear density T. These patterns are essential for assessing and predicting strength and constructing a physically nonlinear law of yarn strain.

4. Results.

The changes in the initial values of the strain modulus E_N depending on the actual linear density T, constructed based on experimental results [10,11], are given in Table 1.

Dependence $E_N(T)$ in the form of graphs is given in [10].

For an analytical description of curves [10], the experimental curve was averaged over the nominal values of the linear densities of cotton yarn. At that, close values of nominal linear densities were combined into one group. As a result, the following six groups of linear densities were obtained.

The first group included all yarns with nominal linear densities of $T = 14.0$; 15.4; 16.5; 18.5 tex. The second group consisted of yarns with $T = 29.0$ tex. The third group included yarns with $T = 50.0$ tex. The fourth group included yarns with $T = 72.0$ tex. The fifth group included yarns with $T = 100.0$ tex, and the sixth group consisted of yarns with $T = 160.0$ tex. For each group, linear density values and parameters E_N, E_e, E_m and E_k were averaged.

Table 1.

Average values of the initial strain modulus E_N and linear density T of cotton yarn by groups

Group No.	1	2	3	4	5	6
T_{cp}, tex	17.0	28.95	49.32	71.42	99.17	162.13
E_N^{cp}, MPa	5532.91	2722.49	2389.64	2031.42	2608.58	2474.86

To approximate curves $E_N(T)$, we chose a decreasing power function in the following form:

$$E_N(T) = E_{Nk}\left(\frac{T}{T_S}\right)^{\chi_1} \tag{3}$$

where E_{Nk}, T_S, and χ_1 – are the coefficients of function (3), to be determined. Ratio T/T_S is taken to have a dimensionless quantity in parentheses in relation (3). For a value of $T_S = 29.0$ tex, in most cases, the value of parameters of dependence $E(\varepsilon)$ becomes steady or begins to increase.

The remaining two parameters of formula (3) E_{Nk} and χ_1 are determined by the least squares method on a computer, and they are $E_{Nk} = 2872.944$ MPa and $\chi_1 = -0.302174$. Here χ_1 – is a dimensionless quantity.

Using formula (3), we can determine the value of the strain modulus E_N, for any value of the yarn linear density obtained by the pneumo-mechanic method of spinning by a carded system.

Table 2 shows changes in the second parameter of $E(\varepsilon)$ - the minimum value of the strain modulus E_e, depending on the linear density of yarns.

Table 2.

Average values of the minimum strain modulus E_e and linear density T of cotton yarn by groups

Group No.	1	2	3	4	5	6
T_{cp}, tex	17.0	28.95	49.32	71.42	99.17	162.13
E_e^{cp}, MPa	2779.46	1507.56	1099.30	1036.51	854.18	767.71

Here, too, for the analytical description of the obtained curves [10,11], the experimental curve was averaged over the nominal values of the linear densities of cotton yarn.

We approximate the curves using a power function in the following form:

$$E_e(T) = E_{ek}\left(\frac{T}{T_S}\right)^{\chi_2} \tag{4}$$

Coefficient values $E_{ek} = 1274.765$ MPa and $\chi_2 = -0.544665$ were obtained using the least squares method.

Table 3 shows similar changes in the parameter of the maximum value of the yarn strain modulus E_m depending on the linear density of yarn T.

Table 3.

Averaged values of maximum strain modulus E_m and linear density T of cotton yarn by groups

Group No.	1	2	3	4	5	6
T_{cp}, tex	17.0	28.95	49.32	71.42	99.17	162.13
E_m^{cp}, MPa	3802.91	2718.37	2524.85	2912.20	1815.86	2524.85

To describe the curves [10,11] for this case, we choose a power function in the following form:

$$E_m(T) = E_{mk}\left(\frac{T}{T_S}\right)^{\chi_3} \tag{5}$$

The values of coefficients $E_{mk} = 2705.089$ MPa and $\chi_3 = -0.202455$ are determined by the least squares method. $T_S = 29.0$ tex.

Table 4 shows changes in the critical strain modulus E_k reached before cotton yarn breakage, depending on its linear density.

Table 4.

Average values of the critical strain modulus E_k and linear density T of cotton yarn by groups

Group No.	1	2	3	4	5	6
T_{cp}, tex	17.0	28.95	49.32	71.42	99.17	162.13
E_k^{cp}, MPa	3513.71	2307.18	2285.46	2273.63	1674.13	1382.22

In this case, function (6) was used to approximate curves $E_k(T)$.

$$E_k(T) = E_{kk}\left(\frac{T}{T_S}\right)^{\chi_4} \tag{6}$$

The values of coefficients $E_{kk} = 2222.351$ MPa and $\chi_4 = -0.365873$ were also determined using the least squares method. Here, $T_S = 29.0$ tex.

Thus, changes in the function parameters of the strain modulus $E(\varepsilon)$, initial modulus E_N, minimum modulus E_e, maximum modulus E_m, and critical modulus E_k depending on the value of the linear density of cotton yarn are determined based on the processing of experimental results in cotton yarn tension to breakage [13].

The pattern of changes in functions $E_N(T)$, $E_e(T)$, $E_m(T)$ and $E_k(T)$ according to the results given in [13] are approximately the same: they generally decrease with an increase in the value of the linear density of cotton yarn.

Formulas (3)-(6) allow us to determine the values of E_N, E_e, E_m, and E_k for any values of the linear density T of the yarn by calculation. The values obtained of the strain moduli E_N, E_e, E_m, and E_k correspond to a certain average value of these moduli for carded yarns with the linear density T obtained by the pneumo-mechanic spinning. For other spinning systems and methods, these parameters must be determined from the results of appropriate experiments on yarn tension to breakage.

5. Discussion.

Based on the processing of the experimental results given in [10-11], formulas were developed to determine analytically the values of parameters E_N, E_e, E_m, and E_k. These parameters characterize changes in the strain modulus of cotton yarn when it is stretched to

breakage. The experimental results [10-12] made it possible to construct analytical functions (3)-(6) to determine the values of these parameters depending on the linear density of cotton yarn.

As noted above, using analytical formulas (3)-(6), it is possible to determine the value of the parameters for changing the strain modulus of yarn of the carded system, produced on an pnuemo-mechanic spinning machine from medium-staple cotton of the 1st grade, 1st maturity group, 4th type fibers Due to the essential importance of these analytical relationships, we present them separately in Table 5.

Table 5.

Formulas for determining the values of parameters for changing the strain modulus depending on linear densities of cotton yarn (T_S=29.0 tex and ε_N=0)

No.	Proposed formula	Coefficients of the formulas and their values	
(3)	$E_N(T) = E_{Nk}\left(\frac{T}{T_S}\right)^{\chi_1}$	$E_{Nk} = 2872.944$ MPa	$\chi_1 = -0.302174$
(4)	$E_e(T) = E_{ek}\left(\frac{T}{T_S}\right)^{\chi_2}$	$E_{ek} = 1274.765$ MPa	$\chi_2 = -0.544665$
(5)	$E_m(T) = E_{mk}\left(\frac{T}{T_S}\right)^{\chi_3}$	$E_{mk} = 2705.089$ MPa	$\chi_3 = -0.202455$
(6)	$E_k(T) = E_{kk}\left(\frac{T}{T_S}\right)^{\chi_4}$	$E_{kk} = 2222.351$ MPa	$\chi_4 = -0.365873$

Thus, using the formulas given in Table 5, the values of the parameters for changing the strain modulus are determined for any values of linear densities when stretching cotton yarn to breakage. This makes it possible to construct a physically nonlinear law of strain of cotton yarn under tension and facilitates its use in practice for strength calculations of yarn.

Comparative graphs of changes in parameters E_N, E_e, E_m and E_k depending on the linear densities of cotton yarn T, are shown in Fig. 4. Here, curves 1-4 are constructed using formulas (3)-(6) from Table 5.

Curve 1 refers to the change in the initial value of strain modulus E_N depending on the linear density of yarn T, i.e. $E_N(T)$; curve 2 refers to function $E_e(T)$; curve 3 – to function $E_m(T)$; and curve 4 – to function $E_k(T)$.

As seen in Fig. 4, changes in the parameters of strain moduli E_N, E_e, E_m and E_k with increasing linear density of yarn decrease monotonically. At high values of the linear density of yarns, for example $T \geq 90$ tex, the values of E_N and E_m converge and become approximately the same.

In these cases, the strain modulus of yarn, after reaching the maximum value, practically remains constant and then, after a slight increase in strain, decreases to a critical value (Fig. 4, curves 1-4).

Based on the analysis of the strain modulus dependences on the tensile strain, the patterns of changes in the function parameters of strain modulus $E(\varepsilon)$ depending on the linear density of yarns were determined. The proposed functional relationships that describe changes in parameters $E_S(\varepsilon)$ make it possible to determine the values of parameters E_N, E_e, E_m and E_k depending on the linear density of yarns.

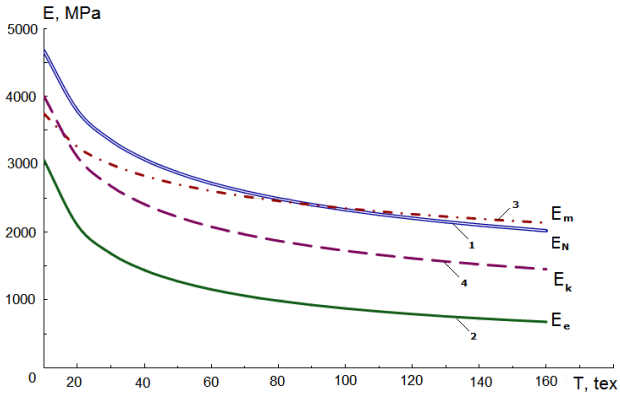

Figure 4. - **Comparative graphs of strain modulus parameters under yarn tension to breakage**

This gives grounds to use the proposed nonlinear law of yarn strain in applied problems of the mechanics of textile threads and yarns in assessing and predicting the strength of cotton yarn. Based on the proposed methodology, it is possible to determine the functional parameters of the nonlinear law for various types of yarns and textile threads and evaluate the applicability of the proposed law under the strain of these materials.

6. Conclusion

1. From the results of experiments on stretching cotton yarn to breaking, changes in the strain modulus of yarn during its strain were determined, as a consequence of changes in its structure; patterns of changes in the parameters of function $E(\varepsilon)$ were also determined. Based on these patterns, specific formulas were obtained for determining the values of these parameters by calculation for any yarn with known linear density.

2. The proposed functional relationships make it possible to determine the values of the parameters of the strain modulus depending on the linear density of yarn. This allows the proposed nonlinear law of cotton yarn strain to be used in applied problems of the mechanics of textile threads and yarns.

3. Based on the methods developed, it is possible to determine the functional parameters of the proposed nonlinear law for various types of yarns and textile threads and evaluate the applicability of the proposed law for materials under strain, which is a task for future research.

References

1. *Jiang Z., Yu C., Yang J., Han G., Xing M.* Estimation of yarn strength based on critical slipping length and fiber length distribution // Textile Research Journal. 2019, 89(2), pp. 182-194.
2. *Zhu L., Marriam I., Xu F.* Experimental and theoretical study on the strain rate dependence of the mechanical properties of Twaron fiber tows with different fiber fineness // Textile Research Journal, 2019, 89(12), pp. 2395-2405.
3. *Sriprateep K.* CAD/CAE for stress–strain properties of a wide range of multifilament twisted man-made filament yarns // Textile Research Journal, 2019,89(2), pp. 204-215.
4. *Grechukhin A.P., Seliverstov V.Yu., Rudovskiy P.N.* The method of determination of yarn bending rigidity and friction factor during interaction of fibers // The Journal of The Textile Institute, 2017, 108:12, pp.2067-2072.
5. *Kovačević S., Schwarz I., Brnada S.* Study of predicting the number of warp thread breaks during the weaving process // Textile Research Journal, 2022, 92(23-24), pp. 4954-4968.
6. *Duo Xu, Ziyi Su, Hang Fan, Wangwang Yang, Jian Fang, Keshuai Liu, Weilin Xu.* Improving spun yarn properties by contacting fiber strand with special-shape condensed surfaces // The Journal of The Textile Institute, 2022, 113:11, pp. 2408-2419.
7. *Li S., Ma X., Hou X., Wang S., Wang Y.* A dynamic modeling approach to the moving filament during high-speed winding by absolute nodal coordinate formulation // Textile Research Journal, 2022, 92(19-20), pp. 3903-3919.
8. *Sultanov K.S., Ismoilova S.I., Mamatova N.R.* Regularities in Variation of Support Functions of Physically Nonlinear Elastic-Visco-Plastic Law of Strain of Cotton Yarn // Journal of Fashion Technology&Textile Engineering, 2018, Vol. 6, No. 1. pp. 45-50.
9. *Sultanov K.S., Ismoilova S.I.* Physically Nonlinear Elastic-Viscoplastic Law of Cotton Yarn under Tension to Breakage // Journal of Fashion Technology&Textile Engineering, 2017, Vol.5, No. 4, pp.10-18.

10. *Baymuratov B., Tulanov Sh., Sultanov K.S., Ismailova S.* Strain characteristics of cotton yarns dependingon the strain rate and methods of their manufacture, In: Proceedings of E3S Web of Conferences 304, 03027. ICECAE 2021.
11. *Sultanov K.S., Ismailova S., Baymuratov B., Tulanov Sh.* Experimental determination of cotton yarn strength at different speeds of movement obtained by various technological methods , In: Proceedings of E3S Web of Conferences 304, 03027. ICECAE 2021.
12. *Sultanov K.S., Ismoilova S.I.* Strength of the yarns at high velocities of their motion in technological processes of textile production, In: Proceedings of the International Conference on Actual Problems of Applied Mechanics - APAM - 2021. 20 October 2022, 2637, 030020. 030020-1-16. https://doi.org/10.1063/5.0118426 (Scopus).
13. *Ismoilova S.I.* Deterministic method to calculate the strength of cotton yarns, In: Proceedings of the International Conference on Actual Problems of Applied Mechanics - APAM - 2021. 20 October 2022, 2637, 030018. 030018-1-9. https://doi.org/10.1063/5.0119210 (Scopus).

SOLUTION OF THE EXTERNAL POCHHAMMER – CHREE PROBLEM AND DERIVATION OF THE PROPORTIONALITY LAW FOR BENDING SEISMIC VIBRATIONS OF A PIPELINE IN AN ELASTIC SOIL

Israilov M.Sh.[1]

[1]*LLC: "Sensor Fusion and Monitoring Technologies". California 94596, USA*

E-mail: israiler@hotmail.com

Abstract: *A formulation is given and an exact analytical solution is obtained for the problem of bending vibrations of an elastic space with a circular cylindrical cavity (called the external Pochhammer-Chree problem). In the classical (internal) Pochhammer-Chree problem of bending vibrations of a circular cylinder, nonzero transverse displacements (eigenfunctions) contain three arbitrary constants and exist at natural frequencies determined from the secular equation (ensuring zero stresses on the cylinder surface). In contrast, in the external problem (for an infinite domain), all frequencies are natural frequencies. In addition, the particles of the medium in the area adjacent to the cylindrical cavity will make approximately transverse vibrations in any one direction (bending direction) if the three constants included in the components of the displacement vector satisfy two relations (meaning that the components of displacement on the cylinder surface in two directions orthogonal to the bending direction are equal to zero). Considering that a pipeline is placed in a cylindrical cavity and that its bending vibrations combined with the medium (soil) are caused by a seismic wave, the law of proportionality of the transverse force acting on the pipeline to the relative transverse displacement of the pipeline is derived.*

Keywords: *Pohhammer - Cree external problem, pipeline, bending seismic vibrations, force of interaction, law of proportionality*

1. Introduction: on existing approaches in the study of flexural seismic vibrations of an underground pipeline.

Much fewer works have been devoted to the topic of bending vibrations of elongated underground structures, in particular pipelines, than to the study of longitudinal seismic motions of such structures in the direction of their length. There are at least two explanations for this ([1], ch. 17). The first of them is that during earthquakes, deformations in the axial direction of the pipe, as a rule, noticeably exceed its deformations from bending. The second explanation is related to the observation, repeatedly confirmed in practice, of approximately the same transverse vibrations of pipelines and soil, except in cases of very strong earthquakes. Even when pipelines connect to inspection wells, both pipelines and wells fluctuate equally with the soil. The latter provision serves as an experimental justification for the simplest engineering theory of "rigidly fixing" of a pipe in the ground (according to which the motions of the soil and the pipeline coincide) for the case of bending vibrations of the pipeline. It is believed that this theory provides an upper bound for seismic loads, and therefore, it is widely used as a calculation base in accepted standards for earthquake-resistant construction [2].

The more complex interaction of the pipeline with the ground during bending vibrations is described by the "beams on an elastic base" model. A fairly complete review of the works in this area is contained in O'Rourke's monograph [3].

T. Rashidov and co-authors proposed a model of interaction with soil in which the forces of interaction during bending vibrations (as well as longitudinal ones) are considered proportional to the relative displacement equal to the difference between the motion of soil in a seismic wave (away

from the pipeline) and the motion of the pipeline itself. A description of the method and references to previous works are contained in the monograph [4]. The differential equations of bending vibrations are written out under the assumption that the bending vibrations of the pipe and the "soil rod" replacing the pipeline are the same if their linear masses are the same. This assumption will be correct if the bending stiffness of the pipe coincides with the bending stiffness of the "soil rod", which can be realized in rare cases.

Bending vibrations of elongated underground pipelines, considered as thin-walled cylindrical shells, were studied by the finite element method in [5, 6]. However, in them, the dynamics of interaction between the pipeline and the soil is completely ignored and it is assumed that seismic waves fall on the shell without distortion.

An attempt to solve the problem of bending vibrations of the pipeline under the influence of seismic waves was made by K. Toki and Sh. Takada [7]. However, the mistakes made by the authors do not make it possible to assume that the task for the soil has been solved and the goal of the authors has been achieved. In the appropriate places, it is indicated below what the fundamental omissions of the work [7] are.

2. Methods

2.1. Formulation and exact solution of the external Pochhammer - Chree problem

In the cylindrical coordinate system (r, θ, z), in which the components of the displacement vector u of the particles of the medium are denoted by u_r, u_θ, u_z the dynamic equations of motion of the elastic medium (Lame equations) are written as (A. Love [8], ch. XII):

$$\begin{cases} \rho \dfrac{\partial^2 u_r}{\partial t^2} = (\lambda + 2\mu)\dfrac{\partial \Delta}{\partial r} - \dfrac{2\mu}{r}\dfrac{\partial \omega_z}{\partial \theta} + 2\mu \dfrac{\partial \omega_\theta}{\partial z}, \\ \rho \dfrac{\partial^2 u_\theta}{\partial t^2} = (\lambda + 2\mu)\dfrac{1}{r}\dfrac{\partial \Delta}{\partial \theta} - 2\mu \dfrac{\partial \omega_r}{\partial \mathrm{z}} + 2\mu \dfrac{\partial \omega_\mathrm{z}}{\partial r}, \\ \rho \dfrac{\partial^2 u_\mathrm{z}}{\partial t^2} = (\lambda + 2\mu)\dfrac{\partial \Delta}{\partial r} - \dfrac{2\mu}{r}\dfrac{\partial}{\partial r}(r\omega_\theta) + \dfrac{2\mu}{r}\dfrac{\partial \omega_r}{\partial \theta}. \end{cases} \tag{1}$$

here

$$\Delta \equiv \operatorname{div} \mathbf{u} = \frac{1}{r}\frac{\partial (r u_r)}{\partial r} + \frac{1}{r}\frac{\partial u_\theta}{\partial \theta} + \frac{\partial u_\mathrm{z}}{\partial \mathrm{z}}, \tag{2}$$

denotes the volumetric expansion, and the components of the rotation vector $2\boldsymbol{\omega} = \operatorname{rot} \mathbf{u}$ are given by the relations

$$2\omega_r = \frac{1}{r}\frac{\partial u_\mathrm{z}}{\partial \theta} - \frac{\partial u_\theta}{\partial \mathrm{z}}, \quad 2\omega_\theta = \frac{\partial u_r}{\partial \mathrm{z}} - \frac{\partial u_z}{\partial r}, \quad 2\omega_z = \frac{1}{r}\left(\frac{\partial (r u_\theta)}{\partial r} - \frac{\partial u_r}{\partial \theta}\right). \tag{3}$$

In this case, the components (3) satisfy identically the equality of $\operatorname{div}(2\boldsymbol{\omega}) = \operatorname{div}(\operatorname{rot} \mathbf{u}) \equiv 0$, i.e., equality

$$\frac{1}{r}\frac{\partial (r\omega_r)}{\partial r} + \frac{1}{r}\frac{\partial \omega_\theta}{\partial \theta} + \frac{\partial \omega_z}{\partial \mathrm{z}} = 0. \tag{4}$$

Thus, only two components of the vector $\boldsymbol{\omega}$ are independent and, therefore, the components of the displacement vector can be expressed in terms of volumetric expansion and any two of the components of the rotation vector.

In [9] we proved that the associated system of equations (1) can be reduced in cylindrical coordinates to a partially separated system of wave equations for Δ and components ω_z, ω_r, namely

$$\frac{\rho}{\lambda + 2\mu}\frac{\partial^2 \Delta}{\partial t^2} = \nabla^2(\Delta), \tag{5}$$

$$\frac{\rho}{\mu}\frac{\partial^2 \omega_z}{\partial t^2} = \nabla^2 \omega_z, \tag{6}$$

$$\frac{\rho}{\mu}\frac{\partial^2 (r\omega_r)}{\partial t^2} = \nabla^2(\mathrm{r}\omega_r) + 2\frac{\partial \omega_z}{\partial z}. \tag{7}$$

The Laplace operator included in the right-hand parts of these equations is defined in cylindrical coordinates by the expression

$$\nabla^2 \equiv \frac{\partial^2}{\partial r^2} + \frac{1}{r}\frac{\partial}{\partial r} + \frac{1}{r^2}\frac{\partial^2}{\partial \theta^2} + \frac{\partial^2}{\partial z^2}\,. \tag{8}$$

Equations (5), (6) are separate wave equations for the volumetric expansion Δ and the third component of the rotation vector ω_z. Equation (7) for the rotation component ω_r can be integrated as an inhomogeneous wave equation after the function ω_z is defined. Finding three functions Δ, ω_z and ω_r is sufficient to calculate the components of the displacement vector of the particles of the medium, since the function ω_θ can be determined from the identity (4) when ω_z and ω_r are known.

By analogy with the formulation of the problem of bending vibrations of an elastic circular cylinder, we formulate the problem of bending vibrations of an unlimited elastic medium occupying a spatial region external to the circular cylinder. The primary sources for the first problem (which we will call the internal problem) are the works of Pochhammer [10] and Chree [11]. A simple way to solve an internal problem is given by A. Love in his treatise on the mathematical theory of elasticity [8].

To arrive at stationary bending vibrations of a region external to a circular cylinder, consider, as in the case of a circular cylinder [8], a class of solutions to the dynamic equations of elasticity theory written out above, in which all components of the displacement vector are harmonic functions of time t and the z coordinate (measured along the axis of the cylinder), assuming, in addition, that u_r and u_z are proportional to $\cos\theta$, and u_θ is proportional to $\sin\theta$, i.e.,

$$u_r = U\cos\theta\, e^{i(\gamma z - pt)},\ u_\theta = V\sin\theta\ e^{i(\gamma z - pt)},\ u_z = W\ \cos\theta\ e^{i(\gamma z - pt)}, \tag{9}$$

where $U,\ V,\ W$ are functions of r. Then, according to formulas (2), (3), we have

$$\Delta = \tilde{\Delta}\cos\theta\, e^{i(\gamma z - pt)} = \cos\theta\, e^{i(\gamma z - pt)}\left(\frac{dU}{dr} + \frac{U}{r} + \frac{V}{r} + i\gamma W\right), \tag{10}$$

$$2\omega_r = -\widetilde{\omega_r}\sin\theta\ e^{i(\gamma z - pt)} = -\ \sin\theta\ e^{i(\gamma z - pt)}\left(i\gamma U - \frac{dW}{dr}\right),$$

$$2\omega_\theta = \widetilde{\omega_\theta}\ \cos\theta\ e^{i(\gamma z - pt)} = \cos\theta\ e^{i(\gamma z - pt)}\left(\frac{W}{r} + i\gamma V\right),$$

$$2\omega_z = \widetilde{\omega_z}\ \sin\theta\ e^{i(\gamma z - pt)} = \sin\theta\ e^{i(\gamma z - pt)}\left(\frac{dV}{dr} + \frac{V}{r} + \frac{U}{r}\right)$$

and the equations (5), (6), (7) (equivalent to the Lame equations in cylindrical coordinates) take the form:

$$\frac{d^2\tilde{\Delta}}{dr^2} + \frac{1}{r}\frac{d\tilde{\Delta}}{dr} - \left(\frac{1}{r^2} - h^2\right)\tilde{\Delta} = 0, \tag{11}$$

$$\frac{d^2\widetilde{\omega_z}}{dr^2} + \frac{1}{r}\frac{d\widetilde{\omega_z}}{dr} - \left(\frac{1}{r^2} - \kappa^2\right)\widetilde{\omega_z} = 0, \tag{12}$$

$$\frac{d^2\Omega_r}{dr^2} + \frac{1}{r}\frac{d\Omega_r}{dr} - \left(\frac{1}{r^2} - \kappa^2\right)\Omega_r + \frac{2}{r}i\gamma\,\widetilde{\omega_z} = 0,\ \Omega_r \equiv r\widetilde{\omega_r}, \tag{13}$$

in which

$$h^2 = \frac{\rho p^2}{\lambda + 2\mu} - \gamma^2 = \left(\frac{p}{c_1}\right)^2 - \gamma^2, \quad \kappa^2 = \frac{\rho p^2}{\mu} - \gamma^2 = \left(\frac{p}{c_2}\right)^2 - \gamma^2. \tag{14}$$

In the ratios (14) c_1 and c_2 there are velocities of propagation of longitudinal and transverse waves in an elastic medium. It is supposed that the right-hand sides of these relations are positive, i.e., that the phase velocity $c = p/\gamma$ of the propagation of disturbances (9) along the z axis is greater than the velocities c_1 and c_2 (this condition is not specified by A. Love [8], however, his reasoning and calculations are valid only in this case). This situation is realized, for example, when an inclined longitudinal wave falls on an underground pipeline [12]. If this is not the case, then only the case when $h^2 < 0$ is possible, i.e., the case $c_2 < c < c_1$.Then the solution of equation (11)

should be taken not in the form of a Hankel function, as below, but in the form of a Bessel function from a purely imaginary argument (i.e. in the form of a modified Bessel function).

Equations (11), (12) are Bessel equations, and (13) reduces to the Bessel equation after substituting solution (12) for $\widetilde{\omega_z}$ into it and finding a partial solution to the inhomogeneous equation, obtained by this way.

A. Love has shown that solutions of equations (11) - (13) limited on the axis of the cylinder $r = 0$ in the form of Bessel functions of the first kind lead to bending vibrations of a circular cylinder.

When solving the problem of stationary oscillations in a region external to a circular cylinder, it is required, in order to ensure uniqueness, to seek a solutions of equations (11) - (13) that satisfy the radiation conditions of Sommerfeld at infinity (see, for example, [13])

$$\lim_{r\to\infty} r\left(\frac{d\tilde{\Delta}}{dr} - ih\tilde{\Delta}\right) = 0,\ \lim_{r\to\infty} r\left(\frac{d\widetilde{\omega_\beta}}{dr} - i\kappa\widetilde{\omega_\beta}\right) = 0\ \ (\beta = z, r). \tag{15}$$

Physically, conditions (15) mean that in order to isolate the unique solutions, it is not enough to require them to decrease for $r \to \infty$ (all Bessel functions, except modified ones of the first kind, disappear at infinity), but they must form waves going to infinity. The solutions of equations (11) - (13) in the form of Bessel functions of the first and second kind (used in the internal problem) form standing waves and do not satisfy the conditions (15) and from the solutions of these equations in the form of Hankel functions, forming traveling waves, only functions of the first kind $H_1^{(1)}(hr)$ and $H_1^{(1)}(\kappa r)$ form waves going to infinity, when multiplied by the exponential time dependence assumed above for all functions Δ, ω_β in the form of e^{-ipt} (formulas (10). The latter statement is easily established using well-known asymptotic representations of Hankel functions for large values of the argument [14] (Hankel functions of the second kind form waves coming from infinity).

Remark 1. Note that if, as in the book by A. Love, we take the time dependence for the functions in (10) in the form e^{+ipt}, then the radiation conditions (15) should be written with a plus sign before the second terms, and solutions of equations (11) - (13) satisfying such conditions will be Hankel functions of the second kind $H_1^{(2)}(hr)$ and $H_1^{(2)}(\kappa r)$.

Considering the above, we have solutions of equations (11) and (12) satisfying the radiation conditions (15) in the following form:

$$\tilde{\Delta} = -\left(\frac{p}{c_1}\right)^2 A\, H_1^{(1)}(hr). \tag{16}$$

$$2\widetilde{\omega_z} = \kappa^2 C\, H_1^{(1)}(\kappa r). \tag{17}$$

In these solutions, for convenience in further calculations, arbitrary constants A and C are taken with multipliers $-(p/c_1)^2$ and κ^2.

Substituting expression (17) for $\widetilde{\omega_z}$ into equation (13) and integrating the inhomogeneous Bessel equation obtained, we arrive at a solution

$$2\,\widetilde{\omega_r} = i\gamma C\frac{d\,H_1^{(1)}(\kappa r)}{dr} + iB\left(\frac{p}{c_2}\right)^2\frac{H_1^{(1)}(\kappa r)}{r}, \tag{18}$$

satisfying the radiation condition (15).

The found values for $\tilde{\Delta}$, $\widetilde{\omega_z}$, $\widetilde{\omega_r}$ (formulas (16) - (18) lead to the following relations for displacements

$$\begin{cases} U = A\dfrac{d\,H_1^{(1)}(hr)}{dr} + B\gamma\dfrac{d\,H_1^{(1)}(\kappa r)}{dr} + C\dfrac{H_1^{(1)}(\kappa r)}{r}, \\ V = -A\dfrac{H_1^{(1)}(hr)}{r} - B\gamma\dfrac{H_1^{(1)}(\kappa r)}{r} - C\dfrac{d\,H_1^{(1)}(\kappa r)}{dr}, \\ W = i\gamma A\,H_1^{(1)}(hr) - iB\kappa^2\,H_1^{(1)}(\kappa r). \end{cases} \tag{19}$$

Substituting these expressions into formulas (9), we obtain solutions of equations (1).

The solution of the internal Pochhammer-Chree problem, similar to (19), instead of Hankel functions contains Bessel functions of the first kind (and first order) [8] and, therefore, by virtue of the equality $J_1(0) = 0$, on the axis $r = 0$ the displacement W (or u_z) is zero. Therefore, the points of the cylinder lying on the axis $r = 0$ move in a plane perpendicular to the axis (perform bending vibrations). Moreover, this position holds for arbitrary constants A and B included in the expression for W. But the points outside the axis do not remain in the process of motion in a plane perpendicular to the axis of the cylinder, i.e., $W \neq 0$ at $r \neq 0$. Or, otherwise, deplanation takes place (violation of the law of flat sections). However, since the arguments of Bessel functions are defined by equalities

$$hr = 2\pi \frac{r}{\Lambda}\sqrt{\left(\frac{c}{c_1}\right)^2 - 1}\,, \quad \kappa r = 2\pi \frac{r}{\Lambda}\sqrt{\left(\frac{c}{c_2}\right)^2 - 1}\,, \tag{20}$$

in which $\Lambda = 2\pi/\gamma$ is the length of waves (9), and $c = p/\gamma$ is the phase velocity of their propagation along the z axis, then $W \approx 0$ if $a/\Lambda \ll 1$. Consequently, in the internal Pochhammer - Chree problem the vibrations of the cylinder will be the closer to purely bending ones the smaller the radius of the cylinder in comparison with the wavelength.

In solving the considered external Pochhammer-Chree problem it is possible to achieve equality $W = 0$ on the surface of the cylinder (cavity) $r = a$, which, according to solution (19), is satisfied if the constants A and B are related by the relation

$$B = A\,\frac{\gamma}{\kappa^2}\frac{H_1^{(1)}(ha)}{H_1^{(1)}(\kappa a)}\,. \tag{21}$$

However, just as in the situation described above in the internal Pochhammer-Chree problem, it is impossible to achieve that $W = 0$ for all $r > a$. But, due to the continuity of the Hankel functions, for any finite value of the argument, the approximate equality $W \approx 0$ will be satisfied if $(r - a)/\Lambda \ll 1$.

Consequently, when the relation (21) is fulfilled, the points of the medium located in the vicinity of a cylindrical surface of small size in comparison with the wavelength will, during motions obeying the laws (19), deviate slightly from the plane perpendicular to the axis of the cylindrical cavity, i.e., they will perform approximately bending vibrations.

Let us now require that these bending vibrations occur (approximately) in one direction, say, in the direction of the straight line from which the angle θ is measured. Let's take this direction as the x-axis of the Cartesian coordinate system (x, y, z), which is introduced here along with the cylindrical one. The specified requirement is fulfilled if the points of the cylinder surface $r = a$ move in the x direction , i.e., when

$$V_y\big|_{r=a} = \cos\theta\ \sin\theta\,(U + V)|_{r=a} = 0. \tag{22}$$

Substituting U and V from (19) into condition (22), we get that it will be satisfied if

$$C = A\frac{P(ha)}{Q(\kappa a)} + B\gamma = = A\left[\frac{P(ha)}{Q(\kappa a)} + \frac{\gamma^2}{\kappa^2}\frac{H_1^{(1)}(ha)}{H_1^{(1)}(\kappa a)}\right], \tag{23}$$

where there are the following notations:

$$P(ha) = \frac{d\,H_1^{(1)}(ha)}{da} - \frac{H_1^{(1)}(ha)}{a},\ Q(\kappa a) = \frac{d\,H_1^{(1)}(\kappa a)}{da} - \frac{H_1^{(1)}(\kappa a)}{a}, \tag{24}$$

$$\frac{d\,H_1^{(1)}(qa)}{da} \equiv \frac{d\,H_1^{(1)}(qr)}{dr}\bigg|_{r=a}, \quad q = (h, \kappa).$$

Thus, formulas (19), in which constants B and C are expressed by relations (21), (23) through a single constant A give a solution to the external Pochhammer-Chree problem of bending vibrations of the exterior of a circular cylinder. The unknown constant A is determined from an

additional boundary condition on a cylindrical surface $r = a$. So, in the problem of joint bending vibrations of an infinite elastic medium and a pipeline such a condition is the condition of continuity (equality) of the displacements of the pipe and the points of the medium adjacent to the surface of the pipe in the direction of bending (i.e., in the direction of the x axis).

In the internal Pochhammer-Chree problem the relation (22), as well as the condition $W = 0$, is fulfilled for arbitrary constants included in expressions for displacements similar to (19). However, equality (22) even for points lying on the axis $r = a$, as well as in the external problem, is already fulfilled only approximately when the radius of the cylinder is small in comparison with the wavelength (this circumstance was not noted by A. Love [8]).

The above difference, consisting in the fact that in the internal Pochhammer-Chree problem all three constants in the expressions for displacements remain undefined during bending vibrations, is due to the fact that there are natural oscillations in it only at certain (fundamental) frequencies derived from the conditions of the absence of stresses on the lateral surface of the cylinder. Whereas in an external problem (with an unlimited domain), any frequency is fundamental.

Remark 2. K. Toki and S. Takada state in [7] that they have found a solution to the problem considered in this section, in which at all points of the region (the exterior of the circular cylinder) the displacements in the direction of the cylinder axis are zero ($W = 0$). As shown above, there is no such solution. It is only possible to achieve that the named displacements are equal to zero on a cylindrical surface (when the relation (21) between the constants is satisfied) and the smallness of W in the vicinity of this surface, the size (diameter) of which is small in comparison with the length of the seismic wave.

2.2. Calculation of the transverse force during bending seismic vibrations of the pipeline in elastic soil

First of all, let us establish that if the conditions of Section *2.1* are satisfied and the constant A remains arbitrary, then the solution of the external Pochhammer – Chree problem, obtained above, is such that the displacements of all points of cross-section $z = \text{const}$ of the cylindrical surface $r = a$ in the direction of the x axis, i.e., in the direction of bend, are the same (they do not depend on the angle θ). Indeed, by virtue of the relations (9) displacements along the axes r and θ are equal to $U_r = U\cos\theta$ and $V_\theta = V\sin\theta$, respectively. Therefore, $U_x = U_r\cos\theta - V_\theta\sin\theta = U\cos^2\theta - V\sin^2\theta$. Now using condition (22) in the resulting expression for U_x, we get

$$U_x|_{r=a} = U|_{r=a} = -V|_{r=a}. \tag{25}$$

Expressions (25) represent one condition (not two) because, due to the dependencies found above between A, B and C ((21), (23)), U and $-V$ coincide when $r = a$.

When a cylindrical rod or pipe of circular cross section is placed in a cylindrical cavity, then the result (25) admits the fulfillment of the stickiness condition, that is, the condition of continuity of displacements of the medium and the rod on its surface. From here, the last undefined constant A can be found in the solution obtained above in Section *2.1*. Indeed, let the displacement of the pipe in an arbitrary cross-section in the direction of the x axis (in the direction of bending) be $\mathcal{U}_a$ (or $u_a = \mathcal{U}_a e^{i(\gamma z - pt)}$. Then, according to (25) and (19),

$$\mathcal{U}_a = \left\{ A\frac{d\,H_1^{(1)}(hr)}{dr} + B\gamma\frac{d\,H_1^{(1)}(\kappa r)}{dr} + C\frac{H_1^{(1)}(\kappa r)}{r} \right\}_{r=a}. \tag{26}$$

Writing down the equalities (21) and (23) in the form $B = m_1 A$, $C = m_2 A$, where denoted

$$m_1 = \frac{\gamma}{\kappa^2}\frac{H_1^{(1)}(ha)}{H_1^{(1)}(\kappa a)}, \quad m_2 = \frac{P(ha)}{Q(\kappa a)} + \frac{\gamma^2}{\kappa^2}\frac{H_1^{(1)}(ha)}{H_1^{(1)}(\kappa a)}, \tag{27}$$

we obtain from (26) the value of the constant A through a given displacement $\mathcal{U}_a$ in the direction of the bend:

$$A = \frac{\mathcal{U}_a}{\dfrac{d\,H_1^{(1)}(ha)}{da} + \gamma m_1 \dfrac{d\,H_1^{(1)}(\kappa a)}{da} + m_2 \dfrac{H_1^{(1)}(\kappa a)}{a}}\,. \tag{28}$$

The calculation of the constant A by formula (28) completes the final solution of the external Pochhammer–Chree problem formulated in Section *2.1*. The radial and tangential displacements of the medium points in this solution take, in accordance with representations (9), the form

$$\begin{cases} u_r = A\left[\dfrac{d\,H_1^{(1)}(hr)}{dr} + \gamma m_1 \dfrac{d\,H_1^{(1)}(\kappa r)}{dr} + m_2 \dfrac{H_1^{(1)}(\kappa r)}{r}\right]\cos\theta\; e^{i(\gamma z - pt)} \\ u_\theta = -A\left[\dfrac{H_1^{(1)}(hr)}{r} - \gamma m_1 \dfrac{H_1^{(1)}(\kappa r)}{r} - m_2 \dfrac{d\,H_1^{(1)}(\kappa r)}{dr}\right]\sin\theta\; e^{i(\gamma z - pt)} \end{cases} \tag{29}$$

In formulas (29), the values m_1, m_2 and A are defined by expressions (27) and (28).

It is easy to establish that the force acting on the pipeline when moving in the direction of the x axis is given by equality (we remind that the angle θ is counted counterclockwise from this axis)

$$\mathcal{F} = -\int_0^{2\pi} (\sigma_{rr}\cos\theta - \sigma_{r\theta}\sin\theta)|_{r=a}\, a d\theta. \tag{30}$$

Here σ_{rr} and $\sigma_{r\theta}$ represent the physical components of the stress tensor in a cylindrical coordinate system; they are expressed in terms of the physical components of the small strain tensor in the same way as the components of the stress tensor are expressed in terms of the components of the strain tensor in the Cartesian coordinate system (however, when writing Hooke's law in the components of stress and strain tensors in a cylindrical coordinate system, as in any curved orthogonal system, it is necessary to replace the unit Kronecker tensor with a metric one which is sometimes mistakenly ignored [15]).

When calculating the physical components of stresses according to Hooke's law, we use the above expression for volumetric expansion (16). In addition, when calculating the physical components of deformations according to known formulas [16]

$$\varepsilon_{rr} = \frac{\partial u_r}{\partial r}\,, \quad 2\varepsilon_{r\theta} = \frac{1}{r}\frac{\partial u_r}{\partial \theta} + \frac{\partial u_\theta}{\partial r} - \frac{u_\theta}{r}$$

they, and hence the corresponding physical stress components, will include the second derivatives of the Hankel functions. We eliminate the second derivatives of the Hankel functions in these expressions, using the fact that the Hankel functions satisfy the corresponding Bessel equations. Further, we eliminate the first derivatives of the first-order Hankel functions using the well-known formula ([17], Part III, formula (3.1.1)).

The expressions for the physical components of stresses, that are simplified in this way, are reduced, after elementary but somewhat long calculations, to the following form

$$\sigma_{rr} = A\,\mu\cos\theta\left\{\left[-\frac{\lambda}{\mu}\left(\frac{p}{c_1}\right)^2 - 2h^2 + \frac{4}{r^2}\right] H_1^{(1)}(hr) - \frac{2}{r}h\,H_0^{(1)}(hr) + 2\left[\gamma m_1\left(\frac{2}{r^2} - \kappa^2\right) - \frac{2m_2}{r^2}\right] H_1^{(1)}(\kappa r) + \frac{2}{r}(-\gamma m_1 + m_2)\kappa\,H_0^{(1)}(\kappa r)\right\} \equiv g_1(r)\cos\theta, \tag{31}$$

$$\sigma_{r\theta} = -A\,\mu\sin\theta\left\{-\frac{4}{r^2}\,H_1^{(1)}(hr) + \frac{2}{r}h\,H_0^{(1)}(hr) + \left(\frac{-4\gamma m_1 + 4m_2}{r^2} - m_2\kappa^2\right) H_1^{(1)}(\kappa r) + \frac{2}{r}(\gamma m_1 - m_2)\kappa\,H_0^{(1)}(\kappa r)\right\} \equiv g_2(r)\sin\theta.$$

Substituting the found stresses (31) into the formula (30), we obtain

$$\mathcal{F} = -ag_1(a)\int_0^{2\pi} \cos^2\theta\, d\theta + ag_2(a)\int_0^{2\pi} \sin^2\theta\, d\theta$$
$$= Aa\pi\left\{\left[\lambda\left(\frac{p}{c_1}\right)^2 + 2\mu h^2\right] H_1^{(1)}(ha) + \mu(2\gamma m_1 + m_2)\kappa^2\, H_1^{(1)}(\kappa a)\right\}$$

Therefore, taking into account the value of the constant A from (28), we have the final result for the linear force (the force acting on the surface of the pipe element of unit length)

$$\mathcal{F} = \pi\rho c_2^2 f\, \mathcal{U}_a, \tag{32}$$

here

$$f = \left\{\left[\left(\left(\frac{c_1}{c_2}\right)^2 - 2\right)\left(\frac{ap}{c_1}\right)^2 + 2\bar{h}^2\right] H_1^{(1)}(\bar{h}) + (2\gamma m_1 + m_2)\bar{\kappa}^2 H_1^{(1)}(\bar{\kappa})\right\} \times \frac{1}{\mathcal{Z}}, \tag{33}$$

$\mathcal{Z} \equiv \bar{h}H_0^{(1)}(\bar{h}) - H_1^{(1)}(\bar{h}) + \gamma m_1\bar{\kappa}H_0^{(1)}(\bar{\kappa}) + (-\gamma m_1 + m_2)H_1^{(1)}(\bar{\kappa})$.

Dimensionless parameters $\bar{h} \equiv ha, \bar{\kappa} \equiv \kappa a$ are introduced in formulas (33). The dimensionless quantity $\mathcal{Z}$ is multiplied by a the denominator of the right side of the relation (28) for the coefficient A, after excluding the derivatives of the Hankel functions from it by formula (3.1.1) from [17].

3. Results and Discussion

Now let's assume that transverse vibrations of the pipeline occur due to the impact of a seismic wave

$$u_0 = \mathcal{U}_0 e^{i(\gamma z - pt)}, \tag{34}$$

in which the displacements of the particles are directed in the direction of the x-axis.

Let us denote the transverse displacements of the pipeline in the direction of the x-axis arising from the incidence of the wave (34) through $\hat{u} = \hat{\mathcal{U}}e^{i(\gamma z - pt)}$. The resulting soil problem differs from the one discussed above in that its solution at infinity ($r \to \infty$) must tend to wave (34). Since there are no Bessel functions that take finite values at infinity (they either tend to zero or are not limited), we represent $\hat{u}$ as $\hat{u} = u_0 + u = (\mathcal{U}_0 + \mathcal{U})e^{i(\gamma z - pt)}$. Then u must disappear at infinity and the task of finding it coincides with the external Pochhammer–Chree problem. Only when recording the stickiness condition on the pipe surface (when finding the constant A), it is necessary to put $\mathcal{U}_a = \mathcal{U} = -\mathcal{U}_0 + \hat{\mathcal{U}}$. Further, taking into account that when the pipeline moves according to the law of the incident wave (34) no forces from the soil would act on it we have, in accordance with (32), the following expression for the force causing bending movements of the pipeline:

$$\hat{\mathcal{F}} = \pi\rho c_2^2 f\,(\mathcal{U}_0 - \hat{\mathcal{U}}), \quad \hat{\mathcal{F}}e^{i(\gamma z - pt)} = \pi\rho c_2^2 f\,(u_0 - \hat{u}), \tag{35}$$

where the multiplier f is defined by formulas (34).

In relation (35), the proportionality coefficient $k_x = \pi\rho c_2^2 f = \pi\mu f$ will be called the coefficient of interaction (of soil and pipeline) during bending vibrations (in the direction of the x-axis). The expression for it is significantly simplified when the ratio of the radius of the pipe to the length of the seismic wave is a small value: $a/\Lambda \ll 1$ or, respectively, $\Lambda/a \gg 1$ (which is exactly the case in practice).To do this, we use the well-known representations of Hankel functions (see, for example, [20])

$$H_0^{(1)}(w) \sim -i\frac{2}{\pi}\ln\frac{2}{w}, \quad H_1^{(1)}(w) \sim -i\frac{2}{\pi}\left(\frac{1}{w}\right)$$

for small values of the argument (in our case these arguments, defined by the equalities (20), are real and positive). Then from (33) we obtain the asymptotic representation

$$k_x \approx \frac{4\pi\mu\left(\frac{c}{c_2}\right)^2}{2\ln\left(\frac{\Lambda}{\pi a}\right) - \ln\left(\sqrt{\left(\frac{c}{c_1}\right)^2 - 1}\sqrt{\left(\frac{c}{c_2}\right)^2 - 1}\right)}. \tag{36}$$

When $\Lambda/a \to \infty$ it follows from formula (36) that $k_x \to 0$ and, therefore, in this limiting case the simplest engineering theory of "rigid fixing" of the pipeline in the soil is valid, which means that the transverse displacements of the pipe coincide with the transverse displacements of soil particles.

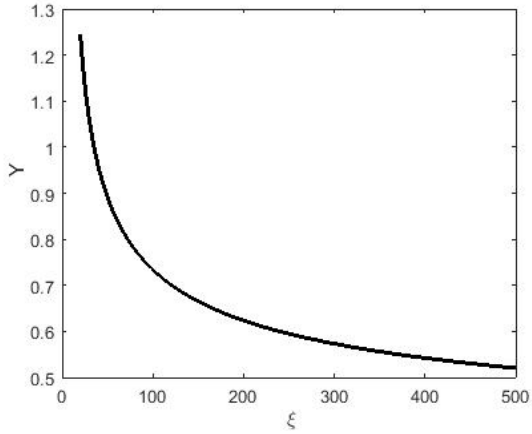

Figure 1. - **Dependence of the interaction coefficient on the ratio of the seismic wave length to the radius of the pipeline**

Figure 1 shows a graph of the dependence (36) of the interaction coefficient ($Y \equiv k_x/(\pi\mu)$) on the ratio $\xi \equiv \Lambda/(\pi a)$ when the soil is dry clay. The numerical values for the velocities of wave propagation in clay are taken from the handbook [21]: $c_1 = 2.0 \cdot 10^3$ m/s, $c_2 = 0.4 \cdot 10^3$ m/s. The velocity of propagation of the incident wave along the x-axis is assumed to be $c = 2.4 \cdot 10^3$ m/s (which corresponds to the incidence of a longitudinal wave on the pipeline at approximately an angle of 35°).

4. Conclusions

1. The external Pochhammer-Chree problem of bending vibrations of an unlimited elastic medium occupying the exterior of a circular cylinder is formulated and solved.

2. Based on the obtained solution of the external Pochhammer-Chree problem for elastic soil, the linear force acting on the pipeline is found when it and the soil perform joint bending vibrations under impact of a seismic wave.

3. It is shown that this force (named as force of interaction between pipeline and soil) is always proportional to the relative transverse displacement of the pipeline (the law of proportionality).

4. An asymptotic formula is obtained and the dependence of the interaction coefficient on large values of the ratio of the seismic wave length to the radius of the pipeline is investigated. It follows from this investigation that at large wavelengths, the bending vibrations of the pipeline approximately coincide with the vibrations in seismic wave.

References

1. *Okamoto S.* Introduction to earthquake engineering. Univ. of Tokyo Press, 1973.

2. Normy proektirovaniya atomnykh stantsii: NP 031–01, M.: 2001. Prilozhenie 6. Osnovnye polozheniya rascheta lineino-protyazhennykh konstruktsii. S. 23-25.

3. *O'Rourke M.J., Liu X.* Response of buried pipelines subject to earthquake effects // Publ. Multidisciplinary Center for Earthq. Engng. Res. (MCEER). Univ. of Buffalo. Buffalo, 1999.

4. *Rashidov T.* Dinamicheskaya teoriya seismostoikosti slozhnykh sistem podzemnykh sooruzhenii. Tashkent: Izd-vo «FAN» UzSSR, 1973.

5. *Kouretzis G.P., Bouckovalas G.D., Gantes C.*J. 3-D shell analysis of cylindrical underground structures under seismic shear (S) wave action // Soil Dynamics and Earthquake Engineering. 2006, 26, p. 909-921. https://doi:10.1016/j.soildyn.2006.02.002

6. *Kouretzis G.P., Bouckovalas G.D., Karamitros D.K.* Seismic verification of long cylindrical underground structures considering Rayleigh wave effects // Tunneling and Underground Space Technology. 2011, 26. Pp. 789-794. https://doi.org/10.1016/j.tust.2011.05.001

7. *Toki T., Takada S.* Earthquake response of underground tubular structures // Bull. Disaster Preventation Res. Inst. Kyoto Univ. 1974, 24(2). No. 221, p. 107-125. https://repository.kulib.kyoto-u.ac.jp/dspace/bitstream/2433/124841/1/b24p2n221p06.pdf

8. *Love A.E.H.* A treatise on the mathematical theory of elasticity. Fourth. ed. Cambridge: Univ. Press, 1927.

9. *Israilov M.Sh.* Solution of the External Pochhammer - Chree Problem and Bending Seismic Vibrations of the Pipeline in Infinite Elastic Continuum // Mechanics of Solids. 2023, 58(1), p. 26-37. DOI: 10.3103/S0025654422700042
10. *Pochhammer L.* Ueber die Fortpflanzungsgeschwindigkeiten kleiner Schwingungen in einem unbegrenzten isotropen Kreiscylinder // J. reine und angewandte Mathematik. Einundachtzigster Band. In vier Heften, 1876. S. 324-336.
11. *Chree C.* Longitudinal vibrations of a circular bar // Quart. J. Pure and Appl. Mathematics. 1886. Vol. XXI. Pp. 287-298.
12. *Israilov M.Sh.* Action of Oblique Seismic Wave on an Underground Pipeline // Mechanics of Solids. 2022, 57(5), p. 1006-1015. DOI: 10.3103/S0025654422050089
13. *Kupradze V.D.* (red.). Trekhmernye zadachi matematicheskoi teorii uprugosti i termouprugosti. M.: Nauka, 1976.
14. *Bell W.W.* Special functions for scientists and engineers. London: Van Nostrand, 1968.
15. *Poruchikov V.B.* Methods of the classical theory of elastodynamics. Berlin: Springer - Verlag, 1993.
16. *Eringen A.C.* Mecanics of continua. N.-Y.: Wiley, 1967.
17. *Magnus W., Oberhettinger F., Soni R.P.* Formulas and theorems of the special functions of mathematical physics. 3-d ed. N.-Y.: Springer – Verlag, 1966.
18. *Miklowitz J.* The theory of elastic waves and waveguides. Amsterdam: North-Holland Publ. Co., 1978.
19. *Israilov M.Sh.* Coupled Seismic Vibrations of a Pipeline in an Infinite Elastic Medium // Mechanics of Solids. 2016, 51(1), p. 46-53. DOI: 10.3103/S0025654416010052
20. *Lebedev N.N.* Special functions and their applications. Prentice-Hall, Inc., 1965.
21. *Clark S.P.* (Ed.). Handbook of the physical constants. Publ. by the Geological Soc. of Am. N.-Y., 1966.

COUPLED PLANE PROBLEM OF DYNAMIC THERMAL ELASTICITY IN STRESSES

Kalandarov A.[1], Khaldjigitov A.[2], Atabayev K.[3]
[1]*Gulistan State Pedagogical Institute, Gulistan, Uzbekistan*
[2]*National University of Uzbekistan, Tashkent, Uzbekistan*
[3]*Andijan Machine-building Institute, Andijan, Uzbekistan*
E-mail: abroshox@mail.ru

Abstract. *This paper proposes a dynamic model of the coupled problem of thermoelasticity in stresses. A coupled boundary value problem consisting of three differential equations for the stress tensor components and temperature, as well as the heat influx equation with the corresponding initial and boundary conditions is formulated. Explicit and implicit finite-difference equations have been developed that can be solved by sequential application of the elimination method and recurrence relations, respectively. The coupled dynamic problem of plane thermoelasticity in stresses is solved numerically. Numerical results show the reliability of the results and the validity of the proposed coupled boundary value problem of thermoelasticity in stresses.*

Keywords. *Thermoelasticity, stresses, deformations, explicit scheme, implicit scheme, convergence.*

1. Introduction

Mathematical and numerical modeling of the deformation process, taking into account the mutual influence of thermal and mechanical factors, is an urgent problem in thermoelasticity and mathematical modeling. In mechanics, usually when solving thermoelastic problems, the temperature field is considered to be known as a solution of the heat equation. But, in order to more adequately describe the deformation process taking into account temperature, along with the motion equations, it is necessary to consider the equation of heat influx. Then the boundary value problem becomes coupled with respect to displacements and temperature. In the static case, the problem becomes uncoupled, and the mechanical and thermal equations can be solved independently of each other[1].

In general, a coupled dynamic boundary value problem of thermoelasticity consists of an equation of motion, a relationship between stresses and strains taking into account temperature, the Cauchy relation, and a heat flow equation with appropriate initial and boundary conditions. All of the above problems of thermoelasticity are usually solved in displacements [2].

Recently, the formulation of related problems of thermoelasticity with respect to stress and temperature, and their numerical solution, has become relevant. Typically, boundary value problems in stresses are considered within the framework of the Beltrami-Michell equations. In this direction, one can note the works of Konovalov [3], [4] and others.

In works [5-20], various mathematical models of the theory of elasticity and thermoelasticity, as well as methods for their solution, are considered.

This work is devoted to the formulation of the coupled problem of dynamic thermoelasticity without using the Beltrami-Michell equations. The plane problem of a free plate initially located in a dome-shaped temperature field is considered. Difference schemes of explicit form have been compiled and their solutions are reduced to recurrence relations.

2. Formulation of the coupled problem of plane thermoelasticity in stress

Typically, the coupled problem of plane thermoelasticity consists of the equation of motion

$$\frac{\partial \sigma_{11}}{\partial x}+\frac{\partial \sigma_{12}}{\partial y}+X_1=\rho\frac{\partial^2 u}{\partial t^2} \tag{1}$$

$$\frac{\partial \sigma_{21}}{\partial x}+\frac{\partial \sigma_{22}}{\partial y}+X_2=\rho\frac{\partial^2 v}{\partial t^2} \tag{2}$$

Duhamel-Neumann relations [1]

$$\sigma_{11}=\left(\lambda+2\mu\right)\varepsilon_{11}+\lambda\varepsilon_{22}-\gamma(T-T_0) \tag{3}$$

$$\sigma_{22}=\left(\lambda+2\mu\right)\varepsilon_{22}+\lambda\varepsilon_{11}-\gamma(T-T_0) \tag{4}$$

$$\sigma_{12}=2\mu\varepsilon_{12} \tag{5}$$

Cauchy relations

$$\varepsilon_{11}=\frac{1}{2}\left(\frac{\partial u}{\partial x}+\frac{\partial u}{\partial x}\right)=\frac{\partial u}{\partial x} \tag{6}$$

$$\varepsilon_{22}=\frac{1}{2}\left(\frac{\partial v}{\partial y}+\frac{\partial v}{\partial y}\right)=\frac{\partial v}{\partial y} \tag{7}$$

$$\varepsilon_{12}=\frac{1}{2}\left(\frac{\partial u}{\partial y}+\frac{\partial v}{\partial x}\right) \tag{8}$$

and, heat flow equation [1]

$$\lambda_0\left(\frac{\partial^2 T}{\partial x^2}+\frac{\partial^2 T}{\partial y^2}\right)-c_\varepsilon\frac{\partial T}{\partial t}-(3\lambda+2\mu)\alpha T\left(\frac{\partial \varepsilon_{11}}{\partial t}+\frac{\partial \varepsilon_{22}}{\partial t}\right)=0 \tag{9}$$

where, $\sigma_{ij}-$ stress tensor, $\varepsilon_{ij}-$ strain tensor, u_i- displacement, $\rho-$ density of the body, $\lambda,\mu-$ Lame constants, $c_\varepsilon-$ denotes heat at a constant deformation, X_i- volume force, $\gamma=(3\lambda+2\mu)\alpha$, $\alpha-$ corresponds to thermal expansion coefficient, λ_0- is the heat flow coefficient with known initial and boundary conditions regarding stress and temperature.

In order to write down problem (1-9) regarding stress and temperature, differentiating (1) with respect to *x* and (2) with respect to *y*, we obtain

$$\frac{\partial^2 \sigma_{11}}{\partial x^2}+\frac{\partial^2 \sigma_{12}}{\partial x\partial y}+X_1=\rho\frac{\partial^2}{\partial t^2}\left(\frac{\partial u}{\partial x}\right) \tag{10}$$

$$\frac{\partial^2 \sigma_{21}}{\partial x\partial y}+\frac{\partial^2 \sigma_{22}}{\partial y^2}+X_2=\rho\frac{\partial^2}{\partial t^2}\left(\frac{\partial v}{\partial x}\right). \tag{11}$$

Taking into account the Cauchy relations (6-7), equations (10-11) take the form

$$\frac{\partial^2 \sigma_{11}}{\partial x^2}+\frac{\partial^2 \sigma_{12}}{\partial x\partial y}+X_1=\rho\frac{\partial^2 \varepsilon_{11}}{\partial t^2} \tag{10}$$

$$\frac{\partial^2 \sigma_{21}}{\partial x\partial y}+\frac{\partial^2 \sigma_{22}}{\partial y^2}+X_2=\rho\frac{\partial^2 \varepsilon_{22}}{\partial t^2} \tag{11}$$

or

$$\frac{\partial^2 \varepsilon_{11}}{\partial t^2} = \frac{1}{\rho}\left(\frac{\partial^2 \sigma_{11}}{\partial x^2} + \frac{\partial^2 \sigma_{12}}{\partial x \partial y} + X_1\right) \tag{12}$$

$$\frac{\partial^2 \varepsilon_{22}}{\partial t^2} = \frac{1}{\rho}\left(\frac{\partial^2 \sigma_{21}}{\partial x \partial y} + \frac{\partial^2 \sigma_{22}}{\partial y^2} + X_2\right) \tag{13}$$

Next, we differentiate equations (3) and (4) twice with respect to time *t*

$$\frac{\partial^2 \sigma_{11}}{\partial t^2} = \left(\lambda + 2\mu\right)\frac{\partial^2 \varepsilon_{11}}{\partial t^2} + \lambda \frac{\partial^2 \varepsilon_{22}}{\partial t^2} - \gamma \frac{\partial^2 T}{\partial t^2} \tag{14}$$

$$\frac{\partial^2 \sigma_{22}}{\partial t^2} = \left(\lambda + 2\mu\right)\frac{\partial^2 \varepsilon_{22}}{\partial t^2} + \lambda \frac{\partial^2 \varepsilon_{11}}{\partial t^2} - \gamma \frac{\partial^2 T}{\partial t^2} \tag{15}$$

Substituting (12) and (13) into (14) and (15), respectively, in the absence of body forces, we obtain

$$\frac{\partial^2 \sigma_{11}}{\partial t^2} = \frac{\lambda + 2\mu}{\rho}\left(\frac{\partial^2 \sigma_{11}}{\partial x^2} + \frac{\partial^2 \sigma_{12}}{\partial x \partial y}\right) + \frac{\lambda}{\rho}\left(\frac{\partial^2 \sigma_{21}}{\partial x \partial y} + \frac{\partial^2 \sigma_{22}}{\partial y^2}\right) - \gamma \frac{\partial^2 T}{\partial t^2} \tag{16}$$

$$\frac{\partial^2 \sigma_{22}}{\partial t^2} = \frac{\lambda + 2\mu}{\rho}\left(\frac{\partial^2 \sigma_{21}}{\partial x \partial y} + \frac{\partial^2 \sigma_{22}}{\partial y^2}\right) + \frac{\lambda}{\rho}\left(\frac{\partial^2 \sigma_{11}}{\partial x^2} + \frac{\partial^2 \sigma_{12}}{\partial x \partial y}\right) - \gamma \frac{\partial^2 T}{\partial t^2} \tag{17}$$

or

$$\frac{\partial^2 \sigma_{11}}{\partial t^2} = \frac{\lambda + 2\mu}{\rho}\frac{\partial^2 \sigma_{11}}{\partial x^2} + \frac{2(\lambda + \mu)}{\rho}\frac{\partial^2 \sigma_{12}}{\partial x \partial y} + \frac{\lambda}{\rho}\frac{\partial^2 \sigma_{22}}{\partial y^2} - \gamma \frac{\partial^2 T}{\partial t^2} \tag{18}$$

$$\frac{\partial^2 \sigma_{22}}{\partial t^2} = \frac{\lambda + 2\mu}{\rho}\frac{\partial^2 \sigma_{22}}{\partial y^2} + \frac{2(\lambda + \mu)}{\rho}\frac{\partial^2 \sigma_{21}}{\partial x \partial y} + \frac{\lambda}{\rho}\frac{\partial^2 \sigma_{11}}{\partial x^2} - \gamma \frac{\partial^2 T}{\partial t^2} \tag{19}$$

Further, differentiating (1) with respect to y and (2) with respect to x, without taking into account body forces, one can find i.e.

$$\frac{\partial^2 \sigma_{11}}{\partial x \partial y} + \frac{\partial^2 \sigma_{12}}{\partial y^2} = \rho \frac{\partial^2}{\partial t^2}\left(\frac{\partial u}{\partial y}\right) \tag{20}$$

$$\frac{\partial^2 \sigma_{21}}{\partial x^2} + \frac{\partial^2 \sigma_{22}}{\partial x \partial y} = \rho \frac{\partial^2}{\partial t^2}\left(\frac{\partial v}{\partial x}\right) \tag{21}$$

Adding (20) and (21) we get

$$\frac{\partial^2 \sigma_{11}}{\partial x \partial y} + \frac{\partial^2 \sigma_{21}}{\partial x^2} + \frac{\partial^2 \sigma_{12}}{\partial y^2} + \frac{\partial^2 \sigma_{22}}{\partial x \partial y} = \rho \frac{\partial^2}{\partial t^2}\left(\frac{\partial u}{\partial y} + \frac{\partial v}{\partial x}\right) \tag{22}$$

Dividing (22) by 2 we have

$$\frac{1}{2\rho}\left(\frac{\partial^2 \sigma_{11}}{\partial x \partial y} + \frac{\partial^2 \sigma_{21}}{\partial x^2} + \frac{\partial^2 \sigma_{12}}{\partial y^2} + \frac{\partial^2 \sigma_{22}}{\partial x \partial y}\right) = \frac{1}{2}\frac{\partial^2}{\partial t^2}\left(\frac{\partial u}{\partial y} + \frac{\partial v}{\partial x}\right) \tag{23}$$

Substituting (8) into (23) we get

$$\frac{1}{2\rho}\left(\frac{\partial^2 \sigma_{11}}{\partial x \partial y} + \frac{\partial^2 \sigma_{21}}{\partial x^2} + \frac{\partial^2 \sigma_{12}}{\partial y^2} + \frac{\partial^2 \sigma_{22}}{\partial x \partial y}\right) = \frac{\partial^2 \varepsilon_{12}}{\partial t^2} \tag{24}$$

Now let us differentiate relation (5) twice with respect to time *t*

$$\frac{\partial^2 \sigma_{12}}{\partial t^2} = 2\mu \frac{\partial^2 \varepsilon_{12}}{\partial t^2} \tag{25}$$

and, substituting (24) into (25) we will have

$$\frac{\partial^2 \sigma_{12}}{\partial t^2} = \frac{\mu}{\rho}\left(\frac{\partial^2 \sigma_{11}}{\partial x \partial y} + \frac{\partial^2 \sigma_{21}}{\partial x^2} + \frac{\partial^2 \sigma_{12}}{\partial y^2} + \frac{\partial^2 \sigma_{22}}{\partial x \partial y}\right) \tag{26}$$

Thus, we have obtained a system of three equations (18,19) and (26) regarding the components of the stress and temperature tensor. Now it remains to attach to this system the equation of heat influx expressed relative to temperature and voltage.

For this purpose, we write the Duhamel-Neumann relation in the stress-resolved form [1]

$$\varepsilon_{ij} = \alpha(T - T_0)\delta_{ij} + \frac{1}{2\mu}(\sigma_{ij} - \frac{\lambda}{3\lambda + 2\mu}\sigma_{kk}\delta_{ij}) \tag{27}$$

and, in the two-dimensional case it has the form

$$\varepsilon_{11} = \alpha(T - T_0) + \frac{1}{2\mu}(\sigma_{11} - \frac{\lambda}{3\lambda + 2\mu}(\sigma_{11} + \sigma_{22})) \tag{28}$$

$$\varepsilon_{22} = \alpha(T - T_0) + \frac{1}{2\mu}(\sigma_{22} - \frac{\lambda}{3\lambda + 2\mu}(\sigma_{11} + \sigma_{22})) \tag{29}$$

$$\varepsilon_{12} = \frac{1}{2\mu}\sigma_{12}. \tag{30}$$

Substituting (28) and (29) into (9) we obtain the required heat influx equation

$$\lambda_0\left(\frac{\partial^2 T}{\partial x^2} + \frac{\partial^2 T}{\partial y^2}\right) - (c_\varepsilon + 2(3\lambda + 2\mu)\alpha T)\frac{\partial T}{\partial t} -$$
$$-(3\lambda + 2\mu)\alpha T\left(\frac{1}{2\mu}(1 - \frac{\lambda}{3\lambda + 2\mu})(\frac{\partial \sigma_{11}}{\partial t} + \frac{\partial \sigma_{11}}{\partial t}) - \frac{\lambda}{3\lambda + 2\mu}(\frac{\partial \sigma_{22}}{\partial t} + \frac{\partial \sigma_{22}}{\partial t})\right) = 0. \tag{31}$$

Differential equations (18), (19), (26) and (31) with the corresponding initial and boundary conditions regarding stress and temperature constitute a new coupled dynamic problem of plane thermoelasticity in stress, i.e.

$$\begin{cases} \dfrac{\partial^2 \sigma_{11}}{\partial t^2} = \dfrac{\lambda + 2\mu}{\rho}\dfrac{\partial^2 \sigma_{11}}{\partial x^2} + \dfrac{2\lambda + 2\mu}{\rho}\dfrac{\partial^2 \sigma_{12}}{\partial x \partial y} + \dfrac{\lambda}{\rho}\dfrac{\partial^2 \sigma_{22}}{\partial y^2} - \gamma\dfrac{\partial^2 T}{\partial t^2} \\ \dfrac{\partial^2 \sigma_{22}}{\partial t^2} = \dfrac{\lambda + 2\mu}{\rho}\dfrac{\partial^2 \sigma_{22}}{\partial y^2} + \dfrac{2\lambda + 2\mu}{\rho}\dfrac{\partial^2 \sigma_{21}}{\partial x \partial y} + \dfrac{\lambda}{\rho}\dfrac{\partial^2 \sigma_{11}}{\partial x^2} - \gamma\dfrac{\partial^2 T}{\partial t^2} \\ \dfrac{\partial^2 \sigma_{12}}{\partial t^2} = \dfrac{\mu}{\rho}\left(\dfrac{\partial^2 \sigma_{11}}{\partial x \partial y} + \dfrac{\partial^2 \sigma_{21}}{\partial x^2} + \dfrac{\partial^2 \sigma_{12}}{\partial y^2} + \dfrac{\partial^2 \sigma_{22}}{\partial x \partial y}\right) \\ \lambda_0\left(\dfrac{\partial^2 T}{\partial x^2} + \dfrac{\partial^2 T}{\partial y^2}\right) - (c_\varepsilon + 2\alpha\gamma T)\dfrac{\partial T}{\partial t} - \\ -\gamma T\left(\dfrac{1}{2\mu}(1 - \dfrac{2\lambda}{3\lambda + 2\mu})(\dfrac{\partial \sigma_{11}}{\partial t} + \dfrac{\partial \sigma_{22}}{\partial t})\right) = 0 \end{cases} \tag{32}$$

with initial

$$\sigma_{11}(x, y, t)\big|_{t=0} = \phi_1, \quad \sigma_{22}(x, y, t)\big|_{t=0} = \phi_2, \quad \sigma_{12}(x, y, t)\big|_{t=0} = \phi_3, \quad T(x, y, t)\big|_{t=0} = T_0,$$
$$\frac{\partial \sigma_{11}}{\partial t}\bigg|_{t=0} = \psi_1, \quad \frac{\partial \sigma_{22}}{\partial t}\bigg|_{t=0} = \psi_2, \quad \frac{\partial \sigma_{12}}{\partial t}\bigg|_{t=0} = \psi_3, \quad \frac{\partial T}{\partial t}\bigg|_{t=0} = \psi_4 \tag{33}$$

and, boundary conditions

$$\sigma_{11}(x, y, t)\big|_{x=\Gamma} = \sigma_0, \quad \sigma_{22}(x, y, t)\big|_{x=\Gamma} = \overline{\sigma}_0, \quad \sigma_{12}(x, y, t)\big|_{x=\Gamma} = \overline{\overline{\sigma}}_0,$$
$$T(x, y, t)\big|_{x=\Gamma} = T_1, \quad T(x, y, t)\big|_{x=\Gamma} = T_2. \tag{34}$$

3. Finite-difference method for solving coupled thermoelasticity problems

For numerical solution of the coupled problem of plane thermoelasticity (32-34) using the finite-difference method, explicit or implicit schemes can be constructed. Replacing the derivatives in equations (32) with finite-difference relations, we obtain an explicit scheme:

$$\frac{\sigma_{11}^{i,j,k+1}-2\sigma_{11}^{i,j,k}+\sigma_{11}^{i,j,k-1}}{\tau^2}=\frac{\lambda+2\mu}{\rho}\frac{\sigma_{11}^{i+1,j,k}-2\sigma_{11}^{i,j,k}+\sigma_{11}^{i-1,j,k}}{h_1^2}+$$
$$+\frac{2\lambda+2\mu}{\rho}\frac{\sigma_{12}^{i+1,j+1,k}-\sigma_{12}^{i+1,j-1,k}-\sigma_{12}^{i-1,j+1,k}+\sigma_{12}^{i-1,j-1,k}}{4h_1^2h_2^2}+$$
$$+\frac{\lambda}{\rho}\frac{\sigma_{22}^{i,j+1,k}-2\sigma_{22}^{i,j,k}+\sigma_{22}^{i,j-1,k}}{h_2^2}-\gamma\frac{T^{i,j,k+1}-2T^{i,j,k}+T^{i,j,k-1}}{\tau^2} \tag{35}$$

$$\frac{\sigma_{22}^{i,j,k+1}-2\sigma_{22}^{i,j,k}+\sigma_{22}^{i,j,k-1}}{\tau^2}=\frac{\lambda+2\mu}{\rho}\frac{\sigma_{22}^{i,j+1,k}-2\sigma_{22}^{i,j,k}+\sigma_{22}^{i,j-1,k}}{h_2^2}+$$
$$+\frac{2\lambda+2\mu}{\rho}\frac{\sigma_{12}^{i+1,j+1,k}-\sigma_{12}^{i+1,j-1,k}-\sigma_{12}^{i-1,j+1,k}+\sigma_{12}^{i-1,j-1,k}}{4h_1^2h_2^2}+$$
$$+\frac{\lambda}{\rho}\frac{\sigma_{11}^{i+1,j,k}-2\sigma_{11}^{i,j,k}+\sigma_{11}^{i-1,j,k}}{h_1^2}-\gamma\frac{T^{i,j,k+1}-2T^{i,j,k}+T^{i,j,k-1}}{\tau^2} \tag{36}$$

$$\frac{\sigma_{12}^{i,j,k+1}-2\sigma_{12}^{i,j,k}+\sigma_{12}^{i,j,k-1}}{\tau^2}=\frac{\mu}{\rho}\left(\frac{\sigma_{11}^{i+1,j+1,k}-\sigma_{11}^{i+1,j-1,k}-\sigma_{11}^{i-1,j+1,k}+\sigma_{11}^{i-1,j-1,k}}{4h_1^2h_2^2}+\frac{\sigma_{21}^{i+1,j,k}-2\sigma_{21}^{i,j,k}+\sigma_{21}^{i-1,j,k}}{h_1^2}+\right.$$
$$\left.+\frac{\sigma_{12}^{i,j+1,k}-2\sigma_{12}^{i,j,k}+\sigma_{12}^{i,j-1,k}}{h_2^2}+\frac{\sigma_{22}^{i+1,j+1,k}-\sigma_{22}^{i+1,j-1,k}-\sigma_{22}^{i-1,j+1,k}+\sigma_{22}^{i-1,j-1,k}}{4h_1^2h_2^2}\right) \tag{37}$$

$$\lambda_0\left(\frac{T^{i+1,j,k}-2T^{i,j,k}+T^{i-1,j,k}}{h_1^2}+\frac{T^{i,j+1,k}-2T^{i,j,k}+T^{i,j-1,k}}{h_2^2}\right)-(c_\varepsilon+2\alpha\gamma T^{i,j,k})\frac{T^{i,j,k+1}-T^{i,j,k}}{\tau}-$$
$$-\gamma T^{i,j,k}\left(\frac{1}{2\mu}(1-\frac{2\lambda}{3\lambda+2\mu})(\frac{\sigma_{11}^{i,j,k}-\sigma_{11}^{i,j,k-1}}{\tau}+\frac{\sigma_{22}^{i,j,k}-\sigma_{22}^{i,j,k-1}}{\tau})\right)=0. \tag{38}$$

Having solved difference equations (35)-(38) for $\sigma_{11}^{i,j,k+1}$, $\sigma_{22}^{i,j,k+1}$, $\sigma_{12}^{i,j,k+1}$ and $T^{i,j,k+1}$, respectively, we obtain

$$\sigma_{11}^{i,j,k+1}=\tau^2\left(\frac{\lambda+2\mu}{\rho}\frac{\sigma_{11}^{i+1,j,k}-2\sigma_{11}^{i,j,k}+\sigma_{11}^{i-1,j,k}}{h_1^2}+\frac{2\lambda+2\mu}{\rho}\frac{\sigma_{12}^{i+1,j+1,k}-\sigma_{12}^{i+1,j-1,k}-\sigma_{12}^{i-1,j+1,k}+\sigma_{12}^{i-1,j-1,k}}{4h_1^2h_2^2}+\right.$$
$$\left.+\frac{\lambda}{\rho}\frac{\sigma_{22}^{i,j+1,k}-2\sigma_{22}^{i,j,k}+\sigma_{22}^{i,j-1,k}}{h_2^2}-\gamma\frac{T^{i,j,k+1}-2T^{i,j,k}+T^{i,j,k-1}}{\tau^2}\right)+2\sigma_{11}^{i,j,k}-\sigma_{11}^{i,j,k-1} \tag{39}$$

$$\sigma_{22}^{i,j,k+1}=\tau^2\left(\frac{\lambda+2\mu}{\rho}\frac{\sigma_{22}^{i,j+1,k}-2\sigma_{22}^{i,j,k}+\sigma_{22}^{i,j-1,k}}{h_2^2}+\frac{2\lambda+2\mu}{\rho}\frac{\sigma_{12}^{i+1,j+1,k}-\sigma_{12}^{i+1,j-1,k}-\sigma_{12}^{i-1,j+1,k}+\sigma_{12}^{i-1,j-1,k}}{4h_1^2h_2^2}+\right.$$
$$\left.+\frac{\lambda}{\rho}\frac{\sigma_{11}^{i+1,j,k}-2\sigma_{11}^{i,j,k}+\sigma_{11}^{i-1,j,k}}{h_1^2}-\gamma\frac{T^{i,j,k+1}-2T^{i,j,k}+T^{i,j,k-1}}{\tau^2}\right)+2\sigma_{22}^{i,j,k}-\sigma_{22}^{i,j,k-1} \tag{40}$$

$$\sigma_{12}^{i,j,k+1}=\frac{\tau^2\mu}{\rho}\left(\frac{\sigma_{11}^{i+1,j+1,k}-\sigma_{11}^{i+1,j-1,k}-\sigma_{11}^{i-1,j+1,k}+\sigma_{11}^{i-1,j-1,k}}{4h_1^2h_2^2}+\frac{\sigma_{21}^{i+1,j,k}-2\sigma_{21}^{i,j,k}+\sigma_{21}^{i-1,j,k}}{h_1^2}+\right.$$
$$\left.+\frac{\sigma_{12}^{i,j+1,k}-2\sigma_{12}^{i,j,k}+\sigma_{12}^{i,j-1,k}}{h_2^2}+\frac{\sigma_{22}^{i+1,j+1,k}-\sigma_{22}^{i+1,j-1,k}-\sigma_{22}^{i-1,j+1,k}+\sigma_{22}^{i-1,j-1,k}}{4h_1^2h_2^2}\right)+2\sigma_{12}^{i,j,k}-\sigma_{12}^{i,j,k-1} \tag{41}$$

$$T^{i,j,k+1}=\frac{\tau}{c_\varepsilon+2\alpha\gamma T^{i,j,k}}\left(\lambda_0\left(\frac{T^{i+1,j,k}-2T^{i,j,k}+T^{i-1,j,k}}{h_1^2}+\frac{T^{i,j+1,k}-2T^{i,j,k}+T^{i,j-1,k}}{h_2^2}\right)-\right.$$

$$\left.-\gamma T^{i,j,k}\left(\frac{1}{2\mu}(1-\frac{2\lambda}{3\lambda+2\mu})(\frac{\sigma_{11}^{i,j,k}-\sigma_{11}^{i,j,k-1}}{\tau}+\frac{\sigma_{22}^{i,j,k}-\sigma_{22}^{i,j,k-1}}{\tau})\right)\right)+T^{i,j,k}. \tag{42}$$

Difference equations (39)-(42) using initial and boundary conditions make it possible to calculate the values of the stresses and temperatures on the *(j+1)* layer over time.

It is known that the convergence of explicit finite-difference schemes imposes a certain limitation on the time step size, similar to the Fredric's-Courant inequalities.

It is possible to construct implicit finite-difference schemes without the above restrictions for the boundary value problem (32-34):

$$\frac{\sigma_{11}^{i,j,k+1}-2\sigma_{11}^{i,j,k}+\sigma_{11}^{i,j,k-1}}{\tau^2}=\frac{\lambda+2\mu}{\rho}\frac{\sigma_{11}^{i+1,j,k+1}-2\sigma_{11}^{i,j,k+1}+\sigma_{11}^{i-1,j,k+1}}{h_1^2}+$$

$$+\frac{2\lambda+2\mu}{\rho}\frac{\sigma_{12}^{i+1,j+1,k}-\sigma_{12}^{i+1,j-1,k}-\sigma_{12}^{i-1,j+1,k}+\sigma_{12}^{i-1,j-1,k}}{4h_1^2h_2^2}+$$

$$+\frac{\lambda}{\rho}\frac{\sigma_{22}^{i,j+1,k}-2\sigma_{22}^{i,j,k}+\sigma_{22}^{i,j-1,k}}{h_2^2}-\gamma\frac{T^{i,j,k+1}-2T^{i,j,k}+T^{i,j,k-1}}{\tau^2} \tag{43}$$

$$\frac{\sigma_{22}^{i,j,k+1}-2\sigma_{22}^{i,j,k}+\sigma_{22}^{i,j,k-1}}{\tau^2}=\frac{\lambda+2\mu}{\rho}\frac{\sigma_{22}^{i,j+1,k+1}-2\sigma_{22}^{i,j,k+1}+\sigma_{22}^{i,j-1,k+1}}{h_2^2}+$$

$$+\frac{2\lambda+2\mu}{\rho}\frac{\sigma_{12}^{i+1,j+1,k}-\sigma_{12}^{i+1,j-1,k}-\sigma_{12}^{i-1,j+1,k}+\sigma_{12}^{i-1,j-1,k}}{4h_1^2h_2^2}+$$

$$+\frac{\lambda}{\rho}\frac{\sigma_{11}^{i+1,j,k}-2\sigma_{11}^{i,j,k}+\sigma_{11}^{i-1,j,k}}{h_1^2}-\gamma\frac{T^{i,j,k+1}-2T^{i,j,k}+T^{i,j,k-1}}{\tau^2} \tag{44}$$

$$\frac{\sigma_{12}^{i,j,k+1}-2\sigma_{12}^{i,j,k}+\sigma_{12}^{i,j,k-1}}{\tau^2}=\frac{\mu}{\rho}\left(\frac{\sigma_{11}^{i+1,j+1,k}-\sigma_{11}^{i+1,j-1,k}-\sigma_{11}^{i-1,j+1,k}+\sigma_{11}^{i-1,j-1,k}}{4h_1^2h_2^2}+\frac{\sigma_{21}^{i+1,j,k+1}-2\sigma_{21}^{i,j,k+1}+\sigma_{21}^{i-1,j,k+1}}{h_1^2}+\right.$$

$$\left.+\frac{\sigma_{12}^{i,j+1,k}-2\sigma_{12}^{i,j,k}+\sigma_{12}^{i,j-1,k}}{h_2^2}+\frac{\sigma_{22}^{i+1,j+1,k}-\sigma_{22}^{i+1,j-1,k}-\sigma_{22}^{i-1,j+1,k}+\sigma_{22}^{i-1,j-1,k}}{4h_1^2h_2^2}\right) \tag{45}$$

$$\lambda_0\left(\frac{T^{i+1,j,k+1}-2T^{i,j,k+1}+T^{i-1,j,k+1}}{h_1^2}+\frac{T^{i,j+1,k}-2T^{i,j,k}+T^{i,j-1,k}}{h_2^2}\right)-(c_\varepsilon+2\alpha\gamma T^{i,j,k})\frac{T^{i,j,k+1}-T^{i,j,k}}{\tau}-$$

$$-\gamma T^{i,j,k}\left(\frac{1}{2\mu}(1-\frac{2\lambda}{3\lambda+2\mu})(\frac{\sigma_{11}^{i,j,k}-\sigma_{11}^{i,j,k-1}}{\tau}+\frac{\sigma_{22}^{i,j,k}-\sigma_{22}^{i,j,k-1}}{\tau})\right)=0. \tag{46}$$

Implicit difference equations (43-46) can be reduced to a system of equations with a three-diagonal matrix and solved by the elimination method: equation (43) has the form

$$a_i^1\sigma_{11}^{i+1,j,k+1}+b_i^1\sigma_{11}^{i,j,k+1}+c_i^1\sigma_{11}^{i-1,j,k+1}=f_i^1 \tag{47}$$

here

$$a_i=\frac{\lambda+2\mu}{\rho h_1^2},\quad b_i=-\frac{2(\lambda+2\mu)}{\rho h_1^2}-\frac{1}{\tau^2},\quad c_i=\frac{\lambda+2\mu}{\rho h_1^2},$$

$$f_i=\gamma\frac{T^{i,j,k+1}-2T^{i,j,k}+T^{i,j,k-1}}{\tau^2}-\frac{\lambda}{\rho}\frac{\sigma_{22}^{i,j+1,k}-2\sigma_{22}^{i,j,k}+\sigma_{22}^{i,j-1,k}}{h_2^2}-$$

$$-\frac{2\lambda+2\mu}{\rho}\frac{\sigma_{12}^{i+1,j+1,k}-\sigma_{12}^{i+1,j-1,k}-\sigma_{12}^{i-1,j+1,k}+\sigma_{12}^{i-1,j-1,k}}{4h_1^2h_2^2}+\frac{2\sigma_{11}^{i,j,k}-\sigma_{11}^{i,j,k-1}}{\tau^2}.$$

Similarly, equations (44)-(46) can be reduced to tridiagonal form

$$a_i^4 T^{i+1,j,k+1} + b_i^4 T^{i,j,k+1} + c_i^4 T^{i-1,j,k+1} = f_i^4 \tag{48}$$

where

$$a_i^4 = \frac{\lambda_0}{h_1^2}, \quad b_i^4 = -\frac{2\lambda_0}{h_1^2} - \frac{c_\varepsilon + 2\alpha\gamma T^{i,j,k}}{\tau}, \quad c_i^4 = \frac{\lambda_0}{h_1^2},$$

$$f_i^4 = \gamma T^{i,j,k}\left(\frac{1}{2\mu}(1-\frac{2\lambda}{3\lambda+2\mu})(\frac{\sigma_{11}^{i,j,k}-\sigma_{11}^{i,j,k-1}}{\tau}+\frac{\sigma_{22}^{i,j,k}-\sigma_{22}^{i,j,k-1}}{\tau})\right)-$$

$$-\lambda_0\frac{T^{i,j+1,k}-2T^{i,j,k}+T^{i,j-1,k}}{h_2^2}-\frac{c_\varepsilon+2\alpha\gamma T^{i,j,k}}{\tau}T^{i,j,k}.$$

Having determined the values of the desired functions $\sigma(x,y,t)$ on the initial layers *j=0* and *j=1* and $T(x,y,t)$ on the layer *j=0* from the initial conditions, then using the boundary conditions, difference equations (47) - (48) can be solved by the elimination or iterative method.

4. Numerical example

Let us consider the coupled thermoelastic problem on the free plate subject to a dome-shaped temperature field specified at the initial moment of time. It is required to study the distribution of temperature stresses over time in the plate. The problem is described by equations (31-33). In this case, the initial and boundary conditions for the problem under consideration have the form:

initial conditions

$$\sigma_{11}(x,y,t)\big|_{t=0}=0,\ \sigma_{22}(x,y,t)\big|_{t=0}=0,\ \sigma_{12}(x,y,t)\big|_{t=0}=0,\ T(x,y,t)\big|_{t=0}=T_0\cdot\sin(\pi x)\sin(\pi y)$$

$$\left.\frac{\partial\sigma_{11}}{\partial t}\right|_{t=0}=0,\quad \left.\frac{\partial\sigma_{22}}{\partial t}\right|_{t=0}=0,\quad \left.\frac{\partial\sigma_{12}}{\partial t}\right|_{t=0}=0,\quad \left.\frac{\partial T}{\partial t}\right|_{t=0}=0$$

boundary conditions

$$\sigma_{11}(x,y,t)\big|_{x=\Gamma}=0,\ \sigma_{22}(x,y,t)\big|_{x=\Gamma}=0,\ \sigma_{12}(x,y,t)\big|_{x=\Gamma}=0,\ T(x,y,t)\big|_{x=\Gamma}=0.$$

Initial data are given as follow

$$\lambda=1.5,\quad \mu=0.5,\quad \lambda_0=0.15,\quad \alpha=0.125,\quad \rho=0.86,\quad c_\varepsilon=3.4,\quad T_0=20,\quad h=0.1,\quad \tau=0.01\,.$$

In tables 1-2 the distribution of the stresses in the middle of the plane rectangle are shown.

Table 1.

Stress values σ_{11} in the middle of the plate

Method of solution y=0.5, t=0,08:	*x=0*	*x=0.1*	*x=0.2*	*x=0.3*	*x=0.4*	*x=0.5*
Recurrence formulas(Explicit scheme)	0	0.382	0.968	1.692	2.283	2.507
Elimination method(Implicit scheme)	0	0.400	0.965	1.642	2.197	2.409

Table 2.

Stress values σ_{22} in the middle of the plate

Method of solution y=0.5, t=0,08:	*x=0*	*x=0.1*	*x=0.2*	*x=0.3*	*x=0.4*	*x=0.5*
Recurrence formulas(Explicit scheme)	0	0.376	0.965	1.692	2.283	2.507
Elimination method(Implicit scheme)	0	0.379	0.947	1.634	2.195	2.409

Table 3 shown the temperature distribution in the center of the plate at time *t=8.* Note that the maximal values of the temperature is reached in the center of the plate.

Table 3.

Temperature values T in the middle of the plate

Method of solution for y=0.5, t=0,08:	*x=0*	*x=0.1*	*x=0.2*	*x=0.3*	*x=0.4*	*x=0.5*
Recurrence formulas(Explicit scheme)	0	5.630	10.321	13.664	16.631	16.279
Elimination method(Implicit scheme)	0	5.616	10.329	13.719	15.722	16.381

5. Conclusion

The paper formulates a coupled problem of thermoelasticity in stresses. In this case, the coupled boundary value problem consisted of four partial differential equations including heat influx one. In the proposed boundary value problem, unlike known problems, three components the stress tensor and temperature are unknown. Discrete equations are compiled using the finite-difference method in the form of explicit and implicit schemes. The plane problem of thermal stresses of a free plate under the influence of temperature effects of a dome-shaped shape is solved, numerically. The presented results using an explicit and implicit schemes show the reliability of the results obtained and the validity of the proposed coupled boundary value problem of thermoelasticity in stresses.

References

1. *Novatsky V.* The Theory of Elasticity. -M.: Mir, 1975. -872 p.
2. *Pobedrya B.E.* Numerical Methods in the Theory of Elasticity and Plasticity. -M.: Moscow State University, 1996.-343 p.
3. *Konovalov, A.N.* Solving problems of elasticity theory under stress. Novosibirsk: NSU, 1979. - 92 p.
4. *Melnik R.V.N.* Discrete models of coupled dynamic thermoelasticity for stress-temperature // Applied Mathematics and Computation.12292001), p.107-132
5. *Kartashov E.M.* Model representations of heat shock in terms of dynamic thermal elasticity // Russian Technological Journal. 2020;8(2), p.85-108
6. *Pobedrya B.E.* On Static Problem in terms of Stresses // Moscow Univ. Mech. Bull. 58 (3), 8-14 (2003).
7. *Borodachev N.M.* Stress Solutions to the Three-Dimensional Problem of Elasticity. Intern. Appl. Mech. 42 (8), 849-878 (2006).
8. *Khaldjigitov A.A., Tilovov O.U.* Numerical solution of the problem of the theory of elasticity in stresses // Problems_Mechanics 2022, No. 2, pp. 12-19
9. *Khaldjigitov A.A., Kalandarov A.A., Djumayozov U.Z.* Numerical modeling of coupled problems of thermo-plasticity on non-uniform meshes // 2nd International Conference on Energetics, Civil and Agricultural Engineering 14-16 Oktober, 2021, Tashkent, AIP Conference Proceedings 2686, 020010 (2022); https://doi.org/10.1063/5.0114013.
10. *Khaldjigitov A.A., Kalandarov A.A., Djumayozov U.Z. Finite-Difference Equations for 2D Elasticity Problems on a Non-Uniform Grid //* International Conference on Actual Problems of Applied Mechanics APAM – 2021, 27-29 October, Samarkand, AIP Conference Proceedings 2637, 030005 (2022) https://doi.org/10.1063/5.0118482
11. *Turimov D., Khaldjigitov A., Djumayozov U., Kim W.* Formulation and Numerical Solution of Plane Problems of the Theory of Elasticity in Strains. Mathematics, 2024, 12, 71. https://doi.org/10.3390/ math12010071
12. *Samarski A.A., Nikolaev E.S.* Methods for Solving Grid Equations.M: «Science», 1978, 592 p.
13. *Rebello M. A., Zdanski P. S. B., Vaz M. Jr.* Considerations on alternative solutions for stress analysis of anisotropic materials: a beam case study. Continuum Mech. Thermodyn. (2021) 33:2123–2140 https://doi.org/10.1007/s00161-021-01012-4
14. *Filonenko-Borodich M.* Theory of Elasticity. University Press of the Pacific. (November 6, 2003), 396 p.
15. *Tauchert T.R.* Publications On Thermal Stresses. // J. Therm. Stress. - 2001. - Vol. 24, № 1. - P. 91-92.
16. *Youssef H. M., Al-Felali A.S.* Generalized Thermoelasticity Problem of Material Subjected to Thermal Loading Due to Laser Pulse. Applied Mathematics, 2012, 3, 142-146.

17. *Youssef, H.M.* Theory of two-temperature-generalized thermoelasticity // IMA J. of APPL. Math., 2006, 71, pp. 383-390.
18. *Ilyushin A.A.* Plastic. Part 1. Elastoplastic deformations / Gostekhizdat, Moscow, 2004 391 p.
19. *Abirov, R.A., Khusanov, B.E., Sagdullaeva, D.A.* Numerical modeling of the problem of indentation of elastic and elastic-plastic massive bodies. In IOP Conference Series: Materials Science and Engineering, 2020, 971(3): 032017. https://doi.org/10.1088/1757-899X/971/3/032017.
20. *Matus P., Mazhukin V., Mozolevsky I.* Stability of Finite Difference Schemes on Non-uniform Spatial-Time-Grids. Conference Paper in Lecture Notes in Computer Science June 2000. DOI: 10.1007/3-540-45262-1_67.

PLANE PROBLEMS IN STRAINS FOR ORTHOPROPIC BODIES

Khaldjigitov A.A.[1], Khasanova Z.Z.[1], Djumayozov U.Z.[2]
[1]*National University of Uzbekistan, Tashkent, Uzbekistan;*
[2]*Samarkand branch of Tashkent University of Information Technologies, Samarkand, Uzbekistan;*
E-mail: djumayozov@bk.ru

Abstract: *The paper proposes differential equations of compatibility in strains for orthotropic bodies. In a particular case, from which the well-known differential equations of compatibility for isotropic bodies follow. A plane problem of elasticity in strains for orthotropic bodies is formulated. The grid equations are compiled using the finite-difference method and solved using the iterative method and the alternative variable method. The validity of the modeling equations and the reliability of the results are substantiated by comparing the solution of rectangular plate problem in different boundary conditions and using various methods.*

Key words: *elasticity, stress, strain, displacements, boundary value problem.*

1. Introduction.

Usually, the problem of studying the stress-strain state (SSS) of structures made of anisotropic (composite) materials is reduced to boundary value problems regarding displacements. In this case, the necessary strains and stresses are determined from known displacements.

The formulation of boundary value problems regarding stresses and strains for the purpose of effectively studying the stress-strain state of structures made of anisotropic materials is an urgent problem of the solid mechanics. Research in the field of boundary value problems regarding stresses originates from the well-known Beltrami-Michell equations [1]. Further problems in stresses were considered in the works of Filonenko-Borodich [2], Konovalov [3], Pobedria [4] and Borodachev [5] and others. In the works of Pobedria [4,6] a new formulation of the problem of the theory of elasticity in stresses was proposed, from which in a particular case follows the classical Beltrami-Michell equations.

The formulation of a boundary value problem regarding deformations is a poorly studied area of solid mechanics. The Saint-Venant compatibility conditions using the equilibrium equations and Hooke's law can be written in the form of a system of six differential equations for strains [1]. These equations, in combination with three equilibrium equations and boundary conditions, constitute the boundary value problem of the theory of elasticity in strains [7]. Boundary value problems in strains are also considered in [8,9]. The formulation and solution of boundary value problems of the theory of elasticity in strains is an important and urgent problem in the solid mechanics.

This work is devoted to the study of the compatibility conditions of Saint-Venant deformations as applied to anisotropic bodies. Beltrami-Michell type equations in strains for orthotropic bodies are proposed. A plane problem in strains for orthotropic bodies is formulated and solved using different numerical methods and boundary conditions.

2. Plane problem in deformations for isotropic bodies.

Let us consider the equilibrium equations in a plane stress case:

$$\frac{\partial \sigma_{11}}{\partial x} + \frac{\partial \sigma_{12}}{\partial y} + X_1 = 0, \tag{1}$$

$$\frac{\partial \sigma_{21}}{\partial x} + \frac{\partial \sigma_{22}}{\partial y} + X_2 = 0. \tag{2}$$

By adding differentiated equilibrium equations (1) and (2) with respect to y and x, respectively, the following equation can be found

$$\nabla^2 \sigma_{12} + \frac{\partial^2 (\sigma_{11} + \sigma_{22})}{\partial x \partial y} = -(\frac{\partial X_1}{\partial y} + \frac{\partial X_2}{\partial x}). \tag{3}$$

Differentiating equation (1) with respect to x, and taking into account the following well-known relation [10]

$$\frac{\partial^2 \sigma_x}{\partial y^2} + \frac{\partial^2 \sigma_y}{\partial x^2} = 2\frac{\partial^2 \sigma_{xy}}{\partial x \partial y}.$$

it can be written in the following form

$$\nabla^2 \sigma_{11} + \frac{\partial^2 (\sigma_{11} + \sigma_{22})}{\partial x^2} = -2\frac{\partial X_1}{\partial x}. \tag{4}$$

Similarly, equation (2) can be represented in the following form

$$\nabla^2 \sigma_{22} + \frac{\partial^2 (\sigma_{11} + \sigma_{22})}{\partial y^2} = -2\frac{\partial X_2}{\partial y}. \tag{5}$$

Note that equation (3-5) can be found from the Beltrami-Mitchell equations at $\nu = 0$. By Timoshenko [11] was noted that the distribution of plane stresses, under certain conditions of load application, does not depend on Poisson's ratio ν.

Substituting Hooke's law

$$\begin{aligned} \sigma_{11} &= (\lambda + 2\mu)\varepsilon_{11} + \lambda \varepsilon_{22}, \\ \sigma_{22} &= \lambda \varepsilon_{11} + (\lambda + 2\mu)\varepsilon_{22}, \\ \sigma_{12} &= 2\mu \varepsilon_{12}. \end{aligned} \tag{6}$$

in (3) the following equation in strains can be find i.e.

$$\nabla^2 \varepsilon_{12} + \frac{\lambda + \mu}{\mu}\frac{\partial^2 \theta}{\partial x \partial y} = -\frac{1}{2\mu}(\frac{\partial X_1}{\partial y} + \frac{\partial X_2}{\partial x}), \quad \theta = \varepsilon_{11} + \varepsilon_{22}. \tag{7}$$

The last equation coincides with the differential equations of compatibility for strains given in [1] at $i = 1,\ j = 1.$ Equation (7), in the case of plane problems, can be considered as a well-known compatibility condition in strains [11,16]

$$\frac{\partial^2 \varepsilon_{11}}{\partial y^2} + \frac{\partial^2 \varepsilon_{22}}{\partial x^2} = 2\frac{\partial^2 \varepsilon_{12}}{\partial x \partial y}. \tag{8}$$

Equation (7), in the absence of body forces, in combination with two equilibrium equations can be considered as a plane boundary problem in deformations [7] i.e.

$$\begin{aligned} &(\lambda + 2\mu)\frac{\partial \varepsilon_{11}}{\partial x} + \lambda \frac{\partial \varepsilon_{22}}{\partial x} + 2\mu \frac{\partial \varepsilon_{12}}{\partial y} = 0, \\ &(\lambda + 2\mu)\frac{\partial \varepsilon_{22}}{\partial y} + \lambda \frac{\partial \varepsilon_{11}}{\partial y} + 2\mu \frac{\partial \varepsilon_{21}}{\partial x} = 0, \\ &\mu(\frac{\partial^2 \varepsilon_{12}}{\partial x^2} + \frac{\partial^2 \varepsilon_{12}}{\partial y^2}) + (\lambda + \mu)(\frac{\partial^2 \varepsilon_{11}}{\partial x \partial y} + \frac{\partial^2 \varepsilon_{22}}{\partial x \partial y}) = 0, \end{aligned} \tag{9}$$

with appropriate boundary conditions

$$\begin{aligned} &(\lambda(\varepsilon_{11} + \varepsilon_{22}) + 2\mu \varepsilon_{11})n_1 + 2\mu \varepsilon_{12} n_2)|_\Gamma = S_1, \\ &(2\mu \varepsilon_{12} n_1 + (\lambda(\varepsilon_{11} + \varepsilon_{22}) + 2\mu \varepsilon_{22})n_2)|_\Gamma = S_2. \end{aligned} \tag{10}$$

To ensure the completeness of the boundary value problem (9-10), it is necessary to add equilibrium equations (1-2) to them as boundary conditions, i.e.

$$\left[(\lambda+2\mu)\frac{\partial\varepsilon_{11}}{\partial x}+\lambda\frac{\partial\varepsilon_{22}}{\partial x}+2\mu\frac{\partial\varepsilon_{12}}{\partial y}\right]|_{\Gamma}=0,$$
$$\left[(\lambda+2\mu)\frac{\partial\varepsilon_{22}}{\partial y}+\lambda\frac{\partial\varepsilon_{11}}{\partial y}+2\mu\frac{\partial\varepsilon_{21}}{\partial x}\right]|_{\Gamma}=0. \tag{11}$$

where Γ is the boundary of a given area. Thus, equations (9-11) represent a plane boundary value problem of the theory of elasticity with respect to deformations.

3. Differential equations of strains for orthotropic bodies.

Usually, when formulating plane problems of the theory of elasticity in stresses and strains, the Saint-Venant compatibility condition (8) is considered together with two equilibrium equations. It is known that plane problems in stresses are solved by reducing them to a biharmonic equation with respect to the Airy stress function [11]. Plane problems in strains for isotropic bodies were formulated in the previous section.

In order to formulate a plane problem for anisotropic bodies, substituting the generalized Hooke's law of orthotropic bodies [12, 17]

$$\sigma_{11}=C_{1111}\varepsilon_{11}+C_{1122}\varepsilon_{22},$$
$$\sigma_{22}=C_{2211}\varepsilon_{11}+C_{2222}\varepsilon_{22}, \tag{12}$$
$$\sigma_{12}=2C_{1212}\varepsilon_{12},$$

in to (3), the following equation can be found

$$2C_{1212}\nabla^2\varepsilon_{12}+(C_{1111}+C_{2211})\frac{\partial^2\varepsilon_{11}}{\partial x\partial y}+(C_{2222}+C_{1122})\frac{\partial^2\varepsilon_{22}}{\partial x\partial y}=-(\frac{\partial X_1}{\partial y}+\frac{\partial X_2}{\partial x}). \tag{13}$$

where $C_{ijkl}-$ tensor of elastic constants for orthotropic bodies, X_i- body forces. The last equation can be considered as a compatibility condition for plane problems in the theory of elasticity of anisotropic bodies.

The compatibility equation (13) should be considered together with two equilibrium equations (1-2) expressed, using Hooke's law for orthotropic bodies, with respect to deformations (12), i.e.

$$C_{1111}\frac{\partial\varepsilon_{11}}{\partial x}+C_{1122}\frac{\partial\varepsilon_{22}}{\partial x}+2C_{1212}\frac{\partial\varepsilon_{11}}{\partial y}+X_1=0,$$
$$C_{2222}\frac{\partial\varepsilon_{22}}{\partial y}+C_{2211}\frac{\partial\varepsilon_{11}}{\partial y}+2C_{1212}\frac{\partial\varepsilon_{21}}{\partial x}+X_2=0. \tag{14}$$

In the numerical implementation of boundary value problems, to increase the of approximation order of the finite-difference equations, equilibrium equations (14) can be used in a differentiated form with respect to *x* and *y*, respectively. If, in differentiated equilibrium equations, the mixed derivatives are replaced using the compatibility condition (8), the following equations can be found

$$C_{1111}\frac{\partial^2\varepsilon_{11}}{\partial x^2}+C_{1212}\frac{\partial^2\varepsilon_{11}}{\partial y^2}+(C_{1122}+C_{1212})\frac{\partial^2\varepsilon_{22}}{\partial x^2}=-2\frac{\partial X_1}{\partial x},$$
$$C_{2222}\frac{\partial^2\varepsilon_{22}}{\partial y^2}+C_{1212}\frac{\partial^2\varepsilon_{22}}{\partial x^2}+(C_{2211}+C_{1212})\frac{\partial^2\varepsilon_{11}}{\partial y^2}=-2\frac{\partial X_2}{\partial y}. \tag{15}$$

Equations (13) and (15) are compatibility differential equations in strains for anisotropic bodies.The elastic constant tensor C_{ijkl} is related to technical constants as follows[12]

$$C_{1111}=\frac{E_1}{1-\nu_{12}\nu_{21}}, C_{1122}=\frac{E_1\nu_{21}}{1-\nu_{12}\nu_{21}},$$
$$C_{1212}=G_{12}=\frac{E_1E_2}{E_1+E_2(1+2\nu_{12})},\ \frac{\nu_{12}}{E_1}=\frac{\nu_{21}}{E_2}, \tag{16}$$
$$C_{2211}=\frac{E_2\nu_{12}}{1-\nu_{12}\nu_{21}},\qquad C_{2222}=\frac{E_2}{1-\nu_{12}\nu_{21}}.$$

where $E_1, E_2 -$ Young's moduli for orthotropic bodies, $\nu_{12}, \nu_{21} -$ Poisson's constants for orthotropic bodies, $G_{12} -$ shear modulus.

In the case of isotropic bodies, these constants have the form

$$C_{1111}=C_{2222}=\lambda+2\mu,\ C_{1122}=C_{2211}=\lambda,\ \ C_{1212}=\mu.$$

and, from equations (13,15) the well-known compatibility differential equations for isotropic bodies follow [1].

4. Differential equations of strains for orthotropic bodies.

For formulation the plane problems in strains, similarly to the Beltrami-Michell equations, following the works [7,8], it is enough to consider equation (13) together with two equilibrium equations expressed with respect to deformations (14) i.e.

$$C_{1111}\frac{\partial\varepsilon_{11}}{\partial x}+C_{1122}\frac{\partial\varepsilon_{22}}{\partial x}+2C_{1212}\frac{\partial\varepsilon_{12}}{\partial y}+X_1=0, \tag{17}$$

$$C_{2222}\frac{\partial\varepsilon_{22}}{\partial y}+C_{2211}\frac{\partial\varepsilon_{11}}{\partial y}+2C_{1212}\frac{\partial^2\varepsilon_{12}}{\partial x}+X_2=0, \tag{18}$$

$$2C_{1212}\nabla^2\varepsilon_{12}+(C_{1111}+C_{2211})\frac{\partial^2\varepsilon_{11}}{\partial x\partial y}+(C_{2222}+C_{1122})\frac{\partial^2\varepsilon_{22}}{\partial x\partial y}=-(\frac{\partial X_1}{\partial y}+\frac{\partial X_2}{\partial x}), \tag{19}$$

with boundary conditions regarding deformations

$$\begin{aligned}&((C_{1111}\varepsilon_{11}+C_{1122}\varepsilon_{22})n_1+2C_{1212}\varepsilon_{12}n_2)\,|_\Gamma=S_1,\\&(2C_{1212}\varepsilon_{12}n_1+(C_{2211}\varepsilon_{11}+C_{2222}\varepsilon_{22})n_2)\,|_\Gamma=S_2.\end{aligned} \tag{20}$$

and, additional boundary conditions

$$\begin{aligned}&\left[C_{1111}\frac{\partial\varepsilon_{11}}{\partial x}+C_{1122}\frac{\partial\varepsilon_{22}}{\partial x}+2C_{1212}\frac{\partial\varepsilon_{12}}{\partial y}+X_1\right]|_\Gamma=0,\\&\left[C_{2222}\frac{\partial\varepsilon_{22}}{\partial y}+C_{2211}\frac{\partial\varepsilon_{11}}{\partial y}+2C_{1212}\frac{\partial\varepsilon_{21}}{\partial x}+X_2\right]|_\Gamma=0.\end{aligned} \tag{21}$$

Thus, equations (17-21) represent a plane boundary value problem in strains for orthotropic bodies. Let us consider the boundary conditions (20) for a rectangular plane stretched along the *OX* axis:

$$\begin{aligned}&for\ x=0,l_1:\ \sigma_{11}\,|_{x=0,l_1}=\varphi,\ \sigma_{12}\,|_{x=0,l_1}=0,\\&for\ y=0,l_2:\ \sigma_{22}\,|_{y=0,l_2}=0,\ \sigma_{21}\,|_{y=0,l_2}=0.\end{aligned} \tag{22}$$

Hooke's law (12) taking into account technical elasticity constants (16 has the form [12]

$$\begin{aligned}&\sigma_{11}=\frac{E_1}{(1-\nu_{12}\nu_{21})}\varepsilon_{11}+\frac{E_1\nu_{21}}{(1-\nu_{12}\nu_{21})}\varepsilon_{22},\\&\sigma_{22}=\frac{E_2\nu_{12}}{(1-\nu_{12}\nu_{21})}\varepsilon_{11}+\frac{E_2}{(1-\nu_{12}\nu_{21})}\varepsilon_{22},\\&\sigma_{12}=2G_{12}\varepsilon_{12}.\end{aligned} \tag{23}$$

Then the boundary conditions regarding strains have the form

$$\varepsilon_{11}|_{x=0}=\frac{1-\nu_{12}\nu_{21}}{E_1}\sigma_{11},\ \varepsilon_{21}|_{x=0}=0,\varepsilon_{22}|_{y=0}=0,\ \varepsilon_{12}|_{y=0}=0,$$
$$\varepsilon_{11}|_{x=l_1}=\frac{1-\nu_{12}\nu_{21}}{E_1}\sigma_{11},\ \varepsilon_{21}|_{x=l_1}=0,\ \varepsilon_{22}|_{y=l_2}=0,\varepsilon_{12}|_{y=l_2}=0, \tag{23}$$

and, additional boundary conditions

$$\left[\frac{\partial\varepsilon_{11}}{\partial y}\right]|_{y=0,l_2}=-\left[\frac{2G_{12}}{C_{1122}}\frac{\partial\varepsilon_{21}}{\partial x}\right]|_{y=0,l_2}, \tag{24}$$

$$\left[\frac{\partial\varepsilon_{22}}{\partial x}\right]|_{x=0,l_1}=-\left[\frac{2G_{12}}{C_{2211}}\frac{\partial\varepsilon_{12}}{\partial y}\right]|_{x=0,l_1}. \tag{25}$$

where C_{1122} and C_{2211} are defined by relation (16).

5. Finite-difference equations and solution methods.

We proceed to the numerical solution of the boundary value problem (17-21). Let us consider the boundary value problem in a rectangle domain $0\le x\le l_1, 0\le y\le l_2$ with a corresponding grid area $\Omega\{x_i=ih_1,\ i=\overline{0,n};\ y_j=jh_2,\ j=\overline{0,n}\}$, where $h_k=l_k/N_k, k=1,2$. Replacing the derivatives in differential equations (17-19) with finite relations [13], we can find that

$$C_{1111}\frac{\varepsilon^{11}_{i+1,j}-\varepsilon^{11}_{ij}}{h_1}+C_{1122}\frac{\varepsilon^{22}_{i+1,j}-\varepsilon^{22}_{i-1,j}}{2h_1}+C_{1212}\frac{\varepsilon^{12}_{i,j+1}-\varepsilon^{12}_{i,j-1}}{2h_2}=0,$$
$$C_{2222}\frac{\varepsilon^{22}_{i,j+1}-\varepsilon^{22}_{ij}}{h_2}+C_{2211}\frac{\varepsilon^{11}_{i,j+1}-\varepsilon^{11}_{i,j-1}}{2h_2}+C_{2121}\frac{\varepsilon^{12}_{i+1,j}-\varepsilon^{12}_{i-1,j}}{2h_1}=0,$$
$$2C_{1212}\frac{\varepsilon^{12}_{i+1,j}-2\varepsilon^{12}_{i,j}+\varepsilon^{12}_{i-1,j}}{h_1^2}+\left(C_{1111}+C_{1122}\right)\frac{\varepsilon^{11}_{i+1,j+1}-\varepsilon^{11}_{i+1,j-1}-\varepsilon^{11}_{i-1,j+1}+\varepsilon^{11}_{i+1,j+1}}{4h_1h_2}+$$
$$+2C_{1212}\frac{\varepsilon^{12}_{i,j+1}-2\varepsilon^{12}_{i,j}+\varepsilon^{12}_{i,j-1}}{h_2^2}+\left(C_{2222}+C_{2211}\right)\frac{\varepsilon^{22}_{i+1,j+1}-\varepsilon^{22}_{i+1,j-1}-\varepsilon^{22}_{i-1,j+1}+\varepsilon^{22}_{i+1,j+1}}{4h_1h_2}=0 \tag{26}$$

Resolving equations $(26)_{1,2}$ for $\varepsilon^{11}_{ij},\varepsilon^{22}_{ij},\varepsilon^{12}_{ij}$, we can find that

$$\varepsilon^{11}_{ij}=\varepsilon^{11}_{i+1,j}+\frac{h_1}{C_{1111}}(C_{1122}\frac{\varepsilon^{22}_{i+1,j}-\varepsilon^{22}_{i-1,j}}{2h_1}+C_{1212}\frac{\varepsilon^{12}_{i,j+1}-\varepsilon^{12}_{i,j-1}}{2h_2}),$$
$$\varepsilon^{22}_{ij}=\varepsilon^{22}_{i,j+1}+\frac{h_2}{C_{2222}}(C_{2211}\frac{\varepsilon^{11}_{i,j+1}-\varepsilon^{11}_{i,j-1}}{2h_2}+C_{2121}\frac{\varepsilon^{12}_{i+1,j}-\varepsilon^{12}_{i-1,j}}{2h_1}),$$
$$\varepsilon^{12}_{ij}=(\frac{C_{1111}+C_{1122}}{2C_{1212}}\frac{\varepsilon^{11}_{i+1,j+1}-\varepsilon^{11}_{i+1,j-1}-\varepsilon^{11}_{i-1,j+1}+\varepsilon^{11}_{i+1,j+1}}{4h_1h_2}+\frac{\varepsilon^{12}_{i+1,j}+\varepsilon^{12}_{i-1,j}}{h_1^2}+$$
$$+\frac{\varepsilon^{12}_{i,j+1}+\varepsilon^{12}_{i,j-1}}{h_2^2}+\frac{C_{2222}+C_{2211}}{2C_{2121}}\frac{\varepsilon^{22}_{i+1,j+1}-\varepsilon^{22}_{i+1,j-1}-\varepsilon^{22}_{i-1,j+1}+\varepsilon^{22}_{i+1,j+1}}{4h_1h_2})/(\frac{2(h_1^2+h_2^2)}{h_1^2h_2^2}). \tag{27}$$

For to ensure the symmetricity of finite-difference equations, we consider two variants of difference equations for equation $(17)_1$, using the right and left relations for derivatives of the first term, respectively, i.e.

$$C_{1111}\frac{\varepsilon^{11}_{i+1,j}-\varepsilon^{11}_{ij}}{2h_1}+C_{1122}\frac{\varepsilon^{22}_{i+1,j}-\varepsilon^{22}_{i-1,j}}{2h_1}+2C_{1212}\frac{\varepsilon^{12}_{i,j+1}-\varepsilon^{12}_{i,j-1}}{2h_2}=0,$$
$$C_{1111}\frac{\varepsilon^{11}_{ij}-\varepsilon^{11}_{i-1,j}}{2h_1}+C_{1122}\frac{\varepsilon^{22}_{i+1,j}-\varepsilon^{22}_{i-1,j}}{2h_1}+2C_{1212}\frac{\varepsilon^{12}_{i,j+1}-\varepsilon^{12}_{i,j-1}}{2h_2}=0. \tag{28}$$

Subtracting the second equation from the first, we can find that [7, 20]

$$\varepsilon^{11}_{i,j}=\frac{\varepsilon^{11}_{i+1,j}+\varepsilon^{11}_{i-1,j}}{2}. \tag{29}$$

Similarly, from equation $(17)_2$ for ε^{22}_{ij} we obtain

$$\varepsilon^{22}_{i,j}=\frac{\varepsilon^{22}_{i,j+1}+\varepsilon^{22}_{i-1,j}}{2}. \tag{30}$$

Then, equations (29, 30) can be considered instead of $(27)_{1,2}$.

In order to increase the order of approximation, we differentiate the equilibrium equations (17-18) with respect to x and y, respectively. Then, the finite-difference analogue of the boundary value problem has the form

$$C_{1111}\frac{\varepsilon^{11}_{i+1,j}-2\varepsilon^{11}_{i,j}+\varepsilon^{11}_{i-1,j}}{h_1^2}+C_{1122}\frac{\varepsilon^{22}_{i+1,j}-2\varepsilon^{22}_{i,j}+\varepsilon^{22}_{i-1,j}}{h_1^2}+C_{1212}\frac{\varepsilon^{12}_{i+1,j+1}-\varepsilon^{12}_{i-1,j+1}-\varepsilon^{12}_{i+1,j-1}+\varepsilon^{12}_{i-1,j-1}}{2h_1h_2}=0,$$
$$C_{2222}\frac{\varepsilon^{22}_{i,j+1}-2\varepsilon^{22}_{i,j}+\varepsilon^{22}_{i,j-1}}{h_2^2}+C_{2211}\frac{\varepsilon^{11}_{i,j+1}-2\varepsilon^{11}_{i,j}+\varepsilon^{11}_{i,j-1}}{h_2^2}+C_{2121}\frac{\varepsilon^{12}_{i+1,j+1}-\varepsilon^{12}_{i-1,j+1}-\varepsilon^{12}_{i+1,j-1}+\varepsilon^{12}_{i-1,j-1}}{2h_1h_2}=0,$$
$$2C_{1212}\frac{\varepsilon^{12}_{i+1,j}-2\varepsilon^{12}_{i,j}+\varepsilon^{12}_{i-1,j}}{h_1^2}+\left(C_{1111}+C_{1122}\right)\frac{\varepsilon^{11}_{i+1,j+1}-\varepsilon^{11}_{i+1,j-1}-\varepsilon^{11}_{i-1,j+1}+\varepsilon^{11}_{i+1,j+1}}{4h_1h_2}+$$
$$+2C_{1212}\frac{\varepsilon^{12}_{i,j+1}-2\varepsilon^{12}_{i,j}+\varepsilon^{12}_{i,j-1}}{h_2^2}+\left(C_{2222}+C_{2211}\right)\frac{\varepsilon^{22}_{i+1,j+1}-\varepsilon^{22}_{i+1,j-1}-\varepsilon^{22}_{i-1,j+1}+\varepsilon^{22}_{i+1,j+1}}{4h_1h_2}=0. \tag{31}$$

It is easy to see that finite-difference equations (27) can be solved by the iterative method with respect to $\varepsilon^{11}_{i,j}$, $\varepsilon^{22}_{i,j}$ and $\varepsilon^{12}_{i,j}$

$$\varepsilon^{k+1}_{11i,j}=\varepsilon^{k}_{11i+1,j}+\frac{h_1}{C_{1111}}(C_{1122}\frac{\varepsilon^{k}_{22i+1,j}-\varepsilon^{k}_{22i-1,j}}{2h_1}+C_{1212}\frac{\varepsilon^{k}_{12i,j+1}-\varepsilon^{k}_{12i,j-1}}{2h_2}),$$
$$\varepsilon^{k+1}_{22i,j}=\varepsilon^{k}_{22i,j+1}+\frac{h_2}{C_{2222}}(C_{2211}\frac{\varepsilon^{k}_{11i,j+1}-\varepsilon^{k}_{11i,j-1}}{h_2^2}+C_{2121}\frac{\varepsilon^{k}_{12i+1,j}-\varepsilon^{k}_{12i-1,j}}{2h_1}),$$
$$\varepsilon^{k+1}_{12i,j}=(\frac{C_{1111}+C_{1122}}{2C_{1212}}\frac{\varepsilon^{k}_{11i+1,j+1}-\varepsilon^{k}_{11i+1,j-1}-\varepsilon^{k}_{11i-1,j+1}+\varepsilon^{k}_{11i+1,j+1}}{4h_1h_2}+\frac{\varepsilon^{k}_{12i+1,j}+\varepsilon^{k}_{12i-1,j}}{h_1^2}+$$
$$+\frac{\varepsilon^{k}_{12i,j+1}+\varepsilon^{k}_{12i,j-1}}{h_2^2}+\frac{C_{2222}+C_{2211}}{2C_{2121}}\frac{\varepsilon^{k}_{22i+1,j+1}-\varepsilon^{k}_{22i+1,j-1}-\varepsilon^{k}_{22i-1,j+1}+\varepsilon^{k}_{22i+1,j+1}}{4h_1h_2})/(\frac{2(h_1^2+h_2^2)}{h_1^2h_2^2}). \tag{32}$$

where $k-$ iteration number.

Boundary and additional boundary conditions regarding nodal points have the form:

$$\varepsilon^{(0)}_{11\ 0j}=\frac{1-\nu_{12}\nu_{21}}{E_1}\sigma_{11},\ \varepsilon^{(0)}_{21\ 0j}=0,\ \varepsilon^{(0)}_{22\ i0}=0,\ \varepsilon^{(0)}_{12\ i0}=0,$$
$$\varepsilon^{(0)}_{11\ N_1j}=\frac{1-\nu_{12}\nu_{21}}{E_1}\sigma_{11},\ \varepsilon^{(0)}_{21\ N_1j}=0,\ \varepsilon^{(0)}_{22\ iN_2}=0,\ \varepsilon^{(0)}_{12\ iN_2}=0, \tag{33}$$

for $y=0$ and $y=l_2$

$$\varepsilon_{11}^{(0)}{}_{i0} = \varepsilon_{11}^{(0)}{}_{i1} + \frac{C_{1212}h_2}{C_{1122}} \frac{\varepsilon_{12}^{(0)}{}_{i+1,0} - \varepsilon_{12}^{(0)}{}_{i-1,0}}{h_1},$$
$$\varepsilon_{11}^{(0)}{}_{iN_2} = \varepsilon_{11}^{(0)}{}_{i,N_2-1} - \frac{C_{1212}h_2}{C_{1122}} \frac{\varepsilon_{12}^{(0)}{}_{i+1,N_2} - \varepsilon_{12}^{(0)}{}_{i-1,N_2}}{h_1}, \tag{34}$$

for $x=0$ and $x=l_1$

$$\varepsilon_{22}^{(0)}{}_{0,j} = \varepsilon_{22}^{(0)}{}_{1,j} + \frac{C_{1212}h_1}{C_{1122}} \frac{\varepsilon_{0,j+1}^{12} - \varepsilon_{0,j-1}^{12}}{h_2},$$
$$\varepsilon_{22}^{(0)}{}_{N_1,j} = \varepsilon_{22}^{(0)}{}_{N_1-1,j} - \frac{C_{1212}h_1}{C_{1122}} \frac{\varepsilon_{12}^{(0)}{}_{N_1,j+1} - \varepsilon_{12}^{(0)}{}_{N_1,j-1}}{h_2}. \tag{35}$$

Note that finite-difference equations (31) can be solved by the elimination method within the framework of the alternating direction method [3, 18, 19].

6. Numerical examples

This section is devoted to substantiating the validity of the formulated boundary value problem in strains for orthotropic bodies. For this purpose, the tension problem for a rectangular plate is considered and solved numerically by two numerical methods under different boundary conditions.

Let a rectangular plate of size *(2a,2b)* be under the action of a uniaxial load of parabolic shape applied on opposite sides perpendicular to the *OX* axis. The remaining sides are free from loads, i.e.

$$\text{for } x = \pm a: \ \sigma_{11} = S_0(1 - \frac{y^2}{a^2}), \quad \sigma_{12} = 0, \tag{36}$$

$$\text{for } y = \pm b: \ \sigma_{22} = 0, \quad \sigma_{12} = 0. \tag{37}$$

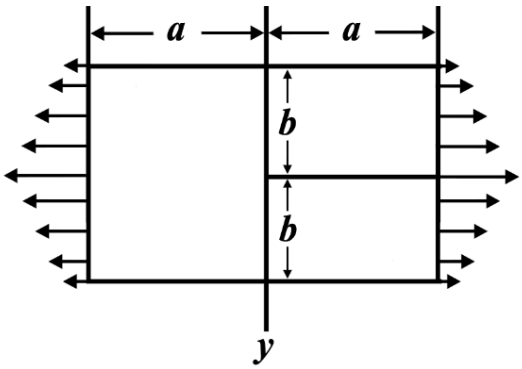

Figure 1. - **Tension of the rectangular plate under parabolic load**

This problem was considered by Timoshenko-Goodier for an isotropic plate [11]. We will consider this problem for orthotropic bodies under various boundary conditions.
The initial data for the orthotropic body had the following dimensionless values:

$$E_1 = 10, \quad E_2 = 5, \quad \nu_{12} = 0.438, \quad \nu_{21} = \frac{E_2\nu_{12}}{E_1}, N_1 = N_2 = 10, \quad a = 1, \quad b = 1, \quad h = 0.2, \quad S_0 = 1. \tag{38}$$

Note that according to [12,14], the shear modulus has the form

$$G_{12} = \frac{E_1E_2}{E_1 + E_2(1 + 2\nu_{12})}.$$

Table 1 compares the of stress values σ_{11} in the middle of a rectangular plate under the action of a tensile parabolic load applied on opposite sides perpendicular to the *OX* axis. Equations (27) were solved using the iteration method, taking into account (29,30). The third line shows solutions corresponding to finite-difference equations (31) using the alternative method. The first row of the table shows the results of Timoshenko-Goodier [11] for isotropic bodies. It should be noted that the results obtained by the alternative variable method are more accurate.

Table 1.

Stress values σ_{11} in the middle of the plate under parabolic load

Solution methods for y=0:	*x=0.0*	*x=0.2*	*x=0.4*	*x=0.6*	*x=0.8*	*x=1*
Timoshenko-Goodier method	1.00	0.97	0.93	0.87	0.84	0.82
Iteration Method	1.00	1.00	0.93	0.85	0.82	0.79
Alternative variable method (along axes)	1.00	1.00	1.00	1.00	1.00	1.00

Let a rectangular plate of size (*a*, *b*) be located in the first quarter of the coordinate system, and be compressed by a uniformly distributed load $S=1$ in the direction of the *OX* axis, i.e.

$$\text{for } x=0,l_1: \ \sigma_{11}=S_0, \quad \sigma_{12}=0, \tag{39}$$

$$\text{for } y=0,l_2: \ \sigma_{22}=0, \quad \sigma_{21}=0. \tag{40}$$

In this case, the initial data had the following values:

$$E=10,\ E_2=5,\ \nu_{12}=0.438,\ N_1=N_2=10,\ l_1=1,\ l_2=1,\ h=0.1. \tag{41}$$

The stress and strain values obtained using the iteration method and the alternative variable method are given in Tables 2 and 3, respectively.

Table 2.

Stress values σ_{11} in the middle of the plate under uniform load

Solution methods for y=0.5:	*x=0*	*x=0.1*	*x=0.2*	*x=0.3*	*x=0.4*	*x=0.5*
Iteration Method	1.000	1.012	0.913	0.884	0.847	0.816
Alternative variable method (along axes)	1.000	1.000	1.000	1.000	1.000	1.000

Table 3.

Strain values ε_{11} in the middle of the plate under uniform load

Solution methods for y=0.5:	*x=0*	*x=0.1*	*x=0.2*	*x=0.3*	*x=0.4*	*x=0.5*
Iteration Method	0.100	0.091	0.083	0.076	0.074	0.071
Alternative variable method (along axes)	0.100	0.100	0.100	0.100	0.100	0.100

Let us consider a tension problem for an orthotropic rectangular plate along the *OX* axis by a sine-shaped load

$$\text{for } x=0,l_1: \ \sigma_{11}=\sin\left(\frac{y\pi}{l_2}\right), \quad \sigma_{12}=0, \tag{42}$$

$$\text{for } y=0,l_2: \ \sigma_{22}=0, \quad \sigma_{21}=0. \tag{43}$$

The initial data is the same as in the previous problem. Table 4 shows the stress values σ_{11} in the middle of the rectangular plate obtained by the iteration method and the alternative variable method.

Table 4.

Stress values σ_{11} in the middle of the plate at (41-42)

Solution methods for y=0.5:	*x=0*	*x=0.1*	*x=0.2*	*x=0.3*	*x=0.4*	*x=0.5*
Iteration Method	*1.000*	*1.000*	*1.000*	*1.000*	*1.000*	*1.000*
Alternative variable method (along axes)	*1.000*	*1.000*	*1.000*	*1.000*	*1.000*	*1.000*

Table 5.

Strain values ε_{11} in the middle of the plate at (41-42)

Solution methods for y=0.5:	*x=0*	*x=0.1*	*x=0.2*	*x=0.3*	*x=0.4*	*x=0.5*
Iteration Method	*0.100*	*0.100*	*0.100*	*0.100*	*0.100*	*0.100*
Alternative variable method (along axes)	*0.090*	*0.090*	*0.090*	*0.090*	*0.090*	*0.090*

Table 5 compares the values of deformations ε_{11} in the middle of a rectangular plate obtained by the iteration method and the elimination method.

7. Conclusion

In the work, within the framework of the Saint-Venant compatibility condition, differential equations in strains for orthotropic bodies are proposed and in a particular case from which, the

well-known differential compatibility equations for isotropic bodies follow. A plane boundary value problem in strains for orthotropic bodies is formulated. The grid equations are compiled be finite-difference method and solved using the iterative method and the alternative variable method. The validity of the modeling equations and the reliability of numerical models are justified by comparing the results of the plate tension problem by various numerical methods and boundary conditions.

References

1. *V. Novatsky /* The Theory of Elasticity, «Mir», M., 1975. 872 p.

2. *M. Filonenko-Borodich.* Theory of Elasticity. University Press of the Pacific. (November 6, 2003), 396 p.

3. *Konovalov, A.N.* Solving problems of elasticity theory under stress. Novosibirsk: NSU, 1979. - 92 p.

4. *B.E. Pobedrya.* On Static Problem in terms of Stresses. Moscow Univ. Mech. Bull. 58 (3), 8-14 (2003).

5. *N.M. Borodachev.* Stress Solutions to the Three-Dimensional Problem of Elasticity. Intern. Appl. Mech. 42 (8), 849-878 (2006).

6. *B.E. Pobedrya.* Numerical Methods in the Theory of Elasticity and Plasticity. -M.: Moscow State University, 1996.-343 p.

7. *Khaldjigitov A.A., Djumayozov U.Z.* Numerical solution of the problem of the theory of elasticity in deformations // Problems of Mechanics No. 3, 2022, pp.56-65.

8. *Khaldjigitov A.A., Djumayozov U.Z.* Model Equations of the Theory of Elasticity in Strains: Classical and New Formulations. E3S Web of Conferences 497, 02015 (2024), https://doi.org/10.1051/e3sconf/202449702015

9. Khaldjigitov Abduvali, Djumayozov Umidjon, *Numerical Solution of the Two-Dimensional Elasticity Problem in Strains. Mathematics and Statistics, Vol. 10, No. 5, pp. 1081 - 1088, 2022. DOI: 10.13189/ms.2022.100518*

10. *Turimov, D.; Khaldjigitov, A.; Djumayozov, U.; Kim, W.* Formulation and Numerical Solution of Plane Problems of the Theory of Elasticity in Strains. Mathematics, 2024, 12, 71. https://doi.org/10.3390/ math12010071

11. *Khaldjigitov A.A., Tilovov O.U.* Numerical solution of the problem of the theory of elasticity in stressess. Problems Mechanics No. 2, 2022, 12-19

12. *S. Timoshenko and J.N. Goodier.* Theory of Elasticity. McGraw-Hill, Boston, 1970.

13. *M. A. Rebello, P. S. B. Zdanski, M. Vaz Jr.* Considerations on alternative solutions for stress analysis of anisotropic materials: a beam case study. Continuum Mech. Thermodyn. (2021) 33:2123–2140 https://doi.org/10.1007/s00161-021-01012-4

14. *Samarski A.A., Nikolaev E.S.* Methods for Solving Grid Equations. – Moscow: «Science», 1978, 592 p.

15. *Lekhnitskii, S.G.* Theory of Elasticity of an Anisotropic Elastic Body. Holden-Day, San Francisco (1963)

16. *Ubaydullaev, M.; Eshpulatov, B.* Inter-zone light absorption in a size quantized wire. In Proceedings of the 2021 International Conference on Information Science and Communications Technologies (ICISCT), Tashkent, Uzbekistan, 3–5 November 2021, pp. 1–5.

17. *Eshpulatov, B., Ubaydullaev, M.* Binding energy of a one-dimensional exciton in a magnetic field. International Conference on Information Science and Communications Technologies (ICISCT), 2020, 9351377.

18. *Ravshanov N., Narzullayeva N., Muradov F.* International Conference on Information Science and Communications Technologies: Applications, Trends and Opportunitles, ICISCT, 2021.

19. *M. Umarov, F. Muradov and T. Azamov*, "Traffic Sign Recognition Method Based on Simplified Gabor Wavelets and CNNs," 2021 International Conference on Information Science and Communications Technologies (ICISCT), Tashkent, Uzbekistan, 2021, pp. 1-5, doi: 10.1109/ICISCT52966.2021.9670118.

20. *F. Muradov and N. Tashtemirova*, "Numerical Algorithm for Calculation the Density of Harmful Substances in the Atmosphere," 2021 International Conference on Information Science and Communications Technologies (ICISCT), Tashkent, Uzbekistan, 2021, pp. 01-03, doi: 10.1109/ICISCT52966.2021.9670278.

NATURAL VIBRATIONS OF SMOKESTACKS OF THERMAL POWER PLANTS

Khudainazarov Sh.[1], Salimov Sh.[2]
[1]*Tashkent Institute of Irrigation and Agricultural Mechanization Engineers"*
National Research University, Tashkent, Uzbekistan
[2]*Tashkent university for applied sciences, Tashkent, Uzbekistan*
E-mail: scherzodshox77@mail.ru.

Abstract*. Natural vibrations of tall smokestacks of thermal power plants are examined in the article. Scientific research is developing in two directions: using methods, algorithms, and programs built by the authors, and using the ANSYS software package. The modes of natural vibrations of tall smokestacks of thermal power plants are constructed. The amplitude-frequency response of natural vibrations of smokestacks is determined. The results obtained are compared with the results of theoretical and experimental studies by well-known authors. The reliability of the results obtained was verified by comparing them with the exact solutions of a number of test problems.*

Keywords*: thermal power plant, smokestack, natural vibrations, natural frequency, amplitude of vibrations, principle of virtual displacements, amplitude-frequency response, ANSYS software package.*

1. Introduction.

Energy provides opportunities for economic development, comfortable living for people, and the creation of conditions for the normal functioning of such important social spheres as education, medical care, social security, and utilities. The energy sector cannot operate without thermal power plants (TPPs), because thermal power plants generate 85.1% of electricity in Uzbekistan. The energy base of the republic consists of 42 power plants with a total installed capacity of more than 12.0 million kW, including 10 thermal power plants with a capacity of 10.6 million kW (85.1%) and 29 hydraulic power plants with a capacity of 1.4 million kW (11 .4%), other stations generate 480 million kW (3.5%). The largest thermal power plants in Uzbekistan have the following installed capacity: Syrdarya Thermal Power Plant - 3000 MW, Novo-Angren Thermal Power Plant - 2100 MW, Tashkent Thermal Power Plant - 1860 MW, Navoi Thermal Power Plant - 1250 MW, and Talimarjan Thermal Power Plant - 800 MW.

Smokestacks of thermal power plants are unique, high-rise structures designed to remove and release combustion product residues from hot water and steam boilers into the atmosphere (Table 1).

There are three types of smokestacks for thermal power plants:

1. Single-pipe type without gas outlet shafts;
2. Single-pipe type with a separate gas outlet shaft;
3. Multi-pipe type.

Smokestacks of thermal power plants operate in difficult conditions, combining changes in temperature, pressure, humidity, aggressive chemical effects of flue gases, wind loads, and loads from their weight.

As the capacity of units and power plants increases, the height of smokestacks increases due to the requirements of permissible air pollution. At modern thermal power plants, the height of the smokestacks reaches 330–420 m and is taken from the unification conditions as a multiple of 30 m. The shell of a reinforced concrete monolithic stack is designed as a truncated cone, cylinder, or a combination of both. The ratio of the height of the shell or its section to the lower diameter of the section should be no more than 20. The slope of the generatrix of the outer surface should be taken no more than 0.1. The minimum thickness of the shell walls is 180-200 mm. The foundation for the smokestack consists of a solid round or annular plate, going into a conical cup.

Smokestacks of thermal power plants are complex engineering structures; therefore, their design, construction, and operation require a comprehensive solution to numerous technical problems.

When calculating smokestacks, in addition to strength and stability, a calculation of dynamic characteristics is required; it determines the eigenmodes and eigenfrequiencies of structure vibrations and compares them with the frequencies of excitation loads. Studies of the basic dynamic characteristics of smokestacks occupy a special place in the dynamics of structures. The eigenfrequency, modes of vibrations, and decrements of vibrations are the passport of a structure

and allow us to examine the dynamic properties of the structure as a whole, without studying its behavior under various impacts. Determining eigenfrequencies and modes of vibrations even for a simple structure is a difficult task. A review of well-known publications shows that the assessment of the dynamic characteristics of various structures in different articles is performed in different ways, and each theory or method used has its advantages and shortcomings.

Table 1

The unique smokestacks of thermal power plants worldwide

№	Name	Pinnacle height		Year	Country	Town
1.	Chimney of GRES-2 Power Station	1.377 ft	419.7 m	1987	Kazakhstan	Ekibastuz
2.	Inco Superstack	1.250 ft	380.1 m	1971	Canada	Sudbury, Ontario
3.	Original Unit 3 chimney of Homer City Generating Station	1.217 ft	371 m	1977	United States	Homer City, Pennsylvania
4.	Kennecott Smokestack	1.215 ft	370.4 m	1974	United States	Magna, Utah
5.	Chimney of Berezovskaya GRES	1.214 ft	370 m	1985	Russia	Sharypovo
6.	Original chimney of Mitchell Power Plant	1.20 ft	367.6 m	1968	United States	Moundsville, West Virginia
7.	Trbovlje Chimney	1.181 ft	360 m	1976	Slovenia	Trbovlje
8.	Chimney of Endesa Power Station	1.168 ft	356 m	1974	Spain	As Pontes, Galicia
9.	Chimney of Phoenix Copper Smelter	1.153 ft	351.5 m	1995	Romania	Baia Mare
10.	3rd chimney of Syrdarya Power Plant	1.148 ft	350 m	1980	Uzbekistan	Shirin

In [1], the authors of the article proposed an original analytical formulation for estimating eigenfrequencies and mode shapes of high-rise buildings. The methodology is intended for engineers to be used in the preliminary design stages as it allows the dynamic performance of high-rise buildings consisting of closed or open retractable walls, frames, frame tubes, and diametrical grid systems to be assessed. The potential of the proposed method is confirmed by a numerical example demonstrating the advantages of this procedure.

The study in [2] investigated the probabilistic analysis of the seismic characteristics of high-rise reinforced concrete buildings using the brittleness assessment method. Three reinforced concrete buildings were designed having the same plan dimensions and height but differing in structural configurations; their seismic characteristics were compared. The brittleness assessment results showed that, in general, retractable walls improve the seismic performance of buildings. However, the configuration of retractable walls also affects seismic performance, which requires further study.

In [3], different configurations of buildings and architectural modifications to the design of tall structures were investigated to reduce vibrations. The results obtained were analyzed and the design parameters of high-rise structures were determined. The results obtained were interpreted for buildings of different configurations, which allowed determining the form of a high-rise building that is the most stable under various dynamic and seismic loads.

The seismic design procedure for a ten-story building with a self-centering wall was comprehensively reviewed in [4] using state-of-the-art design and structural detailing techniques, additional recommendations were put forward. The demonstration project promotes the concept of earthquake-resistant structures and contributes to the most attractive urban planning strategy for sustainable cities. The document can serve as reference material for construction engineers to promote self-centering wall systems worldwide.

In [5-6], the natural frequencies of a cylindrical shell were determined. The influence of variations in shell thickness and boundary conditions on natural oscillations was studied.

The study in [7] is devoted to numerical simulation and field measurements of the dynamic characteristics of a 508 m high skyscraper to confirm the noise stability and accuracy of the combined scheme for estimating the time-varying eigenfrequencies of the structure. The developed

combined scheme is further used to study the time-varying characteristics of the natural frequencies of a skyscraper under the impacts of typhoons and earthquakes. An effective tool is provided to estimate the time-varying eigenfrequencies of tall buildings under strong dynamic impacts.

Articles [8-10] proposed a procedure based on the popular Galerkin method for solving nonlinear oscillations; the nonlinear equation is solved approximately over the fundamental period of oscillation by adding integration with a weighting function and harmonic time terms. Solving a nonlinear eigenvalue problem, the mode shapes of the natural frequency are determined. The procedure can also be applied to linear vibration equations to obtain results identical to the Galerkin method.

Reference [11] presents several methods of dynamic analysis for studying mode shapes and natural frequencies in a car chassis structure. The studies used the finite element method with the *ANSYS v13 APDL Mechanical* software package. A graph of amplitude versus frequency was plotted from harmonic analysis and used to determine the resonant frequency. The highest amplitude was observed at the third natural frequency for the amplitude of 0.375 mm. The results of this analysis can be used as a guide to improve the chassis design and performance, taking into account the dynamic behavior of the structure by introducing a stiffener in the part of the chassis with the largest displacement.

Articles [12, 13] present the dynamic analysis of a cantilever beam subjected to impact loading with and without the mass of the tip (head). The cantilever beam is made by placing a layer of viscoelastic material between the main structure and the piezoelectric layer. The viscoelastic layer contributes to passive damping, while the piezoelectric layer contributes to active damping. Euler-Bernoulli beam theory is used with Hamilton's principle to derive the governing equations of system motion and boundary conditions. The solution to the system is obtained by using the finite element method and the Newmark time integration scheme. The natural frequencies of the system and the displacement of the tip are determined using the finite element method. Parametric studies were performed to determine the influence of some potential design variables on the oscillatory behavior of the system.

In [14-20], the dynamic behavior of high-rise structures was studied within the framework of a one-dimensional model, considering the elastic, viscoelastic, and nonlinear deformation of the material. Problems were solved using the finite element method and the Newmark method. The influence of the nature of the kinematic action and the choice of various laws of material deformation on the dynamic response of the structure was studied.

In [21-24], various engineering structures were studied to determine natural frequencies and vibration modes using the *ANSYS* software package. The vibration modes and graphs of the amplitude-frequency response of structures were constructed. The results obtained were compared with theoretical and experimental studies by known authors.

For the rational design of smokestacks of thermal power plants, it is necessary to conduct theoretical, experimental and numerical studies under static and dynamic influences. Conducting such extensive research allows us to understand a qualitative pattern of the influence of various parameters in a wide range of studies and make grounded recommendations not only at the design stage but also during the operation of various high-rise structures.

Therefore, the development of a mathematical model, an effective methodology and an algorithm for determining the dynamic characteristics of smokestacks, considering the physical and mechanical properties of the material, and the structural and real geometric dimensions of the structure, is an urgent problem in mechanics.

2. Research methods

The purpose of this work is to study the natural vibrations of smokestacks of thermal power plants, considering the physical and mechanical properties of the material, design, and actual geometric dimensions of the smokestacks.

To achieve this goal, the following research was conducted:

1. Familiarization with methods for studying the spectrum of natural frequencies and vibration modes and their features for high-rise buildings;

2. Construction of natural vibration modes and comparison with the experimental and theoretical results obtained by other well-known authors;

3. Determination of natural frequencies of oscillations and comparison with the experimental and theoretical results obtained by other well-known authors;

4. Constructing amplitude-frequency diagrams and comparing them with experimental and theoretical results obtained by other well-known authors;

5. Conducting an analysis of the influence of the physical and mechanical properties of the material, the design, and actual geometric dimensions of the smokestacks of thermal power plants on the natural frequencies of vibration of the shell;

6. Development of recommendations for planned measures to mitigate the risk of developing dangerous vibrations

3. Research method No.1.

The natural frequencies and vibration modes of high-rise smokestacks of the Talimarjan, Syrdarya, and Novo-Angren thermal power plants are studied according to the elastic beam theory using the developed methodology and calculation programs focused on PC-IBM.

The smokestack is modeled by a beam of variable cross-section with a variable slope of the generatrices, the lower part of the structure ($z = 0$) is on a rigid foundation, and the upper part ($z = L$) is free. In the sections of the structure, a longitudinal force acts, which is the weight of the upper part of the structure. The slopes of various sections of the internal and external surfaces of the structure are variable. Figure 1 shows calculation models of smokestacks of thermal power plants.

The following parameters of the physical and mechanical characteristics of the materials of the considered smokestack structures were taken in theoretical and numerical calculations:

$$E=2{,}9\times10^4 MPa;\ \nu=0{,}17;\ \rho=2{,}5\ t/m^3;\ \Gamma^s=0;\ \Gamma^c=0$$

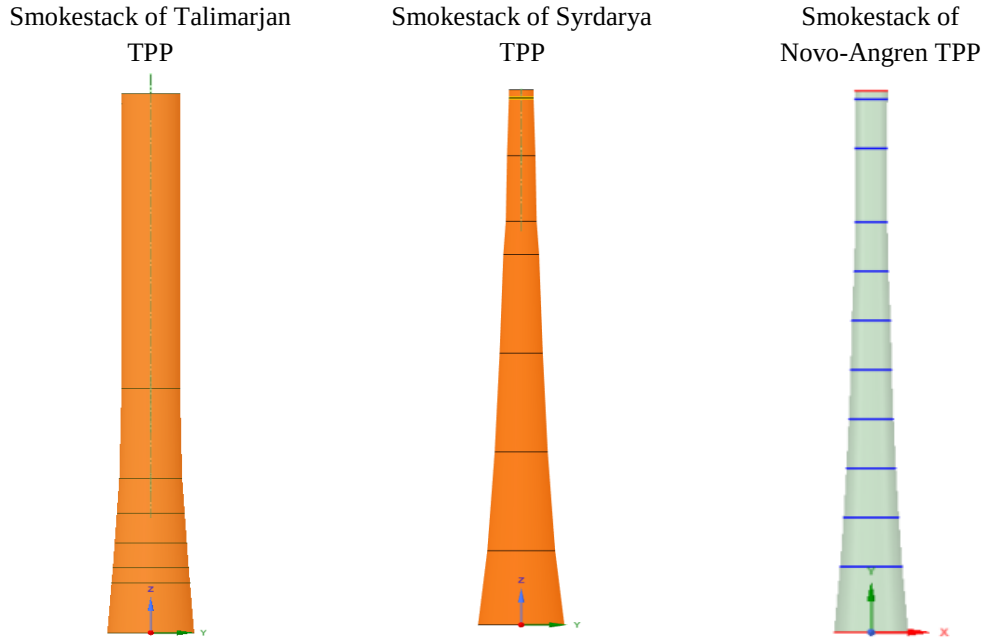

Figure 1. **Calculation models of smokestacks of thermal power plants**

Table 2 shows the geometric dimensions of the smokestacks of the Talimarjan, Syrdarya, and Novo-Angren thermal power plants in their sections.

Using for these structures the methods developed in [14-15] and calculation programs focused on PC-IBM, the authors determined the values of the five lowest frequencies and the corresponding natural vibration modes.

Table 2

Geometric dimensions of smokestacks

Talimarzhan TPP			Syrdarya TPP			Novo-Angren TPP		
z (m)	R^H(m)	h(m)	z (m)	R^H(m)	h(m)	z (m)	R^H(m)	h(m)
0.0	18.00	0.90	0.0	21.00	0.85	0.0	19.00	1.10
25.0	16.25	0.90	45.0	16.50	0.75	40.0	15.90	0.90
32.5	15.725	0.70	65.0	15.30	0.70	70.0	14.15	0.75
45.0	14.975	0.65	105.0	12.90	0.57	100.0	12.65	0.65
60.0	14.075	0.60	125.0	12.10	0.53	130.0	11.40	0.55
77.5	13.025	0.55	165.0	10.50	0.45	160.0	10.50	0.45
90.0	12.775	0.50	205.0	9.30	0.30	190.0	10.00	0.38
105.0	12.475	0.45	225.0	8.70	0.25	220.0	8.70	0.34
122.5	12.125	0.40	245.0	7.50	0.25	250.0	8.25	0.30
135.0	12.125	0.36	285.0	6.90	0.22	295.0	8.25	0.30
150.0	12.125	0.33	320.0	6.00	0.22	325.0	8.35	0.40
167.5	12.125	0.30	325.0	6.00	0.22	330.0	8.35	0.40
251.5	12.125	0.30	-	-	-	-	-	-
265.0	12.125	0.60	-	-	-	-	-	-

4. Research method No. 2.

The natural vibrations of the smokestacks of the Talimarjan, Syrdarya, and Novo-Angren thermal power plants were studied using the *ANSYS* software package. The natural frequencies and vibration modes were determined and the influence of the physical and mechanical properties of the material, and structural and actual geometric dimensions of the smokestack on the natural frequencies of vibration of the smokestack was analyzed.

The *ANSYS* multidisciplinary engineering software includes a set of highly accurate analysis tools that predict product behavior under real-world conditions. These tools combine the open, adaptive architecture of the *ANSYS Workbench* platform and flexible modeling methods with a comprehensive set of solvers for all areas of science: mechanics of deformable rigid body, heat transfer, fluid and gas flow, and electromagnetism. Combining these advanced technologies, we create the foundation for performing interdisciplinary calculations and solving complex engineering problems.

In general, the *ANSYS Workbench* interface includes the following windows:

1. *Project Schematic* – is the main window of the project. The window displays the project diagram (modules and applications of the project); it allows managing project settings and options;

2. *Properties* –is the window of object properties. It is a tabular representation of the properties of the selected object.

3. *Toolbox* –is the window of project tools. It displays integrated modules and applications of the program block. The block includes the following sections:

a) *Analysis Systems.* Contains solvers for all types of numerical (engineering) analysis.

b) *Component Systems*. Includes auxiliary modules for numerical analysis: geometric model, finite element mesh, etc.

c) *Custom Systems*. Contains templates for interdisciplinary analysis.

d) *Design Exploration.* Solves problems of optimization of model parameters;

4. *Window of stage modeling*. Represents the structure of numerical analysis. A project may include several such interconnected windows;

5. *Messages* – message window. Displays all types of service messages and errors.

The study was conducted using the ***ANSYS 2023R*** software package in the following order:

1. Open the ***ANSYS Workbench*** interface.
2. Select the type of software module ***Static Structural***;
3. Using the ***Engineering Data*** block, input the quantities that reflect the physical and mechanical properties of the structural material.
4. Using the ***Geometry*** block, develop three-dimensional 3-D models of the design drawing in accordance with the real geometric dimensions.
5. Select the type of software module ***Modal***;

6. Combine these two modules ***Static Structural*** and ***Modal***. In this case, data about the design project created and its material is displayed in the ***Modal*** module.
7. Using the ***Mesh*** block, select the number and structure of the mesh of finite elements;
8. Using the ***Setup*** block, transfer the geometric model covered with a finite element mesh into a separate module and set the boundary conditions for the smokestack structure;
9. Using the ***Solution*** block, start programs for the calculation;
10. Using the ***Results*** block, perform the processes of comparison and analysis of the results obtained.

Using the *ANSYS 2023R* software package, a design diagram was constructed for each smokestack based on the data presented in Table 1. The characteristics of the stack material were fed into the program and step-by-step calculations were performed.

5. Results and discussion.

In studies conducted by known scientists [25-28], it was determined that the predominant periods of strong ground motion during severe earthquakes were in the range of 0.1-0.5 seconds. Therefore, generally, in dynamic calculations of structures for seismic impacts, several lower frequencies and modes of natural vibration of structures located in the frequency spectrum of 2 - 10 Hz, corresponding to the specified interval, were used.

Table 2 shows the natural frequencies of bending vibrations of some tall smokestacks of thermal power plants obtained using the developed methodology.

Table 3 shows the natural frequencies obtained using the *ANSYS* software package for three tall smokestacks of thermal power plants in Uzbekistan.

Table 2

Natural frequencies of bending vibrations of smokestacks of thermal power plants, (Hz)

No.	Novo-Angren TPP	Syrdarya TPP	Azerbaijan TPP	Ekibastuz TPP
ω_1	0.3065	0.4011	0.2665	0.1840
ω_2	1.0978	1.2488	1.0030	0.6401
ω_3	2.5996	2.9847	2.3482	1.5006
ω_4	4.8791	5.2745	4.3813	2.7639
ω_5	7.8481	8.1401	7.0768	4.4492

Table 3

Values of natural frequencies of smokestacks of thermal power plants in Uzbekistan, (Hz)

No.	No. of natural frequency	Talimarjan TPP	Syrdarya TPP	Novo-Angren TPP
1.	ω_1	0.3798	0.3771	0.3008
2.	ω_2	0.9088	1.1054	1.0739
3.	ω_3	1.1708	1.6977	2.3988
4.	ω_4	1.7003	1.8351	2.5994
5.	ω_5	1.7311	2.1998	3.1356
6.	ω_6	2.5221	2.3948	3.5708
7.	ω_7	2.6302	2.5185	3.9049
8.	ω_8	2.6981	3.0073	4.1944
9.	ω_9	2.9897	3.7310	4.5381
10.	ω_{10}	2.9961	3.8525	4.5861

If we compare the values in Table 2 with the ones given in Table 3, we can see that the lowest numerical values of the vibration frequencies are close to each other; the differences increase as the vibration frequencies increase. The most significant natural frequencies in terms of seismic hazard were identified; the range of predominant seismic frequencies (2 - 10 Hz) includes five frequencies for the smokestack of the Talimarjan Thermal Power Plant, six frequencies for the smokestack of the Syrdarya Thermal Power Plant, and eight frequencies of natural vibrations of the smokestack of the Novo-Angren Thermal Power Plant.

Using the *ANSYS* software package, numerical calculations make it possible to identify more frequencies at which resonance phenomena can occur during real earthquakes.

Analysis of the results obtained shows that there is a possibility that these frequencies coincide with the frequency of an earthquake, which can lead to resonant vibrations of the smokestack. Therefore, for real structures, it is recommended to apply additional measures to prevent dangerous vibrations, such as installing dynamic vibration dampers.

Figures 2-4 show the natural vibration modes obtained using the *ANSYS* software package for three tall smokestacks of thermal power plants.

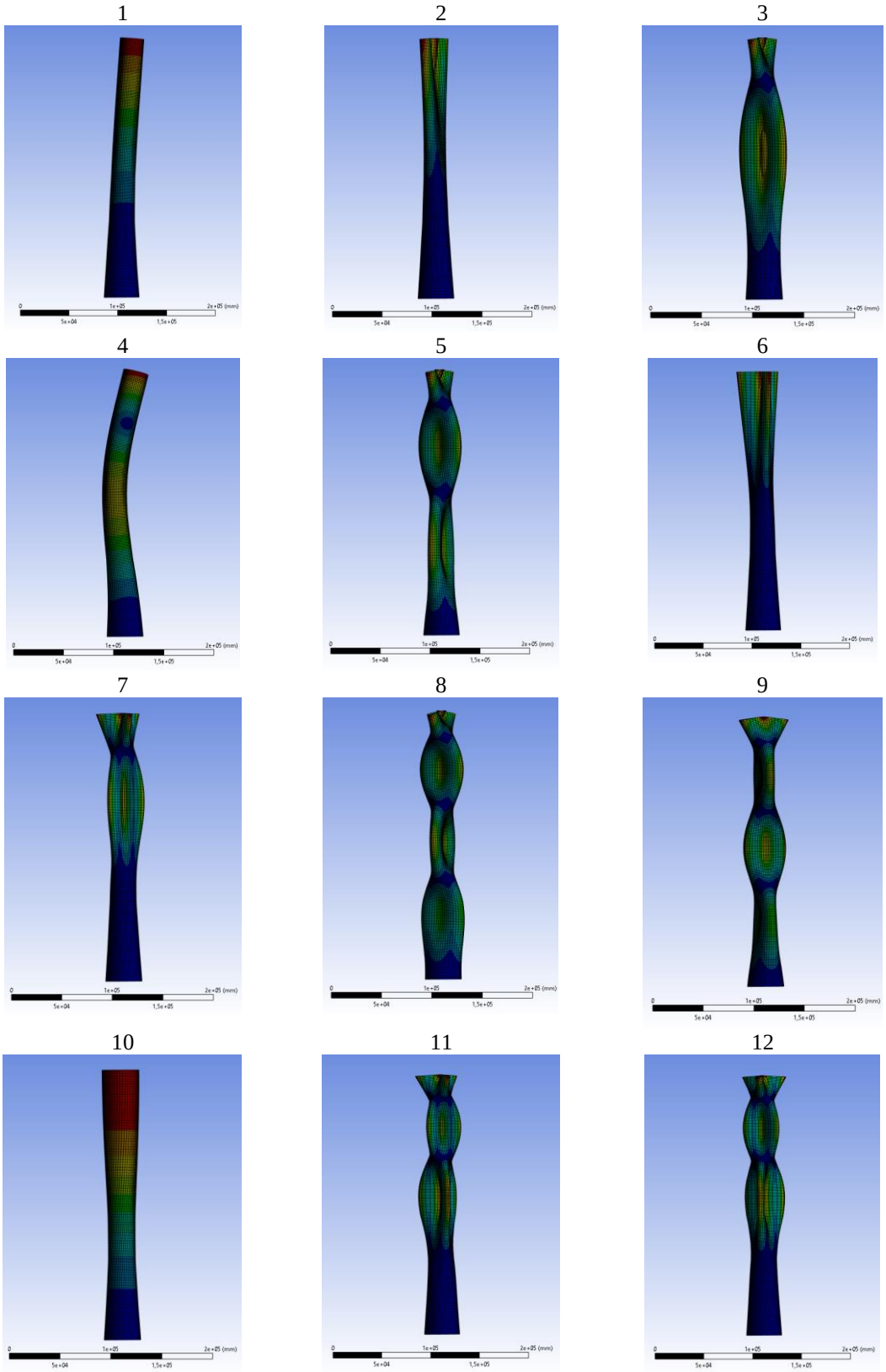

Figure 2. - **Natural vibration modes of the smokestack of the Talimarjan thermal power plant.**

1 2 3

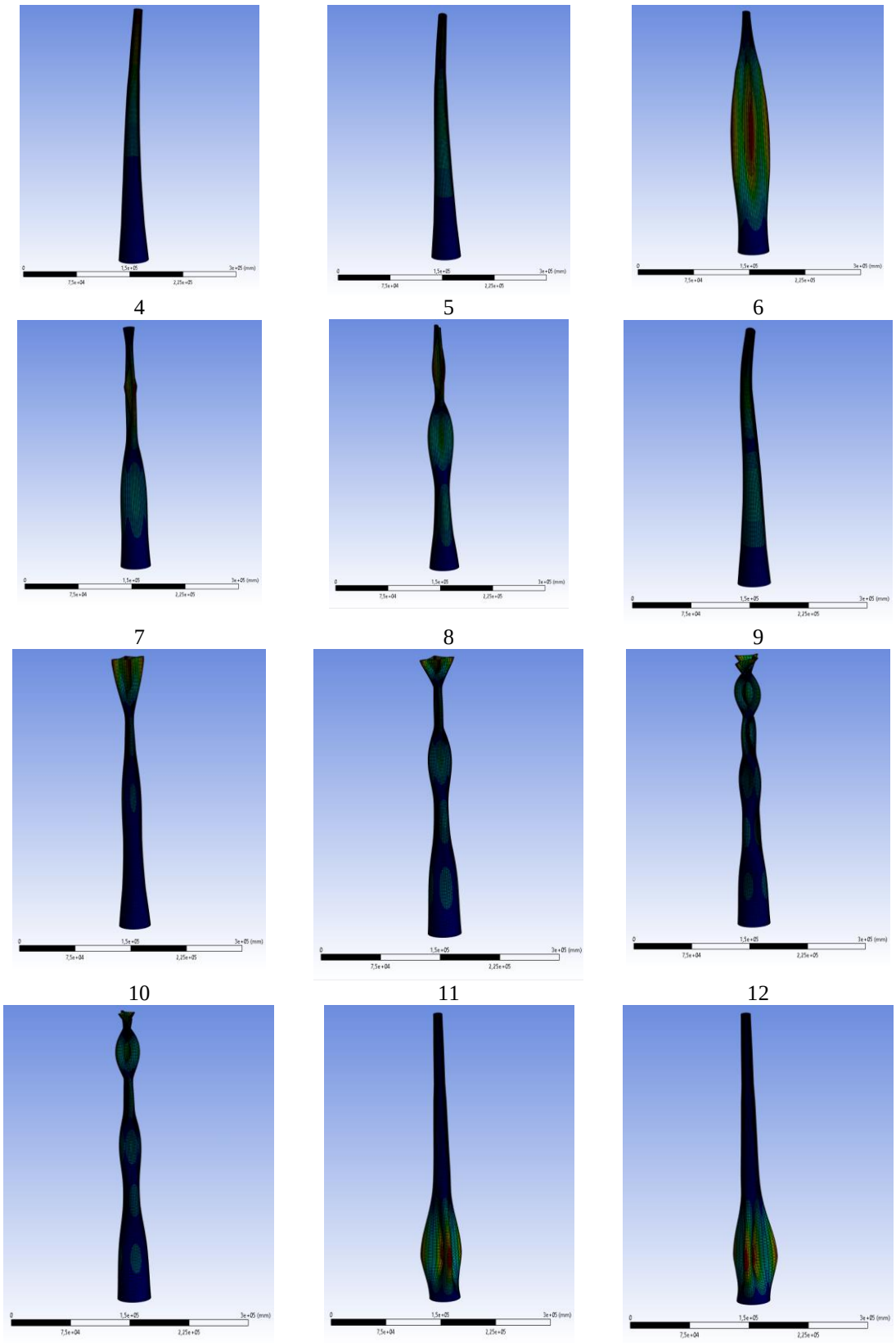

Figure 3. - **Natural vibration modes of the smokestack of the Syrdarya thermal power plant.**

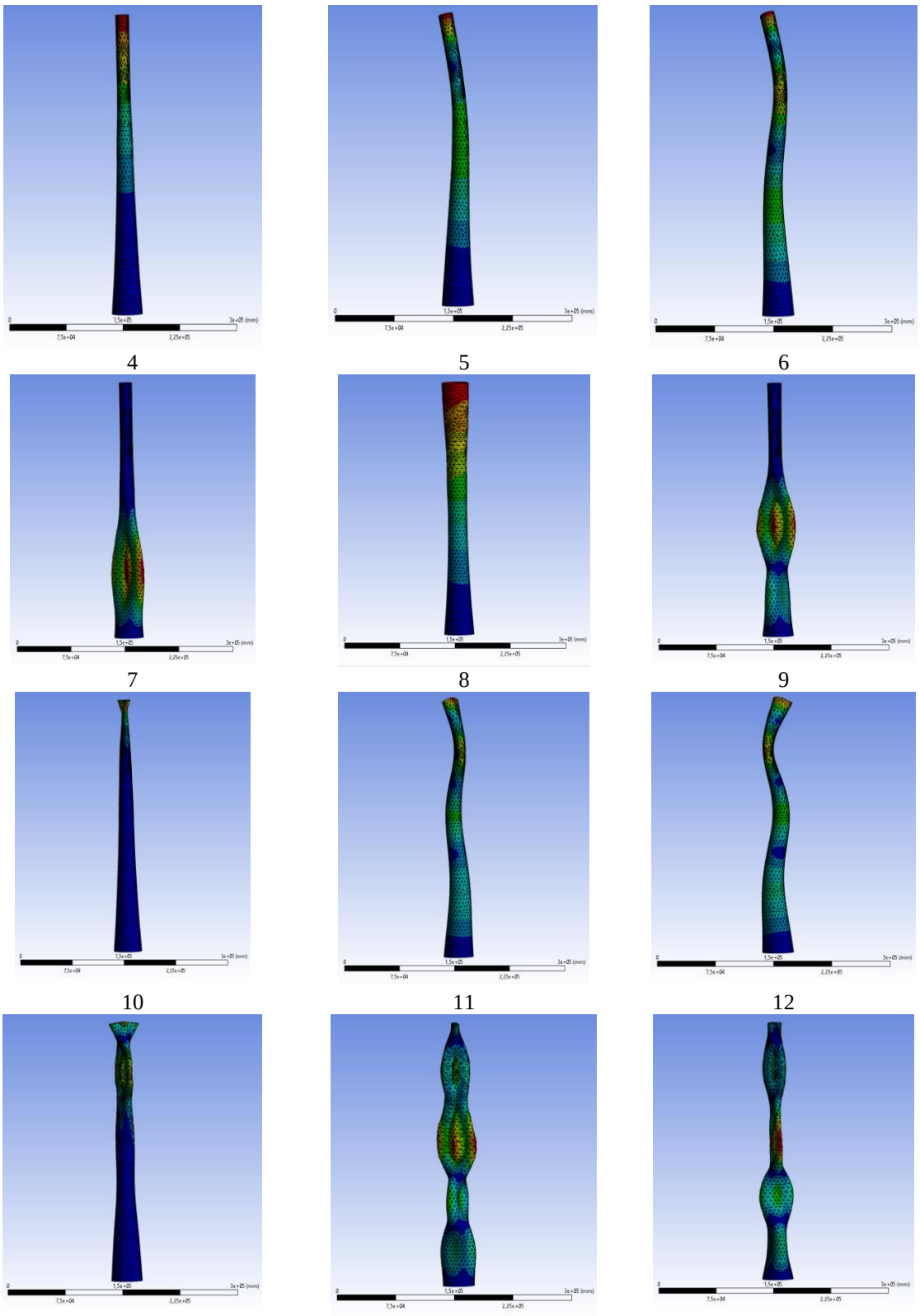

Figure 4. - **Natural vibration modes of the smokestack of the Novo-Angren thermal power plant.**

When comparing the embedded waveforms, it turns out that the vibration mode shape largely depends on the actual geometric dimensions of the structure. In the calculations, the same materials were selected for the three stacks. The Talimarjan smokestack is the shortest, the outer diameter of the upper part is the same, and the thickness of the smokestack does not differ much. Therefore, the vibration modes of this smokestack differ from the vibration modes of the other two smokestacks. The height and wall thickness of these two stacks are close to each other, so similarities are observed in the vibration modes.

Table 4

Periods of bending vibrations of smokestacks of thermal power plants

Smokestacks	No. of periods	Vibration periods (sec)			
		Theoretical		using *ANSYS*	Full-scale experiment
		Beam theory	Shell theory	Beam theory	Beam theory
Novo-Angren TPP	T_1	3.26	3.32	3.32	3.4
	T_2	0.91	0.99	0.93	1.0
	T_3	0.38	0.44	0.42	0.5
	T_4	0.21	0.25	0.38	0.3
Syrdarya TPP	T_1	2.51	2.12	2.65	2.8
	T_2	0.80	0.83	0.90	0.9
	T_3	0.33	0.38	0.59	0.4
	T_4	0.19	0.23	0.55	0.2

The oscillation periods obtained from the theories of beam and shell are compared with the results of full-scale experiments [29-30], see Table 4.

Table 5 shows the periods of vibrations obtained using the *ANSYS* software package for three tall smokestacks of thermal power plants.

Table 5

Periods of natural vibrations of smokestacks of thermal power plants

No. of vibration period	Talimarjan TPP	Syrdarya TPP	Novo-Angren TPP
T_1	2.6333	2.6519	3.3247
T_2	1.1003	0.9047	0.9312
T_3	0.8541	0.5890	0.4169
T_4	0.5881	0.5450	0.3847
T_5	0.5777	0.4546	0.3189
T_6	0.3965	0.4176	0.2801
T_7	0.3802	0.3971	0.2561
T_8	0.3706	0.3325	0.2384
T_9	0.3506	0.2680	0.2250
T_{10}	0.3338	0.2596	0.2181

Analysis of the results shows that the values of the periods of bending vibrations obtained experimentally [29-30] and theoretically using the developed method and the *ANSYS* software package are quite close.

6. Conclusions

As a result of the study, the following conclusions were drawn:

1. A procedure was developed for studying the natural vibrations of smokestacks using the *ANSYS* software package.

2. The vibration modes were constructed using the finite element calculation method in the *ANSYS* software package for different smokestacks. When comparing the embedded waveforms, it turns out that the shape of the vibration modes largely depends on the actual geometric dimensions of the structure.

3. Natural frequencies were determined using the developed methodology and the *ANSYS* software package. Analysis of the results obtained shows that the lowest numerical values of the vibration frequencies are close to each other, the differences increase as the vibration frequencies increase.

4. Natural vibration frequencies corresponding to the seismic hazard range were identified. When using the *ANSYS* software package, numerical calculations made it possible to identify more frequencies at which resonance phenomena occur during real earthquakes.

5. Analysis of the results obtained shows that there is a possibility that these frequencies coincide with the frequency of an earthquake, which can lead to resonant vibrations of the

smokestack. Therefore, for these real structures, it is recommended to apply additional measures to prevent dangerous vibrations, such as installing dynamic vibration dampers.

References

1. Nitti, Giuseppe, Lacidogna, Giuseppe and Carpinteri, Alberto. "An analytical formulation to evaluate natural frequencies and mode shapes of high-rise buildings" *Curved and Layered Structures*, vol. 8, no. 1, 2021, pp. 307-318. https://doi.org/10.1515/cls-2021-0025
2. Sadraddin H (2015) Fragility Assessment of High-Rise Reinforced Concrete Buildings Fragility Assessment of High-Rise Reinforced Concrete Buildings, In Department of Civil and Construction Engineering. Western Michigan University: Western Michigan University. p. 147
3. Rajmani A, Guha P Analysis of wind & earthquake load for different shapes of high-rise building. International Journal of Civil Engineering and Technology (IJCIET), ISSN 0976 – 6308 (Print), ISSN 0976 – 6316(Online), Volume 6, Issue 2, February (2015), pp. 38-45 © IAEME
4. Zhou, Y., Wang, R. & Lu, Y. Seismic design and analysis of a high-rise self-centering wall building: Case study. Front. Struct. Civ. Eng.17, 1690–1706 https://doi.org/10.1007/s11709-023-0022-x
5. Hemmatnezhad M., Rahimi G.H., Ansari R.. On the free vibrations of grid-stiffened composite cylindrical shells. ActaMechanica. 2014, Vol. 225, Iss. 2, Pp 609–623.
6. Zafar Iqbal, Muhammad N. Naeem, Nazra Sultana. Vibration characteristics of FGM circular cylindrical shells using wave propagation approach. ActaMechanica. December 2009, Pp.208-237. https://doi.org/10.1007/s00707-009-0141-z.
7. Mengmeng Sun, Qiusheng Li, Yi Li Investigation of time-varying natural frequencies of high-rise buildings under harsh excitations using a high-resolution combined scheme. Journal of building engineering-Vol. 57,2022. pp 104859-104859. https://doi.org/10.1016/j.jobe.2022.104859
8. Lian, C., Meng, B., Jing, H. *et al.* The Analysis of Higher Order Nonlinear Vibrations of an Elastic Beam with the Extended Galerkin Method. *J. Vib. Eng. Technol.* **12**, 2743–2758 (2024). https://doi.org/10.1007/s42417-023-01011-6
9. Shi B, Yang J, Wang J (2021) Forced vibration analysis of multi-degree-of-freedom nonlinear systems with the extended Galerkin method. Mechanics of Advanced Materials and Structures, 1–9. https://doi.org/10.1080/15376494.2021.2023922
10. Wang J, Wu R (2022) The extended Galerkin method for approximate solutions of nonlinear vibration equations. Appl Sci 12(6):2979. https://doi.org/10.3390/app12062979
11. Marzuki, M. A. B., Halim, M. H. A. & Mohamed, A. R. N. (2015). Determination of Natural Frequencies through Modal and Harmonic Analysis of Space Frame Race Car Chassis Based on ANSYS. *American Journal of Engineering and Applied Sciences*, *8*(4), 538-548. https://doi.org/10.3844/ajeassp.2015.538.548
12. Baro, D.K., Yadav, V. & Mahto, S. Dynamic modelling and analysis of smart cantilever beam using FEM. *Int J Interact Des Manuf* **17**, 1199–1214 (2023). https://doi.org/10.1007/s12008-022-01100-y
13. Özbayrak, A., Ali, M.K. & Çıtakoğlu, H. Buckling Load Estimation Using Multiple Linear Regression Analysis and Multigene Genetic Programming Method in Cantilever Beams with Transverse Stiffeners. *Arab J Sci Eng* **48**, 5347–5370 (2023). https://doi.org/10.1007/s13369-022-07445-6
14. Mirsaidov, M.M., Khudainazarov, Sh.O. Spatial natural vibrations of viscoelastic axisymmetric structures. Magazine of Civil Engineering. No.04. 2020. 96(4). Pp.118– 128. https://doi.org/10.18720/MCE.96.10
15. Sherzod Khudainazarov, Talibjan Sabirjanov and Alisher Ishmatov. Assessment of Dynamic Characteristics of High-Rise Structures Taking into Account Dissipative Properties of the Material. Journal of Physics. 1425. 2020. 012009 https://doi.org/10.1088/1742- 6596/1425/1/012009
16. Mirsaidov M., Abdikarimov R., Khudainazarov S., Sabirjanov T. Damping of vibrations of high-rise structures by viscoelastic dynamic dampers. E3S Web Conference. 2020. 02020. DOI:10.1051/e3sconf/202022402020
17. Sherzod Khudainazarov, Tulkin Mavlanov, Jakhongir Qosimov and Oliya Nurova Forced vibrations of high-rise buildings. IOP Conf. Series: Materials Science and Engineering 869 (2020) 052047 IOP https://doi.org/10.1088/1757-899X/869/5/052047
18. Sh Khudainazarov, B Donaev and J Yarashov Non-stationary oscillations of high-rise axisymmetric structures. IOP Conf. Series: Materials Science and Engineering 883 (2020) 012195 IOP https://doi.org/10.1088/1757-899X/883/1/012195
19. Sherzod Khudainazarov, Burkhon Donayev, Talibjan Sabirjanov and Jahongir Qosimov Dynamics of high-rise structures taking into account the viscoelastic properties of the material. E3S Web of Conferences 304, 02004 (2021) https://doi.org/10.1051/e3sconf/202130402004
20. Khudainazarov, Sh., Donayev, B., Sabirjanov, T., Qosimov, J. Non-Stationary Vibrations of a Viscoelastic Structure *AIP Conference Proceedings*, 2023, 2612, 020015 https://doi.org/10.1063/5.0113281
21. Zheleznyakova E.A., Osintsev A.V. Determination of natural frequencies and visualization of vibration modes of structural elements. Scientific Visualization, 2018, volume 10, number 3, pages 45 - 57, https://doi.org/10.26583/sv.10.3.03

22. Marzuki, M. A. B., Halim, M. H. A. & Mohamed, A. R. N. (2015). Determination of Natural Frequencies through Modal and Harmonic Analysis of Space Frame Race Car Chassis Based on ANSYS. *American Journal of Engineering and Applied Sciences*, *8*(4), 538-548. https://doi.org/10.3844/ajeassp.2015.538.548
23. Zaides, S.A., Nguyen Hyu Hai Effect of the Initial Orientation of a Working Tool on the Stress–Strain State during Reversible Surface Plastic Deformation. *Russ. Metall.* **2023**, 2187–2193 (2023). https://doi.org/10.1134/S0036029523700301
24. Zaides, S.A., Fam Wan An. The Influence of Working Tool Parameters on the Stress State during Orbital Surface Plastic Deformation. *Steel Transl.* **53**, 405–411 (2023). https://doi.org/10.3103/S0967091223050170
25. Koltunov, M.A., Mirsaidov, M.,Troyanovskii, I.E. Transient vibrations of axisymmetric viscoelastic shells. Polymer Mechanics. 1978. 14(2), c. 233-238.
26. Mirsaidov, M.,Troyanovskii, I.E. Forced axisymmetric oscillations of a viscoelastic cylindrical shell. Polymer Mechanics. 1975. 11(6), c. 953-955
27. Mirsaidov, M., Mekhmonov, Ya. Nonaxisymmetric vibrations of axisymmetric structures with associated masses and hollows (protrusions). Strength of Materials. March 1987. Vol.19, Iss. 3, Pp. 424-430. DOI**:** 10.1007/BF01524147
28. Ishmatov, A.N.,Mirsaidov, M.Nonlinear vibrations of an axisymmetric body acted upon by pulse loads. Soviet Applied Mechanics. 1991. 27(4), c. 388-394
29. Mirsaidov M., Abdurashidov K., Khamraev P. On natural vibrations of axisymmetric structures. Journal "Structural Mechanics and Calculation of Structures". M: 1986 No. 5, p. 53-53.
30. Mirsaidov M., Khamraev P., Shalimov A. Experimental and theoretical determination of the dynamic characteristics of smokestacks. Construction and architecture, series 14, issue 4, M.: 1985. P.17-20.

THE INFLUENCE OF SURFACTANTS AND COLLAGEN ON THE CLINKER GRINDING PROCESS

Khudanov U.O.[1], Kadirov T.Zh.[2], Sharifov G.N.[1], Gelchinova S.[1]
[1]*Jizzakh State Pedagogical University, Jizzakh, Uzbekistan*
[2]*Tashkent Institute of Textile and Light Industry, Tashkent, Uzbekistan*
E-mail: uhudanov@mail.ru,

Abstract: *In recent years, the development of directions for increasing the efficiency of grinding cement clinker has become relevant. To increase the efficiency of grinding, physical and chemical intensification methods are introduced, based on the creation of an adsorption-active environment with small additions of surfactants. The chemistry of collagen is mainly concerned with the development of new methods for obtaining complex compounds, studying and modifying structures. The promising and in-depth development of such problems is also determined by polymer chemistry. The intensifying effect of surfactants and collagen, which form an adsorption-active medium, is associated with a decrease in the strength of the ground material at the coarse grinding stage. Reducing sticking and aggregation at the stage of fine grinding, as well as increasing the fluidity of cement.*
Keywords: *cement, intensification, collagen, surfactants, intensifier.*

1. Introduction

The effectiveness of the cement grinding intensifier increases when grinding clinkers with high structural defects and high adhesive and autohesive properties; decreases when grinding clinker with easily crushed porous additives, as well as with additives that reduce the degree of sticking (sand, tripoli, slag) with an increase in the mixture humidity of more than 1.5 -2% [1].

In addition to these studies, we carried out work on the effect of surfactants J -1 on the grinding coefficient of clinker at a cement plant. There are several ways to intensify the grinding of cement clinker. One of them is a method of intensifying the grinding of cement clinker, which consists of joint grinding of clinker, gypsum dihydrate and a surfactant additive - polyconension product of sulfite modified metacresolmeloaminoformaldehyde - resins in an amount of 0.2-1% by weight of cement.

To explain the influence of the surfactant composition on the dispersion of cements, we will focus on the adsorption mechanism. Surfactant on clinker particles. There are two types of active centers on their surface - calcium and oxygen, and to activate the latter, the presence of water is necessary, which ensures their protonation [1-2]. Active centers previously attributed to silicon and aluminum (iron) are now also considered as oxygen ones, the specificity of which is manifested by the presence of incompletely compensated additional valence forces, depending on the central metal atom in the oxygen tetrahedron. The main structural defects of clinker particles - crystal boundaries,

stacking faults, dislocations - are characterized by excess calcium and are predominantly zones of calcium centers.

Anionic surfactants, which include all acids and their salts (including sulfonic acids, lignosulfonic acids, fatty acids, etc.), being sorbed mainly on calcium centers, contribute to the opening of the main structural defects of clinker particles in cracks, thereby anionic surfactants generate a large number of small particles during grinding. An increase in the yield of fine fractions (dusting) is characteristic of an intensifying effect on cement grinding, for example, with the introduction of surfactants such as conventional technical lignosulfonates, fatty acids (water-repellent surfactants), including their water-soluble salts such as soaponaft.

2. Methods

The effectiveness of surfactants was determined by the quality of the residue on sieve No. 008 and the productivity of the grinding unit based on the correction factor for grinding fineness. Grinding of Portland cement clinker was carried out in a laboratory two-chamber ball mill. During the laboratory experiments, the following remained constant: the mill filling factor, the mass of grinding media and clinker, its particle size distribution, and grinding duration. The composition and concentration of surfactants changed. The grinding time both without additives and with additives was the same - 90 minutes.

The additive is supplied to the chamber in a finely dispersed state. The standard of comparison is the grindability of clinker without additives and with the addition of triethanolamine, which is widely used in cement production.

From the results of the sieve analysis it is clear that all the studied surfactants, as well as the widely used TEA, well intensify the grinding process, increase the productivity of the grinding unit by 30-47%. The optimal concentrations are 0.03-0.05% by weight of the clinker.

3. Results

Analysis of the data obtained showed that the use of surfactants in the indicated quantities reduced the specific energy consumption during grinding to a residue on sieve No. 008 R = 10% by 17.5 -25%.

From the table it is clear that o the specific surface area S increases with the addition of J -1 from the clinker of the plant by 350 - -800 cm2/g, with the addition of J -2 - by 15 -600 cm2/g, with the addition of J -3 - by 100 -230 cm2/g . From the clinker of a building materials plant, the value of S increases with the addition of J -1 by 700 - -820 cm2/g, with the addition of J -2 - by 50 -160 cm2/g, with the addition of J -3 by 50 -100 cm2/g, and with the addition of TEA, this value is less than that of cement without additives. This is explained by the fact that TEA, adsorbed on the surface of grains, greatly affects the physical properties, increasing the fluidity of cement [1]. Apparently, with increasing fluidity, cement loses its resistance to air permeability. To study this phenomenon, we conducted an experiment on grinding cements to a specific surface area of approximately 5000 with optimal concentrations of surfactants (Table 1).

Table 1.

The influence of surfactants on the performance of the limestone grinding process

Additive	Number of additives, %	Residue on sieve 008, %	Specific surface area, p cm2/g	Specific consumption: energy, kWh/t	Increased productivity of grinding units, %
Without supplements		14	2500	41,0	-
J -1	0,03	5,00	2600	33,0	30,0
	0,05	4,75	2650	32,5	32,5
J -2	0,03	5,50	2620	33,0	26,0
	0,05	5,00	2680	33,0	30,0
J -3	0,03	5,50	2600	33,0	26,0
	0,05	4,75	2600	32,5	32,5

From the results of the sieve analysis it is clear that all the studied surfactants intensify the grinding process well and increase the productivity of the grinding unit. The table shows that the

specific surface area increases with the addition of d -1 by 100 -150 cm2'/g, with the addition of J -2 by 120 -180 cm2/g, with the addition of J -3 by 100 cm2/g.

When studying the process of grinding limestone with various particles in a laboratory ball mill, it was found that at this stage of the process, the dependence of the change in E materials of the content of particles more than 80 microns on the grinding time is close to linear, and, therefore, can be described by the following equation [1].

$$\Delta R008=K.t$$

From Table 2. It is clear that the additives under study intensify grinding well. After 105 minutes of grinding with surfactant additives, practically nothing remains on the control sieve, while for cement without additives the grinding fineness is 2.3%. The specific surface area of cements with surfactants increases with increasing grinding time.

Table 2.

The influence of surfactants on the performance of the clinker grinding process

Name of additive	Additive concentration, % by weight of cement	Dispersity of cement		Specific energy consumption, kW. h/t	Increased grinding productivity unit, %
		$\sum R_{008}$=10%	S см^2		
1	2	3	4	5	6
Plant clinker without additives	-	10	2650	40,0	-
TEA	0,015	4,25	2600	32,0	37,5
	0,03	4,00	2620	31,5	40,0
	0,05	4,75	2600	32,5	32,5
	0,10	5,50	2640	33,0	26,0
J -1	0,015	4,00	3360	31,5	40,0
	0,03	3,75	3600	31,0	44,0
	0,05	3,50	3650	30,0	44,5
	0,10	4,75	3200	32,5	32,5
J -2	0,015	5,00	2800	33,0	30,0
	0,03	4,50	3200	32,0	35,0
	0,05	4,75	3250	32,5	32,5
	0,10	5,00	3150	33,0	30,0
J -3	0,015	5,50	2750	33,5	26,0
	0,03	4,75	2800	32,5	32,5
	0,05	4,50	2880	32,5	33,0
	0,10	5,50	2700	33,5	26,0

“J” series additives greatly improve the grindability of clinkers. Clinkers with a diameter of 2-7 mm were crushed in a laboratory ball mill. Additives in optimal quantities based on the weight of the clinker were introduced immediately before grinding in sprayed form. To determine the amount of residue on sieve No. 008 every 10 minutes. Samples were taken from the mill. The diagrams show the grindability of clinkers without additives and with additives.

A comparison of the data obtained shows that the influence of the additive on the grindability of clinker, regardless of its mineralogical composition, begins to appear after the first 10 clays of grinding and increases as the dispersion of cement increases.

When grinding cement to the fineness accepted at most plants (8-10% residue on sieve No. 008), the specific energy consumption decreased from J-1 by 50%, from J-2 by 45%, from J-3 by 40% and from TEA - by 30%.

In Table 3. data on the grindability of mixtures according to examples 1-6 are given.

Table 3.

Refining the dispersion of cements with optimal surfactant additives during grinding time

Name of additive	Number of additives, %	Change in dispersion of cements with optimal surfactant additives during grinding time (min)					
		30	45	60	75	90	105
Plant clinker without additives	-	3350	2750	3500	3900	4500	4800
		18,4	7,5	6,5	5,5	4,75	2,3
ТЭА	0,03	2000	2650	3550	.3800	4300	4600
		16,7	6,1	6,6	4,9	4,5	0
J -1	0,05	2150	3900	3800	4000	4600	4900
		17 '	7,60	6,4	4,9	3,5	0
И -2	0,05	2150	2850	3850	3950	4600	4800
		17,1	6,8	5,5	4 , 5	4,5	0
И -3	0,05	3050	2850	3800	3900	4550	4790
		18,1	7,1	6,6	4,8	4,75	0
Note: in the numerator the specific surface area, cm2 /g; the denominator is the residue on sieve No. 008, %.							

However, the existing method of grinding intensification does not allow increasing the clinker grinding coefficient, i.e. the ratio of the grinding time of pure cement to the grinding time of cement with additives at equal specific surface area.

Intensification of grinding of cement clinker is carried out in an overlapping manner.

The triethanolamine-modified bottoms of cottonseed oil production, collagen - gossypol resin (J-1) were introduced together with cement clinker and gypsum dihydrate into a ball mill in an amount of 0.02 -1.00% by weight of Portland cement clinker.

Example I. To obtain Portland cement, the following components are mixed, wt.%: clinker 95.0; gypsum dihydrate 5.0. The mixture is immersed in a laboratory ball mill and crushed to a specific surface area of 3000 cm2/g.

Example 2. To obtain Portland cement, the following components are mixed, wt.%: clinker 94, 085; gypsum dihydrate 5.0; VAT residue of cottonseed oil production modified triethanol - amine (J -1) 0.015. Next, they are subjected to grinding similarly to example I.

Example 3. To obtain Portland cement, the following components are mixed, wt.% clinker 94.97; gypsum dihydrate 4.0; collagen 1.0; And -1 0.03. Next, they are subjected to grinding similarly to example I.

Example 4. To obtain Portland cement, the following components are mixed, wt.%: clinker 94.95; gypsum dihydrate 3.5; collagen 1.5 J -1 0.05. Next, they are subjected to grinding similarly to example I.

Example 5. To obtain Portland cement, the following components are mixed, wt.%: clinker 94.5; gypsum dihydrate 5.0; J -1 0.5.

Next, they are subjected to grinding similarly to example I.

Example 6. To obtain Portland cement, the following components are mixed, wt.%: clinker 94.0; gypsum dihydrate 5.0; J -1 1.0. Next, they are subjected to grinding similarly to example I.

Table 4.

The influence of J -1 on the grinding coefficient of clinker at a cement plant

By example	Specific surface area, cm2/g	Grinding time, min.	Grindability factor
1	3000	120	1,0
2	3000	79	1,52
3	3000	77	1,56
4	3050	75	1,60
5	3070	60	2,0
6	3000	57	2,1

5. Discussion

The data presented in the table show that the surfactant additive J-1 can dramatically increase the grinding coefficient of cement clinker. The use of this additive makes it possible to obtain

cement with a specific surface area of 3000 cm3/g in a short time, a sharp reduction in specific energy consumption in cement production.

As for our intensifiers, these additives, unlike the known ones, are chemisorbed on active surface centers of both types and calcium. And oxygen. Therefore, we can consider the process of clinker grinding in the presence of J -1, J -2, J -3 as a result of activation (i.e. opening into cracks) of structural defects, enhanced or generated by adsorbed surfactant molecules.

Such structural defects can be divided into two groups - those starting on calcium and oxygen atoms, and at the beginning of grinding the number of the former is much greater, thus practically we are dealing with two different materials containing the initial defects and without them, which leads, as is known, to the oscillatory grinding mode. Let's call the grinding mode resonant, in which, under the influence of surfactants, both groups of defects develop into cracks, mutually accelerating the process of destruction of the original grains. Obviously, such a regime can be established by regulating the functional composition of the additive, namely, the molar ratio of anion and cationic groups in it, the inverse in magnitude of the ratio of the number of calcium to oxygen centers, which can be calculated based on the mineralogical composition of the clinker and the density of dislocations on it surfaces. Thus, the introduction of the J series additive, intensifying the grinding of the binder, prevents overgrinding and increases the yield of the middle fraction in cement. When grinding cement to the standard accepted at most plants, the specific consumption of electrical energy also decreased.

References

1 . *Гелчинова С.Р., Худанов У.О.* Интенсификация процесса помола цемента / Ламберт академия, 2024, 116 p.

2. *Anisovich, A.G., Markevich M.I., Zhuravleva V.I., Kodirov T., Khudanov U.O.* Surface morphology of natural lamb leather after tannide tanning and laser exposure // Journal High Temperature Material Processes. 2023, vol. 27, No. 4, pp. 39–44.

3. *Kadirov T. Z., Khudanov U. O.,Ummatova D.* New technologies for skin impregnation using collagen-polymer systems // International Journal of Psychosocial Rehabilitation. 2020, vol. 29, No. 08, pp. 3303-3307.

4. *Riyadi W.B., Sivaraman R., Hussein A.M., Wais, F., Altalbawy M.A., Chaudhary D.K., Khudanov U.O.,* Mechanism of Imprinting Process in the Ni-P Metallic Glass Films: A Molecular Dynamics Stud Journal.Hindawi // Advances in Materials Science and Engineering. 2023,vol. 2023, pp. 1-8.

5. *Kadirov, T.J., Khaitov, A.A., Alimov, O.S., Ruziev, R.R.* Thermal analysis of structural and relaxation changes of collagen and collagen-based modifiers // ALCA. 2002, vol. .XCVII, No. 5, pp. 204

6. *Кадиров Т.Ж., Тошев А.Ю., Худанов У.О. и др.* Патент РУз. IAP 20070038. Пенетратор для отделки кожи. 26.10.2009.

COMPARATIVE ANALYSIS OF TORSIONAL VIBRATION OF CIRCULAR CYLINDRICAL ELASTIC AND VISCO ELASTIC SHELLS

Khudoynazarov Kh.Kh.[1], Akhatov Kh.N.[1]

[1]*Samarkand State University, Samarkand, Uzbekistan*

E mail: khudoynazar92@gmail.com

Abstract*. The specific torsional vibrations of circular-cylindrical elastic and viscoelastic shells are studied in this article. The relationship between frequency and wave number was investigated, when the layer is elastic and viscoelastic. A special case of the author's equations for a three-layer cylindrical shell is considered as a circular cylindrical shell equation. When the circular cylindrical shell is free of external forces, the frequency equation was derived and the obtained numerical results were obtained using the Maple 17 program, and corresponding graphs were constructed. Viscoelastic and elastic cases were compared, based on the results.*

Key words*: shell, frequency, viscoelastic, wave number, stress, deformation.*

1. Introduction.

Studying the issue of wave propagation in elastic and viscoelastic media is one of the main issues of mechanics. Elastic and viscoelasticity in constructions serve to reduce the stresses and deformations generated in the structures to the permissible limit. Therefore, studying the

characteristics of various elements of constructions and obtaining new results has become an urgent problem. Taking into account the viscoelastic properties of structures, more attention is being paid to solving dynamic problems.

The use of layered structures as structural elements in various fields of technology is widely developed, especially in industry, aviation, shipbuilding and agriculture. In the world, great importance is attached to the issues of reducing the material consumption of layered composite structures, which are the main load-bearing elements of engineering objects. For this reason, viscoelastic bodies are widely used as new materials. A mathematical model of longitudinal radial vibrations for a circular cylindrical three-layered viscoelastic body based on exact solutions in the study of the three-dimensional problem of the linear theory was proposed in [1]. Equations allowing to determine the state of stress-deformation in arbitrary cross-sections of the cylindrical shell have been obtained. Equations for calculating a three-layer cylindrical shell under a symmetric load with respect to the axis, taking into account the creep theory, are presented in [2].Longitudinal vibrations of a circular cylindrical elastic shell filled with a viscous liquid were studied in [3]. In this case, the shell is considered free of external loads. In addition, taking into account pure longitudinal vibrations, the radial displacements of the shell points were assumed to be zero. Physical nonlinear equations for torsional vibrations of a body were derived in [4]. In this case, an algorithm was developed to determine the strain-deformation state of arbitrary cross-section points in the body. Torsional vibration equations and stressed-deformed state of a truncated conical rod were considered in [5], taking into account the physical nonlinear relationship. Symmetric and antisymmetric vibrations of a three-layer plate are studied in the article [6,7]. In this work, the theory of transverse vibrations of a three-layer plate is developed based on the exact solutions of the equations of the theory of linear elasticity. The problem of harmonic antisymmetric vibrations of a three-layer elastic plate is solved. Longitudinal-radial vibrations of an elastic shell filled with a viscous liquid are considered in the article [8]. A circular cylindrical three-layer shell made of viscoelastic material was studied in [9]. In this work, there are unique contact conditions between the layers, and the dynamic and kinematic contact conditions of the problem are formed. It was created an algorithm for calculating the torsional vibration equations of a circular cylindrical three-layer shell.

Based on the shell theory, a mathematical model, a numerical algorithm and a computer program were created in [10] to solve the problem of nonlinear vibrations of large-diameter narrow-elastic thin-walled pipes. The results of the assessment of the stress-deformation state of the three-layer cylindrical shell, its structural characteristics, and the physical-mechanical characteristics of the polymer filler are presented in works [11-13]. The outer layers of the three-layer cylindrical shell are made of materials with high mechanical properties (steel, light metal alloys, wood, plastic). Low-density materials, such as rubber materials, are placed in the middle of the load-bearing layers. Wave propagation of an elastic shell with a viscous fluid within the framework of the model of linear equations of the hydrodynamics of a viscous compressible fluid was considered in [14]. This article examines the differences between cylindrical shell (elastic or viscoelastic) and fluid (ideal or viscoelastic) systems. Vibrations of viscoelastic cylindrical panels of variable thickness are considered in [15]. It is determined by a numerical method based on eliminating the singularity in the relaxation kernel of the integral operator.

The vibration of shells is one of the most widely studied areas in mechanics and structural dynamics. The vibration of cylindrical shells has been extensively studied by many researchers. Including two functional gradient layers. The analysis of vibration frequencies of two- and three-layer cylindrical shells is considered in works [16-18]. In the analysis of the literature, one, two and three-layer cylindrical shell equations were considered, but the frequency issue for an arbitrary point of the layer was not considered.

In the following, the equations of elastic and viscoelastic torsional vibrations of a cylindrical shell are considered as a special case of the three-layer cylindrical shell equations derived in [19]:

$$\frac{r_1^2}{4}\lambda_0 v_0^{(0)} + \xi\left(\frac{1}{2}(\lambda_0 - \frac{4}{r_1^2}) + \frac{r_1^2}{8}(\ln\frac{r_1}{\xi} - \frac{1}{4})\lambda_0^2\right)v_0^{(1)} = 0$$
$$\frac{r_2^2}{4}\lambda_0 v_0^{(0)} + \xi\left(\frac{1}{2}(\lambda_0 - \frac{4}{r_2^2}) + \frac{r_2^2}{8}(\ln\frac{r_2}{\xi} - \frac{1}{4})\lambda_0^2\right)v_0^{(1)} = 0 \tag{1}$$

2. Method.

If the circular cylindrical shell is a viscoelastic body we get the λ_n^m -operator as follows.

$$\lambda^n = \left[\frac{1}{b^2}M^{-1}\left(\frac{\partial^2}{\partial t^2}\right) - \frac{\partial^2}{\partial z^2}\right]^n,\ b^2 = \frac{\mu}{\rho},\ (n = 1,2). \tag{2}$$

takes the form, here

$$M(\varsigma) = \varsigma(t) - \int_0^t f(t-\tau)\varsigma(\tau)d\tau, \tag{3}$$

$f(\tau)$ - the kernel of the viscoelasticity operator. The material of the shell is elastic

$$M(\varsigma) = \varsigma(t) \tag{4}$$

Then, if we put expression (2) into the system of equations (1):

$$\frac{r_1^2}{4}\left(\frac{1}{b^2}M^{-1}\left(\frac{\partial^2}{\partial t^2}\right) - \frac{\partial^2}{\partial z^2}\right)v_0^{(0)} + \xi\left(\frac{1}{2}\left(\frac{1}{b^2}M^{-1}\left(\frac{\partial^2}{\partial t^2}\right) - \frac{\partial^2}{\partial z^2} - \frac{4}{r_1^2}\right) + \right.$$
$$\left. + \frac{r_1^2}{8}(\ln\frac{r_1}{\xi} - \frac{1}{4})\left(\frac{1}{b^2}M^{-1}\left(\frac{\partial^2}{\partial t^2}\right) - \frac{\partial^2}{\partial z^2}\right)^2\right)v_0^{(1)} = 0$$
$$\frac{r_2^2}{4}\left(\frac{1}{b^2}M^{-1}\left(\frac{\partial^2}{\partial t^2}\right) - \frac{\partial^2}{\partial z^2}\right)v_0^{(0)} + \xi\left(\frac{1}{2}\left(\frac{1}{b^2}M^{-1}\left(\frac{\partial^2}{\partial t^2}\right) - \frac{\partial^2}{\partial z^2} - \frac{4}{r_2^2}\right) + \right.$$
$$\left. + \frac{r_2^2}{8}\left(\ln\frac{r_2}{\xi} - \frac{1}{4}\right)\left(\frac{1}{b^2}M^{-1}\left(\frac{\partial^2}{\partial t^2}\right) - \frac{\partial^2}{\partial z^2}\right)^2\right)v_0^{(1)} = 0 \tag{5}$$

In particular, for an elastic shell, relation (4) is valid, and the system of equations (5) looks like

$$\frac{r_1^2}{4}\left(\frac{1}{b^2}\left(\frac{\partial^2}{\partial t^2}\right) - \frac{\partial^2}{\partial z^2}\right)v_0^{(0)} + \xi\left(\frac{1}{2}\left(\frac{1}{b^2}\left(\frac{\partial^2}{\partial t^2}\right) - \frac{\partial^2}{\partial z^2} - \frac{4}{r_1^2}\right) + \right.$$
$$\left. + \frac{r_1^2}{8}(\ln\frac{r_1}{\xi} - \frac{1}{4})\left(\frac{1}{b^2}\left(\frac{\partial^2}{\partial t^2}\right) - \frac{\partial^2}{\partial z^2}\right)^2\right)v_0^{(1)} = 0$$
$$\frac{r_2^2}{4}\left(\frac{1}{b^2}\left(\frac{\partial^2}{\partial t^2}\right) - \frac{\partial^2}{\partial z^2}\right)v_0^{(0)} + \xi\left(\frac{1}{2}\left(\frac{1}{b^2}\left(\frac{\partial^2}{\partial t^2}\right) - \frac{\partial^2}{\partial z^2} - \frac{4}{r_2^2}\right) + \right.$$
$$\left. + \frac{r_2^2}{8}\left(\ln\frac{r_2}{\xi} - \frac{1}{4}\right)\left(\frac{1}{b^2}\left(\frac{\partial^2}{\partial t^2}\right) - \frac{\partial^2}{\partial z^2}\right)^2\right)v_0^{(1)} = 0 \tag{6}$$

In the obtained system of equations (5), we pass to dimensionless quantities. For this, we make the following substitutions [20].

$$r_1 = \xi \cdot r_1^*, r_2 = \xi \cdot r_2^*, t = \frac{\xi}{b} \cdot t^*, z = \xi \cdot z^*, v_0^{*(0)} = v_0^{(0)}, v_0^{(1)} = \xi \cdot v_0^{*(1)}.$$

Here b is the transverse wave propagation velocity. We divide both sides of the equation (5) by

$$\frac{r_1^{*2}}{4} M\left(\left(\frac{\partial^2}{\partial t^{*2}}\right) - M\frac{\partial^2}{\partial z^{*2}}\right)v_0^{*(0)} + \left(\frac{1}{2}\left(M\left(\frac{\partial^2}{\partial t^{*2}}\right) - M^2\frac{\partial^2}{\partial z^{*2}} - M^2\frac{4}{r_1^{*2}}\right) + \right.$$

$$\left. + \frac{r_1^{*2}}{8}(\ln\frac{r_1}{\xi} - \frac{1}{4})\left(\left(\frac{\partial^2}{\partial t^{*2}}\right) - M\frac{\partial^2}{\partial z^{*2}}\right)^2\right)v_0^{*(1)} = 0$$

$$\frac{r_2^{*2}}{4} M\left(\left(\frac{\partial^2}{\partial t^{*2}}\right) - M\frac{\partial^2}{\partial z^{*2}}\right)v_0^{*(0)} + \left(\frac{1}{2}\left(\left(M\frac{\partial^2}{\partial t^{*2}}\right) - M^2\frac{\partial^2}{\partial z^{*2}} - M^2\frac{4}{r_2^{*2}}\right) + \right. \tag{7}$$

$$\left. + \frac{r_2^{*2}}{8}\left(\ln\frac{r_2}{\xi} - \frac{1}{4}\right)\left(\left(\frac{\partial^2}{\partial t^{*2}}\right) - M\frac{\partial^2}{\partial z^{*2}}\right)^2\right)v_0^{*(1)} = 0$$

(7) to make the system of equations more convenient, we drop the sign (*) and the general solution of the resulting system of equations

$$v_0^{(0)} = C_1 \exp\left(i(\omega t + kz)\right) \quad \text{and} \quad v_0^{(1)} = C_2 \exp\left(i(\omega t + kz)\right). \tag{8}$$

Here, k - is wave number, ω - is circular frequency of vibrations. Frequency equation for harmonic wave propagation of a circular cylindrical viscoelastic shell

$$\frac{r_1^2}{4}(1 - N(\omega))\left(-\omega^2 + (1 - N(\omega))k^2\right)C_1 + \left(\frac{1}{2}(1 - N(\omega))\left(-\omega^2 + \right.\right.$$

$$\left.\left. + (1 - N(\omega))k^2 - (1 - N(\omega))\frac{4}{r_1^2}\right) + \frac{r_1^2}{8}(\ln\frac{r_1}{\xi} - \frac{1}{4})\left(-\omega^2 + (1 - N(\omega))k^2\right)^2\right)C_2 = 0$$

$$\frac{r_1^2}{4}(1 - N(\omega))\left(-\omega^2 + (1 - N(\omega))k^2\right)C_1 + \left(\frac{1}{2}(1 - N(\omega))\left(-\omega^2 + \right.\right.$$

$$\left.\left. + (1 - N(\omega))k^2 - (1 - N(\omega))\frac{4}{r_2^2}\right) + \frac{r_2^2}{8}(\ln\frac{r_2}{\xi} - \frac{1}{4})\left(-\omega^2 + (1 - N(\omega))k^2\right)^2\right)C_2 = 0 \tag{9}$$

Here

$$N(\omega) = \int_0^\infty f(\varsigma)e^{-i\omega\varsigma}d\xi \tag{10}$$

For numerical calculations, we adopt a viscoelastic regular kernel

$$f(t) = \sum_{n=1}^{\infty}\frac{\alpha_n}{\tau_n}e^{-\frac{t}{\tau_n}}, \sum_{n=1}^{\infty}\alpha_n = 1,$$

Here α_n -are viscoelastic parameters of the layer; τ_n-are relaxation times. Then formula (10) takes the following form

$$N(\omega) = \sum_{n=1}^{\infty}\frac{\alpha_n(1 - i\omega\tau_n)}{1 + \omega^2\tau_n^2},$$

From equations (9) we arrive at two algebraic homogeneous equations with respect to $v_0^{(0)}$ *and* $v_0^{(1)}$. Then we create the system of equations (11).

$$\begin{cases} A_{11}C_1 + A_{12}C_2 = 0 \\ A_{21}C_1 + A_{22}C_2 = 0 \end{cases} \tag{11}$$

Here

$$A_{11} = \frac{r_1^2}{4}\left(-(1-N(\omega))\omega^2 + k^2\right), A_{21} = \frac{r_2^2}{4}\left(-(1-N(\omega))\omega^2 + k^2\right),$$

$$A_{12} = \frac{1}{2}\left(-(1-N(\omega))\omega^2 + k^2 - \frac{4}{r_1^2}\right) + \frac{r_1^2}{8}(\ln\frac{r_1}{\xi} - \frac{1}{4})\left(-(1-N(\omega))\omega^2 + k^2\right)^2$$

$$A_{22} = \frac{1}{2}\left(-(1-N(\omega))\omega^2 + k^2 - \frac{4}{r_2^2}\right) + \frac{r_2^2}{8}(\ln\frac{r_2}{\xi} - \frac{1}{4})\left(-(1-N(\omega))\omega^2 + k^2\right)^2$$

In order for the obtained equations (12) to have a non-zero solution, it is necessary and sufficient that the main determinant of this system is equal to zero. We have the following frequency equation.

$$A_{11} \cdot A_{22} - A_{12} \cdot A_{21} = 0 \tag{12}$$

3. The results.

We solve equations (12) numerically using the "Maple 17" application program package and graph the obtained results using the Excel program.

The geometric characteristics of a single-layer circular cylindrical structure are as follows:

$$r_1 = 0.2\ ,\ r_2 = r_1 + h.\ \ h = r_2 - r_1.$$

Here r_1, r_2 - the inner and outer radii of the layer, h - the thickness of the layer, aluminum ($p_0 = 2700\ kg/m^3, E_0 = 7 \cdot 10^{10} N/m^2, \nu_0 = 0.34$) was taken as a single-layer elastic body. Polypropylene ($E = 5{,}5 \cdot 10^{11} Pa; \rho = 920\, kg/m^3; \nu = 0.35 - 0{,}38.$) was used as a single-layer viscoelastic body material. The following values of viscoelastic parameters and relaxation times were obtained:

$$\alpha_1 = 0{,}6;\ \alpha_2 = 0{,}3;\ \alpha_3 = 0{,}1;\ \tau_1 = 0{,}16 \cdot 10^5\, мкс;\ \tau_2 = 0{,}14 \cdot 10^7\, мкс;\ \tau_3 = 0{,}11 \cdot 10^8\, мкс.$$

Numerical values of frequency in circular cylindrical elastic and viscoelastic shell torsional vibrations are given in the following tables.

Table 1

Values of the frequency when the materials of the circular cylindrical elastic shell are different (*k- wave number*)				
k		aluminum	steel	copper
1	Re	0.5656854302	0.6480740702	0.6164414001
	IM	0	0	0
2	Re	1.131370847	1.296148140	1.232882800
	IM	0	0	0
3	Re	1.697056287	1.944222210	1.849324202
	IM	0		0
4	Re	2.262741720	2.592296278	2.465765596
	IM	0	0	0
5	Re	2.828426853	3.240370355	3.082206986
	IM	0	0	0
6	Re	3.394111895	3.888444464	3.698648427
	IM	0	0	0
7	Re	3.959799361	4.536518450	4.315090020
	IM	0	0	0
8	Re	4.525478182	5.184592566	4.931533776
	IM	0	0	0
9	Re	5.091176557	5.832667599	5.547963667
	IM	0	0	0
10	Re	5.656858695	6.480740556	6.164419139
	IM	0	0	0

Table 2.

Comparison of frequency values in torsional vibrations of circular-cylindrical elastic and viscoelastic shells			
k		elastic	viscoelastic
1	Re	0.5656854302	0
	IM	0	6.221156716
2	Re	1.131370847	0
	IM	0	6.134115576
3	Re	1.697056287	0
	IM	0	5.987417861
4	Re	2.262741720	0
	IM	0	5.778986461
5	Re	2.828426853	0
	IM	0	5.507114125
6	Re	3.394111895	0
	IM	0	5.173111365
7	Re	3.959799361	0
	IM	0	4.787341952
8	Re	4.525478182	0
	IM	0	4.378412610
9	Re	5.091176557	0
	IM	0	3.993803081
10	Re	5.656858695	0
	IM	0	3.675221172

Table 3.

Frequency values in torsional vibrations of a circular cylindrical viscoelastic shell (*k- wave number, ω - circular frequency*)			
k		ω_1	ω_2
1	Re	0	0
	IM	0.02464945949	6.221156716
2	Re	0	0
	IM	0.02453783074	6.134115576
3	Re	0	0
	IM	0.02451738717	5.987417861
4	Re	0	0
	IM	0.02451024858	5.778986461
5	Re	0	0
	IM	0.02450694734	5.507114125
6	Re	0	0
	IM	0.02450515485	5.173111365
7	Re	0	0
	IM	0.02450407431	4.787341952
8	Re	0	0
	IM	0.02450337309	4.378412610
9	Re	0	0
	IM	0.02450289238	3.993803081
10	Re	0	0
	IM	0.02450254857	3.675221172

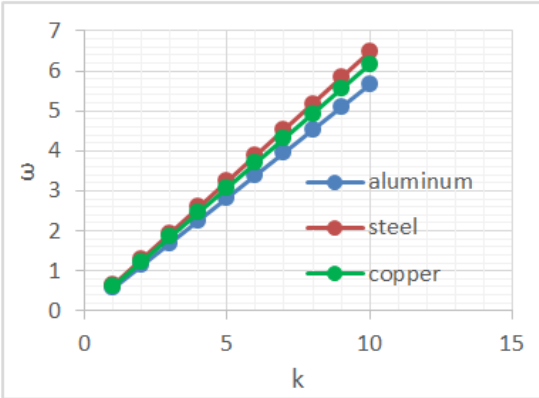

Figure.1. **The relationship between frequency and wave number when the material of a circular cylindrical single-layer cylindrical shell is different**

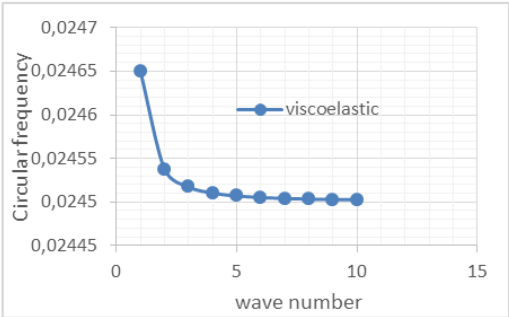

Figure. 2. **Relationship between frequency and wave number when the material of a circular cylindrical one-laverviscoelastic shell is different**

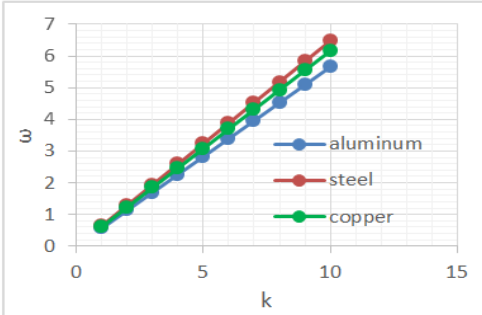

Figure.1. **The relationship between frequency and wave number when the material of a circular cylindrical single-layer cylindrical shell is different**

4. Analysis results.

In torsional vibrations of a circular cylindrical elastic shell, when the elastic material is varied, the values of the frequency are given in fixed values of the wave number. In Fig. 1, when the wave number is equal to *k=4*, we can see an increase in the frequency of the layer material steel and copper compared to aluminum (Table 1). The values of the frequency when the material of the circular cylindrical shell is a viscoelastic body are given in Table 2. It can be seen from Fig.2 that the frequency decreases as the number of waves increases, and in the elastic case, we can see that the frequency increases as the number of waves increases. The solutions of the system of equations (13) of the circular cylindrical elastic and viscoelastic shell consist of a complex root. In Table 3, the value of the circular frequency at the value of *k=6* can be seen to decrease in frequency compared to the elastic state. Figure 3 shows the material of the circular cylindrical shell is viscoelastic and elastic. A graph of the relationship between frequency and wave number was constructed and compared. When using pipe materials in agriculture, it is more convenient to use viscous elastic polypropylene materials than elastic materials (steel, copper, aluminum). Because there is less vibration in the pipes.

5. Conclusions.

In this work, the frequency equations of a circular cylindrical shell were derived. When the material of the layer is elastic and viscoelastic, the numerical results of the frequency were obtained using the Maple 17 mathematical program, and graphs were constructed based on the obtained results. It can be seen from the results that we can observe frequency attenuation in a viscoelastic body compared to an elastic body.

References

1. *Khudoynazarov Kh.* Longitudinal-radial vibrations of a viscoelastic cylindrical three-layer structure // Facta Universitatis, series: Mechanical Engineering. 2024, https://doi.org/10.22190/FUME231219010K
2. *Chepurnenko A.S., Yazыev B.M., Lapina A.P* three-layer cylindrical shell taking into account creep // Construction and Architecture (2018) Vol. 6. Issue 4 (21):
3. *Khudoynazaarov Kh., Yalgashev B.* Longitudinal vibrations of a cylindrical shell filled with a viscous compressible liquid. 2021. E3S Web of Conferences 264, 02017. https://doi.org/10.1051/e3sconf/202126402017
4. *Khudoynazarov Kh.* A mathematical model of physically nonlinear torsional vibrations of a circular elastic rod. Vestnik Tomskogo gosudarstvennogo universiteta. Matematika i mekhanika – Tomsk State University Journal of Mathematics and Mechanics. 2023. 84. pp. 152–166. doi: 10.17223/19988621/84/12
5. *Khudoynazarov Kh*. Modeling of nonlinear torsional vibrations of a truncated conical rod, Vestn. Samar. Gos. Tekhn. Univ., Ser. Fiz.-Mat. Nauki [J. Samara State Tech. Univ., Ser. Phys. Math. Sci.], 2023. vol. 27, no. 4, pp.704-722. https://doi.org/10.14498/vsgtu 2002
6. *Khudoynazarov Kh., Yaxshiboyev Sh.R.* The Mathematical Model of Transverse Vibrations of the Three-Layer Plate. IOP Conf. Ser.: Earth Environ. Sci. 2020. 614 012062. DOI: 10.1088/1755-1315/614/1/012062.
7. *Khudoynazarov Kh., Khudoyberdiyev Z.B.* Unsteady vibrations of a three-layer plate with an asymmetric structure. IOP Conf. Ser.: Earth Environ. Sci. 2020. 614 012061 DOI:10.1088/1755-1315/614/1/012061.
8. *Khudoynazarov Kh.Kh., Khalmuradov R.I., Yalgashev B.F.* 2021 Longitudinal-radial vibrations of a elastic cylindrical shell filled with a viscous compressible liquid. Tomsk State University. Journal of Mathematics and Mechanics. 69, 139-154. DOI: 10.17223/19988621/69/11.
9. *Khudoynazarov K. et al* Mathematical modelling of torsional vibrations of the three-layer cylindrical viscoelastic shell. IOP Conf. Series: Mater. Sci. Eng. 2021 1030 012098 DOI: 10.1088/1757-899X/1030/1/012098
10. *Khudayarov B.A., Turaev F.Z.,* 2019, Mathematical simulation of nonlinear vibrations of viscoelastic pipelines conveying fluid // Applied Mathematical Modelling, 66, pp. 662–679
11. *Gaidaichuk V.V., Kotenko K.E.* Stress - strain state of a three-layer cylindrical shell under internal axisymmetric pulse load // Strength of Materials and Theory of Structures. 2020. № 105
12. *Lugovyi P. Z., Gaidaichuk V. V., Skosarenko Yu. V., and Kotenko K. E.* Stress–strain state of three-layer cylindrical shells with reinforced light core under nonstationary loading // International Applied Mechanics, Vol. 57, No. 4, July, 2021
13. *Ustarkhanov O.M., Muslimov H.M., Yarakhmedov I.T.* Investigation of the stress-strain state of a three-layer cylindrical shell // Izvestiya vuzov. The North Caucasus region. technical sciences. 2021. № 3
14. *Marasulov A.M., Tazhibaeva A. K.* Longitudinal-transverse vibrations in a system of cylindrical shells filled or immersed in a liquid// Young scientist. 2017. No. 11 (145). pp. 86-91.
15. *Abdikarimov R.A., Khudayarov B.A.* Study of vibrations of viscoelastic circular cylindrical panels of variable *thickness, Computational Continuum Mechanics, 2012, vol.5. no.1, pp.11-18. DOI: 10.7242/1999-*6691/2012.5.1.2
16. *Shahid, H.A., Muhammad, N.N.,Nazra, S., Abdul, G.Sh., Zafar, I.,* 2011, Vibration analysis of bi-layered FGM cylindrical shells, Archive of Applied Mechanics, 81, pp. 319–343.
17. *Muhammad N., Naeem A.G.Kh., Shahid H.A., Abdul G.Sh., Madiha G.,* 2014, Vibration of Three-Layered FGM Cylindrical Shells with Middle Layer of Isotropic Material for Various Boundary Conditions // World Journal of Mechanics, 4, pp. 315–331.
18. *Kadir M., Çiğdem D., Ömer C.* Vibration analysis of FG cylindrical shells with power-law index using discrete singular convolution technique // Curved and Layer. Struct. 2016; 3 (1):82–90
19. *Khalmuradov R., Yalgashev B., Akhatov Kh.* Refined equations of torsional vibrations of a three-layer cylindrical viscoelastic shell // AIP Conference Proceedings 2637, 030026 (2022) Published Online: 20 October 2022
20. *Khudoynazarov Kh., Gadayev A., Akhatov Kh.* Torsional vibrations of a rotating viskoelastic rod // E3S Web of Conferences 365, 02016 (2023)

NUMERICAL SOLUTION TO THE DIFFERENTIAL EQUATION OF TRANSVERSE VIBRATIONS OF AN UNDERGROUND PIPELINE

Khusainov R.B.[1,2], Khusainova B.B.[2,3], Khusainov S.B.[4,5]
[1]*Institute of Mechanics and Seismic Stability of Structures, Tashkent, Uzbekistan*
[2]*University of Geological Sciences, Tashkent, Uzbekistan*
[3]*Tashkent branch of Plekhanov Russian University of Economics, Tashkent, Uzbekistan*
[4]*Bauman Moscow State Technical University, Moscow, Russia*
[5]*Tashkent State Transport University, Tashkent, Uzbekistan*
E-mail: r.khusainov89@yandex.com

Abstract. *The pipeline is considered an elastic body having the form of a cylindrical rod. The pipeline is surrounded by soil, therefore, on the surface of the pipeline, due to the influence of soil on the pipeline, normal and shear stresses appear under the interaction of the "pipe-soil" system. The seismic wave propagates along the side surface of the pipeline and lies in a plane parallel to the surface of soil. The problem is solved under the following three types of boundary conditions: simply supported, fixed and unsupported boundary conditions. To solve the equation, an explicit scheme of the finite difference method is used.*

Keywords: *pipe, soil, interaction, bending, vibration, elasticity, strain.*

1. Introduction

Underground pipelines are a key component of critical life support systems such as water supply, gas and liquid fuel pipes, sewerage, electricity, and telecommunications. The interaction with the soil structure under the impact of seismic waves has an important effect on the behavior of the pipeline, and, when integrated throughout the pipeline network, on the performance of the entire system [1, 2].

The effects of wave propagation on underground segmented pipelines have received much attention in recent decades. References [2-6] propose various models for analyzing the interaction of segmented pipelines under wave propagation.

Damage to underground pipelines during an earthquake is associated with a combination of different types of hazards: permanent ground deformations (landslides, liquefaction, and seismic subsidence) and wave propagation effects. The latter is characterized by transient deformation and curvature in soil due to the traveling wave effect. To analyze wave propagation, T.R. Rashidov and N.M. Newmark [7-8] proposed a simple procedure considering one traveling wave of an undamped (traveling) waveform. According to the definition given by T.R. Rashidov, the static theory was first considered in the work of R.M. Mukurdumov [9], and presented in the monographs of Sh.G. Napetvaridze [10]; there, it was proposed that when a wave propagates along a pipe, the pipe and soil move similarly. N.M. Newmark later proposed another assumption that the underground pipeline strictly follows the movement of soil, called the static theory. Therefore, the maximum axial deformation of the pipe is the same as the maximum axial deformation of soil.

However, the above procedures consider infinite pipeline lengths and therefore do not account for their effective length and any engineering works (constraint conditions). In [11], analytical relationships for a finite length of pipe subjected to various combinations of boundary conditions (i.e. free end, fixed, or elastic) for pipelines of various lengths were developed. In 1962, T.R. Rashidov proposed a differential equation for an underground pipeline, which became the basis of the dynamic theory. T.R. Rashidov [7, 11], G.De Martino et al. [12], and V.Corrado et al. [13] developed models of pipe-soil interaction considering the limited length of the pipeline. Assuming a linear elastic model of soil motion and ignoring slip at the pipe-soil interface, the models analyzed the dynamic behavior of a finite-length pipeline with boundary conditions at the ends. The pipeline was expected to be continuous; that is, any fluctuations between the characteristics (parameters) of the pipeline and its connections were considered insignificant. A.A. Ilyushin and T.R. Rashidov [2] proposed a viscoelastic-plastic model of the interaction of an underground structure with soil.

In [14–17], the use of various mechanical and mathematical models was analyzed and a number of pressing problems of underground and surface structures were solved. The model of linear deformation of the rod and the linear relationship between the contact force and the displacement of pipe sections was used to solve problems of seismodynamics of underground pipelines [18-22]. However, analysis of the results of experimental data [2, 23] indicated a more

complex dependence of the contact force of interaction on the displacement of the pipe section relative to soil.

The studies in [23-24] present various models of the interaction of underground structures with soil, taking into account the elastic, viscous, and plastic properties of soils with the transition to Coulomb friction.

In [19-22, 25], the influence of the coefficients of elasticity, viscosity, and plasticity of the pipeline interaction with soil on the stress-strain state of the underground pipeline was studied in detail. In [22], the influence of inertial forces on the strain state of an underground pipeline was considered.

In [26], the behavior of underground structure and soil interaction by Coulomb's law and the nonlinear elastoplastic interaction model [26–28] were studied.

2. Materials, methods and object of study

Consider the problem of the impact of a transverse wave on an underground pipeline of finite length interacting with soil by elastic law. The seismic wave propagates along the side surface of the pipeline and lies in a plane parallel to the surface of soil. To study the transverse vibration of an underground pipeline, we make the following assumptions. The underground pipeline is taken as a straight line, and the seismic wave at each section of the pipeline is directed perpendicular to the axis of the pipeline. The seismic wave is taken in the form of a sine.

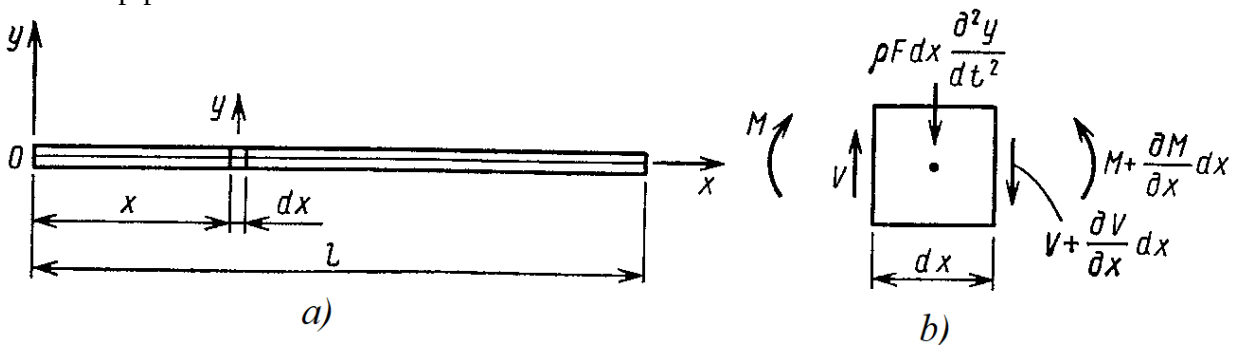

Figure 1. - **Scheme of a pipeline of finite length (*a*) and forces acting on a small element of the pipe (*b*).**

To simplify the statement of the problem, we assume the following: the presence of a pipeline does not affect the wave field near it.

Since the wave field behind the front of surface wave depends on the depth of soil, let us consider the averaged displacements of soil particles along the pipeline axis.

3. Statement of the problem.

The outer surface of the pipeline is in contact with soil along the axis of the pipeline by elastic law; the following three boundary conditions are taken: simply supported, fixed, and unsupported boundary conditions. Considering these assumptions, the equation for transverse vibrations of the pipeline and boundary conditions are written in the following form:

$$\rho F u_{tt} + EJ_y u_{xxxx} + \pi D_t k_y \left(u - u_g\right) = 0, \quad 0 < x < L \tag{1}$$

The conditions on the boundaries are $x = 0$ and $x = L$.

As the first partial case of transverse vibrations of an underground pipeline, we study a simply supported pipeline shown in Fig. 2. The edge conditions for this case are:

$$u(0, t) = 0, \; u_{xx}(0, t) = 0, \quad u(L, t) = 0, \; u_{xx}(L, t) = 0. \tag{2}$$

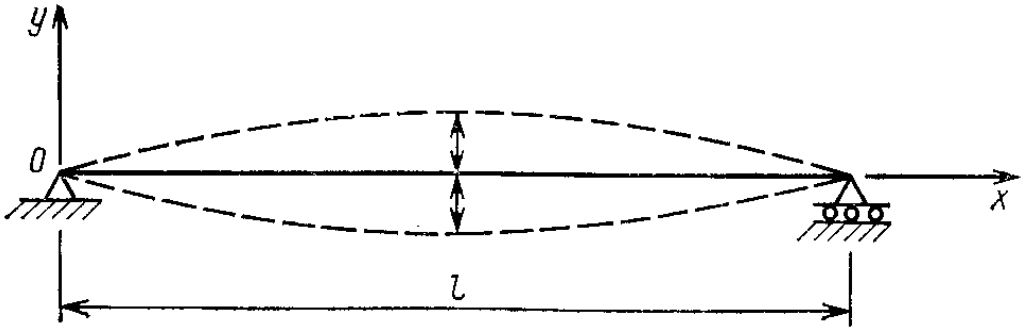

Figure 2. - **Simply supported pipeline**

A pipeline with rigidly fixed ends (see Fig. 3). The edge conditions in this case have the following form:

$$u(0,t)=0,\ u_x(0,t)=0,\quad u(L,t)=0,\ u_x(L,t)=0. \tag{3}$$

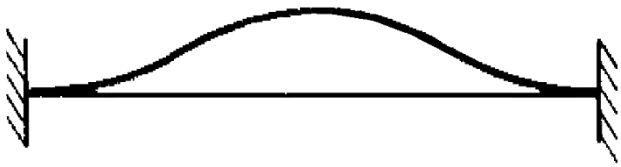

Figure 3. - **Pipeline with rigidly fixed ends**

Figure. 4. - **Pipeline with unsupported ends**

A pipeline with unsupported ends (see Fig. 4). In this case, we have the following edge conditions:

$$u_{xx}(0,t)=0,\quad u_{xxx}(0,t)=0,\ u_{xx}(L,t)=0,\ u_{xxx}(L,t)=0. \tag{4}$$

We take zero initial conditions:

$$u(x,0)=0,\ u_t(x,0)=0. \tag{5}$$

The seismic wave acting on the pipeline is taken in the following form:

$$u_g(t)=A\cdot\sin\omega t, \tag{6}$$

where $u(x,t)$ is the transverse displacement of an arbitrary section of the pipeline; $u_g(t)$ is the displacement of soil particles; A is the maximum ground displacement; ω is the angular velocity of seismic wave oscillations, determined by formula $\omega=2\pi/T$; E and $\rho-$are the Young modulus and density of the pipeline material; E_g is Young's modulus of soil.

4. Solution method

To solve equation (1), we use the following explicit scheme of the finite difference method with error $O(\tau^2+h^4)$.

The partial derivatives used in equation (1) are approximated by the following formulas:

Fourth order derivative of function $u(x,t)$ with respect to x coordinate:

$$\partial^4 u/\partial x^4 \approx \left(u_{i+2}^j-4u_{i+1}^j+6u_i^j-4u_{i-1}^j+u_{i-2}^j\right)/h^4, \tag{7}$$

Third order derivative of function $u(x,t)$ with respect to x coordinate:

$$\partial^3 u/\partial x^3 \approx \left(u_{i+2}^j-2u_{i+1}^j+2u_{i-1}^j-u_{i-2}^j\right)/(2h^3), \tag{8}$$

Second order derivative of function $u(x,t)$ with respect to x coordinate:

$$\partial^2 u/\partial x^2 \approx \left(u_{i+1}^j-2u_i^j+u_{i-1}^j\right)/h^2 \tag{9}$$

Second order derivative of function $u(x,t)$ with respect to time t:

$$\partial^2 u/\partial t^2 \approx \left(u_i^{j+1}-2u_i^j+u_i^{j-1}\right)/\tau^2 \tag{10}$$

First order derivative of function $u(x,t)$ with respect to x coordinate:

$$\partial u/\partial x \approx \left(u_{i+1}^{j} - u_{i-1}^{j}\right)/(2h) \tag{11}$$

First order derivative of function $u(x,t)$ with respect to x coordinate:

$$\partial u/\partial t \approx \left(u_{i}^{j+1} - u_{i}^{j-1}\right)/(2\tau), \tag{12}$$

where τ and h are the time step and the coordinate step.

The displacements are approximated in the following form:

$$u \approx \left(u_{i}^{j+1} + u_{i}^{j-1}\right)/2 \tag{13}$$

Now, we substitute the approximated values of partial derivatives into equation (1) and obtain the following recurrent values:

$$u_{i}^{j+1} = \left[-au_{i}^{j-1} + bu_{i}^{j} + c\left(u_{i+2}^{j} - 4u_{i+1}^{j} - 4u_{i-1}^{j} + u_{i-2}^{j}\right) + d\left(u_{gi}^{j+1} + u_{gi}^{j-1}\right)\right]/a \tag{14}$$

Here $a = \rho F/\tau^2 + \pi D_t k_y/2;\ \ b = 2\rho F/\tau^2 + 6EJ_y/h^4;\ \ c = EJ_y/h^4;\ \ d = \pi D_t k_y/2.$

To approximate the partial derivative of displacement along a coordinate at the boundaries, we use the "fictitious point" method. Let us dwell on recording the difference scheme at irregular nodes (at the boundary or near it). At these nodes, to write difference equations, it is necessary to use boundary conditions [1].

Consider a way to write a difference edge condition with an accuracy of O(h^2). We approximate equation (1) using an explicit scheme.

The fictitious point method is visual. Let us introduce fictitious point $x_{-1} = x_0 - h$ outside segment $0 < x < L$ and assume that the original equation is valid for $x_{-1} \le x$. Then the difference equation (14) can be written for $i = 1$ in the following form:

$$u_{1}^{j+1} = \left[-au_{1}^{j-1} + bu_{1}^{j} + c\left(u_{3}^{j} - 4u_{2}^{j} - 4u_{0}^{j} + u_{-1}^{j}\right) + d\left(u_{g1}^{j+1} + u_{g1}^{j-1}\right)\right]/a$$

Replacing the derivative in the left edge condition (1.2) with a symmetric difference, we obtain the following equations:

$$u_{0}^{j+1} = -u_{0}^{j-1} \text{ and } u_{-1}^{j} = 2u_{0}^{j} - u_{1}^{j}$$

We substitute the resulting value for u_{-1}^{j} into the above recurrent expression. As a result, we obtain the values of u_{0}^{j+1} and u_{1}^{j+1} at the nodes on the left boundary of the pipeline:

$$\begin{cases} u_{0}^{j+1} = -u_{0}^{j-1} \\ u_{1}^{j+1} = \left[-au_{1}^{j-1} + bu_{1}^{j} + c\left(u_{3}^{j} - 4u_{2}^{j} - 2u_{0}^{j} - u_{1}^{j}\right) + d\left(u_{g1}^{j+1} + u_{g1}^{j-1}\right)\right]/a \end{cases} \tag{15}$$

We define it in the same way for u_{n}^{j+1} and u_{n-1}^{j+1} on the right boundary of the pipeline.

Let us introduce fictitious point $x_{n+1} = x_n + h$ outside segment $0 < x < L$ and assume that the original equation is valid for $x_{n+1} \ge x$.

$$u_{n-1}^{j+1} = \left[-au_{n-1}^{j-1} + bu_{n-1}^{j} + c\left(u_{n+1}^{j} - 4u_{n}^{j} - 4u_{n-2}^{j} + u_{n-3}^{j}\right) + d\left(u_{g(n-1)}^{j+1} + u_{g(n-1)}^{j-1}\right)\right]/a$$

Let us replace the derivative in the right edge condition (2) with a symmetric difference and obtain the following equations:

$$u_{n}^{j+1} = -u_{n}^{j-1} \text{ and } u_{n+1}^{j} = 2u_{n}^{j} - u_{n-1}^{j}$$

Eliminating the fictitious point u_{n+1}^{j} from the last two equations, we obtain a difference analog of the edge condition:

$$\begin{cases} u_{n-1}^{j+1} = \left[-au_{n-1}^{j-1} + bu_{n-1}^{j} + c\left(-2u_{n}^{j} - u_{n-1}^{j} - 4u_{n-2}^{j} + u_{n-3}^{j}\right) + d\left(u_{g(n-1)}^{j+1} + u_{g(n-1)}^{j-1}\right)\right]/a \\ u_{n}^{j+1} = -u_{n}^{j-1} \end{cases} \tag{16}$$

Now we determine the difference analog of the edge condition (3) for both ends of the fixed underground pipeline.

Let us introduce the fictitious point $x_{-1} = x_0 - h$ outside segment $0 < x < L$ and assume that the original equation is valid for $x_{-1} \le x$. Then the difference equation (14) can be written for $i = 1$ in the following form:

$$u_1^{j+1} = \left[-au_1^{j-1} + bu_1^j + c\left(u_3^j - 4u_2^j - 4u_0^j + u_{-1}^j\right) + d\left(u_{g1}^{j+1} + u_{g1}^{j-1}\right)\right] / a$$

Let us replace the derivative in the left edge condition (3) with a symmetric difference and obtain the following equations:

$$u_0^{j+1} = -u_0^{j-1} \text{ and } u_{-1}^j = u_1^j .$$

Let us substitute the obtained values for u_{-1}^j into the above recurrent expression. As a result, we obtain the values of u_0^{j+1} and u_1^{j+1} at the nodes on the left boundary of the pipeline

$$\begin{cases} u_0^{j+1} = -u_0^{j-1} \\ u_1^{j+1} = \left[-au_1^{j-1} + bu_1^j + c\left(u_3^j - 4u_2^j + u_1^j - 4u_0^j\right) + d\left(u_{g1}^{j+1} + u_{g1}^{j-1}\right)\right] / a \end{cases} \quad (17)$$

For the right boundary of the pipeline, we define u_n^{j+1} and u_{n-1}^{j+1}.

Let us introduce the fictitious point $x_{n+1} = x_n + h$ outside segment $0 < x < L$ and assume that the original equation is valid for $x_{n+1} \ge x$.

$$u_{n-1}^{j+1} = \left[-au_{n-1}^{j-1} + bu_{n-1}^j + c\left(u_{n+1}^j - 4u_n^j - 4u_{n-2}^j + u_{n-3}^j\right) + d\left(u_{g(n-1)}^{j+1} + u_{g(n-1)}^{j-1}\right)\right] / a$$

Let us replace the derivative in the right edge condition (2) with a symmetric difference and obtain the following equations:

$$u_n^{j+1} = -u_n^{j-1} \text{ and } u_{n+1}^j = u_{n-1}^j$$

Eliminating the fictitious point u_{n+1}^j from the last two equations, we obtain a difference analog of the edge condition:

$$\begin{cases} u_n^{j+1} = -u_n^{j-1} \\ u_{n-1}^{j+1} = \left[-au_{n-1}^{j-1} + bu_{n-1}^j + c\left(-4u_n^j + u_{n-1}^j - 4u_{n-2}^j + u_{n-3}^j\right) + d\left(u_{g(n-1)}^{j+1} + u_{g(n-1)}^{j-1}\right)\right] / a \end{cases} \quad (18)$$

Let us proceed to the definition of a finite-difference analog of the boundary condition (4), i.e. for the case when both ends of the underground pipeline are not fixed.

We introduce fictitious points $x_{-1} = x_0 - h$, $x_{-2} = x_0 - 2h$ outside segment $0 < x < L$ and assume that the original equation is valid for $x_{-1} \le x$ and $x_{-2} \le x$. Then the difference equation (14) can be written for $i = 0$ and $i = 1$ in the following form:

$$u_0^{j+1} = \left[-au_0^{j-1} + bu_0^j + c\left(u_2^j - 4u_1^j - 4u_{-1}^j + u_{-2}^j\right) + d\left(u_{g0}^{j+1} + u_{g0}^{j-1}\right)\right] / a$$

and

$$u_1^{j+1} = \left[-au_1^{j-1} + bu_1^j + c\left(u_3^j - 4u_2^j - 4u_0^j + u_{-1}^j\right) + d\left(u_{g1}^{j+1} + u_{g1}^{j-1}\right)\right] / a$$

Replacing the derivative in the left edge condition (1.4) with a symmetric difference, we obtain the following equations:

$$u_{-1}^j = 2u_0^j - u_1^j \text{ и } u_{-2}^j = u_2^j - 2u_1^j + 2u_{-1}^j$$

We substitute the obtained values for u_{-1}^j and u_{-2}^j into the equations given above, and obtain the values of u_0^{j+1} and u_1^{j+1} at the nodes on the left boundary of the pipeline:

$$\begin{cases} u_0^{j+1} = \left[-au_0^{j-1} + bu_0^j + c\left(2u_2^j - 4u_1^j - 4u_0^j\right) + d\left(u_{g0}^{j+1} + u_{g0}^{j-1}\right)\right]/a \\ u_1^{j+1} = \left[-au_1^{j-1} + bu_1^j + c\left(u_3^j - 4u_2^j - u_1^j - 2u_0^j\right) + d\left(u_{g1}^{j+1} + u_{g1}^{j-1}\right)\right]/a \end{cases} \quad (19)$$

For the right boundary of the pipeline, we define u_n^{j+1} and u_{n-1}^{j+1}.

We introduce fictitious points $x_{n+1} = x_n + h$, $x_{n+2} = x_n + 2h$ outside segment $0 < x < L$ and assume that the original equation is valid for $x_{n+1} \geq x$ and $x_{n+2} \geq x$. Equation (14) is written for $i = n-1$ and $i = n$: $u_{n-1}^{j+1} = \left[-au_{n-1}^{j-1} + bu_{n-1}^j + c\left(u_{n+1}^j - 4u_n^j - 4u_{n-2}^j + u_{n-3}^j\right) + d\left(u_{g(n-1)}^{j+1} + u_{g(n-1)}^{j-1}\right)\right]/a$ and $u_n^{j+1} = \left[-au_n^{j-1} + bu_n^j + c\left(u_{n+2}^j - 4u_{n+1}^j - 4u_{n-1}^j + u_{n-2}^j\right) + d\left(u_{gn}^{j+1} + u_{gn}^{j-1}\right)\right]/a$

Let us replace the derivative in the right edge condition (4) with a symmetric difference and obtain the following equations: $u_{n+1}^j = 2u_n^j - u_{n-1}^j$ and $u_{n+2}^j = 4u_n^j - 6u_{n-1}^j + u_{n-2}^j$

Eliminating fictitious points u_{n+1}^j and u_{n+2}^j, from the last two equations, we obtain a difference analog of the edge condition:

$$\begin{cases} u_{n-1}^{j+1} = \left[-au_{n-1}^{j-1} + bu_{n-1}^j + c\left(-2u_n^j - u_{n-1}^j - 4u_{n-2}^j + u_{n-3}^j\right) + d\left(u_{g(n-1)}^{j+1} + u_{g(n-1)}^{j-1}\right)\right]/a \\ u_n^{j+1} = \left[-au_n^{j-1} + bu_n^j + c\left(2u_{n-2}^j - 6u_{n-1}^j - 4u_n^j\right) + d\left(u_{gn}^{j+1} + u_{gn}^{j-1}\right)\right]/a \end{cases} \quad (18)$$

5. Results and discussion.

We accept the following characteristics of the pipe and soil: density ρ = 7800 kg/m^3, Young's modulus $E = 2.1 \cdot 10^8$ kN/m^2, length $L = 100$ m, diameter $D_t = 200$ mm, thickness $s = 5$ mm, period of fundamental vibrations $T = 0.1$ s, vibration amplitude $A = 4$ mm, Young's modulus of soil $E_g = 20 \cdot 10^4$ kN/m^2.

Let us consider the transverse vibrations of an underground pipeline when the ends of the pipe are simply supported. The research results are presented in the form of graphs in Figures 5-18. If soil particles near an underground pipeline move according to law (6), then the pipeline also vibrates according to the same law, but at a different amplitude.

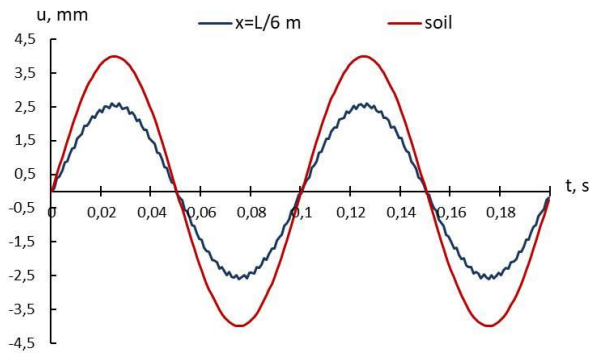

Figure 5. - **Change in displacements over time**

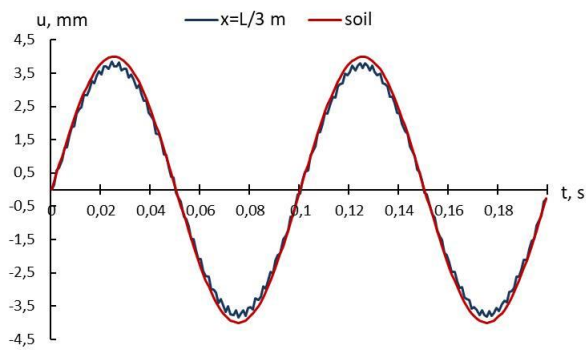

Figure 6. - **Change in displacements over time**

Figures 5 and 6 show changes in displacements over time when comparing the displacement of an underground pipeline and the soil near the pipeline. At the boundaries of the pipeline, the displacement is assumed to be zero with simply supported conditions. In this case, in the middle of the pipeline, the displacement of the pipeline takes on the maximum value. In sections from the boundary to the middle of the pipeline, the maximum displacement increases. This is confirmed by the research results shown in Figures 5, 6, and 9.

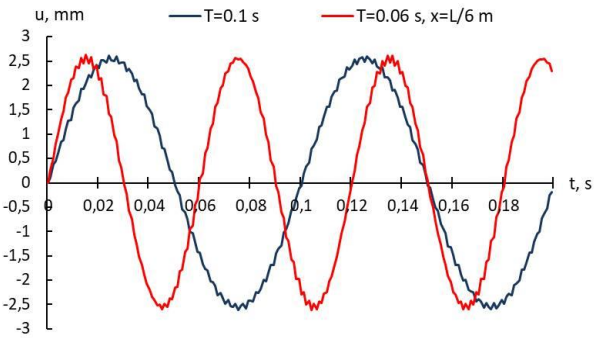

Figure 7. - **Change in displacements over time**

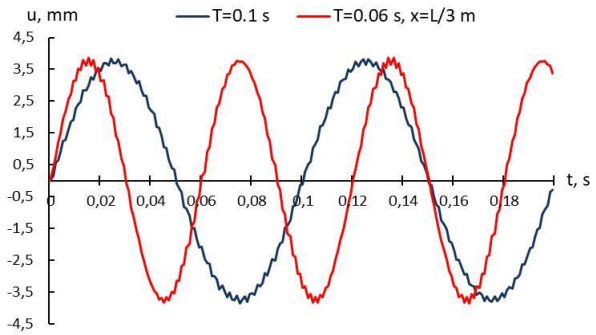

Figure 8. - **Change in displacements over time**

Now let us look at the comparative results for two values of the periods of ground motion oscillations T=0.06 s and T=0.1 s. Changes in the period of oscillation or frequency do not affect the amplitudes of the pipeline oscillations but do affect the oscillation frequency (see Figs. 7-8)

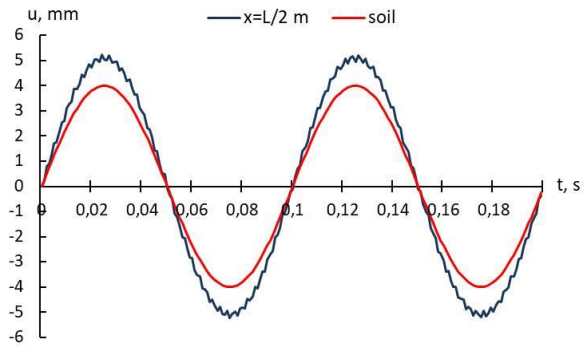

Figure 9. - **Change in displacements over time**

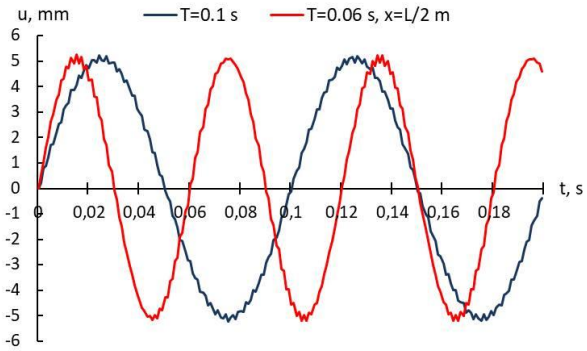

Figure 10. - **Change in displacements over time**

In the middle of the pipeline, the amplitude of pipeline displacement vibrations is greater than the amplitude of the soil displacement vibrations, i.e., in this case, the amplitude of the soil displacement vibrations is 0.004 m, and the amplitude of the pipeline displacement vibrations is approximately 0.005 m (see Figs. 9-10).

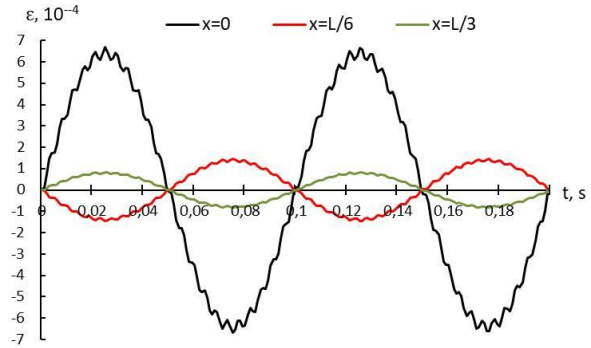

Figure 11. - **Change in strain over time for k_y=4·10^4 kN/m^3**

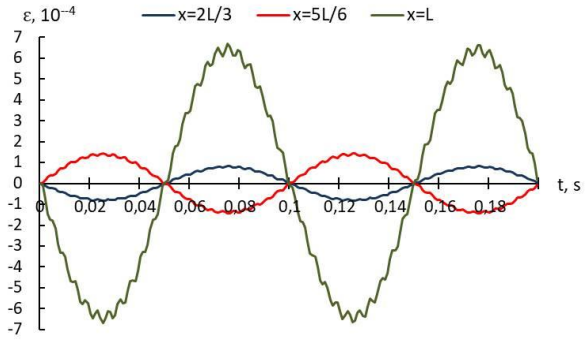

Figure 12. - **Change in strain over time for k_y=4·10^4 kN/m^3**

Figures 11 and 12 show the results of a numerical solution for the transverse vibration of a 100-meter pipe. Analysis of the results leads to the following conclusions: from the boundary to the middle of the pipeline, the maximum value of strain decreases and in the middle of the pipeline, it is zero.

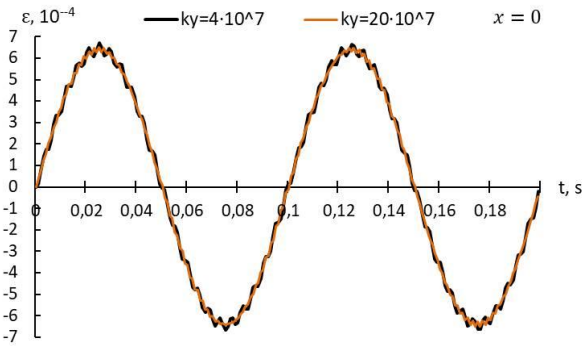

Figure 13. **- Change in strain over time on the left boundary of the pipeline**

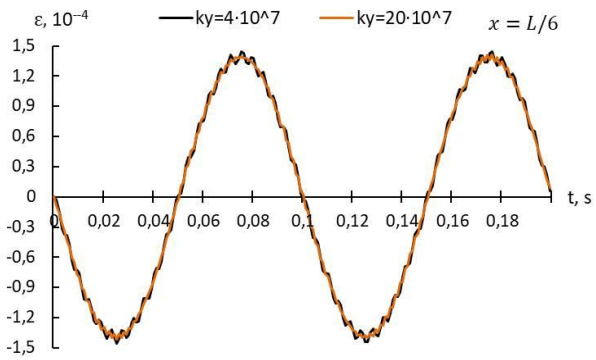

Figure 14. **- Change in strain over time in section x=L/6 m**

Figures 13, 14, and 15 show the change in strain over time. The results of the study show that with an increase in the coefficient of lateral resistance of soil, high-frequency oscillations of the pipeline strain attenuate. Figures 13, 14, and 15 compare the strains that occur in the pipeline for two values of the soil lateral resistance coefficient $k_y = 4 \cdot 10^7$ N/m^3 and $k_y = 20 \cdot 10^7$ N/m^3. Figure 13 shows the comparative result for section $x = 0$ m, and Figures 14 and 15 show comparative results for sections $x = L/6$ m and $x = L/3$ m, respectively.

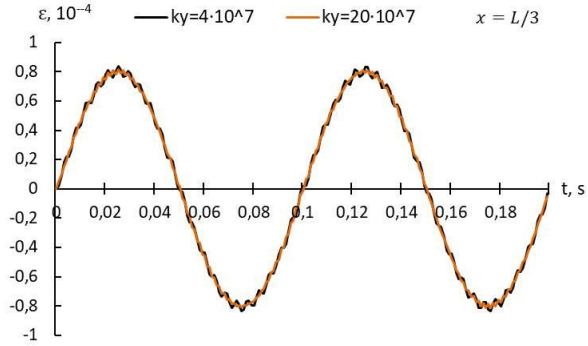

Figure 15. **- Change in strain over time in section *x=L*/3 m.**

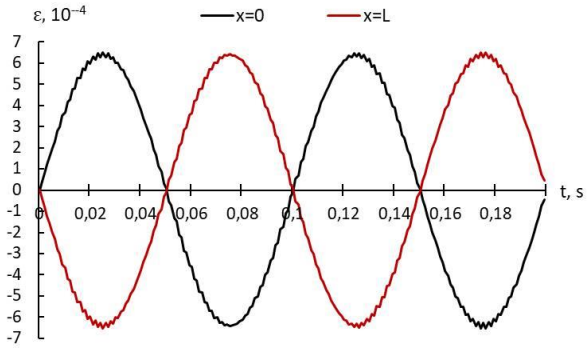

Figure 16. **- Change in strain over time at the ends of the pipeline for k_y=20·10^4 kN/m^3**

At pipeline boundaries, the maximum strain is approximately 0.00065. In the sections of the pipeline *x=L*/6 m and *x=5L*/6 m, the strain of the pipe does not exceed ε_{max}=0.00014, and in sections *x=L/3* m and *x=2L*/3 m, it is ε_{max}=0.00008. These results are shown in Figures 16, 17, and 18.

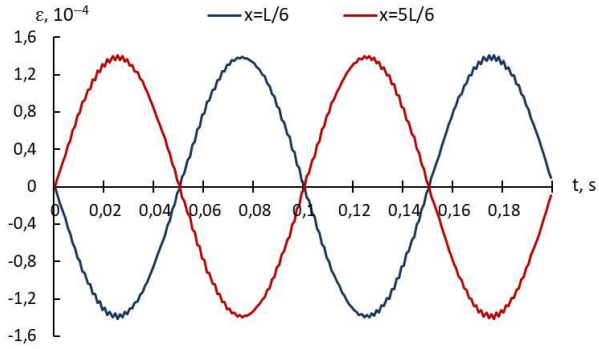

Figure 17. **- Change in strain over time in pipeline sections *x=L*/6 m and *x=5L*/6 m for k_y=20·10^4 kN/m^3**

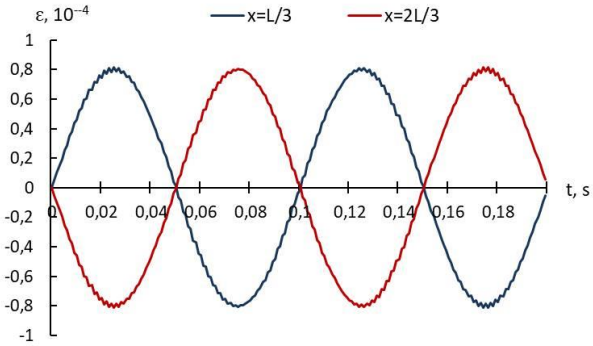

Figure 18. **- Change in strain over time in pipeline sections *x=L*/3 m and *x=2L*/3 m for k_y=20·10^4 kN/m^3**

The study shows that under transverse vibrations, the strain at both ends of a simply supported underground pipeline has the maximum values at the boundaries and zero strain in the middle of the pipeline.

The displacement in the middle of the underground pipeline has the maximum value, and it is greater than the vibration amplitude of the soil particles.

An increase in the coefficient of transverse soil resistance to the pipeline leads to the attenuation of high-frequency vibrations.

6. Conclusion

The maximum displacement in pipeline sections increases with distance from the boundary, and in the middle of the pipeline reaches its maximum value along the length of the pipeline.

Changing the frequency of ground vibrations does not affect the maximum value of displacements occurring in the pipeline.

An increase in the coefficient of lateral resistance of soil to the pipeline leads to the attenuation of high-frequency oscillations in displacement and strain graphs.

The study shows that under transverse vibrations, both ends of a simply supported underground pipeline have the maximum strain at the boundaries and zero strain in the middle of the pipeline.

References

1. *O'Rourke T.D.* Geohazards and large geographically distributed systems. // Geotechnique 2010; 60(7).-p 503-543.

2. *Rashidov T.* Dynamic theory of seismic resistance of complex systems of underground structures. -Tashkent: Fan, 1973. – 180 p.

3. *O'Rourke M.J. and Liu X*. "Response of buried pipelines subject to earthquake effects," // MCEER Monograph 3, Multidisciplinary Center for Earthquake Engineering Research, University at Buffalo, Buffalo, NY, USA, 1999.

4. *Iwamoto T., Wakai N., Yamaji T.* Observation of dynamic behavior of ductile iron pipelines during earthquakes. // In: Proceedings of the 8th World Conference on Earthquake Engineering, Vol. VII. San Francisco, USA; 1984. -p. 231-238.

5. *O'Rourke T.D., Wang Y., Shi P*. Advances in lifeline earthquake engineering. // In: Proceedings of the 13th World Conference on Earthquake Engineering, Vancouver, Canada; 2004. Paper No. 5003

6. *Wang LRL*. Some aspects of seismic resistant design of buried pipelines. // In: Lifeline earthquake engineering: buried pipelines, seismic risk, and instrumentation (PVP-34). American Society of Mechanical Engineers; 1979. -p. 117-131.

7. *Rashidov T.* Differential equation of vibration of an underground pipeline during an earthquake. // Tashkent, Reports of the Academy of Sciences of Uzbekistan, 1962, No. 9. - P.10-12.

8. Newmark N.M. "Problems in wave propagation in soil and rocks," // in Proceedings of the International Symposium on Wave Propagation and Dynamic Properties of Earth Materials, University of New Mexico Press. 1967, pp. 7-26.

9. *Mukurdumov R.M*. Issues of seismic resistance of underground pipelines. // Tashkent. Academy of Sciences of Uzbekistan, 1953.

10. *Napetvaridze Sh.G*. Seismic resistance of hydraulic structures. // M., Gosstroyizdat, 1959. – 216 p.

11. *Rashidov T.*, Calculation of underground pipelines of finite length under the action of short-term seismic load // Tashkent, Reports of the Academy of Sciences of Uzbekistan, 1963, - No. 4, - P. 13-16.

12. *De Martino G., D'Acunto B., Fontana N., and Giugni M*. "Dynamic response of continuous buried pipes in seismic areas," // in ASCE Pipelines Conference, August 2006.

13. *Corrado V., D'Acunto B., Fontana N., and Giugni M.* Inertial Effects on Finite Length Pipe Seismic Response. // MPE. - 2012. - P.14

14. *Mirsaidov M.M., Abdikarimov R.A., Khodzhaev D.A.*, Dynamics of a viscoelastic plate carrying concentrated mass with account of physical nonlinearity of material. PNRPU Mech Bull. № 2. P. 143–155. 2019.

15. *Abirov Rustam*, On metals' properties manifested under complex loading // AIP Conf. Proc. 2369, 020018 (2021), https://doi.org/10.1063/5.0060895

16. *Abirov, R.* On behavior of plasticity functionals at complex loading // *Materials Today: Proceedings*, 2021, 38, P. 1480–1483. https://doi:10.1016/j.matpr.2020.08.132

17. *Mirsaidov M.M., Usarov M.K.*, Bimoment theory construction to assess the stress state of thick orthotropic plates. IOP Conf. Ser.: Earth Environ. Sci. 614. 2020. 012090. https://doi:10.1088/1755-1315/614/1/012090.

18. *Borodavkin P.P.*, Underground main pipelines (design and construction) M.: Nedra, 1982. –384 p.

19. *Khusainov, R., Yarashov, J., Khusainov, S.*(2023) Application of finite difference method for solving problem of seismic resistance of underground pipelines //V International Scientific Conference "Construction Mechanics, Hydraulics and Water Resources Engineering" (CONMECHYDRO - 2023) // E3S Web of Conferences, 2023, 401, 05046. https://doi.org/10.1051/e3sconf/202340105046

20. *Khusainov, R.B., Yuldoshev, B.Sh., Abdullaev, D., Khusainov, S.B.* (2023) Longitudinal vibrations of underground pipelines of finite length in medium surrounded by soil with different properties along pipeline length //V International Scientific Conference "Construction Mechanics, Hydraulics and Water Resources

Engineering" (CONMECHYDRO - 2023)// E3S Web of Conferences, 2023, 401, 04060. https://doi.org/10.1051/e3sconf/202340104060

21. *Rakhmankulova Barna, Mirzaev Sayibdjan, Khusainov Rakhmatjon, Khusainov Saparboy,* Underground main pipeline behavior under a travelling impulse in the form of a triangle. International Scientific Conference CONMECHYDRO - 2021. E3S Web Conf.Volume 264, 2021. https://doi.org/10.1051/e3sconf/202126401006.

22. *Rakhmankulova Barna, Mirzaev Sayibdjan, Aynakulov Sharafidin, Khusainov Rakhmatjon, Khusainov Saparboy,* Inertia force effect on longitudinal vibrations of underground pipelines // International Scientific Conference CONMECHYDRO - 2021. E3S Web Conf.Volume 264, 2021. https://doi.org/10.1051/e3sconf/202126401007.

23. *Sultanov K.S.,* Wave theory of seismic resistance of underground structures. Tashkent: Fan, 2016. – 392 p.

24. *Sultanov K.S., Khusanov B.E., Rikhsieva B.B.* Mathematical model of underground structure-soil interaction // IOP Conf. Ser.: Mater. Sci. Eng.2020. Vol. 962. P 032021 https://doi.org/10.1088/1757-899X/962/3/032021

25. *Khusainov, R.B., Khusainov, S.B. & Khusainova, B.B.* Seismodynamics of Underground Pipelines under Viscous-Elastic-Plastic Interaction with Soil. Soil Mech Found Eng 59, 544–552 (2023). https://doi.org/10.1007/s11204-023-09849-4

26. *Sultanov K.S., Khusanov B.E., Rikhsieva B.B.* Longitudinal waves in a cylinder with active external friction in a limited area // Journal of Physics: Conference Series. 2020. Vol.1546. P.012140, https://doi.org/10.1088/1742-6596/1546/1/012140

27. *Sultanov K.S. Khusanov B.E. Rikhsieva B.B.* Elastic wave propagation in a cylinder with external active friction // Journal of Physics: Conference Series. – 2021. – Vol. 1901 (1), P.012125. – doi:10.1088/1742-6596/1901/1/012125

28. *Sultanov K.S., Khusanov B.E., Rikhsieva B.B.* Stress waves in a cylindrical body interacting with external medium // IOP Conference Series: Materials Science and Engineering.- Vol. 971(4).- P.042036 https://doi.org/10.1088/1757-899X/971/4/042036

OSCILLATIONS OF UNDERGROUND PIPELINES UNDER NONLINEAR INTERACTION WITH SOIL

Khusainov R.[1,2], Khusainova B.[2,3], Khusainov S.[4,5]

[1]*Institute of Mechanics and Seismic Stability of Structures named after M.T. Urazbaev, Tashkent, Uzbekistan*
[2]*University of Geological Sciences, Tashkent, Uzbekistan*
[3]*Tashkent branch of Plekhanov Russian University of Economics, Tashkent, Uzbekistan*
[4]*Bauman Moscow State Technical University, Moscow, Russia*
[5]*Tashkent State Transport University, Tashkent, Uzbekistan*
E-mail: r.khusainov89@yandex.com

Abstract. *The solution to the problem of longitudinal oscillations of an underground pipeline is given, taking into account the viscous-elastic-plastic interaction in the "pipe-soil" system. The seismic impact on soil is taken in the form of a traveling sine wave. Based on the data obtained in the experiments, a nonlinear problem is solved for the model of dry friction. The problem is solved under free and fixed boundary conditions. The stress-strain state of an underground pipeline was studied for linear and non-linear interaction with soil. The problems are solved by the finite difference method, taking into account various soil conditions.*

Keywords: *pipe, soil, interaction, plasticity, viscosity, elasticity, stress, strain.*

1. Introduction

The formulation and solution of any engineering problem are always associated with the idealization of real processes and phenomena since it is impossible to take into account all the factors that have some impact on the course of the process. Therefore, when setting the task, a number of parameters are singled out that play a determinant role in these processes. When solving applied problems of seismic resistance of underground structures, the issue of the nature and magnitude of the forces arising at the contact of the structure surface with the surrounding soil in the presence of relative displacements is of crucial importance. The nature of the seismic motion of soil in the vicinity of the structure is assumed to be known in advance. Thus, the interaction means the nature and magnitude of the friction force acting on the surfaces of the structure in contact with soil in the presence of relative displacements caused by the action of a seismic load considering the differences in their physical and mechanical properties.

The behavior of underground structures under seismic impact is largely determined by the characteristics of soil conditions. When performing seismodynamic calculations, the degree of correspondence between the results obtained and the actual process depends significantly on how the chosen model of structure-soil interaction corresponds to the actual character of the interaction.

In [1], for the first time, a pipe slippage relative to the surrounding soil during seismic wave propagation was taken into account. A differential equation for the longitudinal oscillations of the pipeline was derived and its solution was obtained for a finite and semi-infinite pipeline under harmonic and impulse loads.

It was experimentally determined that the law of interaction of underground structures with various types of soil, in the general case, is non-linear. The parameters characterizing the nonlinear, elastic, plastic, and viscous properties of the underground pipeline interaction with soil were determined in [2].

In [3], studies of the influence of the elastoplastic properties of interaction on seismic oscillations of an underground pipeline system were conducted; a system with a finite number of degrees of freedom was chosen as the design scheme.

In [4–5], a two-dimensional axisymmetric non-stationary wave problem was solved for the "underground pipeline–soil" system. In this case, the pipeline and soil were taken as linearly deformable bodies. The proposed condition (a model) of interaction at the contact boundary takes into account the structural destruction of the soil contact layer and the cyclic nature of the interaction process. On the surface of their contact, the interaction force (friction) is determined by a two-stage law (pre-limit and limit stages). In [6], the problem of building new models of soil and rock strain that take into account structural damage was considered. For this, models of interaction of underground structures with soil were compared with models of soil strain. The transition from strain models to interaction models is shown. In [7], a numerical solution of coupled one-dimensional wave problems on the longitudinal wave propagation in the soil half-space and in the underground pipeline was given. Longitudinal stresses in the pipeline were determined in its various sections beginning from the initial section, which coincides with the initial section of the soil half-space [8].

In [9–13], the use of various mechanical and mathematical models was analyzed and a number of topical problems of underground and surface structures were solved. The influence of the coefficients of elasticity, viscosity, and plasticity of the pipeline interaction in contact with soil on the stress-strain state of the underground pipeline was studied in detail in [14–19]. In [19], the effect of inertia forces on the deformed state of an underground pipeline was studied. The effect of a seismic wave on an underground pipeline was considered in [20]. Accumulated experience demonstrates that direct simulation of real objects in the general case does not ensure the required quality of the relevant analytical models [21].

The seismic stability of an underground pipeline remains one of the urgent problems facing scientists worldwide. In this regard, the studies of foreign scientists deserve attention. They obtained several relationships between shear stress and displacement when studying the elastoplastic pipe-soil interaction. For example, in [15], shear stress was revealed at the contact of the pipeline with sand and clay. Prof. K.S. Sultanov conducted numerous experiments to determine the properties of the pipeline interaction with soils of disturbed and undisturbed structures. Reference [14] presents graphs of dependence of shear stress on the contact surface on displacements, plotted based on the experimental data. Let us present one of the graphs from the monograph [14].

The manifestation of the peak value of shear stress τ_p at the interaction of fragments with soil and at the shear of the soil samples is associated with the process of accumulation of plastic strains and destruction of the soil structure. After the relative displacement reaches the value of u*, the structural bonds of soil with the fragment are completely destroyed and the shear stress at values of τ_r remains constant with a further increase in the displacement of the fragment relative to soil. As the results of experiments on the interaction of fragments with undisturbed soils show, the value of u_* does not change at different interaction rates.

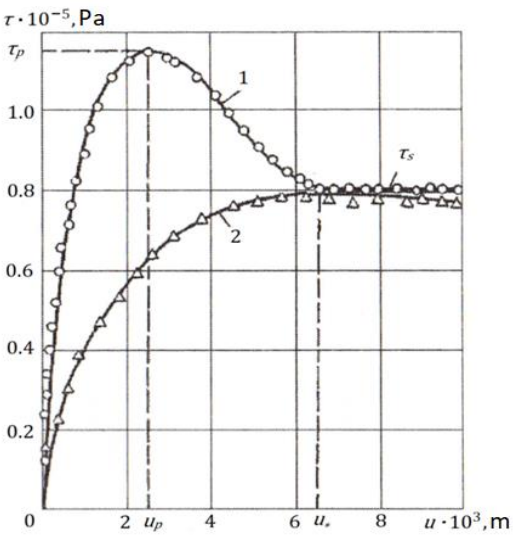

Figure 1. - **Shear stress dependences on relative displacement.**

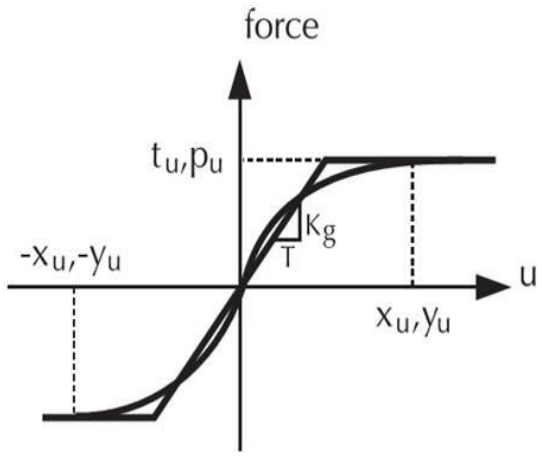

Figure 2. - **Idealized load-deformation relations at the pipe-soil interface**

Curves 1, 2 in Fig. 1 were obtained at the interaction of a smooth-surface fragment with loess soil in a quasi-static mode [14].

The results of experiments on the interaction of fragments of the outer surface of underground structures with soil of disturbed structures show that the change in shear stress, depending on the relative displacement on the fragment–soil contact surface and on the interaction of underground pipes with soil consists of two stages. The first stage is when the value of the shear stress develops depending on the relative displacement, and the second stage is when the shear stress does not depend on the change in the values of relative displacements.

In the case of undisturbed soil, the dependences τ(u) show the peak value of the shear stress. The values of the limit shear stress for the cases of disturbed and undisturbed soil structures at constant roughness of the fragment surface and normal pressure are the same.

Based on the above analysis of the experimental results, it is clear that in the model of the interaction of rigid bodies with soil, the value of shear stress in the first stage of the interaction process should depend on the relative displacement. In the second stage of interaction, obviously, Coulomb's law is fulfilled. The Winkler-type law describes the reverse motion.

The results of experiments on the interaction of underground structures and their fragments with soils show that the interaction rate affects the patterns of interaction, especially in the case of undisturbed soil in the first stage of the interaction process.

In [14], three types of mathematical models of the interaction of rigid bodies with soil are given: Winkler model, Kelvin–Voigt model, and a model of a standard linear body.

In the interaction model of the Kelvin–Voigt type under loading to elastic limit u_*, the shear stress is determined by the Kelvin–Voigt model in the following form:

$$\tau = K_x(\sigma_N, I_s)u + \eta_s(\sigma_N, I_s)du/dt \quad \text{for } du/dt \geq 0,\ 0 \leq u \leq u_*, \tag{1}$$

beyond the elastic limit, the shear stress is determined by the law of dry friction:

$$\tau = f_u \sigma_N \quad \text{for } du/dt \geq 0,\ u > u_*, \tag{2}$$

unloading to the elastic limit is realized by the Winkler model, i.e.

$$\tau = K_x^R(\sigma_N, I_s)u \quad \text{for } du/dt < 0,\ 0 \leq u \leq u_*, \tag{3}$$

beyond the elastic limit, the shear stress under unloading is zero.

$$\tau = 0 \quad \text{for } du/dt < 0,\ u > u_*, \tag{4}$$

where $\sigma_N -$ is the stress normal to the structure–soil contact surface; $\sigma_N^* -$ is the tensile strength of the soil-structure contact; $K_x(\sigma_N, I_s) -$ is the interaction coefficient; $\eta_s(\sigma_N, I_s) -$ is the shear viscosity coefficient; $K_x^R(\sigma_N, I_s) -$ is the coefficient of interaction under the reverse movement of

the structure relative to soil; $f_u -$ is the coefficient of friction; $u_* -$is the critical value of the relative displacement at which there is a transition from one stage of interaction to another. Parameter $I_s = [u / u_*]$ determines the degree of destruction of the soil structure in the process of interaction. For $I_s = 0$, the soil on the contact layer is considered undisturbed, and for $I_s = 1$, it is considered completely destroyed. In other cases, $0 < I_s < 1$. $K_x^D(\sigma_N, I_s)$ is the coefficient of dynamic interaction (as $\dot{u} \to \infty$); $K_x^S(\sigma_N, I_s)$ is the coefficient of quasi-static interaction (as $\dot{u} \to 0$); $\mu_s -$ is the soil shear viscosity parameter related to the soil shear viscosity coefficient η_s.

In [15], the proposed law of interaction, based on the model of a standard linear body and Coulomb's law, has the following form:
under loading to the elastic limit ($du / dt \geq 0,\ 0 \leq u \leq u_*$):

$$\tau_t / K_x^D(\sigma_N, I_s) + \left[\mu_s(\sigma_N, I_s, \dot{u}) / K_x^S(\sigma_N, I_s)\right]\tau = u_t + \mu_s(\sigma_N, I_s, \dot{u})u;$$

beyond the elastic limit under loading ($du / dt \geq 0,\ u > u_*$):

$$\tau = f_u \sigma_N;$$

under unloading to elastic limit ($du / dt < 0,\ 0 \leq u \leq u_*$):

$$\tau_t / K_x^R(\sigma_N, I_s) = u_t;$$

beyond the elastic limit ($du / dt < 0,\ u > u_*$):

$$\tau = 0.$$

American Society of Civil Engineers (ASCE) and American Society of Civil Engineers Technical Council on Lifeline Earthquake Engineering (TCLEE) proposed an idealized elastoplastic model for analysis shown in Fig. 2. Note that the elastoplastic model is completely characterized by two parameters; maximum resistances $t_u,\ p_u,\ q_u$, in the horizontal axial, horizontal transverse, and vertical transverse directions, respectively, having units of force per unit length and maximum elastic displacements $x_u,\ y_u,\ z_u$, having units of distance [15].

Equivalent coefficients of soil spring, having units of force per unit area, are the ratio of the maximum resistance divided by half of the maximum elastic strain, for example $2t_u / x_u$, for a horizontal axial (longitudinal) case. Moreover, this spring coefficient is effective only for relative displacements that are less than the maximum values of $x_u,\ y_u,\ z_u$, after that values the resistance is constant.

Relative displacement parallel to the pipe axis is the result of longitudinal forces of interaction in the pipe-soil system. For elastoplastic models, the ASCE standards provide the following clay and sand ratios:

for sand:

$$t_u = \frac{\pi}{2} D\gamma H(1 + k_0)\tan k\varphi,\ x_u = 2.54 \sim 5.08 \cdot 10^{-3}\,\text{m}, \tag{5}$$

for clay:

$$t_u = \pi D \alpha S_u,\ x_u = 5.08 \sim 10.16 \cdot 10^{-3}\,\text{m}, \tag{6}$$

where $D -$ is the pipe diameter; S_u is the shear force of the surrounding soil; α is the empirical sticking coefficient, varying with S_u; γ is the effective unit weight of soil; $H -$is the depth of embedment from the midline of the pipe; $\phi -$is the sand shear resistance angle; $k_o -$is the coefficient of lateral soil pressure at rest. The value of k_o for normally consolidated loose soils ranges from 0.35 to 0.47. However, the value of k_o may be greater due to joints and strengthening of soil surrounding the pipeline. In [15], $k_o = 1.0$ is recommended for embedment conditions of underground pipelines. Finally, $k -$ is the damping coefficient depending on the external surface

characteristics and the hardness of the pipe. For certain types of pipes, steel or cement-coated cast iron pipes k is 1.0; for cast iron or rough surface steel pipes k ranges from 0.7 to 1.0, and for smooth (even) steel coated pipes or pipes with a smooth surface with relatively hard coating k varies in the range from 0.5 up to 0.7.

It should be emphasized that the model given by formula (5) is a partial case of the Kelvin–Voigt-type interaction model given by (1)–(4) for $\mathrm{I_s} = 1$.

2. Materials, methods and object of study

The solution to the problem of longitudinal oscillations of an underground pipeline is given, taking into account the viscous-elastic-plastic interaction in the "pipe-soil" system. The seismic impact on soil is taken in the form of a traveling sine wave. Based on the data obtained in the experiments, a nonlinear problem is solved for the model of dry friction. The problem is solved under free and fixed boundary conditions. The stress-strain state of an underground pipeline was studied for linear and non-linear interaction with soil. The problems are solved by the finite difference method, taking into account various soil conditions.

3. Formulation of the problem.

Let us consider the problem of longitudinal oscillation of an underground pipeline under viscoelastic-plastic interaction with soil for two types of end fixing. The oscillation equation in relative displacements has the following form:

$$m \cdot \frac{\partial^2 \bar{u}}{\partial t^2} - EF \cdot \frac{\partial^2 \bar{u}}{\partial x^2} + (2\pi R\mu / H) \cdot \frac{\partial \bar{u}}{\partial t} + 2\pi R\tau_i = EF \cdot \frac{\partial^2 u_g}{\partial x^2} - m \cdot \frac{\partial^2 u_g}{\partial t^2}, \tag{7}$$

Boundary conditions are:

$$a)\ \bar{u}(0,t) = 0, \qquad b)\ \bar{u}(l,t) = 0.$$

Initial conditions are zero, i.e.

$$u = 0, \quad u_t = 0 \qquad \text{for} \quad t = 0,$$

where $\bar{u}(x,t) = u(x,t) - u_g(x,t)$ – is the relative displacement between the pipe and soil in the pipeline section x at time t; $u_g(x,t)$ –is the soil displacement in the pipeline section x along the x-axis at time t; $u(x,t)$ – is the absolute displacement of the pipeline section x along the x-axis at time t.

We pass to dimensionless variables using the following formulas:

$$\bar{\bar{u}} = u / A, \ \bar{u}_g = u_g / A, \ \bar{x} = x / a, \ \bar{t} = t / b, \tag{8}$$

where $a = \sqrt{EF / (2\pi R k_x)}, \quad b = \sqrt{m / (2\pi R k_x)}.$

4. Solution methods

To solve equation (7), an implicit scheme of the finite difference method is applied, and the use of the approximations given below leads to second-order accuracy results. The implicit scheme is absolutely stable.

Approximation of the differentials of the function in time and coordinates, (9) and (10), has the following form:

$$\partial^2 \bar{\bar{u}} / \partial \bar{t}^2 \approx \left(\bar{\bar{u}}_i^{j+1} - 2\bar{\bar{u}}_i^{j} + \bar{\bar{u}}_i^{j-1} \right) / \tau^2, \ \partial^2 \bar{\bar{u}} / \partial \bar{x}^2 \approx \left(\bar{\bar{u}}_{i+1}^{j+1} - 2\bar{\bar{u}}_i^{j+1} + \bar{\bar{u}}_{i-1}^{j+1} \right) / h^2, \tag{9}$$

where τ and h – are the time and coordinate steps.

The partial derivative with respect to time and displacement is approximated as follows:

$$\partial \bar{\bar{u}} / \partial \bar{t} \approx \left(\bar{\bar{u}}_i^{j+1} - \bar{\bar{u}}_i^{j-1} \right) / (2\tau), \ \bar{\bar{u}} \approx \left(\bar{\bar{u}}_i^{j+1} + \bar{\bar{u}}_i^{j-1} \right) / 2. \tag{10}$$

To analyze wave propagation, Rashidov and Newmark [15] proposed a simple procedure considering a single traveling wave with an undamped (traveling) waveform. The soil displacement parallel to the pipe can be written as:

$$u_g = A \cdot \sin \omega (t - x / C_p) \cdot H(t - x / C_p), \tag{11}$$

where $H(t-x/C_p)$ – is the Heaviside function, A – is the amplitude of ground motion, ω is the frequency of seismic wave oscillations, determined by formula $\omega = 2\pi / T$; C_p is the “apparent velocity” of wave propagation (hereinafter called the wave propagation velocity in soil). The "apparent velocity" of wave propagation in soil can be large due to the angle of incidence of the wave to the axis of the pipeline or due to the yielding joints of the pipeline.

The law of soil motion under seismic impact is taken as a traveling sine wave given in formula (11).

5. Results and discussion.

The interaction model given in formula (5) for a pipeline with both fixed ends is used. We set the following values of mechanical and geometric parameters: $\gamma_g = 18$ kN/m^3; $\phi = 35^\circ$; $H = 1.2$ m; $x_u = 3 \cdot 10^{-3}$ m; $k_0 = 1$; k=1; $D = 0.4$ m; $s = 0.0095$ m; $A = 0.007$ m; $\rho = 7850$ kg/m^3; $t_u = [\pi D \gamma H (1 + k_0) \tan k\varphi] / 2$; $k_x = 1.266 \cdot 10^4$ kN/m^3.

The wavelength in soil is longer than the length of the pipeline.

For the interaction model according to formula (5), beyond the elastic limit, due to the destruction of the soil structure in areas located closer to the pipeline surface, shear stresses remain constant according to the Coulomb law of dry friction.

Let us present a comparative graph of the results of calculations for models of linear viscoelastic interaction and, in a partial case, for $I_s = 1$, for a model of interaction of the Kelvin-Voigt type according to formulas (1)–(4) [14]. Here, *c* is the coefficient of strengthening of the interaction model, *c*=0 for a viscoelastic model of the interaction of the "pipe-soil" system; *c*=1 for a viscoelastic-plastic model of the interaction of the "pipe-soil" system.

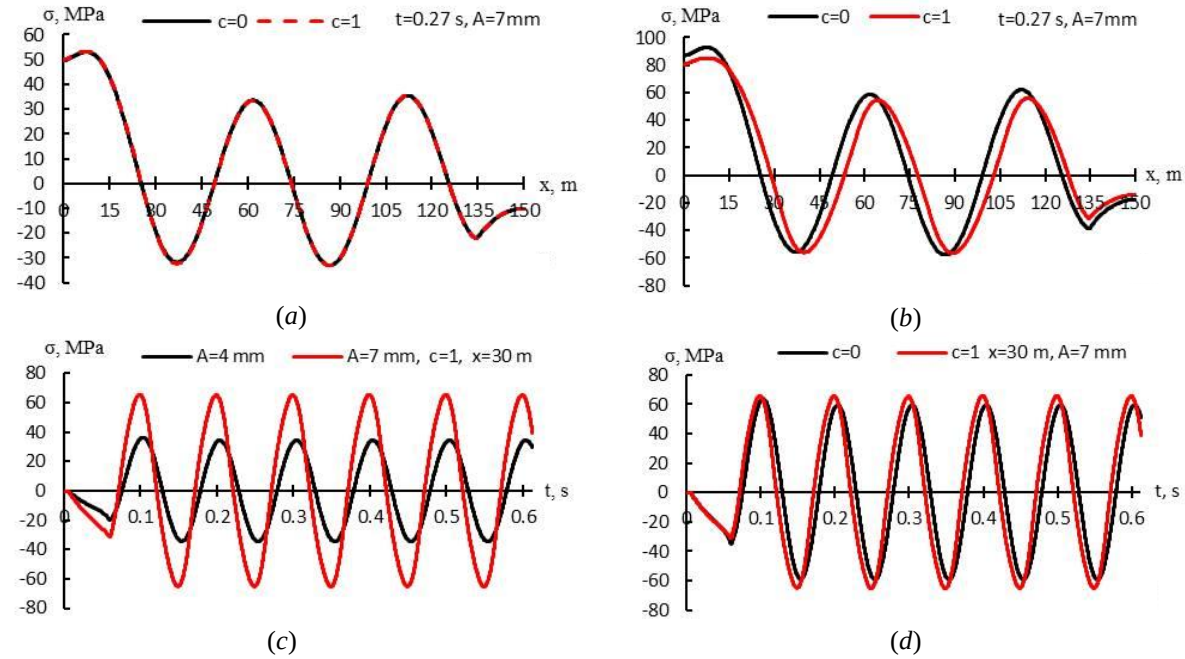

Figure 3. **Comparison of stress changes in coordinate (*a*), (*b*) and in time (*c*), (*d*) for viscoelastic and viscoelastic-plastic interaction of the pipeline with soil**

It was determined that the values of the amplitude of soil vibrations and the elastic limit of interaction play an important role in the stress-strain state (SSS) of an underground pipeline (Figs. 3, *a, b, c, d).*

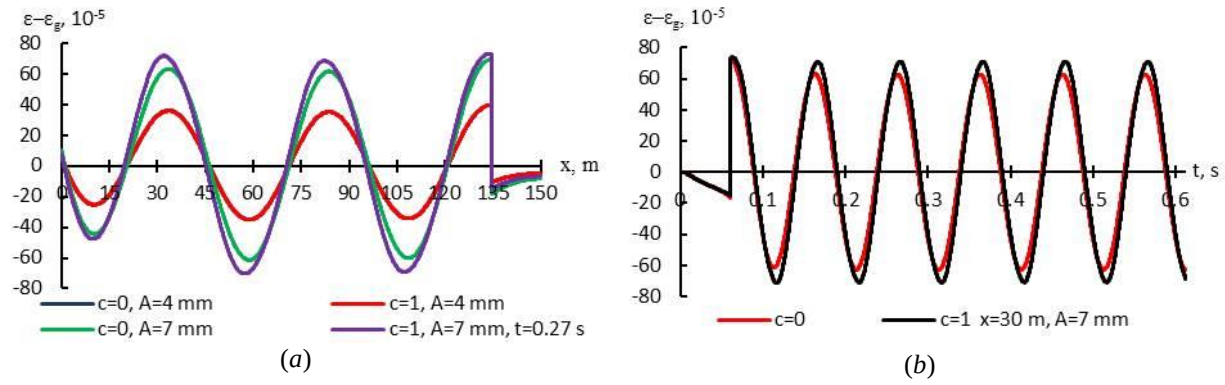

Figure 4. Change in the strain difference of the pipe and soil in coordinate (*a*) and in time (*b*)

The results show that under the interaction in the form of dry friction, the oscillation phase shifts (see Fig. 3, *d*). The amplitude affects the results of the relative displacement and the difference in strains of the pipe and soil, and linear and nonlinear interaction [14]. Comparative results are shown in Figs. 4 and 5.

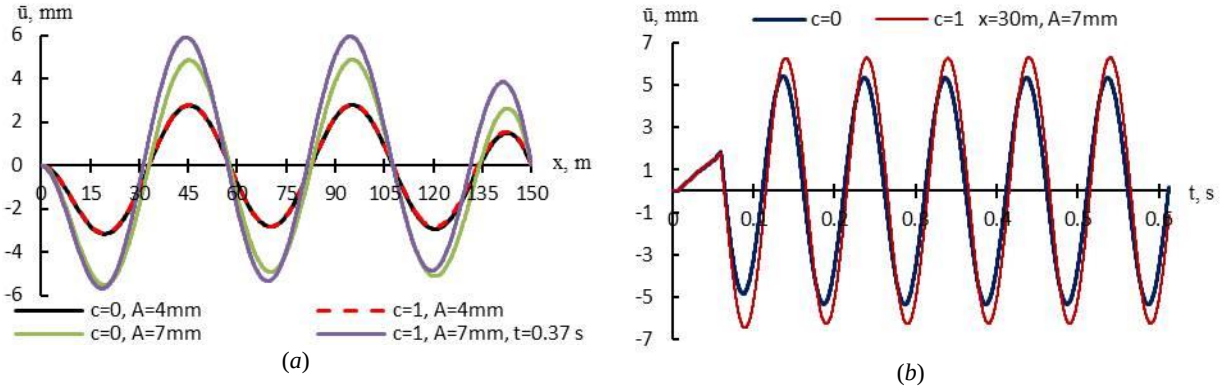

Figure 5. **Change in relative displacement in coordinate (*a*) and in time (*b*)**

The relative displacement of the underground pipeline according to the interaction model by formula (5) is greater than the displacement of the viscoelastic model (see Figs. 5, *a*, *b*).

Figure 6 shows comparative results of viscoelastic and viscoelastic-plastic interaction of an underground pipeline and the phase shift of oscillations.

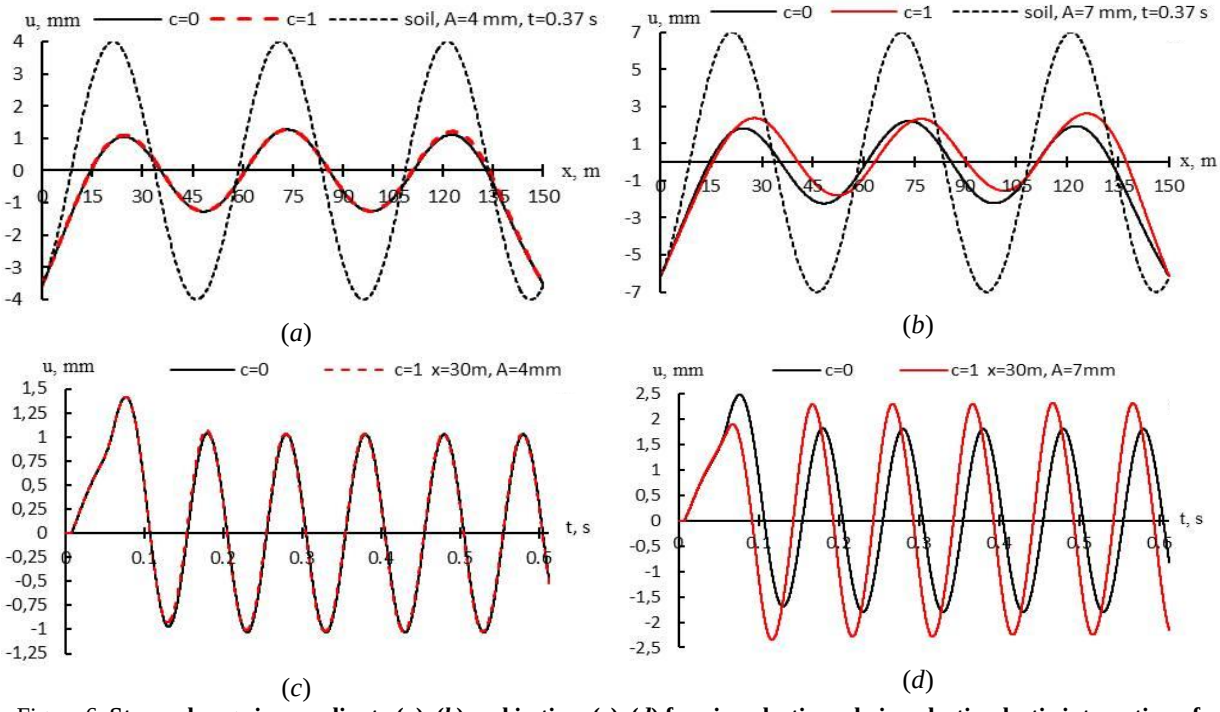

Figure 6. **Stress change in coordinate (*a*), (*b*) and in time (*c*), (*d*) for viscoelastic and viscoelastic-plastic interaction of the pipeline with soil**

Figure 7 shows the interaction cycle of the "pipe-soil" system. To analyze the process, we use the designation R, which takes the following values:
a) for a load up to the elastic limit R=1.1; b) for a load greater than the elastic limit R=1.2;
c) for unloading to the elastic limit R=0.1; d) for unloading lower than the elastic limit R=0.2.

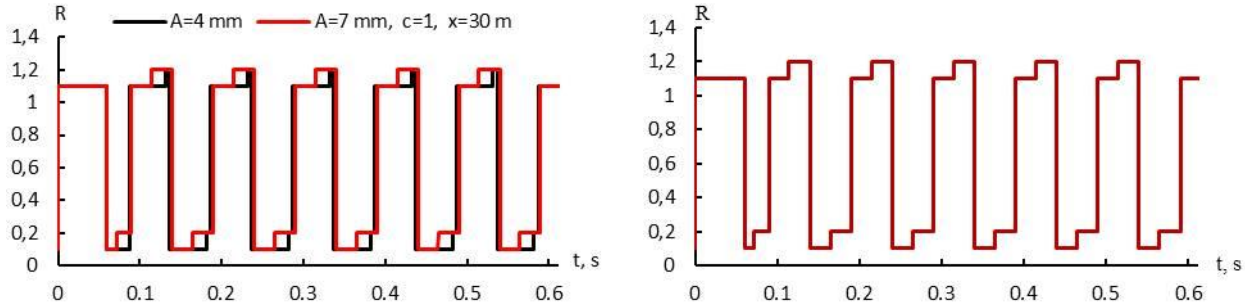

(*a*) (*b*)

Figure 7. **Change in parameter R in time, comparison for A=4 and 7mm (*a*) and for A=7mm (*b*).**

Figure 7, *a* shows a comparison of the load-unload cycle for the amplitudes of ground vibrations for A=4 and 7 mm, and Fig. 7, *b* - for A=7 mm.

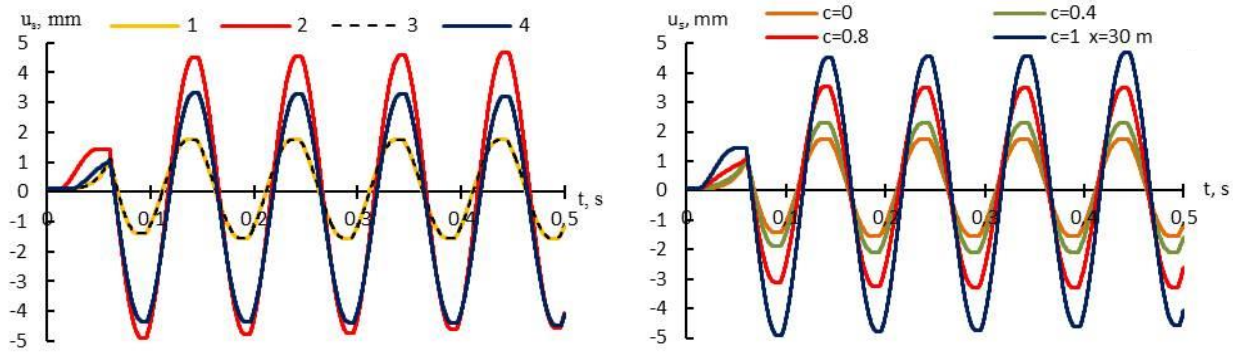

(*a*) (*b*)

Figure 8. **Change in the upper limit of elasticity in time: 1- for c=0, with both ends fixed; 2-for c=1, with both ends fixed; 3 - for c=0, with both ends of the pipeline free; 4 - for c=1, with both ends of the pipeline free**

During cyclic interaction of the "pipe-soil" system, the elastic limit of the interaction changes (Fig. 8).

A comparative analysis shows that an account for the nonlinearity of the pipeline-soil interaction leads to an increase in the relative displacement between the pipe and soil and to a decrease in the normal stress of the pipeline. With both ends of the pipeline fixed to the ground, the maximum relative displacement of the underground pipeline is greater than with the stress-free ends, taking into account the nonlinearity of the interaction.

6. Conclusions

Various patterns of change in displacements and stresses in the sections of steel pipelines in time and coordinate were determined under the influence in the form of a traveling sine wave. In particular, it was shown that the absolute maximum stress values arising when considering the viscoelastic-plastic interaction of the pipeline with soil were less than at viscoelastic interaction, depending on the coefficient of strengthening. The greater the coefficient of strengthening, the lower the stress on the underground pipeline.

A numerical method was developed for solving boundary value problems for partial differential equations, which describes wave processes in pipelines at their viscous-elastic-plastic interaction with the surrounding soil.

Based on the use of data obtained in the experiments, a nonlinear problem was solved for the model of dry friction. The data obtained are illustrated in the form of graphs and substantiated by the analysis of the results.

Embedment of an underground pipeline in a trench in loose and dispersed soils leads to a decrease in strain and, accordingly, in stresses. The use of soil with a lower elastic limit of interaction helps to reduce stresses in the underground pipeline but at the same time, increases the displacement of a pipe.

References

1. *Rashidov T.R.* Dynamic theory of seismic resistance of complex systems of underground structures. Tashkent: Fan, 1973. - 180 p.
2. *Rashidov T.R., Khozhmetov G.Kh.* Seismic resistance of underground pipelines. Tashkent: Fan, 1985. - 152 p.
3. *Seleznev V.E.* Numerical simulation of a gas pipeline network using computational fluid dynamics simulators // Journal of Zhejiang University SCIENCE A. Vol. 5. China, 2007. № 5. P. 755–765.
4. *Sultanov K., Khusanov B., Rikhsieva B.* Underground pipeline strength under non-one-dimensional motion // IOP Conference Series: Materials Science and Engineering 883 (1), 2020. 012023.
5. *Sultanov K.S., Khusanov B.E., Rikhsieva B.B.* Mathematical model of underground structure-soil interaction // IOP Conference Series: Materials Science and Engineering 962 (3), 2020. 032021.
6. *Ronghuan Xu, Ruinian Jiang, Tie-Jun Qu* Review of Dynamic Response of Buried Pipelines // Journal of Pipeline Systems Engineering and Practice, May 2021, Vol. 12, Issue 2.
7. *Sultanov K.S., Loginov P.V., Rikhsieva B.B., Kumakov Zh.Kh.* Destruction of underground extended structures during their contact interaction with soil, XII All-Russian Congress on Fundamental Problems of Theoretical and Applied Mechanics. Ufa, August 19–24, 2019, pp. 803–805.
8. *Sultanov K. S., Vatin N. I.* Wave Theory of Seismic Resistance of Underground Pipelines // Appl. Sci. 2021. (11), №4. 1797. https://doi.org/10.3390/app11041797.
9. *Mirsaidov M., Sultanov T., Yarashov J.* Strength of earth dams considering elastic-plastic properties of soil, Magazine of Civil Engineering, 2021, 108(8), 10813, doi: 10.34910/MCE.108.13
10. Sayapin, S.N., Shkapov, P.M. Application of Bauschinger effect during prolonged storage in stressed state of elements of structures made of fiber reinforced plastic //Journal of Physics: Conference Series, 2019, 1301(1), 012014. https://doi.org/10.1088/1742-6596/1301/1/012014
11. Mirsaidov M.M., Abdikarimov R.A., Khodzhaev D.A., Dynamics of a viscoelastic plate carrying concentrated mass with account of physical nonlinearity of material. PNRPU Mech Bull. № 2. P. 143–155. 2019.
12. Abirov R.A., Khusanov B.E., Sagdullaeva D.A., Numerical modeling of the problem of indentation of elastic and elastic-plastic massive bodies // IOP Conf. Ser.: Mater. Sci. Eng. 971. 2020. 032017. https://doi:10.1088/1757-899X/971/3/032017.
13. Mirsaidov M.M., Usarov M.K., Bimoment theory construction to assess the stress state of thick orthotropic plates // IOP Conf. Ser.: Earth Environ. Sci. 614. 2020. 012090. https://doi:10.1088/1755-1315/614/1/012090.
14. Sultanov K.S., Wave theory of seismic resistance of underground structures. Tashkent: Fan, 2016. - 392 p.
15. *O'Rourke M.J., Liu X.* Response of Buried Pipelines Subject to Earthquake Effects; Monograph Series; Multidisciplinary Center for Earthquake Engineering Research (MCEER), A National Center of Excellence in Advanced Technology Applications: Buffalo, NY, USA, –1999. –249 p.
16. *Khusainov R.B.* Longitudinal Deformation Wave in Buried Pipeline Subject to Viscoelastic Interaction with Soil // Soil Mechanics and Foundation Engineering 2020, vol. 56, pp. 420–426.
17. *Khusainov R.B., Khusainov S.Bu., Khusainova B.B.* Seismodynamics of Underground Pipelines Under Viscous-Elastic-Plastic Interaction with Soil // Soil Mech Found Eng 2023, vol. 59, pp. 544–552.
18. *Khusainov R., Yarashov J., Khusainov S.* Application of finite difference method for solving problem of seismic resistance of underground pipelines // E3S Web of Conferences, 2023, 401, 05046.
19. *Khusainov R.B., Yuldoshev B.Sh., Abdullaev D., Khusainov S.B.* Longitudinal vibrations of underground pipelines of finite length in medium surrounded by soil with different properties along pipeline length // E3S Web of Conferences, 2023, 401, 04060
20. *Ilyushin A.A., Rashidov T.R.* On the effect of a seismic wave on an underground pipeline, News of the AS RUz. Series Tech. Sci. Tashkent, 1971. No. 1. Pp. 37–42.
21. *Shkapov P.M., Sulimov A.V., Sulimov V.D.* Correction of analytical model for lateral-staging rocket with modal data using hybrid optimization algorithms // AIP Conference Proceedings, 2019, 2171, 030013

NONLINEAR WAVE PROCESSES IN RODS WITH EXTERNAL FRICTION.

Loginov P.[1], Akbarov N.[1], Khamidov S.[2]

[1]*Institute of Mechanics and Seismic Stability of Structures named after M.T.Urazbaev, Tashkent, Uzbekistan*

[2]*NRU "Tashkent Institute of Irrigation and Agricultural Mechanization Engineers", Tashkent, Uzbekistan*

E-mail: lopavi88@mail.ru

Abstract. *Numerical solutions to the nonlinear wave problem of longitudinal wave propagation are presented. In this case, soil is an external rod. A wave is initiated on the external rod, and the internal rod is drawn into motion by friction forces that arise between the rods on the surface of their contact, varying according to complex nonlinear laws. The dependences of the stability of numerical solutions on the discretization step of the solution domain in time and space are considered. The optimal values of discretization steps, at which the stability of the numerical results is ensured, are established.*

Keywords: *nonlinear waves, external and internal rods, numerical solution, stability solution.*

1. Introduction

The rod under an impact action is a classical problem, studied by Poisson, Saint-Venant, Navier, and Bernoulli. Saint-Venant considered this problem from the point of view of the theory of wave propagation. Graff [1], Goldsmith [2], Timoshenko [3], Johnson [4], etc. made great contributions to the solution of this problem. The mechanical behavior of rods is quite a complex process, depending on load conditions [5-7], boundary conditions [8-11], and soil parameters [12-18].

In [5], based on Eringen's nonlocal elasticity theory formulated in differential form, the free lateral oscillatory behavior of a functionally graded nanobeam in an elastic matrix with rotationally fixed ends was studied. Euler-Bernoulli beam theory, sine Fourier series, and Stokes transform were used to study the oscillatory behavior of nanobeams with constrained boundary conditions. To study and analyze the effect of deformable boundary conditions on the lateral vibrations of nanobeams, Fourier coefficients obtained by the Stokes transform were used. In [5], explicit formulas for elastic nonlocal boundary conditions at the ends were derived. Using these equations, a useful coefficient matrix was obtained. In addition, the influence of some parameters such as functional gradient index, non-local parameter, and rotation constraints on eigenfrequencies was studied [5] and some conclusions were made.

In [6], the free vibration of a carbon nanotube retained in an elastic matrix subjected to rotational boundary conditions was analyzed based on non-local Eringen’s elasticity. An analytical solution was found for the frequencies of free vibrations of single-walled carbon nanotubes. Using the Fourier series and the Stokes transform a useful coefficient matrix was obtained. The analytical formulation stated in [6] gives a more efficient coefficient matrix for calculating the vibration frequencies of carbon nanotubes with different boundary conditions (rigid or constrained ones). The eigenvalues of this matrix give the oscillation frequencies.

In [7], a nonlocal theory of couple stress was developed to study the static stability and free vibration characteristics of functionally graded nanobeams. The governing equations and the corresponding boundary conditions were derived based on Hamilton's principle and were solved using the Chebyshev-Ritz method, which satisfies different boundary conditions. In [8], based on the nonlocal Eringen theory, longitudinal free vibrations of one-dimensional nanostructures with different boundary conditions were studied. The basic differential equation of motion was solved analytically for different boundary conditions, such as fixed, free, and attached mass and/or spring.

The analysis of free vibrations of embedded carbon and silicon carbide nanotubes lying on an elastic matrix was conducted in [9] based on Eringen’s nonlocal theory of elasticity. The elastic matrix was considered a Winkler–Pasternak elastic foundation and an axial elastic medium for the models of beam and rod, respectively. The beam and rod vibration formulas were obtained using Hamilton's principle. The resulting equations of motion were solved by the separation of variables method and the finite element method based on Hermite polynomials for different boundary conditions. In [10], the free axial vibration of Rayleigh nanorods with axial constraints was studied using Eringen’s nonlocal elasticity theory. The boundary conditions and equation of motion were

obtained using Hamilton's principle. Elastic spring boundary conditions play an important role in the dynamic analysis of nanorods [11].

The results of laboratory experiments on dynamic compression of loess soil samples were presented in [12]. Based on experimental results, preliminary values of the mechanical characteristics of soils were determined. The numerical solution to the wave problem, the statement of which is identical to the experimental conditions, was obtained. Based on the analysis of the results of the numerical solution to the wave problem, the conditions for quasi-static strain of soil under dynamic loading during the experiment were obtained. By comparing the experimental results with numerical calculations and the method of successive approximation, refined values of mechanical characteristics of loess soils were determined based on an elastic-viscous-plastic model of soil strain.

In [13], the mechanical characteristics of soils under static and dynamic strains were determined experimentally. The system of partial differential equations of hyperbolic type, describing the wave process, was solved by the method of characteristics and the finite difference method in an implicit scheme. Using a numerical solution, changes in wave parameters over time were obtained for different sections of the soil layer. The effect of layer thickness on the wave parameters and the quasi-static process was demonstrated experimentally.

In [14], a one-dimensional statement of the nonstationary wave problem on the propagation and reflection of a longitudinal monochromatic wave from a rigid stationary barrier adjacent to an underground pipeline was given. The linear viscoelastic Eyring model, which describes constrained creep and relaxation, was taken as the law of pipeline strain. The problem was solved numerically using the theory of characteristics followed by the finite difference method using an implicit scheme. The study analyzes numerical solutions obtained in the form of dependencies of plane wave parameters: longitudinal stress, velocity, and strain for fixed sections of the pipeline. Analysis of variation in these wave parameters shows that at high frequencies of the dynamic load generating the wave, the stress amplitude in the pipeline increases two or more times compared to the load amplitude. This is due to the superposition of incident and reflected waves in the pipeline and the high rate of pipeline loading. At low frequencies of dynamic loading, such an increase is not observed due to the low rate of loading. The numerical solutions obtained allow one to choose the statement of problems on the dynamic stress state of an underground pipeline depending on the frequency of the incident wave. It is shown that the highest longitudinal stresses in an underground pipeline arise at points (sections) close to its connection with a rigid, stationary solid body.

The reliability of underground main pipelines in most cases is assessed by their strength [15]. When determining the strength of underground pipelines under seismic impacts, the calculations must consider the forces of the longitudinal interaction of the pipe with soil (friction force). As shown in [15], the interaction forces on the contact surface of an underground pipeline with soil are of complex pattern and depend on the parameters of waves in soil and in the pipeline. Based on the numerical results of solving one-dimensional non-stationary problems of coupled waves for the interacting “underground pipeline-soil” system, the pattern of changes in interaction forces in the pipeline-soil contact surface is determined. It was established that an account for static and dynamic soil pressure normal to the contact surface leads to quantitatively different results compared to considering static pressure only. It is shown that when solving problems of reliability of underground main pipelines under seismic impacts, first, it is necessary to consider the dynamic stress-strain state of soil in the vicinity of the pipeline.

Mechanical characteristics of soils under dynamic and static loads were determined in laboratory conditions using special instruments [16]. Dynamic loads were initiated in devices by an impact on a soil sample. Upon impact, waves were initiated in soil; they significantly influence the stress-strain state of soil samples placed in the device. Depending on the parameters of the shock load in the device, stress-strain states of different qualities and quantities arise in different parts of the soil sample. The mechanical characteristics of soils, determined by the stress-strain state, also differ. The effect of the stress-strain state of soil on its mechanical characteristics can be assessed theoretically. The occurrence of the wave process and the dynamic stress-strain state in a soil

sample placed in the device can be theoretically examined in detail. In this regard, a wave problem was posed, corresponding to the formulation of experiments on the device of dynamic loading of soil. The law of soil strain was assumed elastic-viscous-plastic. The numerical solution to the wave equations was obtained by the finite difference method. Based on an analysis of the stress-strain state of soils in various sections, obtained by numerical calculations, a condition was derived under which the influence of wave processes on the mechanical characteristics of soils was excluded. This condition establishes a relationship between the wavelength, the speed of wave propagation in soil, the thickness of the soil sample in the device, and the duration of the dynamic load. Experimental diagrams between stress and strain components for soft soils are nonlinear [17]. Nonlinear diagrams are qualitatively different for soils of undisturbed and disturbed structures.

In addition, numerical methods were used to study the longitudinal impact; for example, the finite difference method [19], the finite element method [20-23], the boundary element method [24], and others.

Using the finite difference method, nonlinear equations describing elastic dynamic strains after buckling were solved for two types of problems related to shock buckling of straight rods [19]. The initial mode of dynamic buckling with a small amplitude parameter, given by the dual-parameter solution, was used as the initial condition for the nonlinear solution after buckling. Particular attention is paid to the mechanism of growth and propagation of buckling strain in the rod and the interaction of the axial stress wave with the buckling strain under the impact process.

In [20], a simulated visualization of wave propagation in an elastic rod with damage was presented to improve the understanding of the physical phenomenon and determine the location and severity of damage. The rod has one end fixed and the other free end is exposed to a rigid mass. Consequently, a longitudinal shock wave is generated at the contact end and passes through the rod. Rods with and without damage were inspected. A finite element model was constructed to simulate wave propagation. The mechanism of initiation and propagation of secondary waves due to damage was identified. It is noteworthy that a standing stress wave is created at the damage location, and resides in. The form of the damage determines the shape of this standing wave.

Finite element formulation to analyze the propagation of a stress wave in an elastic rod hitting a rigid body was developed in [22]. The rod has rigid, free, or deformable conditions of support. The formulation is based on Saint-Venant's contact theory. Accordingly, the equations of motion are introduced and an equivalent finite element formulation is obtained. In this way, the dynamic responses are illustrated and the contact forces are estimated. Some simulation results are compared with the analytical results published. The results demonstrate the influence of conditions of support on the propagating stress wave and consequently on velocities, displacements, and contact forces. To improve the understanding of the phenomenon, a simulated visualization of the reflection and transmission of the stress wave at the end of the constraint is presented.

In [24], using the collocation method, a homogeneous matrix equation was obtained that depends on the frequency and wave number of the guided wave. The dispersion equation for guided waves is then obtained by finding nontrivial solutions to the matrix equation. Numerical results are shown for square bars, rectangular bars, and L-shaped bars. The dispersive properties of guided waves in rods are discussed and compared with results for Lamb modes in a two-dimensional plate.

The solution to the problem of wave propagation in soils received the attention of such scientists as Kh.A. Rakhmatulin, S.S. Grigoryan, G.M. Lyakhov, K.S. Sultanov, et al. In [25, 26], experimental and theoretical interaction of rigid bodies with soil were studied.

In [26], it is shown that seismic resistance of underground pipelines should be considered based on the theory of seismic wave propagation in soil and the interaction of seismic waves with underground pipelines, i.e., on the basis of the wave theory of seismic resistance of underground pipelines. Based on the wave theory, a one-dimensional combined problem of seismic resistance of underground pipelines under seismic impacts was formulated. An algorithm and program for the numerical solution of the wave problems posed using the method of characteristics and the finite difference method were developed. Analysis of the laws of interaction between underground pipelines and soil under seismic impacts shows that in calculations, it is necessary to use interaction

laws that consider all interaction processes observed in experiments. Analysis of the numerical solutions obtained and related problems posed of the wave theory of seismic resistance of underground pipelines shows the mechanisms of the occurrence of longitudinal stresses in underground pipelines under seismic impacts. The calculation results showed that consideration of dynamic stresses normal to the outer surface of the underground pipeline leads to a multiple increase in longitudinal stresses in the underground pipeline. Based on the results of the analysis, a theory of the process of seismic wave propagation in an underground pipeline and the surrounding soil was proposed.

Based on the experimental results, the laws of interaction between underground pipelines [27] and soil were constructed.

In [27], the interaction of a semi-infinite underground pipeline with the surrounding soil under longitudinal seismic wave propagation was considered. The wave propagated in soil with a front perpendicular to the axis of the pipeline, and nonlinear laws of interaction (friction) at the surface of their contact, including the Amonton-Coulomb law, were used to solve related wave problems for the pipeline and soil. To solve these problems numerically, the method of characteristics and the finite difference method were successively used. The implementation of the law of interaction processes (friction) depended on the wave parameters in soil and the mechanical characteristics of soil. It was determined that a wave in soil when contacting a pipeline generates a powerful wave in the pipeline. The amplitude of this wave is many times greater than the wave amplitude in soil, and it propagates through the pipeline without attenuation. The dependences of the amplitude of this wave on the parameters of the law of friction, waves in the soil, and mechanical characteristics of soil were determined. It was shown in [17, 28] that the experimental diagrams between the stress and strain components for soft soils are nonlinear and differ for soils of different structures.

In [28], the propagation of longitudinal waves in a viscoelastic medium was studied. A mathematical model of the problem of a linear viscoelastic medium was developed. The problem under consideration was reduced to solving a system of differential equations, solved by the method of characteristics, with the corresponding boundary conditions. The results were compared with known results obtained by other authors; the comparison shows the adequacy of the problem posed. It was established that the maximum values of stress, strain, and velocity of particles in viscous media vary according to a nonlinear law. In the initial section of the medium and near it, the stress first reaches a maximum, and then strains and particle velocities reach their maximum values.

2. Methods.

The initial sections of the rods under consideration coincide at x=0, but they have significantly different strengths. Here the external rod is soil, and the internal rod is the pipeline. Equations of motion of the rod and soil considering friction have the following form:

$$\begin{aligned} &\rho_{0i}\partial v_i / \partial t - \partial\sigma_i / \partial x + \chi_i \sigma_{\tau i} = 0 \\ &\partial v_i / \partial x - \partial\varepsilon_i / \partial t = 0 \end{aligned} \tag{1}$$

here v_i - is the particle velocity; σ_i - is the longitudinal stress, ε_i - is the longitudinal strain; ρ_{0i} - is the initial density; $\chi_i = sign(v)$ for a rod, $\chi_i = -sign(v)$ for soil; v -is the relative velocity; σ_τ - is the reduced friction force, t - is time.

σ_τ for a pipeline and soil are determined from (2):

$$\sigma_{\tau i} = 4D_{Hi}\tau / (D_{Hi}^2 - D_{Bi}^2) \tag{2}$$

where τ - is the friction force (shear stress) acting between the pipeline and soil; D_{Hi} - are the outer diameters, and D_{Bi} - are the inner diameters of the pipeline and soil.

The equations of state of the rod and soil are taken in the form of (3), where at i = 1 the parameter values relate to the pipeline, and at i = 2, they relate to soil:

$$\frac{d\varepsilon_i}{dt} + \mu_i \varepsilon_i = \frac{d\sigma_i}{E_{Di} dt} + \mu \frac{d\sigma_i}{iE_{Si}} \tag{3}$$

$$\mu_i = E_{Di} E_{Si} / (E_{Di} - E_{Si}) \eta_i$$

The solution to the problem is reduced to the integration of system (1), closed by equation (3), solved separately for the pipeline and for soil. The law of friction, for $\sigma_N > \sigma_N^*$ (for $\sigma_N \le \sigma_N^*$, τ) is represented by the following relations:

for $0 \le u \le u_*$

$$\frac{d\tau}{K_x^D(\sigma_N, I_S) dt} + \mu_S(\sigma_N, I_S, \dot{u}) \frac{\tau}{K_x^S(\sigma_N, I_S)} = \frac{du}{dt} + \mu_S(\sigma_N, I_S, \dot{u}) u \tag{4}$$

for $du/dt \ge 0,\ \ u > u_*$

$$\tau = f_u \sigma_N \tag{5}$$

for $du/dt < 0,\ \ u \ge u_*$

$$\tau = 0 \tag{6}$$

here $K_x^D(\sigma_N, I_S)$ - is the function of dynamic interaction, and $K_x^S(\sigma_N, I_S)$ - is the function of quasi-static interaction; μ_S - is the function of parameter of soil shear viscosity related to the function of soil shear viscosity $\eta_S = (\sigma_N, I_S, \dot{u})$ - by the following relation:

$$\mu_S = K_x^D K_x^S / (K_x^D - K_x^S) \eta_S \tag{7}$$

The wave process is originated in the initial section by a load varying according to the following law:

$$\sigma_i = \sigma_{\max} \sin(2\pi t / T) \qquad 0 \le t \le \theta \tag{8}$$

where $\sigma_{\max}$ - is the amplitude, T - is the period of oscillation, and θ - is the duration of the load.

The boundary conditions for the initial section of soil are (8), and for the rod, they are $\sigma_1 = 0$; at the wave front in the rod:

$$\sigma_1 = -C_{01} \rho_{01} v_1; \quad v_1 = -C_{01} \varepsilon_1; \quad C_{01} = (E_{D1} / \rho_{01})^{1/2} \tag{9}$$

and at the wave front in soil:

$$\sigma_2 = -C_{02} \rho_{02} v_2; \quad v_2 = -C_{02} \varepsilon_2; \quad C_{02} = (E_{D2} / \rho_{02})^{1/2} \tag{10}$$

where c_{0i} - are the wave front velocities in the rod and soil, respectively.

Calculations were conducted using a numerical solution to equations (1)-(3) taking into account (4)-(10), using the method of characteristics and the finite difference method.

3. Results.

The following values were selected as initial data: for the first rod (a pipeline) $D_{H1} = 0.2$ m, $D_{B1} = 0.18$ m, $\rho_{01} = 7800$ kg/m^3, $\mu_1 = 10^4$ s^{-1}, $C_{01} = 5000$ m/s, $\gamma_1 = 1.02$, $E_{D1} = C_{01}^2 \rho_{01}$, $E_{S1} = E_{D1} / \gamma_1$; for the second rod (soil medium) $\rho_{01} = 1800$ kg/m^3, $C_{01} = 1000$ m/s, $K_\sigma = 0.3$, $\mu_2 = 1000$ s^{-1}, $\gamma_2 = 1.1$, $E_{D2} = C_{02}^2 \rho_{02}$, $E_{S2} = E_{D2} / \gamma_2$.

Figure 1. **Changes in particle velocity over time in the rod sections at x = 5 m.**

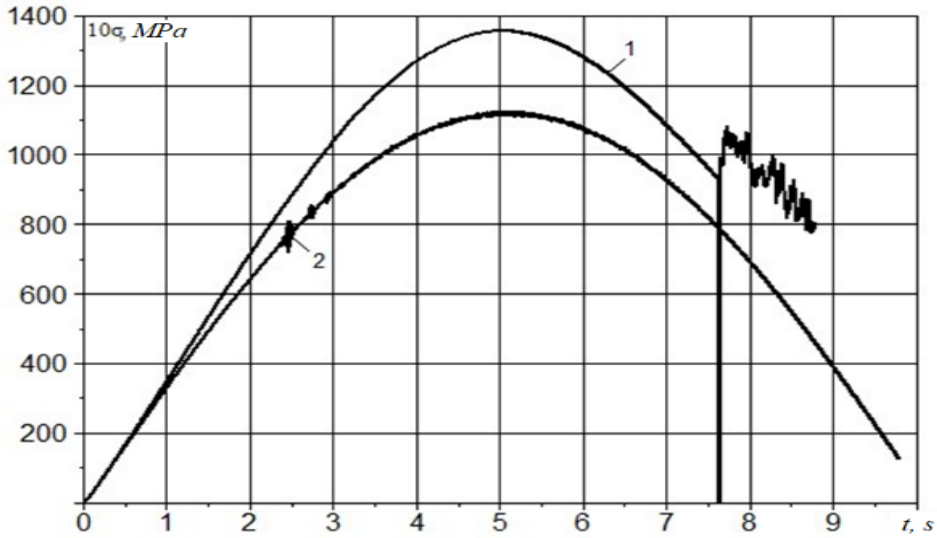

Figure 2. **Changes in longitudinal stress over time in the rod sections at x = 5 m.**

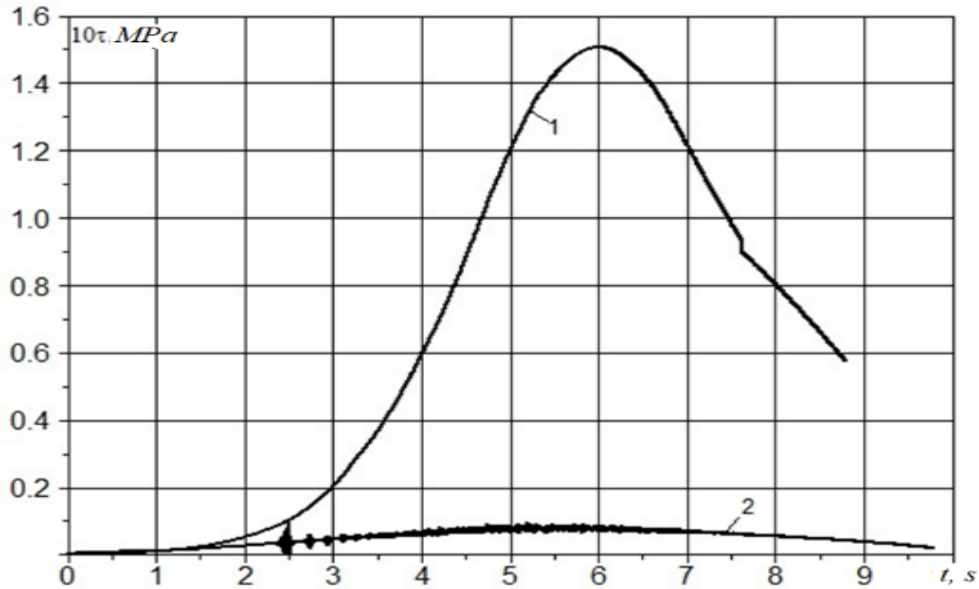

Figure 3. **Changes in friction force in the rod sections at x = 5 m.**

4. Analysis

The calculation results given in Fig 1 were obtained at values $\Delta tr = 10^{-6}$ sec; $\Delta xr_2 = 5*10^{-4}$ m; $\Delta xr_1 = 5*10^{-3}$ m and $\Delta tr = 10^{-5}$ sec; $\Delta xR_2 = 5*10^{-3}$ m; $\Delta xR_1 = 5*10^{-2}$ m. At the oscillation period of a load T = 20 sec, a wave with frequency f = 0.05 sec^{-1} propagates along the rod. Fig 1 shows the

changes in velocity over time in the rod section at x = 5 m. The velocity of the particles smoothly increases from the very beginning, reaches the maximum, and decreases. Here, curve 1 refers to the change in section velocity of the second rod (a leading rod), and curve 2 refers to the first rod (a driven (involved) one). The difference in velocities in the same sections of rods, after the velocities reach maximum values, becomes smaller and alternating in sign. An increase in discretization steps led to bifurcations of wave parameters already in the area of increasing values of velocities and stresses of rod sections (curves 3 and 4 in Fig 1, curve 2 in Fig 2). Then, the bifurcation increases, but occurs over a certain interval of width 0.1-0.4 m/sec in terms of velocity values (Fig 1, curves 3, 4) and over a very small interval in terms of stress values (Fig 2, curve 2). Note that bifurcation in all cases occurs only in the pipeline. No bifurcation is observed in soil (curves 1 and 3, Fig 1). An increase in the values of the discretization steps Δt and Δx_i (second option) by an order of magnitude leads to a decrease in the velocity values by 16% in both rods and the stress by 18% in the first rod in terms of the maximum values. This is associated with the values of the friction force on the contact surface of rods (Fig 3), determined by equations (4) - (6). Here curve 1 shows the changes in shear stress in the first option and curve 2 - in the second option. Reliable values of the parameters of nonlinear wave processes described by nonlinear equations must be obtained by numerical experiments with different discretization steps. Here, the decrease in steps Δt and Δx_i continues until the wave process is stable.

5. Discussion and Conclusions

Numerical analysis shows that in this formulation of the problem when rods with different stiffness characteristics interact, the values of longitudinal stress greatly increase in the pipeline. The longitudinal stress in soil remains almost constant (0.3 MPa). In the first rod, the maximum longitudinal stress increases to 135 MPa, which is 450 times higher than in the second rod. It has been established that in nonlinear wave processes in interacting coaxial rods, a loss of stability of numerical solutions occurs, depending on the discretization steps of the solution domain on characteristic plane t, x. The values of the wave parameters also depend on these steps. A multiple increase in the maximum longitudinal stress in the driven rod is shown during a low-frequency nonlinear wave process in interacting rods with significantly different stiffness characteristics.

References

1. *Graff K.F.* Wave motion in elastic solids / Courier Corporation. 2012, 688 p.
2. *Goldsmith W.* The theory and physical behaviour of colliding solids / Dover Publ. 1999, 379 p.
3. *Timoshenko S.* Vibration problems in engineering. second ed / Wolfenden Press. 2008, 476 p.
4. *Johnson W.* Impact strength of materials / Publisher Hodder Arnold 1972, 376 p.
5. *Yayli M.Ö.* Free vibration analysis of a rotationally restrained (FG) nanotube // Microsystem Technologies. 2019. vol. 25, No 10. P. 3723–3734.
6. *Yayli M.Ö.* Free vibration analysis of a single- walled carbon nanotube embedded in an elastic matrix under rotational restraints // Micro & Nano Letters. 2018. vol. 13, No 2. P. 202–206.
7. *Ebrahimi F., Barati M.R., Civalek Ö.* Application of Chebyshev–Ritz method for static stability and vibration analysis of nonlocal microstructure-dependent nanostructures // Engineering with Computers. 2020. vol. 36, No 3. P. 953–964.
8. *Numanoğlu H.M., Akgöz B., Civalek Ö.* On dynamic analysis of nanorods // International Journal of Engineering Science. 2018. vol. 130. P. 33–50.
9. *Civalek Ö. et al*. Size-dependent transverse and longitudinal vibrations of embedded carbon and silica carbide nanotubes by nonlocal finite element method // The European Physical Journal Plus. 2020. vol. 135, No 4. P. 381.
10. *Yayli M.Ö.* Axial vibration analysis of a Rayleigh nanorod with deformable boundaries // Microsystem Technologies. 2020. vol. 26, No 8. P. 2661–2671.
11. *Yayli M.Ö.* Free longitudinal vibration of a nanorod with elastic spring boundary conditions made of functionally graded material // Micro Nano Lett. 2018. vol. 13, No 7. P. 1031–1035.
12. *Loginov P. V., Salikhova Z.R., Sultanov K.S.* Experimental and Theoretical Method for Determining Mechanical Characteristics of Soils under Dynamic Loads // Mechanics of Solids. 2019. vol. 54, No 6. P. 915–928.
13. *Sultanov, K.S., Loginov, P. V, Ismoilova, S.I., Salikhova, Z.R.* Quasistaticity of the process of dynamic strain of soils. // Magazine of Civil Engineering. 2019. vol. 85, No 1. P. 71–91.

14. *Ismoilova S.I., Loginov P.V., Khamidov S.S., Akbarov N.A., Kumakov J.X.* Dynamic stress state of underground pipelines at junctions // IOP Conference Series: Materials Science and Engineering. 2020. vol. 869, No 5. P. 052013.
15. *Ismoilova S.S., Loginov P.V., Khamidov S.S., Akbarov N.A., Kumakov J.X.* Force properties of longitudinal interaction of the underground pipeline with soil // IOP Conference Series: Materials Science and Engineering. 2020. vol. 869, No 5. P. 052036.
16. *Sultanov K.S., Loginov P.V., Ismoilova S.I., Salikhova Z.R.* Wave processes in determining mechanical characteristics of soils // E3S Web of Conferences / ed. Volkov A. et al. 2019. vol. 97. P. 04009.
17. *Sultanov K.S., Loginov P.V., Ismoilova S.I., Salikhova Z.R.* Variable moduli of soil strain // E3S Web of Conferences / ed. Volkov A. et al. 2019. vol. 97. P. 04013.
18. *Sultanov K.S., Khalikulov E.K., Loginov P. V.* Definition of dynamic loads on conveyor bearing edge of Muruntau open pit // Gorniy Zhurnal. 2013. vol. 8, No 1. P. 36-38.
19. *Wang A., Tian W.* Mechanism of buckling development in elastic bars subjected to axial impact // International Journal of Impact Engineering. 2007. vol. 34, No 2. P. 232–252.
20. *Elkaranshawy H.A.* Stress Waves in a Damaged Rod Subjected to Longitudinal Impact // International Journal of Mechanical Engineering and Robotics Research. 2019. P. 488–493.
21. *Ragab S.A., Fayed H.E.* Introduction to Finite Element Analysis for Engineers // Introduction to Finite Element Analysis for Engineers. CRC Press, 2018.
22. *Etiwa R.M., Elabsy H.M.*, Elkaranshawy H.A. Finite Element Analysis of the Longitudinal Impact of a Rod with Various Support Conditions // International Journal of Mechanical Engineering and Robotics Research. 2021. P. 626–632.
23. *Kulkarni R.B., Gopalakrishnan S., Trikha M.* Impact force identification in structures using time-domain spectral finite elements // Acta Mechanica. 2020. vol. 231, No 11. P. 4513–4528.
24. *Gunawan A., Hirose S.* Boundary element analysis of guided waves in a bar with an arbitrary cross-section // Engineering Analysis with Boundary Elements. 2005. vol. 29, No 10. P. 913–924.
25. *Sultanov K.S.* Wave theory of seismic resistance of underground structures / Tashkent: FAN. 2016, 392 p.
26. *Sultanov K.S., Vatin N.I.* Wave Theory of Seismic Resistance of Underground Pipelines // Applied Sciences 2021. vol. 11, No 4. P. 1797.
27. *Sultanov K.S.* Contact interaction of an underground pipeline with soil under dynamic impacts // Facta Universitatis, Series: Mechanical Engineering. 2024. vol. 23, No 2.
28. *Khamidov S.S., Loginov P.V., Akbarov N.A.*, Propagation of longitudinal waves in a linear viscoelastic medium // E3S Web of Conferences. 2023. vol. 458, 08013

ANALYTICAL METHOD FOR SOLVING THE PROBLEM OF CALCULATING THREE-LAYER PLATES

Mamasoliev K.M.[1], Sindarov J.A.[1]

[1]*Samarkand State University of Architecture and Civil Engineering, Samarkand, Uzbekistan.*

E-mail: q-mamasoliev@mail.ru

Abstract: *Two rectangular plates lying on an elastic half-space, located symmetrically above each other, in the form of layers, are considered. It is assumed that an elastic filler is installed between the plates. Such structures are called three-layer plates lying on an elastic half-space. A closed system of integro-differential equations is obtained that solves the problem in displacements; solutions to the problem in analytical form allow obtaining results that are more exact. The method for solving the problem is based on the approximation of orthogonal polynomials. A test example is provided. Based on the results of a study of the problem of bending of three-layer beam plates lying on an elastic foundation, a corresponding example, and numerical calculations, conclusions were drawn on the influence of the filler and external forces on the internal forces in the plate.*

Keywords: *three-layer plate, filler, half-space, integro-differential equation, closed system, infinite.*

1. Introduction

Multifactor studies of the stress-strain state of contacting bodies are among the pressing problems in the field of mechanics. Among such contacting bodies, structures on a deformable base present a relevant issue.

When assessing various interaction factors of critical parts of engineering structures, modeling and methods for solving contact problems of elasticity theory are widely used. Improving the performance of engineering structures is directly related to the need to improve the level and quality of their design. When performing design and calculation work and constructing structures, it is necessary to consider the multifactorial interactions of structural elements. Such structures include foundations of industrial and civil buildings, airfields and road surfaces, and many others.

The above determines the need to develop multifactor effective mathematical models and calculation methods to implement in the design and calculation work and construction of objects. The proposed models and calculation methods should lead to ones that are more economical.

In [1, 2], an algorithm and program for the numerical solution of wave problems using the method of characteristics and the finite difference method were developed. In [3], the vibrations of a rod protected from vibrations generated by kinematic excitations were studied. In [4], the influence of the interaction of foundation plates with the base was studied, and in [5], the stress-strain state of asymmetrically layered plates with controlled forces interacting with a sandy base was considered.

In [6], the process of free and forced vibrations of a beam system with intermediate supports was studied. Analytical solutions were obtained to ensure effective results in design work.

The dynamic localization of deformations of ductile polymer rods under large tensile strains up to failure was investigated in [7], and in [8], a unified procedure was proposed for analyzing the behavior of free and transient vibrations of a composite laminated beam under general boundary conditions in a thermal scenario.

In [9], the propagation of a longitudinal wave in a cylinder with active external friction over a limited area was considered, and in [10], the propagation of oscillatory waves and assessment of the level of their impact on various objects were studied. Mathematical models and methods for assessing the levels of vibration waves at various distances from the soil base were developed.

In [11], an effective theoretical solution was proposed for studying the time response of an elastic thin plate interacting with multilayer transversally isotropic soils, and in [12], a new method for assessing deformations based on their monitoring was proposed.

The study in [13] presents a comparative analysis of nonlinear vibrations of plates made of pure polymer and three types of plates made of a polymer composite, and in [14, 15], experimental and numerical analyses were conducted to determine the ultimate strength for modeling stiffeners and a support plate.

In [16, 17], the problem of bending of multilayer strip-plates lying on an elastic foundation was studied. An assessment of internal forces in plates was conducted based on the approximation of orthogonal polynomials.

In [18], an interaction function was constructed based on axial compression (tension) and shear loads of orthotropic plates, and in [19], an approach to dynamic modeling of a multi-plate structure connected by nonlinear hinges was presented. It was shown that linear modes play an important role in dynamic analysis.

References [20, 21] provide a brief overview of the development of mathematical models, and methods of elastic analysis of inhomogeneous solids and viscoelastic foundations in oscillatory systems.

In [22, 23], a mathematical model was obtained and an analytical method was used to solve the problem. To estimate the internal forces of the plates, orthogonal polynomials were used. Corresponding conclusions were presented on the influence of base and filler pressure on internal forces in the plate.

In [24], a mathematical model was developed for assessing the stress-strain state of earth dams using a spatial model based on the variational Lagrange equation, considering the real geometry, material properties, and heterogeneous design features of structures.

A model analysis of the honeycomb pattern of the structure was conducted in [25], for various parametric conditions using the finite element method.

In [26], a numerical algorithm for solving odd differential equations using the Runge-Kutta method, suitable for dynamic systems, was created.

In [27, 28], modifications of the structure made from composite laminate plates were studied. The results of experimental and numerical analysis affecting the connection relationships of the structure were presented.

Researchers have developed various calculation methods based on different models. However, there is a need to develop analytical calculation methods that model the interaction between structures and the soil foundation to ensure accurate results.

2. Statement of the problem.

Consider a structure consisting of two plates and an filler between them, working together as a three-layer structure. The structure is free and fits tightly into the elastic half-space. We assume that the top plate is loaded with an external load acting uniformly along any straight guides along the plate, and arbitrarily across the plate. Each plate is affected by the reactive pressures of the filler. To evaluate the reaction of the elastic filler, according to the Winkler-Zimmerman hypothesis, we take a value proportionally equal to the differences in the deflections of the plates. The bottom plate is acted upon from above by the reactions of the filler, and from below by the reactive pressures of the elastic base. To mathematically model the problem, we select from the structure a unit part across it, the width of which is equal to one. In this case, the three-dimensional problem under consideration is reduced to a one-dimensional problem, i.e. to the study of the stress-strain state of three-layer beam plates lying on an elastic foundation (Figure 1).

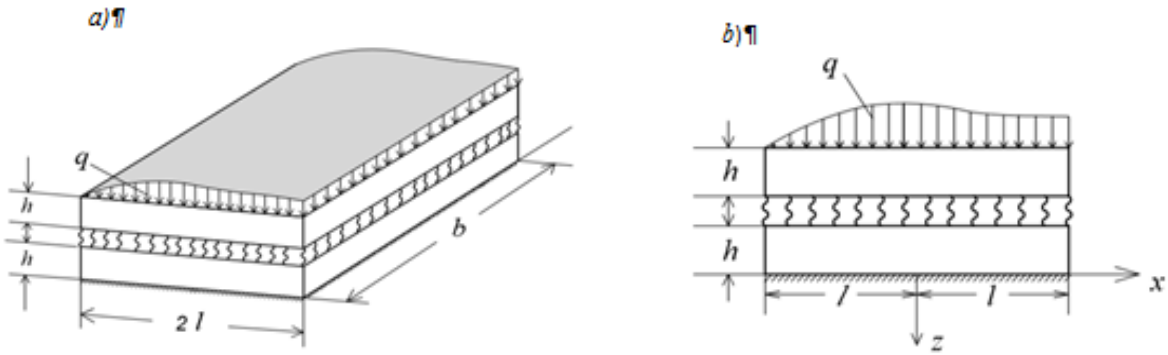

Figure 1. - **a) Design diagram of a three-layer plate, b) Design diagram of three-layer beam plates.**

3. Math modelling

We introduce designations for beam plates:

W_1, W_2 and $D_1, D_2 -$ are the deflections and cylindrical stiffness of the first and second plates; $h, 2l -$ are the height and length of beam plates; $q -$ is the external load; p and $k(W_1 - W_2) -$ are the reactive pressures of the base and filler; $k -$ is the filler hardness coefficient.

For convenience, we set the origin of the Cartesian coordinate system at the center of symmetry of the neutral axis of the first beam plate. Then the deflections of the beam plates, the external load, and the reactive pressures of the foundation will be functions of the variable x, which is $x \in [-l; l]$.

Satisfying the equilibrium conditions of the structure, based on the laws of the theory of elasticity, we derive the following system of fourth-order differential equations regarding the deflections of beam plates:

$$D_r W_r^{IV} = \delta_r q + (-1)^r (W_2 - W_1) - \delta_{r-1} p, \qquad r = 1,2. \tag{1}$$

where δ_1=1, $\delta_0 = \delta_2 = 0$.

To determine precipitation V, for a homogeneous base, we accept the following formula:

$$V = \frac{2(1 - \nu_0^2)}{\pi E_0} \int_{-l}^{l} K(x - s) p(s)\, ds. \tag{2}$$

Here, E_0 and ν_0 are the elastic modulus and Poisson's ratio of the base material, respectively; $K(x - s)$ is the kernel of the integral equation (2), represented in the following form:

$$K(x - s) = ln \frac{1}{|x - s|} \tag{3}$$

Based on the above assumptions, there is a two-way connection between the surface of the first plate and the base. In this case, the relationship between the structure and the base, as a contact condition, is written in the following form:

$$W_1(x) = V(x), \qquad -l \le x \le l\,. \tag{4}$$

In what follows we will use the dimensionless coordinate x, equal to the ratio of the absolute coordinate to the half-length of the beam plate.

4. Method for solving the problem

To integrate the system of differential equations (1), we accept the following substitutions:

$$D_2 = D_1 = D;\, W_2 + W_1 = y_1;\;\; W_2 - W_1 = y_2. \tag{5}$$

Then system (1) takes the form:

$$y_1^{IV} = \frac{l^4}{D}[q(x) - p(x)];\; y_2^{IV} + \frac{2kl^4}{D}\, y_2 = \frac{l^4}{D}[q(x) + p(x)]. \tag{6}$$

The analytical solution of system (1), which determines the deflections of beam plates, based on the general integral of differential equations (6), is presented in the following form:

$$W_r = \frac{l^4}{2D}\left\{\sum_{i=1}^{4}\left[C_i x^{4-i} + (-1)^r \frac{D}{l^4} B_i u_i(\propto_1 x)\right] + f_q(x) - f_p(x) + \right.$$
$$\left. +(-1)^r \frac{D}{l^4}\left[\varphi_q(x) + \varphi_p(x)\right]\right\}, \qquad r = 1{,}2. \tag{7}$$

Where C_i, B_i – are the constants of integration determined from the boundary conditions of the problems under consideration;

$u_1(\propto_1 x) = \cosh(\propto_1 x)\cos(\propto_1 x)$;

$u_2(\propto_1 x) = \sinh(\propto_1 x)\cos(\propto_1 x) + \cosh(\propto_1 x)\sin(\propto_1 x)$;

$u_3(\propto_1 x) = \sin(\propto_1 x)\sinh(\propto_1 x)$;

$u_4(\propto_1 x) = \sinh(\propto_1 x)\cos(\propto_1 x) - \cosh(\propto_1 x)\sin(\propto_1 x)$;

$$\left(f_q^{IV}(x), f_p^{IV}(x)\right) = \left(q(x), p(x)\right);\;\; \propto_1{}^4 = \frac{kl^4}{2D}\,; \tag{8}$$

$$(\varphi_q(x), \varphi_p(x)) = \frac{1}{4\propto_1{}^3}\int_0^x u_4[\propto_1 (x-s)](q(s), p(s))ds; \tag{9}$$

Functions $f_q(x)$ and $\varphi_q(x)$, depending on the patterns of external loads $q(x)$, are considered known since the pattern of external loads is presented in a specific form appropriate in practice. Functions $f_p(x)$ and $\varphi_p(x)$, depending on the patterns of pressure distribution in foundation $p(x)$, are considered unknown since the pattern of distribution of pressure in the foundation is not presented.

Following [16], we assume that the foundation pressure is distributed according to polynomial functional laws that well describe the true nature of the pressure of a homogeneous foundation soil. Based on this, we determine the reactive pressure of the base in the form of a series using the Chebyshev polynomials [16]:

$$p(x) = (1 - x^2)^{-\frac{1}{2}} \sum_{n=0}^{\infty} A_n\, T_n(x). \tag{10}$$

Here: A_n – are the unknown coefficients to be determined; $T_n(x)$ – is the Chebyshev polynomial of the first kind.

If we denote by P_s and M_s –the sum of all vertical forces and the sum of their moments relative to the middle of the beam plates, respectively, then the equilibrium equation of the beam plates can be written in the following form:

$$l\int_{-1}^{1} p(x)\,dx = P_s, \qquad l^2\int_{-1}^{1} xp(x)dx = M_s. \tag{11}$$

Substituting (10) into (11), and considering the orthogonality of the Chebyshev polynomials, we determine the first two unknown coefficients of series (10) in the following form:

$$A_0 = \frac{P_s}{\pi l}\ ;\ \ A_1 = \frac{M_s}{\pi l^2}\ . \tag{12}$$

Let us substitute (10) into (2), and with (3), we obtain the following expression for determining the foundation settlement [16]:

$$V = \frac{2(1-\nu_0^2)l}{E_0}\left[-A_0 ln2 + \sum_{n=1}^{\infty}\frac{A_n}{n}T_n(x)\right]. \tag{13}$$

Expression (7), which determines the deflections of beam plates, and considers (10), takes the following form:

$$W_r = \frac{l^4}{2D}\left\{\sum_{i=1}^{4}\left[C_i x^{4-i} + (-1)^r\frac{D}{l^4}B_i u_i(\propto_1 x)\right] + f_q\,(x) + (-1)^r\frac{D}{l^4}\varphi_q(x) - \right.$$
$$\left. -\sum_{n=0}^{\infty}A_n\left[f_{p,n}(x) - (-1)^r\frac{D}{l^4}\varphi_{p,n}\right]\right\}, r = 1,2. \tag{14}$$

Here

$$\varphi_{p,n}(x) = \frac{1}{4\alpha^4}\int_0^x u_4\,[\propto_1 (x-z)](1-z^2)^{-\frac{1}{2}}T_n(z)dz, \tag{15}$$

$$f_{p,n}(x) = \frac{1}{16n(n-1)(n-2)(n-3)}(1-x^2)^{\frac{7}{2}}P_{n-4}^{(\frac{7}{2},\frac{7}{2})}(x), n > 3. \tag{16}$$

Where $P_j^{(\beta_1,\beta_2)}(x)$ –are the Jacobi polynomials [22]. Function $f_{p,n}(x)$ at $n \le 3$, is determined on the basis of Chebyshev polynomials in explicit form.

Based on the given formula (14), the factors of internal forces in three-layer beam plates are determined by the following formulas:

$$\varphi_r(x) = \frac{D}{l}W_r'(x);\ M_r(x) = -\frac{D}{l^2}W_r''(x);\ Q_r(x) = -\frac{D}{l^3}W_r'''(x), r = 1,2. \tag{17}$$

Foundation settlements (13) and beam plate deflections (14) were expressed through unknown coefficients A_n. To determine coefficients A_n, we use the contact condition (4). We substitute expressions (13) and (14) into equality (4), then multiply both sides of the equalities by the expression $(1-x^2)^{-1/2}T_k(x)$ and integrate in the range from -1 to 1. When integrating, we consider the orthogonality of the polynomials. We obtain an infinite system of algebraic equations with infinite numbers of unknowns relative to unknown coefficients A_n:

$$a_k + \sum_{n=0}^{\infty}a_{n,k}\,A_n = c_k A_k, \qquad k = 2,3,4,\dots n. \tag{18}$$

Here

$$a_k = \frac{l^4}{2D}\int_{-1}^{1}\left\{\sum_{i=1}^{4}\left[C_i x^{4-i} - \frac{D}{l^4}B_i u_i(\propto_1 x)\right] + f_q\,(x) - \frac{D}{l^4}\varphi_q(x)\right\}(1-x^2)^{-\frac{1}{2}}T_k(x)dx; \tag{19}$$

$$a_{n,k} = -\frac{l^4}{2D}\int_{-1}^{1}\left[f_{p,n}(x) + \frac{D}{l^4}\varphi_{p,n}(x)\right](1-x^2)^{-\frac{1}{2}}T_k(x)dx; \tag{20}$$

$$c_k = \frac{2\pi(1-\nu_0^2)l}{E_0 k}. \tag{21}$$

Consider the case of a generalized symmetrical plate barrier, which is often observed in practice.

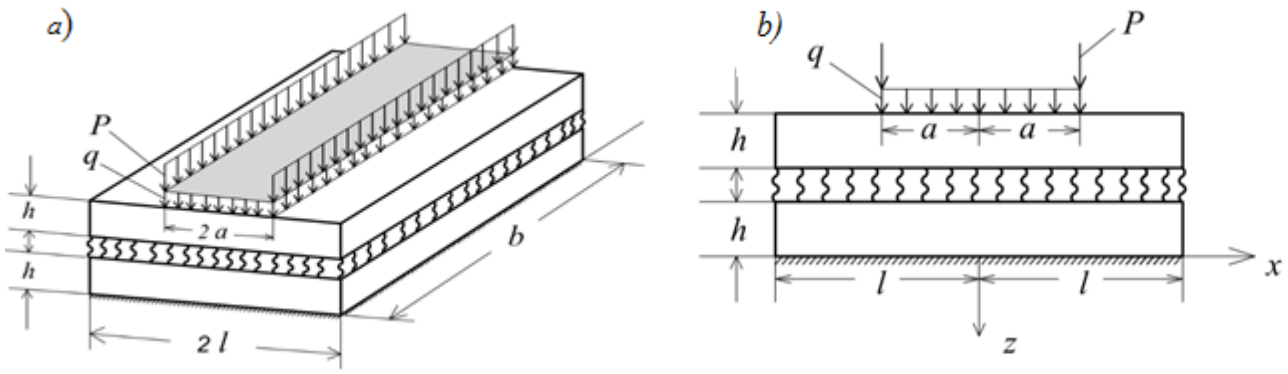

Figure 2. - **a) Design diagram of a three-layer plate under symmetrical loading, b) design diagram of a three-layer beam plate under symmetric loading.**

Let the top plate be loaded with a uniformly distributed external load on the segment $[-a;a]([-a;a]\in[-l;l], a\le l)$ and concentrated external forces at the boundary of this segment, symmetrically relative to its middle (Fig. 2. a, b). In this case, series (10) consists of terms with even polynomials:

$$p(x)=(1-x^2)^{-\frac{1}{2}}\sum_{n=0}^{\infty}A_{2n}\,T_{2n}(x). \tag{22}$$

In this case, expressions (12) and (13), respectively, will take the following form:

$$A_0=\frac{2}{\pi}(a(q+P)); \tag{23}$$

$$V=\frac{2(1-\nu_0^2)l}{E_0}\left[-A_0 ln2+\sum_{n=1}^{\infty}\frac{A_{2n}}{2n}T_{2n}(x)\right]. \tag{24}$$

Expressions (14) that determine the deflections of beam plates, considering (22), for each section separately, are presented in the following form:

$$W_r^I=\frac{l^4}{2D}\left[\sum_{i=1}^{4}C_i^I x^{4-i}+\frac{(q+P)x^4}{24}\right]+(-1)^r\frac{1}{2}\left[\sum_{i=1}^{4}B_i^I u_i(\propto_1 x)-\frac{(q+P)}{4\alpha^4}\left(1-u_1(\propto_1 x)\right)\right]-$$
$$-\frac{1}{2}\sum_{n=0}^{\infty}A_{2n}\left[\frac{l^4}{D}f_{p,2n}(x)-(-1)^r\varphi_{p,2n}(x)\right], x\in[-a;a], r=1,2. \tag{25}$$

$$W_r^{II}=\frac{l^4}{2D}\sum_{i=1}^{4}C_i^{II}x^{4-i}+(-1)^r\frac{1}{2}\sum_{i=1}^{4}B_i^{II}u_i(\propto_1 x)-$$
$$-\frac{1}{2}\sum_{n=0}^{\infty}A_{2n}\left[\frac{l^4}{D}f_{p,2n}(x)-(-1)^r\varphi_{p,2n}(x)\right], x\in[-1;-a]\cup[a;1], r=1,2. \tag{26}$$

Here, symbols I and II indicate the values corresponding to (Fig. 2.b) sections $0\le x\le a$ and $a\le x\le 1$.

Arbitrary constants $C_i^I, C_i^{II}, B_i^I, B_i^{II}, (i=1,2,3,4)$ are determined from the following boundary conditions:

1. For $x=0$,

$$Q_1^I(0)=0;\ Q_2^I(0)=0;\ \varphi_1^I(0)=0;\ \varphi_2^I(0)=0. \tag{27}$$

2. For $x=\pm 1$,

$$Q_1^I(\pm 1)=0;\ Q_2^I(\pm 1)=0;\ M_1^I(\pm 1)=0;\ \varphi_2^I(\pm 1)=0. \tag{28}$$

3. For $x=\pm a$ (conditions for connecting sections),

$$Q_1^I(\pm a)=Q_1^{II}(\pm a);\ \ Q_2^I(\pm a)-Q_2^{II}(\pm a)=P;$$
$$M_1^I(\pm a)=M_1^{II}(\pm a);\ \ M_2^I(\pm a)=M_2^{II}(\pm a);$$
$$W_1^I(\pm a)=W_1^{II}(\pm a);\ \ W_2^I(\pm a)=W_2^{II}(\pm a). \tag{29}$$

Having satisfied conditions (27), we obtain:

$$C_1^I = 0, C_3^I = 0, B_2^I = 0, B_4^I = 0. \tag{30}$$

From the fulfillment of condition (28), we have:

$$C_2^{II} = \frac{1}{2} A_0 f_0''(1), B_2^{II} = 0, B_4^{II} = 0;$$

$$B_1^{II} = A_0 \frac{b^{-1}}{2\alpha^3} [u_1(\propto_1)\varphi_0'''(1) + \alpha u_4(\propto_1)\varphi_0''(1)];$$

$$B_3^{II} = A_0 \frac{b^{-1}}{2\alpha^3} [u_3(\propto_1)\varphi_0'''(1) - \propto_1 u_2(\propto_1)\varphi_0''(1)]. \tag{31}$$

Having satisfied the conjugation condition (29), we will have:

$$B_1^I = \frac{u_1(\propto_1 a)}{2 \propto_1{}^3 b(a)} \left(-2P + \frac{l^4}{D}(q+P)a\right) +$$

$$+ \frac{u_4(\propto_1 a)}{b(a)} \left(\frac{l^4}{2D}(4C_2^I + (q+P)a^2)\right) - \frac{(q+P)}{4 \propto_1{}^4} + B_1^{II},$$

$$B_3^I = \frac{u_3(\propto_1 a)}{2 \propto_1{}^3 b(a)} \left(\frac{l^4}{D}(q+P)a\right) - \frac{u_2(\propto_1 a)}{b(a)} \left(\frac{l^4}{2D}(4C_2^I + (q+P)a^2)\right) + B_3^{II},$$

$$C_2^I = \frac{1}{1 + 2 \propto_1{}^2} C_2^{II} - \frac{(q+P)a^2 \propto_1{}^2}{2}, \qquad C_3^{II} = 0. \tag{32}$$

Here $b = u_1(\propto_1)u_2(\propto_1) + u_3(\propto_1)u_4(\propto_1)$; $b(a) = u_1(\propto_1 a)u_2(\propto_1 a) + u_3(\propto_1 a)u_4(\propto_1 a)$.

Constants of integration C_4^I, C_4^{II} are eliminated when moving to relative deflections of the following form:

$$W_{11}^I(x) = W_1^I(x) - W_1^I(0); \;\; W_{11}^{II}(x) = W_1^{II}(x) - W_1^{II}(0);$$
$$W_{22}^I(x) = W_2^I(x) - W_2^I(0); \;\; W_{22}^{II}(x) = W_2^{II}(x) - W_2^{II}(0).$$

Moving on to relative deflections, we have the following:

$$W_{11}^I = \frac{l^4}{2D}\left(C_2^I x^2 + \frac{(q+P)x^4}{24}\right) - \frac{1}{2}[B_1^I u_1(\propto_1 x) + B_3^I u_3(\propto_1 x) -$$

$$- \frac{(q+P)}{4 \propto_1{}^4}\left(1 - u_1(\propto_1 x)\right)\Big] - \frac{1}{2}\sum_{n=0}^{\infty} A_{2n}\left[\frac{l^4}{D} f_{p,2n}(x) + \varphi_{p,2n}(x)\right]; \tag{33}$$

$$W_{11}^{II} = \frac{l^4}{2D} C_2^{II} x^2 - \frac{1}{2}[B_1^{II} u_1(\propto_1 x) + B_3^{II} u_3(\propto_1 x)] -$$

$$- \frac{1}{2}\sum_{n=0}^{\infty} A_{2n}\left[\frac{l^4}{D} f_{p,2n}(x) + \varphi_{p,2n}(x)\right]; \tag{34}$$

$$W_{22}^I = \frac{l^4}{2D}\left(C_2^I x^2 + \frac{(q+P)x^4}{24}\right) + \frac{1}{2}[B_1^I u_1(\propto_1 x) + B_3^I u_3(\propto_1 x) -$$

$$- \frac{(q+P)}{4 \propto_1{}^4}\left(1 - u_1(\propto_1 x)\right)\Big] - \frac{1}{2}\sum_{n=0}^{\infty} A_{2n}\left[\frac{l^4}{D} f_{p,2n}(x) - \varphi_{p,2n}(x)\right]; \tag{35}$$

$$W_{22}^{II} = \frac{l^4}{2D} C_2^{II} x^2 + \frac{1}{2}[B_1^{II} u_1(\propto_1 x) + B_3^{II} u_3(\propto_1 x)] -$$

$$- \frac{1}{2}\sum_{n=0}^{\infty} A_{2n}\left[\frac{l^4}{D} f_{p,2n}(x) - \varphi_{p,2n}(x)\right]; \tag{36}$$

For convenience, we introduce the following notation:

$$P_1(x) = \frac{l^4}{2D}\left(C_2^I x^2 + \frac{(q+P)x^4}{24}\right) - \frac{1}{2}[B_1^I u_1(\propto_1 x) + B_3^I u_3(\propto_1 x) -$$

$$- \frac{(q+P)}{4 \propto_1{}^4}\left(1 - u_1(\propto_1 x)\right)\Big], \text{at } x \in [-a; a];$$

$$P_2(x) = \frac{l^4}{2D} C_2^{II} x^2 - \frac{1}{2}[B_1^{II} u_1(\propto_1 x) +$$
$$+B_3^{II} u_3(\propto_1 x)] \quad \text{at } x \in [-1; -a] \cup [a; 1]\,. \tag{37}$$
$$P_2(x) = \frac{l^4}{2D}\left(C_2^I x^2 + \frac{(q+P)x^4}{24}\right) + \frac{1}{2}[B_1^I u_1(\propto_1 x) +$$
$$+B_3^I u_3(\propto_1 x) - \frac{(q+P)}{4\,\propto_1{}^4}\big(1 - u_1(\propto_1 x)\big)\Big], \quad \text{at } x \in [-a; a];$$
$$P_2(x) = \frac{l^4}{2D} C_2^{II} x^2 + \frac{1}{2}[B_1^{II} u_1(\propto_1 x) +$$
$$+B_3^{II} u_3(\propto_1 x)], \quad \text{при } x \in [-1; -a] \cup [a; 1]. \tag{38}$$
$$P_{1,2n}(x) = -\frac{1}{2}\left[\frac{l^4}{D} f_{p,2n}(x) + \varphi_{p,2n}(x)\right] \tag{39}$$
$$P_{2,2n}(x) = -\frac{1}{2}\left[\frac{l^4}{D} f_{p,2n}(x) - \varphi_{p,2n}(x)\right]. \tag{40}$$

Then, for the deflections of beam plates, we can write the following expressions:

$$W_{11}(x) = P_1(x) + \sum_{n=0}^{\infty} A_{2n} P_{1,2n}(x); \tag{41}$$
$$W_{22}(x) = P_2(x) + \sum_{n=0}^{\infty} A_{2n} P_{2,2n}(x). \tag{42}$$

The system of algebraic equations (18) will take the following form:

$$a_{2k} + \sum_{n=0}^{\infty} a_{2n,2k}\, A_{2n} = c_{2k} A_{2k}, k = 1,2,3,4, \ldots, \tag{43}$$

here

$$a_{2k} = \frac{l^4}{2D} \int_{-1}^{1} P_1(x)(1-x^2)^{-\frac{1}{2}} T_{2k}(x)dx; \tag{44}$$
$$a_{2n,2k} = -\frac{l^4}{2D} \int_{-1}^{1} P_{1,2n}(x)\,(1-x^2)^{-\frac{1}{2}} T_{2k}(x)dx. \tag{45}$$

By integrating integrals (44) and (45) by parts, we can eliminate the singularity:

$$a_{2k} = \frac{l^4}{2D}\left(-\frac{1}{4k}\right) \int_{-1}^{1} F_1'(x)(1-x^2)^{\frac{1}{2}} P_{2k-1}^{(\frac{1}{2},\frac{1}{2})}(x)dx;$$
$$a_{2n,2k} = -\frac{l^4}{2D}\left(-\frac{1}{4k}\right) \int_{-1}^{1} F_{1,2n}'(x)(1-x^2)^{\frac{1}{2}} P_{2k-1}^{(\frac{1}{2},\frac{1}{2})}(x)dx.$$

It can be noted that the resulting expressions have a more appropriate form and it becomes possible to implement calculations using computer technology.

Now it is convenient to determine the solution to system (43) using the reduction method. According to the principle of the reduction method, we restrict ourselves to the first few unknowns in order $A_2, A_4, \ldots, A_{2r}$ with relevant r equations of the system of equations (43). Defining solutions A_{2r} from the compiled system and, substituting them into (41) and (42), we find the deflections of the beam plate. Then, using deflection formulas, the internal forces of the beam plate can be calculated based on formulas (17). Here we can easily notice that the restrictions relative to r equations with r unknowns in system (43) correspond to those accepted instead of the infinite series (22) in the form of a finite series consisting of r terms.

5. Numerical example

To illustrate the presented methodology, consider a numerical example. We accept the following system characteristics [16]:

for soil - $E_0 = 5 \cdot 10^2 \frac{kg}{cm^2}$; $\nu_0 = 3 \cdot 10^{-1}$;

for plates - $E = 1{,}25 \cdot 10^5 \frac{kg}{cm^2}$; $\nu = 1{,}67 \cdot 10^{-1}$; $l = 4 \cdot 10^2 sm$; $h = 2{,}5 \cdot 10\ cm$;

for filler hardness coefficient k, having the dimension $\frac{kg}{cm^3}$ -

$$1 \cdot 10^{-1};\ 2 \cdot 10^{-1};\ 3 \cdot 10^{-1};\ 4 \cdot 10^{-1};\ 5 \cdot 10^{-1}.$$

To perform calculations, in series (22), we take the first four terms with unknown coefficients $A_0,\ A_2,\ A_4,\ A_6$. The numerical values of the unknown coefficients corresponding to various values of the filler stiffness coefficient k are given in Table 1.

Table 1

Numerical values of unknown coefficients when solving algebraic equations

k	$A_0 l(a(q+P))^{-1}$	$A_2 l(a(q+P))^{-1}$	$A_4 l(a(q+P))^{-1}$	$A_6 l(a(q+P))^{-1}$
0.10	0.636619	-0.079847	-0.006673	0.000546
0.20	0.636619	-0.083365	-0.007134	0.000544
0.30	0.636619	-0.089861	-0.007617	0.000538
0.40	0.636619	-0.091437	-0.007984	0.000549
0.50	0.636619	-0.094783	-0.008132	0.000557

Based on the calculation results, Table 2 shows the maximum values of bending moments in beam plates and their comparison with the results obtained in [16], - $M_1(ql^2)^{-1}, M_2(ql^2)^{-1}$.

Table 2

Maximum values of bending moments in beam plates

k	0.10	0.20	0.30	0.40	0.50
$M_1(ql^2)^{-1}$	0.069591	0.071368	0.072437	0.074981	0.077576
$M_1(a(q+P)l^2)^{-1}$	0.078631	0.081319	0.086109	0.083753	0.083165
$M_2(ql^2)^{-1}$	0.103563	0.103012	0.099073	0.098169	0.091864
$M_2(a(q+P)l^2)^{-1}$	0.119397	0.113721	0.099869	0.099629	0.099427

6. Conclusions drawn from numerical examples

According to Table 1, it can be noted that:

1. Changing the stiffness of the filler does not lead to a noticeable change in the solution of the algebraic equations and, similarly, does not lead to a change in the distribution of the base pressure.

2. To ensure the necessary calculation accuracy, with a uniform distribution of foundation pressure, in the Chebyshev polynomial, it is enough to restrict oneself to the first four terms of the series.

Analyzing the data given in Table 2, it can be noted that:

1. Bending moments in plates increase up to 10%.

2. An increase in the rigidity of the filler leads to the bending moments in the plates approaching each other.

7. Conclusion

Analyzing the results of the study, we can conclude that:

1. A mathematical model and analytical method were developed to assess the bending of three-layer plates interacting with an elastic base.

2. An improved algorithm for calculating three-layer plates freely lying on an elastic foundation was created.

3. The nature of the influence of the filler layer and external forces on the internal forces in three-layer plates lying on an elastic base was determined.

4. Limits of numerical restrictions were determined to ensure accuracy in practical calculations of three-layer plates lying on an elastic half-space.

References

1. *Sultanov K.S., Vatin N.I.* Wave theory of seismic resistance of underground pipelines. Applied Sciences (Switzerland), **2021**, 11(4), Pp. 1–28, 1797. https://doi.org/10.3390/app11041797
2. *Sultanov, Karim.* Contact interaction of an underground pipeline with soil under dynamic impacts. Facta Universitatis, Series: Mechanical Engineering, March 2024. ISSN 2335-0164.
3. *Mirsaidov M., Dusmatov O., Khodjabekov M.* Mode Shapes of Transverse Vibrations of Rod Protected from Vibrations in Kinematic Excitations. Proceedings of FORM **2021** Pp 217-227, https://doi.org/10.1007/978-3-030-79983-0_20
4. *Ikonin S.V., Sukhoterin A.V.* The effect of design on interaction of foundation plates with the base. Magazine of Civil Engineering. **2019**. 89(5). Pp. 141–155. https://doi:10.18720/MCE.89.12
5. *Philip Schreiber, Christian Mittelstedt.* Buckling of shear-deformable unsymmetrically laminated plates. International Journal of Mechanical Sciences Volume 218, 15 March **2022**, https://doi.org/10.1016/j.ijmecsci.2021.106995.
6. *Xingzhuang Zhao, Peter Chang.* Free and forced vibration of double beam with arbitrary end conditions connected with a viscoelastic layer and discrete points. International Journal of Mechanical Sciences. Volume 209, 1 November **2021**, https://doi.org/10.1016/j.ijmecsci.2021.106707.
7. *Longhui Zhang, Antonio Pellegrino, David Townsend, Nik Petrinic.* Temperature Dependent Dynamic Strain Localization and Failure of Ductile Polymeric Rods under Large Deformation. International Journal of Mechanical Sciences Volume 204, 15 August **2021**, https://doi.org/10.1016/j.ijmecsci.2021.106563
8. *Dong Shao, Qingshan Wang, Yongqiang Tao, Wen Shao, Wei Wu.* A unified thermal vibration and transient analysis for quasi-3D shear deformation composite laminated beams with general boundary conditions. International Journal of Mechanical Sciences. Volume 198, 15 May **2021**.
9. *Sultanov K.S., Khusanov B.E., Rikhsieva B.B.* Longitudinal waves in a cylinder with active external friction in a limited area. Journal of Physics: Conference Series, **2020**, 1546(1), 012140. https://doi.org/10.1088/1742-6596/1546/1/012140
10. *Mirsaidov M., Boytemirov M., Yuldashev F.* Estimation of the Vibration Waves Level at Different Distances. Lecture Notes in Civil Engineering, **2022**, 170, Pp. 207–215. https://doi.org/10.1007/978-3-030-79983-0_19
11. *Mincai Jia, Ye Yang, Zhiyong Ai.* Time history response of an elastic thin plate on a transversely isotropic multilayered medium due to vertical loadings. Computers and Geotechnics Volume 134, June **2021**
12. *Wenrui Wang,Yu Lu, Dezong Zhao, Jiaming Zhang, Xuesong Bai.* Research on large deflection deformation reconstruction of elastic thin plate based on strain monitoring. Measurement. Volume 149, January **2020**
13. *Mao J.J., S.K. Lai, W. Zhang, Y.Z. Liu.* Comparisons of nonlinear vibrations among pure polymer plate and graphene platelet reinforced composite plates under combined transverse and parametric excitations. Composite structures. Volume 265, 1 June **2021**. https://doi.org/10.1016/j.compstruct.2021.113767
14. *Linyuan Li., Chang Liu, Weisheng Zhang, Zongliang Du, Xu Guo.* Combined model-based topology optimization of stiffened plate structures via MMC approach. International journal of Mechanical Sciences. Volume 208, 15 October **2021**. https://doi.org/10.1016/j.ijmecsci.2021.106682
15. *Hongyang Ma, Qunfei Xiong, Deyu Wang.* Experimental and numerical study on the ultimate strength of stiffened plates subjected to combined biaxial compression and lateral loads. Ocean Engineering. Volume 228, 15 May **2021**. https://doi.org/10.1016/j.oceaneng.2021.108928
16. *Mirsaidov M., Mamasoliev Q.* Contact problems of multilayer plates interaction on an elastic foundation.2020. IOP Conf. Series: Earth and Environmental Science 614 (**2020**) 012089 IOP Publishing https://doi:10.1088/1755-1315/614/1/012089
17. *Mirsaidov M., Mamasoliev K., Ismayilov K.* (**2022**) Bending of Multilayer Plates Lying on Elastic Half-Space, Considering Shear Stresses. In: Vatin N., Roshchina S., Serdjuks D. (eds) Proceedings of MPCPE 2021. Lecture Notes in Civil Engineering, vol 182. Springer, Cham. https://doi.org/10.1007/978-3-030-85236-8_8)
18. *Binwen Wang, Xiangming Chen, Xiasheng Sun, Puhui Chen, Zhe Wang, Ya'nan Chai.* Interaction formulae for buckling and failure of orthotropic plates under combined axial compression/tension and shear. Chinese Journal of Aeronautics. Volume 35, Issue 3, March **2022**, Pp. 272-280.
19. *Yuteng Cao, Dengqing Cao, Guiqin He, Xinsheng Ge, Yuxin Hao.* Modelling and vibration analysis for the multi-plate structure connected by nonlinear hinges. Journal of Sound and Vibration. Volume 492, 3 February **2021**. https://doi.org/10.1016/j.jsv.2020.115809
20. *Yuriy Tokovyy, Anatoliy Chyzh, Chien-Ching Ma.* An analytical solution to the axisymmetric thermoelasticity problem for a cylinder with arbitrarily varying thermomechanical properties. Acta Mechanica volume 230, Pp.1469–1485 (**2019**), https://doi.org/10.1007/s00707-017-2012-3(2017).
21. *Yuriy Tokovyy, Chien-Ching Ma.* Elastic Analysis of Inhomogeneous Solids: History and Development in Brief. Journal of Mechanics, Volume 35, Issue 5, October **2019**, Pp. 613–626, https://doi.org/10.1017/jmech.2018.57

22. *Mirsaidov M., Mamasoliev K.* Contact interaction of multilayer plates with an inhomogeneous base. Magazine of Civil Engineering, **2022**, 115(7), 11504. https://doi.org/10.34910/MCE.115.4
23. *Mirsaidov M., Mamasoliev K.* Contact interaction of multi-layer plates with a combined base. AIP Conference Proceedings 2637, 050001 (2022). Doi: 10.1063/5.0118870
24. *Jurayev D.J., Vatin N., Sultanov T.Z., Mirsaidov M.M.* Spatial stress-strain state of earth dams. Magazine of Civil Engineering, **2023**, 118(2), 11810. https://doi.org/10.34910/MCE.118.10
25. *Avinash C. D., Narasimhe Gowda, Smitha N.* Modal analysis of honeycomb structure for different parametric conditions using finite element method. Journal: AIP Conference Proceedings, *AIP Conf. Proc.* 2399, 030005 (2023), https://doi.org/10.1063/5.0132658.
26. *Marwa Al Safar, Kais Ibraheem*. Numerical algorithm for solving fuzzy differential equations using Runge-Kutta method RK6, Journal: AIP Conference Proceedings, *AIP Conf. Proc.* 3036, 040020 (2024), https://doi.org/10.1063/5.0203150
27. *Shabbir Ahmed R.M.; Mohammed Haneef.* Experimental and numerical analysis of woven glass-epoxy composite laminates with single lap joints. Journal: AIP Conference Proceedings, *AIP Conf. Proc.* 2399, 030020 (2023), https://doi.org/10.1063/5.0157163
28. *Sridhar N. Shastry, Subrahmanya S. Swamy.* The effects of design modification in a two edge coupled thin composite laminates on SEA. *AIP Conf. Proc.* 2399, 030024 (2023), December 2023, https://doi.org/10.1063/5.0132717

ASSESSMENT OF VIBRATIONS OF SUPERSTRUCTURES OF REINFORCED CONCRETE BRIDGES UNDER THE INFLUENCE OF MOBILE LOADS

Mardonov B.[1], Bekmirzaev D.[1], Berdibaev M.[1], Khurramov A.[1], Botabaev N.[1]
[1]*Institute of Mechanics and Seismic Stability of Structures named after M.T.Urazbaev, Tashkent, Uzbekistan.*
E-mail: mars.berdibaev@mail.ru

Abstract. *The article presents the transverse vibrations of a single-span reinforced concrete bridge, the bearings of which interacts with the superstructure under the concentrated and distributed moving loads. It is accepted that the deformation of the structure does not exceed the elastic limit and the vibrations are linear. The problems posed were analytically solved based on the Fourier method, graphs of changes in deflections and normal stresses of superstructures over time were constructed, and their greatest values were determined.*

Keywords. *Bridge, superstructure, vibration, moving load, normal stress, deflection.*

1. Introduction.

The development of transport infrastructure makes it possible to create large integrated cities, thereby opening up new prospects for the socio-economic development of regions. Bridge constructions, as a type of transport infrastructure, are usually aimed primarily at the internal development of a country, improving transport accessibility and enhancing interregional connections. Currently, in developed countries of the world, improvement of calculation methods is required to ensure the strength, reliability and service life of bridge structures.

Studies have shown that the gross weight, axle weight, and axle configuration of heavy movies loads directly affect the service life of highway bridge superstructures. Damage typically occurs in the bridge deck and in the main superstructure elements, including floor beams and girders, diaphragms, joints, and bearings. With the rapid growth of highway transportation, the increasing frequency of passing heavy movies loads contributes to fatigue damage. As a result, bridge maintenance becomes more difficult and more costly, since maintenance, rehabilitation, and replacement become more frequent.

Bridge structures are one of the most important and integral links of all types of ground transportation systems, including automotive roads, railways, pedestrian roads and pipelines. Bridges, overpasses and similar man-made structures serve to overcome various natural and artificial obstacles [1].

Most transport structures for carrying various moving loads are complex dynamic oscillatory systems with distributed parameters and are therefore continuous. To assess the reliability and load-bearing capacity of such engineering structures under the influence of non-stationary dynamic influences, complex, modern and advanced calculation methods are used [2-10]. The algorithms developed on their basis are implemented using rapidly developing computer technology and application software packages. This allows you to perform a sufficient number of computational

experiments to obtain a complete picture of the stress-strain state of the structure. However, in a number of cases, it is possible to assess the reliability of a structure with sufficient accuracy by wisely using the simplicity of calculation methods in the classical setting without involving complex and modern calculation methods [11-20]. In this case, it is necessary to determine the boundaries of using one or another simplified version of the formulation of such a problem. On the other hand, each of the options can be improved to generalize the problem and expand the scope of its application.

The recent developments in design technology and material qualities in civil engineering enable the construction of more light and slender structures, which causes structures to be vulnerable to dynamic loads, especially moving loads. Large deflections and vibrations induced by heavy and high-speed vehicles affect significantly the safety and serviceability of bridges. Vibrations induced by heavy moving loads may significantly increase the maximum internal stresses of bridges and deteriorate serviceability. Therefore, vibration control using control devices is a very efficient way to suppress the response of bridges, and thus to enhance the structural safety and serviceability of bridges [21]. Moving load problem is generally studied for beam structures. Research on the dynamic response of bridges due to moving loads has received considerable attention with the passing of recent years. Several mathematical models of vehicles were developed with the passing of years [22].

2. Methodology.

Moving load effect on bridges is an important task solving in many workplaces in the world. The task can be solved analytical, numerically and experimentally. In the present time, analytical and numerical modeling of the problems of moving load effect on bridges is an effective tool for the solution of real tasks of engineering practice. To solve this problem it is possible to create various computational models. Models can be planar or spatial. They can be created in the spirit of classical dynamics or in the spirit of the finite element method. The models can be discrete with finite degrees of freedom, or the model parameters can be continually distributed. Discrete computational models are more advantageous from the point of view of the mathematical solution because the equations of motion have the form of ordinary differential equations. The innovative contribution in solving vehicle-bridge interaction is modeling of the vehicles in combination with mass objects, damping and stiffness elements, which can better describe the real vehicle and its movement over the bridge construction [23]. Figure 1 shows a single-span reinforced concrete road bridge. Let us consider the vibrations of a superstructure under the influence of a moving load moving at a constant speed (Fig. 2).

Figure.1. - **General view of a single-span reinforced concrete road bridge**

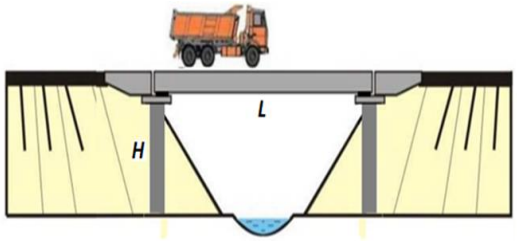

Figure.2. - **Design diagram of a reinforced concrete bridge with a moving load**

The deflection of the superstructure $W(x,t)$ satisfies the equation

$$m_b \frac{\partial^2 W}{\partial t^2} + EJ \frac{\partial^4 W}{\partial x^4} = f(v_0 t - x)\,.\ 0 < x < L\,,\ t > 0 \tag{1}$$

and the following initial and boundary conditions

$$\frac{\partial W}{\partial x} = 0\,,\ EJ \frac{\partial^3 W}{\partial x^3} - k_1 W = 0 \ \text{ for } x=0, \tag{2}$$

$$\frac{\partial W}{\partial x} = 0\,,\ EJ \frac{\partial^3 W}{\partial x^3} + k_2 W = 0 \ \text{ for } x=L, \tag{3}$$

where m_b – is the linear mass of the superstructure, E – is Young's modulus, J – is the moment of inertia of the section, L – is the length of the superstructure, v_0 – is the constant speed of the moving load, k_1 and k_2 – are the stiffness coefficients of the bearings.

Initial conditions are assumed to be zero, i.e

$$W(x,0)=\frac{\partial W(x,0)}{\partial t}=0 \tag{4}$$

The solution of the equation (1) is determined by the Fourier method through the initial and boundary conditions (2) and (3).

$$\overline{W}=\frac{W}{L},\ \overline{W}=\sum T_i(\tau)\varphi_i(\xi). \tag{5}$$

where $T_i(t)$ and $\varphi_i(\xi)$ satisfy these equations

$$\ddot{T}_i=-\omega_i^2 T_i,\ \varphi_i^{IV}(\xi)-\lambda^4\varphi_i=0$$

where $\tau=\frac{v_0 t}{L},\ \xi=\frac{x}{L},\ \omega_i^2=\frac{\lambda_i^4}{L\cdot v_0}\sqrt{\frac{EJ}{m_b}}$

The functions $\varphi_i(\xi)$ are obtained in the following form according to the conditions (2) and (4).

$$\varphi_i(\xi)=\left\{\beta_1\lambda_i^3\cdot Y_{2i}\left[Y_{3i}\cdot Y_1(\lambda_i\xi)-Y_{4i}\cdot Y_4(\lambda_i\xi)\right]+F_i\left[Y_{3i}\cdot Y_3(\lambda_i\xi)-Y_{2i}\cdot Y_4(\lambda_i\xi)\right]\right\}F_i\cdot Y_{3i}$$

where $\beta_1=\frac{EJ}{k_1L^3},\ F_i=Y_{3i}-\beta_1\cdot\lambda_i^3 Y_{4i},$

$Y_i(x)$ – Krylov functions

$Y_{1i}=Y_1(\lambda_i),\ Y_{2i}=Y_2(\lambda_i),\ Y_{3i}=Y_3(\lambda_i),\ Y_{4i}=Y_4(\lambda_i).$

$Y_1(x)=(chx+\cos x)/2,\ Y_2(x)=(shx+\sin x)/2,\ Y_3(x)=(chx-\cos x)/2,\quad Y_4(x)=(shx-\sin x)/2,$

λ_i – are solutions of the transcendental equation

$$Y_i(1)-\beta_2\cdot Y_i''(1)=0,\ \beta_2=\frac{EJ}{k_2L}.$$

where $\varphi_i(\xi)$ functions fulfill the condition of orthogonality:

$$\int_0^1\varphi_i(\xi)\varphi_j(\xi)d\xi,\ i\neq j$$

We put expression (5) into equation (1):

$$\sum\left(\ddot{T}_i+\omega_i^2T_i\right)\phi_i(\xi)=\frac{L}{m_bv_0^2}\cdot f(\tau-\xi)H(\tau-\xi)\cdot H(l_0-\tau+\xi) \tag{6}$$

$$0\le\xi\le1,\ 0\le\tau\le1+l_0 \tag{7}$$

We multiply equation (2.6) by $\varphi_j(\xi)$ and integrate the result in the interval $0\le\xi\le1$:

$$\sum\left(\ddot{T}_i+\omega_i^2T_i\right)\int_0^1\varphi_i(\xi)\cdot\varphi_j(\xi)=\frac{L}{m_bv_0^2c_i}\int_0^1 f(\tau-\xi)\varphi_j(\xi)H(\tau-\xi)H(l_0-\tau+\xi)\alpha\xi \tag{8}$$

Using the orthogonality condition in these expressions, we obtain from it these equations for T_i

$$\ddot{T}_i+\omega_i^2T_i=\frac{L}{m_bv_0^2c_i}\int_0^\tau f(\tau-\xi)\cdot\varphi_i(\xi)d\xi=F_{1i}(\tau),\ 0\le\tau\le l_0 \tag{9}$$

$$\ddot{T}_i+\omega_i^2T_i=\frac{L}{m_bv_0^2c_i}\int_{\tau-l_0}^\tau f(\tau-\xi)\cdot\phi_i(\xi)d\xi=F_{2i}(\tau),\ l_0\le\tau\le1 \tag{10}$$

$$\ddot{T}_i+\omega_i^2T_i=\frac{L}{m_bv_0^2c_i}\int_{\tau-l_0}^1 f(\tau-\xi)\cdot\varphi_i(\xi)d\xi=F_{3i}(\tau),\ 1\le\tau\le1+l_0 \tag{11}$$

$$\ddot{T}_i+\omega_i^2T_i=0,\ \tau\ge1+l_0 \tag{12}$$

where $C_i = \int_0^1 \varphi_i^2(\xi)d\xi$

Let's look at the function $F_i(\tau)$ using this formula.

$$F_i = \begin{cases} F_{1i}(\tau), & 0 \le \tau \le l_0 \\ F_{2i}(\tau), & l_0 \le \tau \le 1 \\ F_{3i}(\tau), & 1 \le \tau \le 1 + l_0 \\ 0, & \tau \ge 1 + l_0 \end{cases} \tag{13}$$

When the initial conditions are zero, the solution of equations (9) - (11) is as follows

$$T_i = \frac{L}{m_b v_0^2 c_i} \int_0^\tau F_i(z) \sin \omega_i (z - \tau) dz, \ 0 \le \tau \le 1 + l_0 \tag{14}$$

Denoting $T_i(\tau)$ in equation (12) by $T_{Li}(\tau)$, its solution can be obtained as follows.

$$T_{Li} = \dot{T}_i(1 + l_0) \frac{\sin \omega_i (\tau - 1 - l_0)}{\omega_i} + T_i(1 + l_0) \cos \omega_i (\tau - 1 - l_0), \ \tau \ge 1 + l_0 \tag{15}$$

Putting the expressions of $T_i(\tau)$ and $T_{Li}(\tau)$ into equation (5), we get the solution of the intermediate device cooling in dimensionless form.

3. Results.

1. We consider the effect of the accumulated moving charge on the intermediate device in the form of the Dirac delta function (Fig. 3). (P_0 is the accumulated moving load).

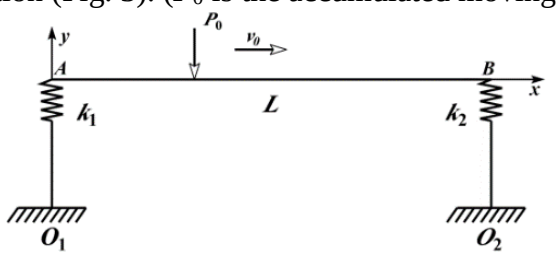

Figure.3. - **Scheme for calculating concentrated moving load on a bridge**

In this case, $f(t)$ is represented by the Dirac delta function.

$$f(\tau - \xi) = \frac{P_0}{L} \delta(\tau - \xi) \tag{16}$$

In this case, with l_0=0, the appearance of the function $F_i(\tau)$ in expression (13) is as follows:

$$F_i = \frac{P_0 L^2}{EJc_i} \varphi_i(\tau), \ 0 \le \tau \le 1, \tag{17}$$

$$F_i = \frac{P_0 L^3}{EJc_i} \varphi_i(1), \ \tau \ge 1. \tag{18}$$

The solution of equations (17) - (18) is as follows

$$T_i = T_{1i} = \frac{L^2 P_0}{EJC_i \omega_i} \left[\int_0^\tau \varphi_i(z) \sin \omega_i (z - \tau) dz \right], \ 0 \le \tau \le 1, \tag{19}$$

$$T_i = T_{2i} = T_{1i}(1) + \frac{L^2 P_0}{EJC_i \omega_i} \left[\int_1^\tau \varphi_i(1) \sin \omega_i (z - \tau) dz \right], \ \tau \ge 1. \tag{20}$$

Figure 4 shows graphs of distributions of deflections $W(\xi,\tau)$ (a) and normal stresses $\sigma(\xi,\tau)$ (b) along the length $\xi = x/L$ of the superstructure at different values of dimensionless time $\tau = v_0 t/L$. In the calculations it was assumed: E=3.45·10^4 MPa, L=24 m, P_0=400 kN, m_b=1517 kg, v_0=25 km/h, J=0.023 m^4, k_1=k_2=10^{10} N/m.

a)

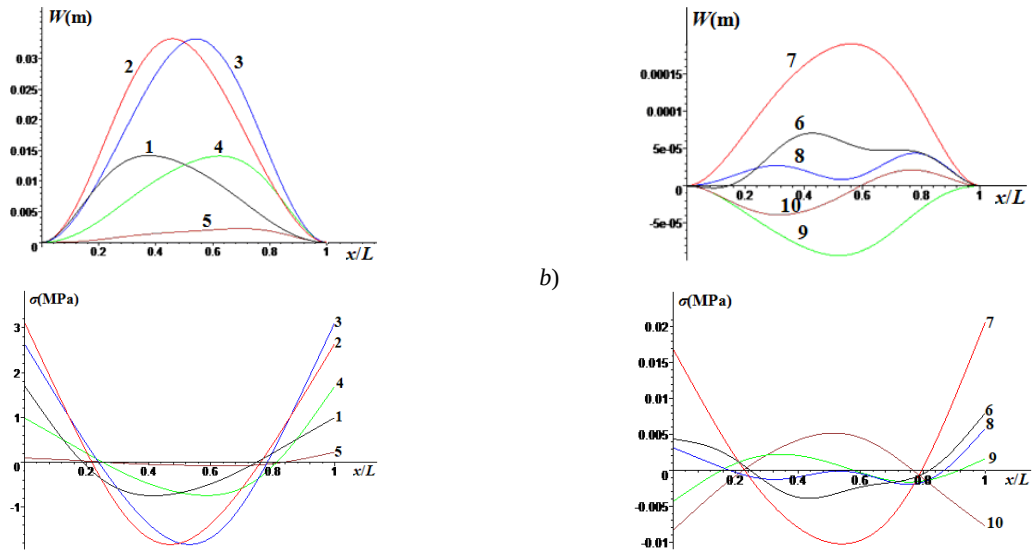

Figure.4. - **Distributions of deflections W(m) (a) and normal stresses σ(MPa) (b) of the superstructure along the length for k=10^{10}(N/m) at different values of dimensionless time τ: 1–t=0.2, 2–t=0.4, 3–t=0.6, 4–t=0.8, 5–t=0.94, 6–t=1.02, 7–t=1.03, 8–t=1.05, 9–t=1.08, 10–t=1.14**

With the value of the stiffness coefficients of the bearings k=10^{10} N/m, it was observed that when exposed to a concentrated moving load on the first half of the length of the superstructure, the deflection reaches the value W=3 cm (Fig. 4 a), and the normal stress σ=3 MPa (Fig. 4 b). And when the load reaches the second end of the superstructure, the values of deflections and normal stresses decrease; at subsequent time values, vibrations with low amplitude continue.

2. Let now the superstructure be subject to a uniformly distributed load P_0 on a section of the span of length L (Fig. 5), determined by the formula (l_0=l_1/L). (P_0 – moving distributed load).

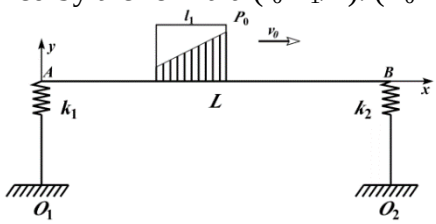

Figure.5. - **Scheme for calculating distributed moving load on a bridge**

In this case, the law of influence on the movement of the distributed moving load along the intermediate device can be determined by the following expressions.

$$f(\tau-\xi)=\frac{P_0}{l},\ 0\le\xi\le\tau-l_0,\ 0\le\tau\le\tau_0 \tag{21}$$

$$f(\tau-\xi)=\frac{P_0}{l},\ \tau-l_0\le\xi\le\tau,\ \tau_0\le\tau\le1 \tag{22}$$

$$f(\tau-\xi)=0,\ 0\le\xi\le1,\ \tau>1+\tau_0 \tag{23}$$

where l_0=τ_0=l_1/L

If we use the expressions in (2.9) – (2.11).

$$F_i=\frac{P_0}{l}\int_0^z\varphi_i(\eta)d\eta=F_{1i}(z),\ 0\le z\le\tau_0 \tag{24}$$

$$F_i=\frac{P_0}{l}\int_{z-l_0}^z\varphi_i(\eta)d\eta=F_{2i}(z),\ \tau_0\le z\le1 \tag{25}$$

$$F_i=\frac{P_0}{l}\int_{z-l_0}^1\varphi_i(\eta)d\eta=F_{3i}(z),\ 1\le z\le1+\tau_0 \tag{26}$$

$$F_i=0,\ z>1+\tau_0 \tag{27}$$

Using the expressions of F_i, we determine the appearance of functions T_i (τ_1≥1+τ_0).

$$T_i = \frac{P_0}{m_b v_0^2 \omega_i l_0 C_i} \int_0^{\tau} F_i(z) \sin \omega_i (\tau - z) dz \,, \; 0 \le \tau \le \tau_1 \tag{28}$$

Intermediate device cooling and normal stresses in the section are determined by the following formulas

$$W = \sum_{i=1}^{\infty} T_i(\tau) \varphi_i(\xi) \tag{29}$$

With the value of the stiffness coefficient of the bearings k=10^{10} N/m, it was observed that when exposed to a distributed moving load on the first half of the superstructure length, the deflection reaches a value of W=3 cm (Fig. 6 *a*), and the normal stress σ=3 MPa (Fig. 6 *b*). And when the load reaches the second end of the superstructure, the values of deflections and normal stresses decrease, with subsequent values of time fluctuations with a small amplitude continue.

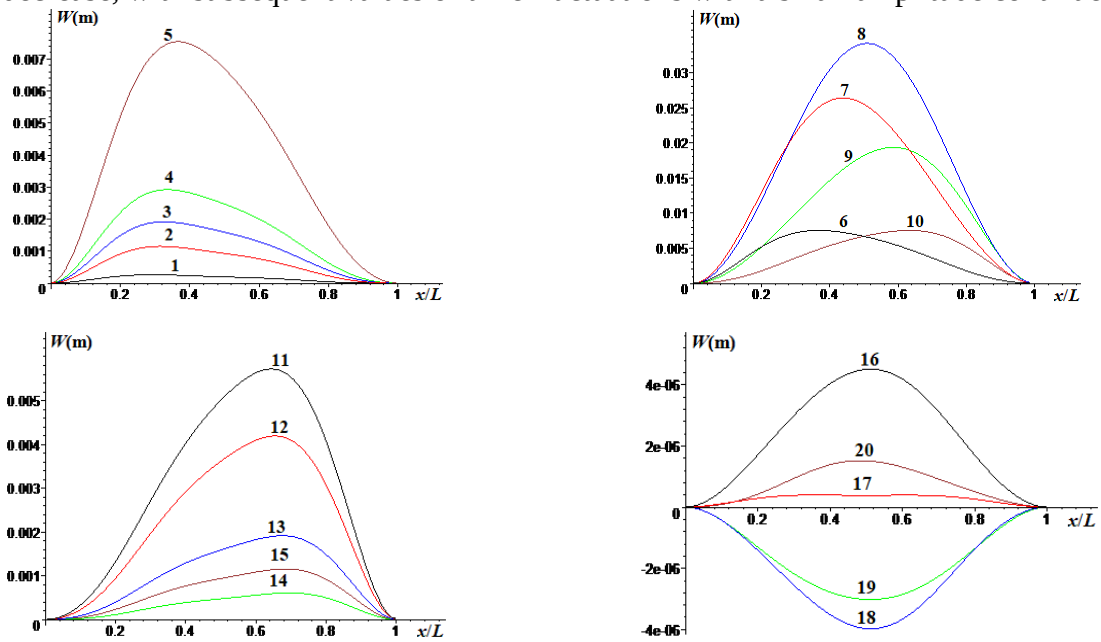

Figure.6. - **Distributions of deflections W(m) of the superstructure along the length for k=10^{10}(N/m) at different values of dimensionless time τ: 1–t=0.3τ_0, 2–t=0.5τ_0, 3–t=0.6τ_0, 4–t=0.7τ_0, 5–t=τ_0, 6–t=τ_0, 7–t=1.8τ_0, 8–t=2.6τ_0, 9–t=3.5τ_0, 10–t=1 τ_0, 11–t=1+0.1τ_0, 12–t=1+0.2τ_0, 13–t=1+0.4τ_0, 14–t=1+0.6τ_0, 15–t=1+0.9τ_0, 16–t=τ_1, 17–t=1.2τ_1, 18–t=1.4τ_1, 19–t=1.8τ_1, 20–t=2τ_1.**

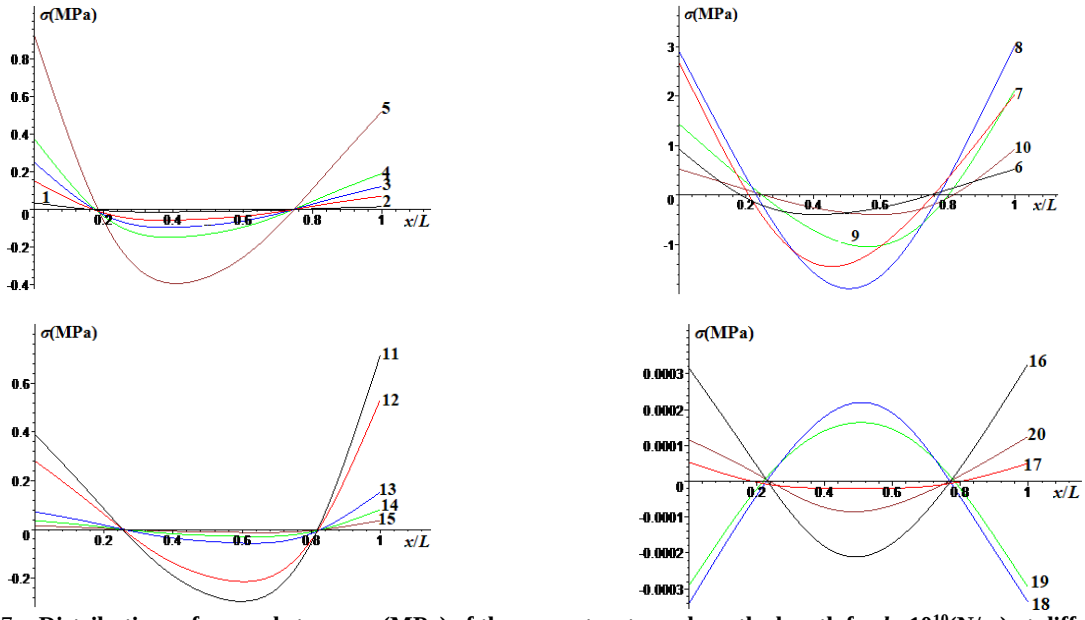

Figure 7. - **Distributions of normal stresses σ(MPa) of the superstructure along the length for k=10^{10}(N/m) at different values of dimensionless time τ: 1–t=0.3τ_0, 2–t=0.5τ_0, 3–t=0.6τ_0, 4–t=0.7τ_0, 5–t=τ_0, 6–t=τ_0, 7–t=1.8τ_0, 8–t=2.6τ_0, 9–t=3.5τ_0, 10–t=1 τ_0, 11–t=1+0.1τ_0, 12–t=1+0.2τ_0, 13–t=1+0.4τ_0, 14–t=1+0.6τ_0, 15–t=1+0.9τ_0, 16–t=τ_1, 17–t=1.2τ_1, 18–t=1.4τ_1, 19–t=1.8τ_1, 20–t=2τ_1.**

It follows from this that with the same values of the stiffness coefficients of the bearings, not very different values of deflections and normal stresses are obtained under the influence of a concentrated or distributed moving load.

4. Conclusion.

Using the Fourier method, an analytical solution to the problem was obtained and the dynamics of the structure under the influence of a moving load was numerically analyzed, taking into account the interaction of the bearing of the bridge with the superstructure. After the end of the action of moving loads, the laws of normal stress distribution along the length of the superstructure are practically independent of time.

Under the influence of moving loads, depending on the stiffness coefficient of the connection between the bearing and the superstructure, a stress may arise in the middle of the section of the superstructure that exceeds the limit. This circumstance indicates the need to take into account the nature of the interaction between the bearing and the superstructure when carrying out calculations of the superstructure under the action of moving loads.

An increase in the stiffness coefficient of the bearings has a different effect on the nature of the stress distribution along the length of the superstructure. Thus, at high values of the coefficient, the laws of stress distribution along the length of the superstructure are practically independent of time. In this case, an increase in the value of this coefficient leads to a decrease in normal stresses in the sections of the superstructure.

References.

1. *Rashidov T., Baybulatov K., Bekmirzayev D., Takhirov S., Gayibov J., Nishonov N.* Comprehensive Program on Structural Assessment of Bridges in Uzbekistan. Vol. 3542. 2020 (Sendai, Japan: The 17th World Conference on Earthquake Engineering). P.3c–0013.
2. *Berdibaev Mars., Mardonov Batir., Nishonov Nematilla., Rakhimjonov Ziyovuddin.* Beam vibration due movement of overweight cargoes on reinforced concrete bridges at different ground conditions. E3S Web of Conferences 401, 01075 / CONMECHYDRO – 2023. https://doi.org/10.1051/e3sconf/202340101075.
3. *Meriem Ouchenane.* Study of the Vibratory Behavior of the Bridge under the Passage of Mobile Loads Convoys: Comparative Study between Unidimensional and Three-dimensional Modeling. Civil Engineering Journal Vol. 4, No. 5, May, 2018.
4. *Lezin Seba Minsili, Gilbert Tchemou, Ayina Ohandja Louis Max, Mandegue Lotin Josette A.* Parametric Analysis of Vertical Deflections of Bridges under Moving Loads. Lezin Seba Minsili et al.; Sch. Bull.; Vol-3, Iss-12 (Dec, 2017):685-694. DOI: 10.21276/sb.2017.3.12.9.
5. *Cantero, Daniel; González, Arturo; O'Brien, Eugene J.* Maximum dynamic stress on bridges traversed by moving loads. Proceedings of the Institution of Civil Engineers Bridge Engineering 162 June 2009 Issue BE2 Pages 75-85 doi: 10.1680/bren.2009.162 .2.75.
6. *Olita S., Ciampa D., Agostinacchio M.* The evaluation of stress-strain state of asphalt bridge joints for high structural durability. 4th International SIIV Congress – Palermo (Italy), 12-14 September 2007.
7. *Yang Liu.* Dynamic Analysis of Elastic Support Beam Subject to Moving Load. Applied Mechanics and Materials 256-259:918-921. December 2012. DOI: 10.4028/www.scientific.net/AMM.256-259.918
8. *Susmita Panda, Arnab Banerjee and Bappaditya Manna.* Effectiveness of an elastically supported beam under the action of moving loads traversing in the opposite direction. Journal of Vibration and Control. April 2023 DOI: 10.1177/10775463231174661.
9. *Mardani E.* The analysis of a beam under moving loads. IJE Transactions B: Applications Vol. 24, No. 3, October 2011 – 227.
10. *Zhenhua Nie, Yongkang Xie, Jun Li, Hong Hao and Hongwei Ma.* Damage detection in bridges under moving loads based on subspace projection residuals. Advances in Structural Engineering 2022, Vol. 0(0) 1–23. DOI: 10.1177/13694332211056107.
11. *Maghsoudi A.A and Azadpour F.* Stress-strain field and theoretical analysis of RC bridge. IJE Transactions B: Applications. Vol. 22, No. 1, April 2009 – 7.
12. *Ruilan Tian, Xinwei Yang, Qin Zhang and Xiuying Guo.* Vibration reduction in beam bridge under moving loads using nonlinear smooth and discontinuous oscillator. Advances in Mechanical Engineering 2016, Vol. 8(6) 1–12. DOI: 10.1177/1687814016652564.
13. *Arshad Mehmood, Ahmad Ali Khan, Husain Mehdi.* Vibration Analysis Of Beam Subjected To Moving Loads Using Finite Element Method. IOSR Journal of Engineering (IOSRJEN) ISSN (e): 2250-3021, ISSN (p): 2278-8719 Vol. 04, Issue 05 (May. 2014).

14. *Petra Bujňáková, Jozef Jošt, and Matúš Farbák.* Load testing of Highway Bridge. MATEC Web of Conferences 196, 02020 (2018) https://doi.org/10.1051/matecconf/201819602020 XXVII R-S-P Seminar 2018, Theoretical Foundation of Civil Engineering.

15. *Khadri Y., Tekili S., Daya E.M., Daouadji A., Guenfoud M., Merzoug B.* Analysis of the Dynamic Response of Bridges Under Moving Loads. International Review of Mechanical Engineering (I.RE.M.E.), Vol. 3, N. 1 January 2009.

16. *Zaki N.* Dynamic response of highway bridges to moving vehicles considering higher modes. Journal of Engineering and Applied Sciences, Vol. 56, Issue 1, 2009, p. 21-38.

17. *Kuchárová D., Melcer J.* Two-span bridge under moving load. Vibroengineering Procedia, Vol. 23, 2019, p. 115-118.

18. *Duc Tran-Van, Toan Nguyen-Xuan, Thao Nguyen-Duy, Loan Nguyen-ThiKim.* Study on dynamic impact factor of girder bridges due to vehicle load model. IOP Conf. Series: Materials Science and Engineering 1289 (2023) 012004. DOI:10.1088/1757-899X/1289/1/012004.

19. *Shermukhamedov U., Sobirova M, Azamov N., Ibrokhimova S.* Analysis of technical and operational condition of urban reinforced concrete bridge structures. E3S Web of Conferences 365, 02015 (2023). https://doi.org/10.1051/e3sconf/202336502015. CONMECHYDRO - 2022.

20. *Shermukhamedov U.Z., Karimova A.B., Abdullaev A.R., Khakimova Ya.T.* Comparison of operating costs of reinforced concrete bridges and overpasses with different static schemes. E3S Web of Conf. Volume 401, V International Scientific Conference "Construction Mechanics, Hydraulics and Water Resources Engineering" (CONMECHYDRO - 2023). https://doi.org/10.1051/e3sconf/202340102035.

21. *Ho-Chul Kwon, Man-Cheol Kim and In-Won Lee.* Vibration control of bridges under moving loads. Computers & Structures Vol. 66, No. 4, pp. 473-480, 1998.

22. *Khadri Y., Tekili S., Daya E.M., Daouadji A., Guenfoud M., Merzoug B.* Analysis of the dynamic response of bridges under moving loads. International Review of Mechanical Engineering (I.RE.M.E.), Vol. 3, N. 1 January 2009.

23. *Veronika Valašková, Daniela Kuchárová, Jozef Melcer.* Two-span bridge under moving load – numerical and experimental approach. Journal of Vibroengineering. May 2020, Volume 22, ISSUE 3.

DYNAMIC SIMULATION OF A HUMAN BODY BY FREQUENCY RESPONSE DATA

Mavlanov T.[1], Khudainazarov Sh.O.[1], Rayimov A.O.[1]

[1]Tashkent Institute of Irrigation and Agricultural Mechanization Engineers" National Research University, Tashkent, Uzbekistan

E-mail: scherzodshox77@mail.ru

Abstract: *It is known that the human body under small vibrations and excitation frequencies can be considered a linear viscoelastic mechanical system. This makes it possible to describe the dynamic properties of a body using frequency response data. This article is devoted to the development of a dynamic model under various influences, considering the viscoelastic properties of the human body. The excitation module represents a dimensionless amplitude-frequency characteristic. The natural vibrations of the human body are examined in the study considering viscoelastic properties. The eigenfrequencies and modes of vibration of a human body are determined.*

Keywords: *the viscoelastic properties, the human body, the classical Boltzmann-Volterra mathematical model, the constructed modeling method, the Maple software, the amplitude-frequency response*

1. Introduction

Modeling is the process of replacing an object of study with some of its models and researching the model to obtain the necessary data about the object. A model is a physical or abstract image of an object to be modeled, appropriate for research that allows one to adequately display the physical properties and characteristics of the object of interest to the researcher. The convenience of conducting research can be determined by various factors: the ease and accessibility of obtaining information, reducing time and material costs for research, etc. We consider a brief classification of types of system modeling. There is physical and mathematical modeling. Physical modeling assumes that either the system under study is used as a model (for example, in the case of a production experiment), or another system with the same or similar physical features. Generally, a prototype of an object is made, tests are conducted, during which its output parameters and characteristics are determined, and the reliability of operation and the degree of fulfillment of the technical requirements presented to the object are assessed. Physical modeling is associated with large time and material costs.

Mathematical modeling is understood as the process of establishing the correspondence of a given real system to a certain mathematical model and the study of this model, which makes it possible to obtain the characteristics of the real system. A mathematical model is an approximate description of a real process, expressed using mathematical relationships. Any mathematical model describes a real process only with a certain degree of approximation to reality. Mathematical models can be systems of differential equations, algebraic equations, matrix equations, linear, and nonlinear equations, etc. Modeling is characterized by the fact that the mathematical model of the system is presented in the form of a computer software or computer model that allows one to perform computational experiments with it. In numerical modeling, methods of computational mathematics are used to build a computer model, and a computational experiment consists of the numerical solution to some mathematical equations for given parameter values and initial conditions.

The study of human posture regulation mechanisms remains one of the most pressing problems in the physiology of movement in recent years. The reason for this lies in valuable theoretical results concerning the general principles of the organization of human movement control. At the current level of understanding of the problem, its analysis is impossible within exclusively physiological studies and requires constructing mathematical models that implement certain physiological hypotheses.

One of the least studied issues of posture regulation is ensuring calm standing. Standing calmly means maintaining an upright posture in the absence of discernible disturbances. The feature of the organization of the posture regulation system is that in response to any identified disturbance, a stereotypical program of compensation is launched. The latter makes it difficult to study the problem.

Currently, there are two main competing points of view regarding the mechanisms of maintaining calm standing. According to one of them, the main role in stabilization is played by the so-called reflex muscle rigidity, supported by the feedback existing in the human body, ensuring muscle force increases (muscle gain) as they lengthen. Another hypothesis is that reflex muscle rigidity is insufficient for stability, and stabilization requires additional mechanisms. The contradiction between the two hypotheses is due to the current lack of methods allowing reliable assessing reflex muscle rigidity.

To experimentally study the mechanisms of ensuring calm standing, two methods were used. The first is to analyze the oscillations of a calmly standing person. These oscillations have a wide spectrum, in which components close to periodic, corresponding to the so-called “fundamental oscillations” are observed, which have a frequency of about 0.35 Hz and, according to several researchers, reflect the dynamics of the stabilization process. The body deviations characteristic of the main vibrations amount to fractions of a degree, which, according to some estimates, corresponds to the sensitivity thresholds of biological sensors in the human body.

At present, there is no consensus regarding the nature of the main oscillations. Some authors believe that the oscillations correspond to the sensitivity thresholds of biological sensors in the human body. According to another point of view, they reflect the natural vibrations of a single-link biomechanical system simulating the human body, stabilized by the viscoelastic properties of muscles.

A common feature of most currently known attempts to mathematically simulate the process of a person standing quietly and describe the biomechanics of the human body is the use of a single-link model, the so-called, inverted pendulum model, which considers mobility only of the ankle joint. However, experimental data was accumulated indicating the active participation of the knee and hip joints in fundamental vibrations during quiet standing. At the same time, interesting results were obtained using three-link mathematical models when studying the human reaction to short-term disturbance. The author is unaware of any currently published articles in which the three-link model is used to analyze the mechanisms of maintaining calm vertical posture, and he believes conducting such a study is of essential interest.

It should be noted that generally in three-link models muscle forces are replaced by moments acting on the joints. Such a replacement is not entirely correct, primarily because in the lower extremities of a person there is a significant number of bi-articular muscles that take an active part in solving various motor tasks. Since muscle rigidity plays an important role in ensuring quiet standing, it is necessary to account for the anthropometric features of the structure of the musculoskeletal system when constructing a three-link model.

The second method of studying the mechanisms of ensuring quiet standing is the consideration of slow disturbances that are not identified by the nervous system as disturbances and do not lead to the launch of compensatory programs. Within this approach, the processes with characteristic times of the order of 10 seconds were revealed in the dynamics of regulation of vertical posture. Such characteristic times are extremely atypical for the human motor system.

Articles [1-3] developed a 3D model of the human body that can simulate movements; these models realized multi-dimensional adjustable functions for creating the human body. Various methods were proposed for creating the human body, allowing one to simulate a database of human movements with high accuracy.

In [4,5], research was conducted on the development of effective damping engineering structures to protect against large vibrations. The basic principles of vibration control are outlined and vibration control strategies for various damping materials and structures are analyzed. Multiple designs of new damping structures and prospects for future developments of engineering structures are presented.

Articles [6-8] overview studies on damping using composite materials. Methods for increasing the damping capacities of structures are described and the physical and mechanical characteristics of materials with better damping properties are given.

The study in [9] comprehensively reviews various methods for studying theoretical calculation models used in mechanical engineering under the static and dynamic vibration characteristics of structures made of viscoelastic damping materials. A classification of conventional viscoelastic damping materials following their physical properties, areas of application, and calculation methods is given.

Articles [10,11] present a calculation methodology for assessing the vibration isolation properties of mechanical systems to reduce vibration. A new technique is proposed for selecting the nonlinear dynamic behavior of passive systems. The mathematical model of the vibration suppression system is developed to simulate its dynamic behavior under various operating conditions. The spectral characteristics of the system's acceleration are presented depending on the acting impacts.

Reference [12] presents a methodology for modeling and analyzing various dynamic systems. Modeling of mechanical, electrical, electromechanical, thermal, and fluid systems is given. For analytical solutions, the Laplace transform is used. Computer solutions are based on *MATLAB* and *Simulink* software. Linear and nonlinear systems are considered as examples. An introduction to modeling and design tools for feedback control systems is provided.

In [13], the use of modal description as an alternative method is presented and its contribution to biodynamic modeling is discussed. Based on experimental data, modal parameters such as natural frequencies, damping coefficients, and modal masses, are determined. The results obtained can be used to develop hardware vibration simulators.

In [14,15], mathematical models of a sitting person's body were developed, using two models with one and two degrees of freedom. The optimal parameters of the models are determined and it is revealed that the model with two degrees of freedom provides an apparent mass similar to the human body mass. Using modal analysis, three states of the human body were associated with resonances in the measured apparent masses.

Article [16] presents a procedure for estimating the dynamic properties of a human body. Excitation is generated by a person moving rhythmically while acting on a flexible structure (for example, a pedestrian overpass). The research was conducted in two directions:

a) determining the modal properties of the elements of a mechanical system;

b) determining the ability of the human body to transmit.

The modal characteristics determined, are vibration frequencies, vibration modes, damping coefficients, and modal mass of the bearing structure.

In [17-21], experimental studies were conducted on biodynamic reactions to vertical vibrations; the influence of vertical excitation on the main resonance manifested in various postures of the human body was studied. It was determined that the transmission of vertical vibration of the seat to the pelvis and upper torso is the same for uniaxial vertical and biaxial vertical excitations, and resonant frequencies manifested in the transmission of vertical vibration of a seat to various parts of the body would decrease with increasing rotation speed of the seat. Test subjects took different sitting postures with different heights of footsteps to ensure different hip contact with the seat. Forces were measured in the vertical direction, in front and rear, in sideward direction on the seat, and the vertical direction on the footstep. The characteristic nonlinear response of the human body with a decrease in resonant frequency at an increase in vibration intensity was observed in all postures, but to a lesser extent at a minimal hip contact.

Reference [22] is devoted to the construction of a mathematical model of a person sitting in a seat with a backrest to assess comfort when driving in a car. In describing the movements of a seated person, two multi-body models representing automotive postures were studied. Both models were modified to best accommodate different driving positions with and without backrest supports. Based on the analytical study and experimental verification, it was found that the fourteen degrees of freedom model proposed in this study best fits the test results. Therefore, this model is recommended for studying the biodynamic responses of a sitting human body subjected to vertical vibrations in various vehicle positions.

The purpose of this work is to construct a mathematical model of the human body based on frequency characteristics to protect against harmful vibrations.

2. Research methods

In theoretical modeling, the human body is represented as a mechanical system consisting of a certain number of solid bodies jointed by elastic and viscous properties. At small oscillations and excitation frequencies, the human body can be considered a linear viscoelastic mechanical system. This makes it possible to describe the dynamic properties of a body using frequency characteristics.

The most general linear theory, which most fully reflects almost all the features of the quasi-static and dynamic behavior of the viscoelastic characteristics of materials, (in our case, a human body), is the Boltzmann-Volterra theory, according to which the relationship between stresses and strains has the following form:

$$\varsigma(t) = E[\varepsilon(t) - \int_0^t R\,(R(t-\tau)\varepsilon(\tau)d\tau]\,, \tag{1}$$

where ς – is the stress, ε - strain, t - observation time, $0 < \alpha < 1$ - intermediate moment, E - instantaneous Young's modulus, R - memory function or relaxation kernel.

The type of kernel R significantly separates both the behavior of the material model and the possibility of using certain methods for solving problems for materials modeled using relation (1). If function R has the form of an exponential or a sum of exponentials, then relations (1) are reduced to differential relations, the order of which is equal to the number of exponentials in the specified sum. The behavior of viscoelastic materials is most adequately described by weakly singular heredities, of which we note the A.P. Bronsky kernel:

$$\mathbf{R}(t-\tau) = \frac{\alpha\lambda e^{-(t-\tau)\alpha}}{(t-\tau)^{1-\alpha}}, 0 < \alpha < 1, \tag{2}$$

Power kernel is

$$K(t-\tau) = \frac{\beta}{(\alpha)(t-\tau)^{1-\alpha}}, 0 < \alpha < 1, \tag{3}$$

To solve the problems posed in this work, the M.A. Koltunov and A.P. Rzhanitsyn kernels were used [23-25]**:**

$$R(t-\tau) = \frac{Ae^{-\beta(t-\tau)}}{(t-\tau)^{\alpha}}, \tag{4}$$

which, on the one hand, very satisfactorily reflects both the quasi-static and dynamic behavior of materials; on the other hand, it is most convenient when conducting quasi-static and dynamic calculations and determining mechanical vibrations.

The problem of oscillations of viscoelastic systems is reduced to a system of integro-differential equations (differential in coordinates and integro-differential in time). The system of equations contains partial derivatives in the case of systems with distributed parameters and ordinary derivatives in the case of systems with a finite number of degrees of freedom. Statements of problems in the theory of viscoelasticity as quasi-static ones are presented with exhaustive detail in the monograph [26].

Dynamic problems with an infinite number of degrees of freedom using some approximate method (Bubnov-Galerkin, Ritz, finite elements) can be reduced to a system of a finite number of differential or integro-differential equations in time. From the concepts of mechanics, this means replacing a system with an infinite number of degrees of freedom with a system with lumped parameters or imposing an infinite number of additional connections on the original system. The vast majority of problems in the nonlinear and linear theory of viscoelasticity were solved in this way. The main difficulty that arises here is the choice of basic coordinate functions into which the sought-for solution is expanded. These functions are quite simple in the case of bodies of simple shape. In the case of a body of more or less complex shapes, the choice of a system of basic coordinate functions of the projection method, which reduces the original system to a system with a finite number of degrees of freedom, is a difficult problem.

Small mechanical vibrations occur in elastic bodies under the influence of variable forces. Vibration is characterized by frequency *f*, i.e. number of oscillations per second (*Hz*), amplitude *A*, i.e. displacement of waves, or height of rise from the equilibrium position (mm), velocity *V* (m/s), and acceleration. The entire range of vibration frequencies is divided into 1, 2, 4, 8, 16, 32, 63 125, 250, 500, 1000, 2000 Hz. The absolute values of the parameters characterizing vibration vary within wide limits.

It is known that the human body can be considered a complex mechanical system. One system is the entire torso with the lower part of the spine and pelvis, another - the upper part of the torso in combination with the upper part of the spine, tilted forward. For a person standing on a vibrating surface, there are 2 resonant peaks at frequencies of 5...12 and 17...25 Hz, for a sitting person - at frequencies of 4...6 Hz. For the head, resonant frequencies are in the range of 20…30 Hz. In this frequency range, the amplitude of head vibrations can exceed the amplitude of shoulder vibrations by 3 times. Vibrations of internal organs, chest and abdominal cavity exhibit resonance at frequencies of 3.0...3.5 Hz.

To protect the human body from vibration, it is necessary to build a mathematical model of the human body. The structure of the human body model must be selected considering the experimental data presented by the frequency characteristics. Moreover, the general principle of modeling is that the theoretical model should have the same dynamic characteristics as the human body. From a mathematical point of view, the task of determining a finite number of model parameters from known frequency characteristics is complex [27-29].

In order to best approximate the properties of the model to the properties of the modeled object, the required parameters are determined from the conditions of minimum error. We will use the standard deviation criterion as an error. The task is formulated as follows. The input mechanical impedance of the human body is specified in the form of graphs or tables of modulus and phase obtained from the experiment. It is required to build a dynamic model of the human body in the form of linear mechanical systems with lumped parameters. In this case, expressions for describing the input pulse are considered given. For example, according to [30], the input impedance is sought in the following form:

$$\mathrm{Z(p)} = \frac{\mathrm{a_n p^n + a_{n-1} p^{n-1} + \cdots + a_0}}{\mathrm{g_l p^l + g_{l-1} p^{l-1} + \cdots + g_0}} \tag{5}$$

here $a_n = f_n(m_i, c_i, b_i)$; $g_l = f_l(m_i, c_i, b_i)$ are the functions depending on the inertial m_i, elastic c_i and damping b_i parameters of the model; *n* and l are positive integers, and $n \leq l$.

The values of a_n and g_l are determined by the criterion of the minimum sum of standard deviations of modulus $|Z(i\omega)|$ and phase $\varphi(\omega)$ of the frequency response:

$$\min K=\min\sum_0^N\left\{\left[|Z(i\omega_j)|-|Z^*(i\omega_j)|\right]^2+\left[\varphi(\omega_j)-\varphi^*(\omega_j)\right]^2\right\}, \quad (6)$$

here, N− is the number of approximation points selected on the frequency axis.

Condition (6) is satisfied for:

$$\frac{\partial K}{\partial(a_n, g_l)}=0 \quad (7)$$

Expression (7) after transformations is reduced to a system of equations for the unknowns a_n and g_l. In particular, in contrast to [30], for a standing person, we will accept a mechanical model in the form of a two-mass oscillatory system. Then for this problem, relations (1-3) will be rewritten as follows:

$$Z(p)=\frac{a_4p^4+a_3p^3+a_2p^2+a_1p}{g_4p^4+g_3p^3+g_2p^2+g_1p+g_0}, (8)$$

Hence,

$$|Z(i\omega)|^2=\frac{(a_4\omega^4-a_2\omega^2)^2+(a_1\omega-a_3\omega^3)^2}{(g_4\omega^4-g_2\omega^2+g_0)^2+(g_1\omega-g_3\omega^3)^2}, (9)$$

$$\varphi(\omega)=arctg\frac{(a_1\omega-a_3\omega^3)(g_4\omega^4-g_2\omega^2+g_0)-(a_4\omega^4-a_2\omega^2)(g_1\omega-g_3\omega^3)}{(a_4\omega^4-a_2\omega^2)(g_4\omega^4-g_2\omega^2+g_0)+(g_1\omega-g_3\omega^3)(a_1\omega-a_3\omega^3)}, \quad (10)$$

3. Results and discussion

Experimental values of mass m[kgf·s^2/m], stiffness coefficient c [kgf/m] and damping coefficient b [kgf·s/m] for a standing person as a two-mass oscillatory system are:

$$m_1=6.2,\ m_2=1.3,\ c_1=6.2\cdot10^3,\ c_2=8\cdot10^3,\ b_1=140;\ b_2=53;$$

The known structure of the model unambiguously determines the functional relationship between a_n and g_l and the parameters of the model:

$$a_1=c_1c_2(m_1+m_2)=3.72\cdot10^7,\qquad a_2=(m_1+m_2)(b_1c_2+b_2c_1)=1.09\cdot10^7,$$
$$a_3=b_1b_2(m_1+m_2)+m_1m_2(c_1+c_2)=1.7\cdot10^5,\ a_4=m_1m_2(b_1+b_2)=1555.58,$$
$$g_0=c_1c_2=4.96\cdot10^7,\qquad g_1=b_1c_2+b_2c_1=1.45\cdot10^6,$$
$$g_2=m_1c_2+m_2c_1+b_1\cdot b_2=65080,\ g_3=m_1b_2+m_2b_1=510.6,\ g_4=m_1m_2=8.06, \quad (11)$$

Let us write equation (10) using experimental data a_n and g_l obtained using (11):

$$\left|z^*(iw_j)\right|=\sqrt{\frac{\left(2.42\,10^6\,w_i^6-4.87\,10^9\,w_i^4-8.52\,10^{12}\,w_i^2+1.38\,10^{17}\right)w_i^2}{64.96\,w_i^8-7.88\,10^5\,w_i^6+3.56\,10^9\,w_i^4-4.36\,10^{12}\,w_i^2+2.46\,10^{15}}}, \quad (12)$$

$$\varphi^*(\omega_j)=-\arctan\left(\frac{5.77\,10^5\,w_i^6-6.27\,10^9\,w_i^4+1.69\,10^{13}\,w_i^2-1.85\,10^{16}}{w_i^3\left(12537.97\,w_i^4-1.02\,10^8\,w_i^2+3.48\,10^{11}\right)}\right), \quad (13)$$

Now we find experimental values of $|z^*(iw_j)|$ and $\varphi^*(\omega_j)$ at fixed frequency values $\omega_j=2\pi f_j$ $(f_j=3,5,6,8,10,12,5\ Hz)$, Table (1).

Table 1

Experimental values of $|z^*(iw_j)|$ and $\varphi^*(\omega_j)$ at fixed frequency values

f_j	3	5	6	8	10	12.5
$\|z^*(iw_j)\|$	190.06	368.59	347.65	278.02	297.21	381.25
$\varphi^*(\omega_j)$	1.41	0.74	0.42	0.29	0.38	0.18

We will plot functions $||z^*(iw_j)|$ and $\varphi*(\omega_j)$ using (7) relative to f_j in Figs.1 and 2.

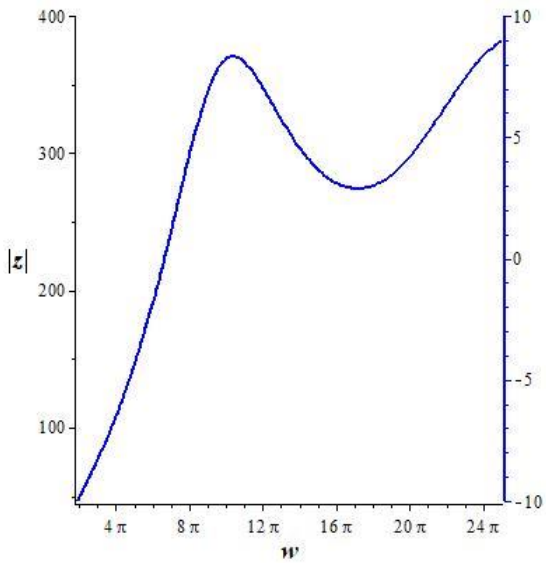

Figure 1. - **Graph of function $\left|z^*(iw_j)\right|$ depending on the oscillation frequency**

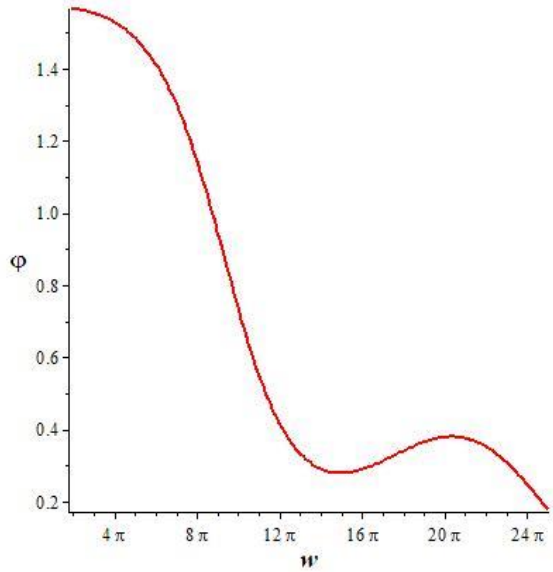

Figure 2. - **Graph of function $\varphi*(\omega_j)$ depending on the oscillation frequency**

graph of the function depending on the oscillation frequency

With (10) at fixed values of frequencies $2\pi f_j$ $\left(f_j \text{ is } 3,5,6,8,10,12,5\ Hz\right)$, and experimental ff_ivalues $\left|z^*(iw_j)\right|$ and $\phi(\omega_j)$ from Table (1) corresponding to these frequencies, function K is obtained in the form:

$$K = \left[\left|Z(i\omega_j)\right| - \left|Z^*(i\omega_j)\right|\right]^2 + \left[\varphi(\omega_j) - \varphi^*(\omega_j)\right]^2 \tag{14}$$

The function obtained in the form (14) using the *"Maple"* software was minimized by the least squares method, the minimum value of function K was obtained, and the partial values of a_n and g_n were determined when minimizing function K:

$$minK = 6939.55,$$
$$a_1 = 5.01 \cdot 10^9, \quad a_2 = 4.72 \cdot 10^7, \quad a_3 = 10^6, \quad a_4 = 286.48,$$
$$g_0 = 4.99 \cdot 10^8, \quad g_1 = 10^7, \quad g_2 = 2.83 \cdot 10^5, \quad g_3 = 0, \quad g_4 = 41.68, \tag{15}$$

The values of a_n and g_l are determined by the criterion of the minimum of sum of standard deviations of module $|Z(i\omega)|$ and phase $\varphi(\omega)$ of the frequency response.

Let us write equation (5) using the calculated data a_n and g_l obtained using (8):

$$\left|z(iw_j)\right| = \sqrt{\frac{\left(82070.79\,w^6 + 9.73\,10^{11}\,w^4 - 7.79\,10^{15}\,w^2 + 2.51\,10^{19}\right)w^2}{1737.22\,w^8 - 2.36\,10^7\,w^6 + 1.22\,10^{11}\,w^4 - 1.82\,10^{14}\,w^2 + 2.49\,10^{17}}}$$

$$\varphi^*(\omega_j) = -\arctan\left(\frac{4.17\,10^7\,w^6 - 4.89\,10^{11}\,w^4 + 1.44\,10^{15}\,w^2 - 2.50\,10^{18}}{w\left(11940.49\,w^6 - 2.05\,10^9\,w^4 + 3.50\,10^{12}\,w^2 + 2.65\,10^{16}\right)}\right) \tag{9}$$

Let us plot functions $|Z(i\omega)|$ and $\varphi(\omega)$ from calculated data using (7) relative to f_j , Figs. 3 and 4 (blue line).

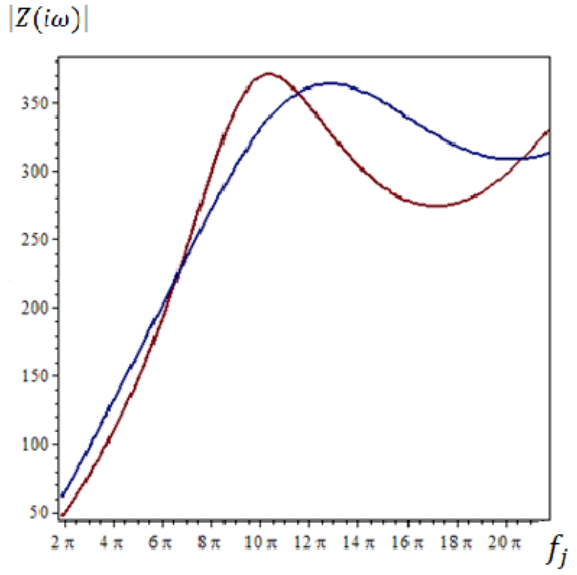

Figure 3. - **Graph of function $|z^*(iw_j)|$ depending on the oscillation frequency**

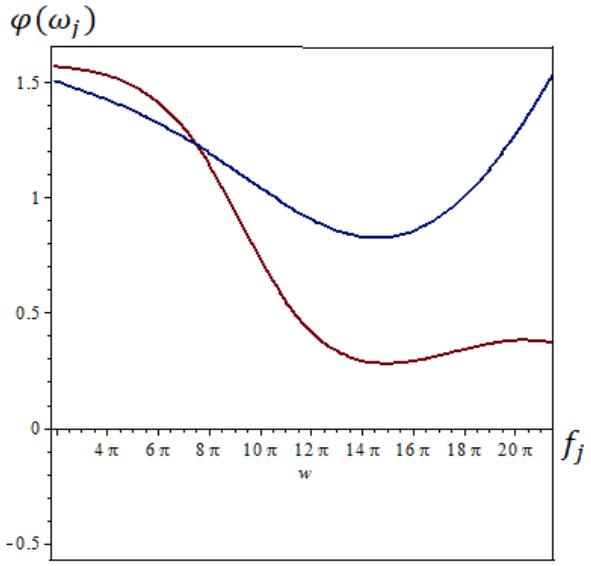

Figure 4. - **Graph of function $\varphi(\omega_j)$ depending on the oscillation frequency**

_____ - experimental data _____ - calculated data

4. Conclusions

As a result of the study, the following conclusions were drawn:

1. To account for the viscoelastic properties of the elements of the human body, the classical Boltzmann-Volterra mathematical model was used;

2. The three-parameter Rzhanitsyn-Koltunov kernel was used as a relaxation kernel, which satisfactorily reflects the quasi-static and dynamic behavior of the parts of the human body;

3. Based on the posture of the person, the constructed modeling method allows us to assess the impact of vibration and reduce them, allowing us to create and implement protective equipment for a person;

4. Using the *Maple* software package, numerical modeling was performed and the amplitude-frequency response was determined.

References

1. *Shen Y., Li C., Guo Y.* Research on 3D Human Body Modeling // Man-Machine-Environment System Engineering. MMESE 2023, Lecture Notes in Electrical Engineering, vol. 1069. Springer, Singapore. https://doi.org/10.1007/978-981-99-4882-6_7
2. *Chi C, Zeng X., Bruniaux P., Tartare G., Jin H.* A new parametric 3D human body modeling approach by using key position labeling and body parts segmentation // Textile Research Journal, 2022, 92(19-20):3653-3679. https://doi.org/:10.1177/00405175221089688
3. *Luo S., Zhang Q. and Feng J.* Automatic location and semantic labeling of landmarks on 3D human body models // Comp. Visual Media **8**, 2022, pp. 553–570. https://doi.org/10.1007/s41095-021-0254-4
4. *Zhang H., Li J., Wang Z. et al.* Biological Vibration Damping Strategies and Mechanisms // J Bionic Eng. **20**, 2023, pp. 1417–1433. https://doi.org/10.1007/s42235-023-00366-6
5. *Chung D.D.L.* Review: Materials for vibration damping // Journal of Materials Science **36**, 2001, pp. 5733–5737. https://doi.org/10.1023/A:1012999616049
6. *Chung D.D.L.* Structural composite materials tailored for damping // Journal of Alloys and Compounds, 2003, vol. 355, pp. 216-223, https://doi.org/10.1016/S0925-8388(03)00233-0.
7. *Luo J. L., Duan Z. D., Xian G. J., Li Q. Y. and Zhao T. J.* Damping performances of carbon nanotube reinforced cement composite // Mechanics of Advanced Materials and Structures, 2015, pp. 224–232. https://doi.org/10.1080/15376494.2012.736052
8. *Chandra R., Singh S.P., Gupta K.* Damping studies in fiber-reinforced composites – a review, Composite Structures, 1999, vol. 46, pp. 41-51, https://doi.org/10.1016/S0263-8223(99)00041-0.

9. *Zhou X.Q., Yu D.Y., Shao X.Y., Zhang S.Q., Wang S.* Research and applications of viscoelastic vibration damping materials // A review, Composite Structures, 2016, vol. 136, pp. 460-480, https://doi.org/10.1016/j.compstruct.2015.10.014.
10. *Maciejewski I., Zlobinski M. and Krzyzynski T.* Optimal design of vibration-isolation systems by means of a numerical simulation // J Mech Sci Technol 35, 2021, pp. 3887–3894. https://doi.org/10.1007/s12206-021-0802-y
11. *Maciejewski I., Meyer L. and Krzyzynski T.* Modelling and multi-criteria optimization of passive seat suspension vibro-isolating properties // Journal of Sound and Vibration, 324, 2009, pp. 520–538.
12. *Close C. M., Frederick D. K. and Newell J. C.* Modeling and Analysis of Dynamic Systems // 3rd Edition, John Wiley, 2001, New York.
13. *Sebastian Rützel, Barbara Hinz, Horst Peter Wölfel* Modal description—A better way of characterizing human vibration behavior // Journal of Sound and Vibration, 2006, vol. 298, pp. 810-823, https://doi.org/10.1016/j.jsv.2006.06.019.
14. *Wei L., Griffin M.J.* Mathematical models for the apparent mass of the seated human body exposed to vertical vibration // Journal of Sound and Vibration, 1998, vol. 212, pp. 855-874, https://doi.org/10.1006/jsvi.1997.1473.
15. *Wu Jun, Qiu Yi, Sun Chao* Modelling and analysis of coupled vibration of human body in the sagittal and coronal planes exposed to vertical, lateral and roll vibrations and the comparison with modal test // Mechanical Systems and Signal Processing, 2022, vol. 166, pp. 1085-1094 https://doi.org/10.1016/j.ymssp.2021.108439.
16. *Wei He, Kewen He, Hang Cui, Guobo Wang* Using a rhythmic human shaker to identify modal properties of a stationary human body on a footbridge // Journal of Sound and Vibration, 2022, vol. 540, 117309, https://doi.org/10.1016/j.jsv.2022.117309.
17. *Zheng Guangtai, Qiu Yi, Griffin Michael J.* Vertical and dual-axis vibration of the seated human body: Nonlinearity, cross-axis coupling, and associations between resonances in transmissibility and apparent mass // Journal of Sound and Vibration, 2012, vol. 331, pp. 5880-5894, https://doi.org/10.1016/j.jsv.2012.07.029.
18. *Fairley Thomas E., Griffin Michael J.* The apparent mass of the seated human body // Vertical vibration, Journal of Biomechanics, 1989, vol. 22, pp. 81-94. ISSN 0021-9290, https://doi.org/10.1016/0021-9290(89)90031-6.
19. *Wu J., Qiu Y.* The Study of Seat Vibration Transmission of a High-speed Train Based on Improved MISO Method // Mechan. Syst. Sign. Process, 2020, 143 p.
20. *Nawayseh N., Griffin M.J.* Non-linear dual-axis biodynamic response to vertical whole-body vibration, // Journal of Sound and Vibration, 2003, vol. 268, pp. 503-523, https://doi.org/10.1016/S0022-460X(03)00254-2.
21. *Wu J. , Qiu Y.* Modelling of seated human body exposed to vertical, lateral and roll vibration // J. Sound Vib., 2020, 485 p.
22. *Liang C.C., Chiang C.F.* Modeling of a seated human body exposed to vertical vibrations in various automotive postures Ind. Health, 46, 2008, pp. 125-137.
23. *Sherzod Khudainazarov, Burkhon Donayev, Talibjan Sabirjanov and Jahongir Qosimov* Dynamics of high-rise structures taking into account the viscoelastic properties of the material // E3S Web of Conferences 304,2021, 02004 https://doi.org/10.1051/e3sconf/202130402004
24. *Khudainazarov Sh., Mavlanov T., Salimov Sh., Ulugova M. and Sabirjanov T.* Simulation of dynamic processes of shell structures with viscoelastic elements // E3S Web of Conferences. 2023, 365, 03040. https://doi.org/10.1051/e3sconf/202336503040
25. *Khudainazarov Sh., Mavlanov T., Umarova F., Sabirjanov T. and Ulugova M.* Evaluation of the dynamic characteristics of complex multiply connected, structurally inhomogeneous systems // E3S Web of Conferences. 2023, 365, 03035 https://doi.org/10.1051/e3sconf/202336503035
26. *Samarskii A.A., Mikhailov A.P.* Mathematical Modeling / Ideas. Methods. Examples. 2nd ed. corr. – M.: FIZMATLIT, 2005. - 320 p.
27. *Khakimzyanov G.S., Chubarov L.B., Voronina P.B.* Mathematical modeling / Novosibirsk, RITC NSU, 2014. – 263 p.
28. *Marion G. and Lawson D.* An Introduction to Mathematical Modelling // Scientific Research Publishing, 2008, pp. 1-32. https://www.scirp.org/reference/referencespapers?referenceid=2416390
29. *Moghadas S.M., Jaberi-Douraki M.* Mathematical modeling / A graduate textbook. John Wiley and Sons, Inc. 2018, 192 p.
30. *Frolov K.V.* Vibrations in technology / M.: “Mechanical Engineering”. 1981, vol. 6, 456 p.

NUMERICAL STUDY OF THE ZONE OF INFLUENCE OF TWO PARALLEL RUNNING TUNNELS.

Miralimov M. [1], Ishanhodjaev A.[1], Normurodov Sh. [1], Usmanov D.[1]
[1]*Tashkent State Transport University, Tashkent, Uzbekistan*
E-mail: rustam_abirov@mail.ru

Abstract. *Problems related to a violation of the stability of the soil mass, engineering structures, communications, etc., arise during the construction of two parallel tunnels using a shield method in weak unstable soils in densely built-up areas are solved here. Existing engineering methods are based on the preliminary determination of loads with the subsequent use of the principles of structural mechanics and soil mechanics [1-3]. Their main drawback is that they do not fully account for the real conditions of the interaction of parallel tunnels with the surrounding soil mass [4, 5]. In addition, the problems of understanding and analyzing a number of physical processes and predicting strains in the rock mass and the ground surface have not been solved before.*

Keywords: *Tunnel, structural, interaction, soil, finite element*

1. Introduction

A more complete analysis of the studies shows that the use of numerical methods of analysis makes it possible to avoid a number of shortcomings of empirical, semi-empirical and analytical methods; however, the scientific studies conducted in this direction are scattered and require generalization and updates. In addition, it practically do not affect the forecast of geo-mechanical processes during the construction of structures of complex spatial configuration. So some solutions was proposed in [6, 7]. To analyze this problem, a numerical approach to investigate additional stresses and displacements in tunnels when the distance between them changes described below. Finite element approach is more conventional for solving of this problem. In order to identify patterns of stress-strain state change in the system “soil mass–two parallel tunnels”, the computational domain was used, shown in Fig. 1.

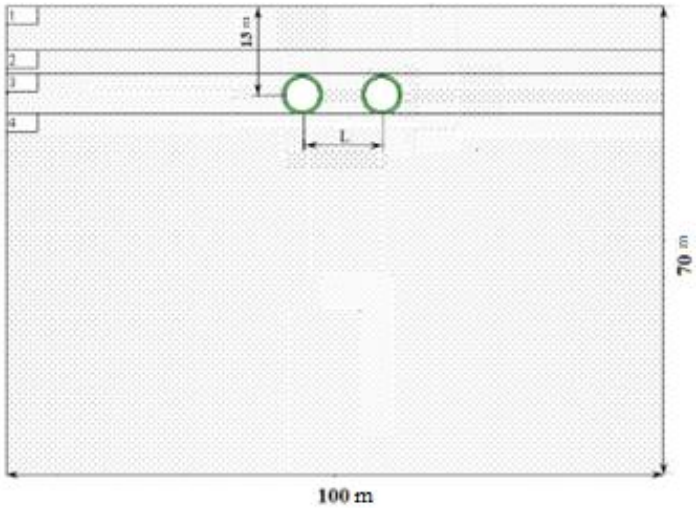

Figure 1. - **Computational domain with parallel tunnels**

2. Methods

The excavation of a working, associated with the removal of a certain volume of soil from the massif, leads to a violation of the equilibrium that existed in the massif and a change in the initial stress field. At the same time, the stress-strain state of an untouched rock mass under the action of initial stresses without a working is first determined, and then a working is carried out in it and an additional stress-strain state of the rocks is determined from the "removal" of stresses on its contour. The sum of the initial and additional stress and strain fields gives a solution to the problem [6].

The desired components of the total stresses in the soil continua can be represented, as indicated above, as the sum of two terms:

$$\sigma_{ij} = \sigma_{ij}^{(o)} + \sigma_{ij}^{(1)} \qquad (1)$$

here $\sigma_{ij}^{(o)}$ are the initial stresses that acted in the undisturbed mass before the formation of the working; $\sigma_{ij}^{(1)}$ are additional (removable) stresses caused by the formation of workings.

Based on the foregoing, the design scheme of a tunnel working is, in the general case, a plane simulating an array weakened by a hole. Relieved stresses are applied to the line of contact of the lining with the array C_L, and external forces can also be applied to the boundary C_P, if necessary.

In a soil massif with an average specific gravity γ, the vertical and horizontal components of the body forces from rock pressure at a certain depth are used by the well-known formulas:

$$\sigma_{yy}^{(o)} = \gamma H; \quad \sigma_{xx}^{(o)} = \lambda \gamma H \tag{2}$$

here H is the excavation depth; γ is the average specific gravity of the array; λ is the lateral pressure coefficient.

The loads applied to the considered part of the massif can be specified both by the boundary normal and tangential forces, and by the distributed mass forces of the weight of the rocks. On the remote lateral boundaries of the considered zone, the corresponding conditions are modeled as rigid one along the normal to these boundaries. The disadvantage of the finite element method is the impossibility to take the conditions at infinity.

If the mass is layered, then the stresses change significantly from layer to layer and the more, the more their elastic characteristics differ. Therefore, when the mine working intersects rock layers with different initial stress state, the stress distribution around the rock contour differs significantly from the homogeneous model.

The elastic linear model is based on Hooke's law of isotropic linear elasticity. Well, known this model includes two constant stiffness parameters: Young modulus and Poisson's ratio.

Analysis of the stress state by the finite element method satisfies the conditions of the static equilibrium condition and makes it possible to evaluate stress changes caused by varying elastic properties, inhomogeneity, and geometric shapes.

Thus, by specifying the forces at each node from the self-weight of the base and at the boundaries of the region, a system of joint equations based on a common stiffness matrix can be resolved with respect to the displacements of each node.

If the calculation results are considered in a different form, then the relationship between the stresses in the Cartesian and polar coordinate systems is obtained as:

$$\left.\begin{matrix}\sigma_r \\ \sigma_\theta\end{matrix}\right\} = \frac{\sigma_1 + \sigma_2}{2} \pm \frac{\sigma_1 - \sigma_2}{2}\cos 2\theta$$
$$\tau_{r\theta} = -\frac{\sigma_1 - \sigma_2}{2}\sin 2\theta \tag{3}$$

Once the displacements are defined, the stresses can be determined for each element. The mesh of the soil area is carried out by isoparametric finite elements. The well-known Mohr-Coulomb model can be considered as a first-order approximation with respect to the real behavior of the soil. This elastoplastic model requires knowledge of four main input parameters, namely, young modulus E, Poisson's ratio υ, cohesion C, and the angle of internal friction φ.

In the general case, when opening a working in a soil mass, two zones are distinguished: elastic - stable 1 and plastic - unstable 2. Elastic zone conforms the Hooke's law and plastic one the Coulomb-Mohr condition ($\tau_{\lim} = \sigma_n tg\varphi + C$). Here $\tau_{\lim}$ is the limiting shear stress, σ_n is the normal stress on the shear areas.

If the strength of the soil material is determined only by the maximum and minimum principal stresses, then the Mohr-Coulomb condition can be written in the following form:

$$\sigma_1 - \sigma_2 = (\sigma_1 + \sigma_2 + 2\sigma_c)\sin\varphi \tag{4}$$

here $\sigma_c = C / tg\varphi$.

In this case, the principal stresses, as is known, are expressed in terms of the stress components along two mutually perpendicular areas by the dependences

$$\left.\begin{matrix}\sigma_1\\ \sigma_2\end{matrix}\right\} = \frac{1}{2}(\sigma_x + \sigma_y) \pm \frac{1}{2}\sqrt{(\sigma_x - \sigma_y)^2 + 4\tau^2_{xy}} \tag{5}$$

In numerical scheme the stresses are calculated at the center of each finite element. With a known stress field within investigated zone and a given yield condition, it is possible to estimate the strength of the rock at each site of the foundation. Assuming, for instance, that the destruction of rocks occurs due to shear, knowing the limiting values of shear resistance for rocks of different sections of the massif, and determining the effective shear stresses for the most dangerous areas in the elements of the mesh, we can find the values of safety factors for these sites:

$$\eta = \frac{\tau_{np}}{\tau} \tag{6}$$

In the simplest case, these data make it possible to construct lines of equal soil safety factors (isolines). Zones with η>l indicate that the soil has a margin of safety; at η=l, the zones are unstable.

By using this approach boundary problem was solved below.

3. Numerical results and analysis

When performing multivariate calculations, three values of distances between the centers of two parallel tunnels were taken: L=12.9 m, L=18 m, and L=24 m. Figure 2 shows the strain pattern for the computational domain, taking into account the distance between the tunnels, where the values of vertical displacements of the ground surface began to decrease with increasing distance (Fig. 3).

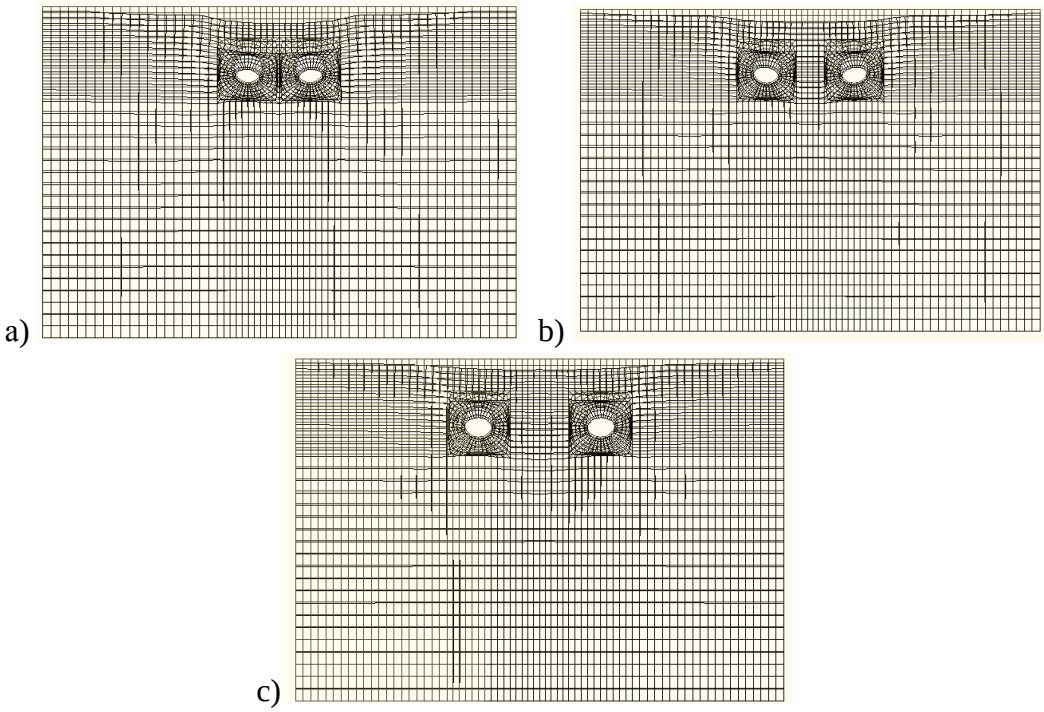

Figure 2. **- Strain pattern of the computational domain for: a) L=12,9 m, b) L =18 m, c) L =24 m**

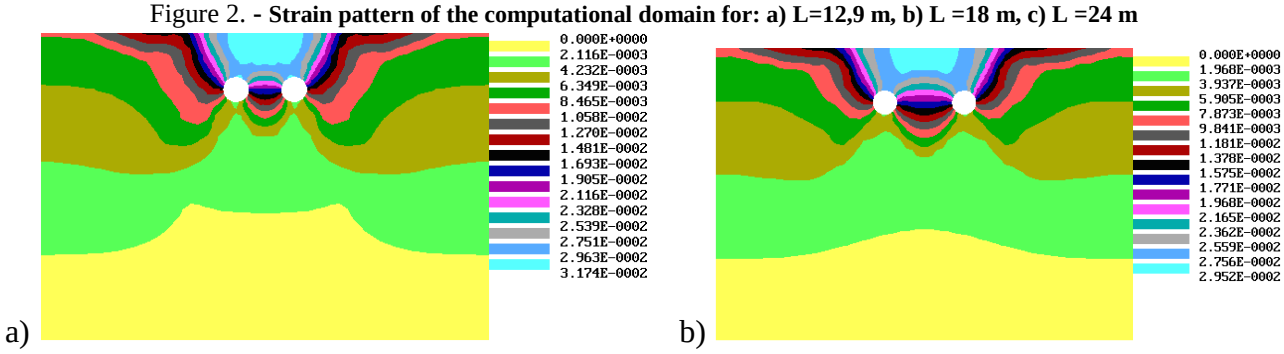

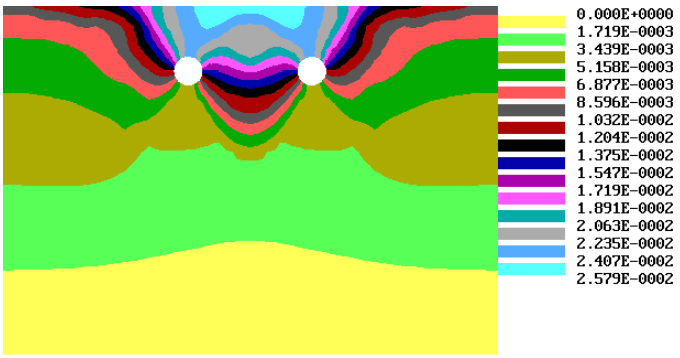

c)

Figure 3. - **Isochromes of vertical displacements of the domain, (m) for: a) L=12,9 m, b) L=18 m, c) L=24 m**

Cauldrons of vertical subsidence of the ground surface during the driving of running tunnels, considering the distance between the tunnels, are shown in Fig. 4.

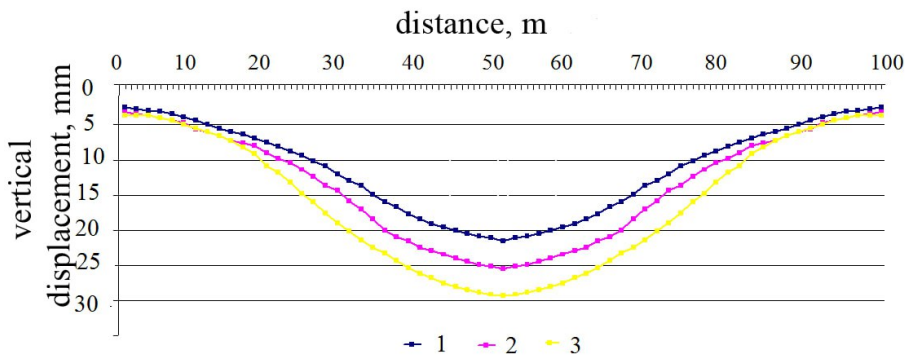

Figure 4. - **Cauldrons of vertical subsidence of the ground surface during the driving of running tunnels, (mm) for: 1 - L=12,9 m, 2 - L=18 m, 3 - L=24 m**

Figure 5 shows the distribution of maximum radial and shear stresses in the soil area between the tunnels depending on their distance.

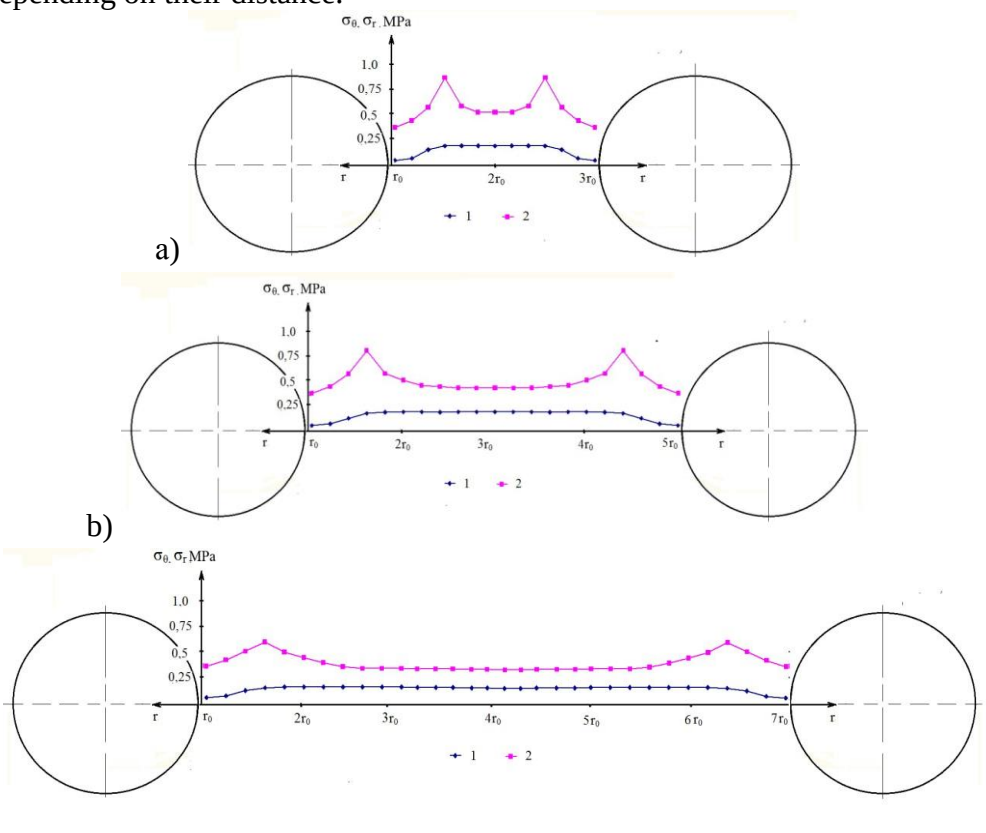

a)

b)

c)

1 - σ_r, 2 - σ_θ

Figure 5. - **Distributions of maximum radial and shear stresses in the soil, (MPa) for: a) L=12,9 m, b) L=18 m, c) L=24 m**

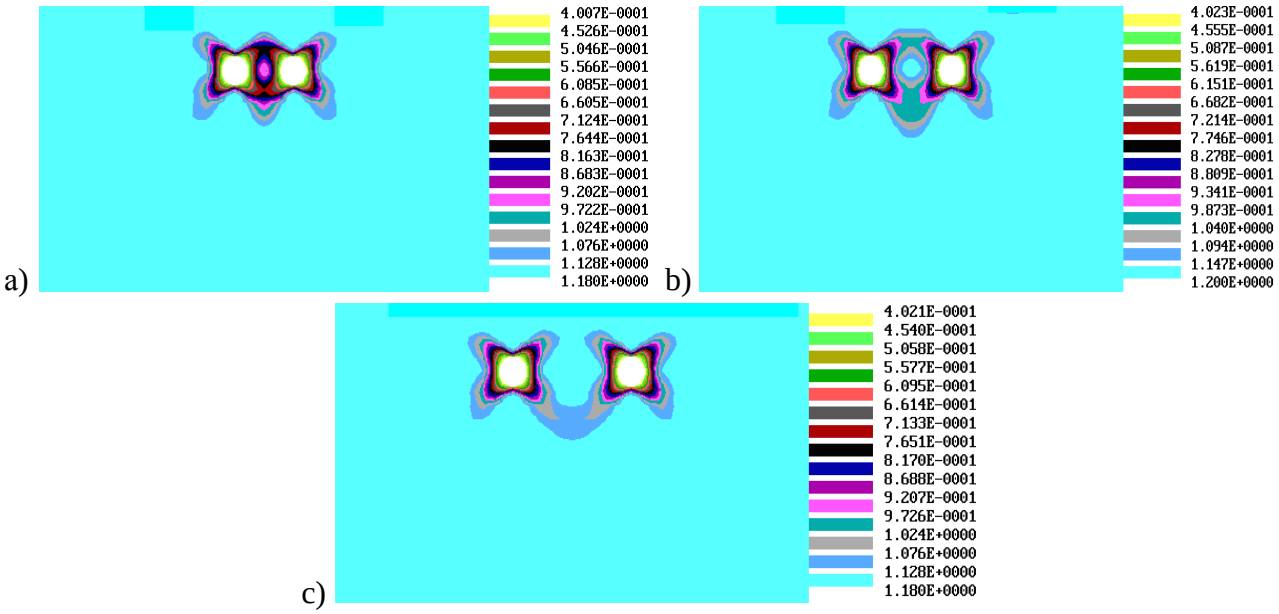

Figure 6. **Isochromes of safety factors η for a given domain for: a) L=12,9 m, b) L=18 m, c) L=24 m**

4. Conclusion

The proposed method for implementing a numerical method for solving integro-differential equations of motion of concentrated masses with account of the viscoelasticity of deformation of materials according to the hereditary theory is satisfactory and can be applied in practice to solve engineering problems. A new opportunity originates can optimize the damping properties of materials of vibrating structures that is important in solving the problem of introducing new materials. In mechanics was proposed a new approach that knowing the rheological parameters of material one can find directly the damping coefficients without resorting to experiment.

References

1. *Rossikhin Y.A.* Reflections on two parallel ways in the progress of fractional calculus in mechanics of solids // Applied Mechanics Reviews. Trans. of the ASME, vol. 63, 2010.
2. *Golub V.P.* Modelling of deformation and fracture processes of structural materials under creep conditions // J. for Applied Mathematics and Mechanics, vol. 76, 1996.
3. *Badalov F.B., Taylakov N.I.* One approach to the numerical solution of nonlinear weakly singular integro-differential equations with partial derivation // The Uzbek mathematical, «TAI» Tashkent, 1999, pp. 15-20.
4. *Shevchenko Y.N., Babeshko M.E., Terekhov R.G.* Thermo viscoplasticity processes of complex deformation in constructions // «Naukova Dumka»,Kiev, 1992, pp. 123-145.
5. *Rabotnov Y.N.* The effect of changing loads during creep // Proc. of a Symposium held at the National Physical Laboratory, «Her Majesty's Stationary Office» London, 1956, pp. 221-225.
6. *Khudayarov B.A.* Nonlinear flattor of viscoelastic plastic plates // PhD thesis, TAI, 2013.
7. *Badalov F.B.* Dynamic absorbers of vibrations of hereditarily deformable systems // The Uzbek mathematical «TAI» Tashkent, 2003.
8. *Mirsaidov M.M., Sultanov T.Z.* Assessment of stress-strain state of earth dams withallowance for non-linear strain of material and large dams // Mag. Civ. Eng. *49 (5), 2014.*
9. *Mirsaidov M. M., Sultanov T. Z., Sadullaev A.* Determination of the stress-strain state ofearth dams with account of elastic-plastic and moist properties of soil and large strain // MagCiv. Eng. *40(5), 2013.*
10. *Adilov F. F., Miralimov M. H., Abirov R. A.* To the stability of the roadbed reinforced with gabions // In IOP Conf. Series: Materials Science and Engineering, *913* (IOP Publishing, 2020).

ASSESSMENT OF STRESS-STRAIN STATE OF EARTH DAMS CONSIDERING THE SPATIAL OPERATION OF STRUCTURES

Mirsaidov M.M.[2]., Matkarimov P.J.[3], Juraev D.[1]

[1]National Research University-Tashkent Institute of Irrigation and Agricultural Mechanization Engineers, Tashkent, Uzbekistan

[2]M.T.Urazbaev Institute of Mechanics and Seismic Stability, Tashkent, Uzbekistan;

[3]Namangan Institute of Engineering and Technology, Namangan, Uzbekistan.

E-mail: mirsaidov1948@mail.ru,

Abstract. *The article presents a mathematical model, methodology, and algorithm for assessing the stress-strain state (SSS) of earth dams in a spatial statement, considering the features of structures, under the influence of their weight and water pressure. The stress-strain state of three earth dams was studied, considering non-homogeneous and structural features in a spatial statement. As a result of the calculations, it was revealed that the displacements in the vertical direction predominate compared to the other two directions; consideration of the mechanical properties of the dam core significantly influences the SSS of earth dams; the pattern of distribution of relative vertical strains in the middle section of the dam and around it differs sharply from the results obtained using a plane scheme for the structure; when the reservoir is completely filled, water pressure has the maximum effect on the SSS of the dam. It was revealed that to assess the stress-strain state under static loads of the Gissarak dam located in a narrow alignment, it is necessary to use a three-dimensional model of structures.*

Keywords*: spatial and three-dimensional model, earth dam, stress state, non-homogeneity, body forces, hydrostatic pressure, stress contour.*

1. Introduction

When designing water-retaining structures in the areas of high seismicity, in most cases, their stress-strain state and dynamic behavior are studied using a plane design scheme, which does not consider many features of the structure.

Today, to evaluate the strength parameters of various structures, the finite difference method (FDM) and the finite element method (FEM) are used [2-14].

In [15], seismic analysis of dams (earth and rockfill ones) was conducted using quasi-static and dynamic methods. The results of seismic analysis show that the settlement of the dam in the vertical direction is substantial relative to the horizontal displacement; horizontal displacements in the upper, middle, and lower sections of the dam are 66%, 55% and 52%, respectively. The highest subsidence rates were observed at the upper levels of the dam under static and dynamic conditions.

The authors of the article [16] studied in the laboratory conditions the dynamic characteristics of a damaged model of an arch dam. As a result of the study, changes in the dynamic characteristics of the dam were determined: eigenfrequencies, nature of vibrations, and damping coefficient before and after modernization. Experimentally determined dynamic characteristics obtained from all variants of the experiment were compared.

Seismic stress in soil [17,27] was determined based on the fundamental equations of continuum mechanics. The problem posed was solved by the FDM, based on exact boundary and zero initial conditions. This method takes into account the moisture regime, elasticity, viscosity, and plasticity of soil.

References [18,19] examine the stressed state of soil joints under static and seismic influences and provide the main conclusions and scientific achievements in assessing the stability of slopes, safety, and other issues related to earth dams.

The study in [20] considers the method for numerical modeling of the motion of the “Foundation–dam–reservoir” spatial system under static and seismic influences. The stress-strain state of arched concrete dams was assessed, their eigenfrequencies were determined and the corresponding vibration modes were constructed. The universal program *ANSYS Mechanical* was used in the research.

In [21], studies of the dynamics of a concrete spillway dam of a river hydroelectric power plant are presented. A detailed review of the method for calculating the dynamic characteristics of structures and the results of assessing the response of structures to time-varying excitation and earthquake accelerograms are provided. The resulting response spectra made it possible to estimate the maximum horizontal accelerations.

In [22], using three-dimensional boundary elements, the dynamic behavior of the Soria arch dam (Gran Canary, Spain) was studied, considering the interaction with the soil foundation, the completeness of the reservoir filling, and the actual geometry of the dam wall. It was established that the influence of the dynamic characteristics of the dam is significantly influenced by the correct consideration of the properties of the material of the structure, the level of water filling, and the correct consideration of the geometry of the dam.

In [23], the dynamic characteristics of the structure of the Indirasagar gravity dam, located in the Andhra Pradesh state (India) were determined, considering the dead weight of the dam and hydrostatic water pressure using the *ANSYS* software package.

As a review of scientific publications presented here shows, studies of the dynamic behavior and stress-strain state of dams built from local soils, considering their design features and the performance of structures, are not enough.

Based on the above, it can be stated that the development of mathematical models, calculation methods for assessing the SSS and determining the strength characteristics of earth dams in a spatial statement, considering design features, real properties of materials and the level of reservoir filling, is an urgent problem in continuum mechanics.

2. Methods

Consider a spatial model of an earth dam of complex geometry (Fig. 1), its volume is $V=V_1+V_2+V_3$ (V_1 is the volume of the upper prism, V_2 is the volume of the core, and V_3 is the volume of the lower prism). The area of the dam along the foundation and the coastal slope $\Sigma_4^{'},\Sigma_4^{''},\Sigma_4^{'''}$ is rigidly fixed, and surfaces $\Sigma_1,\Sigma_2,\Sigma_3$ are stress-free. The structure is under the influence of its weight $\vec{f}$, and the water pressure $\vec{p}$ of the reservoir acts on the surface S_p.

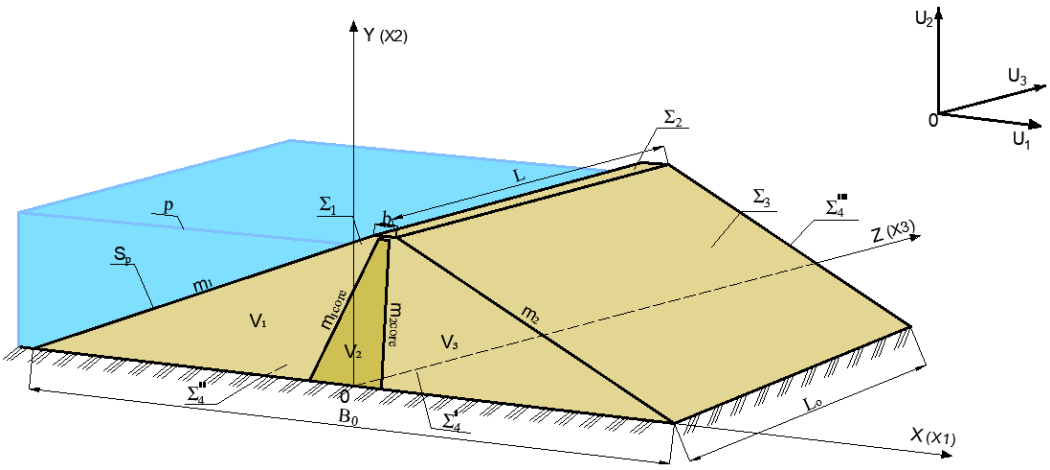

Figure 1. - **Spatial calculation model of an earth dam**

In Fig. 1, it is indicated: L – the length of the crest; L_o – the longitudinal length of the foundation; b – the width of the crest; B_0 – the width of the dam foundation in cross-section; m_1 and m_2 –the upstream and downstream slopes; m_{1core} and m_{2core} the slopes of the dam core.

The statement of the problem is formulated based on Lagrange's variational equation and d'Alembert's principle [1], i.e.:

$$\delta A=-\int_{V_1}\sigma_{ij}\delta\varepsilon_{ij}dV_1-\int_{V_2}\sigma_{ij}\delta\varepsilon_{ij}dV_2-\int_{V_3}\sigma_{ij}\delta\varepsilon_{ij}dV_3+$$
$$+\int_{V_1}\vec{f}\delta\vec{u}dV_1+\int_{V_2}\vec{f}\delta\vec{u}dV_2+\int_{V_3}\vec{f}\delta\vec{u}dV_3+\int_{S_P}\vec{p}\delta\vec{u}dS=0,\quad i,j=1,2,3 \tag{1}$$

under conditions:

$$\vec{x}\in\Sigma_4=\Sigma_4^{'}+\Sigma_4^{''}+\Sigma_4^{'''}\quad:\quad\vec{u}=0\,. \tag{2}$$

The generalized Hooke's law of the following form is used:

$$\sigma_{ij} = \lambda_n \theta \, \delta_{ij} + 2\mu_n \, \varepsilon_{ij} \tag{3}$$

and Cauchy relations

$$\varepsilon_{ij} = \frac{1}{2}\left(\frac{\partial u_i}{\partial x_j} + \frac{\partial u_j}{\partial x_i}\right). \tag{4}$$

The water pressure of the reservoir on the upstream slope of the dam is determined as:

$$p = \rho_0 g(h - x_2) \tag{5}$$

Here $\vec{u}$, ε_{ij}, σ_{ij} , $\delta\vec{u}$, $\delta\varepsilon_{ij}$ are the displacement vectors, components of strain and stress tensors, and their isochronic variations, respectively; $\vec{p}$ is the hydrostatic water pressure, ρ_o is the water density, $\vec{f}$ is the vector of body forces, acting towards surface S_p; λ_n and μ_n are the Lame constants for the ***n***-th element of the dam; $\{x\}=\{x_1,x_2,x_3\}=\{x,y,z\}$, $\{u_1,u_2,u_3\}=\{u,v,w\}$, $\theta = \varepsilon_{kk}$ are the coordinates, components of the displacement vector of a point of the structure body, and volumetric strain, respectively; $i, j, k = 1, 2, 3$.

When solving the variational problem (1) - (4), the domain occupied by the body is divided into subdomains having different physical and mechanical parameters, then, these subdomains are automatically partitioned into the final elements of the tetrahedron.

Using the FEM procedure [24], the variational problem (1)-(4) is reduced to a system of non-homogeneous algebraic equations of high order, i.e.:

$$[K]\{u\} = \{P\}, \tag{6}$$

here $[K]$ are the stiffness matrices of the structure under consideration (Fig. 1); $\{u\}$ are the sought-for components of the displacement vectors in the nodes of the structure; $\{P\}$ are the components of external forces (body forces and water pressure) acting on the nodes of the structure.

The problems posed in a spatial statement were solved using a computer program developed by the authors and the universal program *Abaqus*. When solving specific problems, the order of the system of equations reached 70,000.

3. Results and discussion

The SSS of three different earth dams were studied in the article in a spatial statement, considering the actual design parameters of the structure under the action of body forces and water pressure in reservoirs using the above mathematical model, method, algorithm, and computer calculation program.

The stress-strain state of various earth dams erected in the territory of high seismicity of Central Asia was studied:

1) Gissarak high-rise earth dam (height H=138.5 m).
2) Pachkamar earth dam (height H=70 m).
3) Sokh earth dam (height H=87.3 m).

In the spatial problem posed, first, the stress-strain state of earth structures under the influence of their weight and the water pressure of the reservoir was studied. Then, to analyze in detail and evaluate the strain state of the dams under consideration in a spatial statement, several characteristic transverse sections were selected along their longitudinal axis and isofields of equal levels of distribution of relative strains under their weight were constructed in these sections. Next, the results obtained for each section were compared and the results obtained for the middle section were compared with the ones obtained in a plane statement.

First, the calculations were performed for the stress-strain state of the dams in a spatial statement. For the convenience of analyzing the results in the transverse and longitudinal sections of the dam, isofields of the displacement and stress components were constructed, which are given below.

The fields of equal levels of horizontal (a, d), vertical (b, e) and longitudinal (c, f) displacements in a spatial statement for the Gissarak dam under the pressure impact of reservoir water and the structure's weight are shown in Fig. 2.

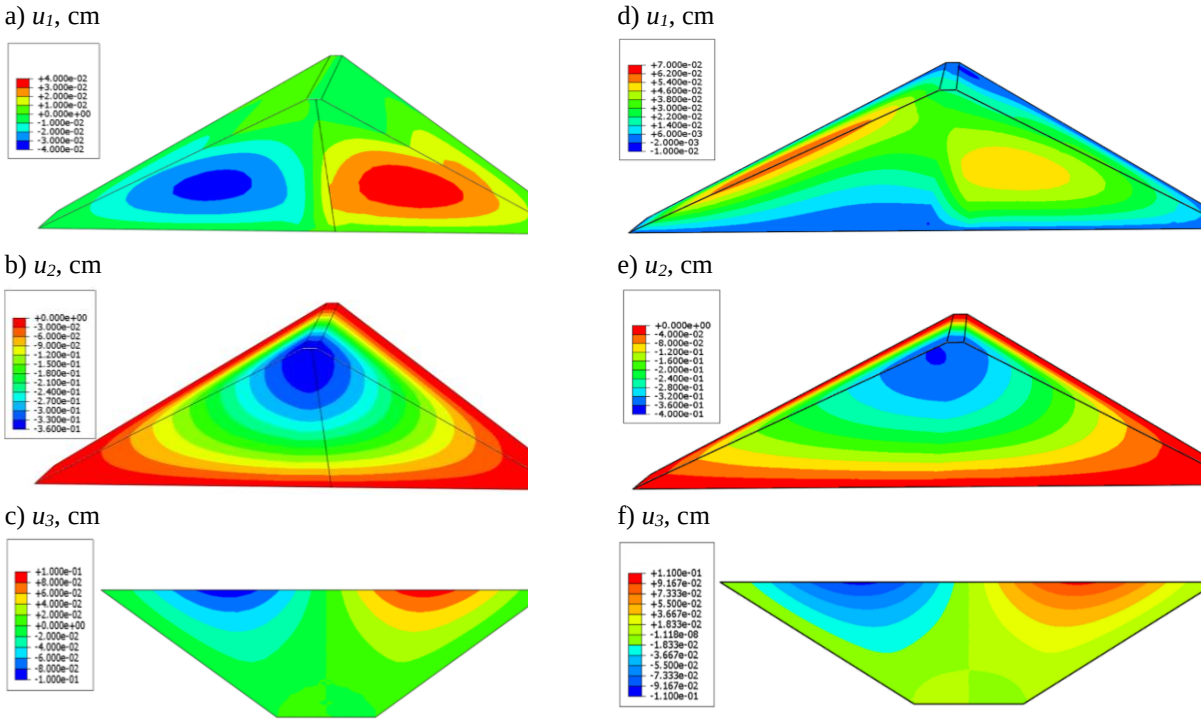

Figure 2. - **Field of equal levels of displacements (u_1, u_2, u_3) in the middle transverse and longitudinal sections of the Gissarak dam in empty reservoir (a, b, c) and completely filled reservoir (d, e, f).**

The fields of equal stress components σ_{ii} for the Gissarak dam under the impact of water pressure when the reservoir is completely filled and the structure's weight are shown in Fig. 3.

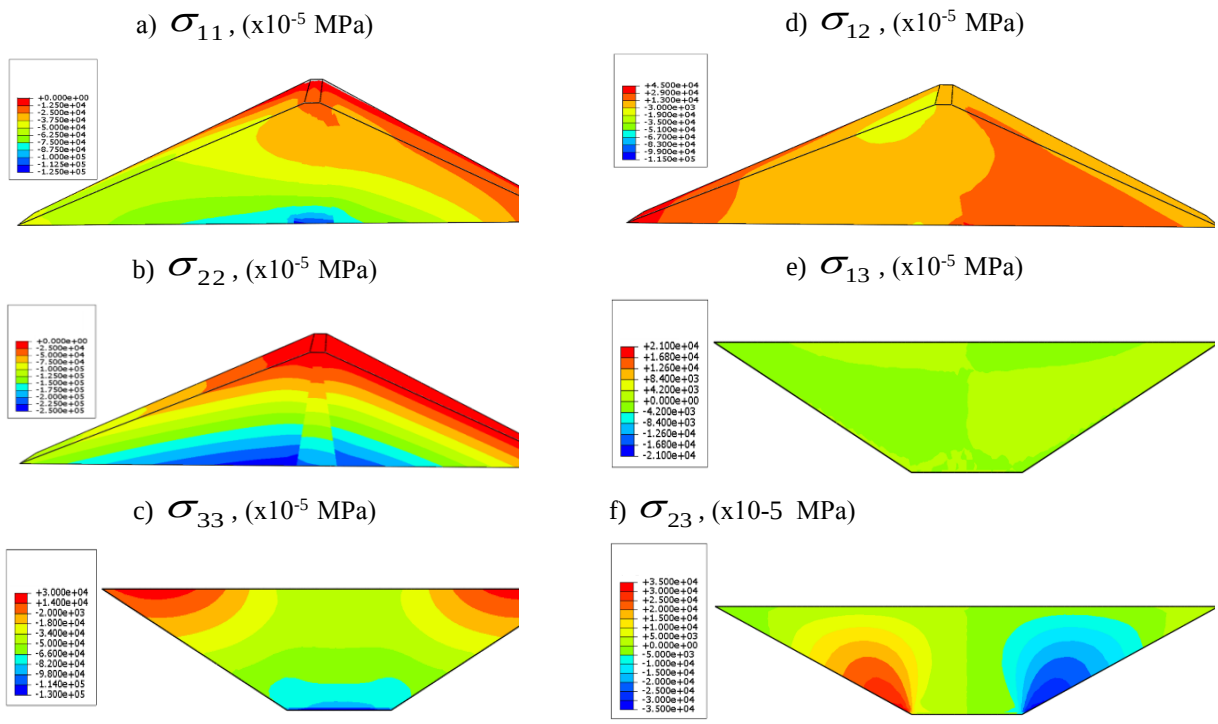

Figure 3. - **Field of equal levels of stress components in the Gissarak dam: a) σ_{11} - horizontal stress; b) σ_{22} - vertical stress; c) σ_{33} - longitudinal normal stress and σ_{12} (d), σ_{13} (e), σ_{23} (f) - shear stress.**

The results obtained (Fig. 2) show that the displacements of points in the dam body relative to the vertical axis are approximately symmetrical. In the core of the dam, the values of horizontal displacements are close to zero, and their values increase towards the centers of the upper and lower

retaining prisms. Here, the displacements of the point in the vertical direction predominate since the calculations were performed considering only the weight of the structure. Analysis of longitudinal displacements (along the x3-axis) shows that in the middle of the Gissarak dam (Fig. 2c) the value of displacement u3 is practically zero, and their values increase towards the left and right banks of the alignment.

The displacement values of the profile points of the dam under study (Fig. 2) significantly depend on the level of reservoir filling. With an increase in water level, the pattern of distribution of displacements $\mathbf{u_1}$ and $\mathbf{u_2}$ along the body of the dam changes, as a result, the symmetrical nature is lost, and the values of displacements $\mathbf{u_1}$ increase by 1.5-2.0 times compared to the case without considering the effect of water.

The results (Fig. 3) presented without considering the water effect, indicate that the stress state is almost symmetrical with respect to the vertical axis of the structure. The core of the dam leads to the appearance of an arched effect and changes the pattern of the stress state in the cross section of the structure as a whole. The value of horizontal stresses σ_{11} is approximately symmetrical relative to the center of the dam core and increases from the top to the dam foundation. The value of the vertical stress σ_{22} decreases around the core of the dam, forming an arch effect. The distribution of shear stresses σ_{12} on the dam body is symmetrical and practically equal to zero in the core and transition zones.

Along with the spatial formulation, these dams have been calculated in the plane-deformed statement.

It was revealed that the plane model could not accurately assess the processes occurring in the dam when evaluating the stress-strain state of the Gissarak dam. It was shown that when assessing the stress-strain state of the Gissarak dam, research should be conducted using a spatial model only since this dam is built on a narrow alignment. The study of the SSS of other dams, i.e. The Sokh and Pachkamar earth dams located in a wide alignment showed that for the calculation of these dams for static loads, it is possible to use a plane model.

At the next stage of calculations, the strain of the dam under the influence of its weight in a spatial statement is considered. To assess in detail the strain state of the Gissarak and Sokh dams arising under the influence of their weight, various transverse sections «A-A'» - «G-G'» of the dam were selected along the longitudinal axis (see Fig. 4), and the isofields of equal levels of distribution of relative vertical strains ε_{22} were constructed in these sections.

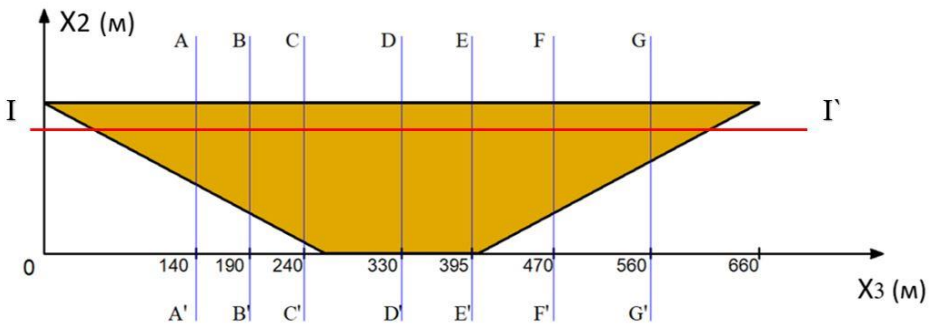

Figure 4. - **Scheme of location of cross sections of the Hissarak dam along the longitudinal X_3-axis**

Fig. 5 shows the isofields of equal levels of distribution of relative vertical strains ε_{22} in Gissarak dam in axonometric form.

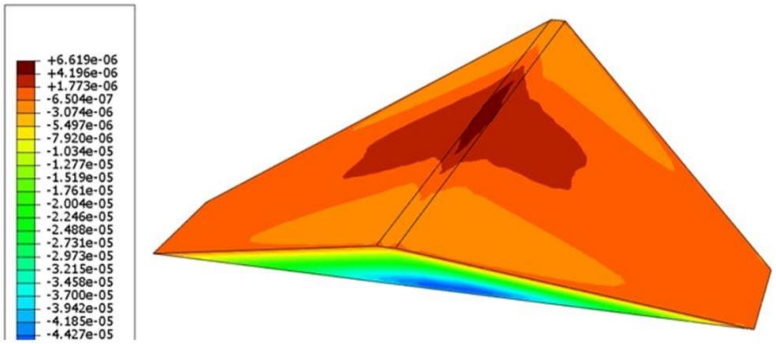

Figure 5. **Isofields of equal levels of distribution of vertical relative strains ε_{22} in axonometric form.**

Analysis and comparison of the results obtained in spatial and plane formulations for the Gissarak dam showed that the pattern of distribution of relative vertical strain ε_{22} around the left and right parts of the dam slopes along the cross section is similar to each other. However, the pattern of distribution of relative strains ε_{22} changes significantly in the middle sections of the dam and around it. Here, the "arch effect" that occurred in the upper part of the dam core in a plane statement is not observed, and the value of the strain ε_{22} decreases and is directed upward (rises) having a positive value. In this part of the dam, the process of extrusion of loamy (relatively soft) soil is observed. The occurrence of such a mechanical phenomenon can be assessed as the influence of soils of the left and right slopes, and the soft and light soils in the core (when compared to the soils of the retaining prisms) on the deformed state of the middle part of the dam.

This mechanical effect was identified during the study of the Gissarak dam using a spatial model. This effect was clearly observed only in the Gissarak dam since its geometric dimensions resembles a volumetric body, unlike the Sokh and Pachkamar dams.

4. Conclusions

1. To assess the SSS of earth structures using spatial schemes, a mathematical model was developed based on the variational principle of virtual displacements, considering the real features of the structure.

2. The spatial stress-strain state of three different earth dams under the impact of body forces and hydrostatic pressure of the reservoir water was studied using a developed method, algorithm, and computer program.

3. Analysis of the results obtained revealed that under the action of body forces in the vertical direction, the displacement of points in the body of the dam predominates; considering the physical and mechanical properties of the core significantly affects the stress state and strain of soil dams; the filling level of the reservoir significantly affects the SSS of the dam, and the maximum effect is observed when it is completely filled.

4. Analysis and comparison of the results obtained for the Gissarak dam in spatial and plane formulations showed that the pattern of distribution of relative vertical strains ε_{22} near the left and right parts of the slopes of the dam along the cross section is similar to each other. However, the pattern of distribution of relative strains ε_{22} changes significantly in the middle sections of the dam and around it. In this case, the "arch effect" observed in the upper part of the core in a plane statement is not observed, and the value of strain ε_{22} decreases and is directed upward (rises), having a positive value. This effect was clearly observed only in the Gissarak dam since in its geometric dimensions, it resembles a volumetric body, unlike the Sokh and Pachkamar dams.

References

1. *Timoshenko S.P., Goodyer J.* Theory of elasticity / «Nauka» M., Main editorial office of physical and mathematical literature, 1979, 560 p.

2. Konstantinov I. A. *Dynamics of hydraulic structures. Part 2 / «Publishing house» L., 1976, 196 p.*
3. Zaretsky Yu.K., Lombardo V.N. *Statics and dynamics of earth dams / «Energoizdat» M., 1983, 256 p.*
4. Lyakhter V.M., Ivashenko I.N. *Seismic resistance of earth dams / «Nauka» M., 1986, 233 p.*
5. Krasnikov N.D. *Seismic resistance of hydraulic structures made of earth materials / «Energoizdat» M., 1981, 240 p.*
6. *Mirsaidov M.M., Sultanov T.Z., Abdikarimov R.A., Ishmatov A.N., Yuldoshev B.Sh., Toshmatov E.S., Jurayev D.P.* Strength parameters of earth dams under various dynamic effects // Magazine of Civil Engineering. 2018. No. 1. pp. 101–111.
7. *Juraev D., Matkarimov P., Mirsaidov M.* Three-Dimensional Stress State of Earth Dams Under Static Loads // Lecture Notes in Civil Engineering Proceedings of MPCPE 2022, 2023,pp. 1-11.
8. *Juraev D.P., Matkarimov P.J.* Stress-strain state and strength of earth dams under static loads // IV International Scientific Conference "Construction Mechanics, Hydraulics and Water Resources Engineering", Tashkent, Uzbekistan, E3S Web of Conferences, 2023, Volume 365, id.03008 https://doi.org/10.1051/e3sconf/202336503008
9. *Kholboev Z., Matkarimov P., Mirzamakhmudov A.* Investigation of dynamic behavior and stress-strain state of soil dams taking into account physically Non-linear properties of soils // E3S Web of Conferences. – EDP Sciences, 2023, vol. 452, P. 02009. https://doi.org/10.1051/e3sconf/202345202009
10. *Il'ichev, V. A., Yuldashev, S. S., Matkarimov, P. Z.* Forced vibrations of an inhomogeneous planar system with passive vibrational insulation // Soil Mechanics and Foundation Engineering, 1999, No. 36(2), pp. 50-54. https://doi.org/10.1007/BF02469084
11. *Mirsaidov M.M., Sultanov T.Z.* Assessment of stress-strain state of earth dams with allowance for non-linear strain of material and large strains // Magazine of civil engineering. 2014, vol. 49, pp. 73-82. DOI 10.5862/MCE.49.8
12. *Mirsaidov M.M., Sultanov T.Z., Sadullaev S.A.* Determination of the stress-strain state of earth dams with account of elastic-plastic and moist properties of soil and large strains // Magazine of civil engineering. 2013, vol. 40, pp. 59-68
13. *Pinyol N.M., Alonso E.E.* Earth dam, spatial model, stress-strain state, dynamic characteristic, natural frequency, modes of oscillations // International Journal of Civil Engineering. 2019, vol. 17. No. 4. pp. 501–513. DOI: 10.18720/MCE.89.1
14. *Mirsaidov M.* Strength of earth dams considering the elastic-plastic properties of soils // E3S Web of Conferences 365, 03001 (2023). https://doi.org/10.1051/e3sconf/202336503001
15. *Ahmad R.M., Mostafa Z.R., Behrang B.* Quasi-static and dynamic analysis of vertical and horizontal displacements in earth dams (case study: Azadi earth dam) // Journal of Civil Engineering and Materials Application. 2020; No. 4(4): pp. 223-232
16. *Ahmet Can Altunişik, Murat Günaydin, Barış Sevim, Alemdar Bayraktar, Süleyman Adanur* // CFRP composite retrofitting effect on the dynamic characteristics of arch dams. Soil Dynamics and Earthquake Engineering, 2015, pp.1-9. DOI:10.1016/j.soildyn.2015.03.008
17. *Sultanov K.S., Khusanov B.E., Loginov P.V., Normatov Sh.* Method for Assessing the Reliability of Earth Dams in Irrigation Systems // Construction of Unique Buildings and Structures, 2020,vol. (4)89 , No. 8901. p. 49. doi:10.18720/CUBS.89.1
18. *Hongqi Ma Fudon Chi.* Major Technologies for Safe Construction of High Earth-Rockfill Dams // Engineering. vol. 2, iss. 4, 2016, pp. 498-509. https://doi.org /10.1016/ J.ENG. 2016.04.001Get rights and content
19. *Kong X., Liu J., Zou D.* Numerical simulation of the separation between concrete face slabs and cushion layer of Zipingpu dam during the Wenchuan earthquake // Science China Technological Sciences. 2016. vol. 59. No. 4. pp. 531–539. doi: 10.1007/s11431-015-5953-6
20. *Belostotsky A.M., Akimov P.A., Nguyen Tai Nang Luong.* Methodology for numerical modeling of a three-dimensional system "foundation–dam–reservoir" under static loads and seismic impacts. // "Issues of applied mathematics and computational mechanics." Collected works No. 20, 2017, pp. 364-377. doi**:** 10.22337/9785432302663-87-94
21. *G.L.Kozinetc, P.V.Kozinetc.* The calculation of the dynamic characteristics of the spillway of the dam // Magazine of Civil Engineering. 2022, 113(5), pp.1-8. doi: 10.34910\MCE.113.12
22. *J .C.Galván, et al.* Boundary element model for the analysis of the dynamic response of the Soria arch dam and experimental validation from ambient vibration tests // Engineering Analysis with Boundary Elements. 2022, vol.144, pp.67-80. https://doi.org/10.1016 /j.enganabound.2022.08.008
23. *Ravindra Vipparthy.* Static and free vibration analysis of gravity dam under the influence of hydrostatic pressure using ANSYS finite element models // GMRIT JNTUK. 2022, https://doi.org/10.21203/rs.3.rs-1823407/v1
24. *Bathe K., Wilson E.* Numerical methods of analysis and FEM / «Stroyizdat» M., 1982, 448 p.
25. *Vasilyeva I.A., Zhuravlev G.I. et al.* Hydraulic structures / «Stroyizdat» M.,, 1978, 647 p.
26. *Grishin M.M.* Hydraulic structures (in two parts). Part I / «Higher school» M., 1979, 615 p.
27. *Sultanov, Karim.* Contact interaction of an underground pipeline with soil under dynamic impacts. Facta Universitatis, Series: Mechanical Engineering, [S.l.], March 2024. ISSN 2335-0164. Available at: http://casopisi.junis.ni.ac.rs/index.php/FUMechEng/article/view/12383.

VIBRATIONS OF PLANE STRUCTURES CONSIDERING THE PHYSICAL NONLINEARITY OF THE MATERIAL

Mirsaidov M.M.[1,2], Ishmatov A.N.[1], Yuldoshev B.Sh.[1], Urinov B.Kh.[1]

[1]National Research University-Tashkent Institute of Irrigation and Agricultural Mechanization Engineer
[2]M.T.Urazbaev Institute of Mechanics and Seismic Stability of Structures, Uzbekistan Academy of Sciences
E-mail: mirsaidov1948@mail.ru,

***Abstract**: The study provides a detailed analysis of the current stress state of various dams. A mathematical model, method, and algorithm are proposed for assessing the dynamic behavior and stress-strain state of earth dams, considering the nonlinear viscoelastic properties of the material under the real conditions of the structure's operation. The viscoelastic properties of the material are described by nonlinear hereditary Boltzmann-Volterra theory. The solution to the problem is performed as linear elastic problem of the natural vibrations of the structure is solved. As a specific example, natural and nonlinear forced vibrations of the Gissarak dam were studied. The dynamic behavior of the structure under consideration was analysed. Near the resonant mode of vibrations, the most stressed areas of the structure body were assessed and dangerous sections were identified. The influence of nonlinear elastic and viscoelastic properties of the material on the dynamics of the structure was assessed.*

***Keywords**: plane structure, dynamic behavior, earth dam, kinematic effects, physical nonlinearity, viscoelasticity, integrodifferential equations, resonant mode.*

1. Introduction

Recently, the construction of various hydraulic structures was conducted on a large scale in areas with high seismicity, rich in hydro-energy resources\; this requires the creation of reliable methods and dynamic calculation algorithms for a number of earth structures, taking into account the elastic properties and viscoelasticity of the material for the actual conditions of the structure's operation.

There are numerous publications considering dynamic calculations of structures of this type; however, the issues of the parameters of oscillatory processes taking into account elastic nonlinearity and viscoelasticity of the material were studied insufficiently. The relevance of solving such problems is primarily explained by the demands of the design, construction, and operation of various types of earth structures.

The purpose of the study is to develop a methodology and algorithm for solving the problem of forced vibrations of inhomogeneous structures that have both nonlinear elastic and viscoelastic properties of the material; to study the dynamics of specific tasks and to analyze the results obtained from the point of view of discovering new mechanical effects.

In recent years, articles have been published that study the stress-strain state and dynamic behavior of various structures.

Such scientific publications include the following:

- in [4], vibrations of dams are considered using various methods. Various types of dam vibrations were studied, such as free, forced vibrations and cases of vibrations in resonant modes. Methods for monitoring dam vibrations are described by installing sensors, data analysis, mathematical modeling, and the use of special control methods. Examples are given of the practical application of methods for monitoring dam vibrations in various countries.

- the study in [5] describes the use of the finite element method for calculating dam vibrations. A new approach to calculating dam vibrations is given, based on the use of the finite element method. A model of the dam is presented, based on the FEM, and its dynamic characteristics are calculated. A new control method is being considered, based on the use of resonant sensors. In conclusion, the results of the study and its practical significance are given.

- reference [6] provides an analysis of dam vibrations that occur during the operation of hydraulic structures, and determines the most optimal conditions for their operation. Methods for mathematical modeling of dam dynamics are described and a comparative analysis of various operating modes is provided, the influence of the following factors: changes in water level, frequency, and amplitude of oscillations, taking into account the impact of hydraulic forces on the

dynamics of dams are described. It is shown that under certain operating conditions of dams, critical conditions arise that lead to the collapse of the structure.

- in [7], the main causes of dam vibrations were studied, such as wind and hydrodynamic loads, the influence of topography on the location of dams. Monitoring methods used to assess dam vibrations are examined, including the use of vibrometric and infrasonic sensors. An analysis of monitoring data collected at several dams is presented. The main causes of dam vibrations at each of the dams, and the influence of dam parameters, such as height and length, on the level of vibrations are identified.

- in [8], the modeling of dam dynamics under conditions of resonant interaction with water is considered. A numerical study examined the influence of various factors on dam vibrations, such as water flow rate, water depth, dam parameters, and others. Computational fluid dynamics and finite element methods were used in modeling. The results show the influence of resonant interaction with water on the dynamics of dams, which can lead to significant vibrations and damage to dams. Several methods were proposed to reduce vibrations and improve the stability of dams, such as changing the dam geometry and selecting optimal dam parameters.

- in [9], studies related to the choice of parameters for dam vibration models were conducted. A principal component method was proposed that allows one to determine the most important parameters influencing dam vibrations and use them as input data for modeling. Data obtained from dam vibration monitoring were used. It is shown that the principal component method is an effective tool for determining the parameters of dam vibration models.

- reference [10] proposes a new approach to analyzing the dynamic characteristics of dams based on their modeling and experimental studies. A technique for modeling dam vibrations using the finite element method is given. Experiments were conducted to obtain data on the dynamic characteristics of dams under different loading conditions. Various parameters of dams that affect their dynamic stability were considered - geometric parameters, material properties, and loading conditions. An analysis of the influence of these parameters on the dynamic characteristics of dams and recommendations for optimizing the dam design are given.

- in [11], the possibility of using artificial neural networks to determine the parameters of dam vibration models was explored. The problem of determining the dynamic parameters of a dam based on available data on its fluctuations using artificial neural networks that can learn from available data and make predictions was considered. The process of collecting data on dam vibrations is described. Several experiments were conducted to evaluate the accuracy and efficiency of the method. It is shown that the use of artificial neural networks makes it possible to achieve high accuracy in determining the parameters of dam vibration models.

- in [12], a system for monitoring and controlling dam vibrations was developed based on unmanned aerial vehicles. The process of monitoring dam vibrations was modeled. Inertial measurement units and high-resolution cameras were used to monitor dam vibrations. The software was used to analyze the data and determine the vibration characteristics of the dams. The system was tested on several dams of various designs.

- article [13] presents a method for mathematical modeling of dam vibrations using the FEM, considering the dissipative properties of materials. A numerical study of dam vibrations is given using the example of a simulated hydroelectric power plant, taking into account the influence of external loads, such as seismic waves and hydrodynamic shocks, and the dissipative properties of materials. The dissipative properties of the material definitely affect the dynamics of dam vibrations; in particular, consideration of dissipation makes it possible to significantly reduce the amplitude of vibrations, which, in turn, increases the dynamic stability of dams.

- reference [14] presents a method for determining the dynamic characteristics of dams based on the Fourier series, which makes it possible to determine the frequency spectrum of dam oscillations and evaluate its dynamic characteristics, such as natural frequencies and damping. The results of numerical simulation of dam vibrations are based on the theory of thin-walled shells. The proposed method is used to analyze the dynamic characteristics of dams using the example of several types of dams, determining the frequencies of natural vibrations and damping of the dams

with high accuracy. It was revealed that the geometric parameters of dams have a significant impact on their dynamic stability.

- in [15], a methodology for assessing the impact of natural disasters on dam vibrations was proposed, which can be used to assess risks and prevent catastrophic events in this area. Various factors influencing the behavior of dams, such as water levels, earthquakes, and other natural phenomena, are described. A mathematical model and numerical methods for assessing the impact of natural disasters on dam vibrations are considered. Research based on this methodology makes it possible to determine possible risks and consequences in the event of catastrophic situations.

- in [16], the dynamic processes occurring in dams during the operation of hydroelectric power plants were studied. A new mathematical model is given that accounts for the free edge effect in dams. The results of numerical modeling are presented for various operating conditions of dams, under various parameters, for example, flow rate, water depth, etc. on the behavior of the dam.

- a study in [17] showed the possibility of using the finite element method to simulate dam vibrations. The efficiency and accuracy of the FEM in solving problems related to the dynamic behavior of dams was studied. Various aspects of the application of the FEM in modeling dam vibrations are considered, including the choice of a mathematical model, the formulation of boundary conditions, and the analysis of results. Conclusions are drawn about the applicability of the FEM for modeling dam vibrations and its advantages and shortcomings are pointed out.

- article [18] is devoted to the analysis of the influence of dynamic loads on the operation of dams during their design and exploitation, taking into account various factors that can cause dynamic loads on dams, such as earthquakes and other natural phenomena. An overview of various methods and approaches to the analysis of dynamic loads on dams is presented, analytical and numerical methods, and the use of computer models and simulations for the analysis of the dynamic behavior of dams are considered.

- in [19], the influence of microseismic vibrations on the operation of dams is considered, taking into account the safety and stability of dams. An overview of microseismic vibrations and their characteristics, such as geological faults, seismic activity and anthropogenic factors, is given. The main attention is paid to the analysis of the influence of microseismic vibrations on the structural elements of dams and their impact on the strength and stability of structures is analyzed. A methodology is presented for assessing the effect of microseismic vibrations on dams, including modeling and numerical analysis.

- the study in [20] provides a calculation of the dynamic characteristics of dams under the interaction with the medium and soil. The influence of soil conditions on the dynamic behavior of dams is investigated and a methodology for calculating these characteristics is given. A review of methods for calculating the dynamic characteristics of dams and their interaction with soil is presented. Various aspects of interaction modeling are considered, including the choice of mathematical models, consideration of dam geometry, soil properties, and boundary conditions. A methodology is given for calculating the dynamic characteristics of dams taking into account interaction with soil.

- reference [21] is devoted to modeling the dynamics of dams under the influence of seismic loads using the finite element method. A review of methods for modeling dam dynamics under seismic loads is presented. The main aspects of using the finite element method are considered, such as the choice of dam geometry, material properties, determination of boundary conditions, and consideration of seismic effects. Numerical models are presented using the finite element method, which allows one to evaluate the dynamic characteristics of dams, such as vibration amplitudes, resonant frequencies, and strains, as well as the influence of various factors - dam geometry, materials, and boundary conditions.

- the study in [22] considers the influence of dynamic loads, such as seismic and wind influences, on the operation of dams and methods of their strengthening. The results of an analysis of various cases of dynamic loads on dams are presented, and methods for modeling such loads and assessing their influence on the design of dams are described. Methods for strengthening dams are

given, including the use of various types of reinforcement, building up dams, installing additional supports, and using damping systems.

- in [23], a mathematical model was used to describe the dynamics of dams, taking into account nonlinearities in the operation of dams, including nonlinearities in materials, hydrodynamic effects and nonlinear effects of contact between the dam and soil. The results of numerical simulation of the dynamic behavior of dams taking into account nonlinear effects are given. The influence of nonlinearities on the vibration characteristics of dams, such as amplitude, frequency and mode of vibrations, was studied. An analysis is given of the influence of nonlinearities on the operation of dams under various types of dynamic loads, such as seismic and water loads.

- in [24], the dynamic parameters of the dam were studied using two main approaches - monitoring and mathematical modeling. Monitoring methods used to collect data on the dynamic pattern of the dam are given. Mathematical models used to estimate the dynamic parameters of the dam are considered. The results of the study are presented, which compare the data obtained from monitoring with the results of mathematical modeling. The importance of combining monitoring and mathematical modeling to accurately assess the dynamic parameters of dams is emphasized.

- in [25], numerical methods and mathematical modeling are used to analyze and obtain quantitative estimates under the influence of soil parameters on the dynamics of dams. Soil models were selected that consider the physical and mechanical properties of soil, and the parameters that could be changed to assess their influence on the dynamics of the dams. The results of studies are given, which show the influence of changes in soil parameters on various dynamic characteristics of dams, such as the amplitude of vibrations, resonant frequencies, forces of interaction with soil, and others. Quantitative assessments of these changes and their impact on the reliability and stability of dams are presented.

- in [26], the influence of the geometric characteristics of dams (height, base width, ramp slope, etc.) on their dynamics is studied using a mathematical model and numerical methods. The results of studies of the influence of various geometric parameters on the dynamics of dams, such as vibration amplitude, resonant frequencies, strains and stresses, quantitative estimates of these changes and their consequences for the reliability and stability of dams are presented.

- in [27], the influence of soil foundations on the dynamics of dams is considered, models of soil foundations are selected taking into account the physical and mechanical properties of soils, as well as the parameters that are used to analyze the influence of soil foundations on the dynamics of dams. Results were obtained in the form of vibration amplitudes, resonant frequencies, strains and stresses in dams, under the influence of soil foundations on the dynamics of dams. Quantitative assessments of these changes with implications for the reliability and stability of dam operation are presented.

- in [28], methods of mathematical modeling and numerical analysis are used to assess the consideration of geometric parameters when modeling the dynamics of dams. In modeling the dynamics of dams, an approach based on the finite element method was chosen. A mathematical model and numerical methods used to simulate the dynamics of dams are presented, taking into account the influence of changes in geometric parameters, such as height, width, ramp slope, and other, on the dynamic behavior of dams. The results of numerical experiments are given in which the influence of changes in these parameters on the amplitudes of vibrations and the stress-strain state of dams is analyzed.

in [29], the dynamics of dams was studied taking into account nonlinear effects. A mathematical model was selected that considers nonlinear effects and numerical methods used to study the dynamics of dams. Nonlinear phenomena such as nonlinear stiffness, nonlinear damping, and nonlinear forces that can arise in the operation of dams are considered. The results are given in which the influence of nonlinear effects on the dynamic behavior of dams is analyzed. The amplitudes of vibrations, stress and strain of dams under various conditions and parameters were studied. Recommendations are proposed for optimizing the operation of dams under these effects.

- in publications [30-38], a number of results are given on the study of the dynamic behavior and the stress-strain state of various structures. The internal force factors and the strength of these structures under various types of influences are assessed.

As the above analysis of well-known scientific works shows, each of these studies has its advantages and shortcomings; despite this, they are used to solve specific practical problems.

Based on this analysis, it can be noted that the development of mathematical models, solution methods and the study of dynamics for earth structures is currently a very relevant and necessary problem worldwide that requires its solution.

2. Methods

2.1. **Mathematical model.** Consider nonlinear forced vibrations of earth structures, occupying the volume $V = V_1 + V_2 + V_3 + V_4 + V_5$ (Fig. 1) under the action of non-periodic kinematic influence $\vec{x} \in \Sigma_u$: $\vec{u}_0(\vec{x},t) = \vec{\psi}_1(t)$ on its lower part. The upper slope of the dam is affected by water pressure $\vec{p}_c = \rho_o g\ (h - x_2)$ on surface S_p. Other surfaces of the dam are stress-free. The material of the structure is considered linearly elastic for domain v_1, linearly viscoelastic for domain v_2, nonlinearly elastic for domains v_3, v_5, and nonlinear viscoelastic for domain v_4. The actual geometry of the structure and the non-homogeneous mechanical properties of the material for individual sections are considered.

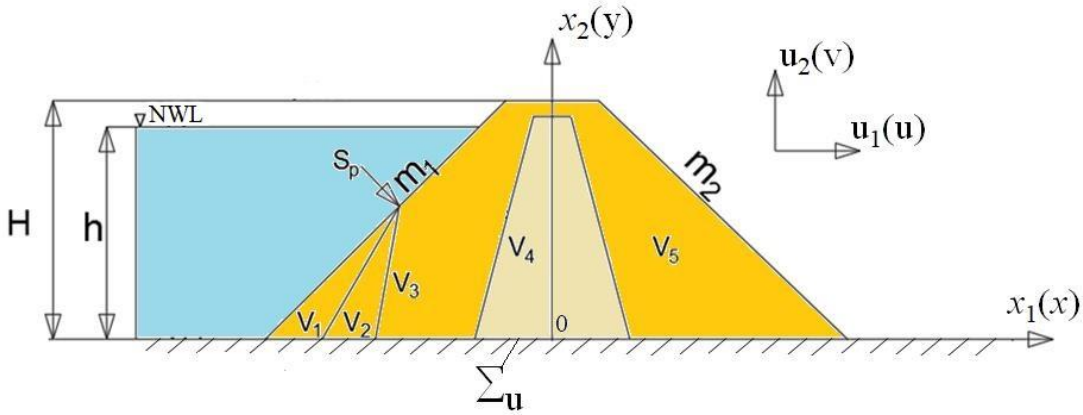

Figure. 1.**-Plane scheme of a non-homogeneous earth dam**

The dynamic behavior and stress-strain state of the structure (Fig. 1) under unsteady forced vibrations and the action of non-periodic kinematic influences $\vec{x} \in \Sigma_u$: $\vec{u}_0(\vec{x},t) = \vec{\psi}_1(t)$, are subject to determination.

To formulate the problem the following relations are used:

linear Cauchy relations:

$$\varepsilon_{ij} = \frac{1}{2}\left(\frac{\partial u_i}{\partial x_j} + \frac{\partial u_j}{\partial x_i}\right), \quad i, j = 1,2 \tag{1}$$

the stress-strain relationship in the following form:

$$\vec{x} \in V_1 : \sigma^1_{ij^{1}_{ij}} = k_1 \varepsilon_{ij}(t)\delta_{ij} + 2G_1\, l_{ij}(t)$$

$$\vec{x} \in V_2 : \sigma^2_{ij} = k_2\, \varepsilon_{ij}(t)\delta_{ij} + 2G_2\, \{l_{ij}(t) - \int_0^t R_1(t-\tau) l_{ij}(\tau) d\tau\}$$

$$\vec{x} \in V_3 : \sigma^3_{ij} = k_3\, \varepsilon_{ij}(t)\delta_{ij} + 2G_3\, \{l_{ij}(t) - \gamma l_{ij}(t) l(t)\} \tag{2}$$

$$\vec{x} \in V_4 : \sigma^4_{ij} = k_4\, \varepsilon_{ij}(t)\delta_{ij} + 2G_4\, \{[l_{ij}(t) - \int_0^t R_1(t-\tau) l_{ij}(\tau) d\tau] - \gamma [l_{ij}(t) l(t) - \int_0^t R_3(t-\tau) l_{ij}(\tau) d\tau]\},$$

$$l_{ij} = \varepsilon_{ij} - \frac{1}{3}\upsilon\delta_{ij}, \qquad l = l_{kl}\, l_{lk}, \qquad v = \varepsilon_{ij}, i, j, k, l = 1,2$$

kinematic boundary conditions:

$$\vec{x} \in \sum_u : \vec{u}_0 \ (\vec{x}, t) = \vec{\Psi}_1(t) \tag{3}$$

initial conditions:

$$\begin{aligned} &\vec{x} \in v : \vec{u}(\vec{x}, 0) = \vec{\Psi}_2(\vec{x}) \\ &\frac{\partial \vec{u}(\vec{x}, o)}{\partial t} = \vec{\Psi}_3(\vec{x}) \end{aligned} \tag{4}$$

the principle of virtual displacements, which considers the work of inertial forces:

$$\delta A_u = -\int_v \rho_n \frac{\partial^2 \vec{u}}{\partial t^2} \delta \vec{u}\, dV \quad , \tag{5}$$

the work of internal stress:

$$\delta A_\sigma = -\int_v \sigma_{ij}^n \delta \varepsilon_{ij} d\,V \tag{6}$$

and the work of hydrostatic pressure:

$$\delta A_p = \int_{S_p} \vec{p}_c \delta \vec{u} dS \quad . \tag{7}$$

To describe the dynamic process in a structure, based on the variational principle of virtual displacements, a variational equation is derived:

$$\delta A = \delta A_u + \delta A_\sigma + \delta A_p = 0 \quad ,$$

where $\vec{u}$, ε_{ij}, σ_{ij}, $\delta\vec{u}$, $\delta\varepsilon_{ij}$ - are the components of the displacement vector, strain and stress tensors, and isochronous variations of these quantities, respectively; ρ_o, ρ_n, K_n, G_n – are the water density, material density, volumetric modulus and instantaneous shear modulus, respectively, of each section of the dam; $V = V_1 + V_2 + V_3 + V_4 + V_5$ is the volume occupied by the elements of the structure; $\vec{\Psi}_1$- is the given vector function of time; $\vec{\Psi}_2, \vec{\Psi}_3$- are the given vector functions of coordinates; R_1, R_3– are the relaxation kernels corresponding to the linear and nonlinear parts of the equation; g – is the free fall acceleration; (h-x_2) – is the depth of various points of the reservoir; $\vec{u} = \{u_1, u_2\} = \{u, \upsilon\}$ - are the components of the displacement vector; $\vec{x} = \{x_1, x_2\} = \{x, y\}$- are the coordinate systems; i, j = 1.2; n = 1,2,3,4,5.

Displacements $\vec{u}(\vec{x}, t)$ and stresses $\sigma_{ij}(\vec{x}, t)$ that satisfy variational equations (5)-(8), (1)-(2) and conditions (3)-(4) must be determined for any virtual displacement $\delta\vec{u}$.

2.2. **Solution method**. The solution to the problem under consideration (5)-(8), (1)-(4) is sought by expanding the solution using previously found eigenmodes of vibrations of elastic structures.

2.2.1. Natural vibrations. To solve the problem of unsteady forced vibrations of a structure, a linear elastic problem of natural vibrations in the absence of external forces is first solved, assuming that the mechanical properties of its sections are non-homogeneous. It is also assumed that homogeneous kinematic boundary conditions are specified on surface $\sum_u$, i.e.:

$$\vec{x} \in \sum_u : \vec{u} = 0, \ \delta\vec{u} = 0 \tag{8}$$

The task is to determine parameters $\vec{u}^*$ and ω (Fig.1):

$$\vec{u}(\vec{x},t)=\vec{u}^{*}(\vec{x})\cos\omega t \quad , \tag{9}$$

where ω - is the eigenfrequency; $\vec{u}^{*}$ - is the natural mode of vibration of the structure.

In the mathematical formulation of the problem, the principle of virtual displacements (5)-(7), (1), and homogeneous kinematic boundary conditions (8) are used. In expression (2), parameters $\gamma=0, R_1=0,\ R_3=0$ are assumed to be zero.

After formulating (9) in Eqs. (1), (5)-(7), the problem of natural vibrations of a non-homogeneous elastic structure (Fig. 1), when considering $\gamma=0, R_1=0,\ R_3=0$, is reduced to a variational equation for its eigenmodes $\vec{u}^{*}(\vec{x})$, i.e.

$$-\int_{V}\sigma_{ij}^{*}\delta\varepsilon_{ij}dV+\omega^2\rho\int_{V}\vec{u}^{*}\delta u^{*}dV=0 \tag{10}$$

$$\vec{x}\in\sum\nolimits_{u}:\vec{u}^{*}=0,\ \delta\vec{u}^{*}=0$$

where $V = V_1 + V_2 + V_3 + V_4 + V_5$ – is the volume occupied by the structure; σ_{ij}^{*} are the stress amplitudes corresponding to $\delta\vec{u}^{*}$.

An auxiliary normalization condition is set when finding eigenforms:

$$\int_{V}\vec{u}^{*2}dV=1 \tag{11}$$

Now the problem of natural oscillations is reduced to finding the parameters ω_n^2 and $\vec{u}^{*}(x)$ that satisfy the variational equation (10), conditions (8) and virtual displacement $\delta\vec{u}^{*}$.

Using the FEM procedure, the variational problem (10) is reduced to the system by the following equation:

$$\left([K]-\omega^2[M]\right)\{\vec{u}^{*}\}=0, \tag{12}$$

here $[K],[M]$- are the stiffness and mass matrices; $\omega,\{\vec{u}^{*}\}$ - are the natural frequency and eigenvector of the structure (Fig. 1).

As a result of solving equations (12), several lower eigenfrequencies of the structure $\omega_1,\omega_2,\varpi_3,\omega_4,\omega_5$ and the corresponding eigenvectors (u,υ) for each grid node of the structure are determined (Fig. 1); they are obtained after finite element discretization, i.e. for each value of $\omega_1,\omega_2,\varpi_3,\omega_4,\omega_5$, the following was determined:

$$\begin{gathered}\omega_1:\{u^{*}{}_1\}=\{u_1^1,\upsilon_1^1,u_1^2,\upsilon_1^2,...,u_1^m,\upsilon_1^m\}\\ \dots\dots\dots\dots\dots\dots\dots\dots\dots\dots\\ \omega_5:\{u^{*}{}_5\}=\{u_5^1,\upsilon_5^1,u_5^2,\upsilon_5^2,...,u_5^m,\upsilon_5^m\}\end{gathered} \tag{13}$$

Based on this, we can write the displacement functions inside each finite element in the following form:

$$\begin{aligned}u_n&=\varphi_1^e u_{i,n}^e+\varphi_2^e u_{j,n}^e+\varphi_3^e u_{k,n}^e\\ \upsilon_n&=\varphi_1^e \upsilon_{i,n}^e+\varphi_2^e \upsilon_{j,n}^e+\varphi_3^e \upsilon_{k,n}^e\end{aligned} \tag{14}$$

The last expressions represent the field of displacements inside the ***e***-th element at the ***n***-th eigenmode (***n***=1, 2, ... , N) of oscillations.

2.2.2. Nonlinear forced oscillations.

The solution to problem (10) is sought using Eqs. (1), (2), (5)-(7) and (3)-(4) in the following form:

$$\vec{u}(\vec{x},t)=\vec{u}_0(\vec{x},t)+\sum_{k=1}^{N}\vec{u}_k^*(\vec{x})y_k(t),$$
$$\delta\vec{u}=\sum_{k=1}^{N}\vec{u}_k^*(\vec{x})\delta y_k(t), \tag{15}$$

where y_n(t) - are the sought-for time functions; $\{\vec{u}^*{}_k\ (\vec{x})\}$ -are the natural vibration modes of the structure found by FEM; $\{\vec{u}_0\ (\vec{x},t)\}$ - are the specified functions (3); δy_k - are the independent isochronous variations of the sought-for function $y_k(t)$; ***N*** - is the number of eigenmodes retained in expansion (15).

When obtaining a system of resolving equations for function $y_k(t)$, it is necessary to calculate the elementary works (5) – (7) of all active forces acting on the system for virtual displacements, and then substitute the expressions of resulting work into the variational equation (10). Equating to zero the factors for independent variations of δy_k, we obtain N of nonlinear systems of integrodifferential equations $y_k(t)$ of the following form:

$$\sum_{n=1}^{N}\left[M_{ij}\ddot{Y}_j+Q_{ij}Y_j-C_{ij}\int_o^t R_1(t-\tau)Y_j(\tau)\,d\,\tau=\Phi_i\ddot{U}_o(t)-\right.$$
$$-\sum_{j=1}^{N}\sum_{k=1}^{N}\sum_{m=1}^{N}L_{ijkm}Y_jY_kY_m+\sum_{j=1}^{N}\sum_{k=1}^{N}\sum_{m=1}^{N}H_{ijkm}\int_o^t R_3(t-\tau)Y_j(\tau)Y_k(\tau)Y_m(\tau)d\,\tau \tag{16}$$

with initial conditions

$$Y_n(0)=Y_{on},\quad \dot{Y}_n(0)=\dot{Y}_{on} \tag{17}$$

The coefficients of system (16) are integrals taken over the volume V of the structure, from combinations of products of eigenmodes and their derivatives.

System (16) is written in the following form:

$$\ddot{Y}_j+\omega_i^2Y_j=B_i\ddot{\vec{U}}_o(t)+\sum_{j=1}^{N}\lambda_{ij}^2\int_o^t R_1(t-\tau)--\sum_{j=1}^{N}\sum_{k=1}^{N}\sum_{m=1}^{N}L_{ijkm}Y_jY_kY_m+\sum_{j=1}^{N}\sum_{k=1}^{N}\sum_{m=1}^{N}H_{ijkm}\int_o^t R(t-\tau)Y_j(\tau)Y_k(\tau)Y_m(\tau)d\,\tau \tag{18}$$
$$Y_i(0)=Y_{io},\quad \dot{Y}_i(0)=\dot{Y}_{io},\quad i=1,2,...$$

where the following notations are accepted:

$$\omega_i^2=\frac{Q_{ii}}{M_{ii}},\ \lambda_i^2=\frac{C_{ii}}{M_{ii}},\ B_i=\frac{\Phi_{ii}}{M_{ii}}$$
$$C_{ijkm}=\frac{L_{ijkm}}{M_{ii}},\ P_{ijkm}=\frac{H_{ijkm}}{M_{ii}}$$

To solve the system of equation (18), quadrature formulas were used [2].

3. Results and discussion

In this section of the article, natural and unsteady forced vibrations of the Gissarak earth dam (as an example) were studied, considering its real geometry and the non-homogeneous features of the structure. The height of the specific earth dam is H = 138.5 m, width along the ridge is 16 m, the slope ratio is m_1 = 2.2, m_2 = 1.9, length along the ridge is 660 m.

Material characteristics for the core (of loamy soil) – elastic modulus of soil E = 2400 MPa, specific gravity γ = 1.7 tf/m, Poisson's ratio μ = 0.35; for the retaining prisms (of rock mass) –E = 3600 MPa, γ = 1.9 tf/m3, μ = 0.35.

Fig.2 shows the results of calculating the natural vibrations of the Gissarak earth dam obtained using the above method, considering the actual properties of the material and design features of the structure.

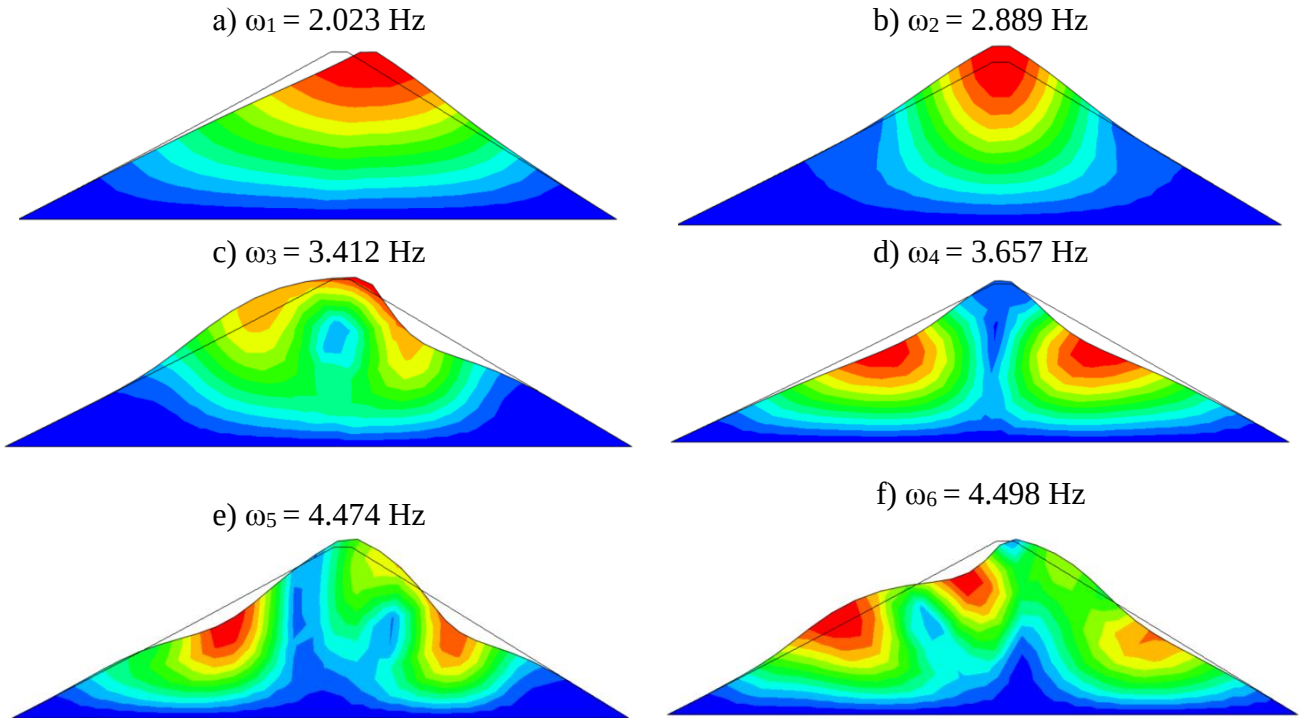

Figure 2. - **The first six eigenfrequencies and modes of vibration of the Gissarak dam**

Next, using the developed methodology and algorithm, we solve the problem of unsteady oscillations of a dam under kinematic excitation of the dam foundation in the following form:

$$x \in \sum_u : \ddot{u}_o(t) = \ddot{\upsilon}_o(t) = F \sin pt, \quad 0 < t \le t^* \tag{19}$$

with initial conditions

$$y_i(0) = y_{io}, \quad \dot{y}_i(0) = \dot{y}_{io} \tag{20}$$

To describe the viscoelastic properties of the dam material, a core of the following form was used:

$$\Gamma(t) = Ae^{-\beta t} t^{\alpha - 1} \qquad (0 < \alpha < 1) \tag{21}$$

with parameters: A=0,074, $\alpha = 0{,}25$, $\beta = 0{,}00243$, which were obtained from experimental creep curves for some types of soils. The nonlinearity coefficient is $\gamma = 50000$.

For specific calculations of the acceleration amplitude at the base of the dam, F=0.2 m/s^2 was taken, and the frequency of the kinematic action p in (19) was taken close to the second eigenfrequency of the structure, i.e. $p = \omega_2$ =3.4 Hz (almost resonance mode of oscillations).

Fig.3 shows graphs of changes in horizontal displacements for the dam point (x_1 = 70.6 m, x_2=14.2 m) under the kinematic influence of the form (19) at t^*=4 sec. As seen from the results, forced oscillations of the system occur with a markedly increasing sweep. After removing the load (i.e. after t=4 seconds), the system performs free oscillations, and for the linear case, these oscillations are almost harmonic. For a dam with nonlinearly elastic materials, the amplitude increases until certain values. This result is characteristic of oscillations damping over time.

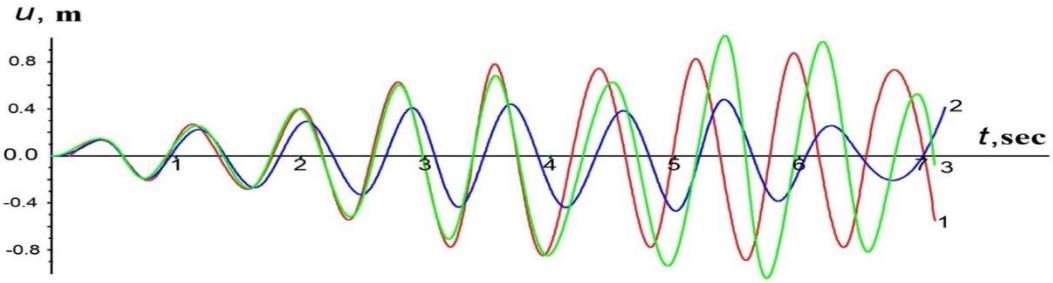

Figure. 3. - **Horizontal displacements of dam points (x1=70.6 м, x2=14.2 m) under unsteady oscillations**

Fig.4 shows the change in stress σ_{11} at the dam point (x_1 =310.8 м, x_2 =39.4 m) under the influence of a pulse of duration t^*= 4 seconds. Designations 1 and 2 refer to the case of linear and nonlinear elastic solutions of the problem, 3 – to the case when the problems are solved in a nonlinear viscoelastic formulation. As seen, the stresses for the linear and nonlinear elastic cases are harmonic, and for the nonlinear viscoelastic case, the stresses decrease, which is a manifestation of viscosity.

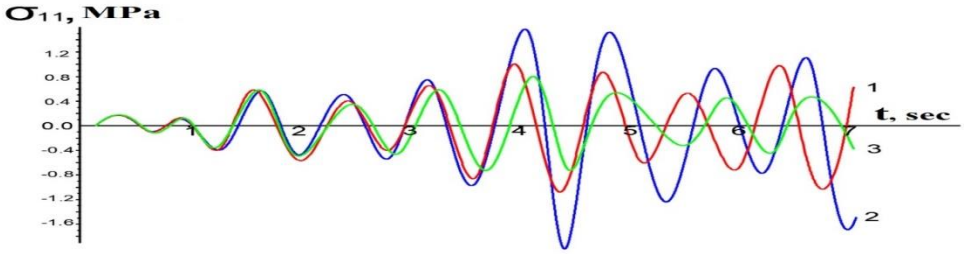

Figure 4. - **Horizontal normal stresses of dam points (x1=310.8 м, x2=39.4 m) under unsteady oscillations**

Studies of forced vibrations of the dam under non-stationary kinematic influences showed that:

- under prolonged kinematic influence, individual sections of the structure experience tensile dynamic stresses, i.e. the dam soil is in tension;

- an account for nonlinear elastic properties leads to a noticeable reduction in stresses arising in the dam body;

- the viscosity of the material leads to a gradual attenuation of vibrations over time, limiting the amplitudes of vibrations throughout the entire body of the dam in resonant modes;

- near the resonant mode of oscillations, considering the physical nonlinearity of the structure material, the occurrence of large stresses in some individual sections of the structure is shown; these stresses can lead to failure of the dam strength.

4. Conclusion

1. The article provides a detailed overview of well-known publications related to the study of the dynamic behavior of several concrete and earth dams.
2. A mathematical model, method, and algorithm for studying forced vibrations of plane structures is presented, considering the nonlinear elastic and viscoelastic properties of the structure material under the impact of various kinematic influences.
3. The natural vibrations of the Gissarak earth dam were determined.
4. Unsteady forced vibrations of the Gissarak dam were studied, considering the nonlinear elastic and viscoelastic properties of the material under various kinematic influences near resonance.
5. It was determined that the physical nonlinearity of the material of the structure leads to the occurrence of large stresses near the resonant mode of oscillations (in some sections of the structure), which can lead to structural damage to the dam.

References

1. *Bate K., Wilson E.* Numerical methods of analysis and the FEM. M.: Stroyizdat, 1982. 448 p.
2. *Badalov F.B., Eshmatov X., Yusupov M.* On some methods for solving systems of integrodifferential equations encountered in viscoelasticity problems. Appl. Math. and Mech., 1987. P. 51, No. 5. pp. 867-871.
3. *Demidovich B.P., Maron I.A., Shuvalova E.Z.* Numerical methods of analysis. Approximation of functions, differential and integral equations. M.: Nauka, 1967. 368 p.
4. *Gubanov I.V., Kovalchuk Yu.M., Pyshnograev A.V., Shutyaev V.G.* Oscillations of dams and the possibilities of their control. Hydraulic engineering. 2016. No. 12. pp. 28-37. DOI: 10.32684/0869-5376-2016-12-28-37
5. *Akhmetov A.S., Klimanov A.V., Khamidullin M.R.* Calculation and study of dam vibrations using the finite element method. Bulletin of the Bashkir University. 2019. V. 24, No. 3. P. 802-808. DOI: 10.33184/bulletin-bsu-2019.3.48
6. *Zlobin V.V., Kosogov N.A., Krylov S.V.* Analysis of dam dynamics under various operating modes. News of the Russian Academy of Sciences. Energy. 2020. No. 3. pp. 89-99. DOI: 10.31857/S0002331020030043
7. *Bronnikov A.V., Polishchuk A.N., Shilokhvostov D.V.* Investigation of the causes of dam vibrations based on monitoring data. Hydraulic engineering. 2014. No. 3. P. 14-25. DOI: 10.32684/0869-5376-2014-3-14-25
8. *Vasin V.I., Maklakova A.S., Nikolaev D.V.* Modeling the dynamics of dams under conditions of resonant interaction with water. Hydraulic engineering. 2015. No. 5. P. 35-45. DOI: 10.32684/0869-5376-2015-5-35-45
9. *Kudashev A.A., Kudasheva V.N., Fedorov I.A.* Determination of parameters of dam vibration models using the principal component method. News of the Russian Academy of Sciences. Mechanics of solids. 2017. No. 5. pp. 32-43. DOI: 10.17586/VNC.2017.05.32.43
10. *Kozlov A.A., Nazarenko A.V., Chernobrovkin V.A.* Development of a technique for monitoring dam vibrations based on the analysis of dynamic characteristics. Engineering and Construction Journal. 2021. No. 8(104). pp. 39-50. DOI: 10.34910/INS.104.8
11. *Pavlov V.V., Chernev A.S., Knyazeva E.A.* Determination of parameters of dam vibration models using artificial neural networks. News of the Russian Academy of Sciences. Theory and control systems. 2016. No. 5. P. 42-55. DOI: 10.7868/S0002338816050059
12. *Gorbunov A.A., Guryev M.Yu., Popov S.A.* Development of a system for monitoring and controlling dam vibrations based on unmanned aerial vehicles. Scientific and technical bulletin of information technologies, mechanics and optics. 2016. No. 1. pp. 1-7.
13. *Kovalev S.V., Laptev A.A., Timofeev M.V.* Modeling of dam vibrations considering external influences and dissipative properties of materials. Engineering and Construction Journal. 2014. No. 7(49). pp. 41-51. DOI: 10.22227/1997-0935.2014.7.41-51
14. *Krivosheev S.V., Suslov A.A., Kozlov A.V.* Determination of dynamic characteristics of dams based on the Fourier series. News of the Russian Academy of Sciences. Theory and control systems. 2019. No. 5. P. 27-39. DOI: 10.7868/S0002338819050032
15. *Kuzmina N.V., Nikolaev A.A., Stepanov O.A.* Assessing the impact of natural disasters on dam vibrations. Scientific and technical bulletin of information technologies, mechanics and optics. 2014. No. 1. pp. 1-7.
16. *Kozlov M.S., Chernov A.A., Bugrinov D.Yu.* Modeling of dynamic processes in dams considering the free edge effect. Scientific and technical bulletin of information technologies, mechanics and optics. 2016. No. 1. pp. 1-7. DOI: 10.17586/2226-1494-2016-16-1-1-7
17. *Panferov A.V., Kiryukhin V.I., Shestakov A.A.* Analysis of the possibilities of using the finite element method for modeling dam vibrations. Scientific and technical bulletin of information technologies, mechanics and optics. 2018. No. 1. pp. 1-7. DOI: 10.17586/2226-1494-2018-18-1-1-7
18. *Chepurnoy A.V., Dmitriev A.A., Zakharov D.A.* Analysis of the influence of dynamic loads on the operation of dams during design and operation. Hydraulic engineering. 2015. No. 5. pp. 2-9. DOI: 10.15407/gts05.02.002
19. *Sergeeva E.S., Moiseev A.A., Bocharov N.N.* Assessment of the influence of microseismic vibrations on the operation of dams. Hydraulic engineering. 2020. No. 11. pp. 2-9. DOI: 10.15407/gts11.02.002
20. *Karpov A.I., Belov A.A., Popov I.N.* Calculation of dynamic characteristics of dams considering the interaction with soil. Hydraulic engineering. 2016. No. 6. pp. 2-9. DOI: 10.1007/s10973-016-5476-9
21. *Zhilenkov M.S., Khlebov A.A., Korotkov A.V.* Modeling the dynamics of dams under the influence of seismic loads based on the finite element method. Hydraulic engineering. 2020. No. 12. pp. 2-9. DOI: 10.15407/gts12.02.002
22. *Kornilov A.S., Rodionov A.A., Shishkina I.V.* The influence of dynamic loads on the operation of dams and measures to strengthen them. Hydraulic engineering. 2015. No. 9. pp. 2-9. DOI: 10.15407/gts09.02.002
23. *Lipov A.A., Suvorov A.V., Khokhlov E.A.* Analysis of dam dynamics considering nonlinear effects in their operation. Hydraulic engineering. 2018. No. 11. pp. 2-9. DOI: 10.15407/gts11.02.002
24. *Maksimov A.V., Rodionov A.A., Kuznetsov I.A.* Assessment of dynamic parameters of dams based on monitoring results and mathematical modeling. Engineering and Construction Journal. 2022. No. 1(117). pp. 3-23. DOI: 10.34910/INS.117.1
25. *Zarembo A.A., Litvinov A.A., Kozhevnikov N.A.* Assessment of the influence of changes in soil parameters on the dynamics of dams. News of higher educational institutions. Construction. 2018. No. 8 (692). pp. 40-50. DOI: 10.32683/0536-1052-2018-8-40-50

26. *Zarembo A.A., Litvinov A.A., Kozhevnikov N.A.* Analysis of the impact of geometric characteristics of dams on their dynamics. Inžinerinė mechanika. 2019. V. 25, No. 3. P. 112-119. DOI: 10.5755/j01.mech.25.3.22206
27. *Khokhlov E.A., Lipov A.A., Suvorov A.V.* The influence of earth foundations on the dynamics of dams. News of higher educational institutions. Geology and exploration. 2016. No. 4. P. 65-70. DOI: 10.32454/0536-1037-2016-4-65-70
28. *Berdnikov V.I., Makarova E.V., Novikov V.P.* Modeling the dynamics of dams considering the influence of changes in geometric characteristics. Hydraulic engineering. 2017. No. 11. pp. 43-51. DOI: 10.32684/0869-5376-2017-11-43-51
29. *Lipov A.A., Suvorov A.V., Khokhlov E.A.* Study of the dynamics of dams considering nonlinear effects in their operation. News of the Russian Academy of Sciences. Mechanics of liquid and gas. 2018. No. 5. pp. 121-129. DOI: 10.20948/hydro-2018-05-121-129
30. *Mirsaidov, M., Mamasoliev, K.* Contact interaction of multilayer slabs with an inhomogeneous base. Magazine of Civil Engineering. 2022. № 115(7). 11504. DOI: 10.34910/MCE.115.7.
31. *Mirsaidov, M., Sultanov, T., Yarashov, J., Kayumov, A.* Strength of earth dams considering the elastic-plastic properties of soils. E3S Web of Conferences. 2023. № 365. 03001. DOI: 10.1051/e3sconf/202236503001.
32. *Mirsaidov, M.M., Toshmatov, E.S.* Dynamic behavior of earth dams under different kinematic impacts. E3S Web of Conferences. 2023. № 376. 01103. DOI: 10.1051/e3sconf/202337601103.
33. *Mirsaidov, M., Sultanov, T., Yarashov, J.* Strength of earth dams considering elastic-plastic properties of soil. Magazine of Civil Engineering. 2021. 108(8). 10813. DOI: 10.34910/MCE.108.8.10813.
34. *Juraev, D.J., Vatin, N., Sultanov, T.Z., Mirsaidov, M.M.* Spatial stress-strain state of earth dams. Magazine of Civil Engineering. 2023. 118(2). 11810. DOI: 10.34910/MCE.118.2.11810.
35. *Mirsaidov, M., Mamasoliev, K., Ismayilov, K.* (2022). Bending of Multilayer Slabs Lying on Elastic Half-Space, Considering Shear Stresses. In: Lecture Notes in Civil Engineering, vol 182, Pp. 93–107. DOI: 10.1007/978-981-16-6269-0_8.
36. *Sultanov, Karim.* Contact interaction of an underground pipeline with soil under dynamic impacts. Facta Universitatis, Series: Mechanical Engineering, [S.l.], mar. 2024. ISSN 2335-0164. http://casopisi.junis.ni.ac.rs/index.php/FUMechEng/article/view/12383>
37. *Mirsaidov M.M., Sultanov T.Z., Sadullaev S.A.* Determination of the stress-strain state of earth dams with account of elastic-plastic and moist properties of soil and large strains. Magazine of civil engineering. 2013. Volume 40. Issue 5. Pp. 59-68. DOI: 10.5862/MCE.40.7
38. *Mirsaidov M.M., Sultanov T.Z.* Assessment of stress-strain state of earth dams with allowance for non-linear strain of material and large strains. Magazine of civil engineering. 2014. Volume 49. Issue 5. Pp. 73-82. DOI 10.5862/MCE.49.8

EFFECT OF THE DEPTH OF CIRCULAR LINING IN AN ELASTIC MEDIUM WITH TRANSPARENT BOUNDARY UNDER THE IMPACT OF SEISMIC WAVES

Mirzaev I.[1], Gainazarov S.M.[2]
[1]*Tashkent State Transport University, Tashkent, Uzbekistan*
[2]*National University of Uzbekistan, Tashkent, Uzbekistan*
E-mail: ibrakhim.mir@mail.ru

Abstract. *The use of numerical methods for solving problems requires bounding the calculation domain and specifying the necessary boundary conditions on artificial boundaries. In contrast to the approximate boundary conditions available in published works, a new mathematical model on artificial boundaries is proposed to ensure the transparency of boundaries for transverse and longitudinal seismic waves. In this article, the finite element method (FEM) in spatial variables and the Bathe method in time are used to study the lining embedded in elastic soil media. As an example, the problem of the impact of a transverse seismic wave on a circular concrete lining based on real earthquake records, specified on the lower artificial boundary of a rectangular domain, was solved. The results of calculations are presented, showing good quality of transparency conditions at artificial boundaries and the dynamics of the structure under the impact of a seismic wave.*

Keywords: *Soil, circular lining, seismic analysis, transparent boundaries, finite element method.*

1. Introduction

When calculating a circular lining in a soil medium under seismic impacts, one of the important conditions is to consider the non-reflection of waves from the boundary of the computational domain, which allows the use of artificial boundaries in numerical calculations.

Reference [1] was the first publication that considered the conditions of non-reflection of waves from the boundary. Formulas for the dependence of stresses on the velocity of particles at the boundary for plane waves were used.

In [2], for the structure-foundation system, the wave energy loss through a non-reflecting boundary was considered using the Lismer conditions [1], and the finite element method was used for calculations. In [3], in the same way, the consideration of wave energy loss was used to study the propagation of vibration waves initiated by the movement of a railway train.

In [4], an inhomogeneous plane dynamic problem of elasticity theory was solved using the finite element method in calculating the propagation of vibrations that occur when metro trains pass in parallel tunnels.

Articles [5, 6] proposed the use of a fictitious domain with special wave absorption properties, which is one of the solutions to the problem of non-reflection at the boundaries of the domain. In these articles, a related problem involving the internal subdomain and absorbing layers was implemented through heterogeneous asynchronous time integrators, which allowed absorbing layers to be processed using an explicit central difference scheme. An exemplar for three-dimensional explicit asynchronous absorbing layers for modeling unbounded domains using a standard displacement-based finite element method was presented.

Reference [7] reviews studies, which present various conditions for non-reflection of waves at the boundaries of a bounded domain.

Review article [8] discusses various methods for numerical solutions to the non-stationary Schrödinger equation in unbounded domains. The most recent approaches to solving the problem of transparency and artificial boundary conditions for linear and nonlinear equations are presented in detail and alternative ideas are briefly described, pointing out the connections between these studies. Finally, several numerical examples from different application areas are given to compare the presented methods.

In [9], a new procedure for incorporating free field effects into a seismic soil-structure interaction (SSSI) model is presented using 8-node finite elements constrained by compatible absorbing infinite elements.

In [10], for a one-dimensional wave equation, a method for obtaining transparent boundary conditions is proposed and its numerical implementation is shown using the finite difference method. An alternative method for constructing transparent boundary conditions using a Dirac-type equation is presented. The proposed method is extended to a three-dimensional wave equation with radial symmetry.

The study in [11] is devoted to the construction and analysis of high-order transparent boundary conditions for a weighted wave equation on a fractal tree, simulating the propagation of sound inside the human lungs. An analysis of stability and convergence is presented. The numerical results obtained, are confirmed by theoretical conclusions.

In [12, 13, 14], a static analysis of the stress state of various metro tunnel linings was performed. An analysis was conducted depending on the tunnel embedment depth.

Reference [15] considered an embedded in soil culvert reinforced with concrete on three sides. A frequency analysis using the finite element method was performed.

In [16], an overview of dynamic soil-structure interaction (SSI) of building units and available modeling methods for solving SSI problems are given. In addition, the main approaches to assessing seismic soil-structure interaction problems using widely used modeling and computational methods are highlighted. Strengths, restrictions, and applications of each model are discussed and compared.

In [17-19], one-dimensional wave problems were studied, where the conditions of non-reflection of waves were taken as boundary conditions.

In [20, 21], the basics of the finite element method and its application in various problems of mechanics are given. These publications consider various finite-difference schemes for solving a system of ordinary differential equations that arise in dynamic problems when applying the FEM.

In [22], the free software *FreeFem++ system* is described, which allows solving various problems of physics and mechanics using the finite element method.

This article presents the exact conditions of transparency at the boundaries, which allow incoming and outgoing waves to freely pass and exit through the boundaries of the domain and make it possible to conduct research in bounded domains of the medium.

2. Materials, methods and object of study.

A two-dimensional isotropic linearly elastic body is considered in the half-plane, bounded by domain Ω, with inclusion in the form of a circular lining (Fig. 1). The wave enters domain Ω through boundary AB, and the conditions at boundaries AC and BD must compensate for the effect of the discarded part of the half-plane. Boundary CD of domain Ω is stress-free, i.e. on this boundary, the condition of a free surface is specified; in the case of the absence of a free surface on this boundary, the conditions for its transparency are specified. Inside the rectangular domain, a circular lining is embedded at different depths from the free surface.

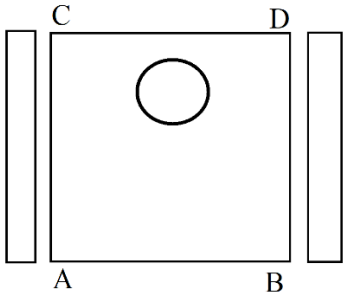

Figure 1 - **View of the fundamental domain and auxiliary domains**

To solve the problem, we use the weak form (variational form) of the equilibrium equations [9]:

$$\int_{\Omega}[\lambda div(u)div(\delta u)+2\mu\varepsilon^{T}\delta\varepsilon-(r-\rho\ddot{u}-c\dot{u})\delta u]d\Omega-\int_{\Gamma}P\delta u d\Gamma=0 \qquad (1)$$

where P is the vector of surface forces per unit area at the boundary of the domain, ρ, c, r are the density of the material, the viscosity parameter of the medium, and the vector of volumetric forces, $u^{T}=\{u_x, u_z\}$ is the displacement vector, ε is the strain tensor, λ and μ are the Lame coefficients. The axes of Cartesian coordinates are directed: *Ox* – from left to right, *Oz* – from bottom to top, the origin of coordinates is located in the center of the free surface.

Transparent boundary conditions are derived by applying exact solutions for a plane wave in the form of a connection between strains and particle velocities and by substituting them into the generalized Hooke's law. In addition, the solution to a one-dimensional plane dynamic problem for the domain without lining is used under the obtained conditions.

Consider the Cauchy relations

$$\varepsilon_{xx}=\frac{\partial u_x}{\partial x}, \varepsilon_{zz}=\frac{\partial u_z}{\partial z}, \varepsilon_{xz}=\frac{\partial u_x}{\partial z}+\frac{\partial u_z}{\partial x} \qquad (2)$$

and generalized Hooke's law

$$\sigma=B\varepsilon, \quad B=\begin{bmatrix}\lambda+2\mu & \lambda & 0\\ \lambda & \lambda+2\mu & 0\\ 0 & 0 & \mu\end{bmatrix}. \qquad (3)$$

The boundary conditions, when longitudinal and transverse waves with particle velocities $f_p(t)$ and $f_s(t)$ enter domain Ω through boundary AB, are:

transparency conditions on AB, with incoming longitudinal and transverse waves, have the following form:

$$\sigma_{zz} = c_p \rho \dot{u}_z + \lambda \frac{\partial u_x}{\partial x} - 2c_p \rho f_p(t);\ \sigma_{xz} = c_s \rho \dot{u}_x + \mu \frac{\partial u_z}{\partial x} - 2c_s \rho f_s(t);$$

$$P_z = -\sigma_{zz};\ P_x = -\sigma_{xz};$$

non-reflection conditions on CD:

$$\sigma_{zz} = -c_p \rho \dot{u}_z + \lambda \frac{\partial u_x}{\partial x};\ \sigma_{xz} = -c_s \rho \dot{u}_x + \mu \frac{\partial u_z}{\partial x};\ \ P_z = \sigma_{zz};\ P_x = \sigma_{xz};$$

or free surface conditions on CD:

$$\sigma_{zz} = 0;\ \sigma_{xx} = 0;\ \ P_z = 0;\ P_x = 0;$$

transparency conditions on AC:

$$\sigma_{xx} = c_p \rho \dot{u}_x + \lambda \frac{\partial u_z}{\partial z} - c_p \rho \dot{u}_x^1;\ \sigma_{xz} = c_s \rho \dot{u}_z + \mu \frac{\partial u_x}{\partial z} - c_s \rho \dot{u}_z^1;$$

$$P_x = -\sigma_{xx};\ P_z = -\sigma_{xz};$$

transparency conditions on BD:

$$\sigma_{xx} = -c_p \rho \dot{u}_x + \lambda \frac{\partial u_z}{\partial z} + c_p \rho \dot{u}_x^1;\ \sigma_{xz} = -c_s \rho \dot{u}_z + \mu \frac{\partial u_x}{\partial z} + c_s \rho \dot{u}_z^1;$$

$$P_x = \sigma_{xx};\ P_z = \sigma_{xz}.$$

Here c_p, c_s are the propagation velocities of longitudinal and transverse waves; $\dot{u}_x^1$ and $\dot{u}_z^1$ are the solutions to the corresponding one-dimensional problems for a plane wave in a rectangular domain with the necessary boundary conditions given below.

Consider the dynamic problem separately from the static one, therefore the initial conditions at t=0 have the following form:

$$u_x = 0, \dot{u}_x = 0, u_z = 0, \dot{u}_z = 0 \qquad .(4)$$

To determine $\dot{u}_x^1, \dot{u}_z^1$, an auxiliary correction domain is introduced (Fig. 1) to calculate the process of propagation of the original wave with the same physical characteristics and with the following geometry and boundaries:

$$\Omega_1 = \{(x,z): x \in [0, \Delta L], z \in [0, -H]\},$$

$$\Gamma_{l1} = \{(x,z): x = 0, z \in [0, -H]\},$$

$$\Gamma_{r1} = \{(x,z): x = \Delta L, z \in [0, -H]\},$$

$$\Gamma_{b1} = \{(x,z): x \in [0, \Delta H], z = -H\},$$

$$\Gamma_{t1} = \{(x,z): x \in [0, \Delta H], z = 0\}.$$

With the following boundary conditions:

for longitudinal wave

$$\sigma_{zz} = c_p \rho \dot{u}_z + \lambda \frac{\partial u_x}{\partial x} - 2c_p \rho f_p(t);\ \sigma_{xz} = c_s \rho \dot{u}_x + \mu \frac{\partial u_z}{\partial x};$$

$$P_z = -\sigma_{zz};\ P_x = -\sigma_{xz} \quad \text{on } \Gamma_{b1},$$

$$\sigma_{zz} = -c_p \rho \dot{u}_z + \lambda \frac{\partial u_x}{\partial x};\ \sigma_{xz} = -c_s \rho \dot{u}_x + \mu \frac{\partial u_z}{\partial x};$$

$P_z = \sigma_{zz};\ P_x = \sigma_{xz}$ conditions of non-reflection on Γ_{t1} or

$\sigma_{zz} = 0;\ \sigma_{xz} = 0$ free surface conditions,

$u_x = 0;\ \sigma_{xz} = 0$ ideal sliding conditions on Γ_{l1} and Γ_{r1},

and for shear wave:

$$\sigma_{xz} = c_s \rho \dot{u}_x + \mu \frac{\partial u_z}{\partial x} - 2c_s \rho f_s(t);\ \sigma_{zz} = c_p \rho \dot{u}_z + \lambda \frac{\partial u_x}{\partial x};$$

$$P_z = -\sigma_{zz};\ P_x = -\sigma_{xz} \text{ on } \Gamma_{b1},$$

$$\sigma_{xz} = -c_s \rho \dot{u}_x + \mu \frac{\partial u_z}{\partial x};\ \sigma_{zz} = -c_p \rho \dot{u}_z + \lambda \frac{\partial u_x}{\partial x};$$

$$P_z = \sigma_{zz};\ P_x = \sigma_{xz} \text{ conditions of non-reflection on } \Gamma_{t1} \text{ or}$$

$$\sigma_{zz} = 0;\ \sigma_{xx} = 0 \text{ free surface conditions,}$$

$$u_z = 0;\ \sigma_{xx} = 0 \text{ conditions on } \Gamma_{l1} \text{ and } \Gamma_{r1}.$$

Consider the problem when a wave at the boundary of the domain is given as a velocigram of the Ghazli earthquake.

Applying the method of partial discretization by finite elements [20] to (1), i.e. presenting the displacements in the element as $u^e = \sum_{i=1}^{n} u_i(t)\varphi_i(x,z)$, where n is the number of degrees of freedom in element e, u_i are the sought-for nodal displacements that depend on time, and $\varphi_i(x,z)$ are the shape functions in the element, we obtain the system of linear ordinary differential equations:

$$M\ddot{U} + C\dot{U} + KU = R \tag{5}$$

With initial conditions

$$U = 0,\ \ \dot{U} = 0 \text{ at } t = 0, \tag{6}$$

where M, C, K – are the matrices of mass, resistance and stiffness, respectively, U is the vector of the sought-for nodal displacements, and R is the load vector.

To solve systems of equations (5) with initial conditions (6), the implicit Bathe finite-difference method is used [21].

The solution algorithm is as follows: at each time step, using the above methods, particle velocities are determined for a one-dimensional domain with the corresponding boundary conditions, modeled by one element in width; and the number of elements in height depends on the finite element mesh of the basic medium. Then the obtained values of particle velocities are substituted into the corresponding boundary conditions of the basic medium.

3. Results and discussions

To substantiate the proposed mathematical model, the fields of a given rectangular domain 50m×50m, and a one-dimensional domain with a height of 50m, were calculated; the area represents a homogeneous soil with the following mechanical characteristics: Young's modulus E=150 MPa, Poisson's ratio ν=0.3, density $\rho = 1800$ kg/m^3. The lining is a reinforced concrete ring with a diameter of 6m and a thickness of 0.3m, Young's modulus E=12000 MPa, Poisson's ratio ν=0.3; in the calculations, the center of the ring is located at different depths: h=8m, h=15m, and h=22m.

The implementation of the problem was conducted using the free software *FreeFem++ system* [22], which has its language for describing the statement of the problem with the corresponding boundary conditions and methods of partitioning into finite elements. A triangular element with six nodes of the second degree of accuracy was used as a finite element.

To solve the static problem and determine the static stress state of the lining in a homogeneous soil, a static calculation of the domain under the influence of its weight was conducted. At the lower boundary of the domain, zero displacements are specified, the upper boundary is stress-free, and ideal sliding conditions are used at the side boundaries. Figure 2 shows the values of displacements u_x and u_z in the calculation domain with the lining at a depth of 15 meters.

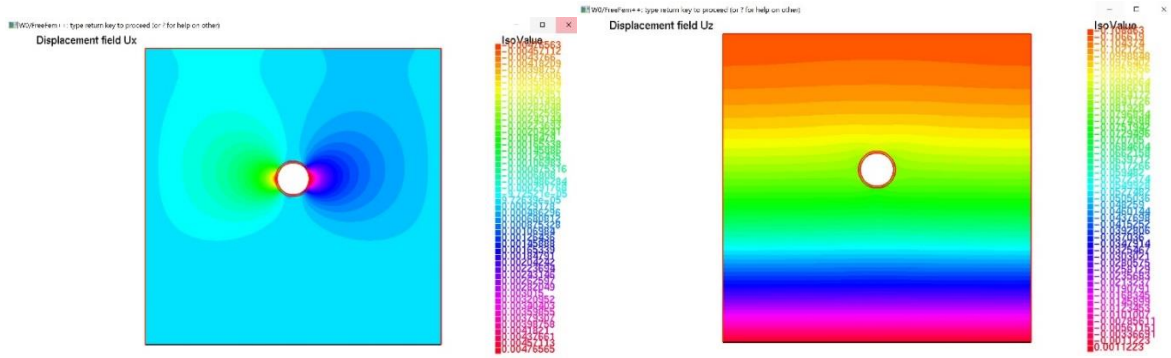

Figure 2 - **Fields of displacement around the circular lining**

The displacement values and the pattern of their distribution correctly reflect the processes occurring in soil. The hoop stresses in the lining along the outer and inner boundaries and inside the lining were calculated. The state of hoop stresses in and around the lining for various depths of bedding is given in Table 1.

The Table shows that the lining is subject to pressure from soil, resulting in compressive stresses in the lining.

Table 1

Values of hoop stresses in circular lining $\sigma_{\theta\theta}$ (MPa)

	h=8m			*h*=15m			*h*=22m		
θ/r	2.7m	2.85m	3.0m	2.7m	2.85m	3.0m	2.7m	2.85m	3.0m
0	-3.123	-1.711	-0.412	-6.193	-3.248	-0.668	-9.198	-4.826	-0.991
45	-0.439	-0.520	-0.604	-1.063	-1.152	-1.251	-1.647	-1.761	-1.838
90	0.466	-0.559	-1.480	1.026	-1.313	-3.409	1.620	-2.032	-5.279
-45	-0.861	-0.772	-0.628	-1.476	-1.382	-1.29	-2.076	-1.992	-1.924
-90	0.614	-0.985	-2.414	1.186	-1.709	-4.312	1.763	-2.419	-6.158

Next, a study of the lining under the impact of seismic loads arising in soil was conducted. The impact of a seismic wave on a circular lining is considered. As an example, we took a digitized recording of the velocigram of the Gazli earthquake, the graph of which is shown in Fig. 3. When specifying the particle velocity as an incoming shear wave into the region through its lower boundary, the velocity values in the velocigram recording are halved, considering further reflection of the wave from the free surface.

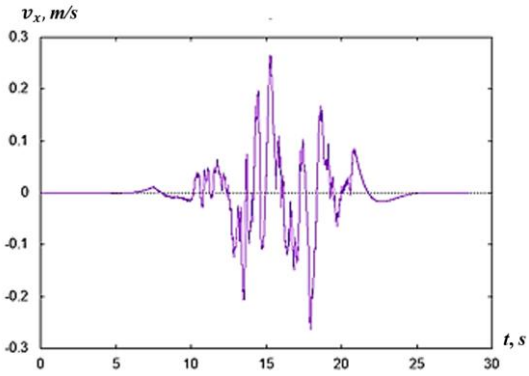

Figure 3 - **Velocigram of the Gazli earthquake**

Table 2 shows the results of calculations of stress intensity and hoop stresses at the outer boundary of the lining.

Table 2

Values of extreme dynamic stresses at the outer boundary of the lining (MPa)

	h=8m			h=15m			h=22m		
θ/r	$\sigma_{\theta\theta}$min	$\sigma_{\theta\theta}$max	σ_{in}max	$\sigma_{\theta\theta}$min	$\sigma_{\theta\theta}$max	σ_{in}max	$\sigma_{\theta\theta}$min	$\sigma_{\theta\theta}$max	σ_{in}max
0	-0.259	0.329	0.426	-0.321	0.359	0.420	-0.477	0.366	0.832
45	-1.213	1.152	1.356	-1.720	1.729	2.002	-1.497	1.712	2.084
90	-0.155	0.165	0.371	-0.267	0.268	0.587	-0.298	0.274	0.651
-45	-0.747	0.068	1.491	-0.179	0.172	2.058	-0.091	0.791	2.171
-90	-0.211	0.231	0.506	-0.303	0.284	0.661	-0.316	0.258	0.690

As seen from the table, the maximum stress intensity occurs at points with angles of 45 and -45 degrees, the highest hoop stresses are observed at horizontal points of the circular lining.

Below are graphs of hoop stresses on the outer boundary of the lining at various points and at different depths.

From Figures 4, 5, and 6, it is clear that the pattern of stresses during an earthquake is highly unsteady. To obtain the stress values, it is necessary to add the static and dynamic stresses, then the maximum hoop stresses will decrease, which is favorable for concrete. The maximum hoop stress, at a lining depth of 8 m, on the central horizontal axis is 2 times greater than the maximum hoop stress on the central vertical axis. At depths of lining 15 m and 22 m, this difference decreases to 1.34 times. An increase in the depth of the lining within the considered limits led to an increase in the intensity of dynamic stresses at the outer boundary of the lining. This process occurs in the epicentral zone of an earthquake. Far from the epicenter of an earthquake, studies must be conducted under the impact of surface waves based on the records of past earthquakes. Since the amplitude of a surface wave decreases exponentially with depth, the deeper the circular lining embedded, the less the impact of surface waves.

The stressed state of the lining strongly depends on the physical and mechanical characteristics of the surrounding soil. If the circular lining is located in soft soil, then tensile hoop stresses appear in the lining and can reach dangerous values for concrete.

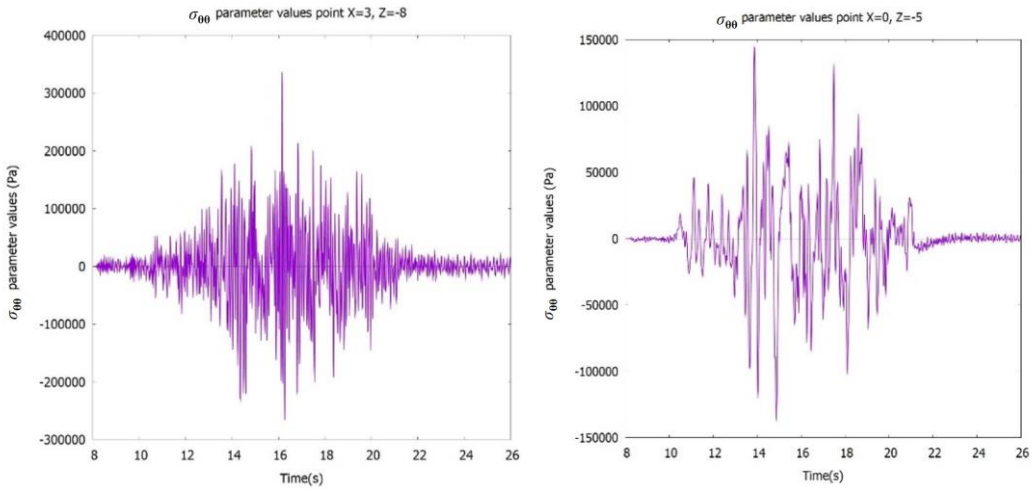

Figure 4 - **Graphs of hoop stresses in various points of the lining at a depth of 8 meters**

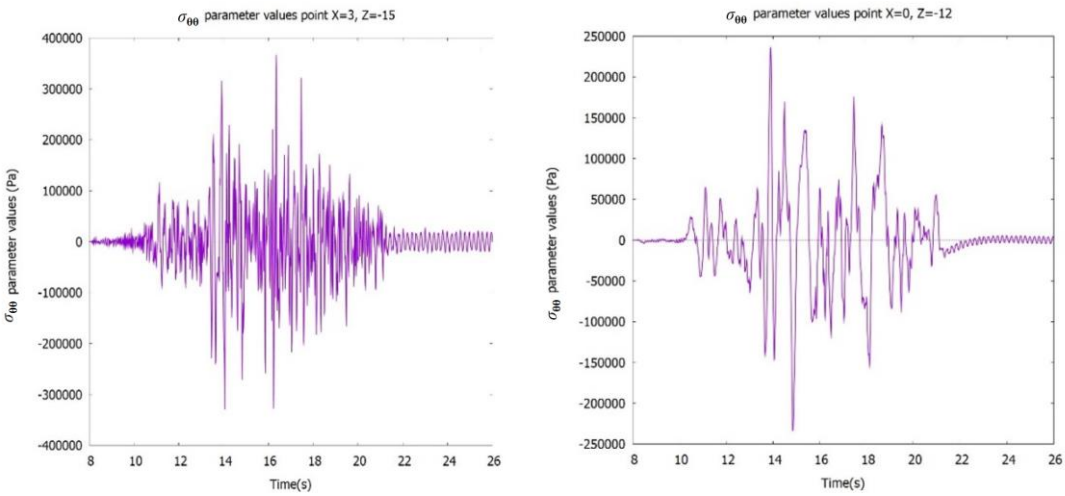

Figure 5 - **Graphs of hoop stress values in various points of the lining at a depth of 15 meters**

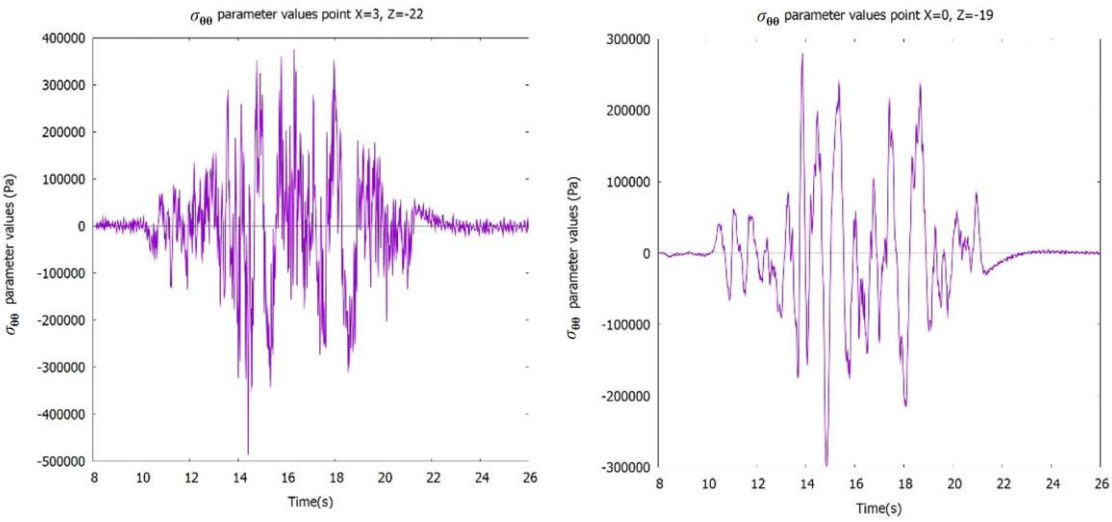

Figure 6 - **Graphs of hoop stresses at various points of the lining at a depth of 22 meters**

As expect, the results of numerical calculations of the transparent upper boundary of the design domain showed that the location of the circular lining from the upper boundary of the domain does not matter, as long as sufficient distance from the upper and lower sides of the computational domain is ensured. This indicates the accuracy of the transparency conditions at the boundaries of the computational domain.

4. Conclusion

Exact conditions on transparent boundaries are obtained when the set longitudinal and transverse waves enter a bounded rectangular domain parallel to the free surface of this domain. Using the free programming software for FEM FreeFem++ and the Bathe method, the problem of the impact of seismic waves on a circular lining in a homogeneous soil medium was solved. As an example, the problem of the impact of a transverse seismic wave based on real records of the Gazli earthquake, specified on the lower artificial transparent boundary of the domain, was solved. Calculation results presented showed good quality of transparency conditions at artificial boundaries; an analysis of the dynamic response of the lining at different depths of embedment was performed. With an increase in the depth of the circular lining from 8 m to 22 m, due to the overlapping of incoming waves and waves reflected from the free surface, the maximum values of the intensity of dynamic stresses in the lining increase. With an increase in the depth of the circular lining, its static stress state favorably affects the hoop stresses at the outer boundary of the lining.

References

1. *Lysmer J., Kyhlemeyer L.* Finite Dynamik Model for Infinite Media // Journal Engineering Mechanics Division, ASCE. 1969, vol 95, Issue 4, pp. 859-887. https://doi.org/10.1061/JMCEA3.000114
2. *Mirsaidov M.M., Sultanov T.Z., Rumi D.F.* An assessment of dynamic behavior of the system "structure – foundation" with account of wave removal of energy // Magazine of Civil Engineering. 2013, No. 4, pp. 94-127. https://doi.org/10.5862/MCE.39.10
3. *Il'ichev V.A., Yuldashev, S.S. and Saidov S.M.* Propagation of vibration from trains in relation to track position. Soil Mech Found Eng 36, 1999, P. 55–56. https://doi.org/10.1007/BF02469085
4. *Yuldashev S.S., & Karabaeva, M.U.* Soil surface vibrations in the training of metro trains in parallel tunnels. // Theoretical & Applied Science, 85 (05). 2020, pp. 117-121. https://doi.org/10.15863/TAS.2020.05.85.24
5. *Li S., Bruna M., Djeran-Maigrea I., Kuznetsov S.* Benchmark for three-dimensional explicit asynchronous absorbing layers for ground wave propagation and wave barriers // Computers and Geotechnics 131. 2021, pp. 1-16. https://doi.org/10.1016/j.compgeo.2020.103808
6. *Bruno Guidio, Boris Jeremić, Leandro Guidio, Chanseok Jeong.* Passive seismic inversion of SH wave input motions in a truncated domain // Soil Dynamics and Earthquake Engineering. 2022, vol. 158, No. 107263 https://doi.org/10.1016/j.soildyn.2022.107263
7. *Dan Givoli.* High-Order Local Non-Reflecting Boundary Conditions: A Review // Wave Motion. 2004, vol. 39, Issue 4, pp. 319-326. https://doi.org/10.1016/j.wavemoti.2003.12.004
8. *Xavier Antoine, Anton Arnold, Christophe Besse, Matthias Ehrhardt and Achim Schadle.* A Review of Transparent and Artificial Boundary Conditions Techniques for Linear and Nonlinear Schrodinger Equations // Communications in Computational Physics. 2008, vol. 4, No. 4, pp.729-796. http://www.global-sci.com
9. *Yacine Bakhtaoui.* New procedure for soil-structure interaction problems incorporating free-field effects by 2D quadratic elements // Computers and Geotechnics. 2024, vol. 165, No. 105843, https://doi.org/10.1016/j.compgeo.2023.105843
10. *Pilar Velasco M., David Usero, Salvador Jim´enez, Luis V´azques.* Transparent boundary conditions for the wave equation in one dimension and for a dirac-like equation // Electronic Journal of Differential Equations, Conference. 2015, 22, pp. 117-137. https://ejde.math.txstate.edu/conf-proc/22/v2/velasco.pdf
11. *Patrick Joly, Maryna Kachanovska.* Local transparent boundary conditions for wave propagation in fractal trees (I). Method and numerical implementation. SIAM Journalon Scientific Computing, 2021. 30p.
12. *Miralimov M., Normuradov Sh.* Ground behaviour and settlements analysis on tunnelling of shallow-buried metro in Tashkent city // E3S Web of Conferences. 2023, vol. 401, No. 01062, CONMECHYDRO-2023, https://doi.org/10.1051/e3sconf/202340101062
13. *Adilov F, Yuldoshev B, Abirov R, Miralimov M.* Numerical approach for estimation of stress strain state of deep tunnels // E3S Web of Conferences. 2019, vol. 97. https://doi.org/10.1051/e3sconf/20199704064
14. *R. Abirov, M. Miralimov.* Calculation of the Lining of Construction of the Shallow Subway Tunnel. Hydraulic and Civil Engineering Technology VIII M. Yang et al. (Eds.) 2023, https: doi:10.3233/ATDE230700
15. *Oztur K.F.* Investigation of dynamic responses of three-sided underpass culvert under near-fault and far-fault ground motions considering soil-structure interaction // Soil Dynamics and Earthquake Engineering. 2024, vol. 177 No. 108446. https://hdl.handle.net/20.500.12440/6143
16. *Bapir B., Abrahamczyk L., Wichtmann T., Prada-Sarmiento F.* Soil-structure interaction: A state-of-the-art review of modeling techniques and studies on seismic response of building structures // Front. Built Environ., 03 February 2023 Sec. Earthquake Engineering. 2023, vol. 9. https://doi.org/10.3389/fbuil.2023.1120351
17. *Mirzaev I., Shomurodov J.F.* Unsteady waves in an extended underground pipeline under seismic action // Computational Technologies. 2023, 28(3), pp. 10-24. https://doi.org/10.25743/ICT.2023.28.3.002 (In Russ.)
18. *Mirzaev I.M.* Reactions of composite structures, with concentrated and distributed parameters, to seismic action (vertical vibrations) // Soviet mining science. 1976, vol. 12, No. 3, pp. 296-300. https://doi.org/10.1007/bf02594874
19. *Mirzaev I. Shomurodov J. F.* Wave processes in an extended underground pipeline interacting with soil according to the model of an “ideal elastoplastic body” // Journal of Physics: Conference Series. 2021, vol. 1902, No. 012017. https://doi.org/10.1088/1742-6596/1902/1/012017
20. *Zienkiewicz O.C., Morgan K.* Finite elements and approximation / “Wiley-Interscience” New York, 1983. 328-p.
21. *Bathe K.J.* Finite Element Procedure Second Edition. / Printed in the United States of America, 2016, 1065-p.
22. *Hecht F., Pironneau O., Le Hyaric A., Ohtsuka K.* FreeFem++. Third Edition, Version 3 / Laboratoire Jacques-Louis Lions, Universite Pierre et Marie Curie, Paris, 390-p. URL: https://freefem.org/

STUDIES ON TRUSS BRIDGES

Mirzakhmedov M.I.[1], Yuvmitov A.S.[2], Khurramov A.Ch.[2]
[1]*Tashkent State Transport University*
[2]*Institute of Mechanics and Seismic Stability of Structures named after M.T. Urazbaev, Tashkent, Uzbekistan*
E-mail: Mirzahmedov75@mail.ru,

Abstract: *The article discusses the possibility of replacing rigid nodes with hinges when calculating trusses used in the construction of bridges, and determining the effective shapes of trusses based on the location of diagonal elements.*

Keywords: *truss, construction, mesh, rod, elements, assembly, hinged connection, single joint, tension, statically definite and indefinite systems, Lira-SAPR, knot cutting method, Ritter, Maxwell-Cremont diagram, efficiency.*

1. Introduction.

Truss structures are considered to be one of the lightweight and material-efficient constructions used in large-span structures. Based on its external appearance, the shape of its panels, and the arrangement of it supports this structure is divided into several types, according to the assigned task it is structured into trusses, cranes, and bridge trusses [1]. Chord trusses are used to cover the roofs of buildings and structures. Crane booms are utilized in crane structures, the construction of transmission towers, and high-voltage electrical line supports. Trusses used in the construction of bridges are called bridge trusses. In many instances, they are formulated in a trapezoidal configuration, see Fig.1(a).

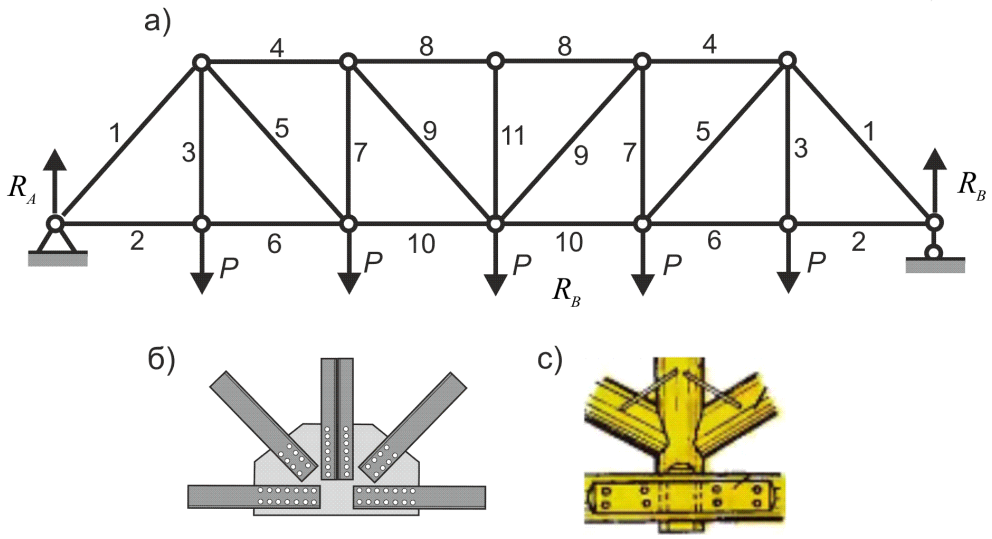

Figure 1. – **The trusses utilized in bridge construction and connection knots.**

The trusses are theoretically considered to be connected by means of hinges. It is believed that the chords of the trusses are only engaged in compression or tension forces and do not undergo deformation such as bending, torsion, or other forms of distortion. In fact, the chords are attached at the nodes by mutual nailing or welding, Fig.1(a) and b) Fig.1(b). If the structure is considered in this way, it is in the form of a static indeterminate system, and its calculation becomes more complicated. For example, if the truss shown in the Fig.1 is analyzed using the force method without hinges, the static uncertainty of the farm will be equal to 30 with three unknowns in each section shown in its main system. Resolving such highly indeterminate problems requires quite intricate calculations.

When the elements in the trusses are interconnected through hinges, this truss becomes statically determinate, and its analysis can be simplified using conventional methods. It is possible to determine reactions by creating sections, as well as by constructing Ritter and Maxwell-Cremona diagrams.

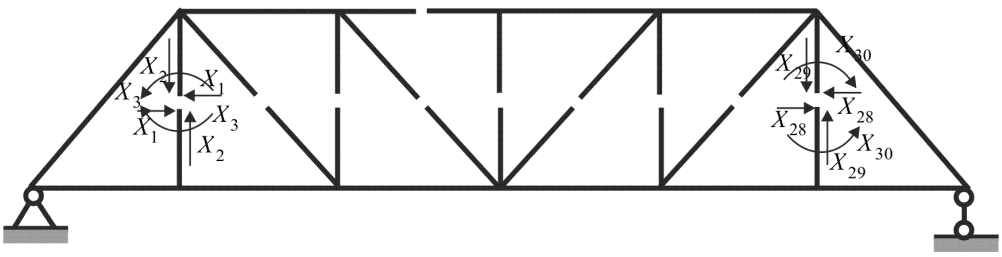

Figure 2. – **Unknowns in truss elements**

2. Materials, methods and object of study.

When analyzing trusses with elements connected in both hinged and pinned conditions, comparing the forces generated in their elements is necessary to distinguish between the two configurations. This involves calculating forces separately for each configuration and then comparing them. For this, we consider that the span of the truss in the Fig.1 is 18 m, the height is 4 m, each of its lower hinges is affected by a force of P=2 kN, we determine the tension in all its struts by the method of cutting nodes, and the results are presented in the Table 1. The forces in the truss and its elements are equal because the forces applied to them are symmetrically distributed.

Table 1.

In the analytical method											
Truss elements	1	2	3	4	5	6	7	8	9	10	11
Forces, (kN)	-6.25	+3.75	+2	-6	+3.75	+3.75	-1	-6.75	+1.25	+6	0
In the LIRA-SAPR software											
Forces, (kN)	-6.24	+3.74	+1.99	-6.24	+3.74	+3.75	-0.991	-6.75	+1.25	+6	+0.001
Difference, %	0.16	0.3	0.5	3.8	0.3	0	0.9	0	0	0	0.1

3. Analysis of results.

As a result of the development of computer technologies in recent years, several programs for analysis and design of building structures have been developed. One of such programs is the engineering program "LIRA- SAPR", based on the finite element method. With the help of this program, we designed the elements of the truss for the case of mutual fixation of elements in the truss (Fig.3) and determined the forces of the rods, presenting the results in Table 1.

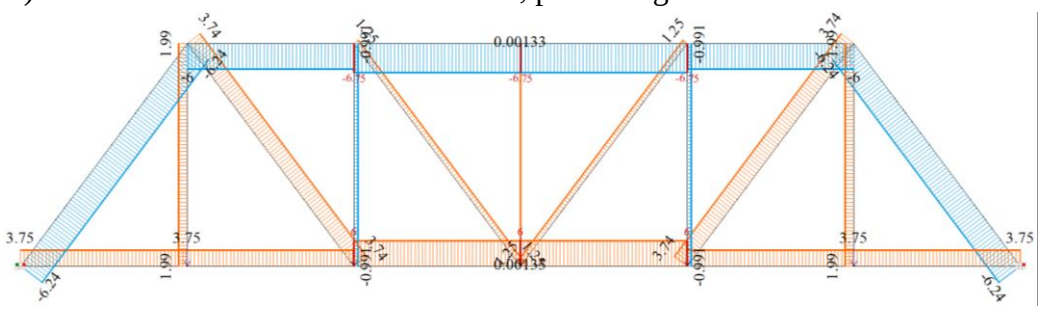

Figure 3. – **Longitudinal force diagram in the truss elements**

Analyzing the results obtained from analytical calculations and the software shows that the difference in forces between the elements does not exceed 3%, excluding the 7th rod. This indicates that in designing structural elements, achieving uniformity in forces is not of significant importance. This suggests that in analyzing truss structures, considering the elements as interconnected by hinges allows for analysis using conventional methods.

When the truss elements are interconnected in the nodes, besides the axial force, there will also be internal shear forces and bending moments within the elements (Fig.4-5). However, their magnitudes being very small, it is not necessary to consider their effects in calculations.

The efficiency of truss structures is evaluated based on their ability to bear loads, their stiffness, the complexity of the technological processes involved in their fabrication, and the design aesthetics of their external appearance. Lightness of construction depends on the amount of deflection in its elements. In other words, the smaller the deflection, the smaller the section of the element, and the structure becomes more compact. This leads to an overall increase in the strength-to-weight ratio of the structure [3].

Research shows that the deflections in structural elements are also dependent on their arrangement, including the positioning of diagonal elements, i.e., trusses [4]. Using the LIRA-SAPR software, we identify and analyze the tensions in the elements of a truss structure with various arrangements of trusses [5]. First, the tension in all the elements of the truss is determined as shown in Fig.6. It is assumed that the span of the truss is 24 m, the size of the panels is 3 m, and the height is 6 m. We assume that all loads acting on it are P = 50 kN and they are applied to the lower nodes. The results obtained from the program are shown in Fig.7, and the values of the tension in the elements are shown in Table 2.

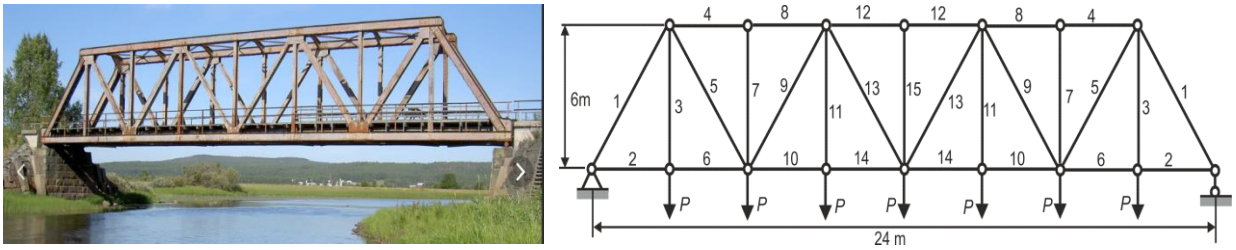

Figure 6. – **The truss and the calculation scheme where the rod forces are determined.**

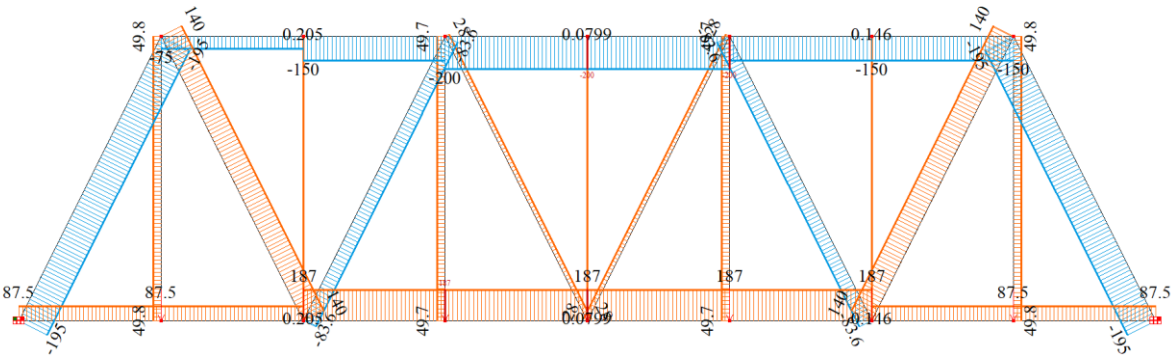

Figure 7. – **The results obtained by the LIRA-SAPR software.**

Table 2

Truss elements	1	2	3	4	5	6	7	8
Forces, (kN)	-195	+87.5	+49.8	-75	+140	+87.5	0.205	-150
Truss elements	9	10	11	12	13	14	15	12
Forces, (kN)	-83	+187	+49.7	-200	+28	+187	0.08	-200

In the first example regarding the shape, we will consider the calculation of yet another truss similar to the one seen from a perspective, but with diagonal elements positioned polygonally. For comparison, we'll first equivalently select all its dimensions and forces acting on the previous truss (Fig.8). Program-based solution of the truss is given in the Fig.9 and the deformation of the elements is represented in Table 3.

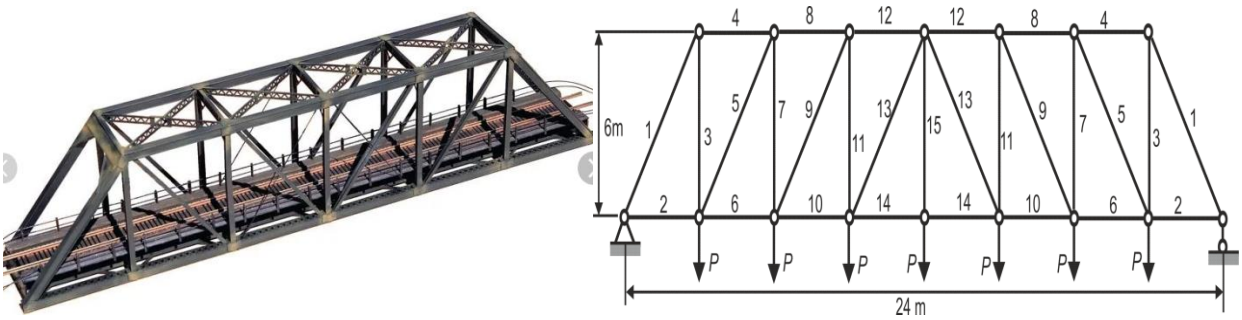

Figure 8. – **The truss and its equivalent calculation scheme**

Table 3

Truss elements	1	2	3	4	5	6	7	8
Forces, (kN)	-195	+87.5	+174	-43.8	+139	+150	125	-150
Truss elements	9	10	11	12	13	14	15	12
Forces, (kN)	-83.6	+187	+74.8	-187	+27.7	+200	49.8	-200

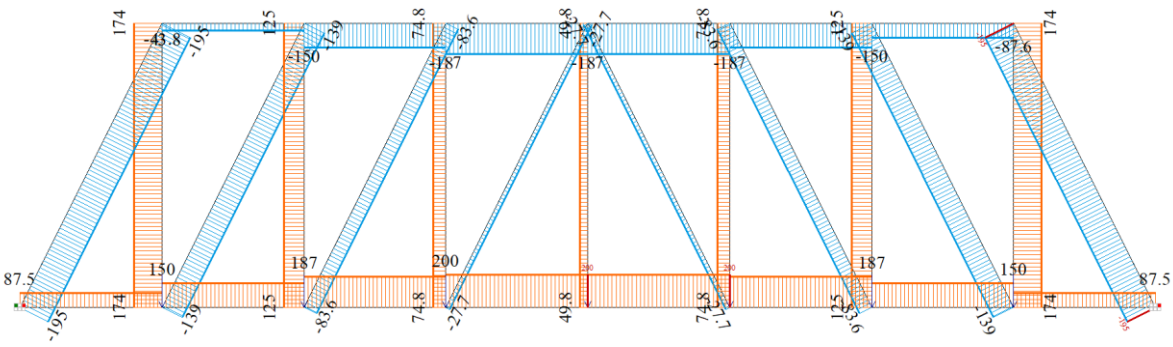

Figure 9. – **Calculation results obtained using Lira-SAPR software**

Comparing the forces shows that the truss in the first view is more efficient compared to the second one. Because in the second truss, the forces of the 3rd elements are 71%, the 7th rod are 123%, the 11th rod are 34%, and the 15th rod is 49% different from the corresponding forces in the first truss, it is possible to observe the variations in the Fig.9.

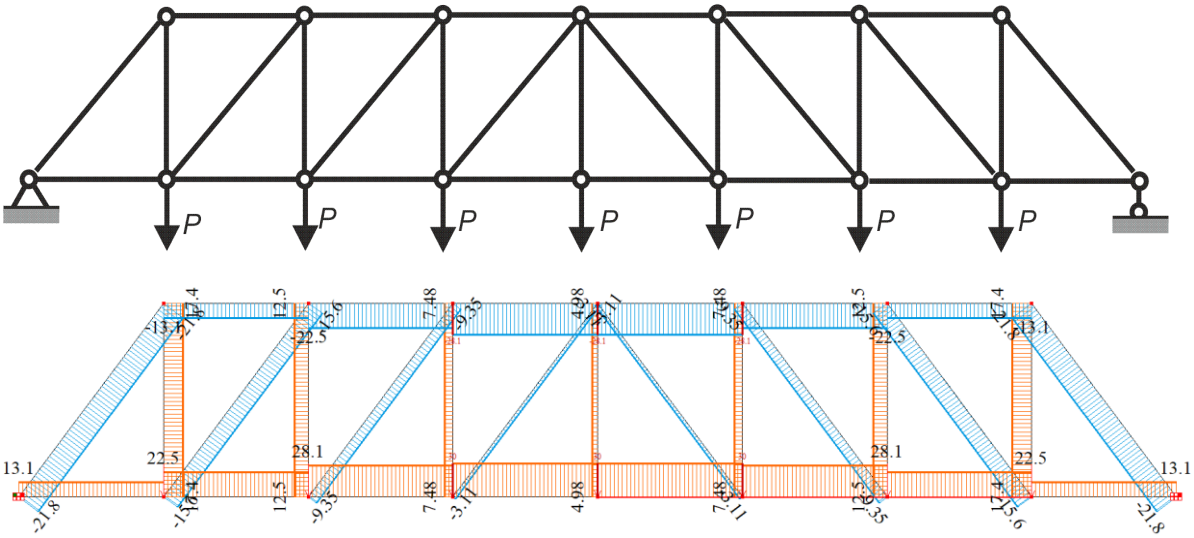

Figure 10. – **The calculation scheme and obtained results for a truss with diagonal elements working under compression**

In determining the effective forms of truss constructions, the tensile or compressive performance of their elements is also of great importance. If the truss is symmetrical, meaning its supports are located at the ends of the structure, and the loads are applied vertically, then all top girder elements of the truss will experience compression, while bottom girder elements will be

subjected to tension of the elements. In general, it is desirable that the struts work in tension in the construction. Because if the elements work under compression, there may also be issues beyond strength, such as buckling, meaning it's necessary to maintain the initial stability condition of the elements. This also requires considering the issue of stability for that particular elements.

It is not possible to ensure that all top chord elements and top elements in trusses work only in compression. Indeed, it is possible to ensure that diagonal elements work only in tension. The diagonal elements within the trusses of Fig.6 and Fig.8, as seen in the calculations above, are indeed subjected to compression. If the truss's diagonal elements are designed similar to Fig.10 and loads are applied to the bottom chords, then it's possible to determine if they are all working under compression through calculations in the program.

Now let us determine the forces in the rod elements using the program of diagonal rod position in the truss, as shown in Fig.11. The calculation results show that all elements of the rods work in tension.

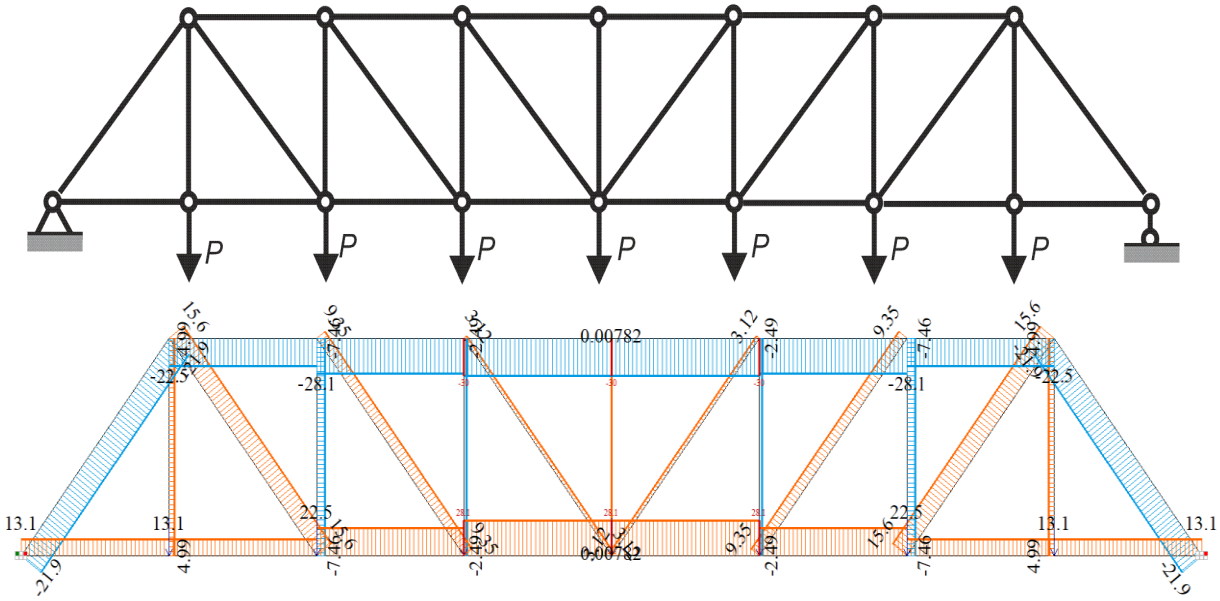

Figure 11. – **Calculation scheme and obtained results for a truss with diagonal elements working under tension.**

4. Conclusion.

It can be concluded that in the configuration where diagonal elements are positioned similar to configuration in the Fig.11 truss, all elements are working under compression. In other words, there is no need to consider stability issues for these elements. The number of compressed elements in the truss shown in the Fig.10 is about 14, in the Fig.11 is 12. This indicates that the truss in the Fig.11 configuration is relatively more efficient compared to the one in the Fig.10 configuration [2].

References.

1. *Abdurashidov K.S. et al.* Structural Mechanics, "Uzbekistan", 1999, pp. 47-70
2. *Torayev X.Sh. et al.* Structural Mechanics. Tashkent - "Finance" -2002, pp. 88-90
3. *Odilkhodjaev E.A. et al.* Examples and Problems from Structural Mechanics. Tashkent, 1985, 526 p.
4. *Mirzakhmedov M.I., Muradov M.M.* Collection of articles of Scientific-Practical Conference with Participation of Foreign Partners on the theme "Technologies of information modeling in the complex "Credo". Tashkent-2022. 63 p.
5. *LIRA-SAPR. Book I.* Fundamentals. E.B. Strelets-Streletsky, A.V. Zhuravlev, R.Y. Vodopyanov. Edited by Academician of RAASN, Doctor of Technical Sciences, Prof. A.S. Gorodetsky. - LIRALAND Publishing House, 2019. 154 p.

ON ANALYTICAL METHOD FOR ASSESSING THE STABILITY OF SOIL SLOPES

Normatov Sh.I.[1], Khusanov B.E.[1], Ganieva B.R.[2]
[1]*Institute of Mechanics and Seismic Stability of Structures named after M.T. Urazbaev, Tashkent, Uzbekistan*
[2]*Institute of Seismology, Uzbekistan Academy of Sciences, Tashkent, Uzbekistan*
E-mail: shovkatnormatov871@gmail.com

Abstract: *The possibility of using analytical methods to determine the parameters of a circular-cylindrical slip surface and evaluate the stability of homogeneous soil slopes is shown in this study. The problem is reduced to solving systems of three or two (when one of the boundaries of the slip surface is known) algebraic equations. As an example, for an elementary homogeneous slope, the parameters of the most dangerous circular-cylindrical slip surfaces of the soil slope and the corresponding values of the stability safety factor were found. Graphs are constructed that show the existence of minimum expressions for the stability coefficient using the MAPLE software package.*

Keywords*: slip surfaces, stability coefficient, soil slopes, analytical solutions.*

1. Introduction

In modern methods of calculation, including building codes SNiP, the stability of soil slopes is based on a simple model - the limit state of soil; this model does not consider the deformed state of soil. Calculations without considering strain but considering the equilibrium of rigid elements, under the assumption that the ultimate stress state was reached along the surface of collapse, allow one to obtain relatively simple solutions for various calculation schemes, which have received good practical confirmation [1-5]. Calculating the stability of slopes using the Terzaghi method is reduced to determining the stability coefficient, which is equal to the ratio of the moment of retaining forces (friction and cohesion) to the moment of shear forces along the slip surface, i.e. the problem comes down to finding a slip surface, in which the stability coefficient has a minimum value [6-9]. This problem is generally solved approximately for several rigid compartments [7-12]. By using numerical (approximate) solutions, a significant success was achieved in the area of application of the results in design and construction practice [13-15]. In this study, analytical methods are used to solve the problem: the equilibrium condition for the moments of forces that act along the slip surface, which is in a state of limited equilibrium, and the most unfavorable slip surfaces are determined.

2. Statement of the problem

When the soil mass is in an extremely stressed state, the formula proposed by K. Terzaghi [7] takes the following form:

$$K = \frac{\int_C M_{uder}\,dl}{\int_C M_{sdvig}\,dl} = \frac{\int_{x_1}^{x_2}\left[f\gamma(y-p)\cos\alpha + \frac{c}{\cos\alpha}\right]dx}{\int_{x_1}^{x_2}\gamma(y-p)\sin\alpha\,dx}, \qquad (1)$$

where γ is the specific gravity of soil, c and f are the cohesion and coefficient of the angle of internal friction $f = tg\varphi$, α is the angle between the lines of the slip surface to the center of the circular cylindrical slip surface (CCSS) and the vertical line to the CCSS, p is the function describing the profile of the slope surface, i.e. CCSS, y is the function expressing the collapse surface, x_1 and x_2 are the ordinates of the boundaries of the collapse surface (Fig. 1).

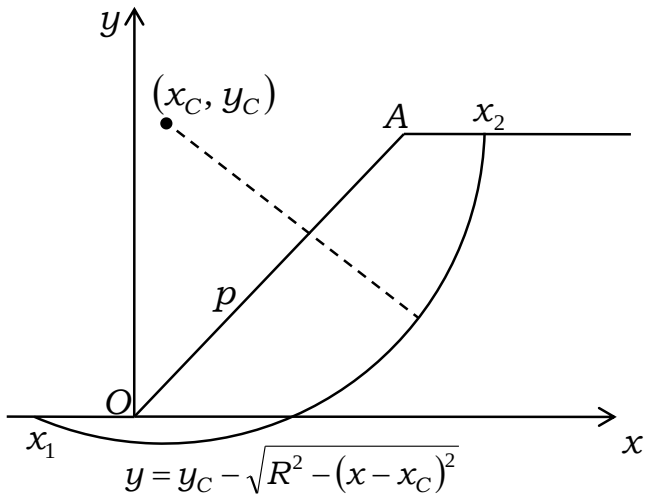

Figure 1. – **Calculation scheme**

Function describing the slope surface profile is:

$$p = \begin{cases} 0 & x < 0, \\ x/m & 0 \le x \le x_A, \\ h & x \ge x_A \end{cases},$$

where $h = y_A$ is the height of the slope, $m = \frac{x_A}{y_A} = \frac{x_A}{h}$ is the slope coefficient. The function describing the profile of the collapse surface, according to the CCSS, has the following form:

$$y = y_C - \sqrt{R^2 - (x - x_C)^2},$$

where (x_C, y_C) and R are the coordinates of the center and the radius of the circle, the arc of which describes the profile of the assumed collapse surface. This shows that function y is continuous and continuously differentiable, and function p is continuously differentiable piecewise. The derivative of this function is:

$$y' = \frac{dy}{dx} = \frac{x - x_C}{\sqrt{R^2 - (x - x_C)^2}} = -\frac{x - x_C}{y - y_C},$$

therefore,

$$tg\alpha = y' = -\frac{x - x_C}{y - y_C}. \tag{2}$$

Using the following trigonometric identities:

$$\sin\alpha = \sqrt{\frac{1 - \cos 2\alpha}{2}}, \quad \cos\alpha = \sqrt{\frac{1 + \cos 2\alpha}{2}}, \quad \cos 2\alpha = \frac{1 - tg^2\alpha}{1 + tg^2\alpha} = \frac{ctg\alpha - tg\alpha}{ctg\alpha + tg\alpha},$$

we obtain:

$$\sin\alpha = \frac{tg\alpha}{\sqrt{1 + tg^2\alpha}}, \quad \cos\alpha = \frac{1}{\sqrt{1 + tg^2\alpha}},$$

or

$$\sin\alpha = -\frac{x - x_C}{R}, \quad \cos\alpha = \frac{y - y_C}{R}. \tag{3}$$

Thus, the force acting on the slip surface, i.e. the integral of the denominator (1) is:

$$F_{sil} = \int_{x_1}^{x_2} \gamma(y-p)\sin\alpha\, dx = -\int_{x_1}^{x_2} \gamma(y-p)\frac{x-x_C}{R}\, dx \quad . \tag{4}$$

The force retaining part of soil is:

$$F_{ush} = \int_{x_1}^{x_2} \left[f\gamma(y-p)\cos\alpha + \frac{c}{\cos\alpha} \right] dx = F_{ush1} + F_{ush2} \tag{5}$$

where

$$F_{ush1} = \int_{x_1}^{x_2} f\gamma(y-p)\cos\alpha\, dx \quad , \quad F_{ush2} = \int_{x_1}^{x_2} \frac{c}{\cos\alpha}\, dx \quad . \tag{6}$$

The last force is:

$$F_{ush2} = \int_{x_1}^{x_2} \frac{c}{\cos\alpha}\, dx = \int_{x_1}^{x_2} \frac{cR}{(y-y_C)}\, dx = -cR\int_{x_1}^{x_2} \frac{dx}{\sqrt{R^2-(x-x_C)^2}} \quad . \tag{7}$$

Thus, for an analytical solution of the Terzaghi method, it is necessary to find parameters R, x_C, y_C of the slip surface that provide the minimum value of relation (1).

3. Analytical solution to the problem

Now for the analytical expression of relation (1), we calculate the integrals (4)-(5). First, we calculate integral (4):

$$F_{sil} = -\int_{x_1}^{x_2} \gamma y \frac{x-x_C}{R}\, dx + \int_{x_1}^{x_2} \gamma p \frac{x-x_C}{R}\, dx =$$

$$= -\frac{\gamma y_C}{R}\left\{ \frac{x_2^2 - x_1^2}{2} - x_C(x_2 - x_1) \right\} - \frac{\gamma y_C}{R}\left\{ \left[R^2 - (x_2 - x_C)^2\right]^{3/2} - \left[R^2 - (x_1 - x_C)^2\right]^{3/2} \right\} +$$

$$+ \frac{\gamma x_A^2}{mR}\left(\frac{x_C}{2} - \frac{x_A}{6} \right) + \frac{\gamma x_A}{mR}\left(\frac{x_2^2}{2} - x_C x_2 \right).$$

From here, considering $R^2 - (x_2 - x_C)^2 = (y_2 - y_C)^2 = (h - y_C)^2 = \left(y_C - \frac{x_A}{m} \right)^2$ and

$R^2 - (x_1 - x_C)^2 = (y_1 - y_C)^2 = (y_C)^2$, we obtain:

$$F_{sil} = -\frac{\gamma y_C}{R}\left\{ \frac{x_2^2 - x_1^2}{2} - x_C(x_2 - x_1) \right\} + \frac{\gamma x_A}{mR}\left(\frac{x_2^2}{2} - x_C x_2 \right) + \frac{\gamma x_A^2}{mR}\left(\frac{x_C}{2} - \frac{x_A}{6} \right) +$$

$$+ \frac{\gamma x_A y_C}{mR}\left\{ \left(y_C - \frac{x_A}{m} \right)^2 + y_C\left(y_C - \frac{x_A}{m} \right) + y_C^2 \right\} =$$

$$= \frac{1}{R}\left\{ A_2 x_1^2 + B_2 x_2^2 + A_1 x_1 + B_1 x_2 + C_1 \right\}, \tag{8}$$

where

$$A_2 = \frac{\gamma y_C}{2}, \qquad A_1 = -\gamma x_C y_C = -2x_C A_2,$$

$$B_2 = -\frac{\gamma y_C}{2} + \frac{\gamma x_A}{2m} = -\frac{\gamma}{2}(y_C - h), \qquad B_1 = \gamma x_C y_C - \gamma x_C \frac{x_A}{m} = \gamma x_C (y_C - h),$$

$$C_1 = \gamma y_C h\left\{ (y_C - h)^2 + y_C(y_C - h) + y_C^2 \right\} + \gamma x_A h\left(\frac{x_C}{2} - \frac{x_A}{6} \right).$$

We calculate integrals (5) or (6) expressing the retaining forces.

Using the following relation

$$\int \frac{dx}{\sqrt{R^2 - x^2}} = \arcsin\frac{x}{R} + const,$$

we determine

$$F_{ush2} = -cR\left\{\arcsin\frac{x - x_C}{R}\Bigg|_{x_1}^{x_2}\right\} = -cR\left\{\arcsin\frac{x_2 - x_C}{R} - \arcsin\frac{x_1 - x_C}{R}\right\}.$$

Now we calculate the 1st integral (6):

$$F_{ush1} = \int_{x_1}^{x_2} f\gamma(y - p)\cos\alpha dx = \frac{f\gamma}{R}\left\{\int_{x_1}^{x_2}\left(R^2 - (x - x_C)^2\right)dx - y_C\int_{x_1}^{x_2}\sqrt{R^2 - (x - x_C)^2}\,dx + \right.$$

$$\left. + \frac{1}{m}\int_0^{x_A} x\sqrt{R^2 - (x - x_C)^2}\,dx + h\int_{x_A}^{x_2}\sqrt{R^2 - (x - x_C)^2}\,dx\right\}.$$

Considering that

$$\int_{x_1}^{x_2}\left(R^2 - (x - x_C)^2\right)dx = R^2 x\Big|_{x_1}^{x_2} - \frac{(x - x_C)^3}{3}\Bigg|_{x_1}^{x_2} = R^2(x_2 - x_1) +$$

$$+ \frac{(x_2 - x_C)^3}{3} - \frac{(x_1 - x_C)^3}{3} = \frac{x_2^3 - x_1^3}{3} - x_C\left(x_2^2 - x_1^2\right) - \left(R^2 + x_C^2\right)(x_2 - x_1);$$

$$- y_C\int_{x_1}^{x_2}\sqrt{R^2 - (x - x_C)^2}\,dx =$$

$$= \frac{y_C}{2}\left\{(h - y_C)x_2 + y_C x_1 - hy_C - R^2\left(\arcsin\frac{x_2 - x_C}{R} - \arcsin\frac{x_1 - x_C}{R}\right)\right\};$$

$$\frac{1}{m}\int_0^{x_A} x\sqrt{R^2 - (x - x_C)^2}\,dx = \frac{2}{3m}\left((h - y_C)^3 - \left(\sqrt{R^2 - x_C^2}\right)^3\right);$$

$$h\int_{x_A}^{x_2}\sqrt{R^2 - (x - x_C)^2}\,dx =$$

$$= -\frac{h}{2}\left\{(h - y_C)x_2 - x_A(h - y_C) - R^2\left(\arcsin\frac{x_2 - x_C}{R} - \arcsin\frac{x_A - x_C}{R}\right)\right\},$$

we obtain:

$$F_{ush1} = \frac{f\gamma}{R}\left(\frac{x_2^3 - x_1^3}{3} - x_C\left(x_2^2 - x_1^2\right) - \left(R^2 + x_C^2\right)(x_2 - x_1) + \right.$$

$$+ \frac{y_C}{2}\left\{(h - y_C)x_2 + y_C x_1 - hy_C - R^2\left(\arcsin\frac{x_2 - x_C}{R} - \arcsin\frac{x_1 - x_C}{R}\right)\right\} + \frac{2}{3m}\left((h - y_C)^3 - \left(\sqrt{R^2 - x_C^2}\right)^3\right) - \tag{9}$$

$$\left. - \frac{h}{2}\left\{(h - y_C)x_2 - x_A(h - y_C) - R^2\left(\arcsin\frac{x_2 - x_C}{R} - \arcsin\frac{x_A - x_C}{R}\right)\right\}\right).$$

Thus, the stability coefficient (1) with (8)-(9) for a slope is expressed by the following formula:

$$K = \frac{\frac{1}{R}\left\{\begin{array}{l} A_3x_1^3 + B_3x_2^3 + A_{21}x_1^2 + B_{21}x_2^2 + A_{11}x_1 + B_{11}x_2 + R^2(x_1 - x_2) + C_2 + \\ + D_1R^2\arcsin\frac{x_1 - x_C}{R} + D_2R^2\arcsin\frac{x_2 - x_C}{R} + D_3R^2\arcsin\frac{x_A - x_C}{R}\end{array}\right\}}{\frac{1}{R}\left\{A_2x_1^2 + B_2x_2^2 + A_1x_1 + B_1x_2 + C_1\right\}}, \tag{10}$$

where coefficients $A_i, B_i, A_{ij}, B_{ij}, C_i, D_i$ are expressed through the physical, mechanical, and geometric parameters of the soil slope:

$$A_3 = -\frac{\gamma f}{3},\ B_3 = \frac{\gamma f}{3} = -A_3,\ A_{21} = \gamma f x_C,\ B_{21} = -\gamma f x_C = -A_{21},$$

$$A_{11} = \gamma f\left(x_C^2 + \frac{y_C^2}{2}\right),\ B_{11} = -\gamma f\left(x_C^2 + \frac{(h-y_C)^2}{2}\right),$$

$$D_1 = \frac{\gamma f}{2} y_C + c,\ D_2 = \frac{\gamma f}{2}(h - y_C) - c,\ D_3 = -\frac{\gamma f}{2} h,$$

$$C_2 = \gamma f\left(\frac{y_C}{3m}\left\{(y_C - h)^3 - \left(\sqrt{R^2 - x_C^2}\right)^3\right\} - \frac{h y_C^2}{2} + \frac{h x_A}{2}(h - y_C)\right);$$

$$A_2 = \frac{\gamma y_C}{2},\ A_1 = -\gamma x_C y_C = -2 x_C A_2,$$

$$B_2 = -\frac{\gamma y_C}{2} + \frac{\gamma x_A}{2m} = -\frac{\gamma}{2}(y_C - h),\ B_1 = \gamma x_C y_C - \gamma x_C \frac{x_A}{m} = \gamma x_C (y_C - h),$$

$$C_1 = \gamma y_C h\left\{(y_C - h)^2 + y_C(y_C - h) + y_C^2\right\} + \gamma x_A h\left(\frac{x_C}{2} - \frac{x_A}{6}\right).$$

In many cases, one of the boundaries of the collapse surface is defined. For example, in the case where the rigidity of the base is much greater than the rigidity of the slope, it can be considered that $x_1 = 0$. Then the stability coefficient is expressed by the following formula (10):

$$K = \frac{\left\{\begin{array}{l} B_3 x_2^3 + B_{21} x_2^2 + B_{11} x_2 - R^2 x_2 + C_2 - D_1 R^2 \arcsin\dfrac{x_C}{R} + \\ + D_2 R^2 \arcsin\dfrac{x_2 - x_C}{R} + D_3 R^2 \arcsin\dfrac{x_A - x_C}{R} \end{array}\right\}}{B_2 x_2^2 + B_1 x_2 + C_1}. \quad (11)$$

Relationship (10) that determines the slope stability coefficient is a function of three independent unknowns. $R,\ x_C,\ y_C$ can be taken as unknowns. In this case, boundaries x_1 and x_2 must be determined through these unknowns. From Fig. 1, it is clear that

$$x_1 = x_C - \sqrt{R^2 - y_C^2},\quad x_2 = x_C + \sqrt{R^2 - (y_C - h)^2}. \quad (12)$$

If $x_1 = 0$, then $x_C = \sqrt{R^2 - y_C^2}$ and $x_2 = \sqrt{R^2 - y_C^2} + \sqrt{R^2 - (y_C - h)^2}$, therefore (11) is the stability coefficient which is a function of two unknowns.

The minimum values of function (10) or (11) provide an assessment of the stability of the soil slope. To do this, it is necessary to find the values of $R,\ x_C,\ y_C$ corresponding to the extreme values of these functions. These values are the solution to the following systems of algebraic equations for (10):

$$\partial K / \partial R = 0,\quad \partial K / \partial x_C = 0,\quad \partial K / \partial y_C = 0 \quad (13)$$

For (11), we obtain:

$$\partial K / \partial R = 0,\quad \partial K / \partial y_C = 0 \quad (14)$$

4. Numerical solution to the problem

For the soil slope 15 m high, with the laying angle of $\alpha = 30°$, composed of semi-solid clay with the following physical and mechanical characteristics: density $\rho = 1{,}89$ g/cm^3; specific gravity $\gamma = 18{,}5$ kN/m^3; specific cohesion $C = 19{,}82$ kPa (2.02 kgf/cm^2); the angle of internal friction $\varphi = 14°$, us consider the behavior of the stability coefficient for two independent variables, i.e. for systems of equations (14). These results, obtained by using *MAPLE 18* software, are shown in Figs. 2-4.

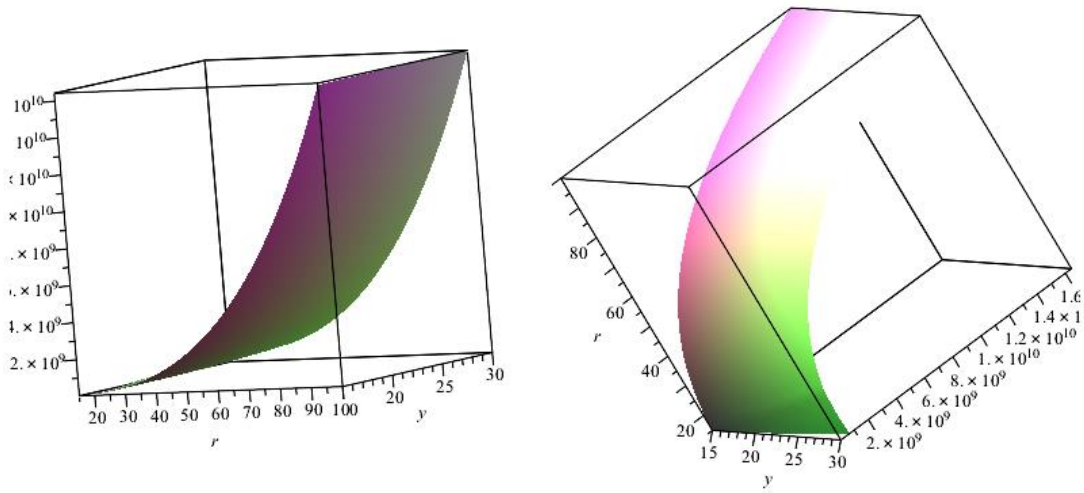

Figure 2. - **Stability coefficient for various values of** $r = R,\ \ y_C$

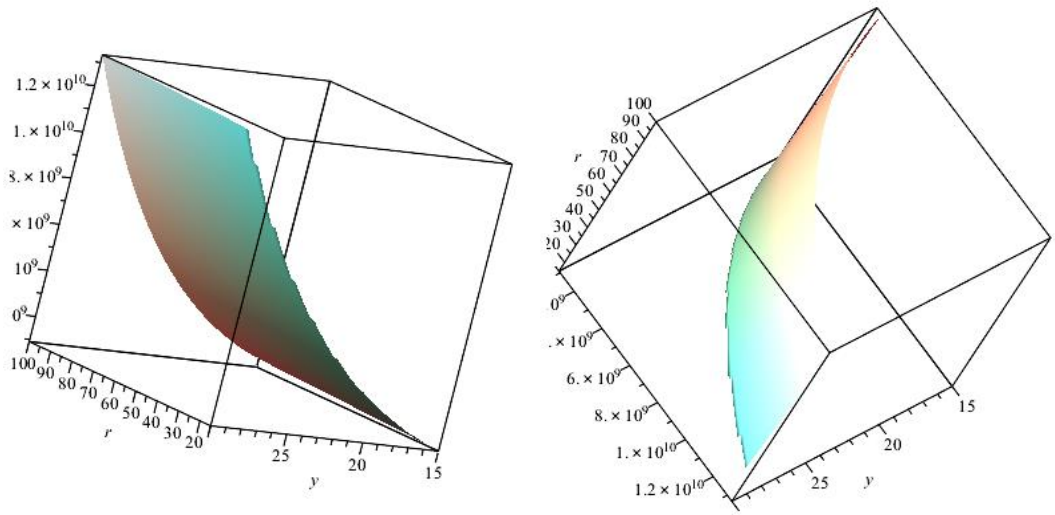

Figure 3. - **Stability coefficient for various values of** $r = R,\ \ y_C$

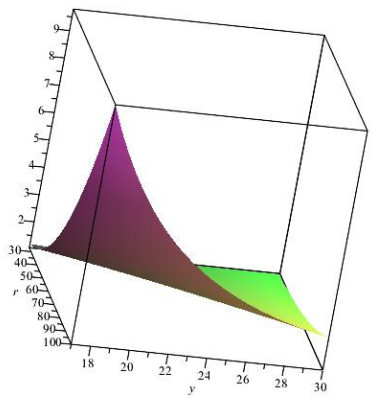

Figure 4. - **Stability coefficient for various values of** $r = R,\ \ y_C$

Thus, by the elementary method of determining the stability of soil slopes, we can use analytical methods to determine parameters R, x_c, y_c - the most dangerous circular cylindrical slip (collapse) surface of the soil slope.

5. Conclusions

The analytical method shows the possibility of assessing the stability and parameters R, x_c, y_c of the assumed slip surface for a homogeneous slope. A method for assessing soil slopes was studied, based on the assumption that the ultimate shear resistance is achieved only on the slip surface; the values are recommended in regulatory documents and widely used in practice. An algebraic expression for the stability coefficient for the C. Terzaghi method is derived. The graphs show the relationship between the stability coefficient and these parameters, i.e. behavior of the stability coefficient for two independent variables R, y_c. The results illustrate that when the stability coefficient reaches a minimum value, the slip surface takes the form of a circular arc. This shows that the radius of the arc does not reach infinity.

References

1. *Bogomolov A.N., Bogomolova O.A., Tsvetkova E.V., Podtelkov V.V.* The features of the calculation stability of homogeneous and layered ground slope laden based on analysis of stress state // PNRPU Bulletin Construction and Architecture, 2016, vol. 7, No. 2, pp. 93–105.
2. *Chubka P.Yu., Chubka Yu.Sh.* Comparison of methods for calculating the stability of soil arrays. // The Eurasian Scientific Journal, 2021, vol. 13, No. 5, pp. 1-11.
3. *Ždankus N. T., Stelmokaitis G.* Clay slope stability computations // Journal of civil engineering and management, 2008, vol. 14, No. 3, pp. 207-212.
4. *Sultanov, Karim.* Contact interaction of an underground pipeline with soil under dynamic impacts. Facta Universitatis, Series: Mechanical Engineering, [S.l.], mar. 2024. ISSN 2335-0164. Available at: <http://casopisi.junis.ni.ac.rs/index.php/FUMechEng/article/view/12383>. Date accessed: 31 mar. 2024.
5. *Sainov M.P.* Influence of the stressed state of a slope of homogeneous soil on its stability // Bulletin of MGSU, 2012, No. 10, pp. 102-108.
6. *Sainov M.P.* Numerical Modeling of the Stress-Strain State of Earth Dams That Have Thin Rigid Seepage Control Elements, Proceedings of Moscow State University of Civil Engineering, 2012, No. 10, pp. 102—108.
7. *Karl Terzaghi,* Theoretical Soil Mechanics. / John Wiley & Sons, Inc. Printed in the USA, 2001, pp 1-526.
8. Ryma A., Smail.G. Finite element slope stability analysis of Souk Tleta dam by shear strength reduction technique // Innov. Infrastruct. Solut, 2018, vol. 6, No.3, pp. 1-10.
9. *Khusanov B., Khaydarova O.* Stress-strain state of earth dam under harmonic effect. E3S Web of Conferences. 2019, vol. 97, P.05043. https://doi.org/10.1051/e3sconf/20199705043
10. *Bakhtiyar K., Barno R.* Numeric Simulation of Subsidence of Loess Soil under Wetting in a Limited Area // Journal of Advanced Research in Fluid Mechanics and Thermal Sciences. 2023, vol. 104, Issue 2, pp.1-18. https://doi.org/10.37934/arfmts.104.2.118
11. *Pendin V.V., Fomenko I.K.* Methodology for assessing and forecasting landslide hazard // M.: LENAD Moscow, 2015, 320 p.
12. *Duncan J.M.* Factors of safety and reliability in geotechnical engineering // Journal of Geotechnical & Geoenvironmental Engineering. 2000, April, pp. 307–316.
13. Nengxiong X., Jiayin Z., Hong T., Gang M., Quan G. Discrete element modeling of strata and surface movement induced by mining under open-pit final slope // International Journal of Rock Mechanics and Mining Sciences. 2016, vol. 88, pp. 61–76.
14. *Karim Sultanov, Sadillakhon Umarkhonov and Shovkat Normatov* Calculation of earth dam strain under seismic impacts // International Conference on Actual Problems of Applied Mechanics - APAM-2021, AIP Conf. Proc. 2637, 030008-1–030008-7.
15. *Bakhtiyar K., Shovkat N., Ozodaxon K.* On one method for assessing the soil slopes stability // AIP Conf. Proc. 2022, vol.2637, P.030012. https://doi.org/10.1063/5.0119155

STABILITY ASSESSMENT OF PIT WALL SIDES DETERMINING PARAMETERS OF SLIP SURFACE

Normatov Sh.I.[1], Rikhsieva B.B.[1]
[1]*Institute of Mechanics and Seismic Stability of Structures named after M.T. Urazbaev, Tashkent, Uzbekistan*
E mail: shovkatnormatov871@gmail.com

Abstract: *The stability of stepped slopes is discussed in this article. To solve the problem, the method of circular cylindrical slip surfaces (CCSS) was used. More than the ten least values of the stability coefficient and the corresponding parameters of the expected slip surface were determined for homogeneous and non-homogeneous stepped slopes with benches that correspond to the sides of deep quarries. The distributions of normal, shear, and retaining stresses along the most possible slip surface are plotted and it is shown that the ratio of the areas of the diagrams of retaining and shear stresses corresponds to the value of the stability coefficient.*

Keywords*: pit wall side, bench, stability, stress, slip surface.*

1. Introduction

The problems of studying the stability of soil slopes arise in the design and operation of structures erected for hydraulic, industrial, civil, transport, and other purposes on foundations with slopes and inclinations. The bases, slopes of dams, embankments and excavations, sides and benches of deep quarries, and natural slopes under their operation act as soil slopes. The stability of soil slopes is generally understood as their ability to withstand shear forces for a long time while maintaining their shape. The stable position of slopes and inclinations is determined by the corresponding stress-strain state formed by force impacts. Under an unfavorable combination of various factors, the soil foundation or massif (the side of a quarry or the slope of a dam), limited by a slope or inclination, can go into a non-equilibrium state and lose stability.

From the literature sources on the issue of priority of soil slopes, it can be seen that in the calculation schemes, limit states are assumed at all points of the potentially unstable part of the soil mass, i.e. at the same time, a limiting stress-strain state arises, obeying the Coulomb-Mohr law [1-2]. There are various methods for assessing the stability of slopes and inclinations [3-8]. The most widely used method for assessing stability is the circular-cylindrical slip surface method [9-12]. In this method, the expected slip surface is considered circular-cylindrical; a surface corresponding to the smallest value of the safety factor is sought for the stability of slopes and inclinations. This article proposes a method for determining such surfaces and assessing the stability of the sides of deep quarries.

2. Statement of the problem

As a rule, the value of the slope stability coefficient is most likely determined as the ratio of the sum of the retaining and shearing factors arising along the surface of the virtual slip; here, the stability coefficient should have a minimum value. In general, the stability margin factor is defined as the ratio of the retaining and shearing factors. In the ultimate stress state, the stability coefficient is expressed as:

$$K = \frac{\Phi_{uder}}{\Phi_{sdvig}} \tag{1}$$

where Φ_{uder}, Φ_{sdvig} are the retaining and shearing factors acting along the most probable slip surface. These factors can be forces acting along a probable slip surface or, in the case of a circular cylindrical slip surface using the Terzaghi method, moment forces relative to the central axis of the cylinder $\Phi_{uder} = \int_s M_{uder} ds$, $\Phi_{sdvig} = \int_s M_{sdvig} ds$, where s is the arc coordinate of the slip line.

Suppose the shape and position of the slip surface are known. In that case, the curvilinear integrals can be replaced with definite ones and the value of the stability margin factor K can be determined by the following formula:

$$K = \frac{\int_s M_{uder} ds}{\int_s M_{sdvig} ds} \quad \text{or} \quad K = \frac{\int_s F_{uder} ds}{\int_s F_{sdvig} ds},$$

and, passing from the contour integral to the definite one, we obtain:

$$K = \frac{\int_{x_1}^{x_2} \left[f\gamma(y_1 - p)\cos\alpha + \frac{c}{\cos\alpha} \right] dx}{\int_{x_1}^{x_2} \gamma(y_1 - p)\sin\alpha dx}, \quad (2)$$

where γ - is the specific gravity of soil; c and f - are the cohesion and the coefficient of internal friction angle $f = tg\varphi$; α is the angle between the tangent lines of the slip surface and the vertical line; p is the function describing the surface profile of a slope or inclination; y_1 is the function expressing the collapse surface: x_1 and x_2 are the ordinates of the boundaries of the collapse surface [13].

Let us recall that due to the non-homogeneity and geological features of the soil slope, the specific gravity, cohesion, and coefficient of internal friction angle depend on the *x, y* coordinates, and the functions p and y_1 are arbitrary functions of *x*. Let the function describing the profile of the plane surface of the side of a deep quarry be a stepped function.

In the case of a circular cylindrical slip surface, the function describing the profile of the collapse surface, according to the circular cylindrical surface (a circular arc) has the form $y = y_c - \sqrt{R^2 - (x - x_c)^2}$, where (x_C, y_C) and R are the coordinates of the center and the radius of the circle, the arc of which describes the profile of the expected collapse surface. This shows that function y_1 is continuous and continuously differentiable, and function p is continuously piece-wise differentiable. Naturally, for function (2), there is point (x_C, y_C) at which the function has a minimum value [13].

To solve this problem, a method was developed for numerically determining the stability coefficient of a circular-cylindrical slip surface and slope. Using this method, we consider the results of determining the slip surface, the stability coefficient, and stresses arising along the slip surface using numerical calculations [13-14].

3. Numerical results and their analysis

Table 1.

Stability coefficient and slip surface parameters

K	*R, m*	R_x, *m*	R_y, *m*	x_1, *m*	x_2, *m*
1.7457	28.6987	-3.2971	28.7349	0.2	24.04
1.7459	28.6067	-3.5190	28.6139	0.2	23.76
1.7466	28.7945	-3.0784	28.8572	0.2	24.32
1.7475	28.5184	-3.7440	28.4944	0.2	23.48
1.7480	31.2393	-4.8915	31.0716	0.2	24.32
1.7485	31.3584	-4.6800	31.2263	0.2	24.6
1.7486	26.4606	-2.1426	26.6067	0.2	23.48
1.7487	31.1242	-5.1062	30.9186	0.2	24.04
1.7487	28.8938	-2.8626	28.9811	0.2	24.6
1.7489	26.5341	-1.9143	26.6997	0.2	23.76

As is known, the sides of deep quarries have highly inclined slopes and benches, and geological features are expressed by the non-homogeneity of the physical and mechanical parameters of the rock. A stepped slope with benches is taken as the sides of deep quarries. Let us consider a soil slope with three benches (the profile of the slope and benches are shown in Fig. 1). For a homogenous slope with benches, the results are shown in Tables 1-2 and Figures 1-3. A soil massif 20 m high and a general angle of slope $\alpha = 45°$ with the following soil characteristics: density - ρ=2000 kg/m^3 ; specific cohesion $c = 30$ kPa (Table 1, Figure 1) and $c = 40$ kPa (Table 2 and Fig. 2-3); the angle of internal friction $\varphi = 30°$, were taken as the initial data. Diagrams of normal, shear, and retaining stresses along the line of the assumed slip surface are shown in linear size for presentation on graphs by multiplying by $1/\rho g$.

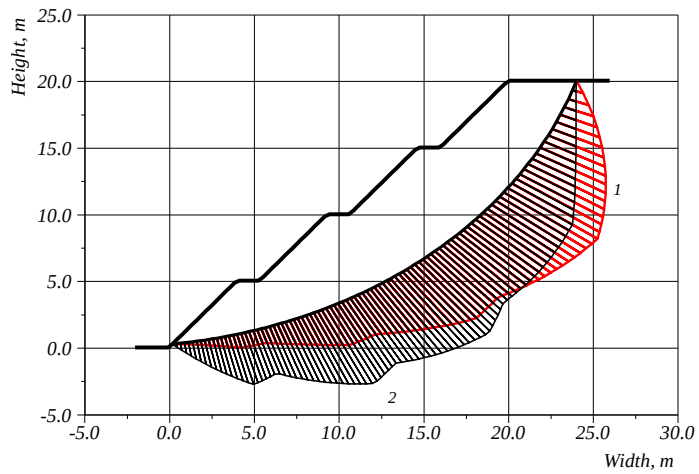

Figure 1. - **Estimated slip surface and diagram of shear (1) and retaining (2) stresses along the surface**

Table 2.

Stability coefficient and slip surface parameters

K	R, m	R_x, m	R_y, m	x_1, m	x_2, m
1.9529	28.9967	-2.6497	29.1063	0.2	24.88
1.9532	28.8938	-2.8626	28.9811	0.2	24.6
1.9538	29.1029	-2.4395	29.2330	0.2	25.16
1.9538	26.6911	-1.4667	26.8890	0.2	24.32
1.9542	26.7744	-1.2471	26.9853	0.2	24.6
1.9547	28.7945	-3.0784	28.8572	0.2	24.32
1.9547	26.6109	-1.6891	26.7938	0.2	24.04
1.9557	29.2125	-2.2320	29.3611	0.2	25.44
1.9558	26.8609	-1.0303	27.0827	0.2	24.88
1.9566	25.3713	0.0837	25.3708	-0.08	24.88

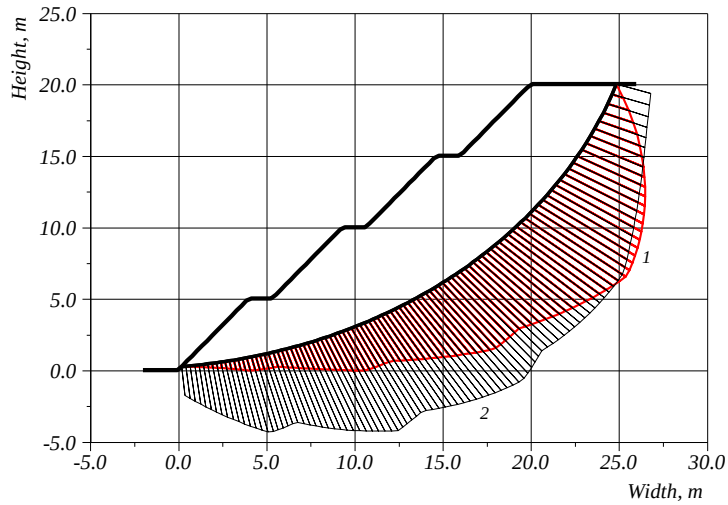

Figure 2. - **Estimated slip surface and diagram of shear (1) and retaining (2) stresses along the surface**

From a comparison of the results with previous calculations, it can be seen that the stability coefficient for a slope with benches (K=1.7457) is 27% higher than the stability coefficient of a homogeneous slope without benches (K=1.3654). The increase in the cohesion value of a homogeneous slope with benches c= 40 kPa exceeds the stability coefficient up to K = 1.9529 (Table 2), which is 12% higher than for c = 30 kPa, i.e. a 33% increase in cohesion leads to an increase in the strength margin factor by 12%. As seen in Figure 2 at an increase in soil cohesion, the retaining forces in almost all areas of the slip surface exceed the shear forces.

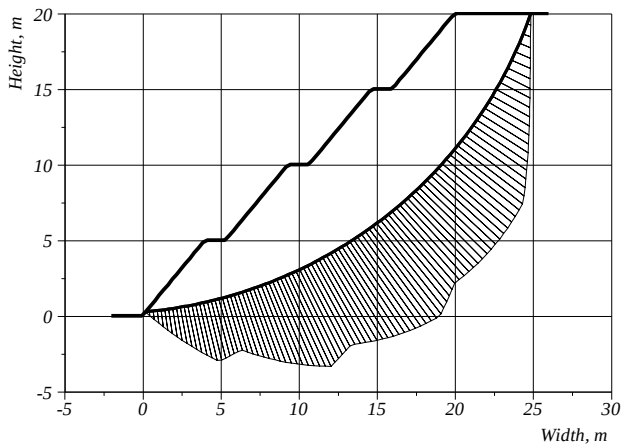

Figure 3. - **Diagram of normal stresses along the assumed slip surface**

Consider a non-homogeneous slope with benches. Let the heterogeneity consist of a uniform layer-by-layer occurrence of soil. We believe that the density and cohesion of soil change with each bench in the direction of increasing depth: the density of the base is 3000 kg/m^3, and then changes in height to 1800 kg/m^3: $y \le 0{,}0$, ρ=3000 kg/m^3, c=300 Pa, 0 < y ≤ 5m, ρ=2600kg/m^3, c = 3000 Pa; $5\,\text{м} < y \le 10\,\text{м}$, 5m < y ≤ 10m, ρ=2300 kg/m^3, c = 25000 Pa; 10m < y ≤ 15m, $\rho = 2000$ кг/м^3 ρ=2000 kg/m^3, c = 25000 Pa; and 15m < y ≤ 20m, ρ=1800 kg/m^3, $c = 15000$ Па c = 1500 Pa; for all values of x. The results of these calculations are presented in Table 3; diagrams of retaining and shear stresses along the assumed slip surface are shown in Figure 4. Here the stability coefficient is K=1.5824 and its value decreases by 23% compared to a homogeneous slope with benches.

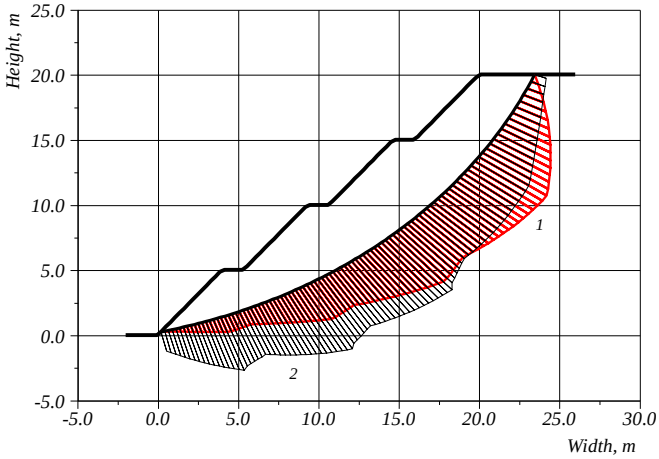

Figure 4. - **Diagrams of retaining and shear stresses along the assumed slip surface**

Table 3.

Stability coefficient and slip surface parameters

K	R, m	R_x, m	R_y, m	x_1, m	x_2, m
1.6421	26.5341	-1.9143	26.6997	0.2	23.76
1.6424	28.6987	-3.2971	28.7349	0.2	24.04
1.6426	26.4606	-2.1426	26.6067	0.2	23.48
1.6427	28.7945	-3.0784	28.8572	0.2	24.32
1.6429	26.6109	-1.6891	26.7938	0.2	24.04
1.6433	28.6067	-3.5190	28.6139	0.2	23.76
1.6442	28.8938	-2.8626	28.9811	0.2	24.6
1.6445	26.3907	-2.3739	26.5149	0.2	23.2
1.6448	26.6911	-1.4667	26.8890	0.2	24.32
1.6456	28.5184	-3.7440	28.4944	0.2	23.48

4. Conclusion

By using the method of circular cylindrical slip surfaces, the possibility of assessing the stability and parameters of the proposed slip surface for a homogeneous and non-homogeneous stepped slope with benches corresponding to the sides of deep quarries is shown. The values of the stability coefficients and parameters of the ten most probable slip surfaces are presented in a tabular form. The distributions of normal, shear, and retaining stresses along the most probable slip surface are presented as graphs. The ratio of the areas of the diagrams of retaining and shear stresses corresponds to the value of the stability coefficient.

References

1. *Huang Y.H.* Slope Stability Analysis by the Limit Equilibrium Method // American Society of Civil Engineers, (Reston, VA 2014), pp. 1-365. https://doi.org/10.1061/9780784412886.
2. *Terzaghi K.* Theoretical Soil Mechanics. / « John Wiley & Sons. Inc. Printed» USA, 2001, 526 p.
3. *Sultanov K.* Contact interaction of an underground pipeline with soil under dynamic impacts // Facta Universitatis, Series: Mechanical Engineering, 2024. <http://casopisi.junis.ni.ac.rs/index.php/FUMechEng/article/view/12383>.
4. *Fomenko I.K., Pendin V.V., Gorobtsov D.N.* Assessment of the stability of quarry sides on rocky soils // Mining Sciences and Technologies. 2016, no. 3, pp. 10-19. https://doi.org/10.17073/2500-0632-2016-3-10-19.
5. *Zerkal O.V., Fomenko I.K.* Landslides in rocky soils and assessment of their stability // Engineering Geology. 2016, No. 4, pp. 4-21.
6. *Pendin V.V., Fomenko I.K.* Methodology for assessing and forecasting landslide hazard / «LENAD» Moscow, 2015, 320 p.
7. *Vanapalli S.K., Fredlund D.G., Pufahl D.E., Clifton A.W.* Model for the prediction of shear strength with respect to soil suction // Canadian Geotechnical Journal, 1996. Vol. 33. pp. 379–392.
8. *Genuchten M.T.* A closed form equation for predicting the hydraulic conductivity of unsaturated soils // Soil Science Society of America Journal, 1980, Vol. 44, pp. 892–898.
9. *Duncan J.M.* Factors of safety and reliability in geotechnical engineering // Journal of Geotechnical & Geoenvironmental Engineering. 2000. pp. 307–316.
10. *Morgenstern N.R., Price V.E.* The analysis of the stability of general-slip surface // Geotechnique. 1965. Vol. 15. No. 1. pp. 70–93.
11. *Barton N.R., Bandis S.* Review of predictive capabilities of JRC-JCS model in engineering practice // Rock joints: Proc. Int. Symp. on Rock Joints, 1990. – pp. 603-610.
12. *Zhang Z., Chang C., Zhao Z.* Influence of the Slope Shape on Seismic Stability of a Slope // Adv. Civ. Eng, 2020, pp. 1-8, https://doi.org/10.1155/2020/8827072
13. *Khusanov B., Normatov Sh., Khaydarova O.* On one method for assessing the soil slopes stability, In: Proceedings of the International Conference on Actual Problems of Applied Mechanics - APAM-2021, 2637, 030012-1–030012-10.
14. *Sultanov K., Umarkhonov S., Normatov Sh.* Calculation of earth dam strain under seismic impacts , In: Proceedings of the International Conference on Actual Problems of Applied Mechanics - APAM-2021, 2637, 030008-1-030008-7.
15. *Zerkal' O.V., Fomenko I. K.* Ocenka vlijanija anizotropii svojstv gruntov na ustojchivost' sklonov [Assessment of the anisotropy of the properties of the soil on the slope stability] // Engineering survey, 2013, No. 9, pp. 44-50.
16. *Markland J.T.* A useful technique for estimating the stability of rock slopes when the rigid wedge sliding type of failure is expected // Imperial College Rock Mechanics Research Report, 1972, No. 19, pp.10.
17. *Chanda N.* Seismic stability analysis of slope assuming log-spiral rupture surface using modified pseudo-dynamic method // Int. J. Geotech. Eng, 2021, Vol.15, pp. 160–170, https://doi.org/10.1080/19386362.2018.1529281
18. *Nalgire T., Dahale P.P., Mehta A.A., Hiwase P.D.* Slope Stability Analysis by GeoSlope, 2020, HELIX. 10, pp 71–75, https://doi.org/10.29042/2020-10-1-71-75.
19. *Lekhanova K.V., Novodzinskiy A.L.* Sravnenie chislennyh i analiticheskih metodov rascheta ustoychivosti gruntovyh otkosov [Comparison of numerical and analytical methods for calculating the stability of soil slopes] // Vestnik PNIPU. Construction and Geotechnics, 2011, No. 1, pp.45-50.
20. *Malinin A.G., Malinin P.A., Chernopazov S.A., Gladkov I.L., Vorob'ev A.V.* Computer programs for geotechnical analyses // Soil Mech. Found. Eng, 2008, No. 45, pp.13–16, https://doi.org/10.1007/s11204-008-0003-z.

NATURAL VIBRATIONS OF CYLINDER AND SPHERICAL SHELL IN ELASTIC MEDIUM

Safarov I.I.[1], Mirzakabilov B.N.[1]
[1]*Tashkent Institute of Chemical Technology, Tashkent, Uzbekistan*
E-mail: safarov54@mail.ru, bmirzakabilov@inbox.ru

Abstract: *An experimental verification of part-homogeneous plane cylinder and spherical sheel connected with boundless media are considered in the paper. Let us consider the natural vibrations of a piecewise homogeneous plane, cylindrical and spherical sheel associated with an infinite medium. The first papers on the vibration of thin, elastic, spherical shells precede the general formulation of the classical bending theory of shells. After simple transformations, a system of differential equations with complex coefficients is obtained, which is further solved using the method of straight lines, which will allow using the software tool of the orthogonal sweep Muller method.*

Keywords: *shells, waves, frequency, viscosity coefficient, oscillation, vibrations.*

1. Introduction

This work examines the vibrations of cylindrical shells in a deformable medium [1,2]. In the case of sufficiently extended underground structures and the impact directed perpendicular to their longitudinal axis, the medium and lining are reduced to a plane problem of the dynamic theory of elasticity (or viscoelasticity). Under the assumption of a generalized plane deformed state, the equation of motion in mixtures has the form [3,4,5]. From a physical point of view, damping in an ideal elastic medium is explained by the radiation of energy excited by natural oscillations due to diverging elastic waves. The behavior of complex natural frequencies depending on the geometric and physical-mechanical parameters of the system has been studied. The medium of cylindrical and spherical shells is considered as elastic, viscoelastic and multicomponent. The multiple results obtained are compared on a computer. A piecewise homogeneous mechanical system is considered as dissipatively homogeneous and inhomogeneous. An ideal elastic body has no losses [6,7,8,9]. Apart from round cylindrical shells, other types of shells such as conical, spherical, elliptical, parabolic and hyperbolic shells are also commonly used in civil, mechanical, aeronautical and marine applications. Radial vibrations of an elastic isotropic hollow sphere are considered, as well as other limiting cases for the first mode of vibrations of a thin spherical shell. Also, curve was plotted for the dependence of the frequency parameter on the ratio of the thickness of the sphere to its radius. The results obtained and their comparison with the results of other authors are presented [10].

2. Materials, methods and object of study

In this work we will limit ourselves to considering the unsteady motions of spherical bodies immersed in a viscoelastic medium under the action of unsteady waves. The relationship between stresses and strains satisfies the hereditary Boltzmann-Volter integral. The main integro-differential equations are obtained on the basis of the principle of possible displacements and differential formulation. During the research, the following methods were used: the method of separation of variables, the freezing method, the Muller method, the Godunov orthogonal sweep method and the methods of equations of mathematical physics. Using the integral Laplace transform, an exact solution of the equations of motion in images is obtained. The integrand in images satisfies Jordan's lemma.

3. Formulation of the problem

Natural vibrations of a composite rod. Let us consider the natural vibrations of a composite rod, with elastic boundary conditions at the left and viscoelastic boundary conditions at the right end.

The equation of free vibrations of a rod of constant cross-section has the form

$$EF\frac{\partial^2 u}{\partial x^2}-\rho\frac{\partial^2 u}{\partial t^2}=0, \tag{1}$$

where $E-$ modulus of elasticity of the rod material; $F-$cross-sectional area, $\rho-$ density of the rod material.

Solution (1) is sought in the form

$$u(x,t) = U(x)\cdot e^{-i\omega t}, \tag{2}$$

where $\omega -$ circular frequency.

To determine $U(x)$ from equation (1) we obtain a system of algebraic equations:

$$\begin{cases} U'' + \dfrac{\omega^2}{c_{p1}^2} U = 0, \text{ at } 0 < x < x_1, \\ U'' + \dfrac{\omega^2}{c_{p2}^2} U = 0, \text{ at } x_1 < x < x_2, \end{cases} \tag{3}$$

where

$$C_{pk} = [(\lambda_k + 2\mu_k)/\rho_k]^{1/2}, \qquad k = 1, 2.$$

System (3) is solved under the following boundary conditions:

$$\begin{aligned} &a\cdot U(0) - b\cdot U'(0) = 0, && U(x_1 - 0) = U(x_1 + 0), \\ &E_1\cdot U'(x_1 - 0) = E_2\cdot U'(x_1 + 0), && E_2\cdot U'(x_2) - i\cdot\omega\cdot\mu\cdot U(x_2) = 0, \end{aligned} \tag{4}$$

where $\mu -$ damper viscosity coefficient.

We write solution (3) in the form

$$U(x) = \begin{cases} C_1\cdot\exp(i\omega x/c_{p1}) + C_2\cdot\exp(-i\omega x/c_{p1}) \text{ at } 0 < x < x_1, \\ C_1'\cdot\exp(i\omega x/c_{p2}) + C_2'\cdot\exp(-i\omega x/c_{p2}) \text{ at } x_1 < x < x_2, \end{cases} \tag{5}$$

Substituting (5) and (4), we obtain a system of homogeneous algebraic equations for the unknowns C_1, C_2, C_1', C_2':

$$\begin{bmatrix} a - b\cdot i\cdot\dfrac{\omega}{c_{p1}} & a + b\cdot i\cdot\dfrac{\omega}{c_{p1}} & 0 & 0 \\ e^{i\cdot\frac{\omega}{c_{p1}}\cdot x_1} & e^{i\cdot\frac{\omega}{c_{p1}}\cdot x_1} & -e^{i\cdot\frac{\omega}{c_{p2}}\cdot x_2} & e^{-i\cdot\frac{\omega}{c_{p2}}\cdot x_2} \\ \dfrac{E_1}{c_{p1}}\cdot e^{i\cdot\frac{\omega}{c_{p1}}\cdot x_1} & -\dfrac{E_1}{c_{p1}}\cdot e^{-i\cdot\frac{\omega}{c_{p1}}\cdot x_1} & -\dfrac{E_2}{c_{p2}}\cdot e^{i\cdot\frac{\omega}{c_{p2}}\cdot x_2} & \dfrac{E_2}{c_{p2}}\cdot e^{-i\cdot\frac{\omega}{c_{p2}}\cdot x_2} \\ 0 & 0 & \left(\dfrac{E_2}{c_{p2}} - \mu\right)\cdot e^{i\cdot\frac{\omega}{c_{p2}}\cdot x_2} & -\left(\dfrac{E_2}{c_{p2}} + \mu\right)\cdot e^{-i\cdot\frac{\omega}{c_{p2}}\cdot x_2} \end{bmatrix} \times \begin{bmatrix} C_1 \\ C_2 \\ C_1' \\ C_2' \end{bmatrix} = 0 \tag{6}$$

Based on this condition, after some transformations we obtain

$$\left(a + b\cdot i\cdot\frac{\omega}{c_{p1}}\right)\cdot\left\{\frac{E_1}{c_{p1}}\left[1 + \beta_1\cdot e^{-2i\cdot\frac{\omega}{c_{p2}}\cdot x_1}\cdot e^{2i\cdot\frac{\omega}{c_{p2}}\cdot x_2}\right] - \frac{E_2}{c_{p2}}\left[1 - \beta_1\cdot e^{-2i\cdot\frac{\omega}{c_{p2}}\cdot x_1}\times e^{2i\cdot\frac{\omega}{c_{p2}}\cdot x_2}\right]\right\}\cdot e^{2i\cdot\frac{\omega}{c_{p1}}\cdot x_1} +$$

$$+\left(a - b\cdot i\cdot\frac{\omega}{c_{p1}}\right)\cdot\left\{\frac{E_2}{c_{p2}}\left[1 - \beta_1\cdot e^{-2i\cdot\frac{\omega}{c_{p2}}\cdot x_1}\cdot e^{2i\cdot\frac{\omega}{c_{p2}}\cdot x_2}\right] + \frac{E_1}{c_{p1}}\left[1 + \beta_1\cdot e^{-2i\cdot\frac{\omega}{c_{p2}}\cdot x_1}\cdot e^{2i\cdot\frac{\omega}{c_{p2}}\cdot x_2}\right]\right\} = 0, \tag{7}$$

where

$$\beta_1 = \left[E_2/C_{p2} - \mu\right]/\left[E_2/C_{p2} + \mu\right]. \tag{8}$$

Now we select the viscosity coefficient μ. To do this, we use the surface discontinuity condition or radiation conditions [1]

$$\frac{\partial u(x_2,t)}{\partial x}+\frac{1}{C_{p2}}\frac{\partial u(x_2,t)}{\partial t}=0 \quad \text{or} \quad U'(x_2)=i\omega\frac{1}{C_{p2}}U(x_2).$$

On the other hand, from the boundary conditions (4) we obtain

$$U'(x_2)=i\omega\frac{\mu}{E_2}U(x_2).$$

By equating the last two equalities, we can determine the coefficient viscosity μ in the form

$$\mu=E_2/C_{p2}. \tag{9}$$

With this choice of the viscosity coefficient μ, it follows from relation (8) that $\beta_1=0$ and the frequency equation (7) do not depend on the distance x_2, i.e.

$$\left(a+b\cdot i\cdot\frac{\omega}{C_{p1}}\right)\cdot\left(\frac{E_1}{C_{p1}}-\frac{E_2}{C_{p2}}\right)\cdot e^{2i\cdot\frac{\omega}{c_{p1}}\cdot x_1}+\left(a-b\cdot i\cdot\frac{\omega}{C_{p1}}\right)\cdot\left(\frac{E_2}{C_{p2}}+\frac{E_1}{C_{p1}}\right)=0 \tag{10}$$

If the left end of the composite rod is stationary, then $b=0$.
The spectrum of eigenvalues is determined by formula

$$\omega=\frac{C_{p1}}{2ix_1}\cdot\ln\frac{E_1\cdot C_{p2}+E_2\cdot C_{p1}}{E_2\cdot C_{p1}-E_1\cdot C_{p2}}, \tag{11}$$

where under the logarithm is a complex infinite-valued function.
There are no natural frequencies at $E_2\cdot C_{p1}=E_1\cdot C_{p2}$.

Taking into account the above, the eigenvalues take the following form:

$$\omega_k=\begin{cases} C_{p1}k\pi/x_1-\left(iC_{p1}/2x_1\right)\cdot\ln\left[\dfrac{E_1\cdot C_{p2}+E_2\cdot C_{p1}}{E_2\cdot C_{p1}-E_1\cdot C_{p2}}\right], & \text{at } E_2\cdot C_{p1}>E_1\cdot C_{p2}, \\ C_{p1}(2k+1)\pi/2x_1-\left(iC_{p1}/2x_1\right)\cdot\ln\left[\dfrac{E_1\cdot C_{p2}+E_2\cdot C_{p1}}{E_2\cdot C_{p1}-E_1\cdot C_{p2}}\right], & \text{at } E_2\cdot C_{p1}<E_1\cdot C_{p2}, \end{cases} \tag{12}$$

where by logarithm we mean the main real branch. The real parts of eigenvalues ω_k have the meaning of natural frequencies. At $E_2\cdot C_{p1}>E_1\cdot C_{p2}$ they coincide exactly with the natural frequencies of the left part of the rod $[0,\ x_1]$ with a fixed right end, a at $E_2\cdot C_{p1}<E_1\cdot C_{p2}$ the real parts of (13) coincide with the natural frequencies of the left part of the rod $[0,\ x_1]$ with a free right end.

Antiplane oscillations of a cylinder immersed in an infinite medium. It can be shown that for $R>>1$ the problem under consideration is equivalent to the problem of natural vibrations of a two-layer cylinder shown in the the following equations of motion and boundary conditions:

$$\frac{\partial^2 u}{\partial r^2}+\frac{1}{r}\frac{\partial u}{\partial r}-\frac{1}{C_{ph}^2}\frac{\partial^2 u}{\partial t^2}=0, \qquad k=1,2, \tag{13}$$

$$\begin{cases} u=0, \text{ at } r=r_1 \\ u(r-0)=u(r+0),\ \sigma_{rz}(r-0)=\sigma_{rz}(r+0) \text{ at } r=r_2 \\ \sigma_{r2}=\mu_2\dfrac{\partial u}{\partial r}, \text{ at } r=R, \end{cases} \tag{14}$$

where μ_2- is Poisson's ratio.

Now we determine the conditions for the absence of reflection at $r = R$. At $R >> 1$ the diverging wave has the form

$$u(r,t) = \frac{1}{\sqrt{ar}} e^{i\left(ar - \frac{\pi}{4} - \omega t\right)}, \tag{15}$$

since the asymptotics Henkel function $H_0^{(1)}(ar) \cong \sqrt{\frac{2}{\pi ar}} e^{i\left(ar - \frac{\pi}{4}\right)}$, is valid, where $a-$ is the wave number; $\omega-$ natural frequency.

Analytical method for solving the problem of diffraction of harmonic waves on a spherical shell. Particular solutions of these equations are spherical Bessel (or Hankel) functions of the first kind (or Hankel).

From relation (15) we have

$$\frac{\partial u}{\partial r} = \frac{ia}{\sqrt{ar}} e^{i\left(ar - \frac{\pi}{2} - \omega t\right)} - \frac{a}{2(ar)^{3/2}} e^{i\left(ar - \frac{\pi}{4} - \omega t\right)} \quad \text{or} \quad \frac{\partial u}{\partial r} = iau - \frac{1}{2r} u \tag{16}$$

Further,

$$\frac{\partial u}{\partial t} = -\frac{i\omega}{\sqrt{ar}} e^{i\left(ar - \frac{\pi}{4} - \omega t\right)} \quad \text{or} \quad \frac{\partial u}{\partial t} = -i\omega u\,. \tag{17}$$

After some transformations we get

$$\frac{\partial u}{\partial r} = -\frac{a}{\omega}\frac{\partial u}{\partial t} - \frac{1}{2r} u \tag{18}$$

So, the condition for the absence of reflection at $r = R$ has the following form:

$$\left.\frac{\partial u}{\partial r}\right|_{r=R} = \left.\left(-\frac{a}{\omega}\frac{\partial u}{\partial t} - \frac{1}{2R} u\right)\right|_{r=R},$$

$$\left.\sigma_{r2}\right|_{r=R} = -\frac{\mu_2}{C_{p2}}\left.\frac{\partial u}{\partial t}\right|_{r=R} - \left.\frac{\mu_2}{2R} u\right|_{r=R}, \tag{19}$$

Under this condition (19), obtaining the frequency equation does not depend on the radius of radius of the outer cylinder.

When $\mu_2 = 1$ from (19) it immediately follows that

$$\left.\sigma_{r2}\right|_{r=R} = -\frac{1}{C_{p2}}\left.\frac{\partial u}{\partial t}\right|_{r=R} - \left.\frac{1}{2R} u\right|_{r=R}. \tag{20}$$

Radial vibrations of a spherical shell. Radial vibrations of an elastic isotropic hollow sphere are considered, as well as other limiting cases for $C_p >> C_s$, the problem under consideration is equivalent to the problem of natural oscillations of a spherical shell shown in the form of a displacement potential $\psi(r,t)$, satisfying equation

$$\frac{\partial^2 \varphi}{\partial r^2} + \frac{2}{r}\frac{\partial \varphi}{\partial r} - \frac{1}{C_p^2}\frac{\partial^2 \varphi}{\partial t^2} = 0. \tag{21}$$

Solution (21), presented in the form

$$\varphi(r,t) = \left[\frac{A}{r} e^{ia} \cdot p^r + \frac{B}{r} e^{-ia} \cdot p^r\right] \cdot e^{-i\omega t}, \tag{22}$$

satisfies the boundary conditions

$$\left.\sigma_{rr}\right|_{r=a} = 0, \tag{23}$$

$$\left.\frac{\partial\varphi}{\partial r}\right|_{r=b}=\left.\left(-\frac{a_p}{\omega}\frac{\partial\varphi}{\partial t}-\frac{1}{r}\right)\right|_{r=b}, \tag{24}$$

where

$$\sigma_{rr}=-\mu\left[a_t^2\varphi+\frac{4}{r}\frac{\partial\varphi}{\partial r}\right], \quad a_p=\frac{\omega}{C_p},\ a_t=\frac{\omega}{C_s},\ C_p^2=\frac{\lambda+2\mu}{\rho},\ C_s^2=\frac{\mu}{\rho}. \tag{25}$$

Substituting (22) into (24), we obtain that $B=0$.

Then the general solution of equation (21) can be represented in the form

$$\varphi(r,t)=\frac{A}{r}e^{i(a_p r-\omega t)}. \tag{26}$$

Substituting (26) into the boundary condition (23), we have

$$\left(aa_p\frac{C_p}{C_s}\right)^2=4\left(1-ia_p a\right), \tag{27}$$

When $C_p >> C_s$ the problem under consideration is equivalent to the problem of the natural oscillations of a spherical shell. The roots of the characteristic equation

$$\begin{aligned}D_n &= xH_{n-1}\left[\left(n^2-1\right)yH_{n-1}(y)-\left(n^3-n+y^2/2\right)H_n(y)\right]-\\ &-H_n(x)\left[\left(n^3-n+y^2/2\right)yH_{n-1}(y)-\left(n^2+n-y^2/4\right)y^2H_n(y)\right]\end{aligned} \tag{28}$$

where

$x=\omega a\left(\rho/\left(\lambda+2\mu\right)\right)^{1/2}$; $y=\omega a\left(\rho/\mu\right)^{1/2}$, λ and $\mu-$Lame coefficients; $\rho-$density of the material. Equation (28) after certain transformations can be written in the following form:

$$\left(n^2-1\right)F(x)F(y)-\left(y^2/2\right)F(x)+F(y)+n^2-\left(n^2-y^2/2\right)^2=0 \tag{29}$$

where $F(x)=xH_n^1(x)/H_n(x)$, $n=1,2,3,\ldots$, and we are found by the Mueller method. On the basis of these studies, it is revealed that the mechanical system under consideration has a discrete complex natural frequency.

$$\omega=\frac{2C_s}{a}\left(1-i\frac{C_s}{C_p}\right). \tag{30}$$

At $a\to\infty$ a natural frequencies $\omega\to 0$; When $C_p\to\infty$ the natural frequency takes the following form $\omega=\frac{2C_s}{a}$. It is clear from (30) that $\omega=\omega_R+i\omega_I$ where $\omega_R=\frac{2C_s}{a}$; $\omega_I=\frac{C_s}{C_p}<<1$.

The resulting expression (30) completely corresponds to the results of the work of Landau and Lifshitz, which are obtained on the basis of the Somerfield radiation condition. Thus, two problems for an infinite and finite domain are equivalent. This is explained by the fact that at the outer boundary conditions are set for the absence of reflection. There is no reflection because the conditions are satisfied by diverging cylindrical and spherical waves, which in the general case are written in the form

$$LU(R_\infty)=lU(R_\infty) \tag{31}$$

Here L and l linear differential operators, $R_\infty-$border selected area of infinite media, $U-$ vector of displacement. Equation (31) replaces the Somerfield radiation condition. Equations (8), (19), and (24) is a particular case of (31). Equation (31) is the nonreflecting condition of the “Troyanovski - Safarov”.

4. Results

The results obtained show that with increasing elastic modulus, the corresponding natural frequencies of the mechanical system slowly increase: Table 1.

Table 1.

Experimental results data - Comparison of results (v = 0.25

№	Our Results	Pao and Mao [10]	Bnron and Parnes [10]
0	0.43832−0.43310i	0.4373− 0.43138i	0.4373 − 0.4320i
1	1.08381−0.78752i	1.08281− 0.7754i	1.0839 − 0.432i
2	1.808553−0.88791i	1.89853− 0.8989i	1.8987 − 0.898i

Let us consider radial oscillations of a cavity in an unbounded medium, accompanied by the emission of longitudinal sound waves, which leads to a loss of energy and, consequently, to the damping of oscillations.

The numerical solution was carried out on a computer with various parameter ratios $\eta = \rho_1 / \rho_2$, $E = E_1 / E_2$, $\nu_1 = \nu_2 = 0.25$ (Fig. 1).

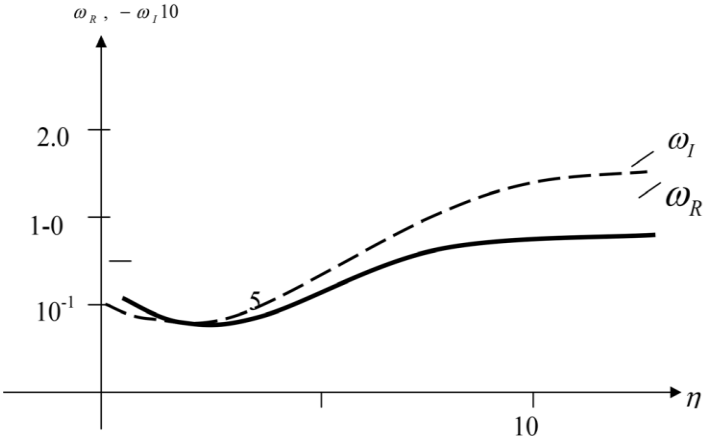

Figure 1. - **Dependence of natural frequencies (ω_R) and deformation coefficients from η to (ω_I)**

5. Analysis of results

It has been established that the kinematic factors: acceleration and velocity of a spherical shell are significantly different from the kinematic factors (acceleration and velocity) of a viscoelastic medium. It was found that under short-term exposure to waves (loads), the picture of the stress-strain state becomes different: at all points of the shell, the maximum values of stress and deformation are significantly higher than the average, and the stress reaches its greatest value at the frontal point.

This section provides an analysis of the results obtained, their interpretation, comparison with the results of other authors, and the reliability of the results obtained.

6. Discussion

The formulation of the problem of investigating energy dissipation in the propagation of waves in an elastic medium with spherical inclusions is proposed. The coefficient of the so-called scattering coefficient is introduced, which expresses the relationship between the energies of the incident and scattered waves in the sphere. Thus, the scattering coefficient is expressed in terms of the characteristics of the incident and scattered waves.

It has been found that taking into account the viscous properties of the material reduces the stress-strain state of the body and the surrounding media by 10–15%, and the frequencies of oscillations of the sphere are closely related to the waves reflected from it. Some differences were also discovered in the nature of the relationship between the displacements of the spherical shell and the surrounding viscoelastic medium as a function of time.

7. Conclusion

The frequency equation is obtained in parametric form and the resulting solutions are analyzed. Examples of the frequency of the first vibration mode of an incompressible material are given. Purely radial vibrations of an elastic isotropic hollow sphere are considered. The frequency equation is derived in a form that allows a very simple solution to be obtained.

8. Acknowledgments

Scientific research aimed at researching the characteristics of wave propagation in visco-elastic shells located in the soil environment is carried out by the world's leading scientific centers and higher education institutions, including the Institute of Mechanics and Seismic Stability of Structures of the Academy of Sciences of the Republic of Uzbekistan, Tashkent Institute of Irrigation and Agricultural Mechanization Engineers, National University of Uzbekistan, Tashkent conducted by Institute of Chemical Technology, Jizzakh Polytechnic Institute, Bukhara Engineering and Technology Institute (Uzbekistan) and others. In their work, propagation of wave diffraction in cylindrical elastic bodies was studied.

References

1. *Safarov I.I.* Oscillations and waves in dissipatively inhomogeneous media and structures. Science, Tashkent, 1992, 250 p.
2. *Horace Lamb MA.* On the vibrations of a spherical shell. Proceedings of the London Mathematical Society, 1882, vol. 14, No. 1, pp. 50-56. https://doi.org/10.1112/plms/s1-14.1.50
3. *Novatsky V.* Theory of elasticity. T.2./ Mir, Moscow, 1975, 872 p.
4. *Guz A.N., Kubenko V.D. Cherevko I.A.* Diffraction of elastic waves / Kiev, Naukova Dumka, 1978, 308 p.
5. *Safarov I.I., Akhmedov M.S., Boltaev Z.I.* Distribution of the Natural Waves of Extended Lamellar Viscoelastic Bodies of Variable Thickness / LAP, Lambert Academic Publishing, Saarbrücken, 2015, 112 p.
6. *Chen WQ, Ding HJ.* Natural frequencies of a fluid-filled anisotropic spherical shell // Journal of the Acoustical Society of America, 1999, vol.105, pp. 174-182. https://doi.org/10.1121/1.424578
7. *F. DiMaggio, R. Rand* Axisymmetric Vibrations of Prolate Spheroidal Shells // J. Acoust. Soc. Am. 1966, vol. 38, pp. 179-186.
8. *Kalnins A.* Effect of Bending on Vibration of Spherical Shells // Journal of Acoustic Society of America, 1964, vol. 36, pp. 74–81.
9. *Lamb H.* On the Vibrations of a Spherical Shell // Procedures of the London Mathematical Society, 1882, vol. 14, pp. 50–56.
10. *Pao Y.H., Mow, C.C.* The Diffraction f Elastic Waves and Dynamic StressConcentrations. 1973, 694 p.

DYNAMIC STRESS-STRAIN STATE OF MULTILAYER CYLINDRICAL SHELL UNDER THE INFLUENCE OF CYLINDRICAL HARMONIC WAVES

Safarov I.I.[1], Teshaev M.Kh[2,3], Rakhmonov B.S.[4], Jalolov F.B.[3]

[1]Tashkent Institute of Chemical Technology, Tashkent, Uzbekistan
[2] Bukhara branch, Institute of Mathematics named after V.I.Romanovskii, Bukhara, Uzbekistan
[3]Bukhara Engineering and Technology Institute, Bukhara, Uzbekistan
[4]Urganch state university, Urganch, Uzbekistan,
4Jizzakh State Pedagogical University named after Abdulla Kadyri, Jizzakh, Uzbekistan,
E-mail: farruhjalolov2@mail.ru

Abstract. *An infinitely long circular multilayer cylinder in a viscoelastic half-space is considered in this paper. The dynamic stress-strain state of the multilayer cylindrical shell under the influence of a cylindrical harmonic wave is investigated. The problem is reduced to the plane problem of elasticity theory. The wave processes of a half-space with a multilayer shell are described by Lame equations with visco-elasticity operator coefficients. The conditions of continuity of stresses and displacements (equality of corresponding stresses and displacements) are fulfilled between the shell and the medium. The Green-Lamb method is applied to solve the Lamé equation. The solutions of the obtained wave equations consist of Bessel and Hankel functions of complex argument. A solution technique and algorithm based on Gauss, Mueller and Laplace methods and the freezing method are developed. Numerical results of the stresses as a function of wavelength, taking into account the distance from the source, are obtained. It is found that the maximum stresses will be contour stresses under the influence of transverse waves and they are 15-20% higher than those under the influence of longitudinal waves.*

Key words: *frequency, wavelength, wave equation, complex argument, harmonic wave.*

1. Introduction

A seismic wave can be divided into a surface wave and a volume wave. The first type of bulk wave is a longitudinal wave (P-wave) whose propagation causes soil particles to move along the line of propagation of the wave. The medium in which this type of wave propagates undergoes compression-extension stresses with a change in its volume. When transverse waves (S-waves) propagate, the particles of the medium are displaced orthogonally to the direction of wave propagation; they are accompanied by a change in the shape of the medium, but the volume is preserved. They are sometimes called distortion waves.

Harmonic waves with different fronts propagate along the surface of an elastic half-space. They can be volume waves or surface waves. Surface waves decay exponentially with depth. These waves are formed as a result of reflection from the boundary of the medium [1-3]. Two main types of surface waves are used in seismology, which differ in the orientation of the plane of polarization: in Rayleigh waves the medium particles move along, and in Love waves - orthogonally to the plane of wave propagation. [4,5]. The Poisson's ratio of materials, which is used in the construction of underground structures, is in the range of 0.20 to 0.49. When Rayleigh wave is approximated as a transverse wave, the error is up to 26% [6,7]. So far, researchers have mainly paid attention to the bulk (longitudinal and transverse) waves. They have hardly investigated the effect of Rayleigh wave on underground structures. The incident waves (seismic wave) are characterized by length, velocity and frequency. In [8,9,10], Rayleigh wave propagation and attenuation were investigated by complex methods. However, to ensure the strength of underground structures, the consideration of Rayleigh waves alone is not sufficient, so together with these waves it is necessary to consider the effects of volume waves.

According to numerous experimental data, as well as theoretical calculations, in the case of a surface or near-surface source, ~60% of the source energy is consumed for the formation of Rayleigh and Love waves [11]. The propagation velocity of surface Rayleigh waves C_R is less than the propagation velocities of P and S waves. Depending on the elastic properties of the soil, the speed of propagation of these waves is different. For example, for rock - 3.5÷5.6 km/s, for clay and sandy soils - 0.7÷1.6 km/s, and for bulk and soil bases - 0.2÷0.5 km/s [12]. Rayleigh waves carry most of the earthquake energy; they cause intense surface vibrations and are the main cause of structural failure. Soil types are characterized by the following ranges of shear velocity of wave: - rocky soil 750 m/s; - hard soil 200-750 m/s; - soft soil 200 m/s [13, 14]. Instrumental measurements are carried out for scientific analysis of seismic vibration processes [15, 16]. Long-term instrumental observations in different seismic zones have established that the patterns of seismic vibrations have a regional character, i.e., ground vibrations are different in different seismic areas.

2. Methods

2.1 Problem Statement

Let a viscoelastic half-space containing a multilayer cylindrical shell be given. A harmonic wave with a cylindrical front is incident on the shell. Along the length of the shell, the incident waves are equally impressed. The longitudinal axes of the cylindrical source and the cylindrical shell are parallel. The problem is reduced to the problem of plane deformed state of visco-elasticity theory. The cylindrical source is characterized by the amplitude φ_0, circular frequency ω (Fig.1). The wave processes of the half-space are described by the Lamé equations. The equations of motion of the shell are also described by equations with operator coefficients.

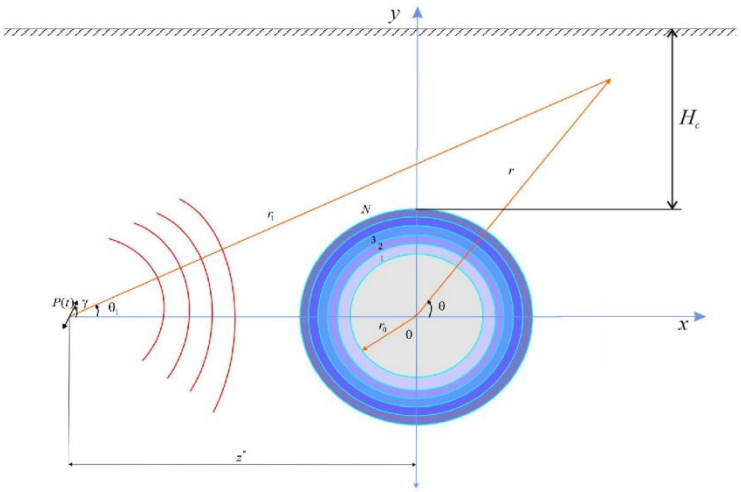

Figure 1. – **Calculation scheme of layered cylindrical shells with fluid in a half-space**

The equation of wave processes assuming a plane deformed state of the half-space takes the following form [17]

$$(\tilde{\lambda}_j + 2\tilde{\mu}_j) grad\, div \vec{u}_j - \tilde{\mu} rot rot \vec{u}_j + \vec{b}_j = \rho_j \frac{\partial^2 \vec{u}_j}{\partial t^2}, \tag{1}$$

where λ_j and μ_j (j = 1,2 ...N, -relate to the environment, $j = 1, 2...., N-1$ - to the layer) are operator modulus of elasticity [18]

$$\tilde{\lambda}_j f(t) = \lambda_{0j} \left[f(t) - \int_{-\infty}^{t} R_{\lambda}^{(i)}(t-\tau) f(\tau) d\tau \right]$$
$$\tilde{\mu}_j f(t) = \mu_{0j} \left[f(t) - \int_{-\infty}^{t} R_{\mu}^{(i)}(t-\tau) f(\tau) d\tau \right]; \tag{2}$$

$\vec{b}_j$ - is the vector of volume force density; $f(t)$ - some function; ρ_j - density, $R_{\mu}^{(i)}(t-\tau)$ and $R_{\lambda}^{(i)}(t-\tau)$ - relaxation kernels, λ_{oj}, μ_{oj} - instantaneous elastic moduli, $\vec{u}_j(u_{rj}, u_{\theta j})$ - components of the displacement vector, which are functions of coordinates and time t. The state of an ideal fluid at pressures up to 100 *MPa* satisfies the wave equation for velocity potentials [2]

$$\Delta \phi_0 = \frac{1}{C_o^2} \frac{\partial^2 \phi_0}{\partial t^2} \tag{3}$$

where $\Delta = \frac{d^2}{dr^2} + \frac{d}{rdr} + \frac{d^2}{r^2 d\theta^2}$; C_o - is the acoustic speed of sound in the liquid. The potential φ_0 and the fluid velocity vector $\vec{V}$ are related by the relation $\vec{V} = grad\phi_0$. The pressure of the liquid at $r = R_0$ the contact with the shell satisfies the Cauchy-Lagrange relation. $P = -\rho_o C_0 \frac{\partial \varphi_0}{\partial t}$, ρ_o - is the density of the liquid.

The cylindrical cloud is filled with an liquid, so at $r = R_0$ should be equal to velocity

$$\left. \frac{\partial \phi_0}{\partial r} \right|_{r=R_0} = \left. \frac{\partial u_{r1}}{\partial t} \right|_{r=R_0} \tag{4}$$

where u_{r1} - displacements of the layer along the normal.

At the interface of two bodies $r = R_j$ the conditions of ideal contact, i.e., the equality of displacements and stresses, are fulfilled:

$$u_{rj} = u_{r(j+1)};\ \sigma_{rrj} = \sigma_{rr(j+1)}\ \ u_{\theta j} = u_{\theta(j+1)};\ \sigma_{r\theta j} = \sigma_{r\theta(j+1)} \tag{5}$$

If sliding exists on the contact surfaces of the shell and the ground, then the following conditions are fulfilled in equality (5) [18]: $\sigma_{r\theta j} = 0$, where, $\sigma_{nn}^{(j)}$ and $\sigma_{ns_1}^{(j)}$ - radial and tangential stresses, $u_n^{(j)}$ and $u_{s_1}^{(j)}$ - radial and tangential displacements. On the free surface the conditions of freedom from stresses are put: $\sigma_{yy} = 0; \sigma_{xy} = 0.$ Also the conditions of limitation of displacements and stresses are put for $r \to 0$ [19].

The displacement potentials of the external medium (1) satisfy in infinity $r \to \infty$ the Somerfield radiation conditions [19]:

$$\lim_{r\to\infty} \varphi_N = 0, \quad \lim_{r\to\infty} (\sqrt{r})^{\kappa} \left(\frac{\partial \varphi_N}{\partial r} + i\alpha_N \varphi_N \right) = 0,$$

$$\lim_{r\to\infty} \psi_N = 0, \quad \lim_{r\to\infty} (\sqrt{r})^{\kappa} \left(\frac{\partial \psi_N}{\partial r} + i\beta_N\ \psi_N \right) = 0. \tag{6}$$

We assume that there is a source of harmonic longitudinal waves of a cylindrical front in a viscoelastic half-space, which is applied at the point $\overline{O}$ (Fig.1).

The displacement potential of the incident wave has the form [19]

$$\varphi_N^P = \varphi_{NO} i\pi H_o^{(1)}(\alpha_N \bar{r})\, e^{-i\omega t} \tag{7}$$

where $H_o^{(1)}$ represents the divergent Hankel functions; φ_{NO} - amplitude of the expansion wave; α_N - compression wave number; $\alpha_N^2 = \omega^2/c^2_\alpha$, ω - circular frequency.

2.1 Solution Methods

Let's represent the displacements through the sum of potentials:

$$\vec{u}_j = grad\ \varphi_j + rot\vec{\psi}_j, \quad (j = 1,2,.....,N),$$

where φ_j - longitudinal wave potential; $\vec{\psi}_j\ (\psi_{rj}, \psi_{\theta j})$ - transverse wave potential.

Then equations (1) are reduced to the equation

$$\left(\lambda_{oj} + 2\mu_{oj}\right)\nabla^2\varphi_j - \lambda_{oj}\int_{-\infty}^{t} R_\lambda^{(j)}(t-\tau)\nabla^2\varphi_j d\tau - 2\mu_{oj}\int_{-\infty}^{t} R_\mu^{(j)}(t-\tau)\nabla^2\varphi_j d\tau = \rho_j \frac{\partial^2\varphi_j}{\partial t^2}$$

$$\mu_{oj}\nabla^2\vec{\psi}_j - \mu_{oj}\int_{-\infty}^{t} R_\mu^{(j)}(t-\tau)\nabla^2\vec{\psi}_j d\tau = \rho_j \frac{\partial^2\vec{\psi}_j}{\partial t^2} \tag{8}$$

where $\nabla^2 = \frac{\partial^2}{\partial r^2} + \frac{1}{r}\frac{\partial}{\partial r} + \frac{1}{r^2} + \frac{\partial^2}{\partial \theta^2}$ - is the differential operator in cylindrical coordinates, ν_j - is the Poisson's coefficient.

At infinity $r \to \infty$, the longitudinal and transverse wave potentials at $j = N$ satisfy the Sommerfeld radiation condition (6).

The solution of equation (8) can be sought in the form:

$$\varphi_j(r,\theta,t) = \sum_{k=1}^{\infty} q_{kj}^{(\varphi)}(r,\theta)e^{-i\omega t};\ \ \psi_j\ (r,\theta,t) = \sum_{k=1}^{\infty} q_{kj}^{(\psi)}(r,\theta)e^{-i\omega t}, \tag{9}$$

where $q_{kj}^{(\varphi)}(r,\theta)$ and $q_{kj}^{(\psi)}(r,\theta)$ are complex functions, which are solutions of the following equations:

$$\nabla^2 q_{kj}^{(\varphi)}(r,\theta) + \alpha_j^2 q_{kj}^{(\varphi)} = 0, \quad \nabla^2 q_{kj}^{(\psi)}(r,\theta) + \beta_j^2 q_{kj}^{(\psi)} = 0,$$

$$\nabla^2 q_{k0}^{(\varphi)}(r,\theta)+\alpha_0^2 q_{k0}^{(\varphi)}=0,\ j=1,2,.....N \tag{10}$$

where $\alpha_j^2=\dfrac{\rho\omega^2}{\lambda_{oj}\left(1-\bar{\lambda}_{oj}\right)+2\mu_{oj}\left(1-\bar{\mu}_{oj}\right)}$, $\beta_j^2=\dfrac{\rho\omega^2}{\mu_{oj}\left(1-\bar{\mu}_{oj}\right)}$, $\alpha_0^2=\dfrac{\omega^2}{C_0{}^2}$,

$\bar{\lambda}_{oj}=a_{\lambda j}(\omega)+ib_{\lambda j}(\omega)$, $\bar{\mu}_{oj}=a_{\lambda\mu}(\omega)+ib_{\mu j}(\omega)$,

$a_{\lambda j}(\omega)=\int_0^\infty R_{\lambda j}(\tau)\sin\omega\tau\, d\tau$, $b_{\lambda j}(\omega)=\int_0^\infty R_{\mu j}(\tau)\cos\omega\tau\, d\tau$.

The solution of equation (8) taking into account (10) is expressed through Hankel functions of the 1-st and 2-nd kind of *n*-th order:

$$\varphi_j=\sum_{n=0}^{\infty}\left[A_{nj}H_n^{(1)}(\alpha_j r)+A'_{nj}H_n^{(2)}(\alpha_j r)\right]\cos n\theta e^{-i\omega t};$$

$$\psi_j=\sum_{n=0}^{\infty}\left[B_{nj}H_n^{(1)}(\beta_j r)+B'_{nj}H_n^{(2)}(\beta_j r)\right]\sin n\theta e^{-i\omega t};\ j=1,2,.....N\text{-}1$$

$$\varphi_N=\sum_{n=0}^{\infty}\left[C_{nN}H_n^{(1)}(\alpha_N r)+D_{nN}H_n^{(2)}(\alpha_N r)\right]\cos n\theta e^{-i\omega t}$$

$$\psi_N=\sum_{n=0}^{\infty}\left[M_{nN}H_n^{(1)}(\beta_N r)+L_{nN}H_n^{(2)}(\beta_N r)\right]\sin n\theta e^{-i\omega t} \tag{11}$$

$$\varphi_0=\sum_{n=0}^{\infty}\left[K_{n0}J_n(\alpha_0 r)+K'_{n0}N_n(\alpha_0 r)\right]\cos n\theta e^{-i\omega t},$$

where $A_{nj},A'_{nj},B_{nj},B'_{nj},C_{nj},D_{nj},L_{nN},A_{nj},A'_{nj},B_{nj},B'_{nj},C_{nj},D_{nj},L_{nN}$ - unknown constants determined from boundary conditions; K_{nN} and K'_{nN} - Hankel functions: $H_n^{(1),(2)}(\alpha r)=J_n(\alpha r)\pm iN_n(\alpha r)$.

The solution (11) for $j=N$ satisfies at infinity r→∞ the Sommerfeld radiation condition (6) and is represented in the form:

$$\varphi_N=\sum^{\infty}C_{nN}H_n^{(1)}(\alpha_N r)\cos(m\theta)e^{-i\omega t};\psi_N=\sum^{\infty}M_{nN}H_n{}^{(1)}(\beta_N r)\sin(n\theta)e^{-i\omega t}.$$

The solution of the problem (8) at $r\to 0$ satisfies the power-law constraint condition [20] and hence it follows that $K'_n=0$, then

$$\varphi_0=\sum_{n=0}^{\infty}K_{n0}J_n(\alpha_0 r)\cos n\theta e^{-i\omega t}$$

The total potential can be determined by superimposing the incident and reflected wave potentials. Thus, the displacement potentials are

$$\phi_N=\sum_{k=0}^{K_1}\varphi_0^{(k)}+\varphi_N,\ \Psi_N=\psi_N,\ \phi_j=\varphi_j,\quad \Psi_j=\psi_j,\quad \phi_0=\varphi_0 \tag{12}$$

where K_1 -is the number of reflected waves, and at *k=0* the reflection from the free surface is not taken into account.

Using the construction in Fig. 1 and passing from $\bar{r},\bar{\theta}$ to coordinates r,θ in the area $r\le r_N$, we obtain

$$\varphi_N^{(p)}=\varphi_0 i\pi\ \sum_{n=1}^{\infty}[(-1)^n E_n J_n(\alpha_N r)H_n^{(1)}(\alpha_N z)]\cos n\theta\, e^{-i\omega t},$$

where $E_n=\begin{cases}1, & n=0\\ 2, & n\ge 1\end{cases}$, J_n - is the Bessel function.

The parametric forms of the Green-Lamb transform take the following form [20],

$$u_{rj} = \frac{\partial \phi_j}{\partial r} + \frac{1}{r}\frac{\partial \psi_j}{\partial \theta}; \quad u_{\theta j} = \frac{1}{r}\frac{\partial \phi_j}{\partial \theta} - \frac{\partial \psi_j}{\partial r},$$

$$\sigma_{rrj} = \bar{\lambda}_j \nabla^2 \phi_j + 2\bar{\mu}_j \left[\frac{\partial^2 \phi_j}{\partial r^2} + \frac{\partial}{\partial r}\left(\frac{1}{r}\frac{\partial \psi_j}{\partial \theta} \right) \right];$$

$$\sigma_{\theta\theta j} = \bar{\lambda}_j \nabla^2 \phi_j + 2\bar{\mu}_j \left[\frac{1}{r}\left(\frac{\partial \phi_j}{\partial r} + \frac{1}{r}\frac{\partial^2 \phi_j}{\partial \theta^2}\right) + \frac{1}{r}\left(\frac{1}{r}\frac{\partial \psi_j}{\partial \theta} - \frac{\partial^2 \psi_j}{\partial r \partial \theta}\right) \right];$$

$$\sigma_{r\theta j} = \bar{\mu}_j \left\{ 2\left[\frac{1}{r}\frac{\partial^2 \phi_j}{\partial \theta \partial r} - \frac{1}{r^2}\frac{\partial \phi_j}{\partial \theta} \right] + \left[\frac{1}{r^2}\frac{\partial^2 \psi_j}{\partial \theta^2} - r\frac{\partial}{\partial r}\left(\frac{1}{r}\frac{\partial \psi_j}{\partial r} \right), \right. \tag{13}$$

where $\bar{\lambda}, \bar{\mu}_j$ – are complex moduli of elasticity [21].

The displacements and stresses are obtained for the case of compression waves ψ falling on the layer.

After substituting (12) into (13), taking into account (10), we obtain the following expressions for displacements and stresses:

$$u_{rN} = r^{-1}\sum_{n=0}^{\infty}\left[\varphi_0 E_n i^n E_{51}^{(1N)}(\alpha_N r) + C_{nN} E_{51}^{(3N)}(\alpha_N r) + M_{nN} E_{52}^{(3N)}(\beta_N r)\right]\cos n\theta e^{i\omega t}$$

$$u_{\theta N} = r^{-1}\sum_{n=0}^{\infty}\left[\varphi_0 E_n i^n E_{61}^{(1N)}(\alpha_N r) + C_{nN} E_{61}^{(3N)}(\alpha_N r) + M_{nN} E_{62}^{(3N)}(\beta_N r)\right]\cos n\theta e^{-i\omega t}$$

$$u_{rj} = r^{-1}\sum_{n=0}^{\infty}\left[A_{nj} E_{51}^{(3j)}(\alpha_j r) + A_{nj}^1 E_{61}^{(4j)}(\alpha_j r) + B_{nj} E_{52}^{(3j)}(\beta_j r) + B_n^1\ E_{52}^{(4j)}\right]\cos n\theta e^{-i\omega t}$$

$$u_{\theta j} = r^{-1}\sum_{n=0}^{\infty}\left[A_{nj} E_{61}^{(3j)}(\alpha_j r) + A_{nj}^1 E_{61}^{(4j)}(\alpha_j r) + B_{nj} E_{62}^{(3j)}(\beta_j r) + B_{nj}^1 E_{62}^{(4j)}(\beta_j r)\right]\sin n\theta\, e^{-i\omega t} \tag{14}$$

$$\sigma_{rrN} = 2\mu_{0N}(1 - M_{kN}) r^{-2}\sum_{n=0}^{\infty}\left[\varphi_0 E_n i^n E_{11}^{(1N)}(\alpha_N r) + C_{nN} E_{11}^{(3N)}(\alpha_N r) + M_{nN} E_{12}^{(3N)}(\beta_N r)\right]\cos n\theta e^{-i\omega t}$$

$$\sigma_{\theta\theta N} = 2\mu_{0N}(1 - M_{kN}) r^{-2}\sum_{n=0}^{\infty}\left[\varphi_0 E_n i^n E_{21}^{(1N)}(\alpha_N r) + C_{nN} E_{21}^{(3N)}(\alpha_N r) + M_{nN} E_{22}^{(3N)}(\beta_N r)\right]\cos n\theta e^{-i\omega t}$$

$$\sigma_{r\theta N} = 2\mu_{0N}(1 - M_{kN}) r^{-2}\sum_{n=0}^{\infty}\left[\varphi_0 E_n i^n E_{41}^{(1N)}(\alpha_N r) + C_{nN} E_{41}^{(3N)}(\alpha_N r) + M_{nN} E_{42}^{(3N)}(\beta_N r)\right]\sin n\theta e^{-i\omega t}$$

$$\sigma_{rrj} = 2\mu_{0j}(1 - M_{kj}) r^{-2}\sum_{n=0}^{\infty}\left[A_{nj} E_{11}^{(3j)}(\alpha_j r) + A_{nj}^1 E_{11}^{(4j)}(\alpha_j r) + B_{nj} E_{12}^{(3j)}(\beta_j r) + B_{nj}^1 E_{11}^{(4j)}(\beta_j r)\right]\cos n\theta e^{-i\omega t}$$

$$\sigma_{\theta\theta j} = 2\mu_{0j}(1 - M_{kj}) r^{-2}\sum_{n=0}^{\infty}\left[A_{nj} E_{21}^{(3j)}(\alpha_j r) + A_{nj}^1 E_{21}^{(4j)}(\alpha_j r) + B_{nj} E_{22}^{(3j)}(\beta_j r) + B_{nj}^1 E_{22}^{(4j)}(\beta_j r)\right]\cos n\theta e^{-i\omega t}$$

$$\sigma_{r\theta j} = 2\mu_{0j}(1 - M_{kj}) r^{-2}\sum_{n=0}^{\infty}\left[A_{nj} E_{51}^{(3j)}(\alpha_j r) + A_{nj}^1 E_{61}^{(4j)}(\alpha_j r) + B_{nj} E_{52}^{(3j)}(\beta_j r) + B_{nj}^1 E_{52}^{(4j)}(\beta_j r)\right]\sin n\theta e^{-i\omega t}$$

where

$$E_{11}^{(kj)} = \left(n^2 + n - \frac{\beta_j^{\ 2} r^2}{2} \right) Y_n^{(kj)}(\alpha_j r) - \alpha_j r Y_{n-1}^{(kj)}(\alpha_j r)$$

$$E_{12}^{(kj)} = n\left[(n+1) Y_n^{(kj)}(\beta_j r) + \beta_j r Y_{n-1}^{(kj)}(\beta_j r)\right]$$

$$E_{21}^{(kj)} = -\left(n^2 + n + \frac{\beta_j^{\ 2} r^2}{2} - \alpha_j^{\ 2} r^2 \right) Y_n^{(kj)}(\alpha_j r) + \alpha_j r Y_{n-1}^{(kj)}(\alpha_j r)$$

$$E_{22}^{(kj)} = n\left[\beta_j r Y_n^{(kj)}(\beta_j r) - (n+1) Y_n^{(kj)}(\beta_j r)\right]$$

$$E_{31}^{(kj)} = \left(\alpha_j{}^2 r^2 - \frac{\beta_j{}^2 r^2}{2}\right) Y_n^{(kj)}(\alpha_j r)$$

$$E_{41}^{(kj)} = n\left[(n+1)Y_n^{(kj)}(\alpha_j r) - \alpha_j r Y_{n-1}^{(kj)}(\alpha_j r)\right]$$

$$E_{42}^{(kj)} = -\left(n^2 + n - \frac{\beta_j{}^2 r^2}{2}\right) Y_n^{(kj)}(\beta_j r) + \beta_j r H_{n-1}^{(kj)}(\beta_j r)$$

$$E_{51}^{(kj)} = \left[\alpha_j r Y_{n-1}^{(kj)}(\alpha_j r) - n Y_n^{(kj)}(\alpha_j r)\right]$$

$$E_{52}^{(kj)} = -n Y_n^{(kj)}(\beta_j r)$$

$$E_{61}^{(kj)} = -n Y_n^{(kj)}(\alpha_j r)$$

$$E_{62}^{(kj)} = \left[n Y_n^{(kj)}(\beta_j r) - \beta_j r Y_{n-1}^{(kj)}(\beta_j r)\right], \quad k = 1,2,3,4$$

Here $Y_n^{(1j)} = J_n, \quad Y_n^{(2j)} = N_n, \quad Y_n^{(3j)} = H_n^{(1)}, \quad Y_n^{(4j)} = H_n^{(2)}.$

The problems are reduced to the solution of algebraic equations

$$\left[[Q] - \Omega^2 [N]\right]\{Z\} = \bar{\mu}_\Gamma [P][F] + \bar{\mu}_\Gamma (1 + \frac{\bar{h}}{2})\{H\}, \tag{15}$$

where $\Omega^2 = \frac{\rho_0 h R}{\bar{G}_{z1}}\omega^2$ - dimensionless parameter, $\bar{\mu} = \bar{\mu}_1 / \bar{G}_{z1}$ and $\rho = \rho_0 / \rho_1$ - ratios of complex moduli of elasticity and densities, respectively; {Z}-matrix-column of arbitrary constants; {F}-matrix-column of external loads; [Q]-square matrix of multilayer shell parameters, {H}-matrix-column with Bessel and Hankel functions, [N]-square matrix of masses.

Equations (15) are solved by Gaussian method with principal element extraction. Displacements and stresses are reduced to dimensionless forms:

$$u_{rj}^* = \frac{u_{rj}}{i\alpha\varphi_A}; \quad u_{\theta j}^* = \frac{u_{\theta j}}{i\alpha\varphi_A}; \quad \sigma_{rrj}^* = \frac{\sigma_{rrj}}{\sigma_0}; \quad \sigma_{r\theta j}^* = \frac{\sigma_{r\theta j}}{\sigma_0}; \quad \sigma_0 = -\bar{\mu}\beta^2\varphi_A$$

In the case when $E_1=E_2\ldots=E_N$, $\rho_1=\rho_2\ldots=\rho_N$ and $\nu_1=\nu_2\ldots=\nu_N$, , we obtain holes ($r=R$) located in an infinitely elastic medium ($a_{\lambda N}(\omega) = 0$, $b_{\lambda N}(\omega) = 0$). The boundary (r=R) is stress free, i.e., there is no fluid. In this case, the circumferential stress on the cavity surface is reduced to:

$$\sigma_{\theta\theta N}(R,\theta,t) = \frac{-4}{\pi}\beta_N{}^2 \mu_N \varphi_0 \left(1 - \frac{1}{k^2}\right) * \sum_{n=0}^{\infty} (-1)^n \in_n H^{(1)}{}_n(\alpha_N Z)\bar{T}_{nN} \cos n\theta\, e^{-i\omega t}, \tag{16}$$

where

$$\bar{T}_{nN} = T_{nN}(R_N) = \left[\alpha_N R_N H_{n-1}(\alpha_N R_N) - H_{n-1}(\alpha_N R_N) + Q_{nN}(\beta_N R_N)\right]^{-1},$$

$$Q_{nN}(\beta_N R_N) = \frac{(n^3 - n + \frac{1}{2}\beta^2{}_N R_N^2)\beta_N R_N H_{n-1}(\beta_N R_N) - (n^2 + n - \frac{1}{4}\beta_N{}^2 R_N^2)\beta_N{}^2 R_N{}^2 H^{(1)}{}_n(\beta_N R_N)}{(n^2 - 1)\beta_N R_N H^{(1)}{}_{n-1}(\beta_N R_N) - (n^2 - n + \frac{1}{2}\beta_N{}^2 R_N^2) H_n^{(1)}(\beta_N R_N)}$$

$$k_N{}^2 = C_{pN}^2 / C_{SN}^2.$$

Now let's analyze a few cases.

When $r \to 0$:

$$H_0^{(1),(2)}(z)\Big|_{r\to 0} = \pm\frac{2i}{\pi}\ln z - i\left(\frac{z}{2}\right)^2\left(1 - \frac{2}{\pi}\ln z\right) + 0\left(z^4 \ln z\right),$$

$$H_m^{(1),(2)}(z)\Big|_{r\to 0} = \mp\frac{i}{\pi}\left(\frac{z}{2}\right)^2 \left\{(n-1)! + n!\, z^2 + 0\left(z^4\right)\right\},$$

and at $r \to \infty$: $H_m^{(1),(2)}(z) = \left(\frac{2}{\pi z}\right)^{1/2} e^{\pm i(kz-\pi/4)}$, used the Hankel asymptotic formulas of the 1-st and 2-nd kind [14]. If in expression (16) Z tends to infinity, we can use the asymptotic expansions of the Hankel function [21]

$$\lim_{Z\to\infty} \sigma^*{}_{\theta\theta}\Big|_{r=R_N} \approx \frac{4}{4}\left[1-\frac{1}{k_N^2}\right]\sum_{n=0}^{\infty} i^{n+1} E_n T_{nN} \cos n\theta\, e^{-i\omega t}$$

The contour stresses of a cylindrical shell under the influence of incident longitudinal waves of harmonic type are obtained [21]. In the case when the limit wave number is equal to zero, then the last formula describes the static contour stress. To obtain the formula for the limiting case the asymptotic expressions of special Bessel and Hankel functions of complex argument (Z is finite) are used:

$$\lim_{\alpha\to o} \sigma_{\theta\theta}\Big|_{r=R_1} \approx 4\left[1+(\frac{R_N}{Z})^2+\frac{4}{Z}\cos\theta\right] * \sum_{m=2}^{\infty}(-1)^{m-2}(-\frac{R_N}{Z})^{m-2}(m-1)\cos m\theta \tag{17}$$

If the cavity is filled with an ideal fluid, then the annular stresses

$$\sigma_{\theta\theta}^* = -\frac{4}{\pi}\sum_{n=0}^{\infty}\frac{\in_n i^{n+1}}{\Delta_n}\{[\left(\frac{1}{\chi_N^2}-1\right)\left(\frac{n\beta_N^2R^2}{2}(n-1)-n^2\left(n^2-1\right)-n\frac{\beta_N^4R^4}{4}\right)+$$

$$+\frac{\beta_N^2R^3}{4}\eta\left(n(n+1)-\frac{1}{2}\beta_N^2R^2\right)]I_n\left(\alpha_0R\right)H_n\left(\beta_NR\right)+$$

$$+[\left(\frac{1}{\chi_N^2}-1\right)\left(n^3-n^2-n\right)-\frac{1}{4}n\beta_N^2R^2]\beta_NRI_n\left(\alpha_0R\right)H_{n-1}(\beta_NR)+$$

$$+\left(\frac{1}{\chi_N^2}-1\right)\left(n^3-n+\frac{1}{2}\beta_N^2R^2\right)\alpha_0RI_{n-1}\left(\alpha_0R\right)H_n(\beta_NR)+$$

$$+\left(\frac{1}{\chi_N^2}-1\right)\left(1-n^2\right)\alpha_0\beta_N^2R^2I_{n-1}\left(\alpha_0R\right)H_{n-1}(\beta_NR)\}\cos n\theta e^{-i\omega t}$$

Table 1.

Information on limit processes

Case 1	Case 2	Case 3	Case 4
$\lim\limits_{Z\to\infty}\left\{\sigma_{\theta\theta}^*\Big\|_{r=R}\right\}$ α -arbitrary	$\lim\limits_{\alpha\to 0}\left\{\sigma_{\theta\theta}^*\Big\|_{r=R}\right\}$ z - finite	$\lim\limits_{Z\to 0}\left\{\sigma_{\theta\theta}\Big\|_{r=R}\right\}$ $\alpha \to 0$	$\lim\limits_{\alpha\to 0}\left\{\lim\limits_{Z\to\infty}\sigma_{\theta\theta}\Big\|_{r=R}\right\}$ α - finite
Dynamic solution for a plane wave	linear expansion wave source	purely shear stress state	plane deformed state problem.

where

$$\chi_N^2 = \frac{2(1-v_N)}{1-2v_N} = \frac{\beta_N^2}{\alpha_N^2}; \qquad \eta = \frac{\rho_0}{\rho_N}.$$

At $\alpha_1 R \to 0$, is the static problem solution:

$$\sigma_{rr}^* = \frac{\lambda_0}{\lambda_0+\mu_N u}; \quad \sigma_{\theta\theta}^* = \frac{1}{1-v_N}\left[\left(1-\frac{2\lambda_0(1-v_1)}{\lambda_0+\mu_N}\right)-(2-4v_N)\cos 2\theta\right].$$

In the limiting cases, formulas (16) and (17) describe the results obtained in Table 1.

$\sigma_{\theta\theta N}^*$ is defined as follows:

$$\sigma_{\theta\theta}^*\Big|_{r=R_N} = \frac{\sigma_{\theta\theta}\Big|_{r=R_N}}{\sigma_{\theta\theta}^{(p)}}$$

where $\sigma_{\theta\theta}^{(p)} = i\,\pi\varphi_0\,\mu\,\alpha^2\,[\,H_2^{(1)}\pi\varphi\mu((\alpha\bar{r})\ +(1-k^2)\,H_o^{(1)}(\alpha\bar{r})\,]\,e^{-i\omega t}$.

If we consider the fluid, then using (3) and (4) we can determine the corresponding stresses $\sigma_{rr\,N}^{*}$ and $\sigma_{\theta\theta N}^{*}$.

3. Results and analysis

Stresses and displacements for these incident waves are determined by series (14), calculated on Matlab, with an accuracy of 10^{-8}.

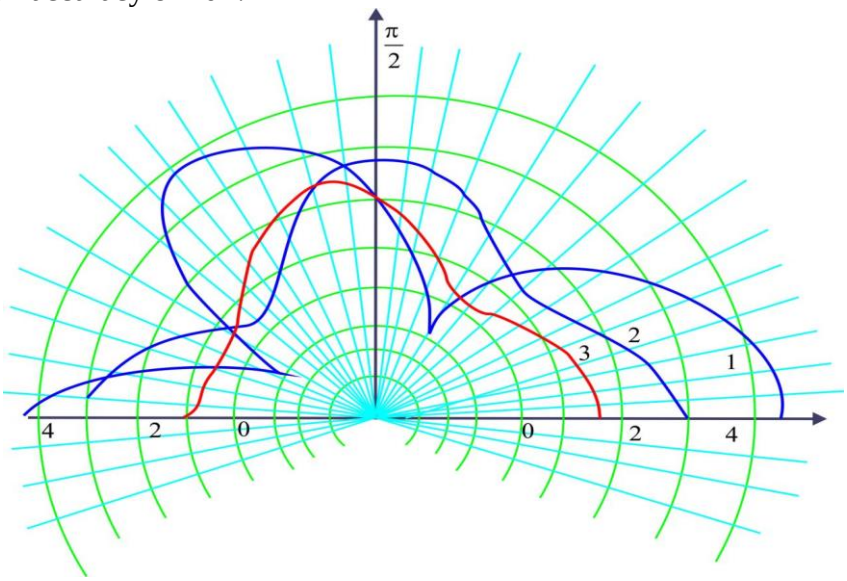

Figure 2. – **Epuray of the effect of source distance on the contour voltages** $\left|\sigma_{\theta\theta}^{*}\right|$ **depending on** $\theta(\alpha R = 0.1)$

$$1.z^{*}/(2r_0) = 5.0; 2.z^{*}/(2r_0) = 10; 3.z^{*}/(2r_0) = 30$$

We take the Rzhanitsyn-Koltunov kernel [21] as the relaxation kernel, where A, α, β - parameters of the material [21]. Let us assume the following parameters: $A = 0{,}048;\quad \beta = 0{,}05;\quad \alpha = 0{,}1$.

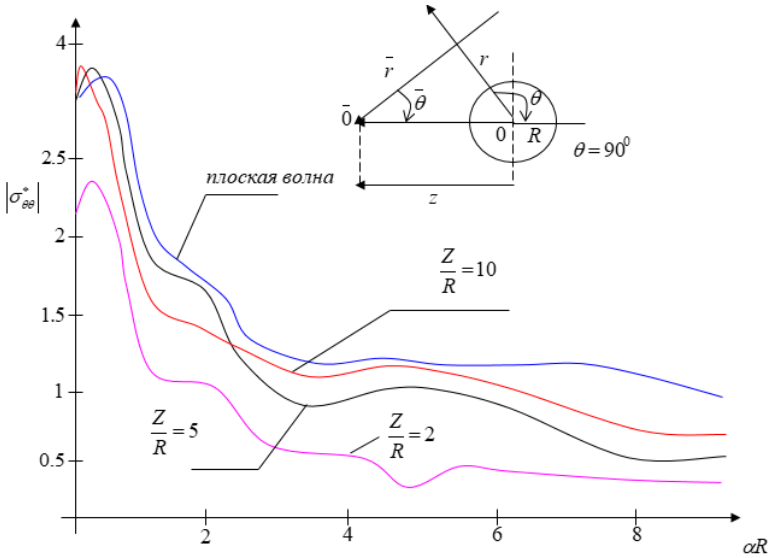

Figure 3. – **Change** $\left|\sigma_{\theta\theta}^{*}\right|$ **from** αR **(wave number) at** $\theta = 90^0;\quad A = 0{,}048;\quad \alpha = 0{,}1;\quad \beta = 0{,}5$

For $E_1=E_2=\ldots E_n$; $\rho_1 = \rho_2 = \ldots = \rho_n$; $\nu_1 = \nu_2 = \nu_3 = \ldots = \nu_n$, then the problem is considered. Fig.2 shows change $\left|\sigma_{\theta\theta}^{*}\right|$ from αR (wave number) at $\frac{Z}{R} = 3.0;\ 30,\ 50,\ \ \alpha R = 0.1$,

$A = 0{,}048;\quad \beta = 0{,}05;\quad \alpha = 0{,}1;\ \nu = 0.25$. Fig. 2 shows that the source distance dependence is to move the maximum value to the point where the ray drawn from the source is tangent to the cavity boundary.

Fig. 3 shows the variation of $\sigma^*_{\theta\theta}\big|_{r=R_N}$ from the αR (wave number) under longitudinal wave action and values of $\dfrac{Z}{R} = 6.0;\ 12;\ 20$, which rapidly tend to the solution under plane wave action when $\alpha R > 0.16$. That is, when the source is more than five radii away from the cavity, the high-frequency wave variation $\sigma^*_{\theta\theta}$ can be replaced by a plane wave variation. The maximum difference at $Z \to \infty$ between the plane wave solution and the investigated solution is observed in the interval $0 \le \alpha R \le 0.22$. It is easy to see that when $\alpha R \to 0$, the dynamic solution is tend to the static value ($\nu = 0.25, \theta = \pi/2$), i.e. to value $\sigma^*_{\theta\theta}$=2.76.

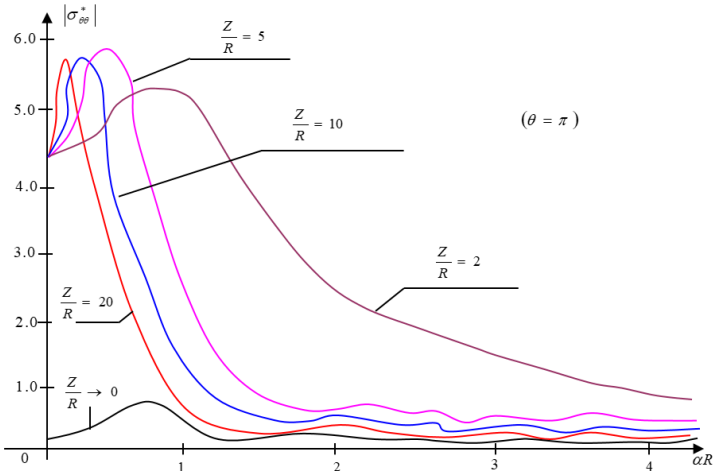

Figure 4. – **Change** $|\sigma^*_{\theta\theta}|$ **on** αR $(\theta = \pi)$

At $\theta = \pi$, for $\sigma^*_{\theta\theta}$, when $\alpha R \ge 1.0$, the solution for the dynamic source also tends to the solution for the plane wave (Fig.4).

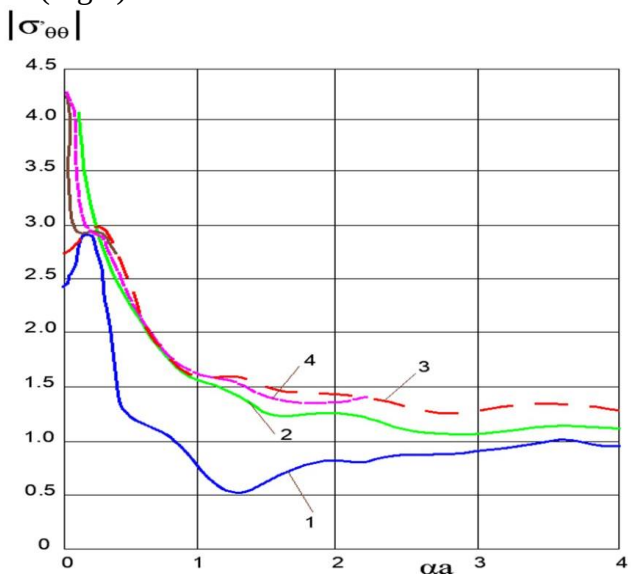

Figure 5. – **Variation** $|\sigma^*_{\theta\theta}|$ **on** αR **at** $\theta = 90^0;\ A = 0{,}048;\quad \alpha = 0{,}1;\quad \beta = 0{,}5$

$1.z^*/2r_0 = 2, 2.z^*/2r_0 = 5, 3.z^*/2r_0 = \infty, 4.z^*/2r_0 = 10$ **(longitudinal wave)**

In Fig. 5 shows the variation $|\sigma^*_{\theta\theta}|$ on αR when $\theta = 90^0;\ A = 0{,}048;\quad \alpha = 0{,}1;\quad \beta = 0{,}5$; $1.z^*/2r_0 = 2, 2.z^*/2r_0 = 5, 3.z^*/2r_0 = \infty, 4.z^*/2r_0 = 10$ (longitudinal wave).

In the case of Z/R = 2 (Fig. 3), the difference between the dynamic concentration curve from the static concentration curve is up to 15%.

When Z / R = 2, in the case of $\alpha R = 2.0$ the results of static and dynamic stress state are sharply different, and at $R_1/Z > 50$, the radius of curvature of the wave can be disregarded.

It is found that when the cylindrical cavity contains fluid, then the dependence of stresses on the parameter $\gamma = \dfrac{C_{p1}}{C_{p2}}$ is observed to be strong (Fig.6., Fig.5).

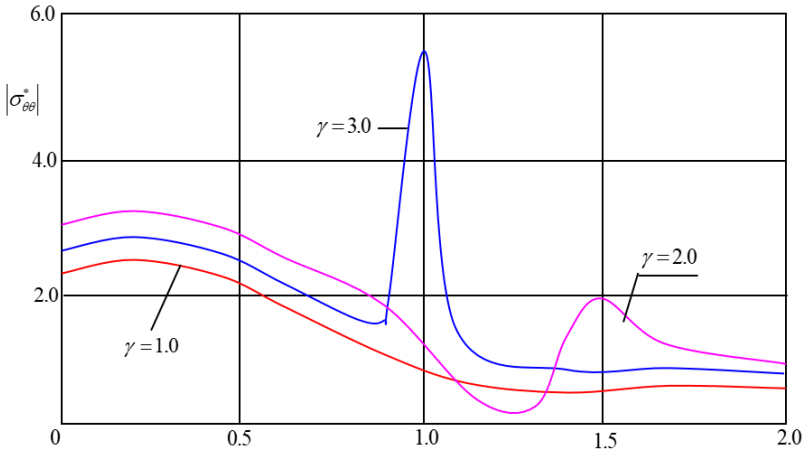

Figure 6. – **Dependence** $|\sigma^*_{\theta\theta}|$ **on** $\alpha_N R$ **(wave number)**

4. Conclusions

1. Methods and algorithms for solving the problem of diffraction of cylindrical harmonic waves on a multilayer viscoelastic cylindrical shell with a liquid in a half-space are developed.
2. The contour forces under the action of bulk waves in a cylindrical shell take their maximum value under the action of transverse waves. When the source of harmonic waves is located at a distance of fifty radii ($Z > 50R$) from the multilayer cylindrical shell, then the radius of curvature of the incident waves can be ignored.

References

1. *Durdiyev, D., Safarov, I., Teshaev, M.* Propagation of Waves in a Fluid in a Thin Elastic Cylindrical Shell // WSEAS Transactions on Fluid Mechanics. 2024, vol. 19, pp. 113–119.

2. *Teshaev, M., Safarov, I., Ibragimova, D., Rayimov, D., Akhmedov, S.* Stationary response of the system cylindrical shell // Viscoelastic filler to the effect of a moving load. Journal of Physics: Conference Series. 2024, vol. 2697, No. 1, 012004. https://doi.org/10.1088/1742-6596/2697/1/012004

3. *Muleski G.E., Ariman T., et al.* A shell model o f a buried pipe in a seismic environment // Journal of Pressure Vessel Technology. 1979, vol. 101, pp. 44-50.

4. *Pao Y.H., Mow C.C.* Diffraction of Elastic Waves and Dynamics Stress Concentrations / Crane, Russak and Company Inc., New York, 1973.

5. *Hindy A., Novak M.* Earthquake response of underground pipeline // Journal of Earthquake Engineering Structure Dynamic. 1979, vol. 7, pp. 451-476.

6. *Sancar S., Pao Y.H.* Spectral analysis of elastic pulses back scattered from two cylindrical cavities in a solid // Journal of the Acoustical Society of America. 1981, vol. 69, pp. 1591-1596.

7. *Davis C.A., Lee V.W.* Transverse response of underground cavities and pipes to incident SV waves // Journal of Earthquake Engineering Structure Dynamic. 2001, vol. 30, pp. 383-410.

8. *Kattis S.E., Beskos D.E., Cheng A.H.D.* 2D dynamic response of unlined and lined tunnels in poroelastic soil to harmonic body waves // Journal of Earthquake Engineering Structure Dynamic. 2003, vol. 32, pp. 97-110.

9. *Liu D.K., Gai B.Z., Tao G.Y.* Applications of the method of complex functions to dynamic stress concentrations // Wave Motion. 1982, vol. 4, pp. 293-307.

10. *Pavic G.* Vibrational energy flow in elastic circular cylindrical shells // Journal of Sound and Vibration. 1990, vol. 142, pp. 293-310.

11. *Cao H., Lee V. W.* Scattering of plane P waves by circular cylindrical canyons with various depth-to-width ratio // Soil Dynamics and Earthquake Engineering. 1990, vol. 9, pp. 141-150.

12. *Beres J.* Characterisation of anisotropy in a karstified carbonate plateform using seismic and electrical resistivity methods: a joint approach. Doctoral dissertation. Paris: University Paris Sud; 2013.

13. *Mesgouez A, Buis S, Lefeuve-Mesgouez G, Micolau G.* Use of global sensitivity analysis to assess the soil poroelastic parameter influence // Wave Motion. 2017, vol. 72, pp. 377-94.
14. *Virieux J, Operto S.* An overview of full-waveform inversion in exploration geophysics // Geophysics. 2009, vol. 74, No. 6, pp. WCC127-52.
15. *Lefeuve-Mesgouez G, Mesgouez A, Ogam E, Scotti T, Wirgin A.* Retrieval of the physical properties of an anelastic solid half space from seismic data // Journal of Applied Geophysics. 2013, vol. 88, pp. 70-82.
16. *Mesgouez A.* Characterization of a viscoelastic heterogeneous object with an effective model by nonlinear full waveform inversion // Journal of Sound and Vibration. 2018, vol. 422, pp. 189-209.
17. *Sidler R, Carcione JM, Holliger K.* A pseudo-spectral method for the simulation of poro-elastic seismic wave propagation in 2D polar coordinates using domain decomposition // Journal of Computational Physics. 2013, vol. 235, pp. 846-64.
18. *Zhou XL, Wang JH, Xu B, Jiang LF.* Dynamic response of a circular pipeline in a poroelastic medium // Mechanics Research Communications. 2009, vol. 36, No. 8, pp. 898-905.
19. *Gao M, Wang Y, Gao GY, Yang J.* An analytical solution for the transient response of a cylindrical lined cavity in a poroelastic medium // Soil Dynamics and Earthquake Engineering. 2013, vol. 46, pp. 30-40.
20. *Yi CP, Lu WB, Zhang P, Johansson D, Nyberg U.* Effect of imperfect interface on the dynamic response of a circular lined tunnel impacted by plane P-waves // Tunnelling and Underground Space Technology. 2016, vol. 51, pp. 68-74.
21. *Safarov, I.I., Teshaev, M.Kh.* Unsteady Motions of Spherical Shells in a Viscoelastic Medium // Vestnik Tomskogo Gosudarstvennogo Universiteta, Matematika i Mekhanika. 2023, vol. 83, pp. 166–179. https://doi.org/10.17223/19988621/83/14

SELECTION OF THE TYPE OF SUPPORTING PARTS FOR THE SEISMIC STABILITY OF CONTINUOUS REINFORCED CONCRETE BRIDGES

Shermukhamedov U.Z.[1], Karimova A.B.[1], Abdullaev A.R.[1], Gulomov D.I.[1]
[1]*Tashkent State Transport University, Tashkent, Uzbekistan*
E-mail: ulugbekjuve@mail.ru

Abstract. *Advanced experience in the study of rubber-metal supporting parts of bridges and overpasses is analyzed in the article. The calculation of a continuous reinforced concrete overpass for seismic impacts presented is implemented by the finite element method within the framework of linear-spectral theory. Numerical calculations have shown that the supporting part of the right end of the overpass does not allow the superstructure to fall from the abutment due to the fact that the maximum displacement of the rubber-metal supporting part is 0.2 m. As a result, the span and supports of the overpass have an overestimated safety factor for an 8-point earthquake on the MSK-64 scale.*

Keywords: *bridges and overpasses, seismic insulation, supporting parts, superstructure, support, compression and tension, monolithic structures.*

1. Introduction

Strong earthquakes (with an intensity of 7.0 and higher) can cause enormous deformations and sometimes destruction. To prevent such consequences, bridges must be able to dissipate energy when vibrating due to internal structural friction in the material from which they are made or under inelastic strains [1]. As is known, in Uzbekistan a significant part of structures are built in seismically hazardous areas. Protecting structures from seismic impacts is an important task in engineering. A study of world experience in the field of seismic protection of bridges shows that the use of the principle of seismic isolation has wide application. Using this method, flexible (rubber-metal) or sliding supporting parts are installed between the supports and spans, working as a seismic isolating element.

It should be noted that currently about twenty monographs have been published on the issues of seismic insulation and seismic damping of bridge structures. Classifications of seismic isolating devices are given in [2-7] and other publications. The study in [6, 14] considers the issues of seismic isolation and seismic damping of bridges, considering the characteristics of seismic vibrations of bridges, assessing seismic loads, and specifying the design impact and coefficients of combined seismic and mobile loads.

Under horizontal excitation of seismic impacts in two directions, Lead Rubber Bearings (LRB) are installed in continuous beam bridges, the nonlinear response of which is given in [8, 9]. Laboratory tests of a model of isolated bridges, the design of which included continuous spans and

LRB supporting parts, were conducted on a vibration stand. The results of tests performed under the influence of corresponding loads were also presented; they were compared with experimental data. A difference in displacements of various types of supporting parts was discovered, which arises when the restoring force in the longitudinal and transverse directions of rubber-metal supporting parts is idealized. Based on this, the bidirectional interaction of LRBs is considered under seismic isolation of bridge structures.

Recently, seismograms of earthquake records have been taken as a seismic effect [10, 11]. In this regard, it is of interest to develop methods and software for performing calculations of bridges and overpasses under the influence of earthquakes based on available seismogram records.

Calculations based on available real records of seismograms [12, 14], registered during strong earthquakes and stored in well-known databases in Europe and the USA, make it possible to study the behavior of the structure in real-time and assess the strength of the bridge and overpass elements. This approach provides a guaranteed assessment of the reliability of bridges and overpasses under seismic impacts of a certain intensity at the construction site. Since the bridge being calculated is equipped with seismic protection devices with nonlinear properties, the calculation must be performed by a direct dynamic method.

2. Materials, methods and object of study.

Considering the seismic activity of the territory of the Republic of Uzbekistan, anti-seismic strengthening becomes a key aspect in the construction and design of bridges and overpasses in the conditions of Uzbekistan

In recent years, for the development of transport infrastructure, on the initiative of the President of the Republic of Uzbekistan, a tourist complex was built in the territory of the rowing canal in the Samarkand region. The first monolithic reinforced concrete overpass in Uzbekistan was built in Samarkand as part of improving the city's transport infrastructure and providing amenities for tourists and residents visiting the new tourist center. For the overpass built on the 1083rd kilometer of the M-39 highway passing through Samarkand, anti-seismic supporting parts with a lead core of the LRB series from the “FIP-Industriale” manufacturer (Fig. 1) were used. In addition, in the capital of the country, at the intersection of the Small Ring Road and Chuponota Street, a continuous type overpass made of monolithic reinforced concrete was realized. This project was developed jointly with the Turkish transport engineering company “Kalyon Ulaştırma”. The total length of the overpass is 788 meters.

Figure 1. - **Modern continuous (monolithic) reinforced concrete bridges and overpasses in Samarkand and Tashkent**

Due to the complexity of the bridge design and the spatial pattern of seismic impact, analytical methods for calculating their stress-strain states do not seem possible. Therefore, numerical methods were used to solve problems. The impact is specified as a series of seismogram records in three directions with amplitude adjustment for different magnitudes. The equation of motion of the structure after applying discretization using the finite element method was reduced to the following form [13-16]:

$$[M]\{\ddot{u}\} + \eta[C]\{\dot{u}\} + [K]\{u\} = \{P\}, \tag{1}$$

with initial conditions from the static solution to the problem

$$\{u(t)\}_{t=0} = \{u(0)\}, \quad \{\dot{u(t)}\}_{t=0} = \{\dot{u}(0)\}, \tag{2}$$

where {u(t)} is the vector of absolute displacements of the nodal points of the finite element model of the structure, for nonlinear problems, matrices [M], [C], [K] depend on the absolute displacement

vector, {P(t)} includes the specified motion of soil and acting forces. Ground motion is specified in the form of seismogram records [14].

The seismic impact is transferred to the structure through the supports in the form of equality of displacements of the support foundations and the base surface, considering the propagation of the seismic wave.

The displacements and rotations of nodal points throughout the structure are calculated based on the solution to the problem with the corresponding boundary conditions at the ends of the span. Then, using the appropriate formulas, the forces, moments of forces in all structural elements, and normal stresses in the span elements are calculated at each time step.

3. Statement of the problem

Two types of rubber-metal support parts were examined in the study:

− insulators with the lead core of the LRB series (Fig. 2);

− rubber-metal insulators of the SI-N (normal) series (Fig. 3).

Figure 2. - **LRB Series Lead Core Rubber Bearings**

Figure 3. - **SI-N Series Rubber Bearings**

Lead core insulators of the LRB series are rubber-metal bearing parts consisting of steel plates alternating with layers of rubber, made with a cylindrical lead core (Fig. 2). Energy dissipation is provided by the lead core under its plastic strain, allowing reaching the values of the equivalent viscous damping coefficient of about 30%. Due to the high capacity of energy dissipation, it becomes possible to reduce horizontal displacements compared to an insulation system with the same equivalent stiffness but at lower energy dissipation capacity [7, 17].

The LRB insulator is made of a rubber mixture with G=0.8 MPa, diameter 900 mm, with rubber layers a lead core with diameters of 160 and 185 mm. A typical hysteresis loop for LRB series insulators can be represented as bilinear. Parameters d_1, F_1, d_2, and F_2, characterizing the bilinear curve, are given for each insulator of the LRB series shown in Table 1 and Fig. 4 [14, 17].

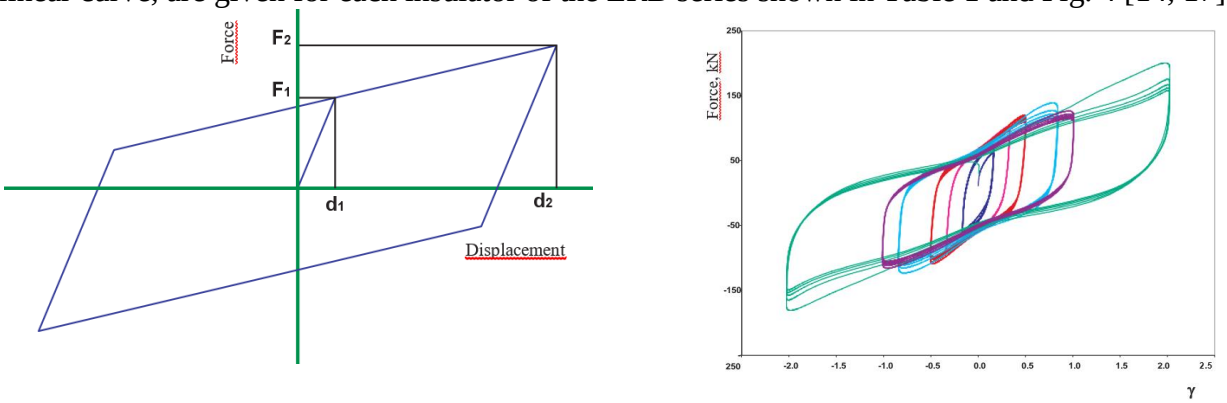

Figure 4. - **Typical hysteresis loops of a rubber-metal insulator with a lead core obtained during dynamic tests at high shear strain amplitude**

The hysteretic behavior of the LRB series isolator can also be given as a single line graph, with the effective stiffness K_e and the equivalent viscous damping coefficient ξ_e, depending on the maximum displacement d_2 and the corresponding force F_2 to which they relate [14, 17]:

$$K_e = \frac{F_2}{d_2}\ ; \tag{3}$$

$$\xi_e = \frac{2}{\pi} * \left[\frac{F_1}{F_2} - \frac{d_1}{d_2}\right]. \tag{4}$$

where K_e is the effective horizontal stiffness (at displacement d_2);

ξ_e is the equivalent viscous damping coefficient (at displacement d_2);

F_2 is the maximum horizontal force (with displacement by value d_2);

F_1 is the resistance limit (yield strength);

d_1 is the displacement to the yield point.

Table 1

Initial parameters of rubber-metal insulators of the LRB-SN and SI-N series for different allowable displacements

Allowable displacement, mm	Type of insulator	K_e	ε_e	F_2	F_1	K_v	D_g
		kN/mm	%	kN	kN	kN/mm	mm
200	LRB-SN 900/144-160	at d_2 =167mm			241	3509	900
		3.83	20	639			
250	LRB-SN 900/171-185	at d_2 =208mm			312	2892	
		3.49	23	728			
300	LRB-S 900/162-150	at d_2 =250mm			312	2892	
		2.27	21	817			
200	SI-N 900/108	4.71	Insulator without lead core			4377	900
250	SI-N 900/132	3.86				3582	
300	SI-N 900/168	3.03				2814	

The second type of insulators of the SI series are rubber-metal supporting parts consisting of steel plates alternating with layers of rubber, combined by hot vulcanization. Typically, SIs are manufactured in a round shape, but can also be square or rectangular in plan. Rubber-metal insulators are designated SI (Seismic Isolator) followed by one of the letters, S (Soft), N (Normal), and H (Hard) [7, 14].

The rubber mixtures used for the production of SI have an equivalent dynamic shear modulus G_{dyn} from 0.4 MPa to 1.4 MPa and an equivalent viscous damping coefficient of 10% or 15%.

To design a continuous monolithic bridge considering seismic insulation, an option comparison of two insulators was performed. Parameters K_e, ξ_e, K_v, F_1, d_2 and F_2, characterizing the bilinear curve, are given for each insulator of the LRB-SN and SI-N series in Table 1, for two rubber-metal supporting parts [17].

4. Results

A reinforced concrete monolithic overpass running at 1083 km of the M-39 highway in the city of Samarkand is made as two separate overpasses, each for one direction of movement. The span structure of the overpass is made of a continuous monolithic reinforced concrete design scheme 33+42+33 m of individual design, 110 m long and 10.5 m wide, and has a variable height along the overpass. Along the facade, the span of the structure is made of a plate of variable height - 1.3 m in the span, 2.3 m above the support (Fig. 5).

The overpass structure is partitioned into finite elements, considering the change in height along the length of the span. The finite element models axial tension–compression, bending relative to axes perpendicular to the longitudinal axis of the overpass, and torsion relative to the longitudinal axis [14, 18].

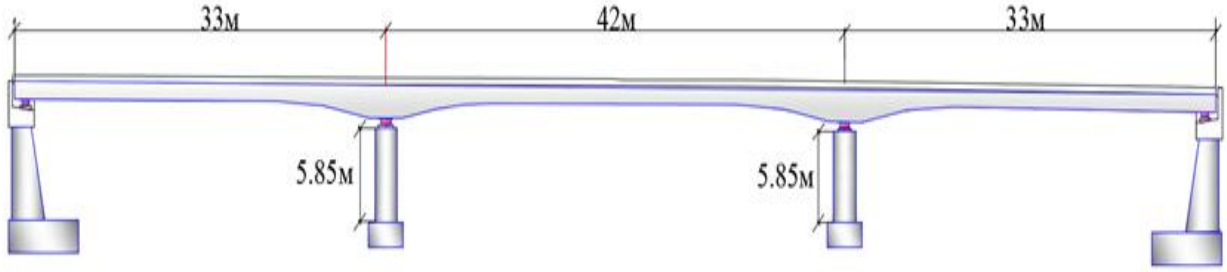

Figure 5. - **Scheme of a monolithic overpass running at 1083 km of the M-39 highway**

Bridge structures consist of many components, the most important of which are spans, supports, and supporting (bearing) parts [7, 17]. The support and supporting parts are the most vulnerable elements of a bridge structure. Thus, seismic isolating devices, in particular rubber-metal ones, are used for the supporting part in earthquake-prone areas. The supporting part is a seismic isolating rubber-metal device that allows the span to move in the longitudinal direction in the range from 0.1 m to 0.35 m, depending on the model used due to low shear rigidity [19, 20]. The supporting part is modeled as a single finite element working in tension-compression, shear in two directions, and torsion. The intermediate supports have dimensions: height 5.85 m, width along the facade - 2 m, and in the lateral direction they have a variable size in height from 5 m to 8.4 m. The supports are partitioned into finite elements working in tension-compression, shear in two directions, and torsion, considering the mass distribution. In this calculation, we assumed that the movements of their bases are equal to the movements of the base at the corresponding points during an earthquake. The material of the composite structures is concrete of strength class B35, with a specific gravity γ = 25000 N/m^3, elastic modulus E = 35200 MPa, Poisson's ratio ν = 0.2. The seismicity of the territory of Samarkand is assumed to be 8 points, according to the seismic microzoning map plotted by the Institute of Seismology in 1980.

Let us consider the behavior of a road overpass with seismic insulation produced by the “FIP-Industriale” Company during earthquakes of varying intensity and frequency. The seismic isolation is a system of bridge spans on longitudinally movable supporting parts. The beginning of the overpass - the left end of the span is rigidly connected to the abutment, and the end of the overpass - the right end - is connected to the abutment with movable supporting parts [14].

5. Analysis of results

The results of calculations of a monolithic overpass under dynamic load, based on records of two real seismograms of severe earthquakes: Tabas (Iran) and Cairano (Italy) [14].

1. Cairano - 000319 (01/16/1981, 8-points on the MSK-64, maximum acceleration - 1.47 m/s^2, maximum displacement - 0.0029 m, digitization step - 0.005 s, duration - 22.175 s);

2. Tabas - 000187 (09/16/1978, higher on the MSK-64 scale, maximum acceleration - 10.17 m/s^2, maximum displacement - 0.3446 m, digitization step - 0.005 s, duration - 78.395 s).

Tables 2 and 3 show the results of the calculated maximum absolute values of normal stresses in the upper and lower sections of spans of the monolithic overpass (Fig. 6). Calculations were performed using the *SHARK* software for structural calculation [14, 16].

As seen from Table 3 (Fig. 6), the maximum tensile stress in the left span of the overpass with rigid supporting parts is 1.7373 MPa. This is due to the fact that the rigid support part transfers the energy of the seismic wave directly to the first span. Note that due to the use of rubber-metal supporting parts with a lead core in three supports of the overpass and energy loss in spans due to viscosity, stresses in the middle span (1.1614 MPa) and the right span (0.41634 MPa) are reduced by 1.5 and 4 times, respectively, compared to stresses in the left span.

Table 2

Normal maximum stresses in the upper section of spans of a monolithic overpass under seismic impacts of past earthquakes

Type of supporting part with different displacements	Name of impact	Maximum stress, MPa					
		in the middle of the left span (16.5m)		in the middle of the overpass (54m)		in the middle of the right span (91.5m)	
		Statics	Dynamics	Statics	Dynamics	Statics	Dynamics
LRB-SN (200mm)	Cairano	-0.048162	0.12632	-0.08188	0.02991	-0.061171	-0.032722
	Tabas	-0.048162	1.537	-0.08188	0.99005	-0.061171	0.27594
LRB-SN (250mm)	Cairano	-0.047916	0.12634	-0.082342	0.029208	-0.061281	-0.032674
	Tabas	-0.047916	1.5452	-0.082342	0.99705	-0.061281	0.28179
LRB-SN (300mm)	Cairano	-0.047916	0.12607	-0.082342	0.029058	-0.061281	-0.03284
	Tabas	-0.047916	1.5388	-0.082342	0.99097	-0.061281	0.27762
SI-N (200mm)	Cairano	-0.048649	0.12404	-0.081699	0.028995	-0.061215	-0.033814
	Tabas	-0.048649	1.5162	-0.081699	0.97082	-0.061215	0.26142
SI-N (250mm)	Cairano	-0.048195	0.12398	-0.081842	0.028587	-0.061165	-0.033766
	Tabas	-0.048195	1.5042	-0.081842	0.9598	-0.061165	0.25565
SI-N (300mm)	Cairano	-0.047645	0.12357	-0.082188	0.027657	-0.061167	-0.033835
	Tabas	-0.047645	1.4913	-0.082188	0.94766	-0.061167	0.24972

An analysis of the maximum values of normal stresses during 10 and 8-point earthquakes showed that the overpass structure can withstand strong and very strong earthquakes. According to design standards, the permissible stress value is 2.73 MPa.

Table 3

Normal maximum stresses in the lower section of spans of a monolithic overpass under seismic impacts of past earthquakes

Type of supporting part with different displacements	Name of impact	Maximum stresses, Mpa					
		in the middle of the left span (16.5m)		in the middle of the overpass (54m)		in the middle of the right span (91.5m)	
		Statics	Dynamics	Statics	Dynamics	Statics	Dynamics
LRB-SN (200mm)	Cairano	0.045901	0.23169	0.079672	0.19604	0.05961	0.09983
	Tabas	0.045901	1.6905	0.079672	1,1525	0.05961	0.41064
LRB-SN (250mm)	Cairano	0.045667	0.23115	0.080134	0.19626	0.059703	0.099983
	Tabas	0.045667	1.7373	0.080134	1.1614	0.059703	0.41634
LRB-SN (300mm)	Cairano	0.045667	0.22838	0.080134	0.19602	0.059723	0.099792
	Tabas	0.045667	1.7299	0.080134	1.1549	0.059723	0.41205
SI-N (200mm)	Cairano	0.045861	0.22976	0.078989	0.19387	0.059362	0.098605
	Tabas	0.045861	1.7066	0.078989	1.1294	0.059362	0.39407
SI-N (250mm)	Cairano	0.045916	0.22905	0.079618	0.194	0.059594	0.098653
	Tabas	0.045916	1.6921	0.079618	1.1191	0.059594	0.38807
SI-N (300mm)	Cairano	0.045863	0.227666	0.080438	0.1939	0.059871	0.098577
	Tabas	0.045863	1.6759	0.080438	1.1088	0.059871	0.38188

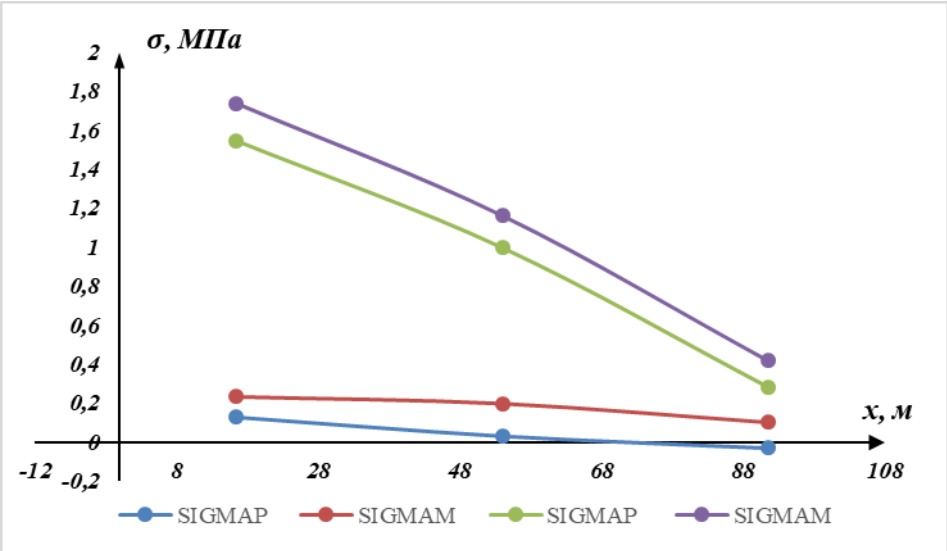

max		16.5	54	91.5
CAIRANO	SIGMAP	0.12634	0.029208	-0.03267
	SIGMAM	0.23115	0.19626	0.099983
TABAS	SIGMAP	1.5452	0.99705	0.28179
	SIGMAM	1.7373	1.1614	0.41634

Figure 6. **Dependence of maximum tensile stresses relative to the horizontal axis along the overpass in the upper and lower sections of spans of the monolithic overpass**

Table 4

Normal minimum stresses in the upper section of spans of a monolithic overpass under seismic impacts of past earthquakes

Type of supporting part with different displacements	Name of impact	Minimum stresses, MPa					
		in the middle of the left span (16.5m)		in the middle of the overpass (54m)		in the middle of the right span (91.5m)	
		Statics	Dynamics	Statics	Dynamics	Statics	Dynamics
LRB-SN (200mm)	Cairano	-0.048162	-0.19897	-0.08188	-0.17515	-0.061171	-0.084392
	Tabas	-0.048162	-1.9828	-0.08188	-1.2716	-0.061171	-0.39983
LRB-SN (250mm)	Cairano	-0.047916	-0.19808	-0.082342	-0.17502	-0.061281	-0.084178
	Tabas	-0.047916	-1.9783	-0.082342	-1.2669	-0.061281	-0.39946
LRB-SN (300mm)	Cairano	-0.047916	-0.1987	-0.082342	-0.1509	-0.061281	-0.075728
	Tabas	-0.047916	-1.9813	-0.082342	-1.2707	-0.061281	-0.40026
SI-N (200mm)	Cairano	-0.048649	-0.20187	-0.081699	-0.17723	-0.061215	-0.085352
	Tabas	-0.048649	-1.9972	-0.081699	-1.2896	-0.061215	-0.40543
SI-N (250mm)	Cairano	-0.048195	-0.20262	-0.081842	-0.1784	-0.061165	-0.085649
	Tabas	-0.048195	-2.0005	-0.081842	-1.2939	-0.061165	-0.40584
SI-N (300mm)	Cairano	-0.047645	-0.2034	-0.082188	-0.17991	-0.061167	-0.086
	Tabas	-0.047645	-2.0043	-0.082188	-1.2992	-0.061167	-0.40676

The results of a comparison of stresses under static and dynamic loading show that when using rubber-metal supporting parts with a lead core (displacement 250 mm) in the overpass during the Tabas earthquake, the maximum values of dynamic stresses in the lower sections of the overpass span were significantly greater than the static one, i.e. in the left span by 37 times, in the middle span by 14 times, and in the right span by 6 times. As for the Cairano earthquake, we can see that in the left span, the dynamics is 5 times greater than the statics, and in the middle and right spans, it is 2 times greater, since this earthquake is 8 points on the MSK-64 scale.

Besides, Tables 4 and 5 show the results of the calculated minimum absolute values of normal stresses in the upper and lower sections of spans of the monolithic overpass (Fig. 7).

Table 5

Normal minimum stresses in the lower section of spans of a monolithic overpass under seismic impacts of past earthquakes

Type of supporting part with different displacements	Name of impact	Minimum stresses, MPa					
		in the middle of the left span (16.5m)		in the middle of the overpass (54m)		in the middle of the right span (91.5m)	
		Statics	Dynamics	Statics	Dynamics	Statics	Dynamics
LRB-SN (200mm)	Cairano	0.045901	-0.097047	0.079672	-0.010447	0.05961	0.030331
	Tabas	0.045901	-1.9589	0.079672	-1.1699	0.05961	-0.3209
LRB-SN (250mm)	Cairano	0.045667	-0.096764	0.080134	-0.009395	0.059723	0.030696
	Tabas	0.045667	-1.9546	0.080134	-1.1647	0.059723	-0.31871
LRB-SN (300mm)	Cairano	0.045667	-0.097456	0.080134	-0.010054	0.059723	0.030397
	Tabas	0.045667	-1.9576	0.080134	-1.1679	0.059723	-0.31985
SI-N (200mm)	Cairano	0.045861	-0.099938	0.078989	-0.01381	0.059362	0.028893
	Tabas	0.045861	-1.9737	0.078989	-1.189	0.059362	-0.32847
SI-N (250mm)	Cairano	0.045916	-0.10152	0.079618	-0.01443	0.059594	0.028519
	Tabas	0.045916	-1.9771	0.079618	-1.1919	0.059594	-0.32742
SI-N (300mm)	Cairano	0.045863	-0.10355	0.080438	-0.015077	0.059871	0.02807
	Tabas	0.045863	-1.981	0.080438	-1.1947	0.059871	-0.32597

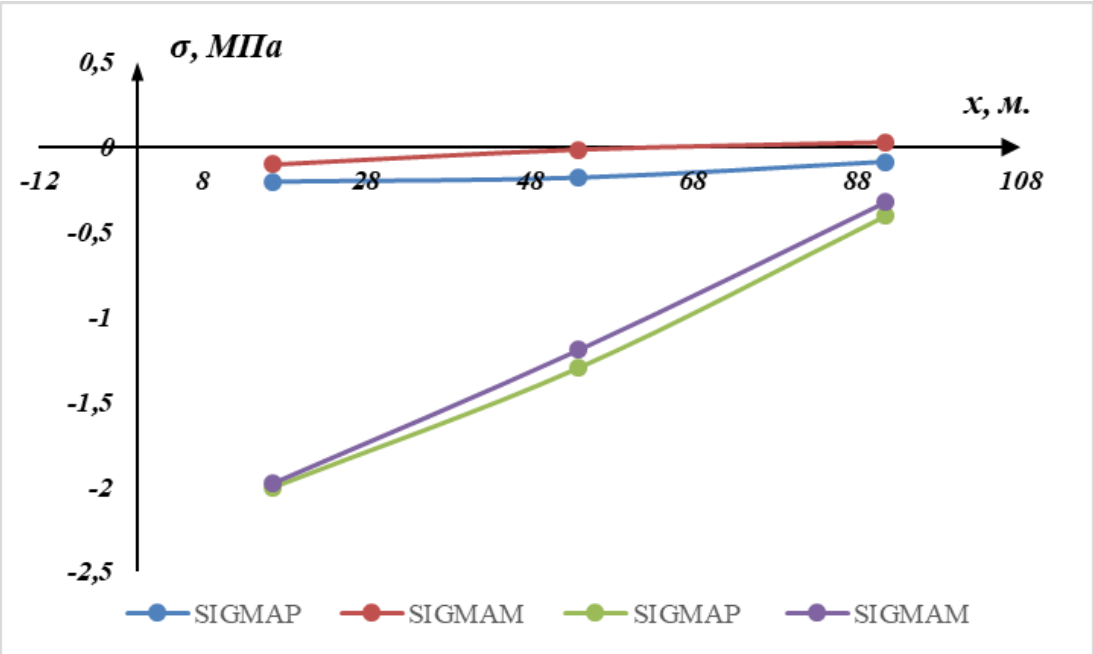

Figure 7. - **Dependence of the minimum tensile stresses relative to the horizontal axis along the overpass in the upper and lower sections of spans of the monolithic overpass**

Table 6 shows the values of the maximum tensile stresses in the upper and lower sections of spans (Fig. 8) relative to the horizontal axis along the overpass on the left (16.5 m), middle (54 m), and right (91.5 m) sides based on real records of the Tabas and Cairano earthquakes using rubber-metal supports of LRB-SN and SI-N types (with different allowable displacements of 200 mm, 250 mm, and 300 mm, respectively).

Table 6

Normal maximum stresses in the upper and lower sections of spans of a monolithic overpass at various allowable displacements according to seismograms of past earthquakes

Maximum stress in span structures, σ, *MPa*	Use of two types of supporting parts for different allowable displacements					
	LRB-SN (200mm)	LRB-SN (250mm)	LRB-SN (300mm)	SI-N (200mm)	SI-N (250mm)	SI-N (300mm)
Sigma P - 16.5	1.537	1.5452	1.5388	1.5162	1.5042	1.49139
Sigma M - 16.5	1.6905	1.7373	1.7299	1.7066	1.6921	1.6759
Sigma P - 54	0.99005	0.99705	0.99097	0.97082	0.9598	0.94766
Sigma M - 54	1.1525	1.1614	1.1549	1.1294	1.1191	1.1088
Sigma P - 91.5	0.27594	0.28179	0.27762	0.26142	0.25565	0.24972
Sigma M - 91.5	0.41064	0.41634	0.41205	0.39407	0.38807	0.38188

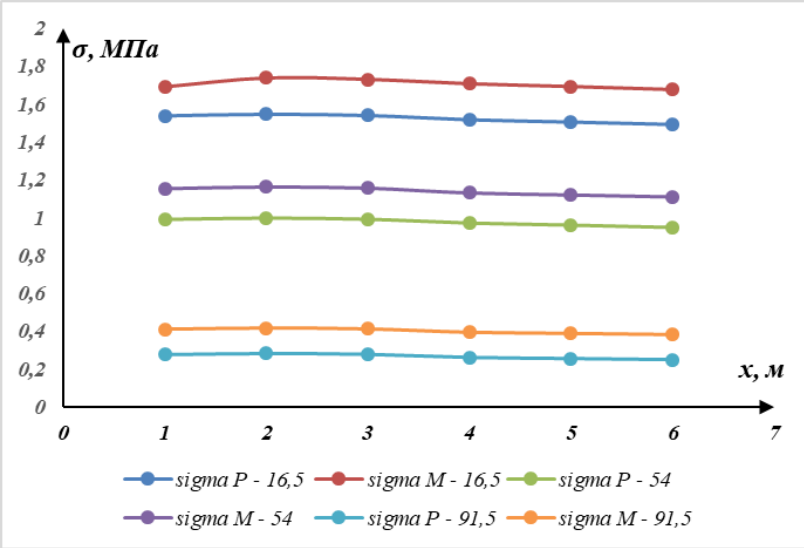

Figure 8. - **Dependence of maximum tensile stresses relative to the horizontal axis along the overpass in the upper and lower sections of spans of a monolithic overpass using two types of supporting parts at different allowable displacements**

The results of a comparison of two types of supporting parts of the overpass at different allowable displacements according to the records of the Tabas and Cairano earthquakes showed that it is appropriate to use a seismic insulator LRB-SN (250 mm) with greater rigidity since this type of insulator has the highest damping coefficient. A higher damping coefficient increases the overall stiffness of the insulator under dynamic impacts but leads to damping of vibrations.

6. Discussion

The selection and substantiation of the parameters of seismic protection bearing parts, considering various real records of earthquakes and assessing their impact explain the research results, allowing the engineer to select and substantiate the parameters of seismic protection means in designing continuous reinforced concrete bridges.

7. Conclusions

1. To ensure guaranteed seismic safety of bridge structures, it is necessary to conduct design calculations based on sets of records of past earthquakes that are close in dominant frequencies to the characteristics of the construction site.

2. The results of normal stresses obtained in span structures under the impact of strong earthquakes show that they do not exceed the allowable values of design standards.

3. The results of a comparison of two types of supporting parts of the overpass under different allowable displacements according to earthquake records showed that it is appropriate to use a seismic insulator LRB-SN (250 mm) with greater rigidity since this type of insulator has the highest

damping coefficient. A higher damping coefficient, in principle, increases the overall stiffness of the insulator under dynamic impacts but leads to damping of vibrations.

4. Comparing the displacements of the right end of the overpass and the corresponding support, the authors concluded that the most effective method of seismic protection of an overpass of a continuous beam span was the use of rubber-metal support parts with a lead core (displacement 250 mm), which provide sufficient damping to attenuate structural vibrations initiated by seismic impacts.

8. Acknowledgments

The research was conducted under financial support of the Fund for Supporting the Field of Seismology, Ensuring the Seismic Resistance of Structures and Seismic Safety under the Cabinet of Ministers of the Republic of Uzbekistan for 2022-2023, grant No. 28/2022 “Creation of a set of programs for calculating railway bridges considering the nonlinear interaction of their elements under real seismic impacts”.

References

1. *Shermukhamedov U.Z., Kadyrova Sh.Sh.* Selection of bridge supports in seismic areas // Uzbek journal “Problems of Mechanics”. IMSS. 2015. Tashkent. No.2. pp. 59-62.

2. *Verkholin V.A.* Features of calculation and selection of seismic isolation parameters for bridges, Earthquake-resistant construction, Structural Safety, 2004. No. 2. pp. 44-48.

3. *Uzdin A.M., Sandovich T.A., Al-Nasser-Mohamad Samih Amin.* Fundamentals of the theory of seismic resistance and earthquake-resistant construction of buildings and structures // Publishing house of VNIIG. 1993. p. 175. St. Petersburg.

4. *Shestoperov G.S.* Overview. Antiseismic devices in bridge construction. // VPTITRANSSTROY, M. 1986. p. 46

5. *Skiner R.I., Robinson W.H., McVerry G.H.* An introduction to seismic isolation. John Wiley & Sons, 1993. p. 353. New Zealand.

6. *Uzdin A.M., Kuznetsova I.O.* Seismic resistance of bridges. Book. Palmarium Academic Publishing, 2014. 456 p.

7. *Shermukhamedov U.Z.* Damping of longitudinal seismic vibrations of beam bridge supports with seismic isolating supporting parts. Monograph. 2020. p. 180. Tashkent.

8. *Qiang Han, Jianian Wen, Xiuli Du*. Nonlinear response of continuous girder bridges with isolation bearings under bi-directional ground motions. Journal of Vibroengineering, Beijing University of Technology, Beijing, 2015. Vol. 17, Issue 2, p. 816-826. China.

9. *Shermukhamedov U.Z., Karimova A.B., Zakirov B.S.* Calculation of Continuous Reinforced Concrete Bridges And Overpasses Inseismically Hazardous Areas. In E3S Web of Conferences, 2023. Vol. 401, p. 01078. EDP Sciences.

10. *Mirzaev I., Anvar Yuvmitov, Malikjon Turdiev and Jakhongir Shomurodov*. Influence of the Vertical Earthquake Component on the Shear Vibration of Buildings on Sliding Foundations. E3S Web of Conferences, 2021. Vol. 264, 02022. CONMECHYDRO.

11. *Elbek Kosimov, Ibrakhim Mirzaev and Diyorbek Bekmirzaev*. Comparison of the impacts of harmonic and seismic waves on an underground pipeline during the Gazli earthquake. IOP Conf. Series: Materials Science and Engineering 1030. 2021. 012082 IOP Publishing.

12. *Ambraseys N.N., Smit P., Douglas J., Margaris B., Sigbjörnsson R., Ólafsson S., Suhadolc P., Costa G.* Internet site for European strong-motion data. Bollettino di Geofisica Teorica ed Applicata. 2004. 45(3). URL: http://www.isesd.hi.is/ESD_local/frameset.htm.

13. *Shermukhamedov U.Z., Karimova A.B., Khakimova Ya.T., Abdusattorov A.A.* Modern techniques for the construction of monolithic bridges // "Science and innovation" international scientific journal. UIF-2022: Volume 1 Issue 8, 8.2. ISSN: 2181-3337. – p. 790-799. https://doi.org/10.5281/zenodo.7441336.

14. *Karimova A.B.* Contents of dissertation abstract of doctor of philosophy (PhD) on technical sciences. Dissertation of Doctor of Philosophy in Technical Sciences. Tashkent. - 118 p.

15. *Shermukhamedov U., Shaumarov S., Uzdin A.* Use of seismic insulation for seismic protection of railway bridges. In E3S Web of Conferences 2021. (Vol. 264, p. 02001). EDP Sciences. doi:10.1051/e3sconf/202126402001.

16. *Rashidov T.R., Kuznetsov S.V., Mardonov B.M., Mirzaev I.* Applied problems of seismodynamics of structures. Book 1. Tashkent. Navruz. 2019. p. 268.

17. http://www.fipindustriale.it.

18. *Myachenkov V.I., Maltsev V.G., Mayboroda V.P. et al.* Calculation of mechanical engineering structures by the finite element method. Directory. Under general ed. by Myachenkov V.I. Moscow. Mechanical engineering. 1989. p. 520.

19. *Raupov C., Shermuxamedov U., Karimova A.* Assessment of strength and deformation of lightweight concrete and its components under triaxial compression, taking into account the macrostructure of the material. In E3S

Web of Conferences, 2021. Vol. 264, p. 02015. CONMECHYDRO-2023, EDP Sciences. https://doi.org/10.1051/e3sconf/202126402015

20. *Shermukhamedov U., Mirzaev I., Karimova A.B., Askarova D.* Calculation of the stress-strain state of monolithic bridges on the action of real seismic impacts. In E3S Web of Conferences, 2023. Vol. 401, p. 05080. EDP Sciences. https://doi.org/10.1051/e3sconf/202340105080.

21. *Shermukhamedov, U., Karimova, A.B., Abdullaev, A.R., & Khakimova, Ya.T.* Comparison of operating costs of reinforced concrete bridges and overpasses with different static schemes. In E3S Web of Conferences, 2023. Vol. 401, p. 02035. EDP Sciences. https://doi.org/10.1051/e3sconf/202340102035.

22. *Raupov C., Karimova A., Zokirov F., Khakimova Y.* Experimental and theoretical assessment of the long-term strength of lightweight concrete and its components under compression and tension, taking into account the macrostructure of the material. In E3S Web of Conferences. 2021, p. 264, 02024 CONMECHYDRO.

STRUCTURAL HEALTH MONITORING OF CHADRA HAULY (KHOREZM, UZBEKISTAN) BY MEANS OF LASER SCANNING.

Takhirov S. M.[1], Rakhmonov B.[2], Akhmedov M. M.[3], Blondet M.[4]

[1]*Structures Lab and Center for Smart Infrastructure, University of California at Berkeley, Berkeley, USA*
[2]*Urgench State University, Urgench, Uzbekistan*
[3]*Miyamoto International Silk Road, Tashkent, Uzbekistan*
[4]*Gerdis Research Group, Pontifical Catholic University of Peru, Lima, Peru*
E-mail: takhirov@berkeley.edu

Abstract: *The paper focused on the structural health monitoring of Chadra Hauli, which is located in the Khorezm. As one of the first steps of the structural health monitoring project, a laser scanning project was conducted. This four-story building was scanned by a terrestrial laser scanner with surveying grade accuracy. As a result, an accurate digital twin of the monument was created. This heritage building represents a common construction method, the so-called pakhsa, that utilizes earthen materials (adobe). The analysis presented herein shows that walls are tapered, and the taper can be quantified for any location throughout the monument. In addition, it shows that there is significant sagging in both floors and ceilings of the building, which might be related to termite infestations. In the next phase of the project, the resonant frequencies of the building will be measured in ambient vibration tests. The performance of the numerical model under various loading will be investigated to develop strategies of its preservation.*

Keywords: *Chadra Hauly, laser scanning, structural assessment, pakhsa construction, earthen materials, adobe, structural health monitoring, preservation strategies.*

1. Introduction

Chadra Hauly (Chodira Hovli, Chandra Hauly, Chadra-Hauly) is a heritage building located about 15 km away from Khiva. It is located in the Khorezm region of Uzbekistan. Chadra Hauly used to be a country palace of Khivan khans in the 18th-19th centuries [1]; it was built on a site surrounded by orchards and far from the cities. An image from Google Maps presented in Fig 1 shows that it is still surrounded by orchards.

Figure 1. – **Google Maps view of the monument**

There are a few publications discussing its structural condition [2,3]. Since the information about the monument was very limited, this project was undertaken to obtain the geometry of the monument with high accuracy and to create a digital 3D twin of the monument that can be studied

in detail. This was achieved by utilizing laser scanning technology. A terrestrial laser scanner, Scan Station C10 [4], was used for the collection of the point clouds. The scans were conducted from 11 positions (the so-called stations), and both the interior and exterior of the building were laser scanned. All these scans were stitched in the Cyclone [5] and Matlab [6] software environments. The fully-stitched point cloud represents an accurate 3D twin of the monument that was studied in detail by means of Matlab [6].

2. Materials, methods, and object of study.

The monument is built as a four-story structure, as presented in Fig. 2. On the ground floor, there are two rooms of normal height, a warehouse, and a stable with a mud-brick staircase to the next level. The main entrance is located on the front side of the building (Fig. 2-left). There are two more entrances: on the left side (when facing the front) and on the rear side of the building. The entrances are not interconnected. The second and third floors are residential; they consist of one room with an open patio (the so-called ayvan). On the second floor, the ayvan is closed on the sides, and it is open on the front side. On the third floor, the van is open from the front and the side. Low-set windows are cut through all the walls of the room's buildings. Communication between the floors is carried out using ladders, through openings of the floors of the ayvans. On the fourth floor, two iwans are blocked, facing south and separated by a transverse partition (Fig. 2-right). A common wall closes them from the north. The foundation and the basement of the monument were built of fire-cured bricks. The walls represent a classic case of construction by utilizing earthen material, the so-called pakhsa. The beams supporting the floor and roof are wooden.

It is worth noting that laser scanning is a commonly used approach for documenting and preserving heritage structures [7-21], but it has never been used for this heritage monument.

Front Side

Figure 2. – **Ground-level views of the monument**

3. Point cloud collection.

As noted earlier, the point cloud collection was conducted from many stations. The project was conducted in the Summer of 2022. Fig. 3 presents a typical view of the point cloud from one of the stations. It shows the collected point cloud in two coloring schemes. In the left image, the points are colored by utilizing the images taken by a still imaging camera of the scanner. The scanning was conducted on a sunny day with sharp differences in color between the shadowed surfaces and surfaces directly exposed to the sun. Hence this image shows these variations of color. The image on the right side shows the same point clouds colored by the intensity of the returned laser beam.

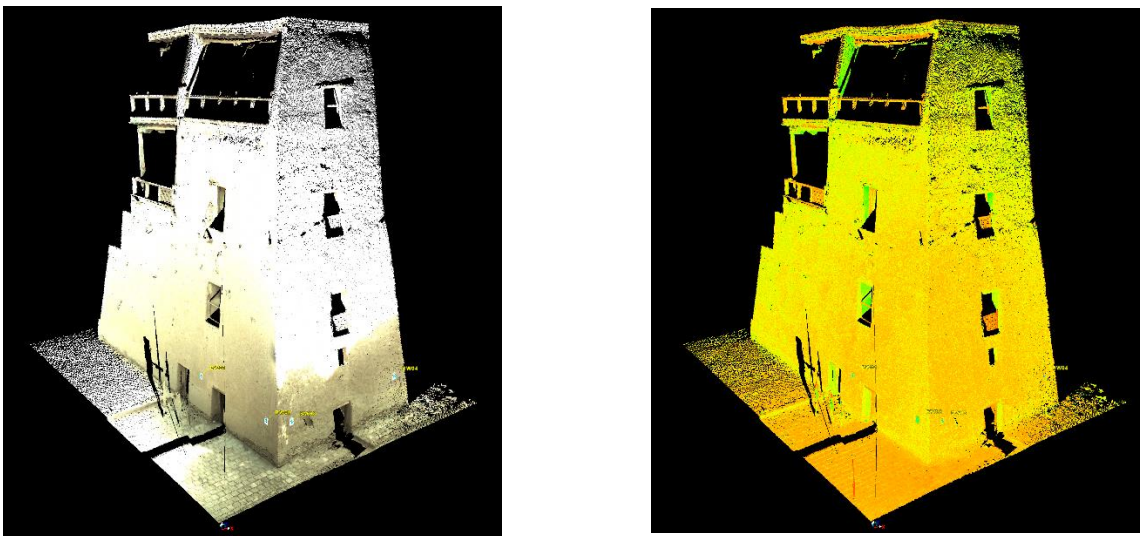

Natural colors Intensity of the returned laser beam

Figure 3. – **A typical point cloud in two coloring schemes (case of Station 1 is shown)**

The interior surface of the monument's third and fourth floors was stitched separately from the rest of it. The interior surface of the upper two levels consisted of about 40.5 billion points, and the point cloud of the rest consisted of about 31.2 billion points. Since the majority of the second point cloud was related to the exterior surface of the monument, it is called the "exterior point cloud" for the purpose of this paper. Both point clouds are presented in Fig. 4. These plots are generated in the Matlab environment, and the color changes based on the elevation from the reference horizontal plane.

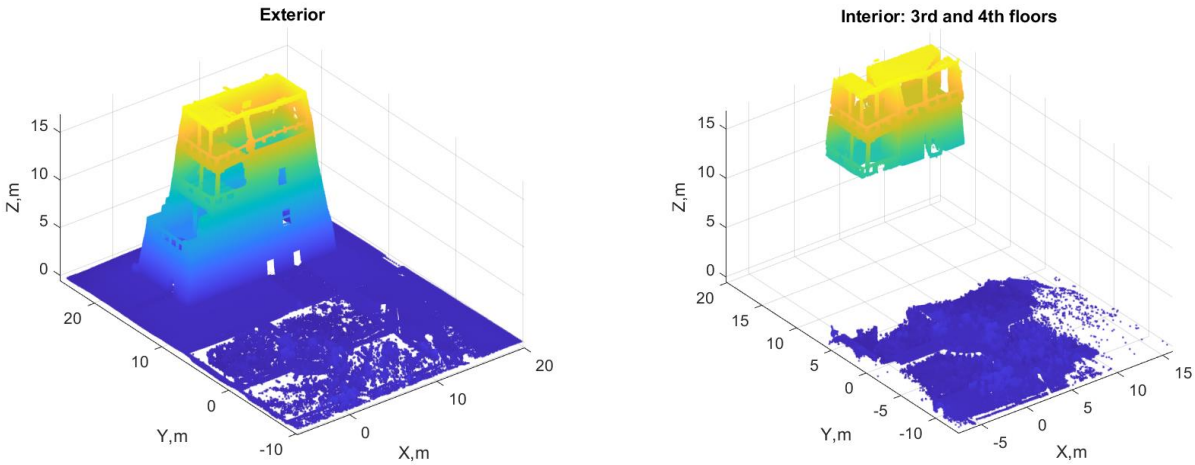

Exterior Interior of 3rd and 4th floors

Figure 4. – **Point cloud of exterior and interior surfaces**

This reference plane coincides with the top surface of the pool, which is shown in Fig. 5. The X-axis is oriented along the building, and the Y-axis is oriented in the traverse direction. As shown in Fig. 5, the origin of the coordinate system is selected on the right corner of the building, when looking from the front side.

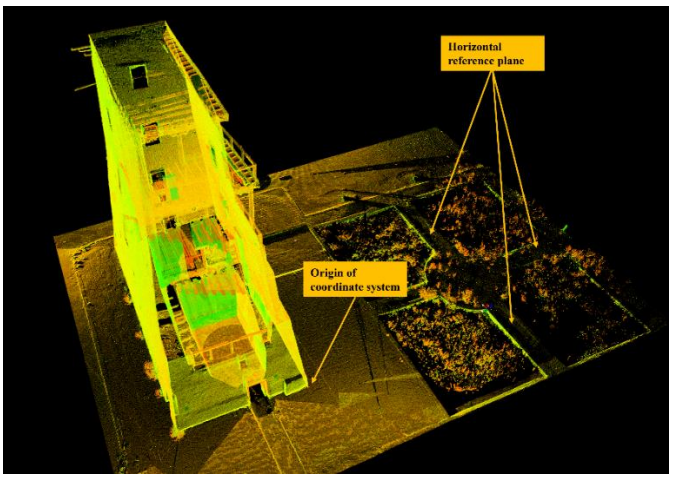

Figure 5. – **Point cloud with a paved pool on the right side where the coordinate system's reference plane is selected**

The final stitching of the exterior and interior surfaces of the upper two levels was conducted in the Matlab environment. It is provided in Fig. 6.

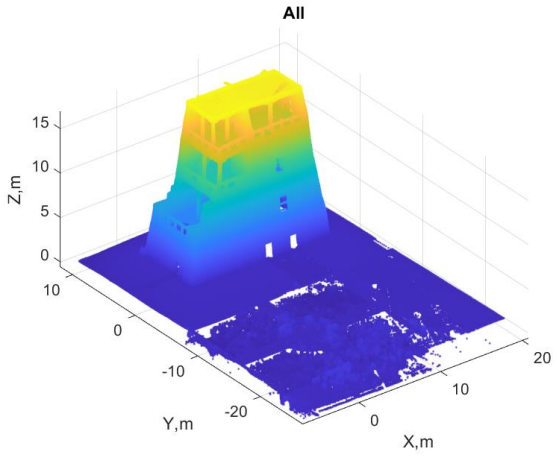

Figure 6. – **Fully-stitched point cloud**

4. Analysis of Obtained Data and Results

Plan views. The rest of the study is focused on the detailed investigation of the obtained digital twin of the monument. A few horizontal sections of the point cloud are investigated in the study, as presented in Fig. 7.

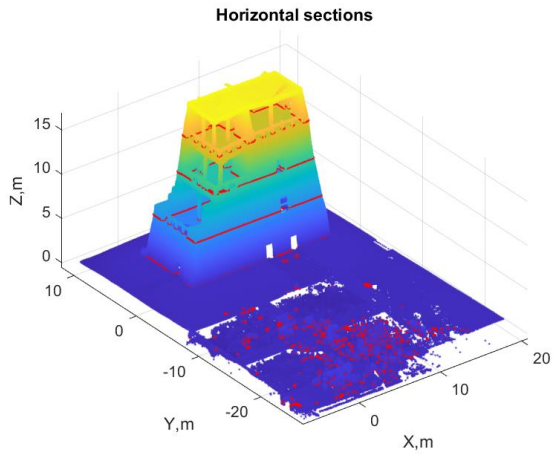

Figure 7. – **Horizontal sections of the point cloud**

Fig. 7 shows the plan view of the first floor at an elevation of 0.2 meters. The latter elevation corresponds to the elevation at which the building's surface meets the horizontal surface of the paved area around the building. As the plot shows, it has some imperfections, and the overall shape is close to a rectangular shape. It shows that the width of the building is very close to 8 meters, and the length of the building is very close to 17 meters.

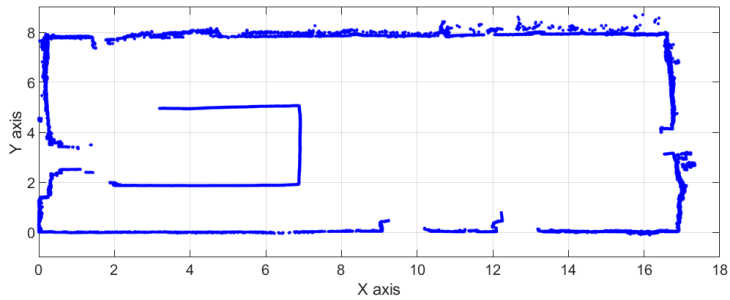

Figure 7. – **Plan view of the building at Z=0.2 m**

Fig. 8 presents the plan views of the building at elevations very close to the floor level of the second, third, and fourth floors. They are compared to the building's plan view at Z=0.2 m. As the plot shows, the overall size of the building's plan reduces when the elevation increases. It is worth noting that the overall shapes of the building's plan remain very close to the rectangular shapes.

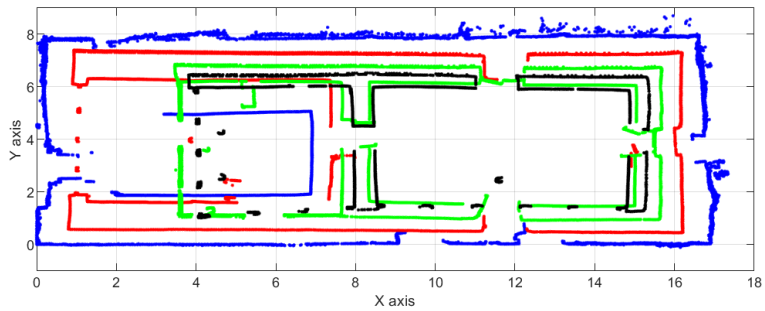

Figure 8. – **Plan view of the building at Z=13.2 m (black), Z=9.0 m (green), Z=4.8 m (red) compared to that at Z=0.2 m (blue)**

Sections by vertical plane across the length of the building. Two sections by a vertical plane at X=5 m and X=14 m were introduced to investigate the building's cross-sections. They correspond to the cross-sections of the front and rear portions of the buildings, respectively. The cross-section at X=5 m is presented in Fig. 9. It corresponds to the portion of the building where ayvans are located on the second, third, and fourth floors.

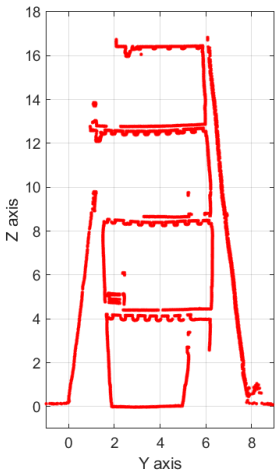

Cross-section in 2D

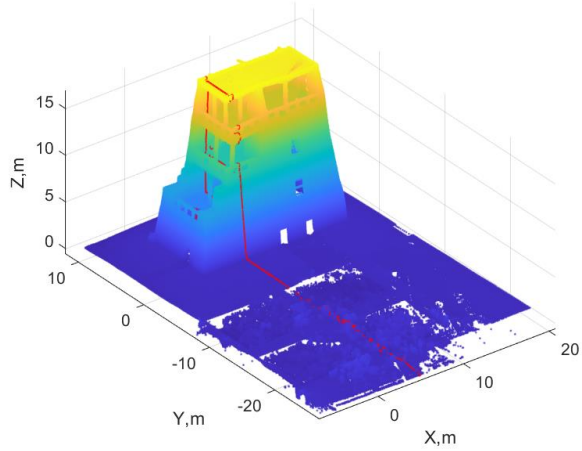

Cross-section in 3D

Figure 9. – **Cross-section of the building at X=5.0 m**

Fig. 10 presents the respective cross-section at X=14 m. Both cross-sections by the vertical planes clearly show that the exterior walls are tapered. In addition, they show that the taper is present only on the exterior surface of the walls so that the interior surface of the walls is close to vertical.

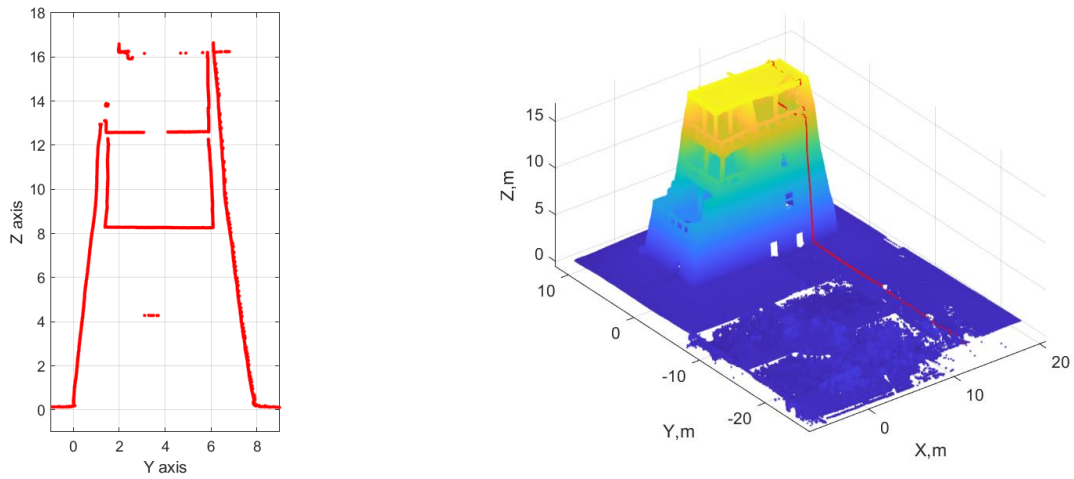

Cross-section in 2D Cross-section in 3D

Figure 10. – **Cross-section of the building at X=14.0 m**

Sections by vertical plane along the length of the building. Two sections by a vertical plane at Y=2.3 m and Y=5.8 m were introduced to investigate the building's cross-sections along its longitudinal direction. The section at Y=2.3 m is presented in Fig. 11. It clearly shows the taper in the rear wall of the building. Although the inner surfaces of the rear side of the building on the second and third floors were not captured, evidence of the taper in all walls is obvious. This cross-section also shows the staircase leading from the second floor to the third floor.

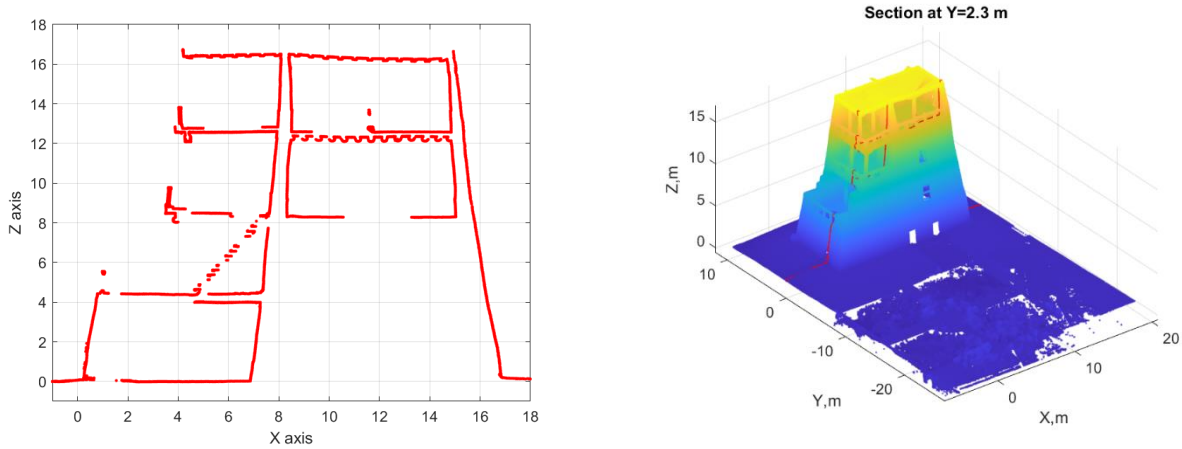

Cross-section in 2D Cross-section in 3D

Figure 11. – **Cross-section of the building at Y=2.3 m**

Fig. 12 presents the section at Y=5.8 m. It also clearly shows the taper in the rear wall of the building. Although the inner surfaces of the rear side of the building on the second and third floors were not captured, evidence of the taper in all walls is obvious. This cross-section also shows two staircases: the first one leading from the first floor to the second floor and the second staircase leading from the third floor to the fourth floor.

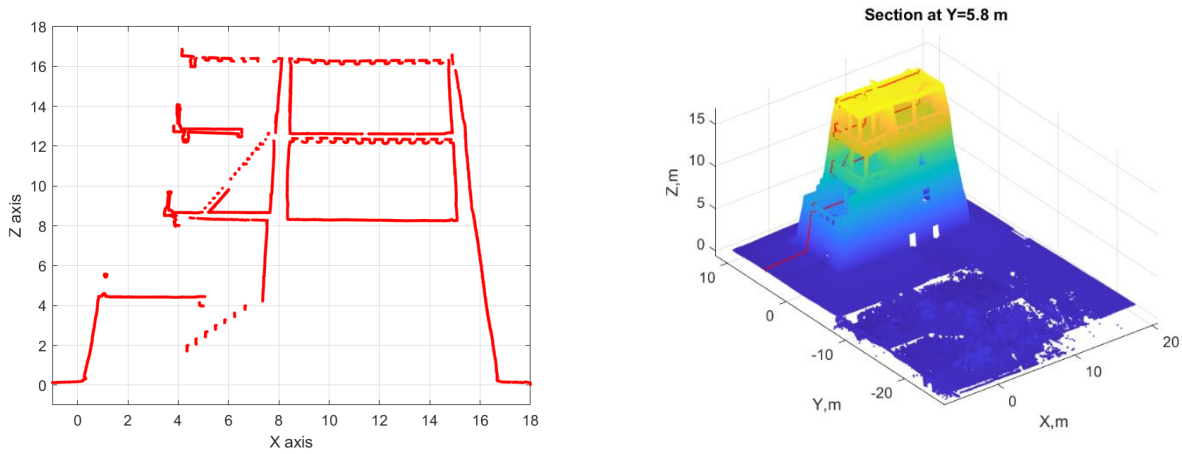

Cross-section in 2D

Cross-section in 3D

Figure 12. – **Cross-section of the building at Y=5.8 m**

Sagging of the ceilings and floors. Some significant sagging was observed in the ceiling of the building, as presented in Fig. 13. The plot shows sagging on the ceiling of the second and the third floors, which were extracted from the cross-section at X=5 m. As shown in the top plot, the sagging in the ceiling of the third floor was about 15 cm. The sagging in the ceiling of the second floor was estimated as 14 cm, as presented in the bottom plot of Fig. 13. The sagging of the floor surface is also evident but is not as significant as the ceilings. Nevertheless, it is quite large for the third floor and somewhat repeats the shape of the ceiling. It can be related to termite infestations of the lumber members supporting the floors. This shows that structural health monitoring of these members is needed for the preservation of this building.

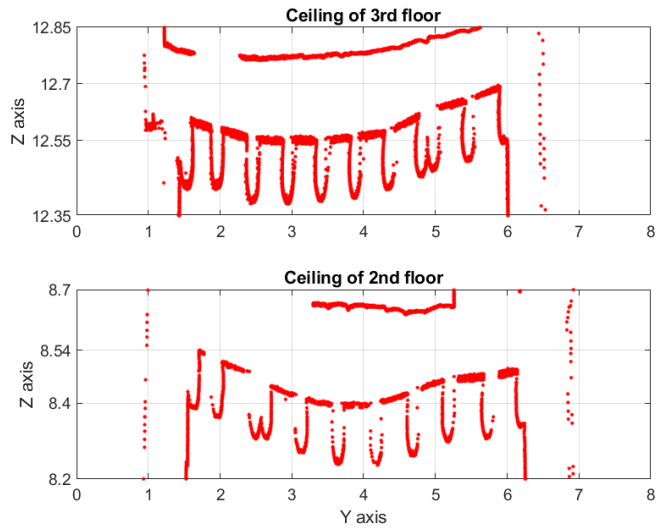

Figure 13. – **Sagging of the ceilings (X=5 m section)**

The taper of pakhsa walls. As observed from the cross-sectional views of the point cloud, the pakhsa walls have a tapered shape. In addition, the taper changes over elevation. An example of the taper estimation is presented in Fig. 14. A portion of the north wall was selected for that, and it was divided into two portions. The first portion (blue points in the right plot) represents the exterior wall for the third and fourth levels. The second portion (red points in the right plot) represents the exterior wall for the bottom two levels. A straight line best fitting each portion of the point cloud was obtained by utilizing the least square method. The inclination of the straight line represents an angle of the wall's taper. Two conclusions were drawn from these computations. First, the point clouds are very close to the straight line, which serves as evidence of the high quality of the ancient craftsmanship. Second, the taper's angle changes after the second level, and the wall has a smaller

taper for the third and fourth floors. For this exterior wall (at the selected cross-section), the difference between the taper angles is about 3 degrees, as shown in Fig. 14.

The same computation procedure can be used for other walls, and this portion of the work is ongoing.

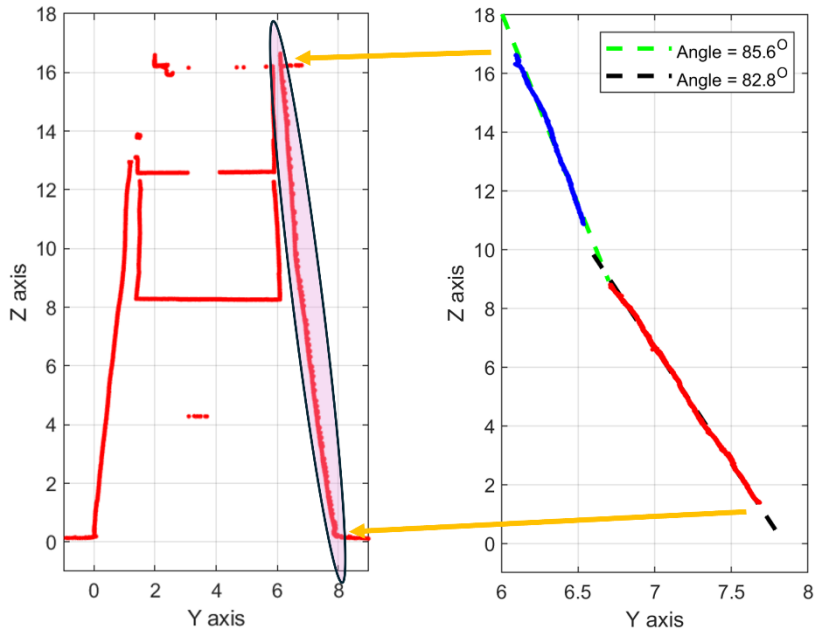

Figure 14. – **Example of taper estimation**

5. Conclusions

The paper focused on laser scanning on the heritage building, which represents a common construction method, the so-called pasha, that utilizes earthen materials. This four-story building was scanned by a terrestrial laser scanner with surveying grade accuracy. As a result, an accurate digital twin of the monument was created. The paper shows only a few examples of the very detailed investigation work that is ongoing. The analysis presented herein shows that walls are tapered, and the taper can be quantified for any location throughout the monument. Two conclusions were drawn from the taper computations of a portion of the exterior wall. First, the slices of point clouds are very close to the straight line, which serves as evidence of the high quality of the ancient craftsmanship. Second, the taper's angle changes after the second level, and the wall has a smaller taper for the third and fourth floors. For this exterior wall, the difference between the taper angles is about 3 degrees. In addition, it shows that there is significant sagging in both floors and ceilings of the building, which is a result of termite infestations. In the next phase of the project, the resonant frequencies of the building will be measured in ambient vibration tests. Based on the collected point clouds and the resonant frequencies, a numerical model of the building will be generated. The performance of the numerical model under various loading will be investigated to develop strategies of its preservation. Frequent laser scanning would be one of the most valuable options (similar to [17]) for monitoring the deterioration of the building under the effects of environmental conditions.

6. Acknowledgements

The authors would like to acknowledge the Urgench State University (Urgench, Uzbekistan) for sponsoring the project. Special thanks are due to Sigma Innovative Tech, Tashkent, Uzbekistan, for providing technical help during the laser scanning activities.

References

1. *Mankovskaya L., Bulatova V.* Monuments of Khorezm architecture. Tashkent, 1978. (In Russian: Маньковская Л., Булатова В. Памятники зодчество Хорезма. – Ташкент, 1978).
2. *Azizova B.* Architectural longevity-in the case of the summer palace Chandra-Hauly in Khiva city, Uzbekistan. MOJ Civil Eng. 2017;2(5):158-160. DOI: 10.15406/mojce.2017.02.00045.
3. *Б.С.Рахмонов, И.М.Хаджиев, К.А.Курьязов, М.М.Жуманиязов.* Изучение технического состояния строительных конструкций памятников Чадра-Хавли города Хивы. Международный сборник научных трудов «Материалы и изделия для ремонта и строительства», 2006. С. 126–128.
4. *Leica Geosystems AG*. Leica ScanStation C10. 2011. Available online: https://w3.leicageosystems.com/downloads123/hds/hds/ScanStation%20C10/brochuresdatasheet/Leica_ScanStation_C10_DS_en.pdf (accessed on 19 October 2021).
5. *Leica Geosystems AG*. Cyclone Version 2022.1.0; 2022.
6. MathWorks. Matlab Version R2020a; 2020.
7. *Remondino, F*. Heritage Recording and 3D Modeling with Photogrammetry and 3D Scanning // Remote Sens. 2011, vol. 3, pp. 1104–1138.
8. *Kęsik, J.; Miłosz, M.; Montusiewicz, J.; Samarov, K.* Documenting the geometry of large architectural monuments using 3D scanning—The case of the dome of the Golden Mosque of the Tillya-Kori Madrasah in Samarkand // Digit. Appl. Archaeol. Cult. Herit. 2021, vol. 22, e00199.
9. *Takhirov, S.; Rakhmonov, B.; Nafasov, R.; Samandarov, A.; Sultanova, S.* Laser Scanning and Ambient Vibration Study of Juma Mosque in Khiva (Uzbekistan) with Subsequent Finite Element Modeling of Its Minaret // Remote Sensing. 2023, vol. 15 No. 6:1632. https://doi.org/10.3390/rs15061632.
10. *Takhirov, S.; Rakhmonov, B.; Nafasov, R.; Samandarov, A.; Sultanova, S.; Musurmanov, J.; Takhirov, B.* Structural health monitoring of Juma Mosque in Itchan Kala, Uzbekistan by laser scanning. In Proceedings of the International Conference on Structural Health Monitoring of Intelligent Infrastructure: Transferring Research into Practice, SHMII, Porto, Portugal, 30 June – 02 July 2021 (ISSN 2564-3738); pp. 1331–1337.
11. *Takhirov, S.; Rakhmonov, B.* Structural Health Monitoring of the Juma Mosque in Itchan Kala in Khiva (Uzbekistan): Laser Scanning Combined with Numerical Modelling. In Proceedings of the 12th International Conference on Structural Analysis of Historical Constructions SAHC, 2020; Roca, P., Pelà, L., Molins, C., Eds.; pp. 3361–3370. https://doi.org/10.23967/sahc.2021.266.
12. *Takhirov, S.M.; Aripov, I.; Matrasulov, D.* Real-time Structural Monitoring of Bibi-Khanum in Samarkand (Uzbekistan) Combined with Subsequent Laser Scans. In Proceedings of the 12th International Conference on Structural Analysis of Historical Constructions SAHC, 2020; Roca, P., Pelà, L., Molins, C., Eds.; pp. 3339–3348.
13. *Takhirov, S. et al.* First Step Toward Preservation of Ancient Toprak Qala in Uzbekistan: Estimation of Erosion and Deterioration Rates by Laser Scanning. In: Endo, Y., Hanazato, T. (eds) Structural Analysis of Historical Constructions. SAHC 2023. RILEM Bookseries, vol 47. Springer, Cham. https://doi.org/10.1007/978-3-031-39603-8_47.
14. *Barton, J.* '3D laser scanning and the conservation of earthen architecture: a case study at the UNESCO World Heritage Site Merv, Turkmenistan' // World Archaeology, 2009, vol. 41 No. 3, pp. 489–504.
15. *Campiani, A.; Lingle, A.; Lercari, N.* Spatial analysis and heritage conservation: Leveraging 3-D data and GIS for monitoring earthen architecture // Journal of Cultural Heritage. 2019, vol. 39, pp. 166-176.
16. *Magnani, M.; Schroder, W.* New approaches to modeling the volume of earthen archaeological features: A case-study from the Hopewell culture mounds // Journal of Archaeological Science, volume 64, 2015, pp. 12-21.
17. *Guo, Z.; Qi, Q.; Zhang, S.; Chen, W.; Wu, C.; Wu, H.* Study on the characterization of differential weathering feature based on surface roughness theory and 3D laser scanning: A case study of the Suoyang Ancient City // Journal of Cultural Heritage, vol. 62, 2023, pp. 449-459.
18. *Fanti, R.; Gigli, G.; Lombardi, L.; Tapete, D.; Canuti, P.* Terrestrial laser scanning for rockfall stability analysis in the cultural heritage site of Pitigliano (Italy) // Landslides, 2013, vol. 10, pp.409-420
19. *Richards, J.; Zhao, G.; Zhang, H.; Viles, H.* A controlled field experiment to investigate the deterioration of earthen heritage by wind and rain // Heritage Science, 2019, vol.7, No. 1.
20. Ikpere, J. A. (2021). Identification and Quantification of the Degradation of Historic Earthen'cob'Structures in Hampshire, United Kingdom, Using a Novel Spray Test Method Incorporating 3-D Laser Scanning / Doctoral dissertation, University of Portsmouth.
21. *Chevance, J.-B.; Evans, D.; Hofer, N.; Sakhoeun, S., Mahendraparvata, C.R.* An early Angkor-period capital defined through airborne laser scanning at Phnom Kulen // Antiquity; 2019. 93(371):1303-1321.

TEMPERATURE MONITORING OF PAVEMENT LAYERS FOR PERFORMANCE IMPROVEMENTS OF AUTOMOTIVE ROADS.

Takhirov Sh.[1], Zakhidov A.[2], Aitbayev K.[3], Nugmanova A.[4]

[1]*Structures Lab and Center for Smart Infrastructure, University of California at Berkeley, Berkeley, California, USA*
[2] *University of Texas at Dallas, Dallas, Texas, USA*
[3] *Kazakh Automobile and Roads Institute, Almaty, Kazakhstan*
[4] *JSC Kazakhstan Highway Research Institute (KazDorNII), Astana, Kazakhstan*
E-mail: takhirov@berkeley.edu

Abstract: *The paper is focused on a detailed analysis of the dataset recorded at one of the 28 monitoring stations in Kazakhstan. Although the dataset contains data for both summer and winter times, a more detailed discussion is provided for summertime measurements. The temperature changes in the pavement and the roadbed were compared to the daily average. It was shown that the temperature changes in the top layers have a cyclicity with a period of about 24 hours. Opposite to that, the temperature changes in the lower layers are controlled by seasonal temperatures with much longer periods. The phase shift between the cyclic temperature changes in the top layers is discussed. The results of the analysis will be used in the future development of the numerical model so the future performance of the road can be predicted.*

Keywords: *roadbed, pavement, automotive roads, embedded temperature sensors, real-time monitoring.*

1. Introduction

The integrity of automotive roads is very important for the economic development and growth of any country [1-3]. The roads should be able to withstand harsh environmental conditions and remain functional to provide passage for trucks and cars without causing dangerous situations leading to monetary losses or fatalities. It is quite challenging to achieve, especially now when global warming results in even more demanding weather conditions. To set priority for maintenance, repair, or replacement, new modern means are needed. Therefore, many countries are looking into the possibility of remote monitoring of the road condition [4-9]. The monitoring can be done on demand by traveling to the site (after a large catastrophic event, for example) or by conducting real-time monitoring of the roads. The latter approach produces much more information that can be used for detailed modeling of the roads and to predict their performance in the future (see [10-13] as representative examples). In addition, it can be used for monitoring how new materials or improvements in the road design (see [14,15] as representative examples) are affecting the performance of the roads. It is envisioned to become a valuable part of the continuous monitoring by other modern means, with a few of them described in [16].

2. Materials, methods, and object of study.

Based on the information from the Bureau of National Statistics, Kazakhstan has a large network of automotive roads with a total length of 94,781 km in 2022 [17]. The total length is more than two times greater than that in the neighboring Uzbekistan which is 42,900 km – as of January 1, 2022 [18]. Although the total length of the roads is greater in Kazakhstan, there is a big difference between the total land areas of these two countries: 2,724,900 km^2 in Kazakhstan and 448,978 km^2 in Uzbekistan [19]. Therefore, the road length to 100 km^2 land area ratio is about 3.48 km^{-1} for Kazakhstan, which is more than three times less than the same ratio for Uzbekistan, 10.91 km^{-1}. This dramatic difference shows the challenges of Kazakhstan, which are related to the maintenance of the roads located in the vast land of the country. On top of that, the population of Kazakhstan is close to 53% of that of Uzbekistan [19], so the roads distributed over much larger land need to be serviced and maintained by fewer people. Therefore, there is a strong need for new modern means of monitoring the condition of the roads.

As one of the steps in addressing the challenges described above, a few automotive roads are instrumented in Kazakhstan, with a total of 28 stations [9]. The monitoring instrumentation consists of two groups aimed at measuring two parameters of the roadbed: the temperature and the moisture content of the road's layers [9]. In the first group, the temperature sensors are installed at different elevations, and a reference temperature gauge monitoring air temperature is installed above the surface near the road. In the second group, moisture content sensors are installed at various elevations, and a reference sensor monitoring the air humidity above the ground is installed near the

road. This paper is focused on the analysis of the data collected from the first group. An example of an instrumented station near Kostanay (Kazakhstan) is discussed herein. Based on Wikipedia [20], Kostanay is located in an area with a warm-summer humid continental climate. As a result, very warm, dry summers and frigid, snowy winters are very common here. The average July temperature is 20.9 °C, and the respective average temperature in January is −14.5 °C [20], although sharp changes in temperature during the day are quite common. The average wind speed is 12 km/h, mainly from the south in winter and from the north in summer [20]. Precipitation averages around 335 millimeters, with a maximum in summertime. The average annual humidity is 71 percent [20].

It is worth noting that because of the challenging climate conditions, the sensors must remain functional in very rough environmental conditions, including the effects of heavy snow and rain, relatively high winds, and a large temperature variation from very warm to very cold, which is significantly below freezing temperatures. As shown in [9] and in this study, the sensors and the data acquisition system were able to overcome these challenges and deliver high-quality data.

3. Problem statement.

At the station described above, temperature changes in the layers of the road pavement structure and points of the roadbed have been monitored since 2021. Figure 1 shows a photo of the external reference measuring node, the design of the road surface, and the depth of the sensors under the road surface. Table 1 provides details of the road payment design. Table 2 shows the depth of each sensor's location. A dataset smaller than the one researched in [9] was selected for this study. The main purpose of this study is to understand the physical mechanism of the heat transfer that will be used for future modeling.

(a) (b)

Figure 1. – **Monitoring station on the section near Kostanay: (a) a photo of the external measuring station; (b) sensor location diagram in the layers of the road pavement [9]**

Table 1.

Pavement design and materials [9]

Layer Number	Material	Layer thickness
1	Asphalt concrete, type B	h_1=5 см
2	Coarse porous asphalt concrete	h_2=13 см
3	Coarse-grained and highly porous asphalt concrete	h_3=9 см
4	Mixture C-4	h_4=35 см
5	Soil sand	h_5=90 см
6	Black soil (chernozem)	h_6=148 см

Table 2.

Sensor locations (measured from the top of the road surface down)

Notations	y_1	y_2	y_3	y_4	y_5	y_6	y_7	y_8	y_9	y_{10}
Value, cm	3	11	22	45	78	111	145	180	240	300

4. Results

The dataset contains the periodic temperature measurements from November 1, 2021, to May 15, 2022. The sampling rate was one record per hour. Each record consists of data from 11 temperature sensors listed in Table 2 and a reference temperature gauge monitoring air temperature. Figure 2 shows the graph of the air temperature change for the whole dataset. It also shows the moving average calculated for 24 samples, which represents a daily moving average.

The coldest period in this dataset corresponds to the end of December 2021, as presented in Figure 3. The coldest temperature of -31.0^{O} C was recorded on December 26, 2021, at 7:58. In the next 39 hours, there was a quick warm-up that resulted in a rapid increase of the air temperature to -6.4^{O} C at 22:58 on the following day. After this, the air temperature started to go down again. This example shows how rapidly the air temperature can change. In this particular case, the temperature difference between the pick and valley was close to 25 degrees Celsius.

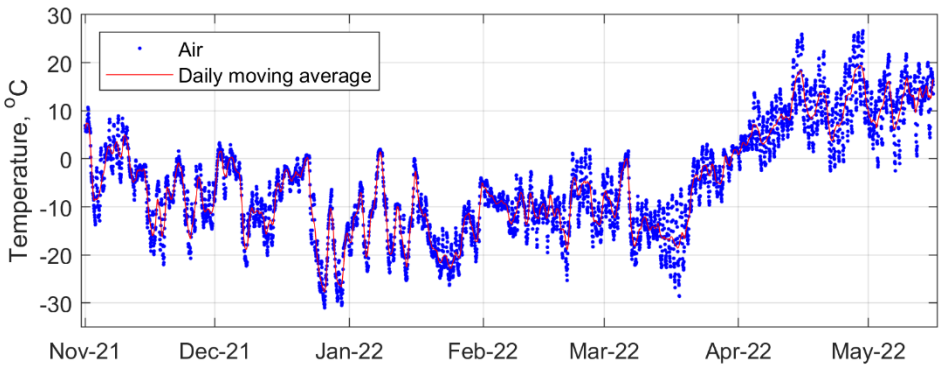

Figure 2. – **Air temperature collected every hour and daily moving average for the duration of the dataset**

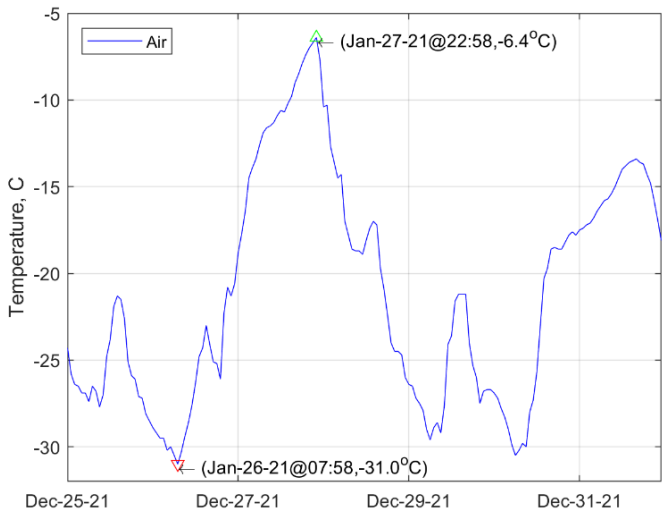

Figure 3. – **The coldest air temperature in the dataset**

Figure 4 shows the results for the warmest temperature in the dataset. As the plot shows, the warmest air temperature in the dataset, 26.6^{O} C, was recorded on April 22, 2022, at 17:58. By the morning of the following day, the air temperature dropped to 7.6^{O} C at 5:58, which corresponds to a 12-hour difference. Therefore, the plot also shows regular cyclic variations of the air temperature with a period of one day (24 hours). Based on these data, the spring air temperature can vary by about 20 degrees Celsius between the daytime and nighttime temperatures.

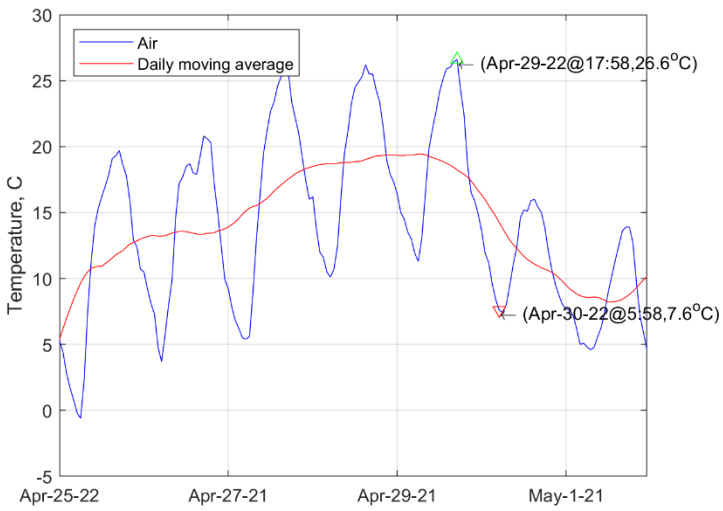

Figure 4. – **The warmest air temperature in the dataset**

As is known, air temperature is only one of many controlling parameters that affect the temperature of the pavement's surface. Wind, rain, snow, and other environmental effects can also affect it. Therefore, as presented in Figure 5a, there is a large difference between the air temperature and the temperature of the pavement's top layer.

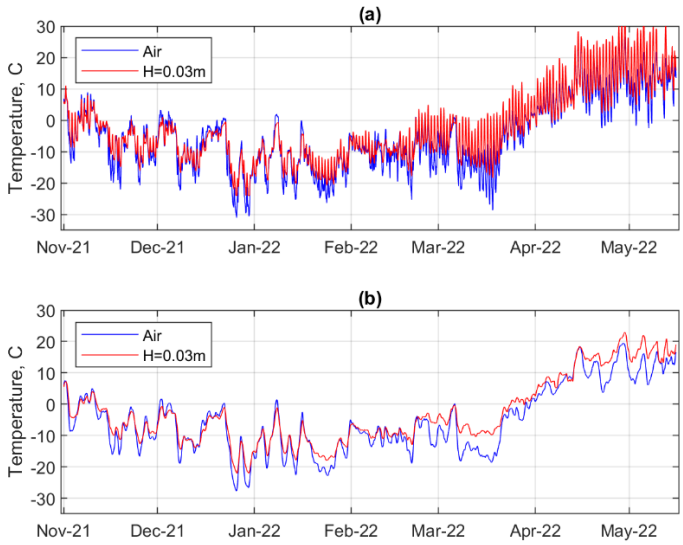

Figure 5. – **The difference between the air temperature and the temperature of the top layer**

The plot in Figure 5a shows that, in general, the top layer of the pavement has greater temperatures than the air above the road. It is more obvious when daily averages are compared, as shown in Figure 5b. On warmer days (starting from the end of February 2001 for this dataset), the air temperature of the top layer of the pavement is greater than the air above the road. On warmer days, it is much greater than the air temperature. This can be related to the much greater capacity of the top layer to store thermal energy.

It is worth noting that the temperature of the air and the top layer varies with the same frequency while there is a small phase shift in the cycles of the top layer, as presented in a typical plot for a small subset of the data in Figure 6. The period of these cycles is very close to 24 hours. The phase shift is related to the slower temperature response of the top layer to the temperature changes in the air.

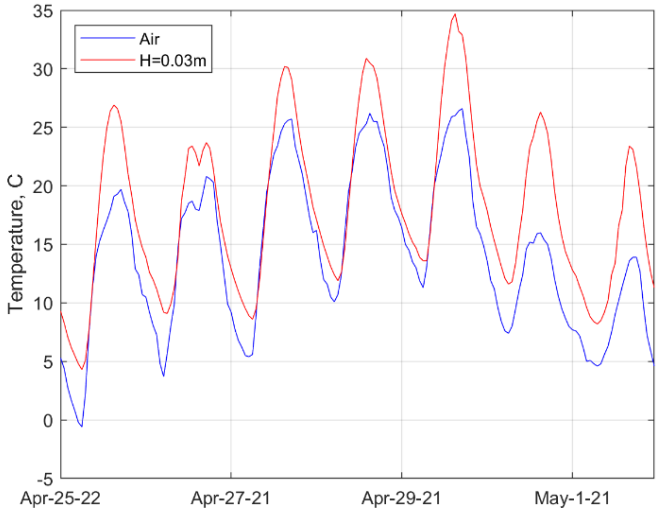

Figure 6. – **Cyclicity of air and top layer temperatures**

The rest of the discussion is based on how the heat transfers downward and upwards and, as such, the temperature of the top layer compared to that of the lower layers. The temperature for the top, the second, and the third layers from the top are presented in Figure 7.

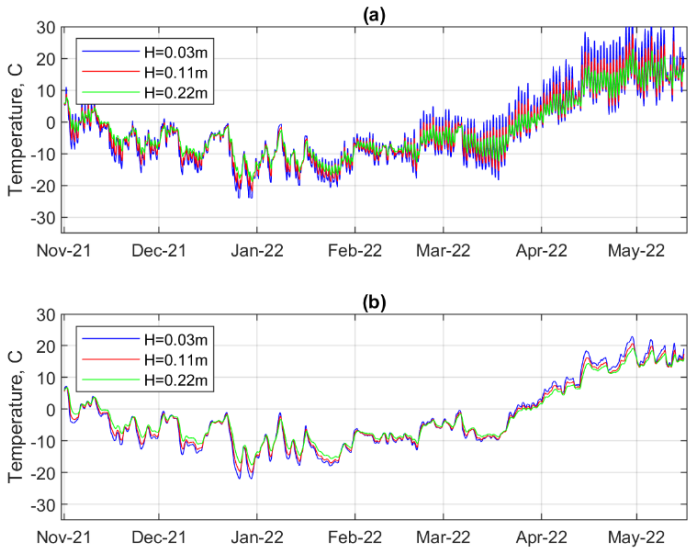

Figure 7. – **Temperature at sensors installed at three top elevations of the pavement**

As presented in Figure 7a, the temperature variability decreases with depth. Figure 7b shows the daily averages for the same sensors. In general, the temperature of the third layer is greater in winter and lower in summer when compared to the two others.

Figure 8 presents a small subset representing springtime temperature changes. It shows the same trend of similar temperature cyclicity between the layers, but it also shows that the cycling period is increasing with depth, in addition to the phase shift that was observed earlier between the air and the top layer.

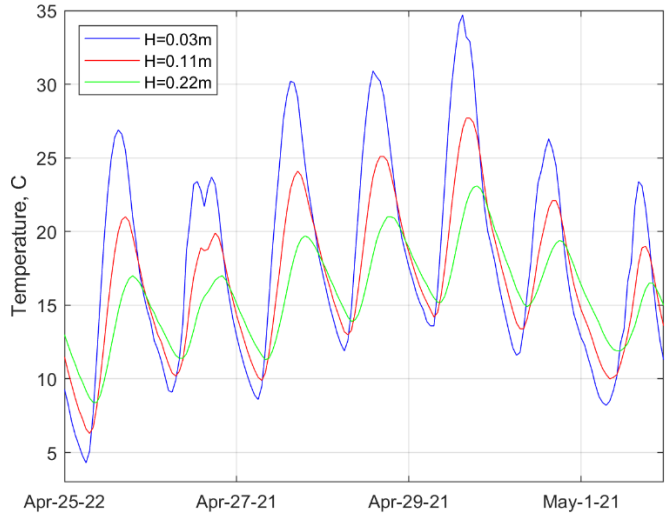

Figure 8. – **Temperature cycles for top three layers: spring**

Figure 9 presents the plot showing the temperature for all layers, starting from layer four. It shows that the fourth layer is the last layer (at a depth of 0.48 m) to be sensitive to daily temperature changes.

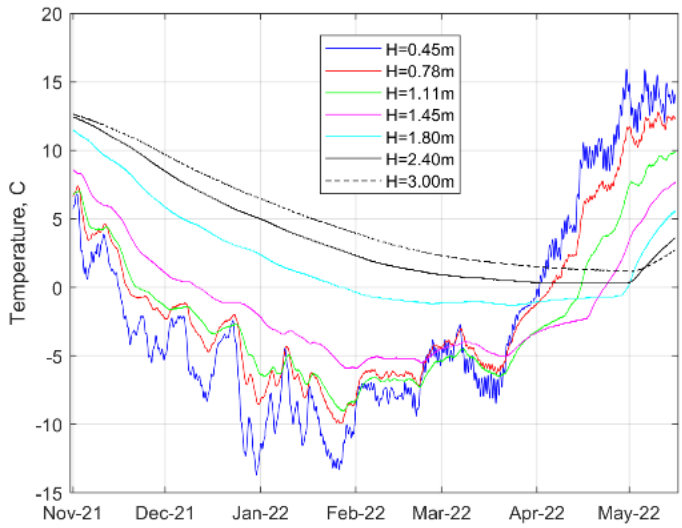

Figure 9. – **Temperature cycles for all other layers starting from number four.**

The plot shows that freezing temperatures can never reach a depth of 2.4 m. In addition, seasonal temperature changes mainly control all layers starting from 1.45 m.

Figure 10 presents a small subset representing springtime temperature changes. It confirms the previous results that there is the same trend of similar temperature cyclicity between the layers, but it also shows that the cycling period is increasing with depth, in addition to the phase shift that was observed earlier between the air and the top three layers.

Figure 11 presents temperatures for 15 days. The hourly changes were modified by subtracting the respective daily temperature changes for each layer, including the air temperature. The resultant temperatures are called relative temperatures in this paper. The relative temperatures for the top four layers and the air are shown in Figure 11. As presented in this plot, an almost perfect periodicity can be observed for all layers. The reduction of the amplitude and phase shift over the depth is more obvious in this plot.

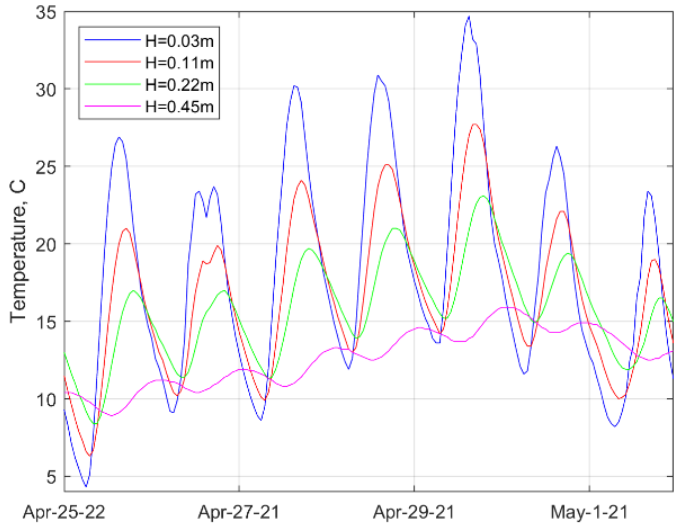

Figure 10. – **Spring temperatures for the top four layers and the air (7 days).**

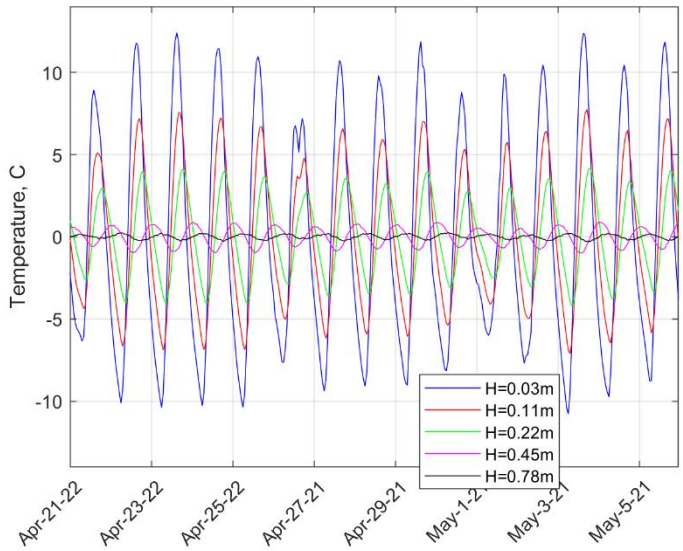

Figure 11. – **Spring temperatures for the top five layers and the air with a daily average removed (15 days).**

5. Conclusions

The following conclusions were drawn from the discussion of the dataset of temperatures for the Kostanay monitoring station:

1. In general, the temperature of the third layer at a depth of 0.22 m is greater in winter and lower in summer than that of the other two closer to the surface.
2. Up to a depth of 0.45 m, it was observed that there is a trend of similar temperature cyclicity between the layers (with an air temperature period of 24 hours), although the cycling period is increasing with depth, in addition to the phase shift and amplitude decrease.
3. Freezing temperatures can never reach a depth of 2.4 m. In addition, seasonal temperature changes mainly control all layers starting from 1.45 m.
4. When daily averages are removed, the temperature variations are very close to periodic temperature changes, with the amplitude reducing over the depth.

6. Acknowledgements

The author would like to acknowledge the management of the Kazakhstan Road Research Institute (Kazakhstan) for providing access to the dataset used in the study. Special thanks are due to Sensor Fusion and Monitoring Technologies, LLC (USA) for partially sponsoring the analysis of the provided dataset.

References

1. *Solodky A.* Organizational and economic basis for the formation of the road network in the context of regional development. Prob. Mod. Econ. 2007; 4, pp. 278–281.
2. *Cantos P., Gumbau-Albert M., Maudos J.* Transport infrastructures, spillover effects and regional growth: Evidence of the Spanish case. Transp. Rev. 2005;25:25–50. doi: 10.1080/014416410001676852.
3. *Calderón C., Servén L.* The Effects of Infrastructure Development on Growth and Income Distribution. World Bank Publications; Washington, DC, USA: 2004. Number 270.
4. *Silveira E., Bonho S.* Temperature Monitoring Through Wireless Sensor Network Using an 802.15. 4/802.11 Gateway; Proceedings of the 4th IFAC Symposium on Telematics Applications TA 2016; Porto Alwegre, Brasil. 6–9 November 2016.
5. *Corej, J., Korenko, M., & Remisova, E.* (2004). Climatic characteristics and the temperature regime of asphalt pavements. Communications - Scientific Letters of the University of Zilina, 6(3), 31-36. doi: 10.26552/com.C.2004.3.31-36.
6. *Wang X., Zhao J., Zhang C., Lu H.* Design and implementation of wireless sensor monitoring system for temperature and humidity based on ZigBee. Int. J. Circuits Syst. Signal Process. 2016;10:414–419.
7. *Fernández-Lozano J., Martín-Guzmán M., Martín-Ávila J., García-Cerezo A.* A wireless sensor network for urban traffic characterization and trend monitoring. Sensors. 2015;15:26143–26169. doi: 10.3390/s151026143.
8. *Godoy J., Milanés V., Pérez J., Villagrá J., Onieva E.* An auxiliary V2I network for road transport and dynamic environments. Transp. Res. Part C Emerg. Technol. 2013;37:145–156. doi: 10.1016/j.trc.2013.09.012.
9. *Teltayev B, Oliviero Rossi C, Aitbayev K, Suppes E, Yelshibayev A, Nugmanova A.* Freezing and Thawing Processes of Highways in Kazakhstan. Applied Sciences. 2022; 12(23):11938. https://doi.org/10.3390/app122311938.
10. *Lukanen E.O., Stubstad R., Briggs R.* Temperature Predictions and Adjustment Factors for Asphalt Pavement. Federal Highway Administration; Washington, DC, USA: 2000. Technical Report.
11. *Yumei Hu, Esben Almkvist, Torbjörn Gustavsson, and Jörgen Bogren* (2019). Modeling Road Surface Temperature from Air Temperature and Geographical Parameters—Implication for the Application of Floating Car Data in a Road Weather Forecast Model. Journal of Applied Meteorology and Climatology.01 May 2019, pp. 1023-1038. DOI:https://doi.org/10.1175/JAMC-D-18-0145.1.
12. *Hu, Y., Almkvist, E., Gustavsson, T. and Bogren, J.* (2019). Modeling Road Surface Temperature from Air Temperature and Geographical Parameters—Implication for the Application of Floating Car Data in a Road Weather Forecast Model. Journal of Applied Meteorology and Climatology 58(5) pp. 1023-1038.
13. *Arian Asefzadeh, Leila Hashemian, Alireza Bayat* (2017). Development of statistical temperature prediction models for a test road in Edmonton, Alberta, Canada. International Journal of Pavement Research and Technology, Volume 10, Issue 5, 2017, pp. 369-382, ISSN 1996-6814, https://doi.org/10.1016/j.ijprt.2017.05.004.
14. *Fei Pan, Jianzhong Pei, Gewei Zhang, Yong Wen, Jiupeng Zhang, Rui Li,* (2022). Building the cooling roads with high thermal conductivity pavements to relieve urban heat island effect, Construction and Building Materials, Volume 346, 2022, 128276, ISSN 0950-0618, https://doi.org/10.1016/j.conbuildmat.2022.128276.
15. *Jian Wei, Dongming Gao, Yuan Wang, Xueting Li, Yupeng Guo, Yi Yao* (2023). Extremely high thermal conductive cement-based composites with diamond/ZnO/expanded graphite thermal conductivity network for cooling road. Construction and Building Materials. Volume 393, 2023, 131968, ISSN 0950-0618, https://doi.org/10.1016/j.conbuildmat.2023.131968.
16. *Takhirov, S., Nugmanova, A., Koshimkhanov, D.* 2023. Application of Multi-Sensor Road Feature Detection and Mapping in Kazakhstan and Development of Pole Detection and Analysis Procedure. Proceedings of ISAS 2023 - 7th International Symposium on Innovative Approaches in Smart Technologies. 23-25 November 2023, ISG Airport Hotel, Istanbul, Turkey.
17. https://stat.gov.kz/upload/iblock/368/a6bkq09o57ao0vuo3myn2qo6z6e0ivd0/Length%20of%20roads.xls?sphrase_id=357546 (last accessed on 04/06/2024).
18. https://daryo.uz/en/2022/12/22/uzbekistan-ranks-4th-among-cis-member-states-in-terms-of-roads-length-in-2022 (last accessed on 04/06/2024).
19. https://en.wikipedia.org/wiki/Central_Asia (last accessed on 04/06/2024).
20. https://en.wikipedia.org/wiki/Kostanay (last accessed on 03/29/2024).

CENTER FOR SMART INFRASTRUCTURE: A COMPREHENSIVE APPROACH FOR WATER INFRASTRUCTURE MONITORING AND PRESERVATION BY TESTING AND MODELING.

Takhirov Sh[1], Soga Kenichi [1], Katzev D.[2]

[1]Structures Lab and Center for Smart Infrastructure, University of California at Berkeley, Berkeley, USA
[2] East Bay Municipal Utility District, Oakland, USA
E-mail: takhirov@berkeley.edu

Abstract: *The preservation of existing infrastructure and the construction of more resilient future infrastructure are two of the main engineering challenges we need to overcome while dealing with shrinking resources worldwide. In addition, global warming imposes new challenges by increasing the demand for structures or changing them in very different ways. One viable and cost-effective way to achieve this goal is to integrate a variety of sensors into infrastructure to monitor their performance over time and provide a new tool for stakeholders in their decision-making process. Real-time or on-demand monitoring turns an object into part of a large interconnected digital system, a smart infrastructure. This paper describes the newly developed experimental capabilities at the Center for Smart Infrastructure (CSI), which was recently established at the University of California, Berkeley. These unique testing capabilities are combined with advanced monitoring and infrastructure modeling. This paper is focused on highlighting CSI's testing capabilities.*

Keywords: *water pipeline, joint performance, experimental study, water industry.*

1. Introduction

The consequences of global warming significantly affect our daily lives. Water resources are shrinking throughout the world, and preservation of this priceless commodity is becoming more important. As a representative example, water reservoirs supplying water to the region of Central Asia have been half-full for many years [1]. As a result, the water dams experience loading conditions quite different from the ones they were designed for. In addition, because of the age of the water infrastructure, the term "infrastructure fatigue" was mentioned in the discussion of the water resources of Central Asia [2]. This falls in line with the main vision of the Center for Smart Infrastructure (CSI) at the University of California, Berkeley (USA). It is aimed at monitoring infrastructure components and systems, developing numerical models based on experimental studies and field data, and predicting infrastructure performance [3]. The main objective is to prolong the life of both existing and upcoming infrastructure and address both aging or performance issues in a timely manner based on the monitoring data and numerical simulations at the system level.

2. Materials, methods, and object of study.

The main vision behind the development of the Center for Smart Infrastructure (CSI) at the University of California, Berkeley, is to find ways to extend the lifeline of the infrastructure. It starts by investigating the performance of its components in situ under real loading conditions and in experimental studies in the laboratory environment. Both these investigations complement each other because the data collected during the tests can help explain the data collected from the in-situ measurements. This paper mainly focuses on the experimental methods and test machines that are used to collect this valuable information.

3. Problem statement.

Pipelines can be subject to various loads. First, the soil surrounding the pipe tends to settle over time. In many cases, the demand imposed on a pipeline by the soil settlement can be quite large, requiring the pipeline to withstand a large vertical deflection of a few meters. For example, the soil settlement in Mexico City can be close to 2.3 m [4]. Second, landslides can impose a similar loading condition with a load parallel to the sliding surface so that it might have both vertical and horizontal components. Depending on the slope of the sliding surface, the demand for differential displacement can be quite large. It is worth noting that landslides are quite common in Uzbekistan and other countries in Central Asia. Third, the pipeline crossing a fault line should be able to withstand a large shear, combined with tension and bending. For example, in the case of the 1906 San Francisco earthquake, the offset along the fault line was about 6.3 m [5].

A few experimental setups are developed at CSI to reproduce this kind of loading and measure the load capacities of the pipelines and their joints via testing up to failure. The best available knowledge and experience are utilized in the development of the laboratory. Many tests were previously conducted at Cornell University, a nationwide center focused on issues related to underground pipelines (see [6-11] for representative examples).

4. Experimental setups

This section discusses experimental setups, which are unique machines for testing pipelines under various loading conditions. These experimental machines reflect the best testing practices recommended for the water industry [12].

4.1 Testing pipelines in tension

In almost all loading cases described above, there is a loading component that will impose tension forces on the pipeline. While the pipe itself can withstand relatively large tension forces, the joints are one of the most vulnerable components of any water network. Hence, tension testing of the pipeline with a joint is one of the main tests conducted for the water industry [12].

Fig. 1 presents a schematic 3D drawing of an experimental tension test machine developed at CSI [13]. As shown in the image, it is designed as a self-reacting frame with a large-capacity actuator. It is designed to accommodate displacements of a pipe up to 0.6 m in diameter and deliver a maximum force of 6.7 MN.

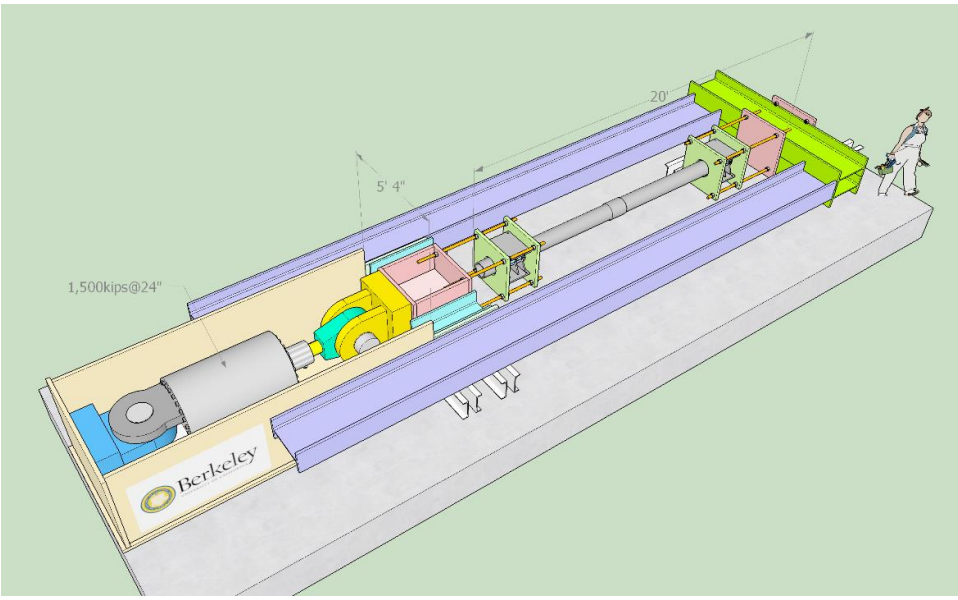

Figure 1. – **Schematic drawing of the tension testing machine.**

The test specimen representing a pipeline with a joint usually consists of two pipes (sticks) connected by a joint. One side of the pipe is attached to the reaction side of the frame, and another is attached to the actuator that is guided to ensure that the force is applied along the pipeline's axis.

Special saddles are introduced to transfer the tension forces to both end ends of the fully assembled pipeline specimen. The saddles are placed right next to the special weld beads with a large shear capacity. In addition, a pre-tension is applied to ensure that the half-shelves of the saddles tightly hug each side of the pipeline. The forces to the saddles are applied via large steel plates, as shown in Fig. 2. The left image shows a schematic drawing with saddles and steel plates used to transfer the tension force to the pipes. The reaction side of the setup is shown here. The load transfer on the loading side was achieved in a similar way. The right image shows the actual photo of the same load-transferring mechanism.

As recommended [12], the pipe is pressurized with water prior to the test, and the water pressure is monitored throughout the test.

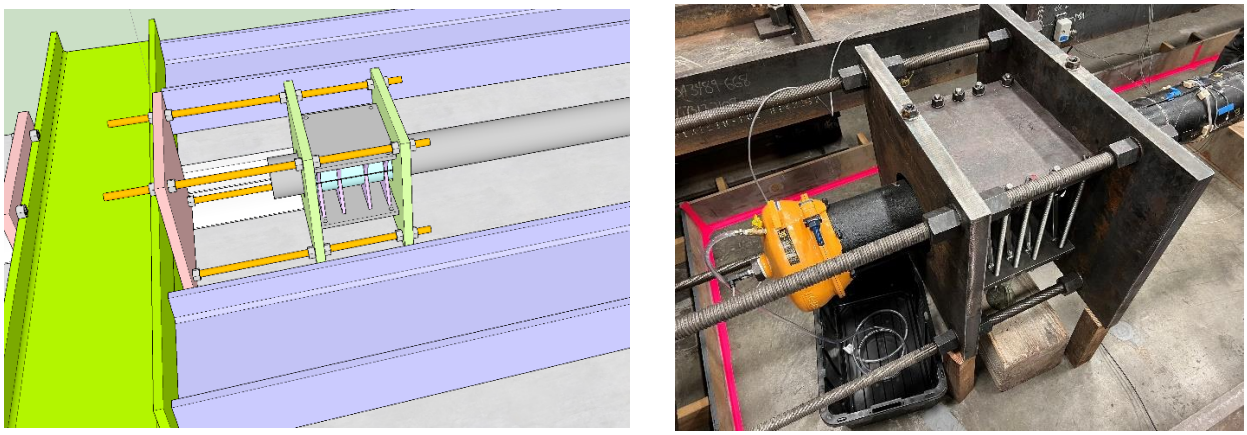

Schematic drawing Photo

Figure 2. – **Schematic drawing and a photo showing saddles and steel plates used to transfer the tension force to the pipes.**

Fig. 3 presents a typical test in action, showing the tension test on the ductile iron pipe with a joint [13]. The photo shows the pipeline with a nominal diameter of 203 mm.

Figure 3. – **Testing ductile iron pipeline with a joint in tension.**

The pipe and the experimental setup are instrumented by conventional instrumentation and an innovative fiber optic sensing (FOS) system. The latter allows monitoring strain along the length of the fiber optic cable, which can be a few kilometers long. This measuring technology is ideal for pipeline monitoring because it can support long fiber optic cables, and as such, it can be used in the in-situ monitoring of buried pipelines. Because of the size limitation of this paper, the results of the tests are not provided here, and they can be obtained from [13].

4.2 Four-point bending of pipeline

As discussed earlier, another type of loading that a pipeline can experience is bending. As an industry standard [12], a four-point bending is used to study the performance of the pipeline with a joint under the effect of bending moment. This type of testing is commonly used because it keeps the bending moment constant over a large portion of the pipe, which includes the joint. It is worth noting that this is a quite common type of testing adopted by many industries (see [14-15] as representative examples).

Four-point bending is a very common testing procedure at CSI, and a typical example [16] is discussed herein. Fig. 4 presents a drawing of the setup.

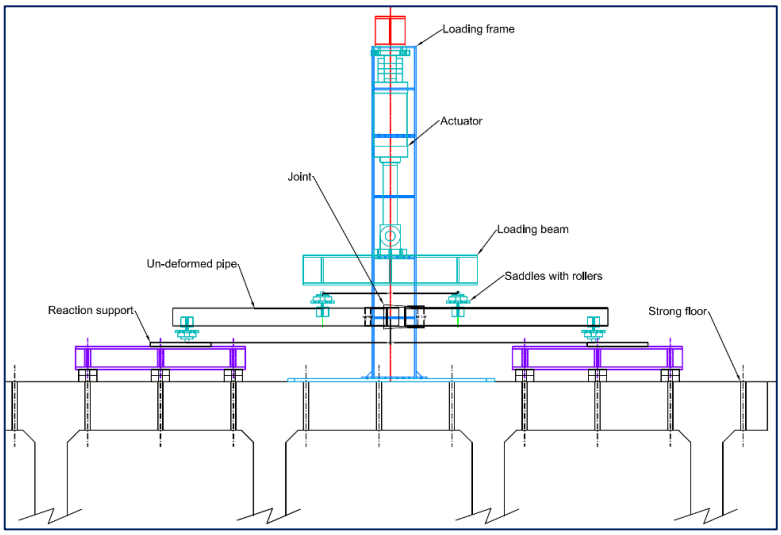

Figure 4. – **Drawing of the experimental setup for four-point bending.**

Similar to the previous case, saddles (although smaller ones) are introduced to distribute the forces over large areas to avoid localized pipe failures. They are installed at two loading points and two reaction points, as shown in Fig. 5. The photos shown herein were taken during the testing of the ductile iron pipe with a nominal diameter of 203 mm.

Figure 5. – **Saddles installed at the loading points (typical).**

Fig. 6 shows a photo of the experimental setup. The photo shows the pipeline's flexed shape with a joint in the four-point loading configuration. Because of the size limitation of this paper, the results of the tests are not discussed herein, and they can be obtained from [16]. A 2.05 MN hydraulic actuator with a stroke of about 0.5 m is installed into the setup.

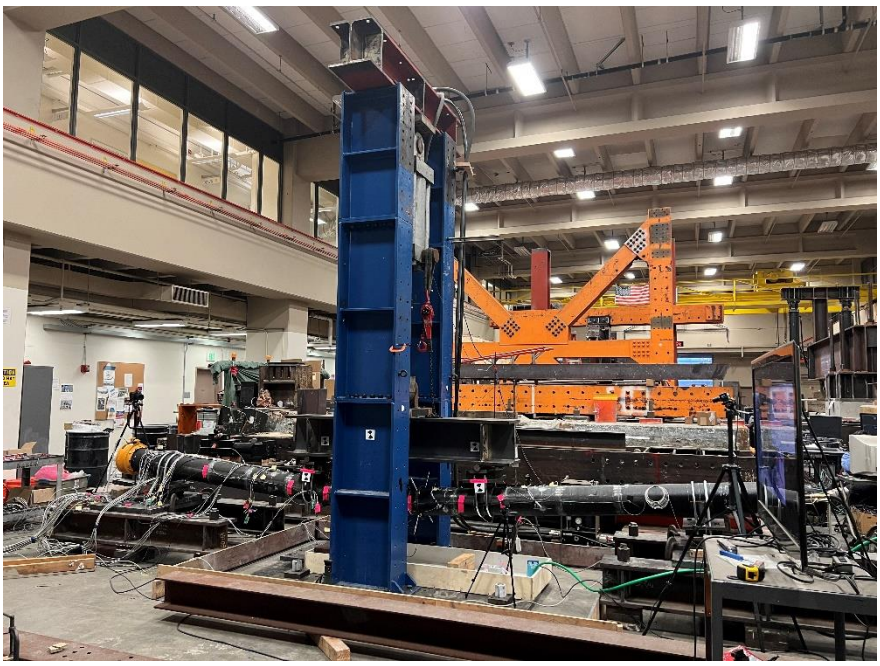

Figure 6. – **Photo of the four-point bending experimental setup.**

4.3 Bi-axial loading of pipeline

A new type of testing has been introduced at CSI [17]. It combines tension and bending loading, and as such, it is called bi-axial loading. It combines the self-reacting frame used for the tension test and the loading frame used in the four-point experimental setup. The drawing is shown in Fig. 7.

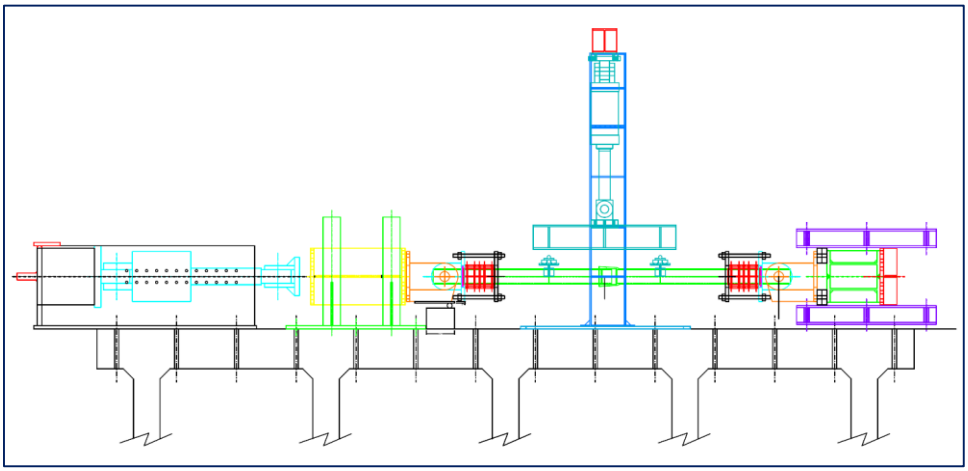

Figure 7. – **Drawing of bi-axial test setup.**

Special clevis systems are introduced, as shown in Fig. 8, to accommodate the rotation of both ends of the pipeline. In addition, a roller is introduced under the pin of the clevis system, as shown in Fig. 9. The left image shows the schematic 3D drawing, whereas the right image shows the photo of how it is implemented in the testing apparatus.

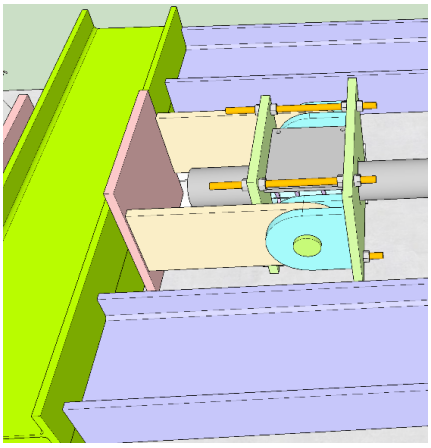

Schematic drawing

Photo

Figure 8. – **Schematic drawing and a photo showing details of clevises for bi-axial testing.**

Figure 9. – **Roller under the pin of clevis system.**

A photo of the experimental setup during the test is presented in Fig. 10. It is worth noting that the bi-axial experimental setup utilizes two independently controlled actuators, and as such, the loading can be conducted in many ways. For example, a testing protocol can start by applying some tension, and then bending can be applied. The second possibility is when the bending is applied first, followed by the application of the tension force until failure. This protocol is used [17] for a better representation of the actual loading of the pipelines (during a landslide, for example).

Because of the size limitation of this paper, the results of the tests are not discussed herein, and they can be obtained from [17].

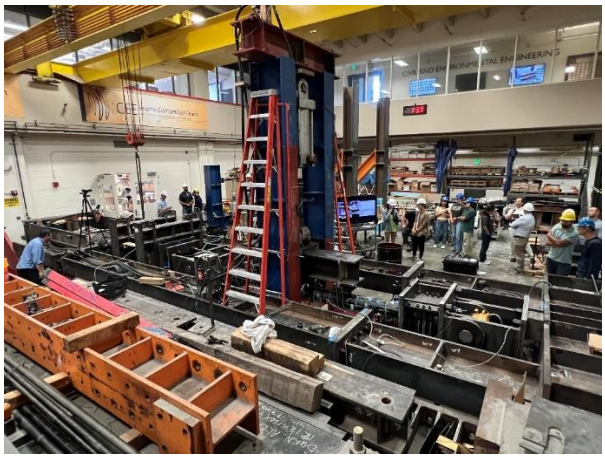

Figure 10. – **A photo of the bi-axial experimental setup during the test.**

4.4 Four-point bending of large diameter pipelines

A special experimental machine was designed and assembled at CSI to test large-diameter pipelines [18]. The drawing of the experimental setup is presented in Fig. 11. It is powered by a 2.05 MN actuator with a stroke of 0.91 m. In the configuration shown below, it is capable of applying a moment up to about 2.7 MN*m. The experimental setup can accommodate all pipe diameters up to 1.75 m. The vertical clearance under is pipe is large enough to accommodate the stroke of the actuator.

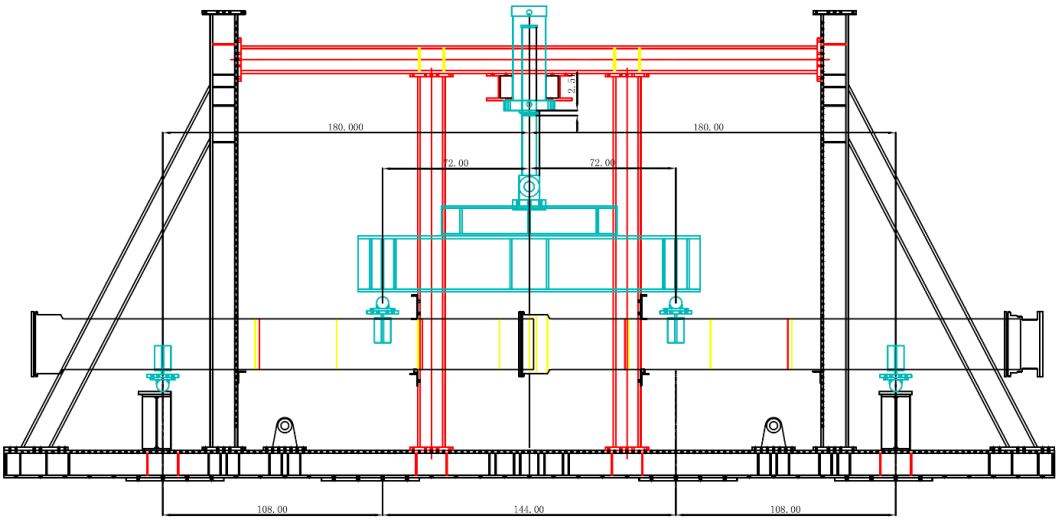

Figure 11. – **Drawing of experimental testing of large-diameter pipes in four-point bending.**

Fig. 12 [19] presents a photo of the experimental setup with a 609 mm pipeline. Because this paper is limited in size, the test results are not discussed here; they can be obtained from [19].

Figure 12. – **Photo of experimental testing of large-diameter pipes in four-point bending**

4.5 Split basin testing

Many split basin tests were conducted at Cornell University (see [19-20] for representative recent examples). In 2022, the experimental setup was moved to CSI to continue research in this direction. Fig. 13 shows a schematic drawing of the split basin test setup with a pipeline crossing the fault line.

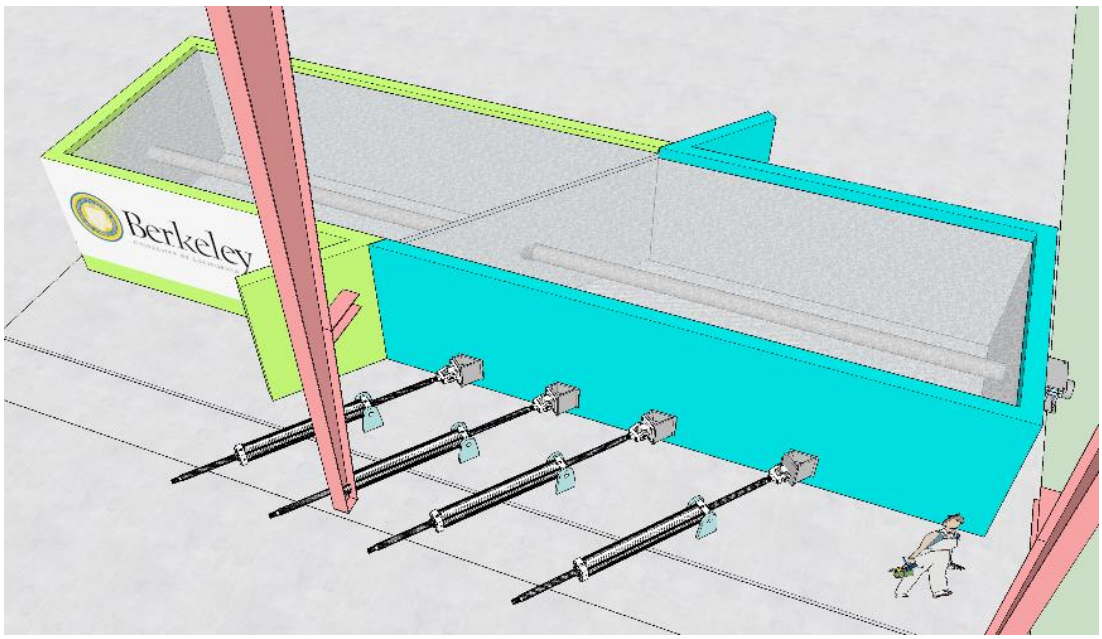

Figure 13. – **A schematic drawing of the split basin experimental setup.**

An experimental setup shown in Fig. 14 utilizes a strong floor. The main approach taken at CSI is to focus on the utilization of self-reacting experimental setups. To accomplish the same idea for the split basin test setup, a special subfloor is introduced. It is built of heavy wide-flange sections and reinforced by braces to provide large shear and flexural resistance.

The sub-floor was fabricated at the beginning of 2024, and the final assembly of the experimental setup is ongoing. It will become fully operational by June 2024.

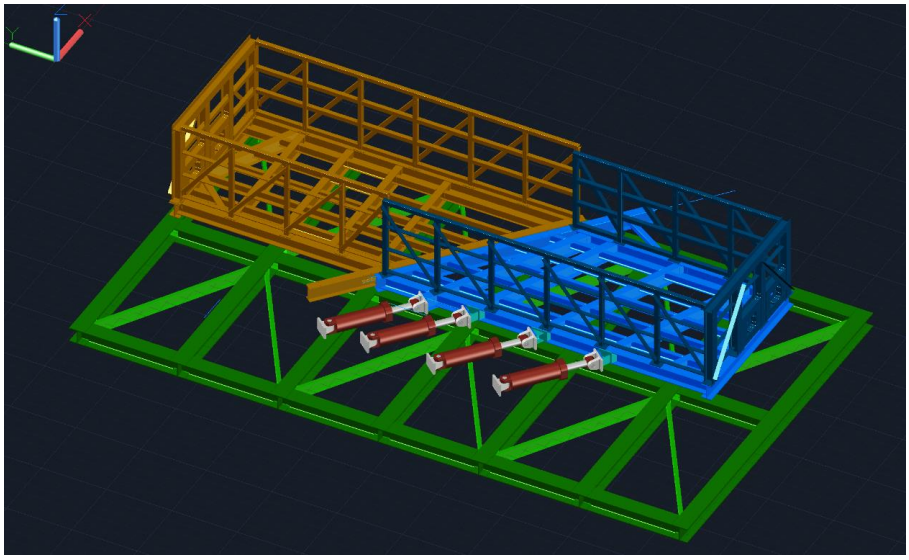

Figure 14. – **3D drawing of the split basin test setup on the subfloor.**

5. Conclusions

The newly developed experimental facility at CSI, the University of California, Berkeley, enables the water industry to perform the tests that have become standard testing routines: tension/compression, four-point bending, bi-axial testing, and split basin testing simulating a fault rupture. In addition, the large square footage of the lab's testing space opens new horizons in experimental studies of seismic performance of very large-diameter pipelines. CSI creates a collaborative space for water utilities and manufacturers of water industries to exchange information about the structural capacities of pipelines and find solutions for improving their performance in the case of deficiencies.

6. Acknowledgements

The authors would like to acknowledge the financial support provided by the East Bay Municipal Utility District (EBMUD). The work at the Center is conducted by a large team. Special thanks are due to Mr. Clifford Chan of EBMUD for the vision that resulted in the establishment of the Center. The authors would like to acknowledge the technical staff of the Department of Civil and Environmental Engineering: Mr. Llyr Griffith, Mr. John Kochan, Mr. Phillip Wong, Mr. Matthew Cataleta, and Mr. Irik Larson. Implementing the Center's vision would not have been possible without their technical support. Special thanks are due to Mr. Shih-Hung Chiu, Mrs. Qinglai Zhang, Mr. Tianyu Han and many other students and postdocs at CSI. The authors would like to acknowledge the faculty of the Department of Civil and Environmental Engineering: Prof. Dimitrios Zekkos, Prof. Matthew DeJong, Prof. Robert E Kayen, Prof. Adda Athanasopoulos-Zekkos, and many others actively participating in the development and projects of the Center. The authors would also like to acknowledge Dr. Blake Berger of Thornton Tomasetti and Dr. Brad Wham of Colorado University for their active participation in the development of CSI.

References

1. *Takhirov Sh., Orunbaev S., Toshmatov E., Shamansurov R., Baiyzbekov Zh.* (2022). Finite Element Model of Kurpsai Dam in Kyrgyzstan Based on Actual Response Measured by Extensive Network of Various Sensors. Accepted for the 8th European Congress on Computational Methods in Applied Sciences and Engineering, ECCOMAS Congress 2022, 5–9 June 2022, Oslo, Norway.
2. *Rakhmatullaev Sh., Frédéric Huneau, Philippe Le Coustumer, Mikael Motelica-Heino, Bakiev M.* (2010). Facts and Perspectives of Water Reservoirs in Central Asia: A Special Focus on Uzbekistan, Water, volume 2, no. 2: 307-320. *https://doi.org/10.3390/w2020307*.
3. https://engineering.berkeley.edu/news/2021/11/uc-berkeley-and-ebmud-announce-new-center-for-smart-infrastructure/.
4. *Flores F.A., Zárate I., Ramírez J., Gordillo N. O.* (2023). Predictions of Settlements of Pond Berms Over Mexico City Clay. R. E. Hammah et al. (Eds.): RIC 2023, AHE 19, pp. 432–438, 2023. https://doi.org/10.2991/978-94-6463-258-3_43.
5. *Schulz S.S., Wallace R.E.* (2016). The San Andreas Fault. Last modified 30-Nov-2016: https://pubs.usgs.gov/gip/earthq3/safaultgip.html (last accessed on 04/14/2024).
6. *Pariya-Ekkasut C., Stewart H. E., Wham B. P., O'Rourke T.D., Argyrou C., Bond T.K.* (2015). Four-Point Bending and Direct Tension Testing of Twelve Inch TR-XTREME™ Pipe Joint. Cornell University School of Civil and Environmental Engineering. Cornell University, September 2015.
7. *Pariya-Ekkasut C., Berger B.A., Stewart H. E., O'Rourke T.D.* (2018). Evaluation of McWane Seismic Flex Coupling for Resistance to Earthquake-Induced Ground Deformation. Cornell University, August 2018.
8. *Wham B.P., Berger B.A., O'Rourke T.D.* (2019). Experimental Performance Evaluation of Seismic-Resilient PVCO Pipeline, in: Pipelines 2019. American Society of Civil Engineers, Reston, VA, pp. 504–514. https://doi.org/10.1061/9780784482506.053.
9. *Pariya-Ekkasut C., Berger B.A. Wham B.P., Stewart H.E., O'Rourke T.D., Bond T.K.* (2017). Four-Point Bending Testing of 6-in. (150-mm), 12-in. (300-mm), and 16-in. (400-mm)-Diameter Kubota Earthquake Resistant Ductile Iron Pipes. Ithaca, NY: Cornell University.
10. *Stewart H. E., Wham B. P., O'Rourke T. D., Bond T. K.* (2013). Task 2 - Four-Point Bending of Bionax Pipe and Pipe Joints. Ithaca, NY: Cornell University.
11. *Wham B.P., Berger B.A., Pariya-Ekkasut C., O'Rourke T.D., Stewart H.E., Bond T.K., Argyrou C.* (2018). Achieving Resilient Water Networks – Experimental Performance Evaluation, in: Eleventh U.S. National Conference on Earthquake Engineering (11NCEE). Los Angeles, CA, p. 11.
12. *Utility Engineering and Surveying Institute (UESI) of the American Society of Civil Engineers (ASCE)* (2024). SEISMIC TESTING AND EVALUATION OF PIPELINE SYSTEMS (STEPS) STANDARD COMMITTEE. DRAFT TESTING STANDARD (Version 5). The draft version of 25 February 2024.
13. *Chiu C.-H., Zhang Q., Takhirov S., Soga K.* (2023): Direct Tension Testing of 8-in. (200-mm) Diameter TR-XTREME Ductile Iron Pipe. Center for Smart Infrastructure, University of California, Berkeley. Report 2023/01. https://doi.org/10.25350/B58G64.
14. *ASTM D790* (2017). Standard Test Methods for Flexural Properties of Unreinforced and Reinforced Plastics and Electrical Insulating Materials.
15. *ASTM C651* (2020). Standard Test Method for Flexural Strength of Manufactured Carbon and Graphite Articles Using Four-Point Loading at Room Temperature.
16. *Chiu C.-H., Zhang Q., Takhirov Sh., Soga K.* (2023): Four-point Bending Testing of 8-in. (200-mm) Diameter TR-XTREME Ductile Iron Pipe. Center for Smart Infrastructure, University of California, Berkeley. Report 2023/04. https://doi.org/10.25350/B51017.

17. *Chiu C.-H., Zhang Q., Takhirov Sh., Soga K.* (2023): Biaxial Tension Testing of 8-in. (200-mm) Diameter TR-XTREME Ductile Iron Pipe. Center for Smart Infrastructure, University of California, Berkeley. Report 2023/02. https://doi.org/10.25350/B54S3V.
18. *Chiu C.-H., Takhirov Sh., Soga K.* (2023): Four-Point Bending Testing of 24-in. (600-mm) Diameter NS-type Ductile Iron Pipe. Center for Smart Infrastructure, University of California, Berkeley. Report 2023/05. https://doi.org/10.25350/B5RG6G.
19. *Pariya-Ekkasut C., Stewart H. E., Wham B.P., O'Rourke T. D., Bond T. K.* (2016). Direct Tension and Split Basin Testing of 6-in. (150-mm) Diameter Kubota Earthquake Resistant Ductile Iron Pipe. Ithaca, NY: Cornell University.
20. *Oda K., Kishi S., Miyazima M., Pariya-Ekkasut C., Wham B.P., O'Rourke T.D.* (2017). "Verification of Design Method of Pipeline Crossing Fault with Earthquake Resistant Ductile Iron Pipe using Large-scale Split-box Test." Proceedings: 10th JWWA/WRF/CTWWA Water System Seismic Conference, Tainan, Taiwan, Oct. 18-20. NCREE-17-013.

ANALYSIS OF ELASTIC PRISMATIC RODS SUBJECTED TO TORSIONAL LOADS

Turdibekov J.E. [1]
[1]*Institute of Mechanics and Seismic Stability of Structures, Tashkent, Uzbekistan*
E-mail: javlonbek.turdibekov9@gmail.com

Abstract. *Understanding the elastic behavior of prismatic rods under torsional loads is crucial in various engineering applications. In this study, we investigate the deformation of an elastic prismatic rod with an arbitrary cross-sectional shape subjected to torsional moments at its ends. The rod's lateral surface is assumed to be free from external forces, while torque forces equivalent to torsional moments are applied to its ends. By establishing a Cartesian coordinate system with its origin at a chosen point on the end cross-section of the rod and aligning the z-axis parallel to the generator of the lateral surface, we formulate the boundary conditions for this problem.*

Keywords: *elastic behavior, prismatic rods, torsional loads, boundary conditions, deformation analysis*

1. Introduction

The relevance of this study lies in its potential applications across diverse engineering disciplines. Whether designing transmission shafts in automotive systems, analyzing the behavior of structural members in buildings, or optimizing the performance of rotating machinery, a comprehensive understanding of the elastic behavior of prismatic rods under torsion is indispensable.

In subsequent sections, we will delve into the mathematical framework governing the behavior of such rods, discussing the derivation of equations governing deformation and exploring solutions to elucidate critical insights. Through this exploration, we aim to provide engineers and researchers with valuable tools for tackling design challenges and optimizing the performance of structures and systems involving prismatic rods under torsional loading.

2. Materials, methods, and object of study

The primary object of study is the elastic deformation of the prismatic rod with an unequal angle cross-section under the action of torsional moments applied at its ends (Fig 1). By investigating the stress distribution and deformation patterns within the rod, we aim to understand how the geometry of the cross-section influences its mechanical response to torsional loading.

Additionally, the study will explore how variations in material properties, such as Young's modulus and Poisson's ratio, affect the stress state within the rod. The ultimate goal is to provide insights into the mechanical behavior of prismatic rods with non-standard cross-sectional shapes under torsional loading, thereby aiding in the design and optimization of such structural elements in engineering applications.

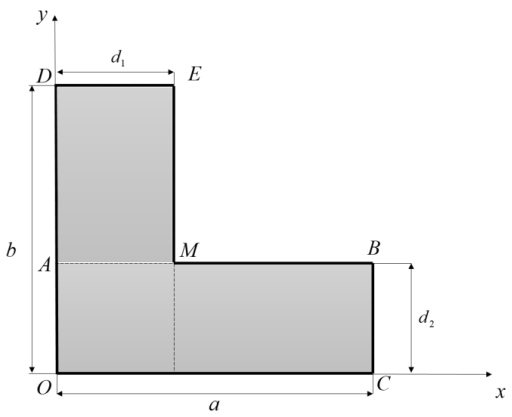

Figure 1. - **Elastic prismatic rod with a non-uniform cross-section in the shape of an unequal angle**

We position the origin of the Cartesian coordinate system at some arbitrary point of the end cross-section of the rod and align the z-axis parallel to the generator of the lateral surface of the rod. Then, the boundary conditions can be expressed as follows [1]:

On the lateral surface:

$$\left.\begin{aligned} \sigma_x \cos(nx) + \tau_{xy} \cos(ny) = 0 \\ \tau_{xy} \cos(nx) + \sigma_y \cos(ny) = 0 \\ \tau_{xz} \cos(nx) + \tau_{yz} \cos(ny) = 0 \end{aligned}\right\} \tag{1}$$

where n is the outward normal to the lateral surface of the rod.

And on the ends of the rod *(z = 0 u z = l):*

$$\left.\begin{aligned} &\iint_A \tau_{xz} dA = 0, \qquad \iint_A \tau_{yz} dA = 0, \\ &\iint_A \sigma_z dA = 0, \qquad \iint_A x\sigma_z dA = 0, \\ &\iint_A y\sigma_z dA = 0 \end{aligned}\right\} \tag{2}$$

Additionally,

$$\iint_A (x\tau_{yz} - y\tau_{xz}) dA = M \tag{3}$$

where M represents the torsional moment applied.

These boundary conditions play a crucial role in determining the behavior of the rod under torsional loading, accounting for stresses and deformations throughout its structure.

We will solve the problem by directly determining stresses using the semi-inverse Saint-Venant method. Let's assume:

$$\sigma_x = \sigma_y = \tau_{xy} = 0 \tag{4}$$

and we attempt to determine the remaining stress components to satisfy all equations of elasticity theory.

According to equation (4), the differential equilibrium equations:

$$\left.\begin{aligned} \frac{\partial \sigma_x}{\partial x} + \frac{\partial \tau_{xy}}{\partial y} + \frac{\partial \tau_{xz}}{\partial z} = 0, \\ \frac{\partial \tau_{xy}}{\partial x} + \frac{\partial \sigma_y}{\partial y} + \frac{\partial \tau_{yz}}{\partial z} = 0, \\ \frac{\partial \tau_{xz}}{\partial x} + \frac{\partial \tau_{yz}}{\partial y} + \frac{\partial \sigma_z}{\partial z} = 0 \end{aligned}\right\} \tag{5}$$

from this

$$\left.\begin{aligned}\frac{\partial \tau_{xz}}{\partial z}=0,\\ \frac{\partial \tau_{yz}}{\partial z}=0,\\ \frac{\partial \tau_{xz}}{\partial x}+\frac{\partial \tau_{yz}}{\partial y}+\frac{\partial \sigma_z}{\partial z}=0\end{aligned}\right\} \tag{6}$$

And the compatibility equations expressed in stresses:

$$\left.\begin{aligned}\nabla^2\sigma_x+\frac{1}{1+\nu}\frac{\partial^2 S}{\partial x^2}=0,\\ \nabla^2\sigma_y+\frac{1}{1+\nu}\frac{\partial^2 S}{\partial y^2}=0,\\ \nabla^2\sigma_z+\frac{1}{1+\nu}\frac{\partial^2 S}{\partial z^2}=0,\\ \nabla^2\tau_{xy}+\frac{1}{1+\nu}\frac{\partial^2 S}{\partial x\partial y}=0,\\ \nabla^2\tau_{xz}+\frac{1}{1+\nu}\frac{\partial^2 S}{\partial x\partial z}=0,\\ \nabla^2\tau_{yz}+\frac{1}{1+\nu}\frac{\partial^2 S}{\partial y\partial z}=0,\end{aligned}\right\} \tag{7}$$

Where $S=\sigma_x+\sigma_y+\sigma_z$, $\nu-$ Poisson's ratio, a $\nabla^2=\frac{\partial^2}{\partial x^2}+\frac{\partial^2}{\partial y^2}+\frac{\partial^2}{\partial z^2}-$ is the Laplace operator, we can rewrite them as:

$$\left.\begin{aligned}\frac{\partial^2\sigma_z}{\partial x^2}=\frac{\partial^2\sigma_z}{\partial y^2}=\frac{\partial^2\sigma_z}{\partial z^2}=\frac{\partial^2\sigma_z}{\partial x\partial y}=0,\\ \nabla^2\tau_{xz}+\frac{1}{1+\nu}\frac{\partial^2\sigma_z}{\partial x\partial z}=0,\\ \nabla^2\tau_{yz}+\frac{1}{1+\nu}\frac{\partial^2\sigma_z}{\partial y\partial z}=0\end{aligned}\right\} \tag{8}$$

since, based on (4), $S=\sigma_z$, and $\nabla^2\sigma_x=\nabla^2\sigma_y=\nabla^2\tau_{xy}=0.$. From the first two equilibrium equations in (6), it follows that the stresses τ_{xz} and τ_{yz} do not depend on the coordinate *z*, meaning these stresses are identical in all sections of the rod.

Directly from the compatibility equations in (8), we deduce that σ_z is a function of coordinates *x*, *y* and *z* of the form:

$$\sigma_z=Azy+Bzx+Dx+Ey+Fz+H. \tag{9}$$

Substituting (9) into the boundary conditions (2) to find the constants, we obtain a homogeneous system of six linear equations, from which it follows that *A* = *B* = *D* = *E* = *F*= *H* = *0*, i. e. σ_z is identically zero in all cross-sections of the rod.

Then, the equilibrium equations (6) and compatibility equations (8) take the form:

$$\frac{\partial \tau_{xz}}{\partial x}+\frac{\partial \tau_{yz}}{\partial y}=0 \tag{10}$$

$$\nabla^2\tau_{xz}=0,\quad \nabla^2\tau_{yz}=0 \tag{11}$$

Thus, assuming that the three stress components σ_x, σ_y, and τ_{xy} are zero, we only need to determine the distributions of shear stresses τ_{xz} and τ_{yz} across the cross-section of the twisted rod

to satisfy the original equations (10) and (11) and the boundary conditions (1)-(3), as the normal stresses σ_z in all sections of the rod are identically zero.

By differentiating the equilibrium equation (10) with respect to *x* and subtracting the first equation in (11), we obtain:

$$\frac{\partial}{\partial y}\left(\frac{\partial \tau_{yz}}{\partial x}-\frac{\partial \tau_{xz}}{\partial y}\right)=0. \tag{12}$$

Similarly, by differentiating equation (10) with respect to *y* and subtracting the second equation in (11), we find:

$$\frac{\partial}{\partial y}\left(\frac{\partial \tau_{xz}}{\partial y}-\frac{\partial \tau_{yz}}{\partial x}\right)=0. \tag{13}$$

Equations (12) and (13) directly lead to:

$$\frac{\partial \tau_{xz}}{\partial y}-\frac{\partial \tau_{yz}}{\partial x}=C, \tag{14}$$

where *C* is an arbitrary constant, to be determined later.

Thus, the system of equations (10) and (11) can be replaced by equivalent equations (10) and (14).

Substituting the expressions for τ_{xz} and τ_{yz} in the left side of equation (14) in terms of displacements, i.e., expressions:

$$\left.\begin{aligned}\tau_{xz}&=G\gamma_{xz}=G\left(\frac{\partial u}{\partial z}+\frac{\partial w}{\partial x}\right),\\ \tau_{yz}&=G\gamma_{yz}=G\left(\frac{\partial v}{\partial z}+\frac{\partial w}{\partial y}\right),\end{aligned}\right\} \tag{15}$$

here *G* is the shear modulus of the rod material, and *u*, *v*, and *w* - are the displacement components of the rod points along the coordinate axes x, y, and z, respectively, we obtain:

$$\frac{\partial \tau_{xz}}{\partial y}-\frac{\partial \tau_{yz}}{\partial x}=G\frac{\partial}{\partial z}\left(\frac{\partial u}{\partial y}-\frac{\partial v}{\partial x}\right). \tag{16}$$

Using the expression for the component of the elementary rotation about the *z* axis:

$$\omega_z=\frac{1}{2}\left(\frac{\partial v}{\partial x}-\frac{\partial u}{\partial y}\right) \tag{17}$$

from (13), we find:

$$\frac{\partial \tau_{xz}}{\partial y}-\frac{\partial \tau_{yz}}{\partial x}=-2G\frac{\partial \omega_z}{\partial z}, \tag{18}$$

Here, $\frac{\partial \omega_z}{\partial z}-$ represents the rate of twist per unit length of the fibers of the rod parallel to the rod axis (this angle is often referred to as the twist). By comparing equations (14) and (18), we obtain:

$$-2G\frac{\partial \omega_z}{\partial z}=C \tag{19}$$

From here, the meaning of the constant *C* becomes clear, namely:

$$C=-2G\theta \tag{20}$$

where $\theta-$ is the twist angle, constant for all fibers of the twisted rod parallel to the rod axis.

According to (19) and (20), for the rotation angle of the rod section ω_z at a distance *z* from the fixed end (*z=0*), we have the following relations:

$$\theta=\frac{\partial \omega_z}{\partial z}, \quad and \quad \omega_z=\theta\cdot z\ . \tag{21}$$

From the above it follows that solving the problem of torsion of prismatic rods reduces to integrating the equations

$$\frac{\partial \tau_{xz}}{\partial x} + \frac{\partial \tau_{yz}}{\partial y} = 0, \tag{22}$$

$$\frac{\partial \tau_{xz}}{\partial y} - \frac{\partial \tau_{yz}}{\partial x} = -2G\theta \tag{23}$$

under the boundary conditions (1) - (3).

We seek the solution to equations (22) and (23) in the form[2-4]:

$$\left.\begin{aligned} \tau_{xz} &= G\theta \frac{\partial \Phi}{\partial y}, \\ \tau_{yz} &= -G\theta \frac{\partial \Phi}{\partial x}, \end{aligned}\right\} \tag{24}$$

where $\Phi(x, y)$– is some function of variables x and y, called the stress function in torsion or the Prandtl stress function. It is easy to see that with this choice of the general solution (24), the equilibrium equation (22) is identically satisfied. Substituting the expressions (24) for stresses τ_{xz} and τ_{yz} into the compatibility equation (23), we obtain the following equation for determining the stress function $\Phi(x, y)$:

$$\nabla^2 \Phi(x, y) = \frac{\partial^2 \Phi}{\partial x^2} + \frac{\partial^2 \Phi}{\partial y^2} = -2. \tag{25}$$

Thus, the stress function $\Phi(x, y)$: in the cross-sectional area of the twisted rod must satisfy the Poisson's equation (25).

3. Statement of the Problem

Let's consider an elastic prismatic rod with a non-uniform cross-section in the shape of an unequal angle (see Fig 1), subjected to torsional moments ***M*** applied to its ends.

The stress state in such a rod is characterized by only two shear stresses τ_{xz} and τ_{yz} which can be expressed through the stress functions (24).

The stress function $\Phi(x, y)$ must satisfy the differential equation (25) in the cross-sectional area of the rod *dA* and the boundary condition $\Phi = 0$ on the contour of the area *dA*. To determine the stress function $\Phi(x, y)$ for twisting rods with polygonal cross-sections, such as for rolled profiles (channel, I-beam, Z-section, etc.), the method proposed by N. H. Arutyunyan is effective, which involves reducing the problem of determining the stress function using auxiliary functions to solving entirely regular infinite systems of linear equations.

For this purpose, the cross-sectional area of the rod is represented as two overlapping areas *OABCO* and *ODEFO* (Fig 1). Suppose that the stress function $\Phi(x, y)$ in the area *OABCO* takes the value $\Phi_1(x, y)$, and in the area *ODEFO* it takes the value $\Phi_2(x, y)$. Since the function $\Phi(x, y)$ satisfies the Poisson's equation, to ensure the continuity of this function and its first derivatives throughout the cross-sectional area, it is sufficient to require that the values of the functions $\Phi_1(x, y)$ and $\Phi_2(x, y)$ on the contour of the common part of the areas *OABCO* and *ODEFO* coincide. Therefore, in expanded form, the boundary conditions for the functions Φ_1 and Φ_2 are as follows:

$$\left.\begin{array}{l}\Phi_1(0,y)=\Phi_1(x,0)=\Phi_1(a,y)=0,\\ \Phi_1(x,d_2)=\begin{cases}0, & x\ge d_1\\ \Phi_2(x,d_2), & x\le d_1,\end{cases}\\ \Phi_2(x,0)=\Phi_2(0,y)=\Phi_2(x,b)=0,\\ \Phi_2(d_1,y)=\begin{cases}0, & y\ge d_2\\ \Phi_1(d_1,y), & y\le d_2.\end{cases}\end{array}\right\} \tag{26}$$

4. Numerical Method

Let's substitute these approximations into the Poisson's equation (25):

$$\frac{\Phi_{i+1,j}-2\Phi_{i,j}+\Phi_{i-1,j}}{h^2}+\frac{\Phi_{i,j+1}-2\Phi_{i,j}+\Phi_{i,j-1}}{k^2}=-2 \tag{27}$$

Now we can rewrite this equation in explicit finite difference form[5]:

$$\Phi_{i,j}=\frac{h^2k^2}{2\left(h^2+k^2\right)}\left(\Phi_{i+1,j}+\Phi_{i-1,j}+\Phi_{i,j+1}+\Phi_{i,j-1}\right)+\frac{hk^2}{h^2+k^2} \tag{28}$$

Now let's refine the program to accommodate your instructions and definitions. We will use the step size h both in the x and y directions. Let the number of grid points in the x direction be N, and in the y direction be M. The grid points are defined by the formula $(x_i,y_j)=(i\cdot h,\ j\cdot h)$ for $i=0,1,....,N\ \ and\ \ j=0,1,...,M$.

5. Results

The stress function $\Phi(x,y)$ exhibits symmetry about the *y*-axis, evident from the fact that the values of $\Phi(x,y)$ are symmetrically distributed about the *y*-axis. Generally, as we move away from the origin along the *x*-axis, the values of $\Phi(x,y)$ tend to increase. This suggests that the stress within the rod increases with increasing distance from the center along the *x*-axis Fig 2.

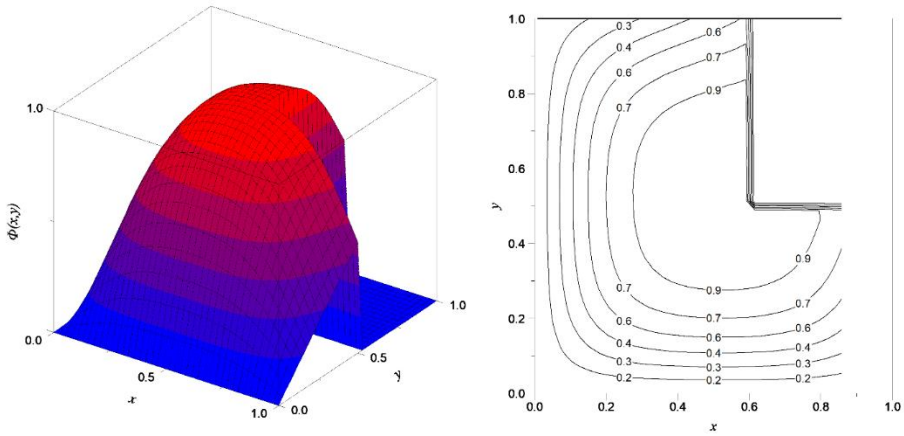

Figure 2. - **The stress function *Φ(x, y)* is dimensionless**

6. Analysis of results

In this project, we addressed the problem of determining the stress distribution in an elastic prismatic rod with a non-uniform cross-section subjected to torsional moments. The stress state in such a rod is characterized by shear stresses τ_{xz} and τ_{yz} which can be expressed through the stress function $\Phi(x,y)$

To solve this problem, we employed the Poisson's equation, which governs the behavior of the stress function $\Phi(x,y)$ within the cross-sectional area of the rod. We also introduced boundary conditions to ensure the continuity of $\Phi(x,y)$ and its derivatives on the contour of the cross-sectional area. To approximate the solution, we discretized the Poisson's equation using finite difference methods. This allowed us to transform the continuous differential equation into a system

of discrete equations, which we solved iteratively. We used a finite grid of points in both the x and y directions, and we updated the solution at each point based on the values of neighboring points.

To assess the convergence of our iterative solution, we calculated the error between consecutive iterations. If this error fell below a specified tolerance level, we terminated the iteration loop, indicating that the solution had converged to an acceptable level.

In conclusion, we have developed a computational approach to determine the stress distribution in a twisted rod with a non-uniform cross-section. By discretizing the governing equations and iteratively solving them, we can obtain an approximate solution that provides valuable insights into the mechanical behavior of such structures. This approach can be further refined and extended for more complex geometries and loading conditions.

References

1. *Bartels S., Reiter P.* Numerical solution of a bending-torsion model for elastic rods // Numerische Mathematik, 2020, https://doi.org/10.1007/s00211-020-01156-6
2. *Сенашов С.И., Савостьянова И.Л.* Elastic-plastic torsion of a multilayer rod // Вестник Чувашского Государственного Педагогического Университета им. И.Я. Яковлева. Серия: Механика Предельного Состояния, 2023, https://doi.org/10.37972/chgpu.2023.56.2.003
3. *Chernyshev A.D.* Solution of the problem of torsion of an elastic rod of s-gonal cross section using the boundary extension method // Journal of Applied Mechanics and Technical Physics, 2009, https://doi.org/10.1007/s10808-009-0144-5
4. *Moayyedian F., Grabski J.K.* Elastic–plastic torsion problem with non-linear hardenings using the method of fundamental solution // Archives of Civil and Mechanical Engineering, 2021, https://doi.org/10.1007/s43452-021-00307-2
5. Numerical Methods for Elliptic and Parabolic Partial Differential Equations. Numerical Methods for Elliptic and Parabolic Partial Differential Equations, 2003, https://doi.org/10.1007/b97419

NUMERICAL MODELING OF THE COUPLED DYNAMIC PROBLEM OF THE STRAIN SPACE THERMOPLASTICITY THEORY

Yusupov Y.[1, 2], Sagdullaeva D.[3], Soliev A.[4]

[1]*Departmend of Applied informatics, Kimyo International university in Tashkent, Tashkent, Uzbekistan.*
[2]*National University of Uzbekistan, Tashkent, Uzbekistan*
[3]*Institute of Mechanics and Seismic Stability of Structure, Tashkent, Uzbekistan.*
[4]*Tashkent State University of Economics, Tashkent, Uzbekistan.*
E-mail: yusabio@gmail.com

Abstract. *The paper is devoted to the formulation and numerical modelling of the coupled dynamic boundary value problems on the strain space thermoplasticity theory. Considered 3D consisting of tree thermoplastic and one heat equations regarding two components of displacements and temperature with a corresponding initial and boundary conditions. Using the finite-difference method, the explicit and implicit schemes are constructed. The solution of the explicit schemes is reduced to the recurrent formulas, whereas the implicit scheme to the elimination method. Comparison of the numerical results obtained by the explicit and implicit schemes show a good coincidence. The distribution of plastic zones is shown.*

Keywords: *coupled, thermoplasticity, explicit and implicit schemes, temperature, displacement, elimination method*

1. Introduction

Investigation of the joint influence of thermomechanical forces on the strength and durability of structures is an actual problem of solid mechanics and engineering. Usually, when solving thermal problems, the temperature is considered given, and the problem is reduced to a separate solution of the thermoelasticity equations. But, in reality, the temperature must be determined based on the solution of the thermal conductivity equation and affects the deformation process. When considering the equations of motion and the heat equation together, taking into account Duhamel-Neumann, we obtain a coupled boundary value of the thermoelasticity.

To investigate the coupled thermoelasticity problems, Biot [1], Lord and Shulman [2], and Youssef [3] introduced a generalized coupled thermoelasticity theory with a wave-type heat equation. Several researchers [4-6] developed a theoretical framework appertaining to coupled

thermomechanical deformations of an inelastic materials at finite strains. The coupled thermoplasticity problem was considered in [7-12]. The coupled and uncoupled thermomechanical boundary value problems were numerically solved in [13-17].

Two types coupled thermomechanical boundary value problems can be formulated based on deformation or incremental (flow) theories of thermoplasticity. The former consists of motion equation, thermoplasticity constitutive relations and heat conduction equations, whereas, the later consists of motion and heat equations, in which the constitutive relations are written in the incremental forms with a corresponding initial and boundary conditions [7]. Note that, in case of strain space plasticity and thermoplasticity theories [18-21] the right side of its constitutive relations depends on strain increments and full strains which is convenient for numerical implementations.

This paper deals with the formulation of coupled thermoplastic boundary value problems based on strain space thermoplasticity theory [16-19] and its numerical treatment.

In Sections 2, based on the strain space thermoplasticity theory, the coupled dynamic boundary value problem regarding to the displacement and temperature increments are formulated. The coupled boundary value problem in two-dimensional case is reduced to the system of two nonlinear motions (hyperbolic) and one heat (parabolic) equations with a corresponding initial and boundary conditions.

In Section 3, using finite difference method an explicit and implicit scheme for coupled boundary value problem based on strain-space thermoplasticity theory are constructed. The finite difference equations using the recurrent formulas and elimination methods, respectively, are solved. Note, the external thermomechanical forces are gradually applied and the values of displacement and temperature are found as a sum of its increments.

In Section 4, numerical examples for a clamped rectangle with the given internal temperature and sinusoidal thermal load are presented. The numerical results on the explicit and implicit schemes are compared and show a good agreement. This section ends with the investigation of temperature distribution and the appearance of plastic zones inside the rectangular region under the given initial and boundary conditions.

2. Coupled boundary value problem of strain space thermoplasticity

The strain-space thermoplasticity constitutive relations are convenient for the formulation and numerical solution of the coupled boundary value problems. Note that the constitutive relations for the flow thermoplasticity theories have incremental form and for that all equations, initial and boundary conditions should be written with respect to the increments of the unknowns.

The coupled boundary value problem of strain-space thermoplasticity theory consists of the motion equation

$$d\sigma_{ij,j} + dX_i = \rho d\ddot{u}_i, \tag{1}$$

the following constitutive equation of the thermoplasticity [17]

$$\begin{gathered} d\sigma_{ij} = \lambda d\theta \delta_{ij} + 2\mu d\varepsilon_{ij} - \alpha\gamma dT\delta_{ij} - \frac{\mu-\mu'}{\varepsilon_u^2}\left(e_{kl}de_{kl}\right)e_{ij} - \frac{\mu-\mu'}{\varepsilon_u^2}e_{ij}\frac{\partial F}{\partial T}dT, \\ F = 0 \quad and \quad dF = e_{ij}de_{ij} + \frac{\partial F}{\partial T}dT \geq 0; \end{gathered} \tag{2}$$

and heat conduction equation [22]

$$\lambda_0 dT_{,ii} - C_\varepsilon d\dot{T} - T_0\alpha\gamma d\dot{\varepsilon}_{ij} = 0 \tag{3}$$

and the Cauchy relations

$$d\varepsilon_{ij} = \frac{1}{2}\left(du_{i,j} + du_{j,i}\right) \tag{4}$$

with initial conditions

$$du_i\big|_{t=t_0}=\phi_i,\quad d\dot{u}_i\big|_{t=t_0}=\psi_i,\quad dT\big|_{t=t_0}=T_0 \tag{5}$$

and boundary conditions

$$du_i\big|_{\Sigma_1}=du_i^0,\qquad d\sigma_{ij}n_j\big|_{\Sigma_2}=dS_i^0,\qquad dT\big|_{\Sigma}=\overline{T}_0 \tag{6}$$

where e_{ij}- a deviator of strain tensor, T- a temperature, C_ε- a heat coefficient, α- a thermal expansion coefficient, λ_0- the heat flow coefficient. If loading function F has following form [32]

$$F\equiv\frac{1}{2}e_{ij}e_{ij}-R(\omega,T)=0 \tag{7}$$

where R the hardening function [24].

Substituting eq. (4) into eq. (2) and eq. (1.3) gives equations for displacement and temperature increments

$$\begin{cases}\eta\dfrac{\partial^2(du)}{\partial x^2}+\mu\dfrac{\partial^2(du)}{\partial y^2}+\mu\dfrac{\partial^2(du)}{\partial z^2}+(\lambda+\mu)\dfrac{\partial^2(dv)}{\partial x\partial y}+(\lambda+\mu)\dfrac{\partial^2(dw)}{\partial x\partial z}-\alpha\gamma\dfrac{\partial(dT)}{\partial x}-\xi=\rho\dfrac{\partial^2(du)}{\partial t^2},\\ \mu\dfrac{\partial^2(dv)}{\partial x^2}+\eta\dfrac{\partial^2(dv)}{\partial y^2}+\mu\dfrac{\partial^2(dv)}{\partial z^2}+(\lambda+\mu)\dfrac{\partial^2(du)}{\partial x\partial y}+(\lambda+\mu)\dfrac{\partial^2(dw)}{\partial y\partial z}-\alpha\gamma\dfrac{\partial(dT)}{\partial y}-\zeta=\rho\dfrac{\partial^2(dv)}{\partial t^2},\\ \mu\dfrac{\partial^2(dw)}{\partial x^2}+\mu\dfrac{\partial^2(dw)}{\partial y^2}+\eta\dfrac{\partial^2(dw)}{\partial z^2}+(\lambda+\mu)\dfrac{\partial^2(du)}{\partial x\partial z}+(\lambda+\mu)\dfrac{\partial^2(dv)}{\partial y\partial z}-\alpha\gamma\dfrac{\partial(dT)}{\partial z}-\chi=\rho\dfrac{\partial^2(dw)}{\partial t^2},\\ \lambda_0\left[\dfrac{\partial^2(dT)}{\partial x^2}+\dfrac{\partial^2(dT)}{\partial y^2}+\dfrac{\partial^2(dT)}{\partial z^2}\right]-C_\varepsilon\dfrac{\partial(dT)}{\partial t}-\alpha\gamma T_0\left[\dfrac{\partial^2(du)}{\partial x\partial t}+\dfrac{\partial^2(dv)}{\partial y\partial t}+\dfrac{\partial^2(dw)}{\partial z\partial t}\right]=0;\end{cases} \tag{8}$$

with the appropriate initial

$$\begin{gathered}du\big|_{t=0}=d\phi,\qquad dv\big|_{t=0}=df,\qquad dT\big|_{t=0}=d\overline{T},\\ \left.\frac{\partial(du)}{\partial t}\right|_{t=0}=d\tilde{\phi},\ \left.\frac{\partial(dv)}{\partial t}\right|_{t=0}=d\tilde{f},\ \left.\frac{\partial(dvw)}{\partial t}\right|_{t=0}=d\tilde{\psi};\end{gathered} \tag{9}$$

and boundary conditions

$$\begin{gathered}du\big|_{x=0/l_1}=du_{1/2},\ dv\big|_{x=0/l_1}=dv_{1/2},\ dw\big|_{x=0/l_1}=dw_{1/2},\\ du\big|_{y=0/l_2}=du_{3/4},\ dv\big|_{y=0/l_2}=dv_{3/4},\ dw\big|_{y=0/l_2}=dw_{3/4},\\ du\big|_{z=0/l_3}=du_{5/6},\ dv\big|_{z=0/l_3}=dv_{5/6},\ dw\big|_{z=0/l_3}=dw_{5/6},\\ dT\big|_{x=0/l_1}=dT_{1/2},\ dT\big|_{y=0/l_2}=dT_{3/4},\ dT\big|_{z=0/l_3}=dT_{5/6};\end{gathered} \tag{10}$$

where $\lambda,\ \mu,\mu',\alpha,\beta,C_\varepsilon,\ \lambda_0$ are the given values, ℓ_1,ℓ_2,ℓ_3 are the length of the parallelepiped, $\varphi,\ \psi,\tilde{\varphi},\ \tilde{\psi},\ T_0,\ T_1,T_2$ are the known values,

$$\xi=\frac{\mu-\mu'}{\varepsilon_u^2}\left[e_{11}\Im+e_{12}\Re+e_{13}\aleph\right],\zeta=\frac{\mu-\mu'}{\varepsilon_u^2}\left[e_{21}\Im+e_{22}\Re+e_{23}\aleph\right],\chi=\frac{\mu-\mu'}{\varepsilon_u^2}\left[e_{31}\Im+e_{32}\Re+e_{33}\aleph\right]$$

$$\begin{cases}\Im=e_{11}\dfrac{\partial(de_{11})}{\partial x}+e_{22}\dfrac{\partial(de_{22})}{\partial x}+e_{33}\dfrac{\partial(de_{33})}{\partial x}+2e_{12}\dfrac{\partial(de_{12})}{\partial x}+2e_{13}\dfrac{\partial(de_{13})}{\partial x}+2e_{23}\dfrac{\partial(de_{23})}{\partial x}+\beta\dfrac{\partial(dT)}{\partial x}\\ \Re=e_{11}\dfrac{\partial(de_{11})}{\partial y}+e_{22}\dfrac{\partial(de_{22})}{\partial y}+e_{33}\dfrac{\partial(de_{33})}{\partial y}+2e_{12}\dfrac{\partial(de_{12})}{\partial y}+2e_{13}\dfrac{\partial(de_{13})}{\partial y}+2e_{23}\dfrac{\partial(de_{23})}{\partial y}+\beta\dfrac{\partial(dT)}{\partial y}\\ \aleph=e_{11}\dfrac{\partial(de_{11})}{\partial z}+e_{22}\dfrac{\partial(de_{22})}{\partial z}+e_{33}\dfrac{\partial(de_{33})}{\partial z}+2e_{12}\dfrac{\partial(de_{12})}{\partial z}+2e_{13}\dfrac{\partial(de_{13})}{\partial z}+2e_{23}\dfrac{\partial(de_{23})}{\partial z}+\beta\dfrac{\partial(dT)}{\partial z}\end{cases} \tag{11}$$

Eqs. (8-10) represent coupled dynamic 3D strain-space thermoplasticity boundary value problem.

3. Finite-difference equations for coupled thermoplasticity boundary value problem

In this section, we construct the explicit and implicit schemes for the finite difference method for coupled strain-space thermoplasticity boundary value problem.

Eqs. (8-10) depend on the displacement and temperature increments du, dv, dw and dT respectively. To construct the finite difference equations, the derivatives of displacement and temperature increments in eqs. (8-10) are replaced by difference quotients i.e.

$$\begin{aligned}
&(\lambda+2\mu)\frac{du^l_{i+1jk}-2du^l_{ijk}+du^l_{i-1jk}}{h_1^2}+\mu\frac{du^l_{ij+1k}-2du^l_{ijk}+du^l_{ij-1k}}{h_2^2}+\\
&+\mu\frac{du^l_{ijk+1}-2du^l_{ijk}+du^l_{ijk-1}}{h_3^2}-\alpha\gamma\frac{dT^l_{i+1jk}-dT^l_{i-1jk}}{2h_1}-\xi^l_{ijk}+\\
&+(\lambda+\mu)\frac{dv^l_{i+1j+1k}-dv^l_{i+1j-1k}-dv^l_{i-1j+1k}+dv^l_{i-1j-1k}}{4h_1h_2}+\\
&(\lambda+\mu)\frac{dw^l_{i+1jk+1}-dw^l_{i-1jk+1}-dw^l_{i+1jk-1}+dv^l_{i-1jk-1}}{4h_1h_3}=\rho\frac{du^{l+1}_{ijk}-2du^l_{ijk}+du^{l-1}_{ijk}}{\tau^2},
\end{aligned} \tag{12}$$

$$\begin{aligned}
&\mu\frac{dv^l_{i+1jk}-2dv^l_{ijk}+dv^l_{i-1jk}}{h_1^2}+(\lambda+2\mu)\frac{dv^l_{ij+1k}-2dv^l_{ijk}+dv^l_{ij-1k}}{h_2^2}+\\
&+\mu\frac{dv^l_{ijk+1}-2dv^l_{ijk}+dv^l_{ijk-1}}{h_3^2}-\alpha\gamma\frac{dT^l_{ij+1k}-dT^l_{ij-1k}}{2h_2}-\xi^l_{ijk}+\\
&+(\lambda+\mu)\frac{du^l_{i+1j+1k}-du^l_{i+1j-1k}-du^l_{i-1j+1k}+du^l_{i-1j-1k}}{4h_1h_2}+\\
&(\lambda+\mu)\frac{dw^l_{ij+1k+1}-dw^l_{ij-1k+1}-dw^l_{ij+1k-1}+dw^l_{ij-1k-1}}{4h_2h_3}=\rho\frac{dv^{l+1}_{ijk}-2dv^l_{ijk}+dv^{l-1}_{ijk}}{\tau^2},
\end{aligned} \tag{13}$$

$$\begin{aligned}
&\mu\frac{dw^l_{i+1jk}-2dw^l_{ijk}+dw^l_{i-1jk}}{h_1^2}+\mu\frac{dw^l_{ij+1k}-2dw^l_{ijk}+dw^l_{ij-1k}}{h_2^2}+\\
&+(\lambda+2\mu)\frac{dw^l_{ijk+1}-2dw^l_{ijk}+dw^l_{ijk-1}}{h_3^2}-\alpha\gamma\frac{dT^l_{ijk+1}-dT^l_{ijk-1}}{2h_3}-\chi^l_{ijk}+\\
&+(\lambda+\mu)\frac{du^l_{i+1jk+1}-du^l_{i+1jk-1}-du^l_{i-1jk+1}+du^l_{i-1jk-1}}{4h_1h_3}+\\
&(\lambda+\mu)\frac{dv^l_{ij+1k+1}-dv^l_{ij-1k+1}-dv^l_{ij+1k-1}+dv^l_{ij-1k-1}}{4h_2h_3}=\rho\frac{dw^{l+1}_{ijk}-2dw^l_{ijk}+dw^{l-1}_{ijk}}{\tau^2},
\end{aligned} \tag{14}$$

$$\begin{aligned}
&\lambda_0\left(\frac{dT^l_{i+1jk}-2dT^l_{ijk}+dT^l_{i-1jk}}{h_1^2}+\frac{dT^l_{ij+1k}-2dT^l_{ijk}+dT^l_{ij-1k}}{h_2^2}+\right.\\
&\left.+\frac{dT^l_{ijk+1}-2dT^l_{ijk}+dT^l_{ijk-1}}{h_3^2}\right)-C_\varepsilon\frac{dT^{l+1}_{ijk}-dT^{l-1}_{ijk}}{2\tau}-\\
&-\alpha\gamma T_0\left(\frac{du^{l+1}_{i+1jk}-du^{l+1}_{i-1jk}-du^{l-1}_{i+1jk}+du^{l-1}_{i-1jk}}{4h_1\tau}+\right.\\
&\left.+\frac{dv^{l+1}_{ij+1k}-dv^{l+1}_{ij-1k}-dv^{l-1}_{ij+1k}+dv^{l-1}_{ij-1k}}{4h_2\tau}+\frac{dw^{l+1}_{ijk+1}-dv^{l+1}_{ijk-1}-dv^{l-1}_{ijk+1}+dv^{l-1}_{ijk-1}}{4h_3\tau}\right)=0.
\end{aligned} \tag{15}$$

we can see that the finite difference equations (12-15) are explicit and can be solved for du_{ijk}^{l+1}, dv_{ijk}^{l+1}, dw_{ijk}^{l+1} and $dT_{i,j}^{l+1}$ respectively. For example, here is shown for eq.(12)

$$\begin{aligned} du_{ijk}^{l+1} = \frac{\tau^2}{\rho}\Bigg(\eta\frac{du_{i+1jk}^{l}-2du_{ijk}^{l}+du_{i-1jk}^{l}}{h_1^2}+\mu\frac{du_{ij+1k}^{l}-2du_{ijk}^{l}+du_{ij-1k}^{l}}{h_2^2}+ \\ +\mu\frac{du_{ijk+1}^{l}-2du_{ijk}^{l}+du_{ijk-1}^{l}}{h_3^2}-\xi_{ijk}^{l}-\alpha\gamma_{\varepsilon}\frac{dT_{i+1jk}^{l}-dT_{i-1jk}^{l}}{2h_1}+ \\ +(\lambda+\mu)\frac{dv_{i+1j+1k}^{l}-dv_{i+1j-1k}^{l}-dv_{i-1j+1k}^{l}+dv_{i-1j-1k}^{l}}{4h_1h_2}+ \\ +(\lambda+\mu)\frac{dw_{i+1jk+1}^{l}-dw_{i+1jk-1}^{l}-dw_{i-1jk+1}^{l}+dw_{i-1jk-1}^{l}}{4h_1h_3}\Bigg)+2du_{ijk}^{l}-du_{ijk}^{l-1}, \end{aligned} \tag{16}$$

with the boundary conditions

$$\begin{aligned} &\left.\begin{aligned} du_{0jk}^{l}&=du_0^x,\ du_{N_1jk}^{n}=d\overline{u}_0^x \\ dv_{0jk}^{l}&=dv_0^x,\ dv_{N_1jk}^{l}=d\overline{v}_0^x \\ dw_{0jk}^{l}&=dw_0^x,\ dw_{N_1jk}^{l}=d\overline{w}_0^x \end{aligned}\right\},\quad \left.\begin{aligned} du_{i0k}^{l}&=du_0^y,\ du_{iN_2}^{n}=d\overline{u}_0^y \\ dv_{i0k}^{l}&=dv_0^y,\ dv_{iN_2}^{n}=d\overline{v}_0^y \\ dw_{i0k}^{l}&=dw_0^y,\ dw_{iN_2}^{l}=d\overline{w}_0^y \end{aligned}\right\}, \\ &\left.\begin{aligned} du_{i0}^{l}&=du_0^z,\ du_{ijN_3}^{l}=d\overline{u}_0^z \\ dv_{ij0}^{l}&=dv_0^z,\ dv_{ijN_3}^{l}=d\overline{v}_0^z \\ dw_{ij0}^{l}&=dw_0^z,\ dw_{ijN_3}^{l}=d\overline{w}_0^z \end{aligned}\right\},\quad \left.\begin{aligned} dT_{0jk}^{l}&=dT_{yz},\ dT_{N_1j}^{l}=d\overline{T}_{yz} \\ dT_{i0k}^{l}&=dT_{xz},\ dT_{iN_2}^{l}=d\overline{T}_{xz} \\ dT_{ij0}^{l}&=dT_{xy},\ dT_{ijN_3}^{l}=d\overline{T}_{xy} \end{aligned}\right\}; \end{aligned} \tag{17}$$

and an initial conditions

$$\begin{aligned} &du_{ijk}^{0}=d\phi_{ijk},\quad dv_{ijk}^{0}=df_{ijk},\quad dw_{ijk}^{0}=d\psi_{ijk}, \\ &du_{ijk}^{1}=du_{ijk}^{0}+\tau d\tilde{\phi}_{ijk},\quad dv_{ijk}^{1}=dv_{ijk}^{0}+\tau d\tilde{f}_{ijk},\quad dw_{ijk}^{1}=dv_{ijk}^{0}+\tau d\tilde{\psi}_{ijk},\ dT_{ijk}^{0}=d\overline{T}_{ijk} \end{aligned} \tag{18}$$

Using the recurrent formula (16) and the initial and boundary conditions (17-18) we can find the displacement du_{ijk}^{l+1}, dv_{ijk}^{l+1}, dw_{ijk}^{l+1} and temperature $dT_{i,j}^{k+1}$ corresponding to the increment of the external forces. The total displacement and temperature are found as a sum of increments i.e.

$$u=\sum_p du,\qquad v=\sum_p dv,\qquad w=\sum_p dw,\qquad T=\sum_p dT\ ,$$

where p is a number of thermomechanical force increments. Note that the finite difference equations, eqs. (12-15), are explicit and the convergence depends on mesh step lengths of h_1, h_2 and τ. In eqs. (12-15) replacing the index k by $k+1$ and we obtain the following equations with a tridiagonal matrices

$$a_{ijk}du_{i+1jk}^{l+1}+b_{ijk}du_{ijk}^{l+1}+c_{ijk}du_{i-1jk}^{l+1}=f_{ijk}, \tag{19}$$

$$A_{ijk}dv_{i,j+1k}^{l+1}+B_{ijk}dv_{ijk}^{l+1}+C_{ijk}dv_{ij-1k}^{l+1}=F_{ijk}, \tag{20}$$

$$\widehat{A}_{ijk}w_{ijk+1}^{l+1}+\widehat{B}_{ijk}w_{ijk}^{l+1}+\widehat{C}_{ijk}w_{ijk-1}^{l+1}=\widehat{F}_{ijk}, \tag{21}$$

$$\tilde{a}_{ijk}dT_{i+1jk}^{l+1}+\tilde{b}_{ijk}dT_{ijk}^{l+1}+\tilde{c}_{ijk}dT_{i-1jk}^{l+1}=\varphi_{ijk}, \tag{22}$$

where $a_{ijk}=c_{ijk}=\dfrac{\lambda+2\mu}{h_1^2}$, $b_{ijk}=-2\dfrac{\lambda+2\mu}{h_1^2}-\dfrac{\rho}{\tau^2}$, $A_{ijk}=C_{ijk}=\dfrac{\lambda+2\mu}{h_2^2}$, $B_{ijk}=-2\dfrac{\lambda+2\mu}{h_2^2}-\dfrac{\rho}{\tau^2}$,

$$f_{ijk} = \alpha\gamma \frac{dT^l_{i+1jk} - dT^l_{i-1jk}}{2h_1} - \mu \frac{du^l_{ij+1k} - 2du^l_{ijk} + du^l_{ij-1k}}{h_2^2} + \xi^l_{ijk} -$$

$$-\mu \frac{du^l_{ijk+1} - 2du^l_{ijk} + du^l_{ijk-1}}{h_3^2} - (\lambda+\mu) \frac{dv^l_{i+1j+1k} - dv^l_{i+1j-1k} - dv^l_{i-1j+1k} + dv^l_{i-1j-1k}}{4h_1h_2} -$$

$$-(\lambda+\mu) \frac{dw^l_{i+1jk+1} - dw^l_{i+1jk-1} - dw^l_{i-1jk+1} + dw^l_{i-1jk-1}}{4h_1h_3} + \rho \frac{u^{l-1}_{ijk} - 2u^l_{ijk}}{\tau^2}$$

$$F_{ijk} = \alpha\gamma \frac{dT^l_{ij+1k} - dT^l_{ij-1k}}{2h_2} - \mu \frac{dv^l_{i+1jk} - 2dv^l_{ijk} + dv^l_{i-1jk}}{h_1^2} + \zeta^l_{ijk} -$$

$$-\mu \frac{dv^l_{ijk+1} - 2dv^l_{ijk} + dv^l_{ijk-1}}{h_3^2} - (\lambda+\mu) \frac{du^l_{i+1j+1k} - du^l_{i+1j-1k} - du^l_{i-1j+1k} + du^l_{i-1j-1k}}{4h_1h_2} -$$

$$-(\lambda+\mu) \frac{dw^l_{ij+1k+1} - dw^l_{ij-1k+1} - dw^l_{ij+1k-1} + dw^l_{ij-1k-1}}{4h_2h_3} + \rho \frac{v^{l-1}_{ijk} - 2v^l_{ijk}}{\tau^2}$$

$$\widehat{A}_{ijk} = \widehat{C}_{ijk} = \frac{(\lambda+2\mu)}{h_3^2}, \quad \widehat{B}_{ijk} = -2\frac{(\lambda+2\mu)}{h_3^2} - \frac{\rho}{\tau^2}, \quad \tilde{a}_{ijk} = \tilde{c}_{ijk} = \frac{\lambda_0}{h_1^2}, \quad \tilde{b}_{ij} = -2\frac{\lambda_0}{h_1^2} - \frac{C_\varepsilon}{2\tau},$$

$$\widehat{F}_{ijk} = \alpha\gamma \frac{dT^l_{ijk+1} - dT^l_{ijk-1}}{2h_3} - \mu \frac{dw^l_{i+1jk} - 2dw^l_{ijk} + dw^l_{i-1jk}}{h_1^2} - \mu \frac{dw^l_{ij+1k} - 2dw^l_{ijk} + dw^l_{ij-1k}}{h_2^2} +$$

$$+ \chi^l_{ijk} - (\lambda+\mu) \frac{du^l_{i+1jk+1} - du^l_{i+1jk-1} - du^l_{i-1jk+1} + du^l_{i-1jk-1}}{4h_1h_3} -$$

$$-(\lambda+\mu) \frac{dv^l_{ij+1k+1} - dv^l_{ij+1k-1} - dv^l_{ij-1k+1} + dv^l_{ij-1k-1}}{4h_2h_3} + \rho \frac{w^{l-1}_{ijk} - 2w^l_{ijk}}{\tau^2},$$

$$\varphi_{ijk} = \alpha\gamma T_0 \left(\frac{du^{l+1}_{i+1jk} - du^{l+1}_{i-1jk} - du^{l-1}_{i+1jk} + du^{l-1}_{i-1jk}}{4h_1\tau} + \frac{dv^{l+1}_{ij+1k} - dv^{l+1}_{ij-1k} - dv^{l-1}_{ij+1k} + dv^{l-1}_{ij-1k}}{4h_2\tau} + \right.$$

$$\left. + \frac{du^{l+1}_{ijk+1} - du^{l+1}_{ijk-1} - du^{l-1}_{ijk+1} + du^{l-1}_{ijk-1}}{4h_3\tau} \right) - \lambda_0 \frac{dT^l_{ij+1k} - 2dT^l_{ijk} + dT^l_{ij-1k}}{h_2^2} -$$

$$-\lambda_0 \frac{dT^l_{ijk+1} - 2dT^l_{ijk} + dT^l_{ijk-1}}{h_3^2} - \frac{C_\varepsilon}{2\tau} dT^{k-1}_{ij}$$

Eqs. (19-22) may be solved numerically using the elimination method [22].

4. Numerical examples

Consider a clamped parallelepiped with an inside temperature T_0 at time $t = 0$. On the opposite surfaces $x = 0, \ell_1$ of the parallelepiped the cupola like temperature T is given. The aforementioned problem may be describe by eqs. (8–10) and with a following initial

$$u(x,y,z,t)\big|_{t=0} = 0,\ v(x,y,z,t)\big|_{t=0} = 0,\ w(x,y,z,t)\big|_{t=0} = 0,$$

$$\left.\frac{\partial u(x,y,z,t)}{\partial t}\right|_{t=0} = 0,\ \left.\frac{\partial v(x,y,z,t)}{\partial t}\right|_{t=0} = 0,\ \left.\frac{\partial w(x,y,z,t)}{\partial t}\right|_{t=0} = 0,$$

$$T(x,y,z,t)\big|_{t=0} = T_0; \tag{23}$$

and boundary conditions

$$
\begin{aligned}
&u(x,y,z,t)\big|_{x,y,z=0}=0,\ v(x,y,z,t)\big|_{x,y,z=0}=0,\ w(x,y,z,t)\big|_{x,y,z=0}=0,\\
&u(x,y,z,t)\big|_{x,y,z=1}=0,\ v(x,y,z,t)\big|_{x,y,z=1}=0,\ w(x,y,z,t)\big|_{x,y,z=1}=0,\\
&T(x,y,z,t)\big|_{x=0}=T_0+T_0\sin(\pi y)\sin(\pi z),\ T(x,y,z,t)\big|_{x=\ell}=T_0+T_0\sin(\pi y)\sin(\pi z),\\
&T(x,y,z,t)\big|_{y=0}=T_0,\ T(x,y,z,t)\big|_{y=\ell}=T_0,\\
&T(x,y,z,t)\big|_{z=0}=T_0,\ T(x,y,z,t)\big|_{z=\ell}=T_0.
\end{aligned}
\tag{24}
$$

For the computation purpose, we use the following data:

$$\lambda=1,\ \mu=0.5,\ \mu'=0.3,\ \ T_0=30,\ \alpha=0.05,\ \lambda_0=1,\ C_\varepsilon=2.7,\ \rho=1.0,$$

$$\ell_i=1,\ n=10,\ h=0.1,\ \tau=0.01$$

In Fig. 1-2 is shown the temperature and displacement distributions at *x=0.9*, *t=0.1*.

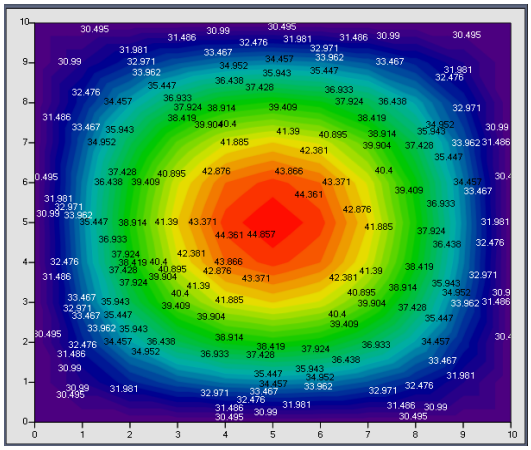

Figure 1. **Temperature distribution *T*(*x, y, z, t*)**

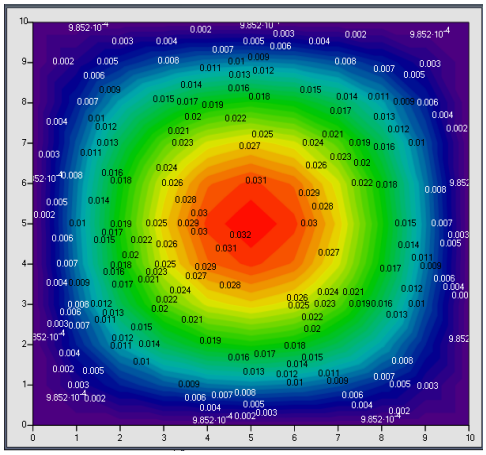

Figure 2. **Distribution of the displacement *u*(*x, y, z, t*)**

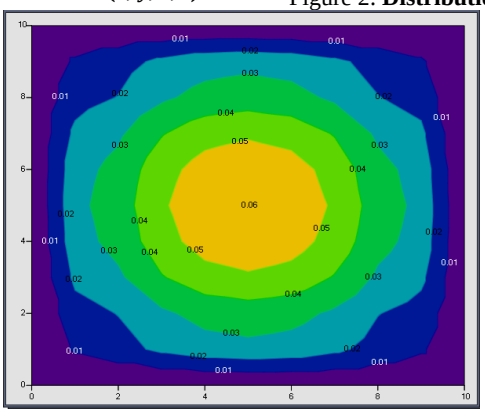

Figure 3. **Distribution of the plasticity zones E_u(*x, y, z, t*)**

Fig. 3 show the distribution of displacement and plasticity zone inside the section *x=0.9*, *t=0.1* under the influence of sinusoidal temperature given at the boundary. From the Figures 1-2, we can see that the temperature and displacement reach their highest value in the vicinity of the corner points, and as expected, the plastic zones appear there.

Tables 1-2 show the temperature distribution, *T* obtained by solving eq. (16) and eqs. (19-22) based on explicit and implicit schemes. The explicit and implicit schemes are solved, using recurrent formulas and elimination method, respectively.

Table 1.

Temperature distribution calculated by the recurrent formulas at *x=0.9, t=0.1*

y / *z*	***0***	***0.1***	***0.2***	***0.3***	***0.4***	***0.5***	***0.6***
0	30	30	30	30	30	30	30
0.1	30	31,52	32,87	33,95	34,65	34,89	34,66
0.2	30	32,87	35,45	37,5	38,83	39,27	38,83
0.3	30	33,95	37,5	40,33	42,14	42,76	42,14
0.4	30	34,65	38,81	42,14	44,26	45	44,26
0.5	30	34,89	39,26	42,76	45	45,77	45
0.6	30	34,66	38,83	42,14	44,26	45	44,26

Table 2.

Temperature distribution obtained by the elimination method at *x=0.9, t=0.1*

y / *z*	***0***	***0.1***	***0.2***	***0.3***	***0.4***	***0.5***	***0.6***
0	30	30	30	30	30	30	30
0.1	30	31,52	32,87	33,95	34,65	34,89	34,65
0.2	30	32,87	35,45	37,49	38,81	39,26	38,81
0.3	30	33,95	37,49	40,31	42,11	42,74	42,11
0.4	30	34,65	38,81	42,11	44,24	44,97	44,24
0.5	30	34,89	39,26	42,74	44,97	45,74	44,97
0.6	30	34,65	38,81	42,11	44,24	44,97	44,24

5. Conclusions

Using the using the strain-space thermoplasticity theory formulated coupled dynamic boundary value problem for isotropic parallelepiped. The discreet equations in the form of explicit and implicit schemes are constructed using the finite-difference method. The explicit and implicit finite difference schemes are solved numerically using the elimination method and recurrent formulas, respectively. The distribution of displacement and plastic zones inside the sections of the parallelepiped under the thermomechanical loads were shown. Comparison of the numerical results obtained using two different methods shows the validity of the formulated coupled strain-space thermoplasticity boundary value problem and the obtained numerical results.

References

1. *Biot, M.A.* Thermoelasticity and irreversible thermo-dynamics. // J. Appl. Phys., 1956, No. 27, pp.240–253.

2. *Lord H.W., Shulman Y.* A generalized dynamical theory of thermoplasticity // J. Mech. Phys. Solids, 1967, vol.15, pp.299-309.

3. *Youssef, H.M.* Theory of two-temperature-generalized thermoelasticity // IMA J. Appl. Math., 2006, No. 71, pp.383-390.

4. *Simo J.C, Miehe C.* Associative coupled thermoplasticity at finite strains: Formulation, numerical analysis and implementation // Computer Methods in Applied Mechanics and Engineering.1992, vol. 98 (1), pp.41-104.

5. *Bertram A. and Krawitietz A.* On the introduction to thermoplasticity //Acta Mech., 2012 , vol. 223, pp.2257-2268.

6. *Helm D.* Stress computation in finite thermoplasticity // Int. J. Plasticity. 2006, vol. 22, pp.1699-1727.

7. *Yusupov Y.S. and Khaldjigitov A.A.,* Mathematical and numerical modelling of the coupled dynamic thermoplastic problem // Universal Journal of Computational Mathematics, 2017, vol. 5(2), pp.34-43.

8. *Khaldjigitov A.A., Qalandarov A.A and Nik Long N.M.A.* Numerical solution of 1D and 2D thermoelastic coupled problems // Int. J. of modern physics, 2012, vol.9, pp. 503-510.

9. *Khaldjigitov A.A., Qalandarov A.A. and Yusupov Y.S.* Coupled problems of thermoelasticity and thermoplasticity. Fan and technology press, Tashkent, 2019, 193 p.

10. *Yanga Q., Stainier L. and Ortiz M.* A variational formulation of the coupled thermo-mechanical boundary-value problem for general dissipative solids // Journal of the Mechanics and Physics of Solids. 2006, vol. 54, pp. 401–424.

11. *Naghdi P.M. and Trapp J.A.,* The significance of formulating plasticity theory with reference to loading surface in strain space // Int. J. Eng. Sci., 1975, vol. 113, pp.785-797.

12. *Khaldjigitov, A.A., Yusupov, Y.S., Adambaev, U.E., Sagdullaeva, D.A.* Numerical solution of two-dimensional coupled thermoplastic problems // In AIP Conference Proceedings. 2022, vol. 2637, No. 1, p. 040007. AIP Publishing LLC.

13. *Shevchenko, Y.N., Babashko, M.E., Piskunov, V.V., Savchenko, V.G.,* Spatial problems of thermoplasticity /

«Nauk. Dumka» Kiev, 1980, p. 262.
14. *Pavlichko, V.M.*, The solution of three-dimensional thermoplastic problem for simple loading. Problems of Strength // 1986, № 1. pp. 77-81.
15. *Tsaplin, A.I.*, To the solution of spatial thermoelasticity problems with variational-difference method. Problems in the theory of elasticity and plasticity / Sverdlovsk, 1978. p. 65-72.
16. *Yusupov Y.S., Babadjanov M.R.* Numerical solution of a Three-Dimensional Coupled thermoplastic problem based on deformation theory // The International Journal of Science & Technoledge 2019, vol. 7, iss. 9.
17. *Madrakhimov Sh., Makharov K., Lolaev M.*. Data preprocessing on input // AIP Conference Proceedings. 2021, 2365, 030003. doi: https://doi.org/10.1063/5.0058132
18. *Casey J. Naghdi P.M.* On the characterization of strain-hardening in plasticity // J. Appl. Mech., ASME, 1981, vol.48(2), pp. 285-296.
19. *Yoder P.J., Iwan W.D.* On the formulation of strain-space plasticity with multiple loading surfaces // J. Appl. Mech., 1981, vol. 48(4), pp.773-778.
20. *Nik Long N.M.A., Khaldjigitov A.A., Adambaev U.* On the constitutive relations for isotropic and transversely isotropic materials // Applied mathematical modeling, 2013, vol. 37, pp. 7726-7740.
21. *Marakhimov A.R., Kudaybergenov J.K., Khudaybergenov K.K., Ohundadaev U.R.* A multivariate binary decision tree classifier based on shallow neural network // Scientific and Technical Journal of Information Technologies, Mechanics and Optics, 2022, vol. 22(4), pp. 725-733.
22. *Khaldjigitov, A.A., Yusupov, Y.S, Khudazarov R.S. Sagdullaeva D.A.* On the thermoplasticity constitutive relations for isotropic and transversely isotropic materials // Int. Journal of Mechanical and Production Engineering Research and Development (IJMPERD) ISSN (P): 2249-6890; ISSN (E):.2019, Vol. 9, Issue 4, pp. 467-478

РАСЧЕТ КОНСТРУКЦИИ ЗЕМЛЯНОГО ПОЛОТНА ЖЕЛЕЗНЫХ ДОРОГ ИЗ БАРХАННЫХ ПЕСКОВ НА УСТОЙЧИВОСТЬ ПО ТИПОВЫМ ТЕХНОЛОГИЧЕСКИМ РЕШЕНИЯМ

Абдураимов У.К.[1]
[1]*Ташкентский государственный транспортный университет, Ташкент, Узбекистан*
E mail: ukabduraimov@mail.ru

Аннотация: *В статье описываются результаты исследованиями и оценками устойчивости откосов земляного полотно непосредственно связаны с проектированием и эксплуатацией железнодорожных пути. С целью оценка устойчивости и безопасной эксплуатации земляного полотно, надежное обеспечение устойчивости откосов грунтов. При этом основной задачей является определение оптимальных параметров откосов с учетом их длительной устойчивости при минимальных объемах работ и различных нагрузках. Для обоснования параметров устойчивости откосов требуется детальное изучение всех факторов, влияющих на процесс сдвига грунтов на откосах.*

Ключевые слова: *Земляное полотно, коэффициент устойчивости, сейсмическая сила.*

1. Введение

Железнодорожный путь, являясь одним из основных технических средств железнодорожного транспорта, должен быть устойчивым и прочным, обеспечивающим надежный, безопасный и своевременный пропуск по нему пассажирских и грузовых поездов с установленными скоростями. При этом обеспечение устойчивости и бесперебойного функционирования железных дорог, является существенным резервом повышения эффективности работы железнодорожного транспорта в целом.

Расчеты устойчивости откосов и насыпей производятся для определения требуемой плотности грунтов насыпей, осадок насыпей и оснований, стабильности (сопротивляемости выпиранию) грунтов основной площадки выемок и оснований насыпей. В нашем случае расчеты производятся для определения устойчивости имеющихся конструкций насыпей, возводимых из барханных песков, а также для определения устойчивости конструкций земляного полотна с применением местных и современных материалов противодефляционного и противодеформационного (ПДПД) укрепления. В отдельных случаях расчеты могут являться основой для оценки устойчивости откосов и склонов[1].

Расчет устойчивости откоса в каждом конкретном случае должен проводиться на основе детального изучения инженерно-геологической обстановки района и участка трассы, а также конкретных особенностей условий работы земляного полотна [2-4].

2. Материалы, методы и объект исследования.

Расчетная схема и метод расчета выбираются в каждом случае индивидуально. При их выборе необходимо учитывать возможность многообразия форм проявления нарушения устойчивости откосов. Выбранная расчетная схема должна соответствовать наиболее вероятной для данного случая форме нарушения устойчивости откоса, определяемой инженерно-геологическими особенностями и особенностями условий работы откоса. Эти особенности отражены в классификации откосов. В тех случаях, когда трудно заранее достоверно определить наиболее вероятную форму нарушения устойчивости откоса, необходимо провести комплексные расчеты, исходя из двух или нескольких наиболее вероятных схем[7-11].

Расчеты устойчивости откосов насыпей и выемок необходимо проводить для расчетных поперечников. В качестве расчетных принимаются поперечники с наиболее неблагоприятным сочетанием различных факторов, таких, как высота и крутизна откоса, величина сдвиговых характеристик грунтов, мощность и расположение слабых прослоек[12].

Для проведения расчета необходимы:

– данные по общим инженерно-геологическим условиям района строительства;
– заданное очертание откоса;
– геотехнический разрез по расчетному поперечнику;
– расчетные значения физико-механических характеристик грунтов, слагающих откос и его основание;
– гидрогеологические данные;
– расчетные временные нагрузки.

Степень достоверности расчета в значительной мере определяется правильностью выбора расчетной схемы и расчетных значений сдвиговых характеристик грунтов откоса и его основания.

При расчете устойчивости откосов земляного полотна железных дорог учитываются возникающие в откосе или в его основании усилия:

– от собственного веса грунтовой толщи;
– от воздействия временной подвижной нагрузки (для насыпей);
– от веса верхнего строения пути (для насыпей).

При расчете устойчивости откосов железнодорожных насыпей величина временной погонной подвижной нагрузки P_n определяется по формуле (рис. 1)

$$P_n = \frac{\Sigma P}{l_{жб}}, \qquad (1)$$

где P - давление на ось расчетного локомотива, т; $l_{жб}$ - длина жесткой базы локомотива, м; ΣP - суммарное давление на оси, составляющие жесткую базу, т.

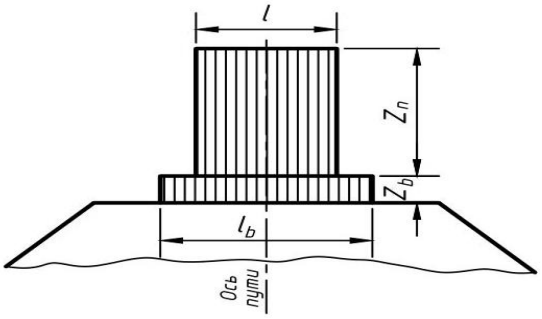

Рисунок 1 – **Учет подвижной нагрузки и нагрузки от верхнего строения пути при расчете устойчивости откосов железнодорожных насыпей**

Для железнодорожных линий I и II категорий величину погонной поездной нагрузки следует назначать равной 23 т, принимая во внимание перспективный тип локомотива с давлением на ось 32 т. Величина постоянной погонной нагрузки на основной площадке от верхнего строения пути устанавливается по заданному типу верхнего строения пути.

В расчетах устойчивости временная подвижная нагрузка и постоянная нагрузка от веса верхнего строения пути заменяются эквивалентным столбом грунта на основной площадке высотой соответственно Z_n и $Z_в$ (см. рис. 1).

Высота фиктивного столба грунта от поездной нагрузки определяется по формуле

$$Z_n = \frac{P_n}{\gamma \cdot l}, \qquad (2)$$

где P_n - погонная поездная нагрузка, т/м; γ - объемный вес грунта под основной площадкой, т/м^3; l - ширина фиктивного столба грунта, м; l = 2,7 + h (h - толщина балластного слоя).

Высота фиктивного столба грунта от веса верхнего строения определяется по формуле

$$Z_в = \frac{P_в}{\gamma \cdot l_б}, \qquad (3)$$

где $P_в$ - погонная нагрузка от верхнего строения пути, т/м; $l_б$ - ширина балластной призмы в м, приведенная к равновеликому прямоугольнику той же высоты; γ - объемный вес грунта под основной площадкой, т/м^3.

Применять для расчета устойчивости один из приведенных методов (табл. 1) допускается лишь в тех случаях, когда заранее можно предвидеть наиболее вероятную форму нарушения устойчивости откоса.

Если откос отличается сложным геологическим строением, подвержен воздействию грунтовых вод и т.п., когда заранее нельзя определить наиболее вероятную форму нарушения устойчивости откоса, следует применять комплексный расчет с использованием двух или более методов, предполагающих различные варианты нарушения устойчивости (см. табл. 1).

Таблица 1.

Выбор методов расчета устойчивости насыпей

Метод расчета	Индекс классификационной группы по табл. 2		Условия применения
	насыпь	выемка	
Расчет по методу круглоцилиндрических поверхностей скольжения	А-1, 2	А-1,2	При заведомо прочном основании
Расчет по методу плоских поверхностей скольжения	-	Б -I, Б -II-1,2	В тех случаях, когда поверхность скольжения явно предопределена геологической структурой откоса, и при заведомо прочном основании откоса
Комплексный расчет по методу круглоцилиндрических поверхностей скольжения и методу плоских поверхностей скольжения	Б-1, 2		При заведомо прочном основании откоса, но когда заранее трудно установить форму наиболее вероятной поверхности скольжения
Комплексный расчет по методу круглоцилиндрических поверхностей скольжения, методу плоских поверхностей скольжения и методу F_p	-	Б -I, II, III, IV-1,2	При заведомо прочном основании откоса, но в случае, когда заранее трудно установить наиболее вероятную форму нарушения устойчивости
Расчет на выдавливание (по коэффициенту безопасности)	А, Б-1, 2	А, Б- I , II , III , IV -1,2	Применяется в комплексе с любым из методов, указанных в данной таблице, - во всех случаях, когда заранее нет уверенности в абсолютной устойчивости основания откоса

3. Постановка задачи.

Для определения устойчивости насыпи земляного полотна высотой 6 метра выполняются расчеты коэффициентов устойчивости по методу Г.М. Шахунянца[2]. Ряд расчетов выполняется для определения критического положения кривой обрушения, которая принимается при минимальном значении коэффициента устойчивости.

$$K_{\text{ст}} = \frac{\sum_{i=1}^{n} M_{i-\text{уд}}}{\sum_{i=1}^{m} M_{i-\text{сдв}}} = \frac{\sum_{i=1}^{n} C_i l_i + \sum_{i=1}^{n} f_i N_i + \sum_{i=1}^{n} T_{i-\text{уд}}}{\sum_{i=1}^{n-m} T_{i-\text{сдв}} + Q_c} \quad (4)$$

где $K_{\text{ст}}$- коэффициент устойчивости; $\Sigma M_{i\text{-уд}}$ *и* $\Sigma M_{i\text{-сдв}}$ – соответственно сумма моментов сил, удерживающих откос от смешения и сдвигающих его; n – суммарное количество отсеков блока смещения; m - количество отсеков блока смещения, в которых действуют удерживающие касательные составляющие силы веса; C_i и f_i – соответственно удельное сцепление (кПа) и коэффициент внутреннего трения грунта в основании i-го отсека составляющие силы его веса, кН; Q_c – сейсмическая сила, кН;

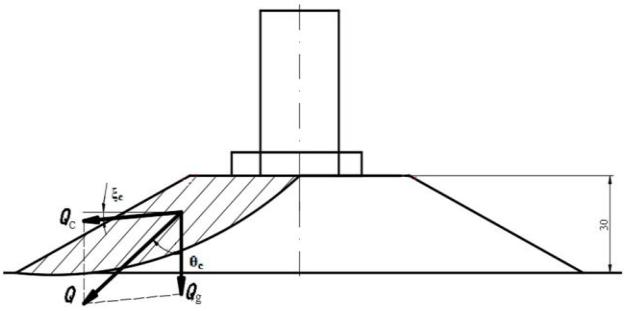

Рисунок 2. **Схема к расчету сейсмической силы**

Учет влияния сейсмичности (землетрясений) на устойчивость откосов регламентируется нормами [5] и обусловлен необходимостью обеспечить устойчивость сооружений при воздействии на них ударных и вибрационных нагрузок, вызываемых землетрясениями. В соответствии со нормам[6] влияние сейсмичности на транспортные сооружения учитывается для железных дорог I - IV категорий в районах с сейсмичностью 7, 8 и 9 баллов.

Рассмотрим, как оценить устойчивость откосов насыпи с учетом сейсмичности [3].

Сейсмическая сила, действующая на блок смещения,

$$Q_c = m n_c \rho \quad (5)$$

где m - масса блока возможного смещения, т; n_c - коэффициент динамичности (зависит от рода грунта, класса сооружения и высоты насыпи; $n_c = 1y$ подошвы насыпи и $n_c = 2 - y$ бровок); ρ - ускорение сейсмической волны, m/c^2.

Сила веса блока смещения (рис.1) $Q_g = mg$, отсюда $m = Q_g/g$. Подставив m в (5), получим

$$Q_c = n_c \frac{Q_g}{g} \rho = n_c \mu_c Q_g = \mu Q_g, \quad (6)$$

где $\mu_c = \rho/g$ - коэффициент сотрясения;

$\mu = n_c \mu_c$ - динамический коэффициент сотрясения.

Направление сейсмической силы Q_c непредсказуемо (угол ξ_c, см. рис.2, неизвестен), поэтому в расчетах обычно принимается сила Q_c, направленная на смещение откоса, практически горизонтальной.

4. Результаты

Проведем расчеты по критическому положению кривой обрушения для насыпи высотой 6 метров без укрепления, с укреплением слоем глинистого грунта толщиной 15 и 20 см, с одной и двумя прослойками. Расчетные схемы приведены на рис. 3, а результаты расчетов в табл. 2.

Исходные данные: $H_н$=6,0м, $B_{оп}$=7,6м, m=2

Параметры нагрузок: $P_п$=80кПа; $b_п$=2,75м, $P_б$=15 кПа, $b_б$=4,3м.

Параметры состояния барханных песков: $\gamma_г$=15,9 кН/м^3; c=2кПа; φ=26˚

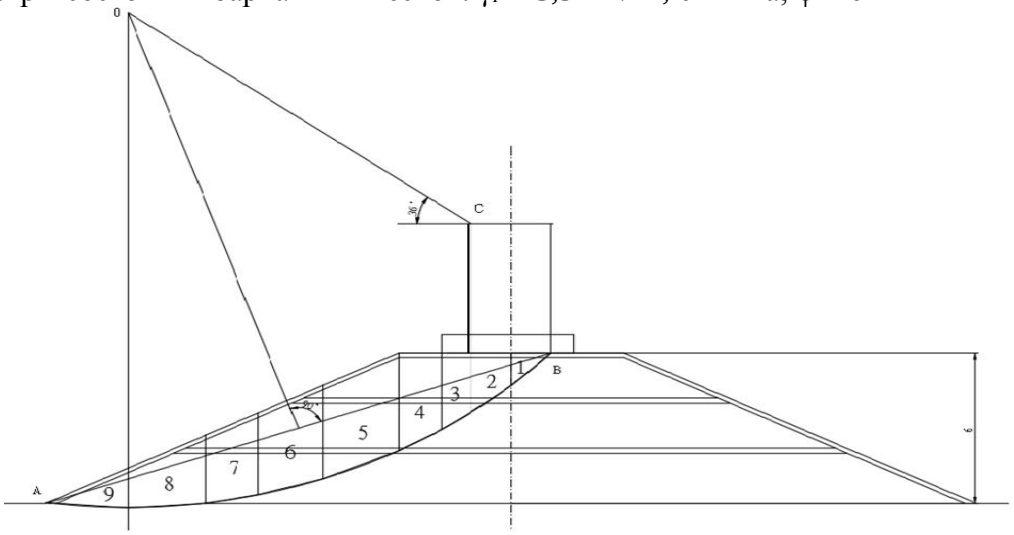

Рисунок 3 – **Схема для расчета коэффициента устойчивости откоса насыпи**

Таблица 2.

Расчет коэффициента устойчивости откоса при высоте насыпи 6 м с укреплением откосов глинистым грунтом и с двумя прослойками

Расчетные величины	Значения расчетных величин по отсекам									сумма
	1	2	3	4	5	6	7	8	9	
Xi	13,66	12,31	11,14	9,92	7,9	5,5	3,51	1,32	1,39	
sinβi	0,692	0,624	0,565	0,503	0,400	0,279	0,178	0,067	0,070	
радиан	0,765	0,674	0,600	0,527	0,412	0,283	0,179	0,067	0,071	
Угол наклона βi	43,816	38,603	34,376	30,184	23,603	16,186	10,247	3,836	4,039	
cosβi	0,721	0,781	0,825	0,864	0,9163	0,960	0,984	0,997	0,997	
F, m²	0,876	2,482	2,712	5,061	9,868	7,786	5,292	5,664	2,082	
F, m² дрен грунт	0,25	0,27	0,199	0,29	0,515	0,443	0,352	0,526	0,523	
F, m² песок	0,626	2,093	2,314	4,482	8,331	6,737	4,588	4,97	1,559	
F, m² глина		0,119	0,199	0,289	1,022	0,606	0,352	0,168		
l, m	1,873	1,728	1,208	1,681	2,815	2,307	1,791	2,638	2,779	
Qi, kN	15,178	38,928	40,952	77,328	143,22	116,37	80,306	90,016	35,718	
Qci, kN	3,035	7,784	8,190	15,464	28,645	23,275	16,061	18,003	7,143	127,60
Ti=∑Qisinβi,	10,508	24,284	23,122	38,878	57,348	32,441	14,286	6,022	2,516	206,89
Ni=∑Qicosβi,	10,952	30,416	33,799	66,840	131,24	111,76	79,024	89,814	35,63	
φNi	5,3337	14,813	16,460	32,551	63,915	54,428	38,485	43,739	17,351	287,07
cili	9,308	8,588	7,115	12,321	20,633	16,910	13,128	13,111	13,811	114,92
$K_{уст}$										1,31

5. Анализ результатов

При расчете вновь проектируемых откосов необходимо обеспечивать определенный коэффициент запаса, величина которого зависит от применяемого метода расчета устойчивости и инженерно-геологических условий. При этом следует руководствоваться данными табл.3.

Таблица 3.+

-Требуемые минимальные значения коэффициентов запаса устойчивости при различных методах расчета

№ пп.	Метод расчета	Однородный сухой откос, сложенный песчаными грунтами при прочном основании	Прочие случаи
1	Метод круглоцилиндрических поверхностей скольжения	-	1,3/1,2
2	Метод горизонтальных сил (метод Маслова-Берера)	1,2/-	1,3/-
3	Метод Г.М. Шахунянца	1,2/1,15	1,25/1,2
4	Метод F_p Н.Н. Маслова	-	1,0
5	Расчет на выдавливание	-	1,0 (коэффициент безопасности)

6. Обсуждение

Расчеты, выполненные по описанной методике, позволили более эффективно назначить и степень устойчивости откоса оценивается в этом случае по величине коэффициента запаса устойчивости земляного полотна.

Требуемые минимальные значения коэффициентов запаса устойчивости при методе Г.М. Шахунянца получаются в результате расчета конструкции насыпи высотой 6 м с укреплением откосов глинистым грунтом и с двумя прослойками.

7. Заключение

Использование в инженерной практике большого числа расчетных методов для оценки устойчивости железнодорожного земляного полотно свидетельствует о сложности задачи и незавершенности процесса поиска ее решения, которое удовлетворяло бы исследователей и проектировщиков.

Существующими методами нахождение наиболее опасной круглоцилиндрической поверхности скольжения путем выделенной области не гарантирует нахождение минимума значения коэффициента устойчивости, поскольку возможно существование в других областях нескольких локальных минимумов.

Литература

1. *Грицык В. И.* Расчеты земляного полотна железных дорог. Учеб. пособие для вузов ж.-д. транспорта. М.: УМКМПС, 1998. 520 с.
2. *Шахунянц Г.М.* Железнодорожный путь: учебник для вузов ж.-д. трансп. - 3-е изд., перераб. и доп. - М.: Транспорт, 1987. 479 с.
3. *Яковлева Т.Г., Шульга В.Я., Амелин С.В. и др.* Основы устройства и расчетов железнодорожного пути. - М.: Транспорт, 1990. 367с.
4. *U Abduraimov, Q Jorayev.*, About the methods for calculation of the stability of slopes of ground massives. Central asian journal of mathematical theory and computer sciences 4 (1),2023 83-88
5. ШНК 2.01.20-16 «Строительство транспортных сооружений в сейсмических районах» Госархитектстрой Республики Узбекистан, г. Ташкент. 2015г, 30 с.
6. КМК 2.01.03-95 Строительство в сейсмических районах, Госкомархитектстрой РУз – Ташкент 1996. 88с.
7. *Меркурьев Ю.С., Стоянович Г.М., Шехтман И.О.* Анализ устойчивости насыпи по методу Г. М. Шахунянца с учётом сейсмических воздействий. Известия Петербургского университета путей сообщения, (1 (42)), 2015. 41-46 с.
8. *Султанов К.С., Вечкина Е.А., Абдураимов У.К.* Методы расчёта устойчивости земляного полотна железных дорог. Вестник ТашИИТ. №1, Ташкент, 2014, 40-45 с.
9. *М.Мирсаидов, А.М.Годованников.* Сейсмостойкость сооружений: Учебное пособие для студентов высших учебных заведений. Ташкент, «Узбекистан», 2008, 203 с.,
10. *Zhussupbekov A., Tulebekova A., Abduraimov U.* Features of laboratory testing methods of clayey soils. Journal of Tashkent Institute of Railway Engineers 16 (3), 2020 9-14
11. *Salikhanov, S., Pulatova, Z., Zakirov, F., Rahimjonov, Z., Abdullayev, A.*, Determination of deformations and self-stress in concrete on stress cement, (2021) E3S Web of Conferences, 264, art. no. 02056.
12. *U. K. Abduraimov; Z. M. Mirzaeva; G. B. Ismailova; Kh. U. Urazov*. On the stability of slopes of the subgrade under seismic impacts. *AIP Conf. Proc.* 3045, 050034 (2024).

МОДЕЛИРОВАНИЕ НЕЛИНЕЙНОГО ДЕФОРМИРОВАНИЯ И ПОВРЕЖДАЕМОСТИ ПОДЗЕМНЫХ ТРУБОПРОВОДОВ – СТЕРЖНЕЙ ПРИ ЦИКЛИЧЕСКИХ НАГРУЖЕНИЯХ С УЧЕТОМ БОЛЬШИХ ДЕФОРМАЦИЙ

Абдусаттаров А.[1], Старовойтов Э.И.[2], Рузиева Н.Б.[1]

Ташкентский государственный транспортный университет, Ташкент, Узбекистан

Белорусский государственный университет транспорта, Гомель, Белоруссия

E-mail: nodi2005@rambler.ru

Аннотация. *В работе приводится математические модели расчета подземных трубопроводов-стержней при циклических нагружениях с учетом больших деформаций и повреждаемости. На основе деформационной теории и вариационного принципа Гамильтона-Остроградского получена система дифференциальных уравнений движения (равновесия) трубопровода-стержня при циклическом нагружении и сформулированы краевые задачи. Рассмотрена методика расчета трубопроводов при динамическом нагружении с учетом вязкоупругого взаимодействия и повреждаемости. Приведена постановка задачи и расчетная схема подземного трубопровода с учетом больших деформации. При построении решений системы дифференциальных уравнений с граничными и начальными условиями применяется разностная схема второго порядка точности. В качестве примера исследована колебания подземной трубы с учетом вязкоупругого взаимодействия с грунтом и повреждаемости.*

Ключевые **слова:** циклическое нагружение, вариационный принцип, пластичность, вязкоупругость, повреждаемость, взаимодействия с грутом, конечная деформация, разностная схема.

1. Введение

Как известно, при действии переменных нагрузок в элементах конструкций и сооружений возникает ряда дополнительных явлений, таких как вторичные пластические деформации, изменение диаграмм деформирования от цикла к циклу, проявление свойств циклического упрочнения-разупрочнения и деформационной анизотропии, накопление повреждений и распространение трещин, расслоение слоев, приводящих к разрушению материала [1].

В работе [2] сформулированы основные уравнения переменной пластичности и вязкопластичности и с учетом накопленных повреждений. Рассмотрены вопросы циклической и длительной прочности элементов конструкций. Введена функция повреждаемости для оценки прочности упругопластических и реономных тел при циклических нагружениях. В работах [3,4] приведены описание диаграмм циклического деформирования для различных конструкционных материалов выполнено и показаны возможные уточнения и интерпретаций диаграмм при решении задач циклической прочности. Создание методов расчета элементов конструкций на прочность при повторно – переменном нагружении стало возможным в результате экспериментального и теоретического изучения закономерности циклического деформирования в упругопластической области, исследований кинетики напряжённо – деформированного состояния и разработки критериев накопления повреждений и разрушения при неоднородном напряженном состоянии.

В работах Т.Буриева [5] рассматривается обеспечение безопасности конструкций сложных объектов. Разрабатаны численные методы решения краевых задач, изложены вопросы реализации и построения алгоритмической системы расчета несущих элементов конструкций в пределах и за пределами упругости при циклических нагружениях.

В работах [6,7] исследованы условия взаимодействия трубы и грунта при продольных перемещениях трубопровода. На основе этих исследований была предложена гипотеза взаимного смещения подземных сооружений относительно грунта. Экспериментально установлено, что закон взаимодействия подземных трубопроводов с различными грунтами носит нелинейный характер, определены параметры, характеризующие нелинейные упругие, упругопластические и вязкопластические свойства взаимодействия подземного трубопровода с грунтом.

В книге [8] излагаются численного моделирования расчета напряженно-деформированного состояния магистральных трубопроводов, оценки их прочности в условиях многофакторного анализа, при этом использованы современные методы

вычислительной механики. В работе [9] рассмотрены учет больших упругопластические деформаций в элементах конструкций.

В работах [10,11] рассмотрены деформирования трехслойных элементов конструкций при переменных нагружениях с учетом упругих, упругопластических и вязкоупругопластических свойств материалов. Численно исследована НДС трехслойных элементов конструкций при действии однократных и циклических нагрузок. На основе вариационного принципа Лагранжа сформулирована краевая задача изгиба трёхслойных стержней при переменном нагружении с учетом повреждаемости материала. Для решения сформулированных задач применен приближенный метод, базирующийся на методе упругих решений Ильюшина. Получены численные результаты расчетных величин для элементов конструкций типа стержней с учетом циклических характеристик материалов и повреждаемости [12-14].

В данной работе рассматривается моделирование нелинейного деформирования и повреждаемости трубопроводов по уточненой теории стержней, взаимодействующих с грунтом и с учетом больших деформаций.

2. Постановка задачи и методы расчета

Приведем математические модели и схема расчета трубопроводов – тонкостенных стержней при циклическом нагружении на основе теории малых упругопластических деформаций А.А.Ильюшина и уточненной теории стержней В.К.Кабулова.

Рассмотрим тонкостенный стержень – трубы произвольного сечения при воздействии внешних переменных сил. Ось OX направим по длине стержня, а оси OZ и OY – по поперечному сечению. Перемещения центральной линии стержня при исходном нагружении обозначим через u_i' , компоненты деформаций и напряжений – через e'_{ij}, σ'_{ij}.

Следуя теории В.В.Москвитина [1], введем разности

$$\bar{u}_i^{(n)} = (-1)^n (u_i^{(n-1)} - u_i^{(n)}),\ \bar{e}_{ij}^{(n)} = (-1)^n (e_{ij}^{(n-1)} - e_{ij}^{(n)}),$$
$$\bar{\sigma}_{ij}^{(n)} = (-1)^n (\sigma_{ij}^{(n-1)} - \sigma_{ij}^{(n)}). \tag{1}$$

Перемещения точек стержня при переменном нагружении представим в цилиндрических координатах:

$$\bar{u}_1^{(n)}(x,r,\gamma,t) = \bar{u}^{(n)}(x,t) - \bar{\alpha}_1^{(n)}(x,t) r\cos\gamma - \bar{\alpha}_2^{(n)}(x,t) r\sin\gamma + \varphi\bar{v}^{(n)}(x,t) + a_1\beta_1^{(n)}(x,t) + a_2\beta_2^{(n)}(x,t),$$
$$\bar{u}_2^{(n)}(x,r,\gamma,t) = \bar{\upsilon}^{(n)}(x,t) - \bar{\theta}^{(n)}(x,t) r\sin\gamma,\ \bar{u}_3^{(n)}(x,r,\gamma,t) = \bar{w}^{(n)}(x,t) + \bar{\theta}^{(n)}(x,t) r\cos\gamma, \tag{2}$$

где $\bar{u}^{(n)}$, $\bar{v}^{(n)}$, $\bar{w}^{(n)}$ – компоненты перемещений при n-ном нагружении; $\alpha_1^{(n)}, \alpha_2^{(n)}$ – углы поворота сечения при чистом изгибе; $\beta_1^{(n)}, \beta_2^{(n)}$ – углы поперечного сдвига; $\theta^{(n)}$ – угол кручения; $\nu_1^{(n)}$ – погонная закрутка при n-ном нагружении; φ – функция кручения Сен-Венана.

Согласно теории переменной пластичности, компоненты напряжений связаны через деформации следующим образом:

а) при переменном нагружении в фиктивных координатах (по Москвитину)

$$\bar{\sigma}_{11}^{(n)} = 3G(1-\omega^{(n)})\bar{e}_{11}^{(n)},\ \bar{\sigma}_{13}^{(n)} = G(1-\omega^{(n)})\bar{e}_{13}^{(n)},\ \bar{\sigma}_{12} = G(1-\omega^{(n)})\bar{e}_{12}^{(n)}; \tag{3}$$

б) при переменном нагружении в текущих величинах (по Буриеву)

$$\sigma_{11}^{(k)} = 3G\left\{e_{11}^{(k)} - \left[\omega^{(k)} e_{11}^{(k)} + \sum_{m=1}^{k-1} \omega^{0(k-m)} \bar{\varepsilon}_{11}^{0(k-m)}\right]\right\},\ \sigma_{13}^{(k)} = G\left\{e_{31}^{(k)} - \omega^{(k)} \bar{\varepsilon}_{31}^{(k)} - \sum_{m=1}^{k-1} \omega^{0(k-m)} \bar{\varepsilon}_{31}^{0(k-m)}\right\},$$
$$\sigma_{12}^{(k)} = G\left\{e_{12}^{(k)} - \omega^{(k)} \bar{\varepsilon}_{12}^{(k)} - \sum_{m=1}^{k-1} \omega^{0(k-m)} \bar{\varepsilon}_{12}^{0(k-m)}\right\}. \tag{4}$$

Здесь аналитический вид функции пластичности принимается в виде [10]

$$\omega^{(n)} = \begin{cases} 0, & \text{при } \bar{\varepsilon}_u^{(n)} \le \bar{\varepsilon}_s^{(n)}(\eta) \\ \bar{A}_n \left[1 - \dfrac{\bar{\varepsilon}_s^{(n)}(\eta)}{\bar{\varepsilon}_u^{(n)}} \right]^{\bar{\alpha}_n}, & \text{при } \bar{\varepsilon}_u^{(n)} > \bar{\varepsilon}_s^{(n)}(\eta) \end{cases}.$$

В случае применения обобщенного принципа Мазинга $\bar{A}_n = \lambda,\ \bar{\alpha}_n = 1, \bar{\varepsilon}_u^{(n)} = \alpha_n \varepsilon_s$, при использовании диаграмм деформирования Гусенкова – Шнейдеровича $\bar{\varepsilon}_s^{(n)} = 2\varepsilon_s$, $\bar{A}_n = 1 - g_n$, где g_n – определяется экспериментально. При учете накопления повреждений:

$$\bar{\varepsilon}_s^{(n)}(\eta) = \alpha_1^{n-z}(1+\alpha_1)\varepsilon_s + (3G)^{-1} B^{1/\alpha} \cdot \left[1 - 0{,}5(1+\alpha_1)\alpha_1^{n-2}\right]\left[1 - (1-\eta)^{1+\alpha}\right]^{1/\alpha} (n-1)^{-1/\alpha}.$$

Функция повреждаемости η определяется из кинетического уравнения [2]:

$$\frac{d\eta}{d\lambda} = f(\bar{\sigma}_u, \eta_n), \tag{5}$$

при условии $\eta(0)=0$, $\eta(N)=1$, где N – число полуциклов до наступления предельного состояния (разрушения).

3. Уравнения движения трубопровода–стержня

Для вывода уравнения движения (равновесия) трубопровода – стержня при пространственном нагружении с учетом повреждаемости и взаимодействий используются вариационный принцип Гамильтона – Остроградского [1]:

$$\delta \int_t (T^{(n)} - \Pi^{(n)} + A^{(n)}) dt = 0 \cdot \tag{6}$$

Для определения вариации кинетической, потенциальной энергии и вариации работы внешних сил в данной постановке имеем соотношения:

$$\delta \int_t T^{(n)} dt = \int_x \tilde{A} \frac{\partial Y^{(n)}}{\partial t} E \delta Y^{(n)} dx \Big|_t - \int_t \int_x \tilde{A} \frac{\partial^2 Y^{(n)}}{\partial t^2} E \delta Y^{(n)}\ dxdt\ ; \tag{7}$$

$$\delta \int_t \Pi^{(n)} dt = \int_t \left\{ \left(A^{уп} - A^{пл} \right) \frac{\partial Y^{(n)}}{\partial x} + \left(B^{уп} - B^{пл} \right) Y^{(n)} \right\} E \delta Y^{(n)} dt \Big|_x + \int_t \int_x \left\{ \frac{\partial}{\partial x} \left(\left(A^{уп} - A^{пл} \right) \frac{\partial Y^{(n)}}{\partial x} + \right.\right.$$

$$\left.\left. + \left(B^{уп} - B^{пл} \right) Y^{(n)} \right) + \left(C^{уп} - C^{пл} \right) \frac{\partial Y^{(n)}}{\partial x} + \left(D^{уп} - D^{пл} \right) Y^{(n)} \right\} E \delta Y^{(n)} dxdt \tag{8}$$

$$\delta \int_t A^{(n)} dt = \int_t Q^{г(n)} \delta Y^{(n)}\ dt \Big|_x + \int_t \int_x Q^{п(n)} \delta Y^{(n)} dxdt, \tag{9}$$

где $Y^{(n)}$ – вектор перемещения, матрицы A, B, C, D – квадратичные матрицы девятого порядка; E – единичная матрица.

В случае учета силы взаимодействия трубопровода с грунтом поверхностные силы $\bar{q}_i^{(n)}$ торцевые силы $\bar{f}_i^{(n)}$ согласно теории [10,11] принимаются в виде:

$$\bar{q}_i^{(n)} = -k_i^{(n)}(\bar{u}_i^{(n)} - \bar{u}_i^{0(n)}) + \tilde{q}_i^{(n)}; \quad \bar{f}_i^{(n)} = -k_i^{гр(n)}(\bar{u}_i^{(n)} - \bar{u}_i^{0(n)}) + \tilde{f}_i^{(n)}, \tag{10}$$

где $k_i^{(n)}$ – коэффициент нелинейного взаимодействия трубопровода с окружающей средой на поверхности при переменном нагружении; $k_i^{гр(n)}$ – коэффициент взаимодействия трубы с окружающей средой на торцах; $\bar{u}_i^{0(n)}$ – составляющая пространственного сейсмического перемещения грунта по координатным осям при переменном нагружении.

Согласно (2) и (10), выражения $\bar{q}_i^{(n)}$, $\bar{f}_i^{(n)}$ представлена в виде:

$$\bar{q}_1^{(n)} = -k_1^{(n)}\Big[(\bar{u}^{(n)} - \bar{u}^{0(n)}) - y(\bar{\alpha}_1^{(n)} - \bar{\alpha}_1^{0(n)}) - z(\bar{\alpha}_2^{(n)} - \bar{\alpha}_2^{0(n)}) + \varphi(\bar{v}^{(n)} - \bar{v}^{0(n)}) + a_1(\bar{\beta}_1^{(n)} - \bar{\beta}_1^{0(n)}) +$$
$$+ a_2(\bar{\beta}_2^{(n)} - \bar{\beta}_2^{0(n)}) + \tilde{q}_1^{(n)}\Big], \quad \bar{q}_2^{(n)} = -k_2^{(n)}\Big[(\bar{v}^{(n)} - \bar{v}^{0(n)}) - z(\bar{\theta}^{(n)} - \bar{\theta}^{0(n)}) + \tilde{q}_2^{(n)}\Big],$$
$$\bar{q}_3^{(n)} = -k_3^{(n)}\Big[(\bar{w}^{(n)} - \bar{w}^{0(n)}) + y(\bar{\theta}^{(n)} - \bar{\theta}^{0(n)}) + \tilde{q}_3^{(n)}\Big] \qquad (11)$$

Учитывая соотношения (10) и (2) и после некоторых преобразований, а также ряд обозначений вариации работ внешних сил приняты в виде

$$\delta\int_t A dt = \int_t\int_x \Big\{\Big(N_x^{об(n)} - N_x^{П(n)} + N_x^{из(n)}\Big)\delta u^{(n)} + \Big(Q_y^{об(n)} + Q_y^{П(n)} + Q_y^{из(n)}\Big)\delta\upsilon^{(n)} + \Big(Q_z^{об(n)} + Q_z^{П(n)} +$$
$$Q_z^{из(n)}\Big)\delta w^{(n)} - \Big(M_z^{об} + M_z^{П(n)} + M_z^{из(n)}\Big)\delta\alpha_1^{(n)} - \Big(M_y^{об(n)} + M_y^{П(n)} + M_y^{из(n)}\Big)\delta\alpha_2^{(n)} -$$
$$-\Big(M_x^{об(n)} + M_x^{П(n)} + M_x^{из(n)}\Big)\delta\theta^{(n)} + \Big(M_\varphi^{об(n)} + M_\varphi^{П(n)} + M_\varphi^{из(n)}\Big)\delta\nu^{(n)} + \Big(M_{a_1}^{об(n)} + M_{a_1}^{П(n)} + M_{a_1}^{из(n)}\Big)\delta\beta_1^{(n)} +$$
$$+\Big(M_{a_2}^{об(n)} - M_{a_2}^{П(n)} + M_{a_2}^{из(n)}\Big)\delta\beta_2^{(n)}\Big\}dxdt + \int_t \Big\{N^{Г(n)}\delta u^{(n)} + Q_y^{Г}\delta\upsilon^{(n)} + Q_z^{Г(n)}\delta w^{(n)} - M_z^{Г(n)}\delta\alpha_1^{(n)} -$$
$$-M_y^{Г(n)}\delta\alpha_2^{(n)} - M_x^{Г(n)}\delta\theta^{(n)} + M_\varphi^{Г(n)}\delta\nu^{(n)} + M_{a_1}^{об(n)}\delta\beta_1^{(n)} + M_{a_2}^{об(n)}\delta\beta_2^{(n)}\Big\}dt\Big|_x .$$

Здесь, например, силы взаимодействия имеет вид:

$$N_x^{из(n)} = -K_{N_x}^{(n)}\Big[(u^{(n)} - u^{0(n)}) + K_{N_{\alpha 1}}^{(n)}(\alpha_1^{(n)} - \alpha_1^{0(n)}) + K_{N_{\alpha 2}}^{(n)}(\alpha_2^{(n)} - \alpha_2^{0(n)}) + K_{N\varphi}^{(n)}(\nu^{(n)} - \nu^{0(n)}) -$$
$$-K_{N_{\beta 1}}^{(n)}(\beta_1^{(n)} - \beta_1^{0(n)}) - K_{N_{\beta 2}}^{(n)}(\beta_2^{(n)} - \beta_2^{0(n)});$$

где $K_{N_x}^{(n)}, K_{N_{\alpha 1}}^{(n)}, K_{N\varphi}^{(n)} \ldots K_{N_{\beta 2}}^{(n)}$ – коэффициенты взаимодействия, определяемые из эксперимента при повторно – переменном нагружении с учетом поврежденности.

Определяя и подставляя векторные выражения вариации кинетической, потенциальной энергий и работы внешних сил в вариационный принцип (6), получим

$$\int_t\int_x \Bigg\{\tilde{A}\frac{\partial^2 Y^{(n)}}{\partial t^2} + \frac{\partial}{\partial x}\Bigg[\Big(A^{уп} - A^{пл}\Big)\frac{\partial Y^{(n)}}{\partial x} + \Big(B^{уп} - B^{пл}\Big)Y^{(n)}\Bigg] +$$
$$+\Big(C^{уп} - C^{пл}\Big)\frac{\partial Y^{(n)}}{\partial x} + \Big(D^{уп} - D^{пл}\Big)Y^{(n)} + Q^{П(n)}\Bigg\}E\,\delta Y^{(n)}\,dx\,dt +$$
$$+\int_t \Bigg\{\Big(A^{уп} - A^{пл}\Big)\frac{\partial Y^{(n)}}{\partial x} + \Big(B^{уп} - B^{пл}\Big)Y^{(n)} + Q^{Г(n)}\Bigg\}E\,\delta Y^{(n)}\,dt\,\Bigg|_x + \int_x \tilde{A}\frac{dY^{(n)}}{dt}E\delta Y^{(n)}\,dx\Bigg|_t = 0$$

Из этого вариационного уравнения получаем следующую краевую задачу:

$$\tilde{A}\frac{\partial^2 Y^{(n)}}{\partial t^2} + \frac{\partial}{\partial x}\Bigg[\Big(A^{уп} - A^{пл}\Big)\frac{\partial Y^{(n)}}{\partial x} + \Big(B^{уп} - B^{пл}\Big)Y^{(n)}\Bigg] + \Big(C^{уп} - C^{пл}\Big)\frac{\partial Y^{(n)}}{\partial x} + \Big(D^{уп} - D^{пл}\Big)Y^{(n)} + Q^{н} = 0; \qquad (12)$$

$$\Bigg\{\Big(A^{уп} - A^{пл}\Big)\frac{\partial Y}{\partial x} + \Big(B^{уп} - B^{пл}\Big)Y + Q^{гр}\Bigg\}\delta Y\Bigg|_x = 0; \;\; \tilde{A}\frac{dY^{(n)}}{dt}E\delta Y^{(n)}\Bigg|_t = 0 \qquad (13)$$

Из сиситемы (12) - (13) вытекает уравнения равновесия трубопровода при повторно-переменном нагружении с граничными условиями в векторной форме. Для решения краевой задачи используется метод конечных разностей и метод упругих решений Ильюшина. На основе приведенных алгоритмов решена ряд краевых задач для анлиза НДС трубопроводов-стержней при циклическом нагружений. Результаты расчета предствлена в виде таблиц и графиков [11-13].

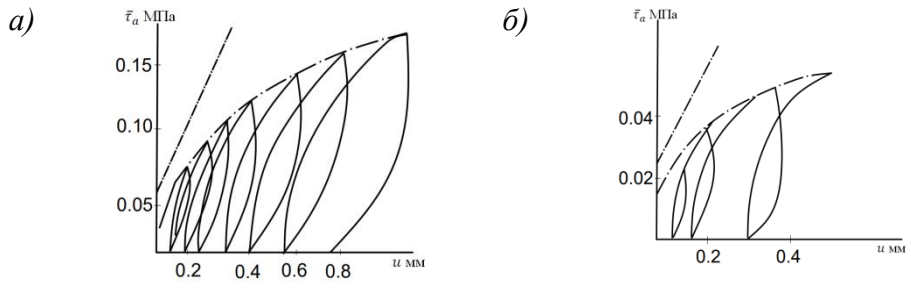

Рисунок 1 – **Диаграмма взаимодействия при многократной нагрузке-разгрузке стальной трбы** $(D_H = 0{,}189\ м,\ l = 3{,}86\ м)$ **с суглинком**

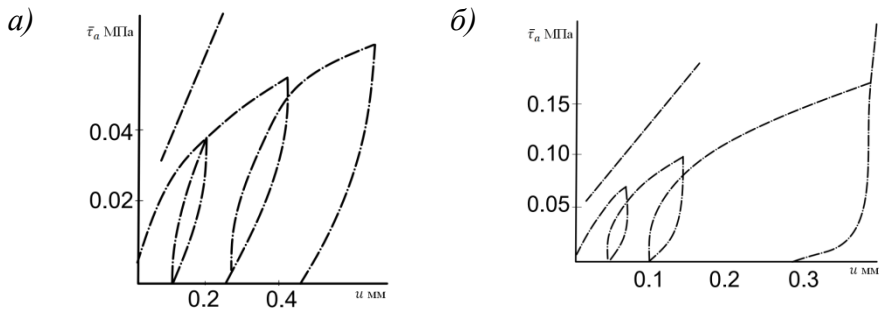

Рисунок 2 – **Диаграмма взаимодействия при многократной нагрузке-разгрузке чугунной трубы** $(D_H = 0{,}169\ м,\ l = 2{,}00\ м)$ **с песком**

Отметим, что некоторые свойства циклического нагружения наблюдается и при переменном нагружении подземных трубопроводов, взаимодействующих с грунтом. Такие результаты были получены в экспериментах [6]. На рис. 1(а,б) и 2(а,б) приведены диаграммы взаимодействия стальной трубы с суглинком и чугунной трубы с песком при многократном цикле нагрузки – разгрузки.

Следуя [1,7] запишим зависимость сопротивления грунта продольному перемещению трубопровода в виде

$$\tau_a = -K_x^0\left[u - \int_0^t R(t'-\tau')u(x,t)d\tau\right] \tag{14}$$

где

$$t' = \int_0^t \frac{d\xi}{a_\eta(\eta(x_\alpha,\xi))},\ \ \tau' = \int_0^\tau \frac{d\xi}{a_\eta(\eta(x_\alpha,\xi))}$$

Функция ползучести $R(t'-\tau')$ определяется экспериментально. В простейшем виде $R(t'-\tau')$ можно представить в виде $R(t'-\tau') = R_0(t'-\tau')^\beta$. В задаче о взаимодействии подземного трубопровода с грунтом, обладающим вязкоупругим свойством, функции повреждаемости можно записать в виде [2]

$$\eta(t) = \frac{(m+1)}{\tilde{B}^{1+m}}\int_0^t (t-\tau)^m \sigma_u^{\alpha_0(1+m)}(\tau)d\tau \tag{15}$$

При вязкоупругом взаимодействии трубопровода с окружающим грунтом для сил взаимодействия, учитывающих повреждаемость грунта по принципу Вольтерра, имеем,

$$P^b(x,t) = D_A^*(Y - Y_0) = D_A\left[(Y - Y_0) - \int_0^t R(t'-\tau')[Y(x,\eta) - Y_0(x,\eta)]d\tau\right], \tag{16}$$

В этом случае, исходя из вариационного принципа и с учетом (16) получена система дифференциальных уравнений трубопровода с учетом вязкоупругого взаимодействия:

$$-A\frac{\partial^2 Y}{\partial t^2}+B\frac{\partial^2 Y}{\partial x^2}+C\frac{\partial Y}{\partial x}+D_n Y+D_A\left(Y-Y_0\right)-D_A\int_0^t R\left(t'-\tau'\right)\left[Y\left(x,\eta\right)-Y_0\left(x,\eta\right)\right]d\tau+F=0; \quad (17)$$

$$\left[-\overline{B}\frac{\partial Y}{\partial x}+\overline{C}_{\Pi}Y+\overline{C}_{\text{A}}\left(Y-Y_0\right)-\overline{C}_{\text{A}}\int_0^t R\left(t'-\tau'\right)\left[Y\left(x,\eta\right)-Y_0\left(x,\eta\right)\right]d\tau+P^{гр}\right]\delta Y\Big|_x=0; \quad (18)$$

$$A\frac{\partial Y}{\partial t}E\delta Y\Big|_t=0. \quad (19)$$

здесь $R\left(t'-\tau'\right)$ – слабосингулярное трехпараметрическое ядро типа Ржаницына – Колтунова, в частности, для первого приближения считается, что $R\left(t'-\tau'\right)=R\left(t-\tau\right)$, где $R\left(t\right)=\overline{A}_b e^{-\overline{\beta}t}t^{\alpha-1}$, $0<\alpha<1$.

Для устранения особенности в подынтегральном выражении, следуя методики [6,7] произведен замена переменных для фиксированных $t_n=\left(n-1\right)\tau$. После некоторых преобразований из (17) - (19) имеем

$$-A\frac{\partial^2 Y}{\partial t^2}+B\frac{\partial^2 Y}{\partial x^2}+C\frac{\partial Y}{\partial x}+D_n Y+D_A\left[\left(Y-Y_0\right)-\frac{A_b}{\alpha}\sum_{k=1}^{n}B_k^b e^{-\beta t_k}\left[Y\left(x,t_n-t_k\right)-Y_0\left(x,t_n-t_k\right)\right]\right]+F=0; \quad (20)$$

$$\left\{-\overline{B}\frac{\partial Y}{\partial x}+\overline{C}_{\Pi}Y+\overline{C}_{A}\left[\left(Y-Y_0\right)-\frac{A_b}{\alpha}\sum_{k=1}^{n}B_k^b e^{-\beta t_k}\left[Y\left(x,t_n-t_k\right)-Y_0\left(x,t_n-t_k\right)\right]\right]+P^{гр}\right\}\delta Y\Big|_x=0; \quad (21)$$

$$A\frac{\partial Y}{\partial t}E\delta Y\Big|_t=0. \quad (22)$$

В случае учета накопления повреждений ядра типа $R\left[t,\tau,\eta\left(\xi\right)\right]$ разлагаются в ряд, здесь ограничимся первым слагаемым:

$$R\left[t-\xi,\eta\left(\xi\right)\right]=R_0\left(t-\xi\right)+\eta\left(\xi\right)R_1\left(t-\xi\right) \quad (23)$$

При пространственном нагружения силы взаимодействия представляем в следующим виде:

$$\tau_a=P^b\left(x,t\right)=R_0\left(0\right)\left[\left(Y-Y_0\right)-\psi_0\left(Y-Y_0\right)\right]-R_1\left(0\right)\psi_1\left(Y-Y_0\right), \quad (24)$$

Здесь

$$\psi_0\left(Y-Y_0\right)=\int_0^t R_0\left(t-\xi\right)\left(Y-Y_0\right)d\xi,\quad \psi_1\left(Y-Y_0\right)=\int_0^t R_1\left(t-\xi\right)\eta\left(\xi\right)\left(Y-Y_0\right)d\xi.$$

Система дифферециальных уравнений (20) - (22) с учетом (24) имеет следующей вид:

$$-A\frac{\partial^2 Y}{\partial t^2}+B\frac{\partial^2 Y}{\partial x^2}+C\frac{\partial Y}{\partial x}+D_n Y+\widetilde{D}_A\left[\left(Y-Y_0\right)-\psi_0\left(Y-Y_0\right)\right]-\widetilde{\widetilde{D}}_A\psi_1\left(Y-Y_0\right)+\overline{F}=0 \quad (25)$$

$$\left\{-\overline{B}\frac{\partial Y}{\partial x}-\widetilde{C}_{\Pi}\left[\left(Y-Y_0\right)-\psi_0\left(Y-Y_0\right)\right]-\widetilde{\widetilde{C}}_A\psi_1\left(Y-Y_0\right)+P^{гр}\right\}\Bigg|_x=0;\ A\frac{\partial Y}{\partial x}E\delta Y\Big|_t=0. \quad (26)$$

Система уравнений решается методом итерации (l – число итерации), при этом, например,

$$\psi_1\left(Y^{(l)}-Y_0^{(l)}\right)=\int_0^t R_0\left(t-\xi\right)\eta^{(l-1)}\left(\xi\right)\left(Y^{(l)}-Y_0^{(l)}\right)d\xi,\quad \eta^{(l-1)}\left(t\right)=\left(1+m\right)\int_0^t\left(t-\xi\right)^m\frac{d\xi}{t_0^{1+m}\left[\sigma_u^{(l-1)}\left(\xi\right)\right]}.$$

При построении решений системы (25) с граничными и начальными условиями (26) применяется разностная схема второго порядка точности. В результате получено система конечно-разностных уравненй, которая решается методом прогонки [1,5].

4. Учет больших деформаций

Теперь рассмотрим один из возможных вариантов учета больших дефорормации при моделирование расчета упругопластического трубопровода.

Перемещения точек трубопровода при циклическом нагружении представим в виде (2), в часности,

$$\bar{u}_1^{(n)} = \bar{u}^{(n)} - \bar{\alpha}_1^{(n)} r\cos\gamma - z\bar{\alpha}_2^{(n)} r\sin\gamma;$$

$$\bar{u}_2^{(n)} = \bar{v}^{(n)} - \bar{\theta}^{(n)} r\sin\gamma;\ \bar{u}_3^{(n)} = \bar{w}^{(n)} + \bar{\theta}^{(n)} r\cos\gamma. \qquad (27)$$

Согласно [1], принимаем нелинейный связь между деформациями и перемещениями в следующем виде (случай *а*-вариант):

$$\bar{\gamma}_{11}^{(n)} = \frac{\partial \bar{u}_1^{(n)}}{\partial x} + \frac{1}{2}\left[\left(\frac{\partial \bar{u}_1^{(n)}}{\partial x}\right)^2 + \left(\frac{\partial \bar{u}_2^{(n)}}{\partial x}\right)^2 + \left(\frac{\partial \bar{u}_3^{(n)}}{\partial x}\right)^2\right],$$

$$\bar{\gamma}_{13}^{(n)} = \frac{\partial \bar{u}_1^{(n)}}{\partial y} + \frac{\partial \bar{u}_2^{(n)}}{\partial x} + \frac{\partial \bar{u}_1^{(n)}}{\partial x}\frac{\partial \bar{u}_1^{(n)}}{\partial y} + \frac{\partial \bar{u}_2^{(n)}}{\partial x}\frac{\partial \bar{u}_2^{(n)}}{\partial y} + \frac{\partial \bar{u}_3^{(n)}}{\partial x}\frac{\partial \bar{u}_3^{(n)}}{\partial y},$$

$$\bar{\gamma}_{12}^{(n)} = \frac{\partial \bar{u}_1^{(n)}}{\partial z} + \frac{\partial \bar{u}_3^{(n)}}{\partial x} + \frac{\partial \bar{u}_1^{(n)}}{\partial x}\frac{\partial \bar{u}_1^{(n)}}{\partial z} + \frac{\partial \bar{u}_2^{(n)}}{\partial x}\frac{\partial \bar{u}_2^{(n)}}{\partial z} + \frac{\partial \bar{u}_3^{(n)}}{\partial x}\frac{\partial \bar{u}_3^{(n)}}{\partial z}. \qquad (28)$$

Для получения уравнения движения трубопровода с учетом больших деформации при циклическом нагружении используем принцип Гамильтона – Остроградского (6). Вариации кинетической и потенциальной энергии, а также работа внешних сил определяются следующими соотношениями:

$$\delta\int_t \bar{T}^{(n)} dt = \int_t\int_v \left[\rho\frac{\partial \bar{u}_1^{(n)}}{\partial t}\delta\frac{\partial \bar{u}_1^{(n)}}{\partial t} + \rho\frac{\partial \bar{u}_2^{(n)}}{\partial t}\delta\frac{\partial \bar{u}_2^{(n)}}{\partial t} + \rho\frac{\partial \bar{u}_3^{(n)}}{\partial t}\delta\frac{\partial \bar{u}_3^{(n)}}{\partial t}\right] dVdt, \qquad (29)$$

$$\delta\int_t \bar{\Pi}^{(n)} dt = \int_t\int_V \left(\bar{\sigma}_{11}^{(n)}\delta\bar{\gamma}_{11}^{(n)} + \bar{\sigma}_{12}^{(n)}\delta\bar{\gamma}_{12}^{(n)} + \bar{\sigma}_{13}^{(n)}\delta\bar{\gamma}_{.13}^{(n)}\right) dVdt, \qquad (30)$$

$$\delta\int_t \bar{A}^{(n)} dt = \int_t\int_V \left(p_1^{(n)}\delta\bar{u}_1^{(n)} + p_2^{(n)}\delta\bar{u}_2^{(n)} + p_3^{(n)}\delta\bar{u}_3^{(n)}\right) dVdt + \int_t\int_S \left(q_1^{(n)}\delta\bar{u}_1^{(n)} + q_2^{(n)}\delta\bar{u}_2^{(n)} + \right.$$

$$\left. + q_3^{(n)}\delta\bar{u}_3^{(n)}\right) dSdt + + \int_t\int_{S_1} \left(f_1^{(n)}\delta\bar{u}_1^{(n)} + f_2^{(n)}\delta\bar{u}_2^{(n)} + f_3^{(n)}\delta\bar{u}_3^{(n)}\right) dS_1 dt\Big|_x. \qquad (31)$$

Подставляя выражения перемещений $\bar{u}_i^{(n)}$ в вариации кинетической энергии и раскрывая скобки под знаком вариации после выполнения операции интегрирования по сечениям трубы и вводя некоторые обозначения, получаем (далее знак «чертой» опускаем):

$$\delta\int_t T^{(n)} dt = \int_x \left\{\left[F\frac{\partial u^{(n)}}{\partial t} - S_z\frac{\partial \alpha_1^{(n)}}{\partial t} - S_y\frac{\partial \alpha_2^{(n)}}{\partial t}\right]\delta u^{(n)} + \left[F\frac{\partial \upsilon^{(n)}}{\partial t} - S_y\frac{\partial \theta^{(n)}}{\partial t}\right]\delta\upsilon^{(n)} + \left[F\frac{\partial w^{(n)}}{\partial t} + S_z\frac{\partial \theta^{(n)}}{\partial t}\right]\delta w^{(n)} + \right.$$

$$+\left[S_y\frac{\partial u^{(n)}}{\partial t} - J_{yz}\frac{\partial \alpha_1^{(n)}}{\partial t} - J_y\frac{\partial \alpha_2^{(n)}}{\partial t}\right]\delta\alpha_2^{(n)} - \left[S_z\frac{\partial u^{(n)}}{\partial t} - J_z\frac{\partial \alpha_1^{(n)}}{\partial t} - J_{yz}\frac{\partial \alpha_2^{(n)}}{\partial t}\right]\delta\alpha_1^{(n)} -$$

$$\left. -\left[S_\varphi\frac{\partial u^{(n)}}{\partial t} - J_{y\varphi}\frac{\partial \alpha_1^{(n)}}{\partial t} - J_{z\varphi}\frac{\partial \alpha_2^{(n)}}{\partial t}\right]\delta\nu^{(n)} + \left[S_z\frac{\partial w^{(n)}}{\partial t} - S_y\frac{\partial \upsilon^{(n)}}{\partial t} + J_\rho\frac{\partial \theta^{(n)}}{\partial t}\right]\delta\theta^{(n)}\right\} dx\Bigg|_t - \qquad (32)$$

$$-\left(\int_t\int_x \left\{\left[F\frac{\partial^2 u^{(n)}}{\partial t^2} - S_z\frac{\partial^2 \alpha_1^{(n)}}{\partial t^2} - S_y\frac{\partial^2 \alpha_2^{(n)}}{\partial t^2}\right]\delta u^{(n)} - \left[S_z\frac{\partial^2 u^{(n)}}{\partial t^2} - J_z\frac{\partial^2 \alpha_1^{(n)}}{\partial t^2} - J_{yz}\frac{\partial^2 \alpha_2^{(n)}}{\partial t^2}\right]\delta\alpha_1^{(n)} - \right.\right.$$

$$-\left[S_y\frac{\partial^2 u^{(n)}}{\partial t^2} - J_{yz}\frac{\partial^2 \alpha_1^{(n)}}{\partial t^2} - J_y\frac{\partial^2 \alpha_2^{(n)}}{\partial t^2}\right]\delta\alpha_2^{(n)} + \left[S_\varphi\frac{\partial^2 u^{(n)}}{\partial t^2} - J_{\varphi z}\frac{\partial^2 \alpha_1^{(n)}}{\partial t^2} - J_{z\varphi}\frac{\partial^2 \alpha_2^{(n)}}{\partial t^2}\right]\delta\nu^{(n)} + \left[S_z\frac{\partial^2 w^{(n)}}{\partial t^2} - \right.$$

$$\left.\left. -S_y\frac{\partial^2 \upsilon^{(n)}}{\partial t^2} + J_\rho\frac{\partial^2 \theta^{(n)}}{\partial t^2}\right]\delta\theta^{(n)} + \left[F\frac{\partial^2 \upsilon^{(n)}}{\partial t^2} - S_y\frac{\partial^2 \theta^{(n)}}{\partial t^2}\right]\delta\upsilon^{(n)} + \left[F\frac{\partial^2 w^{(n)}}{\partial t^2} + S_z\frac{\partial^2 \theta^{(n)}}{\partial t^2}\right]\delta w^{(n)}\right\} dxdt\right),$$

где

$$\int_F dF = F_x; \quad \int_F r\cos\gamma dF = S_z; \quad \int_F r\sin\gamma dF = S_y; \quad \int_F (r\cos\gamma)^2 dF = J_z;$$

$$\int_F (r\sin\gamma)^2 dF = J_y; \quad \int_F (r\cos\gamma)^2 + (r\sin\gamma)^2)dF = J_\rho; \quad \int_F r^2\cos\gamma\sin\gamma dF = J_{yz}. \quad (33)$$

Для определения вариации потенциальной энергии подставляес вариации компонентов деформации в (30) и, приводя подобные слагаемые относительно вариаций $\frac{\partial u_i^{(n)}}{\partial \xi_i}$.

Затем выполняем операции интегрирования по частям и приведя подобные слагаемые относительно вариации перемещений. Вводя ряд обозначений, вариации потенциальной энергии представим в следующем виде:

$$\delta\int_t \Pi^{(n)}dt = \int_t \Big\{\left[N_x^{(n)} + R_1^{(n)}\right]\delta u^{(n)} + \left[M_z^{(n)} + R_5^{(n)}\right]\delta\alpha_1^{(n)} + \left[M_y^{(n)} + R_4^{(n)}\right]\delta\alpha_2^{(n)} + \left[Q_3^{(n)} + R_3^{(n)}\right]\delta w^{(n)} +$$

$$+\left[M_x^{(n)} + R_6^{(n)}\right]\delta\theta^{(n)} + \left[Q_2^{(n)} + R_2^{(n)}\right]\delta\nu^{(n)}\Big|_x\Big\}dt - \int_t\int_x \left\{\left[\frac{\partial N_x^{(n)}}{\partial x} + \frac{\partial R_1^{(n)}}{\partial x}\right]\delta u^{(n)} + \left[\frac{\partial Q_2^{(n)}}{\partial x} + \frac{\partial R_2^{(n)}}{\partial x}\right]\delta\nu^{(n)} +\right.$$

$$\left. + \left[\frac{\partial Q_3^{(n)}}{\partial x} + \frac{\partial R_3^{(n)}}{\partial x}\right]\delta w^{(n)} + \left[\frac{\partial M_z^{(n)}}{\partial x} + \frac{\partial R_5^{(n)}}{\partial x}\right]\delta\alpha_1^{(n)} + \left[\frac{\partial M_y^{(n)}}{\partial x} + \frac{\partial R_4^{(n)}}{\partial x}\right]\delta\alpha_2^{(n)} + \left[\frac{\partial M_x^{(n)}}{\partial x} + \frac{\partial R_6^{(n)}}{\partial x}\right]\delta\theta^{(n)}\right\}dx. \quad (34)$$

Здесь, например,

$$R_1^{(n)} = N_x^{(n)}\frac{\partial u^{(n)}}{\partial x} - M_z^{(n)}\frac{\partial\alpha_2^{(n)}}{\partial x} - M_y^{(n)}\frac{\partial\alpha_1^{(n)}}{\partial x}; \quad R_2^{(n)} = N_x^{(n)}\frac{\partial\nu^{(n)}}{\partial x} + M_z^{(n)}\frac{\partial\theta^{(n)}}{\partial x} + Q_3^{(n)}\theta;$$

$$R_6^{(n)} = M_y^{(n)}\frac{\partial\nu^{(n)}}{\partial x} - M_z^{(n)}\frac{\partial w^{(n)}}{\partial x} + M_{12}^{(n)}\left(\sigma_{12}^{(n)}z\right) - M_{13}^{(n)}\left(\sigma_{13}^{(n)}y\right) + M_{12}^{(n)}\left(\sigma_{12}^{(n)}y\right)\theta^{(n)} + M_{13}^{(n)}\left(\sigma_{13}^{(n)}z\right)\theta^{(n)} +$$

$$+ M_{11}^{(n)}\left(\sigma_{11}^{(n)}z^2\right)\frac{\partial\theta^{(n)}}{\partial x} + M_{11}^{(n)}\left(\sigma_{11}^{(n)}y^2\right)\frac{\partial\theta^{(n)}}{\partial x}.$$

Теперь в вариации работы внешних сил (29) подставляем выражения компонентов перемещений (2), раскрываем скобки и выделяем интеграл по сечению трубы. Вводя некотырых обозначений для вариации работы внешних сил имеем:

$$\delta\int_t Adt = \int_t\int_x \Big\{\left(N^{об(n)} - N^{П(n)}\right)\delta u^{(n)} + \left(Q_y^{об(n)} + Q_y^{П(n)}\right)\delta\upsilon^{(n)} + \left(Q_z^{об(n)} + Q_z^{П(n)}\right)\delta w^{(n)} - \left(M_z^{об} + M_z^{П(n)}\right)\delta\alpha_1^{(n)} +$$

$$+\left(M_y^{об(n)} + M_y^{П(n)}\right)\delta\alpha_2^{(n)} - \left(M_x^{об(n)} + M_x^{П(n)}\right)\delta\theta^{(n)} + \left(M_\varphi^{об(n)} + M_\varphi^{П(n)}\right)\delta\nu^{(n)}\Big\}dxdt + \int_t \Big\{N^{Г(n)}\delta u^{(n)} +$$

$$+ Q_z^{Г(n)}\delta w^{(n)} - M_z^{Г(n)}\delta\alpha_1^{(n)} - M_y^{Г(n)}\delta\alpha_2^{(n)} - M_x^{Г(n)}\delta\theta^{(n)} + M_\varphi^{Г(n)}\delta\nu^{(n)}\Big\}dt\Big|_x \quad (35)$$

где

$$\int_F p_1^{(n)}dF = N_x^{об(n)}, \quad \int_F yp_1^{(n)}dF = M_z^{об(n)}, \quad \int_F zp_1^{(n)}dF = M_y^{об(n)},$$

$$\int_F p_2^{(n)}dF = Q_y^{об(n)}, \quad \int_F p_3^{(n)}dF = Q_z^{об(n)}, \quad \int_F \left(yp_3^{(n)} - zp_2^{(n)}\right)dF = M_x^{об(n)}.$$

В результате из вариационного уравнения получим следующую систему дифференциальных уравнений с соответствующими начальными и граничными условиями:

Уравнения движения:

$$-\left[F\frac{\partial^2 u^{(n)}}{\partial t^2} - S_z\frac{\partial^2\alpha_1^{(n)}}{\partial t^2} - S_y\frac{\partial^2\alpha_2^{(n)}}{\partial t^2} + \frac{\partial N_x^{(n)}}{\partial x} + \frac{\partial R_1^{(n)}}{\partial x} - \left(N^{об(n)} + N^{П(n)}\right)\right] = 0;$$

$$\left[S_z\frac{\partial^2 u^{(n)}}{\partial t^2} - J_z\frac{\partial^2\alpha_1^{(n)}}{\partial t^2} - J_{yz}\frac{\partial^2\alpha_2^{(n)}}{\partial t^2} - \frac{\partial M_z^{(n)}}{\partial x} - \frac{\partial R_5^{(n)}}{\partial x} - \left(M_z^{об} + M_z^{П(n)}\right)\right] = 0;$$

$$\left[S_y\frac{\partial^2 u^{(n)}}{\partial t^2}-J_{yz}\frac{\partial^2\alpha_1^{(n)}}{\partial t^2}-J_y\frac{\partial^2\alpha_2^{(n)}}{\partial t^2}-\frac{\partial M_y^{(n)}}{\partial x}-\frac{\partial R_4^{(n)}}{\partial x}-\left(M_y^{об(n)}+M_y^{П(n)}\right)\right]=0;$$

$$-\left[S_\varphi\frac{\partial^2 u^{(n)}}{\partial t^2}-J_{\varphi z}\frac{\partial^2\alpha_1^{(n)}}{\partial t^2}-J_{z\varphi}\frac{\partial^2\alpha_2^{(n)}}{\partial t^2}-\frac{\partial Q_2^{(n)}}{\partial x}-\frac{\partial R_2^{(n)}}{\partial x}+Q_y^{об(n)}+Q_y^{П(n)}\right]=0; \quad (36)$$

$$\left[S_z\frac{\partial^2 w^{(n)}}{\partial t^2}-S_y\frac{\partial^2\upsilon^{(n)}}{\partial t^2}+J_\rho\frac{\partial^2\theta^{(n)}}{\partial t^2}-\frac{\partial M_x^{(n)}}{\partial x}-\frac{\partial R_6^{(n)}}{\partial x}-M_x^{об(n)}-M_x^{П(n)}\right]=0;$$

$$-\left[F\frac{\partial^2 w^{(n)}}{\partial t^2}+S_z\frac{\partial^2\theta^{(n)}}{\partial t^2}+\frac{\partial Q_3^{(n)}}{\partial x}+\frac{\partial R_3^{(n)}}{\partial x}+Q_z^{об(n)}+Q_z^{П(n)}\right]=0.$$

Начальные условия имеют следующий вид:

$$\left[F\frac{\partial u^{(n)}}{\partial t}-S_z\frac{\partial\alpha_1^{(n)}}{\partial t}-S_y\frac{\partial\alpha_2^{(n)}}{\partial t}\right]\delta u^{(n)}\Bigg|_t=0;\quad -\left[S_z\frac{\partial u^{(n)}}{\partial t}-J_z\frac{\partial\alpha_1^{(n)}}{\partial t}-J_{yz}\frac{\partial\alpha_2^{(n)}}{\partial t}\right]\delta\alpha_1^{(n)}\Bigg|_t=0;$$

$$\left[F\frac{\partial w^{(n)}}{\partial t}+S_z\frac{\partial\theta^{(n)}}{\partial t}\right]\delta w^{(n)}\Bigg|_t=0;\quad -\left[S_y\frac{\partial u^{(n)}}{\partial t}-J_{yz}\frac{\partial\alpha_1^{(n)}}{\partial t}-J_y\frac{\partial\alpha_2^{(n)}}{\partial t}\right]\delta\alpha_2^{(n)}\Bigg|_t=0;$$

$$\left[S_\varphi\frac{\partial u^{(n)}}{\partial t}-J_{y\varphi}\frac{\partial\alpha_1^{(n)}}{\partial t}-J_{z\varphi}\frac{\partial\alpha_2^{(n)}}{\partial t}\right]\delta\nu^{(n)}\Bigg|_t=0;\quad \left[S_z\frac{\partial w^{(n)}}{\partial t}-S_y\frac{\partial\upsilon^{(n)}}{\partial t}+J_\rho\frac{\partial\theta^{(n)}}{\partial t}\right]\delta\theta^{(n)}\Bigg|_t=0. \quad (37)$$

Граничные условия имеют вид

$$-\left[N_x^{(n)}+R_1^{(n)}+N^{\Gamma(n)}\right]\delta u^{(n)}\Big|_x=0;\quad -\left[M_z^{(n)}+R_5^{(n)}-M_z^{\Gamma(n)}\right]\delta\alpha_1^{(n)}\Big|_x=0;$$

$$-\left[M_y^{(n)}+R_4^{(n)}-M_y^{\Gamma(n)}\right]\delta\alpha_2^{(n)}\Big|_x=0;\quad -\left[Q_3^{(n)}+R_3^{(n)}+Q_z^{\Gamma(n)}\right]\delta w^{(n)}\Big|_x=0; \quad (38)$$

$$-\left[M_x^{(n)}+R_6^{(n)}-M_x^{\Gamma(n)}\right]\delta\theta^{(n)}\Big|_x=0;\quad -\left[Q_2^{(n)}+R_2^{(n)}+M_\varphi^{\Gamma(n)}\right]\delta\nu^{(n)}\Big|_x=0.$$

Таким образом, при использовании выражений перемещений (27) и деформаций (28) получена разрешающая система дифференциальных уравнений для геометрически нелинейных задач трубопроводов при циклическом нагружении. Задавая конкретные граничные и начальные условия, задача решается с применением метода последовательных приближений.

5. Результаты расчета

В качестве примера анализируются колебания стальной подземной трубы с учетом повреждаемости при взаимодействии с грунтом. Механические и геометрические характеристики (данные взяты из [6]): E=2.3·10^8 кН/м^2, ρ=7.8 кН·с^2/м^4, R=0.6м, r=0.585 м, L=12 м. Окружающая среда – песчаный грунт с коэффициентом взаимодействия k_x=3.75·10^3 кН/м^3. Параметры ядра для песка: A=0.0748, α=0.2, β=0.048; значение импульса постоянный w_0=0.007 м. Расчет произведен методом конечных разностей по пространству и по времени в явной схеме. Шаги сетки по пространству и времени приняты в безразмерном виде [7]: h=1/N=1/20; τ=h^2/4.

На рис. 3 сплошная линия - 1 соответствует вязкоупругому взаимодействию, а штрих – пунктирная - 2 линейно вязкоупругому случаю с учетом накопленных повреждений

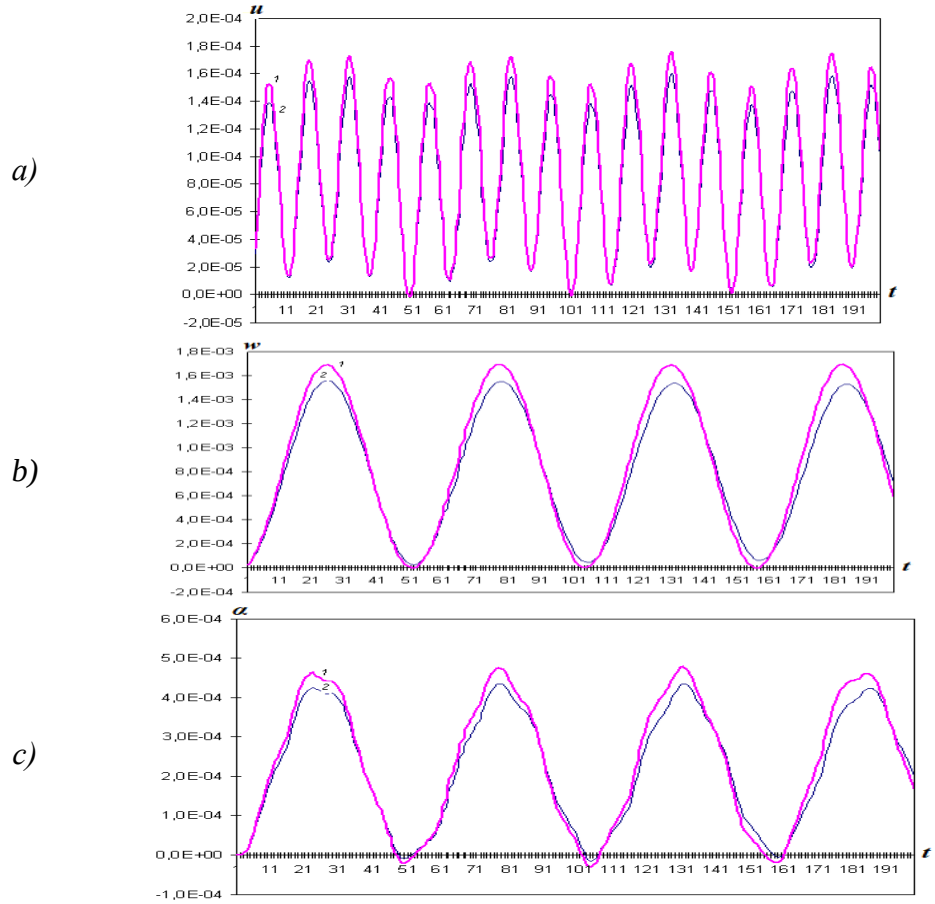

Рисунок 3–**Влияние свойств вязкости взаимодействия и с учетом повреждаенности на кинетику расчётных величин: *a)* перемещения u; *b)* прогиб w; *c)* угль наклона α_2**

Из графиков видно, что в рассмотренных решениях между вязкоупругих (линия-1) и вязкоупругих с учетом накопления повреждаемости (линия-2) разница состовляет до 10-15%.

6. Заключение

На основе вариационного принципа получена система дифференциальных уравнений движения (равновесия) тонкостенных стержней - подземных трубопроводов. Сформированы краевые задачи при циклическом нагружении с учетом обобщенного принципа Мазинга и повреждаемости материала. Приведена результаты расчета трубопровода с учетом взаимодействия с грунтом. Показано изменения расчетных величин по времени с учетом повреждаемости и вязкоупругого взаимодействия при действии внешних сил.

Литература

1. *Абдусаттаров А., Старовойтов Э.И., Рузиева Н.Б.* Деформирование и повреждаемость упругопластических элементов конструкций при циклических нагружениях / Ташкент: «IDEAL PRESS», 2023, 381 с.
2. *Москвитин В.В.* Циклические нагружения элементов конструкций / М.: URSS, 2019, 344 с. (переизд).
3. *Махутов Н.А., Филатов В.М., Раманов А.Н.* Прочность конструций при малоцикловом нагружении / М.: Наука, 1983, 271с.
4. *Гусенков А.П., Москвитин Г.В., Хорошилов В.Н.* Малоцикловая прочность оболочечных конструкций / М.: Наука, 1989, 254 с.
5. *Буриев Т.* Алгоритмизация расчета несущих элементов тонкостенных конструкций / Т.Буриев. – Ташкент:Фан, 1986, 244с.
6. *Рашидов Т.Р., Хожметов Г.Х.* Сейсмостойкость подземных трубопроводов / Т.: Фан, 1985, 152с.
7. *Рашидов Т.Р., Юлдашев Т., Маткаримов А.Х.* Модели сейсмодинамики подземных сооружений при пространственном нагружении // Вестник ТашИИТ. 2006. No. 1. С. 66 – 74.
8. *Селезнев В.Е., Алешин В.В., Прялов С.Н.* Основы численного моделирования магистральных трубопроводов / Изд. 2–е, перераб. и доп., М.: МАКС Пресс., 2009, 436 с.

9. *Поздеев А.А., Трусов П.В., Няшин Ю.И.* Большие упругопластические деформации / М.: Наука, 1986, 232 с.
10. *Старовойтов Э.И., Яровая А.В., Леоненко Д.В.* Деформирование трехслойных элементов конструкции на упругом основании / М.:Физматлит, 2006, 379 с.
11. *Старовойтов Э.И., Абдусаттаров А., Рузиева Н.Б.* Циклическое нагружение упругопластических трёхслойных стержней с учетом их повреждаемости // Узб.журнал «Проблемы механики». 2023, No. 1, С.66-74.
12. *Абдусаттаров А., Исомиддинов А.И., Рузиева Н.Б.*Уравнение движения подземных магистральных трубопроводов при пространственно-переменном упругопластическом нагружении //Матер. Респуб. науч.-прак. конференции «Современная архитектура», прочность зданий и сооружений. Проблемы надежности и сейсмической безопасности. НамИСИ. 2021, С.135 – 137.
13. *Abdusattarov A., Ruzieva N.B and Abdukadirov F.* Deformation and damage capacity of thin–walled rods and tubular conduits under alternating loading // E3S Web of Conferences. 2023, Vol. 401, 03033 https://doi.org/10.1051/e3sconf/202340103033.
14. *Abdusattarov A., Ruzieva N., Abdukadirov F.* Modeling of elastic-plastic deformation of main pipelines under repeated static and dynamic loading // AIP Conference Proceedings. 2023, Vol. 2476, 030016. https://www.scopus.com/record/display.uri?eid=2-s2.0-85160576498&origin=resultslist.

О МЕХАНИЧЕСКИХ СВОЙСТВАХ АРМИРОВАННОГО БЕТОНА

Абиров Р.А.[1]
[1]*Институт механики и сейсмостойкости сооружений, Ташкент, Узбекистан*
E-mail: rustam.abirov@gmail.com

Аннотация: *Мировая практика показала целесообразность использования фибробетонов с цель повышения прочностных свойств, а также ее повышения трещиностойкости изделия. Оптимальные комбинации различных видов фибры и их влияние на прочностные свойства не достаточны изучены. Также нет четких нормативов для использования фибробетонов при различных видах армирования, в том числе и базальтовыми арматурами и фибрами различной длины. В работе приводится метод расчета армированных бетонов на основе метода разрывных смещений. Механические свойства фибробетона определяются на основе свойств входящих в ее состав компонентов: фибры и связующего элемента.*

Ключевые слова: *напряжение, деформация, фибробетон, анизотропия, метод разрывных смещений.*

1. Введение

Одной их основных задач современного строительного материаловедения является создание новых эффективных инновационных материалов с улучшенными эксплуатационными свойствами, с повышенной прочностью. При этом возникает способность создавать материалы с заранее заданными свойствами направленного действия (с доминантой на изгиб, растяжение или кручение). Композиты являются на данном этапе развития самыми перспективными в этой отрасти материаловедения.

Линейка существующих, согласно существующим стандартам, дисперсно-армированных бетонов обладает различными свойствами. Путями, позволяющими значительно улучшить свойства такого рода бетонов, является увеличение прочности сцепления армирующих волокон со строительной матрицей, определение оптимального состава как матрицы, так и армирующих ее волокон, технология изготовления и т.д.

В качестве плюсов таких материалов можно отметить: высокую удельную прочность (прочность 3500 МПа); высокую жёсткость (модуль упругости 130…140 - 240 ГПа); высокую износостойкость; высокую усталостную прочность; легкость. Минусы композитов: высокая стоимость; анизотропия свойств; низкая ударная вязкость; высокий удельный объём; гигроскопичность; токсичность; низкая эксплуатационная технологичность.

Соответственно прочность и уровень свойств волокнистых композитов определяется: природой волокна и матрицы; плотности наполнения и схемой армирования; технологии связи матрица-волокно. При этом схема армирования может быть: хаотической (короткие или непрерывные волокна); одномерной (короткие или непрерывные волокна); двумерной (непрерывные волокна и ткани); объемной (семейства нитей 3D). Под хаотической как правило понимают бетоны с базальтовыми, стальными или иными видами фибры, где

основное это плотность этой фибры, а не ее ориентация. Данная форма заполнения повышает трещиностойкость материалов.

В направлении исследования прочностных свойств фибробетонов проводятся экспериментальные работы [1-3]. Поиск оптимальных соотношений армирующих элементов из аморфной фибры: металлической, базальтовой, полипропиленовой и др. и их применение для сейсмоопасных зон в качестве строительного материала является весьма актуальной задачей. Виды армирования тоже могут значительно отличатся одна от другой, что существенно влияет на свойства материала и соответственно на сферу его применения.

Второй важной частью является разработка методов расчета анизотропных материалов. Большей частью решаются задачи в плоской постановке или на основе теории пластин и оболочек. Решаются эти задачи численно и одним из этих является метод граничных элементов. Применение непрямого метода граничных элементов для решения задачи нелинейного деформирования анизотропных пластин и оболочек рассмотрено в работе [4]. При этом учет сложного нагружения в форме новых определяющих соотношений [5] на данном этапе не рассмотрено.

Целью работы является теоретическое определение физических характеристик материалов с различным уровнем армирования и предложение метода расчета напряженно-деформированного состояния исследуемых материалов. При этом данный подход без проведения экспериментов является однобоким, но может дать предпосылки для создания нормативных методов расчета и включения их в новые разрабатываемые строительные нормы.

2. К определению основных механических характеристик.

При различных выборах армирования бетона и используемого для этого структуры волокнистого материала можно рассматривать в основном два пути – изотропная среда с осредненными физико-механическими свойствами или анизотропная среда. Волокнистую структуру, при расположении волокон вдоль плиты (для панелей) рассматривают как трансверсально-изотропную среду.

Определение пределов прочности на сжатие и на изгиб композитов на основе отходов производства базальтового волокна проведено по ГОСТу 8462-85 [6, 7].

Предел прочности образца при сжатии Rсж вычисляют по формуле:

$$R_{сж} = P/F\,,$$

где P – разрушающая нагрузка, установленная при испытании образца; F– площадь поперечного сечения образца, определяемая как среднее арифметическое значение площадей верхней и нижней его поверхностей,

Предел прочности при трехточечном изгибе образца $R_{изг}$ определяют по формуле:

$$R_{изг} = 3Pl/2bh^2\,,$$

где P – наибольшая нагрузка, установленная при испытании образца на изгиб, l– расстояние между опорами, b– ширина образца, h– высота образца в середине пролета,

В работе Хежеева Х.А. [8] предложено определять прочность полимерфосфогипсовой композиции которая армирована базальтовыми волокнами по следующей формуле:

$$\sigma_k = R_n\left[1+\frac{\gamma_{fib}\rho_c}{1000\rho_f}\left(\frac{E_f}{\nu E_c}-1\right)\right]$$

где E_f - модуль деформации волокна, E_c - модуль деформации связующего, ν - коэффициент учитывающий влияние армирования на величину предельной растяжимости материала матрицы, γ_{fib} - процентное содержание волокна от объема полимера, R_n - прочность волокна на разрыв, ρ_f и ρ_c - плотность волокна и связующего элемента соответственно.

Оригинальный метод предложен в работе Леоновича И.А. [9]. Теоретически проведено прогнозирование и изучение упругих свойств фибробетона в зависимости от объемного

содержания и механических свойств фибры. Материалы, применяемые в качестве фибры, были поделены на три класса по величине собственного модуля упругости в сравнении с модулем продольной упругости бетона: высокомодульную, среднемодульную и низкомодульную фибру. Этот подход является чисто теоретическим, но, однако позволяет оценить влияние каждого компонента на осредненные характеристики материала.

При произвольном расположении строго армированного бетона фиброэлементами, развивая метод Леоновича И.А. [9], предлагается следующая формула:

$$E_{fc} = E_{fc1} - 2\frac{E_{fc1} - E_{fc2}}{\pi}\alpha, \tag{1}$$

где α - угол наклона укладки армирующих элементов к главной оси OX в радианах, где в общем случае, если рассматривать задачу при различных системах координат нужно будет проводить соответствующее преобразование и находить это значение угла. Далее, механические характеристики входящие в (1) определяются как:

$$E_{fc1} = \frac{E_c}{1-\sqrt[3]{\gamma_{fib}}\left(1-E_c/E_{gen1}\right)}, \quad E_{fc2} = E_c + \sqrt[3]{\left(\gamma_{fib}\right)^2}\left(\frac{E_c}{1-\sqrt[3]{\gamma_{fib}}\left(1-E_c/E_{gen2}\right)} - E_c\right), \quad \gamma_{fib} = \frac{V_{fibrous}}{V},$$

$$E_{gen1} = E_c + \sqrt[3]{\left(\gamma_{fib}\right)^2}\left(E_f - E_c\right), \; E_{gen2} = \frac{E_c}{1-\sqrt[3]{\gamma_{fib}}\left(1-E_c/E_f\right)}.$$

В данном подходе предполагалось, что фибра является короткой (значительно корочке длины изделия) и уложена не хаотически. В случае же армирования непрерывными волокнами, аналогично стальной арматуре вдоль всего изделия, формула будет немного иная:

$$E_{fc} = E_{gen1} - 2\frac{E_{gen1} - E_{gen2}}{\pi}\alpha, \tag{2}$$

Таким образом можно определять прочностные характеристики армированных бетонов фибрами различной длины, с различными физико-механическими характеристиками и различной плотности. При данном рассмотрении также можно определить доминантные факторы влияющие на увеличение прочности материала.

3. Численная схема.

Выше был показан метод определения упругих характеристик фибробетонов на основе теоретических моделей, которые предполагали рассмотрении их как изотропной сплошной среды. Этот метод имеет ряд достоинств и одним из них является создание упрощенных методов расчётов том числе и для внесения их в нормативы. Однако рассмотрение среды как анизотропной коей является композит дает возможности не только более точно определять их напряженное и деформированное состояние, но также и определять пути для повышения их прочностных свойств и создания оптимальных композитов, работающих в различных условиях внешнего воздействия.

На примере однонаправленного композита (самая простая форма) можно наблюдать доминантное воздействие внешних нагрузок на материала. При этом неоднородный сплошной материал с армированными элементами и матрицей, обеспечивающей совместную работу армированных элементов можно рассматривать как композит.

При численном решении задач волокна (армирование) моделируются в виде неоднородности (включения). Такой подход, вообще говоря, не дает полной картины напряженно-деформированного состояния, так как не учитываются силы сцепления. Тем не менее, одним из подходов при рассмотрении задач с регулярным армированием можно применить метод граничных элементов в форме разрывных смешений или фиктивных нагрузок.

Этот метод основан на аналитическом решении задачи о бесконечной плоскости, смещения в которой терпят постоянный разрыв. Физически разрыв смещений представляется, вообще говоря, как трещина, противоположные берега которой смещены друг относительно друга.

Метод разрывных смещений основан на представлении, что непрерывно распределенные вдоль линии смещения можно заменить дискретной аппроксимацией [10].

Влияние наличия волокон можно моделировать с помощью метода разрывных смещений (модификация метода граничных интегральных уравнений). Метод разрывных смещений очень удобен при рассмотрении задач как с наличием трещин, так и с наличием включений, так как использует фундаментальное решение, полученное на основе единичного разрыва в пространстве. Применим этот же подход для армированных материалов. Не останавливаясь на выводе формул, для постоянных элементов метод разрывных смещений имеет вид [10]:

$$
\begin{aligned}
u_x &= D_x\left[2(1-\nu)f_{,y} - yf_{,xx}\right] + D_y\left[-(1-2\nu)f_{,x} - yf_{,xy}\right] \\
u_y &= D_x\left[(1-2\nu)f_{,x} - yf_{,xy}\right] + D_y\left[2(1-\nu)f_{,y} - yf_{,yy}\right] \\
\sigma_{xx} &= 2GD_x\left[2f_{,xy} + yf_{,xyy}\right] + 2GD_y\left[f_{,yy} + yf_{,yyy}\right] \\
\sigma_{yy} &= 2GD_x\left[-yf_{,xyy}\right] + 2GD_y\left[f_{,yy} - yf_{,yyy}\right] \\
\sigma_{xy} &= 2GD_x\left[f_{,yy} + yf_{,yyy}\right] + 2GD_y\left[-yf_{,xyy}\right]
\end{aligned}
$$

где $D_i = u_i(x,0_-) - u_i(x,0_+)$ - разность смещений, которые в общем виде могут выступать и как фиктивные смещения (или фиктивные силы при методе фиктивных нагрузок), $f = \dfrac{-1}{4\pi(1-\nu)}\left[y\left(arctg\,\dfrac{y}{x-a} - arctg\,\dfrac{y}{x+a}\right) - (x-a)\ln\sqrt{(x-a)^2+y^2} + (x+a)\ln\sqrt{(x+a)^2+y^2}\right]$.

Производные функции f находятся простым дифференцированием.

Так как ориентация волокон может быть произвольная в плоскости, то удобнее пользоваться локальной системой координат на каждом граничном элементе. Общая формула для расчета напряжений и перемещений на границе, опуская детали вычислений, имеет вид [10]:

$$
\left.
\begin{aligned}
\sigma_s^i &= \sum_{j=1}^{N} A_{ss}^{ij} D_s^j + \sum_{j=1}^{N} A_{sn}^{ij} D_n^j \\
\sigma_n^i &= \sum_{j=1}^{N} A_{ns}^{ij} D_s^j + \sum_{j=1}^{N} A_{nn}^{ij} D_n^j
\end{aligned}
\right\} \tag{3}
$$

$$
\left.
\begin{aligned}
u_s^i &= \sum_{j=1}^{N} B_{ss}^{ij} D_s^j + \sum_{j=1}^{N} B_{sn}^{ij} D_n^j \\
u_n^i &= \sum_{j=1}^{N} B_{ns}^{ij} D_s^j + \sum_{j=1}^{N} B_{nn}^{ij} D_n^j
\end{aligned}
\right\} \tag{4}
$$

Для вычислительных целей включение можно моделировать механической моделью.

Но при наличии множества волокон такой подход обременителен. И в этом случае принимают тело как слоистое. Получается своего рода «слоистый пирог» из заданного материала. И в этом случае удобнее усреднять физико-механические характеристики тела.

В таких случаях слоистую, армированную среду можно рассматривать на основе модели “щелей” Ержанова или, следуя Гудману [11], на основе рассмотрения материала как анизотропного тела [12]. При этом полагается, что слоистость материала регулярна и волокна близко расположены друг к другу (расстояния между ними значительно меньше чем рассматриваемая область). Для такого подхода следует использовать решение Кельвина для анизотропного тела, описанной в работе Крауча [10]. Ниже приведены формулы для рассмотрения задачи в такой постановке.

4. Растяжение однонаправленного композита.

Ниже рассмотрено нагружение плиты (размер 1.6x6 м) в условиях плоского напряженного состояния. Внешняя нагрузка P=20КН, приведенный модуль упругости E=30ГПа, коэффициент Пуассона ν=0.3. Рассматривается изотропный случай с осредненными значениями упругих характеристик. Полагается, в данных задачах, что в уравнении (2) угол $\alpha = 0$.

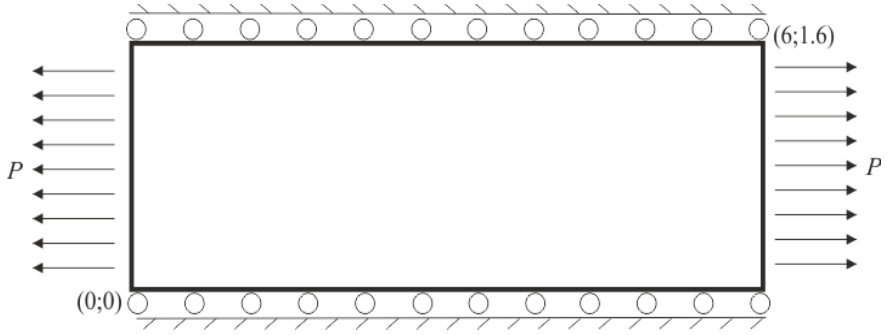

Рисунок 1. - **Нагружение однонаправленного композита**

Задача решена методом разрывных смещений. Результаты представлены в виде изолиний напряжений (рис. 2-4) и смещений (рис. 5).

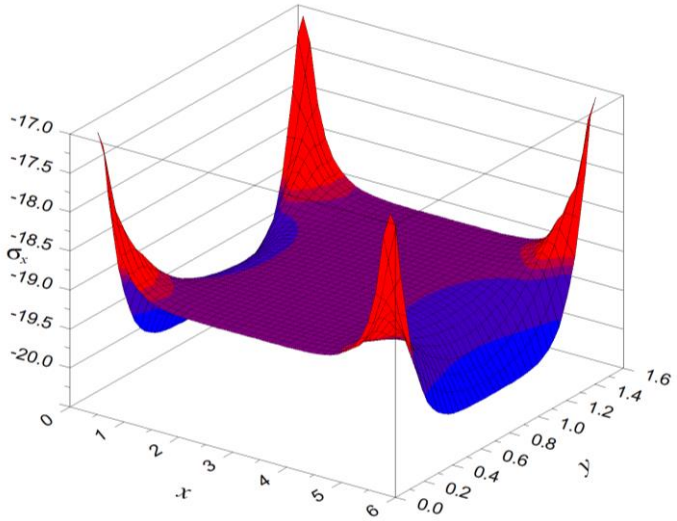

Рисунок 2. - **Распределение напряжений σ_x**

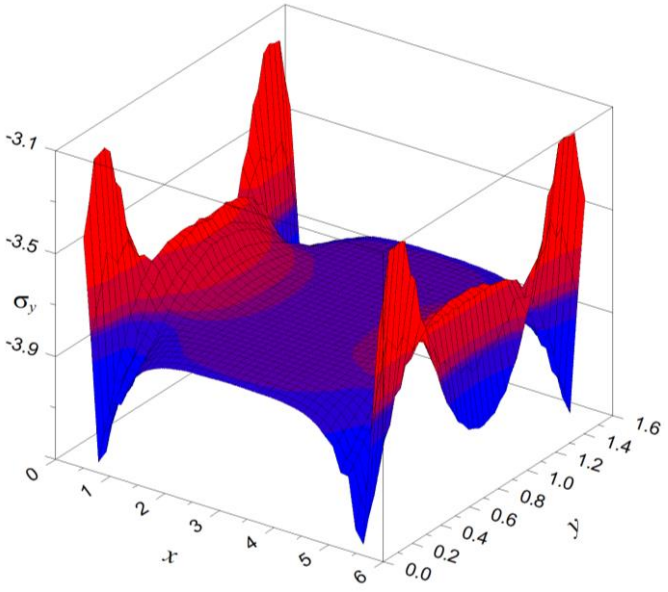

Рисунок 3. - **Распределение напряжений σ_t**

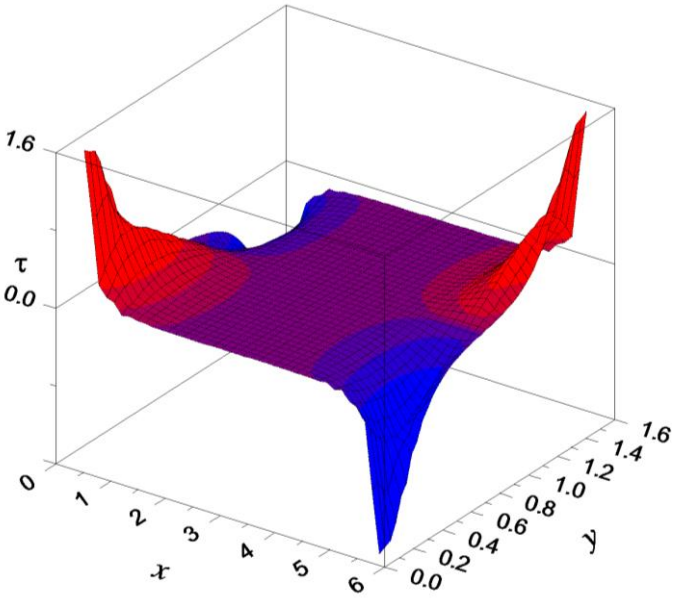

Рисунок 4. - **Распределение касательных напряжений**

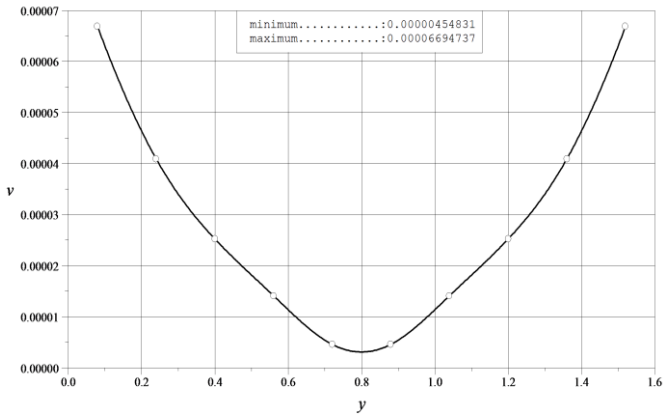

Рисунок 5 – **Вертикальные смещения по центральной оси**

5. Анализ результатов

Полученные результаты согласуются с данными других авторов по расчету композиционных элементов [13-16] и отличие составляет не более 3%. Качественная картина идентична. Отсюда вывод, что предложенный численный подход является приемлемым для расчетов трансверсально изотропных плит на нагружении вдоль их плоскости анизотропии.

6. Обсуждение

Рассмотренный метод определения физико-механических характеристик, представленных формулами (1) и (2) является чисто теоретическим. Тут предполагается строгое армирование, для которого в общем случае технология не разработана. Формулу (2) предлагается использовать для армированных базальтовыми арматурами или сетками бетонных изделий. Пока данные методики не прошли экспериментального подтверждения. Отдельным вопросом стоит разработка определения механических характеристик фибробетонов при хаотическом укладке фибры, что во многом уже применяется в практике строительства. Несмотря, на чисто теоретический подход в данном исследовании, он дает возможность оценить влияние плотности уложения фибры, ее характеристик на прочность изделия в целом. В перспективе данные теоретические выкладки должны замыкаться экспериментальными исследованиями и на их основе создание нормативов для включение их в строительные нормы аналогичные существующим [6, 7].

Литература

1. *Klyuev A.V., Klyuev S.V., Netrebenko A.V., Durachenko A.V.* Fine-grained fiber-reinforced concrete reinforced with polypropylene fiber // Bulletin of BSTU named after V.G. Shukhov. 2014. No. 4, pp.67–72.
2. *Begich Y.E., Klyuev S.V., Jos V.A., Cherkashin A.V.* Fine-Grained Concrete with Various Types of Fibers // Magazine of Civil Engineering. 2020. vol. 97, No. 5, https://doi.org/10.18720/MCE.97.2.
3. *Shirzadi T, F. Ahmadi Danesh Ashtiani, Ehsan Noroozinejad Farsangi*. A novel Ductile Lightweight Fiber-Reinforced Concrete (DLFC) infill for seismic-prone zones: Experimental and numerical investigations // Structures. 2024, vol. 63, https://doi.org/10.1016/j.istruc.2024.106346.
4. *Velikanov P.G., Khalitova D.M.* Solutions of boundary value problems for anisotropic plates and shells by boundary elements method // Vestnik of Samara University. Natural Science Series. 2021, vol. 27, No. 2 pp. 48-61.
5. *Abirov R.A.* On the constitutive relations in plasticity at complex loading. In: ASME International Mechanical Engineering Congress and Exposition, Proceedings. 2009, vol. 12, pp. 557–559.
6. GOST 18105–2010 Concretes. Rules for control and assessment of strength / Interstate council for standardization, metrology and certification
7. Eurocode 2: Design of concretete structures - Part 1-1: General rules and rules for buildings, 2004
8. *Khezheev Kh.A.* Fiber-gypsum concrete composites using volcanic rocks // Building Materials. 2013, No. 11, pp.20–23.
9. *Leonovich I.A., Leonovich A.A.* Influence resilience characteristic of composite materials on properties fibre concretes // Bulletin of the Belarusian-Russian University. 2007, vol. 16, No. 3, pp.148–155.
10. *Crouch S.L., Starfield A.M.* Boundary Element Methods in Solid Mechanics / «George Allen & Unwin» London, 1983, 322 p.
11. *Goodman R.E.* Introduction to Rock Mechanics / John Willey & Sons. New York, 1989, 562 p.
12. *Lekhnitsky S.G.* Theory of an elastic anisotropic body / «Nauka» Moscow, 1977, 411 p.
13. *Spadea G., Bencardino F., Swamy R.N.* Structural Behavior of Composite RC beams with externally bonded CFRP // J. Comp.Constr., ASCE, 1997 vol. 2 No. 3. pp. 132–137.
14. *Ugural Ansel C.* Anisotropic Plates. / In *Stresses in Beams, Plates, and Shells*. 2020, https://doi.org/10.1201/b17516-14.
15. *Stamatelos Dimitrios G., George N. Labeas.* Buckling Analysis of Laminated Stiffened Plates with Material Anisotropy Using the Rayleigh–Ritz Approach. // *Computation*. 2023, https://doi.org/10.3390/computation11060110.
16. *Maksymovych V., Solyar Ya., Kempa Ya.* Investigation of Bending of Anisotropic Plates with Inclusions with the Help of Singular Integral Equations. // Journal of Mathematical Sciences. 2021, vol. 254, pp. 129–141. https://doi.org/10.1007/s10958-021-05293-7.

ИССЛЕДОВАНИЕ НДС И СОБСТВЕННЫХ КОЛЕБАНИЙ ЦИЛИНДРИЧЕСКОЙ ТРУБЫ ИЗ КОМПОЗИТА

Василевич Ю.В.[1], Абдусаттаров А.[2], Сабиров Н.Х.[2]
[1]*Белорусский национальный технический университет, Минск, Белоруссия*
[2]*Ташкентский государственный транспортный университет, Ташкент, Узбекистан*
E-mail: abdusattarov4646@gmail.com

Аннотация. *В процессе деформирования вязкопластических элементов конструкций, особенно высоконаполненных композитных материалах происходит накопления повреждений, которые при определенных условиях приводят к появлению трещин и разрушению. В работе изложены математические модели и методика расчета деформирования и повреждаемости полого цилиндра – трубопровода, взаимодействующего со средой (оболочкой) под действием внутреннего давления из вязкоупругого материала. Изучены радиальные колебания неоднородного многослойного цилиндра и определены собственные частоты рассматриваемого конструкции.*

Ключевые слова: *напряжение, деформирование, повреждаемость, композиционные материалы, слоистые трубы, численный расчет.*

1. Введение

В последнее время особое внимание уделяется разработке и совершенствованию методов расчета деформирования цилиндрических тел из композитных материалов при статических и динамических нагрузок. В связи с этим вопросы повышение прочности, снижение материалоемкости, интенсификация рабочих параметров трубопровода является актуальной задачей [1].

При проектировании и расчета цилиндрической трубы наряду с традиционными материалами широкое применение находят материалы с вязкоупругими свойствами и композиты на их основе. Интерес к этим материалам обусловлен тем, что присущий им комплекс свойств и особенностей существенно отличает их от традиционных материалов. В этих элементах изменяя направления и количество слоёв, можно будет сравнительно в широких пределах моделировать деформационные и прочностные характеристики материалов. В монографии [2] разработаны методы расчета многослойных конструкции на статические, динамические и температурные воздействия. Показаны способы определения эффективных физико-механических характеристик, а также оптимального выбора параметров слоистых композиционных материалов.

В статьях [3,4] отмечено, что создание и развитие новых расчетных методов для исследования напряженно-деформированного состояния труб из композитов с учетом их структурных свойств, а также разработка алгоритмов вычисления и создание комплекс программ, осуществляющих учет, контроль и диагностику трубопроводных систем различного назначения, способствуют повышению их безопасности и эксплуатационной надежности. В монографии [5] рассматривается проблема образования остаточных напряжений и математического моделирования напряжённо-деформированного состояния в упрочнённом слое элементов конструкций после процедуры поверхностного пластического деформирования в условиях ползучести. Решён ряд прикладных задач релаксации остаточных напряжений для толстостенных труб.

В работе [6] изложены результаты теоретических и экспериментальных исследований по оптимизации технических и технологических аспектов производства конструкций из армированных композиционных материалов. Рассмотрены вопросы теории плоского деформирования, прочностные и деформационные характеристики препрегов, находящейся в не отвержденном состоянии композитов. Приведены результаты расчета и анализа напряжений в изделиях из армированных композитов и даны рекомендации по управлению остаточными напряжениями.

В работе [7] рассмотрены методы решения динамических задач упругих и вязкоупругих композитов периодической структуры. На основе метода осреднения, исходная задача сведена к решению двух рекуррентных последовательностей задач. Сформулирована постановка и дано решение ряда новых задач упругопластических и вязкопластических систем при исходном и циклическом нагружениях, в частности упругопластическое решение

полого цилиндра и сферы скрепленного с упругой оболочкой, а также конической трубы при повторном внутреннем давлении [8].

2. Цель задачи

Исследование напряженно-деформированного состояния полого цилиндра – трубы из вязкоупругого материала, взаимодействующей со средой (тонкостенной оболочкой) с учетом повреждаемости материала, а также собственного колебания многослойной трубы.

2.1. Анализ напряженно-деформированного состояния вязкоупругой трубы с учетом повреждаемости.

Рассмотрим задачу о деформировании и длительной прочности трубопровода-полого цилиндра, взаимодействующего с средой. Материал цилиндра считаем несжимаемым и принимаем условия плоской деформации. В этом случае перемещение *U(r,t),* деформации ε_r, ε_θ и интенсивность деформации ε_u определяются соотношениями

$$U(r,t)=\frac{C(t)}{r} \tag{1}$$

$$\varepsilon_r=-\frac{C(t)}{r^2};\ \varepsilon_\theta=\frac{C(t)}{r^2};\ \varepsilon_u=\frac{2}{\sqrt{3}}\frac{|C(t)|}{r^2}. \tag{2}$$

Для связи между компонентами напряжений и деформаций принимаем следующее нелинейное соотношение [1]:

$$S_{ij}=2G\left[Э_{ij}\varphi(\varepsilon_u)-\int_0^t R(t^*-\tau^*)\varphi(\varepsilon_u)Э_{ij}(\tau)d\tau\right] \tag{3}$$

Для определения функции повреждаемости $\omega(t)$ используем кинетическое уравнение [1]

$$\frac{d\omega}{dt}=A\frac{\sigma_u^n}{(1-\gamma\omega)^n}, \tag{4}$$

причем $\omega(0)=0;\ \omega(t_p)=1$, где t_p –время до наступления предельного состояния (разрушения).

Из соотношений (2) и (3) в нашем случае следует:

$$\sigma_\theta-\sigma_r=\frac{4G}{r^2}\left[C(t)\varphi(\varepsilon_u)-\int_0^t R(t^*-\tau^*)\varphi(\varepsilon_u)C(\tau)d\tau\right] \tag{5}$$

Предположим, что

$$\varphi(\varepsilon_u)=B_0\varepsilon_u^{\alpha-1};\ G=G_0(1-\gamma\omega). \tag{6}$$

С учетом соотношений (1) и (6) из (5) получим

$$\sigma_\theta-\sigma_r=a_1(1-\gamma\omega)\frac{C_\alpha(t)}{r^{2\alpha}}, \tag{7}$$

где

$$a_1=4G_0B_0\left[\frac{2}{\sqrt{3}}\right]^{\alpha-1};\ C_\alpha(t)=C^\alpha(t)-\int_0^t R(t^*-\tau^*)C^\alpha(\tau)d\tau. \tag{8}$$

В нашем случае

$$\sigma_u=\frac{2}{\sqrt{3}}(\sigma_\theta-\sigma_r)=\frac{2}{\sqrt{3}}a_1(1-\gamma\omega)\frac{C_\alpha(t)}{r^{2\alpha}} \tag{9}$$

Подставляя (9) в (4), после интегрирования имеем

$$\omega=A\left(\frac{2}{\sqrt{3}}\right)^n\frac{1}{r^{2\alpha n}}\int_0^t C_\alpha^n(\tau)d\tau \tag{10}$$

Используя дифференциальные уравнения равновесия и учитывая (5) и (10), получим

$$\sigma_r = C_1(t) + a_1 C_\alpha(t)\left(\frac{1}{a^{2\alpha}} - \frac{1}{r^{2\alpha}}\right)\frac{1}{2\alpha} - a_1 a_2 C_\alpha(t)\int_0^t C_\alpha^n(\tau)d\tau\left[\frac{1}{a^{2\alpha(n+1)}} - \frac{1}{r^{2\alpha(n+1)}}\right]\frac{1}{2\alpha(n+1)} \quad (11)$$

где

$$a_1 = 4G_0 B_0\left[\frac{2}{\sqrt{3}}\right]^{\alpha-1}.$$

Граничные условия $\sigma_r(a,t) = -P(t)$, $\sigma_r(b,t) = -q(t)$ приводят к следующим соотношениям:

$$\sigma_r = -P(t) + a_3 c_\alpha(t)\left[\frac{1}{a^{2\alpha}} - \frac{1}{r^{2\alpha}}\right] - a_4\left[\frac{1}{a^{2\alpha(n+1)}} - \frac{1}{r^{2\alpha(n+1)}}\right]C_\alpha(t)\int_0^t C_\alpha^n(\tau)d\tau \quad (12)$$

$$\text{P(t)-q(t)=}\ a_3\left[\frac{1}{a^{2\alpha}} - \frac{1}{b^{2\alpha}}\right]\cdot C_\alpha(t) - a_4\left[\frac{1}{a^{2\alpha(n+1)}} - \frac{1}{r^{2\alpha(n+1)}}\right]C_\alpha(t)\int_0^t C_\alpha^n(\tau)d\tau, \quad (13)$$

где

$$a_2 = A\left[\frac{\sqrt{3}}{2}a_1\right]^n;\ a_3 = \frac{a_1}{2\alpha};\ a_4 = \frac{a_1 a_2}{2\alpha(n+1)}.$$

Для определения контактного давления *q(t)* имеем

$$q(t) = \frac{h}{b}\cdot\frac{E_*}{1-\nu_*^2}\frac{C(t)}{b^2} = kU(t) = k\frac{C(t)}{b}. \quad (14)$$

Подставляем выражение (14) в (13):

$$P(t) - \frac{kC(t)}{b} = a_3\left[\frac{1}{a^{2\alpha}} - \frac{1}{b^{2\alpha}}\right]C_\alpha(t) - a_4\left[\frac{1}{a^{2\alpha(n+1)}} - \frac{1}{b^{2\alpha(n+1)}}\right]C_\alpha(t)\int_0^t C_\alpha^n(\tau)d\tau \quad (15)$$

В результате получено нелинейное интегральное уравнение для определения функции *C(t)*.

Для решения уравнения (15) используем метод последовательных приближений. За нулевое приближение принимается решение $C_0(t)$ линейной среды и без учета повреждаемости. В этом случае любое *m*-е приближение строится следующим образом:

$$\frac{kC^{(m)}(t)}{b} = P(t) - a_3\left(\frac{1}{a^{2\alpha}} - \frac{1}{b^{2\alpha}}\right)C_\alpha^{(m-1)}(t) + a_4\left(\frac{1}{a^{2\alpha(n+1)}} - \frac{1}{b^{2\alpha(n+1)}}\right)C_\alpha^{(m-1)}(t)\int_0^t\left[C_\alpha^{(m-1)}(\tau)\right]^n d\tau \quad (16)$$

Представляем уравнение (16) в виде

$$P(t) = a_5 C(t) + a_6 C_\alpha(t) - a_7 C_\alpha(t)\int_0^t C_\alpha^n(\tau)d\tau \quad (17)$$

где

$$a_5 = \frac{k}{b};\ a_6 = a_3\left(\frac{1}{a^{2\alpha}} - \frac{1}{b^{2\alpha}}\right);\ a_7 = a_4\left(\frac{1}{a^{2\alpha(n+1)}} - \frac{1}{b^{2\alpha(n+1)}}\right).$$

В случае отсутствия взаимодействия уравнение (17) имеет следующий вид $(a_5 = 0)$:

$$a_6 C_\alpha(t) - a_7 C_\alpha(t)\int_0^t C_\alpha^n(\tau)d\tau = P(t) \quad (18)$$

Введем следующее обозначение:

$$\phi(t) = \int_0^t C_\alpha^n(\tau)d\tau;\ \frac{d\phi}{dt} = C_\alpha^n(t). \quad (19)$$

Подставляя (19) в (18), получаем дифференциальное уравнение для определения $\phi(t)$:

$$\left(\frac{d\phi}{dt}\right)(a_6 - a_7\phi)^n = P^n(t) \quad (20)$$

Интегрируем это уравнение с учетом начальных условий (при $t=0, \phi=0$). В результате получим ($P(t)=P_0=Const$) аналитическое решение для $\omega(r,t)$:

$$\phi(t)=\frac{a_6}{a_7}+\frac{1}{a_7}\left[P_0^n a_7(n+1)t-a_6^{n+1}\right]^{-1/(n+1)} \tag{21}$$

$$\omega(r,t)=A(3G_0)^n\left(\frac{2}{\sqrt{3}}\right)^{\alpha n}\frac{1}{r^{2\alpha n}}\left\{\frac{a_6}{a_7}+\frac{1}{a_7}\left[P_0^n a_7(n+1)t-a_6^{n+1}\right]^{1/(n+1)}\right\}. \tag{22}$$

Теперь представим уравнение для линейного случая в виде

$$K(t)C(t)-\psi(t)\int_0^t R(t-\tau)C(t)d\tau=P_1(t) \tag{23}$$

где

$$K(t)=1-\psi(t);\psi(t)=\frac{2G}{bK}\left[1-\left(\frac{b}{a(t)}\right)^2\right];\quad P_1(t)=\frac{P_a(t)b}{K}.$$

В качестве ядра релаксации $R(t-\tau)$ принимаем [1] (далее знак «черта» опускаем):

$$R(t-\tau)=\overline{A}e^{-\overline{\beta}(t-\tau)}(t-\tau)^{\overline{\alpha}-1}, A>0, \overline{\beta}>0, 0<\overline{\alpha}<1.$$

К решению (23) применим метод исключения слабо-сингулярных особенностей [7]:

$$C_n=\frac{1}{\left(K_n-\frac{A}{\alpha}\psi_n D_0\right)}\left[P_n+\frac{A}{\alpha}\psi_n\sum_{i=1}^{n}D_i\cdot e^{-\beta t_i}C_{n-i}\right],\quad n=0,1,.... \tag{24}$$

где

$$C(t_n)=C_n,\quad t_n=n\Delta t,\quad K(t_n)=K_n,\quad \psi(t_n)=\psi_n;\ P(t_n)=P_n, D_0=\frac{(\Delta t)^\alpha}{2};$$

$$D_i=\frac{(\Delta t)^\alpha}{2}\left[(i+1)^\alpha-(i-1)^\alpha\right];\quad i=\overline{1,n-1}.\ D_n=\frac{(\Delta t)^\alpha}{2}\left[n^\alpha-(n-1)^\alpha\right];\quad i=n.$$

Здесь ограничимся приведением окончательных формул для деформации ε_θ, принимающей максимальное значение при $r=a(t)$, и для напряжения σ_θ. В этом случае из (24) имеем

$$a_n^2\varepsilon_{\theta n}=C_n,\quad n=0,1,2,.....,$$

$$\overline{\sigma}_{\theta n}=-P_n+\frac{2E}{Kb(1+\nu)a_n^2}\left(C_n-\frac{A}{\alpha}\sum_{i=1}^{n}D_i e^{\beta t_i}C_{n-1}\right) \tag{25}$$

где

$$a(t_n)=a_n;\ t_n=n\Delta t;\ n=0,1,2,...,\ \varepsilon_\theta(t_n)=\varepsilon_{\theta n};$$

$$\overline{\sigma}_\theta(t)=\frac{\sigma_\theta b}{K},\ \overline{\sigma}_\theta(t_n)=\overline{\sigma}_{\theta n}.$$

На основе разработанной методики [7] произведены численные расчеты и анализ напряженно-деформированного состояния полого цилиндра, скрепленного с оболочкой. При этом учитываются вязкоупругих свойств материалов.

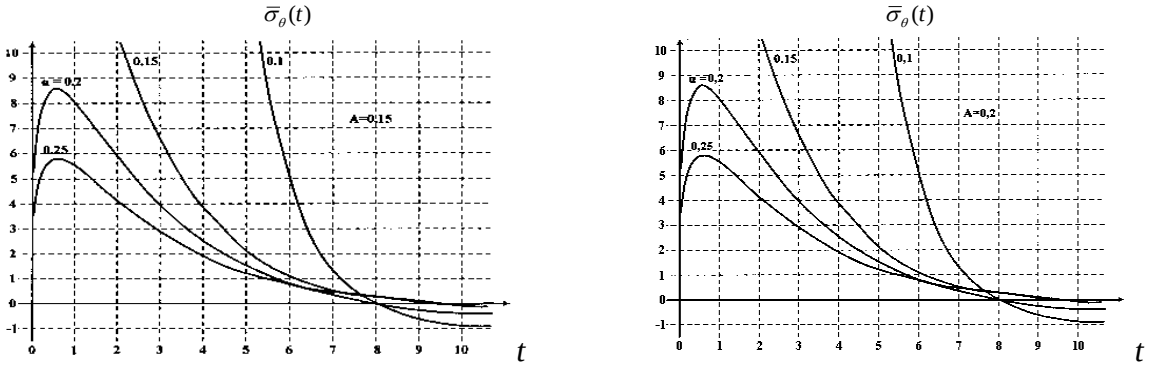

Рисунок 1. – **Графики изменения во времени, характеризующие влияние отдельных параметров на кольцевое напряжение: A=0.15; A=0.20**

На рис. 1 представлены графики изменения по времени кольцевого напряжения при постоянном давлении. Здесь приняты следующие значения параметров: *b/a*=3; *b/h*=10^2; *ν=0.495*; *ν*∗*=0.3*. Эти графики иллюстрируют, на сколько существенное влияние оказывают реологические параметры (A, α, β) на величину кольцевых напряжение (при β=0.05).

2.2. Определение собственных частот трубы. Рассмотрим свободные радиальные колебания толстостенного полого бесконечного неоднородного цилиндра. Цилиндр состоит из упругих изотропных цилиндрических слоев различной толщины с разными механическими свойствами. На границах раздела двух цилиндрических слоев выполняется условия жесткого контакта.

Уравнения движения каждого цилиндрического слоя с учетом осевой симметрии в цилиндрической системе координат имеют вид [7]

$$\frac{\partial^2 u_i}{\partial t^2} = c_i^2\left(\frac{\partial^2 u_i}{\partial r^2} + \frac{1}{r}\frac{\partial u_i}{\partial r} - \frac{u_i}{r^2}\right) \tag{26}$$

при $R_i < r < R_{i+1}$. Здесь u_i - перемещения i - цилиндрического слоя, R_i - радиус внутренней поверхности i-слоя, R_{i+1}- радиус внешней поверхности i-слоя, $c_i = \sqrt{(\lambda_i + 2\mu_i)/\rho_i}$ - скорость распространения продольных волн в материале i-слоя, λ_i, μ_i - коэффициенты Ламе i-слоя, $i = 1,2,3,...,N$, N - число цилиндрических слоев.

Граничные условия имеют вид

$$\sigma_1(R_1,t) = 0, \quad \sigma_N(R_{N+1},t) = 0 \tag{27}$$

Условия непрерывности перемещений $u_i(r,t)$ и напряжений $\sigma_i(r,t)$ на границах раздела цилиндрических слоев дает

$$u_i(R_{i+1},t) = u_{i+1}(R_{i+1},t), \quad \sigma_i(R_{i+1},t) = \sigma_{i+1}(R_{i+1},t), \quad i = 1,2,3,...,N-1 \tag{28}$$

Определяющие соотношения имеют следующий вид

$$\sigma_i(r,t) = (\lambda_i + 2\mu_i)\frac{du_i}{dr} + \lambda_i\frac{u_i}{r}, \quad i = 1,2,3,...,N \tag{29}$$

Решения поставленной задачи (26), (27), (28), (29) ищется в виде

$$u_i(r,t) = U_i(r)e^{i\omega t} \tag{30}$$

где ω - круговая частота, которая считается действительным числом.

Подставляя (30) в (26), (27), (28), (29) получим

$$\frac{d^2U_i(r)}{dr^2} + \frac{1}{r}\frac{dU_i(r)}{dr} - \left(\frac{1}{r^2} - \frac{\omega^2}{c_i^2}\right)U_i(r) = 0 \tag{31}$$

$$\left((\lambda_1+2\mu_1)\frac{dU_1(r)}{dr}+\lambda_1\frac{U_1(r)}{r}\right)_{|r=R_1}=0$$

$$\left((\lambda_N+2\mu_N)\frac{dU_N(r)}{dr}+\lambda_N\frac{U_N(r)}{r}\right)_{|r=R_{N+1}}=0 \tag{32}$$

$$U_i(R_{i+1},t)=U_{i+1}(R_{i+1},t) \tag{33}$$

$$\left((\lambda_i+2\mu_i)\frac{dU_i}{dr}+\lambda_i\frac{U_i}{r}\right)_{/r=R_{i+1}}=\left((\lambda_{i+1}+2\mu_{i+1})\frac{dU_{i+1}}{dr}+\lambda_i\frac{U_{i+1}}{r}\right)_{/r=R_{i+1}} \quad i=1,2,3,...,\mathrm{N}-1$$

Уравнения (31) имеют решения в виде

$$U_i(r)=S_1^{(i)}J_1(\frac{\omega}{c_i}r)+S_2^{(i)}Y_1(\frac{\omega}{c_i}r) \tag{34}$$

где J_1, Y_1- функции Бесселя [7] первого и второго рода соответственно, $S_1^{(i)}$, $S_2^{(i)}$- постоянные.

Используя следующие свойства функции Бесселя

$$\frac{dJ_1(z)}{dz}=-J_2(z)+\frac{1}{z}J_1(z),\ \frac{dY_1(z)}{dz}=-Y_2(z)+\frac{1}{z}Y_1(z)$$

И поставляя (34) в (32), (33) получим

$$\left[\frac{2(\lambda_1+\mu_1)}{R_1}J_1(\frac{\omega}{c_1}R_1)-(\lambda_1+2\mu_1)\frac{\omega}{c_1}J_2(\frac{\omega}{c_1}R_1)\right]S_1^{(1)}+$$

$$+\left[\frac{2(\lambda_1+\mu_1)}{R_1}Y_1(\frac{\omega}{c_1}R_1)-(\lambda_1+2\mu_1)\frac{\omega}{c_1}Y_2(\frac{\omega}{c_1}R_1)\right]S_1^{(1)}=0$$

$$J_1(\frac{\omega}{c_i}R_{i+1})S_1^{(i)}+Y_1(\frac{\omega}{c_i}R_{i+1})S_2^{(i)}-J_1(\frac{\omega}{c_{i+1}}R_{i+1})S_1^{(i+1)}-Y_1(\frac{\omega}{c_{i+1}}R_{i+1})S_2^{(i+1)}=0$$

$$\left[\frac{2(\lambda_i+\mu_i)}{R_{i+1}}J_1(\frac{\omega}{c_i}R_{i+1})-(\lambda_i+2\mu_i)\frac{\omega}{c_i}J_2(\frac{\omega}{c_i}R_{i+1})\right]S_1^{(\mathrm{i})}+$$

$$+\left[\frac{2(\lambda_i+\mu_i)}{R_{i+1}}Y_1(\frac{\omega}{c_i}R_{i+1})-(\lambda_i+2\mu_i)\frac{\omega}{c_i}Y_2(\frac{\omega}{c_i}R_{i+1})\right]S_2^{(\mathrm{i})}-$$

$$\left[\frac{2(\lambda_{i+1}+\mu_{i+1})}{R_{i+1}}J_1(\frac{\omega}{c_{i+1}}R_{i+1})-(\lambda_{i+1}+2\mu_{i+1})\frac{\omega}{c_{i+1}}J_2(\frac{\omega}{c_{i+1}}R_{i+1})\right]S_1^{(\mathrm{i+1})}-$$

$$\left[\frac{2(\lambda_{i+1}+\mu_{i+1})}{R_{i+1}}Y_1(\frac{\omega}{c_{i+1}}R_{i+1})-(\lambda_{i+1}+2\mu_{i+1})\frac{\omega}{c_{i+1}}Y_2(\frac{\omega}{c_{i+1}}R_{i+1})\right]S_2^{(\mathrm{i+1})}=0$$

$$\left[\frac{2(\lambda_N+\mu_N)}{R_{N+1}}J_1(\frac{\omega}{c_N}R_{N+1})-(\lambda_N+2\mu_N)\frac{\omega}{c_N}J_2(\frac{\omega}{c_N}R_{N+1})\right]S_1^{(N)}+$$

$$+\left[\frac{2(\lambda_N+\mu_N)}{R_{N+1}}Y_1(\frac{\omega}{c_N}R_{N+1})-(\lambda_N+2\mu_N)\frac{\omega}{c_N}Y_2(\frac{\omega}{c_N}R_{N+1})\right]S_2^{(N)}=0. \tag{35}$$

Приравнивая к нулю определитель полученной системы уравнений относительно неизвестных $S_1^{(\mathrm{i})}$, $S_2^{(\mathrm{i})}$, получим дисперсионное уравнение рассматриваемой задачи в матричной форме

$$\det a_{ij} = 0 \tag{36}$$

где, например,

$$a_{11} = \frac{2(\lambda_1 + \mu_1)}{R_1} J_1(\frac{\omega}{c_1} R_1) - (\lambda_1 + 2\mu_1) \frac{\omega}{c_1} J_2(\frac{\omega}{c_1} R_1),$$

$$a_{12} = \frac{2(\lambda_1 + \mu_1)}{R_1} Y_1(\frac{\omega}{c_1} R_1) - (\lambda_1 + 2\mu_1) \frac{\omega}{c_1} Y_2(\frac{\omega}{c_1} R_1),$$

$$a_{2N,2N-1} = \frac{2(\lambda_N + \mu_N)}{R_{N+1}} J_1(\frac{\omega}{c_N} R_{N+1}) - (\lambda_N + 2\mu_N) \frac{\omega}{c_N} J_2(\frac{\omega}{c_N} R_{N+1}),$$

$$a_{2N,2N} = \frac{2(\lambda_N + \mu_N)}{R_{N+1}} Y_1(\frac{\omega}{c_N} R_{N+1}) - (\lambda_N + 2\mu_N) \frac{\omega}{c_N} Y_2(\frac{\omega}{c_N} R_{N+1}),\ n = 1, 2, 3, ..., N-1.$$

Теперь переходим к длинноволновому приближению, т.е., рассмотрим случай, когда длина волны существенно превышает характерный размер цилиндра. С учетом следующие свойства функции Бесселя

$$J_1(z) \to \frac{z}{2},\ J_2(z) \to \frac{z^2}{8},\ Y_1(z) \to -\frac{2}{\pi z},\ Y_2(z) \to -\frac{4}{\pi z^2} \quad при \quad z \to 0$$

например, имеем

$$a_{11} = \frac{\omega}{c_1}\left[(\lambda_1 + \mu_1) - \frac{(\lambda_1 + 2\mu_1) R_1^2}{8} \frac{\omega^2}{c_1^2}\right],\ a_{12} = \frac{4\mu_1}{\pi R_1^2} \frac{c_1}{\omega},$$

$$a_{2N,2N-1} = \frac{\omega}{c_N}\left[(\lambda_N + \mu_N) - \frac{(\lambda_N + 2\mu_N) R_{N+1}^2}{8} \frac{\omega^2}{c_N^2}\right],\ a_{2N,2N} = \frac{4\mu_N}{R_{N+1}^2} \frac{c_N}{\omega},$$

Матричное уравнение (36) с найденными элементами позволяет определить собственных частот рассматриваемого многослойного цилиндра.

В качестве примера рассмотрим свободное радиальное колебание двухслойного бесконечного по длине цилиндра. В этом случае на ячейке квазипериодичности находится двух цилиндрических элементов различными механическими и геометрическими свойствами. Тогда, для определения низшей частоты рассматриваемой задачи имеем детерминант четвертого порядка. Разрешив полученного уравнения относительно частоты, находим выражения

$$\omega^2 = \frac{1}{2(A_1 B_3 + A_3 B_1)} (A_2 B_3 + A_3 B_2 - A_1 B_4 - A_4 B_1 - ((A_1 B_4 + A_4 B_1 -$$

$$- A_2 B_3 - A_3 B_2)^2 + 4(A_1 B_3 + A_3 B_1)(A_2 B_4 + A_4 B_2))^{\frac{1}{2}}) \tag{37}$$

где

$$A_1 = \frac{(\lambda_1 + 2\mu_1) R_1^2}{4\pi R_2 c_1^2},\ A_2 = \frac{2}{\pi R_1^2 R_2}\left[2\mu_1 R_2^2 + (\lambda_1 + \mu_1) R_1^2\right],\ A_3 = \frac{\mu_1(\lambda_1 + 2\mu_1)}{2\pi c_1^2}\left(\frac{R_1^2}{R_2^2} - \frac{R_2^2}{R_1^2}\right),$$

$$A_4 = \frac{4\mu_1(\lambda_1 + \mu_1)}{\pi}\left(\frac{1}{R_1^2} - \frac{1}{R_2^2}\right),\ B_1 = \frac{(\lambda_2 + 2\mu_2) R_3^2}{4\pi R_2 c_2^2},\ B_2 = \frac{2}{\pi R_2 R_3^2}\left[2\mu_2 R_2^2 + (\lambda_2 + \mu_2) R_3^2\right],$$

$$B_3 = \frac{\mu_2(\lambda_2 + 2\mu_2)}{2\pi c_2^2}\left(\frac{R_2^2}{R_3^2} - \frac{R_3^2}{R_2^2}\right),\ B_4 = \frac{4\mu_2(\lambda_2 + 2\mu_2)}{\pi}\left(\frac{1}{R_2^2} - \frac{1}{R_3^2}\right).$$

Согласно этому выражению можно исследовать характер зависимости частоты от механических и геометрических параметров рассматриваемого двухслойного полого цилиндра.

3. Заключение.

Разработаны методика расчета напряженно-деформированного состояния вязкоупругой трубы с учетом накопление повреждаемости. Приведены численные результаты расчета и анализ напряжений и деформаций для полого цилиндра, скрепленного с оболочкой. Показано влияние вязкоупругих свойств на кинетику НДС трубопровода. Определены собственные частоты для двухслойного неоднородного композиционного цилиндра.

Литература

1. *Москвитин В. В.* Сопротивление вязкоупругих материалов / М.: URSS, 2019, 328 с.
2. *Болотин В.В., Новичков Ю.Н.* Механика многослойных конструкций / М.: Машиностроение. 1980, 375 с.
3. *Василевич Ю.В., Можаровский В.В.* Математическое моделирование, экспериментальные исследования, расчет на прочность и жесткость труб и резервуаров из композиционных материалов с учетом неоднородности, анизотропии, концентраторов напряжений // Сборник трудов V Белорусского конгресса по теоретической и прикладной механике. Минск, 2011, т. 2, С. 4-8.
4. *Можаровский В.В., Кузьменков Д.С., Василевич Ю.В.* Реализация расчета напряженно-деформированного состояния слоистых цилиндрических труб из полимеров и композитов // «Теоретическая и прикладная механика», Международный научно технический сборник. Минск. БНТУ. 2022, Вып. 37, С. 36-44.
5. *Радченко В.П., Саушкин М.Н.* Ползучесть и релаксация остаточных напряжений в упрочненных конструкциях / М.: Машиностроение-1. 2005, 226 с.
6. *Василевич Ю.В. и др.* Механика препрегов – расчет изделий из армированных композиционных материалов / Минск. БНТУ. 2016, 295 с.
7. *Абдусаттаров А., Каримов А.М.* Методы решения задач механики композитных материалов и неупругих элементов конструкции при циклических нагружениях / Ташкент: Узбекистан. 2020, 198 с.
8. *Абдусаттаров А., Sabirov, N., Ruzieva N.* Mathematical Models of Pipeline Deformation Under Repeated - Variable Loading Taking into Account Damageability // AIP Conference Proceedings. 2022, 030014, https://www.scopus.com/record/display.uri?eid=2-s2.0-85141976410&origin=resultslist.

ПРОБЛЕМЫ АЛГОРИТМИЗАЦИИ В МЕХАНИКЕ РАЗРУШЕНИЯ

Кабулов А.В.[1], Норматов И.Х.[1]

[1]Национальный университет Узбекистан имени Мирзо Улугбека

E-mail: ihnormatov@Gmail.com

***Аннотация**: В статье поставлена задача алгоритмизации в механике декомпозиции и формализована информационная часть символов и банков законов. Исследованы алгоритмизация в механике разрушения, модели вязких и хрупких разрушений, теории трещин методами теории упругости, эластичности и ползучести. Предложено применение алгоритмических методов к установлению законов разрушения, которая получила широкое применение в расчетах на прочность машин и сооружений.*

***Ключевые слова:** алгоритмизация, банки, опыт, законы, метод, модели, разрушения.*

1. Введение

В настоящее время ведутся фундаментальные исследования в области механики разрушения [1-12]. Построении алгоритмических систем применяется метод генерации моделей из общих законов функционирования систем, а частные модели функционирования систем, т.е. конкретных операций выписываются в крайних случаях.

В организационных системах за общие законы можно принять натурально-стоимостные балансы продуктов, балансы мощностей, трудовых ресурсов, доходы и расходы населения и т.д. При исследовании производственных процессов можно взять агрегатные модели [8] ситуационные модели, а также модель массового обслуживания и автоматные модели.

Технологические процессы в основном описываются законами механики сплошных сред и молекулярной физики. Для научных исследований в области механики сплошных сред возможность генерации частных моделей из общих законов сохранения доказана [1].

2. Материалы, методы и объект исследования.

В алгоритмической схеме формализации исследования систем программное обеспечение предлагается строить с помощью шести основных $(Б_1 - Б_6)$ и двух вспомогательных банков ($Б_n$ - постановки, $Б_0$ - операционный) [5]. Каждый основной банк имеет информационную и операционную части и набор модулей; определение состава банков является предметом дальнейших исследований.

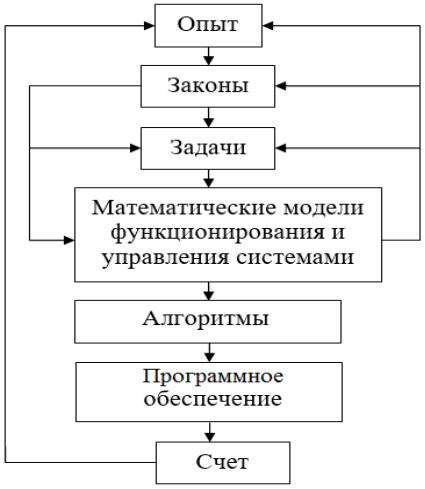

Рисунок 1. - **Основные этапы исследования различных объектов.**

Методы алгоритмизации [2, 6] приобретают особое значение при автоматизации всех этапов исследования систем и построения алгоритмов управления. С этой точки зрения процесс исследования различных объектов можно разбить на семь последовательных этапов [5, 6] (Рис.1), представляющих собой кибернетическую цепь с обратной связью.

В алгоритмизации [1-4] «опыт» предполагается создание информационно-поисковых систем и широкая автоматизация экспериментов с разработкой и внедрением средств сбора, передачи и обработки экспериментальных данных.

В различных отраслях науки на основе универсальных законов решаются разнообразные задачи, принадлежащие разным классам [1-6]. Классификация этих задач и автоматическое распознавание классов выполняются на этапе «задачи» [10]. В научной и инженерной практике повседневно решается множество конкретных локальных задач. Если на основании опыта определены основные параметры задачи, т.е. она поставлена, то по известным законам на ЭВМ можно вывести математические зависимости (логические и аналитические), описывающие эту задачу. Такие зависимости, оформленные в алгебраических, дифференциальных, интегральных и других видах уравнений, являются математическими моделями исследуемого процесса. Вывод математических моделей автоматизируется на этапе «математические модели». Таким образом, образуется множество моделей $M = \{M_1, M_2, ..., M_n\}$.

В вычислительной математике для приближенного решения классов уравнений разработано [2, 6] множество алгоритмов $A = \{A_1, A_2, ..., A_m\}$. Чтобы решить задачи на ЭВМ необходимо предварительно построить отображение множества M на A, т.е. установить сначала применимость алгоритмов из A к операторам из множества математических моделей M. Применимость связана с доказательством сходимости и устойчивостью алгоритма. Так, какой-нибудь одной модели из M соответствует подмножество алгоритмов из A. Для выбора единственного алгоритма следует поставить условия оптимальности алгоритма и проверить их. Данный круг проблем решается на этапе «алгоритмы».

На основе выбора алгоритма необходимо переходить к приближенной системе. К примеру, по методу сеток выбрать сеточную область построить и решить сеточные уравнения. Эти задачи решаются с помощью логических и арифметических операций на

этапе «математическое обеспечение». На этом этапе выбирается также язык программирования и составляются все необходимые программы [2, 6].

На конечном этапе создаются вычислительные комплексы, связанные с опытными установками, и осуществляется увязка счета с опытом [2-9].

При практической реализации этапы алгоритмизации оформляются в виде шести основных и двух вспомогательных алгоритмических банков (АБ). Основные банки названы банками данных (№ 1), законов (№ 2), признаков (№ 3), моделей (№ 4), алгоритмов (№ 5) и прикладных программ (№ 6). Во вспомогательные включены банк постановки и операционный банк. (в настоящей время в научной литературе используется слово блок, однако мы сочли нужным оставить в тексте диссертационном работе слово банк, как исторический факт, связанный с академиком В.К.Кабуловым).

Каждый банк состоит из двух частей: информационной и операционной. В информационной части хранятся численные или символические данные на фиксированных языках, которые вносятся заранее (постоянная информация). Операционная часть алгоритмического банка содержит пакеты программ, перерабатывающие информационные массивы этого банка [2, 6].

Порядок работы банков показан на «Рис.2» [2, 6]. Задача формулируется в банке постановки, а затем вводится в операционный банк и банк признаков. Цифровые исходные данные отправляются в банк данных. В банке признаков условия переводятся в символическую форму, т.е. переписываются на специальном языке, далее вырабатываются признаки задачи, которые передаются в банк законов. С помощью этих признаков в банке законов генерируется математическая модель задачи, которая передается в банк моделей. Здесь модель анализируется, определяются тип оператора и его особенности. Оператор (т.е. математическая модель задачи) с его признаками отправляется в банк алгоритмов, где выбирается оптимальный алгоритм, строится соответствующее уравнение модели. Кроме того, в банке алгоритмов вырабатываются признак для выбора программы счета и сигналы для выборки численных значений коэффициентов. Уравнение модели и вычислительная программа из банка прикладных программ направляются в операционный банк, а признаки для выборки чисел – в банк данных. В операционном банке окончательно формируется уравнение модели и реализуется его численное решение. При этом осуществляется контроль счета и выдачи результатов в заданной форме. В описанной системе обычный счет производится с помощью лишь одного АБ (№ 6), а логические операции выполняются во всех других банках. Банк данных является накопителем всех цифровых характеристик объекта (постоянных и переменных) и заполняется до работы всей системы в целом. Этот банк связывается с экспериментальной системой.

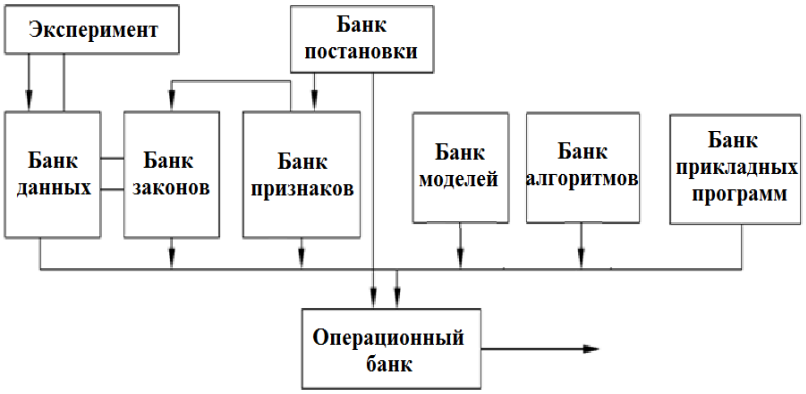

Рисунок 2. - **Схема работы алгоритмических банков**

Применение алгоритмических методов к установлению законов функционирования больших систем, определению стратегии управления, и наконец, к построению управляющих систем имеет большое теоретическое и практическое значение.

Разработка этих проблем приведет к созданию направления, когда автоматизированными будут не только процессы управления, но и процесс проектирования и построения управляющих систем.

Автоматизация на ЭВМ всех этапов исследований по цепочке опыт – законы- математические модели- алгоритмы – программное обеспечение - вычислительный эксперимент является задачей алгоритмизации в механике. При реализации теории формируется шесть основных алгоритмических банков $(Б_1)$ - данных, $(Б_2)$ - законов, $(Б_3)$ - признаков, $(Б_4)$ - моделей, $(Б_5)$ - алгоритмов, $(Б_6)$ - прикладных программ). Все эти банки состоят из информационной и программной частей. В информационной части банков хранятся численные или текстовые данные, оформленные в виде фиксированных форм представления знаний (фреймовые, семантические сети и др.), а в операционной части - программные средства, перерабатывающие эти информации.

Постановка задач оформляется в банке $(Б_0)$, после чего по данным банков $(Б_1 - Б_6)$ в операционном банке $(Б_7)$ собираются исходные данные и программные решения поставленной задачи.

В настоящее время созданы алгоритмические системы для многих областей механики сплошных сред [1-12].

3. Постановка задачи.

Алгоритмизация в механике разрушения начинается с формирования постановки проблемы. Разрушение материалов зависит, прежде всего, от структуры материалов, а также влияния внешних условий - теплового режима, агрессивности среды и характера нагрузок. Теория разрушения -комплексная проблема и изучается на стыке физики твердых тел, материаловедения и механики сплошных сред. Механика разрушения получила широкое применение в расчетах на прочность машин и сооружений. В механике разрушения развиты модели вязких и хрупких разрушений, теории трещин. Все эти процессы исследуются методами теории упругости, эластичности и ползучести. Сначала на основе экспериментальных данных строится континуальная модель разрушения и затем на основе этой модели решаются классы задач. При этом предполагается, что при разрушении исчерпывается несущая способность тела. Это происходит вследствие пластического течения или накопления повреждений. Идеальная пластичность, пластичность с упрочнением ползучести и др. являются моделью течения деформируемого тела.

4. Результаты

Переходим к описанию состава информационной части основных банков.

В информационную часть банка данных $(Б_1)$ записываются значения констант, функций векторов и тензорных величин. Эти данные вводятся заранее при постановке задачи или по результатам вычислений.

В последнее время при создании электронных учебников в $(Б_1)$ добавляется комментарий по содержанию проблемы.

В банк законов $(Б_2)$ прежде всего вводятся законы сохранения механики – массы, импульсов и энергии.

Следующий этап- физические и геометрические законы:

$$Б_{ij} = F(\varepsilon_{ij}, \dot{\varepsilon}_{ij}, \mu), \ \varepsilon_{ij} = \frac{1}{2}\left(\frac{\partial u_i}{\partial x_j} + \frac{\partial u_j}{\partial x_i}\right).$$

При этом рассматриваются законы упругости (изотропные и анизотропные), упругопластичности и ползучести.

В теории разрушения важное значение имеет критерий разрушения из $(Б_2)$.

Приводим перечень критериев по [2].

1. Изотропные материалы (напряжение монотонное, температура обычная, ползучестью пренебрегается).

1.1 Предельная поверхность:

- по инвариантам напряженного состояния $F(I_1(T_\sigma), I_2(T_\sigma), I_3(T_\sigma)) = K$;

- в пространстве напряжений: $F(\sigma_1, \sigma_2, \sigma_3) = K_*$;

- по параметру Моде M_6 и среднему давлению $F(\sigma, T, \mu_\sigma) = K_*$.

1.2. Критерий наибольших нормальных напряжений: $|\sigma_1| = \sigma_*, \quad i = 1, 2, 3.$

1.3. Критерий наибольших касательных напряжений

$$\frac{\tau_{\max}}{2}, \ \max\left(|\sigma_1 - \sigma_2|, |\sigma_2 - \sigma_3|, |\sigma_3 - \sigma_1|\right) = \sigma_*.$$

1.4. Критерий наибольшей интенсивности касательных напряжений

$$T = \frac{\sigma_*}{\sqrt{3}}, \ \left(\sigma_1 - \sigma_2\right)^2 + \left(\sigma_2 - \sigma_3\right)^2 + \left(\sigma_3 - \sigma_1\right)^2 = 2\sigma_*^2.$$

1.5. Критерий Мора $\tau_n = f(\sigma_n)$.

1.6. Критерий Шлейхера - Надаи $T = f(\sigma), \ (T = f(\sigma_{\max}))$.

2. Анизотропные материалы.

2.1. Уравнение предельной поверхности

$$F(\sigma_1, \sigma_2, \sigma_3, \alpha, \beta, \gamma, c_1, c_2, c_3, ...),$$

где $\alpha, \beta, \gamma -$углы, характеризующие положение главных осей напряжений, $c_1, c_2, c_3, ...$ – характеристики механических свойств.

2.2. Условия симметрии:

$$F(J_1, J_2, J_3, ...) = 1,$$

где $J_1, J_2, J_3, ...$ – инварианты, содержащие компоненты напряжений.

3. Критерий длительной и усталостной прочности.

3.1. Критерии длительной прочности: $t_* = A_\alpha^{-45}$, t_* - время до разрушения, A, α - коэффициенты, зависящие от температуры $\sigma_e = f(J_1, J_2, J_3, ...)$.

3.2. Усталостные разрушения при сложных напряжениях:

$$\sigma_e = \max(\bar{\sigma}_1, \bar{\sigma}_2, \bar{\sigma}_3),$$

где $\sigma_e -$максимальное приведенное напряжение, $\bar{\sigma}_i$ - приведенные напряжения в главных направлениях.

4. Упрочняющая среда.

4.1. Пластичное течение

$$f(\sigma_{ij}) = \varphi(q), \ q = S\sqrt{2d\varepsilon_{\ddot{y}} d\varepsilon_{\ddot{y}}} = \Gamma_0,$$

где $q -$ параметры упрочнения.

4.2. Деформационная теория:

$$\varepsilon_1 + \varepsilon_2 + \varepsilon_3 = 0,$$

$$\begin{cases} 3g\left(\Gamma\right)\varepsilon_1 = \sigma_1 - \dfrac{1}{2}\sigma_2, \\ 3g\left(\Gamma\right)\varepsilon_2 = \sigma_2 - \dfrac{1}{2}\sigma_1, \\ 3g\left(\Gamma\right)\varepsilon_3 = -\dfrac{1}{2}(\sigma_1 + \sigma_2). \end{cases}$$

5. Ползучесть.

5.1. Теория течения $i\zeta_{\dot{y}} = f(T)S_y$, T - интенсивность касательных напряжений.

5.2. Теория упрочнения $\psi = \psi(T, \Gamma_0)$, $\Gamma_0 -$ параметр Одквиста.

5.3. Ползуче- пластические среды:

$$\zeta_{ij}^{p} = F(T)\frac{\partial T}{\partial t} S_{\ddot{y}},$$

где $\zeta_{\ddot{y}}^{p} -$скорость мгновенной пластической деформации.

5. Анализ результатов

На основе записанных в $(Б_2)$ законов в банке моделей $(Б_4)$ выводится (или выбирается) математическая модель поставленной задачи. При этом ставятся физические условия (зависимости $\delta_{\ddot{y}}$ и $\varepsilon_{\ddot{y}}$, также условия разрушения), геометрические условия (стрежень, пластинка, оболочка, трехмерные тела), граничные условия (на $\delta_{\ddot{y}}$ и $\varepsilon_{\ddot{y}}$, u_i), выбираются объемные силы (массовые, электродинамические и др), ставится цель вычислений (прочность, устойчивость и др). При этом выполняются аналитические операции (подстановки, дифференцирования, интегрирования и др.).

В банке алгоритмов $(Б_5)$ для выведенной модели выбирается алгоритм, решаются уравнения, затем выполняется вычислительный эксперимент. При этом возможна реализация доказательства теорем по точности и устойчивости выбранных алгоритмов. Алгоритмы сводятся к вариациям, методу сеток и др.

В банке прикладных программ $(Б_6)$ собираются стандартные программы для решения алгебраических уравнений, расчета специальных функций.

Важное значение имеет формирование банка постановки $(Б_0)$ по классам задач механики сплошных сред. Здесь прежде всего учитываются физические законы (упругость, идеальная пластичность, ползучесть и разрушение). Далее ставятся геометрические условия (стрежни, пластинки, оболочки). При этом оформляется конструктивная особенность объекта исследования.

6. Обсуждение

При постановке задачи имеет важное значение выбор материала конструкции.

Например: туго ползучие плавкие конструктивные материалы: сплавы легкие; полимеры; дерево; бетон; горная механика и геофизика.

Хрупкие разрушения (накопление повреждений): специальные жаропрочные сплавы; паровые и газовые турбины; реактивный двигатель и т.д.

В принципе класс задан можно сформулировать по типам разрушений:

- усталостное разрушение при воздействии переменных (циклических) нагрузок;
- медленное изменение механических свойств в металлических сплавах неравномерной структуры (зависящие прежде всего от уровня температуры);
- реакторы из-за дефекта при облучении (атомные факторы);
- коррозионное повреждение;
- циклические напряжения и т.д.

Наконец, в операционном банке $(Б_7)$ формируются программы для решения поставленных задач.

Такова структура информационной части алгоритмических банков при алгоритмизации решения классов задач механики разрушения.

Дальнейшие исследования связаны с формированием программной части алгоритмических банков, составлением конкретных таблиц банка $(Б_0)$ и проведением вычислительных экспериментов $(Б_7)$.

7. Заключение

Исследована алгоритмизация в механике разрушения, которая начинается с формирования постановки проблемы, где разрушение материалов зависит, прежде всего, от структуры материалов, а также влияния внешних условий - теплового режима, агрессивности среды и характера нагрузок. Причем теория разрушения как комплексная проблема изучена на стыке физики твердых тел, материаловедения и механики сплошных сред и получила широкое применение в расчетах на прочность машин и сооружений. В механике разрушения исследованы модели вязких и хрупких разрушений, теории трещин. методами теории упругости, эластичности и ползучести. Предложено применение алгоритмических методов к установлению законов разрушения, которая получила широкое применение в расчетах на прочность машин и сооружений.

8. Благодарности

Авторы искренно благодарны наставникам академикам В.К.Кабулову и Т.Р.Рашидову, которые внесли большой вклад во внедрение алгоритмизации в задачи механики и сейсмостойкости сооружений.

Литература

1. *Кабулов В.К.* Алгоритмизация в механике сплошных сред / «Фан» Ташкент, 1979, 200 р.
2. *Кабулов В.К.* Алгоритмическое направление в кибернетике // Будущее науки: Междунар. ежегодник, Вып.10. 1977. р. 50–58.
3. *Кабулов В.К.* Входной язык алгоритмической системы для автоматизации решения многомерных краевых задач математической физики// – Алгоритмы. Ташкент, Вып.65. 1988. – С. 4–18.
4. *Кабулов В.К., Бузурханов В., Желябин В.Н.* Язык формализации математических понятий // Алгоритмы. Ташкент, 1985. Вып.58. – С. 3–13.
5. *Кабулов В.К., Кабулов А.В., Норматов И.Х.* «Алгоритмические и логические методы в теории управляющих систем», Монография – Т.: «Наврўз», 2019. – 225 с.
6. *Кабулов В.К., Кабулов А.В., Норматов И.Х.* Алгоритмизация в теории управляющих систем// Ташкент–2017. Изд. “Навруз”. – 173 с.
7. *Бриджмен П.* Исследование больших пластических деформаций и разрыва –М.: ИЛ. 1955.
8. *Бусленко Н.П.,* Калапиков В.В., Коваленко И.Н. Лекции по теории сложных систем // М.: Советское радио, 1973. – С. 6–204.
9. *Екоборов Т.* Физика и механика разрушения и прочности твердых тел. –М.: Металлургия. 1971.
10. *Журавлёв Ю.И.* Об алгоритмах распознавания с представительными наборами (о логических алгоритмах) // – ЖВМ и МФ, том 42, № 9. 2002. – С. 1425–1435.
11. *Ильюшин А.А.* Пластичность. –М.: Гостехиздат. 1948.
12. *Качанов Л.М.* Основы механики разрушения. –М.: Наука. 1974.

ОБЕСПЕЧЕНИЕ УСТОЙЧИВОСТИ ОТКОСОВ АВТОМОБИЛЬНЫХ ДОРОГ В УСЛОВИЯХ УЗБЕКИСТАНА

Каюмов А.Д.. Холжигитов Ш.Б., Рахимбаев О.Д.

Ташкентский Государственний Технический Университет, Ташкент, Узбекистан

E-mail: abdubakigmg.@mail.ru

Аннотация: *В сложных условиях рельефа, не менее важным остается обеспечение устойчивости боковых откосов автомобильных дорог. ведущие к эстакадам и мостам, пересекающих высокие отметки и возвышения. В результате совершенствования мероприятий по обеспечению устойчивости откоса дороги, затраты на его строительство и эксплуатацию будут снижены на определенную величину. Поэтому в данной статье рассматриваются вопросы совершенствования методов обеспечения устойчивости бокового откоса земляного полотна автомобильных дорог.*

Ключевые слова: *Автомобильные дороги, сложный рельеф, боковые откосы, местные устойчивости.*

1. Введение.

В последнее время в дорожном строительстве значительно увеличилось количество высоких откосов, вызванных необходимостью располагать земляное полотно в глубоких выемках или устраивать высокие насыпи. Глубина выемок и высота насыпей нередко достигает 30-40 м. В этих случаях важно обеспечить устойчивость их боковых откосов [1-3].

Откосы земляных сооружений - одно из самых уязвимых мест дорожной конструкции, поскольку они испытывают различные воздействия погодно-климатических факторов, силовые, включая напряжения от собственного веса, а также влияние подземных и текучих вод. Конструкции боковых откосов земляного полотна, обычно проектируются с помощью типовых конструкций или индивидуальных решений [4-7].

Объект исследования: Земляное полотно автомобильных дорог.

Предмет исследования: Устойчивость боковых откосов земляного полотна из лессовых грунтов.

Цель исследования: Анализ принципа работы активной зоны боковых откосов автомобильных дорог из лессовых грунтов.

Задачы исследования: изучение проблем обеспечения устойчивости боковых откосов земляного полотна автомобильных дорог, сложенного из лессовых грунтов.

Результаты исследования: С точки зрения обеспечения устойчивости высоких откосов земляного полотна автомобильных дорог целесообразно выделить деформации нарушения общей и местной усойчивости. При нарушении общей устойчивости в движение вовлекаются обычно значительные массы грунта (пород) – весь откос или большая часть его; глубина смещения здесь измеряется часто десятками метров. При нарушении местной устойчивости деформации носят локальный характер, проявляясь в пределах некоторой зоны, прилегающей непосредственно к поверхности откоса. Они имеют гороздо меньшие масштабы, но проявляются с большей частатой в значительном количестве [4, 7].

2. Анализ.

В настоящее время известны и широко применяются более 20 типов укрепления откосов: травосеяние, одерновка, посадка кустарников, лесопосадки, термозащитные и защитные слои с использованием геотекстиля, сборные железобетонные решетки, пневмонабрызг, глинистые грунты, монолитные цементогрунтовые покрытия и решетки, гибкие железобетонные плиты, сборные железобетонные гибкие решетки, сборные бетонные и железобетонные плиты, монолитные железобетонные плиты, каменная наброска, геотекстилы, георешетки, габионы и др [8].

В зависимости от реакции этих укреплений на внешние силовые, погодно-климатические, гидрогеологические, гидрологические и другие воздействия, все конструкции укреплений принято подразделять на следующие три группы:

1 группа – биологические типы конструкций укреплений, предназначенные для защиты откосов от эрозии, сплывов, оплывины в районах с благоприятными грунтовыми и климатическими условиями;

2 группа – несущие конструкции, предназначенные для компенсации сдвигающих усилий, возникающих в грунте поверхностных слоев откосов, а также силовых и других воздействий паводковых и поверхностных вод;

3 группа - защитные и изолирующие конструкции, назначение которых – изолировать поверхностные слои откоса от температурных воздействий, впитывания атмосферных осадков и отводить грунтовые воды.

Необходимо отметить, что основной геотехнической задачей при проектировании высоких насыпей и глубоких выемок является оценка и обеспечение устойчивости откосов. Для решения этой задачи необходимо:

-установить индекс классификационной группы откоса, определяющий особенности строения и гидрогеологического режима грунтовой толщи, слагающий откос и его основание;

-выбрать метод или группу методов расчета для проверки устойчивости откоса, с учетом его классификационной группы;

-провести расчеты по выбранным методам и получить расчетные значения коэффициентов устойчивости;

-сопоставить полученные значения коэффициентов устойчивости с требуемыми значениями и сделать заключение о достаточности или недостаточности степени устойчивости;

-при недостаточной устойчивости необходимо выбрать мероприятие или комплекс мероприятий, обеспечивающих ее повышение наиболее рациональным в данных конкретных условиях способом.

Особенность работы грунтов и пород в поверхностных слоях откосных частей земляных сооружений, а также естественных склонов – это наличие активной зоны, в пределах которой возможно существенное изменение их физико-механические свойства по сравнению с аналогичными свойствами всего массива. Формирование активной зоны происходит под влиянием совокупности внешних и внутренних силовых воздействий (факторов) и физико-химических процессов выветривания.

Для обеспечения устойчивости и стабильности грунта в пределах активной зоны поверхностных слоев откосов, прежде всего необходимо определить его величину $h_{аз}$ и величину Δh, на которую необходимо ограничить рост активной зоны.

Величину Δh можно определить выражениям:

$$\Delta h = h_{аз} - h_0, \tag{1}$$

$$h_0 = \frac{C_{WN} m_0}{\gamma_W \left(1 - tg\varphi_{WN} m_0\right)}, \tag{2}$$

где h_0 – устойчивая часть активной зоны; C_{WN}, $tg\varphi_{WN}$ - величина общего сцепления и коэффициента трения грунта при его начальном состоянии плотности-влажности и исходной структуре; γ_W - плотность влажного грунта, m_0 – крутизна откоса.

Физико-химические процессы выветривания воздействуют на грунты и породы в поверхностных слоях откосных частей как в период строительства, так и на протяжении всего срока службы земляных сооружений. Они обусловлены прежде всего погодно-климатическими факторами: увлажнением, промерзанием, высушиванием.

Погодно-климатические факторы определяют основные, наиболее опасные температурно-влажностные воздействия на грунты и породы поверхностных зон откосов: циклические набухание-высушивание и промерзание-оттаивание, их совместное влияние. В результаты многократных циклических воздействий происходит постепенное уменьшение прочности грунта или пород как за счет изменения их плотности-влажности, так и за счет

более глубоких структурных преобразований. Одновременно наблюдается интенсивный рост активной зоны.

Для проверки вышее отмеченных, предположение о формирование активной зоны в результате многократных циклических воздействий погодно-климатических факторов, прежде всего влажности, в лабораторных и полевых условиях проведены специальные экспериментальные исследования и обсследование существующих откосов автомобильных дорог.

На рис. 1 показан откос автомобильных дорог 4Р10 «Дарбанд-Бойсун-Элбайон», 45 км и на рис. 2 показан откос автомобильных дорог «4Р6 Ташкент-Чимён» на участке дом отдыха Амирсой. Из этих рисунков видно, что в результате многократных циклических воздействий, полностью потеряна сплошность поверхности откосов, сложенная из аргеллитовых и лёссоавх грунтов. Усадочные и морозобойные трещины, объемное набухание, пучение – все это приводило к образованию отдельных агрегатов и прочность по межагрегатным поверхностям снижена за счет нарушения жестких структурных связей и снижения активности связей, имеющих водноколлоидную природу.

Рисунок 1. - **Выветриваемая часть поверхности откосов автодорог 4Р10 «Дарбанд-Бойсун-Элбайон», 47 км.**

Рисунок 2. - **Откос автомобильных дорог «4Р6 Ташкент-Чимён» на участке дом отдыха Амирсой.**

Для экспериментального изучения изменения влажности лессовых грунтов поверхностной зоны откосов насыпей по глубине в зависимости от времени года и по годам.

Исследование проведено в 2021-2023 г.г. на 21 км автомобильной дороги «Тошкентская кольцевая автомобильная дорога» высотой 10 м. Характеристики лессового пылеватого суглинка представлены в таблице 1.

Таблица 1.

Основные характеристик лессового пылеватого суглинка

Количества, %		Предел пластичности			Плот-ность, γW т/м3	Удельный вес т/м3	Показатели прочности	
песок	корбо-наты	Wт, %	Wp, %	PI			Cw, кг/см2	φ, град
0,3	19	29	19	10	1,49	2,67	0,6	30o00′

Расположение мест отбора проб для определения влажности грунта показано на рис. 3. Проба грунта для определения влажности отбиралась до глубины 2,0 м. Для отбора проб

грунта закладывались шурфы, грунт помещался в специальные бюксы и транспортировался в лабораторию. Отбиралось не менее 3-х образцов грунта в каждом 0,2 м.

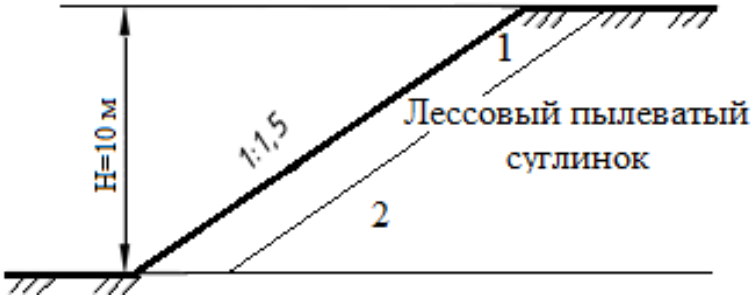

Рисунок 3. - **Поперечные профили участка исследований: 1 – откос земляного полотна; 2 – активная зона глубиной $h_{аз}$**

График изменение влажности грунта в различные месяцы 2022 года по глубине откоса показан на рис. 4.

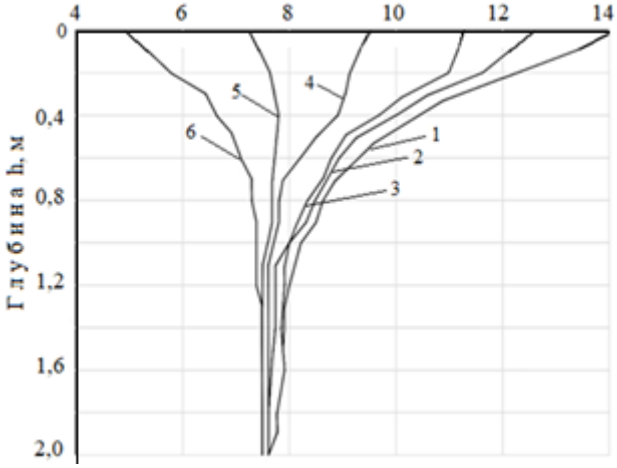

Рисунок 4. - **График распределение влажности по глубине в различные времена 2023 года: 1-март, 2-апрель, 3-май, 4-июнь, 5-июль, 6-август**

Анализ рис. 4 показывает, что влажность лессовых грунтов до глубины 1,2 м колеблется в зависимости от времени года в пределах от 5% до 14%, а глубже 1,2 м практический остаётся постоянным, т.е. 7,8%. Это свидетельствует о том, что до глубины 1,2 м происходит увлажнение-высушивание и нарушение структуры грунта.

Для качественной и количественной оценки местной устойчивости, как выше указано, необходимо определять максимальную величину набухания $a_н$; общее сцепление C и угол внутреннего трения φ лессовых грунтов в зависимости от изменчивости влажности, связанные погодные условия времени года.

В лабораторных условиях, для определения $a_н$ образцы грунта помещали в приборы для набухания. После первого набухания фиксировали по мессуре установившуюся величину деформации набухания и вычисляли величину относительного набухания:

$$a_H = \frac{\Delta h}{h} \cdot 100\% \qquad (3)$$

где Δh – замер на мессуре; h – исходная высота испытываемого образца грунта.

Затем образцы грунта высушивали сначала на воздухе при комнатной температуре, далее в термостатах до влажности на предел усадки. После высушивания образцы набухали повторно. Таким образом, проводили несколько циклов набухания-высушивания.

Результаты опытов, проведенные в лабораторных условиях, по определению относительной набухаемости лессовых грунтов в зависимости от циклов набухание-высушивание представлены на табл. 2.

Анализ табл. 2 показывает, что с увеличением циклов набухание-высушивание увеличивается значение относительное набухание, т.е. уменьшается связь между зернами и

агрегатами лёссового грунта. В связи с этим должны уменьшаться прочностные характеристики.

Таблица 2

Изменение значения относительного набухания от количества циклов набухания-высушивания

Количество циклов набухания-высушивания *N*	Высота образцов до набухания h_0, см	Высота образцов после набухания h_1, см	Относительная набухания $a_н$, %
1	1,1	1,106	0,54
2	1,099	1,231	12,01
3	1,172	1,256	7,16
4	1,145	1,22	6,55
5	1,152	1,21	5,03

Результаты опытов по определению прочностных характеристик угла внутренного трения (φ) и сцепления (С) лессовых грунтов, определенные в лабораторных условиях на приборе Маслова-Лурье при постоянной влажности и плотности, в зависимости от циклов увлажнения-высушивания приведены на рис. 5.

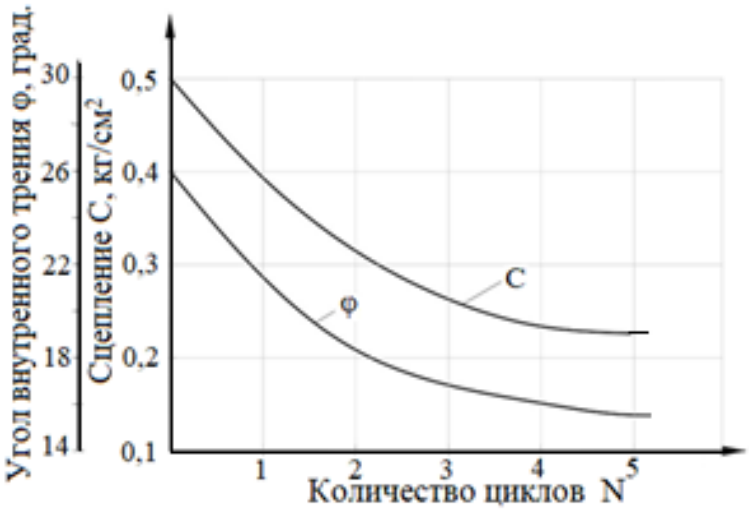

Рисунок 5. - **Зависимость величины угла внутренного трения (φ) и сцепления (С) от количества циклов увлажнение-высушивание (N). W=const=16,0%, γ=const=1,50 г/см³**

Анализ (рис. 5) показывает, что в зависимости от циклов увлажнения-высушивания, уменьшается значение прочностных показателей грунтов: угол внутренного трения (φ) и сцепления (С). Поскольку по глубине в зависимости от времени года, циклически изменяется влажность грунта, это должно привести к изменению, в данном случае, уменьшение прочностных показателей: угол внутренного трения (φ) и сцепления (С). Для проверки этого положения нами определены этих показателей по глубине откоса на каждом 0,2 м.

Таблица 3

Изменение прочностные характеристики лессовых грунтов по глубине откоса

Глубина $h_{гл}$, м	Сцепление С, кг/см²	Угол внутреннего трения φ, град
0,2	0,04	16,0
0,4	0,11	17,8
0,6	0,20	19,6
0,8	0,34	21,9
1,0	0,46	25,2
1,2	0,50	29,0

На табл. 3 приведено изменение прочностных показателей лессовых грунтов по глубине откоса. Анализ табл. 3 также показывают, что с увеличением глубины в пределах активной зоны (до 1,2 м) изменяются прочностные показатели

3. Заключение.

Таким образом под влиянием циклических увлажнений и высушивание поверхностных слоев откосных частей автомобильных дорог, сложенных из лессовых грунтов, а также естественных склонов, существенно изменяются прочностные свойства. В результате этого, возникает опасная зона, т.е. називаемая “Активная зона”, где могут быть нарушены местные устойчивости, приводящие к образованию локальных деформаций и в зависимости от его толщины назначаются укрепительные конструкции.

Литература

1. *Braja M.Das.* Principles of Geotechnical Engineering. 2010. United States. -470 p.
2. *David George Price.* Enjineering Geology principles and practice. 2009. Springer-Verlag Berlin Heidelberg. -450 p.
3. *Craig R.F.* Craig’s soil mexanics. London and New York, 2010. -446 p.
4. *Казарновский В.Д.* «Основы инженерной геологии, дорожного грунтоведения и механики грунтов» (Краткий курс). –М., 2007. -284 с.
5. *Трофимов В.Т. и др.* Грунтоведение. –М., Изд-во МГУ, 2005. -1024 с.
6. *Kayumov A.D.* Muhandislik geologiyasi va gruntshunoslik asoslari. Toshkent. 2012. -160 b.
7. *Добров Э.М.* Механика грунтов. –М.: Изд. сентр “Академия”, 2008. -272 с. ИКН 135-21 «Инструкция по конструкциям укрепления откосов земляного полотна автомобильных дорог», УП «Автодорожный научно-исследовательский институт» Т., 2021г. -77 с.

СОБСТВЕННЫЕ КОЛЕБАНИЯ ПЯТИСЛОЙНОЙ НЕСИММЕТРИЧНОЙ ПО ТОЛЩИНЕ ПЛАСТИНЫ

Лачугина Е.А.

Белорусский государственный университет транспорта, Гомель, Беларусь

E-mail: katherina.lachugina@gmail.com

Аннотация. *Исследованы собственные частоты колебаний упругой круговой несимметричной по толщине пятислойной пластины. Для тонких внешних и внутреннего несущих слоев приняты гипотезы Кирхгофа. В относительно толстых заполнителях справедлива гипотеза Тимошенко о прямолинейности и несжимаемости деформированной нормали. Уравнения движения получены вариационным методом Лагранжа и Даламбера. Аналитическое решение краевой задачи выписано в конечном виде в функциях Бесселя при защемленном контуре пластины. Приведены численные результаты исследования частот собственных колебаний в зависимости от толщины внутреннего несущего слоя.*

Ключевые слова*: пятислойная круговая пластина, собственные колебания, аналитическое решение, численные результаты*

1. Введение

В последнее время в машиностроении и строительстве значительно возрос спрос на использование слоистых тонкостенных элементов конструкций. Это обуславливает необходимость разработки соответствующих математических моделей и методов расчета. Этой проблеме посвящены монографии [1–7]. Динамическое нагружение неоднородных цилиндрических оболочек исследовано в работах [8–11].

Квазистатическому деформированию трехслойных стержней в температурном поле посвящены статьи [12–14]. Изгиб трехслойных пластин, связанных с основанием Пастернака, рассмотрен в публикациях [15, 16]. Решения отдельные краевых задач для трехслойных пластин приведены в работах [17–20]. Циклическое нагружение трехслойных стержней и пластин, в рамах теории Москвитина, рассмотрено в публикациях [21, 22].

Уравнения равновесия и движения круговой пятислойной пластины с жесткими заполнителями в усилиях получены в [23–25]. Решение задачи о собственных колебаниях пятислойной круговой пластины симметричной по толщине приведено в [26, 27].

Здесь предлагается постановка и решение начально краевой задачи о собственных колебаниях пятислойной круговой пластины несимметричной по толщине.

2. Постановка и решение краевой задачи

Рассматривается несимметричная по толщине пятислойная круговая пластина

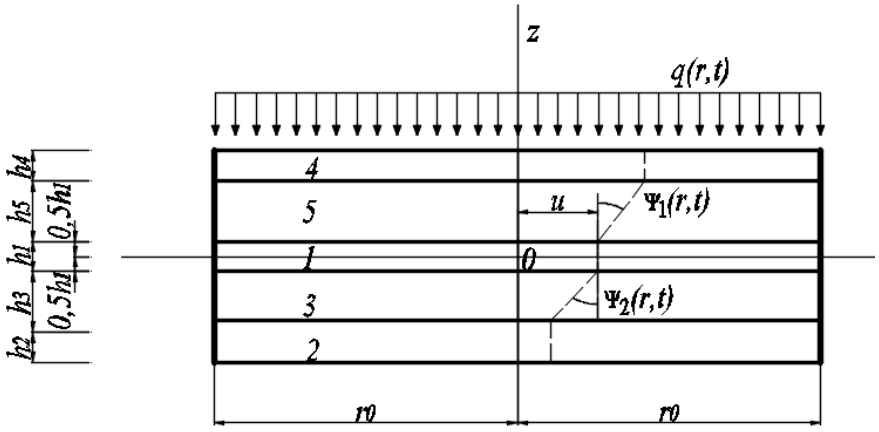

Рисунок 1. – **Расчётная схема несимметричной по толщине пятислойной круговой пластины**

Тонкие несущие слои толщиной h_1, h_2, h_4 выполнены из прочных материалов, для них справедливы гипотезы Кирхгофа. В более толстых заполнителях (h_3, h_5) справедлива гипотеза Тимошенко о прямолинейности и несжимаемости деформированной нормали, которая поворачивается на некоторый дополнительный угол $\psi_i(r, t)$, (i = 1, 2) – относительный сдвиг в заполнителях. Цилиндрическая система координат r, φ, z связывается со срединной плоскостью внутреннего несущего слоя, ось z направлена перпендикулярно вверх, к четвертому слою. Все геометрические размеры пластины отнесены к ее радиусу r_0.

Система дифференциальных уравнений движения в перемещениях, описывающая собственные колебания, получена при отсутствии распределенной нагрузки (q = 0) и при помощи вариационного принципа Лагранжа с учетом сил инерции поперечных колебаний:

$$\mathrm{L}_2(a_1u - a_2w,_r + a_3\psi_1 - a_4\psi_2) = 0,$$

$$\mathrm{L}_2(a_3u - a_5w,_r + a_6\psi_1) = 0,$$

$$\mathrm{L}_2(-a_4u - a_7w,_r + a_8\psi_2) = 0,$$

$$\mathrm{L}_3(a_2u - a_9w,_r + a_{10}\psi_1 + a_{11}\psi_2) - M_0\ddot{w} = 0, \qquad (1)$$

где $M_0\ddot{w}$ – поперечные инерционные силы; $M_0 = (\rho_1h_1 + \rho_2h_2 + \rho_3h_3 + \rho_4h_4 + \rho_5h_5)r_0^2$; запятая в нижнем индексе обозначает операцию дифференцирования по следующей за ней координате; коэффициенты

$$a_1 = \sum_{k=1}^{5} h_kK_k^+, \quad a_2 = \Big[K_4^+h_4(0,5h_4 + 0,5h_1 + h_5) + K_5^+0,5h_5(h_1 + h_5) -$$

$$-K_3^+0,5h_3(h_1 + h_3) - K_2^+h_2(0,5h_2 + 0,5h_1 + h_3)\Big],$$

$$a_3 = \Big[K_4^+h_4h_5 + K_5^+0,5h_5^2\Big], \quad a_4 = \Big[K_2^+h_2h_3 + K_3^+0,5h_3^2\Big],$$

$$a_5 = \left[K_4^+h_4h_5(0,5h_1 + 0,5h_4 + h_5) + K_5^+h_5(\frac{h_1h_5}{4} + \frac{h_5^2}{3})\right],$$

$$a_6 = \left[K_4^+h_5^2h_4 + K_5^+\frac{h_5^3}{3}\right], \quad a_7 = \left[K_2^+h_2h_3(0,5h_1 + 0,5h_2 + h_3) + K_3^+h_3(\frac{h_1h_3}{4} + \frac{h_3^2}{3})\right],$$

$$a_8 = \left[K_2^+h_3^2h_2 + K_3^+\frac{h_3^3}{3}\right], \quad a_9 = \left[K_4^+h_4(\frac{h_4^2}{3} + \frac{h_1^2}{4} + h_5^2 + \frac{h_1h_4}{2} + h_4h_5 + h_1h_5) +\right.$$

$$+K_5^+h_5(\frac{h_1^2}{4}+\frac{h_1h_5}{2}+\frac{h_5^2}{3})+K_3^+h_3(\frac{h_1^2}{4}+\frac{h_1h_3}{2}+\frac{h_3^2}{3})+K_1^+\frac{h_1^3}{12}+K_2^+h_2(\frac{h_2^2}{3}+\frac{h_1^2}{4}+h_3^2+\frac{h_1h_2}{2}+h_2h_3+h_1h_3)\Bigg],$$

$$a_{10}=\left[K_4^+h_4h_5(0,5h_1+0,5h_4+h_5)+K_5^+\frac{h_5^3}{3}\right],\quad a_{11}=\left[K_2^+h_2h_3(0,5h_1+0,5h_2+h_3)+K_3^+\frac{h_3^3}{3}\right],$$

L_2, L_3 – линейные дифференциальные операторы

$$L_2(g)\equiv\left(\frac{1}{r}(rg),_r\right),_r\equiv g,_{rr}+\frac{g,_r}{r}-\frac{g}{r^2},\quad L_3(g)\equiv\frac{1}{r}\left(r\,L_2(g)\right),_r\equiv g,_{rrr}+\frac{2g,_{rr}}{r}-\frac{g,_r}{r^2}+\frac{g}{r^3}.$$

Начальные условия движения принимаем однородными:

$$u=\psi_1=\psi_2=w=\dot{w}=0,\ \text{при}\ t=0. \qquad (2)$$

Кинематические условия заделки контура пластины следующие:

$$u=\psi_1=\psi_2=w=w,_r=0,\ \text{при}\ r=r_0. \qquad (3)$$

После элементарных преобразований, связанных с выделением уравнения для прогиба пластины w, систему (1) можно переписать в виде

$$u=b_1w,_r+C_1r+C_2/r,$$

$$\psi_1=b_2w,_r+C_3r+C_4/r,$$

$$\psi_2=b_3w,_r+C_5r+C_6/r,$$

$$L_3(w,_r)+M^4\ddot{w}=0, \qquad (4)$$

где коэффициенты

$$b_1=\frac{a_8(a_6a_2-a_3a_5)+a_4a_6a_7}{a_8(a_1a_6-a_3^2)-a_4^2a_6},\ b_2=\frac{a_3(a_2a_8+a_4a_7)-a_5(a_1a_8-a_4^2)}{a_3^2a_8-a_6(a_1a_8-a_4^2)};$$

$$b_3=\frac{a_4(a_2a_6-a_3a_5)+a_7(a_1a_6-a_3^2)}{a_8(a_1a_6-a_3^2)-a_4^2a_6};$$

$$M^4=M_0D,\ D=\frac{a_6a_8b_4}{b_4b_7-b_5b_6},$$

$$b_4=a_8(a_2a_6-a_3^2)-a_4^2a_6,\ b_5=a_8(a_2a_6-a_3a_5)+a_4a_6a_7,$$

$$b_6=a_8(a_2a_6-a_3a_{10})+a_4a_6a_{11},\ b_7=a_8(a_6a_9-a_5a_{10})-a_6a_7a_{11}.$$

Так как искомое решение ограничено в начале координат, то для сплошных пластин необходимо обнулить константы интегрирования $C_2 = C_4 = C_6 = 0$.

Искомый прогиб принимается в виде

$$w(r,t)=v(r)(A\cos(\omega t)+B\sin(\omega t)), \qquad (5)$$

где $v(r)$ – искомая координатная функция; ω – частота собственных колебаний пластины; A и B – константы интегрирования, определяемые из начальных условий.

После подстановки выражения (5) в последнее уравнение системы (4) получим бибесселево уравнение для определения координатной функции $v(r)$:

$$L_3(v,_r)-\beta^4v=0. \qquad (6)$$

где $\beta^4=M^4\omega^2$.

Решение уравнения (6) известно:

$$v(\beta r)=C_7J_0(\beta r)+C_8I_0(\beta r)+C_9Y_0(\beta r)+C_{10}K_0(\beta r). \qquad (7)$$

где J_0, I_0 – функции Бесселя первого порядка, K_0, Y_0 – функции Макдональда и Неймана.

Исходя из ограниченности перемещений в начале координат необходимо положить

$C_9 = C_{10} = 0$. В результате решение системы (4) принимает вид:

$$u(r,t) = b_1 w,_r + C_1 r\,,$$

$$\psi_1(r,t) = b_2 w,_r + C_3 r\,,$$

$$\psi_2(r,t) = b_3 w,_r + C_5 r\,,$$

$$w(r,t) = v(r)(A\cos(\omega t) + B\sin(\omega t))\,, \qquad (8)$$

При защемленном контуре пластины должны выполняться условия (3). Подставив в два последних из них прогиб из решения (8), получим однородную систему алгебраических уравнений для определения констант интегрирования C_7, C_8:

$$C_7 J_0(\beta r_0) + C_8 I_0(\beta r_0) = 0\,,$$

$$-C_7 J_1(\beta r_0) + C_8 I_1(\beta r_0) = 0\,, \qquad (9)$$

где J_1, I_1 – функции Бесселя первого порядка.

Система (9) имеет нетривиальное решение при условии равенства нулю ее определителя. Следовательно, получим следующее трансцендентное уравнение

$$I_1(\beta r_0) J_0(\beta r_0) + I_0(\beta r_0) J_1(\beta r_0) = 0\,. \qquad (10)$$

Полученное уравнение (10) служит для вычисления собственных чисел β_n (n = 0, 1, 2, …) уравнения (6). После вычисления β_n частоты собственных колебаний следуют из соотношения, введенного в (6).

$$\omega_n^2 = \frac{\beta_n^4}{M^4} = \frac{\beta_n^4}{M_0 D}\,,$$

где параметр M^4 введен ранее в формуле (4).

3. Численные результаты

Численно исследованы собственные числа и частоты в пятислойной круговой пластине единичного радиуса, несимметричной по толщине. За расчетную модель принята пластина, слои которой набраны из материалов кордиерит – пенополиуретан – титан – пенополиуретан – титан. Толщины несущих слоев и заполнителей, отнесенные к радиусу пластины r_0, следующие: h_4 = 0,02, h_5 = 0,3, h_1 = 0,04, h_3 = 0,4, h_2 = 0,03. Упругие характеристики этих материалов приведены в [1].

В табл. 1 приведены собственные числа и собственные частоты.

Рис. 2 иллюстрирует зависимость первых трех частот собственных колебаний ω_n от толщины внутреннего несущего слоя h_1. С увеличением номера собственных частот колебаний растет нелинейность зависимости их величины от h_1.

Таблица 1.

Собственные числа и собственные частоты пятислойной круговой пластины

Номер n	β_n/ω_n	Номер n	β_n/ω_n
0	3,196 / 689,720	8	28,279 / 53999,221
1	6,306 / 2685,143	9	31,378 / 66482,894
2	9,439 / 6016,049	10	34,561 / 80655,131
3	12,577 / 10681,040	11	37,702 / 95981,643
4	15,716 / 16677,980	12	40,844 / 112646,042
5	18,857 / 24010,688	13	43,985 / 130637,720
6	21,997 / 32672,797	14	47,126 / 149961,770
7	25,138 / 42669,823		

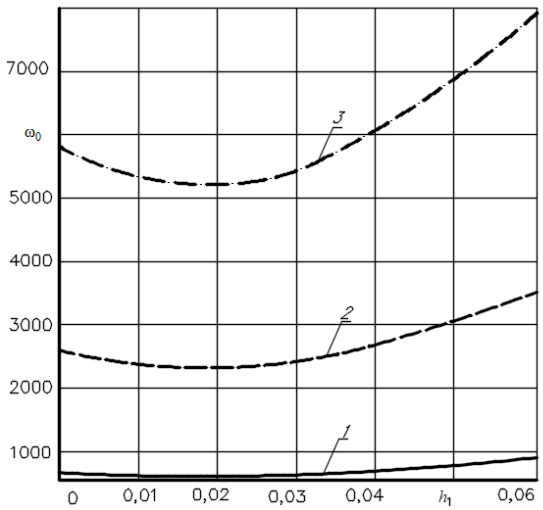

Рисунок 2. – **Зависимость собственных частот ω_n от толщины внутреннего несущего слоя h_1**

1 – ω_0 ; *2* – ω_1 ; *3* – ω_2

Зависимость частот основного тона ω_0 от толщины внутреннего несущего слоя h_1 при различных материалах заполнителей показана на рис. 3. При использовании в качестве заполнителя таких материалов, как пенополиуретан и пенопласт, которые гораздо легче фторопласта-4, частоты нелинейно возрастают.

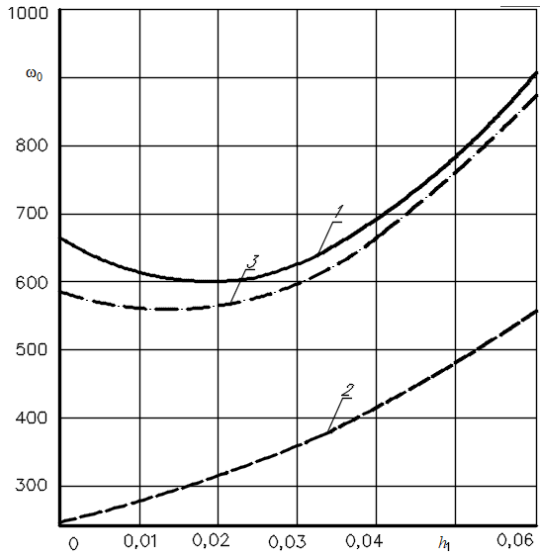

Рисунок 3. – **Зависимость максимальных перемещений от радиуса пятна нагрузки при различной толщине внутреннего несущего слоя**

1 – пенополиуретан; *2* – фторопласт-4; *3* – пенопласт

4. Заключение

Предложенная постановка начально-краевой задачи и ее решение позволяет исследовать собственные частоты и формы колебаний круговых пятислойных пластин, несимметричных по толщине.

Работа выполнена при финансовой поддержке Белорусского республиканского фонда фундаментальных исследований.

Литература

1. *Горшков А.Г., Старовойтов Э.И., Яровая А.В. Механика слоистых вязкоупругопластических элементов конструкций* / Москва, ФИЗМАТЛИТ, 2005, 576 с.

2. *Журавков М.А., Старовойтов Э.И. Математические модели механики твердого тела* / Минск, БГУ, 2021, 535 с.

3. *Zhuravkov M.A., Lyu Yongtao, E.I. Starovoitov.* Mechanics of Solid Deformable Body / Singapore, Springer, 2023, 317 p.
4. *Абдусаттаров А., Старовойтов Э.И., Рузиева Н.Б.* Деформирование и повреждаемость упругопластических элементов конструкций при циклических нагружениях / Ташкент, «IDEAL PRESS», 2023, 381 с.
5. *Aghalovyan L.* Asymptotic theory of anisotropic plates and shells / Singapore–London, World Scientific Publishing; 2015, 376 p.
6. *Старовойтов, Э. И.* Сопротивление материалов / Гомель, БелГУТ, 2004, 376 с.
7. *Старовойтов, Э. И.* Механика материалов / Гомель, БелГУТ, 2011, 380 с.
8. *Старовойтов Э.И., Леоненко Д.В.* Исследование спектра частот трехслойной цилиндрической оболочки с упругим наполнителем // Механика композиционных материалов и конструкций. 2015, vol. 21, No. 2, pp. 162–169.
9. *Bakulin VN, Boitsova DA, Nedbai AYa.* Parametric resonance of a threelayered cylindrical composite rib-stiffened shell // Mechanics of composite materials, 2021, vol. 57, No. 5, pp. 623–634.
10. *Tarlakovskii DV, Fedotenkov GV.* Two-Dimensional Nonstationary Contact of Elastic Cylindrical or Spherical Shells // Journal of Machinery Manufacture and Reliability, 2014, vol, 43, No. 2, pp. 145–152.
11. *Suvorov YeM, Tarlakovskii DV, Fedotenkov GV.* The plane problem of the impact of a rigid body on a half-space modelled by a Cosserat medium // Journal of Applied Mathematics and Mechanics, 2012, vol. 76, No. 5, pp.511–518.
12. *Pradhan M, Dash PR, Pradhan PK.* Static and dynamic stability analysis of an asymmetric sandwich beam resting on a variable Pasternak foundation subjected to thermal gradient // Meccanica, 2016, vol. 51, No. 3, pp.725–739.
13. *Starovoitov É.I., Pleskachevskii Yu.M., Leonenko D.V., Tarlakovskii D.V.* Deformation of a Step Composite Beam in a Temperature Field // Journal of Engineering Physics and Thermophysics, 2015, vol. 88, No. 4, pp. 1023-1029.
14. *Старовойтов Э.И., Леоненко Д.В.* Деформирование трехслойного стержня в температурном поле // Механика машин, механизмов и материалов, 2013, т. 22, С. 31–35.
15. *Старовойтов Э.И., Козел А.Г.* Изгиб упругой круговой трехслойной пластины на основании Пастернака // Механика композиционных материалов и конструкций, 2018, т. 2, No. 3, С. 392–406.
16. *Козел А.Г.* Влияние сдвиговой жёсткости основания на напряжённое состояние сэндвич пластины // Фундаментальные и прикладные проблемы техники и технологии, 2018, т. 332, No. 6, с. 25–34.
17. *Zadeh HV, Tahani M.* Analytical bending analysis of a circular sandwich plate under distributed load // International Journal of Recent Advances in Mechanical Engineering, 2017, vol. 6, No. 1, pp. 01-10.
18. *Yang L, Harrysson O, West H, Cormier D.* A comparison of bending properties for cellular core sandwich panels // Materials Sciences and Applications, 2013, vol. 4, No. 8, pp. 471–477.
19. *Захарчук Ю.В.* Напряженно-деформированное состояние круговой трехслойной пластины со сжимаемым заполнителем. // Механика. Исследования и инновации, 2019, т. 12, No. 12, с. 66–75.
20. *Нестерович, А.В.* Напряженное состояние круговой трехслойной пластины при осесимметричном нагружении в своей плоскости // Механика. Исследования и инновации, 2019, т. 12, No. 12, с. 152–157.
21. *Старовойтов Э.И., Абдусаттаров А., Рузиева Н.Б.* Циклическое нагружение упругопластических трёхслойных стержней с учетом их повреждаемости // Узб. журнал Проблемы механики, 2023, No. 1, с. 66–74.
22. *Старовойтов Э.И., Леоненко Д.В., Абдусаттаров А.* Знакопеременное термосиловое нагружение трёхслойной пластины погонными моментами // Узб. журнал «Проблемы механики», 2023, No. 3, с. 20–30.
23. *Салицкий, В.С.* Изгиб защемлённой по контуру круговой пятислойной пластины // Механика. Исследования и инновации, 2022, т. 15, No. 15, с. 209–213.
24. *Салицкий, В.С.* Изгиб круговой пятислойной пластины // Теоретическая и прикладная механика. Минск, 2023, вып. 38, с. 234 – 239.
25. *Лачугина, Е.А.* Поперечные колебания пятислойной упругой круговой пластины с жесткими заполнителями // Механика. Исследования и инновации. 2022, Вып. 15, С. 212–219.
26. *Лачугина*, Е.А. Частоты собственных колебаний пятислойной круговой пластины // Теоретическая и прикладная механика : международный научно-технический сборник. «БНТУ» Минск, 2023, Вып. 38, С. 227-233.
27. *Лачугина*, Е.А. Собственные колебания пятислойной круговой пластины с легкими заполнителями // Механика. Исследования и инновации. 2023. Вып. 16.

ДИНАМИЧЕСКОЕ НАГРУЖЕНИЕ ТРЕХСЛОЙНОГО СТЕРЖНЯ НА УПРУГОМ ОСНОВАНИИ ЛОКАЛЬНОЙ ИМПУЛЬСНОЙ НАГРУЗКОЙ

Леоненко Д.В.
Белорусский государственный университет транспорта, Гомель, Беларусь
E-mail: leoden@list.ru

Аннотация: *Рассмотрены вынужденные колебания трехслойного стержня на упругом основании. Для описания кинематики несущих слоев приняты гипотезы Бернулли. Заполнитель жесткий, сжимаемый. Реакция основания описывается моделью Винклера. Решение получено при импульсном воздействии синусоидальной и прямоугольной локальной нагрузки. Система уравнений движения получена с помощью вариационного принципа Лагранжа. Найдено ее точное решение в перемещениях. Приведены численные результаты.*

Ключевые слова: *трехслойный стержень, импульс, колебания.*

1. Введение

Трехслойные элементы конструкций широко применяются в современных отраслях промышленности, что обуславливает необходимость разработки методов их расчета [1, 2]. Динамическое нагружение трехслойных оболочек, пластин и стержней рассмотрено в работах [3–5]. Термоупругое деформирование трехслойного стержня исследовано в статье [6]. Колебания стержня без упругого основания описаны в [7]. Здесь рассматриваются колебания трехслойного стержня со сжимаемым заполнителем, возбужденные поверхностными импульсными нагрузками прямоугольной и синусоидальной формы на упругом основании.

2. Постановка задачи

Система координат x, y, z связывается со срединной плоскостью заполнителя. Для изотропных несущих слоёв приняты гипотезы Бернулли, в жёстком заполнителе справедливы точные соотношения теории упругости с линейной аппроксимацией перемещений его точек от поперечной координаты z. На границах контакта слоев используются условия непрерывности перемещений. К внешней поверхности первого несущего слоя приложены динамическая поверхностные нагрузка $q(x, t)$. На нижнюю поверхность второго несущего слоя действует реакция основания $q_r(x,t)$ (рисунок 1). Материалы несущих слоёв несжимаемы в поперечном направлении, в заполнителе учитывается обжатие. Деформации малые. Через h_k и ρ_k –обозначены толщина и плотность материала k-го слоя; $h_3 = 2c$; b_0 – ширина стержня. Все перемещения и линейные размеры стержня отнесены к его длине l.

Искомыми считаются прогибы и продольные перемещения срединных поверхностей несущих слоёв $w_k(x, t)$ и $u_k(x, t)$, (k = 1, 2). Продольные и поперечные перемещения в слоях $u^{(k)}(x, z)$ и $w^{(k)}(x, z)$ можно выразить через четыре искомые функции следующими соотношениями:

▪ в несущих слоях

$$u^{(1)} = u_1 - \left(z - c - \frac{h_1}{2}\right) w_{1,x}, \quad w^{(1)} = w_1 \quad (c \le z \le c + h_1),$$

$$u^{(2)} = u_2 - \left(z + c + \frac{h_2}{2}\right) w_{2,x}, \quad w^{(2)} = w_2 \quad (-c - h_2 \le z \le -c),$$

▪ в заполнителе

$$u^{(3)} = \left(1 + \frac{z}{c}\right)\left(\frac{1}{2}u_1 + \frac{h_1}{4}w_{1,x}\right) + \left(1 - \frac{z}{c}\right)\left(\frac{1}{2}u_2 - \frac{h_2}{4}w_{2,x}\right),$$

$$w^{(3)} = \frac{1}{2}\left(1 + \frac{z}{c}\right)w_1 + \frac{1}{2}\left(1 - \frac{z}{c}\right)w_2 \quad (-c \le z \le c), \qquad (1)$$

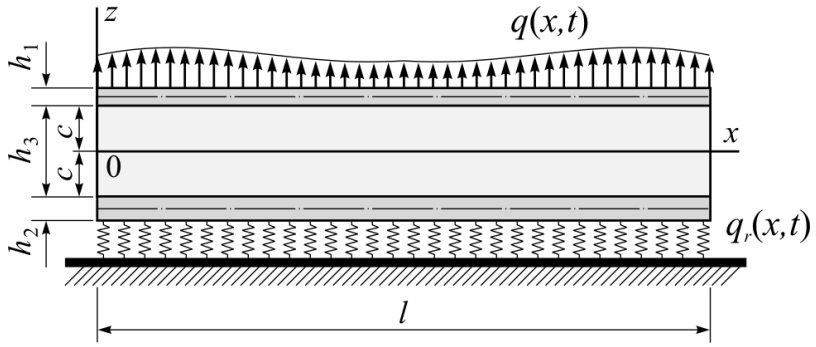

Рисунок 1. – **Расчетная схема стержня**

Уравнения движения следуют из принципа Лагранжа с учетом работы сил инерции

$$\delta A - \delta W = \delta A_I, \tag{2}$$

где δA – вариация работы внешних сил

$$\delta A = b_0 \int_0^l (q\delta w_1 + q_r \delta w_2)dx\,;$$

δW – вариация работы внутренних сил упругости

$$\delta W = b_0 \int_0^l \left[\sum_{k=1}^{3} \int_{h_k} \sigma_{xx}^{(k)} \delta\varepsilon_{xx}^{(k)} dz \; + 2\int_{h_3} \sigma_{xz}^{(3)} \delta\varepsilon_{xz}^{(3)} dz + \int_{h_3} \sigma_{zz}^{(3)} \delta\varepsilon_{zz}^{(3)} dz \right] dx\,;$$

δA_I – вариация работы сил инерции

$$\delta A_I = b_0 \sum_{k=1}^{3} \int_0^l \int_{h_k} \left[\rho_k \left(\ddot{w}^{(k)} \delta w^{(k)} + \ddot{u}^{(k)} \delta u^{(k)} \right) \right] dzdx\,;$$

$\sigma_{ij}^{(k)}$, $\varepsilon_{ij}^{(k)}$ – компоненты тензоров напряжений и деформаций в k-м слое.

В дальнейшем считаем, что стержень прикреплен к основанию и выполняется следующее соотношение

$$q_r = -\kappa_0 w_2\,. \tag{3}$$

где κ_0 – коэффициент жесткости упругого основания (коэффициент постели), w_2 – прогиб второго несущего слоя.

Подставляя выражения вариаций работ в соотношение (2) с учетом физических соотношений теории упругости и выражения (3), получим следующую систему уравнений в частных производных:

$$\begin{gathered}
a_1 u_1 - a_1 u_2 - a_4 u_{1,xx} - a_5 u_{2,xx} + a_2 w_{1,x} + a_3 w_{2,x} - 2a_6 w_{1,xxx} + a_7 w_{2,xxx} + m_1 \ddot{u}_1 = 0\,; \\
-a_1 u_1 + a_1 u_2 - a_5 u_{1,xx} - a_9 u_{2,xx} - a_3 w_{1,x} - a_2 w_{2,x} - a_6 w_{1,xxx} + 2a_7 w_{2,xxx} + m_2 \ddot{u}_2 = 0\,; \\
a_{10} u_{1,x} - a_{17} u_{2,x} + 2a_6 u_{1,xxx} + a_6 u_{2,xxx} + a_{11} w_{1,xx} - a_{12} w_{2,xx} + \\
+ a_{15} w_{1,xxxx} - a_{16} w_{2,xxxx} + a_8 w_1 - a_8 w_2 + m_1 \ddot{w}_1 - m_3 \ddot{w}_{1,xx} = q\,; \\
-a_3 u_{1,x} + a_{17} u_{2,x} - a_7 u_{1,xxx} - 2a_7 u_{2,xxx} - a_{12} w_{1,xx} + a_{14} w_{2,xx} - \\
- a_{16} w_{1,xxxx} + a_{13} w_{2,xxxx} - a_8 w_1 + \left(a_8 + \kappa_0\right) w_2 + m_2 \ddot{w}_2 - m_4 \ddot{w}_{2,xx} = 0\,,
\end{gathered} \tag{4}$$

где a_i и m_j – жесткостные и инерционные коэффициенты системы «стержень–основание».

Граничные условия свободного опирания стержня по торцам на неподвижные в пространстве жесткие опоры в сечениях $x = 0$; l (l – длина стержня) в перемещениях имеют вид:

$$w_k = u_{k,x} = w_{k,xx} = 0 \quad \left(k = 1, 2\right). \tag{5}$$

Начальные условия движения будут следующие (t = 0):

$$u_k(x,0)=u_{k0}(x);\quad \dot{u}_k(x,0)=\dot{u}_{k0}(x);$$
$$w_k(x,0)=w_{k0}(x);\quad \dot{w}_k(x,0)=\dot{w}_{k0}(x)\quad (k=1,2), \tag{6}$$

где $u_{k0}(x)$, $\dot{u}_{k0}(x)$, $w_{k0}(x)$, $\dot{w}_{k0}(x)$ – заданные начальные перемещения и скорости точек срединных поверхностей несущих слоев.

3. Решение задачи

Решение начально-краевой задачи (4)–(6) проводится методом Бубнова –Галеркина. Для этого искомые перемещения $u_1(x)$, $u_2(x)$, $w_1(x)$, $w_2(x)$ и нагрузку $q(x, t)$ представляется в виде разложения в ряды по системам базисных функций, удовлетворяющей принятым граничным условиям:

$$u_1(x,t)=\sum_{m=0}^{\infty}\psi_{1m}(x)T_{m1}(t),\quad u_2(x,t)=\sum_{m=0}^{\infty}\psi_{2m}T_{m2}(t),$$
$$w_1(x,t)=\sum_{m=0}^{\infty}\psi_{3m}T_{m3}(t),\quad w_2(x,t)=\sum_{m=0}^{\infty}\psi_{4m}T_{m4}(t),$$
$$q(x,t)=\sum_{m=0}^{\infty}\psi_{5m}q_m(t), \tag{7}$$

где $T_{mi}(t)$ – неизвестная функция времени, $q_m(t)$ – коэффициенты разложения нагрузки в ряд, ψ_{im} – базисные функции, удовлетворяющие граничным условиям задачи (i = 1…5).

Подстановка выражений (7) в (4), приводит к системе уравнений для определения функций времени $T_{mk}(t)$ (i = 1, 2, 3, 4). В матричном виде она будет следующей (индекс m опущен):

$$[B]\{T\}+[M]\{\ddot{T}\}=\{Q\}, \tag{8}$$

Для замыкания задачи к системе (8) необходимо добавить начальные условия (6).

Функции $T_{mk}(t)$ представляются в виде разложения по собственным формам:

$$T_{mk}=\sum_{i=1}^{4}\delta_{mki}\zeta_{mi}\qquad \left(\sum_{i=1}^{4}\delta_{mik}^2=1\right),$$

где δ_{mki} – амплитуды нормированных собственных форм колебаний.

Функции $\zeta_{mi}(t)$ определяются из системы уравнений

$$\ddot{\zeta}_{mi}+\omega_{mi}^2\zeta_{mi}=\tilde{q}_{mi}(t), \tag{9}$$

где $\tilde{q}_{mi}$ – компоненты приведенной силовой нагрузки.

Общее решение дифференциального уравнения (9) можно принять в виде [8]

$$\zeta_{mi}(t)=A_{mi}\cos(\omega_{mi}t)+B_{mi}\sin(\omega_{mi}t)+\frac{1}{\omega_{mi}}\int_0^t\sin(\omega_{mi}(t-\tau))\tilde{q}_{mi}(\tau)d\tau. \tag{10}$$

После взятия интеграла в (10) искомые перемещения представляются в виде сумм произведений $\zeta_{mi}(t)$ на соответствующие коэффициенты δ_{mki} и исходные базисные координатные функции, указанные в (3).

Рассмотрим частные случаи нагрузки:

1. Мгновенный локальный импульс поверхностной нагрузки действует на стержень в интервале $a \le x \le b$, тогда ее аналитический вид:

$$q(x,t)=q_1\delta(t)(H_0(b-x)-H_0(a-x)),\ q_1=\text{const}, \tag{11}$$

где $H(x)$ – обобщённая функция Хевисайда, $\delta(t)$ – дельта-функция Дирака [9].

Параметры разложения нагрузки в ряд

$$q_m = \frac{2q_1\delta(t)}{\pi m}\left(\cos\frac{\pi m a}{l} - \cos\frac{\pi m b}{l}\right). \qquad (12)$$

Искомая функция времени, соответствующая (12), следует из (10):

$$\zeta_{mi}(t) = \frac{2q_1\delta_{m3i}\sin(\omega_{mi}t)}{\pi m\omega_{mi}\sum_{k=1}^{4} M_{mkk}\delta_{mki}^2}\left(\cos\frac{\pi m a}{l} - \cos\frac{\pi m b}{l}\right).$$

2. Рассмотрим случай действия синусоидальной импульсной нагрузки, приложенной внутри участка $a \le x \le b$.

$$q(x,t) = q_и\delta(t)\left[H_0(b-x) - H_0(a-x)\right]\sin\left[\frac{\pi(x-a)}{b-a}\right],\ q_и = \text{const}. \qquad (13)$$

Параметры разложения нагрузки (13) в ряд будут

$$q_m = q'_m q_и\delta(t) \quad (m = 1, 2, 3, ...), \qquad (14)$$

где коэффициенты q'_m определяются формулjq

$$q'_m = \frac{(b-a)}{\pi}\left\{\frac{1}{m(b-a)-l}\left[\sin\frac{\pi(bm-l)}{l} - \sin\frac{\pi a m}{l}\right] - \right.$$

$$\left. -\frac{1}{m(b-a)+l}\left[\sin\frac{\pi(bm+l)}{l} - \sin\frac{\pi a m}{l}\right]\right\} \quad (m = 1, 2, 3, ...). \qquad (15)$$

Здесь должно выполняться условие $m(b-a) \ne l$, чтобы не возникало деление на ноль.

В сечениях стержня, где $(b-a) = l/p$ (p – натуральное число), при $m \ne p$ работает формула (15), если $m = p$ то

$$q'_p = \frac{2}{l}\int_0^l \left[H_0(b-x) - H_0(a-x)\right]\sin\left[\frac{\pi p(x-a)}{l}\right]\sin\frac{\pi p x}{l}\,dx =$$

$$= \left\{\frac{b-a}{l}\cos\frac{\pi a}{b-a} - \frac{1}{2\pi p}\left[\sin\frac{\pi(2b-a)}{b-a} - \sin\frac{\pi a}{b-a}\right]\right\}.$$

Используя параметры нагрузки q_m (14), функцию времени можно записать в виде

$$\zeta_{mi}(t) = \frac{q'_m q_и\delta_{m3i}\sin(\omega_{mi}t)}{\omega_{mi}\sum_{k=1}^{4} M_{mkk}\delta_{mki}^2}.$$

4. Численное исследование

При *численном исследовании* принимается, что слои стержня выполнены из материалов Д16Т–фторопласт–Д16Т; интенсивность импульса – $q_1 = 1\cdot10^4$ Па·с; относительные толщины слоев – $h_1 = 0{,}01$, $h_2 = 0{,}05$, $c = 0{,}09$.

Прогибы стержня на основаниях различной жесткости при импульсном нагружении прямоугольной нагрузкой ($a = 0$) (*1* – $к_0 = 10^6$ Па/м, *2* – $к_0 = 5\cdot10^8$ Па/м, *3* – $к_0 = 10^{10}$ Па/м) показаны на рисунке 2. Импульсный характер нагрузки оказывает большее влияние на прогибы стержня, особенно на основании высокой жесткости.

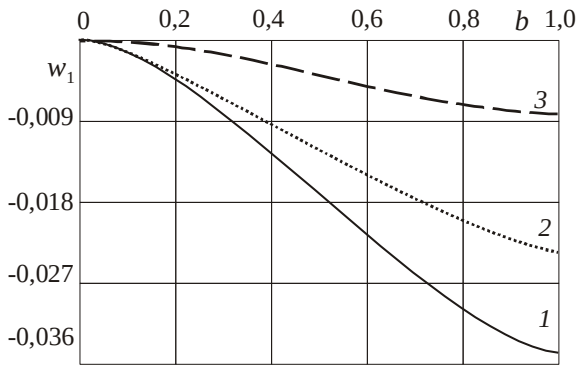

1 – $\kappa_0 = 10^6$ Па/м, *2* – $\kappa_0 = 5 \cdot 10^8$ Па/м, *3* – $\kappa_0 = 10^{10}$ Па/м

Рисунок 2. – **Изменение прогиба первого несущего слоя посередине пролета стержня в зависимости от области нагружения локального прямоугольного импульса при различной жесткости упругого основания**

На рисунке 3 показаны прогиб w_1 (a) и продольное перемещение u_1 (b), взятые в центре и на правом конце стержня соответственно, в зависимости от расположения левого края a пятна импульсной синусоидальной нагрузки ($b - a = 0{,}25$) при $t = 2$ с ($\kappa_0 = 0$): *1*, *3* – перемещения от синусоидальных импульсов с $q'_и = 0{,}5\pi q_и$ и $q_и = 10^4$ Па · с; *2* – прямоугольный импульс $q_и$.

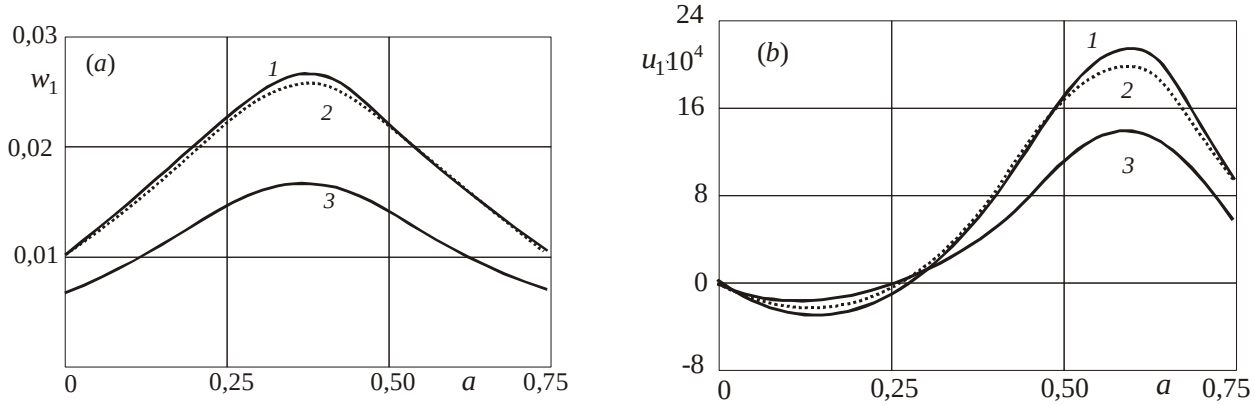

Рисунок 3. – **Прогиб w_1 (a) и продольное перемещение u_1 (b) в зависимости от области нагружения локального синусоидального импульса**

При одинаковой амплитуде нагрузок прогиб *3* от синусоидального импульса значительно меньше по величине, чем от прямоугольного *2*. Если импульсы статически эквивалентны (кривые *1*, *2*), то соответствующие прогибы в центре стержня примерно одинаковы при некотором превосходстве от синусоидального, который достигает максимума при $a = 0{,}375$.

5. Заключение

В работе поставлена и решена задача о вынужденных колебаниях трехслойного стержня, скреплённого с упругим основанием Винклера. Получено решение для случая импульсного локального воздействия. Численный анализ показал, что импульсная нагрузка и очень жесткое основание в совокупности могут оказывать серьезное влияние на напряженно-деформированное состояние трехслойного стержня.

Литература

1. *Болотин В.В., Новичков Ю.Н.* Механика многослойных конструкций / «Машиностроение» Москва, 1980, 375 с.
2. *Старовойтов Э.И.* Вязкоупругопластические слоистые пластины и оболочки / Гомель, 2002, 344 с.
3. *Леоненко Д.В., Старовойтов Э.И.* Исследование спектра частот трехслойной цилиндрической оболочки с упругим наполнителем // Механика композиционных материалов и конструкций. 2015, 21, No. 2, с. 162–169.

4. *Ivanez I., Moure M. M., Garcia-Castillo S. K., Sanchez-Saez S.* The oblique impact response of composite sandwich plates // Composite Structures. 2015, No. 133, pp. 1127– 1136.
5. *Pradhan M., Dash P. R., Pradhan P. K.* Static and dynamic stability analysis of an asymmetric sandwich beam resting on a variable Pasternak foundation subjected to thermal gradient // Meccanica. 2016, vol. 51, No. 3, pp. 725–739.
6. *Старовойтов Э.И., Леоненко Д.В.* Деформирование трехслойного стержня в температурном поле // Механика машин, механизмов и материалов. 2013, No. 1 (22), С. 31–35.
7. *Starovoitov É.I., Leonenko D.V., Yarovaya A.V.* Dynamics of three-layer bars // Strength of Materials. 2006, vol. 41, No. 7, pp. 668–679.
8. *Камке Э.* Справочник по обыкновенным дифференциальным уравнениям / «Наука» Москва, 1976, 576 с.
9. *Корн Г., Корн Т.* Справочник по математике для инженерных работников / «Наука» Москва, 1973, 832 с.

ЧИСЛЕННОЕ РЕШЕНИЕ РАСПРОСТРАНЕНИЯ ПРОДОЛЬНОЙ ВОЛНЫ В НЕЛИНЕЙНОЙ ВЯЗКОУПРУГОЙ СРЕДЕ.

Логинов П.[1], Акбаров Н.[1], Хамидов С.[2]
[1]*Институт механики и сейсмостойкости сооружений им. М.Т. Уразбаева, Ташкент, Узбекистан*
[2]*НИУ "Ташкентский институт инженеров ирригации и механизации сельского хозяйства", Ташкент, Узбекистан*
E-mail: lopavi88@mail.ru

Аннотация. *Данная статья посвящена исследованию распространения продольной волны в нелинейной вязкоупругой среде. Дана математическая постановка задачи распространения продольной волны в нелинейной вязкоупругой среде с использованием уравнения движения за фронтом через переменные Лагранжа. Рассмотренная задача решена методом характеристик. При решении конкретных задач установлено, что: амплитуда первого колебания напряжения в фиксированных сечениях среды больше, чем амплитуда последующих колебаний; структурные изменения среды при деформировании более чувствительны к скорости деформирования; линейная зависимость коэффициента затухания от частоты продольных волн изменяется в широком диапазоне частот.*

Ключевые слова: *грунт; напряжение; деформация; продольная волна; нелинейная вязкоупругая среда; нелинейный закон.*

1. Введение

Исследования Х.А. Рахматуллина, С.С. Григоряна, Г.М Ляхова, К.С. Султонова и многих других авторов посвящены решению волновых задач в грунтах. В их работах особое внимание уделяется изучению распространения волны в грунтах. В [1-5] исследуется экспериментальное и теоретическое взаимодействие твердых тел с грунтом. В рамках исследования волн в грунтах в [6] изучена динамика распространения взрывных волн. В [7] представлена модель распространения продольных волн в горных породах. Известно, что под действием динамических сил они становятся мягкими. То есть скорость звука уменьшается, но размягчение происходит медленно, не мгновенно. Предлагается формулировка, учитывающая вязкоупругое свойство нелинейности. Полученные дифференциальные уравнения линеаризованы с использованием метода Рое. В этом методе использовалось резонансное моделирование, в котором вязкоупругость является линейной. В [8] рассматривается численное моделирование решения проблемы распространения нелинейных сейсмических волн в грунтах. Проблема сейсмической безопасности была частично решена путем обнаружения распространения сильной сейсмической волны в грунте. В [8] также рассматривается одномерная задача распространения волн в линейных и нелинейных средах. В [9] было рассмотрено распространение сейсмических волн в нелинейной вязкоупругой среде с использованием метода вспомогательных дифференциальных уравнений Поланга Мартина. Метод вспомогательных дифференциальных уравнений основан на дифференциальных уравнениях, извлеченных из общего уравнения распространения волны. Также в [9] приведен метод конечных разностей в трехмерном виде. В [10] аналитически была решена задача распространения продольных волн в горных породах. Среда горных пород рассмотрена как состоящая из переменных поперечных сечений. В [10] уравнения непрерывности движения и деформации-напряжения

решены совместно. В частном случае была решена проблема распространения гармонических волн, а также проанализированы результаты, полученные путем решения уравнений, выражающих напряжение и деформацию. Полученные результаты показывают, что коэффициент затухания увеличивается с учетом изменения поперечного сечения. Было показано, что распространение волны в горных породах зависит от частоты. Также для случаев с тремя разными геометриями в средах горных пород затухание распространения волны будет зависеть от статического напряжения, частоты, а также от изменения поперечного сечения. В [11] усовершенствован конечно-разностный метод на основе метода Иванова. По заданным диссипативным свойствам разработан алгоритм вычислений. Вязкоупругое свойство рассматривается через модель Кельвинга-Фойгта. Полученный результат в одномерном случае сравнивался с точным решением. В двумерной задаче полученное уравнение разложено в ряд по пространственным координатам. Для определения достоверности полученного результата задача Лемба решается численным методом с учетом вязкоупругости. В [12-16] исследуется распространения одномерной продольной волны в вязкоупругой среде. В статьях [17-18] исследована одномерная и двумерная нестационарные задачи динамической теории пластичности применительно к расчету параметров среды в случаях распространения и деформации волн от различной поверхности, исходя из деформационной теории с более сложными уравнениями состояний. Решен ряд конкретных задач применительно к исследованию взаимодействия волн со сферической полостью в грунтах с учетом их сложных упругопластических деформаций. В [19] определены механические параметры грунта.

2. Постановка задачи и метод её решения.

Использование моделей с учетом вязких и пластических свойств среды в задачах динамики грунтов затрудняет получение аналитических решений. В таких задачах гораздо эффективнее использовать численные методы для решения проблемы. При решении задач о распространении волн численным методом можно использовать множество методов. В данной работе для оценки распространения продольной волны в нелинейной вязкоупругой среды будем использовать метод характеристик.

Для постановки задачи о распространении продольной волны в нелинейной вязкоупругой среде используем уравнения движения за фронтом в переменных Лагранжа, т.е.:

$$\begin{aligned} &\rho_0 \partial \mathrm{v} / \partial \mathrm{t} - \partial \sigma / \partial \mathrm{r} = 0 \\ &\partial \mathrm{v} / \partial \mathrm{r} - \partial \varepsilon / \partial \mathrm{t} = 0 \end{aligned} \qquad (2)$$

состояние среды в рассматриваемом процессе описывается уравнением

$$\frac{1}{E_D(I_S)}\frac{d\sigma}{dt} + \frac{\mu_0(I_S)}{E_S(I_S)}\sigma = \frac{d\varepsilon}{dt} + \mu_0(I_S)\varepsilon, \qquad (2)$$

При этом в начальном положении t=0 напряжение в скачках увеличивается, а затем его изменение выражается формулой

$$\begin{cases} \sigma = \sigma_m \sin\left(\dfrac{\pi t}{T}\right) t > 0, \\ \sigma = 0, t \le 0 \end{cases} \qquad (3)$$

Решаем характеристическим методом, когда (1) и (2) можно привести к уравнению гиперболического типа. Введем безразмерные переменные Лагранжа и безразмерные величины:

$$x=\frac{\mu_N r}{c_0}, t^0=\mu_N t, \sigma^0=\sigma/\sigma_m, \varepsilon^0=\varepsilon/\varepsilon_m, v^0=v/v_m, v_m=-\sigma_m/(c_0\rho_0);$$
$$f^0=f/\mu_N=1/(2\mu_N T),\ f=1/2T, \varepsilon_m=\sigma_m/E_{DN}, \mu^0=(\mu^0(I_S))/\mu_N, T^0=\mu_N T. \quad (4)$$

С учетом (4) уравнение (1) примет вид:

$$(\partial v^0)/(\partial t^0)+(\partial\sigma^0)/\partial x=0, (\partial v^0)/\partial x+(\partial\varepsilon^0)/(\partial t^0)=0, (\partial\varepsilon^0)/(\partial t^0)+\mu^0\varepsilon^0=(\partial\sigma^0)/(\partial t^0)+\mu^0\gamma\sigma^0;$$
$$d\sigma^0\pm dv^0=(\varepsilon^0-\gamma\sigma^0)\mu^0 dt^0, dx/(dt^0)=\pm 1; \quad (5)$$

$$d\sigma^0+d\varepsilon^0=(\varepsilon^0-\gamma\sigma^0)\mu^0 dt^0, dx/(dt^0)=0; \quad (6)$$

$$x=0:\sigma^0=0, t^0\le 0; \sigma^0=sin(2\pi f^0 t^0), t^0>0; \quad (7)$$

$$x=t^0, \sigma^0=\varepsilon^0=v^0=0; \quad (8)$$

Решение задач (5), (6), (7) и (8) было получено на ЭВМ.

Здесь объемная вязкость принимается как постоянное значение μ_0=1, а значение γ определяется из следующих выражений и оно может принимать значение, большее, чем рассчитанное в процессе расчёта.:

$$\gamma_I=\gamma_*\exp\left(\beta_I\left(1-I_S\right)\right), \beta_I=-\ln\left(\gamma_*/\gamma_N\right) \quad (9)$$

$$\gamma_*=\gamma_N+(\gamma_m-\gamma_N)(d\varepsilon/(\mu_N dt))^\chi \quad (10)$$

В рассматриваемой задаче продольный волновой фронт, распространяющийся в среде, не может разрушить структуру. Это означает, что значение γ_1 будет примерно равно γ_N на основе (9).

При определении параметров волн численным методом скорость деформации в шаге (i+1) расчета имеет вид

$$\frac{d\varepsilon}{dt}\cong\frac{\Delta\varepsilon}{\Delta t}=\frac{\varepsilon_i-\varepsilon_{i-1}}{\Delta t} \quad (11)$$

С учетом (11) выражение (10) примет вид:

$$\gamma_*=\gamma_N+(\gamma_m-\gamma_N)((\varepsilon_i-\varepsilon_{i-1})/(\mu_N\Delta t))^\chi \quad (12)$$

В вычислениях скорость деформации остается неизменной величиной после достижения ею постоянного значения, а значение γ_N находится с помощью (9).

Следует отметить, что при принятых ограничениях модуль динамического сжатия $E_D(I_S)$ становится постоянным, а модуль статического сжатия $E_S(I_S)$ переменным. В этом случае нарушение структуры грунта влияет только на E_S. Однако имеется также влияние на деформацию. Это означает, что значение $\gamma=\gamma_1$ в уравнении (7) является переменным, а характеристические уравнения (1), (2) линейны вдоль характеристических линий.

Таким образом, численное решение рассматриваемой задачи упрощается, но модель (2) для предложенного грунта практически не меняется. Коэффициент поглощения для рассматриваемой среды (без измерения) находится по (13)

$$\alpha_S^0=ln(\sigma_{i-1}^0/\sigma_i^0)/(x_i-x_{i-1}), \alpha_S c_0=\alpha_S^0\mu_N \quad (13)$$

Где i-порядковый номер поперечных сечений среды $\sigma_{i-1}^0, \sigma_i^0$ - амплитуды напряжения в рассматриваемом сечении. На ЭВМ реализованы следующие безразмерные значения расчетных параметров: γ_N=1.1, γ_N=10, χ=0.5, ε_*=0.2, $\mu_N=10^4$ c^{-1}. Эти значения согласно (11) и (4) соответствуют максимальному значению деформации $\dot{\varepsilon}=5*10^{-7}$-$5*10^3 c^{-1}$.

3. Результаты расчетов и их анализ.

В результате расчетов была выявлена связь между безразмерными напряжениями и деформациями в заданных сечениях грунта и волновыми параметрами. Эти параметры будут зависеть от безразмерного времени. Полученные результаты представлены в графическом

виде. Например, на рисунке 1 безразмерное напряжение, при f=5*10^{3}c^{-1} при различных значениях x, определяет изменение в неизменной единице времени. Кривая при x = 0 определяет начальное состояние распространения волны. При этом амплитуда не изменяется на единицу времени. Максимальное значение напряжений здесь меньше, чем в начальном сечении.

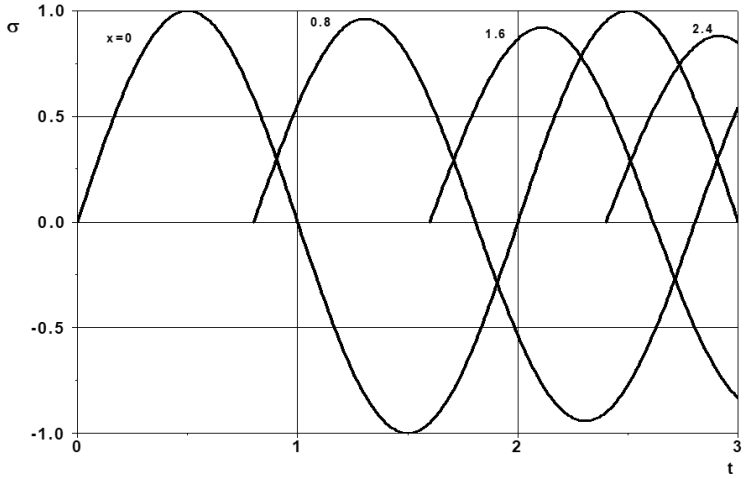

Рисунок 1. **- Зависимость напряжения от времени.**

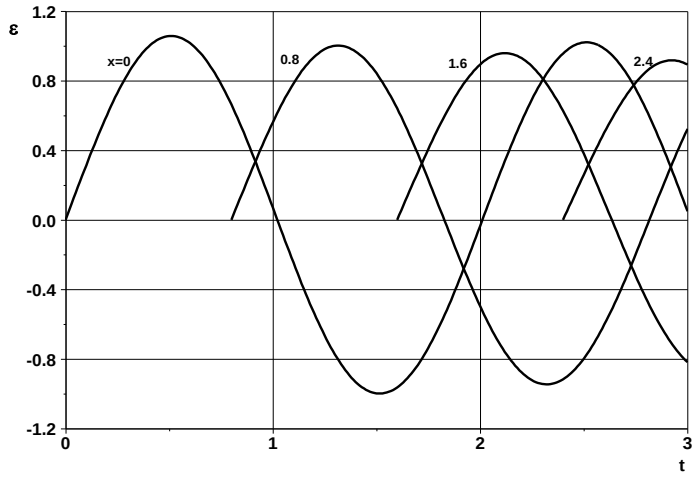

Рисунок 2. **Зависимость деформации от времени.**

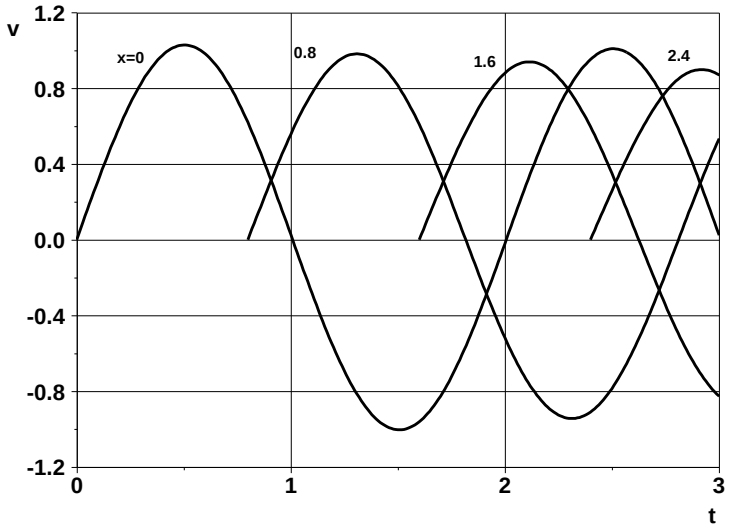

Рисунок 3. **Зависимость скорости от времени.**

Было обнаружено, что амплитуда первого колебательного движения больше, чем амплитуда второго. После 5-7 колебаний амплитуда напряжения остается неизменной. Закон изменения скорости и деформации грунта в фиксированных сечениях будет аналогичен рисункам 1-3. На разных частотах состояние параметров сохраняется. Из параметров волны изменяется только амплитуда колебаний. Затухание частот колебаний волны имеет небольшие изменения. Прирост частоты, затухание волны будут значительными. Дальнейшее увеличение частоты на расстояниях приводит к увеличению длины волны. С помощью максимальных значений амплитуд напряжения, деформации и скорости определяется коэффициент затухания.

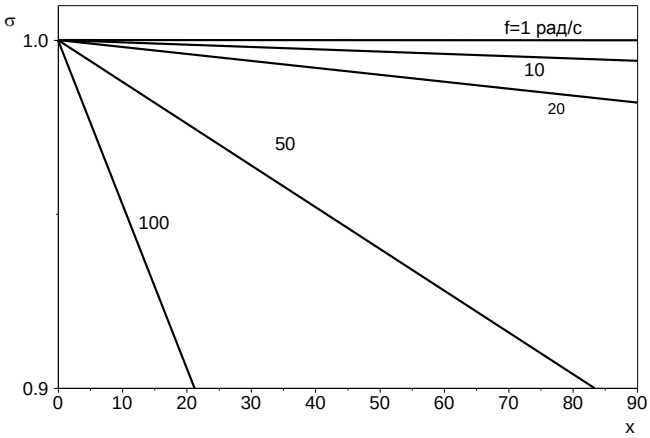

Рисунок 4. **Затухание максимальных напряжений в зависимости от расстояния.**

Для различных значений безразмерной частоты на рис.4 показано уменьшение амплитуды напряжения с расстоянием для первых и стабильных колебаний. На низких частотах затухание волны незначительно (верхние кривые). С увеличением частоты интенсивность затухания волны значительно возрастает (средние кривые). Дальнейшее увеличение частоты приводит к дальнейшему ослаблению напряжения волны с расстоянием (нижние кривые).

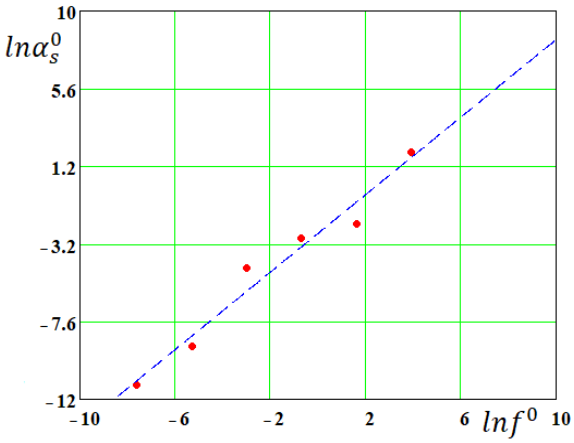

Рисунок 5. **- Зависимость коэффициент затухания от частоты.**

Рисунок 5 соответствует стандартному линейному телу, а его характеристики остаются постоянными. Это, в свою очередь, приводит к тому, что коэффициент затухания для высоких частот остается неизменным. При малых частотах зависимость затухания от частоты линейна начиная с f=5 кГц , а коэффициент затухания не меняется. Такая частотная характеристика является недостатком некоторых моделей.

4. Выводы

1. Дана математическая постановка задачи распространении продольной волны в нелинейной вязкоупругой среде с использованием уравнения движения за фронтом через переменные Лагранжа.

2. Поставленная задача о распространении продольной волны в нелинейной вязкоупругой среде решена методом характеристик.

3. При решение конкретных задач установлено что:

- амплитуды первого колебания напряжения в фиксированных сечениях среды больше, чем амплитуды последующих колебаний;
- структурные изменения среды при деформировании более чувствительны к скорости деформирования;
- линейная зависимость коэффициента затухания от частоты продольных волн изменяется в широком диапазоне частот.

Расчеты показали, что амплитуды первого колебания напряжения в фиксированных сечениях среды больше, чем амплитуды последующих колебаний. Таким образом, предлагаемая модель среды, учитывающая структурные изменения среды при деформировании более чувствительна к скорости деформирования, что дает линейную зависимость коэффициента затухания от частоты продольных волн в широком диапазоне частот.

Литература

1. *Султанов К.С.* Волновая теория сейсмостойкости подземных сооружений /Ташкент. ФАН. 2016, 392 с.
2. *Sultanov K.S., Vatin N.I.* Wave Theory of Seismic Resistance of Underground Pipelines // Applied Sciences. 2021, No 11(4). P. 1797.
3. *Sultanov K.S., Umarkhonov S.I.* Dynamic behavior of earth dams under short-term semi-harmonic loads // E3S Web of Conferences 2023, No 420. P. 07014
4. *Sultanov K.S., Khusanov B.E., Rikhsieva B.B.* Elastic wave propagation in a cylinder with external active friction // J. Phys.: Conf. 2021, No 1901. P. 012125
5. *Sultanov K. S.* Parameters of Nonlinear Laws of Longitudinal Interaction of Underground Pipelines with Soil. // Soil Mechanics & Foundation Engineering, 2022, No 59(4). P. 347.
6. *Ляхов Г.М.* Основы динамики взрывных волн в грунтах и горных породах / Москва. Недра. 1974, 192 с.
7. Berjamin H., Lombard B., Chiavassa G., Favrie N. *Modeling longitudinal wave propagation in nonlinear viscoelastic solids with softening. // International Journal of Solids and Structures, 2018, No 141-142. P. 35-44.*
8. *Oral E. et al.* Spectral element modelling of seismic wave propagation in visco-elastoplastic media including excess-pore pressure development // Geophys. J. Int. 2017. Vol. 211, No 3. P. 1494–1508.
9. *Martin R. et al.* Seismic wave propagation in nonlinear viscoelastic media using the auxiliary differential equation method // Geophys. J. Int. 2019. Vol. 216, No 1. P. 453–469.
10. *Yuan W. et al.* Theoretical Analysis of Longitudinal Wave Attenuation in a Stressed Rock With Variable Cross-Section // Front. Earth Sci. 2019. Vol. 7. P.00270.
11. Садовский В.М., Садовс*кая* О. В. *Вычислительный алгоритм для расчета вязкоупругих волн в среде Кельвина–Фойхта //Вычислительные методы и программирование. 2014. Т. 15. С. 99-108.*
12. *Khamidov S.S., Loginov P.V., Akbarov N.A.* Propagation of longitudinal waves in a linear viscoelastic medium // E3S Web Conf. / ed. Pukhkal V., Uvarova S. 2023. Vol. 458. P. 08013.
13. *Ismoilova S., Loginov P., Khamidov S., Akbarov N., Kumakov J.X.* Dynamic stress state of underground pipelines at junctions // IOP Conf. Ser. Mater. Sci. Eng. 2020. Vol. 869, No 5. P. 052013.
14. *Ismoilova S., Loginov P., Khamidov S., Akbarov N., Kumakov J.* Force properties of longitudinal interaction of the underground pipeline with soil // IOP Conf. Ser. Mater. Sci. Eng. 2020. Vol. 869, No 5. P. 052036.
15. *Кукуджанов В.Н.* Численные методы в механике сплошных сред. Курс лекций /Учебное пособие. МАТИ-РГТУ им. К.Э. Циолковского, Москва 2006, 157 с.
16. *Кукуджанов В.Н.* Компьютерное моделирование деформирования, повреждаемости и разрушения неупругих материалов и конструкций. Учебное пособие / Московский физико-технический институт, Москва, 2008, 212 с.
17. Khudainazarov Sh.O., Donayev B., Ashirov B Propagation of a spherical wave in elastoplastic medium with complex equations of state // E3S Web of Conferences. 2021, No 264(1). P.02041
18. Khudainazarov, S., Donayev, B. Propagation of a Spherical Wave in Elastoplastic Medium with Complex Equations of State // Lecture Notes in Civil Engineering.2022, No 170, P. 403-420.
19. *Loginov P. V., Salikhova Z.R., Sultanov K.S.* Experimental and Theoretical Method for Determining Mechanical Characteristics of Soils under Dynamic Loads // Mechanics of Solids. 2019. vol. 54, No 6. P. 915–928.

ПОСТАНОВКА ЗАДАЧИ ОБ УПРУГОПЛАСТИЧЕСКОМ ИЗГИБЕ ТРЕХСЛОЙНОЙ ПЛАСТИНЫ В ТЕРМОРАДИАЦИОННОМ ПОЛЕ

Мельникова А.С.[1]

[1]*Белорусский государственный университет транспорта, Гомель, Беларусь*

E-mail: lady-nastia@mail.ru

Аннотация: *Рассмотрена постановка задачи об изгибе физически нелинейной прямоугольной трехслойной пластины при действии терморадиационных нагрузок. При получении уравнений использованы соотношения закона Гука. Получены линейные и терморадиационные компоненты тензора напряжений в слоях пластины.*

Ключевые слова: *трехслойная пластина, сжимаемый заполнитель, терморадиационное поле.*

5. Введение

Актуальность темы обоснована широкой областью применения слоистых конструкций. Они используются в машиностроении, авиастроении, приборостроении, строительстве и др. Следовательно, возникает необходимость в новых методах расчета таких конструкций для более эффективного их использования.

В работе [1] рассмотрен изгиб упругопластической прямоугольной трехслойной пластины со сжимаемым заполнителем в температурном поле. В работе [2] исследована деформация трехслойного стержня в температурном поле. В работах [3]–[5] рассмотрены решения ряда задач статики и динамики композитных конструкций при силовых воздействиях.

Здесь рассмотрена постановка задачи об упругопластическом изгибе трехслойной прямоугольной пластины со сжимаемым заполнителем в терморадиационном поле.

6. Материалы, методы и объект исследования.

Рассматривается несимметричная по толщине трехслойная прямоугольная пластина, состоящая из двух несущих слоев, которые выполнены из упругопластического материала, и нелинейно упругого заполнителя. Несущие слои выполнены из материалов высокой прочности и жесткости, так как этими слоями воспринимается основная часть механической нагрузки, приходящейся на пластину. Заполнитель служит для образования монолитной конструкции, гарантирует перераспределение усилий между несущими слоями, тем самым обеспечивает совместную работу слоев пластины (рис. 1).

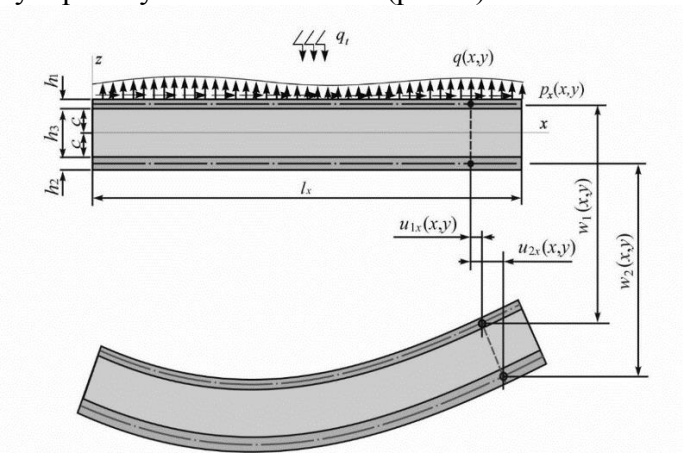

Рисунок 1. – **Расчетная схема пластины**

7. Постановка задачи.

Для изотропных несущих слоев приняты гипотезы Кирхгофа. В жестком заполнителе справедливы точные соотношения теории упругости с линейной аппроксимацией перемещений его точек от поперечной координаты z. На границах контакта перемещения непрерывны. Материалы несущих слоев несжимаемы в поперечном и продольном направлении, в заполнителе учитывается обжатие. Деформации малые. Система координат x, y, z связывается со срединной плоскостью заполнителя. Предположим, что в начальный

момент времени на трехслойную пластину со сжимаемым заполнителем, находящуюся в естественном состоянии, начинают действовать внешняя распределенная нагрузка q, проекции которой на координатные оси: $q(x,y)$, $p_x(x,y)$, $p_y(x,y)$, тепловой поток интенсивностью q_t, направленный перпендикулярно первому несущему слою, а также нейтронный поток.

За искомые функции принимаем продольные перемещения $u_{kx}(x,y)$, $u_{ky}(x,y)$ и прогибы $w_k(x,y)$ срединных поверхностей несущих слоев $(k=1,2)$.

При радиационном (нейтронном) воздействии на упругопластическое тело в функцию пластичности и объемную деформацию вносятся корректировки. Физические уравнения пластичности в радиационном поле принимают вид

$$s_{ij} = 2Gf_1(\varepsilon_u, I)э_{ij}, \qquad \sigma = K(3\varepsilon - BI).$$

Здесь $I = \varphi t$ – интегральный нейтронный поток, который в пределах малых упругопластических деформаций приводит к увеличению радиационного упрочнения материала и росту предела текучести. Радиационное увеличение объемной деформации учитывается величиной BI, где B – константа материала.

При одновременном воздействии теплового и нейтронного потоков уравнения терморадиационной пластичности принимают вид

$$s_{ij} = 2G(T)\, f_1(\varepsilon_u, T, I)э_{ij}, \qquad \sigma = K(3\varepsilon - 3\alpha\Delta T - BI).$$

Предположим, что упругопластическая пластина находится в температурном поле $\boldsymbol{T_k(z)}$ и облучается нейтронным потоком $\boldsymbol{I = \varphi t}$, где $\boldsymbol{\varphi}$ – интенсивность в нейтрон/с, $\boldsymbol{t}$ – время. Соответствующие физические уравнения состояния примут вид

$$s_{ij}^{(k)} = 2G_k\left(T_k\right)\left(1 - \omega^{(k)}\left(\varepsilon_u^{(k)}, T_k, I\right)\right)э_{ij}^{(k)},$$

$$\sigma^{(k)} = 3K_k(T_k)(\varepsilon^{(k)} - \alpha_{0k}\Delta T_k - BI) \quad (i, j = x, y, z,\ k = 1, 2, 3), \tag{1}$$

где $s_{ij}^{(k)}$, $\sigma^{(k)}$ – девиаторная и шаровая части тензора напряжений;

$э_{ij}^{(k)}$, $\varepsilon^{(k)}$ – девиаторная и шаровая части тензора деформаций;

$\varepsilon_u^{(k)}$ – интенсивность деформации в k-м слое; $\omega^{(k)}\left(\varepsilon_u^{(k)}, T_k, I\right)$ – функции Ильюшина пластичности в несущих слоях с учетом зависимости от величины нейтронного потока;

$\omega^{(3)}\left(\varepsilon_u^{(3)}, T_k, I\right)$ – универсальная функция, описывающая физическую нелинейность материала заполнителя с учетом зависимости от величины нейтронного потока;

$G_k(T_k)$, $K_k(T_k)$ – температурно-зависимые модули упругости материалов слоев;

α_{0k} – коэффициент линейного температурного удлинения;

ΔT_k – приращение температуры, отсчитываемое от некоторого начального значения T_0.

Исходя из соотношений (1) выделим в тензоре напряжений упругие (с индексом «0») и нелинейные (с индексом «ω») слагаемые, которые будут включать терморадиационные добавки:

в несущих слоях

$$\sigma_{xx}^{(k)} = \sigma_{xx}^{(k)0} - \sigma_{xx}^{(k)\omega},$$

$$\sigma_{xx}^{(k)0} = 2G_k(T_k)э_{xx}^{(k)} + 3K_k(T_k)\varepsilon^{(k)} = K_k^{+}(T_k)\varepsilon_{xx}^{(k)} + K_k^{-}(T_k)\varepsilon_{yy}^{(k)},$$

$$\sigma_{xx}^{(k)\omega} = 2G_k(T_k)э_{xx}^{(k)}\omega^{(k)} + 3K_k(T_k)\alpha_{0k}\Delta T_k = \frac{2}{3}G_k(T_k)\left(2\varepsilon_{xx}^{(k)} - \varepsilon_{yy}^{(k)}\right)\omega^{(k)} + +3K_k(T_k)\alpha_{0k}\Delta T_k + BI,$$

$$\sigma_{yy}^{(k)} = \sigma_{yy}^{(k)0} - \sigma_{yy}^{(k)\omega},$$

$$\sigma_{yy}^{(k)0} = 2G_k(T_k)э_{yy}^{(k)} + 3K_k(T_k)\varepsilon^{(k)} = K_k^+(T_k)\varepsilon_{yy}^{(k)} + K_k^-(T_k)\varepsilon_{xx}^{(k)},$$

$$\sigma_{yy}^{(k)\omega} = 2G_k(T_k)э_{yy}^{(k)}\omega^{(k)} + 3K_k(T_k)\alpha_{0k}\Delta T_k = \frac{2}{3}G_k(T_k)\left(2\varepsilon_{yy}^{(k)} - \varepsilon_{xx}^{(k)}\right)\omega^{(k)} +$$

$$+3K_k(T_k)\alpha_{0k}\Delta T_k + BI,$$

$$\sigma_{xy}^{(k)} = \sigma_{xy}^{(k)0} - \sigma_{xy}^{(k)\omega}, \quad \sigma_{xy}^{(k)0} = 2G_k(T_k)э_{xy}^{(k)} = 2G_k(T_k)\varepsilon_{xy}^{(k)},$$

$$\sigma_{xy}^{(k)\omega} = 2G_k(T_k)э_{xy}^{(k)}\omega^{(k)} = 2G_k(T_k)\varepsilon_{xy}^{(k)}\omega^{(k)},$$

в заполнителе

$$\sigma_{xx}^{(3)} = \sigma_{xx}^{(3)0} - \sigma_{xx}^{(3)\omega},$$

$$\sigma_{xx}^{(3)0} = 2G_3(T_3)э_{xx}^{(3)} + 3K_3(T_3)\varepsilon^{(3)} = K_3^+(T_3)\varepsilon_{xx}^{(3)} + K_3^-(T_3)\left(\varepsilon_{yy}^{(3)} + \varepsilon_{zz}^{(3)}\right),$$

$$\sigma_{xx}^{(3)\omega} = 2G_3(T_3)э_{xx}^{(3)}\omega^{(3)} + 3K_3(T_3)\alpha_{03}\Delta T_3 =$$

$$= \frac{2}{3}G_3(T_3)\left(2\varepsilon_{xx}^{(3)} - \varepsilon_{yy}^{(3)} - \varepsilon_{zz}^{(3)}\right)\omega^{(3)} + 3K_3(T_3)\alpha_{03}\Delta T_3 + BI,$$

$$\sigma_{yy}^{(3)} = \sigma_{yy}^{(3)0} - \sigma_{yy}^{(3)\omega},$$

$$\sigma_{yy}^{(3)0} = 2G_3(T_3)э_{yy}^{(3)} + 3K_3(T_3)\varepsilon^{(3)} = K_3^+(T_3)\varepsilon_{yy}^{(3)} + K_3^-(T_3)\varepsilon_{xx}^{(3)} + K_3^-(T_3)\varepsilon_{zz}^{(3)},$$

$$\sigma_{yy}^{(3)\omega} = 2G_3(T_3)э_{yy}^{(3)}\omega^{(3)} + 3K_3(T_3)\alpha_{03}\Delta T_3 =$$

$$= \frac{2}{3}G_3(T_3)\left(2\varepsilon_{yy}^{(3)} - \varepsilon_{xx}^{(3)} - \varepsilon_{zz}^{(3)}\right)\omega^{(3)} + 3K_3(T_3)\alpha_{03}\Delta T_3 + BI,$$

$$\sigma_{zz}^{(3)} = \sigma_{zz}^{(3)0} - \sigma_{zz}^{(3)\omega},$$

$$\sigma_{zz}^{(3)0} = 2G_3(T_3)э_{zz}^{(3)} + 3K_3(T_3)\varepsilon^{(3)} = K_3^+(T_3)\varepsilon_{zz}^{(3)} + K_3^-(T_3)\left(\varepsilon_{xx}^{(3)} + \varepsilon_{yy}^{(3)}\right),$$

$$\sigma_{zz}^{(3)\omega} = 2G_3(T_3)э_{zz}^{(3)}\omega^{(3)} + 3K_3(T_3)\alpha_{03}\Delta T_3 =$$

$$= \frac{2}{3}G_3(T_3)\left(2\varepsilon_{zz}^{(3)} - \varepsilon_{xx}^{(3)} - \varepsilon_{yy}^{(3)}\right)\omega^{(3)} + 3K_3(T_3)\alpha_{03}\Delta T_3 + BI,$$

$$\sigma_{xy}^{(3)} = \sigma_{xy}^{(3)0} - \sigma_{xy}^{(3)\omega}, \quad \sigma_{xy}^{(3)0} = 2G_3(T_3)э_{xy}^{(3)} = 2G_3(T_3)\varepsilon_{xy}^{(3)},$$

$$\sigma_{xy}^{(3)\omega} = 2G_3(T_3)э_{xy}^{(3)}\omega^{(3)} = 2G_3(T_3)\varepsilon_{xy}^{(3)}\omega^{(3)},$$

$$\sigma_{xz}^{(3)} = \sigma_{xz}^{(3)0} - \sigma_{xz}^{(3)\omega}, \quad \sigma_{xz}^{(3)0} = 2G_3(T_3)э_{xz}^{(3)} = 2G_3(T_3)\varepsilon_{xz}^{(3)},$$

$$\sigma_{xz}^{(3)\omega} = 2G_3(T_3)э_{xz}^{(3)}\omega^{(3)} = 2G_3(T_3)\varepsilon_{xz}^{(3)}\omega^{(3)},$$

$$\sigma_{yz}^{(3)} = \sigma_{yz}^{(3)0} - \sigma_{yz}^{(3)\omega}, \quad \sigma_{yz}^{(3)0} = 2G_3(T_3)э_{yz}^{(3)} = 2G_3(T_3)\varepsilon_{yz}^{(3)},$$

$$\sigma_{yz}^{(3)\omega} = 2G_3(T_3)э_{yz}^{(3)}\omega^{(3)} = 2G_3(T_3)\varepsilon_{yz}^{(3)}\omega^{(3)},$$

$$K_k^+(T_k) = K_k(T_k) + \frac{4}{3}G_k(T_k), \quad K_k^-(T_k) = K_k(T_k) - \frac{2}{3}G_k(T_k). \tag{2}$$

Введем внутренние усилия и моменты:

$$N_{xx}^{(k)} = \int_{h_k} \sigma_{xx}^{(k)}\,\mathrm{d}z, \quad N_{yy}^{(k)} = \int_{h_k} \sigma_{yy}^{(k)}\,\mathrm{d}z, \quad M_{xx}^{(k)} = \int_{h_k} \sigma_{xx}^{(k)} z\,\mathrm{d}z, \quad M_{yy}^{(k)} = \int_{h_k} \sigma_{yy}^{(k)} z\,\mathrm{d}z,$$

$$M_{xy}^{(k)} = \int_{h_k} \sigma_{xy}^{(k)} z\,\mathrm{d}z, \quad Q_{xy}^{(k)} = \int_{h_k} \sigma_{xy}^{(k)}\,\mathrm{d}z, \quad N_{zz}^{(3)} = \int_{h_3} \sigma_{zz}^{(3)}\,\mathrm{d}z, \quad M_{xz}^{(3)} = \int_{h_3} \sigma_{xz}^{(3)} z\,\mathrm{d}z,$$

$$M_{yz}^{(3)} = \int_{h_3} \sigma_{yz}^{(3)} z\,\mathrm{d}z, \quad Q_{xz}^{(3)} = \int_{h_3} \sigma_{xz}^{(3)}\,\mathrm{d}z, \quad Q_{yz}^{(3)} = \int_{h_3} \sigma_{yz}^{(3)}\,\mathrm{d}z, \tag{3}$$

где $\sigma_{xx}^{(k)}$, $\sigma_{yy}^{(k)}$, $\sigma_{xy}^{(3)}$ $\sigma_{xz}^{(3)}$, $\sigma_{yz}^{(3)}$, $\sigma_{zz}^{(3)}$ – компоненты тензора напряжений; интегралы берутся по толщине k-го слоя.

Выполнив **аналогичные** (1), (2) и (3) действия с внутренними усилиями, получим ($k=1,2,3$):

$$N_{xx}^{(k)}=N_{xx}^{(k)0}-N_{xx}^{(k)\omega},\quad N_{yy}^{(k)}=N_{yy}^{(k)0}-N_{yy}^{(k)\omega},\quad M_{xx}^{(k)}=M_{xx}^{(k)0}-M_{xx}^{(k)\omega},$$

$$M_{yy}^{(k)}=M_{yy}^{(k)0}-M_{yy}^{(k)\omega},\quad M_{xy}^{(k)}=M_{xy}^{(k)0}-M_{xy}^{(k)\omega},\quad Q_{xy}{}^{(k)}=Q_{xy}{}^{(k)0}-Q_{xy}{}^{(k)\omega},$$

$$N_{zz}^{(3)}=N_{zz}^{(3)0}-N_{zz}^{(3)\omega},\quad M_{xz}^{(3)}=M_{xz}^{(3)0}-M_{xz}^{(3)\omega},\quad M_{yz}^{(3)}=M_{yz}^{(3)0}-M_{yz}^{(3)\omega},$$

$$Q_{xz}{}^{(3)}=Q_{xz}{}^{(3)0}-Q_{xz}{}^{(3)\omega},\quad Q_{yz}{}^{(3)}=Q_{yz}{}^{(3)0}-Q_{yz}{}^{(3)\omega}. \tag{4}$$

Входящие в (4) линейные (с индексом «0») и нелинейные (с индексом «ω») составляющие внутренних усилий вычисляются через напряжения и деформации по формулам (2).

Упругие и нелинейные составляющие во внутренних усилиях (4) определяются по **следующим** формулам:

в несущих слоях $(k=1,2)$:

$$N_{xx}^{(k)0}=\int_{h_k}\sigma_{xx}^{(k)0}\,\mathrm{d}z=\int_{h_k}\left(K_k^{+}(T_k)\varepsilon_{xx}^{(k)}+K_k^{-}(T_k)\varepsilon_{yy}^{(k)}\right)\mathrm{d}z,$$

$$N_{xx}^{(k)\omega}=\int_{h_k}\sigma_{xx}^{(k)\omega}\,\mathrm{d}z=\frac{2}{3}\int_{h_k}G_k(T_k)\left(2\varepsilon_{xx}^{(k)}-\varepsilon_{yy}^{(k)}\right)\omega^{(k)}\,\mathrm{d}z+\int_{h_k}\left(3K_k(T_k)\alpha_{0k}\Delta T_k+BI\right)\mathrm{d}z,$$

$$N_{yy}^{(k)0}=\int_{h_k}\sigma_{yy}^{(k)0}\,\mathrm{d}z=\int_{h_k}\left(K_k^{+}(T_k)\varepsilon_{yy}^{(k)}+K_k^{-}(T_k)\varepsilon_{xx}^{(k)}\right)\mathrm{d}z,$$

$$N_{yy}^{(k)\omega}=\int_{h_k}\sigma_{yy}^{(k)\omega}\,\mathrm{d}z=\frac{2}{3}\int_{h_k}G_k(T_k)\left(2\varepsilon_{yy}^{(k)}-\varepsilon_{xx}^{(k)}\right)\omega^{(k)}\,\mathrm{d}z+\int_{h_k}\left(3K_k(T_k)\alpha_{0k}\Delta T_k+BI\right)\mathrm{d}z,$$

$$M_{xx}^{(k)0}=\int_{h_k}\sigma_{xx}^{(k)0}z\,\mathrm{d}z=\int_{h_k}\left(K_k^{+}(T_k)\varepsilon_{xx}^{(k)}+K_k^{-}(T_k)\varepsilon_{yy}^{(k)}\right)z\,\mathrm{d}z,$$

$$M_{xx}^{(k)\omega}=\int_{h_k}\sigma_{xx}^{(k)\omega}z\,\mathrm{d}z=\frac{2}{3}\int_{h_k}G_k(T_k)\left(2\varepsilon_{xx}^{(k)}-\varepsilon_{yy}^{(k)}\right)\omega^{(k)}z\,\mathrm{d}z+\int_{h_k}\left(3K_k(T_k)\alpha_{0k}\Delta T+BI\right)_k z\,\mathrm{d}z,$$

$$M_{yy}^{(k)0}=\int_{h_k}\sigma_{yy}^{(k)0}z\,\mathrm{d}z=\int_{h_k}\left(K_k^{+}(T_k)\varepsilon_{yy}^{(k)}+K_k^{-}(T_k)\varepsilon_{xx}^{(k)}\right)z\,\mathrm{d}z,$$

$$M_{yy}^{(k)\omega}=\int_{h_k}\sigma_{yy}^{(k)\omega}z\,\mathrm{d}z=\frac{2}{3}\int_{h_k}G_k(T_k)\left(2\varepsilon_{yy}^{(k)}-\varepsilon_{xx}^{(k)}\right)\omega^{(k)}z\,\mathrm{d}z+\int_{h_k}\left(3K_k(T_k)\alpha_{0k}\Delta T_k+BI\right)z\,\mathrm{d}z,$$

$$M_{xy}^{(k)0}=\int_{h_k}\sigma_{xy}^{(k)0}z\,\mathrm{d}z=2\int_{h_k}G_k(T_k)\varepsilon_{xy}^{(k)}z\,\mathrm{d}z,\quad M_{xy}^{(k)\omega}=\int_{h_k}\sigma_{xy}^{(k)\omega}z\,\mathrm{d}z=2\int_{h_k}G_k(T_k)\varepsilon_{xy}^{(k)}\omega^{(k)}z\,\mathrm{d}z,$$

$$Q_{xy}^{(k)0}=\int_{h_k}\sigma_{xy}^{(k)0}\,\mathrm{d}z=2\int_{h_k}G_k(T_k)\varepsilon_{xy}^{(k)}\,\mathrm{d}z,\quad Q_{xy}^{(k)\omega}=\int_{h_k}\sigma_{xy}^{(k)\omega}\,\mathrm{d}z=2\int_{h_k}G_k(T_k)\varepsilon_{xy}^{(k)}\omega^{(k)}\,\mathrm{d}z,$$

в заполнителе

$$N_{xx}^{(3)0}=\int_{h_3}\sigma_{xx}^{(3)0}\,\mathrm{d}z=\int_{h_3}\left(K_3^{+}(T_3)\varepsilon_{xx}^{(3)}+K_3^{-}(T_3)\left(\varepsilon_{yy}^{(3)}+\varepsilon_{zz}^{(3)}\right)\right)\mathrm{d}z,$$

$$N_{xx}^{(3)\omega}=\int_{h_3}\sigma_{xx}^{(3)\omega}\,\mathrm{d}z=\frac{2}{3}\int_{h_3}G_3(T_3)\left(2\varepsilon_{xx}^{(3)}-\varepsilon_{yy}^{(3)}-\varepsilon_{zz}^{(3)}\right)\omega^{(3)}\,\mathrm{d}z+\int_{h_3}\left(3K_3(T_3)\alpha_{03}\Delta T_3+BI\right)\mathrm{d}z,$$

$$N_{yy}^{(3)0}=\int\limits_{h_3}\sigma_{yy}^{(3)0}\,\mathrm{d}\,z=\int\limits_{h_3}\left(K_3^{+}(T_3)\varepsilon_{yy}^{(3)}+K_3^{-}(T_3)\left(\varepsilon_{xx}^{(3)}+\varepsilon_{zz}^{(3)}\right)\right)\mathrm{d}\,z\,,$$

$$N_{yy}^{(3)\omega}=\int\limits_{h_3}\sigma_{yy}^{(3)\omega}\,\mathrm{d}\,z=\frac{2}{3}\int\limits_{h_3}G_3(T_3)\left(2\varepsilon_{yy}^{(3)}-\varepsilon_{xx}^{(3)}-\varepsilon_{zz}^{(3)}\right)\omega^{(3)}\,\mathrm{d}\,z+\int\limits_{h_3}\left(3K_3(T_3)\alpha_{03}\Delta T_3+BI\right)\mathrm{d}\,z\,,$$

$$N_{zz}^{(3)0}=\int\limits_{h_3}\sigma_{zz}^{(3)0}\,\mathrm{d}\,z=\int\limits_{h_3}\left(K_3^{+}(T_3)\varepsilon_{zz}^{(3)}+K_3^{-}(T_3)\left(\varepsilon_{xx}^{(3)}+\varepsilon_{yy}^{(3)}\right)\right)\mathrm{d}\,z\,,$$

$$N_{zz}^{(3)\omega}=\int\limits_{h_3}\sigma_{zz}^{(3)\omega}\,\mathrm{d}\,z=\frac{2}{3}\int\limits_{h_3}G_3(T_3)\left(2\varepsilon_{zz}^{(3)}-\varepsilon_{xx}^{(3)}-\varepsilon_{yy}^{(3)}\right)\omega^{(3)}\,\mathrm{d}\,z+\int\limits_{h_3}\left(3K_3(T_3)\alpha_{03}\Delta T_3+BI\right)\mathrm{d}\,z\,,$$

$$M_{xx}^{(3)0}=\int\limits_{h_3}\sigma_{xx}^{(3)0}z\,\mathrm{d}\,z=\int\limits_{h_3}\left(K_3^{+}(T_3)\varepsilon_{xx}^{(3)}+K_3^{-}(T_3)\left(\varepsilon_{yy}^{(3)}+\varepsilon_{zz}^{(3)}\right)\right)z\,\mathrm{d}\,z\,,$$

$$M_{xx}^{(3)\omega}=\int\limits_{h_3}\sigma_{xx}^{(3)\omega}z\,\mathrm{d}\,z=\frac{2}{3}\int\limits_{h_3}G_3(T_3)\left(2\varepsilon_{xx}^{(3)}-\varepsilon_{yy}^{(3)}-\varepsilon_{zz}^{(3)}\right)\omega^{(3)}z\,\mathrm{d}\,z+\int\limits_{h_3}\left(3K_3(T_3)\alpha_{03}\Delta T_3+BI\right)z\,\mathrm{d}\,z\,,$$

$$M_{yy}^{(3)0}=\int\limits_{h_3}\sigma_{yy}^{(3)0}z\,\mathrm{d}\,z=\int\limits_{h_3}\left(K_3^{+}(T_3)\varepsilon_{yy}^{(3)}+K_3^{-}(T_3)\left(\varepsilon_{xx}^{(3)}+\varepsilon_{zz}^{(3)}\right)\right)z\,\mathrm{d}\,z\,,$$

$$M_{yy}^{(3)\omega}=\int\limits_{h_3}\sigma_{yy}^{(3)\omega}z\,\mathrm{d}\,z=\frac{2}{3}\int\limits_{h_3}G_3(T_3)\left(2\varepsilon_{yy}^{(3)}-\varepsilon_{xx}^{(3)}-\varepsilon_{zz}^{(3)}\right)\omega^{(3)}z\,\mathrm{d}\,z+\int\limits_{h_3}\left(3K_3(T_3)\alpha_{03}\Delta T_3+BI\right)z\,\mathrm{d}\,z\,,$$

$$M_{xy}^{(3)0}=\int\limits_{h_3}\sigma_{xy}^{(3)0}z\,\mathrm{d}\,z=2\int\limits_{h_3}G_3(T_3)\varepsilon_{xy}^{(3)}z\,\mathrm{d}\,z\,,\quad M_{xy}^{(3)\omega}=\int\limits_{h_3}\sigma_{xy}^{(3)\omega}z\,\mathrm{d}\,z=2\int\limits_{h_3}G_3(T_3)\varepsilon_{xy}^{(3)}\omega^{(3)}z\,\mathrm{d}\,z\,,$$

$$M_{xz}^{(3)0}=\int\limits_{h_3}\sigma_{xz}^{(3)0}z\,\mathrm{d}\,z=2\int\limits_{h_3}G_3(T_3)\varepsilon_{xz}^{(3)}z\,\mathrm{d}\,z\,,\quad M_{xz}^{(3)\omega}=\int\limits_{h_3}\sigma_{xz}^{(3)\omega}z\,\mathrm{d}\,z=2\int\limits_{h_3}G_3(T_3)\varepsilon_{xz}^{(3)}\omega^{(3)}z\,\mathrm{d}\,z\,,$$

$$M_{yz}^{(3)0}=\int\limits_{h_3}\sigma_{yz}^{(3)0}z\,\mathrm{d}\,z=2\int\limits_{h_3}G_3(T_3)\varepsilon_{yz}^{(3)}z\,\mathrm{d}\,z\,,\quad M_{yz}^{(3)\omega}=\int\limits_{h_3}\sigma_{yz}^{(3)\omega}z\,\mathrm{d}\,z=2\int\limits_{h_3}G_3(T_3)\varepsilon_{yz}^{(3)}\omega^{(3)}z\,\mathrm{d}\,z\,,$$

$$Q_{xy}^{(3)0}=\int\limits_{h_3}\sigma_{xy}^{(3)0}\,\mathrm{d}\,z=2\int\limits_{h_3}G_3(T_3)\varepsilon_{xy}^{(3)}\,\mathrm{d}\,z\,,\quad Q_{xy}^{(3)\omega}=\int\limits_{h_3}\sigma_{xy}^{(3)\omega}\,\mathrm{d}\,z=2\int\limits_{h_3}G_3(T_3)\varepsilon_{xy}^{(3)}\omega^{(3)}\,\mathrm{d}\,z\,,$$

$$Q_{xz}^{(3)0}=\int\limits_{h_3}\sigma_{xz}^{(3)0}\,\mathrm{d}\,z=2\int\limits_{h_3}G_3(T_3)\varepsilon_{xz}^{(3)}\,\mathrm{d}\,z\,,\quad Q_{xz}^{(3)\omega}=\int\limits_{h_3}\sigma_{xz}^{(3)\omega}\,\mathrm{d}\,z=2\int\limits_{h_3}G_3(T_3)\varepsilon_{xz}^{(3)}\omega^{(3)}\,\mathrm{d}\,z\,,$$

$$Q_{yz}^{(3)0}=\int\limits_{h_3}\sigma_{yz}^{(3)0}\,\mathrm{d}\,z=2\int\limits_{h_3}G_3(T_3)\varepsilon_{yz}^{(3)}\,\mathrm{d}\,z\,,$$

$$Q_{yz}^{(3)\omega}=\int\limits_{h_3}\sigma_{yz}^{(3)\omega}\,\mathrm{d}\,z=2\int\limits_{h_3}G_3(T_3)\varepsilon_{yz}^{(3)}\omega^{(3)}\,\mathrm{d}\,z\,.$$

8. Заключение

Выше были рассмотрена постановка задачи об упругопластическом изгибе трехслойной прямоугольной пластины со сжимаемым заполнителем в терморадиационном поле. Приведены результаты, необходимые для дальнейших расчетов и получения системы уравнений в обобщенных усилиях.

Работа выполнена при финансовой поддержке БРФФИ.

Литература

8. *Зеленая А.С.* Изгиб упругопластической прямоугольной трехслойной пластины со сжимаемым заполнителем в температурном поле / А. С. Зеленая // Теоретическая и прикладная механика. 2019, Вып. 34, с. 172–178.

9. *Старовойтов Э.И., Леоненко Д.В.* Деформирование трехслойного стержня в температурном поле // Механика машин, механизмов и материалов. 2013, № 1 (22), с. 31–35.
10. *Леоненко Д.В., Старовойтов Э.И.* Исследование спектра частот трехслойной цилиндрической оболочки с упругим наполнителем // Механика композиционных материалов и конструкций. 2015, 21, № 2, с. 162–169.
11. *Starovoytov E.I., Leonenko D.V., Suleyman M.* Deformation of a composite plate on an elastic foundation by local loads // Mechanics of Composite Materials. 2007. Т. 43. № 1. С. 75-84.
12. *Старовойтов Э.И., Нестерович А.В.* Неосесимметричное нагружение упругопластической трехслойной пластины в своей плоскости // Журнал Белорусского государственного университета. Математика. Информатика. 2022, № 2, с. 57–69.

НЕОСЕСИММЕТРИЧНОЕ ДЕФОРМИРОВАНИЕ ТРЕХСЛОЙНОЙ КРУГОВОЙ ПЛАСТИНЫ ЛИНЕЙНЫМИ НАГРУЗКАМИ

Нестерович А.В.[1]
[1]*Белорусский государственный университет транспорта, Гомель, Беларусь*
E mail: alina_nest92@bk.ru

Аннотация: *Приведена постановка краевой задачи о неосесимметричном деформировании упругой трехслойной круговой пластины в своей плоскости линейными нагрузками. Физические уравнения состояния связывают напряжения и деформации соотношениями линейной теории упругости. Учтено влияние температуры на упругие характеристики материалов слоев. Уравнения равновесия получены вариационным методом Лагранжа. Решение краевой задачи сведено к нахождению двух искомых функций – радиального и тангенциального перемещений в слоях пластины в виде разложения в ряды Фурье. Аналитическое решение этой системы выписано в конечном виде в случае воздействия радиальной и окружной линейных нагрузок. Численно исследована зависимость радиальных и тангенциальных перемещений при различных значениях температуры.*

Ключевые слова: *трехслойная круговая пластина, неосесимметричное нагружение, радиальная нагрузка, тангенциальная нагрузка, температура.*

1. Введение

Разработка новых методик расчетов и уточнения имеющихся связано с широким использованием многослойных элементов конструкций. Методики решения краевых задач о деформировании слоистых элементов приведены в публикациях [1-5]. В работе [6, 7] рассмотрено деформирование прямоугольной и круглой трёхслойных пластины со сжимаемым заполнителем. В работах [8, 9] рассмотрены решения ряда задач статики и динамики композитных конструкций при силовых воздействиях.

Данная работа отличается от проведенных ранее исследований [10, 11] учетом воздействия линейных нагрузок на неосесимметричное деформирование круглой трехслойной пластины с учетом различных температур.

2. Постановка задачи.

Рассматривается несимметричная по толщине круговая трехслойная пластина, с учетом влияния на неё температуры. Пластина состоит из двух тонких высокопрочных несущих слоев и относительно толстого заполнителя, который служит для образования монолитной конструкции и обеспечения совместной работы всей пластины (рис. 1). Для внешних несущих слоев принимаются гипотезы Кирхгофа, для жесткого заполнителя, воспринимающего нагрузку в тангенциальном направлении, справедлива гипотеза о прямолинейности и несжимаемости деформированной нормали. Предполагается, что на контуре пластины имеется жесткая диафрагма, препятствующая относительному сдвигу слоев. На границах слоев перемещения непрерывны.

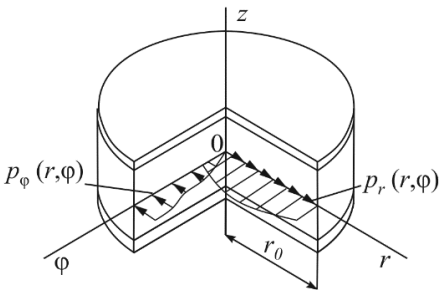

Рисунок 1. – **Расчетная схема круглой трехслойной пластины**

Постановка задачи приводится в полярной системе координат r, φ, которая связана со срединной плоскостью заполнителя. В срединной плоскости заполнителя действует произвольно распределённая неосесимметричная нагрузка, линейно зависящая от радиальной координаты, проекции которой на координатные оси:

$$p_r(x,\varphi) = p_{r1}(1-x)\cos\varphi, \quad p_\varphi(x,\varphi) = p_{\varphi 1}(1-x)\sin\varphi, \tag{1}$$

где $x = r / r_0$ – безразмерная радиальная координата; p_{r1} = const, $p_{\varphi 1}$ = const.

Под действием нагрузки пластина деформируются и в ней возникают радиальные $u_r(r, \varphi)$ и тангенциальные $u_\varphi(r, \varphi)$ перемещения, тогда соответствующие им деформации

$$\varepsilon_{rr} = u_r,_r, \quad \varepsilon_{\varphi\varphi} = \frac{u_\varphi,_\varphi + u_r}{r}, \quad \varepsilon_{r\varphi} = \frac{1}{2r}\left(u_r,_\varphi - u_\varphi + u_\varphi,_r\, r\right), \tag{2}$$

здесь запятая означает дифференцирование по следующей за ней координате.

Напряжения и деформации в пластине связаны известным законом Гука, с учетом температурного воздействия:

$$s_{\alpha\beta}^{(k)} = 2G_k\left(T_k\right)э_{\alpha\beta}^{(k)},$$

$$\sigma^{(k)} = 3K_k\left(T_k\right)\left(\varepsilon^{(k)} - \alpha_0^{(k)}\Delta T_k\right) \quad (\alpha,\beta = r,\varphi,\ k = 1,2,3), \tag{3}$$

где k – номер слоя; $s_{\alpha\beta}^{(k)}$, $э_{\alpha\beta}^{(k)}$, $\sigma^{(k)}$, $\varepsilon^{(k)}$ – девиаторные и шаровые части тензоров напряжений и деформаций; $G_k(T_k)$, $K_k(T_k)$ – сдвиговой и объемный модули упругости материалов, зависящие от температуры; $\alpha_0^{(k)}$ – коэффициент линейного температурного расширения; ΔT_k – приращение температуры в k-м слое.

Внутренние обобщенные усилия в пластине вводятся с помощью компонентов тензора напряжений $\sigma_{\alpha\beta}^{(k)}$:

$$T_{\alpha\beta} \equiv \sum_{k=1}^{3} T_{\alpha\beta}^{(k)} = \sum_{k=1}^{3}\int_{h_k} \sigma_{\alpha\beta}^{(k)}\,\mathrm{d}z\,. \tag{4}$$

Уравнения равновесия рассматриваемой пластины в обобщенных усилиях получены с помощью вариационного принципа Лагранжа:

$$T_{rr},_r + \frac{1}{r}\left(T_{r\varphi},_\varphi + T_{rr} - T_{\varphi\varphi}\right) = -p_r\,,$$

$$T_{r\varphi},_r + \frac{1}{r}\left(T_{\varphi\varphi},_\varphi + 2T_{r\varphi}\right) = -p_\varphi\,. \tag{5}$$

Силовые граничные условия должны выполняться на контуре пластины $r = r_0$:

$$T_{rr} = T_{rr}^0, \quad T_{r\varphi} = T_{r\varphi}^0\,. \tag{6}$$

Выражения внутренних усилий через перемещения выражаются, используя деформации (2) и напряжения (3):

$$T_{rr} = a_1 u_r,_r + \frac{a_2}{r}\left(u_\varphi,_\varphi + u_r\right) - 3\sum_{k=1}^{3}\alpha_0^{(k)}\int_{h_k} K_k\Delta T\,\mathrm{d}z\,,$$

$$T_{\varphi\varphi} = a_2 u_{r,r} + \frac{a_1}{r}\left(u_{\varphi,\varphi} + u_r\right) - 3\sum_{k=1}^{3}\int_{h_k} K_k \alpha_0^{(k)} \Delta T_k \,\mathrm{d}z\,, \tag{7}$$

$$T_{r\varphi} = \frac{a_3}{r}\left(u_{r,\varphi} + r u_{\varphi,r} - u_\varphi\right),$$

где

$$a_1 = \sum_{k=1}^{3}\int_{h_k}\left(K_k(T_k) + \frac{4}{3}G_k(T_k)\right)\mathrm{d}z\,,\quad a_2 = \sum_{k=1}^{3}\int_{h_k}\left(K_k(T_k) - \frac{2}{3}G_k(T_k)\right)\mathrm{d}z\,,\quad a_3 = \sum_{k=1}^{3}\int_{h_k} G_k(T_k)\,\mathrm{d}z\,.$$

Система дифференциальных уравнений равновесия в перемещениях получена подстановкой внутренних усилия (7) в уравнения равновесия (5):

$$u_{r,rr} + \frac{u_{r,r}}{r} - \frac{u_r}{r^2} + \frac{a_3}{a_1 r^2} u_{r,\varphi\varphi} + \frac{a_2 + a_3}{a_1 r} u_{\varphi,\varphi r} - \frac{a_1 + a_3}{a_1 r^2} u_{\varphi,\varphi} = -\frac{p_r}{a_1}\,;$$

$$u_{\varphi,rr} + \frac{u_{\varphi,r}}{r} - \frac{u_\varphi}{r^2} + \frac{a_2 + a_3}{a_3 r} u_{r,r\varphi} + \frac{a_1}{a_3 r^2} u_{\varphi,\varphi\varphi} + \frac{a_1 + a_3}{a_3 r^2} u_{r,\varphi} = -\frac{p_\varphi}{a_3}\,. \tag{8}$$

Добавив к системе дифференциальных уравнений (8) граничные условия в усилиях (6) или перемещениях, получим замкнутую краевую задачу для определения перемещений в трехслойной пластине при неосесимметричном деформировании в своей плоскости.

3. Общее решение краевой задачи

Для решения системы дифференциальных уравнений (8) перемещения и нагрузки представляются в виде разложения в ряды Фурье:

$$u_r(r,\varphi) = u_{r0}(r) + \sum_{n=1}^{\infty}\left[u_{rn}^{(1)}(r)\cos(n\varphi) + u_{rn}^{(2)}(r)\sin(n\varphi)\right],$$

$$u_\varphi(r,\varphi) = u_{\varphi 0}(r) + \sum_{n=1}^{\infty}\left[u_{\varphi n}^{(1)}(r)\cos(n\varphi) + u_{\varphi n}^{(2)}(r)\sin(n\varphi)\right],$$

$$p_r(r,\varphi) = p_{r0}(r) + \sum_{n=1}^{\infty}\left[p_{rn}^{(1)}(r)\cos(n\varphi) + p_{rn}^{(2)}(r)\sin(n\varphi)\right],$$

$$p_\varphi(r,\varphi) = p_{\varphi 0}(r) + \sum_{n=1}^{\infty}\left[p_{\varphi n}^{(1)}(r)\cos(n\varphi) + p_{\varphi n}^{(2)}(r)\sin(n\varphi)\right], \tag{9}$$

где $u_{r0}(r)$, $u_{\varphi 0}(r)$ – перемещения от симметричной части нагрузки, (например, температуры); $u_{rn}^{(1)}(r)$, $u_{rn}^{(2)}(r)$, $u_{\varphi n}^{(1)}(r)$, $u_{\varphi n}^{(2)}(r)$ – амплитудные составляющие асимметричных перемещений; n – номер члена ряда; $p_{r0}(r)$, $p_{\varphi 0}(r)$ – симметричные составляющие нагрузки; $p_{rn}^{(1)}(r)$, $p_{rn}^{(2)}(r)$, $p_{\varphi n}^{(1)}(r)$, $p_{\varphi n}^{(2)}(r)$ – асимметричные составляющие радиальной и тангенциальной внешних нагрузок, которые вычисляются по формулам:

$$p_{rn}^{(1)}(r) = \frac{1}{\pi}\int_0^{2\pi} p_r(r,\varphi)\cos(n\varphi)\,\mathrm{d}\varphi\,,\quad p_{rn}^{(2)}(r) = \frac{1}{\pi}\int_0^{2\pi} p_r(r,\varphi)\sin(n\varphi)\,\mathrm{d}\varphi\,,$$

$$p_{\varphi n}^{(1)}(r) = \frac{1}{\pi}\int_0^{2\pi} p_\varphi(r,\varphi)\cos(n\varphi)\,\mathrm{d}\varphi\,,\quad p_{\varphi n}^{(2)}(r) = \frac{1}{\pi}\int_0^{2\pi} p_\varphi(r,\varphi)\sin(n\varphi)\,\mathrm{d}\varphi\,.$$

После подстановки выражений (9) в систему уравнений (8) и некоторых преобразований получим систему из четырех обыкновенных линейных дифференциальных уравнений для определения искомых амплитудных функций $u_{rn}^{(1)}(r)$, $u_{rn}^{(2)}(r)$, $u_{\varphi n}^{(1)}(r)$, $u_{\varphi n}^{(2)}(r)$:

$$\mathrm{L}_2\left(u_{rn}^{(1)}(r)\right) - \frac{a_3 n^2}{a_1 r^2} u_{rn}^{(1)}(r) + \frac{(a_2 + a_3)n}{a_1 r} u_{\varphi n}^{(2)}{}_{,r}(r) - \frac{(a_1 + a_3)n}{a_1 r^2} u_{\varphi n}^{(2)}(r) = -\frac{1}{a_1} p_{rn}^{(1)}(r),$$

$$\mathrm{L}_2\left(u_{\varphi n}^{(2)}(r)\right)-\frac{a_1 n^2}{a_3 r^2}u_{\varphi n}^{(2)}(r)-\frac{(a_2+a_3)n}{a_3 r}u_{rn}^{(1)},_r(r)-\frac{(a_1+a_3)n}{a_3 r^2}u_{rn}^{(1)}(r)=-\frac{1}{a_3}p_{\varphi n}^{(2)}(r),$$

$$\mathrm{L}_2\left(u_{rn}^{(2)}(r)\right)-\frac{a_3 n^2}{a_1 r^2}u_{rn}^{(2)}(r)-\frac{(a_2+a_3)n}{a_1 r}u_{\varphi n}^{(1)},_r(r)+\frac{(a_1+a_3)n}{a_1 r^2}u_{\varphi n}^{(1)}(r)=-\frac{1}{a_1}p_{rn}^{(2)}(r),$$

$$\mathrm{L}_2\left(u_{\varphi n}^{(1)}(r)\right)-\frac{a_1 n^2}{a_3 r^2}u_{\varphi n}^{(1)}(r)+\frac{(a_2+a_3)n}{a_3 r}u_{rn}^{(2)},_r(r)+\frac{(a_1+a_3)n}{a_3 r^2}u_{rn}^{(2)}(r)=-\frac{1}{a_3}p_{\varphi n}^{(1)}(r). \qquad (10)$$

4. Воздействие линейных нагрузок

Коэффициенты разложения нагрузки (1) в ряды (9) в данном случае будут иметь вид

$$p_{r1}^{(1)}(x)=p_{r1}(1-x),\ p_{\varphi 1}^{(2)}(x)=p_{\varphi 1}(1-x),$$

и система уравнений равновесия (10) при n = 1 примет вид

$$\mathrm{L}_2\left(u_{r1}^{(1)}(x)\right)-\frac{a_3}{a_1 x^2}u_{r1}^{(1)}(x)+\frac{a_2+a_3}{a_1 x}u_{\varphi 1}^{(2)},_x(x)-\frac{a_1+a_3}{a_1 x^2}u_{\varphi 1}^{(2)}(x)=-\frac{r_0^2}{a_1}p_{r1}(1-x),$$

$$\mathrm{L}_2\left(u_{\varphi 1}^{(2)}(x)\right)-\frac{a_1}{a_3 x^2}u_{\varphi 1}^{(2)}(x)-\frac{a_2+a_3}{a_3 x}u_{r1}^{(1)},_x(x)-\frac{a_1+a_3}{a_3 x^2}u_{r1}^{(1)}(x)=-\frac{r_0^2}{a_3}p_{\varphi 1}(1-x),$$

$$\mathrm{L}_2\left(u_{r1}^{(2)}(x)\right)-\frac{a_3}{a_1 x^2}u_{r1}^{(2)}(x)-\frac{a_2+a_3}{a_1 x}u_{\varphi 1}^{(1)},_x(x)+\frac{a_1+a_3}{a_1 x^2}u_{\varphi 1}^{(1)}(x)=0,$$

$$\mathrm{L}_2\left(u_{\varphi 1}^{(1)}(x)\right)-\frac{a_1}{a_3 x^2}u_{\varphi 1}^{(1)}(x)+\frac{a_2+a_3}{a_3 x}u_{r1}^{(2)},_x(x)+\frac{a_1+a_3}{a_3 x^2}u_{r1}^{(2)}(x)=0. \qquad (11)$$

После решения системы (11) с учетом ограниченности перемещений в центре пластины при однородных начальных условиях с учетом граничного условия (жёсткое защемление контура платины) полные перемещения (9) будут

$$u_r(x,\varphi)=\frac{1}{a_1(a_1-a_2)}\left[\left(\frac{1}{32}\left(\left(19a_1^2-14a_1a_2-a_2^2\right)p_{r1}-\left(13a_1^2-18a_1a_2+a_2^2\right)p_{\varphi 1}\right)+\right.\right.$$
$$\left.+\frac{a_1-3a_2}{30}\left(2(2a_1-a_2)p_{r1}+(5a_1-a_2)p_{\varphi 1}\right)\right)\frac{1}{3a_1-a_2}\left(1-x^2\right)-$$
$$\left.-\frac{2}{45}\left((3a_1-4a_2)p_{r1}-2a_2p_{\varphi 1}\right)\left(1-x^3\right)-\frac{1}{16}(a_1-3a_2)\left(p_{r1}+p_{\varphi 1}\right)x^2\ln x\right]r_0^2\cos\varphi,$$

$$u_\varphi(x,\varphi)=\frac{1}{a_1(a_1-a_2)}\left[\left(\frac{1}{32}\left(\left(-19a_1^2+14a_1a_2+a_2^2\right)p_{r1}+\left(13a_1^2-18a_1a_2+a_2^2\right)p_{\varphi 1}\right)+\right.\right.$$
$$\left.+\frac{5a_1+a_2}{30}\left(2(2a_1-a_2)p_{r1}+(5a_1-a_2)p_{\varphi 1}\right)\right)\frac{1}{3a_1-a_2}\left(1-x^2\right)-$$
$$\left.-\frac{1}{45}\left(2(3a_1+a_2)p_{r1}+(15a_1+a_2)p_{\varphi 1}\right)\left(1-x^3\right)-\frac{5a_1+a_2}{16}\left(p_{r1}+p_{\varphi 1}\right)x^2\ln x\right]r_0^2\sin\varphi. \qquad (12)$$

5. Численные результаты

Численная аппрабация получена для трехслойной пластины, выполненной из материалов Д16-Т–фторопласт-4–Д16-Т, при неосесимметричных радиальной и окружной составляющих нагрузки (1) с максимальными значениями p_{r1} = 10 МПа, $p_{\varphi 1}$ = 10 МПа. Все перемещения и линейные размеры пластины отнесены к ее радиусу r_0. Относительные толщины слоев $h_1=h_2=0,02$, $h_3=0,4$; температура принималась однородной.

Рисунок 2 показывает изменение радиальных перемещений $u_r(x, \varphi)$ вдоль радиуса пластины при различных значениях угловой координаты (T = 293 К). Положительный знак радиальных перемещений показывает движение точек вдоль радиуса от центра,

отрицательный – к центру. Экстремальные значения радиальные перемещения достигают по модулю в центре пластины.

Изменение окружных перемещений $u_\varphi(x, \varphi)$ вдоль радиуса пластины (T = 293 К) при различных значениях угловой координаты, иллюстрирует рисунок 3. Максимальные значения окружных перемещений совпадают по модулю с радиальными перемещениями и достигаются в центре пластины. Точки верхней части пластины перемещаются по часовой стрелке, т.к. соответствующие окружные перемещения отрицательные, нижней – против часовой стрелки. В сечении с координатой x = 0,28 окружные перемещения отсутствуют и изменяют направления.

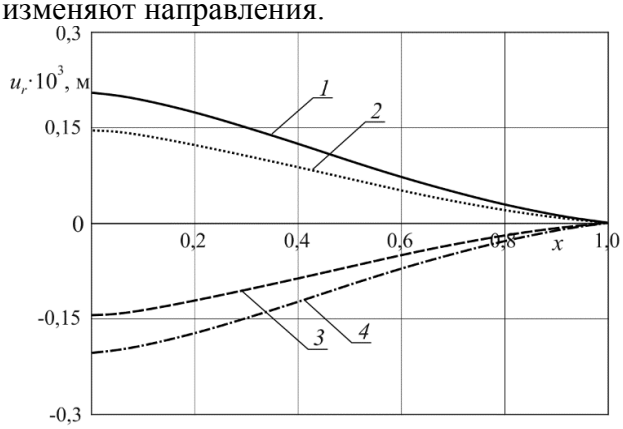

1 – φ = 0, 2π; *2* – φ = π/4, 7π/4; *3* – φ = 3π/4, 5π/4; *4* – φ = π

Рисунок 2. – **Изменение радиальных перемещений $u_r(x, \varphi)$ (T = 293 К)**

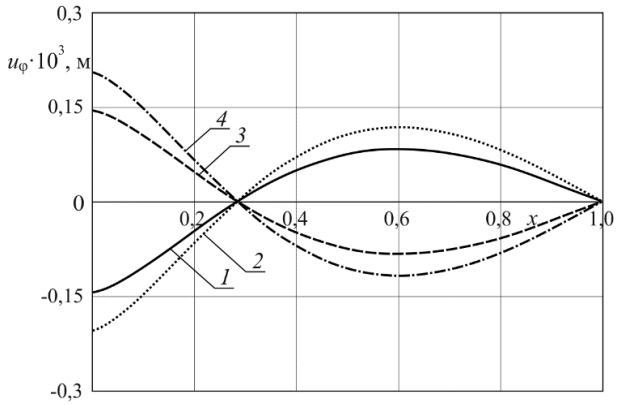

1 – φ = π/4, 3π/4; *2* – φ = π/2; *3* – φ = 5π/4, 7π/4; *4* – φ = 3π/2

Рисунок 3. – **Изменение окружных перемещений $u_\varphi(x, \varphi)$ (T = 293 К)**

Рисунок 4 иллюстрирует изменение радиальных $u_r(x, \varphi)$ – (*а*) и окружных $u_\varphi(x, \varphi)$ – (*б*) перемещений в зависимости от угловой координаты φ в центре пластины (x = 0) при различных температурах. Экстремальные значения радиальных перемещений соответствуют экстремумам используемых тригонометрических функций. При повышенных температурах максимальные перемещения, увеличиваются примерно на 8,7 % и 17,4 % соответственно.

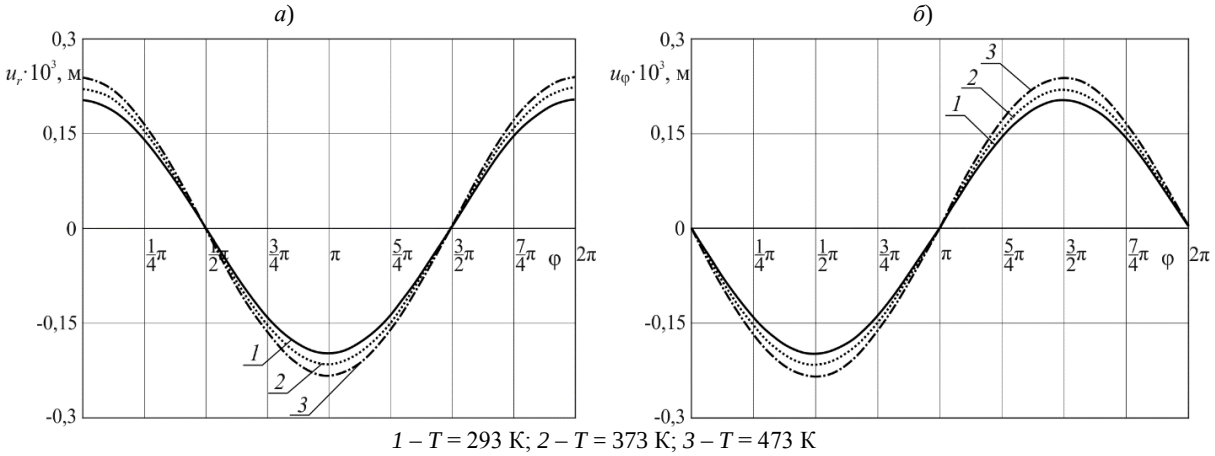

1 – T = 293 К; *2* – T = 373 К; *3* – T = 473 К

Рисунок 4. – **Изменение термосиловых радиальных $u_r(x, \varphi)$ – (*а*) и окружных $u_\varphi(x, \varphi)$ – (*б*) перемещений в центре пластины**

6. Заключение

Предложенная модель деформирования трехслойной круговой пластины при неосесимметричных линейных нагрузках в ее плоскости позволяет проводить анализ напряженно-деформированного состояния при различных температурах. Численная апробация показала, что при увеличении температур перемещения возрастают до 17,4 %.

7. Благодарности

Работа выполнена при финансовой поддержке Белорусского республиканского Фонда фундаментальных исследований.

Литература

13. *Zhuravkov M.A., Lyu Yongtao, Starovoitov E.I.* Mechanics of Solid Deformable Body / Singapore, Springer, 2023, 317 p. https://doi.org/10.1007/978-981-19-8410-5.
14. *Абдусаттаров А., Старовойтов Э.И., Рузиева Н.Б.* Деформирование и повреждаемость упругопластических элементов конструкций при циклических нагружениях / Ташкент, «IDEAL PRESS», 2023, 381 с.
15. *Федоренко А.Н., Федулов Б.Н., Ломакин Е.В.* Задача потери устойчивости тонкостенных конструкций из композиционных материалов, свойства которых зависят от типа нагружения // Вестник Пермского национального исследовательского политехнического университета. Механика. 2019, № 3, с. 104-111. https://doi.org/10.15593/perm.mech/2019.3.11.
16. *Starovoitov E.I., Leonenko D.V.* Deformation of an Elastic Circular Sandwich Plate in a Neutron Flow // Mechanics of Composite Materials. 2022, vol. 57, No. 6, pp. 813-824. https://doi.org/10.1007/s11029-022-10001-w.
17. *Анарова Ш.А., Исмоилов Ш.М., Шокиров Д.А.* Математическая модель деформации трёхслойных стержней при пространственных нагрузках // Проблемы вычислительной и прикладной математики. 2023, № 5(52), с. 56-82.
18. *Леоненко Д.В., Зеленая А.С.* Упругопластический изгиб прямоугольной трехслойной пластины со сжимаемым заполнителем // Теоретическая и прикладная механика. 2018, Вып. 33, с. 65-1.
19. *Starovoitov E.I., Zakharchuk Y.V., Kuznetsova E.L.* Elastic circular sandwich plate with compressible filler under axially symmetrical thermal force load // Journal of the Balkan Tribological Association. 2021, Vol. 27, No. 2, pp. 175-188.
20. *Leonenko D.V., Markova M.V.* Oscillations of a circular three-layer plate under external linear in time load. // Journal of the Belarusian State University. Mathematics and Informatics. 2023, Vol. 1, pp. 49–63. https://doi.org/10.33581/2520-6508-2023-1-49-63.
21. *Козел А.Г.* Об аналитическом решении задачи для шарнирно опертой трехслойной пластины на основании Пастернака // Механика композиционных материалов и конструкций. 2023, Т. 29, № 4, с. 520-537. https://doi.org/10.33113/mkmk.ras.2023.29.04.07.
22. *Starovoitov E.I., Nesterovich A.V.* The non-axisymmetric loading of an elastoplastic three-layer plate in its plane. // Journal of the Belarusian State University. Mathematics and Informatics. 2022, Vol. 2, pp. 57–69. https://doi.org/10.33581/2520-6508-2022-2-57-69.
23. *Starovoitov E.I., Zhuravkov M.A., Nesterovich A.V.* Thermo force loading of an elastic-plastic a three-layer plate. // Journal of the Belarusian State University. Mathematics and Informatics. 2023, Vol. 3, pp. 42–52.

РАСПРОСТРАНЕНИЕ ПРОДОЛЬНЫХ МЕХАНИЧЕСКИХ ВОЛН В УПРУГОЙ ОБЛАСТИ ТРЕУГОЛЬНОЙ ФОРМЫ

Нугужинов Ж.С.[1,2], Ахмедиев С.К.[2], Бекетова М.С.[2], Койшыбай Ж.А.[1,2]

[1]Казахстанский многопрофильный институт реконструкции и развития (КазМИРР), Караганда, Казахстан

[2]НАО «Карагандинский технический университет им. А.С. Сагинова», Караганда, Казахстан

E-mail: kazmirr@mail.ru

Аннотация. *В работе исследованы волновые процессы в виде продольных механических волн, возникающих в условиях внешнего динамического воздействия от удаленных промышленных взрывов. Разработаны теоретические основы для исследования перемещений частиц твердого тела в виде пластин неправильной треугольной формы. При этом получены соответствующие зависимости основных параметров деформированного состояния среды на основе численного метода конечных разностей для упругой области с ортотропными свойствами материала.*

Ключевые слова: *волновые процессы и уравнения, двумерная сетка из разносторонних треугольников, динамические воздействия, сейсмика, скорости деформирования твердого тела, скорость распространения механических волн.*

1. Введение

При значительных динамических воздействиях (сейсмические удары, импульсы, удаленные промышленные взрывы и т.д.) в упругой среде различного очертания возникают механические продольные волны, образующие относительно осей и поверхностей рассматриваемых конструкций поперечные перемещения, волновые параметры которых зависят также и от координаты времени «t».

С точки зрения механики деформируемого твердого тела исследование физико-механических параметров этих волн представляет достаточно сложную техническую

проблему, связанную с интегрированием неоднородных дифференциальных уравнений второго порядка с соответствующими начальными и граничными условиями. В этих случаях наряду с точными аналитическими методами рационально использование и известных численных методов, таких как метод конечных разностей (МКР).

2. Методы

Объектом исследования данной работы являются волновые процессы в тонких пластинах в виде неправильного треугольника, размеры и форма которого определяется следующими параметрами (рис. 1): а* – длина основания треугольника; α – угол наклона левой (боковой) кромки к основанию; β – тоже, правой кромки [3].

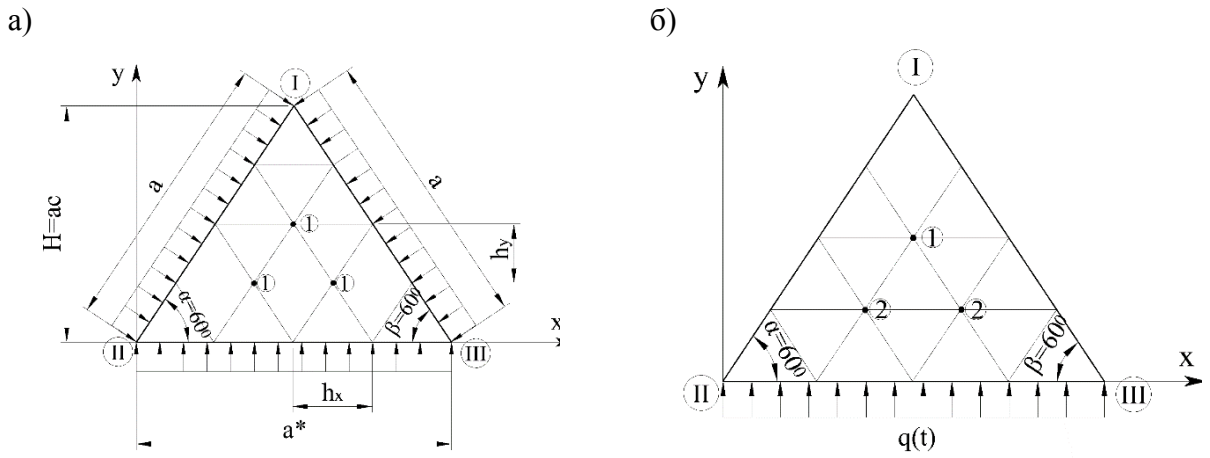

Рисунок 1. - **Расчетные схемы равносторонней треугольной пластины при двух вариантах (а, б) загружения динамической нагрузкой в срединной плоскости**

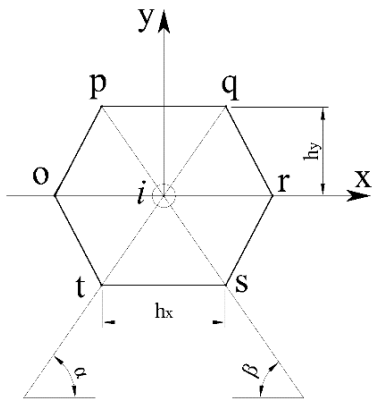

Рисунок 2. - **Фрагмент сетки из разносторонних треугольников**

Исходное дифференциальное уравнение распространения продольных волн в упругих тонких пластинах (двумерная волновая задача) имеет вид [1]:

$$\frac{\partial^2 u}{\partial t^2} = \left(\frac{\partial^2 u}{\partial x^2} + \frac{\partial^2 u}{\partial y^2} \right) + f(x, y, t), \qquad (1)$$

где u=u(x, y, t) – поперечные перемещения вдоль координат x, y срединной поверхности пластины в произвольный момент времени «t».

а – скорость распространения механических волн в упругой среде твердого тела (зависит от вида материала пластины)

Для рассматриваемых пластин (рис. 1) примем их материал в виде стали; тогда:

$$a = \sqrt{\frac{E}{\rho}}, \qquad (2)$$

где $E=2{,}1\cdot 10^{-10}$ кг/м^2 – модуль упругости стали; $\rho = \frac{\gamma}{g} = \frac{7800}{10} = 780 \frac{кгс^2}{м^4}$ – плотность материала (γ – объемный вес стали); тогда по (2) имеем:

$$a = \sqrt{\frac{2{,}1\cdot 10^{10}}{780}} = 5189; \qquad \boxed{a = 5189 м/с} \qquad (3)$$

f(x, y, t) – ускорение, зависящее от внешней динамической нагрузки (например сейсмического воздействия).

В качестве внешней динамической нагрузки $Q(t)$ примем уравнение ударной волны на торцы треугольных пластин площадью ($S=h\cdot a^*$) (h – толщина пластины; a^* – длина основания треугольника). В нашем исследовании примем следующие исходные данные: a^*=6м; h=0,03м;

$$Q(t) = 2{,}782\cdot 10^4 e^{-38{,}18t} \tag{4}$$

– закон изменения во времени давления ударной волны от удаленного взрыва мощностью тротила (1т), на расстоянии (100м) от места расположения конструкции.

Закономерность Q(t) получена на основе исследований [2,5].

Выражение для f(x, y, t) определим по следующей формуле:

$$f(x,y,t) = \frac{Q(t)h}{\rho\cdot S} = \frac{Q(t)}{\rho\cdot a^*} \tag{5}$$

По (5) имеем в нашем случае [с учетом (4)]:

$$f(x,y,t) = \left(\frac{1}{780\cdot 6}\right)(7{,}282\cdot 10^4)e^{-38{,}18t} = 15{,}56e^{-38{,}18t} \text{ (м/с}^2\text{)}$$

$$\boxed{f(x,y,t) = 15{,}56e^{-38{,}18t}} \tag{6}$$

Волновое уравнение (1) должно сопровождаться соответствующими начальными и граничными (краевыми) условиями (рис. 1)[1].

а) Начальные условия (при t=0):

$$u(x_i, y_i, t) = u_{i,0}(t) = 0;\ \left(\frac{\partial u}{\partial t}\right) i = \upsilon_{i,0} \tag{7}$$

($\upsilon_{i,o}$ – начальная скорость упругих волновых деформаций).

б) Граничные условия (кромки треугольных пластин оперты):

$$u(x_i, y_i, t) = u_{i,0}(t) = 0; \tag{8}$$

Для реализации уравнения (1) с начальными и граничными (7,8) применим метод конечных разностей (МКР) с использованием сетки из разносторонних треугольников [3]; Параметры сетки примем следующие для иллюстрации теории МКР применительно к пластинам на рис.1);

N=4 – число делений кромок пластины; для равносторонней треугольной пластины ($\alpha=\beta=60^0$) имеем [3]: $\tau=t_p/M$ – шаг по времени (t_p – расчетное время дин-го воздействия; M – число шагов).

hx=a/N=6/4=1,5м; hy=ac/N=1,3м;

$$A = \frac{\sin\beta\cos\alpha}{\sin(\alpha+\beta)} = 0{,}5; \quad B = \frac{\sin\alpha\cos\beta}{\sin(\alpha+\beta)} = 0{,}5; \tag{9}$$

$$C = \frac{\sin\alpha\cos\beta}{\sin(\alpha+\beta)} = 0{,}5; \quad u = C^2 - AB = -\frac{\sin\alpha\sin\beta\cos(\alpha+\beta)}{\sin^2(\alpha+\beta)} = 0{,}5.$$

При записи конечно-разностного аналога уравнения (1) применим явную разностную схему [4] [j – текущий временной слой, (j-1) – предыдущий слой; (j+1) – последующий временной слой]; тогда для i-го узла сетки (рис. 1) имеем:

$$\begin{aligned}(u_i^{j-1} - 2u_i^j + u_i^{j+1}) &= \tau^2 f(x,y,t) + \\ &+ \frac{\tau^2 a^2}{hy^2}\left[-2(u+1)u_i^j + u(u_o^j + u_r^j) + A(u_p^j + u_s^j) + B(u_q^j + u_t^j)\right]\end{aligned} \tag{10}$$

Из выражения (10) выделим формулу для определения перемещения (u_i^{j+1}):

$$u_i^{j+1} = 2u_i^j - u_i^{j-1} + \tau^2 f(x,y,t) +$$
$$+\frac{\tau^2 a^2}{hy^2}\left[-2(u+1)u_i^j + u(u_o^j + u_r^j) + A(u_p^j + u_s^j) + B(u_q^j + u_t^j)\right]. \quad (11)$$

Также в конечных разностях запишем начальное условие (7):

$$\frac{u_i^{j-1} - u_i^j}{\tau} = \upsilon_{o,i}, \text{ отсюда: } \boxed{u_i^{j-1} = u_i^j + \tau\upsilon_{o,i}} \quad (12)$$

При $\upsilon_{o,i}$=0, из (12) имеем: $\boxed{u_i^{j-1} = u_i^j}$ (13)

I) Рассмотрим 1-й вариант загружения треугольной пластины внешней динамической нагрузкой q(t) (рис. 1, а).

При ($\alpha=\beta=60^0$) [с учетом выражений (3,6,13)] получим [(i=1) – число внутренних расчетных узлов сетки (с учетом симметрии относительно трех медиан равностороннего треугольника)].

$$\boxed{u_i^{j+1} = u_i^j\left[1 - 31{,}88\cdot 10^6(\tau^2)\right] + (\tau^2)\cdot 15{,}56\cdot e^{-38{,}18t}} \quad (14)$$

На рис. 3 и 4 приведены графические зависимости u_1=f(t) и υ_1(t).

Дальнейший расчет по выражению (14) выполним в табличной форме (табл. 1).

По данным табл. 1 вычислим значения механических деформаций и напряжений в конечных разностях:

а) деформации (i-й узел, рис. 2):

$$\xi_x = \frac{\partial u}{\partial x} = \frac{u_2 - u_o}{2hx}; \quad \xi_y = \frac{\partial u}{\partial y} = \frac{1}{2hy}\left[A(u_p^{t*} - u_s^{t*}) + B(u_q^{t*} - u_t^{t*})\right]; \quad (15)$$

u^{t*} – перемещение, соответствующие тому времени нагружения конструкции $t*$, при котором график скорости деформации проходит через нулевые значения абсциссы; по табл. 1: $t*$=0,0015с; u^{t*}=46,5635·10^{-8}(м).

Тогда по (15) получим (ξ^1_{x1} – значение у вершины треугольника (I) => рис. 1, а)
ξ^2_{x1} – то же у вершины II; ξ^3_{x1} – то же у вершины III.

$$\xi^1_{x1} = \frac{0-0}{2(1,5)} = \frac{0}{3,0} = 0,0; \quad \xi^2_{x1} = \xi^3_{x1} = \frac{u_1^* - 0}{3,0} = 15,52\cdot 10^{-8};$$

$$\xi^1_{y1} = \frac{1}{2(1,3)}\left[0,5(-u_1^*) + 0,5(-u_1^*)\right] = -17,91\cdot 10^{-8};$$

$$\xi^2_{y1} = \xi^3_{y1} = \frac{1}{2hy}\left[0,5(0-0) + 0,5(u_1 - 0)\right] = 8,9545\cdot 10^{-8};$$

б) Напряжение

$$\sigma^1_{x1} = E\cdot\xi^1_{x1} = 0,0; \quad \sigma^2_{x1} = \sigma^3_{x1} = 2,1\cdot 10^6\cdot 15,52\cdot 10^{-8} = 0,33 кг/см^2 < (\sigma_{adm}=1600 кг/см^2)$$

$$\sigma^1_{y1} = E\cdot\xi^1_{y1} = -2,1\cdot 10^6\cdot 17,91(10^{-8}) = -0,376 кг/см^2$$

$$\sigma^2_{y1} = \sigma^3_{y1} = (E\cdot\xi^2_{y1} = E\xi^3_{y1} = 2,1\cdot 10^6\cdot 8,9545\cdot 10^{-8} = 0,188 кг/см^2.$$

Налицо, большое недонапряжение при распространении продольных волн по поверхности пластин.

Таблица 1.

Номер шага J	Время, t	$e^{-38,18t}$	$e^{-38,18t}$ $(15,56 \cdot e \cdot 10^8)$	Шаг, τ	D	1+D	$u_1^j(10^8)$	$u_1^j(1+D)$ (10^8)	$u_1^{j+1}(10^8)$	Скорость диформации υ_1^j (10^4)
1	0,0	1,0	15,52	0,001	(-0,3188)= const	(0,6812)=const	0,0	0,0	15,56	-7,03
2	0,001	0,9962	15,50				15,56	10,399	26,099	-7,12
3	0,002	0,9924	15,44				26,099	17,79	33,219	-4,793
4	0,003	0,9886	15,383				33,219	22,629	38,012	-3,205
5	0,004	0,9848	15,323				38,012	25,894	41,217	-2,126
6	0,005	0,9811	15,266				41,217	28,077	43,343	-1,399
7	0,006	0,9774	15,208				43,343	29,525	44,733	-0,889
8	0,007	0,9736	15,15				44,733	30,472	45,622	-0,549
9	0,008	0,9699	15,092				45,622	37,078	46,17	-0,315
10	0,009	0,9662	15,034				46,17	31,451	46,485	-0,157
11	0,001	0,9625	14,97	0,001			46,485	31,666	46,642	0,1544
12	0,002	0,9265	14,416				46,642	31,773	46,189	0,0846
13	0,003	0,8918	13,876				46,189	31,464	45,34	+0,11
14	0,004	0,8584	13,356				46,340	30,866	44,242	0,1245
15	0,005	0,8262	12,86				44,242	30,137	42,997	0,1337
16	0,006	0,7952	12,37				42,977	29,290	41,66	

Построим графики изменения перемещений $[u_1(t)]=[\upsilon_1(t)]$ (по данным табл. 2, а) (рис. 2)

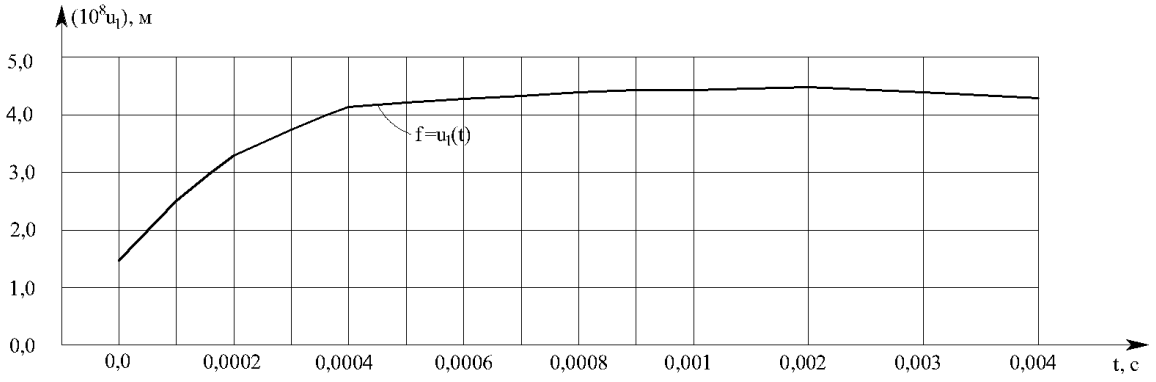

Рисунок 3. - **Изменение перемещений (u_1) от времени (t)**

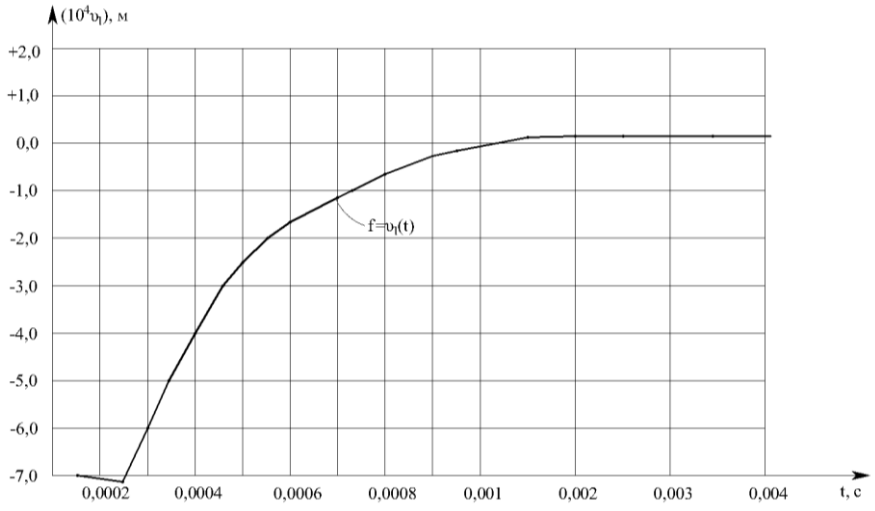

Рисунок 4. - **Изменение скорости деформаций (υ_1) от времени (t)**

II. Рассмотрим 2-й вариант загружения иреугольной равносторонней пластины (рис. 1, б) динамической нагрузкой q(t): в этом случае число внутренних расчетных узлов сетки будет два (i=1,2) (симметрия только по одной медиане, опущенной на основание треугольника).

По типу (11) запишем два разрешающих конечно-разностных уравнений:

а) для узла (i=1) (рис. 1, б)

$(u_i^{j-1} - 2u_1 - u_i^{j+1} = \tau^2 f(x,y,t) + \dfrac{\tau^2 a^2}{hy^2}\left[-2(u+1)u_i^j + Au_2^j + Bu_2^j\right]$, или [по аналогии с (14)]:

$(U_i^{j+1}) = U_i^j + \tau^2(15,56 \cdot e^{-38,18t}) + \tau^2\left(15,94 \cdot 10^6\right) \cdot \left(-3U_1^j + U_2^j\right)$, или (после приведения подобных членов):

$$(U_i^{j+1}) = U_i^j\left[1 - 47,82 \cdot 10^6\left(\tau^2\right)\right] + U_2^j\left[15,94\left(\tau^2\right)\right] + \tau^2\left(15,56 \cdot e^{-38,18t}\right); \quad (16)$$

б) для узла i=2 (рис. 1, б):

$(u_2^{j-1} - 2u_2^j + u_2^{j+1} = \tau^2 f(x,y,t) + \dfrac{\tau^2 a^2}{hy^2}\left[-2(u+2)u_2^j + u(u_2^j) + Bu_1^j\right]$, или

$$(u_2^{j+1}) = u_1^j\left[7,963\left(\tau^2\right)\right] + u_2^j\left[1 - 39,85 \cdot 10^6\left(\tau^2\right)\right] + \left(\tau^2\right)(15,56 \cdot e^{-38,18t}); \quad (17)$$

Уравнения (16,17) надо решать совместно на каждом шаге времени (τ).

Дальнейший расчет выполнен в табличной форме (табл. 2).

Таблица 2.

Шаг по времени	Параметры вершин	$e^{-38,18t}$	$e^{-38,18t}$ $(15,56 \cdot e \cdot 10^8)$	Перемещение (U_2^j), м						Перемещение (U_2^j), м					
				D	1+D	$u_1^j(10^8)$	$u_1^j(1+D)$ (10^8)	$u_1^{j+1}(10^8)$	$u_1^j(10^4)$ (м/с)	D	1+D	$u_1^j(10^8)$	$u_1^j(1+D)$ (10^8)	$u_1^{j+1}(10^8)$	$u_1^j(10^4)$ (м/с)
1	0,0	1,0	15,56	(-0,4782)=const	(-0,5218)=const		0,0	15,56	-8,06	(-0,3985)=const	(-0,6015)=const	0,0	0,0	15,56	-9,3
2	0,0001	0,9962	15,50			15,56	8,1192	23,62	-4,145			15,56	9,359	24,859	-5,533
3	0,0002	0,9924	15,44			23,62	12,325	27,765	-2,106			24,86	14,952	30,392	-3,272
4	0,0003	0,9886	15,383			27,765	14,488	29,871	-1,039			30,392	18,281	33,664	-1,908
5	0,0004	0,9848	15,323			29,871	15,587	30,91				33,664	20,249	35,572	

									-0,485						-1,091
6	0,0005	0,9811	15,266			30,91	16,129	31,395				35,572	21,397	36,663	
									-0,505						-0,598
7	0,0006	0,9774	15,208			31,395	16,382	31,90				36,663	22,053	37,261	
									0,105						-0,301
8	0,0007	0,9736	15,15			31,90	16,645	31,795				37,261	22,412	37,562	
									0,112						-0,124
9	0,0008	0,9699	15,092			31,795	16,591	31,683				37,562	22,594	37,686	
									0,117						-0,016
10	0,0009	0,9692	15,034			31,683	16,532	31,566				37,686	22,668	37,702	
									0,0176						0,005
11	0,001	0,9625	14,976			31,566	16,471	31,447				37,702	22,678	37,654	
									0,062						0,0589
12	0,002	0,9265	14,416			31,447	16,407	30,825				37,654	22,649	37,065	
									0,0865						0,0894
13	0,003	0,8918	13,876			30,825	16,084	29,960				37,065	22,295	36,171	
									0,097						1,058
14	0,004	0,8584	13,356			29,96	15,633	28,989				36,171	21,757	35,113	
									1,003						1,133
15	0,005	0,8262	12,86			28,989	15,126	27,986				35,113	21,12	33,98	
									1,008						1,1711
16	0,006	0,7952	12,37			27,986	14,603	26,978				33,98	20,439	33,809	

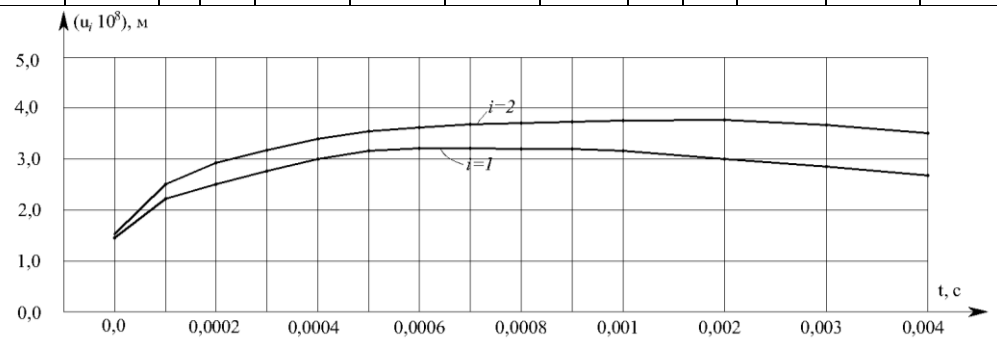

Рисунок 5. - **Изменение перемещений [** $u_i^j\left(i=1,2\right)$ **]**

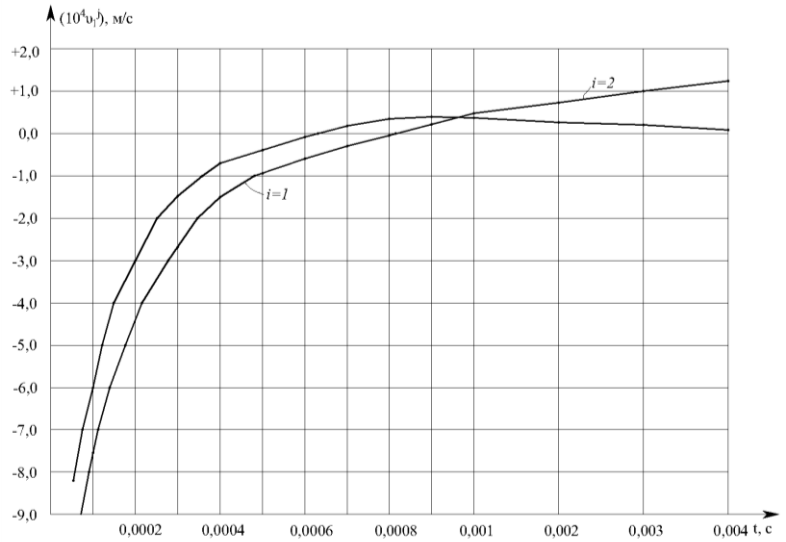

Рисунок 6. - **Изменение скорости деформаций** $\upsilon_i^j\left(i=1,2\right)$

На рис. 5 и 6 приведены графические зависимости $\left[u_i = f(t)\right]$ и $\left[\upsilon_i = f(t)(i=1,2)\right]$.

Вычислим деформации и напряжения в расчетных узлах сетки (i=1,2) для 2-й схемы загружения треугольной пластины (рис. 1, б) по данным табл. 2 и рис. 5,6.

По рис. 6 установим расчетные значения искомых перемещений (u_1, u_2) в тот момент времени (t_0), когда скорости их деформирования (υ_1, υ_2) будут равны между собой (это точка пересечения графиков (υ_1, υ_2) на рис. 6): t*=0,00095с; по данным (таблицы 2) определяем соответствующее значение: $u_1(t^*)=31{,}5065\cdot 10^{-8}$(м); $u_2(t^*)=37{,}678\cdot 10^{-8}$(м).

а) Вычислим деформации в узлах сетки (1,2) (рис. 1.б):

$$\xi_{x1} = \frac{\partial u_1}{\partial x} = \frac{0-0}{2(1,5)} = 0,0; \quad \xi_{x2} = \frac{u_2 - 0}{3,0} = 12,5593\cdot 10^{-8};$$

$$\xi_{y1} = \frac{\partial u_1}{\partial y} = \frac{1}{2hy}\left[A\left(u_p - u_s\right) + B\left(u_q - u_t\right)\right] = \frac{1}{2,6}\left[0,5\left(0-u_2\right) + 0,5\left(0-u_2\right)\right] = -14,4915\cdot 10^{-8};$$

$$\xi_{y2} = \frac{1}{2,6}\left[0,5\left(0-0\right) + 0,5\left(u_1 - 0\right)\right] = 6,0589\cdot 10^{-8};$$

б) Вычислим напряжения

$$\sigma_{x1} = E\cdot\xi_{x1} = 2,1\cdot 10^6\cdot 0,0 = 0,0;$$

$$\sigma_{x2} = E\cdot\xi_{x2} = 2,1\cdot 10^6\cdot 12,5593\cdot 10^{-8} = 0,125\,\text{кг/см}^2 < (\sigma_{adm}=1600\,кг/см^2)$$

$$\sigma_{y1} = E\cdot\xi_{y1} = -2,1\cdot 10^6\cdot(14,4915\cdot 10^{-8}) = -0,304\,кг/см^2$$

$$\sigma_{y1} = (\xi_2 = 2,1\cdot 10^6(6,0589\cdot 10^{-8}) = 0,127\,кг/см^2.$$

Налицо, очень малые величины напряжений.

3. Выводы и заключение

В данной работе выполнено теоретическое исследование распространения продольных механических волн в упругой среде (пластины в неправильной треугольной форме ($\alpha\neq\beta$)) численным методом конечных разностей (МКР) с использованием сетки из разносторонних треугольников, которая наилучшим способом соответствует наличию косых кромок треугольника, при этом:

1. Получены основные конечно-разностные уравнения для определения поперечных перемещении, в произвольный момент времени возникающих при распространении продольных механических волн по срединной поверхности треугольных пластин; применена явная разностная схема.
2. В качестве внешнего динамического нагружения, действующего в плоскости пластины, принято условное давление, возникающего от ударной волны удаленного промышленного взрыва тротила мощностью 1т (на расстоянии 100 м)
3. На основе МКР разработан оригинальный алгоритм расчета, позволяющий получать дискретно-численные величины перемещении на всем временном пространстве, начиная с начального временного слоя с последующим аналитическим переходом в последующие временные слои динамического нагружения.
4. В качестве примера, иллюстрирующего предложенного технические разработки, рассмотрен волновой процесс в равносторонней ($\alpha=\beta=60^0$) треугольной пластине при двух вариантах нагружения (рис.): 1) по всем трем кромкам; 2) лишь по нижней кромке (основанию треугольника); на основании данных «безмашинного» расчета при малой густоте» сетки (N=4) в таблицах 1,2 приведены значения перемещений (u_i) и скоростей деформирования (υ_i) для различных значении времени «t» при двух разных шагах времени (τ_1=0,0001 с) (τ_2=0,001,с); на рис. 3 – 6 приведены графические зависимости [u_i=f(t) и υ_i(t)].
5. На основе анализа полученных результатов исследования (табл. 1,2; рис. 3…6) установленно следующее:

а) с увеличением параметра времени (t) значения (u_i) и (υ_i) монотонно возрастают и приобретают стабильность при шагах времени j>6.

б) скорость деформирования (υ_i) меняются от отрицательных значении (сжатие) (при $\tau \leq 8$) до положительных значений (растяжение) (при $\tau > 8$);

в) при 2-м варианте загружения перемещения (u_i) в узле (i=2) больше по значениям, чем в узле (i=1).

6. Примененная в данном исследовании явная разностная схема характеризуется большим объемом трудоемкости расчета (из-за необходимости принятия малого шага времени «τ»), т. е. для ускорения процесса сходимости результатов целесообразным является применение иной расчетной схемы Кринка-Нильсона (это задача для дальнейших исследований).

7. Предложенные в данной статье теоретические положения и прикладные результаты по изучению волновых процессов треугольных пластин численным методом конечных разностей при действии различных динамических воздействиях (в том числе и от последствий промышленных взрывов) будут полезными как научным работникам в области механики деформируемых твердого тела, так и инженерам-проектировщикам в сфере расчетов и проектирования тонкостенных конструкций (пластин).

Литература

1. *Ржаницын А.Р.* Строительная механика / «Выш. Школа» М., 1982, 400 с.

2. Расчет конструкций убежищ; Авт.: М.Д. Боданский, Л.М. Горшков и др. / «Стройиздат» М., 1974. 207с.

3. *Ахмедиев С.К.* Расчеты треугольных пластин: Караганда: изд-во КарГТУ, 2006. 88 с.

4. *Волков Е.А.* Численные методы / «Наука» М., 1987, 248 с.

5. Убежища гражданской обороны. Конструкции и расчет / под ред. Котляревского В.А. «Стройиздат» М., 1989, 600 с.

6. *Варвак П.М., Варвак Л.П.* Метод сеток в расчетах строительных конструкций / «Строиздат» М.: 1977, 154 с.

7. *Феодосьев В.И.* Сопротивление материалов / «Наука (физматгиз)» М., 1986, 512 с.

8. Справочник проектировщика промышленных и общественных заданий. Расчетно-теоретический / Под ред. А.А. Уманского «Стройиздат», М., кн.2, 1972.

9. *Akhmediyev S.K., Khabidolda O., Vatin N.I., Yessenbayeva G.A., Muratkhan R.* Physical and mechanical state of cantilever triangular plates // Journal of Mathematics, Mechanics and Computer Science, 2023, 118(2), pp. 64–73. https://doi.org/10.26577/JMMCS.2023.v118.i2.07

10. *Ambartsumian S.A.* On the theory of bending of anisotropic plates and shallow shells // Journal of Applied Mathematics and Mechanics, 1960, 24(2), pp. 500–514. https://doi.org/10.1016/0021-8928(60)90052-6

11. *Ambartsumian S.A.* Membrane Theory of Plates // Foundations of Engineering Mechanics pp. 73–103. https://doi.org/10.1007/978-3-030-71326-3_4

12. *Askari H., Saadatnia Z., Esmailzadeh E., Younesian D.* Multi-frequency excitation of stiffened triangular plates for large amplitude oscillations // Journal of Sound and Vibration, 2014, 333(22), pp. 5817–5835. https://doi.org/10.1016/j.jsv.2014.06.026

13. *Brezinski C.* Some pioneers of extrapolation methods // The Birth of Numerical Analysis 2009, pp. 1–22. https://doi.org/10.1142/9789812836267_0001

ЛОКАЛЬНОЕ НАГРУЖЕНИЕ КРУГЛОЙ ПЯТИСЛОЙНОЙ ПЛАСТИНЫ

Салицкий В.С.
Белорусский государственный университет транспорта, Гомель, Беларусь
E-mail: vladislavsalitski@gmail.com

Аннотация. *Исследовано деформирование упругой круглой симметричной по толщине пятислойной пластины локально распределенной по кругу поперечной нагрузкой. Для тонких внешних и внутреннего несущих слоев приняты гипотезы Кирхгофа. В относительно толстых заполнителях справедлива гипотеза Тимошенко о прямолинейности и несжимаемости деформированной нормали. Уравнения равновесия получены вариационным методом. Аналитическое решение краевой задачи выписано в конечном виде в функциях Бесселя. Приведены численные результаты исследования прогибов и относительных сдвигов в зависимости от радиуса силового круга и толщины внутреннего несущего слоя.*

Ключевые слова*: пятислойная круглая пластина, изгиб, локальная круговая нагрузка, аналитическое решение, численные результаты*

1. Введение

В последнее время значительно возрос спрос на использование слоистых тонкостенных элементов конструкций в машиностроении и строительстве. Это обуславливает необходимость разработки их математических моделей и методов расчета на различные виды и типы нагрузок. Методы расчета и постановки краевых задач для расчета слоистых элементов конструкций приведены в монографиях [1–7]. Динамическое нагружение слоистых пластин исследовано в работах [8–12].

Квазистатическому деформированию трехслойных стержней и пластин посвящены статьи [13–15]. Принимались гипотезы ломаной линии, учитывалось воздействие температурного поля и упруго основания.

Решения отдельные краевых задач для трехслойных пластин приведены в статьях [16–20]. Циклическое нагружение трехслойных стержней и пластин, в рамах теории Москвитина, рассмотрено в публикациях [21, 22].

Уравнения равновесия и движения круговой пятислойной пластины получены в [23–25]. Решение задачи об изгибе пятислойной круговой пластины равномерно распределенной нагрузкой приведено в [26, 27]. Здесь предлагается решение краевой задачи об изгибе пятислойной круговой пластины локальной круговой нагрузкой.

2. Постановка и решение краевой задачи

Рассматривается симметричная по толщине пятислойная круговая пластина, деформируемая равномерно распределённой по кругу относительного радиуса $r \le b$ нагрузкой (рис. 1):

$$q(r) = q_0 H_0(b - r)\,, \tag{1}$$

где $H_0(x)$ – функция Хэвисайда; q_0 – интенсивность распределенной нагрузки.

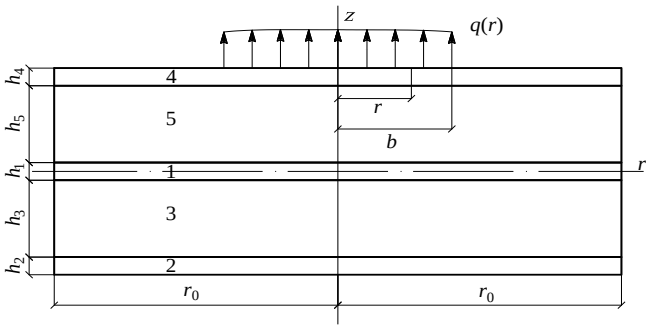

Рисунок 1. – **Расчётная схема симметричной по толщине пятислойной круговой пластины**

Тонкие несущие слои толщиной h_1, $h_2 = h_4$ выполнены из прочных материалов и принимают на себя основную силовую нагрузку. Для них справедливы гипотезы Кирхгофа. В более толстых заполнителях ($h_3 = h_5$) справедлива гипотеза Тимошенко о прямолинейности и несжимаемости деформированной нормали, учитывается относительный сдвиг ψ и работа касательных напряжений. Цилиндрическая система координат r, φ, z связывается со

срединной плоскостью внутреннего несущего слоя, ось z направлена перпендикулярно вверх, к четвертому слою. Все геометрические размеры пластины отнесены к ее радиусу r_0.

Система дифференциальных уравнений равновесия в перемещениях получена в [24, 25] при равномерно распределенной нагрузке. В случае нагрузки (1) она принимает вид

$$\mathrm{L}_2\,(a_4\psi - a_5 w,_r\,) - 2cG_3\psi = 0\,,$$

$$\mathrm{L}_3\,(a_5\psi - a_6 w,_r\,) = -q_0 H_0(b-r)\,, \qquad (2)$$

где запятая в нижнем индексе обозначает операцию дифференцирования по следующей за ней координате; коэффициенты

$$a_4 = \left[2K_2^{+}\ h_2 h_3^{\,2} + 2K_3^{+}\frac{h_3^3}{3}\right],$$

$$a_5 = \left[K_2^{+} h_2 h_3 (h_1 + 2h_3 + h_2) + 2K_3^{+} h_3 (\frac{h_1 h_3}{4} + \frac{h_3^2}{3})\right],$$

$$a_6 = \left[2K_2^{+} h_2 (\frac{h_1^{\,2}}{4} + \frac{h_1 h_2}{2} + h_1 h_3 + \frac{h_2^{\,2}}{3} + h_2 h_3 + h_3^{\,2}) + K_1^{+}\frac{h_1^3}{12} + 2K_3^{+} h_3 (\frac{h_1^2}{4} + \frac{h_1 h_3}{2} + \frac{h_3^2}{3})\right];$$

L_2, L_3 – линейные дифференциальные операторы

$$\mathrm{L}_2(g) \equiv \left(\frac{1}{r}(rg),_r\right),_r \equiv g,_{rr} + \frac{g,_r}{r} - \frac{g}{r^2}\,,\ \ \mathrm{L}_3(g) \equiv \frac{1}{r}\big(r\,\mathrm{L}_2(g)\big),_r \equiv g,_{rrr} + \frac{2g,_{rr}}{r} - \frac{g,_r}{r^2} + \frac{g}{r^3}\,.$$

Краевую задачу о деформировании круговой пятислойной пластины локальной нагрузкой замкнем, добавив к системе уравнений (2) граничные условия. Например, при заделке контура пластины должны выполняться требования

$$u = \psi = w = w,_r = 0\,,\ \text{при}\ r = r_0\,. \qquad (3)$$

После элементарных преобразований, связанных с выделением отдельного уравнения для относительного сдвига ψ, систему (2) можно переписать в виде

$$\mathrm{L}_2(\psi) - \beta^2\psi = f\,,$$

$$\mathrm{L}_3\,(a_5\psi - a_6 w,_r\,) = -q_0 H_0(b-r)\,, \qquad (4)$$

где коэффициенты и функция, входящие в первое уравнение

$$\beta^2 = \frac{2a_6 h_3 G_3}{(a_4 a_6 - a_5^{\,2})}\,,\ \ \gamma_1 = \frac{a_5}{(a_4 a_6 - a_5^{\,2})}\,.$$

$$f(r) = \frac{a_5}{r(a_4 a_6 - a_5^{\,2})}\left(\int q_0 H_0(b-r) r dr - C_1\right) = \frac{\gamma_1}{r}\left(\frac{q_0\left(r^2 - b^2\right)}{2} H_0(b-r) - C_1\right).$$

Решение системы дифференциальных уравнений (4) будет

$$\psi = C_2 I_1(\beta r) + C_3 K_1(\beta r) + \psi_r\,,$$

$$w = \frac{a_5}{a_6}\int \psi dr + \frac{q_0}{a_6}\int \mathrm{L}_3^{-1}(H_0(b-r)) dr - \frac{C_1}{4a_6} r^2 (\ln r - 1) + \frac{C_5 r^2}{4a_6} + C_6 \ln r + C_4\,, \qquad (5)$$

где $I_1(\beta r)$ – модифицированная функция Бесселя; $K_1(\beta r)$ – функция Макдональда; интегралы берутся в пределах от 0 до r; L_3^{-1} – интегральный оператор, обратный соответствующему дифференциальному оператору в (2).

Частное решение первого из уравнений (4) ψ_r получено методом вариации постоянных

$$\psi_r = \frac{\gamma_1 q_0}{2\beta^2} H_0(b-r)\left[\frac{b^2}{r} - r + 2b\big(K_1(\beta b) I_1(\beta r) - I_1(\beta b) K_1(\beta r)\big)\right] + \frac{C_1\gamma_1}{\beta^2 r}\,. \qquad (6)$$

Интегралы, входящие во второе уравнение системы (5) будут

$$\int \mathrm{L}_3^{-1}(q)\,\mathrm{d}\,r = q_0\left(\frac{r^4-5b^4}{64}-\frac{b^4}{16}\ln\left(\frac{r}{b}\right)-\frac{b^2r^2}{8}\ln\left(\frac{r}{b}\right)+\frac{b^2r^2}{16}\right)H_0(b-r)\ ,$$

$$\int \psi dr = \frac{C_2 I_0(\beta r)}{\beta}-\frac{C_3 K_0(\beta r)}{\beta}+\frac{C_1\gamma_1}{\beta^2}\ln(r)+\frac{\gamma_1 q_0}{2\beta^2}H_0(b-r)\times$$

$$\times\left[\frac{b^2-r^2}{2}+b^2\ln\left(\frac{r}{b}\right)+\frac{2b}{\beta}\left(K_1(\beta b)I_0(\beta r)+I_1(\beta b)K_0(\beta r)\right)-\frac{2}{\beta^2}\right]. \qquad (7)$$

Константы интегрирования C_1, …, C_6 – при условии (3) заделки по контуру пятислойной пластины получены следующие:

$$C_1=-\frac{q_0 b^2}{2},\quad C_2=\frac{\gamma_1 q_0}{\beta^2 I_1(\beta)}\left(\frac{b^2}{2}-bK_1(\beta)I_1(\beta b)\right),\quad C_3=\frac{q_0\gamma_1 b I_1(\beta b)}{\beta^2},$$

$$C_4=-\frac{a_5\gamma_1 q_0}{a_6\beta^4 I_1(\beta)}\left(\frac{b^2 I_0(\beta)\beta}{2}-bI_1(\beta b)\right)+\frac{q_0 b^4}{32a_6}+\frac{q_0 b^2}{16a_6},$$

$$C_5=\frac{q_0 b^2}{8}\left(2-b^2\right),\quad C_6=\frac{q_0 b^4}{16a_6}.$$

Решение системы (4) для пластины, заделанной по контуру, принимает следующий конечный вид:

$$\psi=\frac{\gamma_1 q_0}{\beta^2}\left\{\frac{I_1(\beta r)}{I_1(\beta)}\left(\frac{b^2}{2}-bK_1(\beta)I_1(\beta b)\right)+bI_1(\beta b)K_1(\beta r)+\right.$$

$$\left.+\frac{H_0(b-r)}{2}\left[\frac{b^2}{r}-r+2b\left(K_1(\beta b)I_1(\beta r)-I_1(\beta b)K_1(\beta r)\right)\right]-\frac{b^2}{2r}\right\},$$

$$w=\frac{a_5}{a_6}\frac{\gamma_1 q_0}{\beta^2 I_1(\beta)}\left\{\frac{I_0(\beta r)}{\beta I_1(\beta)}\left(\frac{b^2}{2}-bK_1(\beta)I_1(\beta b)\right)-\frac{b^2 I_0(\beta)\beta}{2\beta^2 I_1(\beta)}+\frac{bI_1(\beta b)}{\beta^2 I_1(\beta)}-\frac{bI_1(\beta b)K_0(\beta r)}{\beta}-\right.$$

$$\left.-\frac{b^2}{2}\ln(r)\frac{H_0(b-r)}{2}\left[\frac{b^2-r^2}{2}+b^2\ln\left(\frac{r}{b}\right)+\frac{2b}{\beta}\left(K_1(\beta b)I_0(\beta r)+I_1(\beta b)K_0(\beta r)\right)-\frac{2}{\beta^2}\right]\right\}+$$

$$+\frac{q_0}{8a_6}\left\{\left(\frac{r^4-5b^4}{8}-\frac{b^4}{2}\ln\left(\frac{r}{b}\right)-b^2r^2\ln\left(\frac{r}{b}\right)+\frac{b^2r^2}{2}\right)H_0(b-r)+b^2r^2(\ln r-1)+\frac{b^2}{4}r^2\left(2-b^2\right)+\frac{b^4}{2}\ln r+\frac{b^4}{4a_6}+\frac{b^2}{2a_6}\right\}. \qquad (8)$$

3. Численные результаты

Численно исследован прогиб и сдвиг (8) в пятислойной круговой пластине единичного радиуса, симметричной по толщине. За базовую расчетную модель принята пластина, слои которой набраны из материалов Д16-Т – фторопласт – Д16-Т – фторопласт – Д16-Т. Толщины слоев $h_1 = h_2 = h_4 = 0{,}02$, $h_3 = h_5 = 0{,}1$, величина нагрузки $q_0 = 10$ МПа. Упругие характеристики этих материалов приведены в [1].

Рис. 2 *а*, *б* иллюстрирует изменение перемещений в базовой модели вдоль радиуса пластины при различных радиусах b пятна нагрузки q. При увеличении радиуса нагрузки перемещения увеличиваются нелинейно. При этом экстремум относительного сдвига (*б*) приближается к контуру пластины.

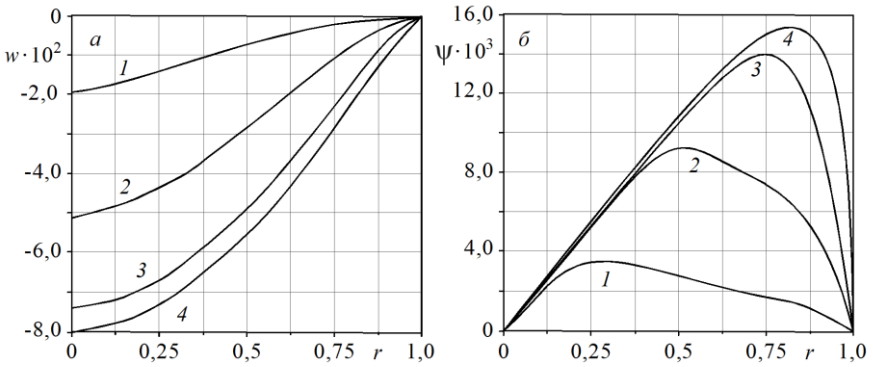

Рисунок 2. – **Перемещения в пластине при различных радиусах *b* пятна нагрузки**

***1* – *b* = 0,25; *2* – *b* = 0,5; *3* – *b* = 0,75; *4* – *b* = 1**

Зависимость максимальных прогиба и относительного сдвига от величины пятна приложенной распределённой нагрузки при различной толщине внутреннего несущего слоя показана на рис. 3 *а, б*. Уменьшение толщины внутреннего несущего слоя в 2 раза приводит к увеличению прогиба на 11,4 процента. Увеличение толщины внутреннего несущего слоя в 1,5 раза приводит к уменьшению прогиба на 15,2 процентов.

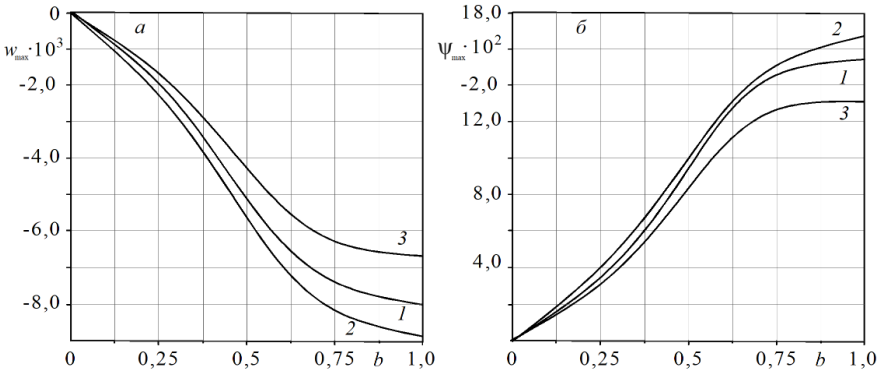

Рисунок 3. – **Зависимость максимальных перемещений от радиуса пятна нагрузки**

при различной толщине внутреннего несущего слоя

***1* – h_1 = 0,02; *2* – h_1 = 0,01; *3* – h_1 = 0,03**

4. Заключение.

Предложенное в работе решение позволяет моделировать напряженно-деформированное состояния круговых пятислойных пластин при локальных поверхностных нагрузках. Численные расчеты показали существенное влияние радиуса пятна нагрузки и

Работа выполнена при финансовой поддержке Белорусского республиканского фонда фундаментальных исследований.

Литература

1. *Горшков А.Г., Старовойтов Э.И., Яровая А.В.* Механика слоистых вязкоупругопластических элементов конструкций / Москва, ФИЗМАТЛИТ, 2005, 576 с.
2. *Журавков М.А., Старовойтов Э.И.* Математические модели механики твердого тела / Минск, БГУ, 2021, 535 с.
3. *Zhuravkov M.A., Lyu Yongtao, E.I. Starovoitov.* Mechanics of Solid Deformable Body // Singapore, Springer, 2023, 317 p.
4. *Абдусаттаров А., Старовойтов Э.И., Рузиева Н.Б.* Деформирование и повреждаемость упругопластических элементов конструкций при циклических нагружениях / Ташкент, «IDEAL PRESS», 2023, 381 с.
5. *Aghalovyan L.* Asymptotic theory of anisotropic plates and shells // Singapore–London, World Scientific Publishing; 2015, 376 p.
6. *Старовойтов, Э. И.* Сопротивление материалов / Гомель, БелГУТ, 2004, 376 с.

7. *Старовойтов, Э. И.* Механика материалов / Гомель, БелГУТ, 2011, 380 с.
8. *Старовойтов Э.И., Леоненко Д.В.* Исследование спектра частот трехслойной цилиндрической оболочки с упругим наполнителем // Механика композиционных материалов и конструкций. 2015, Том 21, No. 2, С. 162–169.
9. *Bakulin VN, Boitsova DA, Nedbai AYa.* Parametric resonance of a three1layered cylindrical composite rib-stiffened shell // Mechanics of composite materials, 2021, vol. 57, No. 5, pp. 623–634.
10. *Tarlakovskii DV, Fedotenkov GV.* Two-Dimensional Nonstationary Contact of Elastic Cylindrical or Spherical Shells // Journal of Machinery Manufacture and Reliability, 2014, vol, 43, No. 2, pp. 145–152.
11. *Suvorov YeM, Tarlakovskii DV, Fedotenkov GV.* The plane problem of the impact of a rigid body on a half-space modelled by a Cosserat medium // Journal of Applied Mathematics and Mechanics, 2012, vol. 76, No. 5, pp.511–518.
12. *Pradhan M, Dash PR, Pradhan PK.* Static and dynamic stability analysis of an asymmetric sandwich beam resting on a variable Pasternak foundation subjected to thermal gradient // Meccanica, 2016, vol. 51, No. 3, pp.725–739.
13. *Starovoitov É.I., Pleskachevskii Yu.M., Leonenko D.V., Tarlakovskii D.V.* Deformation of a Step Composite Beam in a Temperature Field // Journal of Engineering Physics and Thermophysics, 2015, vol. 88, No. 4, pp.
14. *Старовойтов Э.И., Леоненко Д.В.* Деформирование трехслойного стержня в температурном поле // Механика машин, механизмов и материалов, 2013 т, No. 22, С. 31–35.
15. *Старовойтов Э.И., Козел А.Г.* Изгиб упругой круговой трехслойной пластины на основании Пастернака // Механика композиционных материалов и конструкций, 2018, т. 2, No. 3, С. 392–406.
16. *Zadeh HV, Tahani M.* Analytical bending analysis of a circular sandwich plate under distributed load // International Journal of Recent Advances in Mechanical Engineering, 2017, vol. 6, No. 1, pp. 01-10.
17. *Yang L, Harrysson O, West H, Cormier D.* A comparison of bending properties for cellular core sandwich panels // Materials Sciences and Applications, 2013, vol. 4, No. 8, pp. 471–477.
18. *Захарчук Ю.В.* Напряженно-деформированное состояние круговой трехслойной пластины со сжимаемым заполнителем. // Механика. Исследования и инновации, 2019, т. 12, No. 12, С. 66–75.
19. *Козел А.Г.* Влияние сдвиговой жёсткости основания на напряжённое состояние сэндвич пластины // Фундаментальные и прикладные проблемы техники и технологии, 2018, т. 332, No. 6, С. 25–34.
20. *Нестерович, А.В.* Напряженное состояние круговой трехслойной пластины при осесимметричном нагружении в своей плоскости // Механика. Исследования и инновации, 2019, т. 12, No. 12, С. 152–157.
21. *Старовойтов Э.И., Абдусаттаров А., Рузиева Н.Б.* Циклическое нагружение упругопластических трёхслойных стержней с учетом их повреждаемости // Узб. журнал Проблемы механики, 2023, No. 1, С. 66–74.
22. *Старовойтов Э.И., Леоненко Д.В., Абдусаттаров А.* Знакопеременное термосиловое нагружение трёхслойной пластины погонными моментами // Узб. журнал «Проблемы механики», 2023, No. 3, С. 20–30.
23. Лачугина Е.А. Поперечные колебания пятислойной упругой круговой пластины с жесткими заполнителями // Механика. Исследования и инновации, 2022, вып. 15, С. 212–219.
24. Лачугина Е.А. Частоты собственных колебаний пятислойной круговой пластины // Теоретическая и прикладная механика, Минск, БНТУ, 2023, вып. 38, С. 227-233.
25. *Салицкий, В.С.* Уравнения равновесия круговой пятислойной пластины в усилиях / В.С. Салицкий // Мат. XXVII Междунар. симпозиума «Динамические и технологические проблемы механики конструкций и сплошных сред» им. А.Г. Горшкова, 2021, т. 1, С. 199–201.
26. *Салицкий, В.С.* Изгиб защемлённой по контуру круговой пятислойной пластины // Механика. Исследования и инновации, 2022, т. 15, No. 15, С. 209–213.
27. *Салицкий, В.С.* Изгиб круговой пятислойной пластины // Теоретическая и прикладная механика. Минск, 2023, вып. 38, С. 234 – 239.

ДЕФОРМИРОВАНИЕ ТРЕХСЛОЙНЫХ ПЛАСТИН В НЕЙТРОННОМ ПОТОКЕ

Старовойтов Э.И.[1]

[1]*Белорусский государственный университет транспорта, Гомель, Беларусь*

E-mail: edstar0@yandex.by

Аннотация. *Рассмотрен изгиб упругой круговой несимметричной по толщине трехслойной пластины локальной равномерно распределенной по кольцу нагрузкой в нейтронном потоке. Для описания кинематики пакета используются гипотезы ломаной линии. В тонких несущих слоях справедливы гипотезы Кирхгофа, в несжимаемом по толщине относительно толстом заполнителе – гипотеза Тимошенко. Учитывается работа касательных напряжений заполнителя. Принято, что дополнительное изменение объема материалов прямо пропорциональным интегральному нейтронному потоку. Затухание интенсивности нейтронного потока при прохождении через слои пластины предполагается по экспоненциальному закону. Система дифференциальных уравнений равновесия пластины получена вариационным методом Лагранжа. На контуре пластины приняты граничные условия шарнирного опирания. Решение краевой задачи получено в конечном виде. Проведен его численный параметрический анализ*

Ключевые слова: *трехслойная пластина, локальная кольцевая нагрузка, нейтронный поток, численный анализ.*

1. Введение

Потребность оценки напряженно-деформированного состояния композитных, в том числе слоистых, элементов конструкций, работающих в условиях комплексных внешних воздействий, вызвана их широким применением в технике, строительстве и транспортировке энергоресурсов. Это обуславливает необходимость создания расчетных механико-математических моделей для описания их деформирования при различных нагрузках, включая радиационно-силовые. Указанной проблеме посвящен ряд работ.

Влиянию нейтронного облучения на механические свойства материалов и построению соответствующих математических моделей деформирования твердых тел посвящены монографии [1–3].

Общие подходы к построению математических моделей многослойных конструкций при квазистатических и динамических нагрузках изложены в монографиях [4–10]. Свободные, вынужденные и нестационарные колебания неоднородных сферических и цилиндрических оболочек рассмотрены в статьях [11–14]. Колебания трехслойных и пятислойных круговых пластин исследованы в [15–17]. Деформирование трехслойных стержней и пластин в температурных полях исследовано в работах [18–21]. Публикации [22–26] посвящены аналитическому анализу изгиба трехслойных пластин, в том числе связанных с упругим основанием. Квазистатическое деформирование пятислойной круговой пластины исследовано в статьях [27, 28].

Работы [29–31] посвящены развитию математических моделей переменного квазистатического нагружения упругопластических трехслойные стержней и пластин. Физические уравнения состояния принимались соответствующими теории малых упругопластических деформаций. За основу принята теория переменного нагружения однородных тел В.В. Москвитина [32].

В данной работе приведена постановка и получено аналитическое решение краевой задачи о локальном нагружении трехслойной упругой круговой пластины в условиях нейтронного облучения. Исследовано прохождение нейтронного потока через пластину и влияние на ее деформирование.

2. Постановка краевой задачи

В несимметричной по толщине трехслойной круговой пластине принимаются внешние несущие слои тонкими, толщиной $h_1 \neq h_2$, подчиняющимися гипотезам Кирхгофа о несжимаемости, прямолинейности и перпендикулярности деформированных нормалей к срединной поверхности слоев. В жестком достаточно толстом заполнителе ($h_3 = 2c$) учитывается работа в тангенциальном направлении, для него справедлива гипотеза о прямолинейности и несжимаемости деформированной нормали, которая поворачивается относительно срединной поверхности на некоторый дополнительный угол $\psi(r)$. Постановка

задачи и ее решение проводятся в цилиндрической системе координат r, φ, z, которая связывается со срединной плоскостью заполнителя (рис. 1).

Предполагается, что в начальный момент времени перпендикулярно внешней поверхности верхнего слоя $z = c + h_1$ пластины воздействует осесимметричная распределенная по кругу силовая нагрузка $q(r)$ и падает *нейтронный поток* плотностью φ_0 = const в направлении, противоположном внешней нормали (см. рис. 1). В силу осесимметричности нагрузки тангенциальные перемещения в слоях отсутствуют: $u_\varphi^{(k)} = 0$ (k = 1, 2, 3 – номер слоя), а прогиб пластины $w(r, t)$, относительный сдвиг в заполнителе $\psi(r, t)$ и радиальное перемещение координатной поверхности $u(r, t)$, которые в дальнейшем считаются искомыми, не зависят от координаты φ. Их зависимость от времени t определяется интегральным нейтронным потоком $I_k(z,t)$. На контуре жесткая диафрагма, препятствующая относительному сдвигу слоев ($\psi = 0$ при $r = r_0$).

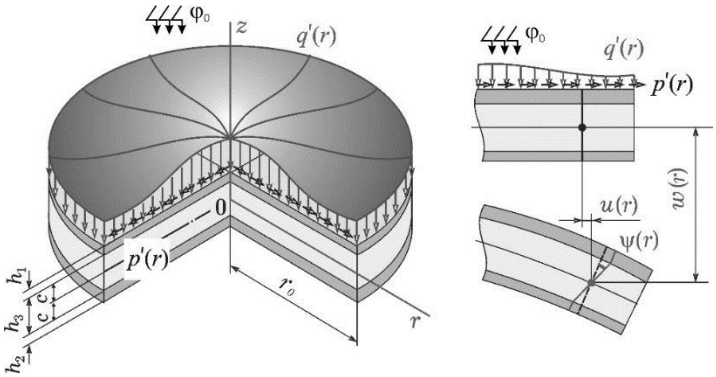

Рисунок 1. - **Расчетная схема трехслойной пластины**

Как указано в работе [1], согласно экспериментальным данным при малых деформациях в линейном приближении можно считать, что изменение объема материала в слоях θ_{Ik} прямо пропорционально интегральному нейтронному потоку

$$\theta_{Ik} = B_k I_k(z,t), \quad I_k(z,t) = \varphi_k(z)t, \tag{1}$$

где φ_k – интенсивность потока, нейтрон/(м^2·с), дошедшего за время t к поверхности с координатой z в k-ом слое; B_k – константа материала, получаемая из опыта.

Пусть на верхнюю поверхность пластины $z = c + h_1$, параллельно оси z падают нейтроны с интенсивностью φ_0. Тогда интенсивность потока нейтронов, доходящих до плоскости, параллельной границе $z = const$, будет убывать по экспоненте [1]. В рассматриваемом случае к моменту t через сечение с координатой z в верхнем слое пройдет интегральный поток

$$I_1(z,t) = \varphi_0 t \exp(-\mu_1(c + h_1 - z)), \tag{2}$$

где μ_1 – величина макроскопического эффективного сечения (1/см).

В заполнителе интегральный поток к этому моменту будет

$$I_3(z,t) = \varphi_{13} t \exp(-\mu_3(c - z)), \tag{3}$$

где $\varphi_{13} = \varphi_0 \exp(-\mu_1 h_1)$.

В нижнем слое интегральный поток

$$I_2(z,t) = \varphi_{32} t \exp(\mu_2(c + z)), \tag{4}$$

где $\varphi_{32} = \varphi_{13} \exp(-2\mu_{31} c)$.

В зависимости от энергии нейтронов и облучаемого материала величина параметра B_k в формуле (1) может быть порядка 10^{-28}–10^{-23} м^2 / нейтрон. При этом значение μ_k обратно величине свободного пробега нейтронов, который в алюминии – λ_1 = 14,1–15,9 см, в полиэтилене – λ_3 =5,5–13,9 см.

Приведенные формулы (2)–(4) позволяют рассчитать интегральный нейтронный поток, прошедший за время t через плоскость с координатой z в трехслойной пластине.

В соответствии с принятыми кинематическими гипотезами радиальные перемещения в слоях $u_r^{(k)}$ выражаются через искомые функции

$$u_r^{(1)} = u + c\psi - zw,_r\,, \qquad c \le z \le c + h_1\,,$$

$$u_r^{(3)} = u + z\psi - zw,_r\,, \qquad -c \le z \le c\,,$$

$$u_r^{(2)} = u - c\psi - zw,_r\,, \qquad -c - h_2 \le z \le -c\,, \tag{5}$$

где запятая в нижнем индексе обозначает производную, по следующей за ней координате.

Для описания связи напряжений с деформациями в слоях пластины используются физические уравнения состояния, учитывающие радиационное изменение объема (1),

$$s_\alpha^{(k)} = 2G_k э_\alpha^{(k)}\,, \quad s_{rz}^{(3)} = 2G_3 э_{rz}^{(3)}\,,$$

$$\sigma^{(k)} = K_k(3\varepsilon^{(k)} - B_k I_k) \quad (k = 1,\,2,\,3;\ \alpha = r, \varphi)\,, \tag{6}$$

где $s_\alpha^{(k)}$, $э_\alpha^{(k)}$ – девиаторные, $\sigma^{(k)}$, $\varepsilon^{(k)}$ – шаровые части тензоров напряжений и деформаций; G_k, K_k – модули сдвига и объемного деформирования, влияние нейтронного облучения на которые незначительно и в дальнейшем не учитывается [1–3]; $s_{rz}^{(3)}$, $э_{rz}^{(3)}$ – касательное напряжение и сдвиговая деформация в заполнителе.

Обобщенные внутренние усилия и моменты вводятся соотношениями

$$T_\alpha \equiv \sum_{k=1}^{3} T_\alpha^{(k)} = \sum_{k=1}^{3} \int_{h_k} \sigma_\alpha^{(k)}\,\mathrm{d}\,z\,, \quad M_\alpha \equiv \sum_{k=1}^{3} M_\alpha^{(k)} = \sum_{k=1}^{3} \int_{h_k} \sigma_\alpha^{(k)} z\,\mathrm{d}\,z\,,$$

$$H_\alpha = M_\alpha^{(3)} + c\left(T_\alpha^{(1)} - T_\alpha^{(2)}\right), \quad Q = \int_{-c}^{c} \sigma_{rz}^{(3)}\,\mathrm{d}\,z \quad (\alpha = r, \varphi)\,, \tag{7}$$

где $\sigma_\alpha^{(k)}$, $\sigma_{rz}^{(k)}$ – компоненты тензора напряжений.

Подставив в (7) выражения напряжений через деформации из (6), а затем с помощью соотношений Коши выразив деформации через перемещения (5), получим для обобщенных внутренних усилий формулы, связывающие их с искомыми функциями:

$$T_r = \sum_{k=1}^{3}\left[h_k(K_k^+ u,_r + \frac{u}{r}K_k^-) - K_k B_k \int_{h_k} I_k\,\mathrm{d}\,z\right] + c(K_1^+ h_1 - K_2^+ h_2)\psi,_r + c(K_1^- h_1 - K_2^- h_2)\frac{\psi}{r} -$$

$$-\left[K_1^+ h_1\left(c + \frac{h_1}{2}\right) - K_2^+ h_2\left(c + \frac{h_2}{2}\right)\right] w,_{rr} - \left[K_1^- h_1\left(c + \frac{h_1}{2}\right) - K_2^- h_2\left(c + \frac{h_2}{2}\right)\right]\frac{w,_r}{r}\,,$$

$$M_r = \left[K_1^+ h_1\left(c + \frac{h_1}{2}\right) - K_2^+ h_2\left(c + \frac{h_2}{2}\right)\right] u,_r + \left[K_1^- h_1\left(c + \frac{h_1}{2}\right) - K_2^- h_2\left(c + \frac{h_2}{2}\right)\right]\frac{u}{r} +$$

$$+\left[cK_1^+ h_1\left(c + \frac{h_1}{2}\right) + cK_2^+ h_2\left(c + \frac{h_2}{2}\right) + \frac{2}{3}c^3 K_3^+\right]\psi,_r + \left[cK_1^- h_1\left(c + \frac{h_1}{2}\right) + cK_2^- h_2\left(c + \frac{h_2}{2}\right) + \frac{2}{3}c^3 K_3^-\right]\frac{\psi}{r} -$$

$$-\left[K_1^+ h_1\left(c^2 + ch_1 + \frac{h_1^2}{3}\right) + K_2^+ h_2\left(c^2 + ch_2 + \frac{h_2^2}{3}\right) + \frac{2}{3}c^3 K_3^+\right] w,_{rr} -$$

$$-\left[K_1^- h_1\left(c^2 + ch_1 + \frac{h_1^2}{3}\right) + K_2^- h_2\left(c^2 + ch_2 + \frac{h_2^2}{3}\right) + \frac{2}{3}c^3 K_3^-\right]\frac{w,_r}{r} - \sum_{k=1}^{3} K_k B_k \int_{h_k} I_k z\,\mathrm{d}\,z\,.$$

$$H_r = c(K_1^+ h_1 - K_2^+ h_2)u,_r + c(K_1^- h_1 - K_2^- h_2)\frac{u}{r} +$$

$$+\left[c^2(K_1^+ h_1 + K_2^+ h_2) + \frac{2}{3}c^3 K_3^+\right]\psi,_r + \left[c^2(K_1^- h_1 + K_2^- h_2) + \frac{2}{3}c^3 K_3^-\right]\frac{\psi}{r} -$$

$$-\left[c\left(K_1^+ h_1(c+\frac{h_1}{2}) + K_2^+ h_2(c+\frac{h_2}{2})\right) + \frac{2}{3}c^3 K_3^+\right]w,_{rr} -$$

$$-\left[c\left(K_1^- h_1(c+\frac{h_1}{2}) + K_2^- h_2(c+\frac{h_2}{2})\right) + \frac{2}{3}c^3 K_3^-\right]\frac{w,_r}{r} -$$

$$-K_3 B_3 \int_{h_3} I_3 z dz - c\left(K_1 B_1 \int_{h_1} I_1 dz - K_2 B_2 \int_{h_2} I_2 \,\mathrm{d}z\right),$$

$$Q = 2cG_3\psi\,,\ \ K_k + \frac{4}{3}G_k \equiv K_k^+,\ \ K_k - \frac{2}{3}G_k \equiv K_k^-. \tag{8}$$

Выражения для обобщенных внутренних усилий M_φ, H_φ и T_φ следуют из (8), если в одноименных величинах поменять местами параметры K_k^+ и K_k^-.

Пусть на рассматриваемую трехслойную пластину действует локальная поверхностная нагрузка $q(r)$, равномерно распределенная внутри кольца относительного радиуса $a \le r_0 \le b$:

$$q(r) = q_0\left(H_0(b-r) - H_0(a-r)\right) \quad (q_0 = \mathrm{const}), \tag{9}$$

где $H_0(r)$ – функция Хэвисайда.

Система уравнений равновесия упругой трехслойной пластины в обобщенных усилиях приведена в [4]. Она получена с помощью вариационного принципа Лагранжа и справедлива в рассматриваемом случае. Подставив в нее обобщенные усилия (8), получим систему обыкновенных дифференциальных уравнений равновесия для определения искомых функций в задаче о деформировании трехслойной круговой пластины в нейтронном потоке:

$$\mathrm{L}_2(a_1 u + a_2\psi - a_3 w,_r) = 0,$$

$$\mathrm{L}_2(a_2 u + a_4\psi - a_5 w,_r) - 2cG_3\psi = 0,$$

$$\mathrm{L}_3(a_3 u + a_5\psi - a_6 w,_r) = q_0\left(H_0(b-r) - H_0(a-r)\right), \tag{10}$$

где дифференциальные операторы L_2 (*оператор Бесселя*), L_3 и коэффициенты a_i определяются соотношениями

$$\mathrm{L}_2(g) \equiv \left(\frac{1}{r}(rg),_r\right),_r \equiv g,_{rr} + \frac{g,_r}{r} - \frac{g}{r^2},\ \ \mathrm{L}_3(g) \equiv \frac{1}{r}\left(r\,\mathrm{L}_2(g)\right),_r \equiv g,_{rrr} + \frac{2g,_{rr}}{r} - \frac{g,_r}{r^2} + \frac{g}{r^3}.$$

$$a_1 = \sum_{k=1}^{3} h_k K_k^+,\ \ a_2 = c(h_1 K_1^+ - h_2 K_2^+),\ a_3 = h_1\left(c + \frac{1}{2}h_1\right)K_1^+ - h_2\left(c + \frac{1}{2}h_2\right)K_2^+,$$

$$a_4 = c^2\left(h_1 K_1^+ + h_2 K_2^+ + \frac{2}{3}cK_3^+\right),\ \ a_5 = c\left[h_1\left(c + \frac{1}{2}h_1\right)K_1^+ + h_2\left(c + \frac{1}{2}h_2\right)K_2^+ + \frac{2}{3}c^2 K_3^+\right],$$

$$a_6 = h_1\left(c^2 + ch_1 + \frac{1}{3}h_1^2\right)K_1^+ + h_2\left(c^2 + ch_2 + \frac{1}{3}h_2^2\right)K_2^+ + \frac{2}{3}c^3 K_3^+.$$

Следует отметить, что интегральный нейтронный поток в систему (10) явным образом не входит, как ранее в подобной задаче [16] и температура.

3. Общее решение краевой задачи.

Общее аналитическое решение системы уравнений (10) будет следующим:

$$\psi = C_2 I_1(\beta r) + C_3 K_1(\beta r) +$$

$$+\frac{\gamma_1 q_0}{2\beta^2} H_0(b-r)\left[\frac{b^2}{r} - r + 2b\left(K_1(\beta b) I_1(\beta r) - I_1(\beta b) K_1(\beta r)\right)\right] -$$

$$-\frac{\gamma_1 q_0}{2\beta^2} H_0(a-r)\left[\frac{a^2}{r} - r + 2a\left(K_1(\beta a) I_1(\beta r) - I_1(\beta a) K_1(\beta r)\right)\right] + \frac{C_1\gamma_1}{\beta^2 r},$$

$$w = \frac{b_2}{b_3}\left[\frac{C_2 I_0(\beta r)}{\beta} - \frac{C_3 K_0(\beta r)}{\beta} + \frac{C_1\gamma_1}{\beta^2}\ln r + \frac{\gamma_1 q_0}{2\beta^2} H_0(b-r)\times\right.$$

$$\left.\times\left[\frac{b^2 - r^2}{2} + b^2\ln\left(\frac{r}{b}\right) + \frac{2b}{\beta}\left(K_1(\beta b) I_0(\beta r) + I_1(\beta b) K_0(\beta r)\right) - \frac{2}{\beta^2}\right]\right] -$$

$$-\frac{\gamma_1 q_0}{2\beta^2} H_0(a-r)\left[\frac{a^2}{r} - r + 2a\left(K_1(\beta a) I_1(\beta r) - I_1(\beta a) K_1(\beta r)\right)\right] + \frac{C_1\gamma_1}{\beta^2 r} +$$

$$+\frac{q_0}{b_3}\left(\frac{r^4 - 5b^4}{64} + \frac{b^2 r^2}{16} - \left(\frac{b^4}{16} + \frac{b^2 r^2}{8}\right)\ln\left(\frac{r}{b}\right)\right) H_0(b-r) -$$

$$-\frac{q_0}{b_3}\left(\frac{r^4 - 5a^4}{64} + \frac{a^2 r^2}{16} - \left(\frac{a^4}{16} + \frac{a^2 r^2}{8}\right)\ln\left(\frac{r}{a}\right)\right) H_0(a-r) - -\frac{1}{4b_3} C_1 r^2(\ln r - 1) + \frac{C_5 r^2}{4b_3} + C_6 \ln r + C_4,$$

$$u = \frac{a_3}{a_1} w,_r - \frac{a_2}{a_1}\psi + \frac{C_7 r}{2} + \frac{C_8}{r}, \qquad (11)$$

где $C_1, C_2, ..., C_8$ – константы интегрирования, определяемые из граничных условий; $I_1(\beta r)$, $K_1(\beta r)$ – функции Бесселя; интегралы берутся в пределах от 0 до r; коэффициенты

$$\beta^2 = \frac{2cb_3 G_3}{b_1 b_3 - b_2^2},\ \ b_1 = \frac{a_1 a_4 - a_2^2}{a_1},\ \ b_2 = \frac{a_1 a_5 - a_2 a_3}{a_1},\ \ b_3 = \frac{a_1 a_6 - a_3^2}{a_1},\ \gamma_1 = \frac{b_2}{(b_1 b_3 - b_2^2)}.$$

Из граничных условий интерес представляет шарнирное опирание контура пластины, т.к. при этом ограничения накладываются на обобщенный радиальный момент M_r (8), что позволяет учесть влияние нейтронного облучения в явном виде. В этом случае на контуре должны выполняться условия

$$u = \psi = w = M_r = 0 \ \text{ при } \ r = r_0. \qquad (12)$$

Константы интегрирования следуют из граничных условий на контуре (12) и требований ограниченности решения (11) в центре пластины. Из ограниченности решения имеем

$$C_1 = -\frac{q_0 b^2}{2},\ \ C_3 = \frac{q_0\gamma_1 b I_1(\beta b)}{\beta^2},\ \ C_6 = \frac{q_0 b^4}{16 b_3},\ \ C_8 = 0. \qquad (13)$$

В случае шарнирного опирания контура из условий (12) получим

$$C_2 = \frac{\gamma_1 q_0}{\beta^2 I_1(\beta r_0)}\left(\frac{b^2}{2} - bK_1(\beta r_0) I_1(\beta b)\right),\ \ C_4 = -\frac{C_5}{4b_3} - \frac{b_2}{b_3}\int \psi\, \mathrm{d}r\Big|_{r=r_0},$$

$$C_5 = \left(\frac{C_1}{2} + 2b_3 C_6\right)\frac{a_1 b_3 - a_7 a_1 - a_3^2}{a_1(a_6 + a_7)} -$$

$$-\frac{2b_3 t}{a_6 + a_7}\left[\frac{\varphi_0 K_1 B_1}{\mu_1}\left(h_1 + c - \frac{1}{\mu_1} - \left(c - \frac{1}{\mu_1}\right)\exp(-\mu_1 h_1)\right) +\right.$$

$$+\frac{\varphi_{32}K_2B_2}{\mu_2}\left(c\left(c+h_2+\frac{1}{\mu_2}\right)\exp(-\mu_2 h_2)-c-\frac{1}{\mu_2}\right)+$$

$$\frac{\varphi_{13}K_3B_3}{\mu_3}\left(c-\frac{1}{\mu_3}+\left(c+\frac{1}{\mu_3}\right)\exp(-2\mu_3 c)\right)\Bigg],\ C_7=-\frac{2a_3}{a_1}\left(\frac{C_6}{r_0^2}+\frac{C_5}{2b_3}\right). \qquad (14)$$

Таким образом, искомые перемещения в пластине при локальной круговой нагрузке (9) определяются формулами (11) с константами интегрирования (13), (14).

Численные результаты получены для пластины единичного радиуса, материалы слоев которой Д16Т–фторопласт–Д16Т. Принимались: $B_1 = B_2 = B_3 = 10^{23}$ м^2/нейтрон, что обеспечивает объемную деформацию в слоях порядка 3–3,5 %; для дюралюминия – $\mu_1 = 1{,}26$ см; для фторопласта $\mu_3 = 3{,}21$ см; интенсивности распределенной круговой нагрузки $q_0 = -1$ МПа, толщины слоев $h_2 = 0{,}04$, $h_3 = 0{,}4$. Константы упругости материалов заимствованы из работ [4, 5].

На рис. 2 показано изменение вдоль радиуса прогиба w – (*а*) и распределение по высоте поперечного сечения на контуре пластины ($r = r_0$) линейных деформаций ε_r^k – (*б*) при облучении нейтронными потоками различных интенсивностей (нейтрон / (м^{2}с)): *1* – $\varphi_1 = 10^{17}$, 2 – $\varphi_2 = 10^{18}$. Силовая нагрузка отсутствует. Толщины слоев: $h_1 = 0{,}02$; $h_2 = 0{,}06$; $h_3 = 0{,}4$. Усиление интенсивности потока на порядок вызывает примерно такое же увеличение прогиба и радиальной деформации.

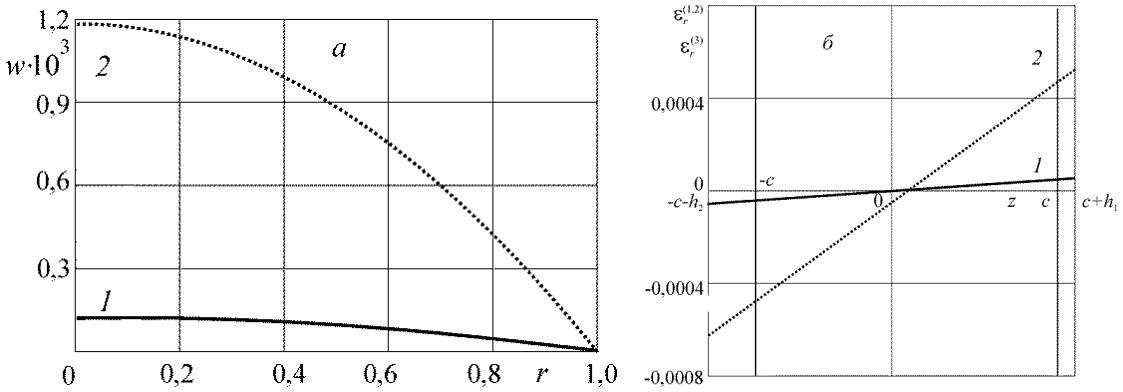

***1* – $\varphi_1 = 10^{17}$, 2 – $\varphi_1 = 10^{18}$ (нейтрон / (м^{2}с))**

Рисунок 2 – **Прогиб *w* – (*а*) и радиальная деформация ε_r^k – (*б*) при нейтронном облучении**

Следует отметить, при воздействии нейтронного облучения происходит увеличение объемной деформации в каждом слое, при этом верхний слой облучается потоком большей интенсивности, что вызывает его распухание и прогиб, в ряде случаев направленный вверх. Существует такое значение толщины верхнего слоя $h_1 = h_1^*$, при котором прогиб обращается в ноль. При выбранных параметрах пластины ($h_3 = 0{,}4$, $h_2 = 0{,}04$) и величины нейтронного потока критическая толщина верхнего слоя $h_1^* \approx 0{,}012$. Если $h_1 < h_1^*$, то прогиб направлен вниз, при $h_1 > h_1^*$ пластина выпукла вверх.

Радиальная деформация в верхнем слое и примыкающей части заполнителя положительна, что говорит об их растяжении. Нейтронное облучение не вызывает относительный сдвиг в заполнителе.

Графики зависимости максимального прогиба w в центре трехслойной пластины от положения кольца нагрузки постоянной ширины $b - a = 0{,}25$ при различных величинах интенсивности нейтронного потока (нейтрон / (м^{2}с)): *1*– $\varphi_1 = 0$, *2* – $\varphi_2 = 10^{17}$, 3 – $\varphi_3 = 10^{18}$ показаны на рис. 3 ($h_1 = 0{,}01$ м) и 4 ($h_1 = 0{,}02$ м).

Здесь, если толщина верхнего несущего слоя меньше критической $h_1 < h_1^* \approx 0{,}012$, то увеличение интенсивности нейтронного потока приводит к смещению прогиба в сторону

действия локальной нагрузки. Максимум абсолютной величины прогиба достигается при кольцевой нагрузке с внутренним радиусом a = 0,25.

В случае толщины $h_1 > h_1^*$ график прогиба с ростом интенсивности нейтронного потока смещается вверх. Максимум абсолютной величины прогиба достигается при кольцевой нагрузке с внутренним радиусом a = 0,75. В этом случае при интенсивности нейтронного потока φ_3 прогиб от нейтронного облучения превосходит прогиб от кольцевой нагрузки и направлен в сторону противоположную ее действию.

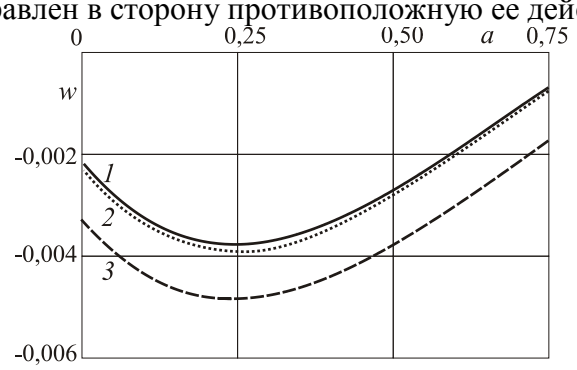

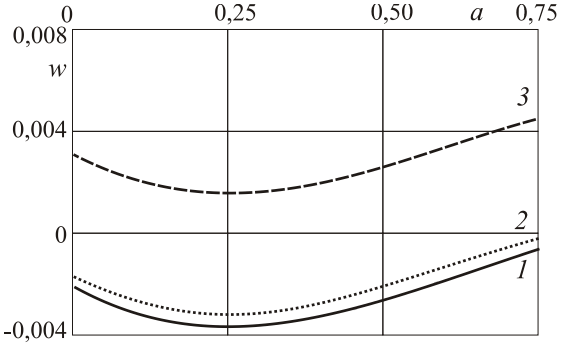

***1*– φ_1 = 0, *2* – $\varphi_2 = 10^{17}$, 3 – $\varphi_3 = 10^{18}$**

Рисунок 3 – **Максимальный прогиб в зависимости от координаты начала кольца нагрузки (h_1 = 0,01)**

Рисунок 4 – **Максимальный прогиб в зависимости от координаты начала кольца нагрузки (h_1 = 0,02)**

4. Заключение

Предложенная постановка краевой задачи и полученное общее решение уравнений равновесия позволяют исследовать напряженно-деформированное состояние упругих трехслойных круговых пластин под действием локальных нагрузок и с учетом нейтронного облучения. Численные результаты показали возможность возникновения напряженно-деформированного состояния в пластине только за счет нейтронного воздействия и его существенную зависимость от геометрических и упругих параметров материалов слоев.

Работа выполнена при финансовой поддержке Белорусского республиканского фонда фундаментальных исследований.

Литература

1. *Ильюшин А. А., Огибалов П. М.* Упругопластические деформации полых цилиндров / Москва, Изд-во МГУ, 1960, 224 с.
2. *Платонов, П. А.* Действие облучения на структуру и свойства металлов. Москва, Машиностроение, 1971, 40 с.
3. *Куликов И.С., Нестеренко В.Б., Тверковкин Б.Е.* Прочность элементов конструкций при облучении / Минск, Навука і тэхніка, 1990, 144 с.
4. *Горшков А.Г., Старовойтов Э.И., Яровая А.В.* Механика слоистых вязкоупругопластических элементов конструкций / Москва, ФИЗМАТЛИТ, 2005, 576 с.
5. *Журавков М.А., Старовойтов Э.И.* Математические модели механики твердого тела / Минск, БГУ, 2021, 535 с.
6. *Zhuravkov M.A., Lyu Yongtao, E.I. Starovoitov.* Mechanics of Solid Deformable Body / Singapore, Springer, 2023, 317 p.
7. *Абдусаттаров А., Старовойтов Э.И., Рузиева Н.Б.* Деформирование и повреждаемость упругопластических элементов конструкций при циклических нагружениях / Ташкент, «IDEAL PRESS», 2023, 381 с.
8. *Aghalovyan L.* Asymptotic theory of anisotropic plates and shells / Singapore–London, World Scientific Publishing; 2015, 376 p.
9. *Старовойтов, Э. И.* Сопротивление материалов / Гомель, БелГУТ, 2004, 376 с.
10. *Старовойтов, Э. И.* Механика материалов / Гомель, БелГУТ, 2011, 380 с.
11. *Старовойтов Э.И., Леоненко Д.В.* Исследование спектра частот трехслойной цилиндрической оболочки с упругим наполнителем // Механика композиционных материалов и конструкций. 2015, vol. 21, No. 2, pp. 162–169.
12. *Bakulin VN, Boitsova DA, Nedbai AYa.* Parametric resonance of a three1layered cylindrical composite rib-stiffened shell // Mechanics of composite materials, 2021, vol. 57, No. 5, pp. 623–634.

13. *Tarlakovskii DV, Fedotenkov GV.* Two-Dimensional Nonstationary Contact of Elastic Cylindrical or Spherical Shells // Journal of Machinery Manufacture and Reliability, 2014, vol, 43, No. 2, pp. 145–152.
14. *Suvorov YeM, Tarlakovskii DV, Fedotenkov GV.* The plane problem of the impact of a rigid body on a half-space modelled by a Cosserat medium // Journal of Applied Mathematics and Mechanics, 2012, vol. 76, No. 5, pp.511–518.
15. *Леоненко Д.В., Маркова М.В.* Колебания круговой трехслойной пластины под действием внешней нагрузки // Журнал Белорусского государственного университета. Математика. Информатика, 2023, т. 1, С. 49–63.
16. *Лачугина Е.А.* Поперечные колебания пятислойной упругой круговой пластины с жесткими заполнителями // Механика. Исследования и инновации, 2022, вып. 15, С. 212–219.
17. *Лачугина Е.А.* Частоты собственных колебаний пятислойной круговой пластины // Теоретическая и прикладная механика, Минск, БНТУ, 2023, вып. 38, С. 227-233.
18. *Pradhan M, Dash PR, Pradhan PK.* Static and dynamic stability analysis of an asymmetric sandwich beam resting on a variable Pasternak foundation subjected to thermal gradient // Meccanica, 2016, vol. 51, No. 3, pp.725–739.
19. *Starovoitov É.I., Pleskachevskii Yu.M., Leonenko D.V., Tarlakovskii D.V.* Deformation of a Step Composite Beam in a Temperature Field // Journal of Engineering Physics and Thermophysics, 2015, vol. 88, No. 4, pp. 1023-1029.
20. *Старовойтов Э.И., Леоненко Д.В.* Деформирование трехслойного стержня в температурном поле // Механика машин, механизмов и материалов, 2013, т. 22, С. 31–35.
21. *Старовойтов Э.И., Козел А.Г.* Изгиб упругой круговой трехслойной пластины на основании Пастернака // Механика композиционных материалов и конструкций, 2018, т. 2, No. 3, С. 392–406.
22. *Zadeh HV, Tahani M.* Analytical bending analysis of a circular sandwich plate under distributed load // International Journal of Recent Advances in Mechanical Engineering, 2017, vol. 6, No. 1, pp. 01-10.
23. *Yang L, Harrysson O, West H, Cormier D.* A comparison of bending properties for cellular core sandwich panels // Materials Sciences and Applications, 2013, vol. 4, No. 8, pp. 471–477.
24. *Захарчук Ю.В.* Напряженно-деформированное состояние круговой трехслойной пластины со сжимаемым заполнителем. // Механика. Исследования и инновации, 2019, т. 12, No. 12, С. 66–75.
25. *Козел А.Г.* Влияние сдвиговой жёсткости основания на напряжённое состояние сэндвич пластины // Фундаментальные и прикладные проблемы техники и технологии, 2018, т. 332, No. 6, С. 25–34.
26. *Нестерович, А.В.* Напряженное состояние круговой трехслойной пластины при осесимметричном нагружении в своей плоскости // Механика. Исследования и инновации, 2019, т. 12, No. 12, С. 152–157.
27. *Салицкий, В.С.* Изгиб защемлённой по контуру круговой пятислойной пластины // Механика. Исследования и инновации, 2022, т. 15, No. 15, С. 209–213.
28. *Салицкий, В.С.* Изгиб круговой пятислойной пластины // Теоретическая и прикладная механика. Минск, 2023, вып. 38, С. 234 – 239.
29. *Старовойтов Э. И., Леоненко Д. В.* Переменный изгиб трехслойного стержня со сжимаемым заполнителем в нейтронном потоке // Изв. Сарат. ун-та. Нов. сер. Сер. Математика. Механика. Информатика, 2017, т. 17, вып. 2, С. 196–208.
30. *Старовойтов Э.И., Абдусаттаров А., Рузиева Н.Б.* Циклическое нагружение упругопластических трёхслойных стержней с учетом их повреждаемости // Узб. журнал Проблемы механики, 2023, No. 1, С. 66–74.
31. *Старовойтов Э.И., Леоненко Д.В., Абдусаттаров А.* Знакопеременное термосиловое нагружение трёхслойной пластины погонными моментами // Узб. журнал «Проблемы механики», 2023, No. 3, С. 20–30.
32. *Москвитин В.В.* Циклическое нагружение элементов конструкций / Москва, Наука, 1981, 344 с.

ИЗУЧЕНИЕ ДЕФОРМАЦИОННЫХ ХАРАКТЕРИСТИК ДВУХСЛОЙНОГО ТРИКОТАЖНОГО ПЕРЕПЛЕТЕНИЕ

Убайдуллаева Д.Х.[1], Ахмедова М.Ф[1]., Ортикова Н.[1]

[1]Ташкентский институт текстильной и легкой промышленности, Ташкент,
E-mail: begmanov701@gmail.com

Аннотация. *В статье для изучения влияние изменения структуры двухслойного переплетение, были исследованы и сопаставлены технологические и физико-механические свойства 4 вариантов трикотажных полотен, выработанных на плоскофанговой машине.*

Ключевые слова: *переплетения, футер, воздухопроницаемость, разрывное удлинение, разрывная нагрузка, деформационная свойство.*

1. Введение

Износ одежды в основном вызван силами растяжения, сжатия, изгиба и силами трения. Поэтому устойчивость изделие к различным механическим воздействиям, т. е. его механические свойства, имеет большое значение для хорошего и длительного сохранения формы и формы одежды.

К механическим свойствам текстильных изделий относятся прочность, удлинение, износостойкость, сменяемость, жесткость, драпируемость и другие свойства [1-6].

Прочность текстильной продукции на разрыв является одним из важнейших показателей, определяющих ее качество. При оценке качества текстильных изделий в лаборатории определяют предел прочности и сравнивают с нормативными нормами. Прочность текстильных изделий на разрыв зависит от содержания в них волокон, количества или количества пряжи, плотности, вид переплетение и характера отделки [7-8]. С целью изучения свойств сохранения формы трикотажных полотен были получены новые варианты двухслойного трикотажного полотна с новой структурой.

2. Материалы, методы и объект исследования.

Изучены показатели качества новых 4-х видов двухслойных трикотажных полотен, полученных с использованием технологических возможностей плосковязальных машин 10-го класса с электронным управлением «LONG XING», а также влияние изменения структура переплетение на деформационные свойства [9].

Состав разработанной переплетение – 100% пряжа ПАН 32х2 текс. Образцы отличаются друг от друга по строению переплетение.

Отобранные для эксперимента образцы выдерживали 24 часа в климатических условиях по ГОСТ 10681 [10-16]. Образцы представленных вариантов двухслойного трикотажного полотна были отобраны согласно требованиям, ГОСТ 8844, а их технологические параметры, физико-механические свойства определены стандартным методом в лаборатории качества «Cen-Tex» ТИТЛП, представлены полученные результаты в таблице 1.

3. Постановка задачи.

Составные части деформации и другие одно цикловые характеристики текстильных полотен определяют на приборах релаксометр стойках.

Растяжение трикотажных полотен нагрузками, меньшими разрывных, в цикле нагрузка-разгрузка-отдых дает возможность определить величины полной деформации, ее составные части и доли их в полной деформации.

Определению компонентов деформации текстильных полотен на растяжение полную деформацию разделяют на быстро обратимую, медлен обратимую и остаточную части. За быстро обратимую деформацию принимают часть деформации, исчезающую за 2-5 с отдыха после разгрузки образца; часть деформации, исчезающую за время наблюдения за вычетом быстро обратимой деформации, принимают за медленнообратимую часть деформации, и наконец, деформацию, оставшуюся к моменту окончания наблюдений, за остаточную [17].

4. Результаты.

Таблица 1.

Физико-механические параметры двухслойных трикотажных полотен.

Параметры		Варианты				ГОСТ
		I	II	III	IV	
Тип и линейная плотность нитей, текс	Передний слой	ПАН 32,5 текс х2	ПАН32,5 текс х2	ПАН 32,5текс х2	ПАН 32,5 текс х2	
	Задний слой	ПАН 35текс х2	ПАН 35текс х2	ПАН 35 текс х2	ПАН 35 текс х2	
Воздухопроницаемость В, sm^3/sm^2 s		180,9	99,6	95,5	98,2	ГОСТ 12088-77 30 -100
Теплопроводность, %		26%	37,5%	38%	28%	28%
Устойчивость к истиранию, И, цикл		28500	35000	36000	32500	ГОСТ 16486-93 30-60
пиллинг		-	-	1	12	
Усадка, У %	По вертикале	0,8	1,4	1,6	1,2	ГОСТ 26667-85 5-8%
	По горизонтале	1,5	2	1,8	2	Кўпи б-н 8-10%
Разрывная нагрузка, Р N	По вертикале	289,76	354,66	452,665	479,26	479,26
	По горизонтале	415,4	321,73	363,435	301,03	301,03
Разрывная удлинение, L,%	По вертикале	14	13	17	16	ГОСТ 8847-85 6 N да 40-100% 2 гр
	По горизонтале	15	22	18	20	
Пластик деформация, $\varepsilon_п$, %	По вертикале	14	14	8,3 (17,1)	14	ГОСТ 28882-90 До 15-20%
	По горизонтале	15	13	16(0,19)	30	
Упругая деформация, $\varepsilon_у$, %	По вертикале	43	28	32,7(67,8)	39	
	По горизонтале	29	49	52,3(0,63)	78	
Эластический деформация, $\varepsilon_э$ %	По вертикале	16	11	7,3(15,1)	10	
	По горизонтале	16	15	15(0,18)	30	

5. Анализ результатов.

Для исследуемого ассортимента необходимо проанализировать ряд факторов, формирующих свойства и структуру трикотажных полотен трикотажа. К ним относятся легкость трикотажного полотна, воздухопроницаемость трикотажного полотна, прочность на разрыв и удлинение при разрыве, упругая деформация и усадка.

Показатель воздухопроницаемости образцов двухслойного трикотажного полотна изменился от 180,9 до 95,5 $см^3/см^2 \cdot с$ за счет изменения структуры полотна трикотажного полотна, то есть воздухопроницаемость изменилась на 48 % (табл. 2).

В результате сравнения вариантов двухслойного трикотажного полотна по показателю теплопроводность образец варианта III оказался образцом с самым высоким показателем теплопроводности по сравнению с образцами других вариантов и составил 38%.

Прочность на разрыв двухслойного трикотажного полотна составляла от 479,26 до 289,76 N, полотно 4 было на 39,6% выше, чем полотно 1. Разрывная нагрузка по горизонтали двухслойного трикотажного полотна изменилась с 415,4 N до 301,03 N при этом вариант 1 оказался на 28% выше по длине полотна. (Табл. 1).

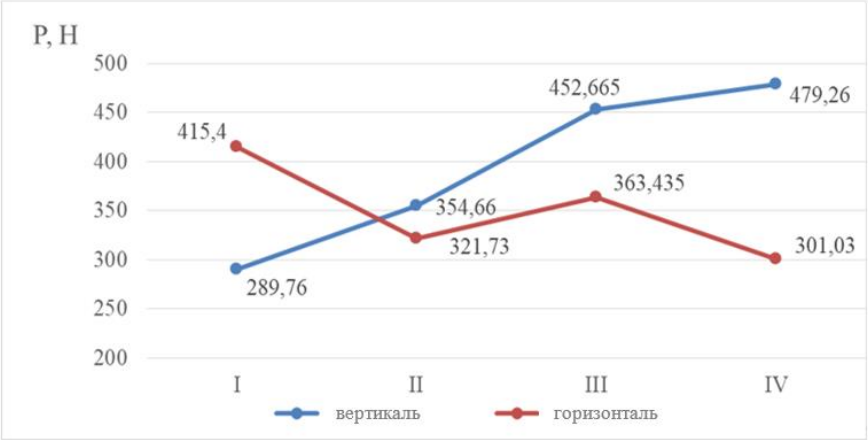

Рисунок 1. - **Зависимость прочности двухслойного переплетения по длине и ширине от структуры трикотажа**

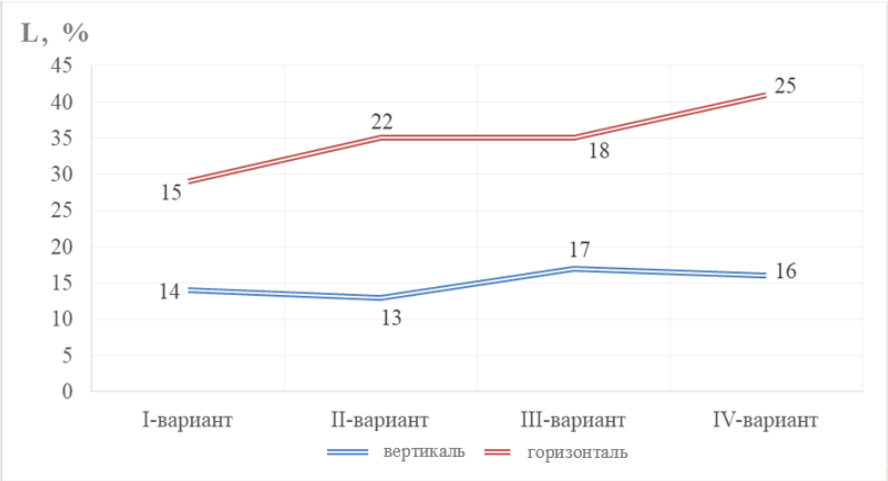

Рисунок 2. - **Зависимость растяжимости двухслойного переплетения по длине и ширине от структуры трикотажного полотна**

6. Обсуждение.

С целью определения деформационных свойств образцов проводились эксперименты на релаксометр «стойка» устройстве, для чего каждый вариант подвергался нагрузке, равной 5 % от предела прочности трикотажного полотно, и изучались их упругие, эластические и пластические деформации, а результаты представлены в таб.-2.

Таблица 2.

Определения деформационных свойств экспериментов

Вар -ты	Направ время	По вертикале							По горизонтале						
		1^1	1	10	20	30	40	60	1^1	1	10	20	30	40	60
1-вар	нагруз	164	167	171	171	172	173	173	156	158	159	159	160	160	160
	без нагруз	130	125	121	119	118	116	114	131	126	122	118	116	115	115
2-вар	нагруз	140	141	145	145	147	147	148	144	145	148	149	150	152	153
	без нагруз	125	120	118	117	115	114	114	125	120	118	117	116	114	114
3- вар	нагруз	147,3	147,5	148	148	148	148	179	181	182	182	182	183	183	183
	без нагруз	114,6	111,6	111,3	110	108,6	108	106	131	126	124	122	119	117	116
4- вар	нагруз	155	158	160	160	162	162	163	210	218	222	222	225	225	228
	без нагруз	126	121	119	117	115	115	114	150	140	135	130	125	123	120

Таблица 3.

Определение одно циклового деформация по вертикале

Деформация	Варианты			
	I	II	III	IV
Общий деформаци	73	48	79	63
Упругая	43	23	64,4	37
Эластическая	16	11	8,6	12
Пластическая	14	14	6	14

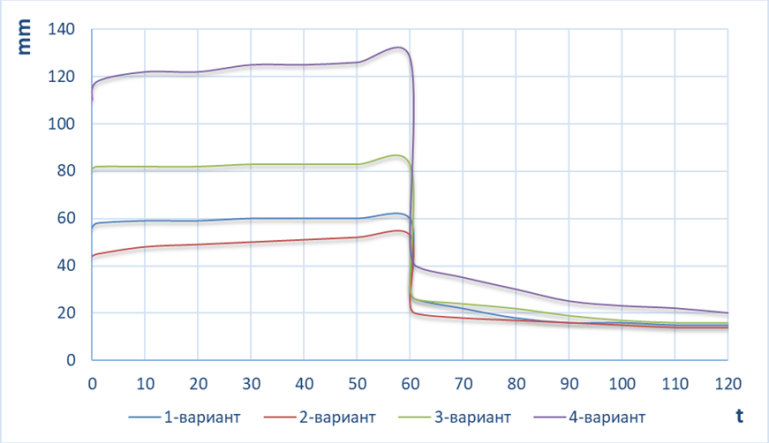

Рисунок 3. - **Одноцикловая деформация по вертикали**

При анализе одно циклового деформация по вертикале общая деформация растяжения в первом образце составила 73 %, из них упругая деформация 43 % (58,9 %), эластическая деформация 16 % (21,9 %), пластическую деформацию 14 % (19,2 %).

Во втором образце общая деформация составила 48 %, из них упругая деформация - 23% (47,9 %), эластическая деформация – 11 % (22,9 %), пластическая деформация – 14 % (29,2 %).

В третьем варианте общая деформация образца составила 79 %, из них упругая деформация 64,4 % (81,5 %), эластическая деформация 8,6 % (10,9 %) и пластическая деформация 6 % (7,6 %).

Четвертый вариант имеет общую деформацию 63 %, из них 37 % (58,7 %) — упругая деформация, 12 % (19,1 %), 12 % (19,1 %) — упругая деформация и 14 % (19,1 %) пластическая деформация. (рис. 3).

Таблица 4.

Определение одно циклового деформация по горизонтале

Деформация	Варианты			
	I	II	III	IV
Общая деформация	60	53	83	128
Упругая	29	28	52	78
Эластическая	16	11	15	30
Пластическая	15	14	16	20

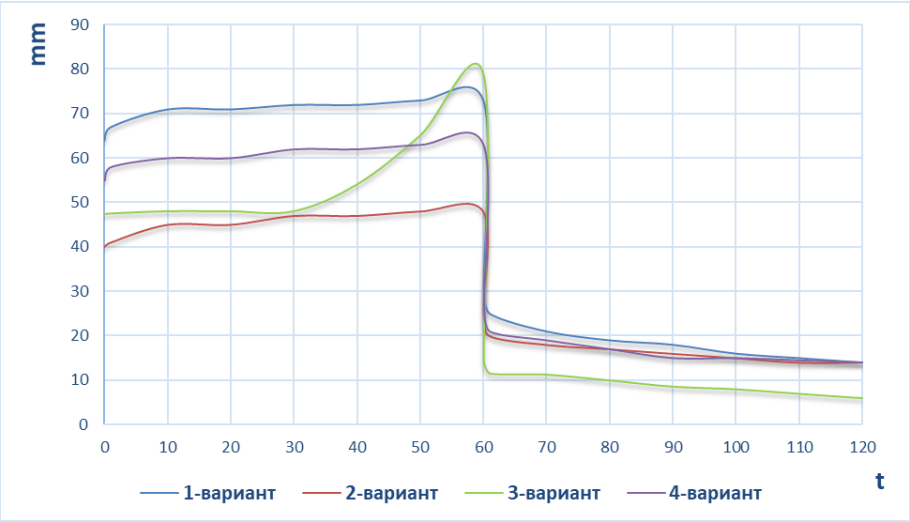

Рисунок 4. - **Одноцикловая деформация по горизонтале**

При анализе поперечного одно циклового деформации по горизонтали IV варианта составила 78 % (61 %), из них 48 % (48,3) по сравнению с I вариантом, 50 % (52,8 %) по сравнению с I вариантом. II варианта, а 50% (52,8%), по сравнению с III вариантом она оказалась выше на 26% (62,6%) (рис. 2).

По результатам эксперимента по стойкости к истиранию трикотажного полотна было показано, что стойкость к истиранию исследуемых двухслойных трикотажных полотен изменяется в зависимости от типа переплетения полотна. Было обнаружено, что этот вариант меняет стойкость трикотажа к истиранию с 28 000 циклов до 36 000 циклов. Самый высокий показатель составил 36 000 циклов, или на 45,5% выше базового показателя, для трикотажа варианта 3.

По результатам анализа физико-механических свойств двухслойного трикотажного полотна установлено, что изменение объемной плотности и толщины трикотажного полотна наблюдается за счет изменения структуры полотна. Высокие показатели сохранения формы и истирания достигаются за счет изменения структуры вязания двухслойных трикотажных полотен.

7. Заключение.

В заключение можно сказать, что при получении трикотажных полотен и производстве из них готовой одежды изучение их деформационных характеристик позволяет заранее спрогнозировать место и срок использования.

В заключение можно сказать, что слои предлагаемых двухслойных трикотажных полотен также позволяют использовать пряжу различного состава и линейной плотности. Уменьшить себестоимость изготавливаемого изделия можно за счет использования дешевой пряжи при вязании заднего (внутреннего) слоя трикотажа, а улучшить гигиенические свойства трикотажа за счет использования натуральных нитей.

Анализ физико-механических свойств двухслойных трикотажных полотен показывает, что эти полотна могут найти широкое применение при производстве верхних трикотажных изделий.

Литература

1. Убайдуллаева Д.Х., Жуманиязов М.Б.. Физико-механического свойство нового футерного трикотажа Ж. "Экономика и социум" Россия 2022.
2. *Ubaydullayeva D.Kh., Begmanov R.A., Abdurasulov I.V. Djalilova Z.A., Nazarova D.T.* Quality Assessment and Forecasting the Properties of Press Weaving Knitting. International Journal of Advanced Research in Science, Engineering and Technology 2022/1 18828-18831
3. *Valieva Z. F., Akhmedov A.A., Ochilov T., Ubaydullayeva D.* Possibility to Use Acoustic Device Pam-1 to Determine Quality Characteristics of Wool Fiber. Received 25 2021/5/8 10166 – 10173
4. *Шустов Ю.С.* Основы текстильного материаловедения. –М.: ООО «Совъяж Бево», 2007.

5. *Hankhadjaeva* N., *Mukimov M.* “Flat knitting interlock structures” Indian Textile Journal №1.14-18 бет.www.indiantextilejournal.com
6. *Ubaydullaeva D. X.* et al. Change efficiency of cleaning cotton from small and large pollutions //International Journal of Advanced Research in Science, Engineering and Technology. – 2020. – Т. 7. – №. 9. – С. 14781-14784.
7. *Убайдуллаева Д. Х., Валиева З. Ф., Бегманов Р. А.* Применение управления качеством продукции текстильной промышленности //Экономика и социум. – 2022. – №. 9 (100). – С. 647-653.
8. *Д.Ҳ.Убайдуллаева, М.Б.Жаниева, М.Ф.Аҳмедова, Н.Ортиқова, Рустамова С* “Икки қавватли трикотаж тўқимасининг деформация хусусиятларини тадқиқи” “Soxa korxonalari uchun yuqori malakali kadrlar tayyorlashda dual ta’limning o‘rni hamda fan, ta’lim, ishlab chiqarish klasterlarini rivojlantirishda innovatsion yondoshuvlar” mavzusiga bag‘ishlangan xalqaro ilmiy-amaliy anjumani to‘plami.1-qism. Toshkent 28-noyabr. 323.б.
9. *Убайдуллаева Д. Х., Бегманов Р. А., Ахмедова М.Ф.* “Саноат ва қишлоқ хўжалик тармоқларида экология ва меҳнат муҳофазаси муоммалари” Республика илмий амалий конференция. Бухоро. 2023. 19-20 октябрь. 310 б.
10. ГОСТ 28554-90. ТРИКОТАЖ. Основные Характеристики
11. ГОСТ 8844-87.отбор проб.
12. ГОСТ 8845-87.Определение поверхностной плотности и влажности полотна, массы куска
13. ГОСТ 8846-87.Определение перекоса, ширины полотна, количества петельных рядов и петель.
14. ГОСТ 8847-87.Определение разрывной нагрузки по длине полотна по растяжимости полотна при нагрузках меньше разрывных
15. ГОСТ 12739-85.Определение стойкости полотна к истиранию
16. ГОСТ 30157.0-85.Определение измерения линейных размеров полотна после мокрой обработки
17. Кирюхин С.М., Шустов Ю.С. Текстильное материаловедение. Москва «Колос-С», 2011. 248 стр.

ЭКСПЕРИМЕНТАЛЬНЫЕ ИССЛЕДОВАНИЯ КОНТАКТНОЙ ЗАДАЧИ БАЛКИ И ГРУНТОВОГО ОСНОВАНИЯ.

Хасанов А.З.[1], Хасанов З.А.[2], Турсунов Ш.А.[3]
[1] СамГУ. Самарканд, Узбекистан
[2] ООО «Геофундаментпроект», [3]СамГАСУ , Самарканд, Узбекистан.
E-mail: ussmge@gmal.com

Аннотация. *В статье рассмотрены вопросы экспериментальных исследований прогибов балки, расположенной на грунтовом основании при воздействии часто встречающихся на практике нагрузок: равномерно распределенной, сосредоточенной по середине и с краю балки нагрузкой. Предложены математические и механические модели позволяющие учитывавать сдвиговую жесткость грунта, изгибную жесткость балки и расчетные схемы для определения прогибов и усилий в балке.*

Ключевые слова: *грунт, балка, эксперимент.*

1. Введение

Основные принципы расчета контактных задач конструкции и грунтового основания. Основные задачи теории контактных задач взаимодействия (лежащей или внедренный в массив грунта, строительных конструкций, нагруженных внешними или гравитационными нагрузками) конструкции и грунтового основания:

a. Конструкции, взаимодействующие с грунтовым основанием воспринимают внешние $q(x)$ и реактивные усилия $P(x)$ грунта, от разности которых в теле конструкции возникают изгибающие моменты $M(x)$ и перерезывающие усилия $Q(x)$. При этом расчет перемещений и усилий балки должен удовлетворять двум основным требованиям: при расчете прогибов балки должно удовлетворятся требования статики $q(x) = P(x)$.

b. Прогибы балки необходимо расчитывать с учётом упруго-пластической работы грунтового основания соотвествующего моменту стабилизации ее осадок. В зависимости от вида нагружения, на определенном растоянии l от оси нагружения будет иметься ограничения по перемещениям $0 \leq w(x) \leq f_{max}$. Осадка системы фундаментов в целом производится с учетом основных закономерностей механики грунтов, в частности согласно упруго-пластическим моделям.

c. Прогиб строительных конструкций и (деформации) грунта в области контакта отвечает требованиям неразрывности, т.е. $0 \leq P(x) \leq 1{,}2R$, где R-реактивные напряжения не превышающие квазилинейную область деформирования грунта. Функционал реактивного давления $P(x)$ зависит от вида нагружения и вида грунта, расположеного в контактной области H_s балки.

d. Итоговая или суммарная жесткость лежащей или внедренной в грунт конструкции (EI) и квазилинейно деформируемого грунтового основания t (сдвиговая жесткость грунта) формирует функцию прогиба конструкции $0 \leq w(x) \leq f_{max}$и функцию радиуса кривизны $\rho(x) = W^1(x)$. Функция реактивного давления грунта на конструкцию $P(x)$ совместно с внешними усилиями $q(x)$ при сохранении условия равновесия формируют функцию внутренних усилий и влияет на величину изгибающих моментов M и перерезывающих сил Q.

Из классической механики известно, что расчетные деформации и внутренние усилия нагруженной балки (плиты), жесткостью EI лежащей на упругом основании зависит от принятой контактной модели. В контактных моделях реактивное давление $p(x)$ принимается постоянным как линейно зависящее от жесткости грунта местному смятию C_1 [1] (предложенной Фуссом, Винклером – Цимерманом, Пастернак П.Л.). Математическое выражение этой модели имеет следующий вид

$$\frac{d^4Y}{dX^4} = \frac{qb}{EI} - \frac{4}{s^4}Y \tag{1}$$

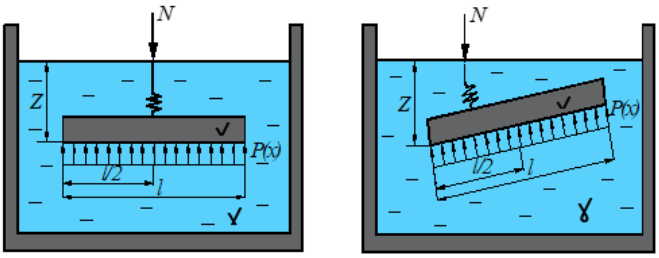

Рисунок 1. - **Модель предложенная Винклером – Цимерманом. а-при центральном нагружении и в-при внецентренном нагружении**

Дифференциальное уравненение (1) характеризует изгиб балки нагруженной внешними q и реактивными нагрузками $P(x)$. Функция реактивного давления считается неизвестной, по этой причине его величина подбирается в соотвествии с принятыми моделями или в виде функционала. В частности в выражении (1) его величина принята в соотвествии с моделью Винклера (рис.1). При этом по закону статики балка по краям условно закреплена на неподвижные шарнирные опоры. Если $\frac{dY}{dX} = 0$ прогиб и $\frac{d^4Y}{dX^4} = 0$ реактивное давление под балкой равномерная, в этом случае выполняется условие модели Винклера – Цимермана.

Учитывая схожесть функций производных $w^{IV}(x)$ и $w^1(x)$ и для упрощения задачи определения величины реактивного давления Пастернак П.Л.[1] сводит задачу к виду

$$P(x) = C_1 w(x) + C_2 \dot{w}(x) \tag{2}$$

Вторая часть уравненеия (2) позволяет учитывать прогиб балки при действии на балку равномерно распределенной нагрузки. При описании выражения (2) авторы предполагали, что первая часть уравнения соответствует модели Винклера и характеризует реактивное давление $P(x)$ пропорциональной величине вертикальной осадки балки за счет сжатия грунта (осадки) [1]. Ее можно представить в виде модели погружения деревянной балки в водной среде (Рис 1).

$$P(x) = N/l = (\gamma_w - \gamma_c)z = Cw(x) \tag{3}$$

где $C = (\gamma_w - \gamma_c)$ –разница жидкой и твердой составляющей плотности.

Вторая его часть характеризует величину реактивного давления $P(x)$ пропорциональная радиусу кривизны, т.е. за счет сопротивления грунтов сдвигу возникающие при изгибе балки $w(x)$. Если предположить что на балку воздействует равномерно распределенная нагрузка интенсивностью q то при симметричном ее изгибе [8].

$$P(x) = C_2 \frac{f}{l} = C_2 \varepsilon \quad (4)$$

коэффициент характеризующий жесткость конструкции изгибу

$$C_2 \cong 4 \frac{EI}{l^3} \quad (5)$$

где $\varepsilon = \frac{f}{l}$ - относительный прогиб балки.

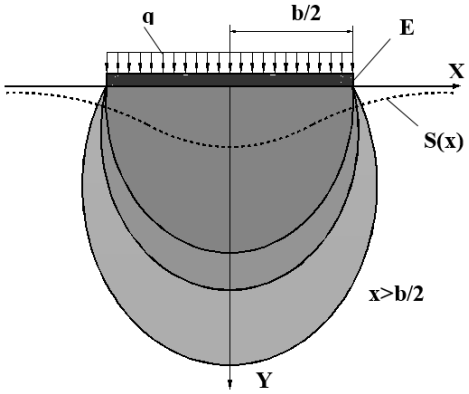

Рисунок 2. – **Расчетная модель упругого полупространства**

В соответствии с (2 и 3) такое возможно, только при $q(x) - P(x) = const$ для балки по кантакту, которой возникают дополнительные сдвиговые напряжения, направленные с краев к его центру. Прогиб, установленной внутри водной среды балки, так же можно смоделировать при помощи ограничивания перемещения связями, установленными по ее краям. В обоих случаях от равномерно распределенной нагрузки в теле балки возникнут деформации прогиба. И так, выражения П.Л. Пастернака [1] в отличии от модели Винклера дополнительно характеризует и изгиб конструкции при равномерной нагрузке. Основным недостатком этого выражения (2) является, то что функция реактивного давления $P(x)$ искусственно, от постоянной величины, поднимается до степенной пропорциональной коэффициенту C_2. Вторая часть уравненеия (2) может исказить реальный прогиб балки при других видов нагрузок, поскольку прогиб балки будет возникать как за счет неравномерного сжатия так и за счет сдвига грунта под балкой.

В работе Симвулиди И.А. [11] реакция грунта в контактной области заменяется функцией реактивного давления в виде степенного ряда. Усилия и перемещения в балке определяются методом интегрирования дифференциального уравненеия, а неизвестные прараметры ряда определябтся по граничным условиям.

Таким образом решение дифференциального уравненеия (1) с учетом граничных условий сводится к определению функции перемешений $w(x)$ или функции реактивных усилий $P(x)$ от реактивный отпор среды считается упругим. Если считать хорошо изученным функцию прогиба балки от различных видов нагружений то уравненеие (1) предпочтительно характеризовать как прогиб части балки как от внешних нагрузок и заданных реактивных сил $P(x)$. В этом случае прогиб балки будет зависеть только от ее конструкционной жесткости.

Более общий случай дифференциального уравнения предложена вработе [3, 4].

$$\frac{d^4Y}{dX^4} = \frac{qa^4}{(1-\mu^2)^2 h^2 EI} + 2r^2 \frac{d^2Y}{dX^2} - s^2 Y \quad (6)$$

Например, такое может произойти, когда на защемленную с двух сторон балку воздействует распределенные или сосредоточенные силы.

Основной задачей решения уравнений (1, 6) является математический метод подбора наиболее приемлемой универсальной функции перемещения $w(x)$ или реактивных давлений и определение численных значений параметров уравненеия.

Для определения усилий (Q и M), прогиба и перемещений (ρ, w) принятое математическое выражение в виде многочлена выражение (3, 6) интегрируют а функцию

перемещений $\mathrm{w}(x)$ наоборот дифференцируют. При этом исходные функции в обоих случаях принимается различными [2, 3, 4]. Неизвестные параметры этих уравнении определяются исходя из граничных и контурных условий. Математическая постановка исходных уравненеий в частном случае может удовлетворить граничные условия, но и проявить побочные нежелательные эффекты в межграничных условиях, что может проитиворечить реальным физическим процессам. Таким образом пути решения поставленной задачи сводится к методам строительной механики, по результатам которой и определяется основные усилия в балке. Решение задачаи сводится к определению функции $\mathrm{w}(x)$ или $\mathrm{P}(x)$ в зависимости от его жесткости $\mathrm{E_c}I_\mathrm{c}$. Во всех этих моделях функция $\mathrm{P}(x)$ остается неизвестной, причем сопротивления грунта сдвигу возникающая при изгибе конструкции полностью игнорируется.

Известны модели, когда систему «здание – основание» принимают как единое целое; при этом трехмерное грунтовое основание под зданием рассматривают как упругую неразрывную среду [6, 4] (Рис. 2). В этом случае распределяющая способность упругой среди считается бесконечным, отсюда и большие расчетные прогибы балок, что противоречит с реальными наблюдаемыми на практике.

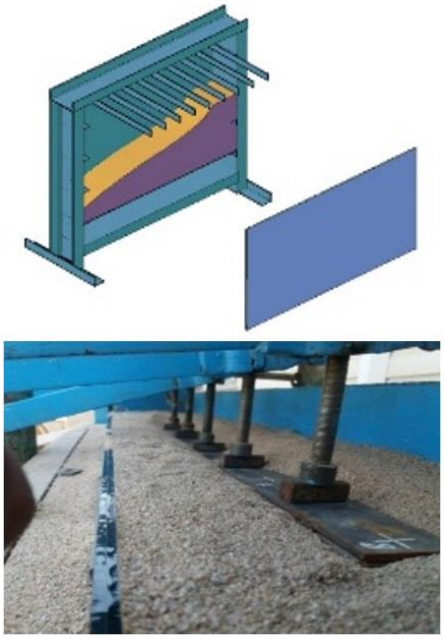

Рисунок 3. – **Конструкция лотка для определения прогибов балки лежащей на грунтовом основании**

В данной статье предпринята попытка решить эту сложную задачу путем экспериментального определения эпюры прогибов балки $\mathrm{w}(x)$, лежащей на грунтовом основании от различных внешних нагрузок. В этом случае интегральная величина изгибной жесткости принимается как сумма конструктивной жесткости балки $E_\mathrm{c}I_\mathrm{c}$ и сдвиговой жесткости грунтового основания- t. Жесткость балки, перемещение которой ограничено по концам определяется известными в механике методами. Что касасается сдвиговой жесткости грунта, то она определяется экспериментально в специальном плоском лотке. В отличии от традиционных методов испытаний металлическая балка (полоса) устанавливается снизу лотка и опирается на две шарнирные опоры. Эксперимент проводится с измерением максимального перемещения (прогиба) балки (полосы) $\mathrm{w}(L/2)$ или при ее отсутствии с измерением реактивного усилия в центре балки $\mathrm{P}(L/2)$ (рис-3) в процессе засыпки слоя грунта. Методика определения сдвиговой жесткости грунта и максимального ее прогиба балки авторами рассмотрена в работе [9]. В соответствии с этими исследованиями установлено, что величина приведенной жесткости балки $E_\mathrm{c}I_\mathrm{c}$ и грунтового основания t принимается как единое и определяется по выражению

$$EI = (E_\mathrm{c}I_\mathrm{c} + t) = E_\mathrm{c}I_\mathrm{c} + kE_0\frac{bH_s^3}{12} \qquad (7)$$

где $H_s \cong tg\varphi\ (l/2)$ –толщина активного слоя жёсткость грунта; -поправочный коэффициент. Модель составной балки (полосы) учитывающая сдвигувую жесткость грунта t принимается как совметсная работа упругой балки жесткостью $E_c I_c$ пролетом L и слоя грунта толщиной H_s , шириной b.

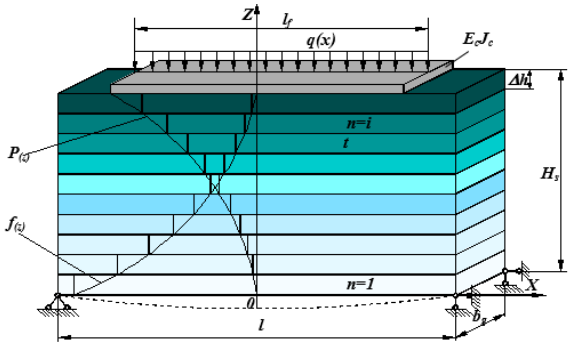

Рисунок 4. - **Механическая модель для определения сдвиговой жесткости грунта и используемая при расчете балок на грунтовом основании**

Максимальный прогиб составной балки, из условия равенства внешних (включая гравитационных) и реактивных усилий зависит от вида нагружения (Рис.4).

1-случай. Распределенная нагрузка интенсивностью q (симметричная задача). (Рис 5).

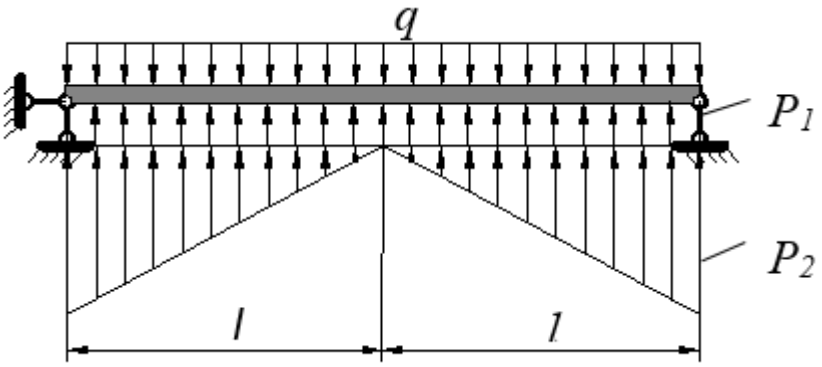

Рисунок 5. - **Расчетная модель влияния нагрузки, равномерно распределенной на балке**

Считается, что при внешненй равномерно распределеной нагрузкой q под балкой длиной L=2l появляется реактивное напряжение в виде суммы равномерной интенсивностью $P_1 = kq$ и неравномерной, состоящей из двух перевернутых треугольников с максимумом у краевой части $P_2 = 2q(1-k)$. Определим возможный максимальный прогиб балки с использованием известных в механике выражений:

- Для распределенных нагрузок $f_{max} = \frac{5q(2l)^4}{384EI} = \frac{80ql^4}{384EI}$.
- Разница, как $f_{\max(q)} - f_{\max(kq)} = \frac{80ql^4}{384EI}(1-k) = \frac{5ql^4}{24EI}(1-k)$
- Прогиб балки от краевых реактивных усилий в виде перевернутых двух треугольников с $P_2 = 2q(1-k)$:

$$f_{max} = 2\frac{P_2 l^3}{360EI * 2l}(40l^2 - 3l^2 - 10l^2) = 2\frac{P_2 l^3}{360EI * 2l}(40l^2 - 3l^2 - 10l^2) = \frac{27ql^4}{180EI}(1-k)$$

Итоговый максимальный прогиб балки от внешних и реактивных усилий (рис.5).

$$f_{max} = \frac{5ql^4}{24EI}(1-k) - \frac{27ql^4}{180EI}(1-k) = \frac{ql^4}{17EI}(1-k) \quad (8)$$

При $k = 0$

$$f_{max} = \frac{ql^4}{17EI}$$

При $k = 1$ выполняется условие модели Винклера.

$$f_{max} = 0$$

Соотвественно так же определяются и усилия в теле балки

$$M_x = \frac{qx^2}{6l}[(k-1)(3l-2x)] \; при \; x = l \; M_{max} = \frac{ql^2}{6}(k-1)$$

$$Q_x = \frac{qx}{l}[(k-1)(l-x)] \; при \; x = 0 \text{ и } l, \; Q_{x=l} = 0$$

2-случай. Сосредоточенная нагрузка N (симметричная задача). (Рис 6). Считается, что при внешненй точечной нагрузки N установленной по центру балки длиной L=2l появляется реактивное напряжение в виде суммы равномерной интенсивностью $P_1 = k\frac{N}{2l}$ и неравномерной, состоящей из одного перевернутого треугольника с максимумом в центральной части $P_2 = \frac{N}{l}(1-k)$.

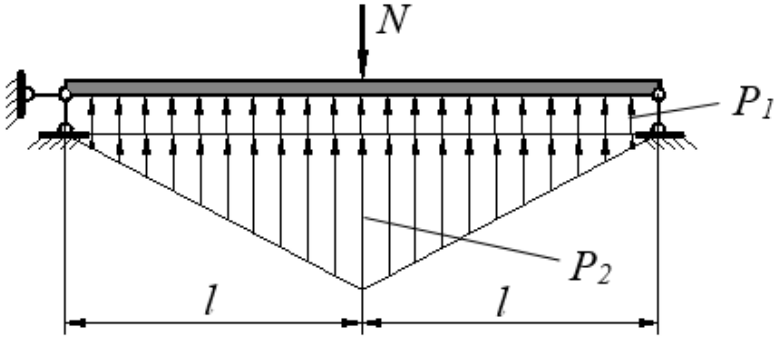

Рисунок 6. - **Расчетная модель влияния нагрузки, сосредоточенной в середине балки**

Определим возможный максимальный прогиб балки с использованием известных в механике выражений.

- Для сосредоточенной внешней нагрузки $f_{max} = \frac{8Nl^3}{48EI}$.
- Для распределенных реактивных нагрузок $f_{max} = \frac{5P_1(2l)^4}{384EI} = \frac{80l^4}{384EI}k\frac{N}{2l} = \frac{5l^3}{48EI}kN$.
- Разница, $f_{\max(N)} - f_{\max(kq)} = \frac{8Nl^3}{48EI} - \frac{5l^3}{48EI}kN = \frac{Nl^3}{48EI}(8-5k)$
- Прогиб балки от реактивных усилий в виде одного перевернутого треугольника с - $P_2 = \frac{N(1-k)}{l}$ максимальная величина эпюры распределенного реактивного усилия треугольной формы длиной $L = 2l$:

$$f_{max} = \frac{P_2(2l)^4}{120EI} = \frac{16(l)^3}{120EI}\,N\,(1-k) = \frac{4Nl^3}{30EI}(1-k)$$

- Итоговый максимальный прогиб балки от внешних и реактивных усилий

$$f_{max} = \frac{Nl^3}{48EI}(8-5k) - \frac{4Nl^3}{30EI}(1-k) = \frac{Nl^3}{240EI}(8+7k) \qquad (9)$$

(Рис.6). При $k = 0$

$$f_{max} = \frac{Nl^3}{30EI}$$

При $k = 1$ выполняется условие модели Винклера.

$$f_{max} = \frac{15Nl^3}{240EI} = \frac{Nl^3}{16EI}$$

Уравнения момента и поперечной силы определяются следующими математическими выражениями;

$$M_x = \frac{Nx^2}{12l^2}(2x + 3lk - 2kx) \text{ при } k = 0 \; x = 0 \text{ и } l, \; M_{max} = 0, M_x = \frac{Nl^2}{6};$$

$$\text{При } k = 1 \; x = 0 \text{ и } l, \; M_{max} = 0, M_x = \frac{N(2l^2+l)}{12};$$

$$\mathrm{Q_x} = \frac{\mathrm{Nx}}{2\mathrm{l}^2}[\mathrm{x} + \mathrm{lk} - \mathrm{kx}] \text{ при } \mathrm{k} = 0 \text{ и } 1 \; \mathrm{Q_{x=0}} = 0, \mathrm{Q_{x=l}} = \frac{\mathrm{N}}{2}$$

3-случай. Сосредоточенная нагрузка приложена с краю балки. (не симметричная задача) Рис.7.

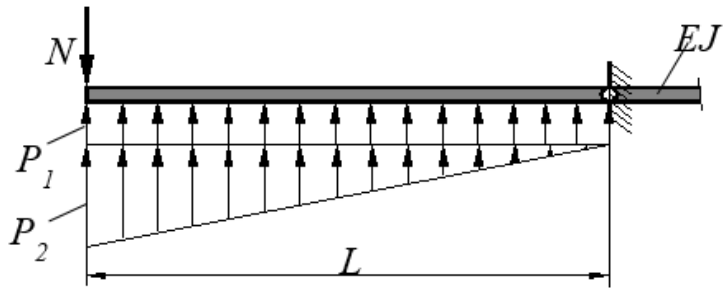

Рисунок 7. - **Сосредоточенная нагрузка N установлена по ее краю**

Экспериментально установлено, что зона влияния прогибов в одну сторону от нагрузки, приложенной с краю, не превышает $l \leq 5b$. На основании этого определены функции перемещения и усилия, результаты которых представлены ниже.

$$f_x = -\frac{N(L-x)^3}{240EJL^2}(3kL^2 + 14L^2 + 3kx^2 - 6x^2 + 12Lx + 4kxL) \quad (10)$$

Краевые реактивные напряжения примем в виде:

$$P_1 = \frac{kN}{l};\ P_2 = \frac{3\,N\left(1-\frac{k}{2}\right)}{l} \quad (11)$$

величина P_2 определена из условия равенства $\mathrm{M}_{(x=l)} = 0$. Определим величину моментов и перерезывающих сил по длине балки:

$$M_x = \frac{Nx(L-x)}{4L^2}(4L - 2x + kx); \quad (12)$$

$$Q_x = -\frac{N}{4L^2}(4L^2 - 3kx^2 + 6x^2 - 12Lx + 2Lkx) \quad (13)$$

Сравнивая выражения (8), (9) и (10) можно констатировать факт, что наибольшая сдвиговая жесткость грунта проявляется при интенсивной нагрузки q и минимальная при действии сосредоточенной нагрузки N, установленной по краю балки. При симметричном точечным нагружении балки она составляет промежуточное значение.

Функция перемещений *W(x)* для различных видов нагружения определяется экспериментально и математически аппроксимируется как ряд в виде многочлена шестой степени с f_{max}. Остальные неизвестные (угол поворота $\dot{w}(x)$, момент *M(x)*, перерезывающие *Q(x)* и реактивные *P(x)* усилия определяются с использованием методов численного или аналитического дифференцирования функции перемещений *W(x)*.

2. Выводы

1. Контактные однопараметровые упругие модели с постоянной жесткостью более достоверно характеризуют вертикальные линейные перемещения основания для достаточно жестких балок (полос). Эта модель не описывает прогибы балки при равномерно-распределённой нагрузке, поскольку считается, что реактивные давления $P(x)$ вдоль балки не меняется.

2. Контактные двухпараметровые модели с постоянной изгибной жесткостью C_2 соответствующие упругим законам хотя и формально учитывают распределительную свойства основания, тем не менее она предполагает что радиус кривизны (первая производная от перемещений) и численное значение параметра C_2 считается известной. Кроме того в уравнении (4) функция перемещений $\mathrm{w}(x)$ имеет жесткую зависимость с ее первой производной $\mathrm{w}^I(x)$. По этой причине она характеризует прогиб балки и не может быть использована для определения общих вертикальных перемещений, присущей модели Винклера – Цимермана. По существу, уравнение (4) характеризует одно-параметровую C_2 модель для определения изгиба балок $\mathrm{w}^I(x)$и функции усилий (M,Q), что приводит к появлению расхождения между расчетными и реально наблюдаемыми на практике результатов.

3. Широко распространенная модель упругого полупространства в отличие от выше рассмотренных контактных отличается, тем что напряжения распространяются по

всему объему. В этом случае распределяющая способность грунта принимается как для сплошной среды. Сравнивая результаты расчетов с результатами экспериментов несложно увидеть, что в первом случае деформация балки нагруженная распределенной нагрузкой ожидается большие, намного превышающие реальные прогибы балки в грунтах.

4. Известно, что при расчете балки, плиты на грунтовом основании используется конструкционная жесткость. Сдвиговая жесткость грунтового основания в расчетах полностью игнорируется. Предложенное расчетное выражение сдвиговой жесткости грунта позволяет более точно вычислять функцию перемещения и максимальный прогиб конструкции фундамента.

5. Предствленная авторами модель грунтового основания позволяет более реально принимать функцию реактивного давления грунта. Причем в зависимости от выбранного коэфиициента k модель транформируется между моделью Винклера и прдложенного авторами модель, характеризующий реактивное давление.

Литература

1. *Пастернак П.Л.* Основы нового метода расчета фундаментов на упругом основании при помощи двух коэффициентов постели. . М.:Госстройиздат, 1954, 56 с.
2. *Филоненко-Бородич М.М.* Простейшая модель упругого основания, способная распределять нагрузку // Труды МЭМИИТ, 1945, Вып.53, с.16-25.
3. *Власов В.З., Леонтьев Н.Н.* Балка и плиты оболочки на упругом основании /М.:Физматгиз, 1960, 492 с.
4. *Горбунов-Пасадов М.И., Маликова Т.А.* Расчет конструкций на упругом основании / М., Стройиздат, 1973.
5. *Гильман Л.С.* К вопросу об определении напряжений на поверхности упругой среды // Труды ЛИИПС, 1934, Вып.1.
6. *Хасанов А.З., Хасанов З.А.* Основания и фундаменты на лессовых просадочных гуртах /Ташкент:ИПТД «Узбекистон», 2006, 158 с.
7. *Хасанов А.З.,Турсунов Ш., Хасанов З.А.* Экспериментальные и теоретические исследования расчетных параметров жесткости грунтов // Труды конференции Новочеркаск, 2018.
8. *Хасанов А.З., Хасанов З.А.и др.* Определение напряжений в массиве грунта от действия внешних нагрузок // Узбекский Журнал «Проблемы механики». 2017, No. 2-3.
9. *Симвулиди И.А.* Расчет инженерных конструкций на упругом основании / М., Высшая школа, 1979, 479 с.

ВЛИЯНИЕ СЖИМАЕМОСТИ ЗАПОЛНИТЕЛЯ И ТЕМПЕРАТУРНОГО ПОЛЯ НА ДЕФОРМИРОВАНИЕ ТРЕХСЛОЙНОЙ ПЛАСТИНЫ

Шафиева Ю.В.

Белорусский государственный университет транспорта, г. Гомель, Беларусь
E-mail:zakharchuk.julia2@mail.ru

Аннотация. *Исследованы перемещения в упругой круговой трехслойной пластине со сжимаемым заполнителем. Поверхностная нагрузка принята осесимметричной. В тонких несущих слоях справедливы гипотезы Кирхгофа, в легком сжимаемом заполнителе – гипотеза Тимошенко. Обжатие заполнителя принимается линейным по толщине. Краевая задача сведена к нахождению четырех функций перемещений. Соответствующая система дифференциальных уравнений равновесия получена вариационным методом Лагранжа. Получены аналитические формулы для вычисления перемещений, включающие температуру. Проведена численная апробация решений.*

Ключевые слова*: трехслойная пластина, сжимаемый заполнитель, температурное поле*

1. Введение.

Разработке математических моделей деформирования трехслойных элементов конструкций в связи с их повсеместным распространением в машиностроении и строительстве, посвящен ряд публикаций. Постановки и методики решения краевых задач о деформировании слоистых элементов конструкций приведены в монографиях [1–8].

Исследование свободных и вынужденных колебаний трехслойных и неоднородных цилиндрических оболочек и пластин проведено статьях [9–14]. Публикации [15–21] посвящены квазистатическому изотермическому и термосиловому нагружению трехслойных стержней и пластин с несжимаемым заполнителем. В работах [22, 23] рассмотрено циклическое нагружение трехслойных стержней и пластин. Напряженно-деформированное состояние трехслойной круговой пластины со сжимаемым заполнителем при изотермических нагрузках исследовано в работах [24–32].

Предлагаемая работа отличается от проведенных ранее исследований учетом воздействия нестационарного температурного поля на деформирование трехслойной пластины со сжимаемым заполнителем.

2. Постановка краевой задачи.

Рассматривается круговая трехслойная несимметричная по толщине пластина со сжимаемым заполнителем (рис. 1), находящаяся под действием осесимметричной распределенной нагрузки q = q(r) и теплового потока qt.

Цилиндрическая система координат связана со срединной плоскостью заполнителя. В тонких внешних несущих слоях справедливы гипотезы Кирхгофа. В легком заполнителе нормаль остается прямолинейной, поворачивается на некоторый дополнительный угол ψ(r, t). Обжатие по толщине принимается линейным. Деформации малые.

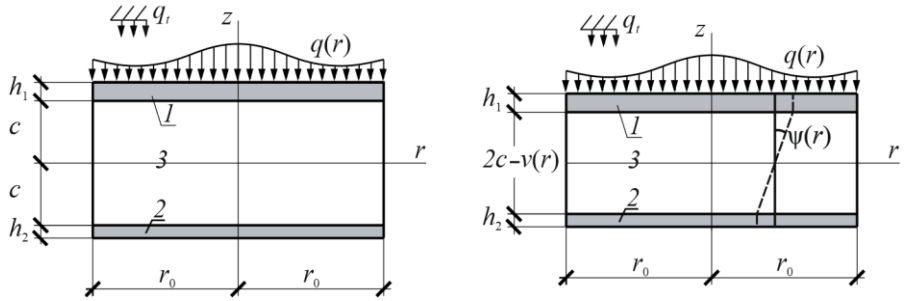

Рисунок 1 – **Расчетная схема круговой трехслойной пластины со сжимаемым заполнителем**

На контуре пластины предполагается наличие жесткой диафрагмы, препятствующей Через $w(r, t)$ и $u(r, t)$ обозначены прогиб и радиальное перемещение срединной плоскости заполнителя, $v(r, t)$ – функция обжатия заполнителя.

Пусть на внешнюю поверхность пластины падает тепловой поток, интенсивность которого q_t. Нижняя поверхность $z = -c - h_2$ и контур $r = 1$ теплоизолированы. Тогда температурное поле $T(z)$ изменяется по толщине пластины во времени t с достаточной степенью точности в соответствии с формулой [1]:

$$T = \frac{qH}{\lambda}\left\{\tau + \frac{1}{2}(s + \frac{c+h_2}{H})^2 - \frac{1}{6} - -\frac{2}{\pi^2}\sum_{n=1}^{\infty}\frac{(-1)^n}{n^2}\cos\left[\pi n\left(s + \frac{c+h_2}{H}\right)\right]e^{-n^2\pi^2\tau}\right\}, \qquad (1)$$

где $\tau = at/H^2$; $s = z/H$; $\lambda = \sum_{k=1}^{3}\lambda_k h_k / H$; $H = h_1 + h_2 + h_3$, $C = \sum_{k=1}^{3} C_k h_k \rho_k / H$; $a = \lambda / C$;

коэффициенты: λ_k – теплопроводности, C_k теплоемкости; ρ_k – плотность материала; $k = 1, 2, 3$ – здесь и далее номер слоя; $h_1 \neq h_2$ – толщины несущих слоев, $h_3 = 2c$ – толщина заполнителя.

В силу осесимметричности нагрузки, окружные перемещения отсутствуют $u_\varphi^{(k)} = 0$, а искомые величины – $w(r, t)$, $u(r, t)$, $\psi(r, t)$, $v(r, t)$ не зависят от координаты φ. Радиальные перемещения $u^{(k)}(r, z)$ и прогибы $w^{(k)}(r, z)$ в k-ом слое можно выразить через эти четыре искомые функции следующими формулами:

▪ в несущих слоях ($k = 1, 2$)

$$u_r^{(1)}(r,z) = u + c\psi - z\left(w,_r + v,_r\right), \quad w^{(1)}(r,z) = w + v, \quad \left(c \le z \le c + h_1\right);$$

$$u_r^{(2)}(r,z) = u - c\psi - zw,_r, \quad w^{(2)}(r,z) = w, \quad \left(-c - h_2 \le z \le -c\right);$$

▪ в заполнителе ($k = 3$)

$$u_r^{(3)}(r,z) = u + z\psi - z\left[w,_r + \frac{v,_r}{2c}(z + c)\right],$$

$$w^{(3)}(r,z) = w + \frac{v}{2c}(z + c) \quad \left(-c \le z \le c\right), \qquad (2)$$

где z – координата; запятая в нижнем индексе обозначает операцию дифференцирования по следующей за ней координате.

Используя перемещения (2) и соотношения Коши в цилиндрической системе координат [1] получим деформации в слоях. Отметим, что перемещения (2) и деформации изменяются во времени вместе с температурой (1). Для связи напряжений и деформаций воспользуемся термоупругими соотношениями закона Гука в девиаторно-шаровой форме:

$$s_\alpha^{(k)} = 2G_k э_\alpha^{(k)}, \quad \sigma^{(k)} = 3K_k\left(\varepsilon^{(k)} - \alpha_{0k}T_k\right),$$

$$s_{rz}^{(3)} = 2G_3 э_{rz}^{(3)}, \quad s_z^{(3)} = 2G_3 э_z^{(3)}, \quad \sigma^{(3)} = 3K_3\left(\varepsilon^{(3)} - \alpha_{03}T_3\right), \qquad (3)$$

где $s_\alpha^{(k)}, э_\alpha^{(k)}$ – девиаторные ($\alpha = r, \varphi$) и $\sigma^{(k)}, \varepsilon^{(k)}$ – шаровые части тензоров напряжений и деформаций; $G_k(T_k), K_k(T_k)$ – температурно зависимые модули сдвига и объемного деформирования, T_k – температура в k –ом слое; α_{0k} – коэффициент линейного температурного расширения материала.

С помощью вариационного принципа Лагранжа получена система уравнений равновесия, при этом работа касательных $\sigma_{rz}^{(3)}$ и нормальных $\sigma_z^{(3)}$ напряжений в заполнителе, в силу принятых гипотез, пренебрегается. В результате имеем следующую систему дифференциальных уравнений для нахождения искомых функций:

$$\mathrm{L}_2(a_1u + a_2\psi - a_3w,_r - a_4v,_r) + K_3^- v,_r = 0,$$

$$\mathrm{L}_2(a_2u + a_5\psi - a_6w,_r - a_7v,_r) = 0,$$

$$\mathrm{L}_3(a_3u + a_6\psi - a_8w,_r - a_9v,_r) = -q, \qquad (4)$$

$$\mathrm{L}_3(a_4u + a_7\psi - a_9w,_r - a_{10}v,_r) + \frac{c}{6}K_3^-\left(v,_{rr} + \frac{v,_r}{r}\right) = -q\,,$$

где a_i – коэффициенты

$$a_1 = \sum_{k=1}^{3} K_{k0}\,,\quad a_2 = c(K_{10} - K_{20})\,,\quad a_3 = \sum_{k=1}^{3} K_{k1}\,,$$

$$a_4 = K_{11} + \frac{1}{2c}K_{32}\,,\quad a_5 = K_{32} + c^2(K_{10} + K_{20})\,,\quad a_6 = K_{32} + c(K_{11} + K_{21})\,,$$

$$a_7 = ca_4\,,\quad a_8 = \sum_{k=1}^{3} K_{k2}\,,\quad a_9 = K_{12} + \frac{1}{2}K_{32}\,,\quad a_{10} = K_{12} + \frac{2}{5}c^3K_{32}\,,$$

$$K_{km} = \int_{h_k}\left[K_k(T_k) + \frac{4}{3}G_k(T_k)\right]z^m\,\mathrm{d}z \quad (m = 0,\,1,\,2);\quad K_k^- = K_k(T_k) - \frac{2}{3}G_k(T_k)\,;$$

L_2, L_3 – дифференциальные операторы

$$\mathrm{L}_2(g) \equiv \left(\frac{1}{r}(rg),_r\right),_r \equiv g,_{rr} + \frac{g,_r}{r} - \frac{g}{r^2}\,,\quad \mathrm{L}_3(g) \equiv \frac{1}{r}\big(r\,\mathrm{L}_2(g)\big),_r \equiv g,_{rrr} + \frac{2g,_{rr}}{r} - \frac{g,_r}{r^2} + \frac{g}{r^3}\,.$$

Краевая задача замыкается добавлением к уравнениям равновесия (4) силовых (7) или кинематических граничных условий на контуре ($r = r_0$) и условий ограниченности решения в центре пластины ($r = 0$):

Если контур жестко заделан, то должны выполняться условия

$$u = \psi = w = v = w,_r = v,_r = 0 \ \text{ при } \ r = r_0\,. \tag{5}$$

В случае шарнирного опирания контура нужно принять

$$u = \psi = w = v = v,_{rr} = 0,\quad M_r = 0 \ \text{ при } \ r = r_0\,. \tag{6}$$

Следует отметить, что если в (7) положить функцию сжимаемости равной нулю, то первые три уравнения совпадут с известной системой уравнений равновесия круговой пластины в случае легкого несжимаемого заполнителя [1].

2. Аналитическое решение краевой задачи

Аналитическое решение системы дифференциальных уравнений (4) следующее:

$$\psi = -\frac{1}{a_6}\mathrm{L}_3^{-1}(q) - \frac{1}{a_6}(a_3u - a_8w,_r - a_9v,_r) + \frac{C_1r}{4a_6}\big(2\ln r - 1\big) + C_3\frac{r}{2} + C_4\frac{1}{r}\,,$$

$$w = \frac{a_2a_6 - a_3a_5}{a_6^2 - a_5a_8}\int u\,\mathrm{d}r - \frac{a_6a_7 - a_5a_9}{a_6^2 - a_5a_8}v - \frac{a_5}{\left(a_6^2 - a_5a_8\right)}\int \mathrm{L}_3^{-1}(q)\,\mathrm{d}r +$$

$$+ \frac{C_1a_5}{\left(a_6^2 - a_5a_8\right)}\frac{r^2}{4}\big(\ln r - 1\big) + C_{10}\frac{r^2}{4} + C_{11}\ln r + C_{12}\,,$$

$$u = b_1v,_r + \big(b_2 + b_3\big)\mathrm{L}_3^{-1}(q) - \frac{r}{4}\big(2\ln r - 1\big)\big(b_2C_1 + b_3C_2\big) + C_5\frac{r}{2} + C_6\frac{1}{r}\,,$$

$$v = -\frac{C_7}{\beta}J_0(\beta r) - \frac{C_8}{\beta}Y_0(\beta r) + \frac{\pi}{2}\Big(\int Y_1(\beta r)\int J_1(\beta r)q_1(r)r\,\mathrm{d}r\,\mathrm{d}r -$$

$$-\int J_1(\beta r)\int Y_1(\beta r)q_1(r)r\,\mathrm{d}r\,\mathrm{d}r\Big) + C_9\,, \tag{7}$$

где $J_0(\beta r), J_1(\beta r)$ – функции Бесселя; $Y_0(\beta r), Y_1(\beta r)$ – функции Неймана; C_i – константы интегрирования; где q_1 – коэффициент, выражаемый через a_i, введенные в (4).

Для сплошных круговых пластин, исходя из требования ограниченности искомого решения в начале координат (деление на ноль, особенности логарифма и функции Неймана в

нуле), следует положить $C_1 = C_2 = C_4 = C_6 = C_8 = C_{11} = 0$. Если контур заделан, то при равномерно распределенной поперечной поверхностной нагрузке $q = q_0$ из граничных условий (5) следуют оставшиеся константы интегрирования:

$$C_3 = \frac{q_0 r_0^2}{8a_6}, \quad C_5 = -\left(b_2 + b_3\right)\frac{q_0 r_0^2}{8}, \quad C_7 = -\frac{q_0}{2\beta^2 J_1(\beta r_0)}\left(p_1 + p_2\right),$$

$$C_9 = \frac{C_7}{\beta} J_0(\beta r_0) - \frac{q_0 r_0}{2\beta^2}\left(p_1 + p_2\right), \quad C_{10} = \frac{a_5}{8\left(a_6^2 - a_5 a_8\right)} q_0 r_0^2,$$

$$C_{12} = -\frac{a_2 a_6 - a_3 a_5}{a_6^2 - a_5 a_8}\left(\frac{\left(b_2 + b_3\right) q_0 r_0^4}{64} + C_5 \frac{r_0^2}{4}\right) + \frac{a_5}{64\left(a_6^2 - a_5 a_8\right)} q_0 r_0^4 - C_{10}\frac{r_0^2}{4}. \qquad (9)$$

В случае шарнирного опирания контура константы определяются из граничных условий (6) и включают температуру в явном виде. Решение (8), (9) отличается от полученных ранее учетом зависимости упругих параметров материалов слоев от температуры, которая рассчитывается по формуле Белла [1].

3. Численные результаты

Численные результаты приведены для пластины со слоями, выполненными из материалов Д16-Т–фторопласт-4–Д16-Т. Механические характеристики материалов приведены в [1]. Толщины слоев, отнесенные к радиусу пластины, c = 0,23, h_1 = 0,03, h_2 = 0,03. Контур жестко заделан. Радиус пластины r_0 = 1 м.

Сравнение прогибов пластин со сжимаемым (*1*, *2*) и несжимаемым (*3*) заполнителями показано на рис. 2: *1* – верхний слой; *2* – нижний слой; *3* – несжимаемый заполнитель (q_0 = –0,5 МПа). Максимальное отличие прогибов составляет около 42 %. Следует отметить, что прогиб пластины с несжимаемым заполнителем практически совпадает с прогибом срединной плоскости заполнителя при учете его сжимаемости.

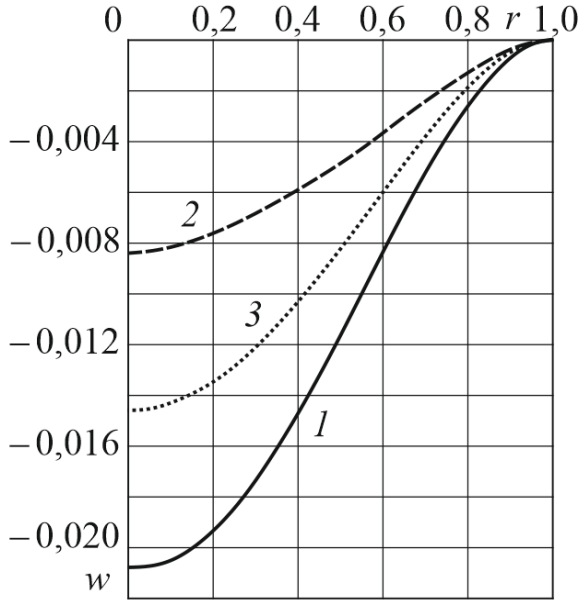

Рисунок 2 – **Прогибы пластин со сжимаемым и несжимаемым заполнителями**

Далее приведены графики перемещений при изгибе пластины в стационарных температурных полях при интенсивности равномерно-распределенная нагрузки q = 1 МПа. Температура в пластине принималась однородной. Ее увеличение на каждом шаге составляет 60 К: *1* – 293 К, *2* – 353 К, *3* – 413 К.

На рис. 3. 4 показано изменение прогиба нижнего слоя $w(r)$ и функции сжимаемости $v(r)$ при различных температурах в пластине. Рост температуры на 60 градусов приводит каждый раз к увеличению прогиба на 5,0 %, обжатия заполнителя – на 7,5%.

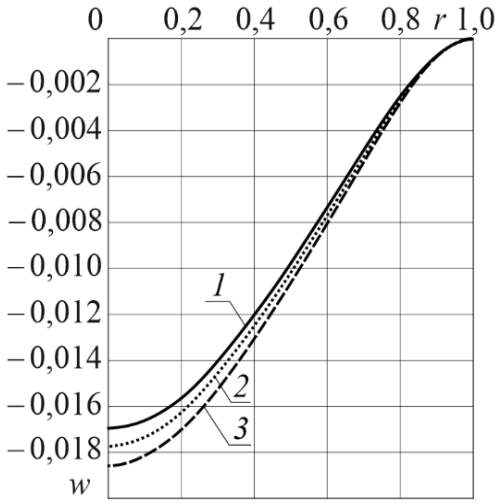

Рисунок 3. – **Прогиб при различных температурах**

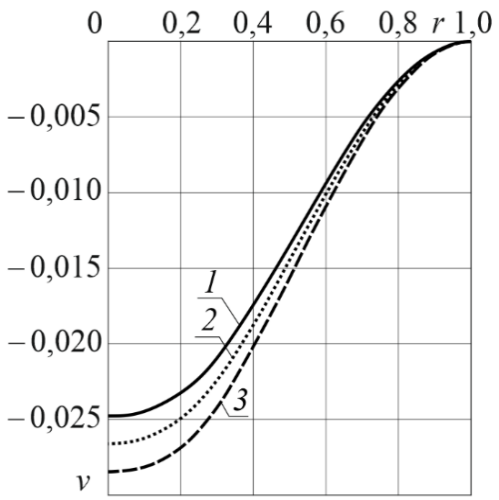

Рисунок 4. – **Функция обжатия**

4. Заключение

Приведенные постановка и аналитическое решение краевой задачи позволяют исследовать напряженно-деформированное состояние круговой несимметричной по толщине трехслойной пластины со сжимаемым легким заполнителем в температурном поле. Необходимость учета сжимаемости материала заполнителя подчеркивают численные результаты, которые иллюстрируют увеличение прогиба верхнего несущего слоя на 42 % при изотермическом нагружении. С ростом температуры все перемещения увеличиваются однотипно в соответствии с уменьшением характеристик упругости материалов слоев.

Работа выполнена при финансовой поддержке Белорусского республиканского Фонда фундаментальных исследований.

Литература

1. *Горшков А.Г., Старовойтов Э.И., Яровая А.В.* Механика слоистых вязкоупругопластических элементов конструкций / Москва, ФИЗМАТЛИТ, 2005, 576 с.
2. *Журавков М.А., Старовойтов Э.И.* Математические модели механики твердого тела / Минск, БГУ, 2021, 535 с.
3. *Яровая, А.В.* Строительная механика. Статика стержневых систем / *УО БелГУТ Гомель, 2013.*
4. *Zhuravkov M.A., Lyu Yongtao, E.I. Starovoitov.* Mechanics of Solid Deformable Body / Singapore, Springer, 2023, 317 p.
5. *Абдусаттаров А., Старовойтов Э.И., Рузиева Н.Б.* Деформирование и повреждаемость упругопластических элементов конструкций при циклических нагружениях / Ташкент, «IDEAL PRESS», 2023, 381 с.
6. *Aghalovyan L.* Asymptotic theory of anisotropic plates and shells / Singapore–London, World Scientific Publishing; 2015, 376 p.
7. *Старовойтов, Э. И.* Сопротивление материалов / Гомель, БелГУТ, 2004, 376 с.
8. *Старовойтов, Э. И.* Механика материалов / Гомель, БелГУТ, 2011, 380 с.
9. *Bakulin VN, Boitsova DA, Nedbai AYa.* Parametric resonance of a three layered cylindrical composite rib-stiffened shell // Mechanics of composite materials, 2021, vol. 57, No.5, pp. 623–634.
10. *Tarlakovskii DV, Fedotenkov GV.* Two-Dimensional Nonstationary Contact of Elastic Cylindrical or Spherical Shells // Journal of Machinery Manufacture and Reliability, 2014, vol, 43, No. 2, pp. 145–152.
11. *Suvorov YeM, Tarlakovskii DV, Fedotenkov GV.* The plane problem of the impact of a rigid body on a half-space modelled by a Cosserat medium // Journal of Applied Mathematics and Mechanics, 2012, vol. 76, No. 5, pp.511–518.
12. *Старовойтов Э.И., Леоненко Д.В.* Исследование спектра частот трехслойной цилиндрической оболочки с упругим наполнителем // Механика композиционных материалов и конструкций. 2015, vol. 21, No. 2, pp. 162–169.
13. *Леоненко Д.В., Маркова М.В.* Колебания круговой трехслойной пластины под действием внешней нагрузки // Журнал Белорусского государственного университета. Математика. Информатика, 2023, т. 1, С. 49–63.

14. *Pradhan M, Dash PR, Pradhan PK.* Static and dynamic stability analysis of an asymmetric sandwich beam resting on a variable Pasternak foundation subjected to thermal gradient // Meccanica, 2016, vol. 51, No. 3, pp. 725–739.
15. *Starovoitov É.I., Pleskachevskii Yu.M., Leonenko D.V., Tarlakovskii D.V.* Deformation of a Step Composite Beam in a Temperature Field // Journal of Engineering Physics and Thermophysics, 2015, vol. 88, No. 4, pp. 1023-1029.
16. *Старовойтов Э.И., Леоненко Д.В.* Деформирование трехслойного стержня в температурном поле // Механика машин, механизмов и материалов, 2013, т. 22, С. 31–35.
17. *Старовойтов Э.И., Козел А.Г.* Изгиб упругой круговой трехслойной пластины на основании Пастернака // Механика композиционных материалов и конструкций, 2018, т. 2, No. 3, С. 392–406.
18. *Нестерович, А.В.* Напряженное состояние круговой трехслойной пластины при осесимметричном нагружении в своей плоскости // Механика. Исследования и инновации, 2019, т. 12, No. 12, С. 152–157.
19. *Козел А.Г.* Влияние сдвиговой жёсткости основания на напряжённое состояние сэндвич пластины // Фундаментальные и прикладные проблемы техники и технологии, 2018, т. 332, No. 6, С. 25–34.
20. *Zadeh HV, Tahani M.* Analytical bending analysis of a circular sandwich plate under distributed load // International Journal of Recent Advances in Mechanical Engineering, 2017, vol. 6, No. 1, pp. 01-10.
21. *Yang L, Harrysson O, West H, Cormier D.* A comparison of bending properties for cellular core sandwich panels // Materials Sciences and Applications, 2013, vol. 4, No. 8, pp. 471–477.
22. *Старовойтов Э.И., Абдусаттаров А., Рузиева Н.Б.* Циклическое нагружение упругопластических трёхслойных стержней с учетом их повреждаемости // Узб. журнал Проблемы механики, 2023, No. 1, С. 66–74.
23. *Старовойтов Э.И., Леоненко Д.В., Абдусаттаров А.* Знакопеременное термосиловое нагружение трёхслойной пластины погонными моментами // Узб. журнал «Проблемы механики», 2023, No. 3, С. 20–30.
24. *Захарчук Ю.В.* Уравнения равновесия упругопластической круговой пластины со сжимаемым заполнителем // Механика. Исследования и инновации, 2018, т. 11, No. 11, С. 80–87.
25. *Старовойтов Э.И., Захарчук Ю.В.* Изгиб круговой трехслойной пластины с легким сжимаемым заполнителем // Проблемы машиностроения и автоматизации, 2018, No. 4, С. 88–97.
26. *Захарчук Ю.В.* Перемещения в упругой круговой трехслойной пластине со сжимаемым заполнителем // Теоретическая и прикладная механика. Международный научно-технический сборник. Минск, БНТУ, 2020, вып. 34, С. 61-69.
27. *Старовойтов Э.И., Захарчук Ю.В.* Изгиб упругопластической круговой трехслойной пластины со сжимаемым заполнителем // Механика композиционных материалов и конструкций, 2020, Т. 26, No. 1, С. 58–73.
28. *Starovoitov E.I., Zakharchuk Y.V., Kuznetsova E.L.* Elastic circular sandwich plate with compressible filler under axially symmetrical thermal force load // Journal of the Balkan Tribological Association, 2021, vol. 27, No. 2, pp.175–188.
29. *Захарчук Ю.В.* Упругое деформирование круговых трехслойных пластин со сжимаемым заполнителем осесимметричными нагрузками // Теоретическая и прикладная механика. Международный научно-технический сборник. Минск, БНТУ, 2022, вып. 36, С. 34-41.
30. *Старовойтов Э.И., Захарчук Ю.В.* Нелинейное деформирование трехслойной пластины со сжимаемым заполнителем // Механика машин, механизмов и материалов, 2019, т. 48, No. , С. 26-33.
31. *Захарчук Ю.В.* Напряженно-деформированное состояние круговой трехслойной пластины со сжимаемым заполнителем // Механика. Исследования и инновации, 2019, No. 12, С. 66-75.
32. *Захарчук Ю.В.* Трехслойная круговая упругопластическая пластина со сжимаемым заполнителем // Проблемы физики, математики и техники. 2018, No. 4(37), С. 72-79.

ДЕФОРМИРОВАНИЕ УПРУГОЙ ТРЕХСЛОЙНОЙ ПЛАСТИНЫ В ТЕМПЕРАТУРНОМ ПОЛЕ

Яровая А.В.[1]
[1]*Белорусский государственный университет транспорта, Гомель, Беларусь*
E-mail: av.yar@yandex.by

Аннотация. *Исследовано деформирование упругой круговой несимметричной по толщине трехслойной пластины локальной равномерно распределенной по кольцу нагрузкой в температурном поле. Для описания кинематики пакета используются гипотезы ломаной линии. В тонких несущих слоях справедливы гипотезы Кирхгофа, в несжимаемом по толщине относительно толстом заполнителе – гипотеза Тимошенко. Учитывается работа касательных напряжений заполнителя. Учтена зависимость упругих свойств материалов слоев от температуры. Система дифференциальных уравнений равновесия пластины получена вариационным методом Лагранжа. На контуре пластины приняты граничные условия шарнирного опирания. Решение краевой задачи получено в конечном виде. Проведен его численный параметрический анализ.*

Ключевые слова: *трехслойная пластина, локальная кольцевая нагрузка, температурное поле, численные результаты*

1. Введение

Актуальность разработки новых математических моделей для исследования упругого деформирования композитных стержней, пластин и оболочек при термосиловых нагрузках, определяется их повсеместным распространением в машиностроении и строительстве.

В монографиях [1–9] разрабатываются общие подходы к созданию механико-математических моделей деформирования слоистых упругих и неупругих элементов конструкций при квазистатических и динамических нагрузках. Приведены постановки соответствующих краевых задач, рассмотрены примеры решения и их численная апробация. Работы В статьях [10–12] исследуется динамическое поведение неоднородных цилиндрических оболочек и стержней при резонансной и нестационарной нагрузках. Работы [13–17] посвящены анализу собственных и вынужденных колебаний трехслойных и пятислойных пластин.

Поведение трехслойных стержней с несжимаемым заполнителем в температурном поле исследовано в [18, 19]. Изгибу трехслойных и пятислойных пластин с несжимаемым заполнителем, в том числе связанных с упругим основанием Пастернака, посвящены работы [20–27]. Деформирование трехслойных круговых пластин со сжимаемым заполнителем при симметричных нагрузках рассмотрен в публикациях [28, 29]. Квазистатическое деформирование слоистых стержней и пластин с упругопластическими слоями в температурном и радиационном полях исследовано в [30–37].

Предлагаемая работа отличается от известных решений учетом воздействия нестационарного температурного поля на деформирование трехслойной упругой пластины локальной круговой кольцевой нагрузкой.

2. Постановка краевой задачи

Рассматривается деформирование упругой круговой трехслойной пластины. Все линейные перемещения, размеры и радиальная координата отнесены к радиусу пластины r_0 (рис. 1). При постановке краевой задачи используется цилиндрическая система координат, связанная со срединной плоскостью заполнителя, перпендикулярно которой ось z направлена вверх. Для несущих внешних достаточно тонких слоев, толщины которых $h_1 \neq h_2$, принимаются кинематические гипотезы Кирхгофа о прямолинейности, перпендикулярности и несжимаемости деформированной нормали. В относительно толстом жестком заполнителе, толщиной $h_3 = 2c$, деформированная нормаль остается прямолинейной, не изменяет своей длины, но поворачивается на некоторый дополнительный угол $\psi(r)$, т.е. справедлива гипотеза Тимошенко.

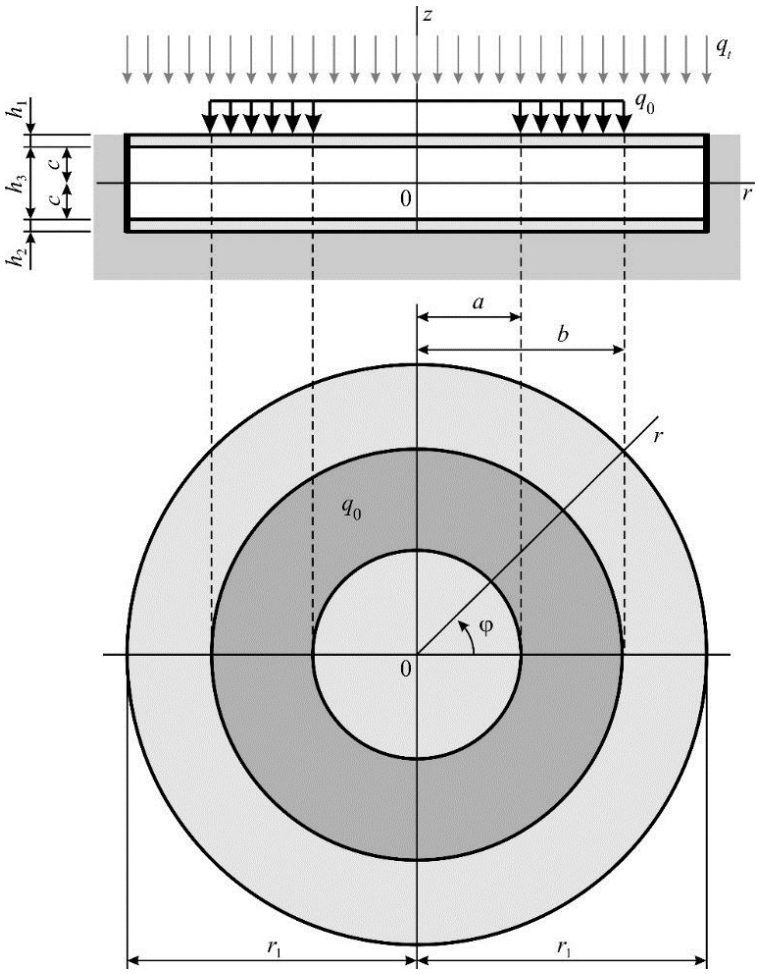

Рисунок 1 – **Схема нагружения трехслойной пластины кольцевой нагрузкой**

Рассматриваемая трехслойная несимметричная по толщине круглая пластина (рис.1), нагружена равномерно распределенной кольцевой нагрузкой постоянной интенсивности q_0:

$$q = q_0(H_0(b-r) - H_0(a-r)), \qquad (1)$$

где $H_0(r)$ функция Хэвисайда нулевого порядка

$$H_0(r) = \begin{cases} 1, & r \geq 0, \\ 0, & r < 0. \end{cases}.$$

Пусть на внешнюю поверхность пластины падает тепловой поток, интенсивность которого q_t. Нижняя поверхность $z = -c - h_2$ и контур $r = 1$ теплоизолированы. Тогда температурное поле в пластине $T(z)$ определяется с достаточной степенью точности по формуле, заимствованной в [1]:

$$T = \frac{qH}{\lambda}\left\{\tau + \frac{1}{2}(s + \frac{c+h_2}{H})^2 - \frac{1}{6} - -\frac{2}{\pi^2}\sum_{n=1}^{\infty}\frac{(-1)^n}{n^2}\cos\left[\pi n\left(s + \frac{c+h_2}{H}\right)\right]e^{-n^2\pi^2\tau}\right\}, \qquad (2)$$

где $\tau = at/H^2$; $s = z/H$; $\lambda = \sum_{k=1}^{3}\lambda_k h_k / H$; $H = h_1 + h_2 + h_3$, $C = \sum_{k=1}^{3} C_k h_k \rho_k / H$; $a = \lambda / C$; коэффициенты λ_k – теплопроводности, C_k теплоемкости; ρ_k – плотность материала; k = 1, 2, 3 – здесь и далее номер слоя; t – время.

Нагрузка принята осесимметричной, поэтому окружные перемещения отсутствуют $u_\varphi^{(k)} = 0$, а искомые функции – радиальное перемещение срединной плоскости заполнителя u, относительный сдвиг ψ и прогиб пластины w зависят только от радиальной координаты и не зависят от φ. Предполагается, что жесткая диафрагма на контуре препятствует относительному сдвигу слоев ($\psi = 0$ при $r = 1$).

Радиальные перемещения, в силу принятых гипотез, изменяются по толщине слоев линейно, деформации следуют из перемещений и соотношений Коши [2]. С помощью напряжений в слоях $\sigma_\alpha^{(k)}$ ($\alpha = r, \varphi$), $\sigma_{rz}^{(3)}$, вводятся обобщенные внутренние силы и моменты:

$$T_\alpha \equiv \sum_{k=1}^{3} T_\alpha^{(k)} = \sum_{k=1}^{3} \int_{h_k} \sigma_\alpha^{(k)} \, \mathrm{d}z, \quad M_\alpha \equiv \sum_{k=1}^{3} M_\alpha^{(k)} = \sum_{k=1}^{3} \int_{h_k} \sigma_\alpha^{(k)} z \, \mathrm{d}z,$$

$$H_\alpha = M_\alpha^{(3)} + c\left(T_\alpha^{(1)} - T_\alpha^{(2)}\right), \quad Q = \int_{-c}^{c} \sigma_{rz}^{(3)} \, \mathrm{d}z. \tag{3}$$

Напряжения вычисляются через деформации с помощью закона Гука:

$$s_\alpha^{(k)} = 2G_k э_\alpha^{(k)}, \quad \sigma^{(k)} = 3K_k(\varepsilon^{(k)} - \alpha_{0k}T^{(k)}), \quad s_{rz}^{(3)} = 2G_3 э_{rz}^{(3)} \quad (k = 1, 2, 3;\ \alpha = r, \varphi), \tag{4}$$

где $s_\alpha^{(k)}, э_\alpha^{(k)}$, $s_{rz}^{(3)}$, $э_{rz}^{(3)}$ – компоненты девиаторов и $\sigma^{(k)}, \varepsilon^{(k)}$ – шаровые части тензоров напряжений и деформаций; $G_k(T_k)$, $K_k(T_k)$ – температурно зависимые модули сдвига и объемного деформирования; α_{0k} – коэффициент линейного температурного расширения материала k-го слоя.

Уравнения равновесия рассматриваемой пластины получены вариационным методом Лагранжа с учетом работы касательных напряжений в заполнителе. При произвольной осесимметричной изотермической поверхностной нагрузке они приведены в [1]. В нашем случае кольцевой нагрузки (1) система уравнений принимает вид

$$\begin{gathered} \mathrm{L}_2(a_1 u + a_2\psi - a_3 w,_r) = -p, \\ \mathrm{L}_2(a_2 u + a_4\psi - a_5 w,_r) - 2cG_3\psi = 0, \\ \mathrm{L}_3(a_3 u + a_5\psi - a_6 w,_r) = q_0(H_0(b-r) - H_0(a-r)), \end{gathered} \tag{5}$$

где запятая в индексе обозначает производную по следующей за ней координате; a_i – коэффициенты, определяемые через модули упругости материалов и толщины слоев при температуре T; L_2, L_3 – линейные дифференциальные операторы

$$a_1 = \sum_{k=1}^{3} K_{k0}, \quad a_2 = c(K_{10} - K_{20}), \quad a_3 = \sum_{k=1}^{3} K_{k1}, \quad a_4 = K_{32} + c^2(K_{10} + K_{20}),$$

$$a_5 = K_{32} + c(K_{11} + K_{21}), \quad a_6 = \sum_{k=1}^{3} K_{k2}, \quad K_{km} = \int_{h_k} \left[K_k(T^{(k)}) + \frac{4}{3} G_k(T^{(k)}) \right] z^m \, \mathrm{d}z \quad (m = 0, 1, 2);$$

$$\mathrm{L}_2(g) \equiv g,_{rr} + \frac{g,_r}{r} - \frac{g}{r^2}, \quad \mathrm{L}_3(g) \equiv g,_{rrr} + \frac{2g,_{rr}}{r} - \frac{g,_r}{r^2} + \frac{g}{r^3}.$$

Для замыкания краевой задачи по определению функций $u(r)$, $\psi(r)$, $w(r)$ к уравнениям (5) необходимо добавить условия ограниченности решения в центре пластины и граничные условия на контуре. При заделке контура пластины должны выполняться кинематические условия при $r = 1$:

$$u = \psi = w = w,_r = 0. \tag{6}$$

При шарнирном опирании

$$u = \psi = w = 0, \ M_r = 0, \text{ при } r = 1, \tag{7}$$

где M_r – обобщенный изгибающий момент, введенный в (3).

3. Аналитическое решение краевой задачи

Решение системы уравнений (5) при изотермическом упругом деформировании пластины кольцевой нагрузкой известно [1]. В случае воздействия кольцевой нагрузки интенсивностью q_0 = const решение задачи термоупругости будет

$$\psi = C_2 I_1(\beta r) + C_3 K_1(\beta r) + \frac{\gamma_1 q_0}{2\beta^2} \left\{ H_0(b-r) \left[\frac{b^2}{r} - r + 2b\left(K_1(\beta b) I_1(\beta r) - I_1(\beta b) K_1(\beta r)\right) \right] - \right.$$

$$-H_0(a-r)\left[\frac{a^2}{r}-r+2a\left(K_1(\beta a)I_1(\beta r)-I_1(\beta a)K_1(\beta r)\right)\right]\Bigg\}+\frac{C_1\gamma_1}{\beta^2 r},$$

$$w=\frac{b_2}{b_3}\Bigg\{\frac{C_2 I_0(\beta r)}{\beta}-\frac{C_3 K_0(\beta r)}{\beta}+\frac{C_1\gamma_1}{\beta^2}\ln(r)+\frac{\gamma_1 q_0}{2\beta^2}H_0(b-r)\times$$

$$\times\left[\frac{b^2-r^2}{2}+b^2\ln\left(\frac{r}{b}\right)+\frac{2b}{\beta}\left(K_1(\beta b)I_0(\beta r)+I_1(\beta b)K_0(\beta r)\right)-\frac{2}{\beta^2}\right]-\frac{\gamma_1 q_0}{2\beta^2}\times$$

$$\times H_0(a-r)\left[\frac{a^2-r^2}{2}+a^2\ln\left(\frac{r}{a}\right)+\frac{2a}{\beta}\left(K_1(\beta a)I_0(\beta r)+I_1(\beta a)K_0(\beta r)\right)-\frac{2}{\beta^2}\right]\Bigg\}+$$

$$+\frac{1}{b_3}\int L_3^{-1}(q_0(H_0(b-r)-H_0(a-r)))dr-\frac{C_1}{4b_3}r^2(\ln r-1)+\frac{C_5 r^2}{4b_3}+C_6\ln r+C_4,$$

$$u=\frac{a_3}{a_1}w,_r-\frac{a_2}{a_1}\psi+\frac{C_7 r}{2}+\frac{C_8}{r}, \qquad (8)$$

где $I_0(\beta r)$, $I_1(\beta r)$ – модифицированные функции Бесселя; $K_0(\beta r)$, $K_1(\beta r)$ – функции Макдональда нулевого и первого порядков; C_1, C_2, …, C_8 – константы интегрирования; L_3^{-1} – интегральный оператор

$$\mathrm{L}_3^{-1}(f)\equiv\frac{1}{r}\int r\int\frac{1}{r}\int rf(r)\,\mathrm{d}r\,\mathrm{d}r\,\mathrm{d}r;$$

$$\int L_3^{-1}(q_0(H_0(b-r)-H_0(a-r)))dr=q_0\left[\frac{r^4-5b^4}{64}-\frac{b^4}{16}\ln\left(\frac{r}{b}\right)-\frac{b^2r^2}{8}\ln\left(\frac{r}{b}\right)+\frac{b^2r^2}{16}\right]H(b-r)-$$

$$-q_0\left[\frac{r^4-5a^4}{64}-\frac{a^4}{16}\ln\left(\frac{r}{a}\right)-\frac{a^2r^2}{8}\ln\left(\frac{r}{a}\right)+\frac{a^2r^2}{16}\right]H(a-r),$$

$$\beta^2=\frac{2cb_3G_3}{b_1b_3-b_2^2},\ \ b_1=\frac{a_1a_4-a_2^2}{a_1},\ \ b_2=\frac{a_1a_5-a_2a_3}{a_1},\ \ b_3=\frac{a_1a_6-a_3^2}{a_1}.$$

При защемленном контуре пластины константы интегрирования следуют из условия (6):

$$C_1=-\frac{q_0(b^2-a^2)}{2},\ \ C_2=\frac{\gamma_1 q_0}{\beta^2 I_1(\beta)}\left(\frac{b^2-a^2}{2}-bK_1(\beta)I_1(\beta b)+aK_1(\beta)I_1(\beta a)\right),$$

$$C_3=\frac{q_0\gamma_1}{\beta^2}\left(bI_1(\beta b)-aI_1(\beta a)\right),$$

$$C_4=-\frac{b_2\gamma_1 q_0}{b_3\beta^4 I_1(\beta)}\left(\frac{I_0(\beta)\beta\left(b^2-a^2\right)}{2}-bI_1(\beta b)+aI_1(\beta a)\right)+$$

$$+\frac{q_0\left(b^4-a^4\right)}{32b_3}+\frac{q_0\left(b^2-a^2\right)}{16b_3},$$

$$C_5=\frac{q_0}{8}\left(2b^2-b^4-2a^2+a^4\right),$$

$$C_6=\frac{q_0}{16b_3}\left(b^4-a^4\right),\ C_7=\frac{a_3q_0}{4b_3a_1}\left(b^2-a^2\right),\ C_8=0. \qquad (9)$$

При шарнирно опертом контуре константы интегрирования следуют из (7), при этом C_1, C_2, C_3, C_6, C_8 охраняют вид (9), а остальные

$$C_4 = \frac{b_2}{b_3}\left(-\frac{C_2 I_0(\beta)}{\beta} + \frac{C_3 K_0(\beta)}{\beta}\right) - \frac{1}{4b_3}\left(C_1 + C_5\right),$$

$$C_5 = q_0 \frac{a_3^2 - a_1 b_3 + a_7 a_1}{4a_1(a_6 + a_7)}\left(b^2\left(1 - \frac{b^2}{2}\right) - a^2\left(1 - \frac{a^2}{2}\right)\right) - \frac{6b_3}{a_6 + a_7}\sum_{k=1}^{3}\alpha_{0k}\int_{h_k} K_k T_k z\,\mathrm{d}z\,,$$

$$C_7 = \frac{2a_3}{a_1\left(a_6 + a_7\right)}\left(3\sum_{k=1}^{3}\alpha_{0k}\int_{h_k} K_k T_k z\,\mathrm{d}z + \frac{q_0 b^2}{4}\left(1 - \frac{b^2}{2}\right) - \frac{q_0 a^2}{4}\left(1 - \frac{a^2}{2}\right)\right). \qquad (10)$$

При заделке контура перемещения в пластине (8), (9) зависят от температуры неявным образом через модули упругости материалов. При шарнирном опирании температура в решение (8), (10) входит явно через константы интегрирования C_4, C_5, C_6.

4. Численные результаты

Численные результаты получены для пластины, слои которой выполнены из материалов Д16-Т–фторопласт-4–Д16-Т. Интенсивность кольцевой нагрузки принята q_0 = 1·МПа, толщины слоев – h_1 = 0,02; h_2 = 0,06; h_3 = 0,4. Параметры упругости материалов приведены в [1]. Температура при расчетах усреднялись по толщине пластины. Для описания зависимости параметров упругости от температуры использовалась формула Белла [1].

На рисунке 2 показано изменение прогиба пластины в зависимости от положения силового кольца нагрузки постоянной толщины $b - a$ = 0,25, при продвижении его к контуру: *1* – T_1 = 293 К, *2* – T_2 = 233 К. При a = 0 нагрузка распределена по кругу радиуса b, при a = 0,75 кольцо нагрузки примыкает к контуру пластины.

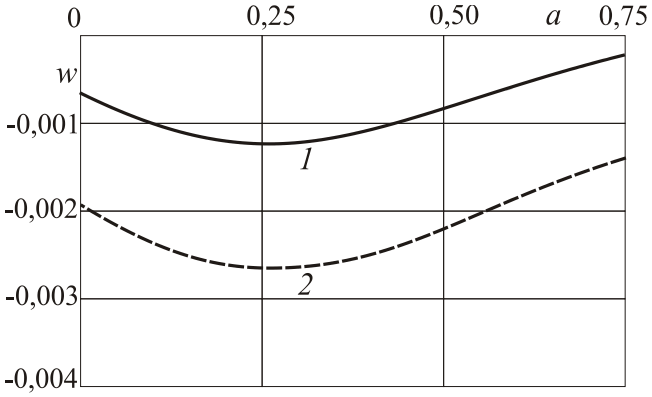

Рисунок 2 – **Прогиб пластины в зависимости от положения пятна кольцевой нагрузки (T_1 = 293 К, T_2 = 233 К)**

На рисунке 3 *а, б* показано изменение относительного сдвига и прогиба пластины вдоль ее радиуса. Кривые построены при различных радиусах b (a = 0) пятна локальной равномерно распределенной нагрузки: *1*– b = 0,5; *2* – b = 0,75; без штриха – T_1 = 293 К, со штрихом – T_2 = 323 К. С увеличением площади нагрузки экстремум на рисунке 3 *а* сдвигается к контуру пластины.

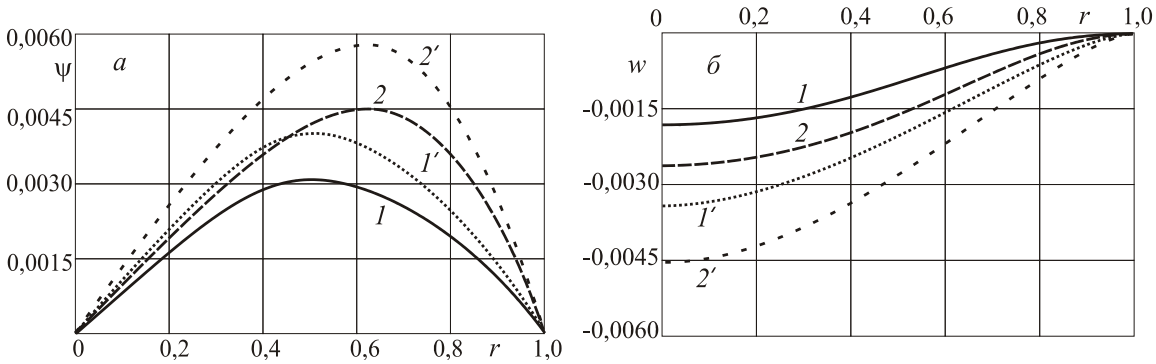

Рисунок 3 – **Перемещения в пластине при различных радиусах пятна нагрузки**

При нагревании пластины прогибы и сдвиги в обоих случаях увеличиваются пропорционально.

5. Заключение

методика решения краевых задач для трехслойных упругих пластин позволяет строить аналитическое решение при осесимметричных локальных равномерно распределенных по кольцу или кругу нагрузках в нестационарном температурном поле. Полученные аналитические результаты позволили провести численный анализ, подтвердивший

Работа выполнена при финансовой поддержке Белорусского республиканского фонда фундаментальных исследований.

Литература

1. *Горшков А.Г., Старовойтов Э.И., Яровая А.В.* Механика слоистых вязкоупругопластических элементов конструкций / Москва, ФИЗМАТЛИТ, 2005, 576 с.
2. *Яровая, А.В.* Строительная механика. Статика стержневых систем / УО БелГУТ Гомель, 2013.
3. *Журавков М.А., Старовойтов Э.И.* Математические модели механики твердого тела / Минск, БГУ, 2021, 535 с.
4. *Zhuravkov M.A., Lyu Yongtao, E.I. Starovoitov.* Mechanics of Solid Deformable Body / Singapore, Springer, 2023, 317 p.
5. *Абдусаттаров А., Старовойтов Э.И., Рузиева Н.Б.* Деформирование и повреждаемость упругопластических элементов конструкций при циклических нагружениях / Ташкент, «IDEAL PRESS», 2023, 381 с.
6. *Aghalovyan L.* Asymptotic theory of anisotropic plates and shells / Singapore–London, World Scientific Publishing; 2015, 376 p.
7. *Старовойтов, Э. И.* Сопротивление материалов / Гомель, БелГУТ, 2004, 376 с.
8. *Старовойтов, Э. И.* Механика материалов / Гомель, БелГУТ, 2011, 380 с.
9. *Старовойтов Э.И., Леоненко Д.В.* Исследование спектра частот трехслойной цилиндрической оболочки с упругим наполнителем // Механика композиционных материалов и конструкций. 2015, vol. 21, No. 2, pp. 162–169.
10. *Bakulin VN, Boitsova DA, Nedbai AYa.* Parametric resonance of a three1layered cylindrical composite rib-stiffened shell // Mechanics of composite materials, 2021, vol. 57, No. 5, pp. 623–634.
11. *Tarlakovskii DV, Fedotenkov GV.* Two-Dimensional Nonstationary Contact of Elastic Cylindrical or Spherical Shells // Journal of Machinery Manufacture and Reliability, 2014, vol, 43, No. 2, pp. 145–152.
12. *Suvorov YeM, Tarlakovskii DV, Fedotenkov GV.* The plane problem of the impact of a rigid body on a half-space modelled by a Cosserat medium // Journal of Applied Mathematics and Mechanics, 2012, vol. 76, No. 5, pp.511–518.
13. *Pradhan M, Dash PR, Pradhan PK.* Static and dynamic stability analysis of an asymmetric sandwich beam resting on a variable Pasternak foundation subjected to thermal gradient // Meccanica, 2016, vol. 51, No. 3, pp.725–739.
14. *Gorshkov A.G. Starovoitov E.I., Yarovaya A.V.* Vibrations of a Circular Linear-Viscoelastic Three-Layered Plate // Strength of materials, 2001, vol. 33, No. 3, pp. 270–276.
15. *Леоненко Д.В., Маркова М.В.* Колебания круговой трехслойной пластины под действием внешней нагрузки // Журнал Белорусского государственного университета. Математика. Информатика, 2023, т. 1, С. 49–63.
16. *Лачугина Е.А.* Поперечные колебания пятислойной упругой круговой пластины с жесткими заполнителями // Механика. Исследования и инновации, 2022, вып. 15, С. 212–219.
17. *Лачугина Е.А.* Частоты собственных колебаний пятислойной круговой пластины // Теоретическая и прикладная механика, Минск, БНТУ, 2023, вып. 38, С. 227-233.
18. *Starovoitov É.I., Pleskachevskii Yu.M., Leonenko D.V., Tarlakovskii D.V.* Deformation of a Step Composite Beam in a Temperature Field // Journal of Engineering Physics and Thermophysics, 2015, vol. 88, No. 4, pp. 1023-1029.
19. *Старовойтов Э.И., Леоненко Д.В.* Деформирование трехслойного стержня в температурном поле // Механика машин, механизмов и материалов, 2013, т. 22, С. 31–35.
20. *Zadeh HV, Tahani M.* Analytical bending analysis of a circular sandwich plate under distributed load // International Journal of Recent Advances in Mechanical Engineering, 2017, vol. 6, No. 1, pp. 01-10. doi: 10.14810/ijmech.2017.6101.
21. *Yang L, Harrysson O, West H, Cormier D.* A comparison of bending properties for cellular core sandwich panels // Materials Sciences and Applications, 2013, vol. 4, No. 8, pp.
22. *Старовойтов Э.И., Козел А.Г.* Изгиб упругой круговой трехслойной пластины на основании Пастернака // Механика композиционных материалов и конструкций, 2018, т. 2, No. 3, С. 392–406.

23. *Козел А.Г.* Влияние сдвиговой жёсткости основания на напряжённое состояние сэндвич пластины // Фундаментальные и прикладные проблемы техники и технологии, 2018, т. 332, No. 6, С. 25–34.
24. *Козел, А.Г.* Уравнения равновесия упругопластической круговой пластины на основании Пастернака // Механика. Исследования и инновации, 2018, т. 11, No. 11, С. 127–133.
25. *Нестерович, А.В.* Напряженное состояние круговой трехслойной пластины при осесимметричном нагружении в своей плоскости // Механика. Исследования и инновации, 2019, т. 12, No. 12, С. 152–157.
26. *Нестерович, А.В.* Напряжения в круговой пластине типа Тимошенко при неосесимметричном растяжении-сжатии // Механика. Исследования и инновации, 2018, т. 11, No. 11, С. 195–203.
27. *Салицкий В.С.* Изгиб круговой пятислойной пластины // Теоретическая и прикладная механика, Минск, БНТУ, 2023, вып. 38, С. 234–239.
28. *Захарчук Ю.В.* Напряженно-деформированное состояние круговой трехслойной пластины со сжимаемым заполнителем. // Механика. Исследования и инновации, 2019, т. 12, No. 12, С. 66–75.
29. *Захарчук Ю.В.* Деформирование круговой трехслойной пластины с легким сжимаемым заполнителем // Теоретическая и прикладная механика, Минск, БНТУ, 2018, вып. 33, С. 363–369.
30. *Старовойтов Э. И., Леоненко Д. В.* Переменный изгиб трехслойного стержня со сжимаемым заполнителем в нейтронном потоке // Изв. Сарат. ун-та. Нов. сер. Сер. Математика. Механика. Информатика, 2017, т. 17, вып. 2, С. 196–208.
31. *Старовойтов Э.И., Абдусаттаров А., Рузиева Н.Б.* Циклическое нагружение упругопластических трёхслойных стержней с учетом их повреждаемости // Узб. журнал Проблемы механики, 2023, No. 1, С. 66–74.
32. *Старовойтов Э.И., Леоненко Д.В., Абдусаттаров А.* Знакопеременное термосиловое нагружение трёхслойной пластины погонными моментами // Узб. журнал «Проблемы механики», 2023, No. 3, С. 20–30.
33. *Старовойтов Э.И., Яровая А.В.* Вязкоупругопластический трехслойный стержень при термосиловых нагрузках // Изв. РАН, Механика твердого тела. 1998, №3, С. 109–116.
34. *Yarovaya, A.V.* Thermoelastic bending of a sandwich plate on a deformable foundation // International Applied Mechanics, 2006, vol. 42, No. 2, pp. 206-213.
35. *Яровая* А.В. Термоупругопластический изгиб трехслойного стержня в условиях абляции // Материалы, технологии, инструменты, 2000, т. 5, No. 5, С. 23-25.
36. *Яровая А.В.* Перемещения в трехслойной ортотропной пластине с усиливающей накладкой // Механика. Исследования и инновации, 2017, т. 10, No. 10, С. 224-232.
37. *Yarovaya A.V* Deformation of layered structural elements in a temperature-radiation field // Strength of Materials, 2004, vol. 36, No. 6, pp. 630-635.

ЗАКОНОМЕРНОСТИ ДЕФОРМИРОВАНИЯ И РАЗРУШЕНИЯ АСФАЛЬТОБЕТОНА

Телтаев Б.Б.[1,2], Искакбаев А.И.[1,3], Айтбаев Е.Е.[1,2], Жайсанбаев А.С.[2]

[1]*Институт механики и машиноведения им.академика У.А.Жолдасбекова, Алматы, Казахстан*

[2]*Дорожный научно-производственный центр, Алматы, Казахстан*

[3]*Казахский национальный университет им. аль-Фараби, Алматы, Казахстан*

E-mail: bagdatbt@yahoo.com

Аннотация: *Представлены экспериментально установленные закономерности деформирования и разрушения плотного мелкозернистого асфальтобетона типа Б, приготовленного с применением окисленного битума марки БНД 100/130, при ползучести при одноосном растяжении. Предложены модели деформирования для разных стадий ползучести.*

Ключевые слова: *асфальтобетон, ползучесть, одноосное растяжение, аппроксимация, модели деформирования.*

1. Введение

Асфальтобетон является одним из основных дорожных материалов в мире. Он главным образом используется для устройства верхних прочных слоев дорожной одежды автомобильных дорог [1]. Дорожное асфальтобетонное покрытие в течение длительного периода, называемого сроком службы, постоянно подвергается к совместному воздействию механических нагрузок от автомобилей и атмосферных (климатических, погодных) факторов сверху [2-4]. На его работу также оказывают влияние грунтовые и гидрологические факторы снизу. Чтобы асфальтобетонное покрытие в течение всего срока службы сохранило прочность под воздействием указанных выше факторов, асфальтобетон должен иметь ряд важных характеристик. В этом вопросе, имеющем важное практическое значение, основой

является знание закономерностей деформирования и разрушения асфальтобетонов под действием механических сил.

В настоящей работе представлены экспериментально установленные закономерности деформирования и разрушения плотного мелкозернистого асфальтобетона типа Б, приготовленного с применением окисленного битума марки БНД 100/130, при ползучести при одноосном растяжении. Предложены модели деформирования для разных стадий ползучести.

2. Характеристики кривой ползучести

Кривая ползучести асфальтобетона имеет три характерных участка (рисунок 1): участок I неустановившейся ползучести; участок II установившейся ползучести; участок III ускоренной ползучести. На участке I деформация увеличивается со временем, но скорость деформирования со временем уменьшается. На участке II деформация увеличивается с постоянной скоростью. На третьем участке скорость деформирования со временем увеличивается и в конце участка испытываемый образец разрушается. Названия всех характеристик кривой ползучести асфальтобетона, приведенных на рисунке 1, представлены в таблице 1.

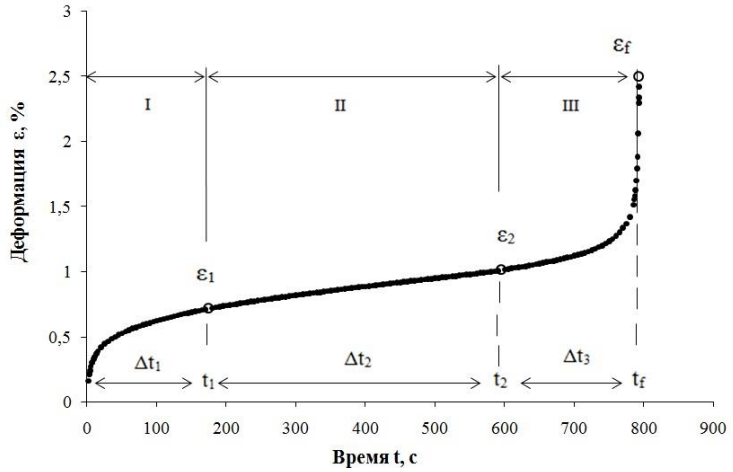

Рисунок 1. Кривая ползучести асфальтобетона под напряжением σ = 0,041 МПа при температуре T = 48ºC

Таблица 1. Описание характеристик кривой ползучести

Обозначение характеристики	Наименование характеристики
I	участок неустановившейся ползучести
II	участок установившейся ползучести
III	участок ускоренной ползучести
Δt_1	длительность участка неустановившейся ползучести
Δt_2	длительность участка установившейся ползучести
Δt_3	длительность участка ускоренной ползучести
ε_1	деформация в конце участка I (в начале участка II) кривой ползучести
ε_2	деформация в конце участка II (в начале участка III) кривой ползучести
ε_3	деформация разрушения, соответствующая моменту разрушения

3. Неустановившейся ползучесть

На рисунке 2 представлены кривые неустановившейся ползучести асфальтобетона, построенные по экспериментальным данным, полученным при разных напряжениях и при

разных температурах. На этих рисунках точками обозначены экспериментально определенные значения деформации, а линии представляют собой соответствующие аппроксимации по следующему выражению:

$$\varepsilon_I(t) = \varepsilon_0 \left[1 + \frac{\delta}{1-\alpha} t^{(1-\alpha)}\right], \quad (1)$$

где $\varepsilon_I(t)$ - деформация в момент времени t;

ε_0 - условно мгновенная деформация;

α, δ - параметры аппроксимации.

Как видно, соответствие аппроксимирующих кривых и экспериментальных деформаций очень хорошее. Такое хорошее соответствие экспериментальных и рассчитанных деформаций получено практически при всех рассмотренных напряжениях и температурах.

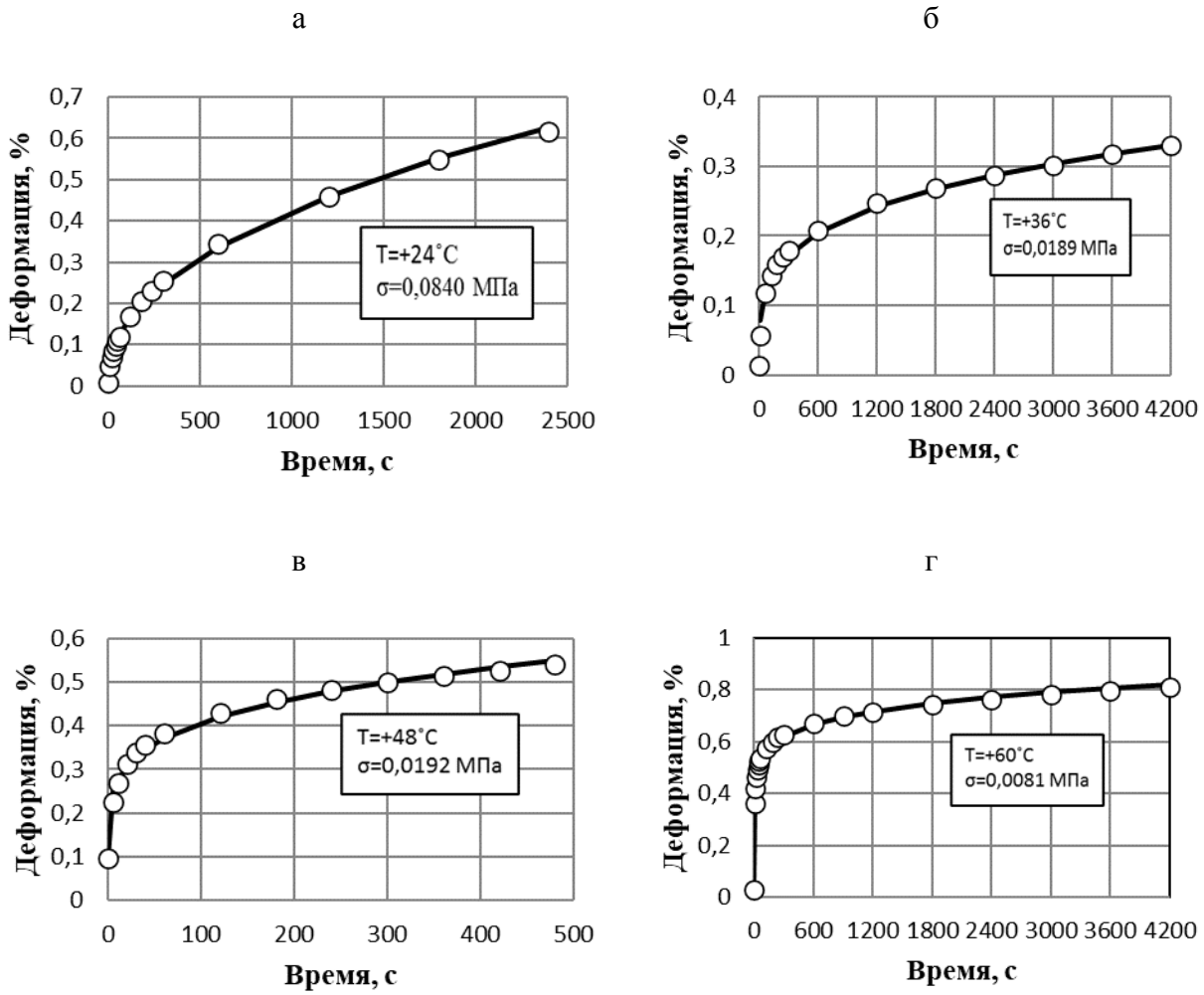

Рисунок 2. Кривые неустановившейся ползучести асфальтобетона:
◦ эксперимент – аппроксимация

Значения параметров ε_0, α и δ для кривых неустановившейся ползучести, показанных на рисунк2, даны в таблице 2.

Таблица 2. Значения параметров ε_0, α, δ

Температура, ˚С	Напряжение σ, МПа	Параметры		
		ε_0, %	α	δ
+24	0,0840	0,0066	0,54	1,23
+36	0,0189	0,0139	0,74	0,67
+48	0,0192	0,0954	0,76	0,26
+60	0,0081	0,0297	0,89	1,17

Можно утверждать, что выражение (1) с параметрами ε_0, α и δ, описывает неустановившуюся ползучесть асфальтобетона с высокой точностью; мы располагаем аналитическим выражением (1) для неустановившейся ползучести асфальтобетона, которое может быть использовано при изучении его других физических и механических характеристик.

Важной характеристикой неустановившейся ползучести материала является ее длительность t_1. Весь процесс ползучести, включая и процесс неустановившейся ползучести, происходит во времени. Неустановившаяся ползучесть продолжается только до времени t_1, за которым начинается другой характерный вид ползучести - установившаяся ползучесть материала с другими физическими механизмами и параметрами. Поэтому очень важно изучить зависимость длительности неустановившейся ползучести от влияющих факторов и желательно иметь для практического использования математическое выражение, описывающее ее. Экспериментально установлено, что длительность неустановившейся ползучести t_1 с увеличением напряжения и повышением температуры уменьшается и удовлетворительно описывается следующим выражением:

$$t_1 = 1.3 \cdot 10^{-25} \cdot \exp\left(\frac{16\,733.96}{T_K}\right) \cdot \sigma^{-(15.05-0.038 \cdot T_K)}. \qquad (2)$$

где t_1 - длительность неустановившейся ползучести, с; σ - напряжение, МПа; $T_к$ - термодинамическая температура, К.

Как видно, полученное выражение состоит из произведения экспоненциальной и степенной функций. У обеих функций аргументом является температура, что указывает на исключительно важное значение температуры при любых значениях напряжения.

Еще одной важной характеристикой деформирования вязкоупругих материалов является скорость деформации. Хорошо известно, что она как физико-механическая характеристика материала входит в разрешающие уравнения в фундаментальных теориях вязкого течения жидкостей и пластического деформирования вязких твердых тел [5, 6]. В нашем случае скорость деформации покажет: как быстро изменяется величина деформации асфальтобетона во времени на участке неустановившейся ползучести.

Продифференцировав уравнение (1) для деформации неустановившейся ползучести, получим следующее выражение для скорости неустановившейся ползучести асфальтобетона:

$$\dot{\varepsilon}_I(t) = \frac{\varepsilon_0 \cdot \delta}{t^{\alpha}}, \quad (0 < t \le t_1). \qquad (3)$$

Из выражения (3) видно, что в начальный момент времени (t=0) скорость деформации (теоретически) бесконечна; с течением времени она уменьшается по степенной зависимости и в конце участка неустановившейся ползучести ($t=t_1$) имеет значение, равное скорости установившейся ползучести на втором участке кривой ползучести.

4. Установившейся ползучесть

Подставив выражение (2) для длительности неустановившейся ползучести в выражение (3), получим следующее выражение для скорости установившейся ползучести асфальтобетона:

$$\dot{\varepsilon}_{II} = \varepsilon_0 \cdot \delta \left[1{,}3 \cdot 10^{-25} \cdot \exp\left(\frac{16\,733{,}96}{T_k}\right) \cdot \sigma^{-(15{,}05-0{,}038 \cdot T_k)}\right]^{-\alpha}. \qquad (4)$$

Скорость установившейся ползучести является важным показателем асфальтобетона, так как она напрямую характеризует процесс пластического деформирования. В дальнейшем она может быть включена в модели по прогнозу колеи на асфальтобетонном покрытии автомобильной дороги.

Обычно чтобы экспериментально определить значение скорости установившейся ползучести, испытание материала на ползучесть должно выполняться до конца участка установившейся ползучести, т.е. требуется большая продолжительность эксперимента. Особенностью выражения (4) является то, что оно дает возможность определения численного значения скорости установившейся ползучести по результатам испытания асфальтобетона на ползучесть только до конца участка I (участок неустановившейся ползучести). Это позволяет существенно сократить затраты времени и материальных ресурсов, а также объемы вычислительных работ. Так, например, экспериментальные результаты показали, что при температуре 20ºС средние относительные длительности участков I, II и III кривой ползучести асфальтобетона равны 13%, 63% и 24 % соответственно [7]. Другими словами, методический подход, по которому получено выражение (4), дает возможность сократить продолжительность экспериментов почти до 5 раз.

Другой важной особенностью выражения (15) является то, что все параметры, входящие в него, имеют ясный физический смысл: термодинамическая температура $T_к$, напряжение σ, параметры ползучести ε_0, δ, α. Из выражения (4) видно, что скорость установившейся ползучести прямо пропорциональна скорости деформации при длительности действия нагрузки 1 секунда ($\varepsilon_0 \cdot \delta$) и влияние на нее длительности неустановившейся ползучести характеризуется параметром α (логарифмическим замедлением).

Предлагается рассматривать весь процесс ползучести вязко-упруго-пластического материала (в том числе асфальтобетона) как течение вязкой жидкости и характеризовать его посредством вязкости. Тогда участок I неустановившейся ползучести и участок II установившейся ползучести кривой ползучести материала можно называть участками переменной (участок I) и постоянной (участок II) вязкости.

Механическое (реологическое) поведение исследуемого асфальтобетона может быть описано следующей моделью:

$$\begin{cases} \lambda(t) = \dfrac{10^2}{\varepsilon_0 \cdot \delta} \cdot \sigma \cdot t^{\alpha} \qquad (0 \le t < t_1), \\ \eta = \dfrac{10^2}{3 \cdot \varepsilon_0 \cdot \delta} \left[1{,}3 \cdot 10^{-25} \cdot \exp\left(\dfrac{16733{,}96}{T_k} \right) \cdot \sigma^{-(15{,}05 - 0{,}038 \cdot T_k)} \right]^{\alpha} \qquad (t_1 \le t \le t_2). \end{cases} \tag{5}$$

где λ(t) - вязкость на участке неустановившейся ползучести, МПа·с; η - вязкость на участке установившейся ползучести, МПа·с.

Эта модель имеет важное практическое значение, так как она напрямую характеризует способность асфальтобетона к сдвиговым деформациям и может быть использована при прогнозе накопления пластических деформаций (глубина колеи) в нежестких дорожных одеждах автомобильных дорог. В дальнейшем, она может быть увязана с выражениями для вязкости жидкостей, полученными Я.И. Френкелем на основе кинетической теории жидкостей [8] и Г. Эйрингом на основе теории абсолютных скоростей реакции (the theory of rate processes) [9, 10], что позволит объяснить явления вязкого и пластического деформирования асфальтобетонов на основе положений молекулярной физики, термодинамики и квантовой физики.

5. Ускоренная ползучесть

Как было отмечено выше, при температуре 20ºС продолжительность периода ускоренной ползучести асфальтобетона составляет почти четверть ее длительной прочности. В этом периоде идет ускоренное накопление повреждений, возникает магистральная трещина и разрушение материала (разделение на части) в конце периода. Нами предложено деформацию ускоренной ползучести описывать следующим выражением:

$$\varepsilon_{III}(t) = B * \sigma^{m} \frac{(n+1)\cdot t_f}{(n+1-q)} \left[1 - \left(1 - \frac{t}{t_f} \right)^{\left(\frac{n+1-q}{n+1}\right)} \right], \quad (6)$$

где t_f - длительная прочность асфальтобетона, с; B, m - параметры установившейся ползучести.

Комплексный параметр q определяется по выражению:

$$q = n + 1 - \frac{1}{\varepsilon_f} \left(\frac{B}{A} \right) \sigma^{(m-n)}, \quad (7)$$

где ε_f - деформация разрушения, %; A, n - параметры длительной прочности.

Выражение (6) включает длительную прочность, деформацию разрушения, параметры установившейся ползучести и длительной прочности, т.е. оно представляет собой не только подходящую для аппроксимации математическую функцию времени, но и аналитическое выражение, имеющее ясный физический смысл и включающее параметры деформирования предшествующего периода (участка установившейся ползучести) и момента разрушения (длительной прочности) асфальтобетона.

На рисунке 3 представлены несколько кривых ускоренной ползучести асфальтобетона при разных напряжениях при температуре 22-24℃. Аппроксимация экспериментально полученных значений деформаций осуществлено выражением (6). Как видно, точность аппроксимации высокая.

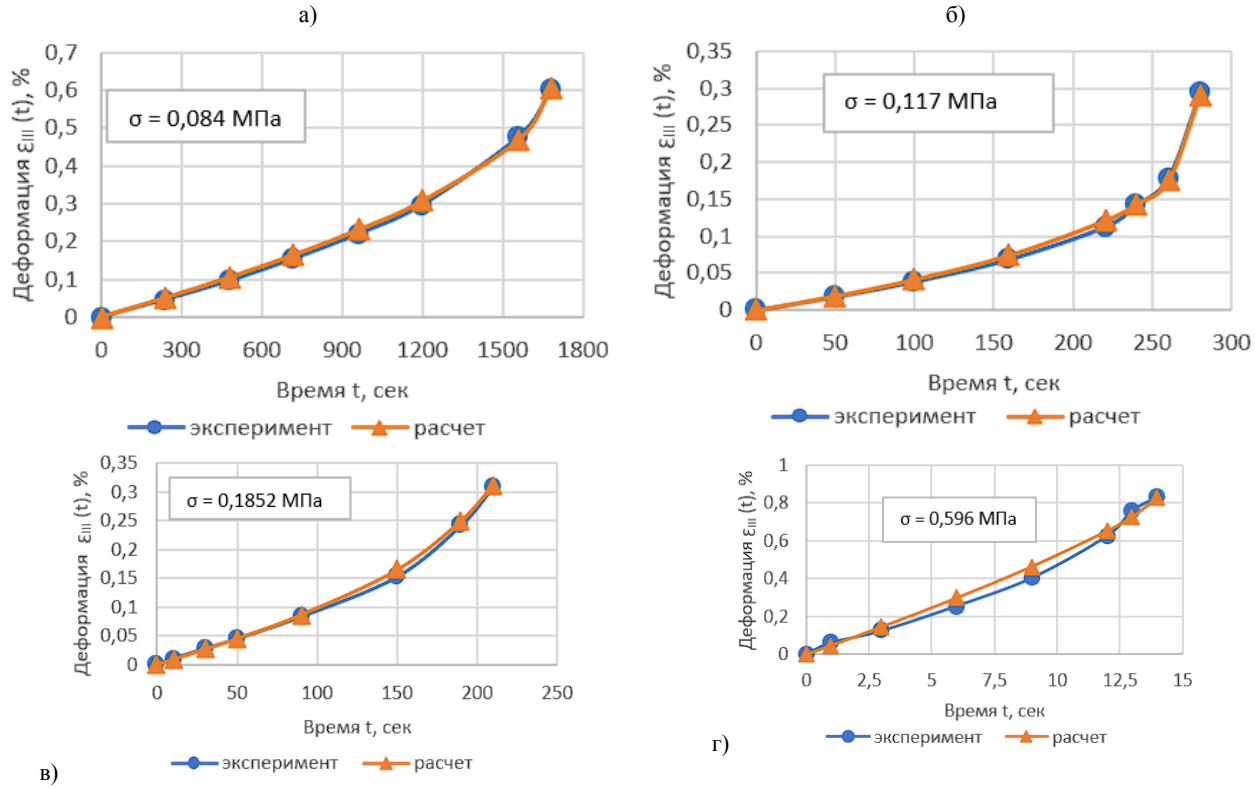

Рисунок 3. Кривые ускоренной ползучести асфальтобетона

6. Заключение

Представленные закономерности деформирования и разрушения асфальтобетона служат основой для более глубокого понимания работы дорожных асфальтобетонных покрытий в сложных условиях их эксплуатации.

Предложенные модели деформирования на разных характерных стадиях ползучести могут быть использованы при прогнозе характеристик работоспособности асфальтобетонных покрытий.

7. Благодарность

Авторы выражают искреннюю благодарность за финансовую поддержку фундаментальных исследований Министерству науки и высшего образования Республики Казахстан (номер гранта: BR20280990).

Литература

1. *MS-4. The asphalt handbook. 7th Edition. Lexington, Asphalt Institute, 2007. 788 p.*

2. *Yoder E.J., Witczak M.W. Principles of pavement design. John Wiley & Sons Inc., New Jersey. 1975. 736 p.*

3. *Huang Y.H. Pavement analysis and design. 2nd Edition. Pearson Education, Inc. Upper Saddle River. New Jersey. 2004. 775 p.*

4. *Papagiannakis A.T., Masad E.A. Pavement design and materials. New Jersey, John Wiley &Sons Inc., 2008. 542 p.*

5. *Nadai A. Theory of flow and fracture of solids. MacGraw-Hill. New York. 1963.*

6. *Hill R. Mathematical theory of plasticity. Oxford University Press Inc. New York. 1950.*

7. *Teltayev B.B., A. Iskakbayev, F. Andriadi, K. Estayev, E. Suppes, A. Iskakbayeva. Experimental research of creep, recovery and fracture processes of asphalt concrete under tension. Proceedings of the 24th International Congress of Theoretical and Applied Mechanics (XXIV ICTAM, 2016), Monreal, Canada.*

8. *Френкель Я.И. Кинетическая теория жидкостей. Ленинград: Наука, 1975.-592 с.*

9. *Glasstone S., Laidler K., Eyring H. The theory of rate processes, McGraw-Hill, New York, 1941.*

10. *Fox T.G., Gratch S., Loshaek S. Viscosity relationship for polymers in bulk and concentrated solutions, in: F.R. Eirich (Ed.), Rheology. Theory and applications. Volume 1, Academic Press Inc., New York, 1956, pp. 431-492.*

DISPLACEMENTS IN THE TORSIONAL VIBRATIONS OF A ROUND ELASTIC ROD IN A VISCOUS FLUID FLOW

Khudoynazarov Kh.[1], Gadayev A.B.[2]

[1]*Samarkand State University, Samarkand, Uzbekistan*

E-mail: gadayevaziz@gmail.com.

Abstract. *In the presented article, the issue of calculation is solved, taking into account the torsional displacements that occur in the cross-sections of the circular elastic rod in the flow of a viscous fluid moving at a constant velocity, and the dynamic forces acting on the surface and the free end of the rod. As the main vibration equations, the refined equation derived by the authors was adopted. The solution of the problem was obtained by a numerical method, and based on the obtained results, were constructed graphs dependent from longitudinal coordinates and time of torsional displacements of the surface points .*

Keywords: *circular steering wheel, torsional vibrations, displacement, kinematic impact, head parts.*

1. Introduction.

In the construction of the main relations of the rod theory, the problem consists in transferring the spatial three-dimensional coordinates to two-dimensional or one-dimensional [1-4]. In this way, researchers [5,6] have obtained refined differential equations of vibrations taking into account certain physical, mechanical or geometrical factors. In the work presented [7], two-layer elastic cylindrical shells are considered, between which there is a viscous incompressible fluid layer, and a mechanical model of a pipe with free ends is considered.

In some research studies, in order to consider the actions of the drilling rig in the modeling of its torsional vibrations, the classical equations of vibrations of the rod theory are presented in [8-9]. The problem [10] of the interaction of an elastic circular-cylindrical shell with an ideal incompressible fluid flow was considered. Oscillation behavior of fluid-filled circular cylindrical layer [11] was studied. Analytical and numerical studies [12] were conducted for the vibrations of cylindrical shells. The equations of motion of a solid body (shell) and a liquid are based on the

equations of motion of an isotropic cylindrical three-dimensional body and viscous fluid particles, respectively. It is important to study the effect of fluid on the axisymmetric vibrations of an elastic circular cylindrical shell with fluid inside and around it [13]. In the article [14], thick circular cylindrical shells were numerically analyzed using the theory of high-order shells. In recent years, the study of longitudinal waves in physically nonlinear elastic shells containing a viscous incompressible fluid between the shells [15] has been given great importance.

2. The imposition of the issue and its solution.

A circular elastic rod with a radius r_0 and length equal to l initially at rest is placed in a viscous liquid stream moving at a constant velocity V. In addition to the effect of viscous fluid on the surface of the rod $f_{r\theta}(z,t)$, dynamic stress also affects it. One end of the rod $z=0$ is free, and the other end $z=l$ is clamped. A kinematic shock given as the amplitude $g(t)$ is applied to the free end of the rod $z=0$. Determine the torsional displacement of a point on an arbitrary cross-section of the rod depending on the spatial coordinate z and time t.

Taking into account the external stress set in the condition of the problem, we accept the equation of torsional vibrations of the rod in the following form [16]

$$\frac{r_0}{2}\lambda U_{\theta,0}+\frac{8\mu_2'}{r_0\mu}\left(\frac{\partial}{\partial t}-V\frac{\partial}{\partial z}\right)U_{\theta,0}=\frac{2}{\mu r_0}M_0^{-1}\left[f_{r\theta}(z,t)\right]. \tag{1}$$

It consists of the λ^n differential operator included in equation (1) and has the following form [17]

$$\lambda^n=\left[\frac{1}{b^2}\left(\frac{\partial^2}{\partial t^2}\right)-\frac{\partial^2}{\partial z^2}\right]^n,\ b^2=\frac{\mu}{\rho},\ n=0,1,2,... \tag{2}$$

here $b^2=\frac{\mu}{\rho}$ - is velocity of propagation of transverse waves in layer material; μ - is shear coefficient (Lame coefficient) of the layer material; ρ - density of layer material; $U_{\theta,0}$ - the main part of the torsional displacement U_θ of the rod points.

Now let's find out what the main researcher $U_{\theta,0}$ of unknown function means for a circular rod. For this we use the following expression of transition [17]

$$U_\theta=2\sum_{n=0}^{\infty}\frac{(r/2)^{2n+1}}{n!(n+1)!}\lambda^n U_{\theta,0}. \tag{3}$$

If here $n=0$ it follows that

$$U_\theta=rU_{\theta,0}, \tag{4}$$

Hence, it follows from equation (4) that the torsional displacements of the rod points are directly proportional to the introduced new function, and this new function is a dimensionless quantity. If we recall Euler's formula for rotational motion, it turns out that the newly introduced function $U_{\theta,0}$ is the torsion angle.

The received equation (1) was written in the following form, taking into account the formula (2) for the operator λ^n:

$$\frac{r_0^2}{4}\left(\frac{1}{b^2}\frac{\partial^2 U_{\theta.0}}{\partial t^2}-\frac{\partial^2 U_{\theta.0}}{\partial z^2}\right)+\frac{4\mu_2'}{\mu}\left(\frac{\partial U_{\theta.0}}{\partial t}-V\frac{\partial U_{\theta.0}}{\partial z}\right)=\frac{1}{\mu}f_{r\theta}(z,t) \tag{5}$$

Using the following formulas, we transfer this equation to dimensionless coordinates:

$$t=\frac{l}{b}t^*,\qquad z=l\cdot z^*.$$

Then, after a number of substitutions, we form this equation:

$$\frac{\partial^2 U_{\theta.0}}{\partial t^2}-\frac{\partial^2 U_{\theta.0}}{\partial z^2}+\frac{16\mu_2'\cdot l\cdot b}{\mu\cdot r_0^2}\left(\frac{\partial U_{\theta.0}}{\partial t}-\frac{V}{b}\frac{\partial U_{\theta.0}}{\partial z}\right)=\frac{4l^2}{r_0^2}\frac{1}{\mu}f_{r\theta}(z,t). \tag{6}$$

Here $\frac{16\mu_2'\cdot l\cdot b}{\mu\cdot r_0^2}$, the quantity is a dimensionless quantity, because the unit of measurement $[\mu_2']=Pa\cdot s$, of the coefficient of dynamic viscosity of a viscous liquid is the unit of measurement of the coefficient (Lame) of displacement of a circular viscoelastic material $[\mu]=Pa$. If these units of measurement are put in their place, the above claim is correct.

We can see the voltage function $f_{r\theta}(z,t)=\frac{P(z,t)}{S_{yon}}$, on the right side of this equation. Here $P(z,t)$ is the force acting on the side surface of the rod. It is known that the surface of the side of the rod is calculated using the formula $S_{yon}=2\pi\, r_0\, l$. Then the right-hand side of the basic equation (6) of torsional vibrations of a circular rod will have the following form

$$\frac{4}{\mu}\frac{l^2}{r_0^2}f_{r\theta}(z,t)=\frac{2l\,P(z,t)}{\pi\, r_0^3\mu}. \tag{7}$$

Substituting the resulting expression (7) into equation (6), we get the following vibration equation that needs to be solved

$$\frac{\partial^2 U_{\theta.0}}{\partial t^2}-\frac{\partial^2 U_{\theta.0}}{\partial z^2}+\frac{16\mu_2'\cdot l\cdot b}{\mu\cdot r_0^2}\left(\frac{\partial U_{\theta.0}}{\partial t}-\frac{V}{b}\frac{\partial U_{\theta.0}}{\partial z}\right)=\frac{2l\,P(z,t)}{\pi\, r_0^3\mu}. \tag{8}$$

We set the initial and boundary conditions of the issue according to the conditions given in the formulation of the problem. At the beginning of time $t=0$ the rod is at rest, i.e., its twist and velocity are zero at the initial position, i.e., the initial conditions are as follows

$$U_\theta(r,z,t)\big|_{t=0}=0,\qquad \left.\frac{\partial U_\theta(r,z,t)}{\partial t}\right|_{t=0}=0,\qquad 0\le z\le l. \tag{9}$$

Similarly, the shock from the free end of the rod and the no-twisting conditions at the clamped end take these forms

$$U_\theta(r_0,z,t)\big|_{z=0}=g(t),\qquad U_\theta(r,z,t)\big|_{z=l}=0,\qquad 0\le t\le T. \tag{10}$$

Here, $T=l/b$ – is the time taken for a transverse wave to travel a distance of l-length from one end of the rod to the other.

Considering the expression (4) of the torsional displacement in the initial and boundary conditions formed by (9) and (10), they can be written as follows.

Initial conditions

$$U_{\theta.0}(z,t)\big|_{t=0}=0,\qquad \left.\frac{\partial U_{\theta.0}(z,t)}{\partial t}\right|_{t=0}=0,\qquad 0\le z\le 1; \tag{11}$$

Boundary conditions

$$U_{\theta.0}(z,t)\big|_{z=0}=\frac{1}{r_0}g(t),\qquad U_{\theta.0}(z,t)\big|_{z=1}=0,\qquad 0\le t\le 1. \tag{12}$$

In further numerical calculations, we get the function *g(t)* representing the kinematic impact from the rod tip in the following form

$$g(t)=A\sin(\pi\, t) \tag{13}$$

We also assume that the external force applied to the surface of the rod is $p(z,t)$ =*constant*.

In the conditions (11) and (12) above, we have transferred to dimensionless coordinates with the above formulas, and therefore, we specify that the fields of change of dimensionless and longitudinal coordinates are $0\le t^*\le 1,\ 0\le z^*\le 1$.

In that case, we determine the numerical solution of equation (8) with conditions (11) and (12) using the mathematical package of the Maple-17 program. The following quantities were selected for numerical calculations:

$$l=10\ m;\ r_0=0.02\ m;\ P=4\cdot 10^3\,[N]=4[kN];\ A\approx 2\cdot 10^{-3}m.$$

Steel was chosen as the material of the rod and these values were adopted for its physical and mechanical characteristics

$$E=2\cdot 10^{11}Pa\ ;\ \ \mu=8\cdot 10^{10}\ Pa;\quad \nu=0{,}32;\quad \rho=7800\,kg/m^3\ .$$

The constant velocity and dynamic viscosity coefficient of the viscous liquid (Glycerin) flowing from the outside of the rod is as follows

$$V=10\frac{m}{s};\quad \mu_2'=1{,}480\ \ Pa\cdot s\ .$$

Calculations were carried out based on these accepted parameters.

3. Numerical results and discussion.

Below, graphs constructed on the basis of numerical values of torsional displacement of the rod points U_θ calculated by formula (3) on the basis of solutions of equation (8) satisfying conditions (11) - (12) are presented in figures 1 and 2.

In the presented figure 1, the point (*r=0.02 m*) on the edges of different sections of the rod (*z=0.2; 0.4; 0.6; 0.8*), the external force P is not taken into account ($P=0$) and the reaction R of the viscous fluid is taken into account for the obtained ($R\neq 0$) case, graphs of time-dependent changes of torsional displacement U_θ are presented (tables 1, 2). Graphs have a sinusoidal character, regardless of which section they are in. This result is a consequence of the kinematic shock from the rod tip being given by the sine function.

We would also like to note that the torsional displacement of the edge point of the arbitrary cross-section of the rod is explained by the harmonic function of the kinematic impact placed on the rod tip, the fact that the excitations in this cross-section have the character of a sinusoidal wave. The reason that the graph of displacement fades with time is also due to the exponential nature of the same function.

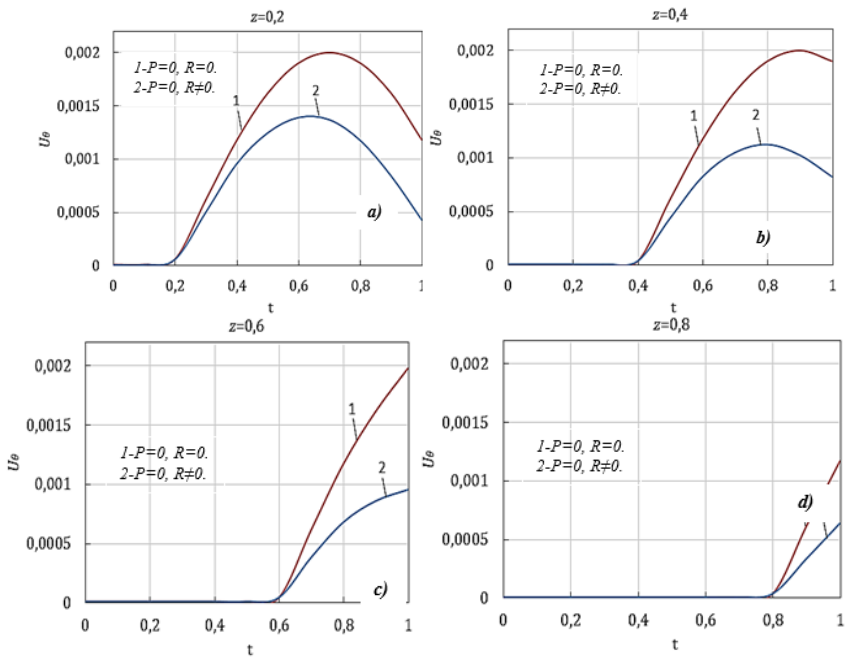

Figure 1 - In the cases where the external force P is not taken into account ($P=0$) and the reaction R of the viscous fluid is taken into account ($R\neq 0$), the torsion coefficient of the point (r = 0.02 m) on the edges of different sections of the stern (z=0.2; 0.4; 0.6; 0.8) graphs of time-dependent changes U_θ.

The time of the initial displacement of the excitation depends on the cross-section of the point under investigation. For example, this excitation $z = 0{,}2$ starts at the approximate moment of time $t \le 0{,}2$ in the section (Fig. 1.a) and so on. When the external force and fluid reaction are not taken into account ($P = 0, R = 0$), the displacement U_θ reaches its maximum value of *0.002000* in the section (Fig. 1.b) at time *t=0.9* in the interval *0.8< t <1.0* , etc.

The fluid flow reaction outside the rod leads to a sharp decrease in the value of the torsional displacement amplitude (Figures 1.a,b,c,d). In this case, the difference in amplitudes is 43% in the section z=0.2, and this difference reaches 81% in the section z=0.4.

In the presented Figure 2, at different times of time (t=0.3; 0.5; 0.7; 1.0), the external force P of the points on the edges of the section (r=0.02 m) is not taken into account ($P = 0$) and the reaction R of the viscous fluid is taken into account graphs of the changes of the torsional displacements U_θ depending on the coordinate are depicted in the cases obtained ($R \neq 0$). It can be seen from the given graphs (Figures 2.a, b, c, d) that the changes of torsional displacement along the longitudinal coordinate are also sinusoidal in nature. The presence of a small liquid flow under the rod leads to a sharp decrease in the amplitudes of torsional displacements at any time (Fig. 2.c, d), that is, the liquid flow causes the damping of vibrations.

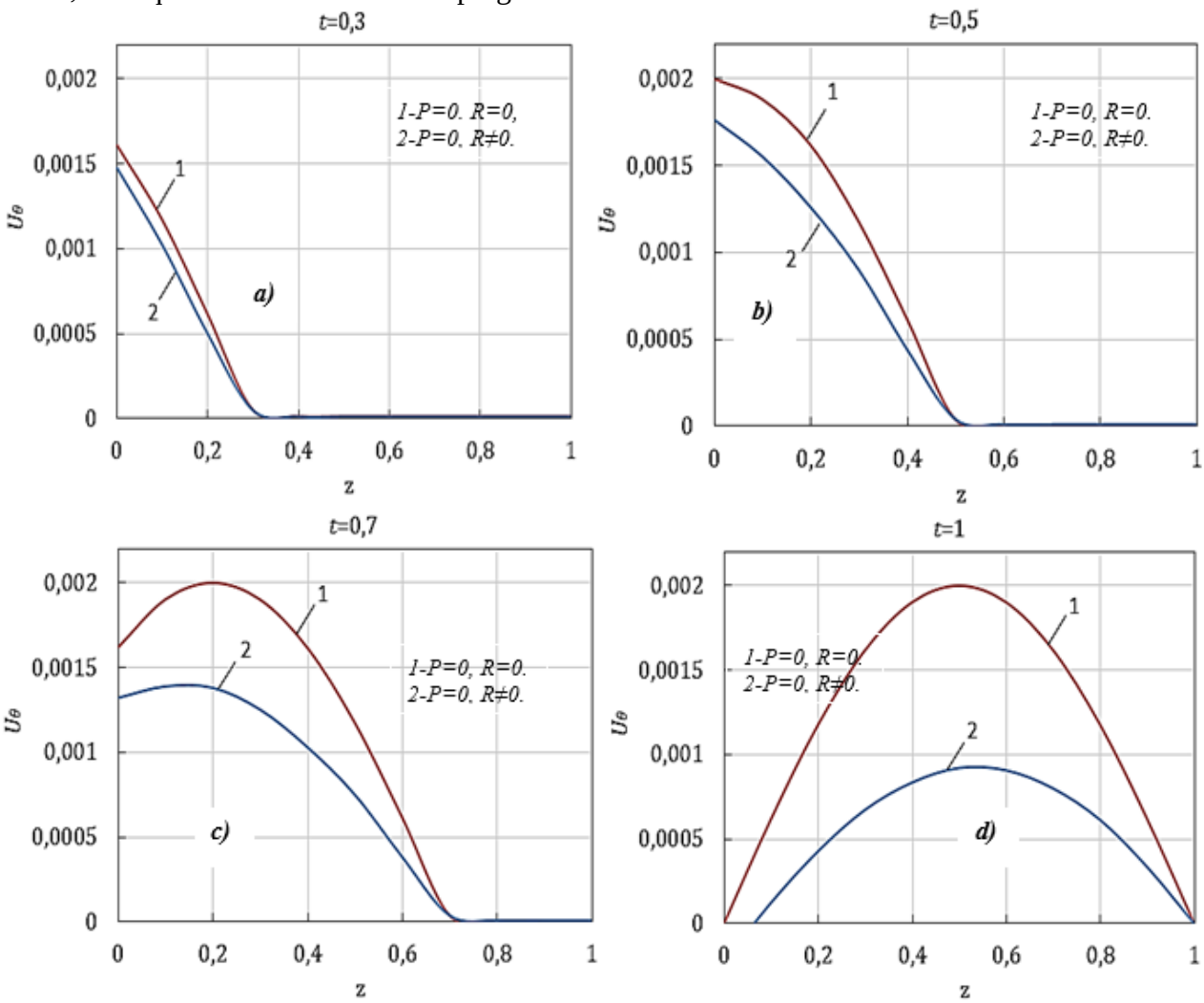

Figure 2. In the cases where the external force P is not taken into account ($P = 0$) and the reaction R of the viscous fluid is taken into account ($R \neq 0$), the torsion coefficient of the point (r = 0.02 m) on the edges of different sections of the stern (t=0,3; 0,5; 0,7; 1,0) graphs of time-dependent changes U_θ .

References.

1. Khudoynazarov Kh. (2024) Longitudinal-radial vibrations of a viscoelastic cylindrical three-layer structure // *Facta Universitatis Series: Mechanical Engineering* https://doi.org/10.22190/FUME231219010K

2. Khudoynazarov, Kh. (2023) A mathematical model of physically nonlinear torsional vibrations of a circular elastic rod. //*Vestnik Tomskogo gosudarstvennogo universiteta. Matematika i mekhanika – Tomsk State University Journal of Mathematics and Mechanics.* 84. pp. 152–166. doi: 10.17223/19988621/84/12
3. Khudoynazarov Kh. (2023) Modeling of nonlinear torsional vibrations of a truncated conical rod, Vestn. Samar. Gos. Tekhn. Univ., Ser. Fiz.-Mat. Nauki [J. Samara State Tech. Univ., Ser. Phys. Math. Sci.], vol. 27, no. 4, pp.704-722. https://doi.org/10.14498/vsgtu 2002
4. Khudoynazarov Kh.Kh., Khalmuradov R.I., Yalgashev B.F. (2021) Longitudinal-radial vibrations of a elastic cylindrical shell filled with a viscous compressible liquid. //*Tomsk state university. Journal of Mathematics and Mechanics.* 69. 139-154. doi 10.17223/19988621/69/11.
5. R.I.Khalmuradov, and B.F.Yalgashev (2020) "Frequency analysis of longitudinal-radial vibrations of a cylindrical shell" IOP Conf. Series: Earth and Environmental Science 614 012087 doi:10.1088/1755-1315/614/1/012087
6. R.I.Khalmuradov and E.A.Ismoilov (2020) Nonlinear vibrations of a circular plate reinforced by ribs. IOP Conf IOP Conf. Ser.: Earth Environ. Sci. 614 012071. DOI: 10.1088/1755-1315/614/1/012071
7. Kondratov D., Kondratova Yu.N., Mogilevich L.I., Khristoforova A.V. (2016) Mathematical modeling of the interaction of two coaxial cylindrical shells with a liquid layer between them under vibration conditions, taking into account shell wear.// *Online journal "NAUKOVEDENIE".* Volume 8, No. 4. http://naukovedenie.ru/PDF/90TVN416.
8. Han J.H., Kim Y.J., Karkoub M. (2013) Modeling of wave propagation in drill strings using vibration transfer matrix methods. // *Journal of the Acoustical Society of America, September*, no. 134 (3), pp. 1920-1931.
9. Ulitin G.M., Pettik Yu.V. (2009) Zbirnik naukovikh prats (galuzeve mashinobuduvannya, budivnitstvo) - Industrial Machine Building, Civil Engineering, Poltava. //*Poltava National Technical Yuri Kondratyuk University Publ*., no. 3 (25), vol. 2, pp. 214-218.
10. Smetanin B.I., Tarasov A.E. Dynamic interaction of a cylindrical shell with a liquid flow. // *ISSN 0321-3005 Izvestiya vuzov. The North Caucasus region. natural sciences.* 2014. No 2, pp. 27-32
11. Kh.Kh. Khudoynazarov, Sh.M. Burkutboyev (2017) Matematicheskaya model krutilnykh kolebaniy vrashayushegosya silindricheskogo sloya s uchetom vnutrenney vyazkoy jidkosti [Mathematical modeling of the rotating cylindrical shell torsional vibrations factored in the internal viscous fluid]. *Matematicheskoe modelirovaniye i chislennye metody-Mathematical modeling and numerical methods*. No 16. pp. 31-47.
12. Syed Ahmed Shah Vibration Analysis of an Infinite Poroelastic Circular Cylindrical Shell Immersed in Fluid. // *Open Journal of Acoustics*, 2012, n 2, c 86-93 39
13. Payal Desai and Tarun Kant. On numerical analysis of axisymmetric thick circular cylindrical shells based on higher order shell theories by segmentation method. // *Journal of Sandwich Structures and Materials* 2015, Vol. 17(2) 130-169 40
14. Lev Mogilevich and Sergey Ivanov, Waves in Two Coaxial Elastic Cubically Non-linear Shells with Structural Damping and Viscous Fluid Between Them. // *www.mdpi.com/journal/Symmetry* 2020, 12, 335; doi:10.3390/*sym*12030335 41
15. Rui Nie, Tianyun Li, Xiang Zhu and Cheng Zhang Analysis of Free Vibration Characteristics of Cylindrical Shells with Finite Submerged Depth Based on Energy Variational Principle. // *Symmetry* 2021, 13, 2162.
16. Khudoynazarov K., Yalgashev B.F. and Mavlonov T. (2021) Mathematical modelling of torsional vibrations of the three-layer cylindrical viscoelastic shell. // *IOP Conf. Series: Mater. Sci. Eng.* 1030 012098 DOI: 10.1088/1757-899X/1030/1/ 012098
17. Khudoynazarov Kh. Unsteady interaction of cylindrical shells and rods with a deformable medium. // *Tashkent: Publisher by name. Abu Ali Ibn Sino*, 2003, 326 c. 6

СОДЕРЖАНИЕ

Секция С – Механика деформируемого твердого тела, геотехника

1. Abdikarimov R.A., Ishmatov A.N., Khodzhaev D.A., Normuminov B.A. Parametric vibrations of a viscoelastic shell of variable thickness 5
2. Abdukadirov F.E., Hasanov T.M. Design and calculation of surface road conductors... 11
3. Adilov F.F. On strengthening of materials with one central crack 15
4. Akhmedov A.B. Applied problems of equilibrium plates in stresses 22
5. Akhmedov A.B., Kuldibaeva L.A. Non-classical theory of the equilibrium of layered plates…….. 31
6. Bekmirzaev D.A., Mansurova N.Sh. Mathematical modeling and numerical solution of problems of underground pipelines under spatial seismic effect …… 38
7. Belyi A.A., Antonyuk A.A., Makhonko A.A. Rationale for structural health monitoring systems implementation on movable bridges ……. 46
8. Bondar I.S., Mamedova J.E. Ensuring the strength of cohesive clay soils railway embankment ……..... 55
9. Djumaev Kh. On the rheological model of asphalt concrete …….. 62
10. Dostanova S.Kh., Issakhanov Y., Kasymova G.T., Tokpanova K.E. Elastic-pliable links to regulate the forces in the superstructures of transport structures …….. 66
11. Eshmatov B.Kh., Abdikarimov R.A. Bending of fiber-reinforced composite wing-like plates ……. 75
12. Eshmuradov D.E., Dzhumamuratov B.A., Elmuradov T.D., Sharipov G.N. Simulation of a dynamic conflict situation in real time flight of a restored aircraft vessel ……. 83
13. Ibragimov B.T., Nishonboev Sh.Z., Abdusattorov A.A., Rashidov J. Evaluation of strength properties in soils enhanced by large crushed stone particles ……. 90
14. Indiaminov R., Djuraev A., Shodmonov J., Indiaminov M. Nonlinear strain of flexible shells in a magnetic field …… 97
15. Ishankhodjayev A.A., Akhmedov Sh.B. On the methodology of reinforcement of t-shaped reinforced concrete beams with carbon fiber materials…… 105
16. Ismoilova S.I., Khazratova T.Ya., Begmanov R.A. Influence of elastic, viscous, and plastic properties on the stress-strain state of yarns under irregular dynamic loads… 112
17. Ismoilova S.I., Khazratova T.Ya., Begmanov R.A., Mamatova N.R. Determination of strain moduli parameters of cotton yarn under the change in its structure…… 120
18. Israilov M.Sh. Solution of the external pochhammer – chree problem and derivation of the proportionality law for bending seismic vibrations of a pipeline in an elastic soil ……. 128
19. Kalandarov A., Khaldjigitov A., Atabayev K. Coupled plane problem of dynamic thermal elasticity in stresses …….. 137
20. Khaldjigitov A.A., Khasanova Z.Z., Djumayozov U.Z. Plane problems in strains for orthopropic bodies ……. 145
21. Khudainazarov Sh., Salimov Sh. Natural vibrations of smokestacks of thermal power plants ……. 154
22. Khudanov U.O., Kadirov T.Zh., Sharifov G.N., Gelchinova S. The influence of surfactants and collagen on the clinker grinding process …….. 165
23. Khudoynazarov Kh.Kh., Akhatov Kh.N. Comparative analysis of torsional vibration of circular cylindrical elastic and visco elastic shells ……. 169
24. Khusainov R.B., Khusainova B.B., Khusainov S.B. Numerical solution to the differential equation of transverse vibrations of an underground pipeline…… 175
25. Khusainov R., Khusainova B., Khusainov S. Oscillations of underground pipelines under nonlinear interaction with soil …….. 185

26. Loginov P., Akbarov N., Khamidov S. Nonlinear wave processes in rods with external friction ……..……. 194
27. Mamasoliev K.M., Sindarov J.A. Analytical method for solving the problem of calculating three-layer plates ……..... 201
28. Mardonov B., Bekmirzaev D., Berdibaev M., Khurramov A., Botabaev N. Assessment of vibrations of superstructures of reinforced concrete bridges under the influence of mobile loads ……. 211
29. Mavlanov T., Khudainazarov Sh.O., Rayimov A.O. Dynamic simulation of a human body by frequency response data ……... 218
30. Miralimov M., Ishanhodjaev A., Normurodov Sh., Usmanov D. Numerical study of the zone of influence of two parallel running tunnels …… 227
31. Mirsaidov M.M., Matkarimov P.J., Juraev D. Assessment of stress-strain state of earth dams considering the spatial operation of structures …….. 232
32. Mirsaidov M.M., Ishmatov A.N., Yuldoshev B.Sh., Urinov B.Kh. Vibrations of plane structures considering the physical nonlinearity of the material 239
33. Mirzaev I., Gainazarov S.M. Effect of the depth of circular lining in an elastic medium with transparent boundary under the impact of seismic waves 250
34. Mirzakhmedov M.I., Yuvmitov A.S., Khurramov A.Ch. Studies on truss bridges 259
35. Normatov Sh.I., Khusanov B.E., Ganieva B.R. On analytical method for assessing the stability of soil slopes 264
36. Normatov Sh.I., Rikhsieva B.B. Stability assessment of pit wall sides determining parameters of slip surface 271
37. Safarov I.I., Mirzakabilov B.N. Natural vibrations of cylinder and spherical shell in elastic medium 276
38. Safarov I.I., Teshaev M.Kh., Rakhmonov B.S., Jalolov F.B. Dynamic stress-strain state of multilayer cylindrical shell under the influence of cylindrical harmonic waves 282
39. Shermukhamedov U.Z., Karimova A.B., Abdullaev A.R., Gulomov D.I. Selection of the type of supporting parts for the seismic stability of continuous reinforced concrete bridges 293
40. Takhirov S.M., Rakhmonov B., Akhmedov M. M., Blondet M. Structural health monitoring of chadra hauly (Khorezm, Uzbekistan) by means of laser scanning 303
41. Takhirov Sh., Zakhidov A., Aitbayev K., Nugmanova A. Temperature monitoring of pavement layers for performance improvements of automotive roads 312
42. Takhirov Sh, Soga Kenichi, Katzev D. Center for smart infrastructure: a comprehensive approach for water infrastructure monitoring and preservation by testing and modeling 320
43. Turdibekov J.E. Analysis of elastic prismatic rods subjected to torsional loads 329
44. Yusupov Y., Sagdullaeva D., Soliev A. Numerical modeling of the coupled dynamic problem of the strain space thermoplasticity theory 335
45. Абдураимов У.К. Расчет конструкции земляного полотна железных дорог из барханных песков на устойчивость по типовым технологическим решениям... 343
46. Абдусаттаров А., Старовойтов Э.И., Рузиева Н.Б. Моделирование нелинейного деформирования и повреждаемости подземных трубопроводов – стержней при циклических нагружениях с учетом больших деформаций 349
47. Абиров Р.А. О механических свойствах армированного бетона 359
48. Василевич Ю.В., Абдусаттаров А., Сабиров Н.Х. Исследование НДС и собственных колебаний цилиндрической трубы из композита 366
49. Кабулов А.В., Норматов И.Х. Проблемы алгоритмизации в механике разрушения 373

50. Каюмов А.Д.. Холжигитов Ш.Б., Рахимбаев О.Д. Обеспечение устойчивости откосов автомобильных дорог в условиях Узбекистана 380
51. Лачугина Е.А. Собственные колебания пятислойной несимметричной по толщине пластины 385
52. Леоненко Д.В. Динамическое нагружение трехслойного стержня на упругом основании локальной импульсной нагрузкой …….. 391
53. Логинов П., Акбаров Н., Хамидов С. Численное решение распространения продольной волны в нелинейной вязкоупругой среде 396
54. Мельникова А.С. Постановка задачи об упругопластическом изгибе трехслойной пластины в терморадиационном поле 402
55. Нестерович А.В. Неосесимметричное деформирование трехслойной круговой пластины линейными нагрузками 407
56. Нугужинов Ж.С., Ахмедиев С.К., Бекетова М.С., Койшыбай Ж.А. Распространение продольных механических волн в упругой области треугольной формы 412
57. Салицкий В.С. Локальное нагружение круглой пятислойной пластины 421
58. Старовойтов Э.И. Деформирование трехслойных пластин в нейтронном потоке…… 426
59. Убайдуллаева Д.Х., Ахмедова М.Ф., Ортикова Н. Изучение деформационных характеристик двухслойного трикотажного переплетение 434
60. Хасанов А.З., Хасанов З.А., Турсунов Ш.А. Экспериментальные исследования контактной задачи балки и грунтового основания 439
61. Шафиева Ю.В. Влияние сжимаемости заполнителя и температурного поля на деформирование трехслойной пластины 447
62. Яровая А.В. Деформирование упругой трехслойной пластины в температурном поле…… 453
63. Телтаев Б.Б., Искакбаев А.И., Айтбаев Е.Е., Жайсанбаев А.С. Закономерности деформирования и разрушения асфальтобетона…….. 459
64. Khudoynazarov Kh., Gadayev A.B. Displacements in the torsional vibrations of a round elastic rod in a viscous fluid flow…….. 465